# CHEMO-RADIATION-RESISTANCE IN CANCER THERAPY

EDITED BY: Zhe-Sheng Chen, Xiaoping Lin and Dexin Kong
PUBLISHED IN: Frontiers in Pharmacology and Frontiers in Oncology

frontiers Research Topics

# frontiers



ISSN 1664-8714
ISBN 978-2-88976-334-4
DOI 10.3389/978-2-88976-334-4

## About Frontiers

Frontiers is more than just an open-access publisher of scholarly articles: it is a pioneering approach to the world of academia, radically improving the way scholarly research is managed. The grand vision of Frontiers is a world where all people have an equal opportunity to seek, share and generate knowledge. Frontiers provides immediate and permanent online open access to all its publications, but this alone is not enough to realize our grand goals.

## Frontiers Journal Series

The Frontiers Journal Series is a multi-tier and interdisciplinary set of open-access, online journals, promising a paradigm shift from the current review, selection and dissemination processes in academic publishing. All Frontiers journals are driven by researchers for researchers; therefore, they constitute a service to the scholarly community. At the same time, the Frontiers Journal Series operates on a revolutionary invention, the tiered publishing system, initially addressing specific communities of scholars, and gradually climbing up to broader public understanding, thus serving the interests of the lay society, too.

## Dedication to Quality

Each Frontiers article is a landmark of the highest quality, thanks to genuinely collaborative interactions between authors and review editors, who include some of the world's best academicians. Research must be certified by peers before entering a stream of knowledge that may eventually reach the public - and shape society; therefore, Frontiers only applies the most rigorous and unbiased reviews.
Frontiers revolutionizes research publishing by freely delivering the most outstanding research, evaluated with no bias from both the academic and social point of view. By applying the most advanced information technologies, Frontiers is catapulting scholarly publishing into a new generation.

## What are Frontiers Research Topics?

Frontiers Research Topics are very popular trademarks of the Frontiers Journals Series: they are collections of at least ten articles, all centered on a particular subject. With their unique mix of varied contributions from Original Research to Review Articles, Frontiers Research Topics unify the most influential researchers, the latest key findings and historical advances in a hot research area! Find out more on how to host your own Frontiers Research Topic or contribute to one as an author by contacting the Frontiers Editorial Office: frontiersin.org/about/contact

# CHEMO-RADIATION-RESISTANCE IN CANCER THERAPY

Topic Editors:
**Zhe-Sheng Chen,** St. John's University, United States
**Xiaoping Lin,** Sun Yat-sen University Cancer Center (SYSUCC), China
**Dexin Kong,** Tianjin Medical University, China

**Citation:** Chen, Z.-S., Lin, X., Kong, D., eds. (2022). Chemo-Radiation-Resistance in Cancer Therapy. Lausanne: Frontiers Media SA. doi: 10.3389/978-2-88976-334-4

# Table of Contents

frontiers | Frontiers in Pharmacology

EDITORIAL
published: 18 May 2022
doi: 10.3389/fphar.2022.904063

# Editorial: Chemo-Radiation-Resistance in Cancer Therapy

*Xiaoping Lin*[1]*, *Dexin Kong*[2] and *Zhe-Sheng Chen*[3]*

[1]State Key Laboratory of Oncology in South China, Department of Nuclear Medicine, Collaborative Innovation Center for Cancer Medicine, Sun Yat-Sen University Cancer Center, Guangzhou, China, [2]Tianjin Key Laboratory on Technologies Enabling Development of Clinical Therapeutics and Diagnostics, School of Pharmacy, Tianjin Medical University, Tianjin, China, [3]Department of Pharmaceutical Sciences, College of Pharmacy and Health Sciences, Institute for Biotechnology, St. John's University, Queens, New York, NY, United States

**Keywords: chemothearpy resistance, radiationtherapy resistance, cancer, chemoradiation resistance, therapy**

## Editorial on the Research Topic

## Chemo-Radiation-Resistance in Cancer Therapy

In recent years, technical advances in chemotherapy and radiotherapy have helped substantially improve the treatment outcome and quality of life of cancer patients. Nevertheless, successful cancer therapy remains a major challenge, particularly in tumors that are resistant to chemotherapy or radiation therapy. Searching the topic "Chemoradiation Resistance in Cancer Therapy" results in 34 articles (six reviews, 27 original research, and one brief research report) contributed by more than 262 authors with over 90000 views in all of time until 20 April 2022, in the fields of cancer diagnosis and therapeutics. Our aim was to generate a collaborative discussion contributing to the future direction of overcoming chemoradiation resistance and improve cancer patient care during chemo- and/or radiation therapy.

Characteristics of chemo-and radiation-resistant cells include altered membrane transporter expressions and functions, enhanced DNA repair activity, apoptotic pathway defects, alteration of target molecules, or enzymatic deactivation. There are two general causes of failure of antineoplastic therapy: Inherent genetic characteristics that induce resistance in cancer cells and acquired resistance after drug exposure and radiation exposure. As the primary anti-cancer therapies, ionizing radiation and chemotherapeutic agents induce cell death by directly or indirectly causing DNA damage, dysregulation of the DNA damage response may contribute to hypersensitivity or resistance of cancer cells to genotoxic agents. Targeting DNA repair pathway can therefore increase the tumor sensitivity to cancer therapies. While more attention have been paid lately to the relationship between defective nuclear DNA repair pathway and therapeutic resistance, less is known about the role of mitochondrial repair pathways. Lan-Ya Li et al. (Li et al., 2021) reviewed the biology and the regulatory mechanisms of DNA repair pathways, which has the potential to facilitate the development of inhibitors of nuclear and mitochondria DNA repair pathways for enhancing anticancer effect of DNA damage-based therapy.

Platinum resistance poses a significant problem for oncology clinicians. The role of epigenetics and DNA methylation in platinum-based chemoresistance has gained increasing attention from researchers in recent years. Ruizheng Sun et al. (Sun et al., 2021) analyzed the platinum chemotherapy response-related methylation patterns from different perspectives of 618 patients across 13 cancer types and integrated transcriptional and clinical data. They indicated that the methylation-transcription axis exists and participates in the complex biological mechanism of platinum resistance in various cancers. Six methylated positions (differentially methylated positions,



***Edited and reviewed by:***
*Olivier Feron,*
*Université catholique de Louvain, Belgium*

***Correspondence:**
*Xiaoping Lin*
*linxp@sysucc.org.cn*
*Zhe-Sheng Chen*
*chenz@stjohns.edu*

***Specialty section:***
*This article was submitted to Pharmacology of Anti-Cancer Drugs, a section of the journal Frontiers in Pharmacology*

***Received:*** *25 March 2022*
***Accepted:*** *27 April 2022*
***Published:*** *18 May 2022*

***Citation:***
*Lin X, Kong D and Chen Z-S (2022) Editorial: Chemo-Radiation-Resistance in Cancer Therapy. Front. Pharmacol. 13:904063. doi: 10.3389/fphar.2022.904063*

DMPs) and four associated genes may have the potential to serve as promising epigenetic biomarkers for platinum-based chemotherapy and guide clinical selection of optimal treatment.

Cisplatin (DDP) is commonly used for gastric cancer treatment, whereas recurrence and metastasis are common because of intrinsic and acquired DDP-resistance. Experiments by Yingying Kou et al. (Kou et al., 2020) suggested that berberine improves chemo-sensitivity to cisplatin by enhancing cell apoptosis and repressing PI3K/AKT/mTOR signaling pathway.

Cisplatin-based regimens also commonly applied for nasopharyngeal carcinoma (NPC) patients receiving concurrent chemotherapy and radiation. The sensitivity of cisplatin is closely associated with the efficacy of radiation therapy. Wenwen Hao et al. (Hao et al., 2021) found that Solute Carrier Family 1 Member 6 (SLC1A6) contributed to reducing cisplatin sensitivity in radioresistant NPC cells by altering drug metabolism profiles and genes.

Carboplatin is the cornerstone of chemotherapy for ovarian cancer. However, drug resistance to this agent continues to present challenges, and the mechanism of resistance to carboplatin in ovarian cancer has become a focus of research in recent years. Increasing evidence has shown that collagen type I alpha 1 chain (COL1A1) has an important role in chemoresistance and could represent a potential therapeutic target, but the mechanism of COL1A1 in carboplatin-resistant ovarian cancer has remained unclear. Feng Yang et al. (Yang et al., 2021) discovered that COL1A1 had a pivotal role in carboplatin resistance in ovarian cancer and identified two key pathways involving COL1A1 in carboplatin resistance: the "extracellular matrix (ECM)-receptor interaction" and "focal adhesion" Kyoto Encyclopedia of Genes and Genomes pathways. Furthermore, they proposed that ZINC000085537017 and quercetin were potential drugs for COL1A1 based on virtual screening and the TCMSP database, respectively.

Besides platinum, paclitaxel (PTX) is a first-line chemotherapeutic drug for the treatment in many different types of cancer, but drug resistance seriously limits its clinical use. Fenfen Xiang et al. (Xiang et al., 2021) showed that DNA-methyltransferase 1 (DNMT1) mediated hypermethylation of Krüppel-like factor 4 (KLF4) promoter leads to downregulation of KLF4 in breast cancer. The level of KLF4 is correlated with the sensitivity of MCF-7 and T47D cells to PTX 3,3′-diindolylmethane (DIM) could enhance the antitumor efficacy of PTX on MCF-7 and T47D cells by regulating DNMT1 and KLF4. In ovarian cancer, Yaqing Zhang et al. (Zhang et al., 2021) found that the drug resistance protein CSAG2 is translationally induced by cytoplasmic polyadenylation element binding protein 4 (CPEB4), which underlies CPEB4-promoted paclitaxel resistance in ovarian cancer *in vitro*. They found interfering CPEB4/CSAG2 axis might be of benefit to overcome paclitaxel-resistant ovarian cancer.

Doxorubicin (DOX) is a first-line chemotherapeutic drug for breast cancer, which can kill tumor cells but it causes multidrug resistance (MDR) if used for a long period of time, resulting in chemotherapy failure. In DOX-resistant breast cancer cells, P-glycoprotein protein can pump DOX out of MCF-7/DOX cells, as a result, DOX fails to exert effective cytotoxic effect and breast cancer cells can evade attack of chemotherapeutics. Reversal of drug resistance can be realized by repressing P- glycoprotein protein. Ting Wang et al. (Wang et al., 2021a) identified that a new chalcone derivative, C49, reverses DOX resistance in MCF-7/DOX cells by inhibiting P-glycoprotein expression.

Despite chemotherapy is the most effective treatment for breast cancer, many patients develop chemoresistance. Early indicator of therapy efficacy might aid in the search for better treatment and patient survival. Emerging evidence indicates a key role of the purinergic receptors P2X7 and A2A in cancer. Victor Manuel Ruiz-Rodríguez (Ruiz-Rodríguez et al., 2020) explored the purinergic receptors P2X7 and A2A in cancer and their involvement in breast cancer chemoresistance, demonstrating the importance of purinergic signaling in $CD8^+$ T cells during chemoresistance as the chemotherapeutic treatment stimulates immune system response, and how it could be considered for implementing personalized therapeutic strategies.

Both long-term anti-estrogen therapy and estrogen receptor-negative breast cancer contribute to drug resistance, causing poor prognosis in breast cancer patients. Breast cancer resistance protein (BCRP) plays an important role in multidrug resistance. The study by Wenting Ni et al. (Ni et al., 2021) suggested that cryptotanshinone (CPT) is a novel BCRP inhibitor that blocks the oligomer formation of BCRP on the cell membrane. CPT can inhibit the activity of BCRP in an ERα-dependent and -independent manner, sensitizing breast cancer cells to chemotherapy.

Histone deacetylases and histone acetylases (HDACs) are important enzymes participating in the regulation of gene expression by acetylating and deacetylating of histones. Specifically, HDACs are the enzymes controlling the epigenetic modifications of histone. In recent years, inhibition of HDACs has exhibited potency for the treatment tumors. Nitrogen mustard anticancer drugs were used clinically since 1942, which effectively bind and cross-link to DNA, resulting in prevention of DNA replication and cell proliferation. Yiming Chen et al. (Chen et al., 2020b) discovered that N-(2-amino-4-fluorophenyl)-4-[bis-(2-chloroethyl)-amino]-benzamide (FNA) was a potent HDAC3 inhibitor by inhibiting tumor growth and promoting apoptosis and G2/M phase arrest, which improved the anticancer activity of paclitaxel and camptothecin.

Overexpression of nucleophosmin (NPM) is involved in the MDR development during acute lymphoblastic leukemia (ALL). Donghui Gan et al. (Gan et al., 2021) identified that doxorubicin/nucleophosmin binding protein-conjugated nanoparticle (DOX-PMs-NPMBP) was able to significantly exert growth inhibition and apoptosis induction, and markedly enhance anti-leukemia activity in acute lymphoblastic leukemia cells *in vitro* and *in vivo*. Mechanistically, p53-driven apoptosis induction and cell cycle arrest played essential role in DOX-PMs-NPMBP-induced anti-leukemia effects.

Nowadays, many natural-derived drugs serve as sources of novel drug discovery and are tested clinically. However, the efficacy of certain natural products could be compromised by MDR-associated ATP-binding cassette (ABC) transporters. ABC subfamily C member 1 (ABCC1, multidrug resistance protein 1/

MRP1), ABC sub-family B member 1 (ABCB1, multidrug resistance protein 1/MDR1, P-glycoprotein/P-gp), and ABC sub-family G member 2(ABCG2, breast cancer resistance protein/BCRP, mitoxantrone-resistant protein/MXR) are extensively studies, and are commonly responsible for MDR. Betulin is susceptible to drug resistance mediated by ABCC1 overexpression, and a known ABCC1 inhibitor, MK571, can sensitize the cells expressing ABCC1 to betulin. Xuan-Yu Chen et al. (Chen et al., 2021) explored ABCC1-induced resistance to betulin by its upregulated protein expression of ABCC1 and found that betulin at high concentration had the ability to inhibit ABCC1 transport function, which may affect the pharmacokinetic profile of other ABCC1 drug substrates, such as vincristine.

Sorafenib, a multireceptor tyrosine kinase inhibitor is FDA approved first-line drug for the treatment of advanced liver cancer and is reported to extend the overall survival in individuals with advanced hepatocellular carcinoma (HCC). However, the primary or acquired resistance to sorafenib is gradually increasing, leading to failure of HCC treatment with sorafenib. Wubin He et al. (He et al., 2021) reported that artesunate regulates neurite outgrowth inhibitor protein B receptor (NgBR) to overcome resistance to sorafenib of HCC in a cell culture model.

Typically, renal cell carcinoma (RCC) is insensitive to traditional chemo- and radio-therapeutic treatments. Moreover, the use of targeted treatment options as first- and second-line treatments have limited effect on the survival rates. Dian Fu et al. (Fu et al., 2020) explored low-toxicity novel treatment strategies for RCC and investigated costunolide (Cos), a natural sesquiterpene compound isolated from various medicinal plants, and found that it exerted autophagic and apoptotic effects on renal cancer through the ROS/JNK-dependent signal route.

Chemoresistance has become a prevalent phenomenon in cancer therapy, which alleviates the effect of chemotherapy and makes it difficult to break the bottleneck of the survival rate of tumor patients. Jin-Feng Xu et al. (Xu et al., 2021) reviewed the functional roles of ginsenosides in chemoresistance reversal. Its underlying mechanism is correlated with inhibition of drug transporters, induction of apoptosis, and modulation of the tumor microenvironment(TME), as well as the modulation of signaling pathways, such as nuclear factor erythroid-2 related factor 2 (NRF2)/AKT, lncRNA cancer susceptibility candidate 2(CASC2)/protein tyrosine phosphatase gene (PTEN), AKT/sirtuin1(SIRT1), epidermal growth factor receptor (EGFR)/PI3K/AKT, PI3K/AKT/mTOR and nuclear factor-κB (NF-κB).

Modulated electro-hyperthermia (mEHT), induced by 13.56 MHz radiofrequency, has been demonstrated both in preclinical and clinical studies to efficiently induce tumor damage and complement other treatment modalities. Tamás Vancsik et al. (Vancsik et al., 2021) used a mouse xenograft model of human melanoma (A2058) to test mEHT (~42°C), both alone and combined with NK-cell immunotherapy. They found that mEHT monotherapy of melanoma xenograft tumors induced irreversible heat and cell stress leading to caspase-dependent apoptosis to be driven by p53. mEHT could support the intra-tumoral attraction of distantly injected NK cells, contributed by CXCL11 and MMP2 upregulation, resulting in additive tumor destruction and growth inhibition.

Many cancer patients who are treated with chemotherapy and/or radiotherapy eventually become resistant, and acquired resistance accounts for the majority of cases. One of the most well understood mechanisms of chemoresistance is the overexpression of ABC transporters. Zhuo-Xun Wu et al. (Wu et al., 2021) reported how to establish a novel irinotecan-resistant human colon cell line to investigate the underlying mechanism(s) of irinotecan resistance, particularly the overexpression of ABC transporters.

Radiotherapy is recommended as an important and effective method for malignant treatment in about half of cancer patients during clinical treatment. Esophageal squamous cell carcinoma (ESCC) patients who have contraindications for surgery or locally advanced disease have a treatment option through Radiotherapy. However, radioresistance is a major cause of treatment failure, contributing to inadequate cure, relapse, and metastasis. Zuoquan Zhu et al. (Zhu et al., 2021) provided evidence that the FMS-related tyrosine kinase 3 ligand (FL) increases the radioresistance of esophageal cancer cells and that FL-related tyrosine kinase 3 (Flt-3) could be a potential target for enhancing radiosensitivity in ESCC.

More attentions have been attracted to radiosensitizers because of their abilities to increase the radiosensitivity of cancer cells and reduce the side effects on normal cells. In order to identify promising radiosensitivity agents, a large number of natural products with anti-inflammatory, antioxidant, and antitumor activations have been considered. The major treatment modality for non-small-cell lung carcinoma (NSCLC) is radiotherapy. However, radiotherapy can induce radioresistance in cancer cells, thereby resulting in a poor response rate. Yarong Du et al. (Du et al., 2021) demonstrated the effects of isorhamnetin (ISO), which is a naturally occurring radiosensitizer, and its impact on the responsiveness of lung cancer cells to irradiation through IL-13 and the NF-κB signaling pathway.

Protein turnover is a dynamically regulated process influencing many important biological functions, including DNA damage response (DDR), cell cycling, and signaling transductions. Pharmacological intervention of protein turnover offers a new therapeutic window for radiosensitization. Driven by their unique cytotoxic mechanisms, the novel strategies targeting the ubiquitin-proteasome system (UPS) with NEDDylation inhibitors and the PROteolysis TArgeting Chimeras (PROTACs) carry great potential as radiosensitizers to improve the efficacy of radiotherapy. The NEDDylation inhibitor MLN4924 exerts several cytotoxic functions, including DNA damage, cell cycle checkpoints dysregulation, and inhibition of NF-κB, and mTOR pathways. Preclinical studies had validated the efficacy of NEDDylation inhibitors as radiosensitizers. Meanwhile, recent progress in PROTAC technology has shown significant improvements in terms of the cellular permeability and substrate specificity. The PROTACs can selectively recruit key proteins related to radioresistance, such as EGFR, androgen

receptor (AR) and estrogen receptor (ER), cyclin-dependent kinases (CDKs), MAP kinase kinase 1 (MEK1), and MEK2, for the cullin-RING E3 ligase (CRL)-mediated polyubiquitin conjugation and subsequent degradation. Shuhua Zheng et al. (Zheng and Tao, 2020) summarized basic and preclinical investigations on NEDDylation inhibitors and PROTACs as radiosensitizers.

Chemotherapy is the backbone of subsequent treatment for patients with lung adenocarcinoma (LUAD) exhibiting radiation resistance, and pemetrexed plays a critical role in this chemotherapy. Yuqing Wang et al. (Wang et al., 2021b) assessed changes in the sensitivity of LUAD cells to pemetrexed under radioresistant circumstances. They showed the much lower efficacy of pemetrexed in radioresistant cells than in parental cells, and that the mechanism of action was the significant downregulation of folate receptor alpha (FRα) by long-term fractionated radiotherapy, which resulted in less cellular pemetrexed accumulation. The activation of FRα by decitabine can sensitize radioresistant LUAD cells to pemetrexed both *in vitro* and in xenografts.

NPC is endemic in southern China and South-East Asia. Radiotherapy is the primary treatment for the non-metastatic disease. Although the local control of NPC can be increased by intensity-modulated radiation therapy (IMRT) rather than conventional radiotherapy, approximately 20% of the patients still present locoregional recurrence following radical IMRT. Tumor recurrence has been recommended to have relationship strong association with radio-resistance. Shan-Shan Guo et al. (Guo et al., 2021b) demonstrated the radioresistant function of angiogenin, as a biomarker that can help identify radio-sensitivity, and showed the clinical prognostic significance of ANG, which could help predict radiosensitivity and stratify high-risk patients or tumor recurrence.

Identifying metastasis-associated genes and finding effective targets is the main strategy to prevent metastasis and improve survival of breast cancer. On the explore of putative tumor suppressor protein, Xin An et al. (An et al., 2020) confirmed that Cavin3 expression is significantly downregulated in breast cancer, and correlated with distant metastasis and worse survival. Cavin3 functions as a metastasis suppressor by downregulating the Akt pathway, which suggests that cavin3 can be a potential prognostic biomarker and a target for breast cancer treatment. Studies by Xin Hua et al. (Hua et al., 2020) suggested that IQ motif-containing GTPase activating protein 3 (IQGAP3), the latest identified member of the IQGAP family, was significantly upregulated in breast cancer cell lines and human tumor tissues at both the mRNA and protein level compared to controls, and the expression was an independent prognostic factor among all 257 breast cancer patients in their cohort. Therefore, IQGAP3 may be a reliable prognostic biomarker in breast cancer.

E3 ubiquitin ligases (E3s) are a large class of proteins, and there are over 800 putative functional E3s. E3s play a crucial role in substrate recognition and catalyze the final step of ubiquitin transfer to specific substrate proteins. The diversity of the set of substrates contributes to the diverse functions of E3s, indicating that E3s could be desirable drug targets. The E3s MDM2, FBWX7, and SKP2 have been well studied and have shown a relationship with drug resistance. Strategies targeting E3s to combat drug resistance include interfering with their activators, degrading the E3s themselves and influencing the interaction between E3s and their substrates. Yuanqi Liu et al. (Liu et al., 2021) summarize the role of E3s in cancer drug resistance from the perspective of drug class and the most important research findings of targeting the cullin-RING E3 ligases for radiosensitization.

The crosstalk between cancer cells and their microenvironment triggers a variety of critical signaling cues and promotes the malignant phenotype of cancer. As a type of transmembrane protein, integrin-mediated cell adhesion is essential in regulating various biological functions of cancer cells. Integrins are the adhesion molecules and receptors of ECM. They mediate the interactions between cells-cells and cells-ECM. Recent evidence has shown that integrins present on tumor cells or tumor-associated stromal cells are involved in ECM remodeling, and as mechanotransducers sensing changes in the biophysical properties of the ECM, which contribute to cancer metastasis, stemness and drug resistance. Chao-Yue Su et al. (Su et al., 2020) outlined the mechanism of integrin-mediated effects on biological changes of cancers and highlight the current status of clinical treatments by targeting integrins.

Most tumor cells are in a hypoxic microenvironment that promotes resistance to radiation therapy. In addition to radiation resistance, the hypoxic microenvironment also promotes cancer proliferation and metastasis. Cordell Gilreath et al. (Gilreath et al., 2021) reviewed the hypoxic microenvironment of breast cancer tumors, related signaling pathways, breast cancer stem-like cells, and the resistance to radiation therapy.

Microenvironmental serine may alter cancer proliferation and invasion. A high serine content in body fluid was identified in a portion of patients with gastric cancer, but its biological significance, such as cell growth, migration and invasion, and drug resistance, was not clearly. Jun Li et al. (Li et al., 2020) characterized the basal gene expressing profiles of MGC803 and HGC27. The HGC27 cells were more differentiated than MGC803 cells while MGC803 cells were more sensitive to the change of serine content. They demonstrated that genetic profiles can affect the biological effects of serine on gastric cancer cells.

The tumor immunological microenvironments of gliomas differ based on their molecular properties. In glioblastoma (GBM), Ji Zhang et al. (Zhang et al., 2020) profiled the immune status of O-6-methylguanine-DNA methyltransferase (MGMT) promoter methylation in GBM and established a local immune signature for GBM that could independently identify patients with a favorable prognosis, indicating a relationship between prognosis and GBM immune signature. MGMT promoter methylation with lower Tim-3 expression was significantly associated with better survival.

Tumorigenesis is strongly associated with a series of cumulative genetic and epigenetic changes occurring in a normal cell; it is also closely related to the body's microenvironment and immunity. The immune system recognizes and kills cancerous cells and their precursors, while cancerous cells develop strategies to escape from immune-surveillance thereby promoting tumorigenesis. Recently,

long non-coding RNA (lncRNA) was proven to play an active part in the regulation of the immune system by affecting tumor microenvironment, epithelial-mesenchymal transition, dendritic cell and myeloid-derived stem cell regulation, and T and B cell activation and differentiation. Immune-related lncRNAs, which were identified as a prognostic marker of various types of cancer, are markedly connected with immune cell infiltration, and might be a potential target for cancer treatment. Peijie Chen et al. (Chen et al., 2020a) constructed a prognostic model and explored the immune characteristics of different risk groups in cervical cancer patients to analyze the relationship between immune-related lncRNAs and the prognosis.

Inherent gene/protein-associated drug and radiation resistance is largely rooted in cancer cell heterogeneity. For this type of resistance, we may be able to detect variants through gene sequencing, flow cytometry, and microarray to determine their mechanisms of resistance, and guide physicians in choosing the right approach for their individual patients. While variants identified for leukemia and lung cancer have improved our ability to predict prognoses and provide personalized medical care, there remain other types of cancer where many new advances could be made.

The efficiency and safety of hypofractionated radiotherapy (HFR) combined with paclitaxel chemotherapy for the treatment of post surgery tracheoesophageal groove lymph node (TGLN) metastasis in patients with esophageal cancer were investigated by Jian Wang et al. (Wang et al., 2020). They found that the combination of hypofractionated radiotherapy (HFR) and chemotherapy improved the prognosis of esophageal cancer patients with tracheoesophageal groove lymph node (TGLN) metastasis with no increased adverse events.

In recent years, multimodal approaches are recommended in unresectable hepatocellular carcinoma (HCC), either as first-line or subsequent therapy. Some studies have shown that the combination of transarterial chemoembolization (TACE) and sorafenib or TACE and thermal ablation is superior to monotherapy. However, few data are available on patients with huge unresectable HCCs treated by TACE and sorafenib, with or without thermal ablation. Ying Wu et al. (Wu et al., 2020) retrospectively evaluate and compare the benefits of TACE and sorafenib with or without thermal ablation in the management of patients with huge unresectable HCCs. They provided a promising strategy of TACE-sorafenib-thermal ablation, which demonstrated extended long-term overall survival in patients with huge unresectable HCC, and this may be a better choice than TACE-sorafenib alone.

Esophageal cancer is one of the most common cancer types, with its most common distant metastatic site being the lung. Currently, population-based data regarding the proportion and prognosis of patients with esophageal cancer with lung metastases (ECLM) at the time of diagnosis is insufficient. Analyses conducted by Jida Guo et al. (Guo et al., 2021a) on Surveillance, Epidemiology, and End Results (SEER) database from 2010 to 2016 of ECLM indicated that age, number of extrapulmonary metastatic sites, treatment three factors as independent predictors for esophageal cancer-specific survival (CSS). Considering the factors that may predict the occurrence of lung metastasis at diagnosis, high-risk patients should undergo a 64-slice multidetector CT (MDCT) examination for small lung nodules screening. According to their findings, chemotherapy or chemoradiotherapy may represent the most advantageous treatments for patients with ECLM.

In conclusion, the "Chemoradiation Resistance in Cancer Therapy" research topic highlights the complex phenomenon of resistance to anticancer therapy in cancer cells. The recent research implies the need to continue improving our understanding into the fundamental mechanisms of chemoradiation resistance related to target mutations, tumor microenvironment, undiscovered genes and signaling pathways in cancers, with the aim of identifying relevant new biomarkers and to develop the strategies that can overcome chemoradiation resistance or improve patient care during chemo- and/or radiation therapy.

## AUTHOR CONTRIBUTIONS

Conceptualization: Writing - original draft preparation: XL; Writing - review and editing: DK and Z-SC. All authors read and approved the final manuscript.

## FUNDING

The authors did not receive financial support from any organization for the submitted work.

## ACKNOWLEDGMENTS

We thank the Frontiers for the opportunity.

## REFERENCES

An, X., Lin, X., Yang, A., Jiang, Q., Geng, B., Huang, M., et al. (2020). Cavin3 Suppresses Breast Cancer Metastasis via Inhibiting AKT Pathway. *Front. Pharmacol.* 11. doi:10.3389/fphar.2020.01228

Chen, P., Gao, Y., Ouyang, S., Wei, L., Zhou, M., You, H., et al. (2020a). A Prognostic Model Based on Immune-Related Long Non-coding RNAs for Patients with Cervical Cancer. *Front. Pharmacol.* 11. Epub 2020/11/30. doi:10.3389/fphar.2020.585255

Chen, X-Y., Yang, Y., Wang, J-Q., Wu, Z-X., Jing, L., and Chen, Z-S. (2021). Overexpression of ABCC1 Confers Drug Resistance to Betulin. *Front. Oncol. Epub* 11, 640656. doi:10.3389/fonc.2021.640656

Chen, Y., Feng, J., Hu, Y., Wang, X., Song, W., and Zhang, L. (2020b). Discovery of N-(2-Amino-4-Fluorophenyl)-4-[bis-(2-Chloroethyl)-Amino]-Benzamide as a Potent HDAC3 Inhibitor. *Front. Oncol.* 10. Oncol. Epub 2020/10/15. doi:10.3389/fonc.2020.592385

Du, Y., Jia, C., Liu, Y., Li, Y., Wang, J., and Sun, K. (2021). Isorhamnetin Enhances the Radiosensitivity of A549 Cells through Interleukin-13 and the NF-Kb Signaling Pathway. *Front. Pharmacol.* 11. Epub 2021/01/25. doi:10.3389/fphar.2020.610772

Fu, D., Wu, D., Cheng, W., Gao, J., Zhang, Z., Ge, J., et al. (2020). Costunolide Induces Autophagy and Apoptosis by Activating ROS/MAPK Signaling Pathways in Renal Cell Carcinoma. *Front. Oncol.* 10. Epub 2020/10/26. doi:10.3389/fonc.2020.582273

Gan, D., Chen, Y., Wu, Z., Luo, L., Yirga, S. K., Zhang, N., et al. (2021). Doxorubicin/Nucleophosmin Binding Protein-Conjugated Nanoparticle Enhances Anti-leukemia Activity in Acute Lymphoblastic Leukemia Cells In Vitro and In Vivo. *Front. Pharmacol.* 12. Epub 2021/02/28. doi:10.3389/fphar.2021.607755

Gilreath, C., Boerma, M., Qin, Z., Hudson, M. K., and Wang, S. (2021). The Hypoxic Microenvironment of Breast Cancer Cells Promotes Resistance in Radiation Therapy. *Front. Oncol.* 10. doi:10.3389/fonc.2020.629422

Guo, J., Zhang, S., Li, H., Omar Hassan, M. O., Lu, T., Zhao, J., et al. (2021a). Lung Metastases in Newly Diagnosed Esophageal Cancer: A Population-Based Study. *Front. Oncol.* 11, 603953. Epub 2021/02/25. doi:10.3389/fonc.2020.603953

Guo, S.-S., Liang, Y.-J., Liu, L.-T., Chen, Q.-Y., Wen, Y.-F., Liu, S.-L., et al. (2021b). Increased Angiogenin Expression Correlates with Radiation Resistance and Predicts Poor Survival for Patients with Nasopharyngeal Carcinoma. *Front. Pharmacol.* 12. doi:10.3389/fphar.2021.627935

Hao, W., Wu, L., Cao, L., Yu, J., Ning, L., Wang, J., et al. (2021). Radioresistant Nasopharyngeal Carcinoma Cells Exhibited Decreased Cisplatin Sensitivity by Inducing SLC1A6 Expression. *Front. Pharmacol.* 12. Epub 2021/04/13. doi:10.3389/fphar.2021.629264

He, W., Huang, X., Berges, B. K., Wang, Y., An, N., Su, R., et al. (2021). Artesunate Regulates Neurite Outgrowth Inhibitor Protein B Receptor to Overcome Resistance to Sorafenib in Hepatocellular Carcinoma Cells. *Front. Pharmacol.* 12. Epub 2021/02/25. doi:10.3389/fphar.2021.615889

Hua, X., Long, Z.-Q., Guo, L., Wen, W., Huang, X., Zhang, W.-W., et al. (2020). IQGAP3 Overexpression Correlates with Poor Prognosis and Radiation Therapy Resistance in Breast Cancer. *Front. Pharmacol.* 11. doi:10.3389/fphar.2020.584450

Kou, Y., Tong, B., Wu, W., Liao, X., and Zhao, M. (2020). Berberine Improves Chemo-Sensitivity to Cisplatin by Enhancing Cell Apoptosis and Repressing PI3K/AKT/mTOR Signaling Pathway in Gastric Cancer. *Front. Pharmacol.* 11. doi:10.3389/fphar.2020.616251

Li, J., Xue, H., Xiang, Z., Song, S., Yan, R., Ji, J., et al. (2020). Genetic Profiles Affect the Biological Effects of Serine on Gastric Cancer Cells. *Front. Pharmacol.* 11. doi:10.3389/fphar.2020.01183

Li, L.-y., Guan, Y.-d., Chen, X.-s., Yang, J.-m., and Cheng, Y. (2021). DNA Repair Pathways in Cancer Therapy and Resistance. *Front. Pharmacol.* 11, 629266. doi:10.3389/fphar.2020.629266

Liu, Y., Duan, C., and Zhang, C. (2021). E3 Ubiquitin Ligase in Anticancer Drugdsla Resistance: Recent Advances and Future Potential. *Front. Pharmacol.* 12. Epub 2021/04/15. doi:10.3389/fphar.2021.645864

Ni, W., Fan, H., Zheng, X., Xu, F., Wu, Y., Li, X., et al. (2021). Cryptotanshinone Inhibits ERα-dependent and -Independent BCRP Oligomer Formation to Reverse Multidrug Resistance in Breast Cancer. *Front. Oncol.* Epub 2021/04/22 11, 624811. doi:10.3389/fonc.2020.624811

Ruiz-Rodríguez, V. M., Turiján-Espinoza, E., Guel-Pañola, J. A., García-Hernández, M. H., Zermeño-Nava, J. d. J., López-López, N., et al. (2020). Chemoresistance in Breast Cancer Patients Associated with Changes in P2X7 and A2A Purinergic Receptors in CD8+ T Lymphocytes. *Front. Pharmacol.* 11. Epub 2020/11/30. doi:10.3389/fphar.2020.576955

Su, C.-y., Li, J.-q., Zhang, L.-l., Wang, H., Wang, F.-h., Tao, Y.-w., et al. (2020). The Biological Functions and Clinical Applications of Integrins in Cancers. *Front. Pharmacol.* 11. Epub 2020/09/15. doi:10.3389/fphar.2020.579068

Sun, R., Du, C., Li, J., Zhou, Y., Xiong, W., Xiang, J., et al. (2021). Systematic Investigation of DNA Methylation Associated with Platinum Chemotherapy Resistance across 13 Cancer Types. *Front. Pharmacol.* 12. Epub 2021/04/29. doi:10.3389/fphar.2021.616529

Vancsik, T., Máthé, D., Horváth, I., Anna Várallyaly, A., Benedek, A., and Bergmann, R. (2021). Modulated Electro-Hyperthermia Facilitates NK-Cell Infiltration and Growth Arrest of Human A2058 Melanoma in a Xenograft Model. *Front. Oncol. Epub* 11, 590764. doi:10.3389/fonc.2021.590764

Wang, J., Yu, J., Jiang, Y., Pei, D., Zhu, H., and Wang, J. (2020). Hypofractionated Radiotherapy in Combination with Chemotherapy Improves Outcome of Patients with Esophageal Carcinoma Tracheoesophageal Groove Lymph Node Metastasis. *Front. Oncol.* 10. doi:10.3389/fonc.2020.01540

Wang, T., Dong, J., Yuan, X., Wen, H., Wu, L., Liu, J., et al. (2021a). A New Chalcone Derivative C49 Reverses Doxorubicin Resistance in MCF-7/DOX Cells by Inhibiting P-Glycoprotein Expression. *Front. Pharmacol.* 12. Epub 2021/04/13. doi:10.3389/fphar.2021.653306

Wang, Y., Huang, J., Wu, Q., Zhang, J., Ma, Z., Zhu, L., et al. (2021b). Decitabine Sensitizes the Radioresistant Lung Adenocarcinoma to Pemetrexed through Upregulation of Folate Receptor Alpha. *Front. Oncol. Epub* 11, 668798. doi:10.3389/fonc.2021.668798

Wu, Y., Qi, H., Cao, F., Shen, L., Chen, S., Xie, L., et al. (2020). TACE-sorafenib with Thermal Ablation Has Survival Benefits in Patients with Huge Unresectable Hepatocellular Carcinoma. *Front. Pharmacol.* 11. doi:10.3389/fphar.2020.01130

Wu, Z-X., Yang, Y., Zeng, L., Patel, H., Bo, L., Lin, L., et al. (2021). Establishment and Characterization of an Irinotecan-Resistant Human Colon Cancer Cell Line. *Front. Oncol.* 10, 624954. Epub 2021/02/22. doi:10.3389/fonc.2020.624954

Xiang, F., Zhu, Z., Zhang, M., Wang, J., Chen, Z., Li, X., et al. (2021). 3,3'-Diindolylmethane Enhances Paclitaxel Sensitivity by Suppressing DNMT1-Mediated KLF4 Methylation in Breast Cancer. *Front. Oncol.* 11. Epub 2021/06/03. doi:10.3389/fonc.2021.627856

Xu, J.-F., Wan, Y., Tang, F., Chen, L., Yang, Y., Xia, J., et al. (2021). Emerging Significance of Ginsenosides as Potentially Reversal Agents of Chemoresistance in Cancer Therapy. *Front. Pharmacol.* 12. doi:10.3389/fphar.2021.720474

Yang, F., Zhao, Z., Cai, S., Ling, L., Hong, L., Tao, L., et al. (2021). Detailed Molecular Mechanism and Potential Drugs for COL1A1 in Carboplatin-Resistant Ovarian Cancer. *Front. Oncol.* 10. Epub 2021/02/17. doi:10.3389/fonc.2020.576565

Zhang, J., Sai, K., Wang, X. l., Ye, S. q., Liang, L. j., Zhou, Y., et al. (2020). Tim-3 Expression and MGMT Methylation Status Association with Survival in Glioblastoma. *Front. Pharmacol.* 11. Epub 2020/09/15. doi:10.3389/fphar.2020.584652

Zhang, Y., Gan, H., Zhao, F., Ma, X., Xie, X., Huang, R., et al. (2021). CPEB4-Promoted Paclitaxel Resistance in Ovarian Cancer In Vitro Relies on Translational Regulation of CSAG2. *Front. Oncol.* 11, 600994. Epub 2020/10/15. doi:10.3389/fonc.2020.59238

Zheng, S., and Tao, W. (2020). Targeting Cullin-RING E3 Ligases for Radiosensitization: From NEDDylation Inhibition to PROTACs. *Front. Oncol.* 10. Epub 2020/08/21. doi:10.3389/fonc.2020.01517

Zhu, Z., Song, J., Gu, J., Xu, B., Sun, X., and Zhang, S. (2021). FMS-related Tyrosine Kinase 3 Ligand Promotes Radioresistance in Esophageal Squamous Cell Carcinoma. *Front. Pharmacol.* 12. doi:10.3389/fphar.2021.659735

**Conflict of Interest:** The authors declare that the research was conducted in the absence of any commercial or financial relationships that could be construed as a potential conflict of interest.

**Publisher's Note:** All claims expressed in this article are solely those of the authors and do not necessarily represent those of their affiliated organizations, or those of the publisher, the editors and the reviewers. Any product that may be evaluated in this article, or claim that may be made by its manufacturer, is not guaranteed or endorsed by the publisher.

frontiers in Pharmacology

ORIGINAL RESEARCH
published: 29 July 2020
doi: 10.3389/fphar.2020.01130

# TACE-Sorafenib With Thermal Ablation Has Survival Benefits in Patients With Huge Unresectable Hepatocellular Carcinoma

*Ying Wu*[1,2†], *Han Qi*[1,2†], *Fei Cao*[1,2†], *Lujun Shen*[1,2], *Shuanggang Chen*[1,2], *Lin Xie*[1,2], *Tao Huang*[1,2], *Ze Song*[3], *Danyang Zhou*[1,3] *and Weijun Fan*[1,2*]

[1] Department of Minimally Invasive Interventional Therapy, Sun Yat-sen University Cancer Center, Guangzhou, China, [2] Department of Medical Oncology, Sun Yat-sen University Cancer Center, Guangzhou, China, [3] State Key Laboratory of Oncology in South China, Collaborative Innovation Center of Cancer Medicine, Sun Yat-sen University, Guangzhou, China

**Purpose:** To investigate the effectiveness and safety of transarterial chemoembolization (TACE) combined with sorafenib and thermal ablation in patients with huge hepatocellular carcinoma (HCC).

**Materials and Methods:** This retrospective study examined 50 patients with huge unresectable HCC treated from January 2009 to December 2015. Among them, 28 cases received TACE-sorafenib treatment (TACE-sorafenib group), and 22 cases received TACE-sorafenib plus thermal ablation treatment (TACE-sorafenib-thermal ablation group). The Overall survival (OS), progression-free survival (PFS), and adverse events (AEs) were compared.

**Results:** The median follow-up was 13.5 months (ranges 4.2 to 96.7 months). The median OS was significantly longer in the TACE-sorafenib-thermal ablation group than that in the TACE-sorafenib group (20.8 vs. 10.4 months, $P$=0.003). The median PFS of the ablation and no ablation groups were 4.3 vs. 7.1 months ($P$=0.546). The treatment modality was an independent predictor of OS ($P$=0.004). There were no notable drug-related high grade adverse events or permanent adverse sequelae.

**Conclusion:** TACE-sorafenib-thermal ablation provided extended OS to patients with huge unresectable HCC and could be a better choice than TACE-sorafenib.

**Keywords: hepatocellular carcinoma, transarterial chemoembolization, thermal ablation, sorafenib, treatment, drug resistance**

OPEN ACCESS

***Edited by:***
*Zhe-Sheng Chen,*
*St. John's University, United States*

***Reviewed by:***
*Xiaoguang Li,*
*Beijing Hospital, China*
*Xin Ye,*
*Shandong University, China*

****Correspondence:***
*Weijun Fan*
*fanwj@sysucc.org.cn*

*†These authors have contributed equally to this work*

***Specialty section:***
*This article was submitted to Pharmacology of Anti-Cancer Drugs, a section of the journal Frontiers in Pharmacology*

***Received:*** *15 June 2020*
***Accepted:*** *10 July 2020*
***Published:*** *29 July 2020*

***Citation:***
*Wu Y, Qi H, Cao F, Shen L, Chen S, Xie L, Huang T, Song Z, Zhou D and Fan W (2020) TACE-Sorafenib With Thermal Ablation Has Survival Benefits in Patients With Huge Unresectable Hepatocellular Carcinoma. Front. Pharmacol. 11:1130. doi: 10.3389/fphar.2020.01130*

## INTRODUCTION

Hepatocellular carcinoma (HCC) is the second most common cause of cancer-related mortality in China (Jemal et al., 2011). Huge unresectable HCC (i.e., >10 cm in its larger axis) is encountered in a considerable portion of patients at diagnosis.

Huge HCCs have specific features that need to be taken into account for successful management. Firstly, HBV-related liver cirrhosis is the predominant underlying cause of HCC in China (Chen et al., 2016). Secondly, huge HCCs always show an incomplete capsule and are prone to invade local vasculature, increasing the risk of tumor thrombus and metastasis (Xue et al., 2015). Thirdly, huge HCCs have an increased risk of rupture, which may accelerate their local spread and deterioration of liver function (Poon et al., 2002). Hence, adequate management of huge HCCs is a challenge.

For unresectable huge HCC, multiple approaches such as sorafenib adminstration, transarterial chemoembolization (TACE), and thermal ablation can be used for its management. Sorafenib, is approved in patients with unresectable HCC based on two phase III randomized trials (Llovet et al., 2008; Cheng et al., 2009) and is the recommended treatment for patients with advanced HCC (Omata et al., 2010; European Association For The Study Of The et al., 2012). However, the efficacy of sorafenib monotherapy is generally limited. Sorafenib is beneficial in only approximately 30% of patients, and acquired resistance often develops within 6 months, with a mean overall survival (OS) and time to progression of 10.7 and 5.5 months, respectively, in the SHARP study (Cheng et al., 2009), and 6.5 and 2.8 months, respectively, in the Asia-Pacific study (Llovet et al., 2008).

TACE is considered as the standard treatment for unresectable HCC (Llovet et al., 2002; Llovet and Bruix, 2003), but TACE monotherapy rarely results in complete necrosis of the lesions (Han et al., 2019). In addition, TACE increases VEGF levels, and VEGF is known to stimulate tumor angiogenesis, thereby contributing to tumor invasion and metastasis (Sergio et al., 2008; Shim et al., 2008). Thermal ablation therapies such as radiofrequency ablation (RFA) and microwave ablation (MWA) have been shown to be safe and effective for local control in patients with HCC (Lee et al., 2014; Hernandez et al., 2015). For early-stage HCC, thermal ablation has been shown to have similar OS compared with surgical resection (Lee et al., 2014; Hernandez et al., 2015). For moderate to advanced stage HCC, thermal ablation can provide a good local control (Lee et al., 2014; Hernandez et al., 2015). Both TACE and thermal ablation are local therapies, and they have limited preventive effect against tumor recurrence and metastasis.

In recent years, multimodal approaches are recommended in unresectable HCC, either as first-line or subsequent therapy. Some studies have shown that the combination of TACE and sorafenib or TACE and thermal ablation (Cabrera et al., 2011; Kim et al., 2011; Kudo et al., 2011) is superior to monotherapy. However, few data are available on patients with huge unresectable HCCs treated by TACE and sorafenib, with or without thermal ablation. In the present study, we retrospectively evaluate and compare the benefits of TACE and sorafenib with or without thermal ablation in the management of patients with huge unresectable HCCs.

**Abbreviations:** AEs, adverse events; AFP, alpha-fetoprotein; CT, computed tomography; HCC, hepatocellular carcinoma; mRECIST, modified Response Evaluation Criteria in Solid Tumors; MWA, microwave ablation; OS, overall survival; PFS, progression-free survival; RFA, radiofrequency ablation; TACE, transarterial chemoembolization.

## MATERIALS AND METHODS

### Patients

This study followed the requirements of the Declaration of Helsinki and was approved by the Institutional Review Board of Sun Yat-sen University Cancer Center. This single-center retrospective study examined the clinical data of patients with huge unresectable HCC treated from January 2009 to December 2015 at Sun Yat-sen University Cancer Center.

The inclusion criteria were: (1) diagnosis of HCC confirmed by liver biopsy or clinically according to the American Association for the Study of Liver Diseases (AASLD) criteria (Llovet et al., 2008); (2) original tumor ≥10 cm in diameter, and satellite foci ≤2 cm; (3) All target lesions that could be measured according to the modified Response Evaluation Criteria in Solid Tumors Group (mRECIST) guidelines (Lencioni and Llovet, 2010); (4) 18–80 years of age; and (5) underwent TACE with sorafenib or TACE, sorafenib, and thermal ablation treatment. The exclusion criteria were: (1) procedure other than TACE and thermal ablation; (2) extrahepatic HCC metastases; (3) portal vein tumor thrombus beyond type IIa (Chan et al., 2016); or (4) previous treatment for HCC.

A total of 533 patients with HCC were treated with sorafenib in our cancer center during the study period. According to the inclusion/exclusion criteria, only 50 patients with huge HCC were included in the present analysis.

### Treatment Option

Prior to their treatment, the patients were fully informed of the specific implications of TACE-sorafenib and TACE-sorafenib-thermal ablation therapies, as well as the possible adverse effects (AEs). The fact that there is limited evidence on the treatment effect was emphasized. Then, the patient received the treatment he/she selected. Informed treatment consent was obtained from all patients before treatment.

### Transarterial Chemoembolization

All TACE treatments were performed by three physicians who have at least 5 years of experience. Under local anesthesia, a 5F French catheter (Yashiro type; Terumo Corporation, Tokyo, Japan) was introduced into the abdominal aorta *via* the femoral artery using the Seldinger technique. Hepatic arterial angiography was performed using fluoroscopy to guide the catheter into the celiac and superior mesenteric arteries. The feeding arteries, tumor, and vascular anatomy surrounding the tumor were identified. A microcatheter (Renegade Hi Flo; Boston Scientific Corporation, Boston MA, USA) was super-selectively inserted into the feeding arteries. A solution

containing pirarubicin (10–40 mg, Shenzhen Main Luck Pharmaceuticals Inc., China), lobaplatin (50 mg/m$^2$, Hainan Changan International Pharmaceutical Co., Ltd., China), and 10 mg of mitomycin c (Zhejiang Hisun pharmaceutical Co., Ltd., China) in iodized oil (Lipoid ultra-fluid, Guerbet, France) was infused into the arteries according to the number and size of the lesions. Liver and kidney function of the patient, and blood supply of the tumors (Chung et al., 2011) were evaluated. Follow-up imaging was performed 1–3 months later to evaluate the effects of TACE. The treatment was repeated once every 1–2 months. Reexamination was conducted one month after TACE. If there were still enhanced tumors, repeated thermal ablation therapy was required. Treatments were discontinued in the presence of significant liver function deterioration or complete elimination of the liver tumors.

## Thermal Ablation

All thermal ablation treatments were performed by three physicians who have at least 5 years of experience. For patients who were willing to receive thermal ablation therapy, we usually performed 3–4 TACE sessions for hypervascular HCCs and 2–3 TACE sessions for hypovascular HCCs before performing thermal ablation based on our experience. Patients were instructed to fast from all foods for 12 h before the procedure. Computed tomography (CT) (Brilliance CT Big Bore; Philips, Best, The Netherlands) was used to locate the liver tumors and to design the optimal route for puncture needle. Routine disinfection and local anesthesia were applied around the puncture points. A microwave antenna (FORSEA; Qinghai Microwave Electronic Institute, Nanjing, China) or RFA (RITA2000, Mountain View. California, USA) was gradually inserted into the tumor along the predetermined angle. The whole MWA procedure was conducted under intravenous anesthesia (propofol; AstraZeneca, London, UK). Vital signs were monitored during the procedure. The settings of the ablation parameters depended upon the manufacturer's recommendation and our experience. An upper abdominal CT scan was carried out immediately after the procedure to evaluate the ablation area and complications. Routine blood and biochemical tests were performed on the first day after ablation treatment to monitor for eventual complications. After the first thermal ablation, TACE was repeated according to the proportion of residual tumor or disease status. If the proportion of residual tumor was >50% or new tumors appeared in the liver, additional TACE were performed.

## Sorafenib Treatment

All patients received continuous standard doses of sorafenib (400 mg twice a day, orally). Sorafenib was started from 3 days to 2 months after the TACE treatment or when tumor progression was found. During sorafenib treatment, the patients visited the outpatient clinic every three or four weeks for AE and tolerability assessments. Dose adjustments were made based on clinically significant toxicity (grade 3 or 4 according to the National Cancer Institute Common Terminology Criteria for Adverse Events Version 4.0) or the determination of patient tolerance by clinicians. For patients who have grades 3 and 4 toxicities, sorafenib was withdrawn until the symptoms improved to grade 2 or lower. Sorafenib was reintroduced at a dose of 200 mg bid for 5 days and then increased back to 400 mg bid if well tolerated. Otherwise, sorafenib was continued at 200-mg bid. Sorafenib was continued until toxicities were unmanageable.

## Follow-Up

OS was calculated from the date of treatment of HCC until the date of the final follow-up or death (no patient was lost in follow-up). Progression-free survival (PFS) was calculated from the day of diagnosis to radiologic progression based on the modified Response Evaluation Criteria in Solid Tumors (mRECIST) evaluation (Lencioni and Llovet, 2010). The procedure-related complications of TACE and thermal ablation were evaluated based on the guidelines for trans-catheter therapy and image-guided tumor ablation (Brown et al., 2009; Goldberg et al., 2009). Major complications were defined as events that led to substantial morbidity or disability, required hospital admission, or substantially lengthened hospital stay (Sacks et al., 2003). All other complications were considered minor. The drug-related toxicity was observed and recorded according to the National Cancer Institute Common Terminology Criteria for Adverse Events Version 4.0.

Liver function, blood coagulation profile, and serum alpha-fetoprotein (AFP) levels were examined monthly. A three-phase helical CT (HiSpeed or LightSpeed QX/I; GE Medical Systems, Milwaukee, WI, USA) or MRI (Discovery MR750 3.0T; GE Medical Systems, Milwaukee, WI, USA) examination was carried out every month for the first 3 months post-operatively. Patients with residual tumor were re-treated with the original procedure. If no residual tumor or tumor recurrence was found, re-examinations were carried out every 3–6 months. Follow-up was censored on June 30, 2017.

## Statistical Analysis

Continuous variables were presented as mean ± standard deviation (SD) and analyzed using the Student's $t$ test. Categorical variables were analyzed using the Chi-square or Fisher's exact test, as appropriate. Survival rates were estimated by the Kaplan-Meier method. Differences in OS were assessed for significance using the log-rank test. The Cox proportional hazards regression model was used to determine the factors associated with survival. As per initial design, all variables with a $P<0.05$ by univariable analysis were entered in the multivariable analysis; finally, only one variable was found to be associated with survival and multivariable analysis could not be performed. All analyses were performed using SPSS 13 (SPSS, Inc., Chicago, IL, USA). Two-tailed $P$-values <0.05 were considered statistically significant.

# RESULTS

## Baseline Clinical Characteristics

Among 533 patients with HCC who were treated with sorafenib at our hospital between January 2009 and December 2015, 28

and 22 patients with huge HCCs were treated with TACE-sorafenib and TACE-sorafenib-thermal ablation therapy, respectively. The baseline characteristics of these patients are shown in **Table 1**. In the TACE-sorafenib group, the 28 patients with 56 liver tumors received 72 TACE treatments (2.6 ± 1.3, range: 1–7). In the TACE-sorafenib-thermal ablation group, 22 patients with 40 liver tumors received 88 TACE treatments and 71 ablations. The specific information about RFA and MWA procedures are provided in **Table 2**.

## Patient Survival and Tumor Progression

The median follow-up of the entire cohort was 13.5 months (ranges 4.2–96.7 months). During follow-up, 28 (100%) and 18 (81.8%) patients died in the TACE-sorafenib and TACE-sorafenib-thermal ablation group, respectively. The median OS was significantly longer in the TACE-sorafenib-thermal ablation group than in the TACE-sorafenib group (20.8 vs. 10.4 months, $P$=0.003) (**Figure 1**). The 1-, 2-, and 3-year cumulative survival rates in the TACE-sorafenib-thermal ablation and TACE-sorafenib groups were 68.2%, 40.9%, and 31.8% vs. 46.4%, 10.7%, and 3.6%, respectively (all $P$<0.05). The median PFS of the TACE-sorafenib-thermal ablation and TACE-sorafenib groups were 4.3 vs. 7.1 months, respectively ($P$=0.546) (**Figure 2**).

In the subgroup analysis, the median OS of the patients without and with vascular invasion/metastasis were 14.0 vs. 9.8 months ($P$=0.648) in the TACE-sorafenib group, and 22.2 vs. 13.7 months ($P$=0.55) in the TACE-sorafenib-thermal group (**Figure 3**). The median OS of the patients who received RFA and MWA alone were 25.0 vs. 10.5 months ($P$=0.18) in the TACE-sorafenib-thermal ablation group (**Figure 4**).

**TABLE 1** | Baseline characteristics of the patients.

| Variables | TACE-sorafenib-thermal ablation (n=22) | TACE-sorafenib (n=28) | P |
|---|---|---|---|
| **Sex** | | | >0.999* |
| Female | 0 | 1 (3.6%) | |
| Male | 22 (100%) | 27 (96.4%) | |
| **Age (years)** | 46.4 ± 11.9 | 48.8 ± 12.3 | 0.479 |
| <50 | 15 (68.2%) | 15 (53.6%) | 0.295 |
| ≥50 | 7 (31.8%) | 13 (46.4%) | |
| **HBV infection** | | | >0.999* |
| Positive | 22 (100%) | 27 (96.4%) | |
| Negative | 0 | 1 (3.6%) | |
| **AFP (ng/ml)** | | | 0.522 |
| <400 | 9 (40.9%) | 9 (32.1%) | |
| ≥400 | 13 (59.1%) | 19 (67.9%) | |
| **Child-Pugh grade** | | | 0.246* |
| A | 22 (100%) | 25 (89.3%) | |
| B | 0 (0%) | 3 (10.7%) | |
| **BCLC stage** | | | 0.749* |
| A | 4 (18.2%) | 3 (10.7%) | |
| B | 6 (27.3%) | 8 (28.6%) | |
| C | 12 (54.5%) | 17 (60.7%) | |
| **Tumor diameter (cm)** | 12.3 ± 2.5 | 12.3 ± 2.4 | 0.988 |
| **Tumor number** | 1.82 ± 0.8 | 1.96 ± 1.0 | 0.559 |
| 1 | 9 (40.9%) | 13 (46.4%) | 0.696 |
| 2–3 | 13 (59.1%) | 15 (53.6%) | |
| **Growth pattern** | | | 0.481* |
| Infiltrative | 5 (22.7%) | 4 (14.3%) | |
| Noninfiltrative | 17 (77.3%) | 24 (85.7%) | |
| **Vascular invasion** | | | 0.449 |
| Present | 11 (50.0%) | 11 (39.3%) | |
| Absent | 11 (50.0%) | 17 (60.7%) | |

*The Fisher exact test was used.*

**TABLE 2** | Procedure-related information about radiofrequency ablation (RFA) and microwave ablation (MWA) in the transarterial chemoembolization (TACE)-sorafenib-thermal ablation group.

| Variables | TACE-sorafenib-thermal ablation | | P |
|---|---|---|---|
| | RFA (n=11) | MWA (n=9) | |
| **Number of procedures** | | | 0.702 |
| Range | 1–7 | 2–5 | |
| Mean ± SD | 2.8 ± 1.9 | 3.1 ± 1.3 | |
| **Procedure duration (min)** | | | 0.385 |
| Range | 8–110 | 6–118 | |
| Mean ± SD | 45.6 ± 31.4 | 39.0 ± 25.3 | |
| **Number of ablation sites** | | | 0.306 |
| Range | 1–7 | 1–8 | |
| Mean ± SD | 3.4 ± 1.8 | 3.9 ± 2.0 | |
| **Ablation duration at each site (min)** | | | <0.01 |
| Range | 5–25 | 3–20 | |
| Mean ± SD | 13.2 ± 4.7 | 9.0 ± 3.5 | |
| **Hospital stays (days)** | | | <0.01 |
| Range | 1–7 | 1–5 | |
| Mean ± SD | 3.48 ± 1.1 | 2.46 ± 0.9 | |

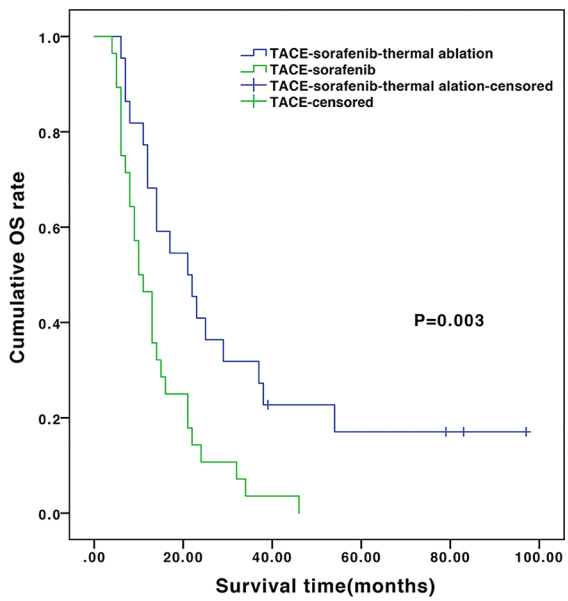


**FIGURE 1** | Overall survival of the transarterial chemoembolization (TACE)-sorafenib-thermal ablation and TACE-sorafenib groups.

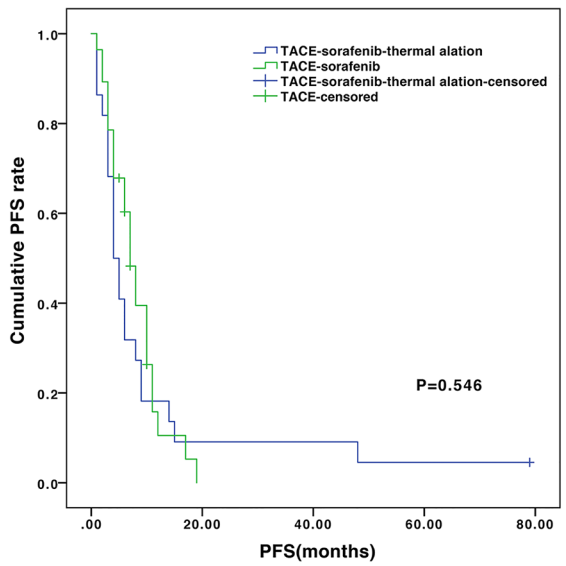


**FIGURE 2 |** Progression-free survival of the transarterial chemoembolization (TACE)-sorafenib-thermal ablation and TACE-sorafenib groups.

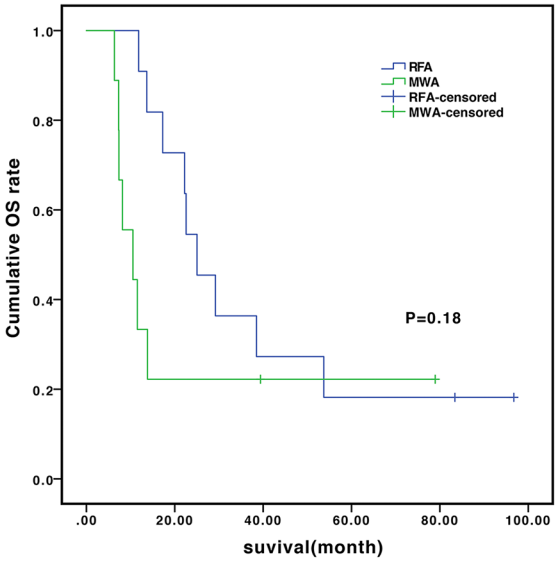


**FIGURE 4 |** Overall survival of patients who received radiofrequency ablation (RFA) and microwave ablation (MWA) in the transarterial chemoembolization (TACE)-sorafenib-thermal ablation group.

## Cox Analysis

The predictors of OS in the Cox analysis are shown in **Table 3**. Multivariate analysis was not performed because only the choice of treatment had a *P*-value <0.05 in univariable analyses. HBV status and Child-Pugh grades could not be analyzed because the number of patients in some categories are too small. TACE-sorafenib-thermal ablation (HR=2.512, 95%CI:1.348–4.680, *P*=0.004) was found to be a predictor of OS.

## Adverse Events

The most common drug-related toxicities were hand-foot syndrome (HFS, 86.4% vs. 85.7%), alopecia (31.8% vs. 39.3%), diarrhea (18.2% vs. 35.7%), and hypertension (13.6% vs. 3.6%) in the TACE-sorafenib-thermal ablation and TACE-sorafenib groups, respectively. Most adverse events were grade 1 or 2. Four cases of drug-related grade 3 toxicitiy were reported, including one case of HFS in the TACE-sorafenib-thermal ablation group and three cases

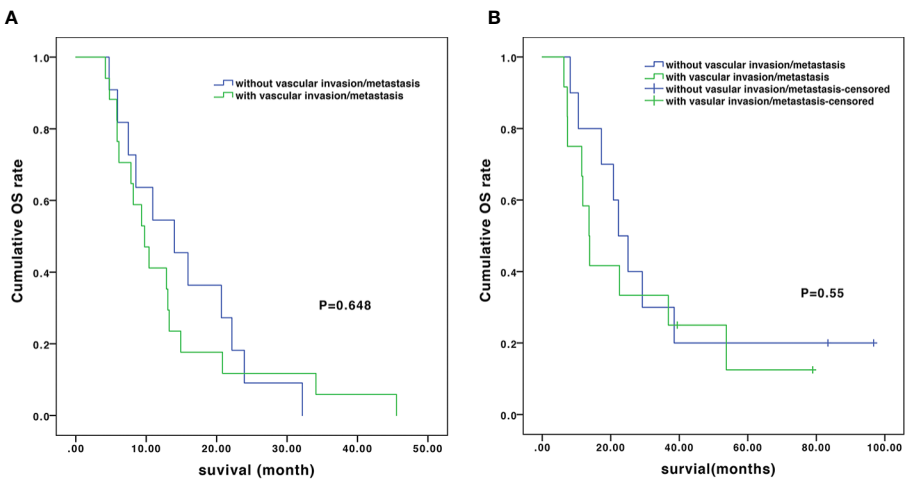


**FIGURE 3 |** Overall survival of patients with and without vascular invasion/metastasis in the transarterial chemoembolization (TACE)-sorafenib group **(A)** and the TACE-sorafenib-thermal ablation group **(B)**.

**TABLE 3 |** Factors influencing overall survival according to the Cox analysis.

| Variables | HR (95% CI) | *P* |
|---|---|---|
| **AFP (ng/ml)** | | |
| <400 | 1.000 | |
| ≥400 | 1.317 (0.772–2.401) | 0.369 |
| **BCLC stage** | | |
| A | 1.000 | |
| B | 2.097 (0.791–5.558) | 0.137 |
| C | 2.108 (0.865–5.137) | 0.101 |
| **Tumor number** | | |
| Single | 1.000 | |
| Multiple | 1.385 (0.768-2.498) | 0.279 |
| **Growth pattern** | | |
| Non-infiltrative | 1.000 | |
| Infiltrative | 1.555 (0.743–3.255) | 0.241 |
| **Vascular invasion** | | |
| Absent | 1.000 | |
| Present | 1.259 (0.701–2.262) | 0.441 |
| **Therapy** | | |
| TACE-sorafenib-thermal ablation | 1.000 | |
| TACE-sorafenib | 2.512 (1.348–4.680) | 0.004 |

*Multivariate analysis was not performed because only the choice of treatment had a P-value <0.05 in univariable analyses. HBV status and Child-Pugh grades could not be analyzed because of the too small number of patients in some categories.*

**TABLE 4 |** Drug-related toxicity.

| Adverse event | TACE-sorafenib-ablation (n=22) | | TACE-sorafenib (n=28) | |
|---|---|---|---|---|
| | Any grade | Grade 3 | Any grade | Grade 3 |
| Hand-foot reaction | 19 (86.4%) | 1 (4.5%) | 24 (85.7%) | 1 (3.6%) |
| Rash | 8 (36.4%) | 0 | 6 (21.4%) | 0 |
| Diarrhea | 4 (18.2%) | 0 | 10 (35.7%) | 0 |
| Hypertension | 3 (13.6%) | 0 | 1 (3.6%) | 0 |
| Voice changes | 1 (4.5%) | 0 | 2 (7.1%) | 0 |
| Bleeding | 0 | 0 | 1 (3.6%) | 1 (3.6%) |
| Liver dysfunction | 0 | 0 | 1 (3.6%) | 1 (3.6%) |
| Alopecia | 7 (31.8%) | 0 | 11(39.3%) | 0 |

(one with HFS, one with bleeding, and one with liver dysfunction) in the TACE-sorafenib group. No drug-related grade 4–5 AEs were recorded. All drug-related toxicities are listed in **Table 4**.

The most common minor complications were post-embolization/ablation syndrome which includes fever (37.7% vs. 83.3%), pain (28.9% vs. 15.3%), and vomiting (7.5% vs. 4.2%) in the TACE-sorafenib-thermal ablation and TACE-sorafenib group, respectively. Meanwhile, two cases of minor bleeding (one thoracic hemorrhage and one liver subcapsule hemorrhage) were observed in the TACE-sorafenib-thermal ablation group; both cases resolved without special treatment. Four major complications were reported, including two cases of liver dysfunction in the TACE-sorafenib-thermal ablation group and two cases of myelosuppression in the TACE-sorafenib group. No permanent adverse sequelae or treatment-related death were observed. All procedure-related complications are listed in **Table 5**.

**TABLE 5 |** Procedure-related complications.

| Procedure-related complications | TACE-sorafenib-thermal ablation | TACE-sorafenib |
|---|---|---|
| | (n=159) | (n=72) |
| **Minor complications** | | |
| **Postembolization/ablation syndrome** | | |
| Fever | 60 (37.7%) | 60 (83.3%) |
| Pain | 46 (28.9%) | 11 (15.3%) |
| Vomiting | 12 (7.5%) | 3 (4.2%) |
| **Bleeding** | | |
| Thoracic hemorrhage | 1 (0.6%) | 0 |
| Liver subcapsule hemorrhage | 1 (0.6%) | 0 |
| **Major complications** | | |
| **Liver dysfunction** | 2 (1.3%) | 0 |
| **Myelosuppression** | 0 | 2 (2.8%) |

## DISCUSSION

Few data are available on the treatment strategies for huge HCC. This study compares the effectiveness and adverse events (AEs) of TACE combined with sorafenib and with or without thermal ablation in patients with huge unresectable HCC. The results suggest that TACE-sorafenib-thermal ablation provided an extended long-term OS to patients with huge unresectable HCC. TACE-sorafenib-thermal ablation may be a better choice than TACE-sorafenib for huge unresectable HCC.

TACE-sorafenib therapy has received more and more acceptance for the treatment of HCC. Compared with the studies of TACE monotherapy for huge HCCs by Xue et al. (2015) and Min et al. (2014), the present study suggests that the TACE-sorafenib group had a higher 1-year survival rate than the studies by Xue et al. (2015) and Min et al. (2014) (46.4% vs. 33% and 37.8%), despite the fact that the patients in the present study had a high risk of vessel invasion and multiple tumors. Hence, TACE-sorafenib therapy could provide survival benefits for patients with huge unresectable HCC. However, TACE is not a curative treatment and the rates of objective response range from 16% to 60% (Llovet and Bruix, 2003), suggesting limited benefits for huge HCC, particularly for hypovascular HCC. In addition, post-TACE vascular changes and hepatic dysfunction caused by sequential TACEs ultimately limit the number of TACE treatments that a patient can receive. Thus, TACE-sorafenib could only provide limited survival benefits for huge unresectable HCC.

Thermal ablation is a minimally invasive technique and is increasingly being used in managing HCCs. The present study provided evidence that thermal ablation plus TACE and sorafenib could be used for the treatment of huge unresectable HCC. In the present study, patients in the TACE-sorafenib-thermal ablation group had significantly higher 1-, 2-, and 3-year survival rates and longer median survival than those in the TACE-sorafenib group. Moreover, although all patients included in the present study had unresectable huge HCCs, Mok et al. (2003) and Hwang et al. (2015) reported that patients treated with TACE+MWA had a similar 1-year OS survival rate (68.6%) compared with surgical resection. TACE-sorafenib-thermal ablation has the following advantages. Firstly, increased levels of proangiogenic factors following thermal ablation have been reported and may be a potential reason for tumor recurrence (Dong et al., 2015). As reported by Dong et al. (2015), sorafenib inhibits the up-regulation of p-Akt and p-ERK1/2 in HCC cells after insufficient RFA, and further down-regulates the expression

of N-cadherin, vimentin, and snail, resulting in enhanced migration and invasion of HCC cells after insufficient RFA. Secondly, thermal ablation can directly and efficiently kill tumor cells and lighten tumor load, especially for hypovascular HCC or HCC with arteriovenous fistula, in which failures to TACE are common. Thermal ablation can specifically eliminate residual tumor tissues after TACE, which could increase the local control rate and reduce neovascularization. Thirdly, thermal ablation causes little damage on liver function and allows an extension of the time interval between two TACE treatments, thus protects liver function. Finally, thermal ablation, especially RFA, could enhance various TAA-specific T cell response and release tumor antigen, heat shock protein, etc., thereby improving tumor-specific immunity, killing residual tumor cells, and reducing recurrence (Mizukoshi et al., 2013). Therefore, TACE-sorafenib-thermal ablation therapy could have great benefits for the treatment of huge unresectable HCC.

In the present study, TACE-sorafenib therapy was the only independent predictor for poor prognosis according to the Cox analysis, suggesting that the addition of thermal ablation is of vital importance in treating huge unresectable HCC. In the ablation procedure, the following principles are taken into account at our hospital and may contribute to the survival benefits. Firstly, for huge HCCs with satellite foci, the original or relatively larger tumor is always the first MWA target. Secondly, MWA should be performed first in the center of the tumor, then in the peripheral residual lesions. Finally, MWA ablation should be given to tumor located in a relatively safe place, then in the tumor that is adjacent to susceptible organs such as the intestines and gallbladder.

The difference of PFS between the TACE-sorafenib-thermal ablation and TACE-sorafenib groups was not statistically significant. We noticed that the median PFS and the 1-year PFS rates were longer in the TACE-sorafenib group, which may be caused by different sorafenib treatment time. The patients in the TACE-sorafenib-thermal ablation group began to take sorafenib at a later time than the patients in the TACE-sorafenib group. Kudo et al. (2011) reported that sorafenib did not significantly prolong survival in patients who responded well to TACE, due to delays in starting sorafenib (>9 weeks) after TACE. Therefore, we recommend starting sorafenib as soon as possible.

In the subgroup analysis, as in the study by Qu et al. (2012), we observed that there was no significant difference in OS between patients with and without vascular invasion in the two groups. Meanwhile, there was no significant difference in OS between patients who received only MWA and RFA treatment in the TACE-sorafenib-thermal ablation group. Nevertheless, patients who received MWA treatment had a slightly shorter time of ablation per site, and this may be due to its advantages over RFA, i.e., more rapid heating rate, higher intratumor temperature (reaching 130°C), larger ablation range, deeper tissue penetration, and smaller influence of blood flow (Hernandez et al., 2015). Hence, it is suggested that priority should be given to MWA for the treatment of huge unresectable HCCs, but this has to be validated by future studies.

In terms of AEs, the present study suggests that TACE-sorafenib-thermal ablation was well tolerated and led to only manageable side effects in patients with huge unresectable HCC. The most common reported drug-related toxicities were HFS, alopecia, diarrhea, and hypertension, similar to previous studies (Abdel-Rahman and Elsayed, 2013). Furthermore, TACE-sorafenib-thermal ablation did not increase the procedure-related complications in patients with huge unresectable HCC. The most common reported procedure-related complications were post-embolization/ablation syndrome, similar to a study by Yao et al. (2015). The major complications in the TACE-sorafenib-thermal ablation and TACE-sorafenib groups were liver dysfunction (n=2) and myelosuppression (n=2), similar to the 4.6% incidence reported for large HCCs by previous studies (Paul et al., 2011; Liang et al., 2013), but lower than in another study by Dong et al. (2016), which could be due to the choice of drugs for TACE. Meanwhile, no permanent adverse sequelae or treatment-related death were observed. Thus, these results suggest that TACE-sorafenib-thermal and TACE-sorafenib are well tolerated by patients with huge unresectable HCC.

There are some limitations in the current study. Firstly, it was a retrospective study and treatment strategy was determined by the choice of patients. Secondly, it was a single-center study in China. The HBV infection rate was higher in China than in Western countries. Thirdly, the sample size might not be large enough. In addition, our study failed to reveal the difference of RFA and MWA and risks factors for prognosis, maybe due to the relatively small sample size. Fourthly, the duration of sorafenib use in these two groups was not the same, which may have affected the OS. Therefore, a prospective trial with a larger sample size is needed.

In conclusion, the present study provides the evidence that TACE-sorafenib and TACE-sorafenib-thermal ablation are well-tolerated and beneficial in patients with huge unresectable HCC. TACE-sorafenib-thermal ablation is associated with significant survival benefits for patients with huge unresectable HCCs compared with TACE-sorafenib.

## DATA AVAILABILITY STATEMENT

The raw data supporting the conclusions of this article will be made available by the authors, without undue reservation.

## ETHICS STATEMENT

This study met the requirements of the Declaration of Helsinki and was approved by the Institutional Review Board of Sun Yat-sen University Cancer Center.

## AUTHOR CONTRIBUTIONS

WF: Study conception. YW, HQ, FC: Analysis and interpretation of data. All authors contributed to the article and approved the submitted version.

## FUNDING

This work was funded by the National Natural Science Foundation of China. Grant number: 81771954.

## REFERENCES


Abdel-Rahman, O., and Elsayed, Z. A. (2013). Combination trans arterial chemoembolization (TACE) plus sorafenib for the management of unresectable hepatocellular carcinoma: a systematic review of the literature. *Dig. Dis. Sci.* 58 (12), 3389–3396. doi: 10.1007/s10620-013-2872-x

Brown, D. B., Gould, J. E., Gervais, D. A., Goldberg, S. N., Murthy, R., Millward, S. F., et al. (2009). Transcatheter therapy for hepatic malignancy: standardization of terminology and reporting criteria. *J. Vasc. Interv. Radiol.* 20 (7 Suppl), S425–S434. doi: 10.1016/j.jvir.2009.04.021

Cabrera, R., Pannu, D. S., Caridi, J., Firpi, R. J., Soldevila-Pico, C., Morelli, G., et al. (2011). The combination of sorafenib with transarterial chemoembolisation for hepatocellular carcinoma. *Aliment. Pharmacol. Ther.* 34 (2), 205–213. doi: 10.1111/j.1365-2036.2011.04697.x

Chan, S. L., Chong, C. C., Chan, A. W., Poon, D. M., and Chok, K. S. (2016). Management of hepatocellular carcinoma with portal vein tumor thrombosis: Review and update at 2016. *World J. Gastroenterol.* 22 (32), 7289–7300. doi: 10.3748/wjg.v22.i32.7289

Chen, W., Zheng, R., Baade, P. D., Zhang, S., Zeng, H., Bray, F., et al. (2016). Cancer statistics in China 2015. *CA Cancer J. Clin.* 66 (2), 115–132. doi: 10.3322/caac.21338

Cheng, A. L., Kang, Y. K., Chen, Z., Tsao, C. J., Qin, S., Kim, J. S., et al. (2009). Efficacy and safety of sorafenib in patients in the Asia-Pacific region with advanced hepatocellular carcinoma: a phase III randomised, double-blind, placebo-controlled trial. *Lancet Oncol.* 10 (1), 25–34. doi: 10.1016/S1470-2045(08)70285-7

Chung, G. E., Lee, J. H., Kim, H. Y., Hwang, S. Y., Kim, J. S., Chung, J. W., et al. (2011). Transarterial chemoembolization can be safely performed in patients with hepatocellular carcinoma invading the main portal vein and may improve the overall survival. *Radiology* 258 (2), 627–634. doi: 10.1148/radiol.10101058

Dong, S., Kong, J., Kong, F., Kong, J., Gao, J., Ji, L., et al. (2015). Sorafenib suppresses the epithelial-mesenchymal transition of hepatocellular carcinoma cells after insufficient radiofrequency ablation. *BMC Cancer* 15, 939. doi: 10.1186/s12885-015-1949-7

Dong, J., Zhai, X., Chen, Z., Liu, Q., Ye, H., Chen, W., et al. (2016). Treatment of Huge Hepatocellular Carcinoma Using Cinobufacini Injection in Transarterial Chemoembolization: A Retrospective Study. *Evid. Based. Complement. Alternat. Med.* 2016:2754542. doi: 10.1155/2016/2754542

European Association For The Study Of The, , L., European Organisation For, , R., and Treatment Of, , C. (2012). EASL-EORTC clinical practice guidelines: management of hepatocellular carcinoma. *J. Hepatol.* 56 (4), 908–943. doi: 10.1016/j.jhep.2011.12.001

Goldberg, S. N., Grassi, C. J., Cardella, J. F., Charboneau, J. W., Dodd, G. D. 3rd, Dupuy, D. E., et al. (2009). Image-guided tumor ablation: standardization of terminology and reporting criteria. *J. Vasc. Interv. Radiol.* 20 (7 Suppl), S377–S390. doi: 10.1016/j.jvir.2009.04.011

Han, T., Yang, X., Zhang, Y., Li, G., Liu, L., Chen, T., et al. (2019). The clinical safety and efficacy of conventional transcatheter arterial chemoembolization and drug-eluting beads-transcatheter arterial chemoembolization for unresectable hepatocellular carcinoma: a meta-analysis. *Biosci. Trends* 13 (5), 374–381. doi: 10.5582/bst.2019.01153

Hernandez, J. I., Cepeda, M. F., Valdes, F., and Guerrero, G. D. (2015). Microwave ablation: state-of-the-art review. *Onco. Targets Ther.* 8, 1627–1632. doi: 10.2147/OTT.S81734

Hwang, S., Lee, Y. J., Kim, K. H., Ahn, C. S., Moon, D. B., Ha, T. Y., et al. (2015). Long-Term Outcome After Resection of Huge Hepatocellular Carcinoma >/= 10 cm: Single-Institution Experience with 471 Patients. *World J. Surg.* 39 (10), 2519–2528. doi: 10.1007/s00268-015-3129-y

Jemal, A., Bray, F., Center, M. M., Ferlay, J., Ward, E., and Forman, D. (2011). Global cancer statistics. *CA Cancer J. Clin.* 61 (2), 69–90. doi: 10.3322/caac.20107

Kim, J. H., Won, H. J., Shin, Y. M., Kim, S. H., Yoon, H. K., Sung, K. B., et al. (2011). Medium-sized (3.1-5.0 cm) hepatocellular carcinoma: transarterial chemoembolization plus radiofrequency ablation versus radiofrequency ablation alone. *Ann. Surg. Oncol.* 18 (6), 1624–1629. doi: 10.1245/s10434-011-1673-8

Kudo, M., Imanaka, K., Chida, N., Nakachi, K., Tak, W. Y., Takayama, T., et al. (2011). Phase III study of sorafenib after transarterial chemoembolisation in Japanese and Korean patients with unresectable hepatocellular carcinoma. *Eur. J. Cancer* 47 (14), 2117–2127. doi: 10.1016/j.ejca.2011.05.007

Lee, D. H., Lee, J. M., Lee, J. Y., Kim, S. H., Yoon, J. H., Kim, Y. J., et al. (2014). Radiofrequency ablation of hepatocellular carcinoma as first-line treatment: long-term results and prognostic factors in 162 patients with cirrhosis. *Radiology* 270 (3), 900–909. doi: 10.1148/radiol.13130940

Lencioni, R., and Llovet, J. M. (2010). Modified RECIST (mRECIST) assessment for hepatocellular carcinoma. *Semin. Liver Dis.* 30 (1), 52–60. doi: 10.1055/s-0030-1247132

Liang, H. Y., Lu, L. G., Hu, B. S., Li, Y., and Shao, P. J. (2013). Effects of sorafenib combined with chemoembolization and radiofrequency ablation for large, unresectable hepatocellular carcinomas. *Chin. Med. J. (Engl.)* 126 (22), 4270–4276. doi: 10.3760/cma.j.issn.0366-6999.20120478

Llovet, J. M., and Bruix, J. (2003). Systematic review of randomized trials for unresectable hepatocellular carcinoma: Chemoembolization improves survival. *Hepatology* 37 (2), 429–442. doi: 10.1053/jhep.2003.50047

Llovet, J. M., Real, M. I., Montana, X., Planas, R., Coll, S., Aponte, J., et al. (2002). Arterial embolisation or chemoembolisation versus symptomatic treatment in patients with unresectable hepatocellular carcinoma: a randomised controlled trial. *Lancet* 359 (9319), 1734–1739. doi: 10.1016/S0140-6736(02)08649-X

Llovet, J. M., Ricci, S., Mazzaferro, V., Hilgard, P., Gane, E., Blanc, J. F., et al. (2008). Sorafenib in advanced hepatocellular carcinoma. *N. Engl. J. Med.* 359 (4), 378–390. doi: 10.1056/NEJMoa0708857

Min, Y. W., Lee, J. H., Gwak, G. Y., Paik, Y. H., Lee, J. H., Rhee, P. L., et al. (2014). Long-term survival after surgical resection for huge hepatocellular carcinoma: comparison with transarterial chemoembolization after propensity score matching. *J. Gastroenterol. Hepatol.* 29 (5), 1043–1048. doi: 10.1111/jgh.12504

Mizukoshi, E., Yamashita, T., Arai, K., Sunagozaka, H., Ueda, T., Arihara, F., et al. (2013). Enhancement of tumor-associated antigen-specific T cell responses by radiofrequency ablation of hepatocellular carcinoma. *Hepatology* 57 (4), 1448–1457. doi: 10.1002/hep.26153

Mok, K. T., Wang, B. W., Lo, G. H., Liang, H. L., Liu, S. I., Chou, N. H., et al. (2003). Multimodality management of hepatocellular carcinoma larger than 10 cm. *J. Am. Coll. Surg.* 197 (5), 730–738. doi: 10.1016/j.jamcollsurg.2003.07.013

Omata, M., Lesmana, L. A., Tateishi, R., Chen, P. J., Lin, S. M., Yoshida, H., et al. (2010). Asian Pacific Association for the Study of the Liver consensus recommendations on hepatocellular carcinoma. *Hepatol. Int.* 4 (2), 439–474. doi: 10.1007/s12072-010-9165-7

Paul, S. B., Gamanagatti, S., Sreenivas, V., Chandrashekhara, S. H., Mukund, A., Gulati, M. S., et al. (2011). Trans-arterial chemoembolization (TACE) in patients with unresectable Hepatocellular carcinoma: Experience from a tertiary care centre in India. *Indian J. Radiol. Imaging* 21 (2), 113–120. doi: 10.4103/0971-3026.82294

Poon, R. T., Fan, S. T., and Wong, J. (2002). Selection criteria for hepatic resection in patients with large hepatocellular carcinoma larger than 10 cm in diameter. *J. Am. Coll. Surg.* 194 (5), 592–602. doi: 10.1016/S1072-7515(02)01163-8

Qu, X. D., Chen, C. S., Wang, J. H., Yan, Z. P., Chen, J. M., Gong, G. Q., et al. (2012). The efficacy of TACE combined sorafenib in advanced stages hepatocellullar carcinoma. *BMC Cancer* 12:263. doi: 10.1186/1471-2407-12-263

Sacks, D., McClenny, T. E., Cardella, J. F., and Lewis, C. A. (2003). Society of Interventional Radiology clinical practice guidelines. *J. Vasc. Interv. Radiol.* 14 (9 Pt 2), S199–S202. doi: 10.1097/01.RVI.0000094584.83406.3e

Sergio, A., Cristofori, C., Cardin, R., Pivetta, G., Ragazzi, R., Baldan, A., et al. (2008). Transcatheter arterial chemoembolization (TACE) in hepatocellular carcinoma (HCC): the role of angiogenesis and invasiveness. *Am. J. Gastroenterol.* 103 (4), 914–921. doi: 10.1111/j.1572-0241.2007.01712.x

Shim, J. H., Park, J. W., Kim, J. H., An, M., Kong, S. Y., Nam, B. H., et al. (2008). Association between increment of serum VEGF level and prognosis after

transcatheter arterial chemoembolization in hepatocellular carcinoma patients. *Cancer Sci.* 99 (10), 2037–2044. doi: 10.1111/j.1349-7006.2008.00909.x

Xue, T., Le, F., Chen, R., Xie, X., Zhang, L., Ge, N., et al. (2015). Transarterial chemoembolization for huge hepatocellular carcinoma with diameter over ten centimeters: a large cohort study. *Med. Oncol.* 32 (3), 64. doi: 10.1007/s12032-015-0504-3

Yao, X., Yan, D., Liu, D., Zeng, H., and Li, H. (2015). Efficacy and adverse events of transcatheter arterial chemoembolization in combination with sorafenib in the treatment of unresectable hepatocellular carcinoma. *Mol. Clin. Oncol.* 3 (4), 929–935. doi: 10.3892/mco.2015.554

**Conflict of Interest:** The authors declare that the research was conducted in the absence of any commercial or financial relationships that could be construed as a potential conflict of interest.

frontiers in Pharmacology

ORIGINAL RESEARCH
published: 31 July 2020
doi: 10.3389/fphar.2020.01183

# Genetic Profiles Affect the Biological Effects of Serine on Gastric Cancer Cells

*Jun Li[1†], Hongzhang Xue[2†], Zhen Xiang[1†], Shuzheng Song[1], Ranlin Yan[1], Jun Ji[1], Zhenggang Zhu[1], Chaochun Wei[2,3] and Yingyan Yu[1*]*

*[1] Department of Surgery of Ruijin Hospital, Shanghai Institute of Digestive Surgery, and Shanghai Key Laboratory for Gastric Neoplasms, Shanghai Jiao Tong University School of Medicine, Shanghai, China, [2] Department of Bioinformatics and Biostatistics, School of Life Sciences and Biotechnology, Shanghai Jiao Tong University, Shanghai, China, [3] SJTU-Yale Joint Center for Biostatistics and Data Science, Shanghai Jiao Tong University, Shanghai, China*

A high serine content in body fluid was identified in a portion of patients with gastric cancer, but its biological significance was not clear. Here, we investigated the biological effect of serine on gastric cancer cells. Serine was added into the culture medium of MGC803 and HGC27 cancer cells, and its influence on multiple biological functions, such as cell growth, migration and invasion, and drug resistance was analyzed. We examined the global transcriptomic profiles in these cultured cells with high serine content. Both MGC803 and HGC27 cell lines were originated from male patients, however, their basal gene expression patterns were very different. The finding of cell differentiation-associated genes, ALPI, KRT18, TM4SF1, KRT81, A2M, MT1E, MUC16, BASP1, TUSC3, and PRSS21 in MGC803 cells suggested that this cell line was more poorly differentiated, compared to HGC27 cell line. When the serine concentration was increased to 150mg/ml in medium, the response of these two gastric cancer cell lines was different, particularly on cell growth, cell migration, and invasion and 5-FU resistance. In animal experiment, administration of high concentration of serine promoted cancer cell metastasis to local lymph node. Taken together, we characterized the basal gene expressing profiles of MGC803 and HGC27. The HGC27 cells were more differentiated than MGC803 cells. MGC803 cells were more sensitive to the change of serine content. Our results suggested that the responsiveness of cancer cells to microenvironmental change is associated with their genetic background.

**Keywords: gastric cancer, MGC803, HGC27, microenvironment, serine**

OPEN ACCESS

***Edited by:***
*Zhe-Sheng Chen,*
*St. John's University, United States*

***Reviewed by:***
*Hongxiu Han,*
*Tongji Hospital Affiliated to Tongji University, China*
*Guanzhen Yu,*
*Shanghai University of Traditional Chinese Medicine, China*

****Correspondence:***
*Yingyan Yu*
*yingyan3y@sjtu.edu.cn*

*[†]These authors have contributed equally to this work*

***Specialty section:***
*This article was submitted to Pharmacology of Anti-Cancer Drugs, a section of the journal Frontiers in Pharmacology*

***Received:*** *15 June 2020*
***Accepted:*** *20 July 2020*
***Published:*** *31 July 2020*

***Citation:***
*Li J, Xue H, Xiang Z, Song S, Yan R, Ji J, Zhu Z, Wei C and Yu Y (2020) Genetic Profiles Affect the Biological Effects of Serine on Gastric Cancer Cells. Front. Pharmacol. 11:1183. doi: 10.3389/fphar.2020.01183*

## INTRODUCTION

Gastric cancer (GC), which ranks the fifth in incidence and the third in mortality worldwide, is one of the most common malignant tumors of digestive tract. This malignancy commonly occurs in Asian countries, especially in China, Japan, and South Korea (Torre et al., 2015; Bray et al., 2018). Because there is no sensitive and specific diagnostic method for GC, most patients have developed to advanced stage and lost the best time for surgical treatment when they were diagnosed. Therefore,

novel detection methods and molecular biomarkers for early diagnosis have been extensively explored (Dou et al., 2018; Song et al., 2019).

Our team has been working on translational research and exploring the pathogenesis of gastric cancer. In a previous study on urine metabolites, a group of amino acids were found to be abnormally elevated in GC patients than that in healthy controls. Those amino acids include alanine, glycine, valine, serine, isoleucine, threonine, proline, methionine, tyrosine, and tryptophan. Among them, all the values of the area under curve (AUC) of the diagnostic curves of threonine, serine, and alanine were above 0.8, indicating the good diagnostic value for GC. Moreover, some of the amino acids showed predictive potential for prognosis (Chen et al., 2016). These findings implied that increased certain amino acids in body fluid might have biological significance on GC development.

Tumor is the overgrowth of cell clusters and the result of abnormal metabolism. Compared with normal cells, tumor cells demand more nutrients for their rapid proliferation and metastasis, and reshape a variety of anabolic and catabolic pathways in the nutrient-deficient microenvironment (Davidson et al., 2016; Bubnovskaya and Osinsky, 2020). Amino acids are important metabolites of tumor cells. Elevation of some amino acids in microenvironment could provide favorable conditions for tumor growth, metastasis, drug resistance, and others. For example, Saito et al. reported that elevated leucine in microenvironment can promote cell proliferation in breast cancer, and induce resistance to tamoxifen (Saito et al., 2019). Engel et al. found that serine content of microenvironment determined the growth and survival of glioblastoma (Engel et al., 2020). In lung cancer, the imbalance of kynurenine to tryptophan ratio in microenvironment was closely related to the resistance for immune checkpoint inhibitor (Li et al., 2019). In this study, we explored the influence of high serine concentration on multiple biological behaviors, as well as the possible molecular mechanisms for GC.

# MATERIALS AND METHODS

## Cell Culture and Reagents

GC cell lines MGC803 and HGC27 were stored at the Shanghai Institute of Digestive Surgery. Both cell lines were cultured in RPMI-1640 medium (Gibco, USA) supplemented with 10% fetal bovine serum (Gibco, USA) and 5 μg/ml penicillin-streptomycin in a humidified incubator at 37°C with 5% CO2. In addition, RPMI-1640 medium supplemented with 1% fetal bovine serum was prepared for experiments and stored at 4°C.

Serine (Purity>98.5%, LR, BBI Life Sciences, China) was fully dissolved with phosphate buffer (1 x PBS) to the concentration of 150 mg/ml and was filtered with 0.22 μm aperture needle filter (Millipore, United States) and then stored at 4°C. Puromycin (Cat. #ANT-PR-5B, Invivogen, USA), rabbit GFP monoclonal antibody (Proteintech, 50430-2-AP, China), HRP-labeled goat anti-rabbit antibody (Servicebio, GB23305, China), 5-Fluorouracil (5-FU, Shanghai Xudong Haipu Pharmaceutical Co., Ltd., China) and Cryptotanshinone (2.5 μM, S2285, SELLECK, Houston, USA) were stored at −20°C.

## Determining the Serine Concentration

In order to find proper concentration of serine in functional experiments, we designed five serine concentrations of 0, 30, 150, 300, and 600 μg/ml. Then we calculated migration cells through transwell experiment. Briefly, MGC803 or HGC27 cells ($8\times10^4$/well) were added onto a 24-well plate (Corning Life Science, Acton, MA, USA). A 700-μl RPMI-1640 medium complemented with 10% fetal bovine serum (FBS), and different concentration of serine was added to the lower chamber of the 24-well plate, and 300 μl FBS-free medium to the upper chamber. After incubation for 24 h, we stained the GC cells on the inserts by 0.5% crystal violet for 20 min at room temperature. The upper remaining cells of the inserts were removed with cotton swabs. Finally, the migrated GC cells were counted at the 200× under the Olympus BX50 microscope (Olympus Optical Co. Ltd., Tokyo, Japan), and photographed by Nikon Digital Sight DS-U2 (Nikon, Tokyo, Japan) camera. Five visual fields were randomly chosen to calculate the number of migrated cells.

## RNA Sequencing and Data Analysis

HGC27 and MGC803 cells ($1\times10^6$) were planted in 10cm dish with RPMI-1640 medium and 10% FBS. The next day, the cells were divided into two groups. One is in standard RPMI-1640 medium plus with serine 30 μg/ml and 1% FBS. The other is in standard RPMI-1640 medium with 1% FBS and an additional serine of 150 μg/ml. Three repeated wells were set for each group. After incubation for 48h, cells were collected into 1.5ml tube with 1 ml Trizol (Invitrogen, USA) for RNA extraction. RNA purification was checked by NanoPhotometer® spectrophotometer (IMPLEN, CA, USA), and RNA integrity was evaluated by Bioanalyzer 2100 system (Agilents, CA, USA). After the RNA quality control, sequencing libraries were generated using NEBNext® UltraTM RNA Library Kit for Illumina® (NEB, USA). RNA sequencing was performed on Illumina Novaseq6000 platform (Jiayin Biomedical Technology Co., Ltd., Shanghai, China). Indexes clustering were performed on cBot Cluster System using TruSeq PE Cluster Kit v3-cBot-HS (Illumia). HTSeq v0.6.0 was used to count the reads numbers mapped to each gene, and then the FPKM (Fragments Per Kilobase per Millions base pairs) of each gene was calculated based on the length of each gene and reads counts. The DESeq2 algorithm was used to filter the expression of differential genes. Differential genes between MGC803 and HGC27 cell lines were plotted with R software (version, R i386.3.6.3). The differential genes (at the standard $|\log2 \text{ (fold change)}| > 0.585$ and $P<0.001$) between high-serine medium group and standard medium group were analyzed. The RNA-seq data of cancer cell lines treated by serine could be found in SRA database (PRJNA638214).

## Cell Proliferation Assay

In the CCK8 assays, MGC803 or HGC27 cells ($2\times10^3$/well) were added into the 96-well plate with six repeated wells for each condition under RPMI-1640 medium 100 μl with 10% FBS incubation for 24 h. Then, the medium was replaced by RPMI-1640 medium with 1% FBS. The experimental groups were

divided as above. On the first, second, and third days, each well was added 100 μl 10% CCK8 solution diluted in medium with 1% FBS for 2 h incubation. The OD values at 450nm wavelength were measured by a spectrophotometry (BioTek, Vermont, USA).

## Colony Formation Assay

In the colony formation assay, cancer cells ($1 \times 10^3$/well) were added to six-well plate, and incubated with 2.5 ml mediums with 1% FBS for 3 days. And then, the medium was replaced with 2.5 ml above medium for another four days. The chemical cryptotanshinone was added at the 7th day. On the 14th day, the cell colony were fixed and dyed with 0.5% crystalline purple diluted in methanol for 20 min. After washing with clean water, the colony was photographed and counted by observing visible colony units in five fields.

## Cell Migration and Invasion Assays

Cell migration and invasion assay were performed by using transwell chambers (Corning, Lowell, MA, USA) coated with or without matrigel (BD Biosciences, Bedford, MA). MGC803 or HGC27 cells ($8\times 10^4$/well) were added to the upper chamber and cultured for 48 h at 37°C with 5% CO2. RPMI-1640 medium 700 μl with 10% FBS and different serine concentration was added to lower chambers and 200 μl medium without FBS but containing different serine concentration or cryptotanshinone was added to upper chamber. After incubation for 48 h, cells on the inserts were fixed and stained with 0.5% crystal violet diluted by methanol for 20 min at room temperature. The upper remaining cells of the inserts were removed with cotton swabs. Permeating cells were counted under the inverted microscope in five random fields. The photographs were taken under the 200× field (Nikon, Tokyo, Japan).

## 5-FU Sensitivity Assay

MGC803 or HGC27 cells ($5 \times 10^3$/well) were added into 96-well plates, and incubated in 100 μl high serine medium (150 μg/ml) or standard medium with 1% FBS for 24 h. Then, the medium was replaced with above two mediums containing gradient concentrations of 5-FU (0, 0.25, 0.5, 1, 2, 4, and 8 μg/ml). After incubation for 48 h, 100-μl solution of 10% CCK8 was added for 2 h, and OD values at 450nm were measured by a spectrophotometry (BioTek, Vermont, USA).

## Popliteal Lymph Node Metastasis

A total of twelve 5-week-old female nude mice (BALB/C nude, Beijing Vitolihua Experimental Animal Technology Co., Ltd.) were randomly divided into two groups. One is high serine group, and another is standard group (Normal). The mice were raised at the Shanghai Experimental Animal Research Center. The experiment was approved by the Research Ethics Committee of Shanghai Jiaotong University School of Medicine. A total of $5 \times 10^6$ HGC27 cells were injected into the left rear foot pad. The detailed steps were reported in the previous study (Xiang et al., 2019). The experimental animals were injected intraperitoneally with serine solution (2g/kg) (Sasaki et al., 2017), and control animals were injected intraperitoneally with 150-μl PBS solution. The first three injections were given every two days, then changed to every three days. Four weeks later, the mice were sacrificed, and primary tumors in foot pad and popliteal lymph nodes were removed for analysis. The size of the popliteal lymph nodes were calculated using the formula (volume=length ×width ×width/2). The popliteal lymph nodes were fixed with 4% formalin and slices were made for examination.

All removed lymph nodes were fixed by formalin and embedded in paraffin. The 4-μm thick slices were made to perform H&E and IHC staining by streptavidin-peroxidase method. Rabbit anti-GFP monoclonal antibody (1:100, Proteintech, 50430-2-AP, China) and HRP-labeled goat anti-rabbit antibody (1: 200, Servicebio, GB23305, China) were used. After staining, semi-quantitative analysis of GFP was conducted according to the proportion and intensity of stained tumor cells. The photographs were taken under the Nikon Digital Sight DS-U2 (Nikon, Tokyo, Japan) at low- and high-power fields.

## Statistical Analysis

All data were performed using GraphPad Prism 8.0 (Inc., La Jolla, CA, USA). The inter-group differences were analyzed by the Student's t test. The positive popliteal lymph node metastasis was analyzed by $\chi 2$ test. $P<0.05$ was considered statistically significant.

# RESULTS

## The Effect of Serine on Cancer Cell Migration

Five concentrations of serine (0, 30, 150, 300, and 600 μg/ml) were added to RPMI-1640 medium. After incubating MGC803 or HGC27 cells with the above five mediums for 24 h, the medium with 150 μg/ml serine showed the highest effect in promoting cell migration (69.2 ± 5.4) compared to that in RPMI-1640 medium (28.8 ± 5.3) in HGC27 cells ($P<0.0001$). The similar trend was observed in MGC803 cells (146.6 ± 11.5 vs 71.6 ± 6.2, $P<0.0001$) (**Figure 1**). In addition, the MGC803 cells showed more migrating cells than that of HGC27 cells in high serine culture medium (146.6 ± 11.5 vs. 69.2 ± 5.4, $P<0.0001$).

## The Effect of Serine on Global Transcriptomic Profiles on Gastric Cancer Cells

Because 150 μg/ml serine promoted cancer cell migration, we analyzed the effect of serine on global transcriptomic profiles of these two cancer cells. By RNA-Seq analysis, although the basal expression of Y chromosome-located genes of MGC803 and HGC27 cells were highly associated (coefficient R=0.794), the expression of thousands of autosomal genes were very different. For instance, the top ten highly expressed genes in HGC27 cells were ALPI, KRT18, TM4SF1, KRT81, A2M, MT1E, MUC16, BASP1, TUSC3 and PRSS21. The expression levels of each of those genes in HGC27 cells were over ten thousand-fold higher than that in MGC803 cells (**Figure 2A**). We separately analyzed

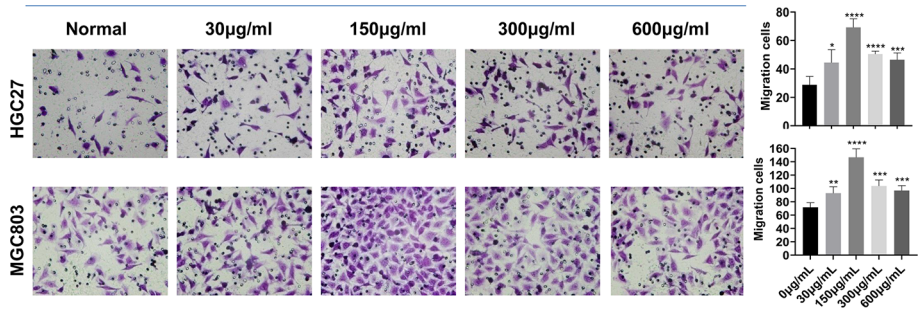


**FIGURE 1 |** The effect of different serine concentration on cancer cell migration. Five serine concentrations from 0 to 600 μg/ml in culture medium were set. After incubating MGC803 or HGC27 cells in mediums with different serine concentrations for 24 h, the optimum serine concentration of 150 μg/ml medium was observed in both cancer cell lines. In addition, the migratory ability of MGC803 cells was higher than that in HGC27cells at high serine condition. These data are representative examples taken from one of the three experiments. "*" represents $P < 0.05$, comparing to "Normal" group, **$P < 0.01$, ***$P < 0.001$, ****$P < 0.0001$.

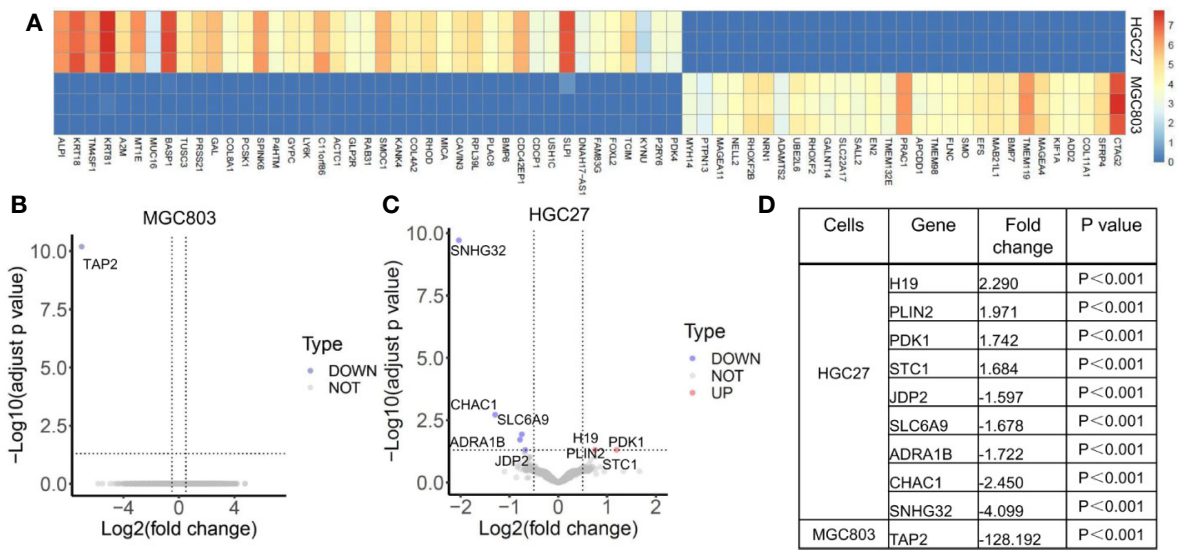


**D**

| Cells | Gene | Fold change | P value |
|---|---|---|---|
| HGC27 | H19 | 2.290 | P<0.001 |
| | PLIN2 | 1.971 | P<0.001 |
| | PDK1 | 1.742 | P<0.001 |
| | STC1 | 1.684 | P<0.001 |
| | JDP2 | -1.597 | P<0.001 |
| | SLC6A9 | -1.678 | P<0.001 |
| | ADRA1B | -1.722 | P<0.001 |
| | CHAC1 | -2.450 | P<0.001 |
| | SNHG32 | -4.099 | P<0.001 |
| MGC803 | TAP2 | -128.192 | P<0.001 |

**FIGURE 2 |** The effect of serine on global transcriptomic profiles of MGC803 and HGC27 cells. **(A)** Image of hierarchical clustering analysis for basal expression profiles of MGC803 and HGC27 cancer cells. The heatmap is presented by the FPKM of each differential gene. Row represents experimental cells, and column represents genes. The up-regulated genes are marked by light red color, and down-regulated genes are marked by dark blue color. **(B, C)** The volcano plots of differential gene expression of MGC803 cells and HGC27 cells in high serine group and standard medium group. **(D)** The fold change of differential genes in MGC803 and HGC27 cells. These data are representative examples taken from one of the three experiments.

the effect of high serine on MGC803 cells and HGC27 cells. Under the strict condition, only one gene TAP2 was differentially expressed between high-serein group and standard medium group in MGC803 cells (**Figure 2B**), while nine genes were differentially expressed in HGC27 cells. Among those different genes, four were up-regulated, and five were down-regulated (**Figure 2C**). The fold changes of different genes in both cell lines were presented in **Figure 2D**. Notably, gene PDK1, which involves in the JAK/STAT3 molecular pathway and associates with cell growth and invasion, was one of the differentially increased genes in the high serine group.

## The Effect of Serine on Cell Growth

CCK-8 assay showed that the cell proliferation ability of HGC27 and MGC803 cells were significantly increased in high serine group (1.69 ± 0.07, 72 h and 1.96 ± 0.01, 72 h, respectively), compared with that in standard medium (1.22 ± 0.05, 72 h, and 1.62 ± 0.05, 72 h, respectively, p<0.0001). The cell proliferative ability could be suppressed by cryptotanshinone (0.52 ± 0.01, 72 h, P<0.0001) in high-serine condition (0.57 ± 0.01, 72 h, 0.55 ± 0.01, 72 h, respectively, $P < 0.0001$, **Figure 3A**). The cell proliferation promoting effect of high serine in MGC803 cells was stronger than that in HGC27 cells (P<0.001, **Figure 3B**). In

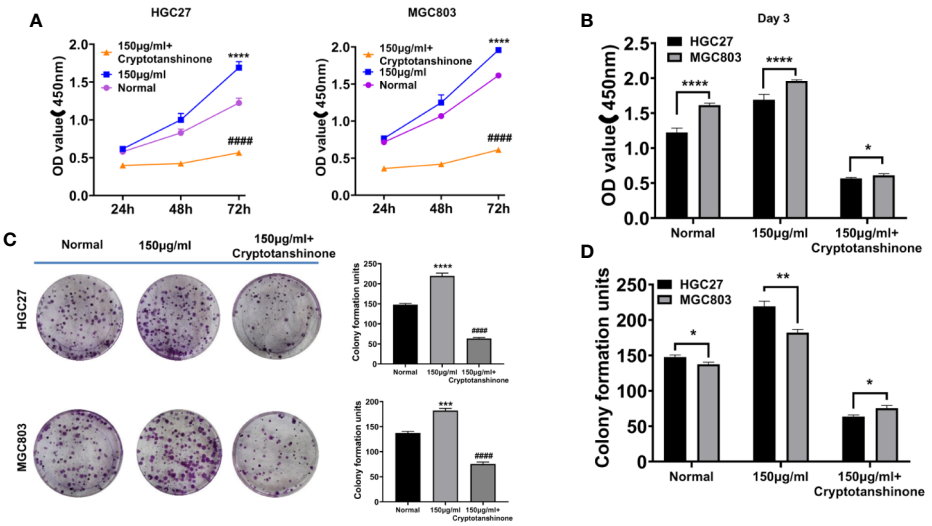


**FIGURE 3 |** The proliferation-enhancing effect of high serine on HGC27 and MGC803 cells. **(A)** CCK8 assay on the proliferation-enhancing effect of high serine on HGC27 and MGC803 cells. **(B)** CCK8 assay on the cell growth of HGC27 and MGC803 cells. **(C)** Colony formation assay on the proliferation-enhancing effect on HGC27 and MGC803 cells. **(D)** The comparison of different effects on colony formation between HGC27 and MGC803 cells. These data are representative examples taken from one of the three experiments. "*" represents $P < 0.05$, comparing to "Normal" group, **$P < 0.01$, ***$P < 0.001$, ****$P < 0.0001$. "####" represent $P < 0.0001$, compared to high-serine group.

addition, we observed much more colony formation of HGC27 cells in high serine group (219.3 ± 5.7), compared with that in standard medium (147.7 ± 2.5, p<0.001). The cryptotanshinone could suppress colony formation in high serine condition (47.3 ± 3.7, P<0.001, **Figure 3C**). In MGC803 cells, colony formation was higher in high serine group (182.3 ± 3.7), compared with that in standard medium (137.3 ± 2.5, p<0.01). The cryptotanshinone suppressed colony formation in high-serine-condition (51.7 ± 2.5, P<0.001). There are more colony formation in HGC27 cells that in MGC803 cells with high serine concentration (P<0.01, **Figure 3D**).

## The Effect of Serine on Cell Migration and Invasion

High serine promoted cell migration of HGC27 cells (58.0 ± 4.4), compared to standard medium (41.8 ± 5.9 cells, P<0.0001), The cryptotanshinone significantly suppressed cell migration in high-serine condition (5.2 ± 1.2, P<0.0001). Similar experimental results were obtained in MGC803 cancer cells (**Figure 4A**). In addition, the migration cells of MGC803 in high serine group were much more than that in HGC27 cells (138.2 ± 8.5 vs. 58.0 ± 4.4, P < 0.0001, **Figure 4B**). In cell invasion assay, the strongest invasion ability of HGC27 cells (102.6 ± 7.3) was observed in high serine group, compared with that in standard medium (62.4 ± 5.2 cells, P < 0.0001). The cryptotanshinone significantly suppressed cell invasion of HGC27 cells in high-serine condition (14 ± 1.7, P < 0.0001). Similar experimental results were obtained in MGC803 cells (**Figure 4A**). We noticed that the cell invasion ability in high serine group in MGC803 were stronger than that of HGC27 cells (149.8.2 ± 10.0 vs. 102.6 ± 7.3, P<0.0001, **Figure 4C**).

## The Effect of Serine on 5-FU Sensitivity

To evaluate the effect of high serine on chemosensitivity, MGC 803 and HGC27 cells were treated with 5-FU. The IC50 of 5-FU on HGC27 cells was higher in high serine group (1.46 ± 0.06 μg/ml), compared to standard medium group (0.76 ± 0.02 μg/ml, p<0.01) (**Figure 5A**). Similarly, the IC50 of 5-FU on MGC803 cells was higher in high serine group (1.01 ± 0.03 μg/ml) than that in standard medium group (0.89 ± 0.03 μg/ml, p<0.05) (**Figure 5B**). In standard medium, the IC50 of 5-FU in MGC803 cells (0.89 ± 0.03 μg/ml) was higher than that in HGC27 cells (0.76 ± 0.02 μg/ml, P<0.05, **Figure 5C**). However, in high serine condition, the IC50 of 5-FU in MGC803 cells (1.01 ± 0.03 μg/ml) was lower than that in HGC27 cells (1.46 ± 0.06 μg/ml, P<0.01) (**Figure 5D**). It means that the sensitivity to 5-FU on MGC803 cells was 1.45-fold higher than that in HGC27 cells in high-serine condition.

## The Effect of Serine on Lymph Node Metastasis In Vivo

To examine the possible effect of serine on promoting cancer cell metastasis *in vivo*, we established a popliteal lymph node metastatic model in nude mice. In experimental group, high concentration of serine (2g/kg) was administrated *via* abdominal cavity, while PBS was administrated *via* abdominal cavity as control (**Figure 6A**). After ten times administration of serine, the mice were sacrificed, and the popliteal lymph nodes were examined (**Figure 6B**). It was found that the sizes of the popliteal lymph nodes in high serine group were significantly larger than that in controls (4.29 ± 1.56 $mm^3$ vs.1.54 ± 0.67 $mm^3$, P<0.01, **Figures 6C, D**). We further detected the metastatic

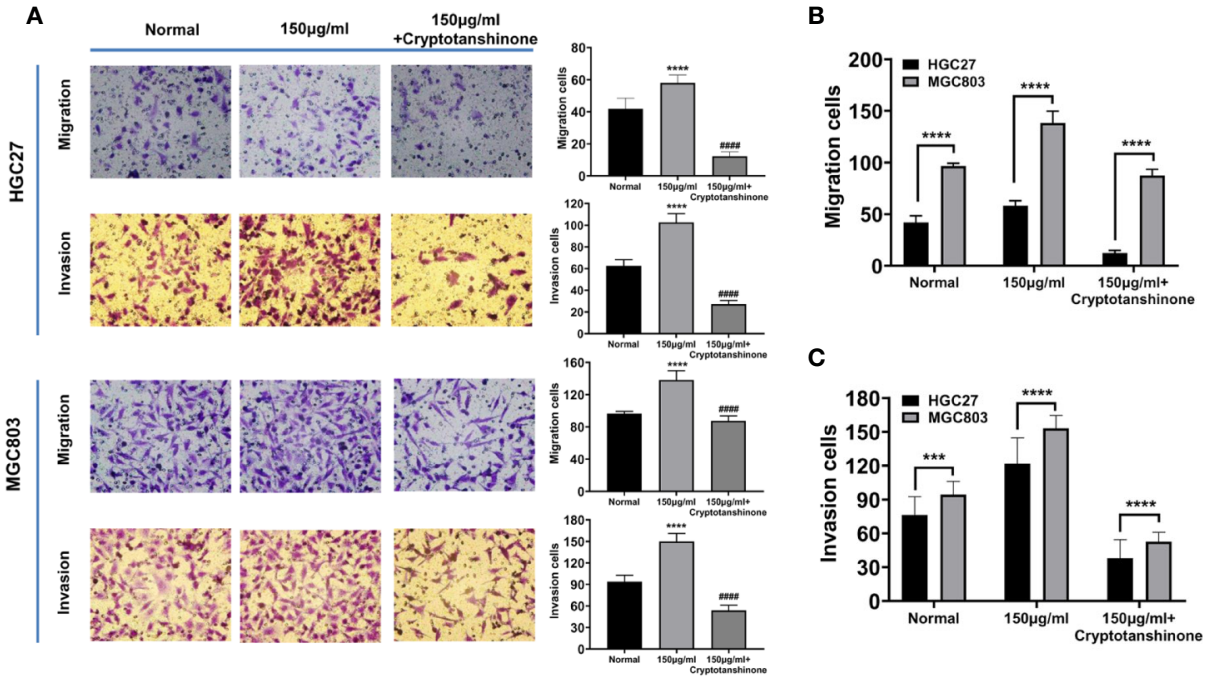


**FIGURE 4 |** Effects of high serine condition on cell migration and invasion of MGC803 and HGC27 cells. **(A)** The enhancing effect on cell migration and invasion under high serine condition. High serine in medium significantly promotes migration and invasion of HGC27 and MGC803 cells. Incubation with chemical cryptotanshinone suppresses cell migration and invasion. **(B)** Comparison of the difference on cell migration between HGC27 and MGC803 cells under the same cell culture conditions. **(C)** Comparison of the difference on cell invasion between HGC27 and MGC803 cells under the same cell culture conditions. These data are representative examples taken from one of the three experiments. "****" and "*****" represent $P < 0.001$, and $P < 0.0001$, compared to normal group. "#####" represent $P < 0.0001$, compared to high-serine group.

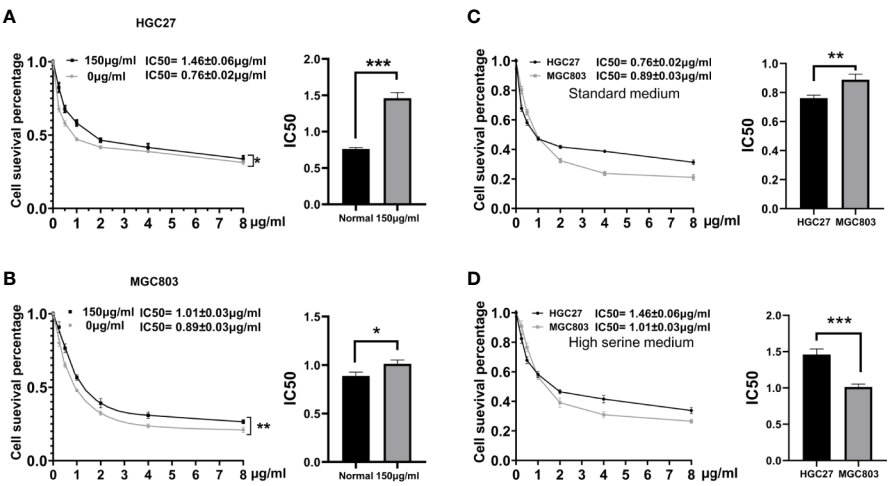


**FIGURE 5 |** Drugs sensitivity analyzed by CCK8 assay. **(A, B)** Dose-response curves and drug concentration of IC 50 of 5-FU between high serine group and standard medium in HGC27 and MGC803 cells. The sensitivity to 5-FU is reduced in high serine condition. **(C)** The difference of IC50 between HGC27 and MGC803 cells in standard medium. **(D)** The difference of IC50 between HGC27 and MGC803 in high serine medium. These data are representative examples taken from one of the three experiments. "*" represents $P < 0.05$, comparing to "Normal" group, **$P < 0.01$, ***$P < 0.001$,

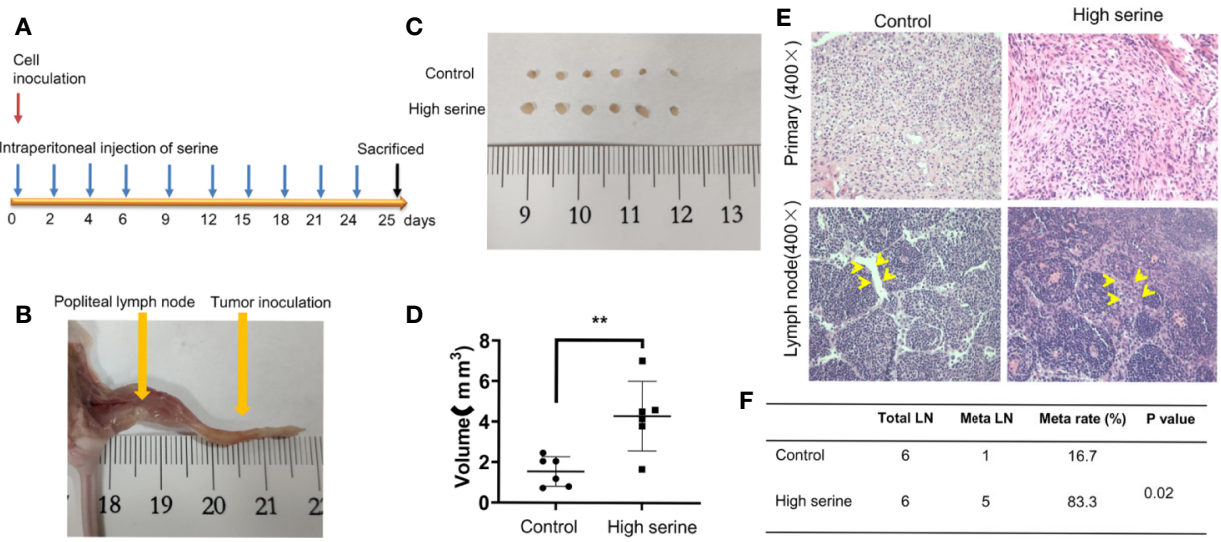


**FIGURE 6 |** Cancer metastasis analysis in nude mice. **(A)** The schematic of time points for cancer inoculation and serine administration. **(B)** Examination of foot pad and popliteal lymph nodes in nude mice. **(C)** The size differences of popliteal lymph nodes between experimental group and control group. **(D)** The volume differences of popliteal lymph nodes measured between experimental group and control group. **(E)** The primary tumor (up) and nodal metastases (down) were examined by H&E staining (400X). Compared to control, more metastatic cancer cells were observed in lymphatic sinuses (arrows). **(F)** The metastatic rate of popliteal lymph nodes was significantly different between the two groups. **P < 0.01.

cancer cells histologically, and found that the metastatic rate of cancer cells in lymph nodes of high serine group was significantly higher than that in controls (83.3% vs 16.7%, P<0.05, **Figures 6E, F**).

## DISCUSSION

Gastric cancer is the most common primary malignancy of digestive tract with a dismal prognosis. Multimodal therapeutic approaches have been used in gastric cancer treatment, such as surgical resection, chemotherapy, and radiotherapy. However, the response to therapies is very different, which could be attributed to different genetic background of individuals. Cancer cells are frequently used as experimental model in basic and clinical studies. MGC803 and HGC27 cell lines have been used for many years in gastric cancer research, however, the difference of their genetic background have not been reported (Tamura et al., 1996; Zhang et al., 2004; Jin et al., 2015). By global transcriptomics profiling for both cell lines, we characterized the differential expression of genes between these two cell lines. Among those, HGC27 cell line showed much more expression of differentiated genes compared to MGC803 cells. MGC803 cells had more genes of poorly differentiated cells. Cancer cells with different genetic backgrounds may response differently to external stimulation, including drug treatment. There were reports indicated that microenvironmental serine may alter cancer proliferation and invasion. For instance, Engel and colleagues reported that tumor microenvironment with high serine concentration contributed to rapid cell growth in glioblastoma. Interfering serine metabolism could be a plausible therapeutic target (Engel et al., 2020). It was reported that the proliferative ability of cancer cells could be enhanced by high content of microenvironmental serine (Labuschagne et al., 2014). Serine promoted cancer growth in prostate cancer (Reina-Campos et al., 2019). Up to date, there is no report on the biological effects of microenvironmental serine on gastric cancer.

In our previous study, significantly increased amino acids, including serine, were found in urine of patients with gastric cancer, implying a disturbed metabolism of amino acids (Chen et al., 2016). Amino acids serve the essential functions of redox balance, energetic regulation, biosynthesis, and homeostatic maintainence for living things (Lieu et al., 2020; Vettore et al., 2020). Serine is one of the pivotal nutrients for cell growth in routine RPMI-1640 culture medium with 30 μg/ml concentration (Mossinger, 1991). In the current study, in order to find out a proper high serine environment, we screened several concentrations and found that 150 μg/ml serine is the optimal concentration on enhancing cell growth and invasiveness of cancer cells. Our study showed that MGC803 cells and HGC27 cells had different biological behaviors no matter in standard condition or in high serine condition. This phenomenon could be explained by their different genetic backgrounds. These two cell lines were established from male patients, because they showed similar expression of genes of Y chromosome. However, the top ten significantly decreased genes (ALPI, KRT18, TM4SF1, KRT81, A2M, MT1E, MUC16, BASP1, TUSC3 and PRSS21) in MGC803 cell were over ten thousand-fold lower than that in HGC27 cells. Most of those genes were closely related to epithelium differentiation (Wang et al., 2008; Green et al., 2009; Shin et al., 2014; Kratochvilova et al., 2015; Wang et al., 2016; Conway et al., 2019; Golob-Schwarzl et al., 2019). This result

indicated that the MGC803 cell originated from poorly differentiated gastric cancer, while HGC27 cell might come from relatively differentiated gastric cancer. Our results will provide important reference for selecting proper cell models for future research. The higher proliferating and invasive ability of MGC-803 cells may attribute to its lower differentiation.

We treated MGC803 and HGC27 cells with same concentration of serine *in vitro*. The change of gene expression pattern was very different. Upon analysis, only TAP2 (transporter 2, an ATP binding cassette subfamily B member) gene showed significant down-regulation in high serine condition in MGC803 cells. TAP2 encodes a membrane-associated protein, which is a member of the MDR/TAP subfamily. Members of the MDR/TAP subfamily are involved in multidrug resistance (Lage et al., 2001). Since high serine stimulation significantly reduced TAP2 expression, the MGC803 cells showed increased sensitivity to 5-FU treatment after up-regulation of microenvironmental serine content. However, the molecular mechanisms should be explored further. In HGC27 cells, high serine condition resulted in different gene expression pattern. The increased expression of genes included oncogenic gene PDK1. PDK1 encodes a pyruvate dehydrogenase kinase 1, which is one of the major enzymes responsible for the regulation of homeostasis of carbohydrate fuels in mammals (Ba et al., 2020). The aberrant activation of PDK1 and its downstream effectors has been reported to involving in pathological phenotypes such as uncontrolled cell proliferation, apoptosis escape, invasion, and metastasis (Qian et al., 2020a), which may explain why HGC-27 cells showed higher metastatic ability in high serine administration in animal experiment. Some researches showed that PDK1 plays a role in chemoresistance in different types of malignancies, and targeting PDK1 could be a selection for promoting chemosensitization (Emmanouilidi and Falasca, 2017; Qian et al., 2020b). Recently, Yuan and colleagues reported that cryptotanshinone, originally a STAT3 inhibitor showed multiple suppressing activity on eight targets with anticancer potential, including MAP2K1, RARalpha, RXRalpha, PDK1, CHK1, AR, Ang-1 R, and Kif11 (Yuan et al., 2014). Those targets are related to promoting cancer growth. Their results provided a clue for the study of the anticancer effects and mechanisms of cryptotanshinone (Gagliardi et al., 2018). In our study, cryptotanshinone showed the suppressing effect on both cancer cell lines. It implied that microenvironmental high serine may activate multiple pathways. The biological behaviors observed in our study suggested that cancer cells might respond differently to microenvironmental serine and the difference might be related to different genetic background and original histological classification. Carter and coworkers reported that sensitivity of radiotherapy of colorectal cancer depended on the genetic background of cancers (Carter et al., 2019).

## CONCLUSIONS

This study demonstrated the global basal expression profiles of MGC803 and HGC27 cells. We found HGC27 cell was more differentiated than MGC803 cell. Although high serine condition could enhance the malignant behaviors in both cancer cells, MGC803 cells are more sensitive to change of serine concentration. This discrepancy could be attributed to different genetic background of cells. Since MGC803 and HGC27 cell lines are commonly used in basic experiments of gastric cancer. This finding will provide important references for cell selection for future research. Moreover, microenvironmental serine content could affect multiple biological behaviors, such as cell growth, cell migration, and invasion, and chemoresistance. Altering serine content of tumor microenvironment could be a new direction for cancer therapy in future.

## DATA AVAILABILITY STATEMENT

The sequencing data has been deposited into BioProject (https://www.ncbi.nlm.nih.gov/sra/?term=PRJNA638214).

## ETHICS STATEMENT

The animal study was reviewed and approved by Shanghai Jiao Tong University School of Medicine.

## AUTHOR CONTRIBUTIONS

YY and JL designed the study. JL, ZX, SS, RY, and JJ performed the experiments. HX and CW processed sequencing data and analyzed data. JL and YY wrote the manuscript. All authors contributed to the article and approved the submitted version.

## FUNDING

This project was partially supported by the Chinese National Key Program (2016YFC1303200 and MOST-2017YFC0908300), the National Natural Science Foundation of China (81772505), Shanghai Science and Technology Committee (18411953100), the cross-institute innovation foundation of Shanghai Jiao Tong University (YG2017ZD01), the Innovation Foundation of Translational Medicine of Shanghai Jiao Tong University School of Medicine (15ZH4001, TM201617 and TM 201702), and Technology Transfer Project of Science & Technology Dept. Shanghai Jiao Tong University School of Medicine. The funders had no role in study design, data collection and analysis, decision to publish, or preparation of the manuscript.

## ACKNOWLEDGMENTS

We thank the High Performance Computing Center (HPCC) at Shanghai Jiao Tong University for the computation.

## REFERENCES


Ba, M. C., Ba, Z., Long, H., Cui, S. Z., Gong, Y. F., Yan, Z. F., et al. (2020). LncRNA AC093818.1 accelerates gastric cancer metastasis by epigenetically promoting PDK1 expression. *Cell Death Dis.* 11, 64. doi: 10.1038/s41419-020-2245-2

Bray, F., Ferlay, J., Soerjomataram, I., Siegel, R. L., Torre, L. A., and Jemal, A. (2018). Global cancer statistics 2018: GLOBOCAN estimates of incidence and mortality worldwide for 36 cancers in 185 countries. *CA Cancer J. Clin.* 68, 394–424. doi: 10.3322/caac.21492

Bubnovskaya, L., and Osinsky, D. (2020). Tumor microenvironment and metabolic factors: contribution to gastric cancer. *Exp. Oncol.* 42, 2–10. doi: 10.32471/exp-oncology.2312-8852.vol-42-no-1.14056

Carter, R., Cheraghchi-Bashi, A., Westhorpe, A., Yu, S., Shanneik, Y., and Seraia, E. (2019) Identification of anticancer drugs to radiosensitise BRAF-wild-type and mutant colorectal cancer. *Cancer Biol, Med.* 16, 234–246.

Chen, Y., Zhang, J., Guo, L., Liu, L., Wen, J., Xu, L., et al. (2016). A characteristic biosignature for discrimination of gastric cancer from healthy population by high throughput GC-MS analysis. *Oncotarget* 7, 87496–87510. doi: 10.18632/oncotarget.11754

Conway, G. D., Buzza, M. S., Martin, E. W., Duru, N., Johnson, T. A., Peroutka, R. J., et al. (2019). PRSS21/testisin inhibits ovarian tumor metastasis and antagonizes proangiogenic angiopoietins ANG2 and ANGPTL4. *J. Mol. Med. (Berl)* 97, 691–709. doi: 10.1007/s00109-019-01763-3

Davidson, S. M., Papagiannakopoulos, T., Olenchock, B. A., Heyman, J. E., Keibler, M. A., Luengo, A., et al. (2016). Environment Impacts the Metabolic Dependencies of Ras-Driven Non-Small Cell Lung Cancer. *Cell Metab.* 23, 517–528. doi: 10.1016/j.cmet.2016.01.007

Dou, Y., Lv, Y., Zhou, X., He, L., Liu, L., Li, P., et al. (2018). Antibody-sandwich ELISA analysis of a novel blood biomarker of CST4 in gastrointestinal cancers. *Oncol. Targets Ther.* 11, 1743–1756. doi: 10.2147/OTT.S149204

Emmanouilidi, A., and Falasca, M. (2017). Targeting PDK1 for Chemosensitization of Cancer Cells. *Cancers (Basel)* 9, 140. doi: 10.3390/cancers9100140

Engel, A. L., Lorenz, N.II, Klann, K., Munch, C., Depner, C., Steinbach, J. P., et al. (2020). Serine-dependent redox homeostasis regulates glioblastoma cell survival. *Br. J. Cancer* 122, 1391–1398. doi: 10.1038/s41416-020-0794-x

Gagliardi, P. A., Puliafito, A., and Primo, L. (2018). PDK1: At the crossroad of cancer signaling pathways. *Semin. Cancer Biol.* 48, 27–35. doi: 10.1016/j.semcancer.2017.04.014

Golob-Schwarzl, N., Bettermann, K., Mehta, A. K., Kessler, S. M., Unterluggauer, J., Krassnig, S., et al. (2019). High Keratin 8/18 Ratio Predicts Aggressive Hepatocellular Cancer Phenotype. *Transl. Oncol.* 12, 256–268. doi: 10.1016/j.tranon.2018.10.010

Green, L. M., Wagner, K. J., Campbell, H. A., Addison, K., and Roberts, S. G. (2009). Dynamic interaction between WT1 and BASP1 in transcriptional regulation during differentiation. *Nucleic Acids Res.* 37, 431–440. doi: 10.1093/nar/gkn955

Jin, Z. T., Li, K., Li, M., Ren, Z. G., Wang, F. S., Zhu, J. Y., et al. (2015). G-protein coupled receptor 34 knockdown impairs the proliferation and migration of HGC-27 gastric cancer cells in vitro. *Chin Med. J. (Engl)* 128, 545–549. doi: 10.4103/0366-6999.151114

Kratochvilova, K., Horak, P., Esner, M., Soucek, K., Pils, D., Anees, M., et al. (2015). Tumor suppressor candidate 3 (TUSC3) prevents the epithelial-to-mesenchymal transition and inhibits tumor growth by modulating the endoplasmic reticulum stress response in ovarian cancer cells. *Int. J. Cancer* 137, 1330–1340. doi: 10.1002/ijc.29502

Labuschagne, C. F., van den Broek, N. J., Mackay, G. M., Vousden, K. H., and Maddocks, O. D. (2014). Serine, but not glycine, supports one-carbon metabolism and proliferation of cancer cells. *Cell Rep.* 7, 1248–1258. doi: 10.1016/j.celrep.2014.04.045

Lage, H., Perlitz, C., Abele, R., Tampe, R., Dietel, M., Schadendorf, D., et al. (2001). Enhanced expression of human ABC-transporter tap is associated with cellular resistance to mitoxantrone. *FEBS Lett.* 503, 179–184. doi: 10.1016/S0014-5793(01)02722-3

Li, H., Bullock, K., Gurjao, C., Braun, D., Shukla, S. A., Bosse, D., et al. (2019). Metabolomic adaptations and correlates of survival to immune checkpoint blockade. *Nat. Commun.* 10, 4346. doi: 10.1038/s41467-019-12361-9

Lieu, E. L., Nguyen, T., Rhyne, S., and Kim, J. (2020). Amino acids in cancer. *Exp. Mol. Med.* 52, 15–30. doi: 10.1038/s12276-020-0375-3

Mossinger, J. (1991). In vitro cultivation of adult Litomosoides carinii: evaluation of basic culture media, gas phases and supplements. *Parasitology* 103 Pt 1, 85–95. doi: 10.1017/S0031182000059321

Qian, Y., Wu, X., Wang, H., Hou, G., Han, X., and Song, W. (2020a). PAK1 silencing is synthetic lethal with CDK4/6 inhibition in gastric cancer cells via regulating PDK1 expression. *Hum. Cell.* 33, 377–385. doi: 10.1007/s13577-019-00317-6

Qian, Y., Wu, X., Wang, H., Hou, G., Han, X., and Song, W. (2020b). MicroRNA-4290 suppresses PDK1-mediated glycolysis to enhance the sensitivity of gastric cancer cell to cisplatin. *Braz. J. Med. Biol. Res.* 53, e9330. doi: 10.1590/1414-431x20209330

Reina-Campos, M., Linares, J. F., Duran, A., Cordes, T., L'Hermitte, A., Badur, M. G., et al. (2019). Increased Serine and One-Carbon Pathway Metabolism by PKClambda/iota Deficiency Promotes Neuroendocrine Prostate Cancer. *Cancer Cell.* 35, 385–400 e389. doi: 10.1016/j.ccell.2019.01.018

Saito, Y., Li, L., Coyaud, E., Luna, A., Sander, C., Raught, B., et al. (2019). LLGL2 rescues nutrient stress by promoting leucine uptake in ER(+) breast cancer. *Nature* 569, 275–279. doi: 10.1038/s41586-019-1126-2

Sasaki, T., Yasoshima, Y., Matsui, S., Yokota-Hashimoto, H., Kobayashi, M., and Kitamura, T. (2017). Intraperitoneal injection of d-serine inhibits high-fat diet intake and preference in male mice. *Appetite* 118, 120–128. doi: 10.1016/j.appet.2017.08.011

Shin, J., Carr, A., Corner, G. A., Togel, L., Davalos-Salas, M., Tran, H., et al. (2014). The intestinal epithelial cell differentiation marker intestinal alkaline phosphatase (ALPi) is selectively induced by histone deacetylase inhibitors (HDACi) in colon cancer cells in a Kruppel-like factor 5 (KLF5)-dependent manner. *J. Biol. Chem.* 289, 25306–25316. doi: 10.1074/jbc.M114.557546

Song, S., Xiang, Z., Li, J., Ji, J., Yan, R., Zhu, Z., et al. (2019). A Novel Citrullinated Modification of Histone 3 and Its Regulatory Mechanisms Related to IPO-38 Antibody-Labeled Protein. *Front. Oncol.* 9, 304. doi: 10.3389/fonc.2019.00304

Tamura, G., Sakata, K., Nishizuka, S., Maesawa, C., Suzuki, Y., Iwaya, T., et al. (1996). Inactivation of the E-cadherin gene in primary gastric carcinomas and gastric carcinoma cell lines. *Jpn J. Cancer Res.* 87, 1153–1159. doi: 10.1111/j.1349-7006.1996.tb03125.x

Torre, L. A., Bray, F., Siegel, R. L., Ferlay, J., Lortet-Tieulent, J., and Jemal, A. (2015). Global cancer statistics 2012. *CA Cancer J. Clin.* 65, 87–108. doi: 10.3322/caac.21262

Vettore, L., Westbrook, R. L., and Tennant, D. A. (2020). New aspects of amino acid metabolism in cancer. *Br. J. Cancer* 122, 150–156. doi: 10.1038/s41416-019-0620-5

Wang, Y., Cheon, D. J., Lu, Z., Cunningham, S. L., Chen, C. M., Luo, R. Z., et al. (2008). MUC16 expression during embryogenesis, in adult tissues, and ovarian cancer in the mouse. *Differentiation* 76, 1081–1092. doi: 10.1111/j.1432-0436.2008.00295.x

Wang, C., Zhao, Y., Ming, Y., Zhao, S., and Guo, Z. (2016). A polymorphism at the microRNA binding site in the 3'-untranslated region of C14orf101 is associated with the risk of gastric cancer development. *Exp. Ther. Med.* 12, 1867–1872. doi: 10.3892/etm.2016.3521

Xiang, Z., Li, J., Song, S., Wang, J., Cai, W., Hu, W., et al. (2019). A positive feedback between IDO1 metabolite and COL12A1 via MAPK pathway to promote gastric cancer metastasis. *J. Exp. Clin. Cancer Res.* 38, 314. doi: 10.1186/s13046-019-1318-5

Yuan, D. P., Long, J., Lu, Y., Lin, J., and Tong, L. (2014). The forecast of anticancer targets of cryptotanshinone based on reverse pharmacophore-based screening technology. *Chin J. Nat. Med.* 12, 443–448. doi: 10.1016/S1875-5364(14)60069-8

Zhang, L., Jia, G., Li, W. M., Guo, R. F., Cui, J. T., Yang, L., et al. (2004). Alteration of the ATM gene occurs in gastric cancer cell lines and primary tumors associated with cellular response to DNA damage. *Mutat. Res.* 557, 41–51. doi: 10.1016/j.mrgentox.2003.09.012


**Conflict of Interest:** The authors declare that the research was conducted in the absence of any commercial or financial relationships that could be construed as a potential conflict of interest.

frontiers in Oncology

REVIEW
published: 21 August 2020
doi: 10.3389/fonc.2020.01517

# Targeting Cullin-RING E3 Ligases for Radiosensitization: From NEDDylation Inhibition to PROTACs

*Shuhua Zheng*[1]* *and Wensi Tao*[2]*

[1] College of Osteopathic Medicine, Nova Southeastern University, Fort Lauderdale, FL, United States, [2] Department of Radiation Oncology, University of Miami-Miller School of Medicine, Coral Gables, FL, United States

As a dynamic regulator for short-lived protein degradation and turnover, the ubiquitin-proteasome system (UPS) plays important roles in various biological processes, including response to cellular stress, regulation of cell cycle progression, and carcinogenesis. Over the past decade, research on targeting the cullin-RING (really interesting new gene) E3 ligases (CRLs) in the UPS has gained great momentum with the entry of late-phase clinical trials of its novel inhibitors MLN4924 (pevonedistat) and TAS4464. Several preclinical studies have demonstrated the efficacy of MLN4924 as a radiosensitizer, mainly due to its unique cytotoxic properties, including induction of DNA damage response, cell cycle checkpoints dysregulation, and inhibition of NF-κB and mTOR pathways. Recently, the PROteolysis TArgeting Chimeras (PROTACs) technology was developed to recruit the target proteins for CRL-mediated polyubiquitination, overcoming the resistance that develops inevitably with traditional targeted therapies. First-in-class cell-permeable PROTACs against critical radioresistance conferring proteins, including the epidermal growth factor receptor (EGFR), androgen receptor (AR) and estrogen receptor (ER), cyclin-dependent kinases (CDKs), MAP kinase kinase 1 (MEK1), and MEK2, have emerged in the past 5 years. In this review article, we will summarize the most important research findings of targeting CRLs for radiosensitization.

**Keywords: NEDDylation, EGFR, PROTAC, cullin-RING E3 ligase, MLN4924**

OPEN ACCESS

***Edited by:***
*Zhe-Sheng Chen,*
*St. John's University, United States*

***Reviewed by:***
*Tarek Abbas,*
*University of Virginia, United States*
*Mikihiko Naito,*
*National Institute of Health Sciences (NIHS), Japan*

***Correspondence:**
*Shuhua Zheng*
*sz227@mynsu.nova.edu*
*Wensi Tao*
*wtao@med.miami.edu*

***Specialty section:***
*This article was submitted to Pharmacology of Anti-Cancer Drugs, a section of the journal Frontiers in Oncology*

***Received:*** *17 June 2020*
***Accepted:*** *15 July 2020*
***Published:*** *21 August 2020*

***Citation:***
*Zheng S and Tao W (2020) Targeting Cullin-RING E3 Ligases for Radiosensitization: From NEDDylation Inhibition to PROTACs. Front. Oncol. 10:1517. doi: 10.3389/fonc.2020.01517*

## INTRODUCTION

Over 60% of cancer patients undergo radiotherapy (RT) during their course of illness, with an estimated 40% contribution toward curative cancer treatment (1, 2). While RT is an essential element for curative, adjuvant, and palliative treatment of a range of human malignancies, a key challenge in RT is to maximize radiation doses to the tumor mass while sparing the surrounding healthy tissue (1). To that end, various approaches combining RT with chemotherapies as radiosensitizers have been explored, which led to improvements in tumor response and higher overall survival (OS) rates (3). Despite a clear success, the favorable clinical outcome of chemoradiotherapy still comes at the sacrifice of increased toxicity in many clinical contexts, mainly due to the limited specificity of conventional chemotherapies (4). In the past two decades, several clinical trials have been conducted to test combining RT with targeted therapies against radioresistance conferring proteins such as epidermal growth factor receptor (EGFR), histone deacetylase (HDAC) and the B-rapidly accelerated fibrosarcoma (BRAF), aiming to develop combined-modality treatment regimens with fewer side effects (5–7). Clinical studies consistently

suggested increased efficacy and improved survival rates of these new strategies, highlighting the clinical importance of using targeted agents as radiosensitizers (4). However, cancer cells will inevitably develop resistance toward these targeted therapies, leading to disease progression and relapse (8). Therefore, there is an urgent need to develop new strategies for radiosensitization.

In the past decade, targeting the activities of cullin-RING (really interesting new gene) E3 ligases (CRLs) in the ubiquitin-proteasome system (UPS) has gained considerable momentum for cancer treatment with the entry of several late-phase clinical trials of its first-in-class inhibitor MLN4924 (pevonedistat) (9). As early as the 1990s, the implication of targeting CRL for radiosensitization was suggested when its key component RING box protein 2 (Rbx2, a.k.a., SAG, ROC2) was identified as a redox inducible antioxidant protein (10). In recent years, studies showed that CRLs carry out the turnover of vital proteins involved in DNA damage response (DDR), as well as those in cell signaling pathways that are critical for radiosensitization (9, 11). Furthermore, in the past 5 years, the development of cell-permeable PROteolysis TArgeting Chimeras (PROTACs), which can selectively recruit radioresistance conferring proteins for CRL-mediated polyubiquitination, paved new methods in developing radiosensitizers that are less likely to develop chemoresistance (12). As such, it is crucial to systematically overview the mechanism of actions of CRL inhibitors for radiosensitization.

In this review article, we will summarize major strategies targeting CRLs and evaluate their potential as radiosensitizers based on the revised framework of the Steel hypothesis, originally described by George Steel in the 1970s (4). The revised hypothesis describes the scenario whereby combined-modality of targeted therapies and RT can improve the therapeutic outcomes by five mechanisms: (1) spatial cooperation, (2) temporal modulation, (3) biological cooperation, (4) cytotoxic enhancement, and (5) normal tissue protection (4).

## A GLIMPSE OF TRADITIONAL RADIOSENSITIZERS

Typical RT involves ionizing radiation (IR), which uses high-energy photon radiation, such as X-rays and gamma ($\gamma$) rays, and particle radiation, such as electron (e), carbon ion and proton (13, 14). The IR exerts cytotoxic effects via direct DNA damage, or indirectly via generation of free radicals, particularly reactive oxygen species (ROS) (15–17). Therefore, the radiosensitivity of cancer cells can be influenced by biological factors that regulate DNA damage repair, oxygen perfusion levels, and cell cycle stage (16). Traditional radiosensitizers target these underlying parameters for radiosensitization.

Platinum analogs, 5-fluorouracil (5-FU), and taxanes are the most common clinically used radiosensitizers. Platinum analogs, such as cisplatin and oxaliplatin, can bind to DNA and produce DNA-DNA crosslinking, which will lead to cell cycle arrest and exacerbating the radiation-induced DNA damage (18). Meanwhile, 5-FU, capecitabine (a 5-FU oral prodrug), and gemcitabine act as pseudo-substrates, incorporation of these nucleoside analogs can dysregulate cell cycle checkpoint in the S phase, disabling DNA damage repair machinery in cancer cells upon IR administration (19, 20). On the other hand, taxanes, such as paclitaxel and docetaxel, synchronize tumor cells at cell cycle G2-M phase and trigger chromosomal missegregation (21, 22). Meanwhile, tumors in the hypoxic microenvironment (low $pO_2$) are more radioresistant than those well-oxygenated (13). At the presence of oxygen, RT-induced DNA damages will be "fixed" via the formation of peroxyl radicals in DNA that had been insulted by free radicals (23). The oxygen mimics such as nitroimidazole derivatives (i.e., pimonidazole and nimorazole), and hypoxia-specific toxins were investigated in clinical trials as radiosensitizers (24, 25). Wang et al. (16) provided a comprehensive review on the recent development of radiosensitizers based on these principles.

The therapeutic potential of radiosensitizer is largely determined by the enhanced efficacy and selectivity against cancer cells but not normal tissue. However, traditional radiosensitizers are also chemotherapeutic drugs, which can cause prominent side effects. For example, cisplatin can cause intolerable nausea, vomiting, hearing loss, and kidney damage (26). Targeted therapies, such as MLN4924 and PROTACs are highly selective and would have fewer side effects. In fact, clinical trials of MLN4924 showed that this compound is well-tolerated (27).

## TARGETING THE UBIQUITIN-PROTEASOME SYSTEM (UPS)

Cellular protein levels are tightly controlled by both protein synthesis and degradation. The ubiquitin-proteasome system (UPS), first characterized in the mid-20th century, is a dynamically regulated multi-enzyme process that earmarks substrate proteins for proteasomal-mediated degradation via polyubiquitination (28). Targeted inhibition of the UPS via direct eradication of the proteasome activities using bortezomib, carfilzomib, or ixazomib has been proven clinically effective for treating multiple myeloma (MM) (29). Several clinical trials also investigated the UPS inhibitors for their potential as radiosensitizers in the treatment of metastatic melanoma (Phase I), head and neck cancer (Phase I), and glioblastoma multiforme (GBM; Phase II) (30–32). However, unexpected earlier tumor progression as a result of EGFR stabilization has been reported with the combined administration of bortezomib and conventional radiochemotherapy in head and neck cancer (32, 33). Such suboptimal response is conceivable as proteasome inhibition indiscriminately stabilizes the substrates, including EGFR and other oncogenic proteins, limiting the clinical applications in targeting proteasome as a radiosensitizing strategy (32). Instead of directly inhibiting the proteasome, recent studies have employed alternative strategies such as targeting the UPS via inhibition of the upstream ubiquitin (Ub) conjugation events or directly recruiting specific substrate protein for polyubiquitination using PROteolysis TArgeting Chimeras (PROTACs) (**Figures 1**, **2**).

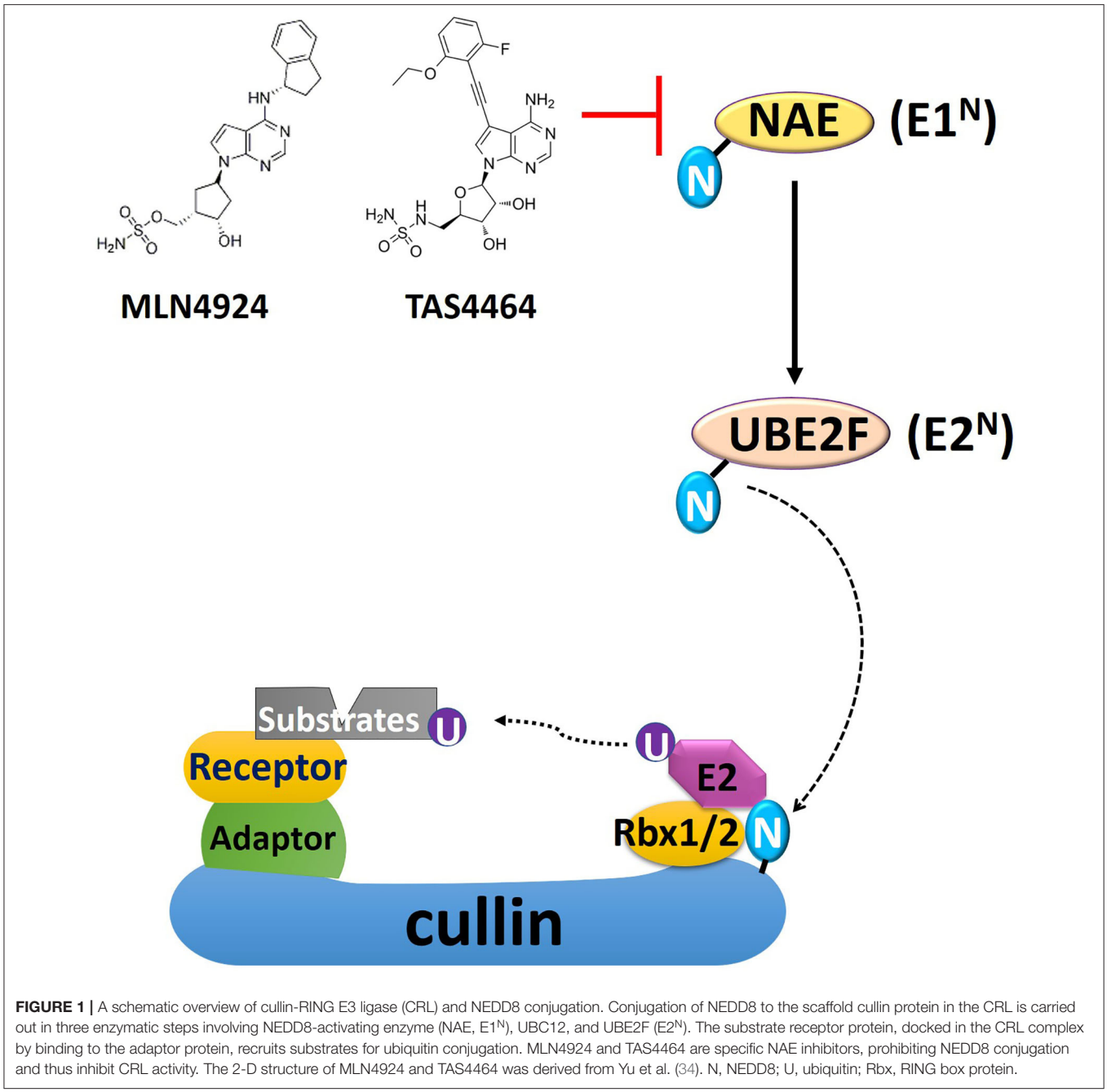


**FIGURE 1 |** A schematic overview of cullin-RING E3 ligase (CRL) and NEDD8 conjugation. Conjugation of NEDD8 to the scaffold cullin protein in the CRL is carried out in three enzymatic steps involving NEDD8-activating enzyme (NAE, $E1^N$), UBC12, and UBE2F ($E2^N$). The substrate receptor protein, docked in the CRL complex by binding to the adaptor protein, recruits substrates for ubiquitin conjugation. MLN4924 and TAS4464 are specific NAE inhibitors, prohibiting NEDD8 conjugation and thus inhibit CRL activity. The 2-D structure of MLN4924 and TAS4464 was derived from Yu et al. (34). N, NEDD8; U, ubiquitin; Rbx, RING box protein.

## NEDDYLATION INHIBITION

### NEDD8 Conjugation Pathway

The cullin-RING E3 ligases (CRLs) are responsible for polyubiquitination of about 20% of cellular proteins degraded via the UPS, most of which are critically involved in cell cycle progression, DDR, and oncogenic signaling cascades (9). The CRL complex's core structure is formed with a scaffold protein cullin bound with the RING-finger containing proteins (Rbx1 or Rbx2) at the C-terminus of cullin (35). This core complex will be joined by the adaptor protein, which binds the cullin's N-terminus domain to form a complete CRL complex (**Figure 1**) (35). Fully activation of CRLs requires conjugation of an Ub-like protein called neural precursor cell-expressed developmentally downregulated 8 (NEDD8) to near the C-terminus of the cullin in the CRL complex (11). Conjugation of NEDD8 to cullins is carried out in three enzymatic steps involving NEDD8-activating enzyme (NAE; E1), UBC12 and UBE2F (E2s), and E3s (**Figure 1**). NAE adenylates NEDD8 on its C-terminal glycine, forming a NEDD8-NAE complex via a covalent thiol-ester bond, and then transfers NEDD8 to the E2s via another thiol-ester bond (36, 37). NEDD8 E3 ligases execute the final step in conjugating

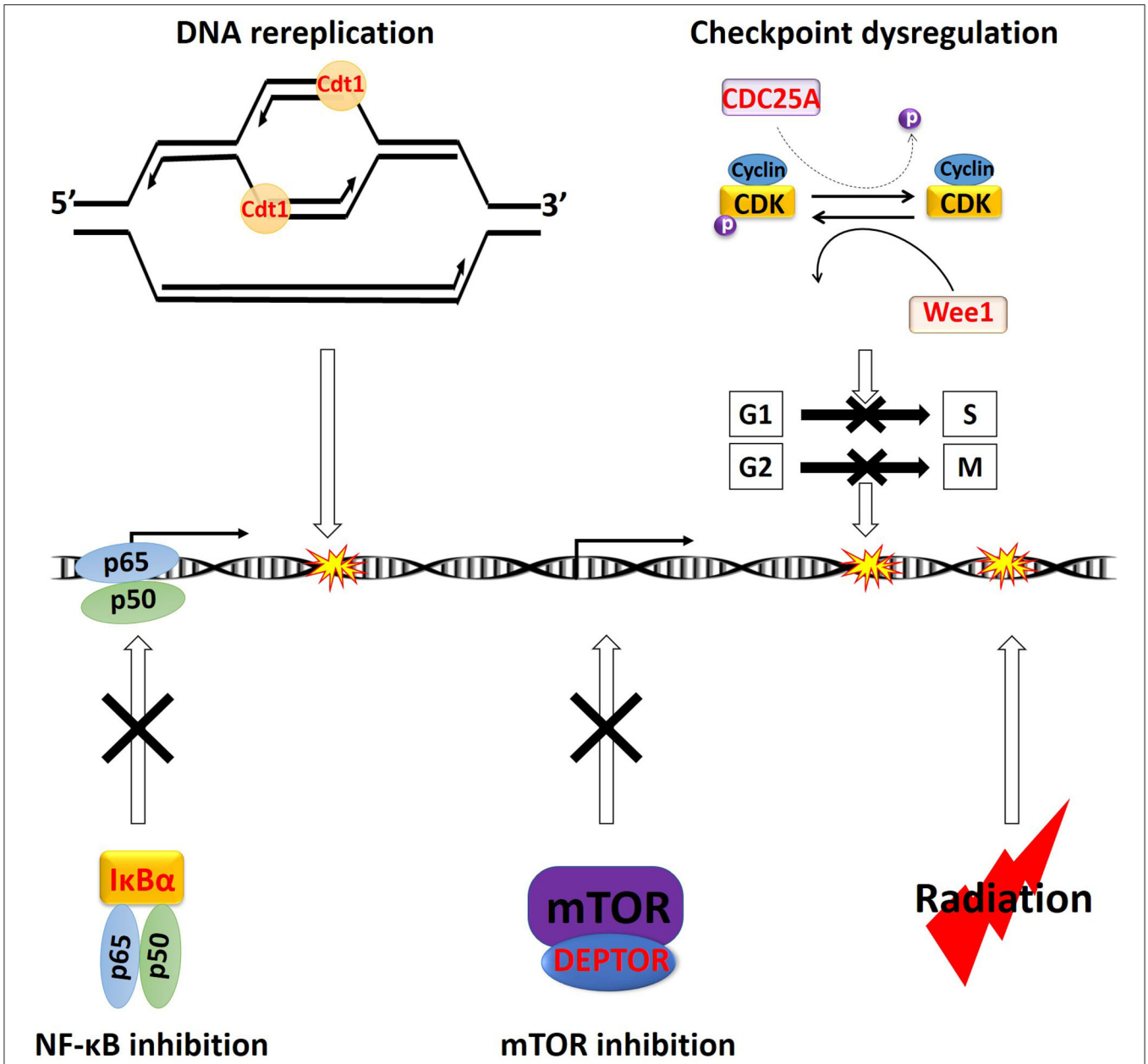


**FIGURE 2 |** Overview of the major cytotoxic mechanism of NEDDylation inhibition. All the characters in "Red" color are CRL substrates. Accumulation of Cdt1 can trigger DNA rereplication, resulting in DNA damages. Stabilization of CDC25A can potentially cause dysregulation of both early (G1 phase to S phase) and late (G2 phase to M phase) cell cycle checkpoints (dash arrow). Meanwhile, the accumulation of Wee1, p21, and p27 will trigger cell cycle arrest at the G1 or G2 phase. Stabilization of IκBα will lead to sequestration NF-κB p65 and p50 heterodimer in the cytosol, leading to inhibition of its transcriptional activities. Stabilization of DEPTOR can directly inhibit mTOR. Ionizing radiation also triggers cell death via induction of DNA damages. p, phosphor group.

NEDD8 to cullins, forming an isopeptide bond with the $\varepsilon$-amino group of a substrate lysyl residue (38, 39). NEDD8 conjugation facilitates the CRL structural remodeling that will juxtapose the substrate toward the catalytically active ubiquitylation site of CRL (40–42). The substrate receptor protein, docked in the CRL complex by binding to the adaptor protein, recruits substrates for Ub conjugation once CRL is fully functional (43) (**Figure 1**). So far, seven different types of human cullin proteins (CUL1, 2, 3, 4A, 4B, 5, 7) have been identified, and new members of the receptor and adaptor proteins are emerging (44). A more detailed overview of NEDD8 conjugation in CRLs has been summarized by Petroski and Deshaies in their review paper (45).

MLN4924 is an adenosine sulfamate analog that inhibits NEDDylation via the formation of an MLN4924-NEDD8 adduct, blocking the downstream NEDD8 conjugation cascade within a few hours after administration (46) (**Figure 1**). TAS4464 is

another NAE inhibitor recently developed with more potent inhibitory effects and prolonged duration of target-binding compared with MLN4924 (47, 48). NAE inhibitors MLN4924 and TAS4464 targeting the process of NEDD8 conjugation have shown particularly promising results in several clinical trials (phase I/II/III) for cancer treatment (46). NEDDylation inhibition appears to have a unique profile of sensitivity toward various types of malignancies. So far, the primary identified cytotoxic mechanisms of MLN4924 include induction of DNA rereplication, senescence, dysregulation of cell cycle checkpoints control, as well as inhibition of mTOR and NF-κB pathways (**Figure 2**) (46, 49–55). Substrates of CRLs, such as Wee1, checkpoint kinase 1 (CHK1), p21, and cell division cycle 25A (CDC25A), are key components of double-strand breaks (DSBs) repair proteins (56–60) (**Figure 2**). Mainly, the degradation of cell cycle proteins Cdt1, p21, and Set8 is mediated by $CRL4^{Cdt2}$, in which Cdt2 plays as a substrate recognition protein (61–63). Genotoxic insults trigger binding of Cdt2 on to the DNA sliding clamp—proliferating cell nuclear antigen (PCNA)—loading $CRL4^{Cdt2}$ on to DNA for the substrate degradation (61–63). Set8 stabilization leads to lysine 20 of histone H4 (H4K20) hypermethylation, triggering transcriptional downregulation of histone with the resultant chromatin decompaction and DNA damage activation, as depicted elegantly by Abbas et al. (61). Driven by the fact that the development of radioresistance is largely determined by factors such as DNA damage response DDR activation after ionizing radiation (IR), cell cycle checkpoints controls, and anti-apoptotic pathways dysregulation, it is essential to investigate the potential of using NEDDylation inhibitors as radiosensitizers (64).

## NEDDylation Inhibitors as Radiosensitizers—DNA Damage Response

One of the major cytotoxic effects of MLN4924 is achieved through the stabilization of its substrate Cdt1, a so-called "DNA replication licensing factor," which tightly regulates the cell cycle progression by facilitating the formation of the pre-replicative complexes (pre-RC) at the G1 phase of cell cycle (46, 65). To prevent relicensing, which will lead to multiple rounds of DNA replication initiation per cell cycle, Cdt1 is rapidly degraded by the CRL Skp1-cullin1-F-box protein (SCF) right after G1 phase (66) (**Figure 2**). MLN4924-mediated inhibition of SCF will lead to the accumulation of Cdt1, causing firing of several rounds of DNA replication initiations without cell division, as evidenced by the accumulation of cells with > 4N DNA in flow cytometry (46) (**Figure 2**). This process will lead to the collision of replication forks and the induction of overwhelming both single- and double-strand DNA damage (67).

The majority of IR-mediated cell killing is mediated by the massive induction of DNA DSBs (64). Radiosensitivity of tumor cells is largely decided by their ability to trigger the DDR, via activation of cell cycle checkpoints and DNA damage repair (64). MLN4924 functions as a radiosensitizer in several types of cancer by potentiating DNA damage and interfering with DDR activation. In the orthotopic xenograft mouse models of human pancreatic cancer and head and neck squamous cell carcinoma (HNSCC), MLN4924 overcame radioresistance via induction of DNA rereplication, leading to prominent induction of DSBs (68, 69). In pancreatic cancer cells, the maximal radiosensitizing effects of MLN4924 was achieved when MLN4924 was administered 24 h prior to receiving RT (69). MLN4924 pretreatment before RT administration will allow time for CRL substrates' accumulation. The radiosensitizing effect of MLN4924 was partially reversed in pancreatic cancer cells with Cdt1 knockdown (69). However, the exact involvement of Cdt1 stabilization in MLN4924-induced radiosensitization needs further investigation.

Expression levels of CRL components were significantly elevated in HNSCC cells compared with those in adjacent normal squamous mucosa of the oral cavity and nasopharynx (68). As a result, DNA rereplication was not observed in the cells of normal tissue (68). Besides HNSCC, hyperactivation of CRLs was also observed in GBM, breast cancer, and liver cancer (70). Therefore, the unique cytotoxic mechanism highlights the potential of NEDDylation inhibitors as radiosensitizers from the perspectives of "*spatial cooperation*," "*biological cooperation*," "*normal tissue protection*," and "*cytotoxic enhancement*" based on the revised Steel framework.

## MLN4924 as a Radiosensitizer—Cell Cycle Arrest

Due to the lethality of unrepaired DNA DSBs, developing new agents to prevent activation of cell cycle checkpoints in response to IR is critical to overcoming radioresistance (71). DDR is initiated by activation of ataxia-telangiectasia mutated (ATM) and ataxia-telangiectasia and RAD3-related (ATR), which will locate the DNA damage and activate various downstream proteins (72). ATM is the major regulator of DDR following IR-induced DSBs, leading to phosphorylation of downstream CHK1 and CHK2 (72). Activated CHKs will then phosphorylate the isoforms of CDC25 phosphatases, triggering their polyubiquitination and degradation (73). Meanwhile, the dephosphorylation and activation of CDK2-cyclinE and CDK1-cyclinB depend on the phosphatase activities of CDC25 (73). As a result, with activation of DDR and subsequent CDC25 degradation, cell cycle arrest will occur at the end of G1 phase or the end of G2 phase to allow time for DNA repair (73) (**Figure 2**). Among the three isoforms of CDC25s (CDC25A, B, C), CDC25A regulates both early (G1 phase to S phase) and late (G2 phase to M phase) cell cycle checkpoints (**Figure 2**) (73). Rapid degradation of CDC25A is critical for activating cell cycle arrest upon IR-induced DNA damages (72). The ubiquitination of CDC25A is carried out by the CRL E3 ligase $SCF^{beta-TrCP}$, in which the beta-TrCP (β-transducin repeat-containing protein) facilitates the recruitment of the CDC25A for Ub conjugation (74). MLN4924-mediated inhibition of $SCF^{beta-TrCP}$ will stabilize the CDC25A protein, causing cell cycle checkpoint dysregulation and potentially radiosensitization (**Figure 2**).

Accumulation of CRL substrates may also induce cell cycle arrest via checkpoint activation. The Wee1 kinase, which phosphorylates and keeps CDK1 in inactive form for activation of cell cycle checkpoints, is another major CRL substrate (**Figure 2**)

(75). Meanwhile, degradation of members of the universal cyclin-dependent kinase inhibitors (CDKIs) family p21 (Cip1) and p27 (Kip1) is also mediated by CRLs (76). As such, several studies reported the activation of cell cycle checkpoints with MLN4924 treatment (77–79). In cell lines of hormone-refractory prostate cancer (HRPC), MLN4924 triggered cell cycle arrest at the G2 phase due to Wee1, p21, and p27 accumulation (79). In the colorectal cancer cell lines of HT-29 and HCT-116, and breast cancer cell lines of SK-BR-3 and MCF7, MLN4924 induced stabilization of p27 and p21, respectively, leading to cell cycle G2/M arrest (77, 78). MLN4924 and RT cotreatment induced a more significant accumulation of Wee1, p21, and p27 than either treatment modality alone, leading to prominent cell cycle arrest and unanimous sensitization all these types of cancer cells toward RT (77–79).

## MLN4924 as a Radiosensitizer—Anti-apoptotic Pathways

Increased radioresistance of cancer cells is developed by the activation of several compensatory pro-survival cell signaling pathways, including phosphatidylinositol 3-kinase (PI3K)/AKT/mTOR pathway, EGFR/mitogen-activated protein kinase (MAPK) pathway and NF-κB signaling pathway (80, 81). The classical theories of how radiation activates these anti-apoptotic pathways state that ionizing events in the cytosol and the mitochondria will generate large quantities of reactive oxygen species (ROS) and reactive nitrogen species (RNS) that will inhibit protein phosphatase (PTPase) activities (81). Radiation can also promote membrane-associated receptor activation by lipid rafts aggregation, leading to activation of downstream pathways (82). Activation of the PI3K/AKT/mTOR, EGFR/MAPK, and NF-κB pathways can facilitate the development of radioresistance by promoting DNA damage repair, and transcriptional upregulation of a myriad of stress-responsive proteins (83, 84) (**Figure 2**). Therefore, it is critical to understand the impact of NEDDylation inhibition on these compensatory pro-survival pathways activated by RT.

Inhibition of NF-κB pathway is one of the major causes of MLN4924 induced cytotoxicity, as evidenced in the initial studies in acute myeloid leukemia (AML) (49). The inhibitor of nuclear factor kappa B (IκBα) binds to the NF-κB p65 and p50 complex and keeps the heterodimer in the cytosol as an inactive form (85). Activation of the pathway triggers rapid degradation of IκBα via the $SCF^{\beta-TrCP}$ E3 ligase, releasing the p65 and p50 heterodimer for nuclear translocation and transcriptional upregulation of its target genes (86). Treatment of MLN4924 will inhibit the $SCF^{\beta-TrCP}$ and prohibit RT-induced IκBα degradation, with resultant sequestration of p65 and p50 in the cytoplasm (49, 52, 87) (**Figure 2**). This mechanism is validated in studies showing that eradication of the RING-box protein Rbx2 in the $SCF^{\beta-TrCP}$ complex triggered IκBα stabilization and NF-κB pathway inhibition, leading to re-sensitization of cancer cells toward RT (88) (**Figure 2**). Furthermore, the existing studies also suggested that the radiosensitizing effect of bortezomib is largely due to the inhibition of the NF-κB pathway (89). As a result, another major radiosensitizing mechanism of MLN4924 is achieved through the NF-κB pathway inhibition (**Figure 2**).

Several mTOR inhibitors, including everolimus and temsirolimus, are under early Phase (I/II) clinical trials as a radiosensitizer to treat several cancer types such as prostate cancer, GBM, and lung cancer (90–92). In human cancer cell lines of acute lymphoblastic leukemia (ALL), AML, cervical, breast, colon, GBM, and kidney, the activity of mTOR is downregulated by MLN4924 in an almost dose-dependent manner, as evidenced with dephosphorylation of mTOR downstream targets such as p70S6 kinase (51, 93–95). Intrinsic mTOR's upstream inhibitors, including the DEP domain containing MTOR interacting protein (DEPTOR) and the regulated in development and DNA damage responses 1 (REDD1), are substrates for $SCF^{\beta TrCP}$ and cullin4A-RING (CRL4A), respectively. These protein-drug interactions largely explain the unanimous response of mTOR inhibition toward NEDDylation inhibition (50, 51, 55). The significant inhibitory effect of MLN4924 on the PI3K/AKT/mTOR axis has implicated the NEDDylation inhibitors as potential therapeutic radiosensitizers (**Figure 2**).

In summary, NEDDylation inhibition can block key pro-survival pathways activated with RT via stabilization of their intrinsic upstream inhibitory proteins. The unique role of MLN4924 in blocking these compensatory pathways demonstrated its potential application as a radiosensitizer via "*spatial cooperation*," "*biological cooperation*," and "*cytotoxic enhancement*" (4).

# PROTEOLYSIS TARGETING CHIMERAS (PROTACS)

Neither bortezomib nor MLN4924 addresses specific proteins as they broadly inhibit the general machinery necessary for protein degradation. MLN4924 is not selective since all the CRL complexes in the cells are inhibited, blocking the activities of over 400 enzymes (70). The PROteolysis TArgeting Chimeras (PROTACs) technology was developed in recent years to overcome these limitations of targeting the protein degradation machinery (96). PROTACs are heterobifunctional molecules with two different ligands connected via a linker (**Figure 3**). One end of the PROTAC, i.e., the "warhead," binds to the protein of interest (POI), and the other end binds to the receptor protein in the CRL complex, thereby promoting the physical interaction of the target protein with the E3 ligase for polyubiquitination (**Figure 3**) (97). Traditional targeted therapies using occupancy driven pharmacology only affect enzymatic function via competitive inhibition, which requires druggable active sites in those enzymes that are susceptible to mutations and protein overexpression (8). Whereas, polyubiquitinated POIs will be degraded by the proteasome with the eradication of both the enzymatic activities and the scaffold functions of target proteins (97). Furthermore, PROTACs-induced protein degradation is a catalytic process, as PROTACs will dissociate from the CRL complex after POI polyubiquitination and binds to a new target. This unique catalytic property of PROTACs

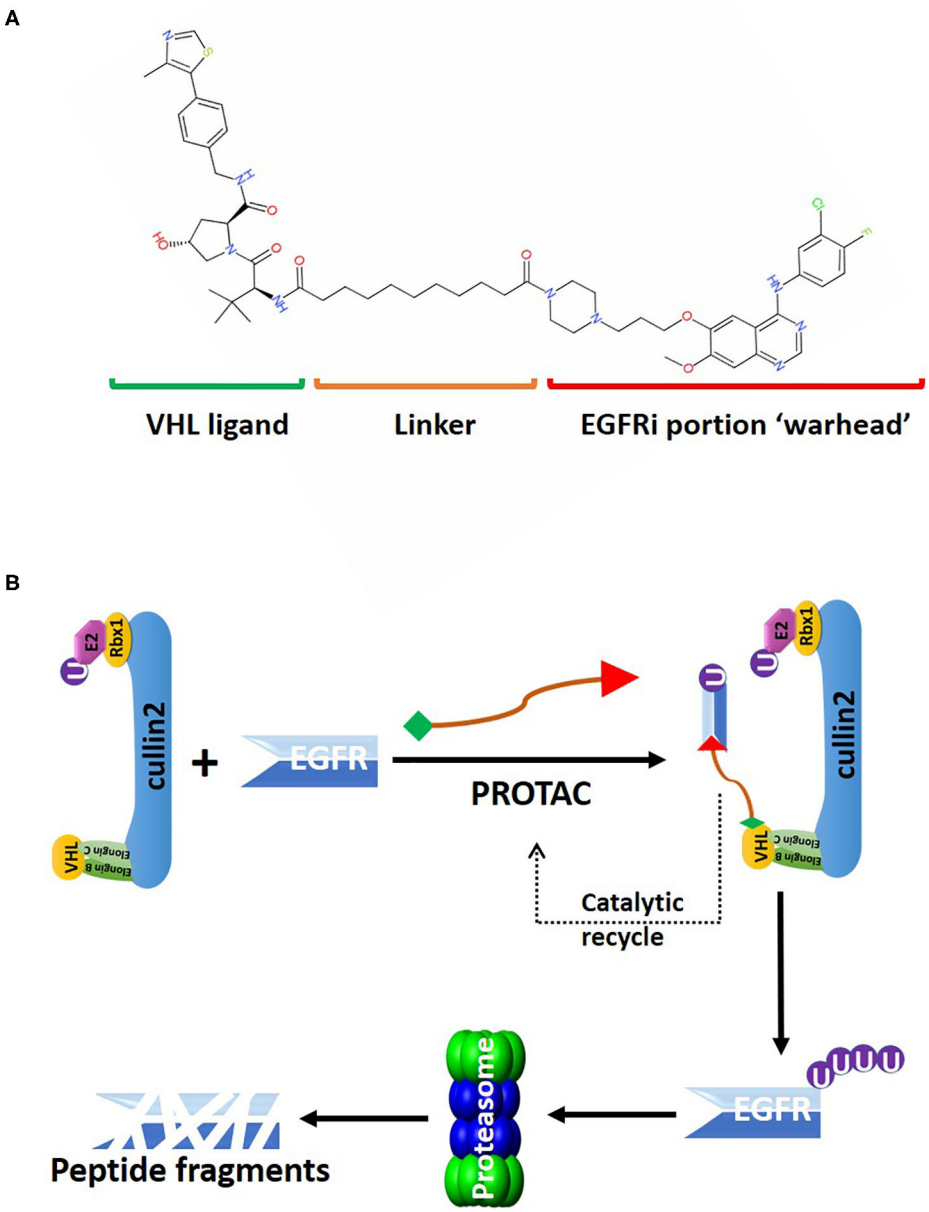


**FIGURE 3 |** An overview of the PROTAC targeting EGFR for $CRL2^{VHL}$-mediated polyubiquitination. **(A)** 2D structure of the PROTAC MS39 that targets EGFR. The "warhead" potion of the PROTAC is based on EGFR inhibitor (EGFRi) gefitinib. **(B)** MS39 can recruit EGFR for polyubiquitin conjugation by the $CRL2^{VHL}$. MS39 mediated EGFR degradation is a catalytic process, as evidenced with dissociation of the PROTAC from the $CRL2^{VHL}$ complex after EGFR polyubiquitination.

can lead to efficient POI clearance at a very low dose 5 (98) (**Figure 3**).

Due to these unique characteristics, targeting CRL substrates related to the development of radioresistance with PROTACs could provide a new strategy to sensitize cancer cells toward RT (70) (**Figure 4**). Since 2015, over 30 small-molecule PROTACs have been reported, most of them utilize substrate receptor proteins von Hippel-Lindau (VHL) in the CRL2 complex ($CRL2^{VHL}$), and cereblon (CRBN) in the cullin4-RING complex ($CRL4^{CRBN}$) as the PROTAC binding sites in the E3 ligase (99) (**Figure 4**). PROTACs against radioresistance-related key substrates of CRL2 and CRL4 have been developed. These substrates include the EGFR, androgen (AR) and estrogen (ER) receptors, CDKs, MAP kinase kinase 1 (MEK1) and MEK2, anaplastic lymphoma kinase (ALK), Bruton tyrosine kinase (BTK), bromodomain and extra-terminal motif (BET) proteins, and bromodomain (BRD) proteins (**Figure 4**) (100–107). Since all these PROTACs are first-in-class protein degraders developed within the past 5 years, a comprehensive understanding of the underlying molecular

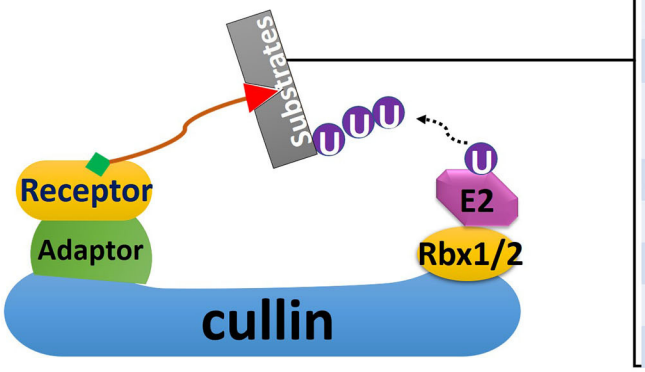


| Substrates | PROTAC | E3 Ligase |
|---|---|---|
| EGFR | MS39/PROTAC3 | $CRL2^{VHL}$ |
| EGFR | MS154 | $CRL4^{CRBN}$ |
| ER | ERD-308 | $CRL2^{VHL}$ |
| AR | ARD-69/ARD-266 | $CRL2^{VHL}$ |
| CDK4/CDK6 | BSJ-03-204 | $CRL4^{CRBN}$ |
| CDK8/9 | JH-XI-10-02/ THAL-SNS-032 | $CRL4^{CRBN}$ |
| ALK | TL13-112 | $CRL4^{CRBN}$ |
| MEK1/2 | MS432 | $CRL2^{VHL}$ |
| BTK | DD-03-171 | $CRL4^{CRBN}$ |
| pan-BET | ARV-771 | $CRL2^{VHL}$ |
| BRD4/9 | dBET6/dBRD9 | $CRL4^{CRBN}$ |

**FIGURE 4 |** A non-exhaustive list of PROTACs targeting proteins related with the development of radioresistance. Corresponding CRLs that mediate polyubiquitination of these proteins were also identified. EGFR, epidermal growth factor receptor; ER, estrogen receptor; AR, androgen receptor; CDK, cyclin-dependent kinase; ALK, anaplastic lymphoma kinase; MEK, mitogen-activated protein kinase kinase; BTK, Bruton tyrosine kinase; BET, bromodomain and Extra-Terminal motif; BRD, bromodomain.

mechanism of these novel compounds is essential for developing next-generation radiosensitizers.

## PROTACs as Radiosensitizers—Targeting Receptors

Targeting EGFR using traditional targeted therapies, such as monoclonal antibodies or tyrosine kinase inhibitors (TKIs), as radiosensitizers have gained moderate success in non-small-cell lung cancer (NSCLC), but failed in GBM and HNSCC to improve OS rates (108, 109). Genetic alterations, including amplification, rearrangement, altered splicing, and mutations, that regulate *EGFR* expression levels and protein activities in GBM and HNSCC, will eventually lead to the development of resistance toward EGFR inhibitors (108, 110). Lysosome-independent degradation of EGFR is mediated by $CRL2^{VHL}$, consistent with the report in clinical trial showing stabilization of EGFR with bortezomib-mediated proteasome inhibition (32, 111). Recently, several PROTACs were developed to target EGFR for $CRL2^{VHL}$-mediated degradation. PROTAC-based technology offers great flexibility in choosing the clinically relevant forms of EGFR proteins targeted for degradation by changing the "warhead" of the degrader (**Figure 3**). For example, the lapatinib-based PROTAC largely degraded the wildtype, and exon-20 insertion mutant forms of EGFR; the gefitinib-based PROTAC selectively degraded EGFR with exon-19 deletion, and L858R point mutation; afatinib-based PROTAC degraded double mutant (L858R/T790M) EGFR (112). All these PROTACs can efficiently eliminate EGFR at low-nanomolar concentrations, and exerted sustained inhibitory effects on cancer cell proliferation and downstream kinases signaling of EGFR (112).

RT-induced overexpression of hormonal receptors, including AR and ER, plays a vital role in mediating radioresistance in prostate and breast cancers, respectively (113, 114). In castration-resistant prostate cancer (CRPC) cells, the PROTAC ARD-61 can efficiently degrade AR and inhibited cancer cell proliferation with half-maximum inhibitory concentration (IC:50) values $<$ 500 nM, regardless of AR mutations, and expression status of AR splice variants, such as AR splice variant-7 (AR-V7) (102). Meanwhile, the viability of cells not expressing AR was not affected (102). Another AR degrader ARD-69 has DC50 values of $<$ 1 nM in prostate cancer cell lines LNCaP and VCaP (DC50: the concentration at which 50% of the target protein has been degraded) (115). The importance of these PROTACs as potential radiosensitizers for prostate cancer is emphasized by the study showing that targeted degradation of RT-increased AR with FDA-approved AR degradation enhancer, dimethylcurcumin (ASC-J9), significantly sensitized prostate cancer toward radiation in xenograft models, while conventional anti-androgen drugs, such as enzalutamide, has no radiosensitizing effects (114). Meanwhile, the ER degrader ERD-308 can induce over 95% of ER degradation at concentrations of $<$ 5 nM in ER+ breast cancer cell lines of MCF-7 and T47D (101). Given the synergistic effect of typical anti-estrogenic drugs with RT in the breast, and cervical cancers, these ER degraders can also be used as potential radiosensitizers alongside with RT (116). More importantly, these degraders can overcome the common resistant mechanism developed during anti-hormonal therapy.

## PROTACs as Radiosensitizers—Targeting Oncogenic Kinases

It is well-known that many patients will eventually become drug resistant and develop disease relapse with prolonged

treatment of protein kinase inhibitors (117). The mechanism of drug resistance is mainly attributed to the kinome rewiring effect, whereby reactivation of the oncogenic pathways restored via compensatory feedback activation of alternative kinases (117). Particularly, RT-induced activation of MEK1/2 is associated with radioresistance is found in several human malignancies (118, 119). Targeted inhibition of MEK1/2 using kinase inhibitors led to radiosensitization in several types of cancer, such as astrocytoma and pancreatic tumor (120, 121). Meanwhile, CDK inhibitors, especially those against CDK4 and CDK6, synergized with RT in killing GBM cells and prolonged survival in the orthotopic GBM model (122). However, resistance toward MEK1/2 and CDK inhibitors will inevitably occur with prolonged treatment (123).

Treatment with PROTACs will lead to catalytic degradation of specific kinases, offering sustained inhibition on their downstream targets (112). PROTACs for kinases critical for radioresistance, including CDKs, MEK1/2, ALK, and BTK, have been recently developed (103, 105–107). Given their unique pharmacological characteristics, these PROTACs carry great potential as radiosensitizers. For example, the PROTAC MS432 recruits MEK1/2 for $CRL2^{VHL}$-mediated polyubiquitination (105). It can suppress extracellular signal-regulated kinase (ERK) phosphorylation and efficiently inhibit colorectal cancer cell proliferation with DC50 values of 31 nM and 17 nM for MEK1 and MEK2 in HT-29 cells, respectively (105). Meanwhile, the CDK6 degrader was recently developed by linking the FDA-approved CDK6 inhibitor palbociclib with a thalidomide derivative for targeted CDK6 polyubiquitination by $CRL4^{CRBN}$ (124). Given that the combination treatment of RT with CDK inhibitors palbociclib and ribociclib are well-tolerated in malignancies such as breast cancer and glioma (NCT 02607124), CDKs-targeting PROTACs are great pharmaceutical candidates for radiosensitizers (125).

## CONCLUSION AND DISCUSSION

In summary, protein turnover is a dynamically regulated process influencing many important biological functions, including DDR, cell cycling, and signaling transductions. Pharmacological intervention of protein turnover offers a new therapeutic window for radiosensitization. Driven by their unique cytotoxic mechanisms, the novel strategies targeting the UPS with NEDDylation inhibitors and the PROTACs carry great potential as radiosensitizers to improve the efficacy of RT. The NEDDylation inhibitor MLN4924 exerts several cytotoxic functions, including DNA damage, cell cycle checkpoints dysregulation, and inhibition of NF-κB, and mTOR pathways (**Figure 2**). Preclinical studies had validated the efficacy of NEDDylation inhibitors as radiosensitizers. Meanwhile, recent progress in PROTAC technology has shown significant improvements in terms of the cellular permeability and substrate specificity. The PROTACs can selectively recruit key proteins related to radioresistance, such as EGFR, AR, ER, MEK1/2, and CDKs, for CRL-mediated polyubiquitin conjugation and subsequent degradation. Based on these strong basic and preclinical investigations hereby summarized, further clinical studies using NEDDylation inhibitors and PROTACs as radiosensitizers are warranted for the therapeutic gain of human malignancies.

## AUTHOR CONTRIBUTIONS

SZ wrote the original manuscript. WT edited and wrote the manuscript. All authors contributed to the article and approved the submitted version.

## FUNDING

This work was supported by SCCC American Cancer Society (IRG) Pilot Project Grants (PI:WT).

## REFERENCES

1. Barnett GC, West CM, Dunning AM, Elliott RM, Coles CE, Pharoah PD, et al. Normal tissue reactions to radiotherapy: towards tailoring treatment dose by genotype. *Nat Rev Cancer.* (2009) 9:134–42. doi: 10.1038/nrc2587
2. Jagodinsky JC, Harari PM, Morris ZS. The promise of combining radiation therapy with immunotherapy. *Int J Radiat Oncol Biol Phys.* (2020). doi: 10.1016/j.ijrobp.2020.04.023. [Epub ahead of print].
3. Qin A, Lusk E, Daignault-Newton S, Schneider BJ. Chemotherapy and radiation versus chemotherapy alone for elderly patients with N3 stage IIIB NSCLC. *Clin Lung Cancer.* (2019) 20:e495–503. doi: 10.1016/j.cllc.2019.04.003
4. Morris ZS, Harari PM. Interaction of radiation therapy with molecular targeted agents. *J Clin Oncol.* (2014) 32:2886–93. doi: 10.1200/JCO.2014.55.1366
5. Anker CJ, Grossmann KF, Atkins MB, Suneja G, Tarhini AA, Kirkwood JM. Avoiding severe toxicity from combined BRAF inhibitor and radiation treatment: consensus guidelines from the eastern cooperative oncology group (ECOG). *Int J Radiat Oncol Biol Phys.* (2016) 95:632–46. doi: 10.1016/j.ijrobp.2016.01.038
6. Clement-Zhao A, Tanguy ML, Cottu P, De La Lande B, Bontemps P, Lemanski C, et al. Toxicity of locoregional radiotherapy in combination with bevacizumab in patients with non-metastatic breast cancer (TOLERAB): final long-term evaluation. *PLoS ONE.* (2019) 14:e0221816. doi: 10.1371/journal.pone.0221816
7. Barazzuol L, Jeynes JC, Merchant MJ, Wera AC, Barry MA, Kirkby KJ, et al. Radiosensitization of glioblastoma cells using a histone deacetylase inhibitor (SAHA) comparing carbon ions with X-rays. *Int J Radiat Biol.* (2015) 91:90–8. doi: 10.3109/09553002.2014.946111
8. Ferguson FM, Gray NS. Kinase inhibitors: the road ahead. *Nat Rev Drug Discov.* (2018) 17:353–77. doi: 10.1038/nrd.2018.21
9. Zhao Y, Sun Y. Cullin-RING ligases as attractive anti-cancer targets. *Curr Pharm Des.* (2013) 19:3215–25. doi: 10.2174/1381612811319990300
10. Duan H, Wang Y, Aviram M, Swaroop M, Loo JA, Bian J, et al. SAG, a novel zinc RING finger protein that protects cells from apoptosis induced by redox agents. *Mol Cell Biol.* (1999) 19:3145–55. doi: 10.1128/MCB.19.4.3145
11. Zhou L, Zhang W, Sun Y, Jia L. Protein neddylation and its alterations in human cancers for targeted therapy. *Cell Signal.* (2018) 44:92–102. doi: 10.1016/j.cellsig.2018.01.009
12. Reynders M, Matsuura BS, Berouti M, Simoneschi D, Marzio A, Pagano M, et al. PHOTACs enable optical control of protein degradation. *Sci Adv.* (2020) 6:eaay5064. doi: 10.1126/sciadv.aay5064
13. Wardman P. Chemical radiosensitizers for use in radiotherapy. *Clin Oncol (R Coll Radiol).* (2007) 19:397–417. doi: 10.1016/j.clon.2007.03.010

14. Imai R, Kamada T, Araki N, Working Group for Bone and Soft Tissue Sarcomas. Carbon ion radiation therapy for unresectable sacral chordoma: an analysis of 188 cases. *Int J Radiat Oncol Biol Phys.* (2016) 95:322–7. doi: 10.1016/j.ijrobp.2016.02.012
15. Lin A, Maity A. Molecular pathways: a novel approach to targeting hypoxia and improving radiotherapy efficacy via reduction in oxygen demand. *Clin Cancer Res.* (2015) 21:1995–2000. doi: 10.1158/1078-0432.CCR-14-0858
16. Wang H, Mu X, He H, Zhang XD. Cancer radiosensitizers. *Trends Pharmacol Sci.* (2018) 39:24–48. doi: 10.1016/j.tips.2017.11.003
17. Buckley AM, Lynam-Lennon N, O'Neill H, O'Sullivan J. Targeting hallmarks of cancer to enhance radiosensitivity in gastrointestinal cancers. *Nat Rev Gastroenterol Hepatol.* (2020) 17:298–313. doi: 10.1038/s41575-019-0247-2
18. Wilson GD, Bentzen SM, Harari PM. Biologic basis for combining drugs with radiation. *Semin Radiat Oncol.* (2006) 16:2–9. doi: 10.1016/j.semradonc.2005.08.001
19. McGinn CJ, Lawrence TS. Recent advances in the use of radiosensitizing nucleosides. *Semin Radiat Oncol.* (2001) 11:270–80. doi: 10.1053/srao.2001.26002
20. Boeckman HJ, Trego KS, Turchi JJ. Cisplatin sensitizes cancer cells to ionizing radiation via inhibition of nonhomologous end joining. *Mol Cancer Res.* (2005) 3:277–85. doi: 10.1158/1541-7786.MCR-04-0032
21. Orth M, Unger K, Schoetz U, Belka C, Lauber K. Taxane-mediated radiosensitization derives from chromosomal missegregation on tripolar mitotic spindles orchestrated by AURKA and TPX2. *Oncogene.* (2018) 37:52–62. doi: 10.1038/onc.2017.304
22. Hei TK, Piao CQ, Geard CR, Hall EJ. Taxol and ionizing radiation: interaction and mechanisms. *Int J Radiat Oncol Biol Phys.* (1994) 29:267–71. doi: 10.1016/0360-3016(94)90273-9
23. Grimes DR, Partridge M. A mechanistic investigation of the oxygen fixation hypothesis and oxygen enhancement ratio. *Biomed Phys Eng Express.* (2015) 1:045209. doi: 10.1088/2057-1976/1/4/045209
24. Metwally MA, Frederiksen KD, Overgaard J. Compliance and toxicity of the hypoxic radiosensitizer nimorazole in the treatment of patients with head and neck squamous cell carcinoma (HNSCC). *Acta Oncol.* (2014) 53:654–61. doi: 10.3109/0284186X.2013.864050
25. Dische S, Bennett MH, Orchard R, Stratford MR, Wardman P. The uptake of the radiosensitizing compound Ro 03-8799 (Pimonidazole) in human tumors. *Int J Radiat Oncol Biol Phys.* (1989) 16:1089–92. doi: 10.1016/0360-3016(89)90923-1
26. Astolfi L, Ghiselli S, Guaran V, Chicca M, Simoni E, Olivetto E, et al. Correlation of adverse effects of cisplatin administration in patients affected by solid tumours: a retrospective evaluation. *Oncol Rep.* (2013) 29:1285–92. doi: 10.3892/or.2013.2279
27. Shah JJ, Jakubowiak AJ, O'Connor OA, Orlowski RZ, Harvey RD, Smith MR, et al. Phase I study of the novel investigational NEDD8-activating enzyme inhibitor pevonedistat (MLN4924) in patients with relapsed/refractory multiple myeloma or lymphoma. *Clin Cancer Res.* (2016) 22:34–43. doi: 10.1158/1078-0432.CCR-15-1237
28. Meyer-Schwesinger C. The ubiquitin-proteasome system in kidney physiology and disease. *Nat Rev Nephrol.* (2019) 15:393–411. doi: 10.1038/s41581-019-0148-1
29. Dimopoulos MA, Goldschmidt H, Niesvizky R, Joshua D, Chng WJ, Oriol A, et al. Carfilzomib or bortezomib in relapsed or refractory multiple myeloma (ENDEAVOR): an interim overall survival analysis of an open-label, randomised, phase 3 trial. *Lancet Oncol.* (2017) 18:1327–37. doi: 10.1016/S1470-2045(17)30578-8
30. Lao CD, Friedman J, Tsien CI, Normolle DP, Chapman C, Cao Y, et al. Concurrent whole brain radiotherapy and bortezomib for brain metastasis. *Radiat Oncol.* (2013) 8:204. doi: 10.1186/1748-717X-8-204
31. Kong XT, Nguyen NT, Choi YJ, Zhang G, Nguyen HN, Filka E, et al. Phase 2 study of bortezomib combined with temozolomide and regional radiation therapy for upfront treatment of patients with newly diagnosed glioblastoma multiforme: safety and efficacy assessment. *Int J Radiat Oncol Biol Phys.* (2018) 100:1195–203. doi: 10.1016/j.ijrobp.2018.01.001
32. Argiris A, Duffy AG, Kummar S, Simone NL, Arai Y, Kim SW, et al. Early tumor progression associated with enhanced EGFR signaling with bortezomib, cetuximab, and radiotherapy for head and neck cancer. *Clin Cancer Res.* (2011) 17:5755–64. doi: 10.1158/1078-0432.CCR-11-0861
33. Pugh TJ, Chen C, Rabinovitch R, Eckhardt SG, Rusthoven KE, Swing R, et al. Phase I trial of bortezomib and concurrent external beam radiation in patients with advanced solid malignancies. *Int J Radiat Oncol Biol Phys.* (2010) 78:521–6. doi: 10.1016/j.ijrobp.2009.07.1715
34. Yu Q, Jiang Y, Sun Y. Anticancer drug discovery by targeting cullin neddylation. *Acta Pharm Sin B.* (2020) 10:746–65. doi: 10.1016/j.apsb.2019.09.005
35. Jia L, Sun Y. SCF E3 ubiquitin ligases as anticancer targets. *Curr Cancer Drug Targets.* (2011) 11:347–56. doi: 10.2174/156800911794519734
36. Walden H, Podgorski MS, Huang DT, Miller DW, Howard RJ, Minor DL, et al. The structure of the APPBP1-UBA3-NEDD8-ATP complex reveals the basis for selective ubiquitin-like protein activation by an E1. *Mol Cell.* (2003) 12:1427–37. doi: 10.1016/S1097-2765(03)00452-0
37. Huang DT, Ayrault O, Hunt HW, Taherbhoy AM, Duda DM, Scott DC, et al. E2-RING expansion of the NEDD8 cascade confers specificity to cullin modification. *Mol Cell.* (2009) 33:483–95. doi: 10.1016/j.molcel.2009.01.011
38. Xirodimas DP, Saville MK, Bourdon JC, Hay RT, Lane DP. Mdm2-mediated NEDD8 conjugation of p53 inhibits its transcriptional activity. *Cell.* (2004) 118:83–97. doi: 10.1016/j.cell.2004.06.016
39. Kamura T, Conrad MN, Yan Q, Conaway RC, Conaway JW. The Rbx1 subunit of SCF and VHL E3 ubiquitin ligase activates Rub1 modification of cullins Cdc53 and Cul2. *Genes Dev.* (1999) 13:2928–33. doi: 10.1101/gad.13.22.2928
40. Duda DM, Borg LA, Scott DC, Hunt HW, Hammel M, Schulman BA. Structural insights into NEDD8 activation of cullin-RING ligases: conformational control of conjugation. *Cell.* (2008) 134:995–1006. doi: 10.1016/j.cell.2008.07.022
41. Saha A, Deshaies RJ. Multimodal activation of the ubiquitin ligase SCF by Nedd8 conjugation. *Mol Cell.* (2008) 32:21–31. doi: 10.1016/j.molcel.2008.08.021
42. Baek K, Krist DT, Prabu JR, Hill S, Klugel M, Neumaier LM, et al. NEDD8 nucleates a multivalent cullin-RING-UBE2D ubiquitin ligation assembly. *Nature.* (2020) 578:461–6. doi: 10.1038/s41586-020-2000-y
43. Sailo BL, Banik K, Girisa S, Bordoloi D, Fan L, Halim CE, et al. FBXW7 in cancer: what has been unraveled thus far? *Cancers.* (2019) 11:246. doi: 10.3390/cancers11020246
44. Petroski MD, Deshaies RJ. Mechanism of lysine 48-linked ubiquitin-chain synthesis by the cullin-RING ubiquitin-ligase complex SCF-Cdc34. *Cell.* (2005) 123:1107–20. doi: 10.1016/j.cell.2005.09.033
45. Petroski MD, Deshaies RJ. Function and regulation of cullin-RING ubiquitin ligases. *Nat Rev Mol Cell Biol.* (2005) 6:9–20. doi: 10.1038/nrm1547
46. Soucy TA, Smith PG, Milhollen MA, Berger AJ, Gavin JM, Adhikari S, et al. An inhibitor of NEDD8-activating enzyme as a new approach to treat cancer. *Nature.* (2009) 458:732–6. doi: 10.1038/nature07884
47. Muraoka H, Yoshimura C, Kawabata R, Tsuji S, Hashimoto A, Ochiiwa H, et al. Activity of TAS4464, a novel NEDD8 activating enzyme E1 inhibitor, against multiple myeloma via inactivation of nuclear factor kappaB pathways. *Cancer Sci.* (2019) 110:3802–10. doi: 10.1111/cas.14209
48. Yoshimura C, Muraoka H, Ochiiwa H, Tsuji S, Hashimoto A, Kazuno H, et al. TAS4464, A highly potent and selective inhibitor of NEDD8-activating enzyme, suppresses neddylation and shows antitumor activity in diverse cancer models. *Mol Cancer Ther.* (2019) 18:1205–16. doi: 10.1158/1535-7163.MCT-18-0644
49. Swords RT, Kelly KR, Smith PG, Garnsey JJ, Mahalingam D, Medina E, et al. Inhibition of NEDD8-activating enzyme: a novel approach for the treatment of acute myeloid leukemia. *Blood.* (2010) 115:3796–800. doi: 10.1182/blood-2009-11-254862
50. Gu Y, Kaufman JL, Bernal L, Torre C, Matulis SM, Harvey RD, et al. MLN4924, an NAE inhibitor, suppresses AKT and mTOR signaling via upregulation of REDD1 in human myeloma cells. *Blood.* (2014) 123:3269–76. doi: 10.1182/blood-2013-08-521914
51. Zhao Y, Xiong X, Jia L, Sun Y. Targeting cullin-RING ligases by MLN4924 induces autophagy via modulating the HIF1-REDD1-TSC1-mTORC1-DEPTOR axis. *Cell Death Dis.* (2012) 3:e386. doi: 10.1038/cddis.2012.125
52. Godbersen JC, Humphries LA, Danilova OV, Kebbekus PE, Brown JR, Eastman A, et al. The Nedd8-activating enzyme inhibitor MLN4924 thwarts microenvironment-driven NF-kappaB activation and induces apoptosis in

chronic lymphocytic leukemia B cells. *Clin Cancer Res.* (2014) 20:1576–89. doi: 10.1158/1078-0432.CCR-13-0987
53. Jia L, Li H, Sun Y. Induction of p21-dependent senescence by an NAE inhibitor, MLN4924, as a mechanism of growth suppression. *Neoplasia.* (2011) 13:561–9. doi: 10.1593/neo.11420
54. Lin JJ, Milhollen MA, Smith PG, Narayanan U, Dutta A. NEDD8-targeting drug MLN4924 elicits DNA rereplication by stabilizing Cdt1 in S phase, triggering checkpoint activation, apoptosis, and senescence in cancer cells. *Cancer Res.* (2010) 70:10310–20. doi: 10.1158/0008-5472.CAN-10-2062
55. Zhao Y, Xiong X, Sun Y. DEPTOR, an mTOR inhibitor, is a physiological substrate of SCF(betaTrCP) E3 ubiquitin ligase and regulates survival and autophagy. *Mol Cell.* (2011) 44:304–16. doi: 10.1016/j.molcel.2011.08.029
56. Jin J, Shirogane T, Xu L, Nalepa G, Qin J, Elledge SJ, et al. SCFbeta-TRCP links Chk1 signaling to degradation of the Cdc25A protein phosphatase. *Genes Dev.* (2003) 17:3062–74. doi: 10.1101/gad.1157503
57. Zhong W, Feng H, Santiago FE, Kipreos ET. CUL-4 ubiquitin ligase maintains genome stability by restraining DNA-replication licensing. *Nature.* (2003) 423:885–9. doi: 10.1038/nature01747
58. Lovejoy CA, Lock K, Yenamandra A, Cortez D. DDB1 maintains genome integrity through regulation of Cdt1. *Mol Cell Biol.* (2006) 26:7977–90. doi: 10.1128/MCB.00819-06
59. Bendjennat M, Boulaire J, Jascur T, Brickner H, Barbier V, Sarasin A, et al. UV irradiation triggers ubiquitin-dependent degradation of p21(WAF1) to promote DNA repair. *Cell.* (2003) 114:599–610. doi: 10.1016/j.cell.2003.08.001
60. Zhang YW, Brognard J, Coughlin C, You Z, Dolled-Filhart M, Aslanian A, et al. The F box protein Fbx6 regulates Chk1 stability and cellular sensitivity to replication stress. *Mol Cell.* (2009) 35:442–53. doi: 10.1016/j.molcel.2009.06.030
61. Abbas T, Shibata E, Park J, Jha S, Karnani N, Dutta A. CRL4(Cdt2) regulates cell proliferation and histone gene expression by targeting PR-Set7/Set8 for degradation. *Mol Cell.* (2010) 40:9–21. doi: 10.1016/j.molcel.2010.09.014
62. Jin J, Arias EE, Chen J, Harper JW, Walter JC. A family of diverse Cul4-Ddb1-interacting proteins includes Cdt2, which is required for S phase destruction of the replication factor Cdt1. *Mol Cell.* (2006) 23:709–21. doi: 10.1016/j.molcel.2006.08.010
63. Abbas T, Sivaprasad U, Terai K, Amador V, Pagano M, Dutta A. PCNA-dependent regulation of p21 ubiquitylation and degradation via the CRL4Cdt2 ubiquitin ligase complex. *Genes Dev.* (2008) 22:2496–506. doi: 10.1101/gad.1676108
64. Morgan MA, Lawrence TS. Molecular pathways: overcoming radiation resistance by targeting DNA damage response pathways. *Clin Cancer Res.* (2015) 21:2898–904. doi: 10.1158/1078-0432.CCR-13-3229
65. Nishitani H, Taraviras S, Lygerou Z, Nishimoto T. The human licensing factor for DNA replication Cdt1 accumulates in G1 and is destabilized after initiation of S-phase. *J Biol Chem.* (2001) 276:44905–11. doi: 10.1074/jbc.M105406200
66. Li X, Zhao Q, Liao R, Sun P, Wu X. The SCF(Skp2) ubiquitin ligase complex interacts with the human replication licensing factor Cdt1 and regulates Cdt1 degradation. *J Biol Chem.* (2003) 278:30854–8. doi: 10.1074/jbc.C300251200
67. Paiva C, Godbersen JC, Berger A, Brown JR, Danilov AV. Targeting neddylation induces DNA damage and checkpoint activation and sensitizes chronic lymphocytic leukemia B cells to alkylating agents. *Cell Death Dis.* (2015) 6:e1807. doi: 10.1038/cddis.2015.161
68. Vanderdys V, Allak A, Guessous F, Benamar M, Read PW, Jameson MJ, et al. The neddylation inhibitor pevonedistat (MLN4924) suppresses and radiosensitizes head and neck squamous carcinoma cells and tumors. *Mol Cancer Ther.* (2018) 17:368–80. doi: 10.1158/1535-7163.MCT-17-0083
69. Wei D, Li H, Yu J, Sebolt JT, Zhao L, Lawrence TS, et al. Radiosensitization of human pancreatic cancer cells by MLN4924, an investigational NEDD8-activating enzyme inhibitor. *Cancer Res.* (2012) 72:282–93. doi: 10.1158/0008-5472.CAN-11-2866
70. Fouad S, Wells OS, Hill MA, D'Angiolella V. Cullin ring ubiquitin ligases (CRLs) in cancer: responses to ionizing radiation (IR) treatment. *Front Physiol.* (2019) 10:1144. doi: 10.3389/fphys.2019.01144
71. Maier P, Hartmann L, Wenz F, Herskind C. Cellular pathways in response to ionizing radiation and their targetability for tumor radiosensitization. *Int J Mol Sci.* (2016) 17:102. doi: 10.3390/ijms17010102
72. Stracker TH, Roig I, Knobel PA, Marjanovic M. The ATM signaling network in development and disease. *Front Genet.* (2013) 4:37. doi: 10.3389/fgene.2013.00037
73. Donzelli M, Draetta GF. Regulating mammalian checkpoints through Cdc25 inactivation. *EMBO Rep.* (2003) 4:671–7. doi: 10.1038/sj.embor.embor887
74. Busino L, Donzelli M, Chiesa M, Guardavaccaro D, Ganoth D, Dorrello NV, et al. Degradation of Cdc25A by beta-TrCP during S phase and in response to DNA damage. *Nature.* (2003) 426:87–91. doi: 10.1038/nature02082
75. Jang SM, Redon CE, Aladjem MI. Chromatin-bound cullin-ring ligases: regulatory roles in DNA replication and potential targeting for cancer therapy. *Front Mol Biosci.* (2018) 5:19. doi: 10.3389/fmolb.2018.00019
76. Lu Z, Hunter T. Ubiquitylation and proteasomal degradation of the p21(Cip1), p27(Kip1) and p57(Kip2) CDK inhibitors. *Cell Cycle.* (2010) 9:2342–52. doi: 10.4161/cc.9.12.11988
77. Wan J, Zhu J, Li G, Zhang Z. Radiosensitization of human colorectal cancer cells by MLN4924: an inhibitor of NEDD8-activating enzyme. *Technol Cancer Res Treat.* (2016) 15:527–34. doi: 10.1177/1533034615588197
78. Yang D, Tan M, Wang G, Sun Y. The p21-dependent radiosensitization of human breast cancer cells by MLN4924, an investigational inhibitor of NEDD8 activating enzyme. *PLoS ONE.* (2012) 7:e34079. doi: 10.1371/journal.pone.0034079
79. Wang X, Zhang W, Yan Z, Liang Y, Li L, Yu X, et al. Radiosensitization by the investigational NEDD8-activating enzyme inhibitor MLN4924 (pevonedistat) in hormone-resistant prostate cancer cells. *Oncotarget.* (2016) 7:38380–91. doi: 10.18632/oncotarget.9526
80. Hein AL, Ouellette MM, Yan Y. Radiation-induced signaling pathways that promote cancer cell survival (review). *Int J Oncol.* (2014) 45:1813–9. doi: 10.3892/ijo.2014.2614
81. Valerie K, Yacoub A, Hagan MP, Curiel DT, Fisher PB, Grant S, et al. Radiation-induced cell signaling: inside-out and outside-in. *Mol Cancer Ther.* (2007) 6:789–801. doi: 10.1158/1535-7163.MCT-06-0596
82. Zeng J, Zhang H, Tan Y, Sun C, Liang Y, Yu J, et al. Aggregation of lipid rafts activates c-met and c-Src in non-small cell lung cancer cells. *BMC Cancer.* (2018) 18:611. doi: 10.1186/s12885-018-4501-8
83. Karimian A, Mir SM, Parsian H, Refieyan S, Mirza-Aghazadeh-Attari M, Yousefi B, et al. Crosstalk between phosphoinositide 3-kinase/Akt signaling pathway with DNA damage response and oxidative stress in cancer. *J Cell Biochem.* (2019) 120:10248–72. doi: 10.1002/jcb.28309
84. Bai M, Ma X, Li X, Wang X, Mei Q, Li X, et al. The accomplices of NF-κB lead to radioresistance. *Curr Protein Pept Sci.* (2015) 16:279–94. doi: 10.2174/1389203716041504291523328
85. Giridharan S, Srinivasan M. Mechanisms of NF-kappaB p65 and strategies for therapeutic manipulation. *J Inflamm Res.* (2018) 11:407–19. doi: 10.2147/JIR.S140188
86. Yaron A, Hatzubai A, Davis M, Lavon I, Amit S, Manning AM, et al. Identification of the receptor component of the IkappaBalpha-ubiquitin ligase. *Nature.* (1998) 396:590–4. doi: 10.1038/25159
87. Russell JS, Raju U, Gumin GJ, Lang FF, Wilson DR, Huet T, et al. Inhibition of radiation-induced nuclear factor-kappaB activation by an anti-Ras single-chain antibody fragment: lack of involvement in radiosensitization. *Cancer Res.* (2002) 62:2318–26.
88. Tan M, Zhu Y, Kovacev J, Zhao Y, Pan ZQ, Spitz DR, et al. Disruption of Sag/Rbx2/Roc2 induces radiosensitization by increasing ROS levels and blocking NF-kappaB activation in mouse embryonic stem cells. *Free Radic Biol Med.* (2010) 49:976–83. doi: 10.1016/j.freeradbiomed.2010.05.030
89. Pordanjani SM, Hosseinimehr SJ. The role of NF-kB inhibitors in cell response to radiation. *Curr Med Chem.* (2016) 23:3951–63. doi: 10.2174/0929867323666160824162718
90. Narayan V, Vapiwala N, Mick R, Subramanian P, Christodouleas JP, Bekelman JE, et al. Phase 1 trial of everolimus and radiation therapy for salvage treatment of biochemical recurrence in prostate cancer patients following prostatectomy. *Int J Radiat Oncol Biol Phys.* (2017) 97:355–61. doi: 10.1016/j.ijrobp.2016.10.013
91. Chinnaiyan P, Won M, Wen PY, Rojiani AM, Werner-Wasik M, Shih HA, et al. A randomized phase II study of everolimus in combination with chemoradiation in newly diagnosed glioblastoma: results of NRG oncology RTOG 0913. *Neuro Oncol.* (2018) 20:666–73. doi: 10.1093/neuonc/nox209

92. Waqar SN, Robinson C, Bradley J, Goodgame B, Rooney M, Williams K, et al. A phase I study of temsirolimus and thoracic radiation in non–small-cell lung cancer. *Clin Lung Cancer.* (2014) 15:119–23. doi: 10.1016/j.cllc.2013.11.007
93. Guo N, Azadniv M, Coppage M, Nemer M, Mendler J, Becker M, et al. Effects of neddylation and mTOR inhibition in acute myelogenous leukemia. *Transl Oncol.* (2019) 12:602–13. doi: 10.1016/j.tranon.2019.01.001
94. Zheng S, Leclerc GM, Li B, Swords RT, Barredo JC. Inhibition of the NEDD8 conjugation pathway induces calcium-dependent compensatory activation of the pro-survival MEK/ERK pathway in acute lymphoblastic leukemia. *Oncotarget.* (2018) 9:5529–44. doi: 10.18632/oncotarget.23797
95. Leclerc GM, Zheng S, Leclerc GJ, DeSalvo J, Swords RT, Barredo JC. The NEDD8-activating enzyme inhibitor pevonedistat activates the eIF2α and mTOR pathways inducing UPR-mediated cell death in acute lymphoblastic leukemia. *Leuk Res.* (2016) 50:1–10. doi: 10.1016/j.leukres.2016.09.007
96. Sun X, Gao H, Yang Y, He M, Wu Y, Song Y, et al. PROTACs: great opportunities for academia and industry. *Signal Transduct Target Ther.* (2019) 4:64. doi: 10.1038/s41392-019-0101-6
97. Liu J, Chen H, Ma L, He Z, Wang D, Liu Y, et al. Light-induced control of protein destruction by opto-PROTAC. *Sci Adv.* (2020) 6:eaay5154. doi: 10.1126/sciadv.aay5154
98. Paiva SL, Crews CM. Targeted protein degradation: elements of PROTAC design. *Curr Opin Chem Biol.* (2019) 50:111–9. doi: 10.1016/j.cbpa.2019.02.022
99. Cully M. PROTAC moves in on lymphoma. *Nat Rev Drug Discov.* (2019) 18:584. doi: 10.1038/d41573-019-00113-9
100. Cheng M, Yu X, Lu K, Xie L, Wang L, Meng F, et al. Discovery of potent and selective epidermal growth factor receptor (EGFR) bifunctional small-molecule degraders. *J Med Chem.* (2020) 63:1216–32. doi: 10.1021/acs.jmedchem.9b01566
101. Hu J, Hu B, Wang M, Xu F, Miao B, Yang CY, et al. Discovery of ERD-308 as a highly potent proteolysis targeting chimera (PROTAC) degrader of estrogen receptor (ER). *J Med Chem.* (2019) 62:1420–42. doi: 10.1021/acs.jmedchem.8b01572
102. Kregel S, Wang C, Han X, Xiao L, Fernandez-Salas E, Bawa P, et al. Androgen receptor degraders overcome common resistance mechanisms developed during prostate cancer treatment. *Neoplasia.* (2020) 22:111–9. doi: 10.1016/j.neo.2019.12.003
103. Brand M, Jiang B, Bauer S, Donovan KA, Liang Y, Wang ES, et al. Homolog-selective degradation as a strategy to probe the function of CDK6 in AML. *Cell Chem Biol.* (2019) 26:300–6.e9. doi: 10.1016/j.chembiol.2018.11.006
104. Gechijian LN, Buckley DL, Lawlor MA, Reyes JM, Paulk J, Ott CJ, et al. Functional TRIM24 degrader via conjugation of ineffectual bromodomain and VHL ligands. *Nat Chem Biol.* (2018) 14:405–12. doi: 10.1038/s41589-018-0010-y
105. Wei J, Hu J, Wang L, Xie L, Jin MS, Chen X, et al. Discovery of a first-in-class mitogen-activated protein kinase kinase 1/2 degrader. *J Med Chem.* (2019) 62:10897–911. doi: 10.1021/acs.jmedchem.9b01528
106. Dobrovolsky D, Wang ES, Morrow S, Leahy C, Faust T, Nowak RP, et al. Bruton tyrosine kinase degradation as a therapeutic strategy for cancer. *Blood.* (2019) 133:952–61. doi: 10.1182/blood-2018-07-862953
107. Powell CE, Gao Y, Tan L, Donovan KA, Nowak RP, Loehr A, et al. Chemically induced degradation of anaplastic lymphoma kinase (ALK). *J Med Chem.* (2018) 61:4249–55. doi: 10.1021/acs.jmedchem.7b01655
108. Byeon HK, Ku M, Yang J. Beyond EGFR inhibition: multilateral combat strategies to stop the progression of head and neck cancer. *Exp Mol Med.* (2019) 51:1–14. doi: 10.1038/s12276-018-0202-2
109. Su Y, Cui J, Xu D, Wang M, Xu T, Tian H, et al. p16(INK4a) status and survival benefit of EGFR inhibitors in head and neck squamous cell cancer: a systematic review and meta-analysis. *Crit Rev Oncol Hematol.* (2018) 124:11–20. doi: 10.1016/j.critrevonc.2018.02.006
110. Eskilsson E, Rosland GV, Solecki G, Wang Q, Harter PN, Graziani G, et al. EGFR heterogeneity and implications for therapeutic intervention in glioblastoma. *Neuro Oncol.* (2018) 20:743–52. doi: 10.1093/neuonc/nox191
111. Cai W, Yang H. The structure and regulation of cullin 2 based E3 ubiquitin ligases and their biological functions. *Cell Div.* (2016) 11:7. doi: 10.1186/s13008-016-0020-7
112. Burslem GM, Smith BE, Lai AC, Jaime-Figueroa S, McQuaid DC, Bondeson DP, et al. The advantages of targeted protein degradation over inhibition: an RTK case study. *Cell Chem Biol.* (2018) 25:67–77.e3. doi: 10.1016/j.chembiol.2017.09.009
113. Rong C, Meinert E, Hess J. Estrogen receptor signaling in radiotherapy: from molecular mechanisms to clinical studies. *Int J Mol Sci.* (2018) 19:713. doi: 10.3390/ijms19030713
114. Chou FJ, Chen Y, Chen D, Niu Y, Li G, Keng P, et al. Preclinical study using androgen receptor (AR) degradation enhancer to increase radiotherapy efficacy via targeting radiation-increased AR to better suppress prostate cancer progression. *EBioMedicine.* (2019) 40:504–16. doi: 10.1016/j.ebiom.2018.12.050
115. Han X, Wang C, Qin C, Xiang W, Fernandez-Salas E, Yang CY, et al. Discovery of ARD-69 as a highly potent proteolysis targeting chimera (PROTAC) degrader of androgen receptor (AR) for the treatment of prostate cancer. *J Med Chem.* (2019) 62:941–64. doi: 10.1021/acs.jmedchem.8b01631
116. Segovia-Mendoza M, Jurado R, Mir R, Medina LA, Prado-Garcia H, Garcia-Lopez P. Antihormonal agents as a strategy to improve the effect of chemo-radiation in cervical cancer: *in vitro* and *in vivo* study. *BMC Cancer.* (2015) 15:21. doi: 10.1186/s12885-015-1016-4
117. Wilson LJ, Linley A, Hammond DE, Hood FE, Coulson JM, MacEwan DJ, et al. New perspectives, opportunities, and challenges in exploring the human protein kinome. *Cancer Res.* (2018) 78:15–29. doi: 10.1158/0008-5472.CAN-17-2291
118. Barker FG II, Simmons ML, Chang SM, Prados MD, Larson DA, Sneed PK, et al. EGFR overexpression and radiation response in glioblastoma multiforme. *Int J Radiat Oncol Biol Phys.* (2001) 51:410–8. doi: 10.1016/S0360-3016(01)01609-1
119. Kim DW, Choy H. Potential role for epidermal growth factor receptor inhibitors in combined-modality therapy for non-small-cell lung cancer. *Int J Radiat Oncol Biol Phys.* (2004) 59(Suppl. 2):11–20. doi: 10.1016/j.ijrobp.2003.11.042
120. Studebaker A, Bondra K, Seum S, Shen C, Phelps DA, Chronowski C, et al. Inhibition of MEK confers hypersensitivity to X-radiation in the context of BRAF mutation in a model of childhood astrocytoma. *Pediatr Blood Cancer.* (2015) 62:1768–74. doi: 10.1002/pbc.25579
121. Estrada-Bernal A, Chatterjee M, Haque SJ, Yang L, Morgan MA, Kotian S, et al. MEK inhibitor GSK1120212-mediated radiosensitization of pancreatic cancer cells involves inhibition of DNA double-strand break repair pathways. *Cell Cycle.* (2015) 14:3713–24. doi: 10.1080/15384101.2015.1104437
122. Whittaker S, Madani D, Joshi S, Chung SA, Johns T, Day B, et al. Combination of palbociclib and radiotherapy for glioblastoma. *Cell Death Discov.* (2017) 3:17033. doi: 10.1038/cddiscovery.2017.33
123. Poulikakos PI, Solit DB. Resistance to MEK inhibitors: should we co-target upstream? *Sci Signal.* (2011) 4:pe16. doi: 10.1126/scisignal.2001948
124. Su S, Yang Z, Gao H, Yang H, Zhu S, An Z, et al. Potent and preferential degradation of CDK6 via proteolysis targeting chimera degraders. *J Med Chem.* (2019) 62:7575–82. doi: 10.1021/acs.jmedchem.9b00871
125. Ippolito E, Greco C, Silipigni S, Dell'Aquila E, Petrianni GM, Tonini G, et al. Concurrent radiotherapy with palbociclib or ribociclib for metastatic breast cancer patients: Preliminary assessment of toxicity. *Breast.* (2019) 46:70–4. doi: 10.1016/j.breast.2019.05.001


**Conflict of Interest:** The authors declare that the research was conducted in the absence of any commercial or financial relationships that could be construed as a potential conflict of interest.

frontiers in Oncology

ORIGINAL RESEARCH
published: 28 August 2020
doi: 10.3389/fonc.2020.01540

# Hypofractionated Radiotherapy in Combination With Chemotherapy Improves Outcome of Patients With Esophageal Carcinoma Tracheoesophageal Groove Lymph Node Metastasis

*Jian Wang[1], Jingping Yu[2], Youqin Jiang[3], Dong Pei[3], Haiwen Zhu[3]* and Jianlin Wang[2]**

*[1] Department of Radiotherapy, Jiangyin People's Hospital, Jiangyin, China, [2] Department of Radiotherapy, The Affiliated Changzhou No. 2 People's Hospital, Nanjing Medical University, Changzhou, China, [3] Department of Radiotherapy, Yancheng No. 3 People's Hospital, Yancheng, China*

OPEN ACCESS

**Edited by:**
*Zhe-Sheng Chen,*
*St. John's University, United States*

**Reviewed by:**
*Ji-Ye Yin,*
*Central South University, China*
*Ru Li,*
*Stony Brook University, United States*

***Correspondence:**
*Haiwen Zhu*
*zhuhaiwen163zxm@126.com*
*Jianlin Wang*
*691883422@qq.com*

**Specialty section:**
*This article was submitted to Pharmacology of Anti-Cancer Drugs, a section of the journal Frontiers in Oncology*

**Received:** *23 May 2020*
**Accepted:** *20 July 2020*
**Published:** *28 August 2020*

**Citation:**
*Wang J, Yu J, Jiang Y, Pei D, Zhu H and Wang J (2020) Hypofractionated Radiotherapy in Combination With Chemotherapy Improves Outcome of Patients With Esophageal Carcinoma Tracheoesophageal Groove Lymph Node Metastasis. Front. Oncol. 10:1540. doi: 10.3389/fonc.2020.01540*

This study investigated the efficiency and safety of hypofractionated radiotherapy (HFR) combined with paclitaxel chemotherapy for the treatment of postsurgery tracheoesophageal groove lymph node (TGLN) metastasis in patients with esophageal cancer (EC). Fifty-three EC patients with TGLN metastasis after surgery admitted to the Yancheng Third People's Hospital from January 2013 to June 2015 were included in this study. They were randomly divided into the HFR group ($n$ = 25) and conventional fractioned radiotherapy (CFR) group ($n$ = 28) based on the random grouping method. Patients in the HFR group received treatment with radiation of 60 Gy (5 fractions per week, total 20 fractions) combined with paclitaxel chemotherapy at a dose of 50 mg once per week for 4 weeks. Patients in the CFR group received radiation of 60 Gy (5 fractions per week, total 30 fractions) combined with paclitaxel chemotherapy at a dose of 50 mg once per week for 6 weeks. The adverse events and treatment outcomes in these two groups were analyzed. It was found that there was no significant difference in the incidence of radiation esophagitis in the HFR group compared with that of the CFR group (grades 3–4, 44.0 vs. 25.0%; $P$ = 0.149). There was no statistical difference in the incidence of radiation pneumonitis between these two groups (grades 3–4, 16.0 vs. 7.1%; $P$ = 0.314). No statistical difference was noticed in complete response (CR), partial response (PR), and no response (NR) between these two groups. The median overall survival (OS) in the HRF group was significantly longer compared with that of the CRF group (24.2 months (95% CI, 16.2–32.1 months) vs. 11.8 months (95% CI, 9.2–14.4 months); $P$ = 0.024). Our results indicated that the combination of HFR and chemotherapy improved the prognosis of EC patients with TGLN metastasis with no increased adverse events.

**Keywords: esophageal cancer, tracheoesophageal groove lymph node metastasis, hypofractionated radiotherapy, conventional fractioned radiotherapy, chemotherapy, prognosis**

## INTRODUCTION

Esophageal cancer (EC), the common malignancy in China, is one of the leading causes of cancer-related death (1). Currently, surgery is preferred for the treatment of EC; however, a larger number of patients may present tracheoesophageal groove lymph node (TGLN) metastasis after surgery, with an incidence of 12–80% (2–5). Most of these patients are featured by hoarseness, bucking, and dyspnea, which hamper their quality of life. Furthermore, TGLN is also a negative prognostic factor for patients with EC. Radiotherapy is a major treatment option for TGLN metastasis in EC patients (6). Recently, the application of intensity-modulated radiation therapy (IMRT) contributes to target conformance and dose homogeneity, which reduces the dose of radiation to normal tissues and increases the local control and survival rate (7).

In a previous study, the efficiency and prognosis of EC patients who underwent chemoradiotherapy (CRT) were superior to that of the radiation monotherapy, and the related adverse events were tolerable (8). In clinical practice, conventional fractionated radiotherapy (CFR) has been commonly used for the treatment of EC. In recent years, it has been reported that hypofractionated radiotherapy (HFR) is feasible for treating moderate and advanced EC as it contributes to the overall survival (OS) (9, 10).

In this study, we investigate whether HFR could be used to improve the treatment efficacy in EC patients with TGLN metastasis after surgery. EC patients with TGLN metastasis were divided into two groups and treated with HFR or CFR, combined with paclitaxel chemotherapy. The treatment efficiency, toxicity, and prognosis of patients who underwent these two different treatment options were analyzed.

## MATERIALS AND METHODS

### Patients

Postoperative EC patients with TGLN metastasis admitted to the Yancheng Third People's Hospital from January 2013 to June 2015 were included in this study. The inclusion criteria were as follows: (1) patients aged less than 75 years, with clinical symptoms of hoarseness and bucking, after excluding vocal cord lesions; (2) patients who were diagnosed with TGLN metastasis using CT, MRI, and/or PET-CT; (3) patients with no severe cardiovascular diseases (CVDs), renal or splenic dysfunction; and (4) patients with an expected survival duration of at least 3 months. The exclusion criteria were as follows: (1) women with pregnancy or lactation; (2) patients complicated with concurrent malignancies; (3) patients with metastasis in the other organs and/or lymph nodes; (4) patients with CRT contraindications; and (5) patients with inadequate follow-up data. The following variables were gathered for analysis: age, gender, previous history, clinical symptoms, laboratory test results, and imaging findings. All participants provided informed consent. The study protocol was approved by the Ethical Committee of Yancheng Third People's Hospital. This clinical trial was registered in the Chinese Trial Registry (ID: CTR1800016848).

### Grouping of Patients

As the radiation frequency in both groups was different in this study, we could not arrange the blinded study. Instead, an open-label study was conducted. The patients were randomly divided into two groups: the HFR group and the CFR group. Patients in the HFR group received radiation of 60 Gy/20 fractions (3 Gy/fraction, 5 fraction/week) combined with chemotherapy using paclitaxel with a dose of 50 mg once per week for 4 weeks. Patients in the CFR group received radiation of 60 Gy/30 fractions (2 Gy/fraction, 5 fraction/week) combined with chemotherapy using paclitaxel with a dose of 50 mg once per week for 6 weeks.

For the radiotherapy, all the patients were fixed with a thermoplastic head mask, followed by cervical and thoracic scanning with a slice thickness of 2.5 mm. The CT images were delivered to the Eclipse system. The gross tumor volume (GTV) was defined as TGLN shown on CT, MRI, and/or PET-CT scans. Planning target volume (PTV) was termed by adding a 1-cm margin around the GTV. The maximal doses for the spinal cord in the CRT and HRT groups were less than 45 and 40 Gy, respectively. The average dose for lung in the CRT and HRT groups were less than 13 and 10 Gy, respectively. The volume of the whole lung receiving $\geq$20 Gy ($V_{20}$) in the CRT and HRT groups was less than 25 and 20%, respectively. The treatment was carried out in a linear accelerator (Varian Unigue) using a photon beam of 6 MV. For the chemotherapy, paclitaxel was given via intravenous drip (50 mg) before radiotherapy for 4 weeks in the HFR group and 6 weeks in the CFR group.

### Patients Follow-Up

The evaluation for the acute radiation-induced esophageal and/or pulmonary injury was based on the standards proposed by the Radiation Therapy Oncology Group (RTOG) in 1997 (11). The lymph node metastasis was evaluated using the Response Evaluation Criteria in Solid Tumors (RECIST, version 1.1). After treatment, the patients were followed up every 3 months within the first 2 years and 6 months once after 2 years. The follow-up data included case history, physical examination, laboratory test results, electrocardiogram, cervical CT, and thoracic CT. The primary endpoint was OS. All the patients were followed up until November 30, 2017.

### Statistical Analysis

The SPSS 19.0 software was used for the statistical analysis. Measurement data were presented as mean $\pm$ standard deviation and were compared using the Student's *t* test. The numeration data were compared using the *Chi* square test. Non-parametric statistics was used for the analysis of ranked data. *Kaplan-Meier* method was used to calculate the OS and PFS. *Log rank* test was used for the analysis of prognosis, and *Cox* regression analysis was used for the multivariate analysis. $P < 0.05$ was considered to be statistically significant.

# RESULTS

## Patients' Characteristics and Adverse Events of Radiotherapy

Fifty-three patients were included in the study. Among them, 25 patients were in the HFR group and 28 in the CFR group. There was no statistical difference in the demographic characteristics of patients, such as sex, age, site of lymph nodes, diameter of lymph node, and clinical TNM stage between the two groups ($P > 0.05$; **Table 1**).

The adverse events of radiotherapy for patients with EC were mainly manifested by radiation esophagitis and pneumonitis. HFR caused no alternation to the incidence of radiation esophagitis and pneumonitis compared with CFR. The incidence of grades 1–2 or 3–4 radiation esophagitis in the HFR group showed no statistical difference compared with that of the CFR group (44.0 vs. 25.0%; $P = 0.149$). Similarly, no statistical difference was noticed in the incidence of grades 0–2 or 3–4 radiation pneumonitis between these two groups ($P = 0.314$; **Table 2**).

## HFR Showed Similar Short-Term Efficiency Compared With CFR

Two months after radiotherapy, the complete response (CR) and partial response (PR) rate of HFR was 36 and 44%, while that of CFR was 21.4 and 53.6%, respectively. There was no statistical difference in the treatment efficiency between these two groups ($P = 0.314$; **Table 3**). The treatment efficiency in patients with lymphatic lesion with a diameter of ≤2 cm was significantly higher than those with lymphatic lesion with a diameter of >2 cm ($P < 0.001$; **Table 4**).

## HFR Treatment Prolonged OS and Reduced Mortality

The 1- and 2-year survival rate of patients was 56.6 and 35.6%, respectively (median OS, 14.7 months; 95% CI, 9.6–19.8 months). The median OS was significantly higher in the HFR group compared with that in the CFR group (24.2 months (95% CI, 16.2–32.1 months) vs. 11.8 months (95% CI, 9.2–14.4 months); $P = 0.024$; **Figure 1**). For the patients with lymphatic metastatic lesion ≤2 cm, the median OS was 24.1 months (95% CI, 12.0–36.1 months), which was significantly higher than those with a lymphatic metastatic lesion >2 cm, who had a median OS of 7.3 months (95% CI, 6.2–8.2 months; $P = 0.001$; **Figure 2**). Patients with a lymphatic metastatic lesion ≤2 cm in the HFR group showed a longer OS compared with those of the CFR group (31 vs. 7.3 months; $P = 0.039$; **Figure 3**). Meanwhile, patients with a lymphatic metastatic lesion >2 cm in the HFR group showed a longer OS compared with those of the CFR group (12.1 vs. 6.9 months; $P = 0.027$; **Figure 4**). Univariate analysis indicated that TGLN diameter ($P < 0.001$) and fractioned types ($P = 0.028$) were risk factors for the prognosis. After adjusting with the age, gender, TGLN, and fractioned types, multivariate analysis indicated that TGLN with a diameter ≤2 cm (HR = 0.108; 95% CI, 0.047–0.249) and HFR (HR = 0.236;

**TABLE 1 |** Patients' characteristics.

| Variables | *N* | Test group (*n* = 25) | Control (*n* = 28) | $\chi^2$ value | *P* value |
|---|---|---|---|---|---|
| Sex | | | | 0.007 | 1.000 |
| Male | 40 | 19 | 21 | | |
| Female | 13 | 6 | 7 | | |
| Age (years) | | | | 1.002 | 0.365 |
| 37–59 | 39 | 20 | 19 | | |
| 60–75 | 14 | 5 | 9 | | |
| Site of lymph nodes | | | | – | 0.856 |
| Left | 28 | 12 | 16 | | |
| Right | 19 | 10 | 9 | | |
| Both | 6 | 3 | 3 | | |
| Diameter of lymph nodes (cm) | | | | 0.335 | 0.769 |
| ≤2 | 17 | 9 | 8 | | |
| >2 | 36 | 16 | 20 | | |
| T stage | | | | – | 0.784 |
| T1–2 | 16 | 7 | 9 | | |
| T3 | 31 | 16 | 15 | | |
| T4 | 6 | 2 | 4 | | |
| N stage | | | | 00.061 | 1.000 |
| N0 | 14 | 7 | 7 | | |
| N1 | 39 | 18 | 21 | | |
| TNM stage | | | | – | 0.452 |
| I | 3 | 2 | 1 | | |
| II | 36 | 15 | 21 | | |
| III | 14 | 8 | 6 | | |

**TABLE 2 |** Comparison of radiation-induced adverse events.

| Groups | *N* | Radiation esophagitis | | Radiation pneumonitis | |
|---|---|---|---|---|---|
| | | Grades 1–2 | Grades 3–4 | Grades 0–2 | Grades 3–4 |
| HFR group | 25 | 56.0 | 44.0 | 84.0 | 16 |
| CFR group | 28 | 75.0 | 25.0 | 92.9 | 7.1 |
| *Z* value | | −1.444 | | −1.006 | |
| *P* value | | 0.149 | | 0.314 | |

*HFR, hypofractionated radiotherapy; CFR, conventional fractionated radiotherapy.*

**TABLE 3 |** Comparison of short-term efficiency between two groups.

| Group | *N* | CR | PR | SD | *Z* value | *P* value |
|---|---|---|---|---|---|---|
| HFR group | 25 | 36.0% | 44.0% | 20.0% | −1.006 | 0.314 |
| CFR group | 28 | 21.4 | 53.6 | 25.0 | | |

*HFR, hypofractionated radiotherapy; CFR, conventional fractionated radiotherapy.*

**TABLE 4 |** Comparison of short-term efficiency in patients with a lymphatic metastatic lesion of different diameters.

| Tumor diameter (cm) | *N* | CR | PR | SD | *Z* value | *P* value |
|---|---|---|---|---|---|---|
| ≤2 | 36 | 36.1 | 55.6 | 8.3 | −3.741 | <0.001 |
| >2 | 17 | 0.0 | 52.9 | 47.1 | | |

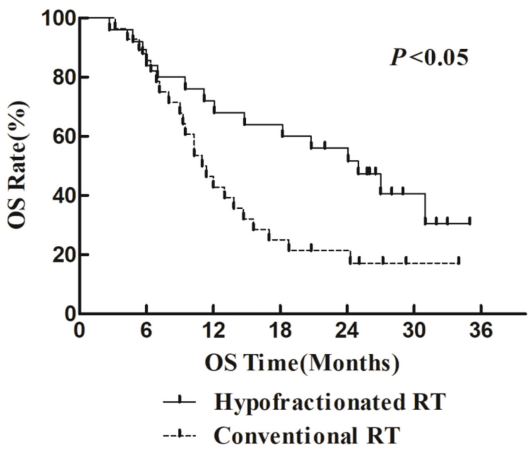


**FIGURE 1 |** Comparison of OS between HFR group and CFR group. Patients who received HFR treatment have better OS than those treated with CFR.

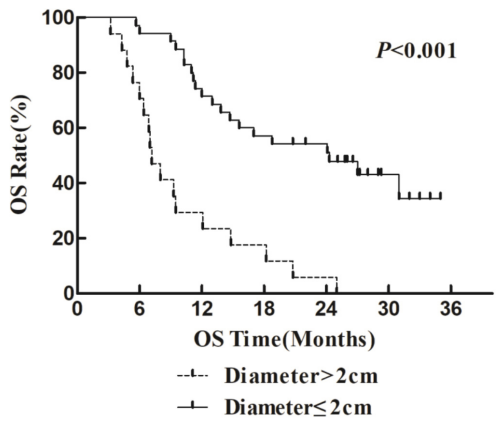


**FIGURE 2 |** Comparison of OS in patients with various lymph node metastases. Patients with lymph node diameter ≤2 cm have better OS than those with >2 cm.

95% CI, 0.105–0.528) were independent risk factors for better prognosis (**Table 5**).

There were 38 deaths in total (71.70%) during the study period. Among the death cases, 3 cases died from TGLN recurrence in the HFR group, while in the CFR group, 12 cases died from TGLN recurrence. In each group, five cases died from metastasis to other organs. In the HFR group, one died from pulmonary embolism and one died from cardiac failure. In the CFR group, one died from pulmonary embolism. Five cases died from unknown causes in each group. The TGLN recurrence in the HFR group was significantly lower than that of the CFR group (12.0 vs. 42.9%; $P = 0.016$).

## DISCUSSION

Surgery is commonly used for the treatment of EC, while lymphadenectomy is used for the resection of TGLN (12–15). However, TGLN metastasis after surgery is the major cause of treatment failure of EC, with an incidence of 12–80% (2–5), especially the right lymph node metastasis (16, 17). The diagnosis of TGLN metastasis is mainly relied on CT and PET-CT scans (6, 18–21), where there is a presence of a short diameter ≥0.5 cm and/or high uptake of 18F-PDG (22). In clinical practice, lymph node metastasis may induce injury of laryngeal nerve, which results in hoarseness and bucking and a poor prognosis.

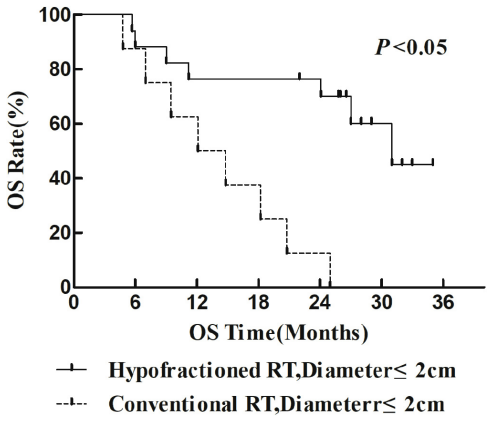


**FIGURE 3 |** Comparison of OS between HFR group and CFR group in patients with lymph node diameter ≤2 cm.

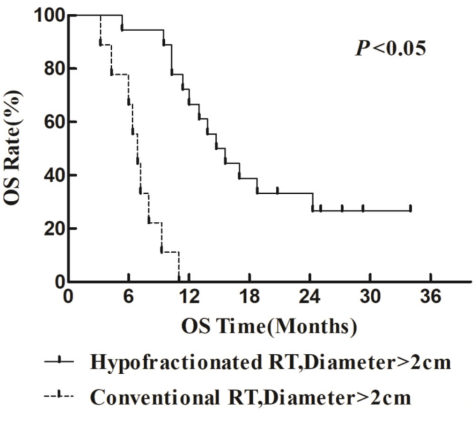


**FIGURE 4 |** Comparison of OS between HFR group and CFR group in patients with lymph node diameter >2 cm.

There is no consensus on the treatment of TGLN metastasis after surgery. Local radiotherapy and adjuvant chemotherapy are usually used for treating TGLN metastasis. After surgery, there is a decrease in blood supply to the TGLN leading to lower sensitivity of radiotherapy. Thus, the treatment efficiency of CFR is not satisfactory. Currently, HFR has rarely been used for the treatment of TGLN metastasis, because severe tracheal and/or esophageal perforation might occur. In a previous study, Song et al. showed that a daily dose of radiation ≤5 Gy was feasible for treating patients with advanced EC with satisfactory tolerance (10). Besides, Ma et al. showed that a dose of 54–60 Gy/18–20 fractions induced no obvious adverse events and may contribute to improving efficiency. Radiotherapy was used for the management of local tumor and peripheral infiltration, and it could not control distal metastasis (23). Several studies had tried the combination of radiotherapy and chemotherapy using low-dose paclitaxel to improve the sensitivity of radiation of EC cells, which could inhibit the metastasis and improve the OS (24, 25). In this study, the major effects of paclitaxel were to sensitize radiation rather than its chemotherapy-related features.

In this study, we compared the treatment efficacy using either HFR or CFR combined with chemotherapy in patients with TGLN metastasis after surgery. The dose used in the HFR group was about 80 Gy. The incidence of radiation esophageal and pulmonary injury in the HFR group was slightly higher than those of the CFR group, but there was no statistical significance. The median OS in the patients with a lymph node diameter ≤2 cm was significantly higher than that of the counterparts with a lymph node diameter >2 cm

**TABLE 5 |** Univariate and multivariate analyses of OS covariants.

| Variable | Univariate analysis | | | Multivariate analysis | | |
|---|---|---|---|---|---|---|
| | HR | 95% CI | *P* value | HR | 95% CI | *P* value |
| **Gender** | | | | | | |
| M/F | 1.326 | 0.639–2.749 | 0.449 | 1.371 | 0.626–3.002 | 0.429 |
| **Age (years)** | | | | | | |
| <60 vs. ≥60 | 0.832 | 0.393–1.761 | 0.832 | 0.537 | 0.247–1.164 | 0.115 |
| **T staging, postoperative** | | | | | | |
| $T_{3-4}$ vs. $T_{1-2}$ | 1.262 | 0.610–2.613 | 0.530 | | | |
| **N staging, postoperative** | | | | | | |
| $N_+$ vs. $N_0$ | 1.457 | 0.685–3.096 | 0.328 | | | |
| **TNM staging, postoperative** | | | | | | |
| I–II vs. III | 1.117 | 0.541–2.304 | 0.765 | | | |
| **Diameter of lymph nodes** | | | | | | |
| ≤2 vs. ≥2 cm | 0.217 | 0.110–0.426 | <0.001 | 0.108 | 0.047–0.249 | <0.001 |
| Fractioned types | | | | | | |
| HFR vs. CFR | 0.474 | 0.244–0.921 | 0.028 | 0.236 | 0.105–0.528 | <0.001 |

*HFR, hypofractionated radiotherapy; CFR, conventional fractionated radiotherapy.*

(24.1 months (95% CI, 12.0–36.1 months) vs. 7.3 months (95% CI, 6.2–8.2 months), $P < 0.05$). This demonstrated that it would be beneficial for EC patients to receive regular thoracic CT or PET/CT in order to monitor TGLN metastasis at an early stage. The median OS in the HFR group was higher than those of the CFR group (24.2 months (95% CI, 16.2–32.1 months) vs. 11.8 months (95% CI, 9.2–14.4 months), $P < 0.05$). Patients with a lymph node metastasis of $\leq$2 cm in the HFR group showed a longer OS compared with those of the CFR group (31 months vs. 7.3 months, $P = 0.039$). In addition, patients with a lymph node metastasis of >2 cm in the HFR group showed a longer OS compared with those of the CFR group (12.1 vs. 6.9 months, $P = 0.027$). These demonstrated that patients with TGLN metastasis may benefit from the HFR. This was not consistent with the previous description in which a higher radiotherapy dose was required for the patients with a large tumor size (26). As previously described, pathological staging was a prognostic factor for EC (27, 28). Nevertheless, in this study, TGLN with a diameter $\leq$2 cm (HR = 0.108; 95% CI, 0.047–0.249) and HFR (HR = 0.236; 95% CI, 0.105–0.528) were independent risk factors for better prognosis.

There are some limitations in this study. The sample size is small because the incidence of TGLN is usually low. Studies involving a larger sample size are required to further validate the efficiency and safety of the combination of HFR and chemotherapy for the treatment of TGLN metastasis after surgery.

In conclusion, EC patients with TGLN metastasis after surgery may benefit from the combinational treatment using HFR and paclitaxel chemotherapy. This study would help clinicians to make individual treatment decisions on late-stage cancer patients.

## DATA AVAILABILITY STATEMENT

The original contributions presented in the study are included in the article/supplementary material, further inquiries can be directed to the corresponding authors.

## ETHICS STATEMENT

The studies involving human participants were reviewed and approved by the Ethical Committee of Yancheng Third People's Hospital. The patients/participants provided their written informed consent to participate in this study.

## AUTHOR CONTRIBUTIONS

JW was responsible for data analysis and manuscript writing. JY, YJ, and DP were responsible for data collection. HZ and JLW designed the study and revised the manuscript. All authors contributed to the article and approved the submitted version.

## FUNDING

This study was supported by the National Natural Science Foundation of China (grant no. 11705095), the Key Science & Technology Program of Changzhou Municipal Commission of Health and Family Planning (grant no. ZD201710), and the Changzhou Scientific and Technological Support Social Development Project (grant no. CE20165024).

## REFERENCES

1. Chen W, Zheng R, Baade PD, Zhang S, Zeng H, Bray F, et al. Cancer statistics in China, 2015. *CA Cancer J Clin*. (2016) 66:115–32.
2. Altorki NK, Skinner DB. Occult cervical nodal metastasis in esophageal cancer: preliminary results of three-field lymphadenectomy. *J Thorac Cardiovasc Surg*. (1997) 113:540–4.
3. Igaki H, Kato H, Tachimori Y, Nakanishi Y. Cervical lymph node metastasis in patients with submucosal carcinoma of the thoracic esophagus. *J Surg Oncol*. (2000) 75:37–41. doi: 10.1002/1096-9098(200009)75:1<37::aid-jso7>3.0.co;2-5
4. Kato H, Igaki H, Tachimori Y, Watanabe H, Tsubosa Y, Nakanishi Y. Assessment of cervical lymph node metastasis in the staging of thoracic esophageal carcinoma. *J. Surg. Oncol.* (2000) 74:282–5.
5. Luo Y, Wang X, Liu Y, Wang C, Huang Y, Yu J, et al. Identification of risk factors and the pattern of lower cervical lymph node metastasis in esophageal cancer: implications for radiotherapy target delineation. *Oncotarget*. (2017) 8:43389–96.
6. Li X, Zhao J, Liu M, Zhai F, Zhu Z, Yu F, et al. Determination of radiotherapeutic target zones for thoracic esophageal squamous cell cancer with lower cervical lymph node metastasis according to CT-images. *Oncotarget*. (2016) 7:35865–73.
7. Lin XD, Shi XY, Zhou TC, Zhang WJ. [Intensity-modulated or 3-D conformal radiotherapy combined with chemotherapy with docetaxel and cisplatin for locally advanced esophageal carcinoma]. *Nan Fang Yi Ke Da Xue Xue Bao*. (2011) 31:1264–7.
8. Cooper JS, Guo MD, Herskovic A, Macdonald JS, Martenson JA Jr., Al-Sarraf M, et al. Chemoradiotherapy of locally advanced esophageal cancer: long-term follow-up of a prospective randomized trial (RTOG 85-01). Radiation therapy oncology group. *JAMA*. (1999) 281:1623–7.
9. Ma JB, Wei L, Chen EC, Qin G, Song YP, Chen XM, et al. Moderately hypofractionated conformal radiation treatment of thoracic esophageal carcinoma. *Asian Pac J Cancer Prev*. (2012) 13:4163–7.
10. Song YP, Ma JB, Hu LK, Zhou W, Chen EC, Zhang W. Phase I/II study of hypofractionated radiation with three-dimensional conformal radiotherapy for clinical T3-4N0-1M0 stage esophageal carcinoma. *Technol Cancer Res Treat*. 2011) 10:25–30. doi: 10.7785/tcrt.2012.500176
11. Al-Halabi H, Paetzold P, Sharp GC, Olsen C, Willers H. A contralateral esophagus-sparing technique to limit severe esophagitis associated with concurrent high-dose radiation and chemotherapy in patients with thoracic malignancies. *Int J Radiat Oncol Biol Phys*. (2015) 92:803–10.
12. Fang Q, Han YT, Wang SX, Ren GG, Peng L, Xiao WG, et al. [Clinical outcomes and selection conditions of three-field lymph node dissection for thoracic esophageal squamous cell carcinoma]. *Zhonghua Zhong Liu Za Zhi*. (2012) 34:212–5.
13. Li B, Xiang J, Zhang Y, Li H, Zhang J, Sun Y, et al. Comparison of Ivor-Lewis vs sweet esophagectomy for esophageal squamous cell carcinoma: a randomized clinical trial. *JAMA Surg*. (2015) 150:292–8.
14. Mao Y, Yang D, Gao S, Xue QH, He J. Consensus and controversies of surgical approach selection in the treatment for thoracic esophageal cancers. *Zhonghua Wei Chang Wai Ke Za Zhi*. (2016) 19:961–4.
15. Yang X, Zhan C, Sun F, Chen L, Shi M, Jiang W, et al. [Efficacy comparison of sweet versus Ivor-Lewis esophagectomy in the treatment of middle-lower

esophageal squamous cell carcinoma]. *Zhonghua Wei Chang Wai Ke Za Zhi*. (2016) 19:979–84.
16. Mao YS, He J, Dong JS, Cheng GY, Sun KL, Liu XY, et al. Comparison of the results of lymph node dissection via left versus right thoracotomy. *Zhonghua Zhong Liu Za Zhi*. (2012) 34:296–300.
17. Xue HC, Wu CR, Zhang ZB, Zhu ZH, Ma ZK, Lin AM. Right para-tracheal triangle lymphadenectomy for esophageal carcinoma. *Zhonghua Zhong Liu Za Zhi*. (2003) 25:397–400.
18. Fencl P, Belohlavek O, Harustiak T, Zemanova M. FDG-PET/CT lymph node staging after neoadjuvant chemotherapy in patients with adenocarcinoma of the esophageal-gastric junction. *Abdom Radiol*. (2016) 41:2089–94.
19. Foley KG, Lewis WG, Fielding P, Karran A, Chan D, Blake P, et al. N-staging of oesophageal and junctional carcinoma: is there still a role for EUS in patients staged N0 at PET/CT? *Clin Radiol*. (2014) 69:959–64.
20. Goel R, Subramaniam RM, Wachsmann JW. PET/Computed tomography scanning and precision medicine: esophageal cancer. *PET Clin*. (2017) 12:373–91.
21. Yap WK, Chang YC, Hsieh CH, Chao YK, Chen CC, Shih MC, et al. Favorable versus unfavorable prognostic groups by post-chemoradiation FDG-PET imaging in node-positive esophageal squamous cell carcinoma patients treated with definitive chemoradiotherapy. *Eur J Nucl Med Mol Imaging*. (2018) 45:689–98.
22. Zhao KL, Ma JB, Liu G, Wu KL, Shi XH, Jiang GL. Three-dimensional conformal radiation therapy for esophageal squamous cell carcinoma: is elective nodal irradiation necessary? *Int J Radiat Oncol Biol Phys*. (2010) 76:446–51.
23. Denham JW, Burmeister BH, Lamb DS, Spry NA, Joseph DJ, Hamilton CS, et al. Factors influencing outcome following radio-chemotherapy for oesophageal cancer. The trans tasman radiation oncology group (TROG). *Radiother Oncol*. (1996) 40:31–43. doi: 10.1016/0167-8140(96)01762-8
24. Jeremic B, Milicic B, Acimovic L, Milisavljeviæ S. Concurrent hyperfractionated radiotherapy and low-dose daily carboplatin/paclitaxel in patients with early-stage (I/II) non-small-cell lung cancer: long-term results of a phase II study. *J Clin Oncol*. (2005) 23:6873–80.
25. Tu L, Sun L, Xu Y, Wang Y, Zhou L, Liu Y, et al. Paclitaxel and cisplatin combined with intensity-modulated radiotherapy for upper esophageal carcinoma. *Radiat Oncol*. (2013) 8:75. doi: 10.1186/1748-717x-8-75
26. MacCarthy P, Isaac P, Frost G, Stokes G. Clinical dose-response studies with guanfacine (BS 100-141), a new antihypertensive agent. *Clin Exp Pharmacol Physiol*. (1978) 5:187–90.
27. Blackham AU, Sm HN, Schell MJ, Jin W, Gangi A, Almhanna K, et al. Recurrence patterns and associated factors of locoregional failure following neoadjuvant chemoradiation and surgery for esophageal cancer. *J Surg Oncol*. (2018) 117:150–9. doi: 10.1002/jso.24808
28. Valmasoni M, Pierobon ES, De Pasqual CA, Zanchettin G, Moletta L, Salvador R, et al. Esophageal cancer surgery for patients with concomitant liver cirrhosis: a single-center matched-cohort study. *Ann Surg Oncol*. (2017) 24:763–9.

**Conflict of Interest:** The authors declare that the research was conducted in the absence of any commercial or financial relationships that could be construed as a potential conflict of interest.

frontiers in Pharmacology

ORIGINAL RESEARCH
published: 15 September 2020
doi: 10.3389/fphar.2020.584652

# Tim-3 Expression and MGMT Methylation Status Association With Survival in Glioblastoma

*Ji Zhang[1†], Ke Sai[1†], Xiao li Wang[2†], Sheng quan Ye[3], Li jiao Liang[1], Yi Zhou[3], Zhi jie Chen[1], Wan-Ming Hu[4*] and Jian min Liu[5*]*

*[1] Department of Neurosurgery, State Key Laboratory of Oncology in South China, Collaborative Innovation Center for Cancer Medicine, Sun Yat-sen University Cancer Center, Guangzhou, China, [2] Department of General Surgery, Shang Jin Nan Fu Hospital of West China Hospital of Sichuan University, Chengdu, China, [3] Department of Anesthesiology, Sun Yat-sen University Cancer Center, State Key Laboratory of Oncology in South China, Collaborative Innovation Center for Cancer Medicine, Guangzhou, China, [4] Department of Pathology, Sun Yat-sen University Cancer Center, State Key Laboratory of Oncology in South China, Collaborative Innovation Center for Cancer Medicine, Guangzhou, China, [5] Department of Neurosurgery, The First Affiliated Hospital of Guangzhou University of Traditional Chinese Medicine, Guangzhou, China*

OPEN ACCESS

**Edited by:**
*Zhe-Sheng Chen,*
*St. John's University, United States*

**Reviewed by:**
*Feng Ye,*
*People's Hospital of Deyang City, China*
*Hongtao Rong,*
*Tianjin Medical University General Hospital, China*

***Correspondence:**
*Jian min Liu*
*solarjm@sina.com*
*Wan-Ming Hu*
*huwm@sysucc.org.cn*

*[†]These authors have contributed equally to this work*

**Specialty section:**
*This article was submitted to Pharmacology of Anti-Cancer Drugs, a section of the journal Frontiers in Pharmacology*

**Received:** *17 July 2020*
**Accepted:** *28 August 2020*
**Published:** *15 September 2020*

**Citation:**
*Zhang J, Sai K, Wang Xl, Ye Sq, Liang Lj, Zhou Y, Chen Zj, Hu W-M and Liu Jm (2020) Tim-3 Expression and MGMT Methylation Status Association With Survival in Glioblastoma. Front. Pharmacol. 11:584652. doi: 10.3389/fphar.2020.584652*

**Background:** A profound understanding of the molecular landscape of glioblastoma multiforme (GBM) will make it possible to develop better and more intelligent therapies directed toward specific molecular targets and may one day yield better prognostic capabilities. Immune checkpoint molecules have inspired the emergence of immune checkpoint-targeting therapeutic strategies. However, the prognostic significance of the immune checkpoint molecule T cell immunoglobulin mucin-3 (Tim-3) on tumor-infiltrating immune cells (TIICs) and O-6-methylguanine-DNA methyltransferase (MGMT) promoter methylation status has not yet been fully elucidated. We aimed to develop an MGMT promoter methylation status-associated immune prognostic signature for GBM.

**Patients and Methods:** A total of 84 patients with newly diagnosed GBM were included in this study. MGMT promoter methylation status was retrospectively analyzed, and the expression level of Tim-3 was investigated using immunohistochemistry (IHC). The correlation between Tim-3 expression combined with MGMT promoter methylation status and prognosis was explored.

**Results:** Tim-3 expression varied in GBM patients. Mesenchymal expression of Tim-3 in GBM tissues was present 73.81% (62/84) of patients, and these were subdivided into groups based on low 15.48% (13/84), moderate 7.14% (6/84), or strong expression 51.19% (43/84). Forty-eight patients had tumors that tested positive for MGMT promoter methylation, while the remaining 36 patients tested negative.

**Conclusions:** We profiled the immune status of MGMT promoter methylation in GBM and established a local immune signature for GBM that could independently identify patients with a favorable prognosis, indicating a relationship between prognosis and GBM immune signature. MGMT promoter methylation with lower Tim-3 expression was significantly associated with better survival.

**Keywords: glioblastoma multiforme, O-6-methylguanine-DNA methyltransferase, prognosis, immune, T cell immunoglobulin mucin-3**

# INTRODUCTION

Glioblastoma is the most common and devastating primary brain tumor in adults (Wirsching et al., 2016). Despite recent advances, only a few treatment strategies are available for GBMs, and their outcomes remain dismal (Stupp et al., 2015). There are few effective treatment options for GBMs, and these carry high risks of relapse and short survival periods. Because the biology of GBM at the cellular and molecular levels is not well understood, especially in relation to treatment, the development of novel therapeutic approaches requires a deeper understanding of the tumor's nature (Yu et al., 2017). In addition to standard treatment involving surgery, radiotherapy and chemotherapy, immunotherapy has been rapidly identified as a promising modality to treat GBM (Deng et al., 2019). A number of immune-related parameters have been reported to be predictive of outcomes for patients with GBM (Han et al., 2014; Han et al., 2015). In particular, MGMT promoter methylation status was reported to be significantly related to GBM prognosis (Rao et al., 2018). However, there is still a lack of studies that systematically explore the effects of MGMT promoter methylation status on the immune microenvironment and on the associations between MGMT promoter methylations status, immune microenvironment, and prognosis.

Tim-3 is widely expressed by mature T lymphocytes and macrophages (Sabatos et al., 2003). Of note, with the exception of the immune response, increasing evidence has suggested that Tim-3 has functional roles in tumor biology (Yan et al., 2015). Previous studies suggest that Tim-3 is a negative immune regulator that may be upregulated in the GBM tumor environment, so Tim-3 is a promising target in glioma treatment. However, until now, no evidence has revealed the value of Tim-3 as a prognostic biomarker in GBM patients. The present study aimed to investigate the influence of MGMT promoter methylation on the immune microenvironment and to develop an MGMT-associated immune prognostic signature for GBM.

# MATERIALS AND METHODS

## Patients and Specimens

A cohort of patients with newly histologically diagnosed GBM (WHO grade IV) was studied consecutively from July 2016 to January 2018. We only included patients for whom affirmatory MGMT promoter methylation status, treatment course, and survival outcome were known. Patients with a mixed history of cancer other than GBM and previous adjuvant radiotherapy or chemotherapy were excluded. Patients who died of diseases unrelated to glioma were also excluded from the study. Patient age ranged from 18 to 70 years at the time of diagnosis. Neurological status was assessed before and after neurosurgery, and Karnofsky performance status (KPS) was not less than 70 in all patients. A series of 84 eligible patients who had tumor tissue available for testing were included in this study. These patients received standard subsequent treatment according to the Stupp protocol (Stupp et al., 2005). Follow-up was carried out regularly. The overall survival (OS) was defined as the interval from GBM diagnosis until either death or, for those who were removed, until the last known follow-up.

**Abbreviations:** Tim-3, T cell immunoglobulin mucin-3; GBM, glioblastoma multiforme; OS, overall survival; IHC, immunohistochemistry.

## Immunohistochemistry (IHC)

Tim-3 was immunohistochemically stained using a previously described standard technique (Li et al., 2018). Briefly, slides were deparaffinized in xylene and rehydrated in graded alcohol. Antigen retrieval was performed in tris-ethylenediaminetetraacetic acid (EDTA; pH 9.0) buffer at 95°C for 20 min. Slides were incubated in tris-buffered saline (TBS) for 5 min. Endogenous peroxidase blocking was performed in 3% $H_2O_2$ for 10 min. Subsequently, the slides were incubated in a rabbit polyclonal antibody against Tim-3 (1:500; Abcam, Inc., Cambridge, MA) overnight at 4°C. The slides were rinsed five times with 0.01 M phosphate-buffered saline (PBS; pH 7.4) for 10 min. Sections were incubated with primary antibodies against Tim-3 (1:1,000; catalog no. ab185703, Abcam) and with a horseradish peroxidase (HRP)–tagged secondary antibody (1:1,000; catalog no. sc-3836, Santa Cruz Biotechnology, Inc.) for another 1 hour at 37°C. Subsequently, the slides were washed in PBS and stained with 3,3-diaminobenzidine (DAB). Finally, the slides were counterstained, dehydrated, and mounted.

## IHC Assessment

The degree of Tim-3 protein expression was independently reviewed by two neuropathologists. The number of stained cells was designated as unexpressed (0), weak (1–5 cells/HPF), moderate (5–10 cells/HPF), or strong (>10 cells/HPF). The model of the microscope was a BX53, Olympus.

## MGMT Promoter Methylation

For the subset of patients who had documented positive MGMT promoter methylation of their initially resected tumor tissues, MGMT promoter methylation was further confirmed by methylation-specific real-time PCR, according to our institutional practice.

## Statistical Analysis

Statistical analyses were performed using GraphPad Prism version 7.0.0. The correlation between Tim-3 expression intensity combined with MGMT promoter methylation status and prognosis was calculated using a chi-square test. Spearman's correlation analysis and the corresponding statistical significance were used to evaluate correlations with gene expression. Independent prognostic factors for OS were identified using the Cox's proportional hazards model. The OS curves were plotted using the Kaplan-Meier method, and log-rank tests were employed to assess the resulting survival curves. A probability value of less than 0.05 was regarded as significant.

# RESULTS

## Clinicopathological Characteristics

Archival tissue samples from 84 patients with GBM were enrolled in the study. Of the 84 GBM patients, 43 were men

(51.19%) and 41 were women (49.81%). The median age at diagnosis was 41 years (range, 18–70 years), and the median KPS was 90 (range, 70–100). All specimens were obtained from the supratentorial area as identified by preoperative MRI. The follow-up duration ranged from 4 to 47 months, and the median OS was 17.3 months.

## Tim-3 Expression

The expression status of specific inhibitory receptors, including Tim-3, programmed cell death 1 (PD-1), cytotoxic T-lymphocyte-associated protein 4 (CTLA4), and lymphocyte-activation gene 3 (LAG-3), are associated with T cell exhaustion and immune escape. The Oncomine database was used to investigate the mRNA levels of these molecules in GBMs and normal tissues (**Figure 1C**). As shown in **Figure 1A**, Tim-3 expression was markedly higher in GBM than in corresponding normal tissue. To validate the relationships between the immune checkpoint molecules Tim-3 and LAG-3 and between Tim-3 and PD-1, RNA-seq data from the TCGA database (https://cancergenome.nih.gov/) were analyzed. As shown in **Figure 1B**, with a p-value threshold of 0.05, Tim-3 expression was significantly related to both LAG-3 and PD-1 expression in GBM. Further, Tim-3 and other exhausting immune molecules (LAG-3, PD-1, CTLA4, CD244, and PD-1) exhibited significantly different expression profiles between normal brain tissues and GBM tissues according to the TCGA database, indicating their potential correlation with glioma progression (**Figure 1**). According to our immunohistochemical analysis, mesenchymal expression of the immune checkpoint molecule Tim-3 in tumor-infiltrating immune cells (TIICs) was not observed in 22/84 patients (26.19%), weak in 13/84 patients (15.48%), moderate in 6/84 patients (7.14%), and strong in 43/84 patients (51.19%) (**Figure 2** and **Table 1**). Notably, strong expression of Tim-3 was more frequently observed in GBM than it was in other tissues.

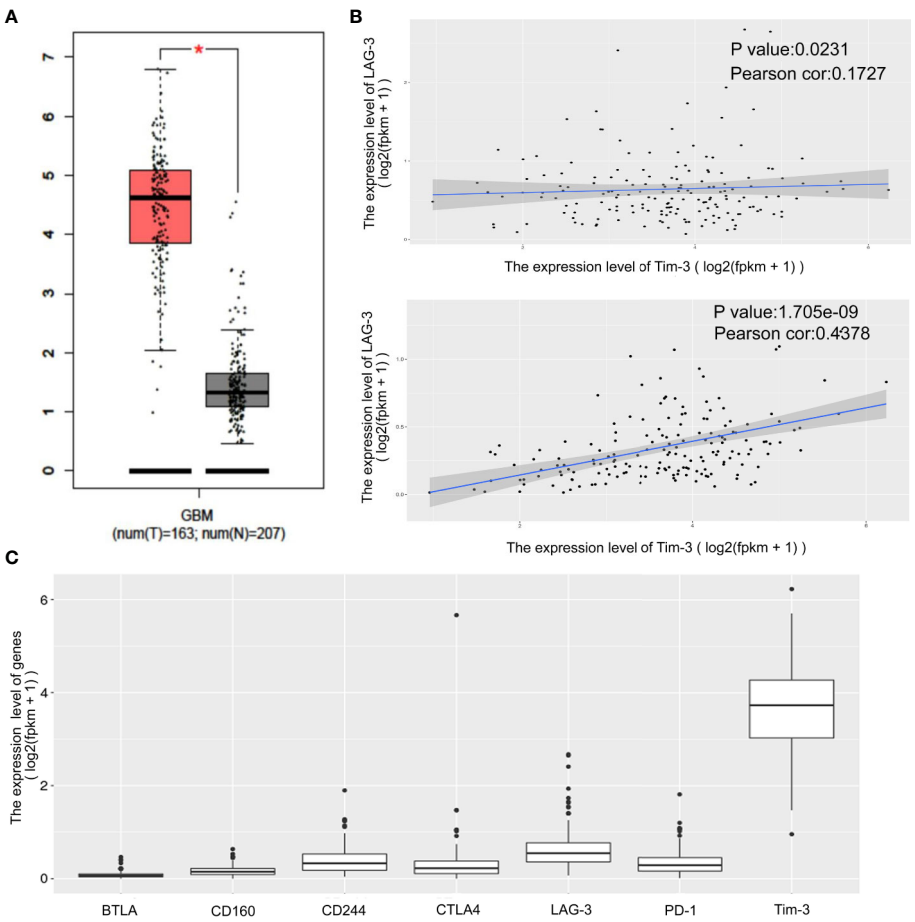


**FIGURE 1** | Differential expression of the immune checkpoint molecules PD-1, CTLA4, Tim-3 and LAG-3 in GBM tissues compared to corresponding normal adjacent tissues by TIMER analysis. Tim-3 expression in GBM compare with normal adjacent tissues **(A)**. Tim-3 expression is significantly associated with LAG-3 and PD-1 in GBM according to the TCGA database **(B)**. Tim-3 is one of the genes expressed differentially in exhausted T cells in GBM according to the TCGA database **(C)**.

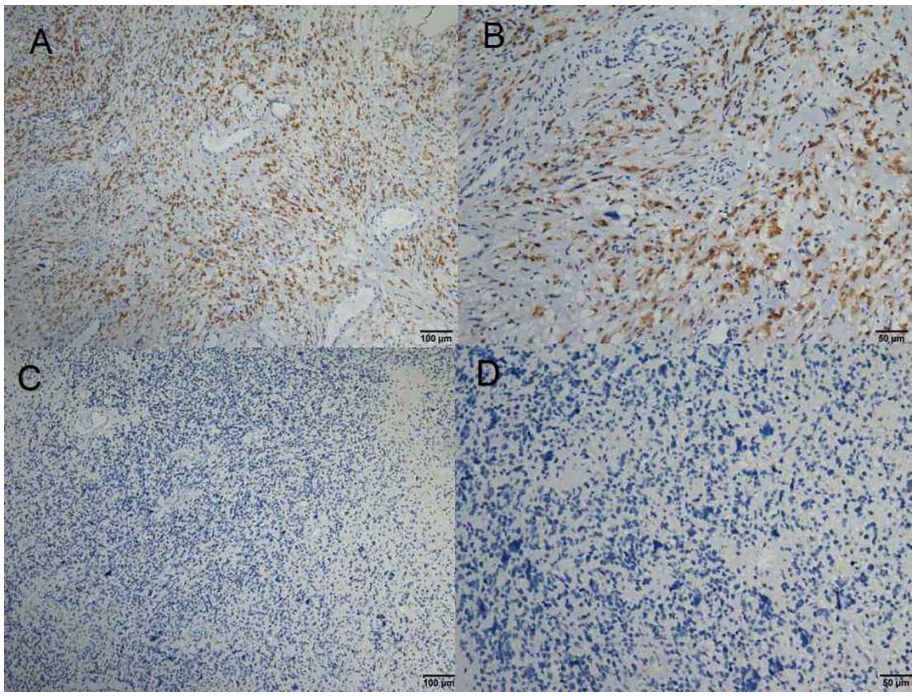


**FIGURE 2** | **(A–D)** Immunohistochemical staining of Tim-3 expression in formalin-fixed, paraffin-embedded GBM tissues.

**TABLE 1** | Tim-3 expression in 84 GBM samples.

| No. of cases (84) | NE (22) | Tim-3 expression | | Strong (43) |
|---|---|---|---|---|
| | | Weak (13) | Moderate (6) | |
| Methylation | 14 | 10 | 2 | 22 |
| Non-methylation | 8 | 3 | 4 | 21 |

*NE, no expression.*

## MGMT Methylation Status in 84 GBM Samples

MGMT methylation status was analyzed for the 84 patients included in this study. All patients had MGMT promoter methylation test results. Testing was performed *via* methylation specific real-time PCR at the time of diagnosis. Forty-eight patients (57.14%) were determined to have MGMT methylated tumors, and 36 patients (42.76%) were determined to have MGMT unmethylated tumors (**Figure 3** and **Table 1**).

## Correlations Between MGMT Methylation Status Combined With Tim-3 Expression and Survival

The relationship between Tim-3 expression and MGMT promoter methylation status is shown in **Table 1** and **Figure 3**. A low expression of Tim-3 in TIICs was associated with MGMT promoter methylation status. Univariate analysis revealed a significant correlation between low expression of Tim-3 in TIICs in combination with MGMT promoter methylation and a better prognosis. We summarized the correlation between Tim-3 expression combined with MGMT promoter methylation and GBM patient prognosis (**Figure 4**). Increased expression of Tim-3 combined with MGMT promoter nonmethylation was significantly associated with a poor prognosis. No significant correlations between Tim-3 expression level and either gender ($P = 0.846$) or tumor location ($P = 0.447$) were observed. However, moderate or strong expression of Tim-3 with either MGMT promoter methylation or nonmethylation was associated with a poor prognosis. In patients with no Tim-3 expression in combination with MGMT promoter nonmethylation, there was a similar association with prognosis, while MGMT promoter methylation was associated with a good prognosis.

Multivariate Cox regression analyses confirmed that a combination of Tim-3 expression and MGMT promoter methylation status was an independent risk factor for survival in GBM patients. Strong expression of Tim-3 in combination with MGMT promoter nonmethylation correlated significantly with shorter OS in each of the four subgroups ($p < 0.05$, **Figure 4**). The median survival was 16.9 and 16.4 months for patients whose tumor had unexpressed and moderate levels of Tim-3, respectively, whereas the median survival was 7.6 months for those who showed high

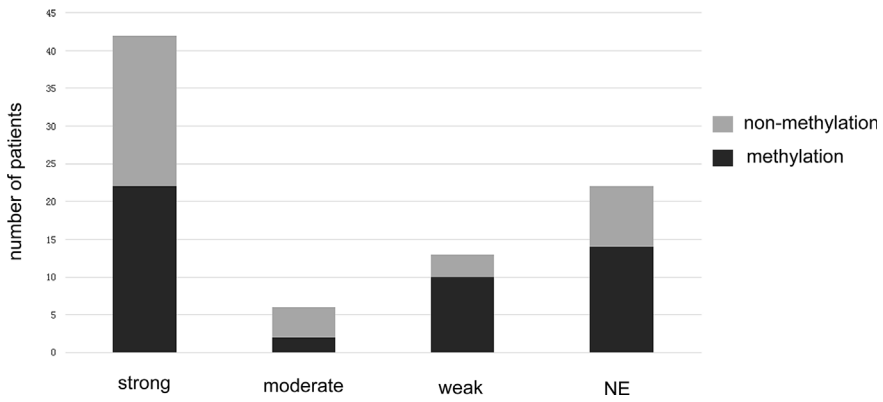


**FIGURE 3** | The bar graph shows the methylated and unmethylated MGMT distributions in different Tim-3 expression groups.

levels of Tim-3 expression and MGMT promoter nonmethylation. In patients with low expression of Tim-3 and with MGMT promoter methylation, the average survival time was 21.8 months.

## DISCUSSION

Glioblastoma is the most common and lethal primary brain tumor, with a high risk of recurrence and a short survival period, and finding the cure for this formidable disease is a daunting task (Stupp et al., 2015; Li et al., 2018). Recent developments in glioblastoma research emphasize targeting the molecular characteristics of the tumor as well as various approaches related to immunotherapy. Many new molecular markers have been identified, but MGMT promoter methylation status in particular is commonly used in GBM studies (Guo et al., 2019).

The discovery that differential MGMT promoter methylation in GBM plays a key role in the understanding of glioma biology (Chai et al., 2019). Increasing numbers of studies indicate that the tumor immunological microenvironments of gliomas differ based on their molecular properties (Berghoff et al., 2017). However, the mechanism that regulates the relationship between MGMT promoter methylation status and the immune microenvironment is still unknown. The current study systematically investigated the prognostic impact of GBM of immune checkpoint molecule Tim-3 expression and MGMT promoter methylation status in TIICs. We identified Tim-3 expression in combination with MGMT promoter methylation status as a novel prognostic parameter for GBM. MGMT promoter methylation status was related to Tim-3 expression in immune cell infiltrating GBM. Our data demonstrated that Tim-3 is differentially expressed in most GBM tissues. Further, we observed that the checkpoint molecule Tim-3 in combination with MGMT promoter methylation status showed significant prognostic potential. Interestingly, strong expression of Tim-3 in combination with MGMT promoter nonmethylation showed a poor effect on survival. Thus, expression of Tim-3 with MGMT promoter methylation status has potential to be a prognostic predictor in immune cell infiltrating GBM.

To the best of our knowledge, the present study is the first to report that Tim-3 expression in combination with MGMT promoter methylation status is a critical prognostic variable for patients with GBM. Tim-3 is an immune regulatory molecule that motivates downstream cascade events upon stimulation by

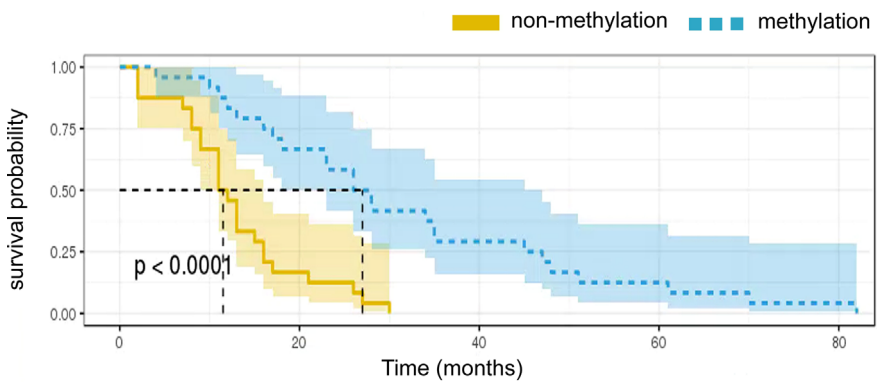


**FIGURE 4** | Kaplan-Meier survival curves showing overall survival according to MGMT promoter methylation status.

its ligand (Liu et al., 2014; Yan et al., 2015). Emerging research has demonstrated the importance of Tim-3 in human tumorigenesis. However, no studies have been performed which investigate the role of Tim-3 expression in combination with MGMT promoter methylation status in GBM patient prognosis. Aberrant expression of Tim-3 has been reported to boost tumor progression and to be associated with unfavorable prognosis in many types of cancers (Piao et al., 2014; Yan et al., 2015; Zheng et al., 2015; Tawk et al., 2016; Zhang et al., 2019).

Tim-3 has previously been reported to be highly expressed in prostate cancer, hepatocellular carcinoma, and melanoma (Piao et al., 2014; Yan et al., 2015; Zheng et al., 2015; Tawk et al., 2016; Zhang et al., 2019). We initially examined Tim-3 protein levels in GBM tissues using immunohistochemical analysis and observed the expression of Tim-3 in GBM interstitial tissue. In line with previous reports, the present study found that expression of Tim-3 was significantly stronger in GBM samples without MGMT methylation. Tim-3 can efficiently predict the aggressive behavior of head and neck squamous cell carcinomas (Chakravarthi et al., 2014). In prostate cancer, Tim-3 overexpression results in an attenuated level of tumor suppressor FLRT3 and increased expression of genes that trigger invasion and metastasis, such as MMPs (Kim et al., 2017). One study reported that Tim-3 promotes glioma cell proliferation, and increased levels of Tim-3 enhance angiogenesis by inducing transdifferentiation of glioma stem cells into endothelial cells and by stabilizing vascular base membranes, which was implicated as a mechanism by which Tim-3 furthers the progression of gliomas (Hegi et al., 2005). However, that study did not explore the association between Tim-3 levels and prognosis in glioma patients, probably due to the limited number of glioma specimens available. Therefore, the prognostic significance of Tim-3 in glioma remains unclear.

Molecular genetic testing, in particular testing for MGMT promoter methylation, is currently performed to predict the success of standard chemotherapy in GBM (Wick et al., 2010). In one study, 57.14% of responders exhibited MGMT promoter methylation. The same study concluded that patients with MGMT promoter methylation had better outcomes following treatment with temozolomide (Malmstrom et al., 2010). Another single-center study reported that MGMT promoter methylation is an independent prognostic factor for positive outcomes in GBM, including prolonged progression-free survival (PFS) and OS (Dunn et al., 2009). To further investigate the relationship between MGMT promoter methylation status and the expression of Tim-3 in GBM, we retrieved 84 specimens from a tumor tissue bank. In line with previous findings, Tim-3 was expressed at differing levels in GBM tissues. High Tim-3 expression was more frequently observed in GBMs from patients who did not show MGMT promoter methylation, which itself was capable of predicting poor prognosis. Among the 84 patients included in this study, the median OS was 17.3 months. The survival time for the subset of GBM patients with low Tim-3 expression and MGMT promoter methylation was longer than those with moderate or strong Tim-3 expression. Subsequent multivariate cox regression analyses confirmed that Tim-3 expression with MGMT promoter methylation was an independent prognostic factor for GBM patients. The subgroup analysis revealed that strong Tim-3 expression together with MGMT promoter nonmethylation was strongly correlated with shorter survival time. The average survival time, however, hardly differed between patients with unexpressed and those with moderate Tim-3 expression.

We also observed that high-risk GBM patients had higher levels of Tim-3 and unmethylated MGMT. We then constructed an MGMT-associated immune prognostic signature which demonstrated the potential to provide novel insights into the GBM immune microenvironment and possible immunotherapies. This enabled us to classify patients into subgroups with distinct outcomes and immunophenotypes, signifying that this signature may be used to delimit the current prognostic model and facilitate further stratification of patients with GBM and improve the accuracy of prognoses. The results of the current study integrate the complementary values of molecular pathology and immune checkpoint molecule Tim-3 expression to develop a novel model which provides superior survival prediction.

## CONCLUSION

Our data demonstrate that Tim-3 expression together with MGMT promoter methylation status is correlated with survival in GBM, indicating that Tim-3 is a promising target. Our study assessed the association between clinical prognosis and Tim-3 expression in combination with MGMT promoter methylation. For the first time, we report an association between high levels of Tim-3 expression without MGMT promoter methylation in GBM tissues and worse prognoses. More importantly, univariate and multivariate analyses revealed that a high expression of Tim-3 with MGMT promoter methylation status was a clear prognostic factor for patients with GBM. Moreover, the checkpoint molecule Tim-3 is clearly associated with treatment response and offers prompt, meaningful information for selecting chemotherapeutic drugs.

## LIMITATIONS

The current study has several limitations. First, it was a retrospective study. Second, the number of patients was limited. Third, selection bias could not be avoided completely. In addition, there may be other parameters we did not consider that could have influenced the study's results.

## DATA AVAILABILITY STATEMENT

The raw data supporting the conclusions of this article will be made available by the authors, without undue reservation.

## ETHICS STATEMENT

The studies involving human participants were reviewed and approved by the Institutional Review Board of the First Affiliated

Hospital of Guangzhou University of Traditional Chinese Medicine. The patients/participants provided their written informed consent to participate in this study.

## AUTHOR CONTRIBUTIONS

All authors contributed equally to the paper. JZ, KS, XW, and SY drafted the article. LL and YZ performed data collection and statistics. ZC, W-MH, and JL supervised the data collection and revised this article. All authors contributed to the article and approved the submitted version.

## FUNDING

The study was supported by Project of Guangdong Medical Science and Technology Research Foundation (A2018017), Special fund for clinical research of Wu jieping medical foundation (320.6750.19093-12), Fundamental Research Funds for the Central Universities (19ykpy190), Foundation of the Science and Technology Program of Guangzhou, People's Republic of China (201607010365), and High Level University Construction Project of Guangzhou University of Traditional Chinese Medicine (A1-AFD018171Z11072). This article has been released as a pre-print at (https://www.researchsquare.com/article/rs-22637/v1).

## REFERENCES

Berghoff, A. S., Kiesel, B., Widhalm, G., Wilhelm, D., Rajky, O., Kurscheid, S., et al. (2017). Correlation of immune phenotype with IDH mutation in diffuse glioma. *Neuro Oncol.* 19, 1460–1468. doi: 10.1093/neuonc/nox054

Chai, R. C., Chang, Y. Z., Wang, Q. W., Zhang, K. N., Li, J. J., Huang, H., et al. (2019). A Novel DNA Methylation-Based Signature Can Predict the Responses of MGMT Promote Unmethylated Glioblastomas to Temozolomide. *Front. Genet.* 10, 910. doi: 10.3389/fgene.2019.00910

Chakravarthi, B. V., Pathi, S. ,. S., Goswami, M. ,. T., Cieslik, M., Zheng, H., Nallasivam, S., et al. (2014). The miR-124-prolyl hydroxylase P4HA1-MMP1 axis plays a critical role in prostate cancer progression. *Oncotarget* 5, 6654–6669. doi: 10.18632/oncotarget.2208

Deng, X., Lin, D., Chen, B., Zhang, X., Xu, X., Yang, Z., et al. (2019). Development and Validation of an IDH1-Associated Immune Prognostic Signature for Diffuse Lower-Grade Glioma. *Front. Oncol.* 9, 1310. doi: 10.3389/fonc.2019.01310

Dunn, J., Baborie, A., Alam, F., Joyce, K., Moxham, M., Sibson, R., et al. (2009). Extent of MGMT promoter methylation correlates with outcome in glioblastomas given temozolomide and radiotherapy. *Br. J. Cancer* 101 (1), 124–131. doi: 10.1038/sj.bjc.6605127

Guo, G., Sun, Y., Hong, R., Xiong, J., Lu, Y., Liu, Y., et al. (2019). IKBKE enhances TMZ-chemoresistance through upregulation of MGMT expression in glioblastoma. *Clin. Transl. Oncol.* 21, 1252–1262. doi: 10.1007/s12094-019-02251-3

Han, S., Zhang, C., Li, Q., Dong, J., Liu, Y., Huang, Y., et al. (2014). Tumour-infiltrating CD4(1) and CD8(1) lymphocytes as predictors of clinical outcome in glioma. *Br. J. Cancer* 110, 2560–2568. doi: 10.1038/bjc.2014.162

Han, S., Liu, Y., Li, Q., Li, Z., Hou, H., and Wu, A. (2015). Pre-treatment neutrophil-to-lymphocyte ratio is associated with neutrophil and T-cell infiltration and predicts clinical outcome in patients with glioblastoma. *BMC Cancer* 15, 617. doi: 10.1186/s12885-015-1629-7

Hegi, M. E., Diserens, A. C., Gorlia, T., Hamou, M. F., de Tribolet, N., Weller, M., et al. (2005). MGMT gene silencing and benefit from temozolomide in glioblastoma. *N. Engl. J. Med.* 352 (10), 997–1003. doi: 10.1056/NEJMoa043331

Kim, J. E., Patel, M. A., Mangraviti, A., Kim, E. S., Theodros, D., Velarde, E., et al. (2017). Combination Therapy with Anti-PD-1, Anti-Tim-3, and Focal Radiation Results in Regression of Murine Gliomas. *Clin. Cancer Res.* 23 (1), 124–136. doi: 10.1158/1078-0432

Li, X., Wang, B., Gu, L., Zhang, J., Li, X., Gao, L., et al. (2018). Tim-3 expression predicts the abnormal innate immune status and poor prognosis of glioma patients. *Clin. Chimica Acta* 476, 178–184. doi: 10.1016/j.cca.2017.11.022

Liu, L., Zhang, X., Lou, Y., Rao, Y., and Zhang, X. (2014). Cerebral microdialysis in GBM studies from theory to application. *J. Pharm. BioMed. Anal.* 96, 77–89. doi: 10.1016/j.jpba.2014.03.026

Malmstrom, A., Gronberg, B. H., Stupp, R., Marosi, C., Frappaz, D., Schultz, H. P., et al. (2010). Glioblastoma in elderly patients: a randomized phase III trial comparing survival in patients treats with 6-week radiotherapy versus hypofractionated RT over 2 week versus temozolomide single agent. *J. Clin. Oncol.* 28, LBA2002. doi: 10.1200/jco.2010.28.18_suppl.lba2002

Piao, Y. R., Jin, Z. H., Yuan, K. C., and Jin, X. S. (2014). Analysis of Tim-3 as a therapeutic target in prostate cancer. *Tumour Biol.* 35, 11409–11414. doi: 10.1177/1010428317716628

Rao, A. M., Quddusi, A., and Shamim, M. S. (2018). The significance of MGMT methylation in glioblastoma Multiforme prognosis. *J. Pak. Med. Assoc.* 68 (7), 1137–1139.

Sabatos, C. A., Chakravarti, S., Cha, E., Schubart, A., Sánchez-Fueyo, A., Zheng, X. X., et al. (2003). Interaction of Tim-3 and Tim-3 ligand regulates T helper type 1 responses and induction of peripheral tolerance. *Nat. Immunol.* 4, 1102–1110. doi: 10.1038/ni988

Stupp, R., Mason, W. P., van den Bent, M. J., Weller, M., Fisher, B., Taphoorn, M. J., et al. (2005). Radiotherapy plus concomitant and adjuvant temozolomide for glioblastoma. *N. Engl. J. Med.* 352, 987–996. doi: 10.1056/NEJMoa043330

Stupp, R., Taillibert, S., Kanner, A. A., Kesari, S., Steinberg, D. M., Toms, S. A., et al. (2015). Maintenance therapy with tumor-Treating fields plus temozolomide vs temozolomide alone for glioblastoma: a randomized clinical trial. *JAMA* 314, 2535–2543. doi: 10.1001/jama.2015.16669

Tawk, B., Schwager, C., Deffaa, O., Dyckhoff, G., Warta, R., Linge, A., et al. (2016). Comparative analysis of transcriptomics based hypoxia signatures in head- and neck squamous cell carcinoma. *Radiother. Oncol.* 118, 350–358. doi: 10.1016/j.radonc.2015.11.027

Wick, W., Engel, C., Combs, S. E., Stoffels, M., Felsberg, J., Stockhammer, F., et al. (2010). NOA-08 randomized phase III trial of 1-week-on/1-week-off temozolomide versus involved field radiotherapy in elderly (older than age 65) patients with newly diagnosed glioblastoma. *J. Clin. Oncol.* 28, LBA2001. doi: 10.1200/jco.2010.28.18_suppl.lba2001

Wirsching, H. G., Galanis, E., and Weller, M. (2016). Glioblastoma. *Handb. Clin. Neurol.* 134, 381–397. doi: 10.1016/B978-0-12-802997-8.00023-2

Yan, W., Liu, X., Ma, H., Zhang, H., Song, X., Gao, L., et al. (2015). Tim-3 fosters HCC development by enhancing TGF-$\beta$-mediated alternative activation of macrophages. *Gut* 64, 1593–1604. doi: 10.1136/gutjnl-2014-307671

Yu, M., Lu, B., Liu, Y., Me, Y., Wang, L., and Zhang, P. (2017). Tim-3 is upregulated in human colorectal carcinoma and associated with tumor progression. *Mol. Med. Rep.* 15, 689–695. doi: 10.3892/mmr.2016.6065

Zhang, J., Zhu, Z. Q., Li, Y. X., Zhuang, Q. F., Lai, Y., Li, S. F., et al. (2019). Tim'3 expression in glioma cells is associated with drug resistance. *J. Can. Res. Ther.* 15 (4), 882–888. doi: 10.4103/jcrt.JCRT_630_18

Zhang, J., Sai, K., Wang, X. L., Ye, S. Q., Liang, L. J., Zhou, Y., et al. (2020). Tim-3 protein expression with MGMT methylation status in glioblastoma and association with survival. *Front. Pharmacol.* doi: 10.21203/rs.3.rs-22637/v1

Zheng, H., Guo, X., Tian, Q., Li, H., and Zhu, Y. (2015). Distinct role of Tim-3 in systemic lupus erythematosus and clear cell renal cell carcinoma. *Int. J. Clin. Exp. Med.* 8, 7029–7038.

**Conflict of Interest:** The authors declare that the research was conducted in the absence of any commercial or financial relationships that could be construed as a potential conflict of interest.

frontiers in Pharmacology

REVIEW
published: 11 September 2020
doi: 10.3389/fphar.2020.579068

# The Biological Functions and Clinical Applications of Integrins in Cancers

*Chao-yue Su[1†], Jing-quan Li[2†], Ling-ling Zhang[1†], Hui Wang[3], Feng-hua Wang[3], Yi-wen Tao[1], Yu-qing Wang[1], Qiao-ru Guo[1], Jia-jun Li[1], Yun Liu[1*], Yan-yan Yan[4*] and Jian-ye Zhang[1,2*]*

[1] The Fifth Affiliated Hospital, Key Laboratory of Molecular Target and Clinical Pharmacology and the State Key Laboratory of Respiratory Disease, School of Pharmaceutical Sciences, Guangzhou Medical University, Guangzhou, China, [2] The First Affiliated Hospital, Hainan Medical University, Haikou, China, [3] Guangzhou Institute of Pediatrics/Guangzhou Women and Children's Medical Center, Guangzhou Medical University, Guangzhou, China, [4] Institute of Immunology and School of Medicine, Shanxi Datong University, Datong, China

OPEN ACCESS

**Edited by:**
Xiaoping Lin,
Sun Yat-sen University Cancer Center (SYSUCC), China

**Reviewed by:**
Zhi Shi,
Jinan University, China
Longyang Liu,
Southern Medical University, China

***Correspondence:**
Jian-ye Zhang
jianyez@163.com
Yan-yan Yan
zwsanyan@163.com
Yun Liu
liokvie@163.com

[†]These authors have contributed equally to this work

**Specialty section:**
This article was submitted to Pharmacology of Anti-Cancer Drugs, a section of the journal Frontiers in Pharmacology

**Received:** 01 July 2020
**Accepted:** 24 August 2020
**Published:** 11 September 2020

**Citation:**
Su C-y, Li J-q, Zhang L-l, Wang H, Wang F-h, Tao Y-w, Wang Y-q, Guo Q-r, Li J-j, Liu Y, Yan Y-y and Zhang J-y (2020) The Biological Functions and Clinical Applications of Integrins in Cancers. Front. Pharmacol. 11:579068. doi: 10.3389/fphar.2020.579068

Integrins are the adhesion molecules and receptors of extracellular matrix (ECM). They mediate the interactions between cells-cells and cells-ECM. The crosstalk between cancer cells and their microenvironment triggers a variety of critical signaling cues and promotes the malignant phenotype of cancer. As a type of transmembrane protein, integrin-mediated cell adhesion is essential in regulating various biological functions of cancer cells. Recent evidence has shown that integrins present on tumor cells or tumor-associated stromal cells are involved in ECM remodeling, and as mechanotransducers sensing changes in the biophysical properties of the ECM, which contribute to cancer metastasis, stemness and drug resistance. In this review, we outline the mechanism of integrin-mediated effects on biological changes of cancers and highlight the current status of clinical treatments by targeting integrins.

**Keywords: integrins, cancer metastasis, drug resistance, stemness, extracellular matrix, therapeutic targeting**

## INTRODUCTION

The transformation process from normal cells to malignant cancer cells involves a series of complex pathological mechanisms, including the abnormal activation/deactivation of various cancer-related signaling molecules and signaling pathways (Cooper and Giancotti, 2019). Incipient cancer cells acquire multiple biological functions during their evolution that enable them to become tumorigenic and ultimately malignant (Hanahan and Weinberg, 2011). Integrins are widely present on the surface of cells and mediate the adhesion between cells -to -cells and cells to ECM (Hamidi and Ivaska, 2018). Accumulating evidence showed that integrins and integrin-dependent biological process play vital roles in mediating cancer stem-like property, cancer metastasis and drug resistance (Seguin et al., 2015; Hamidi et al., 2016; Cooper and Giancotti, 2019). Interaction between integrins and ECM enhances cell adhesion and activates cancer cell pro-survival and anti-apoptotic programs, resulting in the development of drug resistance (Leask, 2019). In addition, integrins are involved in the regulation of survival signaling of cancer stem cells (CSCs), which is another reason for developing cancer drug resistance (Seguin et al., 2015). A number of studies in recent years have reported that integrins on exosomes make a significant contribution in mediating cancer organotropic metastasis and preparing pre-metastatic niche (Hoshino et al., 2015;

Paolillo and Schinelli, 2017; Shimaoka et al., 2019). Hoshino et al. (2015) first demonstrated that tumor exosomal integrins mediated organotropic metastasis. Given the multiple biological functions mediated by integrins in cancers, integrins have been regarded as a promising target for cancer treatment. Although there are few successful clinical trials, many preclinical studies have shown encouraging results (Hamidi and Ivaska, 2018). Additionally, integrins, such as integrin αvβ3, integrin α6 and integrin α7 might have potential as cancer diagnostic and prognostic biomarkers (Seguin et al., 2015; Haas et al., 2017). In this review, we summarized current studies on the roles of integrins in cancer progression and its clinical value.

## INTEGRINS: AN OVERVIEW

Integrins consist of 18 α and 8 β subunits, that pair to form at least 24 different functional heterodimeric receptors (Humphries et al., 2006). Integrin heterodimers are transported from the endoplasmic reticulum to Golgi apparatus, where they are further post-translationally modified and transferred to the cell surface in an inactive state (De Franceschi et al., 2015). The integrin α and β subunits are both glycosylated, and their amino acid terminals are bonded to each other by a non-covalent bond, thereby forming αβ integrin heterodimers (Seguin et al., 2015). Some integrin subunits only appear in a single heterodimer, 12 integrins contain β1-subunits and five contain αv-subunits (Kechagia et al., 2019). As a receptor on the cell membrane, integrins mainly interact with ECM components to mediate cell adhesion (Dustin, 2019). According to different types of ECM components, integrins can be classified into two main categories: receptors that recognize Arg-Gly-Asp (RGD) peptide motifs and receptors that independent on RGD binding region (collagen receptors, laminin receptors and leukocyte-specific integrins) (Hamidi and Ivaska, 2018). On one hand, different types of integrins can recognize and bind the same ligand (Kechagia et al., 2019). For example, all five αv integrins (αvβ1, αvβ3, αvβ5, αvβ6, and αvβ8) and two β1 integrins (α5β1 and α8β1) and αIIbβ3 are RGD-binding integrins (Humphries et al., 2006). Integrins α1β1, α2β1, α10β1, and α11β1 binding to laminins and collagens (Humphries et al., 2006). The common feature of these integrins is that they contain an α-subunit of the αA-domain, which specifically bind to β1-subunit. Additionally, three β1 integrins (α3β1, α6β1, and α7β1) and α6β4 are highly selective laminin receptors (Marsico et al., 2018). Interestingly, the α-subunits of these integrins do not contain αA-domain (Marsico et al., 2018). Moreover, α4β1, α4β7, α9β1, and αEβ7 recognize similar sequences in their ligands. On the other hand, the same integrins can bind to multiple ligands (Kechagia et al., 2019). For instance, αvβ3 not only recognizes RGD peptide motifs but also binds to other ligands, including ADAM (a disintegrin and metalloprotease) family members, COMP (cartilage oligomeric matrix protein), connective tissue growth factor, ICAM-4 (intercellular cell adhesion molecule-4), and MMP-2 (Seguin et al., 2015). Other integrins that have been identified but less reported include αDβ2, αLβ2, αMβ2, and αXβ2 (Hamidi et al., 2016). Compare with RGD-independent integrins receptors, 8 types of integrins that recognize RGD motifs constitute a most important integrin receptor subfamily instrumental in cancers and their metastasis (Kechagia et al., 2019). However, not all integrins exert a tumor-supporting role in tumorigenesis. Studies have reported that laminin-binding integrins (α3β1 and α6β4) have opposite roles in tumors (Ramovs et al., 2017). Laminin-binding integrins have high affinity to the tetraspanin CD151, which in turn regulate the binding properties of integrin and ECM (Ramovs et al., 2017).

Integrins switch specific ligands from an inactive low avidity state to a high avidity state when binding with them (Shattil et al., 2010). Integrins with altered configuration mediate signal transduction from "outside-in" through physical connection between intracellular domain and actin cytoskeleton, and subsequently activate focal adhesion kinase (FAK) and SRC family kinase (SFK) (Seguin et al., 2015; Cooper and Giancotti, 2019). The activation of intracellular signals can mediate signal transduction from "inside-out," resulting in increased affinity of integrins and ligands. In conclusion, integrins act as "intermediate contacts" to transmit bidirectional transmembrane signals, thereby affecting the biological functions of cancer cells, including proliferation, metastasis, drug resistance, metabolism and cancer cell stemness (Seguin et al., 2015).

## INTEGRINS AND CANCER METASTASIS

Cancer metastasis is a complex multi-step process that requires cancer cells to invade from their primary tumor site, survive in the circulation, and eventually colonize on nearby or distant organs (Hoshino et al., 2015). It has gradually become clear that integrins participate in various aspects of these steps in tumor metastasis (Casal and Bartolomé, 2018). Integrins are the main receptors of ECM molecules, and cell adhesion mediated by them is crucial for the spread of cancer cells (Casal and Bartolomé, 2018). In addition, integrins participate in ECM remodeling, provided cancer pre-metastatic niche, and promote survival of circulating cancer cells (CTCs) and colonization of cancer cells in new metastatic sites (Wortzel et al., 2019). However, recent studies have reported that certain integrins, such as integrin α3β1 and α6β4, might exert an inhibitory role in cancer metastasis (Ramovs et al., 2017).

### Integrins Involve in ECM Remodeling

The TME is rich of ECM components, such as collagens, fibronectin, and laminins, and is the key regulator of cancer metastasis (Hamidi and Ivaska, 2018). In recent years, various studies have reported that integrins are involved in ECM remolding that provide a favorable microenvironment for tumor metastasis (Kai et al., 2019). For example, cancer-associated fibroblasts (CAFs), the most abundant tumor stromal cells in TME, mediated matrix remodeling and matrix deposition through integrins, resulting in increased tumor tissue stiffness (Handorf et al., 2015; Attieh et al., 2017; Jang and

Beningo, 2019). CAFs express a variety of integrins, such as integrin αvβ3 (Attieh et al., 2017), α5β1 (Erdogan et al., 2017), and α11 (Primac et al., 2019; Zeltz et al., 2019), that participate in the assembly of fibronectin in ECM and facilitate the conversion of fibronectin matrix to fibronectin and the deposition of CAFs on tumor stroma (Cavaco et al., 2018). Studies have shown that platelet-derived growth factor receptor (PDGFR) is an important intermediate mediator of integrin-mediated ECM remodeling (Erdogan et al., 2017). CAFs aligned fibronectin matrix by increasing non-muscle myosin II and PDGFRα-mediated contractility and traction forces and then converted it to fibronectin by α5β1 integrin (Erdogan et al., 2017). A study performed by Primac and colleagues showed that the crosstalk between CAFs-integrin α11 and PDGFRβ activated downstream JNK signaling pathway, leading to the production of tenascin C (an ECM molecule) (Primac et al., 2019). In addition, pericyte integrin α6β1, a laminin receptor, has been reported to control PDGFRβ and basement membrane structure, which plays a vital role in the stability of tumor blood vessels and the recruitment of pericytes (Reynolds et al., 2017). It is worth noted that tumor cells recruit CAFs and promote their survival by expressing integrins (Peng et al., 2018). Peng et al. (2018) showed that integrin αvβ6 on colon cancer cells induced inactive fibroblasts to become CAFs. Overexpression of integrin α9β1 in breast cancer promoted the recruitment of CAFs (Ota et al., 2014). Briefly, these findings indicated that integrin-mediated ECM remodeling in the TME enables CAFs and cancer cells to communicate with each other, consequently supporting cancer progression and metastasis (**Figure 1**).

## Interaction Between Integrins and ECM Promotes Cancer Invasion and Migration

Cell migration occurs in a variety of physiological and pathological processes, including wound healing, development, induction of immune response, and cancer metastasis (Maritzen et al., 2015). The invasion and migration of tumor cells not only allow cancer cells to spread to distant organs, but more importantly, the increased cell motility permits tumors to grow rapidly by avoiding the steric hindrance and crowding (Waclaw et al., 2015). In the complex regulatory network of tumor metastasis, integrin, as a key regulatory molecule, connects ECM and actin cytoskeleton to support tumor spread (Manninen, 2015). Accumulated studies have shown that integrins interact with a variety of ECM components, activate metastasis-related signaling pathways or molecules, and trigger cancer cell invasion and migration to adjacent tissues. For example, the interaction between integrin α9β1 and tenascin-C promoted the migration of glioblastoma and osteosarcoma cells as well as induced lung metastasis (Sun et al., 2018). Poor cell adhesion mediated by tenascin-C and integrin α9β1 inhibited actin stress fibers, resulting in decreased activity of MKL1 and YAP (Sun et al., 2018). In addition, the combination of integrin αvβ3 and ECM prote*in vitro*nectin upregulates mTOR activity, which overrides the inhibition by hypoxia and facilitates tumor

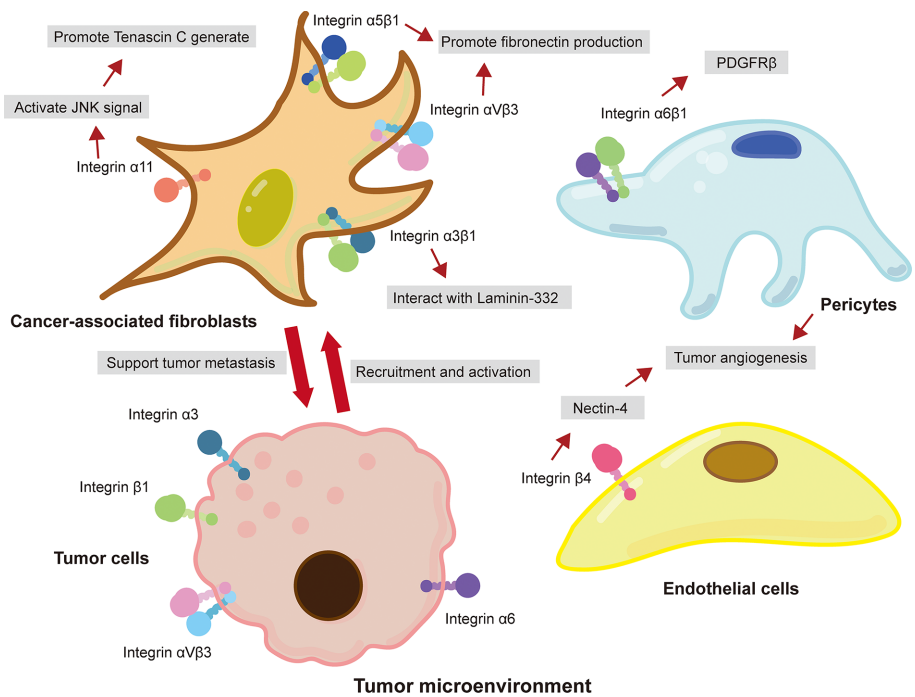


**FIGURE 1 |** Integrin-mediated crosstalk between cancer cells and tumor-associated stromal cells in the TME promotes cancer metastasis. Integrins expressed on CAFs interacted with ECM and promoted the metastasis of cancer cells. Cancer cells also expressed integrins to recruit and promote the activation of fibroblast. Moreover, pericytes and epithelial cells in TME promoted tumor angiogenesis through the interaction of integrins and ECM.

cell invasion (Pola et al., 2013). In oral squamous cell carcinoma, integrin α3 combines with laminin γ2 rich extracellular vesicles (EVs) is absorbed by lymphatic endothelial cells, resulting in enhanced lymphangiogenesis and tumor metastasis to lymph nodes (Wang S. H. et al., 2019). Interestingly, the α5 subunit of integrin α5β1 can be replaced by c-Met to form a c-Met/β1 complex, which has a much greater affinity for fibronectin than α5β1 integrin (Jahangiri et al., 2017). In addition, integrin-linked kinase phosphorylates c-Met, leading to ligand-independent receptor activation (Jahangiri et al., 2017). Crystallography showed that the c-Met/β1 complex could maintain a high-affinity β1 integrin conformation (Jahangiri et al., 2017). The cross-activation of c-Met/β1 integrin complex and its high affinity for fibronectin together drive invasive oncologic processes (Jahangiri et al., 2017).

In addition to activating metastasis-related signaling pathways, the interaction between integrins and ECM has also been reported to promote the intracellular circulation and plasma membrane expression of integrins *via* the endosomal pathway (Novo et al., 2018). The integrins produced through the endosomal pathway can regulate the accumulation and remodeling of proteins in the ECM, thereby facilitating the invasion of tumor cells into adjacent tissues (Novo et al., 2018). Mutant p53 tumor cells showed enhanced invasiveness, characterized by the recycling of Rab-coupling protein (RCP) and diacylglycerol kinase-α (DGKα)–dependent endosomal pathway (Novo et al., 2018). RCP is known for its ability to control integrin recycling (Muller et al., 2009). Mutant p53 tumor cells produced exosomes, which were transmitted horizontally to other tumor cells, and mediated invasiveness and migratory function by activating RCP-dependent integrin recycling (Novo et al., 2018). RCP-driven endocytic recycling of integrin α5β1 promoted actin-related protein 2/3 (ARP2/3) complex-independent ovarian cancer cell migration in 3D ECM rich in fibronectin (Paul et al., 2015). Further research found that ROCK-dependent phosphorylation and FH1/FH2 domain-containing protein 3 (FHOD3)–dependent activation were key mechanisms for cancer cells to mediate invasive migration *via* the RCP-α5β1 integrin pathway (Paul et al., 2015). These findings suggest that integrins play important roles in cancer migration and invasion, mainly through interaction with ECM.

## Integrin Mediates Organ-Specific Metastasis of Cancer Cells

The formation of a pre-metastatic niche is conducive to cancer metastasis to specific sites and colonization of distant organs. Recent evidence has shown that integrins on extracellular vesicles, especially exosomes, promote the establishment of pre-metastatic niche by interacting with cells or ECM at specific tissue sites (Hoshino et al., 2015; Huang et al., 2020). Hoshino and his collages first revealed that exosomal integrins secreted by tumor cell is the decisive factor for tumor organotropic metastasis (Hoshino et al., 2015). Lung-tropic cancer cells secreted α6β1- and α6β4-bearing exosomes preferentially transported to the lungs and were mainly taken up by $S100A4^+$ fibroblasts and $SPC^+$ epithelial cells (Hoshino et al., 2015). Similarly, liver-tropic cancer cells secreted αvβ5-bearing exosomes, which were preferentially distributed in the liver and were mainly taken up by $F4/80^+$ macrophages (Hoshino et al., 2015). Further research found that integrins α6β1 and α6β4 located in the lung bind to laminin in the lung microenvironment, while integrins αvβ5 located in the liver bind to fibronectin (Hoshino et al., 2015). In a study of colorectal cancer, it was found that the primary tumor secreted integrin β1-rich EVs were taken up by resident fibroblasts of remote organs (Ji et al., 2020). Fibroblasts were activated to secrete proinflammatory cytokines (IL-6, IL-8, IL-1β, α-SMA, TGF-β, and CXCL12) to induce the formation of pre-metastatic niche (Ji et al., 2020). It was worth noting that exosomes derived from CAFs also possessed ability to induce the formation of lung pre-metastatic niche (Kong et al., 2019). Exosomal integrin α2β1 of CAFs were uptaken by lung fibroblasts and activated TGF-β signaling pathway, which led to metastasis of salivary adenoid cystic carcinoma (Kong et al., 2019). In a nutshell, tumor exosome integrins are key molecules that mediate tumor cells organ-specific metastasis.

In addition, it has been reported that the integrins expressed on circulating tumor cells (CTC) also made a significant contribution to organ-specific metastasis of primary tumor cells (Aceto et al., 2014). For example, melanoma is prone to metastasize to different organs in human body, depending on the type of integrins expressed on circulating melanoma tumor cells (Huang and Rofstad, 2018). Melanoma cells expressing integrin β3 tend to metastasize to lungs, while melanoma cells expressing integrin β1 preferentially undergo lymph node metastasis (Vink et al., 1993; Hieken et al., 1999). Additionally, integrin of target organ endothelial cells can help infiltration of CTCs. The underlying mechanism may be related to regulating microvasculature (Huang and Rofstad, 2018). In conclusion, integrins interact with specific ECM components in the tissue microenvironment to promote the formation of pre-metastatic niche, thereby providing a favorable "soil" for cancer cells to metastasis and colonize in specific organs (**Figure 2**).

## The Opposing Roles of Integrins in Cancer Metastasis

Most studies have shown that upregulation/overexpression of integrins is closely associated with cancer metastasis. However, several studies reported that the role of integrins in different types of tumors and different stages of tumor development might be different, meaning that the role of integrins in tumors was complex (Longmate and Dipersio, 2017; Ramovs et al., 2019). For example, in HER2-driven breast cancer, downregulation of integrin α3β1 not only reduced the survival of mice, but also increased tumor growth and vascularization, resulting in an increased burden of lung metastasis (Ramovs et al., 2019). Another study on prostate cancer reported that integrin α3β1 inhibited cancer cell metastasis by regulating Hippo signaling pathway (Varzavand et al., 2016). Integrin α3β1 signals by Abl family kinases to suppress Rho GTPase activity, leading to the inhibition of Hippo pathway, and restrain prostate cancer

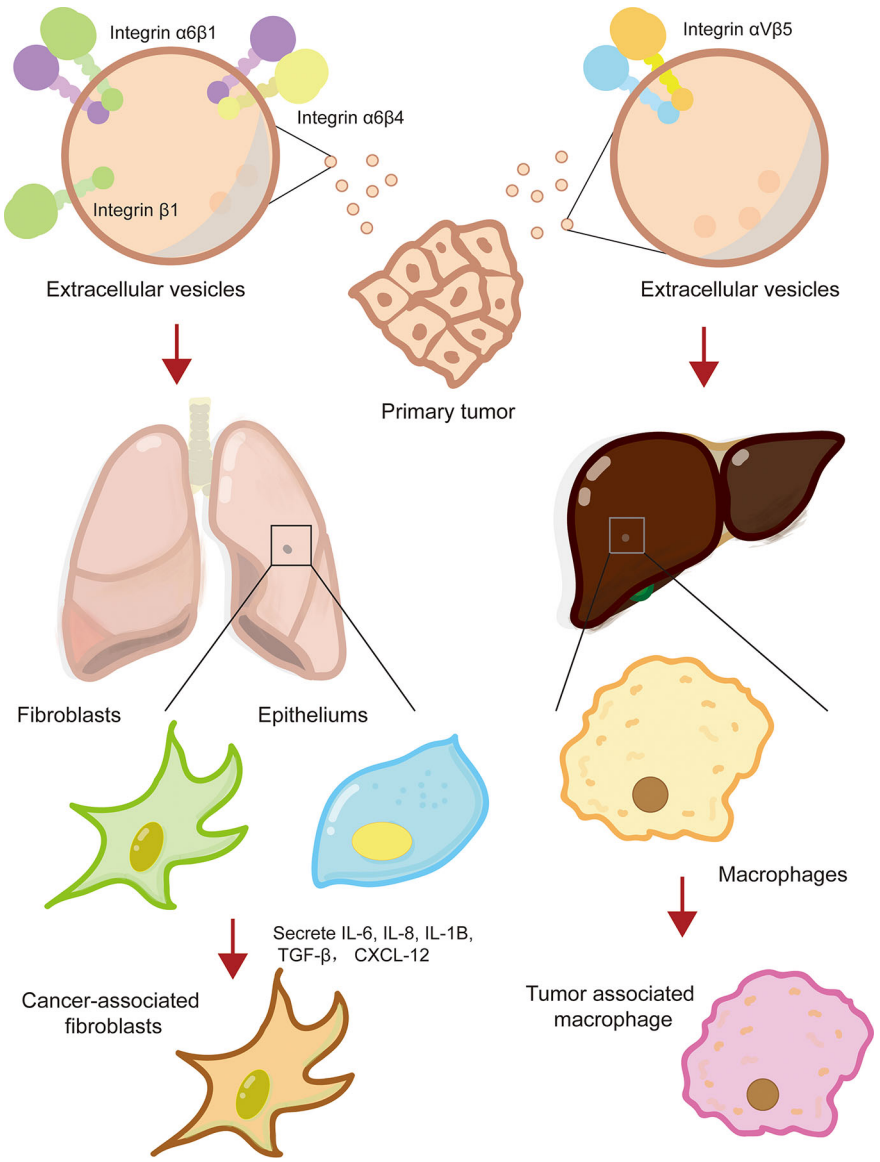


**FIGURE 2 |** Integrin mediates the formation of cancer pre-metastatic niche. Primary cancer cells secreted extracellular vesicles-containing multiple types of integrins, such that integrin α6β1, α6β4, and αvβ5, which reprogramed lung or live resident fibroblasts, epitheliums, and macrophage to cancer-supporting phenotype and facilitated the formation of cancer pre-metastatic niche.

migration and invasion (Varzavand et al., 2016). Moreover, integrin α9, a molecule related to cell adhesion, mobility and angiogenesis, has been reported to play opposite role in different types of cancers (Zhang et al., 2018; Wang Z. S. et al., 2019). The depletion of integrin α9 in triple-negative breast cancer significantly reduced tumor angiogenesis and metastasis (Wang Z. S. et al., 2019). Mechanistically, knockout of integrin α9 caused integrin-linked kinase (ILK) to relocate from cell membrane to cytoplasm. ILK interacted with protein kinase A (PKA) and inhibited its activity, subsequently increased activity of glycogen synthase kinase 3 (GSK3) and promoted the degradation of β-catenin (Wang Z. S. et al., 2019). However, in HCC, the overexpression of integrin α9 significantly suppressed cancer cell migration *in vitro* and tumor metastasis *in vivo* (Zhang et al., 2018). Thus, attention should be paid to the inhibitory effect of certain integrins in tumors when targeting integrins are used for tumor treatment. More studies are warranted to clarify the mechanisms (**Table 1**).

## INTEGRINS AND CANCER STEMNESS

Accumulating evidence suggested that crosstalk between integrins and cancer cells activated cancer cell stemness-related

**TABLE 1** | Role of integrins in cancer metastasis.

| Type of integrins | Cancer cell type/source | Ligand/downstream target | Functions | Ref. |
|---|---|---|---|---|
| α6β1/α6β4/αvβ5 | Breast cancer-Exo/Pancreatic cancer-Exo | S100 | Promote the formation of pre-metastasis niche | (Hoshino et al., 2015) |
| β1 | Colorectal cancer-EVs | IL-6, IL-8, IL-1β, α-SMA, TGF-β and CXCL12 | Promote the formation of pre-metastasis niche | (Ji et al., 2020) |
| | Hepatocellular carcinoma-Exo | IL-6/IL-8/NF-κB | Promote the formation of pre-metastasis niche | (Fang et al., 2018) |
| | Gastric cancer | Galectin-1 | Promote migration and invasion | (Kwan et al., 2017) |
| α2β1 | CAFs | TGF-β | Promote the formation of pre-metastasis niche | (Kong et al., 2019) |
| αvβ3 | CAFs | Fibronectin | Promote tumor invasion | (Attieh et al., 2017) |
| | Breast cancer | Vitronectin/mTOR; IL-8/PI3K/Akt/NF-κB | Promote tumor metastasis | (Pola et al., 2013) |
| | Pancreatic cancer-EVs | – | Promote tumor metastasis | (Shao et al., 2015) |
| α5β1 | CAFs | Fibronectin | Promote tumor migration | (Erdogan et al., 2017) |
| | Ovarian cancer | Rab-coupling protein | Promote tumor migration and invasion | (Paul et al., 2015) |
| α3β1 | Pancreatic duct adenocarcinoma | Laminin-332 | Promote tumor invasion | (Cavaco et al., 2018) |
| | Breast cancer | – | Inhibit tumor growth and vascularization | (Ramovs et al., 2019) |
| | Prostate cancer | Abl/Rho GTPase/Hippo | Inhibit tumor metastasis | (Varzavand et al., 2016) |
| αvβ6 | Colon cancer | TGF-β | Induce fibroblasts to CAFs and promote tumor metastasis | (Peng et al., 2018) |
| α11 | CAFs | PDGFRβ/JNK | Promote tumor metastasis | (Primac et al., 2019) |
| α6β1 | Pericyte | PDGFRβ/Akt-mTOR | Promote tumor angiogenesis | (Reynolds et al., 2017) |
| α5 | Ovarian cancer | – | Promote tumor metastasis | (Gao et al., 2019) |
| β3 | Breast cancer | IL-32/p38-MAPK | Promote EMT and invasion | (Wen et al., 2019) |
| α9β1 | Breast cancer | – | Promote lymphatic metastasis | (Ota et al., 2014) |
| α3 | Lymphatic endothelial cells | Laminin γ2 | Promote tumor metastasis to lymph nodes | (Wang S. H. et al., 2019) |
| β4 | Endothelial cells | Src, PI3K, Akt, and iNOS | Promote tumor angiogenesis | (Siddharth et al., 2018) |
| αx | HUVEC | VEGFR2/VEGF-A/PI3K/Akt/ | Promote tumor angiogenesis | (Wang J. S. et al., 2019) |
| α9β1 | Breast cancer | Tenascin-C | Promote migration and metastasis | (Sun et al., 2018) |
| α9 | Breast cancer | ILK/PKA/GSK3/β-catenin | Promote tumor angiogenesis and metastasis | (Wang Z. S. et al., 2019) |
| | Hepatocellular carcinoma | – | Inhibit tumor migration and metastasis | (Zhang et al., 2018) |

*Exo, exosomes; CAF, cancer-associated fibroblasts; TGF-β, transforming growth factor-β; α-SMA, α-smooth muscle actin; PDGFRβ, platelet-derived growth factor receptor β; HUVEC, human umbilical vein endothelial cell; VEGF, vascular endothelial growth factor; ILK, integrin-linked kinase; PKA, protein kinase A; GSK3, glycogen synthase kinase 3; "-", not mention.*

signaling pathways, which promoted the transformation of stem-like phenotype and caused the transformation of non-CSCs to CSCs (Seguin et al., 2015). In addition, integrins are biomarkers for normal adult stem and progenitor cells. Recent studies have found that these integrins, such as integrin β1, β4, α6, and α7 also exist on CSCs, that could help identify CSC phenotype (Bierie et al., 2017; Moon et al., 2019; Ge et al., 2020).

## INTEGRINS AS BIOMARKER OF CANCER STEM CELLS

Cancer cells with overexpression of certain specific integrins exhibit the characteristics of CSCs, suggesting that integrins may become potential biomarkers of CSCs (Haas et al., 2017; Krebsbach and Villa-Diaz, 2017). In fact, integrins β1, α6, and β3 have been found to be overexpressed in normal adult stem and progenitor cells, and recent studies have shown that they are also biomarkers of CSCs. Enrichment of integrin α6 is found in a variety of CSCs, including breast cancer (Brantley et al., 2016), glioblastoma (GSC) (Herrmann et al., 2020), colorectal cancer (Haraguchi et al., 2013) and squamous cell carcinoma (Schober and Fuchs, 2011). Moreover, the overexpression of integrin β4 is associated with enhanced self-renewal ability and chemotherapy resistance in lung cancer cells. Similarly, integrin β4 is overexpressed in GSCs and breast CSCs (Ma et al., 2019). Inhibiting the expression of integrin β4 reduced the self-renewal capacity and tumorigenicity of CSCs (Bierie et al., 2017; Ma et al., 2019). These findings suggest that integrin β4 may be used as a novel biomarker for CSCs. In addition, studies showed that integrin α7 might be a potential biomarker for CSCs (Haas et al., 2017). Integrin α7 is usually up-regulated in CSCs and tumor tissues, which associated with poor clinical characteristics and poor prognosis of patients (Ming et al., 2016; Ge et al., 2020; Lv et al., 2020). Thus, specific integrins can help identify a small subset of the most aggressive and dangerous cancer cells, and provide beneficial information for the diagnosis and prognosis of tumor patients.

### Activation of Integrin Signaling Promotes Cancer Stemness

Recent studies have shown that activation of integrin signaling pathways plays crucial roles in the regulation of cancer cell stemness (Cooper and Giancotti, 2019). Interestingly, current

studies indicate that integrins regulate tumor stemness in either a ligand-dependent or a ligand-independent manner. For example, GSCs grown on laminin-coated dishes showed overexpression of integrin αvβ3 and αvβ5, which was related to phosphorylation of FAK and protein kinase B (Paolillo et al., 2018). This result indicates that the interaction of integrins αvβ3 and αvβ5 with laminin is necessary for regulating the stemness of GSCs. Breast CSCs produced Laminin 511, which acted as a ligand for α6Bβ1 integrin and subsequently activated Hippo transducer TAZ to promote the self-renewal ability of cancer cells (Chang et al., 2015). Moreover, colorectal cancer cells cultured on 2D collagen showed enhanced cancer stemness (Wu X. et al., 2019). Mechanistic studies have shown that the interaction of collagen-integrin α2β1 activates the PI3K/Akt/Snail signaling pathway, resulting in enhanced metastasis and stemness of colorectal cancer cells (Wu X. et al., 2019). In pancreatic cancer, integrin αvβ3 interacted with osteopontin on pancreatic stellate cells, which led to the activation of αvβ3-Akt/Erk-FOXM1 (forkhead box protein M1) cascade and promoted CSC-like properties of pancreatic cancer (Cao et al., 2019). However, Seguin et al. (2014) showed that integrin αvβ3 promoted the stemness and drug resistance of lung and pancreatic cancer in a ligand-independent manner. The unliganded integrin αvβ3 had the ability to recruit KRAS and RalB to the plasma membrane of tumor cells, which subsequently led to the activation of TBK1 and NF-κB (Seguin et al., 2014). Indeed, several studies have found that integrins may affect CSCs independent of their capacity to interact with the ECM ligands. Ge et al. (2020) demonstrated that integrin α7 regulated the stemness of HCC by activating PTK2-PI3K-Akt signaling pathway. GSCs used integrin αvβ8 to drive tumor initiation and progression (Guerrero et al., 2017). The activation of integrin αvβ8-TGFβ1 signaling pathway was crucial for the self-renewal of GSCs (Guerrero et al., 2017). Additionally, activation of integrin β1-Notch1 signaling pathway promoted the self-renewal ability and xenograft tumorigenicity of head and neck squamous cell carcinoma (Moon et al., 2019). It is worth noting that integrin α6 and fibroblast growth factor receptor 1 (FGFR1) play a synergistic role in enhancing the expression of glioblastoma stem-related factors and the growth of tumor spheroids (Kowalski-Chauvel et al., 2019). The activation of integrin α6-FAK-STAT3 signaling pathway significantly increased the tumorigenicity and drug resistance of GSCs. (Herrmann et al., 2020). To sum up, integrins activate a variety of downstream signaling pathways in a ligand-dependent or ligand-independent manner, thereby regulating the stemness of tumor cells (**Table 2**).

## INTEGRINS AND CANCER DRUG RESISTANCE

More and more studies have elucidated the mechanisms of acquisition and development of cancer drug resistance (Naci et al., 2015; Cruz Da Silva et al., 2019). It is known that resistance to anti-cancer therapies is driven by not only internal factors, such as genetic mutations and epigenetics but also external factors (Seguin et al., 2015). Tumor cells acquired drug resistance by adaptive responses to external stimuli, activation of certain pro-survival signals/anti-apoptotic programs, selection of drug-resistant subpopulations, and alteration of microenvironmental features (Eke and Cordes, 2015; Seguin et al., 2015). Cell adhesion mediated by the interaction between integrins and ECM has been proved to be one of the strategies for tumor cells to evade anti-tumor therapies (Eke and Cordes, 2015).

### Abnormal Activation of Integrin-Driven Signals Leads to Tumor Drug Resistance

Tumor cells often develop resistance to certain targeted drugs (such as tyrosine kinase inhibitors) (Wu and Fu, 2018). One of the reasons is that tumor cells overexpress integrin molecules and activate downstream signaling pathways, thereby triggering cell proliferative signals independent of receptor tyrosine kinase and bypassing the blocking effect of targeted drugs (Kim et al., 2017). It has been reported that activation of integrin β1-driven signal plays a key role in resistance to tumor treatment (Kim et al., 2017; Yang et al., 2018). For example, integrin β1-driven Src-Akt hyperactivation triggered EGFR ligand-independent proliferation signaling in PDAC, resulting in the failure of cetuximab treatment (Kim et al., 2017). Interestingly, Neuropilin-1 (NRP1) physically interacted with active integrin β1, which could be blocked by NRP1 targeting peptide TPP11 (Kim et al., 2017). Therefore, co-targeting EGFR and integrin β1 could produce a synergistic effect, reversing the resistance of PDAC to cetuximab therapy (Kim et al., 2017). In addition, integrin β1 promoted PDAC resistance to gemcitabine by activating the Cdc42 molecule on the PI3Kp110β signaling

**TABLE 2** | Role of integrins in the maintenance of tumor stemness.

| Type of integrins | Cancer cell type/source | Ligand/downstream target | Functions | Ref. |
|---|---|---|---|---|
| α7 | Tongue squamous cell carcinoma | FAK | Enhance tumor stemness, EMT | (Ming et al., 2016) |
| | Hepatocellular carcinoma | PTK2-PI3K-Akt | Enhance tumor stemness | (Ge et al., 2020) |
| α6 | Breast cancer | HIF | Enhance tumor stemness | (Brooks et al., 2016) |
| | Breast cancer | AhR | Promote mammospheres formation | (Brantley et al., 2016) |
| | Glioblastoma | FGFR1/FOXM1 | Enhance tumor stemness | (Kowalski-Chauvel et al., 2019) |
| | Glioblastoma | FAK-STAT3 | Enhance tumorigenicity and resistance | (Herrmann et al., 2020) |
| αvβ3 | Pancreatic cancer | OPN/Akt-Erk-FOXM1 | Enhance tumor stemness | (Cao et al., 2019) |
| αvβ8 | Glioblastoma stem cells | TGFβ1 | Promote self-renewal | (Guerrero et al., 2017) |
| β4 | Breast cancer | – | Enhance tumorigenicity | (Ma et al., 2019) |
| α6Bβ1 | Breast cancer stem cells | Laminin 511/Hippo/TAZ | Promote self-renewal | (Chang et al., 2015) |

*HIF, hypoxia inducible factor; AhR, aryl hydrocarbon receptors; FGFR1, fibroblast growth factor receptor 1; FOXM1, Fokhead Box M1; OPN, osteopontin; "-", not mention.*

pathway (Yang et al., 2018). In head and neck cancer, targeting integrin β1 enhanced the sensitivity on cancer cells (Eke et al., 2012; Koppenhagen et al., 2017). c-Abl tyrosine kinase is an important mediator of β1-integrin signaling for radioresistance. AIIB2 (targets integrin β1)/imatinib (targets c-Abl) dual-targeted therapy has radiosensitization effect on tumor cells that grown on 3D laminin-rich ECM cultures and significantly inhibited the DNA damage repair ability of head and neck cancer cells (Koppenhagen et al., 2017). Additionally, a study performed by Eke et al. (2015) showed that simultaneous targeting integral β1 and EGFR had a radiosensitization effect on head and neck cancer. AIIB2 combined with cetuximab and X-ray enhanced cytotoxicity and radiosensitization in various head and neck cancer cells (Eke et al., 2015). Moreover, studies have shown that long-term use of trastuzumab + pertuzumab + buparlisib (PI3K inhibitors) combination treatment in $HER2^+$/PIK3CAH1047R transgenic mice with breast cancer produces buparlisib resistant tumors (Hanker et al., 2017; Wang and Xu, 2019). RNA sequencing showed that the genes of ECM and cell adhesion were significantly up-regulated, accompanied by activation of integrin β1/Src signaling pathway (Hanker et al., 2017). It was worth mentioning that this drug-resistant tumor only showed resistance to buparlisib when cells were coated on collagen or re-introduced into mice, while those cells were sensitive to buparlisib *in vitro* 2D culture (Hanker et al., 2017). This result indicated that collagen/integrin β1/Src signal transduction was a key regulatory pathway that mediated the resistance of $HER2^+$ breast cancer to anti-HER and anti-PI3K inhibitor combination therapy. In addition to integrin β1, another study found that activation of the integrin α6/Src/Akt signal transduction pathway mediated the resistance of breast cancer cells to tamoxifen (Campbell et al., 2018). Upregulation of integrin α6 was found both in tamoxifen-resistant breast cancer cells and tumor tissue sections from patients who relapsed on tamoxifen treatment (Campbell et al., 2018). In short, integrin is a promising anti-tumor target, and the combination of targeted integrin and other anti-tumor therapies (radiotherapy, chemotherapy, and targeted therapy) has the potential to reverse tumor resistance.

## Crosstalk Between Integrins and ECM Promotes Tumor Drug Resistance

A number of studies have shown that interaction between integrin and ECM is crucial for cancers to develop drug resistance (Azzariti et al., 2016; Jin et al., 2019). Jin et al. (2019) identified that integrin β8 in ECM-based 3D cell culture regulated PDAC resistance to ionizing radiation and cytotoxic drugs. Clinically, patients with HCC often show resistance to sorafenib (Azzariti et al., 2016). Recent studies have shown that HCC resistance to sorafenib is associated with the ECM protein laminin-332 produced by hepatic stellate cells in the HCC TME (Azzariti et al., 2016). The activation of laminin-332-integrin α3 signaling axis reversed the dephosphorylation of sorafenib on FAK, leading to drug resistance (Azzariti et al., 2016). Indeed, ECM stiffening endows tumor cells a strong resistance to chemotherapy. In the collagen-rich microenvironment, the activation of integrin β1 and its downstream effector JNK mediated resistance to sorafenib in triple-negative breast cancer (Nguyen et al., 2014). In addition, resistance to Adriamycin in patients with T-cell acute lymphoblastic leukemia might be due to the interaction between integrin β1 and matrigel that activated the ABCC1 drug transporter (Berrazouane et al., 2019). Glucocorticoid drugs are often used to reduce the toxic and side effects of chemotherapeutic drugs (Chen et al., 2010). However, recent studies have found that dexamethasone increased the levels of integrin β1, α4, and α5 in ovarian cancer cells and enhanced the cancer cells adherent to ECM, thereby mediating resistance to cisplatin and paclitaxel-induced apoptosis (Chen et al., 2010). Another study in ovarian cancer revealed that the combination of ECM protein TGFBI (transforming growth factor beta induced) and integrin β3 mediated the resistance of cancer cells to paclitaxel (Tumbarello et al., 2012). The RGD motif present in the carboxy-terminus of TGFBI is essential for cell adhesion (Tumbarello et al., 2012; Zou et al., 2018) (**Figure 3**). Thus, it would be a promising strategy to reduce or inhibit integrin-mediated ECM stiffness and degradation to achieve homeostasis in ECM, which will increase the penetration of anti-tumor drugs (**Table 3**).

# CURRENT CANCER THERAPEUTIC STRATEGIES BY TARGETING INTEGRINS: CHALLENGES AND OPPORTUNITIES

The interaction between integrins and their ligands activates downstream signaling molecules and leads to a series of cell biological processes, such as proliferation, differentiation, migration, invasion and development of drug resistance (Huang and Rofstad, 2018). With the elucidation of the mechanisms of integrin-ligand interaction and the encouraging results shown by *in vitro* experiments, integrin targeted drugs and the clinical trials are developed (Stupp et al., 2014). Despite the small number of successful clinical trials, integrins are considered as potential targets for cancer treatment (Hamidi and Ivaska, 2018). More importantly, integrins are also valuable probes in cancer imaging studies and can be used to determine prognosis and therapeutic efficacy (Haas et al., 2017; Huang et al., 2017).

## Main Challenges of Integrins as Therapeutic Targets

Currently, drugs or inhibitors are primarily designed to interfere with integrin-ligand interactions, with the treatment strategy targets integrin itself. However, such treatment strategy has encountered challenges in clinical trials. Multiple clinical studies have shown that integrin-selective inhibitors have not achieved the expected efficacy, whether used alone or in combination with chemoradiation. A multicenter, open-label, phase III study

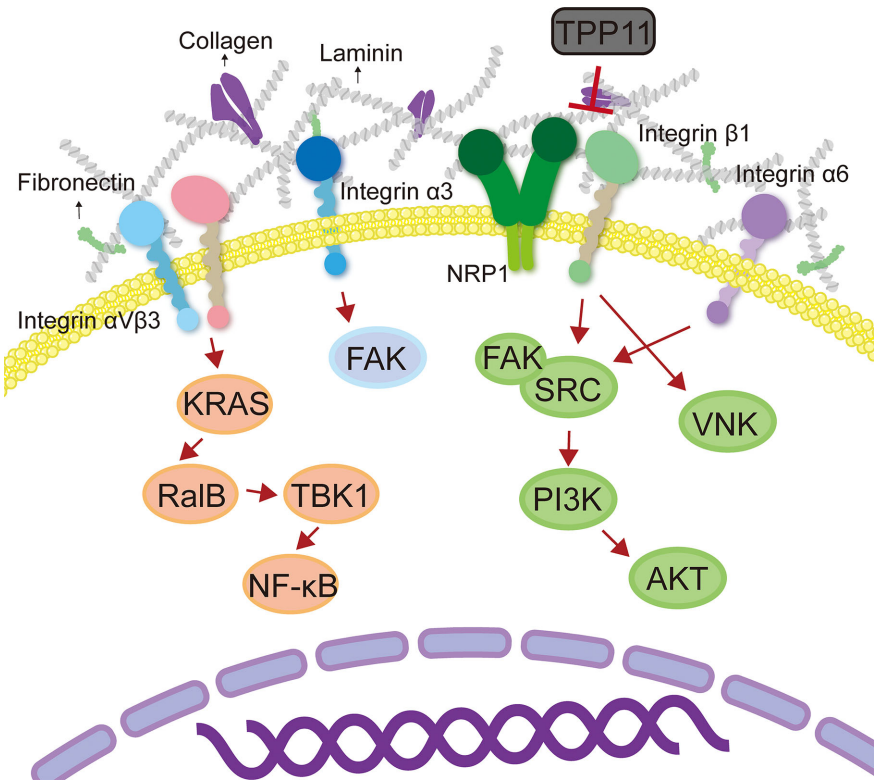


**FIGURE 3 |** Integrin mediates tumor therapy resistance. Crosstalk between integrins and ECM promoted tumor drug resistance by activating the downstream signaling pathways.

**TABLE 3 |** Role of integrins in cancer therapy resistance.

| Type of integrins | Cancer cell type/source | Ligand/downstream target | Functions | Ref. |
|---|---|---|---|---|
| β1 | Pancreatic ductal carcinoma | EGFR/Src-Akt | Promote proliferation; and cetuximab resistance | (Kim et al., 2017) |
| | Pancreatic ductal carcinoma | Cdc42/PI3Kp110β | Gemcitabine resistance | (Yang et al., 2018) |
| | Head and neck cancer | c-Abl | Enhance DNA damage repair and radioresistance | (Koppenhagen et al., 2017) |
| | Head and neck cancer | EGFR | Cetuximab resistance and radioresistance | (Eke et al., 2015) |
| | Breast cancer | Src/PI3K | Resistance to anti-HER and anti-PI3K inhibitor | (Hanker et al., 2017) |
| | Breast cancer | JNK | Sorafenib resistance | (Nguyen et al., 2014) |
| | T-cell acute lymphoblastic leukemia cells | ABCC1 | Doxorubicin resistance | (Berrazouane et al., 2019) |
| α6 | Breast cancer | Src-Akt | Tamoxifen resistance | (Campbell et al., 2018) |
| α3 | Hepatocellular carcinoma | Laminin-332/FAK | Sorafenib resistance | (Azzariti et al., 2016) |
| β3 | Ovarian cancer cells | TGFBI | Paclitaxel resistance | (Tumbarello et al., 2012) |
| | Melanoma stem cell-like cells | – | Doxorubicin and methotrexate resistance | (Zhu et al., 2019) |
| β8 | Glioblastoma-initiating cells | – | Radioresistance | (Jin et al., 2019) |
| αvβ3 | Lung cancer, breast cancer and pancreatic cancer | KRAS/RalB/TBK1/NF-κB | Enhance tumor stemness and resistance | (Seguin et al., 2014) |

*EGFR, epidermal growth factor receptor; TGFBI, transforming growth factor beta induced; "-", not mention.*

(NCT00689221) evaluated the efficacy of cilengitide (a selective αvβ3 and αvβ5 integrin inhibitor) and standard treatment (temozolomide combined with radiochemotherapy) in newly diagnosed glioblastoma (particularly in tumors with methylated MGMT promoter) (Stupp et al., 2014). Unfortunately, cilengitide has not shown significant benefits for treatment, neither the overall survival nor the prognosis was improved (Stupp et al., 2014; Nabors et al., 2015). Another phase I study (NCT00979862)

on cilengitide also yielded frustrating results (Gerstner et al., 2015). Cilengitide plus cediranib was used for the treatment of recurrent glioblastoma showed well tolerance, but the survival and response rate did not warrant further development of this combination (Gerstner et al., 2015). Given the current clinical trial data, cilengitide has been discontinued for the treatment of glioblastoma. However, a phase II clinical trial (CERTO) showed that cilengitide plus cetuximab and platinum-based chemotherapy used in advance NSCLC patients showed potential clinical significance (Vansteenkiste et al., 2015). Compared with the control group, the cilengitide combined group had an improved progression-free survival (PFS) trend (Vansteenkiste et al., 2015). Another phase I study (NCT01118676) for stage III NSCLC patients found that continuous infusion of cilengitide plus chemoradiotherapy showed remarkably favorable clinical response, with a PFS and OS of 14.4 and 29.4 months, respectively (Massabeau et al., 2018). Therefore, although cilengitide has not been further developed as an anti-cancer drug, integrins are still potentially interesting therapeutic targets (Vansteenkiste et al., 2015; Haddad et al., 2017; Yuan et al., 2019).

In addition to cilengitide, several clinical trials have also investigated the efficacy of other integrin-targeted drugs combined with chemotherapeutic drugs, such as abituzumab (a humanized antibody specific for αv integrin) and MINT1526A (an anti-α5β1 monoclonal antibody) (Wirth et al., 2014; Élez et al., 2015; Hussain et al., 2016; Weekes et al., 2018). NCT01008475 was a randomized phase I/II POSEIDON trial that evaluated the efficacy and safety of abituzumab combined with cetuximab plus irinotecan in KRAS wild-type metastatic colorectal cancer (Élez et al., 2015). Although abituzumab did not show improved PFS, it produced an overall survival benefit for patients with high expression of integrin αvβ6 (Élez et al., 2015). In addition, two other clinical trials of castration-resistant prostate cancer (NCT00958477 and NCT01360840) showed that abituzumab was not significantly extended PFS but had potential clinical activity and was worthy of further study (Wirth et al., 2014; Hussain et al., 2016). Moreover, a phase I study (NCT01139723) showed that MINT1526A with or without bevacizumab was well-tolerant and had a preliminary combined effect, although it could not be distinguished from bevacizumab monotherapy (Weekes et al., 2018). In conclusion, the combination of integrin-targeted therapy and chemotherapeutics has potential clinical application value, but there is still a need to develop more effective integrin-specific targeted drugs.

## Potential Treatment Opportunities

Since inhibitors that directly target integrin have not been successfully reflected in clinical treatment, other alternative strategies for inhibiting integrin were developed. Gao et al. (2016) combined integrin-targeted treatment strategy with tumor photodynamic therapy, with the goal of triggering the host immune response to achieve tumor clearance. They used phthalocyanine dye-labeled probes to perform photodynamic therapy on tumors targeted by integrin αvβ6, which significantly inhibit lung metastasis in the mouse breast cancer model (Gao et al., 2016). In addition, the treatment promoted the maturation of dendritic cells and the killing activity of $CD8^+$ T cells (Gao et al., 2016). Combining integrin-targeted therapy with cancer immunotherapy is another potential strategy. Kwan et al. (2017) prepared an integrin-binding peptide fused to the antibody Fc-domain and used it together with the engineered mouse serum albumin/IL-2 fusion, which significantly improve the survival of various types of tumor mouse models. This treatment strategy promoted the activation of $CD8^+$ T cells and natural killer cells by activating the host immune system, rather than blocking the integrin function to achieve therapeutic effects (Kwan et al., 2017).

The overexpression of integrin in cancer cells makes it a promising molecular target in integrin targeting-probes for non-invasive medical imaging and development of biomarkers (Cooper and Giancotti, 2019; Xiao et al., 2019). Recently, the development of radiotracers for integrin targets was used to predict the overall survival and prognosis of patients (Huang et al., 2017). An early phase I clinical trial (NCT04289532) was the first to use 99mTc-RWY, a radiotracer targeting integrin α6, to conduct SPECT (single-photon emission computed tomography) imaging in breast cancer patients. Moreover, Huang et al. (2017) used the integrin α2β1 targeting 68Ga-DOTA-A2B1-PET (positron emission tomography) imaging to identify the phenotypes of aggressive lung cancer and monitor drug responses. Interestingly, PET imaging of the RGD motif-containing αvβ6 integrin-binding peptides SFLAP3 also showed the potential for diagnosing head and neck squamous cell carcinoma (Roesch et al., 2018). Other similar radiotracers include RDG-K5 PET/CT for integrin αvβ3, which has the potential to identify patients with incomplete response to concurrent chemoradiotherapy (Chen et al., 2016). In addition to being a molecular targeted probe, integrins can also be used for cancer diagnosis and prognosis by directly detecting the expression level of specific integrins in serum or tissues. For example, integrin αvβ3 has been shown to be a potential diagnostic and prognostic biomarker in a variety of cancers, including gastric cancer (Böger et al., 2015), breast cancer (Radwan et al., 2019), glioblastoma (Zhang et al., 2019), and lung cancer (Schniering et al., 2019). It is worth noting that new anti-cancer therapies targeting integrins using nanoparticles as carriers are emerging. The treatment strategy is to use integrin-specific ligands to engineer nanoparticles, thereby increasing their affinity for cancer cells (Wu P. H. et al., 2019). In summary, integrins have shown great potential in the diagnosis, prognosis, and treatment of cancer. However, more clinical trials are needed for further verification.

# CONCLUSIONS

As a cell membrane receptor, crosstalk between integrin and ECM is crucial for cancer metastasis, maintenance of cancer stemness, and drug resistance. Integrin-targeted treatment strategy is an emerging cancer treatment concept. Because of

the remarkable therapeutic effect of targeting integrin in preclinical research, more *in vitro* and preclinical studies are warranted to fully understand the mechanisms of integrin-mediated biological behavior of cancer cells, which will facilitate further development of drugs targeting integrin signaling pathways.

## AUTHOR CONTRIBUTIONS

CS, JL, and LZ wrote the first draft of the manuscript. HW, FW, YT, YW, QG, and JL organized the structure of the manuscript. JZ, YY and YL contributed conception of the work. All authors contributed to the article and approved the submitted version.

## FUNDING

This work was supported by National Natural Science Foundation of China (U1903126, 81773888, and 81902152), Natural Science Foundation of Guangdong Province (2020A151501005 and 2020A1515010605), Fund from Guangzhou Institute of Pediatrics/Guangzhou Women and Children's Medical Center (nos. YIP-2018-031 and IP-2018-012).

## REFERENCES

Aceto, N., Bardia, A., Miyamoto, D. T., Donaldson, M. C., Wittner, B. S., Spencer, J. A., et al. (2014). Circulating tumor cell clusters are oligoclonal precursors of breast cancer metastasis. *Cell* 158, 1110–1122. doi: 10.1016/j.cell.2014.07.013

Attieh, Y., Clark, A. G., Grass, C., Richon, S., Pocard, M., Mariani, P., et al. (2017). Cancer-associated fibroblasts lead tumor invasion through integrin-β3-dependent fibronectin assembly. *J. Cell Biol.* 216, 3509–3520. doi: 10.1083/jcb.201702033

Azzariti, A., Mancarella, S., Porcelli, L., Quatrale, A. E., Caligiuri, A., Lupo, L., et al. (2016). Hepatic stellate cells induce hepatocellular carcinoma cell resistance to sorafenib through the laminin-332/α3 integrin axis recovery of focal adhesion kinase ubiquitination. *Hepatology* 64, 2103–2117. doi: 10.1002/hep.28835

Berrazouane, S., Boisvert, M., Salti, S., Mourad, W., Al-Daccak, R., Barabé, F., et al. (2019). Beta1 integrin blockade overcomes doxorubicin resistance in human T-cell acute lymphoblastic leukemia. *Cell Death Dis.* 10, 357. doi: 10.1038/s41419-019-1593-2

Bierie, B., Pierce, S. E., Kroeger, C., Stover, D. G., Pattabiraman, D. R., Thiru, P., et al. (2017). Integrin-β4 identifies cancer stem cell-enriched populations of partially mesenchymal carcinoma cells. *Proc. Natl. Acad. Sci. U. S. A.* 114, E2337–E2346. doi: 10.1073/pnas.1618298114

Böger, C., Warneke, V. S., Behrens, H.-M., Kalthoff, H., Goodman, S. L., Becker, T., et al. (2015). Integrins αvβ3 and αvβ5 as prognostic, diagnostic, and therapeutic targets in gastric cancer. *Gastric Cancer* 18, 784–795. doi: 10.1007/s10120-014-0435-2

Brantley, E., Callero, M. A., Berardi, D. E., Campbell, P., Rowland, L., Zylstra, D., et al. (2016). AhR ligand Aminoflavone inhibits α6-integrin expression and breast cancer sphere-initiating capacity. *Cancer Lett.* 376, 53–61. doi: 10.1016/j.canlet.2016.03.025

Brooks, D. L. P., Schwab, L. P., Krutilina, R., Parke, D. N., Sethuraman, A., Hoogewjis, D., et al. (2016). TGA6 is directly regulated by hypoxia-inducible factors and enriches for cancer stem cell activity and invasion in metastatic breast cancer models. *Mol. Cancer* 15, 26. doi: 10.1186/s12943-016-0510-x

Campbell, P. S., Mavingire, N., Khan, S., Rowland, L. K., Wooten, J. V., Opoku-Agyeman, A., et al. (2018). AhR ligand aminoflavone suppresses α6-integrin-Src-Akt signaling to attenuate tamoxifen resistance in breast cancer cells. *J. Cell Physiol.* 234, 108–121. doi: 10.1002/jcp.27013

Cao, J., Li, J., Sun, L., Qin, T., Xiao, Y., Chen, K., et al. (2019). Hypoxia-driven paracrine osteopontin/integrin αvβ3 signaling promotes pancreatic cancer cell epithelial-mesenchymal transition and cancer stem cell-like properties by modulating forkhead box protein M1. *Mol. Oncol.* 13, 228–245. doi: 10.1002/1878-0261.12399

Casal, J. I., and Bartolomé, R. A. (2018). RGD cadherins and α2β1 integrin in cancer metastasis: A dangerous liaison. *Biochim. Biophys. Acta Rev. Cancer* 1869, 321–332. doi: 10.1016/j.bbcan.2018.04.005

Cavaco, A. C. M., Rezaei, M., Caliandro, M. F., Lima, A. M., Stehling, M., Dhayat, S. A., et al. (2018). The Interaction between Laminin-332 and α3β1 Integrin Determines Differentiation and Maintenance of CAFs, and Supports Invasion of Pancreatic Duct Adenocarcinoma Cells. *Cancers* 11, 14. doi: 10.3390/cancers11010014

Chang, C., Goel, H. L., Gao, H., Pursell, B., Shultz, L. D., Greiner, D. L., et al. (2015). A laminin 511 matrix is regulated by TAZ and functions as the ligand for the α6Bβ1 integrin to sustain breast cancer stem cells. *Genes Dev.* 29, 1–6. doi: 10.1101/gad.253682.114

Chen, Y. X., Wang, Y., Fu, C. C., Diao, F., Song, L. N., Li, Z.-B., et al. (2010). Dexamethasone enhances cell resistance to chemotherapy by increasing adhesion to extracellular matrix in human ovarian cancer cells. *Endocr. Relat. Cancer* 17, 39–50. doi: 10.1677/ERC-08-0296

Chen, S.-H., Wang, H.-M., Lin, C.-Y., Chang, J. T.-C., Hsieh, C.-H., Liao, C.-T., et al. (2016). RGD-K5 PET/CT in patients with advanced head and neck cancer treated with concurrent chemoradiotherapy: Results from a pilot study. *Eur. J. Nucl. Med. Mol. Imaging* 43, 1621–1629. doi: 10.1007/s00259-016-3345-1

Cooper, J., and Giancotti, F. G. (2019). Integrin Signaling in Cancer: Mechanotransduction, Stemness, Epithelial Plasticity, and Therapeutic Resistance. *Cancer Cell.* 35, 347–367. doi: 10.1016/j.ccell.2019.01.007

Cruz Da Silva, E., Dontenwill, M., Choulier, L., and Lehmann, M. (2019). Role of Integrins in Resistance to Therapies Targeting Growth Factor Receptors in Cancer. *Cancers* 11, 692. doi: 10.3390/cancers11050692

De Franceschi, N., Hamidi, H., Alanko, J., Sahgal, P., and Ivaska, J. (2015). Integrin traffic - the update. *J. Cell Sci.* 128, 839–852. doi: 10.1242/jcs.161653

Dustin, M. L. (2019). Integrins and Their Role in Immune Cell Adhesion. *Cell* 177, 499–501. doi: 10.1016/j.cell.2019.03.038

Eke, I., and Cordes, N. (2015). Focal adhesion signaling and therapy resistance in cancer. *Semin. Cancer Biol.* 31, 65–75. doi: 10.1016/j.semcancer.2014.07.009

Eke, I., Deuse, Y., Hehlgans, S., Gurtner, K., Krause, M., Baumann, M., et al. (2012). $\beta_1$Integrin/FAK/cortactin signaling is essential for human head and neck cancer resistance to radiotherapy. *J. Clin. Invest.* 122, 1529–1540. doi: 10.1172/JCI61350

Eke, I., Zscheppang, K., Dickreuter, E., Hickmann, L., Mazzeo, E., Unger, K., et al. (2015). Simultaneous β1 integrin-EGFR targeting and radiosensitization of human head and neck cancer. *J. Natl. Cancer Inst.* 107, dju419. doi: 10.1093/jnci/dju419

Élez, E., Kocáková, I., Höhler, T., Martens, U. M., Bokemeyer, C., Van Cutsem, E., et al. (2015). Abituzumab combined with cetuximab plus irinotecan versus cetuximab plus irinotecan alone for patients with KRAS wild-type metastatic colorectal cancer: the randomised phase I/II POSEIDON trial. *Ann. Oncol.* 26, 132–140. doi: 10.1093/annonc/mdu474

Erdogan, B., Ao, M., White, L. M., Means, A. L., Brewer, B. M., Yang, L., et al. (2017). Cancer-associated fibroblasts promote directional cancer cell migration by aligning fibronectin. *J. Cell Biol.* 216, 3799–3816. doi: 10.1083/jcb.201704053

Fang, T., Lv, H., Lv, G., Li, T., Wang, C., Han, Q., et al. (2018). Tumor-derived exosomal miR-1247-3p induces cancer-associated fibroblast activation to foster lung metastasis of liver cancer. *Nat. Commun.* 9, 191. doi: 10.1038/s41467-017-02583-0

Gao, L., Zhang, C., Gao, D., Liu, H., Yu, X., Lai, J., et al. (2016). Enhanced Anti-Tumor Efficacy through a Combination of Integrin αvβ6-Targeted Photodynamic Therapy and Immune Checkpoint Inhibition. *Theranostics* 6, 627–637. doi: 10.7150/thno.14792

Gao, Q., Yang, Z., Xu, S., Li, X., Yang, X., Jin, P., et al. (2019). Heterotypic CAF-tumor spheroids promote early peritoneal metastatis of ovarian cancer. *J. Exp. Med.* 216, 688–703. doi: 10.1084/jem.20180765

Ge, J. C., Wang, Y. X., Chen, Z. B., and Chen, D. F. (2020). Integrin alpha 7 correlates with poor clinical outcomes, and it regulates cell proliferation, apoptosis and stemness via PTK2-PI3K-Akt signaling pathway in hepatocellular carcinoma. *Cell Signal.* 66, 109465. doi: 10.1016/j.cellsig.2019.109465

Gerstner, E. R., Ye, X., Duda, D. G., Levine, M. A., Mikkelsen, T., Kaley, T. J., et al. (2015). A phase I study of cediranib in combination with cilengitide in patients with

recurrent glioblastoma. *Neuro Oncol.* 17, 1386–1392. doi: 10.1093/neuonc/nov085

Guerrero, P. A., Tchaicha, J. H., Chen, Z., Morales, J. E., Mccarty, N., Wang, Q., et al. (2017). Glioblastoma stem cells exploit the αvβ8 integrin-TGFβ1 signaling axis to drive tumor initiation and progression. *Oncogene* 36, 6568–6580. doi: 10.1038/onc.2017.248

Haas, T. L., Sciuto, M. R., Brunetto, L., Valvo, C., Signore, M., Fiori, M. E., et al. (2017). Integrin α7 Is a Functional Marker and Potential Therapeutic Target in Glioblastoma. *Cell Stem Cell.* 21, 35–50.e39. doi: 10.1016/j.stem.2017.04.009

Haddad, T., Qin, R., Lupu, R., Satele, D., Eadens, M., Goetz, M. P., et al. (2017). A phase I study of cilengitide and paclitaxel in patients with advanced solid tumors. *Cancer Chemother. Pharmacol.* 79, 1221–1227. doi: 10.1007/s00280-017-3322-9

Hamidi, H., and Ivaska, J. (2018). Every step of the way: integrins in cancer progression and metastasis. *Nat. Rev. Cancer* 18, 533–548. doi: 10.1038/s41568-018-0038-z

Hamidi, H., Pietilä, M., and Ivaska, J. (2016). The complexity of integrins in cancer and new scopes for therapeutic targeting. *Br. J. Cancer* 115, 1017–1023. doi: 10.1038/bjc.2016.312

Hanahan, D., and Weinberg, R. A. (2011). Hallmarks of cancer: the next generation. *Cell* 144, 646–674. doi: 10.1016/j.cell.2011.02.013

Handorf, A. M., Zhou, Y., Halanski, M. A., and Li, W.-J. (2015). Tissue stiffness dictates development, homeostasis, and disease progression. *Organogenesis* 11, 1–15. doi: 10.1080/15476278.2015.1019687

Hanker, A. B., Estrada, M. V., Bianchini, G., Moore, P. D., Zhao, J., Cheng, F., et al. (2017). Extracellular Matrix/Integrin Signaling Promotes Resistance to Combined Inhibition of HER2 and PI3K in HER2 Breast Cancer. *Cancer Res.* 77, 3280–3292. doi: 10.1158/0008-5472.CAN-16-2808

Haraguchi, N., Ishii, H., Mimori, K., Ohta, K., Uemura, M., Nishimura, J., et al. (2013). CD49f-positive cell population efficiently enriches colon cancer-initiating cells. *Int. J. Oncol.* 43, 425–430. doi: 10.3892/ijo.2013.1955

Herrmann, A., Lahtz, C., Song, J., Aftabizadeh, M., Cherryholmes, G. A., Xin, H., et al. (2020). Integrin α6 signaling induces STAT3-TET3-mediated hydroxymethylation of genes critical for maintenance of glioma stem cells. *Oncogene* 39, 2156–2169. doi: 10.1038/s41388-019-1134-6

Hieken, T. J., Ronan, S. G., Farolan, M., Shilkaitis, A. L., and Das Gupta, T. K. (1999). Molecular prognostic markers in intermediate-thickness cutaneous malignant melanoma. *Cancer* 85, 375–382. doi: 10.1002/(sici)1097-0142(19990115)85:2

Hoshino, A., Costa-Silva, B., Shen, T.-L., Rodrigues, G., Hashimoto, A., Tesic Mark, M., et al. (2015). Tumour exosome integrins determine organotropic metastasis. *Nature* 527, 329–335. doi: 10.1038/nature15756

Huang, R., and Rofstad, E. K. (2018). Integrins as therapeutic targets in the organ-specific metastasis of human malignant melanoma. *J. Exp. Clin. Cancer Res.* 37, 92. doi: 10.1186/s13046-018-0763-x

Huang, C. W., Hsieh, W. C., Hsu, S. T., Lin, Y. W., Chung, Y. H., Chang, W. C., et al. (2017). The Use of PET Imaging for Prognostic Integrin αβ Phenotyping to Detect Non-Small Cell Lung Cancer and Monitor Drug Resistance Responses. *Theranostics* 7, 4013–4028. doi: 10.7150/thno.19304

Huang, W., Yan, Y., Liu, Y., Lin, M., Ma, J., Zhang, W., et al. (2020). Exosomes with low miR-34c-3p expression promote invasion and migration of non-small cell lung cancer by upregulating integrin α2β1. *Signal Transduct. Target Ther.* 5:39. doi: 10.1038/s41392-020-0133-y

Humphries, J. D., Byron, A., and Humphries, M. J. (2006). Integrin ligands at a glance. *J. Cell Sci.* 119, 3901–3903. doi: 10.1242/jcs.03098

Hussain, M., Le Moulec, S., Gimmi, C., Bruns, R., Straub, J., and Miller, K. (2016). Differential Effect on Bone Lesions of Targeting Integrins: Randomized Phase II Trial of Abituzumab in Patients with Metastatic Castration-Resistant Prostate Cancer. *Clin. Cancer Res.* 22, 3192–3200. doi: 10.1158/1078-0432.CCR-15-2512

Jahangiri, A., Nguyen, A., Chandra, A., Sidorov, M. K., Yagnik, G., Rick, J., et al. (2017). Cross-activating c-Met/β1 integrin complex drives metastasis and invasive resistance in cancer. *Proc. Natl. Acad. Sci. U. S. A.* 114, E8685–E8694. doi: 10.1073/pnas.1701821114

Jang, I., and Beningo, K. A. (2019). Integrins, CAFs and Mechanical Forces in the Progression of Cancer. *Cancers* 11:721. doi: 10.3390/cancers11050721

Ji, Q., Zhou, L., Sui, H., Yang, L., Wu, X., Song, Q., et al. (2020). Primary tumors release ITGBL1-rich extracellular vesicles to promote distal metastatic tumor growth through fibroblast-niche formation. *Nat. Commun.* 11, 1211. doi: 10.1038/s41467-020-14869-x

Jin, S., Lee, W.-C., Aust, D., Pilarsky, C., and Cordes, N. (2019). β8 Integrin Mediates Pancreatic Cancer Cell Radiochemoresistance. *Mol. Cancer Res.* 17, 2126–2138. doi: 10.1158/1541-7786.MCR-18-1352

Kai, F., Drain, A. P., and Weaver, V. M. (2019). The Extracellular Matrix Modulates the Metastatic Journey. *Dev. Cell.* 49, 332–346. doi: 10.1016/j.devcel.2019.03.026

Kechagia, J. Z., Ivaska, J., and Roca-Cusachs, P. (2019). Integrins as biomechanical sensors of the microenvironment. *Nat. Rev. Mol. Cell Biol.* 20, 457–473. doi: 10.1038/s41580-019-0134-2

Kim, Y. J., Jung, K., Baek, D. S., Hong, S. S., and Kim, Y. S. (2017). Co-targeting of EGF receptor and neuropilin-1 overcomes cetuximab resistance in pancreatic ductal adenocarcinoma with integrin β1-driven Src-Akt bypass signaling. *Oncogene* 36, 2543–2552. doi: 10.1038/onc.2016.407

Kong, J., Tian, H., Zhang, F., Zhang, Z., Li, J., Liu, X., et al. (2019). Extracellular vesicles of carcinoma-associated fibroblasts creates a pre-metastatic niche in the lung through activating fibroblasts. *Mol. Cancer* 18, 175. doi: 10.1186/s12943-019-1101-4

Koppenhagen, P., Dickreuter, E., and Cordes, N. (2017). Head and neck cancer cell radiosensitization upon dual targeting of c-Abl and beta1-integrin. *Radiother. Oncol.* 124, 370–378. doi: 10.1016/j.radonc.2017.05.011

Kowalski-Chauvel, A., Gouaze-Andersson, V., Baricault, L., Martin, E., Delmas, C., Toulas, C., et al. (2019). Alpha6-Integrin Regulates FGFR1 Expression through the ZEB1/YAP1 Transcription Complex in Glioblastoma Stem Cells Resulting in Enhanced Proliferation and Stemness. *Cancers* 11, 406. doi: 10.3390/cancers11030406

Krebsbach, P. H., and Villa-Diaz, L. G. (2017). The Role of Integrin α6 (CD49f) in Stem Cells: More than a Conserved Biomarker. *Stem Cells Dev.* 26, 1090–1099. doi: 10.1089/scd.2016.0319

Kwan, B. H., Zhu, E. F., Tzeng, A., Sugito, H. R., Eltahir, A. A., Ma, B., et al. (2017). Integrin-targeted cancer immunotherapy elicits protective adaptive immune responses. *J. Exp. Med.* 214, 1679–1690. doi: 10.1084/jem.20160831

Leask, A. (2019). A centralized communication network: Recent insights into the role of the cancer associated fibroblast in the development of drug resistance in tumors. *Semin. Cell Dev. Biol.* 101, 111–114. doi: 10.1016/j.semcdb.2019.10.016

Longmate, W., and Dipersio, C. M. (2017). Beyond adhesion: emerging roles for integrins in control of the tumor microenvironment. *F1000Res.* 6, 1612. doi: 10.12688/f1000research.11877.1

Lv, Z., Yang, Y., and Yang, C. (2020). Integrin α7 correlates with worse clinical features and prognosis, and its knockdown inhibits cell proliferation and stemness in tongue squamous cell carcinoma. *Int. J. Oncol.* 56, 69–84. doi: 10.3892/ijo.2019.4927

Ma, B., Zhang, L., Zou, Y., He, R., Wu, Q., Han, C., et al. (2019). Reciprocal regulation of integrin β4 and KLF4 promotes gliomagenesis through maintaining cancer stem cell traits. *J. Exp. Clin. Cancer Res.* 38, 23. doi: 10.1186/s13046-019-1034-1

Manninen, A. (2015). Epithelial polarity–generating and integrating signals from the ECM with integrins. *Exp. Cell Res.* 334, 337–349. doi: 10.1016/j.yexcr.2015.01.003

Maritzen, T., Schachtner, H., and Legler, D. F. (2015). On the move: endocytic trafficking in cell migration. *Cell Mol. Life Sci.* 72, 2119–2134. doi: 10.1007/s00018-015-1855-9

Marsico, G., Russo, L., Quondamatteo, F., and Pandit, A. (2018). Glycosylation and Integrin Regulation in Cancer. *Trends Cancer* 4, 537–552. doi: 10.1016/j.trecan.2018.05.009

Massabeau, C., Khalifa, J., Filleron, T., Modesto, A., Bigay-Gamé, L., Plat, G., et al. (2018). Continuous Infusion of Cilengitide Plus Chemoradiotherapy for Patients With Stage III Non-Small-cell Lung Cancer: A Phase I Study. *Clin. Lung Cancer* 19, e277–e285. doi: 10.1016/j.cllc.2017.11.002

Ming, X. Y., Fu, L., Zhang, L. Y., Qin, Y. R., Cao, T. T., Chan, K. W., et al. (2016). Integrin α7 is a functional cancer stem cell surface marker in oesophageal squamous cell carcinoma. *Nat. Commun.* 7, 13568. doi: 10.1038/ncomms13568

Moon, J. H., Rho, Y. S., Lee, S. H., Koo, B. S., Lee, H. J., Do, S. I., et al. (2019). Role of integrin β1 as a biomarker of stemness in head and neck squamous cell carcinoma. *Oral. Oncol.* 96, 34–41. doi: 10.1016/j.oraloncology.2019.07.001

Muller, P., Caswell, P. T., Doyle, B., Iwanicki, M. P., Tan, E. H., Karim, S., et al. (2009). Mutant p53 drives invasion by promoting integrin recycling. *Cell* 139, 1327–1341. doi: 10.1016/j.cell.2009.11.026

Nabors, L. B., Fink, K. L., Mikkelsen, T., Grujicic, D., Tarnawski, R., Nam, D. H., et al. (2015). Two cilengitide regimens in combination with standard treatment

for patients with newly diagnosed glioblastoma and unmethylated MGMT gene promoter: results of the open-label, controlled, randomized phase II CORE study. *Neuro Oncol.* 17, 708–717. doi: 10.1093/neuonc/nou356

Naci, D., Vuori, K., and Aoudjit, F. (2015). Alpha2beta1 integrin in cancer development and chemoresistance. *Semin. Cancer Biol.* 35, 145–153. doi: 10.1016/j.semcancer.2015.08.004

Nguyen, T. V., Sleiman, M., Moriarty, T., Herrick, W. G., and Peyton, S. R. (2014). Sorafenib resistance and JNK signaling in carcinoma during extracellular matrix stiffening. *Biomaterials* 35, 5749–5759. doi: 10.1016/j.biomaterials.2014.03.058

Novo, D., Heath, N., Mitchell, L., Caligiuri, G., Macfarlane, A., Reijmer, D., et al. (2018). Mutant p53s generate pro-invasive niches by influencing exosome podocalyxin levels. *Nat. Commun.* 9, 5069. doi: 10.1038/s41467-018-07339-y

Ota, D., Kanayama, M., Matsui, Y., Ito, K., Maeda, N., Kutomi, G., et al. (2014). Tumor-α9β1 integrin-mediated signaling induces breast cancer growth and lymphatic metastasis via the recruitment of cancer-associated fibroblasts. *J. Mol. Med. (Berl).* 92, 1271–1281. doi: 10.1007/s00109-014-1183-9

Paolillo, M., and Schinelli, S. (2017). Integrins and Exosomes, a Dangerous Liaison in Cancer Progression. *Cancers* 9, 95. doi: 10.3390/cancers9080095

Paolillo, M., Galiazzo, M. C., Daga, A., Ciusani, E., Serra, M., Colombo, L., et al. (2018). An RGD small-molecule integrin antagonist induces detachment-mediated anoikis in glioma cancer stem cells. *Int. J. Oncol.* 53, 2683–2694. doi: 10.3892/ijo.2018.4583

Paul, N. R., Allen, J. L., Chapman, A., Morlan-Mairal, M., Zindy, E., Jacquemet, G., et al. (2015). α5β1 integrin recycling promotes Arp2/3-independent cancer cell invasion via the formin FHOD3. *J. Cell Biol.* 210, 1013–1031. doi: 10.1083/jcb.201502040

Peng, C., Zou, X. Q., Xia, W. Y., Gao, H. J., Li, Z. Q., Liu, N. Q., et al. (2018). Integrin αvβ6 plays a bi-directional regulation role between colon cancer cells and cancer-associated fibroblasts. *Biosci. Rep.* 38, BSR20180243. doi: 10.1042/BSR20180243

Pola, C., Formenti, S. C., and Schneider, R. J. (2013). Vitronectin-αvβ3 integrin engagement directs hypoxia-resistant mTOR activity and sustained protein synthesis linked to invasion by breast cancer cells. *Cancer Res.* 73, 4571–4578. doi: 10.1158/0008-5472.CAN-13-0218

Primac, I., Maquoi, E., Blacher, S., Heljasvaara, R., Van Deun, J., Smeland, H. Y., et al. (2019). Stromal integrin α11 regulates PDGFR-β signaling and promotes breast cancer progression. *J. Clin. Invest.* 130, 4609–4628. doi: 10.1172/JCI125890

Radwan, A. F., Ismael, O. E., Fawzy, A., and El-Mesallamy, H. O. (2019). Evaluation of Serum Integrin αvβ3 & Vitronectin in the Early Diagnosis of Breast Cancer. *Clin. Lab.* 65. doi: 10.7754/Clin.Lab.2019.181219

Ramovs, V., Te Molder, L., and Sonnenberg, A. (2017). The opposing roles of laminin-binding integrins in cancer. *Matrix Biol.* 57-58, 213–243. doi: 10.1016/j.matbio.2016.08.007

Ramovs, V., Secades, P., Song, J.-Y., Thijssen, B., Kreft, M., and Sonnenberg, A. (2019). Absence of integrin α3β1 promotes the progression of HER2-driven breast cancer in vivo. *Breast Cancer Res.* 21, 63. doi: 10.1186/s13058-019-1146-8

Reynolds, L. E., D'amico, G., Lechertier, T., Papachristodoulou, A., Muñoz-Félix, J. M., De Arcangelis, A., et al. (2017). Dual role of pericyte α6β1-integrin in tumour blood vessels. *J. Cell Sci.* 130, 1583–1595. doi: 10.1242/jcs.197848

Roesch, S., Lindner, T., Sauter, M., Loktev, A., Flechsig, P., Müller, M., et al. (2018). Comparison of the RGD Motif-Containing αβ Integrin-Binding Peptides SFLAP3 and SFITGv6 for Diagnostic Application in HNSCC. *J. Nucl. Med.* 59, 1679–1685. doi: 10.2967/jnumed.118.210013

Schniering, J., Benešová, M., Brunner, M., Haller, S., Cohrs, S., Frauenfelder, T., et al. (2019). Visualisation of interstitial lung disease by molecular imaging of integrin αvβ3 and somatostatin receptor 2. *Ann. Rheum. Dis.* 78, 218–227. doi: 10.1136/annrheumdis-2018-214322

Schober, M., and Fuchs, E. (2011). Tumor-initiating stem cells of squamous cell carcinomas and their control by TGF-β and integrin/focal adhesion kinase (FAK) signaling. *Proc. Natl. Acad. Sci. U. S. A.* 108, 10544–10549. doi: 10.1073/pnas.1107807108

Seguin, L., Kato, S., Franovic, A., Camargo, M. F., Lesperance, J., Elliott, K. C., et al. (2014). An integrin $\beta_3$-KRAS-RalB complex drives tumour stemness and resistance to EGFR inhibition. *Nat. Cell Biol.* 16, 457–468. doi: 10.1038/ncb2953

Seguin, L., Desgrosellier, J. S., Weis, S. M., and Cheresh, D. A. (2015). Integrins and cancer: regulators of cancer stemness, metastasis, and drug resistance. *Trends Cell Biol.* 25, 234–240. doi: 10.1016/j.tcb.2014.12.006

Shao, N., Lu, Z. H., Zhang, Y. J., Wang, M., Li, W., Hu, Z. Y., et al. (2015). Interleukin-8 upregulates integrin β3 expression and promotes estrogen receptor-negative breast cancer cell invasion by activating the PI3K/Akt/NF-κB pathway. *Cancer Lett.* 364, 165–172. doi: 10.1016/j.canlet.2015.05.009

Shattil, S. J., Kim, C., and Ginsberg, M. H. (2010). The final steps of integrin activation: the end game. *Nat. Rev. Mol. Cell Biol.* 11, 288–300. doi: 10.1038/nrm2871

Shimaoka, M., Kawamoto, E., Gaowa, A., Okamoto, T., and Park, E. J. (2019). Connexins and Integrins in Exosomes. *Cancers* 11, 106. doi: 10.3390/cancers11010106

Siddharth, S., Nayak, A., Das, S., Nayak, D., Panda, J., Wyatt, M. D., et al. (2018). The soluble nectin-4 ecto-domain promotes breast cancer induced angiogenesis via endothelial Integrin-β4. *Int. J. Biochem. Cell. Biol.* 102, 151–160. doi: 10.1016/j.biocel.2018.07.011

Stupp, R., Hegi, M. E., Gorlia, T., Erridge, S. C., Perry, J., Hong, Y.-K., et al. (2014). Cilengitide combined with standard treatment for patients with newly diagnosed glioblastoma with methylated MGMT promoter (CENTRIC EORTC 26071-22072 study): a multicentre, randomised, open-label, phase 3 trial. *Lancet Oncol.* 15, 1100–1108. doi: 10.1016/S1470-2045(14)70379-1

Sun, Z., Schwenzer, A., Rupp, T., Murdamoothoo, D., Vegliante, R., Lefebvre, O., et al. (2018). Tenascin-C Promotes Tumor Cell Migration and Metastasis through Integrin α9β1-Mediated YAP Inhibition. *Cancer Res.* 78, 950–961. doi: 10.1158/0008-5472.CAN-17-1597

Tumbarello, D. A., Temple, J., and Brenton, J. D. (2012). ß3 integrin modulates transforming growth factor beta induced (TGFBI) function and paclitaxel response in ovarian cancer cells. *Mol. Cancer* 11, 36. doi: 10.1186/1476-4598-11-36

Vansteenkiste, J., Barlesi, F., Waller, C. F., Bennouna, J., Gridelli, C., Goekkurt, E., et al. (2015). Cilengitide combined with cetuximab and platinum-based chemotherapy as first-line treatment in advanced non-small-cell lung cancer (NSCLC) patients: results of an open-label, randomized, controlled phase II study (CERTO). *Ann. Oncol.* 26, 1734–1740. doi: 10.1093/annonc/mdv219

Varzavand, A., Hacker, W., Ma, D., Gibson-Corley, K., Hawayek, M., Tayh, O. J., et al. (2016). α3β1 Integrin Suppresses Prostate Cancer Metastasis via Regulation of the Hippo Pathway. *Cancer Res.* 76, 6577–6587. doi: 10.1158/0008-5472.CAN-16-1483

Vink, J., Thomas, L., Etoh, T., Bruijn, J. A., Mihm, M. C., Gattoni-Celli, S., et al. (1993). Role of beta-1 integrins in organ specific adhesion of melanoma cells in vitro. *Lab. Invest.* 68, 192–203.

Waclaw, B., Bozic, I., Pittman, M. E., Hruban, R. H., Vogelstein, B., and Nowak, M. A. (2015). A spatial model predicts that dispersal and cell turnover limit intratumour heterogeneity. *Nature* 525, 261–264. doi: 10.1038/nature14971

Wang, J. N., and Xu, B. H. (2019). Targeted therapeutic options and future perspectives for HER2-positive breast cancer. *Signal Transduct. Target Ther.* 4, 34. doi: 10.1038/s41392-019-0069-2

Wang, J. S., Yang, L., Liang, F., Chen, Y. P., Yang, G., et al. (2019). Integrin alpha x stimulates cancer angiogenesis through PI3K/Akt signaling-mediated VEGFR2/VEGF-A overexpression in blood vessel endothelial cells. *J. Cell Biochem.* 120, 1807–1818. doi: 10.1002/jcb.27480

Wang, S. H., Liou, G. G., Liu, S. H., Chang, J. S., Hsiao, J. R., Yen, Y. C., et al. (2019). Laminin γ2-enriched extracellular vesicles of oral squamous cell carcinoma cells enhance in vitro lymphangiogenesis via integrin α3-dependent uptake by lymphatic endothelial cells. *Int. J. Cancer* 144, 2795–2810. doi: 10.1002/ijc.32027

Wang, Z. S., Li, Y. F., Xiao, Y. J., Lin, H. P., Yang, P., Humphries, B., et al. (2019). Integrin α9 depletion promotes β-catenin degradation to suppress triple-negative breast cancer tumor growth and metastasis. *Int. J. Cancer* 145, 2767–2780. doi: 10.1002/ijc.32359

Weekes, C. D., Rosen, L. S., Capasso, A., Wong, K. M., Ye, W., Anderson, M., et al. (2018). Phase I study of the anti-α5β1 monoclonal antibody MINT1526A with or without bevacizumab in patients with advanced solid tumors. *Cancer Chemother. Pharmacol.* 82, 339–351. doi: 10.1007/s00280-018-3622-8

Wen, S. Y., Hou, Y. X., Fu, L. X., Xi, L., Yang, D., Zhao, M. J., et al. (2019). Cancer-associated fibroblast (CAF)-derived IL32 promotes breast cancer cell invasion and metastasis via integrin β3-p38 MAPK signalling. *Cancer Lett.* 442, 320–332. doi: 10.1016/j.canlet.2018.10.015

Wirth, M., Heidenreich, A., Gschwend, J. E., Gil, T., Zastrow, S., Laniado, M., et al. (2014). A multicenter phase 1 study of EMD 525797 (DI17E6), a novel humanized monoclonal antibody targeting αv integrins, in progressive castration-resistant prostate cancer with bone metastases after chemotherapy. *Eur. Urol.* 65, 897–904. doi: 10.1016/j.eururo.2013.05.051

Wortzel, I., Dror, S., Kenific, C. M., and Lyden, D. (2019). Exosome-Mediated Metastasis: Communication from a Distance. *Dev. Cell.* 49, 347–360. doi: 10.1016/j.devcel.2019.04.011

Wu, S. C., and Fu, L. W. (2018). Tyrosine kinase inhibitors enhanced the efficacy of conventional chemotherapeutic agent in multidrug resistant cancer cells. *Mol. Cancer* 17, 25. doi: 10.1186/s12943-018-0775-3

Wu, P.-H., Opadele, A. E., Onodera, Y., and Nam, J.-M. (2019). Targeting Integrins in Cancer Nanomedicine: Applications in Cancer Diagnosis and Therapy. *Cancers* 11, 1783. doi: 10.3390/cancers11111783

Wu, X., Cai, J., Zuo, Z., and Li, J. (2019). Collagen facilitates the colorectal cancer stemness and metastasis through an integrin/PI3K/AKT/Snail signaling pathway. *BioMed. Pharmacother.* 114, 108708. doi: 10.1016/j.biopha.2019.108708

Xiao, W., Ma, W., Wei, S., Li, Q., Liu, R., Carney, R. P., et al. (2019). High-affinity peptide ligand LXY30 for targeting α3β1 integrin in non-small cell lung cancer. *J. Hematol. Oncol.* 12, 56. doi: 10.1186/s13045-019-0740-7

Yang, D. J., Tang, Y., Fu, H. B., Xu, J. P., Hu, Z. Q., Zhang, Y., et al. (2018). Integrin β1 promotes gemcitabine resistance in pancreatic cancer through Cdc42 activation of PI3K p110β signaling. *Biochem. Biophys. Res. Commun.* 505, 215–221. doi: 10.1016/j.bbrc.2018.09.061

Yuan, M., Huang, L. L., Chen, J. H., Wu, J., and Xu, Q. (2019). The emerging treatment landscape of targeted therapy in non-small-cell lung cancer. *Signal Transduct. Target Ther.* 4, 61. doi: 10.1038/s41392-019-0099-9

Zeltz, C., Alam, J., Liu, H., Erusappan, P. M., Hoschuetzky, H., Molven, A., et al. (2019). α11β1 Integrin is Induced in a Subset of Cancer-Associated Fibroblasts in Desmoplastic Tumor Stroma and Mediates In Vitro Cell Migration. *Cancers* 11, 765. doi: 10.3390/cancers11060765

Zhang, Y. L., Xing, X., Cai, L. B., Zhu, L., Yang, X. M., Wang, Y. H., et al. (2018). Integrin 9 Suppresses Hepatocellular Carcinoma Metastasis by Rho GTPase Signaling. *J. Immunol. Res.* 2018, 4602570. doi: 10.1155/2018/4602570

Zhang, L., Shan, X., Meng, X., Gu, T., Guo, L., An, X., et al. (2019). Novel Integrin αvβ3-Specific Ligand for the Sensitive Diagnosis of Glioblastoma. *Mol. Pharm.* 16, 3977–3984. doi: 10.1021/acs.molpharmaceut.9b00602

Zhu, X. X., Tao, X. H., Lu, W., Ding, Y., Tang, Y., et al. (2019). Blockade of integrin β3 signals to reverse the stem-like phenotype and drug resistance in melanoma. *Cancer Chemother. Pharmacol.* 83, 615–624. doi: 10.1007/s00280-018-3760-z

Zou, Y., Wei, J. J., Xia, Y. F., Meng, F. H., Yuan, J. D., and Zhong, Z. Y. (2018). Targeted chemotherapy for subcutaneous and orthotopic non-small cell lung tumors with cyclic RGD-functionalized and disulfide-crosslinked polymersomal doxorubicin. *Signal Transduct. Target Ther.* 3, 32. doi: 10.1038/s41392-018-0032-7

**Conflict of Interest:** The authors declare that the research was conducted in the absence of any commercial or financial relationships that could be construed as a potential conflict of interest.

frontiers in Pharmacology

ORIGINAL RESEARCH
published: 30 September 2020
doi: 10.3389/fphar.2020.01228

# Cavin3 Suppresses Breast Cancer Metastasis *via* Inhibiting AKT Pathway

*Xin An[1,2,3†], Xi Lin[1,4†], Anli Yang[1,5], Qiwei Jiang[3], Bingchuan Geng[3], Mayan Huang[1,6], Jiabin Lu[1,6], Zhicheng Xiang[1], Zhongyu Yuan[1,2], Shusen Wang[1,2], Yanxia Shi[1,2*] and Hua Zhu[3*]*

[1] State Key Laboratory of Oncology in South China, Collaborative Innovation Center for Cancer Medicine, Guangzhou, China, [2] Department of Medical Oncology, Sun Yat-sen University Cancer Center, Guangzhou, China, [3] Department of Surgery, Davis Heart and Lung Research Institute, The Ohio State University Wexner Medical Center, Columbus, OH, United States, [4] Departments of Ultrasound, Sun Yat-sen University Cancer Center, Guangzhou, China, [5] Department of Breast Oncology, Sun Yat-sen University Cancer Center, Guangzhou, China, [6] Department of Pathology, Sun Yat-sen University Cancer Center, Guangzhou, China

OPEN ACCESS

**Edited by:**
Zhe-Sheng Chen,
St. John's University, United States

**Reviewed by:**
Yunkai Zhang,
Vanderbilt University Medical Center, United States
Zhijun Liu,
University of Massachusetts Medical School, United States
Elgene Lim,
Garvan Institute of Medical Research, Australia

***Correspondence:**
Yanxia Shi
shiyx@sysucc.org.cn
Hua Zhu
Hua.Zhu@osumc.edu

[†]These authors have contributed equally to this work

**Specialty section:**
This article was submitted to Pharmacology of Anti-Cancer Drugs, a section of the journal Frontiers in Pharmacology

**Received:** 19 May 2020
**Accepted:** 28 July 2020
**Published:** 30 September 2020

**Citation:**
An X, Lin X, Yang A, Jiang Q, Geng B, Huang M, Lu J, Xiang Z, Yuan Z, Wang S, Shi Y and Zhu H (2020) Cavin3 Suppresses Breast Cancer Metastasis via Inhibiting AKT Pathway. Front. Pharmacol. 11:01228. doi: 10.3389/fphar.2020.01228

**Objective:** Cavin3 is a putative tumor suppressor protein. However, its molecular action on tumor regulation is largely unknown. The aim of the current study is to explore the implication of cavin3 alteration, its clinical significance, and any potential molecular mechanisms in the regulation of breast cancer (BC).

**Methods:** TCGA (The Cancer Genome Atlas) and GTEx (Genotype-Tissue Expression) data bases, and 17 freshly paired BC and adjacent normal tissues were analyzed for mRNA levels of *Cavin3*. Furthermore, cavin3 protein expression from 407 primary BC samples were assessed by immunohistochemistry (IHC) and measured by H-score. The clinical significance of cavin3 expression was explored by Kaplan-Meier analysis and the Cox regression method. *In vitro* biological assays were performed to elucidate the function and underlying mechanisms of cavin 3 in BC cell lines.

**Results:** *Cavin3* mRNA was dramatically down-regulated in BC compared with the negative control. The median H-score of cavin3 protein by IHC was 50 (range 0-270). There were 232 (57%) and 175 (43%) cases scored as low (H-score≤50) and high (H-score >50) levels of cavin3, respectively. Low cavin3 was correlated with a higher T and N stage, and worse distant metastasis-free survival (DMFS) and overall survival (OS). Multivariate survival analysis revealed low cavin3 was an independent fact for worse DMFS. In BC cells, an overexpression of cavin3 could inhibit cell migration and invasion, and significantly decreased the level of p-Akt. Knockout of cavin3, meanwhile, promoted cell invasion ability and increased the level of p-AKT.

**Conclusion:** Cavin3 expression is significantly lower in BC and is correlated with distant metastasis and worse survival. Cavin3 functions as a metastasis suppressor *via* inhibiting the AKT pathway, suggesting cavin3 as a potential prognostic biomarker and a target for BC treatment.

**Keywords: Akt, breast cancer, cavin3, metastasis, human patient**

## INTRODUCTION

Breast cancer (BC) is the most common cancer and the second leading cause of cancer death in women worldwide (DeSantis et al., 2016; Bray et al., 2018). Distant metastases account for more than 90% of BC death. Therefore, identifying metastasis-associated genes and finding effective targets is the main strategy to prevent metastasis and improve survival of BC.

Caveolae are special lipid rafts located on plasma membranes. As signal transducing organelles, caveolae play an essential role in cell physiology through the regulation of molecule trafficking and signaling, and are involved in a host of human diseases, such as diabetes, cardiovascular disease, muscular dystrophy, pulmonary fibrosis, and cancers (Razani and Lisanti, 2001; Fridolfsson et al., 2014). There are two crucial components for caveolae formation and function: caveolin and cavin proteins. The caveolin family consists of caveolin-1 (Cav-1), caveolin-2 (Cav2), and caveolin-3 (Cav-3). The cavin family includes cavin1 (Polymerase 1 and Transcript Release Factor, PTRF), cavin2 (Serum-Deprivation Response Protein, SDPR), cavin3 (SDR-related gene product that binds to c-kinase, SRBC), and cavin4 (Muscle-Restricted Coiled-Coil Protein, MURC). Increasing evidence indicates the important role of caveolin and cavin family members in cancer regulation. Thus, they are regarded as new "tumor and metastasis-modifying genes" which might be targeted in cancer therapies (Gupta et al., 2014; Martinez-Outschoorn et al., 2015). However, heterogeneity expression patterns and paradoxical roles of these proteins on tumor suppression and oncogenesis have been reported on different tumor types and stages (Zhang et al., 2008; Di Vizio et al., 2009; Witkiewicz et al., 2009a), suggesting the dual role of these caveolin and cavin family members in cancer regulation.

The two most studied cavin family members in cancer regulation are cavin1 and cavin2. Cavin1 serves as a tumor suppressor in prostate cancer, but acts as a tumor promoter in pancreatic cancer (Aung et al., 2011; Liu et al., 2014). Several recent studies showed that cavin2 functioned as a metastasis suppressor in BC (Ozturk et al., 2016) and hepatocellular carcinoma (HCC) (Jing et al., 2016). Loss of expression of cavin2 was correlated with poor survival both in BC and HCC (Ozturk et al., 2016; Jing et al., 2016). Moreover, cavin1 and cavin2 were reported to be expressed in MDR cell lines and to be involved in drug resistance. In contrast to cavin1 and cavin2, cavin3's function in cancer is not well established. Loss of cavin3 was demonstrated in lung, gastric, ovarian, and colorectal cancers (Zochbauer-Muller et al., 2005; Lee et al., 2008; Tong et al., 2010; Lee et al., 2011), suggesting the tumor suppressing role of cavin3 in these tumors. Cavin3 inactivation was shown to be associated with the acquisition of chemoresistance to oxaliplatin in colorectal cancers (Moutinho et al., 2014). Inactivation of cavin3 was first reported in BC cell lines (Xu et al., 2001). A later study by Lin Bai et al. observed the down-regulation of cavin3 protein in human BC tissue compared with adjacent normal tissue. However, only 40 pairs of samples were tested in this study. Also, the clinical relevance of this down-regulation and related signal pathway were not investigated (Bai et al., 2012). The current study enrolled a large number of BC patients, and conducted analysis to explore the expression, clinical relevance, and possible molecular mechanism of cavin3 in BC. In vitro studies were performed to determine the potential molecular actions of cavin3.

## METHOD

### Databases for Bio-Informatics Analysis

Datasets from the Genotype Tissue Expression project (GTEx) (dbGaP, http://www.ncbi.nlm.nih.gov/gap) and The Cancer Genome Atlas (TCGA) project (CGHub, https://cghub.ucsc.edu) were obtained to compare *Cavin3* mRNA expression from BC tissue and matched normal breast tissue.

### Tissue Specimens and Cancer Cell Lines

Paired fresh-frozen breast tumor and adjacent normal tissues from 17 BC patients who had undergone BC surgery at Sun Yat-Sen University Cancer Center (SYSUCC) were obtained for *Cavin3* mRNA assay.

Paraffin-embedded (FFPE) specimens from 407 stage I-IV BC patients who were diagnosed and treated at SYSUCC during 2011, and had complete clinical and pathological follow-up data were collected. Duplicate tissue microarray (TMA) was constructed for immunohistochemistry (IHC) analysis. Ethical approval for the study was provided by the independent ethics committee of SYSUCC.

BC (MCF7, MDA-MB-231) and 293FT cell lines were purchased from the American Type Culture Collection (ATCC), and cultured in Dulbecco's Modified Eagle's Medium containing 10% fetal bovine serum, 1% L-glutamine, and 1% penicillin/streptomycin. Cells were cultured at 37°C in 5% CO2.

### Real-Time Quantitative PCR (qPCR)

Total RNA was isolated from fresh tissue samples using Trizol Reagent (Invitrogen, USA). cDNA was synthesized via "5X All-In-One MasterMix (with AccuRT Genomic DNA Removal Kit)" (G492, ABM Company, Vancouver, Canada) according to the manufacturer's instructions. qPCR analysis was performed in Roche Light Cycler 480 Real-Time PCR system. The cycling program was 10 min at 95°C one cycle, 10 seconds at 95°C, 20 seconds at 60°C, and 30 seconds at 72°C, for 45 cycles. Primer pairs for Cavin3 were: 5'- CACGTTCTGCTCTTCAAGGAG -3' (forward); 5'- TGTACCTTCTGCAATCCGGTG -3' (reverse). Primer pairs for β-actin were: 5'-ACCTTCTACAATGAGC TGCG-3'(forward); 5'- CCTGGATAGCAACGTACATGG -3' (reverse). Relative expression (RE) of Cavin3 was calculated with the formula: $\Delta Ct = Ct\ (Cavin3) - Ct\ (\beta\text{-actin})$. Fold change expression of Cavin3 mRNA in BC tissue compared with the normal control was calculated by the standard $2^{-\triangle\triangle Ct}$ method (Giulietti et al., 2001).

### Immunohistochemistry (IHC)

IHC staining was performed on an automatic immune stainer (BenchMark XT; Ventana Medical Systems, Tucson, Ariz) according to the manufacturer's instructions. The primary

antibodies used were anti-total cavin3 (PRKCDBP) antibody (Cat# PA534523, Invitrogen, USA)). Expression of cavin3 protein was semi-quantified using H-scores (range 0–300), which incorporate the staining intensity (range 0–3) and the percentage of positively-stained tumor cells (range 0–100%). The average H-score of the duplicate tissue microarray for each tumor was calculated as the final score.

## Construction of Cavin3 Overexpression or Knockout Cell Lines

Cavin3 overexpression plasmid (cavin3-pLVX) was created by cloning the protein coding sequence of cavin3 into the pLVX-puro lentiviral vector (Invitrogen: Thermo Fisher Scientific, Inc., USA). A blank lentiviral vector was used as negative control. The constructs were then transducted into 293FT cells with lentiviral packaging vectors by using Lipofectamine 2000 (Invitrogen: Thermo Fisher Scientific, Inc., USA) based on the manufacturer's instructions. Cavin3 knockout plasmid was generated using the clustered regularly interspaced short palindromic repeats (CRISPR) RNA-guided Cas9 nucleases technique.

## Cell Proliferation and Viability Assays

The cell proliferation was evaluated by Cell Counting Kit-8 (CCK-8) assay (Sigma-Aldrich; Merck KGaA, Germany.). Cells were grown in 96-well plates ($2\times10^3$ cells/well) and incubated overnight. CCK-8 solution (10 μl) was added to each well, followed by incubation for 2 h at 37°C. After that, a microplate reader (Thermo Fisher Scientific, Inc, USA.) was applied to record the absorbance value of each well at 450 nm. Cell viability was expressed as a percentage of that of the control cells. The viability of cancer cells was measured by clonogenic assay. Cells in a logarithmic growth period were plated in a 6-well plate (about 600 cells each plate) and incubated for 14 days at 37C in a 5% CO2 incubator. Thereafter, cells were fixed with methanol/acetic acid and stained with crystal violet. The number of colonies was counted manually.

## Cell Migration and Invasion Assays

Migration and invasion assays were performed using a Transwell system (BD Biosciences, USA). About $5\times10^5$ cells were seeded into the upper chamber with serum-free medium, and DMEM with 20% FBS was added into the lower chamber. After incubation for 24 h, cells on the upper surface of the filter were removed and the cells on the lower surface were stained with 1% crystal violet for quantification. The invading cells were counted under an optical microscope (Olympus Corporation, Japan). The number of transferred cells was determined in 10 randomly selected fields.

## Western Blotting

Cells were lysed in sample buffer and subjected to sodium dodecyl sulfate-polyacrylamide gel electrophoresis, and then transferred to a polyvinylidene fluoride (PVDF) membrane. The primary antibodies used included: anti-Akt rabbit mAb (Cat# 4685S, Cell Signaling Technolog, USA), anti-phospho Akt rabbit mAb (Cat# 4060S,Cell Signaling Technology, USA), anti-Vimentin rabbit mAb (Cat# 5741S, Cell Signaling Technology, USA), anti-E-Cadherin rabbit mAb (Cat# 3195, Cell Signaling Technology, USA), anti-PTEN rabbit mAb (Cat# 9188S,Cell Signaling Technology, USA), and anti-p53 rabbit mAb (Cat# 2527S, Cell Signaling Technology, USA). The secondary horseradish peroxidase-conjugated antibody used was HRP-Goat Anti-Rat IgG (H+L) (Cat# SA00001-2, ProteintechGroup, USA). Bands were detected by enhanced chemiluminescence (Amersham, Bucks, UK). Densitometric values were normalized to GAPDH levels.

## Statistical Analysis

We used SPSS software for Windows (V16.0; SPSS Inc., Chicago, IL) for all statistical analyses. All data were expressed as the means ± standard deviations (SD). Student's *t* test was used to compare mean values between the two groups. The correlation of cavin3 with clinicopathological factors was analyzed by chi-square test. Survival curves were plotted using the Kaplan-Meier method and compared by log-rank test. The Cox proportional hazards model was used for the univariate and multivariate survival analyses, and hazard ratios and 95% confidence intervals (CIs) were calculated. Breast Cancer Gene-Expression Miner v4.4 (bc-GenExMiner v4.4) was used to explore RNA-seq of cavin3 of different molecular subtypes of BC. A $P$ value of <0.05 was considered statistically significant.

# RESULTS

## *Cavin3* mRNA Is Significantly Lower in BC Compared With Adjacent Normal Control

We first analyzed TCGA and GTEx datasets and found expression of *Cavin3* mRNA was significantly lower in BC tumors compared with normal tissues, $P<0.05$ (**Figures 1A, B**). *Cavin3* mRNA levels were further analyzed in 17 paired fresh-frozen breast tumor and tumor-adjacent tissues collected in SYSUCC, which showed the relative *Cavin3* mRNA leves to β-actin were significantly lower in 14 out of 17 pairs of BC tissues compared with normal control, $P=0.0047$(**Figure 1C**).

## Reduced Cavin3 Protein Expression in BC Tissue Is Correlated With Advanced Tumor Stage and Poor Survival

IHC analysis of cavin3 was performed in all 407 of the enrolled patients. The median H-score was 50 (range 0-270). There were 175 (43%) and 232 (57%) cases scored as high (H-score >50) and low (H-score ≤50) levels of cavin3 expression, respectively. Representative IHC images for high and low levels of cavin3 expression were shown in **Figures 2A, B**. Low cavin3 expression was found to be correlated with a higher pathologic T and N stage, and poor recurrence-free survival (RFS) and distant metastasis-free survival (DMFS) (**Figures 2C, D**). No significant association between cavin3 expression and tumor grade, hormone receptor, and HER2 expression was found (**Table 1**). Patients with luminal (HR+/HER2-) subtype showed a relative low level of cavin3

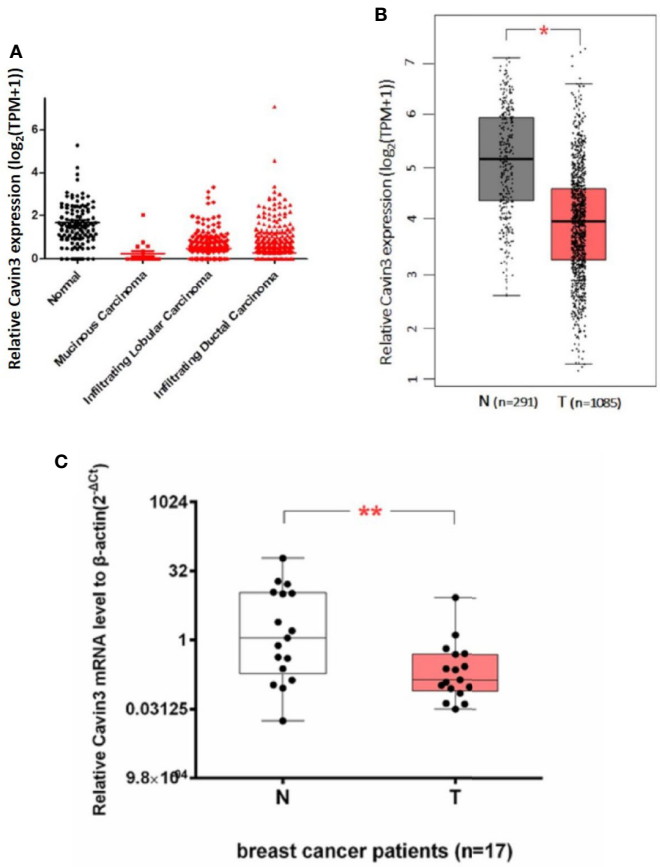


**FIGURE 1** | Lower expression of *Cavin3* mRNA in breast cancer samples compared with normal control. **(A)** TCGA database; **(B)** GTEx database; **(C)** 17paired fresh-frozen breast tumor and adjacent normal tissues. *p<0.05; **p<0.01.

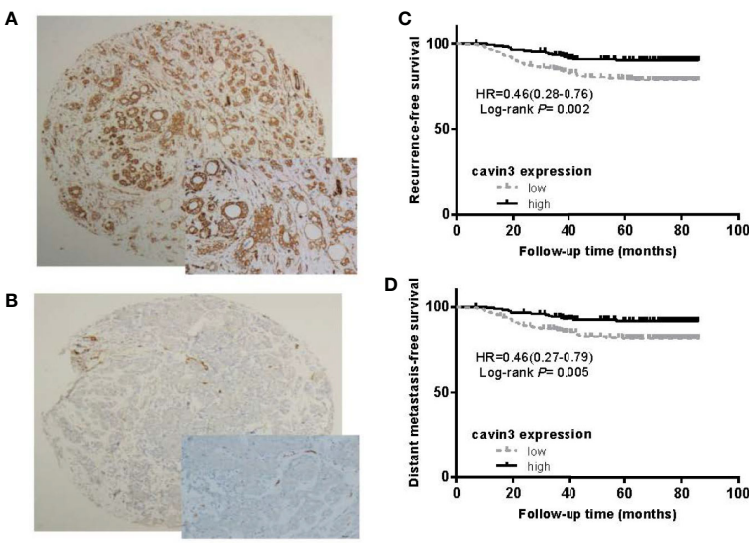


**FIGURE 2** | Expression of cavin3 in breast cancer and its impact on cancer survival. **(A)** Diffusely and strongly positive expression of cavin3 (H-score was 270); **(B)** completely negative expression of cavin3 (H-score was 0); **(C)** Low cavin3 (H-score≤50) is associated with worse recurrence free survival; **(D)** Low cavin3 (H-score≤50) is associated with worse distant metastasis-free survival.

**TABLE 1 |** Comparison of baseline characteristics between patients with high and low expressions of cavin3.

| | All patients | Cavin3 expression | | P value |
|---|---|---|---|---|
| | n=407 (100) | High (H-score>50) n=175 (43.0) | Low (H-score≤50) n=232 (57.0) | |
| Median age (range)* | 49(26-76) | 50 (26-75) | 49 (29-76) | 0.399 |
| Age at surgery (yr) | | | | 0.918 |
| ≤40 | 65(16.0) | 29 (16.6) | 36 (15.5) | |
| >40,<60 | 281 (69.0) | 121 (69.1) | 160 (69.0) | |
| >=60 | 61 (15.0) | 25 (15.5) | 36 (14.3) | |
| Breast surgery# | | | | 0.347 |
| Lumpectomy | 31 (7.7) | 16 (9.3) | 15 (6.6) | |
| Mastectomy | 370 (92.3) | 156 (90.7) | 214(93.4) | |
| Histologic subtype | | | | 0.566 |
| Ductal | 395 (97.1) | 171(97.7) | 224(96.6) | |
| Other | 12 (2.9) | 4 (2.3) | 8 (3.4) | |
| T stage | | | | **0.022** |
| 1 | 180 (44.2) | 88 (50.3) | 92 (39.7) | |
| 2 | 203 (49.9) | 82 (46.9) | 121 (52.2) | |
| 3 | 10 (2.5) | 1 (0.6) | 9 (3.9) | |
| 4 | 14 (3.4) | 4 (2.3) | 10 (4.3) | |
| N stage | | | | **0.000** |
| 0 | 177 (43.5) | 94 (53.7) | 83 (35.8) | |
| 1 | 128 (31.4) | 52 (29.7) | 76 (32.8) | |
| 2 | 60 (15.2) | 19 (10.9) | 41 (17.7) | |
| 3 | 42 (9.8) | 10 (5.7) | 32 (13.8) | |
| LVI | | | | 0.481 |
| Yes | 60(16.5) | 23 (13.1) | 37 (15.9) | |
| No | 347(83.5) | 152 (86.9) | 195 (84.1) | |
| Grade | | | | 1.000 |
| 1-2 | 336 (82.6) | 145 (82.9) | 191 (82.3) | |
| 3 | 71 (17.4) | 30 (17.1) | 41 (17.7) | |
| Ki67 | | | | 0.536 |
| <20% | 154 (37.8) | 70 (40.0) | 84 (36.2) | |
| ≥20%, | 253 (62.2) | 105 (60.0) | 148 (63.8) | |
| HR | | | | 0.246 |
| Positive | 305 (75.1) | 126 (72.0) | 179 (77.5) | |
| Negative | 101 (24.9) | 49 (28.0) | 52 (22.5) | |
| HER2 | | | | 0.163 |
| Positive | 119 (29.2) | 58 (33.1) | 61 (26.3) | |
| Negative | 288 (70.8) | 117(66.9) | 171 (73.7) | |
| Adjuvant CT* | | | | 0.137 |
| Yes | 359 (89.6) | 149 (86.6) | 210 (91.7) | |
| No | 42 (10.4) | 23 (13.4) | 19 (8.3) | |

*Including neoadjuvant chemotherapy.*

*#Five patients with metastatic and one patient with locally advanced disease at diagnosis had no surgery.*

*CT, chemotherapy; LVI, lymphovascular invasion; PR, progesterone receptor.*

*Bold type indicates statistical significance.*

expression compared with those in other subtypes, but the difference did not reach statistical significance (**Supplementary Table 1**). RNA-seq analysis by bc-GenExMiner v4.4 also demonstrated significantly lower levels of *Cavin3* RNA in luminal A and B subtypes as compared with those in basal- like and HER2 over-expression subtypes (**Supplementary Figure 1**). The worse prognosis of low cavin3 seemed to not depend on T and N stages (**Supplementary Figure 2**), but was more remarkable in luminal (HR+/HER2-) subtype (**Figure 3**). No association between cavin3 expression and a specific metastatic site was found (**Supplementary Table 2**). Multivariate analysis showed low cavin3 was an independently worse predictor for DMFS. Other risk factors for distant metastasis included positive lymph nodes and negative hormone receptors (**Table 2**).

## Cavin3 Suppresses BC Metastasis by Down-Regulating AKT Pathway

In vitro studies were based on two BC cell lines: the hormone receptor–positive MCF7 and triple-negative MDA-MB-231cell lines. A lack of baseline cavin3 expression was observed in the MCF7 cell line. Therefore, the MCF7 cell line with cavin3 overexpression and MDA-MB-231cell lines with cavin3 overexpression and knockout were generated. As a result, we found overexpression of cavin3 inhibited cell invasion, while knockout of cavin3 promoted cell invasion ability by transwell assay (**Figure 4**). No effect of cavin3 expression on overall cell proliferation rate (**Supplementary Figure 3**) or migration (**Supplementary Figure 4**) were observed. Western blot study showed the loss of cavin3 increased the level of p-AKT, while gain of cavin3 decreased the level of p-AKT (**Figure 5**). Thus, these results suggested that the metastasis suppressive function of cavin3 might be carried out by inhibiting the AKT signaling pathway.

# DISCUSSION

Cavin3 was originally called SRBC (SDR-related gene product that binds to c-kinase) or protein kinase C delta binding protein (PRKCDBP), due to its high similarity with the serum deprivation response (SDR) gene product and its ability to bind protein kinase C delta (PKCdelta) (Izumi et al., 1997). The gene is located in the 11p15.5 tumor suppressor region (Xu et al., 2001). Loss of cavin3 expression has been observed in several human malignancies including lung cancer (Xu et al., 2001), gastric cancer (Lee et al., 2008), colorectal cancer (Moutinho et al., 2014), ovarian cancer (Tong et al., 2010), and BC (Xu et al., 2001; Bai et al., 2012). Therefore, it is regarded as a potential tumor suppressor gene. However, till now there has been no large-scale study involving a high volume of patients to confirm the tumor suppressive role of cavin3. Moreover, the clinical utility and molecular function of cavin3 in cancer remains unclear. The inactivation of *Cavin3* gene was first reported in BC cell lines in 2001. Down-regulation of cavin3 protein in human BC tissue compared with adjacent normal tissue was later reported in 2012 by Lin Bai et al. (Bai et al., 2012). However, only 40 pairs of samples were detected in Lin Bai's study. Also, the clinical relevance of this down-regulation was not investigated. In the current study, by using the largest available data resources of TCGA and GTEx and by analyzing more than 1000 patients, we confirmed that expression of *Cavin3* mRNA was significantly lower in BC compared with normal breast tissue. In line with this result, among the 17 paired fresh-frozen breast tumor and tumor-adjacent samples from our cancer center, 14 showed significantly lower expression levels of *Cavin3* mRNA in BC compared with adjacent normal tissue. All these observations

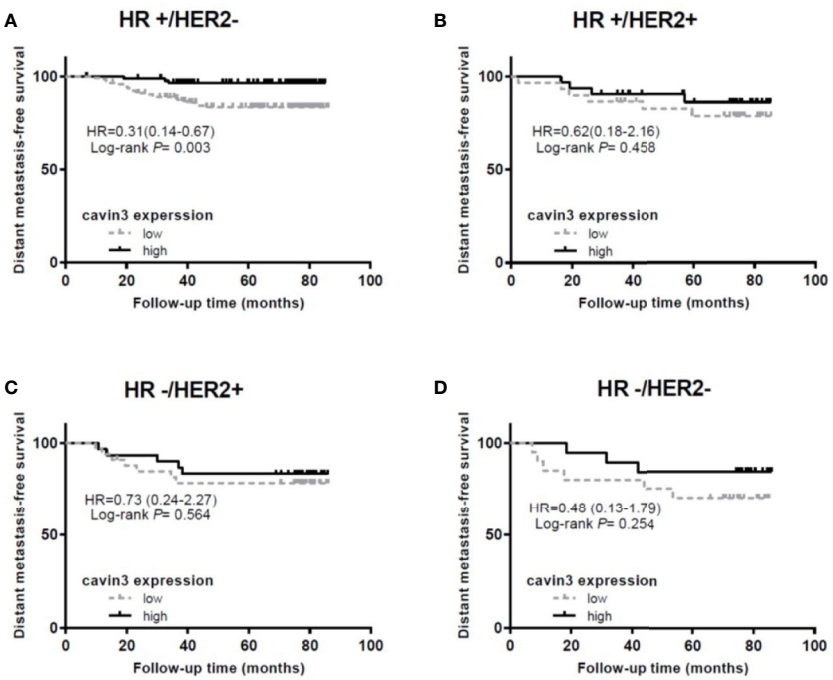


**FIGURE 3** | Impact of cavin3 protein expression on distant metastasis-free survival stratified by IHC-based molecular subtypes. **(A)** HR+/HER2- subtype; **(B)** HR +/HER2+ subtype; **(C)** HR-/HER2+ subtype; **(D)** HR-/HER2- subtype; HR, hormone receptor; HER2, human epidermal growth factor receptor-2.

**TABLE 2** | Univariate and Multivariate analysis of factors for distant metastasis-free survival (DMFS).

| Variable | Univariate | Multivariate | |
|---|---|---|---|
| | P value | HR (95% CI) | P value |
| Age<br>≤40 vs. >40,<60<br>>60 vs. >40,<65 | 0.946 | | |
| Breast surgery<br>Lumpectomy vs. Mastectomy | 0.384 | | |
| T stage<br>T3-4 vs. T1-2 | **0.000** | 2.413 (1.129-5.518) | **0.023** |
| N stage<br>N+ vs. N0 | **0.000** | 3.779 (1.878-7.607) | **0.000** |
| Grade<br>3 vs. 1-2 | 0.087 | | |
| Ki67<br>≥20% vs. <20% | 0.086 | 0.693 (0.375-1.281) | 0.242 |
| LVI<br>positive vs. negative | 0.415 | | |
| ER<br>negative vs. positive | 0.214 | | |
| PR<br>negative vs. positive | **0.021** | 2.168(1.250-3.758) | **0.006** |
| HER2<br>positive vs. negative | 0.324 | | |
| Adjuvant CT<br>no vs. yes | 0.252 | | |
| Cavin3<br>low vs. high | **0.005** | 1.911 (1.034-3.530) | **0.039** |

*HR indicates hazard ratio; CI, confidence interval; CT, chemotherapy; ER, estrogen receptor; HER2, LVI, lymphovascular invasion; PR, progesterone receptor.*
*Bold type indicates statistical significance.*

suggest cavin3 functions as a tumor suppressor and is involved in breast tumorigenesis. However, whether cavin3 can be used as a marker for the early diagnosis of BC remains unclear. Another caveolar protein caveolin1 has been reported to be a useful biomarker for early prediction of ductal carcinoma *in situ* (DCIS) progression to invasive BC (Witkiewicz et al., 2009b). Since the current study did not enroll hyperplasia and DCIS populations, the role of cavin3 as an early diagnosis biomarker remains to be investigated.

To further explore the function of cavin3 in established BC, expression of cavin3 in BC tissues was examined and compared with clinicopathologic data. As a result, we found over 50% of BC patients showed undetectable or low expression of cavin3. Loss or reduction of cavin3 expression correlated with advanced T and N stage and distant metastasis. DMFS was significantly decreased in patients with low cavin3 expression, suggesting the metastasis suppressive function of cavin3. It is noteworthy that low expression of cavin3 was more prominent in the HR+/HER2- subgroup of BC. Moreover, the worse impact of lower cavin3 on DMFS was also more significant in this subtype, indicating cavin3 will probably serve as a promising prognostic marker and therapeutic target for the HR+/HER2- subtype of BC. Harriet Wikman et al. reported the *Cavin3* (*PRKCDBP*) gene was significantly down-regulated in BC with brain metastases compared to BC without relapse or with bone-only metastasis (Wikman et al., 2012). In the current study, we analyzed the correlation between cavin3 expression and initial metastatic sites, and found five out of six patients with brain metastasis showed lower cavin3. However, due to

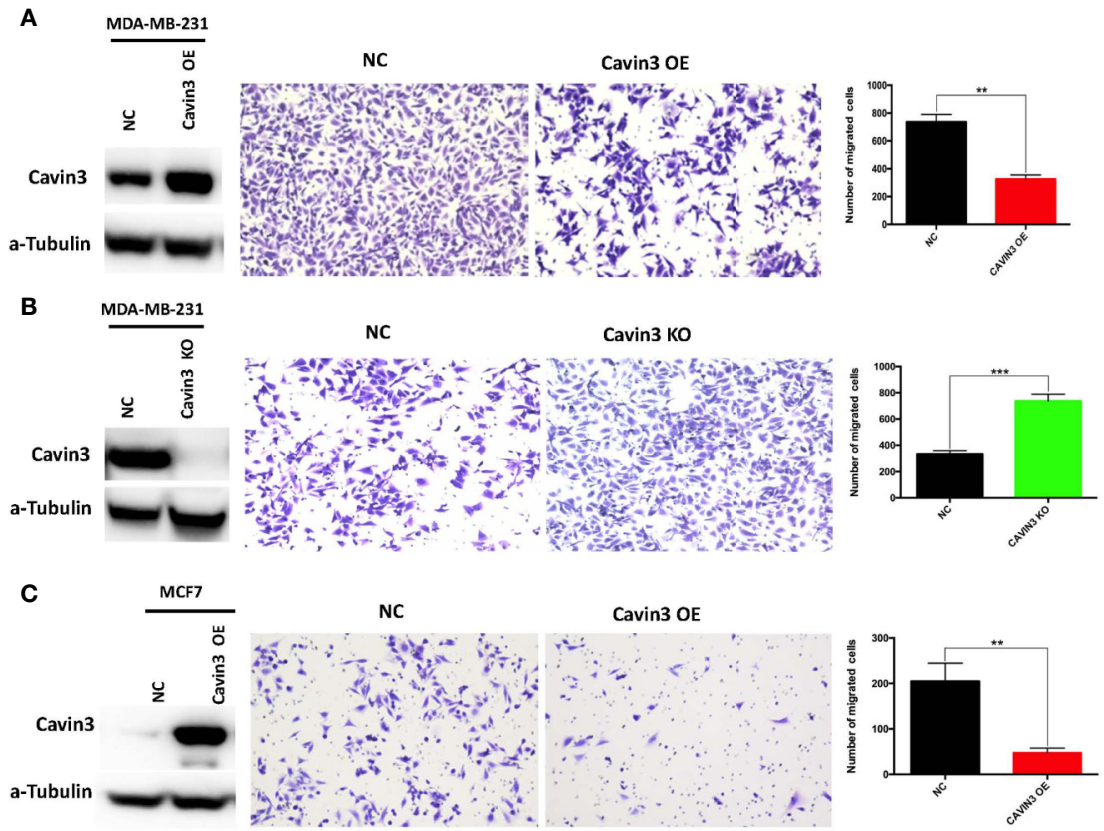


**FIGURE 4** | Impact of cavin3 on cell migration. Overexpression of cavin3 inhibits cancer cell migration **(A, C)**; **(B)** Knockout of cavin3 promote breast cancer cell migration. **p<0.01; ***p<0.001. KO, knockout; NC, normal control; OE, overexpression.

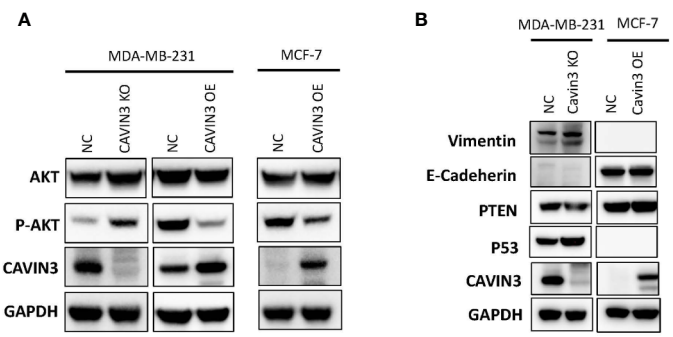


**FIGURE 5** | Cavin3 suppresses breast cancer metastasis by down-regulating the AKT pathway. **(A)** Loss of cavin3 increases the level of p-AKT and gain of cavin3 decreases the level of p-AKT; **(B)** No effect of cavin3 expression on PTEN expression, and EMT markers were observed. KO, knockout; NC, normal control; OE, overexpression.

the small number of events, we could not confirm such a relationship.

In order to elucidate the potential signaling cascade associated with the metastasis suppression role of cavin3, *in vitro* cell lines studies were performed. Consistent with human studies, the overexpression of cavin3 inhibited cell migration, while knockout of cavin3 by CRISPR increased the invasion ability of BC cells. These results further indicate cavin3 is a metastasis suppressor in BC. Moreover, we found the loss of cavin3 increased the level of active p-AKT, while gain of cavin3 decreased p-AKT. It

is well known that AKT is a serine/threonine kinase with a crucial role in major cellular functions. As a key element of the PI3K/AKT/mTOR signaling pathway, AKT is one of the most important pathways involved in BC survival, invasiveness, metastasis, and drug-resistance (Hinz and Jucker, 2019; Khan et al., 2019). Besides the PI3K/AKT/mTOR pathway, activated p-AKT also regulates many other signal molecules in metabolism, proliferation, apoptosis, and migration, such as GSK3, Mdm2, BAD, pro-caspase 9, NFKB, Bcl-XL, MMP2, MMP9, and many more (Khan et al., 2019). The study by Hernandez et al. reported cavin3 suppressed p-AKT signaling by promoting EGR1 and PTEN expression (Hernandez et al., 2013). However, we could not find a change of PTEN in cavin3 overexpressed or knockout breast cell lines. The exact molecular mechanism of cavin3 on the AKT pathway in BC requires further investigation.

Previous studies showed epigenetic inactivation of cavin3 due to aberrant promoter hypermethylation was the main mechanism for the loss of cavin3 (Lee et al., 2011; Wikman et al., 2012). Meanwhile, both the demethylation drug Decitabine (methylation inhibitor 5-aza-2'-deoxycytidine) and chemopreventive agent Anethole Dithiolethione could restore cavin3 expression (Primiano et al., 1996; Moutinho et al., 2014). Actually, many clinical trials concerning cancer treatment or prevention of these two drugs are ongoing (Nervi et al., 2015; Ramakrishnan et al., 2017; Ansari et al., 2018), which makes cavin3 a promising target for the development of new and more efficient therapies.

In summary, our current study suggests that cavin3 serves as a metastasis suppressor in BC and might be a potential prognostic marker and potential target for treating metastatic BC.

## DATA AVAILABILITY STATEMENT

The raw data supporting the conclusions of this article will be made available by the authors, without undue reservation.

## ETHICS STATEMENT

The studies involving human participants were reviewed and approved by the independent ethics committee of Sun Yat-sen University Cancer Center (SYSUCC). The patients/participants provided written informed consent to participate in this study.

## AUTHOR CONTRIBUTIONS

XA, AL, AY, QJ, BG, MH, JL, ZX, ZY, SW, and HZ performed the experiments. XA, XL, YS, and HZ analyzed the data. XA, YS, and HZ wrote the manuscript.

## SUPPLEMENTARY MATERIAL

The Supplementary Material for this article can be found online at: https://www.frontiersin.org/articles/10.3389/fphar.2020.01228/full#supplementary-material

**SUPPLEMENTARY FIGURE 1 |** Violin plot of *Cavin3* RNA expression (all RNA-seq data) according to molecular subtypes of breast cancer by bc-GenExMiner v4.4. *Cavin3 RNA* levels in luminal A and B subtypes are significantly lower than those in basal-like and HER2 over-expression subtypes.

**SUPPLEMENTARY FIGURE 2 |** Impact of cavin3 protein expression on distant metastasis-free survival (DMFS) stratified by tumor size and lymph node status.

**SUPPLEMENTARY FIGURE 3 |** Cavin3 has no effect on breast cancer cells' proliferation by cell counting assay. KO, knockout; OE, overexpression.

**SUPPLEMENTARY FIGURE 4 |** Cavin3 has no effect on breast cancer cells' viability by colony-forming assay. KO, knockout; OE, overexpression.

**SUPPLEMENTARY TABLE 1 |** Comparison of cavin3 protein expression among different molecular subtypes of breast cancer based on IHC. HR: hormone receptor, HER2: Human epidermal growth factor receptor 2.

**SUPPLEMENTARY TABLE 2 |** Correlation between cavin3 expression and initial recurrence pattern. *including 57 patients with distant recurrence.

## REFERENCES


Ansari, M. I., Khan, M. M., Saquib, M., Khatoon, S., and Hussain, M. K. (2018). Dithiolethiones: a privileged pharmacophore for anticancer therapy and chemoprevention. *Future Med. Chem.* 10 (10), 1241–1260. doi: 10.4155/fmc-2017-0281

Aung, C. S., Hill, M. M., Bastiani, M., Parton, R. G., and Parat, M. O. (2011). PTRF-cavin-1 expression decreases the migration of PC3 prostate cancer cells: role of matrix metalloprotease 9. *Eur. J. Cell Biol.* 90 (2-3), 136–142. doi: 10.1016/j.ejcb.2010.06.004

Bai, L., Deng, X., Li, Q., Wang, M., An, W., Deli, A., et al. (2012). Down-regulation of the cavin family proteins in breast cancer. *J. Cell Biochem.* 113 (1), 322–328. doi: 10.1002/jcb.23358

Bray, F., Ferlay, J., Soerjomataram, I., Siegel, R. L., Torre, L. A., and Jemal, A. (2018). Global cancer statistics 2018: GLOBOCAN estimates of incidence and mortality worldwide for 36 cancers in 185 countries. *CA Cancer J. Clin.* 68 (6), 394–424. doi: 10.3322/caac.21492

DeSantis, C. E., Fedewa, S. A., Goding Sauer, A., Kramer, J. L., Smith, R. A., and Jemal, A. (2016). Breast cancer statistics, 2015: Convergence of incidence rates between black and white women. *CA Cancer J. Clin.* 66 (1), 31–42. doi: 10.3322/caac.21320

Di Vizio, D., Morello, M., Sotgia, F., Pestell, R. G., Freeman, M. R., and Lisanti, M. P. (2009). An absence of stromal caveolin-1 is associated with advanced prostate cancer, metastatic disease and epithelial Akt activation. *Cell Cycle* 8 (15), 2420–2424. doi: 10.4161/cc.8.15.9116

Fridolfsson, H. N., Roth, D. M., Insel, P. A., and Patel, H. H. (2014). Regulation of intracellular signaling and function by caveolin. *FASEB J.* 28 (9), 3823–3831. doi: 10.1096/fj.14-252320

Giulietti, A., Overbergh, L., Valckx, D., Decallonne, B., Bouillon, R., and Mathieu, C. (2001). An overview of real-time quantitative PCR: applications to quantify cytokine gene expression. *Methods* 25 (4), 386–401. doi: 10.1006/meth.2001.1261

Gupta, R., Toufaily, C., and Annabi, B. (2014). Caveolin and cavin family members: dual roles in cancer. *Biochimie* 107 Pt B, 188–202. doi: 10.1016/j.biochi.2014.09.010

Hernandez, V. J., Weng, J., Ly, P., Pompey, S., Dong, H., Mishra, L., et al. (2013). Cavin-3 dictates the balance between ERK and Akt signaling. *Elife* 2, e00905. doi: 10.7554/eLife.00905

Hinz, N., and Jucker, M. (2019). Distinct functions of AKT isoforms in breast cancer: a comprehensive review. *Cell Commun. Signal* 17 (1), 154. doi: 10.1186/s12964-019-0450-3

Izumi, Y., Hirai, S., Tamai, Y., Fujise-Matsuoka, A., Nishimura, Y., and Ohno, S. (1997). A protein kinase Cdelta-binding protein SRBC whose expression is induced by serum starvation. *J. Biol. Chem.* 272 (11), 7381–7389. doi: 10.1074/jbc.272.11.7381

Jing, W., Luo, P., Zhu, M., Ai, Q., Chai, H., and Tu, J. (2016). Prognostic and Diagnostic Significance of SDPR-Cavin-2 in Hepatocellular Carcinoma. *Cell Physiol. Biochem.* 39 (3), 950–960. doi: 10.1159/000447803

Khan, M. A., Jain, V. K., Rizwanullah, M., Ahmad, J., and Jain, K. (2019). PI3K/AKT/mTOR pathway inhibitors in triple-negative breast cancer: a review on drug discovery and future challenges. *Drug Discovery Today* 24 (11), 2181–2191. doi: 10.1016/j.drudis.2019.09.001

Lee, J. H., Byun, D. S., Lee, M. G., Ryu, B. K., Kang, M. J., Chae, K. S., et al. (2008). Frequent epigenetic inactivation of hSRBC in gastric cancer and its implication in attenuated p53 response to stresses. *Int. J. Cancer* 122 (7), 1573–1584. doi: 10.1002/ijc.23166

Lee, J. H., Kang, M. J., Han, H. Y., Lee, M. G., Jeong, S. I., Ryu, B. K., et al. (2011). Epigenetic alteration of PRKCDBP in colorectal cancers and its implication in tumor cell resistance to TNFalpha-induced apoptosis. *Clin. Cancer Res.* 17 (24), 7551–7562. doi: 10.1158/1078-0432.CCR-11-1026

Liu, L., Xu, H. X., Wang, W. Q., Wu, C. T., Chen, T., Qin, Y., et al. (2014). Cavin-1 is essential for the tumor-promoting effect of caveolin-1 and enhances its prognostic potency in pancreatic cancer. *Oncogene* 33 (21), 2728–2736. doi: 10.1038/onc.2013.223

Martinez-Outschoorn, U. E., Sotgia, F., and Lisanti, M. P. (2015). Caveolae and signalling in cancer. *Nat. Rev. Cancer* 15 (4), 225–237. doi: 10.1038/nrc3915

Moutinho, C., Martinez-Cardus, A., Santos, C., Navarro-Perez, V., Martinez-Balibrea, E., Musulen, E., et al. (2014). BRCA1 interactor SRBC and resistance to oxaliplatin in colorectal cancer. *J. Natl. Cancer Inst.* 106 (1), djt322. doi: 10.1093/jnci/djt322

Nervi, C., De Marinis, E., and Codacci-Pisanelli, G. (2015). Epigenetic treatment of solid tumours: a review of clinical trials. *Clin. Epigenet.* 7, 127. doi: 10.1186/s13148-015-0157-2

Ozturk, S., Papageorgis, P., Wong, C. K., Lambert, A. W., Abdolmaleky, H. M., Thiagalingam, A., et al. (2016). SDPR functions as a metastasis suppressor in breast cancer by promoting apoptosis. *Proc. Natl. Acad. Sci. U. S. A.* 113 (3), 638–643. doi: 10.1073/pnas.1514663113

Primiano, T., Gastel, J. A., Kensler, T. W., and Sutter, T. R. (1996). Isolation of cDNAs representing dithiolethione-responsive genes. *Carcinogenesis* 17 (11), 2297–2303. doi: 10.1093/carcin/17.11.2297

Ramakrishnan, S., Hu, Q., Krishnan, N., Wang, D., Smit, E., Granger, V., et al. (2017). Decitabine, a DNA-demethylating agent, promotes differentiation via NOTCH1 signaling and alters immune-related pathways in muscle-invasive bladder cancer. *Cell Death Dis.* 8 (12), 3217. doi: 10.1038/s41419-017-0024-5

Razani, B., and Lisanti, M. P. (2001). Caveolin-deficient mice: insights into caveolar function human disease. *J. Clin. Invest.* 108 (11), 1553–1561. doi: 10.1172/JCI200114611

Tong, S. Y., Ki, K. D., Lee, J. M., Kang, M. J., Ha, T. K., Chung, S. I., et al. (2010). Frequent inactivation of hSRBC in ovarian cancers by promoter CpG island hypermethylation. *Acta Obstet. Gynecol. Scand.* 89 (5), 629–635. doi: 10.3109/00016341003678443

Wikman, H., Sielaff-Frimpong, B., Kropidlowski, J., Witzel, I., Milde-Langosch, K., Sauter, G., et al. (2012). Clinical relevance of loss of 11p15 in primary and metastatic breast cancer: association with loss of PRKCDBP expression in brain metastases. *PloS One* 7 (10), e47537. doi: 10.1371/journal.pone.0047537

Witkiewicz, A. K., Dasgupta, A., Sotgia, F., Mercier, I., Pestell, R. G., Sabel, M., et al. (2009a). An absence of stromal caveolin-1 expression predicts early tumor recurrence and poor clinical outcome in human breast cancers. *Am. J. Pathol.* 174 (6), 2023–2034. doi: 10.2353/ajpath.2009.080873

Witkiewicz, A. K., Dasgupta, A., Nguyen, K. H., Liu, C., Kovatich, A. J., Schwartz, G. F., et al. (2009b). Stromal caveolin-1 levels predict early DCIS progression to invasive breast cancer. *Cancer Biol. Ther.* 8 (11), 1071–1079. doi: 10.4161/cbt.8.11.8874

Xu, X. L., Wu, L. C., Du, F., Davis, A., Peyton, M., Tomizawa, Y., et al. (2001). Inactivation of human SRBC, located within the 11p15.5-p15.4 tumor suppressor region, in breast and lung cancers. *Cancer Res.* 61 (21), 7943–7949.

Zhang, H., Su, L., Muller, S., Tighiouart, M., Xu, Z., Zhang, X., et al. (2008). Restoration of caveolin-1 expression suppresses growth and metastasis of head and neck squamous cell carcinoma. *Br. J. Cancer* 99 (10), 1684–1694. doi: 10.1038/sj.bjc.6604735

Zochbauer-Muller, S., Fong, K. M., Geradts, J., Xu, X., Seidl, S., End-Pfutzenreuter, A., et al. (2005). Expression of the candidate tumor suppressor gene hSRBC is frequently lost in primary lung cancers with and without DNA methylation. *Oncogene* 24 (41), 6249–6255. doi: 10.1038/sj.onc.1208775

**Conflict of Interest:** The authors declare that the research was conducted in the absence of any commercial or financial relationships that could be construed as a potential conflict of interest.

frontiers in Oncology

ORIGINAL RESEARCH
published: 15 October 2020
doi: 10.3389/fonc.2020.592385

# Discovery of N-(2-Amino-4-Fluorophenyl)-4-[*bis*-(2-Chloroethyl)-Amino]-Benzamide as a Potent HDAC3 Inhibitor

*Yiming Chen*[1†], *Jinhong Feng*[2†], *Yajie Hu*[1], *Xuejian Wang*[1], *Weiguo Song*[1*] *and Lei Zhang*[1*]

[1] Department of Medicinal Chemistry, School of Pharmacy, Weifang Medical University, Weifang, China, [2] Key Laboratory for Applied Technology of Sophisticated Analytical Instruments of Shandong Province, Analysis and Test Center, Qilu University of Technology (Shandong Academy of Sciences), Jinan, China

In discovery of HDAC inhibitors with improved activity and selectivity, fluorine substitution was performed on our previously derived lead compound. The synthesized molecules N-(2-amino-4-fluorophenyl)-4-[*bis*-(2-chloroethyl)-amino]-benzamide (FNA) exhibited class I (HDAC1, 2, and 3) selectivity in the *in vitro* enzymatic assay and especially potent against HDAC3 activity ($IC_{50}$: 95.48 nM). The results of *in vitro* antiproliferative assay indicated that FNA exhibited solid tumor cell inhibitory activities with $IC_{50}$ value of 1.30 μM against HepG2 cells compared with SAHA (17.25 μM). Moreover, the *in vivo* xenograft model study revealed that FNA could inhibit tumor growth with tumor growth inhibition (TGI) of 48.89% compared with SAHA (TGI of 48.13%). Further HepG2 cell–based apoptosis and cell cycle studies showed that promotion of apoptosis and G2/M phase arrest make contributions to the antitumor activity of FNA. In addition, drug combination results showed that 0.5 μM of FNA could improve the anticancer activity of taxol and camptothecin. The present studies revealed the potential of FNA utilized as a high potent lead compound for further discovery of isoform selective HDAC inhibitors.

**Keywords: 4-fluorine-benzamide, nitrogen mustard, HDAC, antitumor activity, isoform selectivity**

OPEN ACCESS

***Edited by:***
*Zhe-Sheng Chen,*
*St. John's University, United States*

***Reviewed by:***
*Li Tan,*
*University of Michigan, United States*
*Junjie Zhu,*
*University of Pittsburgh, United States*

***Correspondence:**
*Weiguo Song*
*songwg@139.com*
*Lei Zhang*
*leizhangchemical@gmail.com*

[†] *These authors have contributed equally to this work*

***Specialty section:***
*This article was submitted to Pharmacology of Anti-Cancer Drugs, a section of the journal Frontiers in Oncology*

***Received:*** *06 August 2020*
***Accepted:*** *01 September 2020*
***Published:*** *15 October 2020*

***Citation:***
*Chen Y, Feng J, Hu Y, Wang X, Song W and Zhang L (2020) Discovery of N-(2-Amino-4-Fluorophenyl)-4-[bis-(2-Chloroethyl)-Amino]-Benzamide as a Potent HDAC3 Inhibitor. Front. Oncol. 10:592385. doi: 10.3389/fonc.2020.592385*

## INTRODUCTION

Histone deacetylases and histone acetylases are important enzymes participating in the regulation of gene expression by acetylating and deacetylating of histones (1, 2). Specifically, HDACs are the enzymes controlling the epigenetic modifications of histone, along with more than 50 nonhistone proteins (3, 4). So far, a total of 18 different HDACs isoforms have been identified and classified into four classes according to their size, distribution in cells, and homology (5–8). Among the four classes, classes I (HDAC1, 2, 3, and 8), II (HDAC4, 5, 6, 7, 9, and 10), and IV (HDAC11) HDACs require zinc ion as cofactor and thus are known as zinc-dependent enzymes. On the other hand, class III HDACs are a group of NAD+-dependent enzymes (also known as sirtuins), whose activity does not require the presence of zinc iron (9–13).

In recent years, inhibition of HDACs has exhibited potency for the treatment tumors (14, 15), diabetes (16), Parkinson disease (17), inflammation (18, 19), HIV (20), and heart disease (21). In tumor cells, it had been shown that overexpression of HDACs led to increased deacetylation of histones, which increases the gravitational pull between DNA and histones by

restoring the positive charge of the histones, making the relaxed nucleosomes very tight and unfavorable for the expression of specific genes, including some tumor suppressor genes (22–28).

In the field of epigenetics, HDAC inhibitors (HDACIs) have been successfully developed in the antitumor therapy, and several HDACIs have been developed into the market (29). Vorinostat (SAHA) is the first approved HDACI, which has been administered clinically for the treatment of cutaneous T-cell lymphoma (CTCL) (30). Afterward, romidepsin (FK-228), belinostat (PXD101), and panobinostat (LBH589) were approved for the treatment of CTCL, peripheral T-cell lymphoma (PTCL), and multiple myeloma, respectively (31–33). Chidamide (CS055) was approved by the Chinese Food and Drug Administration for the treatment of PTCL (34). Generally, pharmacophores of HDACIs are consist of three structural elements: a capping group, which recognizes the hydrophobic region at the opening of HDAC active site; a linker, which connects the hydrophobic ring and the zinc-binding group (ZBG) via occupation of the tubular channel; a ZBG, whose functions include binding to the zinc ion located in the active center of HDACs, as well as forming hydrogen bonds with certain amino acid residues of active sites (35–37).

Nitrogen mustard anticancer drugs were used clinically since 1942, which effectively bind and cross-link to DNA, resulting in prevention of DNA replication and cell proliferation (38). Nitrogen mustard antitumor drugs are mainly composed of alkylation part and carrier part. According to different carriers, they can be divided into aliphatic nitrogen mustard and aromatic nitrogen mustard (39). Aromatic nitrogen mustard is still used in clinical because of its relatively low toxicity such as chlormethine (40), chlorambucil (41), and melphalan (42).

In discovery of novel and potent HDACIs, aromatic nitrogen mustard parts were integrated into the structure of HDACI CI994 in our previous study (43). The resulting molecule, N-(2-aminophenyl)-4-(*bis*(2-chloroethyl)amino)benzamide (NA) exhibited class I selectivity in the enzymatic assay and potent *in vitro* antitumor activity in the cell based assay. However, NA exhibited lower potency than SAHA in the *in vivo* assay using nude mice xenograft model with inoculation of HepG2 cells. Fluorine substitution in the benzamide ZBG was discovered to improve the metabolic stability of HDACIs, such as the design of chidamide (44, 45). In the present study, to improve the selectivity, activity, and *in vivo* stability of NA, fluorine was introduced to the *para*-position of amide bond in the phenyl ring of ZBG considering the structure of chidamide (**Figure 1**). The designed compound N-(2-amino-4-fluorophenyl)-4-[*bis*-(2-chloroethyl)-amino]-benzamide (FNA) was synthesized and evaluated in the antitumor assay.

## RESULTS AND DISCUSSION

### Chemistry

The designed compound FNA was synthesized as described in **Scheme 1**. Methyl esterification was performed to protect the starting material 4-aminobenzoic acid (a). To synthesize intermediate methyl 4-(*bis*(2-hydroxyethyl)amino)benzoate (c), 2-hydroxyethyl groups were added by reaction of intermediate **b** with ethylene oxide. Subsequent chlorine substitution and

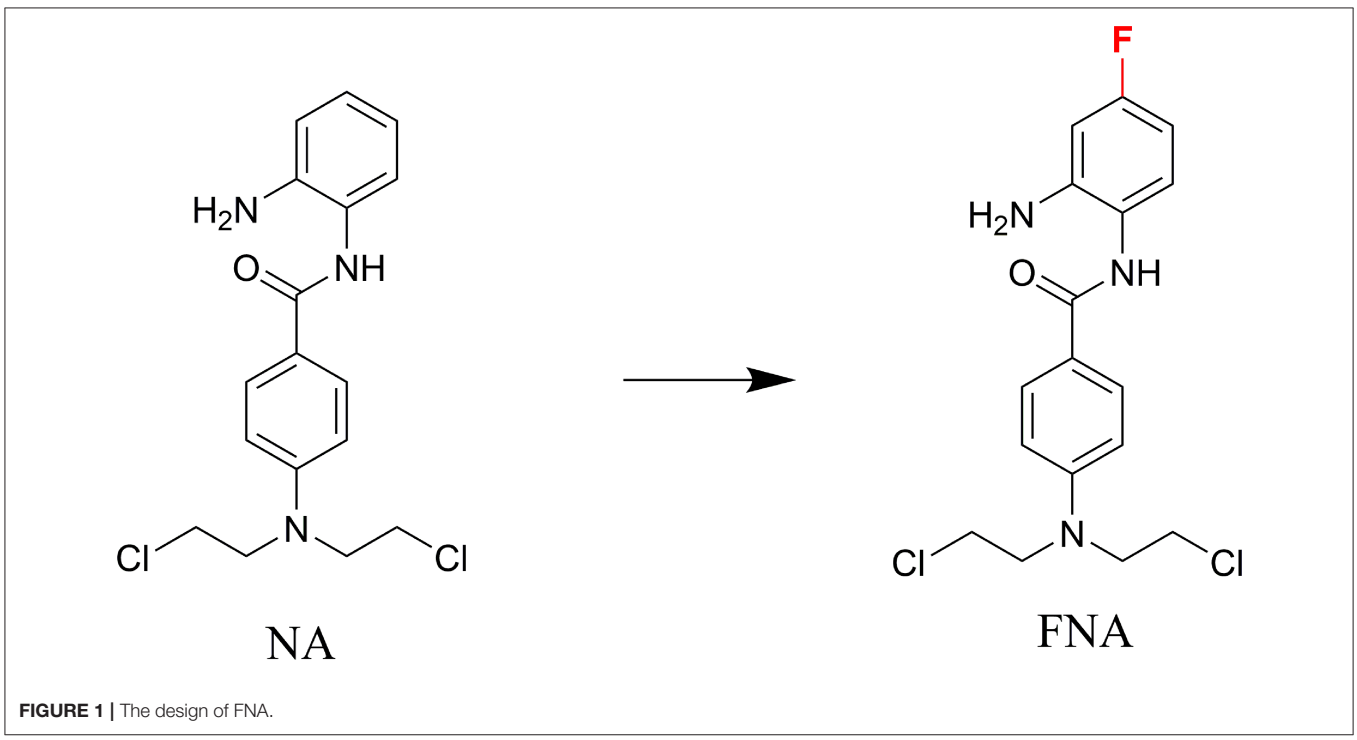


**FIGURE 1 |** The design of FNA.

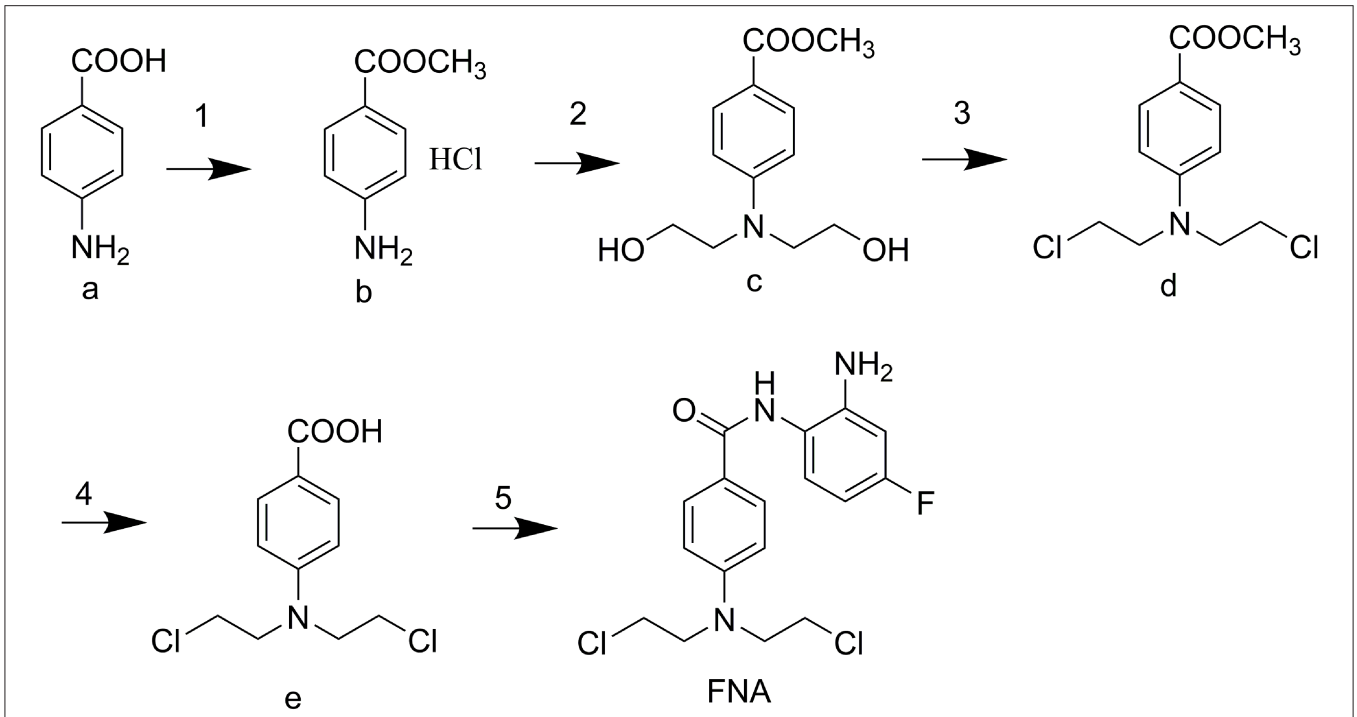


**SCHEME 1 |** (1) $CH_3COCl$, MeOH, reflux 5 h. (2) oxirane, $H_2O/CH_3COOH$, 0°C 48 h. (3) $POCl_3$, MB, reflux 4 h. (4) 4 M HCl, reflux 4 h. (5) 1,2-diamino-4-fluorobenzene, CDI, THF (dry), rt overnight.

**TABLE 1 |** Enzyme inhibitory activity of FNA compared with MS275 and SAHA ($IC_{50}$, nM)[a].

| HDACs | HDAC1 | HDAC2 | HDAC3 | HDAC4 | HDAC6 | HDAC7 | HDAC8 | HDAC9 |
|---|---|---|---|---|---|---|---|---|
| FNA | 842.80 | 949.15 | 95.48 | >5,000 | >5,000 | >5,000 | >5,000 | >5,000 |
| MS275 | 46.17 | 100.90 | 43.89 | >5,000 | >5,000 | >5,000 | >5,000 | >5,000 |
| SAHA | 52.90 | 90.78 | 167.24 | >5,000 | 172.10 | >5,000 | 4,120 | >5,000 |

[a]*Assays were performed in replicate ($n \geq 2$), the SD values are <10% of the mean.*

deprotection of carboxyl group afforded key intermediate 4-(*bis*(2-chloroethyl)amino)benzoic acid (e). Target compound FNA was synthesized by condensation of intermediate **e** with 1,2-diamino-4-fluorobenzene.

## Enzyme Inhibitory Selectivity of FNA

To assess the isoform selectivity and the inhibitory activity of the derived FNA, enzymatic assay was performed against HDAC1, 2, 3, 4, 6, 7, 8, and 9 using SAHA (nonselective inhibitor) and MS275 (class I selective inhibitor) as positive control drugs. The selectivity of isoforms and $IC_{50}$ of the tested compounds were displayed in **Table 1**. According to the results, FNA exhibited $IC_{50}$ values of 842.80, 949.15, and 95.48 nM against HDAC1, 2, and 3, respectively. While in inhibition of HDAC4, 6, 7, 8, and 9, FNA exhibited more than 5,000 nM of $IC_{50}$ values. It is suggested that FNA is a highly class I–selective inhibitor. Nevertheless, in the inhibition of HDAC1, 2, and 3, it is remarkable that FNA showed 8.83- and 9.94-fold of HDAC3 selectivity vs. HDAC1 and HDAC2, respectively. The results suggested that FNA has the potential to be utilized as a lead compound for the discovery of HDAC3-selective inhibitors.

Among all the HDAC isoforms found in human, HDAC3 is unique for its expression in the nucleus, cytoplasm, or membrane. As a single HDAC isoform, HDAC3 was revealed to promote the phosphorylation and activation of AKT, which specifically binds to HDAC3, participate in the self-renewal of liver cancer stem cells, and engage in the growth of triple-negative breast cancer cells (15). Therefore, discovery of selective HDAC3 inhibitors make contributions to the treatment of specific diseases related to the abnormal function of HDAC3. As a potent lead compound, FNA could be utilized for further structural modification in discovery of HDAC3-selective inhibitors.

## Antiproliferative Activity of FNA

The *in vitro* antiproliferative activities of target compound FNA along with the positive control SAHA were tested against multiple tumor cell lines, including the lung cancer (H460, H322, and A549), colon carcinoma SW480, renal carcinoma (OS-RC-2, SK-NEP-1), thyroid cancer (FTC-133, SW-579), breast cancer (MDA-MB-231), ovarian cancer (A2780), cervical carcinoma (Hela), myeloma (U266), liver cancer (HepG2), and leukemic (U937 and K562) cells. According to the results shown in **Table 2**, potent antiproliferative activities against most of the tumor cell lines tested (except SW480 and OR-RC-2) were observed from FNA, as evidenced by the low $IC_{50}$ values. Compared with SAHA, it is obvious that FNA could effectively inhibit the growth of

HepG2, U937, H460, FTC-133, HELA, and K562 cells with $IC_{50}$ values of 1.30, 0.55, 4.73, 9.09, 1.41, and 1.31 μM, respectively. It showed that FNA has a significant inhibitory effect on both solid tumor cells and nonsolid tumor cells. Remarkably, in inhibition the growth of HepG2 cells, FNA (similar to NA) was revealed to be 13.3-fold ($IC_{50}$ value of 1.30 μM) more potent relative to SAHA, whose $IC_{50}$ value is 17.25 μM. The present results indicate the future of development of FNA analogs for the treatment of liver cancer.

**TABLE 2 |** Antiproliferative activities of compound FNA against human cancer cells ($IC_{50}$, μM)[a].

| Cell line | FNA (μM) | SAHA (μM) |
|---|---|---|
| HepG2 | 1.30 ± 0.25 | 17.25 ± 0.46 |
| U937 | 0.55 ± 0.03 | 0.86 ± 0.03 |
| H460 | 4.73 ± 0.05 | 7.63 ± 0.03 |
| SW480 | >100 | 2.91 ± 0.04 |
| OS-RC-2 | >100 | >100 |
| H322 | 6.36 ± 0.07 | 2.54 ± 0.06 |
| SK-NEP-1 | 8.32 ± 0.18 | 3.68 ± 0.02 |
| FTC-133 | 9.09 ± 0.13 | 24.30 ± 0.10 |
| SW579 | 52.40 ± 0.13 | 24.30 ± 0.07 |
| MDA-MB-231 | 35.29 ± 0.03 | 5.82 ± 0.08 |
| A549 | 33.74 ± 0.04 | 4.92 ± 0.04 |
| A2780 | 4.30 ± 0.12 | 2.71 ± 0.09 |
| Hela | 1.41 ± 0.04 | 1.89 ± 0.05 |
| K562 | 1.31 ± 0.05 | 2.52 ± 0.05 |
| U266 | 0.63 ± 0.32 | 0.22 ± 0.03 |

[a]*Assays were performed in replicate (n ≥ 2).*

## *In vivo* Antitumor Activity

To further investigate the anticancer activity of FNA, HepG2 xenograft nude mice model was utilized to assess the *in vivo* antitumor activity of compound FNA. Mice were injected intraperitoneally with FNA and SAHA, both at 100 mg/kg, once a day for 15 days. When the tumor is prominent, the BALB/c female mice were randomly assigned into control and treatment groups (six mice per group). As shown in **Figure 2A**, all the mice in the treatment groups displayed no significant change in body weight. The results showed that both FNA and SAHA can inhibit tumor growth compared with the control group (**Figures 2B–D**). Compound FNA effectively inhibited the tumor growth with tumor growth inhibition (TGI) rate of 48.89% compared with SAHA (with TGI of 48.13%). Although FNA exhibited improved inhibitory activity compared with SAHA in the *in vitro* test, the activity improvement was not obvious in the *in vivo* study. It is suggested that further structural modification of FNA is needed to improve the activity and pharmacokinetic properties. To improve the *in vivo* activity of FNA, introduction of bioactive

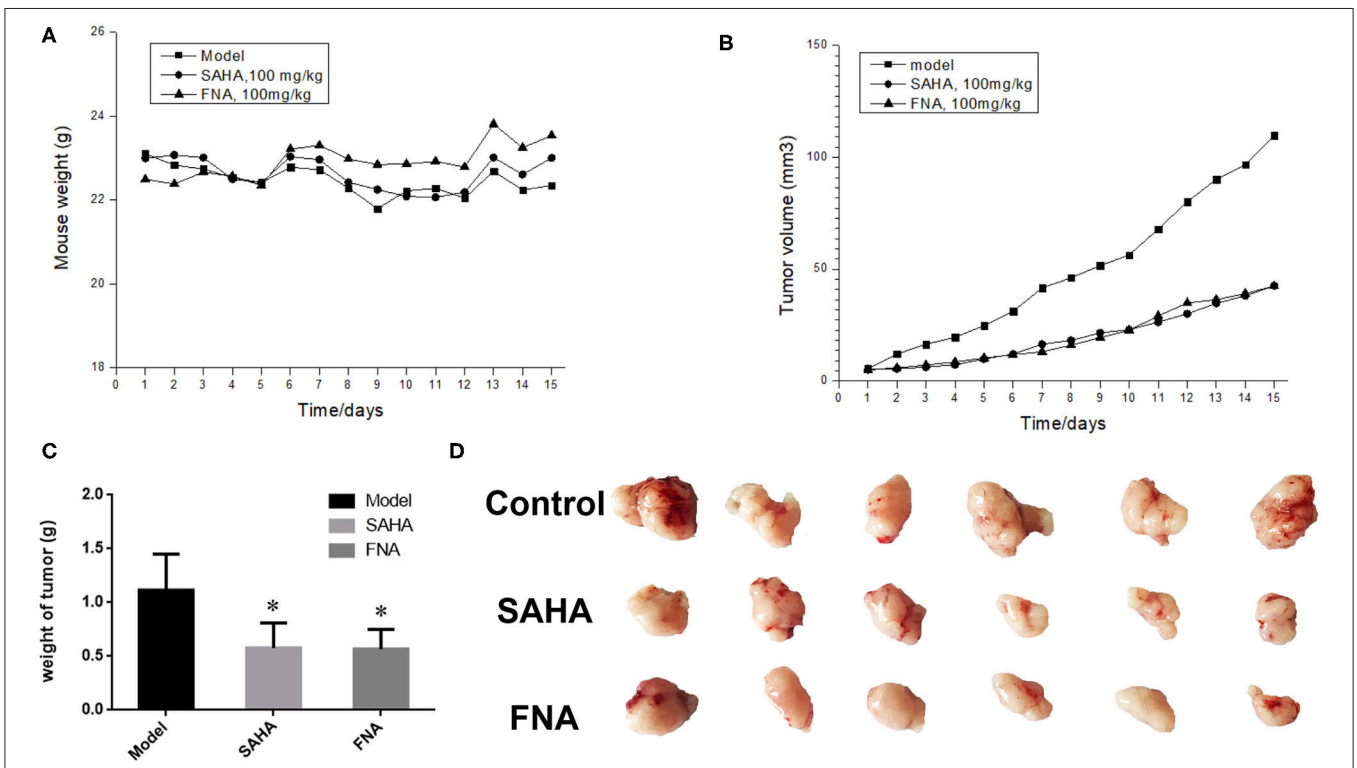


**FIGURE 2 |** Results of *in vivo* evaluation of FNA in the HepG2 xenografts mouse model. **(A)** Body weight of mice. **(B)** Tumor volume measurements from HepG2 xenografts mice in each group. **(C)** The final tumor weights in each group. *$p < 0.05$ compared with the control group. **(D)** Images of the excised tumors in each group.

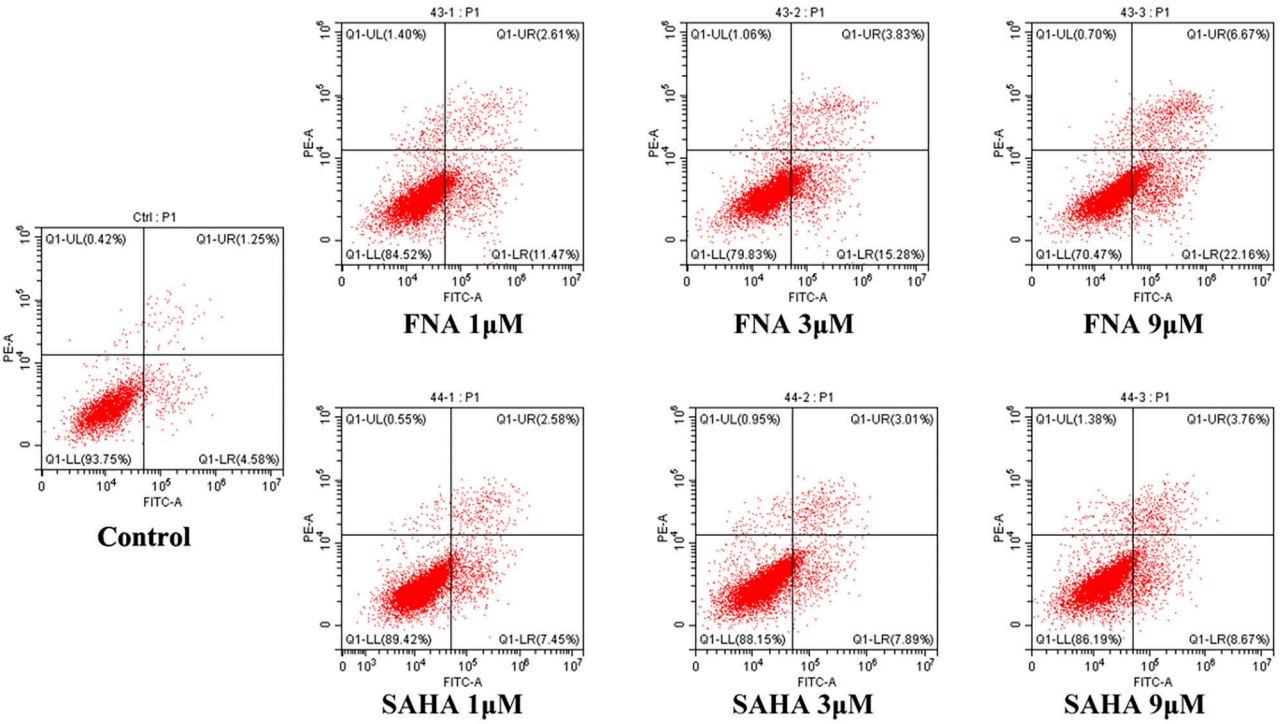


**FIGURE 3 |** Proapoptotic effect of molecule FNA. HepG2 cells were exposed to FNA and SAHA at concentrations of 1, 3, and 9 μM for 24 h. Then cells were stained with annexin V–FITC/PI, and the apoptotic status of the cells was assessed with flow cytometry analysis.

groups with anticancer activities to the structure of FNA will be performed in further studies.

## Cell Apoptosis Analysis

In order to confirm whether apoptosis contributes to the observed antiproliferative activities of FNA, apoptosis study was performed using HepG2 cells. Flow cytometry analysis was shown in **Figure 3**. From the annexin V–fluorescein isothiocyanate/propidium iodide (FITC/PI) stating data, it is obvious that compound FNA promoted cell apoptosis against HepG2 cells dose-dependently. Following treatment with different doses of FNA (1, 3, and 9 μM), the apoptosis rate of HepG2 cells was significantly elevated from 5.83% of the normal group to 14.08, 19.11, and 28.83% compared with SAHA (apoptosis rate of 10.03, 10.91, and 12.43% at concentrations of 1, 3, and 9 μM), respectively. It is suggested that apoptosis plays a role in the HepG2 cell inhibitory activity of FNA.

## Cell Cycle Analysis

Generally, the cell cycle consists of three phases: G0/G1, S, and G2/M phase. A characteristic change in tumor cells is dysregulated cell cycle due to genetic mutations, resulting in uncontrolled cell proliferation. The designed compound FNA was evaluated for the cell cycle effect on HepG2 with various doses (0.125, 0.25, and 0.5 μM). As shown in **Figure 4**, it is significant that FNA increased cell number at G2/M phase with raising concentrations. The percentage of cells in G2/M phase was increased from 18.84 to 59.36% in the FNA (with concentration increase from 0.125 to 0.5 μM) group. However, at the tested concentrations, SAHA did not exhibit any effects in the regulation of HepG2 cell cycle. The results indicated that induction of the G2/M phase arrest also plays a significant role in the antiproliferative effects of molecule FNA.

## Antiproliferative Activities of FNA in Combination With Taxol and Camptothecin

It had been reported that HDACIs (HDACIs) may work as chemosensitizers when used together with other antitumor drugs (8). Because of the high cell cycle arrest ability of FNA, drug combination investigation was performed by combining FNA with the G2/M phase arrest drug taxol and camptothecin. HepG2 cells were used for the test, and percentage inhibition rate (PIR) was used as a measure of potency. As shown in **Figure 5**, it is revealed that the PIRs of FNA (0.5 μM) in combination with taxol and camptothecin are higher than that of the single-drug groups on HepG2 cells. The PIRs of taxol were 57.07 and 62.41 at the concentrations of 0.1 and 0.2 μM, respectively. Addition of 0.5 μM of FNA increased the PIR to 62.43 (0.1 μM of taxol) and 67.23 (0.2 μM of taxol), respectively. The PIRs of camptothecin at doses of 0.25 and 0.5 μM were 61.70 and 60.86, respectively. Improved activities were obtained by addition of FNA (0.5 μM) with PIR values of 67.07 (0.25 μM of camptothecin) and 75.52 (0.5 μM of camptothecin), respectively. It is suggested that FNA could synergistically improve the antiproliferative ability of the cell cycle arrest drugs such as taxol and camptothecin.

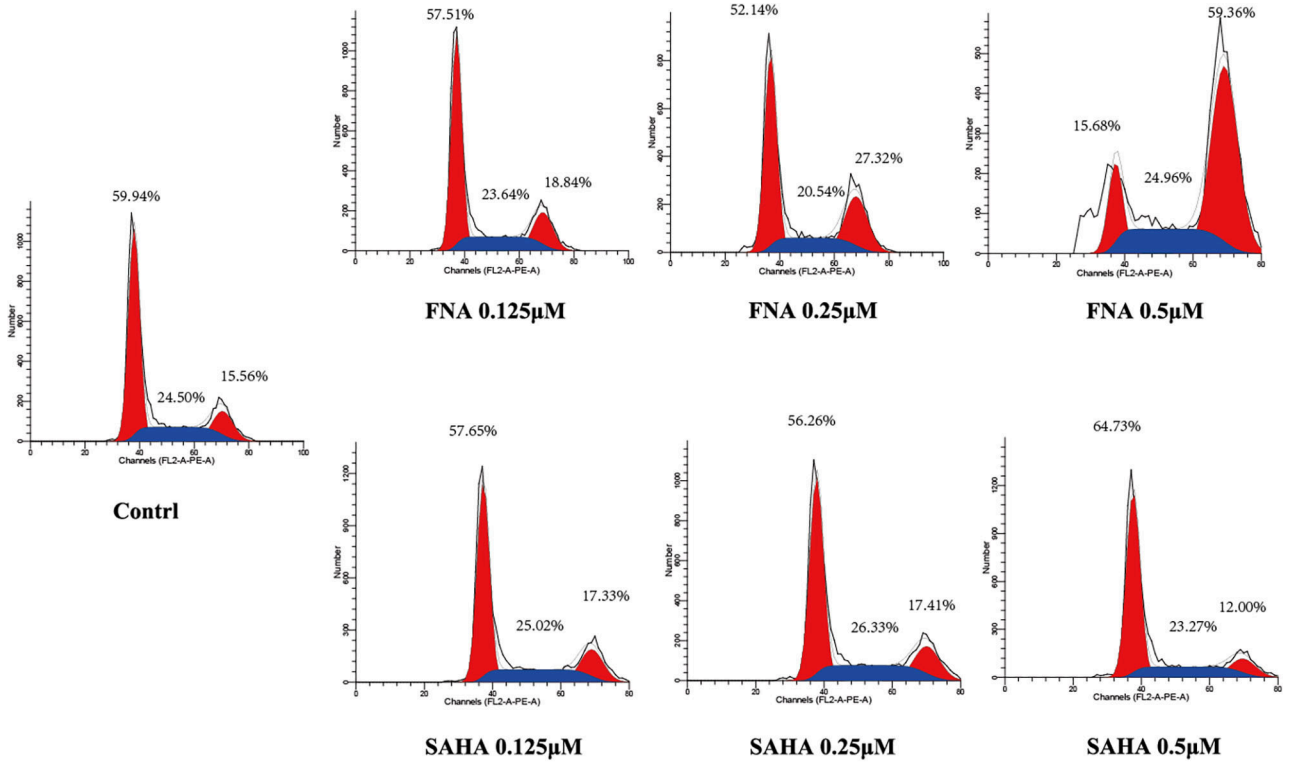


**FIGURE 4 |** Cell cycle analysis on HepG2 cells treated with FNA. Cells were treated with FNA and SAHA at concentrations of 0.125, 0.25, and 0.5 μM for 6 h. The results were evaluated with flow cytometry analysis.

## CONCLUSION

Benzamide HDACIs exhibited the advantage of class I selectivity compared with HDACIs with hydroxamic acid as their ZBGs. However, none of the benzamide HDACIs have been approved by US Food and Drug Administration (FDA) yet. The fluorine substituted benzamide HDACI, chidamide, approved by the CFDA, exhibited advantage of high pharmacokinetic properties compared with the unsubstituted benzamide (such as MS275). Therefore, fluorine substituted was performed on the previous lead compound NA. The derived FNA exhibited HDAC3 selectivity and high HepG2 cell inhibitory activity. Moreover, FNA was also effective in the HepG2 nude mice xenograft model–based assay. Further investigations revealed that promotion of apoptosis and cell cycle arrest at G2/M phase both contributed to the antitumor activity of FNA. Moreover, in combination with FNA, taxol and camptothecin exhibited improved antiproliferative activities against HepG2 cells. Collectively, a potent HDAC3 inhibitor was discovered, which could be utilized as a lead compound in the development of new drugs for cancer treatments.

## MATERIALS AND METHODS

### Chemistry

All the starting materials and reagents commercially available were used in the current study without further purifications. The dry THF was used by heating reflux with sodium. TLC with 0.25-mm silica gel plates (60GF-254) was used to monitor all the reactions. The sports were visualized with UV light and ferric chloride. With a Burker DRX spectrometer, the $^1$H NMR spectra were recorded at 500 MHz, using TMS as an internal standard. High-resolution mass spectra were performed at Weifang Medical University in Weifang, China. The derived target compound (FNA) is of 95.48% purity analyzed by ultraperformance liquid chromatography (UPLC), which was performed on a Waters Acquity H class UPLC instrument using an Acquity UPLC®BEH C18 (150 × 2.1 mm). The mobile phase was acetonitrile–water (90:10), and detection wavelength was 254 nm.

The synthesis and description of 4-(*bis*(2-chloroethyl)amino)benzoic acid (e) were presented in our previous work (43).

### (2-Aminophenyl)-4-(*bis*(2-Chloroethyl)Amino)Benzamide

To a solution of compound e (2.00 g, 7.7 mmol) in THF (50 mL), CDI (1.87 g, 11.6 mmol) was added, and the solution was refluxed for 3 h. 1,2-Diamino-4-fluorobenzene (3.8 g, 30.6 mmol) and TFA (1.1 g, 9.24 mmol) were added with stirring, and the mixture was kept for 16 h at room temperature. The solvent was then evaporated with the residue being dissolved in EtOAc (50 mL). The resulting EtOAc solution was washed with $NaHCO_3$ (3 × 20 mL), 1 M citric acid (3 × 20 mL), and brine (3 × 20 mL),

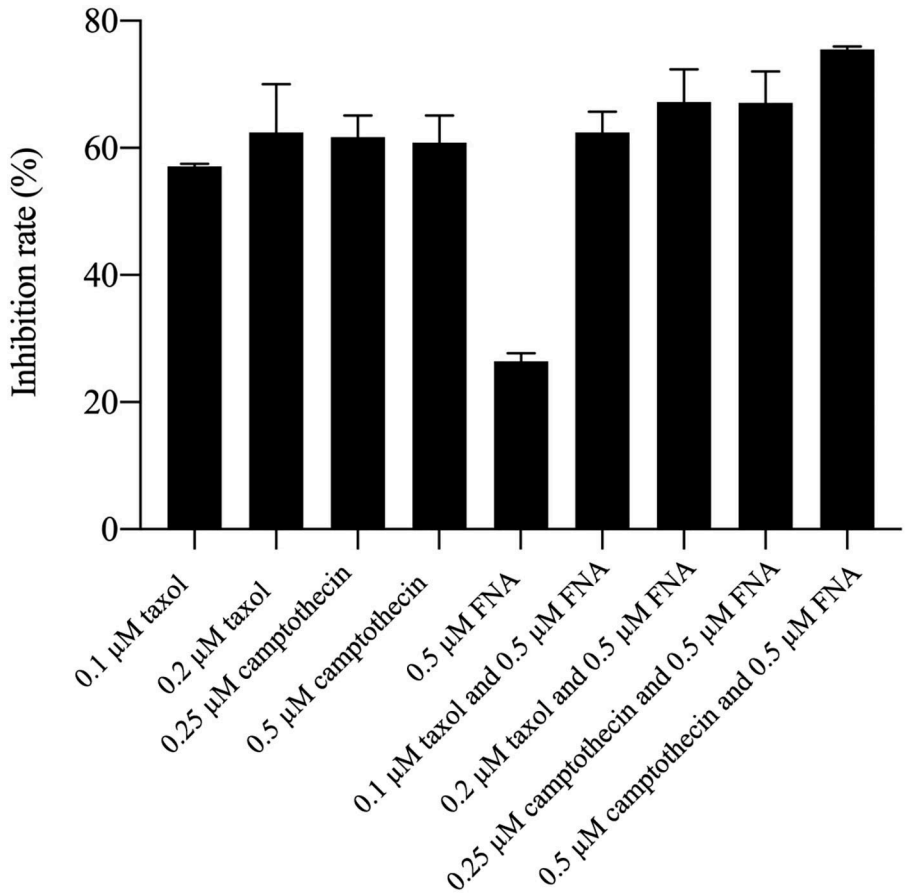


**FIGURE 5 |** Antiproliferative activities of taxol and camptothecin alone and in combination with FNA.

dried over $MgSO_4$, and evaporated under vacuum. The desired compound FNA was obtained by crystallization in EtOAc under 4°C as brown powder. HRMS (AP-ESI) m/z calculated for $C_{17}H_{19}Cl_2FN_3O$ $[M+H]^+$ 370.0889 found 370.0870. $^1H$ NMR (400 MHz, (CD3)2SO): $\delta = 9.33$ (s, $^1H$), 7.86 (d, $J = 8.8$ Hz, $^2H$), 7.08 (dd, $J_1 = 2.3$ Hz, $J_2 = 6.4$ Hz, $^1H$), 6.83 (d, $J = 8.8$ Hz, $^2H$), 6.54 (dd, $J_1 = 2.6$ Hz, $J_2 = 11.2$ Hz, $^1H$), 6.35 (td, $J_1 = 2.8$ Hz, $J_2 = 8.5$ Hz, $^1H$), and 5.14 (s, $^2H$), 3.86–3.75 (m, 8H). $^{13}C$ NMR (400 MHz, (CD3)2SO): $\delta = 165.60$, 161.32, 149.41, 145.81, 130.06, 127.80, 122.59, 120.42, 111.39, 102.60, 102.09, 52.33, and 41.52 ppm.

## Enzyme Inhibitory Selectivity of FNA

All of the HDAC enzymes tested were purchased from BPS Bioscience. First, 20 μL of each recombinant HDAC enzyme solution (HDAC1, 2, 3, 4, 6, 7, 8, and 9) was mixed with various concentrations of tested compound samples (20 μL) in a 96-well plate. The mixture was incubated at 30°C for 1 h for the dose-dependent assay. Additionally, mixtures were incubated for 15, 30, 60, and 90 min, for the time-dependent assay, and then 10 μL of fluorogenic substrate [3 mM Boc-Lys(acetyl)-AMC or Boc-Lys (trifluoroacetyl)-AMC for HDAC1/2/3/6 or HDAC4/7/8/9, respectively] was added. Then, the acetylation reaction was initiated by adding HDAC substrate working solution and incubating at 30°C for 2 h. After the desired time, 10 μL developer with trypsin and trichostatin A was added to stop the reaction, and then the mixture was incubated at 30°C for another 30 min.

A microplate reader was used to determine fluorescence intensity at excitation: 360 nm and emission: 460 nm. The inhibition ratios were calculated by comparing the fluorescence intensities from tested wells to those of controls. The $IC_{50}$ curves and values were then obtained with GraphPad Prism 6.0 software.

## Antiproliferative Activity of FNA

Antiproliferative activities of FNA were evaluated with cell viability assay (MTT assay) with SAHA as the control drug (46). The stock solutions of compounds to be tested were prepared in culture medium. Tumor cell lines were cultured in 96-well plates at a density of $5 \times 10^3$ cells per well and incubated until 90–95% confluence, and then each well received 100 μL medium containing desired concentrations of test compounds, and then incubated at 37°C and 5% $CO_2$ for 48 h. To determine cell viability, 20 μL MTT working solution (5 mg/mL) was then added to each well and incubated for another 4 h. After this incubation, the medium was carefully aspirated, and 200 μL

dimethyl sulfoxide (DMSO) was added to each well and vibrated for 10 min to make sure formed formazans were completely dissolved. The optical densities (ODs) at 490 and 630 nm were counted by Universal Microplate Spectrophotometer. The cell growth inhibition rate was calculated with the following equation: % inhibition = [1–(sample group $OD_{490}$-sample group $OD_{630}$)/(control group $OD_{490}$-control group $OD_{630}$)] × 100%. Origin 7.5 software was used to calculate the $IC_{50}$ values from at least three independent experiments.

## *In vivo* Antitumor Activity

All animal experiments were performed in compliance with the Animal Experiment Ethical Review Board of Weifang Medical University. For *in vivo* antitumor efficacy studies, male athymic nude mice (5–6 weeks old, Slac Laboratory Animals, Shanghai, China) were inoculated subcutaneously in the right shoulder with $1.8 \times 10^7$ HepG2 cells.

Injected mice were kept for 10 days; those with palpable tumors were then randomly assigned into treatment and control groups (six mice per group). The treatment groups were administrated with 100 mg/kg/d test compound intragastrically, whereas the control group was administered with an equal volume of phosphate-buffered saline (PBS) solution. The tumor size and body weight were assessed every day. After 15 days of treatment, the mice were euthanized, and tumor weights were acquired with an electronic balance. The TGI was calculated using the following formula: $TGI = 100\% \times [1 - (TV_{t(T)} - TV_{initial(T)})/(TV_{t(C)} - TV_{initial(C)})]$, where $TV_{t(T)}$ and $TV_{initial(T)}$ stand for the mean tumor volume measured at final time and at initial time for the treatment groups, respectively, and $TV_{t(C)}$ and $TV_{initial(C)}$ represent the mean tumor volume for the control group.

## Cell Apoptosis Assay

HepG2 cells in logarithmic growth phase were cultured in 6-well plates ($4 \times 10^5$ cells per well).Various doses of FNA and SAHA (1, 3, and 9 μM) were added and incubated for 24 h. Then cells were washed with PBS, collected, and resuspended with binding buffer from a commercially available annexin V–FITC kit (Thermo Fisher Co., USA) and mixed with 5 μL of annexin V–FITC gently. Following 10 min of incubation, 1 μL of propidium iodide was added to the samples and incubated for another 20 min while avoiding light. Flow cytometry was used to determine cell apoptosis status (CytoFLEX, Beckman Coulter).

## Cell Cycle Analysis

HepG2 cells in logarithmic growth phase were cultured in 6-well plates with $6 \times 10^5$ cells per well and incubated with different doses of FNA and SAHA (0.125, 0.25, and 0.5 μM). Following 6-h incubation, cells were washed twice with cold PBS and then fixed in 70% precooled ethanol at 4°C for 12 h. The fixed cells were washed again and then stained with PI/RNase A for 30 min at room temperature.

## Drug Combination Analysis

The efficacy of drug combination of FNA with taxol and camptothecin was evaluated via cell viability assay (MTT assay). The stock solutions of tested compounds were diluted to the desired concentrations with culture medium. The cells were cultured in 96-well plates at a density $5 \times 10^3$ cells per well and incubated until 90–95% confluence, and then 100 μL of medium containing desired concentrations of test compounds was added to the wells. Following 48-h incubation, 10 μL of MTT working solution was added to each well and incubated for another 4 h. After removal of the medium, 200 μL DMSO was added to each well to dissolve the formed formazan. The plates were vortexed for 10 min to ensure complete dissolution. Then the OD was acquired with a microplate reader at 490 and 630 nm. The cell growth inhibition rate was calculated with the following equation: % inhibition = [1 – (sample group $OD_{490}$ – sample group $OD_{630}$)/(control group $OD_{490}$ – control group $OD_{630}$)] × 100%.

# DATA AVAILABILITY STATEMENT

The raw data supporting the conclusions of this article will be made available by the authors, without undue reservation.

# ETHICS STATEMENT

The animal study was reviewed and approved by Weifang Medical University Ethics Committee.

# AUTHOR CONTRIBUTIONS

LZ and WS designed the project. YC synthesized the molecules. JF performed the enzymatic screening and performed the *in vivo* antitumor experiment. YH and XW performed the *in vitro* antitumor experiments. YC and LZ analyzed the data and wrote the manuscript. All authors contributed to the article and approved the submitted version.

# FUNDING

This work was supported by Science and technology support plan for youth innovation in universities of Shandong Province (Grant No. 2019KJM001), Natural Foundation of Shandong Province (Youth Found, Grant No. ZR2019QH005), National Natural Science Foundation of China (Youth Found, Grant No. 81803343), International Visiting Scholar Program of Weifang Medical University (No. 20194-05). The English langue of the whole manuscript was revised by Qixiao Jiang.

# SUPPLEMENTARY MATERIAL

The Supplementary Material for this article can be found online at: https://www.frontiersin.org/articles/10.3389/fonc.2020.592385/full#supplementary-material

## REFERENCES


1. Zhang L, Zhang YJ, Chou CJ, Inks ES, Wang XJ, Li XG, et al. Histone deacetylase inhibitors with enhanced enzymatic inhibition effects and potent *in vitro* and *in vivo* antitumor activities. *Chemmedchem*. (2014) 9:638–48. doi: 10.1002/cmdc.201300297
2. Cheng CH, Yun F, He J, Ullah S, Yuan QP. Design, synthesis and biological evaluation of novel thioquinazolinone-based 2-aminobenzamide derivatives as potent histone deacetylase (HDAC) inhibitors. *Eur J Med Chem*. (2019) 173:185–202. doi: 10.1016/j.ejmech.2019.04.017
3. Luan YP, Li J, Bernatchez JA, Li RS. Kinase and histone deacetylase hybrid inhibitors for cancer therapy. *J Med Chem*. (2019) 62:3171–83. doi: 10.1021/acs.jmedchem.8b00189
4. Yun F, Cheng C, Ullah S, He J, Zahi MR, Yuan Q. Thioether-based 2-aminobenzamide derivatives: Novel HDAC inhibitors with potent *in vitro* and *in vivo* antitumor activity. *Eur J Med Chem*. (2019) 176:195–207. doi: 10.1016/j.ejmech.2019.05.007
5. Bernstein BE, Tong JK, Schreiber SL. Genomewide studies of histone deacetylase function in yeast. *Proc Natl Acad Sci USA*. (2000) 97:13708–13. doi: 10.1073/pnas.250477697
6. de Ruijter AJ, van Gennip AH, Caron HN, Kemp S, van Kuilenburg AB. Histone deacetylases (HDACs): characterization of the classical HDAC family. *Biochem J*. (2003) 370(Pt 3):737–49. doi: 10.1042/bj20021321
7. Foglietti C, Filocamo G, Cundari E, De Rinaldis E, Lahm A, Cortese R, et al. Dissecting the biological functions of Drosophila histone deacetylases by RNA interference and transcriptional profiling. *J Biol Chem*. (2006) 281:17968–76. doi: 10.1074/jbc.M511945200
8. Zhang L, Han Y, Jiang Q, Wang C, Chen X, Li X, et al. Trend of histone deacetylase inhibitors in cancer therapy: isoform selectivity or multitargeted strategy. *Med Res Rev*. (2015) 35:63–84. doi: 10.1002/med.21320
9. Gao L, Cueto MA, Asselbergs F, Atadja P. Cloning and functional characterization of HDAC11, a novel member of the human histone deacetylase family. *J Biol Chem*. (2002) 277:25748–55. doi: 10.1074/jbc.M111871200
10. North BJ, Verdin E. Sirtuins: Sir2-related NAD-dependent protein deacetylases. *Genome Biol*. (2004) 5:224. doi: 10.1186/gb-2004-5-5-224
11. Haigis MC, Guarente LP. Mammalian sirtuins–emerging roles in physiology, aging, and calorie restriction. *Genes Dev*. (2006) 20:2913–21. doi: 10.1101/gad.1467506
12. Bottomley MJ, Lo Surdo P, Di Giovine P, Cirillo A, Scarpelli R, Ferrigno F, et al. Structural and functional analysis of the human HDAC4 catalytic domain reveals a regulatory structural zinc-binding domain. *J Biol Chem*. (2008) 283:26694–704. doi: 10.1074/jbc.M803514200
13. Liu T, Liu PY, Marshall GM. The critical role of the class III histone deacetylase SIRT1 in cancer. *Cancer Res*. (2009) 69:1702–5. doi: 10.1158/0008-5472.CAN-08-3365
14. Marks P, Rifkind RA, Richon VM, Breslow R, Miller T, Kelly WK. Histone deacetylases and cancer: causes and therapies. *Nat Rev Cancer*. (2001) 1:194–202. doi: 10.1038/35106079
15. Zhang L, Chen Y, Jiang Q, Song W, Zhang L. Therapeutic potential of selective histone deacetylase 3 inhibition. *Eur J Med Chem*. (2019) 162:534–42. doi: 10.1016/j.ejmech.2018.10.072
16. Patel MM, Patel BM. Repurposing of sodium valproate in colon cancer associated with diabetes mellitus: role of HDAC inhibition. *Eur J Pharm Sci*. (2018) 121:188–99. doi: 10.1016/j.ejps.2018.05.026
17. Mai A, Rotili D, Valente S, Kazantsev AG. Histone deacetylase inhibitors and neurodegenerative disorders: holding the promise. *Curr Pharm Des*. (2009) 15:3940–57. doi: 10.2174/138161209789649349
18. Cantley MD, Haynes DR. Epigenetic regulation of inflammation: progressing from broad acting histone deacetylase (HDAC) inhibitors to targeting specific HDACs. *Inflammopharmacology*. (2013) 21:301–7. doi: 10.1007/s10787-012-0166-0
19. Cao FY, Zwinderman MRH, van Merkerk R, Ettema PE, Quax WJ, Dekker FJ. Inhibitory selectivity among class I HDACs has a major impact on inflammatory gene expression in macrophages. *Eur J Med Chem*. (2019) 177:457–66. doi: 10.1016/j.ejmech.2019.05.038
20. Margolis DM. Histone deacetylase inhibitors and HIV latency. *Curr Opin HIV AIDS*. (2011) 6:25–9. doi: 10.1097/COH.0b013e328341242d
21. Gallo P, Latronico MV, Gallo P, Grimaldi S, Borgia F, Todaro M, et al. Inhibition of class I histone deacetylase with an apicidin derivative prevents cardiac hypertrophy and failure. *Cardiovasc Res*. (2008) 80:416–24. doi: 10.1093/cvr/cvn215
22. Choi JH, Kwon HJ, Yoon BI, Kim JH, Han SU, Joo HJ, et al. Expression profile of histone deacetylase 1 in gastric cancer tissues. *Jpn J Cancer Res*. (2001) 92:1300–4. doi: 10.1111/j.1349-7006.2001.tb02153.x
23. Pflum MK, Tong JK, Lane WS, Schreiber SL. Histone deacetylase 1 phosphorylation promotes enzymatic activity and complex formation. *J Biol Chem*. (2001) 276:47733–41. doi: 10.1074/jbc.M105590200
24. Weichert W, Denkert C, Noske A, Darb-Esfahani S, Dietel M, Kalloger SE, et al. Expression of class I histone deacetylases indicates poor prognosis in endometrioid subtypes of ovarian and endometrial carcinomas. *Neoplasia*. (2008) 10:1021–7. doi: 10.1593/neo.08474
25. Weichert W, Roske A, Niesporek S, Noske A, Buckendahl AC, Dietel M, et al. Class I histone deacetylase expression has independent prognostic impact in human colorectal cancer: Specific role of class I histone deacetylases *in vitro* and *in vivo*. *Clin Cancer Res*. (2008) 14:1669–77. doi: 10.1158/1078-0432.CCR-07-0990
26. Witt O, Deubzer HE, Milde T, Oehme I. HDAC family: what are the cancer relevant targets? *Cancer Lett*. (2009) 277:8–21. doi: 10.1016/j.canlet.2008.08.016
27. Jayani RS, Ramanujam PL, Galande S. Studying histone modifications and their genomic functions by employing chromatin immunoprecipitation and immunoblotting. *Nucl Mech Genome Regul*. (2010) 98:35–56. doi: 10.1016/S0091-679X(10)98002-3
28. Dawson MA, Kouzarides T. Cancer epigenetics: from mechanism to therapy. *Cell*. (2012) 150:12–27. doi: 10.1016/j.cell.2012.06.013
29. De Souza C, Chatterji BP. HDAC inhibitors as novel anti-cancer therapeutics. *Recent Pat Anticancer Drug Discov*. (2015) 10:145–62. doi: 10.2174/1574892810666150317144511
30. Marks PA. Discovery and development of SAHA as an anticancer agent. *Oncogene*. (2007) 26:1351–6. doi: 10.1038/sj.onc.1210204
31. Grant C, Rahman F, Piekarz R, Peer C, Frye R, Robey RW, et al. Romidepsin: a new therapy for cutaneous T-cell lymphoma and a potential therapy for solid tumors. *Expert Rev Anticancer Ther*. (2010) 10:997–1008. doi: 10.1586/era.10.88
32. Rashidi A, Cashen AF. Belinostat for the treatment of relapsed or refractory peripheral T-cell lymphoma. *Future Oncol*. (2015) 11:1659–64. doi: 10.2217/fon.15.62
33. Greig SL. Panobinostat: a review in relapsed or refractory multiple myeloma. *Target Oncol*. (2016) 11:107–14. doi: 10.1007/s11523-015-0413-6
34. Xu Y, Zhang P, Liu Y. Chidamide tablets: HDAC inhibition to treat lymphoma. *Drugs Today*. (2017) 53:167–76. doi: 10.1358/dot.2017.53.3.2595452
35. Mai A, Massa S, Rotili D, Pezzi R, Bottoni P, Scatena R, et al. Exploring the connection unit in the HDAC inhibitor pharmacophore model: novel uracil-based hydroxamates. *Bioorg Med Chem Lett*. (2005) 15:4656–61. doi: 10.1016/j.bmcl.2005.07.081
36. Abdizadeh T, Kalani MR, Abnous K, Tayarani-Najaran Z, Khashyarmanesh BZ, Abdizadeh R, et al. Design, synthesis and biological evaluation of novel coumarin-based benzamides as potent histone deacetylase inhibitors and anticancer agents. *Eur J Med Chem*. (2017) 132:42–62. doi: 10.1016/j.ejmech.2017.03.024
37. Traore MDM, Zwick V, Simoes-Pires CA, Nurisso A, Issa M, Cuendet M, et al. Hydroxyl ketone-based histone deacetylase inhibitors to gain insight into class I HDAC selectivity versus that of HDAC6. *ACS Omega*. (2017) 2:1550–62. doi: 10.1021/acsomega.6b00481
38. Singh RK, Kumar S, Prasad DN, Bhardwaj TR. Therapeutic journery of nitrogen mustard as alkylating anticancer agents: historic to future perspectives. *Eur J Med Chem*. (2018) 151:401–33. doi: 10.1016/j.ejmech.2018.04.001
39. Chen YM, Jia YP, Song WG, Zhang L. Therapeutic potential of nitrogen mustard based hybrid molecules. *Front Pharmacol*. (2018) 9:1453. doi: 10.3389/fphar.2018.01453
40. Goodman LS, Wintrobe MM, Dameshek W, Goodman MJ, Gilman A, McLennan MT. Nitrogen mustard therapy; use of methyl-bis (beta-chloroethyl) amine hydrochloride and tris (beta-chloroethyl) amine hydrochloride for Hodgkin's disease, lymphosarcoma, leukemia and certain

allied and miscellaneous disorders. *J Am Med Assoc.* (1946) 132:126–32. doi: 10.1001/jama.1946.02870380008004
41. Galton DA, Wiltshaw E, Szur L, Dacie JV. The use of chlorambucil and steroids in the treatment of chronic lymphocytic leukaemia. *Br J Haematol.* (1961) 7:73–98. doi: 10.1111/j.1365-2141.1961.tb00321.x
42. Sarosy G, Leyland-Jones B, Soochan P, Cheson BD. The systemic administration of intravenous melphalan. *J Clin Oncol.* (1988) 6:1768–82. doi: 10.1200/JCO.1988.6.11.1768
43. Zhang LH, Lin XY, Chen YM, Wan MH, Jiang QX, Zhang L, et al. Discovery of N-(2-Aminophenyl)-4-(bis(2-chloroethyl)amino) benzamide as a potent histone deacetylase inhibitor. *Front Pharmacol.* (2019) 10:957. doi: 10.3389/fphar.2019.00957
44. Gao S, Li X, Zang J, Xu W, Zhang Y. Preclinical and clinical studies of chidamide (CS055/HBI-8000), an orally available subtype-selective HDAC inhibitor for cancer therapy. *Anticancer Agents Med Chem.* (2017) 17:802–12. doi: 10.2174/1871520616666160901150427
45. Yuan XG, Huang YR, Yu T, Jiang HW, Xu Y, Zhao XY. Chidamide, a histone deacetylase inhibitor, induces growth arrest and apoptosis in multiple myeloma cells in a caspase-dependent manner. *Oncol Lett.* (2019) 18:411–9. doi: 10.3892/ol.2019.10301
46. Lv N, Yuan J, Ji A, Shi L, Gao M, Cui L, et al. Perfluorooctanoic acid-induced toxicities in chicken embryo primary cardiomyocytes: Roles of PPAR alpha and Wnt5a/Frizzled2. *Toxicol Appl Pharmacol.* (2019) 381:114716. doi: 10.1016/j.taap.2019.114716

**Conflict of Interest:** The authors declare that the research was conducted in the absence of any commercial or financial relationships that could be construed as a potential conflict of interest.

frontiers in Oncology

ORIGINAL RESEARCH
published: 26 October 2020
doi: 10.3389/fonc.2020.582273

# Costunolide Induces Autophagy and Apoptosis by Activating ROS/MAPK Signaling Pathways in Renal Cell Carcinoma

*Dian Fu, Ding Wu, Wen Cheng, Jianping Gao, Zhengyu Zhang, Jingping Ge, Wenquan Zhou and Zhenyu Xu**

*Department of Urology, Jinling Hospital, Medical School of Nanjing University, Nanjing, China*

Although costunolide (Cos), a natural sesquiterpene compound isolated from various medicinal plants, exhibits antiproliferative and pro-apoptotic effects in diverse types of cancers, the mechanism associated with the anticancer property of Cos has not been elucidated. The present investigation was carried out to study the anticarcinogenic influence of Cos on kidney cancer cells. Several human renal cancer cell lines were used and biological and molecular studies were conducted. It was found that Cos significantly suppressed renal carcinoma cell growth *via* stimulation of apoptosis and autophagy in a concentration-dependent manner. Further studies revealed that Cos increased Bax/Bcl-2 ratio, decreased mitochondrial transmembrane potential (MMP), and enhanced cytoplasmic levels of cytochrome *c*, and activation of caspase-9, caspase-3, and cleaved PARP, resulting in cell apoptosis. The autophagy induced by Cos resulted from the formation of GFP-LC3 puncta and upregulation of LC3B II and Beclin-1 proteins. Compared with Cos treatment, the autophagy inhibitor 3-MA or ROS scavenger NAC significantly inhibited apoptosis and autophagy. Moreover, NAC and JNK-specific inhibitor SP600125 attenuated the effect of Cos. Taken together, Cos exerted autophagic and apoptotic effects on renal cancer through the ROS/JNK-dependent signal route. These findings suggest that Cos could be a beneficial anticarcinogenic agent.

**Keywords: costunolide, renal cancer, ROS – reactive oxygen species, apoptosis, autophage**

OPEN ACCESS

***Edited by:***
*Zhe-Sheng Chen,*
*St. John's University, United States*

***Reviewed by:***
*Kaisheng Liu,*
*Jinan University, China*
*Jin-Jian Lu,*
*University of Macau, China*

****Correspondence:***
*Zhenyu Xu*
*1625688850@qq.com;*
*xuzhenyu1978@126.com*

***Specialty section:***
*This article was submitted to Pharmacology of Anti-Cancer Drugs, a section of the journal Frontiers in Oncology*

***Received:*** *11 July 2020*
***Accepted:*** *02 September 2020*
***Published:*** *26 October 2020*

***Citation:***
*Fu D, Wu D, Cheng W, Gao J, Zhang Z, Ge J, Zhou W and Xu Z (2020) Costunolide Induces Autophagy and Apoptosis by Activating ROS/MAPK Signaling Pathways in Renal Cell Carcinoma. Front. Oncol. 10:582273. doi: 10.3389/fonc.2020.582273*

## INTRODUCTION

Renal cell carcinoma (RCC) comprises 3–4% of all human cancers, and it is the most lethal kidney malignant tumor (1). Surgical intervention is the most effective therapeutic strategy for RCC. However, up to 30% of RCC cases are diagnosed at the stage of metastasis (2). The 5-year overall survival of metastatic RCC patients is below 10%. Typically, RCC is insensitive to traditional chemo- and radio-therapeutic treatments (3). Moreover, the use of targeted treatment options as first and second-line treatments have limited effect on the survival rates. Therefore, there is need for exploring low-toxicity novel treatment strategies for RCC.

Costunolide (Cos) is a naturally occurring sesquiterpene compound present in various medicinal plants, including *Magnolia sieboldii*, *L aurus nobilis*, and *Saussurea lappa* (4, 5). It has various effects such as anti-inflammatory and antifungal properties (6, 7). Recently, Cos has been

reported to be able to assist chemotherapeutic agents in overcoming multidrug resistance in cancer cells (8). Although some studies have shown that Cos exhibits potent anticarcinogenic activity in human cancer cells through induction of cell cycle arrest and apoptosis (9, 10), its effect on human renal cancer cells and the possible associated mechanisms have not been unraveled.

Cell death can be classified according to the classical morphological criteria as apoptotic or autophagic. Apoptotic cell death is a tightly regulated event, which is important for sustaining tissue constancy *via* removal of genetically compromised cells. The typical features of apoptosis are membranous blebs and nuclear fragments (11). It has been established that apoptosis may occur through either extrinsic or intrinsic route (12). Both pathways may lead to the activation of a related group of caspases involved in the initiation (caspases-8 and -9) and execution (caspases-3) phases of apoptosis (13). Autophagy is an evolutionarily preserved process by which cells degrade macromolecules, unwanted organelles and certain types of bacteria *via* double-membrane structures termed autophagosomes (14). Autophagy performs a complex function in cancer development and treatment (15). It can function as a cytoprotective mechanism that protects cancer cells from apoptotic cell death induced by various anticancer drugs (16). On the other hand, excessive autophagy can cause cell death and arrest tumor progression. Therefore, extensive attention has been paid to redefining the precise function of autophagic processes in malignancy therapy, so as to enhance the designing, selection, and utilization of autophagy-regulating agents (autophagy inducers or inhibitors) (17). In addition, increasing evidence have shown that apoptosis and autophagy may be cooperative or antagonistic to determine cell fate depending on cell types, strength, and duration of the stress-inducing signals, and influence of other signaling routes (18).

In this study, it was found that Cos exerted reactive oxygen species (ROS)-induced autophagic and apoptotic effects on renal cancer cells through ROS induction, resulting in stimulation of JNK signal pathway. Thus, Cos could be a promising inducer of autophagy and apoptosis, which can be used for targeting human cancers.

# MATERIALS AND METHODS

## Materials and Chemicals

Cos, 3-methyladenine, and inhibitors of JNK, MAPK, and ERK1/2 were purchased from Selleck. Cos was dissolved in dimethyl sulfoxide (DMSO) and preserved at −20°C. RPMI-1640, DMEM, and FBS were products of Thermo Fisher, while N-acetyl-L-cysteine was obtained from Sigma (St. Louis, MO, United States). Immunoglobulins against caspases-3, -9, and -8; and Bax, PARP, Bcl-2, Cyt c, CoxIV, JNK, p-JNK, p38, p-p38, ERK, phospho-ERK, LC3B, Beclin-1, and β-actin were products of Cell Signaling Technology (Shanghai, China). Reagents for mitochondrial transmembrane potential (MMP) and apoptosis were obtained from Beyotime Inst. Biotech (Beijing, China). Polyvinylidene difluoride membrane was product of Millipore Corp, United States.

## Cell Maintenance and Cultural Conditions

Four human RCC cells (786-O, A-498, ANCH, and 769-P) were supplied by American Type Culture Collection (Manassas, Virginia, United States). The cell lines were cultured in medium (786-O and 769-P in RPMI-1640; A-498 and ANCH in DMEM) with fetal calf serum and antibiotics. The cell culture was done in a 37°C and 5% $CO_2$ humidified atmosphere. The cells were grown to confluence before drug treatment. Cos was solubilized in DMSO.

## Cell Viability Assay

The CCK8 assay was used. The cells in suspension were exposed to graded doses of Cos (5, 10, 20, and 40 μM) for 24 h, followed by incubation with 10 μL CCK8 solution for 180 s at 37°C and measurement of absorbance at 455 nm.

For cell counting, cell suspension was incubated for 24 h with the same doses of Cos as in CCK8 assay. Thereafter, the population of dead cells was determined with trypan blue dye exclusion procedure.

## Nuclear Morphologies of Apoptotic Cells

Cell suspension treated with graded doses of Cos were subjected to fixation in paraformaldehyde and stained with DAPI away from light. Nuclear fluorescence intensities were obtained using Nikon fluorescence microscopy (Nikon Inc., Japan).

## Flow Cytometry Analysis of Apoptosis

After treatment with Cos, the cells were rinsed in phosphate-buffered saline (PBS) and resuspended in 200-μL binding solution that contained 5 μL Annexin V-FITC and 10 μL propidium iodide for 20 min away from light. All samples were subjected to flow cytometric analysis.

## Caspase Activity Assay

Caspase-3, caspase-8, and caspase-9 were assayed fluorometrically using Beyotime kits (Beijing, China) in line with respective manual protocols.

## Measurement of Mitochondrial Transmembrane Potential

The MMP ($\Delta\psi m$) was measured using JC-1 Assay Kit (Beyotime, Beijing, China) in line with the manufacturer's protocol. The Cos treatment was followed with JC-1 staining for 30 min away from light at 37°C. Cellular fluorescent photographs obtained with microscope (Nikon Inc., Japan) were analyzed with flow cytometry.

## RNA Isolation and Real-Time Quantitative PCR Assays

The 769-P cells were plated in six-well plates. After 12-h incubation, the cells were exposed to Cos (10, 20, and 40 μM) for

24 h, followed by extraction of total RNA and cDNA generation, and RT-PCR with Bio-Rad iQ5 System, with β-actin as control. The β-actin primers were generated as outlined previously (19). Relative abundances of the target mRNAs were calculated.

## ROS Generation

The generation of intracellular ROS was determined with a cell-permeable probe, DCFH-DA. Following treatment of the cells with Cos, they were subjected to incubation with the fluorescent probe at 37°C for ½ h away from light. Fluorescent photographs of cells were analyzed with flow cytometry.

## GFP-LC3 Puncta Assay

The 769-P cells with stable expression of GFP-LC3 were plated in six-well plates. After treatment with Cos, the cells were PBS-rinsed and paraformaldehyde-fixed at room temperature for 10 min. Following removal of paraformaldehyde, the cells were washed thrice with PBS and then stained with DAPI away from light at room temperature. Fluorescent images were captured with a fluorescence microscope.

## Western Blotting

Extraction of total protein from Cos-treated 769-P cells followed the method outlined earlier (19). Moreover, proteins from mitochondria and cytosol were extracted using appropriate Kits (Pierce, Rockford, IL, United States). Bicinchoninic assay method was used for determination of protein levels. Then, equal amounts of protein were subjected to 12% SDS-PAGE and electro-transferred to PVDF membranes, the membranes were blocked in 5% non-fat dry milk at room temperature for 1 h, and then incubated with primary antibodies for overnight at 4°C. Thereafter, the membranes were subjected to

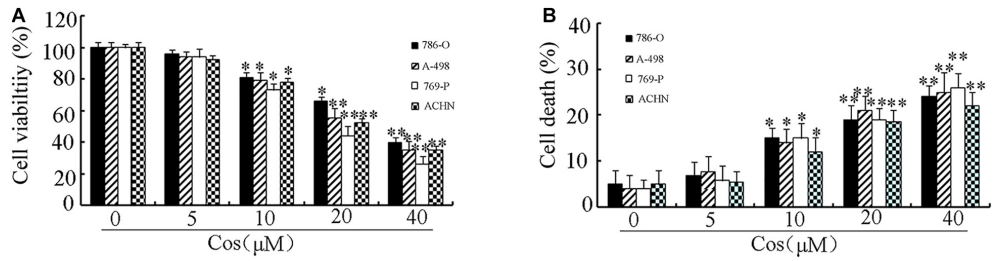


**FIGURE 1 |** Treatment with Cos decreased cell viability and induced cell death. **(A)** Cell viability, as determined with CCK8 assay. **(B)** Cell death, as measured using trypan blue exclusion assay. All results are presented as mean ± SD ($n$ = 3). *$p$ < 0.05; **$p$ < 0.01, vs the control.

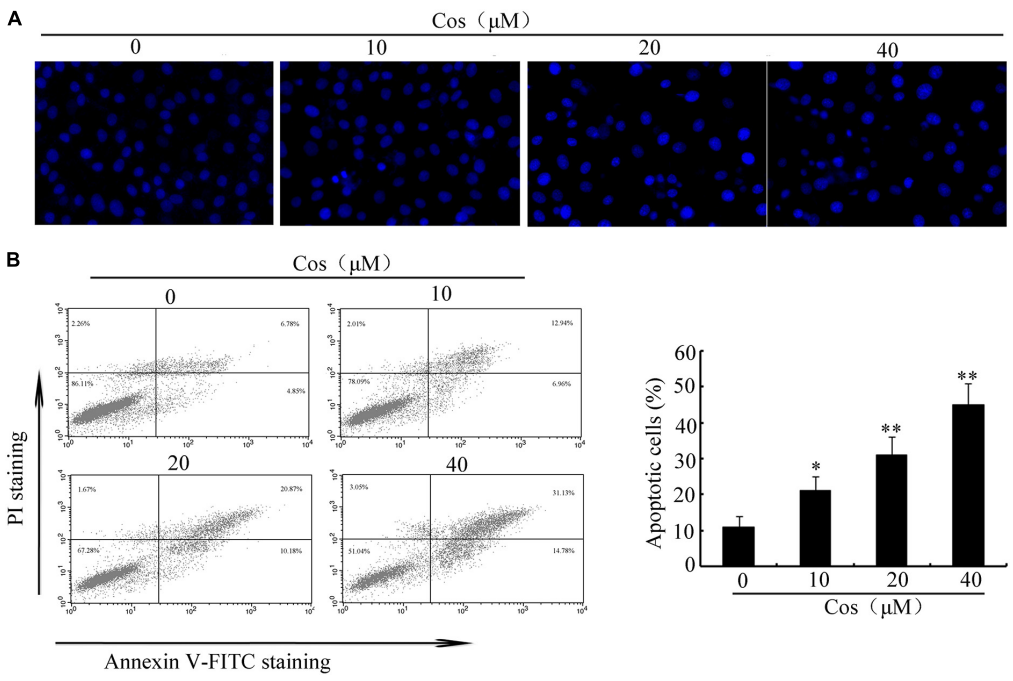


**FIGURE 2 |** Cos induced apoptosis in 769-P cells. **(A)** Apoptotic nuclear morphology, as assessed using DAPI staining and visualized using fluorescence microscopy. **(B)** Percentage of Cos-induced apoptosis in 769-P cells, as measured using Annexin V-FITC/PI staining and flow cytometry. The histograms indicate the percentage of early apoptosis and late apoptosis. All results are presented as mean ± SD ($n$ = 3). *$p$ < 0.05; **$p$ < 0.01, vs the control.

incubation with HRP-linked 2° conjugated secondary antibodies at room temperature for 1 h. The signals were detected using chemiluminescence (ECL).

## Statistical Analysis

All data are expressed as mean ± SD of three independent experiments. Student's *t*-test and one-way ANOVA were employed for statistical analyses. Values of $p$ less than 0.05 were considered statistically significant.

# RESULTS

## Cos Decreased Cell Viability via Induction of Apoptosis in RCC

To determine the cytotoxic influence of Cos on RCC cells, the 786-O, A-498, 769-P, and ACHN cells were exposed to different concentrations of Cos (10, 20, and 40 μM) for 24 h, followed by CCK8 and Trypan blue exclusion assays. **Figure 1A** shows that Cos significantly decreased viability of RCC cells concentration-dependently. Moreover, Cos enhanced apoptosis in a concentration-based fashion (**Figure 1B**). The occurrence of apoptosis in Cos-treated RCC cells was determined with DAPI staining and flow cytometry. Results revealed that the cells without Cos treatment had rounded nuclei with well distributed chromatin, whereas typical apoptotic features of condensed chromatin and nuclear fragmentation were seen following treatment with Cos (10, 20, and 40 μM) (**Figure 2A**). Flow cytometric analysis showed that significant and dose-based increases in apoptotic cell number were observed after Cos exposure (**Figure 2B**).

Previous studies have demonstrated that apoptosis involves stimulation of cysteine proteases, including both initiators and executors of cell death (13). Thus, further evaluation was done on the effects of Cos on the levels of caspases-8, -9, and -3 using caspase fluorometric assay kits. No significant change was observed in the activity of caspase-8 in the Cos-treated cells, when compared with cells with no Cos treatment. Interestingly, Cos treatment markedly enhanced levels of caspases 9 and 3 (**Figure 3A**). Consistent with these results, procaspases-9 and -3 levels were lowered with increase in Cos concentration, while the cleaved forms of caspase-9 and caspase-3 increased (**Figure 3B**).

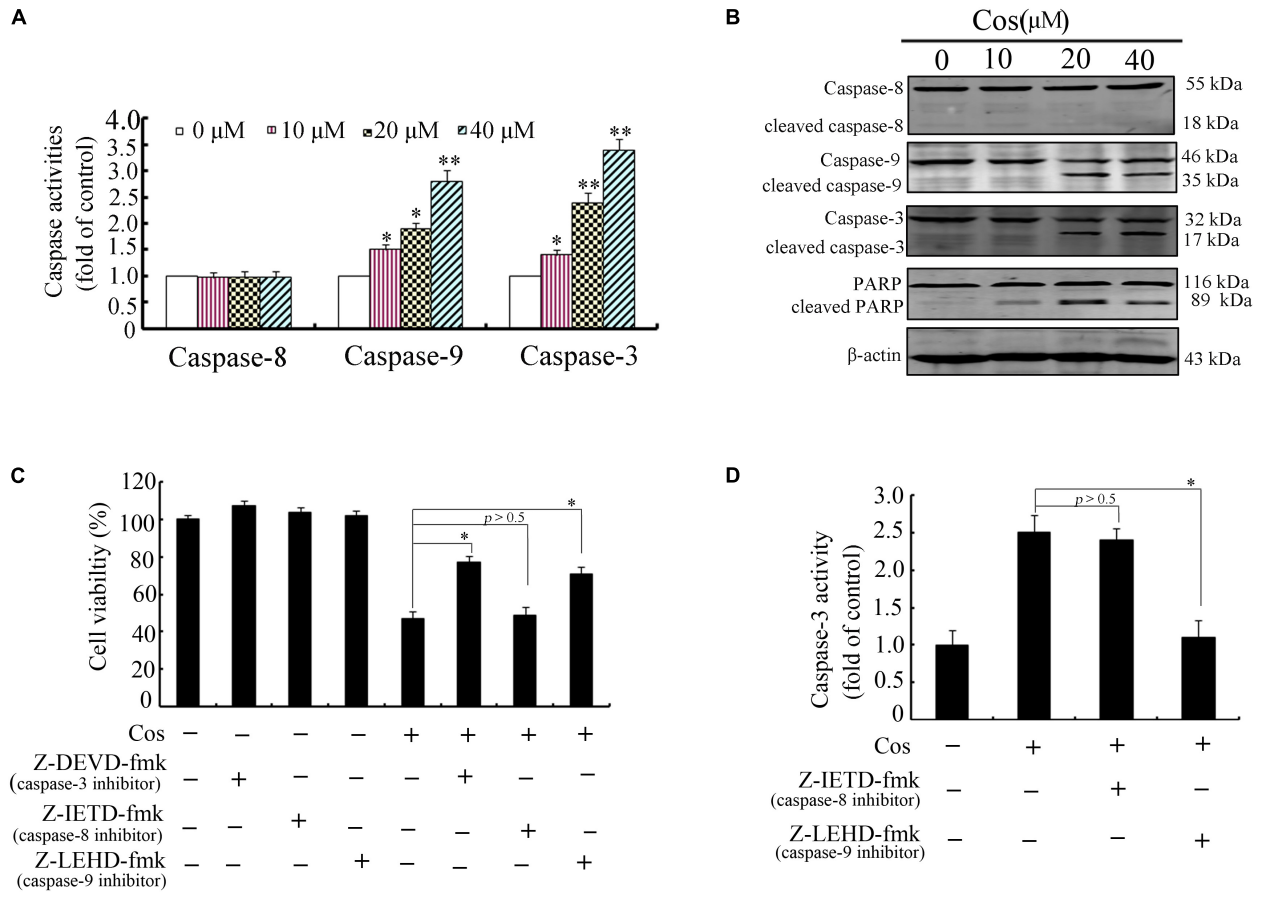


**FIGURE 3 |** Cos-induced apoptosis was mediated by caspases 9 and 3 in 769-P cells. **(A)** Activities of caspase-3, caspase-8, and caspase-9 as measured using the colorimetric assay kits. **(B)** Caspases-8, -9, and -3, and PARP in 769-P cells treated with various concentrations of Cos for 24 h. **(C)** Effect of caspase inhibitors on Cos-induced cell viability, as measured with CCK8 assay. **(D)** Inhibitory effects of caspase-8 and caspase-9 inhibitors on caspase-3 activity. The activity of caspase-3 was assayed using colorimetric assay kit. All results are presented as mean ± SD ($n$ = 3). *$p$ < 0.05; **$p$ < 0.01, vs the control.

Procaspase-8 was not affected, while PARP was apparently cleaved following Cos treatment for 24 h (**Figure 3B**). In addition, specific inhibitors of caspase-9 or caspase-3, not caspase-8, significantly attenuated Cos-provoked apoptosis (**Figure 3C**). Caspase-3 was also significantly inhibited with treatment of caspase-9 inhibitor, but not caspase-8 inhibitor (**Figure 3D**). The observations provide evidence that Cos enhanced apoptosis *via* stimulation of caspases-9 and -3 only.

## Cos-Activated Mitochondrial Apoptotic Route in RCC Cells

To determine whether mitochondrial pathway mediated Cos-induced apoptosis, MMP ($\Delta\psi$m) was determined with JC-1. In normal cells, JC-1 aggregates in normal mitochondria emit red fluorescence. In contrast, JC-1 aggregates in cytosol emit green fluorescence when the mitochondria membrane is depolarized. The results obtained in this study showed a clear change from red to green fluorescence after Cos treatment, indicating that a change in $\Delta\psi$m was triggered by Cos treatment in 769-P cells (**Figure 4A**). Flow cytometric analysis showed that MMP-depolarized cells were enhanced from 6.83% (normal level) to 12.99, 22.77, or 37.70% after Cos treatment (**Figure 4B**).

It is known that $\Delta\psi$m is controlled by the Bcl-2 proteins. Therefore, the expressions of Bax and Bcl-2 were assayed using quantitative RT-PCR and Western blot. Results showed that the expression of Bcl-2 was significantly decreased at both mRNA and protein levels (**Figures 5A,C**). In contrast, Cos treatment significantly increased the mRNA and protein expressions of Bax (**Figures 5B,C**). Moreover, Bax/Bcl-2 was elevated in Cos-exposed cells, relative to control, indicating enhancement of occurrence of apoptosis (**Figure 5D**). In addition, Cos enhanced transfer of Bax from the cytosol to the mitochondrion, and enhanced the release of cytochrome *c* from mitochondria (**Figures 5E,F**). Thus, Cos provoked apoptosis through the mitochondrial pathway.

## Cos Induced Autophagy in RCC Cells

To determine whether Cos induced autophagy in 769-P cells, GFP-LC3 dot formation was performed. The results showed that Cos treatment accentuated GFP-LC3 puncta generation in 769-P cells in a dose-based fashion (**Figures 6A,B**). Moreover, the expression of several protein biomarkers of autophagy were assayed with Western blot analysis. The results revealed that Cos treatment increased the protein expressions of LC3B II and Beclin-1 (**Figures 6C–E**). It is known that

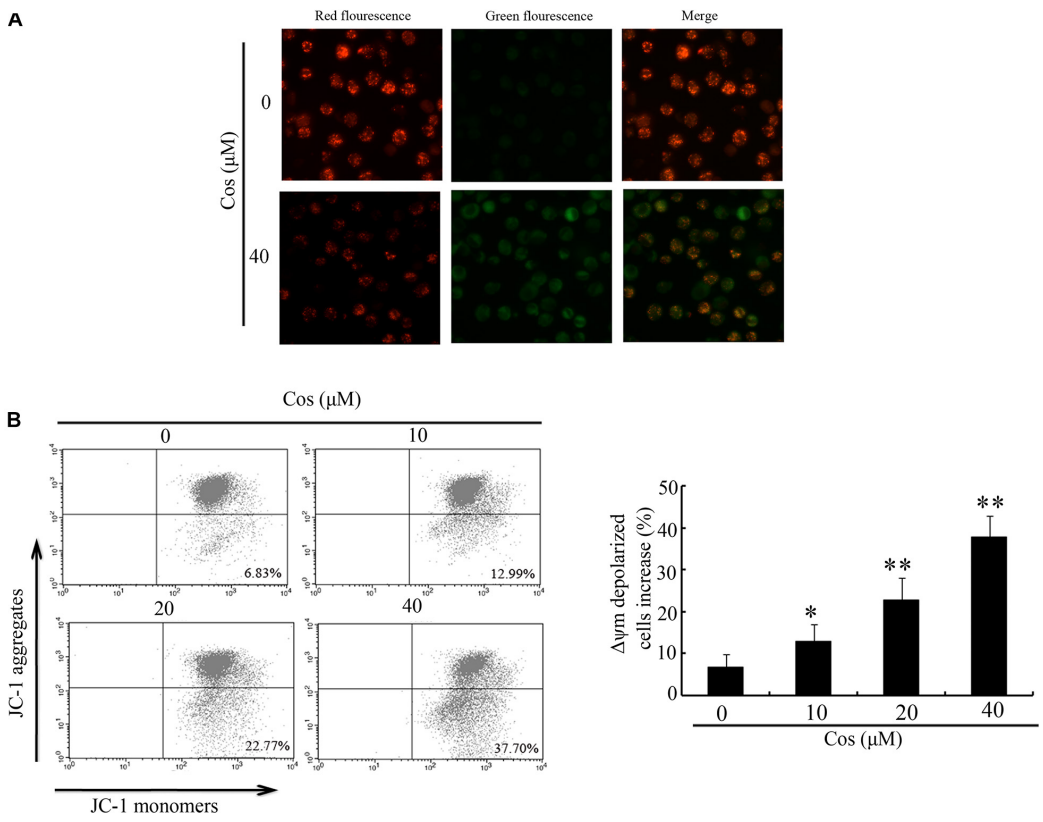


**FIGURE 4 |** Influence of Cos on mitochondrial membrane potential in 769-P cells. **(A)** 769-P cells exposed to Cos (40 μM) for 24 h and observed under fluorescent microscope after JC-1 staining. Untreated cells served as control. Red fluorescence = normal $\Delta\psi$m; green fluorescence = damaged $\Delta\psi$m. **(B)** $\Delta\psi$m after Cos exposure and JC-1 treatment, as determined flow cytometrically, showing that $\Delta\psi$m-depolarized cells increased by about 26.2 and 61.3% at 12 and 24 h, respectively. All results are presented as mean ± SD ($n$ = 3). *$p$ < 0.05; **$p$ < 0.01, vs the control.

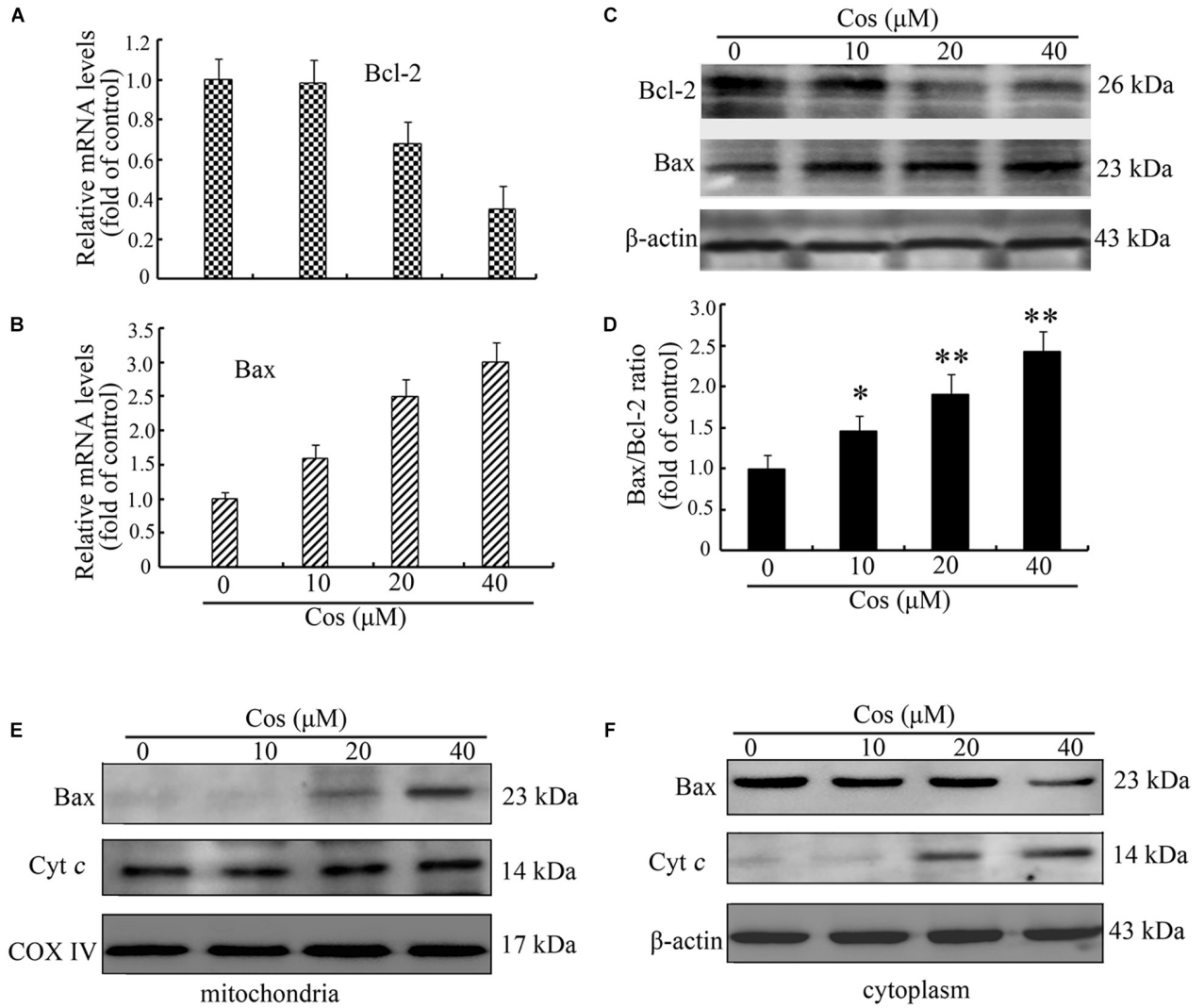


**FIGURE 5 |** Cos-mediated 769-P cell apoptosis was mediated via mitochondrial route. Bcl-2 mRNA **(A)** and **(B)** Bax mRNA levels, as determined with qRT-PCR. **(C)** Bax and Bcl-2 proteins. **(D)** Bax/Bcl-2 ratio. **(E)** Bax and cyt *c* in 769-P cells. All results are presented as mean ± SD ($n = 3$). *$p < 0.05$; **$p < 0.01$, vs the control. **(F)** Cytosolic proteins were isolated and analyzed by Western blot to measure the localization of Bax and cyt c.

autophagy may exert protective effect on cells or contribute to apoptosis (16). Treatment of 769-P cells with 3-MA, an autophagic suppressor, resulted in marked increase in viability (**Figure 6F**). Furthermore, 3-MA markedly decreased Cos-induced mitochondrial depolarization (**Figures 6G,H**). These results suggest that inhibiting autophagy could attenuate apoptosis induced by Cos in 769-P cells.

## Cos Induced Autophagy-Associated Cell Death Through ROS

It is established that ROS are involved in apoptosis and autophagy (20–22). In this study, ROS generation was determined in 769-P cells with the ROS probe DCFH-DA. Treatment with Cos increased ROS in a concentration-dependent fashion (**Figures 7A–C**). Furthermore, the increases in ROS were significantly attenuated by pretreating the cells with the ROS scavenger N-Acetyl-cysteine (NAC) (**Figure 7D**). Moreover, NAC treatment attenuated the decrease in cell viability (**Figure 8A**) and apoptosis (**Figure 8B**) caused by Cos treatment, and NAC significantly decreased the levels of Bax and LC3-II and increased Bcl-2 level (**Figures 8C,D**). Thus, ROS are implicated in autophagy and cell death induced by Cos.

## Cos Induced Apoptotic and Autophagic Changes *via* the JNK Signaling Pathway

The MAPK signaling route is linked to apoptosis and autophagy (23). Levels of p-ERK1/2, p-JNK, and p38 were assayed in this study. As shown in **Figures 9A–C**, Cos treatment markedly increased the level of phosphorylated JNK in a concentration-dependent manner. Furthermore, pretreatment

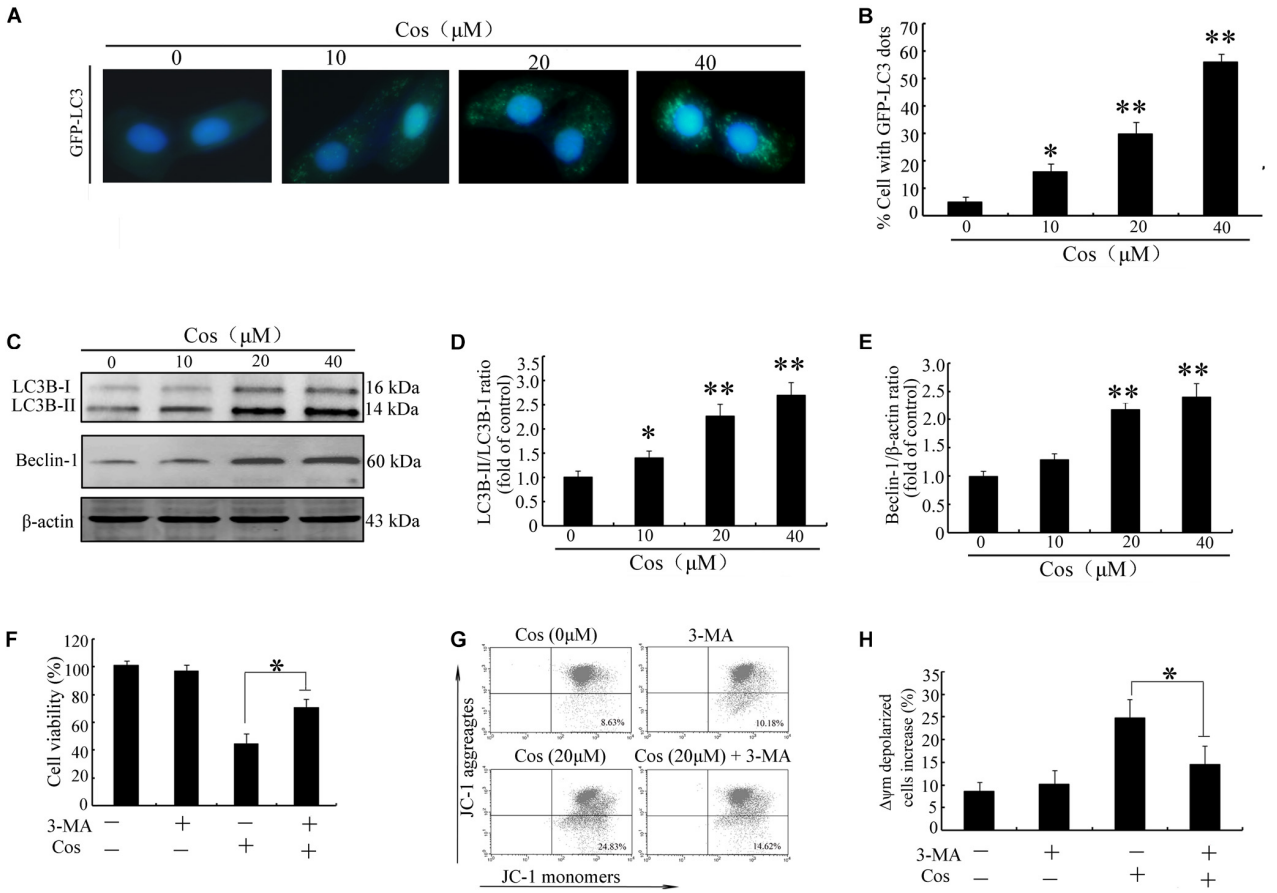


**FIGURE 6 |** Cos exerted autophagy-mediated cell death through ROS production in 796-P cells. **(A)** Photomicrograph of cells showing GFP-LC3 and indicating formation of autophagosomes. Cos-exposed cells had a punctate profile of GFP-LC3B expression. **(B)** Protein expressions of LC3B-I/IC3-II and Beclin-1, as assayed using Western blot. **(C)** LC3-II/LC3-I ratio and **(D)** Beclin-1/β-actin ratio in Cos-treated 769-P cells, as determined with Image J. **(E)** Cell viability, as measured using CCK8. **(F)** Mitochondrial membrane potential. All results are presented as mean ± SD ($n = 3$). *$p < 0.05$; **$p < 0.01$, vs the control. **(G)** The mitochondrial membrane potential were measured using JC-1 staining by flow cytometry. **(H)** The histograms indicate the ratio of green in JC-1 fluorescence.

with JNK inhibitor (SP600125), but not ERK1/2 inhibitor (SCH772984) or p38 MAPK inhibitor (SB203580), significantly attenuated cell viability caused by Cos treatment (**Figure 9D**). The Cos-stimulated apoptosis was mitigated by SP600125 (**Figure 9E**). In addition, SP600125 decreased the protein expressions of LC3-II and Beclin-1 (**Figure 9F**). Taken together, these results indicate the involvement of JNK in Cos-mediated autophagy and cell death.

## ROS Production Preceded JNK Stimulation in Cos-Provoked Apoptosis

**Figure 10A** shows that the JNK inhibitor SP600125 did not affect Cos-induced ROS generation, suggesting that JNK did not enhance ROS levels. Interestingly, suppression of ROS with NAC eliminated Cos-associated JNK2 phosphorylation (**Figure 10B**), indicating that ROS generation preceded the activation of JNK in Cos-treated 769-P cells. Taken together, these findings indicate that ROS/JNK pathway activated by Cos treatment is involved in the induction of apoptosis and autophagy (**Figure 11**).

# DISCUSSION

Cos is a sesquiterpene lactone isolated from the stem bark of *M. sieboldii*. It exhibits various biological and immunological properties. Previous studies showed that Cos exerted various anticancer effects such as blockage of the angiogenic factor (VEGFR) signaling pathway (24), disruption of microtubule proteins (25), inhibition of telomerase activity (26), and triggering of apoptosis and arrest of the cell cycle (9). However, the association between Cos-induced cell death and autophagy has not been reported. The present study has provided evidence, indicating that Cos induced apoptosis and autophagy in human renal cancer cells *via* ROS/JNK signaling pathway.

It is well-known that apoptosis is a basic event needed for maintenance of tissue constancy (11). Earlier reports have shown that Cos induced apoptotic cell death in different cancers such as breast, lung, bladder, and esophageal cancers (9, 27–30). Consistent with these reports, the results obtained in this study showed that Cos decreased RCC cell viability and increased cell death. Chromatin condensation and presence of

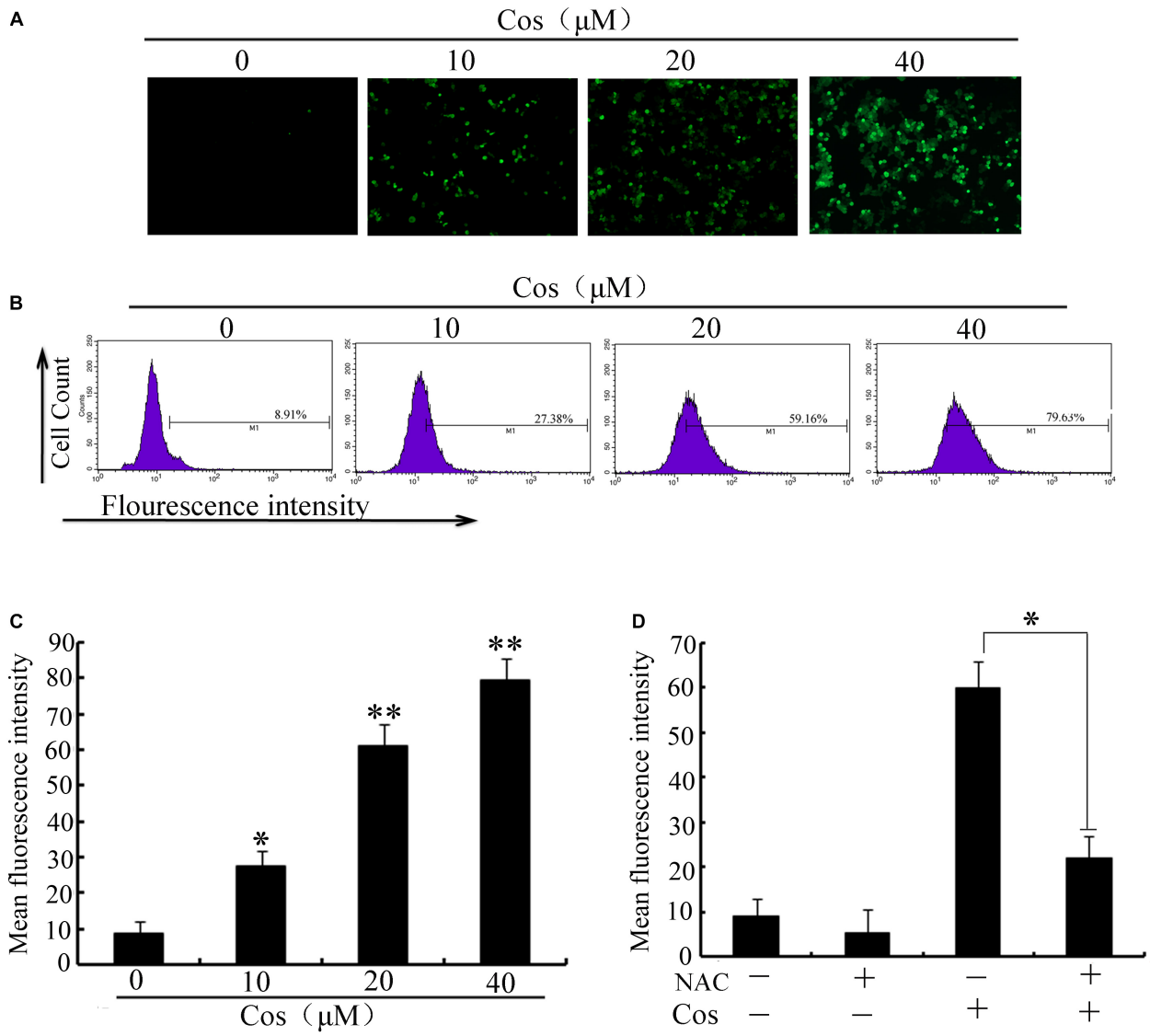


**FIGURE 7 |** Cos increased ROS generation in 769-P cells. **(A)** ROS levels. **(B)** ROS levels measured as fluorescent intensity. **(C)** ROS of cells pretreated with NAC prior to Cos exposure for 24 h. The histograms indicate the change of fluorescent intensity in Cos treated cells. **(D)** Cells were pretreated with NAC (5 mM) for 2 h and then treated with Cos for 24 h. Fluorescent intensity was detected using flow cytometry. All results are presented as mean ± SD ($n = 3$). *$p < 0.05$; **$p < 0.01$, vs the control.

phosphatidylserine on the exterior of the cell are crucial indices of apoptosis. These features were present in RCC cells 24 h after Cos treatment, indicating that Cos induced RCC cell apoptosis.

The possible mechanisms underlying Cos-induced apoptosis in 769-P cells were investigated. Cascade activation of caspases plays important roles in apoptosis. The two major caspase activation pathways (death receptor and mitochondrial pathways) have been well described (12). The death receptor pathway is initiated by binding of ligands to death receptors, resulting in caspase-8 activation (13). Mitochondria pathway depends on Cyt c release from mitochondrion into the cytoplasm, leading to caspase-9 stimulation and activation of capase-3 associated with generation of typical apoptotic features. Previous studies showed that Cos induced cancer cell death *via* stimulation of caspase-8 or caspase-9, depending on cancer cell types or other factors. For instance, it has been reported that Cos induced apoptosis of breast and leukemia cancer cells through the extrinsic route (9, 31). Moreover, Cos induced apoptosis in bladder and lung cancer cells through the mitochondrial pathway (28, 29). The results of the present study revealed that Cos promoted caspases-9 and -3, and cleaved PARP in 769-P cells, but caspase-8 was not affected. In addition, the caspase-8 specific inhibitor (z-IETD-fmk) did not attenuate cell death induced by Cos treatment. Western blot and other assays revealed that Cos treatment enhanced Bax/Bcl-2, reduced mitochondrial membrane potential, and resulted in cytochrome

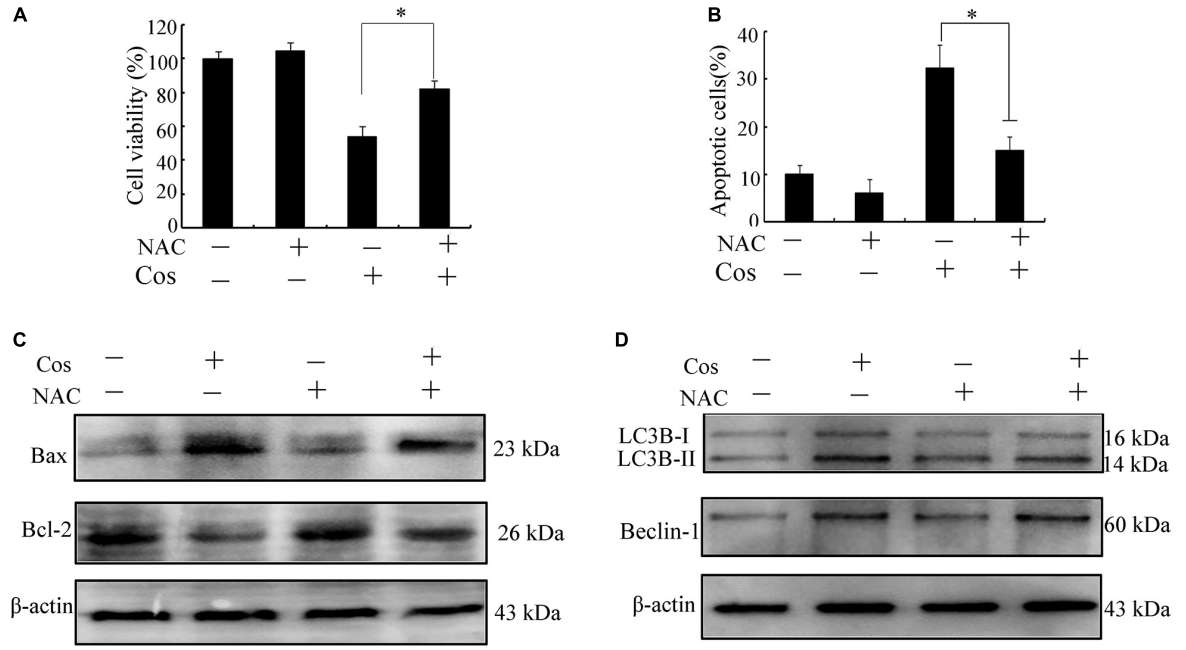


**FIGURE 8 |** Cos exerted apoptotic and autophagic effects in 769-P cells *via* ROS generation. **(A)** Cell viability. **(B)** Cell apoptosis was evaluated by flow cytometry. **(C,D)** Protein expressions of Bax, Bcl-2, Beclin-1, and LC3B-I/LC3B-II ratio. All results are presented as mean ± SD ($n = 3$). *$p < 0.05$; **$p < 0.01$, vs the control.

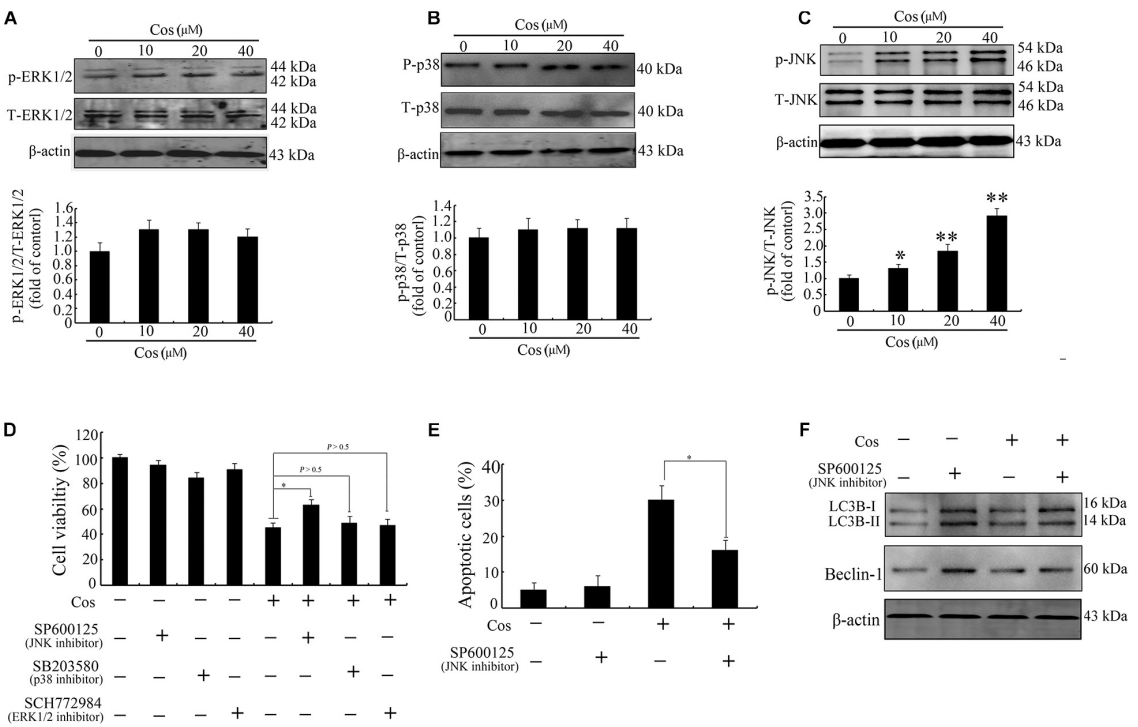


**FIGURE 9 |** Cos-induced apoptosis and autophagy were associated with JNK activation in 769-P cells. Western-blotting results on protein expressions of ERK1/2 and p-ERK1/2 **(A)**, p38 and p-p38 **(B)**, and JNK and p-JNK **(C)**. Phosphorylated proteins in each immunoblot were normalized to total protein content of the respective protein. **(D)** Results CCK8 assay on 769-P cells pretreated with MEK1/2 inhibitor PD98059 (10 μM), JNK inhibitor SP600125 (10 μM), or the p38 inhibitor SB203580 (10 μM) for 2 h prior to treatment with or without Cos (20 μM), for 24 h. **(E)** Apoptosis of 769-P cells pretreated with JNK inhibitor SP600125 (10 μM) for 2 h prior to treatment with or without Cos (20 μM). **(F)** Expression levels of autophagy-related proteins, as assayed using Western blot. All results are presented as mean ± SD ($n = 3$). *$p < 0.05$; **$p < 0.01$, vs the control.

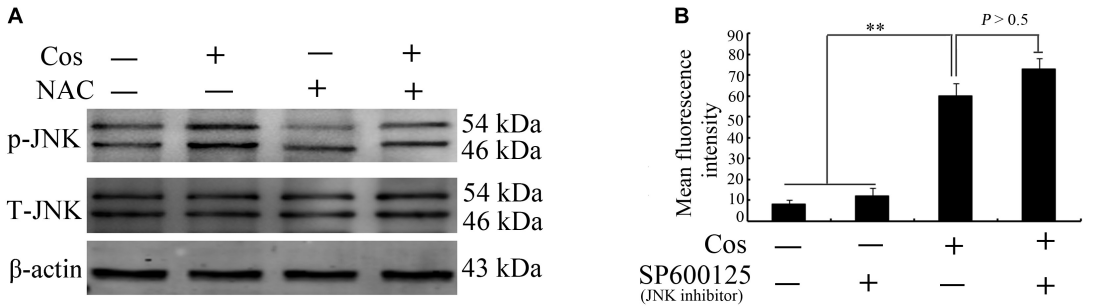


**FIGURE 10 |** ROS production preceded JNK activation in Cos-provoked apoptosis and autophagy in 769-P cells. **(A)** Effect of NAC (5 mM) on expressions of phospho-JNK1/2 and total JNK1/2 in 769-P cells exposed to Cos (20 μM) for 24 h. **(B)** ROS levels in 769-P cells pretreated with SP600125 (10 μM) for 2 h prior to treatment with or without Cos (20 μM). All results are presented as mean ± SD ($n$ = 3). *$p < 0.05$; **$p < 0.01$, vs the control.

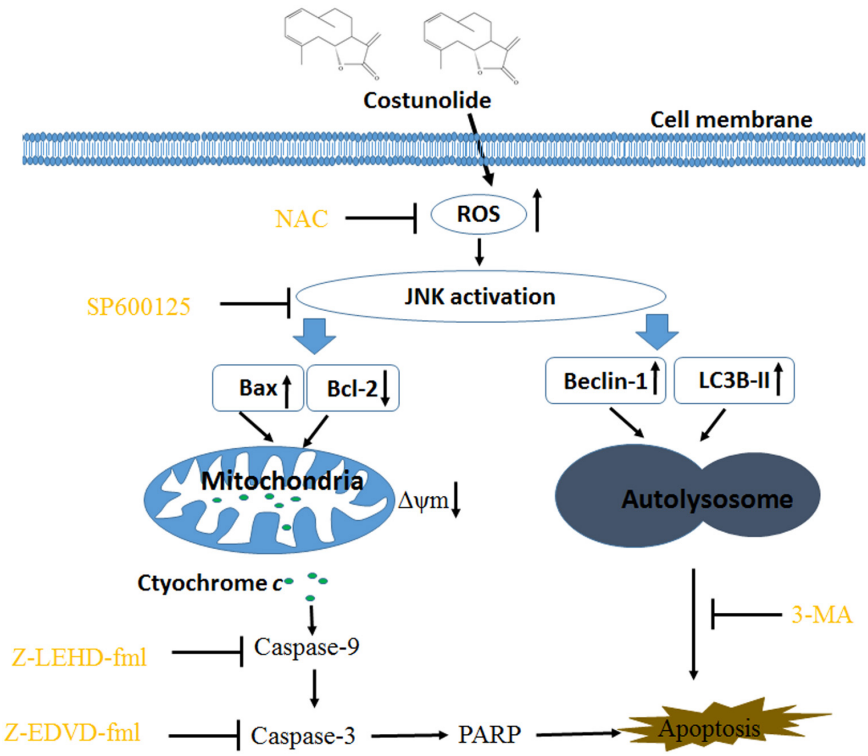


**FIGURE 11 |** Costunolide induced autophagy and apoptosis via ROS/JNK signaling pathway.

*c* release from mitochondrion into the cytosol. These data indicate that Cos induced apoptosis in 769-P cells through mitochondrial pathway.

Protracted exposure of cancerous cells to chemotherapy makes them resist apoptosis. Previous studies have demonstrated that modulation of autophagic processes could be useful for circumventing chemoresistance and enhancing the effects of chemotherapeutics (32, 33). Autophagy is a cellular process for clearance of damaged organelles, and it is involved in carcinogenesis and sensitivity of cancer to therapy (16). Due to different cell types as well as genetic factors, autophagy performs dual roles in cancers. On the one hand, tumor cells can activate autophagy to survive under metabolic and therapeutic conditions by limiting tumor necrosis and mitigating genome damage, such that cancer fighting strategy can be improved by blocking autophagy (15, 34, 35). On the other hand, autophagy may be beneficial in treatment of insensitive cancers (36). In recent years, a great variety of natural products or chemotherapeutic drugs have been demonstrated to participate in the modulation of autophagy through different molecular mechanisms (17, 36–38). For instance, hernandezine, an alkaloid, mediated autophagy in drug-resistant fibroblasts or cancer cells *via* direct stimulation of AMPK (39). Pirarubicin induced an autophagic cytoprotective response *via* inhibition of mTOR/p70S6K signal route in human

bladder carcinoma (40). In this study, the results showed that Cos-induced autophagy was evidenced by the increased autophagic vesicle formation and LC3 conversion in 769-P cells. Moreover, 3-MA decreased Cos-provoked cell death, suggesting that autophagy due to Cos was involved in the cell death. These results suggest that Cos induced pro-apoptotic autophagy in 769-P cells.

ROS have been identified as important molecules in the regulation of cell survival or cancer cell death (29, 36). Low ROS concentrations participate in cellular signaling, whereas excessive ROS impair proteins and DNA in the cell, eventually causing autophagy or cell death (32, 41). This study has shown that Cos induced significant increases in ROS, but pretreatment with NAC markedly reversed Cos-associated apoptosis and autophagy, indicating that Cos exerts apoptotic and autophagic influences through the generation of ROS in 769-P cells. It is well-known that ROS, acting as second messengers, exert their biological effects *via* activation of downstream molecules, mainly MAPK signaling pathways (21, 42, 43). Cinobufagin exerted apoptotic and autophagic cell death *via* the ROS/JNK/p38 signaling pathway (44). The ROS-mediated JNK signal route can also modulate autophagic cyto-protection in Ciclopirox olamine-administered rhabdomyosarcoma (45). The results of this study are consistent with these reports, in that among the members of the MAP kinase family studied, only JNK, but not ERK or p38 was activated in Cos-treated 769-P cells. The JNK inhibitor SP600125 significantly reversed Cos-mediated apoptotic and autophagic lesions. In addition, the stimulation of JNK pathway regulated Beclin-1 expression thereby triggering autophagy. Consistent with this finding, Cos significantly increased Beclin-1 expression, and the increases in Becline-1 expression were blocked by SP600125. These results showed that prior NAC exposure attenuated p-JNK. These findings indicate that Cos induced apoptotic and autophagic changes *via* the activation of ROS/JNK signal route.

In summary, the results of this study have demonstrated that Cos treatment exerted apoptotic and autophagic effects *via* ROS/JNK-linked signaling route. Therefore, Cos could be a novel antitumor drug candidate for therapy of renal cell carcinoma and other cancers.

## DATA AVAILABILITY STATEMENT

All datasets presented in this study are included in the article/supplementary material.

## AUTHOR CONTRIBUTIONS

DF, ZYX, and DW developed the project. DF, ZYX, WC, and JGa performed experiments and wrote the manuscript. JGe, ZYZ, and WQZ supervised the work. All authors read and approved the final manuscript.

## REFERENCES


1. Chen W, Zheng R, Baade PD, Zhang S, Zeng H, Bray F, et al. Cancer statistics in China, 2015. *CA Cancer J Clin*. (2016) 66:115–32. doi: 10.3322/caac.21338
2. Dagher J, Delahunt B, Rioux-Leclercq N, Egevad L, Srigley JR, Coughlin G, et al. Clear cell renal cell carcinoma: validation of WHO/ISUP grading. *Histopathology*. (2017) 71:918–25. doi: 10.1111/his.13311
3. Hollingsworth JM, Miller DC, Dunn RL, Montgomery JS, Roberts WW, Hafez KS, et al. Surgical management of low-stage renal cell carcinoma: technology does not supersede biology. *Urology*. (2006) 67:1175–80. doi: 10.1016/j.urology.2006.01.008
4. Robinson A, Kumar TV, Sreedhar E, Naidu VG, Krishna SR, Babu KS, et al. A new sesquiterpene lactone from the roots of *Saussurea lappa*: structure-anticancer activity study. *Bioorg Med Chem Lett*. (2008) 18:4015–7. doi: 10.1016/j.bmcl.2008.06.008
5. Matsuda H, Shimoda H, Uemura T, Yoshikawa M. Preventive effect of sesquiterpenes from bay leaf on blood ethanol elevation in ethanol-loaded rat: structure requirement and suppression of gastric emptying. *Bioorg Med Chem Lett*. (1999) 9:2647–52. doi: 10.1016/s0960-894x(99)00442-4
6. Kassuya CA, Cremoneze A, Barros LF, Simas AS, Lapa Fda R, Mello-Silva R, et al. Antipyretic and anti-inflammatory properties of the ethanolic extract, dichloromethane fraction and costunolide from Magnolia ovata (Magnoliaceae). *J Ethnopharmacol*. (2009) 124:369–76. doi: 10.1016/j.jep.2009.06.003
7. Wedge DE, Galindo JC, Macias FA. Fungicidal activity of natural and synthetic sesquiterpene lactone analogs. *Phytochemistry*. (2000) 53:747–57. doi: 10.1016/s0031-9422(00)00008-x
8. Yang YI, Kim JH, Lee KT, Choi JH. Costunolide induces apoptosis in platinum-resistant human ovarian cancer cells by generating reactive oxygen species. *Gynecol Oncol*. (2011) 123:588–96. doi: 10.1016/j.ygyno.2011.08.031
9. Choi YK, Seo HS, Choi HS, Choi HS, Kim SR, Shin YC, et al. Induction of Fas-mediated extrinsic apoptosis, p21WAF1-related G2/M cell cycle arrest and ROS generation by costunolide in estrogen receptor-negative breast cancer cells, MDA-MB-231. *Mol Cell Biochem*. (2012) 363:119–28. doi: 10.1007/s11010-011-1164-z
10. Zhang C, Lu T, Wang GD, Ma C, Zhou YF. Costunolide, an active sesquiterpene lactone, induced apoptosis via ROS-mediated ER stress and JNK pathway in human U2OS cells. *Biomed Pharmacother*. (2016) 80:253–9. doi: 10.1016/j.biopha.2016.03.031
11. Burgess DJ. Apoptosis: refined and lethal. *Nat Rev Cancer*. (2013) 13:79. doi: 10.1038/nrc3462
12. Huang P, Oliff A. Signaling pathways in apoptosis as potential targets for cancer therapy. *Trends Cell Biol*. (2001) 11:343–8. doi: 10.1016/s0962-8924(01)02063-3
13. Siegel RM, Lenardo MJ. Apoptosis signaling pathways. *Curr Protoc Immunol*. (2002) Chapter 11:Unit 11.9C.
14. Ouyang L, Shi Z, Zhao S, Wang FT, Zhou TT, Liu B, et al. Programmed cell death pathways in cancer: a review of apoptosis, autophagy and programmed necrosis. *Cell Prolif*. (2012) 45:487–98. doi: 10.1111/j.1365-2184.2012.00845.x
15. Yang ZJ, Chee CE, Huang S, Sinicrope FA. The role of autophagy in cancer: therapeutic implications. *Mol Cancer Ther*. (2011) 10:1533–41. doi: 10.1158/1535-7163.mct-11-0047
16. Rubinsztein DC, Gestwicki JE, Murphy LO, Klionsky DJ. Potential therapeutic applications of autophagy. *Nat Rev Drug Discov*. (2007) 6:304–12.
17. Zhou M, Wang R. Small-molecule regulators of autophagy and their potential therapeutic applications. *ChemMedChem*. (2013) 8:694–707. doi: 10.1002/cmdc.201200560
18. Maiuri MC, Zalckvar E, Kimchi A, Kroemer G. Self-eating and self-killing: crosstalk between autophagy and apoptosis. *Nat Rev Mol Cell Biol*. (2007) 8:741–52. doi: 10.1038/nrm2239
19. Li W, Yu KN, Bao L, Shen J, Cheng C, Han W. Non-thermal plasma inhibits human cervical cancer HeLa cells invasiveness by suppressing the

MAPK pathway and decreasing matrix metalloproteinase-9 expression. *Sci Rep*. (2016) 6:19720.
20. Kumar B, Iqbal MA, Singh RK, Bamezai RN. Resveratrol inhibits TIGAR to promote ROS induced apoptosis and autophagy. *Biochimie*. (2015) 118:26–35. doi: 10.1016/j.biochi.2015.07.016
21. Mi Y, Xiao C, Du Q, Wu W, Qi G, Liu X. Momordin Ic couples apoptosis with autophagy in human hepatoblastoma cancer cells by reactive oxygen species (ROS)-mediated PI3K/Akt and MAPK signaling pathways. *Free Radic Biol Med*. (2016) 90:230–42. doi: 10.1016/j.freeradbiomed.2015.11.022
22. Shi JM, Bai LL, Zhang DM, Yiu A, Yin ZQ, Han WL, et al. Saxifragifolin D induces the interplay between apoptosis and autophagy in breast cancer cells through ROS-dependent endoplasmic reticulum stress. *Biochem Pharmacol*. (2013) 85:913–26. doi: 10.1016/j.bcp.2013.01.009
23. Sui X, Kong N, Ye L, Han W, Zhou J, Zhang Q, et al. p38 and JNK MAPK pathways control the balance of apoptosis and autophagy in response to chemotherapeutic agents. *Cancer Lett*. (2014) 344:174–9. doi: 10.1016/j.canlet.2013.11.019
24. Jeong SJ, Itokawa T, Shibuya M, Kuwano M, Ono M, Higuchi R, et al. Costunolide, a sesquiterpene lactone from Saussurea lappa, inhibits the VEGFR KDR/Flk-1 signaling pathway. *Cancer Lett*. (2002) 187:129–33. doi: 10.1016/s0304-3835(02)00361-0
25. Bocca C, Gabriel L, Bozzo F, Miglietta A. A sesquiterpene lactone, costunolide, interacts with microtubule protein and inhibits the growth of MCF-7 cells. *Chem Biol Interact*. (2004) 147:79–86.
26. Choi SH, Im E, Kang HK, Lee JH, Kwak HS, Bae YT, et al. Inhibitory effects of costunolide on the telomerase activity in human breast carcinoma cells. *Cancer Lett*. (2005) 227:153–62.
27. Wang Z, Zhao X, Gong X. Costunolide induces lung adenocarcinoma cell line A549 cells apoptosis through ROS (reactive oxygen species)-mediated endoplasmic reticulum stress. *Cell Biol Int*. (2016) 40:289–97.
28. Rasul A, Bao R, Malhi M, Zhao B, Tsuji I, Li J, et al. Induction of apoptosis by costunolide in bladder cancer cells is mediated through ROS generation and mitochondrial dysfunction. *Molecules*. (2013) 18:1418–33.
29. Hua P, Zhang G, Zhang Y, Sun M, Cui R, Li X, et al. Costunolide induces G1/S phase arrest and activates mitochondrial-mediated apoptotic pathways in SK-MES 1 human lung squamous carcinoma cells. *Oncol Lett*. (2016) 11:2780–6.
30. Hua P, Sun M, Zhang G, Zhang Y, Song G, Liu Z, et al. Costunolide induces apoptosis through generation of ROS and activation of P53 in human esophageal cancer Eca-109 cells. *J Biochem Mol Toxicol*. (2016) 30:462–9.
31. Kanno S, Kitajima Y, Kakuta M, Osanai Y, Kurauchi K, Ujibe M, et al. Costunolide-induced apoptosis is caused by receptor-mediated pathway and inhibition of telomerase activity in NALM-6 cells. *Biol Pharm Bull*. (2008) 31:1024–8.
32. Kaminskyy VO, Piskunova T, Zborovskaya IB, Tchevkina EM, Zhivotovsky B. Suppression of basal autophagy reduces lung cancer cell proliferation and enhances caspase-dependent and -independent apoptosis by stimulating ROS formation. *Autophagy*. (2012) 8:1032–44.
33. Ganguli A, Choudhury D, Datta S, Bhattacharya S, Chakrabarti G. Inhibition of autophagy by chloroquine potentiates synergistically anti-cancer property of artemisinin by promoting ROS dependent apoptosis. *Biochimie*. (2014) 107(Pt B):338–49.
34. Wang J, Tan X, Yang Q, Zeng X, Zhou Y, Luo W, et al. Inhibition of autophagy promotes apoptosis and enhances anticancer efficacy of adriamycin via augmented ROS generation in prostate cancer cells. *Int J Biochem Cell Biol*. (2016) 77:80–90.
35. Wang C, Li T, Tang S, Zhao D, Zhang C, Zhang S, et al. Thapsigargin induces apoptosis when autophagy is inhibited in HepG2 cells and both processes are regulated by ROS-dependent pathway. *Environ Toxicol Pharmacol*. (2016) 41:167–79.
36. Zhang M, Su L, Xiao Z, Liu X, Liu X. Methyl jasmonate induces apoptosis and pro-apoptotic autophagy via the ROS pathway in human non-small cell lung cancer. *Am J Cancer Res*. (2016) 6:187–99.
37. Wang P, Zhu L, Sun D, Gan F, Gao S, Yin Y, et al. Natural products as modulator of autophagy with potential clinical prospects. *Apoptosis*. (2017) 22:325–56.
38. Shin D, Kim EH, Lee J, Roh JL. RITA plus 3-MA overcomes chemoresistance of head and neck cancer cells via dual inhibition of autophagy and antioxidant systems. *Redox Biol*. (2017) 13:219–27.
39. Law BY, Mok SW, Chan WK, Xu SW, Wu AG, Yao XJ, et al. Hernandezine, a novel AMPK activator induces autophagic cell death in drug-resistant cancers. *Oncotarget*. (2016) 7:8090–104.
40. Li K, Chen X, Liu C, Gu P, Li Z, Wu S, et al. Pirarubicin induces an autophagic cytoprotective response through suppression of the mammalian target of rapamycin signaling pathway in human bladder cancer cells. *Biochem Biophys Res Commun*. (2015) 460:380–5.
41. Xu J, Wu Y, Lu G, Xie S, Ma Z, Chen Z, et al. Importance of ROS-mediated autophagy in determining apoptotic cell death induced by physapubescin B. *Redox Biol*. (2017) 12:198–207.
42. Zhang L, Wang K, Lei Y, Li Q, Nice EC, Huang C. Redox signaling: potential arbitrator of autophagy and apoptosis in therapeutic response. *Free Radic Biol Med*. (2015) 89:452–65.
43. Zhang XY, Wu XQ, Deng R, Sun T, Feng GK, Zhu XF. Upregulation of sestrin 2 expression via JNK pathway activation contributes to autophagy induction in cancer cells. *Cell Signal*. (2013) 25:150–8.
44. Ma K, Zhang C, Huang MY, Li WY, Hu GQ. Cinobufagin induces autophagy-mediated cell death in human osteosarcoma U2OS cells through the ROS/JNK/p38 signaling pathway. *Oncol Rep*. (2016) 36:90–8.
45. Zhou HY, Shen T, Shang CW, Lou Y, Liu L, Yan JM, et al. Ciclopirox induces autophagy through reactive oxygen species-mediated activation of JNK signaling pathway. *Oncotarget*. (2014) 5:10140–50.

**Conflict of Interest:** The authors declare that the research was conducted in the absence of any commercial or financial relationships that could be construed as a potential conflict of interest.

frontiers in Pharmacology

ORIGINAL RESEARCH
published: 30 November 2020
doi: 10.3389/fphar.2020.576955

# Chemoresistance in Breast Cancer Patients Associated With Changes in P2X7 and A2A Purinergic Receptors in CD8$^+$ T Lymphocytes

*Victor Manuel Ruiz-Rodríguez[1], Eneida Turiján-Espinoza[1], Jaime Arturo Guel-Pañola[2], Mariana Haydee García-Hernández[3], José de Jesús Zermeño-Nava[1], Nallely López-López[1], Sofia Bernal-Silva[1], Esther Layseca-Espinosa[1], Ezequiel M. Fuentes-Pananá[4], Ana María Estrada-Sánchez[5] and Diana Patricia Portales-Pérez[1]**

[1]Translational and Molecular Medicine Laboratory, Research Center for Health Sciences and Biomedicine, Autonomous University of San Luis Potosí, San Luis Potosí, México, [2]Central Hospital Dr. Ignacio Morones Prieto, San Luis Potosí, México, [3]Unidad de Investigacion Biomédica de Zacatecas, Delegación Zacatecas, Instituto Mexicano del Seguro Social (IMSS), Zacatecas, México, [4]Research Unit in Virology and Cancer, Children's Hospital of México Federico Gómez, México City, México, [5]División de Biología Molecular, Instituto Potosino de Investigación Científica y Tecnológica (IPICYT), San Luis Potosí, México

Breast cancer (BRCA) is the most frequent cancer type that afflicts women. Unfortunately, despite all the current therapeutic strategies, many patients develop chemoresistance hampering the efficacy of treatment. Hence, an early indicator of therapy efficacy might aid in the search for better treatment and patient survival. Although emerging evidence indicates a key role of the purinergic receptors P2X7 and A2A in cancer, less is known about their involvement in BRCA chemoresistance. In this sense, as the chemotherapeutic treatment stimulates immune system response, we evaluated the expression and function of P2X7 and A2A receptors in CD8$^+$ T cells before and four months after BRCA patients received neoadjuvant chemotherapy. The results showed an increase in the levels of expression of P2X7 and a decrease in the expression of A2A in CD8$^+$ T cells in non-chemoresistant (N-CHR) patients, compared to chemoresistant (CHR) patients. Interestingly, in CHR patients, reduced expression of P2X7 occurs along with a decrease in the CD62L shedding and the production of IFN-$\gamma$. In the case of the A2A function, the inhibition of IFN-$\gamma$ production was not observed after chemotherapy in CHR patients. A possible relationship between the modulation of the expression and function of the P2X7 and A2A receptors was found, according to the molecular subtypes, where the patients that were triple-negative and human epidermal growth factor receptor 2 (HER2)-enriched presented more alterations. Comorbidities such as overweight/obesity and type 2 diabetes mellitus (T2DM) participate in the abnormalities detected. Our results demonstrate the importance of purinergic signaling in CD8$^+$ T cells during chemoresistance, and it could be considered to implement personalized therapeutic strategies.

**Keywords: chemoresistance, P2X7 receptor, A2A receptor, CD8$^+$ T cells, obesity, diabetes, BMI**

OPEN ACCESS

***Edited by:***
*Xiaoping Lin,*
*Sun Yat-sen University Cancer Center (SYSUCC), China*

***Reviewed by:***
*Huan Lin,*
*Guangdong Provincial Hospital of Chinese Medicine, China*
*Jing Wen,*
*Sun Yat-sen University Cancer Center, China*

****Correspondence:***
*Diana Patricia Portales Pérez*
*dportale@uaslp.mx*

***Specialty section:***
*This article was submitted to Pharmacology of Anti-Cancer Drugs, a section of the journal Frontiers in Pharmacology*

***Received:*** *03 July 2020*
***Accepted:*** *23 October 2020*
***Published:*** *30 November 2020*

***Citation:***
*Ruiz-Rodríguez VM, Turiján-Espinoza E, Guel-Pañola JA, García-Hernández MH, Zermeño-Nava JDJ, López-López N, Bernal-Silva S, Layseca-Espinosa E, Fuentes-Pananá EM, Estrada-Sánchez AM and Portales-Pérez DP (2020) Chemoresistance in Breast Cancer Patients Associated With Changes in P2X7 and A2A Purinergic Receptors in CD8$^+$ T Lymphocytes. Front. Pharmacol. 11:576955. doi: 10.3389/fphar.2020.576955*

## INTRODUCTION

Breast cancer (BRCA) is the most common type of cancer in women, both in developed and underdeveloped countries. The World Health Organization (WHO) estimates that 627,000 women died worldwide in 2018 due to this type of cancer. The BRCA incidence rates range from 25.9 cases per 100,000 in South-Central Asia to 94.2 cases per 100,000 in Western Europe (GCO, 2018). In 2015, Mexicos' BRCA incidence was 27.70 new cases per 100,000 women aged 20 years and older (INEGI, 2016). According to its origin, BRCA can develop in the milk ducts (ductal cancers) or the milk-producing glands (lobular cancers). Biopsy evaluation provides information about the degree of aggressiveness of the tumor and the presence or absence of specific markers that aid in making decisions about the best chemotherapy option. In this sense, patients might fall into one of the four intrinsic molecular groups depending on the presence of estrogen receptor (ER), progesterone (PR) or human epidermal growth factor receptor 2 (HER2): luminal A (ER+, PR+, HER2−), luminal B (ER+, PR+/−, HER2+/−), HER2-enriched (ER−, PR−, HER2+), and triple-negative (ER−, PR−, HER2−) (Breastcancer.org, 2018).

To date, chemotherapy is the most effective treatment for BRCA, which can be adjuvant, applied to patients after mastectomy to avoid a recurrence or neoadjuvant, that targets large tumors to reduce its size before the mastectomy. According to Mexican guidelines, neoadjuvant therapy for BRCA includes fluorouracil, cyclophosphamide, and doxorubicin (Secretaría de Salud, 2017). These drugs favor the death of cancer cells due to their cytotoxic mechanism of action, such as intercalating into DNA, inhibiting pyrimidine synthesis or adding alkyl groups to DNA. In this sense, chemotherapeutic treatment has a stimulating effect on the immune system and its cytotoxic action on the tumor cells (Haynes et al., 2008). One of these effects is observed with doxorubicin or oxaliplatin, where the cancer cells release the alarmin high-mobility group box protein 1 (HMGB1), which acts upon the immune cell patter recognition receptors (PRR). High levels of alarmins are found in patients with BRCA after chemotherapeutic treatment (Apetoh et al., 2007; Stoetzer et al., 2013). On the other hand, doxorubicin induces greater involvement of the $CD8^+$ T cells that produce IFN-$\gamma$ and increases the production of IL-1β and IL-17 in murine models of BRCA. In samples from BRCA patients, higher expression of genes for CD8α, CD8β, and IFN-$\gamma$ is associated with a better response to treatment with doxorubicin (Mattarollo et al., 2011). However, despite all the available therapeutic strategies, many patients do not adequately respond to chemotherapy and develop chemoresistance (Ji et al., 2019).

ATP also functions as an alarmin and emerging evidence suggests that purinergic signaling pathways play a crucial role in the development of various types of cancer and immune activation (Buxton et al., 2010; Adinolfi et al., 2012; Zhou et al., 2015). In this regard, ATP activation of P2X7 receptors, an ionotropic receptor that belongs to the P2X family, by ATP, promotes the process of metastasis in a BRCA cell line (Xia et al., 2015). In contrast, in glioma patients, higher expression of P2X7 receptors favors radiotherapy's effectiveness by inducing apoptosis (Gehring et al., 2012). The efficiency of anticancer treatment (oxaliplatin, doxorubicin, thapsigargin, staurosporine, or cisplatin) relates to the degree of ATP released by cancerous cells, which promotes the activation of the P2X7 receptor. P2X7 activation contributes to the activation of the NLRP3-inflammasome pathway and the production of IL-1β, favoring antitumor activity, and better treatment efficiency (Ghiringhelli et al., 2009). Therefore, there is conflicting evidence to the prognosis value of P2X7 expression, due to its pro-tumoral or anti-tumoral functions depending its expression in cancer cells or in immune cells.

The A2A and A2B receptors signaling, which belongs to the P1 receptor family, is activated mainly by adenosine, and it also poses immunosuppressive activity. The A2A receptor is the most studied of the P1 receptor family in the regulation of T cell responses. Adenosine is produced from AMP, mainly by CD73, an ecto-5'-nucleotidase. The A2A/A2B receptors antagonists on CD73-positive cancer cells induce a reduction on metastasis while A2A receptor antagonist increases the cytotoxic capacity of the NK cells (Beavis et al., 2013). In triple-negative BRCA (TNBC) that expresses high levels of CD73, conventional chemotherapy is not effective (Spychala et al., 2004; Mittal et al., 2014). In this case, activation of A2B and A2A receptors leads to metastasis and an immune ineffective antitumor activity, which suppresses the efficacy of anthracyclines (doxorubicin), leading to a worse outcome for patients (Loi et al., 2013). These data together suggest that purinergic signaling might influence the efficacy of chemotherapy in BRCA, which might lead to tumor chemioresistance. Because few studies have been conducted with patients, it is crucial to determine the possible involvement of purinergic signaling in chemoresistance mechanisms in BRCA patients and to generate relevant information on the efficacy of first-line drugs to understand better the role of the immune system in the evolution of patients during chemotherapy.

## MATERIAL AND METHODS

### Study Group

This study included 50 newly diagnosed BRCA women that received neoadjuvant chemotherapy with 5-fluorouracil, adriamycin, and cyclophosphamide (FAC) scheme, which is administered for six cycles consisting of one administration every four weeks at doses of 600 $mg/m^2$ of five- fluorouracil and cyclophosphamide, and 60 $mg/m^2$ of doxorubicin according to the body surface area (BSA) of each patient (Arun et al., 2011). A peripheral venous blood sample was taken before the start of neoadjuvant chemotherapy (C0) and four months later, before administering of the fourth cycle of chemotherapy (C4). The response to chemotherapy was evaluated at the clinic following the Response Evaluation Criteria in Solid Tumors (RECIST), considering the reduction in initial tumor size measured by clinical oncology doctors (Eisenhauer et al., 2009). The patients with a tumor size reduction equal to or less than 30% at C4 were considered chemo-resistant (CHR), including patients who presented tumor enlargement. The molecular identification

of each patient's type of cancer was carried out in the pathology service of the Central Hospital Dr. Ignacio Morones Prieto, San Luis Potosí, using the immunohistochemical or fluorescence *in situ* hybridization (FISH) technique to identify the presence of hormone receptors and HER2; Luminal A (ER+, PR+, HER2−), Luminal B (ER+, PR+/−, HER2+/−), HER2-enriched (ER−, PR−, HER2+), and triple-negative (ER−, PR−, HER2−). All patients signed an informed consent letter before the collection of blood samples. Our study was approved by the Research Committee of the Central Hospital (COFEPRIS 14 CI 24 028 083) and the Committee of Ethics in Research (CONBIOETICA-24-CEI-001-20160427).

## Isolation of Peripheral Blood Mononuclear Cells

The hospital's nursing staff collected the peripheral blood samples during the morning, and patients were no fasting. The blood sample for C0 was collected before the first administration of chemotherapy, and C4 blood was drawn before administering the fourth cycle of chemotherapy. The blood samples were diluted with PBS in a 1:2 ratio and placed in 3 ml of Ficoll per 10 ml of diluted blood. Then, the cells were centrifuged at 2,500 rpm for 20 min, and the fraction of the PBMC was separated and placed in a new tube. Then, a PBS wash was performed at 1,500 rpm for 5 min, and a cell button was obtained and resuspended in RPMI culture medium for the experiments using different stimuli or in PBS, to carry out the analyzes by flow cytometry. Cell viability was determined by trypan blue staining; viable samples were considered when ≥ 95% of living cells were present.

## Flow Cytometry Analysis

The PBMC were placed in a tube (at $2 \times 10^5$ cells), washed with PBS, centrifuged at 1,500 rpm for 5 min, and the supernatant was discarded to resuspend the cell button. Surface labeling was performed to determine the expression of P2X7 or A2A receptors on CD8 T cells, incubating the samples with anti-CD8 antibody FITC (BD Bioscience™) or anti-CD8 PE (BD Bioscience™) respectively, for 20 min at 4°C in the dark; the determination of each receptor was performed in separate tubes. After washing with PBS, the cells were fixed with 4% paraformaldehyde (PFA) for 15 min at 4°C in the dark. Subsequently, for P2X7 detection, 0.1% saponin was added for 10 min, then the sample was centrifuged at 1,500 rpm for 5 min, and the supernatant discarded. Rabbit anti-P2X7-human intracellular primary antibody (Sigma-Aldrich) was added and incubated for 30 min at 4°C in the dark. After washing with PBS and discarding the supernatant, the cell button was incubated with the secondary anti-rabbit-PerCP antibody (Santa Cruz Biotechnology) for 30 min at 4°C in the dark. A wash step was then carried out with PBS, and 1% PFA was added and preserved at 4°C. For A2A detection, Triton X-100 was added and incubated for 5 min at 4°C and washed with PBS + 1% albumin at 1,500 rpm for 5 min. The supernatant was discarded, and the cell button was resuspended and incubated with 0.1% saponin for 5 min. Then, the cells were centrifuged at 1,500 rpm for 5 min, and the supernatant discarded. The anti-A2A-PE antibody (Santa Cruz Biotechnology) was added and incubated for 30 min at 4°C in the dark, then 1% PFA was added, and samples were preserved at 4°C. The cells were analyzed in a FACSCanto II flow cytometer (BD Biosciences™) using FlowJo software (Becton, Dickinson and Company). To determine the expression of the P2X7 or A2A receptors in $CD8^+$ T lymphocytes by flow cytometry, the following analysis strategy was followed: first, the singlets were selected, and the doublets were discarded with the forward scatter-height (FSC-H) vs. forward scatter-area (FSC-A) analysis. Then, the population of lymphocytes was analyzed based on their size (FSC) and granularity side scatter (SSC), the $CD8^+$ T cells were subsequently determined as well as the expression of each receptor.

## Determination of the Shedding of CD62L by Flow Cytometry

The PBMC were incubated in the presence or absence of 100 ng/ml Phorbol 12-myristate-13-acetate (PMA) (as a positive control) or 3 mM ATP at 37°C and 5% $CO_2$ for 30 min. The cells were washed with PBS and incubated in the presence of anti-CD8-PE (BD Bioscience™) and anti-CD62L-FITC antibody (BD Bioscience™) for 30 min. After washing with PBS, the cells were analyzed by flow cytometry, and the percentages of $CD8^+$ cells that were positive for CD62L were obtained in the presence and absence of ATP. The results are expressed as the percentage of CD62L + cells of $CD8^+$ and as the percentage of shedding of CD62L, according to the following formula: percent shedding of CD62L = percentage of CD62L + cells of $CD8^+$ without ATP–the percentage of CD62L + cells of $CD8^+$ stimulated with ATP.

## Determination of the synthesis of IFN-γ by flow cytometry

The PBMC were incubated in the presence or absence of the CD3/CD28 antibodies (5 μg/ml) for 5 days to favor cell activation at 37°C and 5% $CO_2$. Besides, they were incubated separately and simultaneously with the A2A receptor agonist and antagonist, called CGS-21680 (70 μM) and ZM-241385 (10 μM), respectively, these stimuli were used for 1 h before stimulation with the CD3/CD28 antibodies. Cells were washed with PBS and incubated in the presence of an anti-IFN-γ-FITC antibody (BioLegend™) for 30 min. After washing with PBS, the cells were analyzed by flow cytometry.

## Statistical Analysis

The data are shown as the mean ± the standard error of the mean, and the data were analyzed using the GraphPad Prism v.5 program (GraphPad Software Inc., San Diego, CA). The Kolmogorov-Smirnov test determined the distribution of each of the variables. For the analysis of parametric data, a paired Student t-test was performed, and for the case of non-parametric data, a Wilcoxon matched-pairs test was performed. A one-way ANOVA test was performed with a Bonferroni post-hoc test or a Kruskal-Wallis test with Dunn's post-hoc test to determine the differences between the variables and a Spearman r correlation test to determine the correlation between the variables. A

**TABLE 1** | Anthropometric parameters of the individuals included in this study

| Patients | |
|---|---|
| *n* | 50 |
| Age (Years) | 49.9 ± 9.6 |
| BMI (Kg/m$^2$) | |
| Before chemotherapy (C0) | 30.5 ± 6.6 |
| After chemotherapy (C4) | 31 ± 6.6 |
| Normal weight | 23.3 ± 1.25 (24%) |
| Overweight | 27.4 ± 1.42 (22%) |
| Obesity | 35.0 ± 5.56 (54%) |
| T2DM | 30.9% |
| Hypertension | 31.7% |
| Tumor size (cm) | 2 × 2–12 × 12 |
| Luminal A (ER+, PR+, HER2–) | 36% |
| Luminal B (ER+, PR+/–; HER2+/–) | 24% |
| HER2-enriched (ER–, PR–, HER2+) | 20% |
| Triple-negative (ER–, PR–, HER2–) | 20% |
| Chemo-resistant | 20% |

*Values are presented as the mean ± standard deviation (SD) or percentage. BMI (body mass index); T2DM (type two diabetes mellitus); estrogen receptor (ER), progesterone receptor (PR) or human epidermal growth factor receptor 2 (HER2).*

statistically significant difference with a value of $P<0.05$ was considered.

# RESULTS

## Patient Characteristics

The BRCA study group was 49.9 ± 9.6 years old and presented an average body mass index (BMI) of 30.4 ± 6.7. According to the WHO classification of obesity, 54% of the studied patients presented obesity. Also, 30.9% showed comorbidity with type 2 diabetes mellitus (T2DM), and 31.7% with hypertension. All patients received chemotherapy followed the Mexican guide using FAC therapy (5-fluorouracil, adriamycin, and cyclophosphamide). The patients were classified by the intrinsic molecular type; 36% were luminal A, 24% were luminal B, and 20% of the patients were triple-negative, and HER2 enriched represented a 20% (**Table 1**).

## Effect of Chemotherapy on P2X7 Expression in CD8$^+$ T Cells

We assessed how purinergic signaling influences the efficacy of chemotherapy in the BRCA patients, as this pathway has been linked to carcinogenic breast processes. We initially evaluated the expression of P2X7 receptors before and after receiving the FAC chemotherapy (C0 and C4, respectively; see methods). An unmarked control and isotype control were used to finally determine the expression of the P2X7 receptors (**Figure 1A**). There was a significant increase in P2X7 expression in CD8$^+$ T cells at C4 (**Figure 1B**). However, as 20% of patients developed chemoresistance, we evaluated P2X7 expression within each group. Interestingly, CD8$^+$ T cells of non-chemoresistant (N-CHR) patients showed the significant increase in P2X7 positivity (**Figure 1C**). In contrast, CHR patients showed similar frequencies of P2X7 positive CD8$^+$ T cells (**Figure 1D**). When we evaluated the four intrinsic molecular cancer subtypes, significant increased frequency of P2X7 positivity was observed in luminal B and HER2-enriched BRCA (**Figure 1E,F**), while no significant changes were detected in luminal A or triple-negative patients (**Figure 1G,H**).

## Relationship between P2X7 expression, metabolic alterations and tumor size

As 76% of BRCA patients were overweight or obese, we analyzed whether there was a relationship between P2X7 expression in CD8$^+$ T lymphocytes and BMI levels. Interestingly, we found a positive correlation before starting chemotherapy ($r=0.2970$; $p=0.04$, **Figure 2A**). However, this correlation was not observed at C4, presumably due to the increase in P2X7 expression in CD8$^+$ T cells ($r=0.07$; $p=0.63$, **Figure 2B**); also, there were no changes in the BMI of patients after chemotherapy (see **Table 1**). Subsequently, when patients were classified depending on their response to chemotherapy, only the N-CHR at C0 showed a correlation between P2X7 expression and BMI (**Figure S1B**). There was not a correlation between P2X7 and BMI in N-CHR at C4, or CHR at C0 and C4 (**Supplementary Figure S1A,B**).

As BMI emerged as an influential component of our study, we evaluated P2X7 expression in patients classified accordingly to their BMI (Normal weight ≤ 24.9; Overweight 25-29.9, Obesity ≥ 30), and whether they also presented T2DM. The normal weight and obesity group showed a significant increase in the frequency of P2X7 expression in CD8$^+$ T cells in the T2DM group (**Supplementary Figure S2A**). This difference was maintained only in the group of normal weight when T2DM patients were excluded from the analysis (**Supplementary Figure S2B**), demonstrating that obesity could play a role in the regulation of P2X7 expression after chemotherapy. On the other hand, when the analysis was performed with BRCA patients who also suffer from T2DM, a significant increase in the expression of P2X7 after chemotherapy in both T2DM and non T2DM (N-T2DM) patients was detected (**Supplementary Figure S2C,D**), which shows that T2DM has no effect in the regulation of P2X7 expression.

Finally, we explore the change of P2X7 expression in CD8$^+$ T cells according to the initial tumors size -the variable that reveals the effectiveness of chemotherapy, as well as disease progression- and a significant increase in P2X7 expression only was observed in patients with initial tumors size ≤ 5 cm (**Figure 2C**).

## Alterations in the Function of P2X7 in Chemo-Resistant Patients

Next, we determined the function of the P2X7 receptor in CD8$^+$ T lymphocytes treated with ATP by flow cytometry measuring two markers of activation, CD62L down-regulation and IFN-$\gamma$ production. The following analysis strategy was carried out to determine shedding of CD62L. First, the singlets were selected, and the doublets were discarded with the analysis of FSC-H vs. FSC-A. Then, the lymphocyte population was analyzed, considering their size (FSC) and granularity (SSC), in which

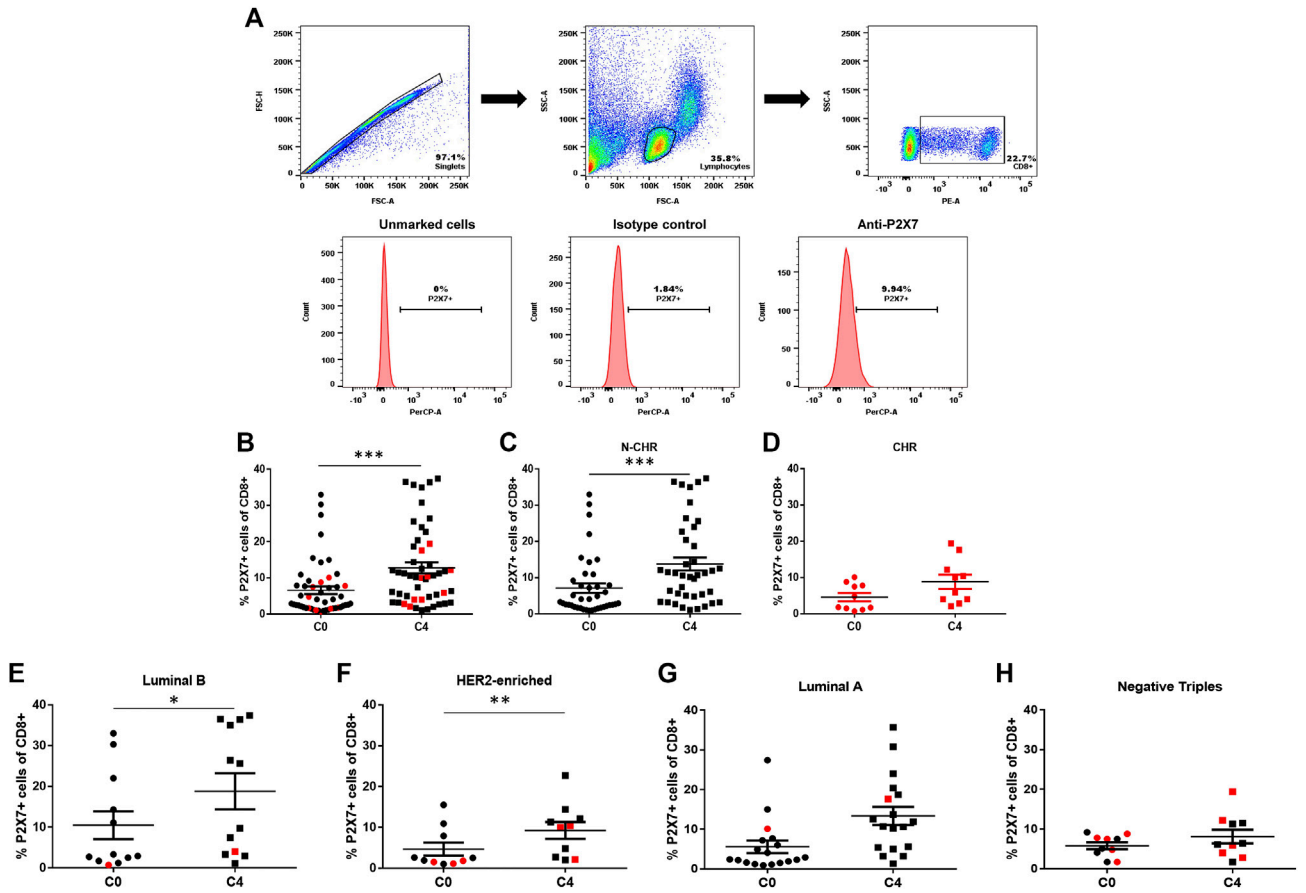


**FIGURE 1 |** Expression of the P2X7 purinergic receptor in CD8$^+$ T cells from Breast cancer (BRCA) patients by flow cytometry. The graphic representations of peripheral blood cells depict the flow cytometry analysis. The singlets were selected, and the lymphocyte population based on cell size and granularity characteristics (FSC and SSC, respectively) was selected. The population of CD8$^+$ T cells was determined using specific CD8 staining, and then the expression levels of the P2X7 receptor **(A)** were obtained. Expression levels of P2X7 in CD8$^+$ T cells from total samples before the start of neoadjuvant chemotherapy (C0) and four months later, before the administration of the fourth cycle of chemotherapy (C4) **(B)** and non-chemo-resistant (N-CHR) **(C)** or chemo-resistant (CHR) patients **(D)** are shown. P2X7 receptor expression is shown in CD8$^+$ T cells in different groups according to their molecular type; luminal A **(E)**, luminal B **(F)**, HER2-enriched **(G)** and triple-negative **(H)** patients. The results correspond to the mean ± SEM. *p<0.05, ***p<0.001. In graphs and onward, CHR is in red while N-CHR is in black symbols.

the population of CD8$^+$ T cells and the expression of CD62L was determined (**Figure 3A**). It is expected that activation of the P2X7 receptor with ATP reduces the expression of CD62L. In N-CHR patients, we found a significant decrease in the frequency of CD62L positive CD8$^+$ T cells at C0 and C4 when activating the P2X7 receptor with 3 mM ATP (**Figure 3B**). In the case of CHR patients, this P2X7 function was lost. No difference in the expression of CD62L was observed in the presence of 3 mM ATP (**Figure 3C**). The shedding of CD62L calculated at C0 in N-CHR patients was greater than that in CHR patients (**Figure 3D**); therefore, the activation of P2X7 is diminished in patients with CHR.

The analysis of the P2X7 receptor activation, when divided by the molecular tumor type, showed a significant decrease in the expression of CD62L only in patients classified as luminal A or in ER + patients (**Supplementary Figure S3**). Regarding the role of P2X7 in patients with metabolic disorders, we only found a significant decrease in the frequency of CD62L positive CD8$^+$ T cells in the group of BRCA patients with normal weight or obesity at C0. However, this P2X7 activation was not observed at C4 (**Supplementary Figure S4A,B**). Additionally, by eliminating the group of patients who also suffer from T2DM to determine the effect of this comorbidity, we were unable to observe any difference (**Supplementary Figure S4C,D**). In contrast, the analysis of data obtained from T2DM or N-T2DM patients showed a decrease in the levels of expression of CD62L only in the group of N-T2DM patients (**Supplementary Figure S4E,F**).

The second strategy to study the influence of P2X7 expression in T cell activation was through the production of IFN-$\gamma$ using the same flow cytometry analysis described above to determine the population of CD8$^+$ T cells (**Figure 3E**). The percentage of IFN-$\gamma$ producing CD8$^+$ T cells was evaluated in a control condition stimulated with anti-CD3/CD28. The N-CHR group presented similar production of IFN-$\gamma$ between C0 and C4 (**Figure 3F**). In contrast, the production of IFN-$\gamma$ was less at C4 in the group of

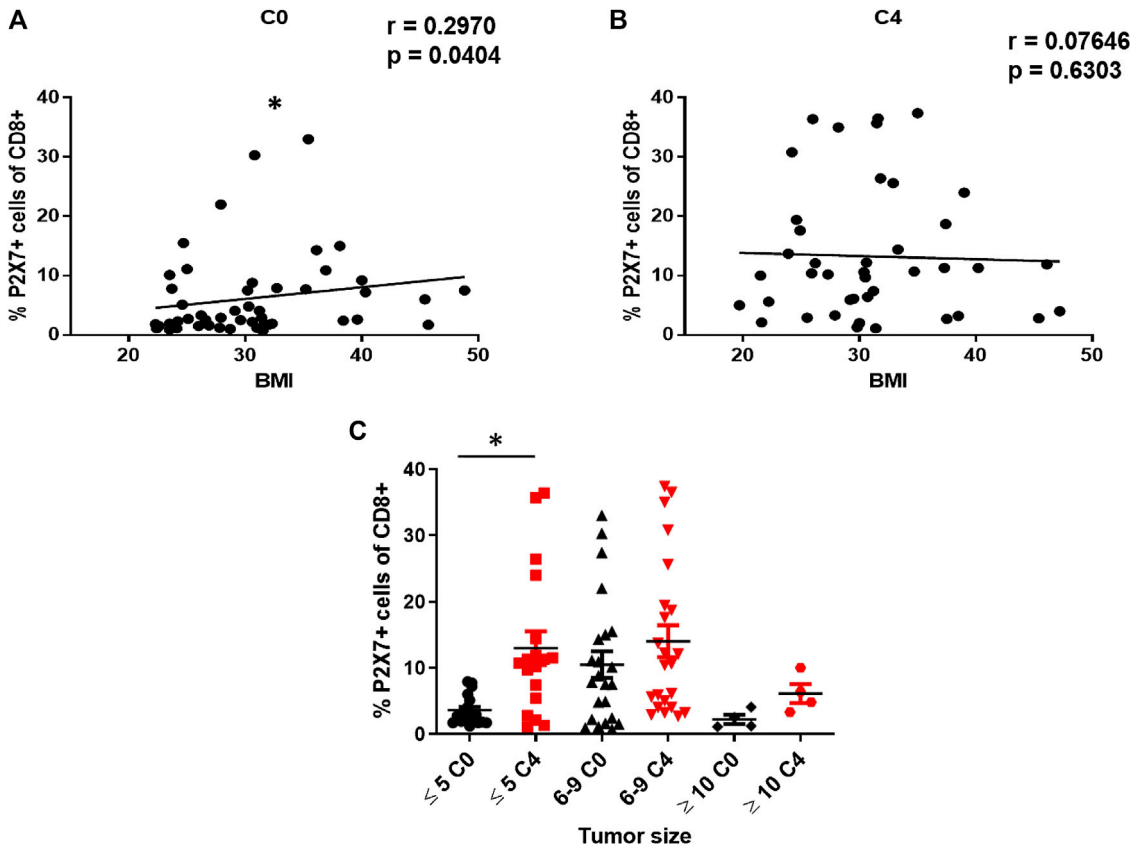


**FIGURE 2 |** Effect of BMI and tumor size on the expression of P2X7 in CD8$^+$ T cells from BRCA patients. Correlation analysis between the expression of the P2X7 receptor and the BMI of patients at C0 **(A)** or C4 **(B)**. Expression of P2X7 in CD8$^+$ T cells from patients classified into three groups according to the size of the tumor (≤5 cm, 6–9 cm, ≥10 cm) before starting treatment. Values are shown as the mean ± SEM. *p<0.05.

CHR patients (**Figure 3G**) or triple-negative patients (**Figure 3H**), compared to C0. Additionally, when comparing the percentage of IFN-$\gamma$ producing CD8$^+$ T cells between N-CHR and CHR patients at C0, we found an increase in the percentage of IFN-$\gamma$ in CHR vs. N-CHR patients. However, at C4, a significant decrease was observed in the CHR patients compared to N-CHR (**Figure 3I**).

## Effect of Chemotherapy on A2A Expression in CD8$^+$ T Cells

The expression of the A2A receptor in CD8$^+$ T lymphocytes by flow cytometry was determined using an unmarked control as shown in **Figure 4A**. It has been shown that A2A receptors regulate the antitumor immune response. Contrary to what we observed with the P2X7, we found a significant decrease in the frequency of A2A positive CD8$^+$ T cells at C4 compared with the same patient at C0 (**Figure 4B**). When analyzing the expression of A2A only in N-CHR patients (**Figure 4C**), a significant decrease was also observed. However, when the CHR patients were analyzed (**Figure 4D**), no differences were detected. When analyzing A2A expression in the different intrinsic molecular subtypes, we found that A2A positive CD8$^+$ T cells decreased significantly at C4 in groups of patients classified as ER+, luminal A, and luminal B patients (**Figure 4F–H**).

## Relationship Between A2A Receptor in Patients With Metabolic Disorders

When comparing the expression of A2A relative to the BMI, no correlation was found at C0 or C4 (data not shown). However, when A2A expression levels were analyzed in patients with BRCA who also have T2DM, overweight or obesity, we found a significant difference in the expression of A2A between C0 and C4 only in the group of normal-weight patients (**Supplementary Figure S5A**). Also, by excluding patients who also suffer from T2DM, the significant decrease in A2A expression in patients with normal weight was preserved (**Supplementary Figure S5B**). On the other hand, if we compared the A2A levels of expression in T2DM (**Supplementary Figure S5C**) or N-T2DM (**Supplementary Figure S5D**) patients, we found a significant decrease only in the group of N-T2DM patients.

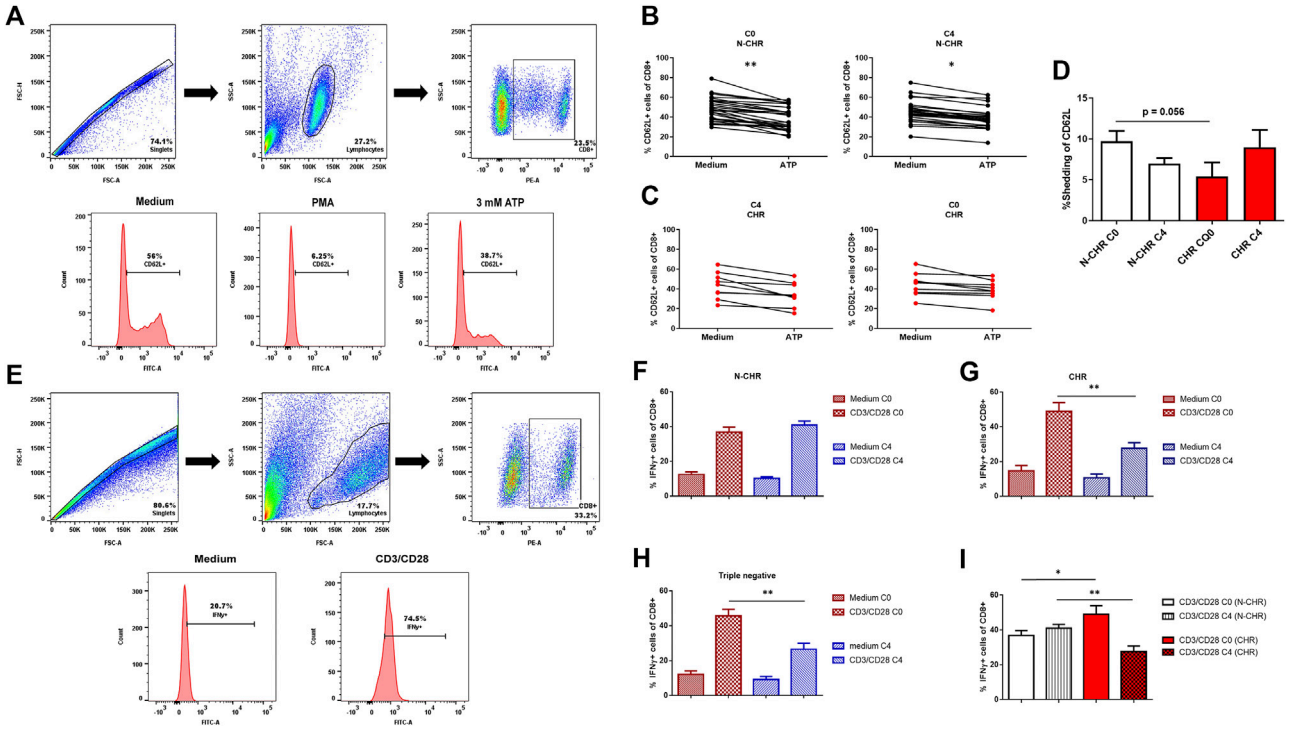


**FIGURE 3 |** Role of the P2X7 receptor in CD8$^+$ T cells from BRCA patients through the shedding of CD62L and the production of IFN-$\gamma$. Dot plots representative of the analysis strategy to determine the shedding of CD62L in CD8$^+$ T cells are shown. The following different culture conditions were used: RPMI-1640 medium, a positive control, with 100 ng/ml PMA and a condition with 3 mM ATP to stimulate the P2X7 receptor **(A)**. CD62L expression in CD8$^+$ T cells at C0 or C4 in N-CHR **(B)** or CHR **(C)** BRCA patients. Comparison analysis of the shedding of CD62L in N-CHR and CHR breast cancer patients at C0 and C4 **(D)**. Dot plots representative of the analysis strategy to determine IFN-$\gamma$ expression in CD8$^+$ T cells under two culture conditions: RPMI-1640 medium and with anti-CD3/CD28 **(E)**. The IFN-$\gamma$ expression levels in CD8$^+$ T cells in the absence or presence of stimulation at C0 and C4 in N-CHR **(F)** or CHR **(G)** patients and triple-negative patients **(H)**. Comparison analysis of IFN-$\gamma$ expression in CD8$^+$ T cells with prior stimulation in N-CHR and CHR patients **(I)**. Values are shown as the mean ± SEM. *p<0.05, **p<0.01.

## Alterations in A2A Function in Chemo-Resistant Patients

To determine the function of the A2A receptor, the inhibition in the production of IFN-$\gamma$ in CD8$^+$ T cells was determined by flow cytometry (**Figure 5A**). The same flow cytometry analysis strategy previously described was followed to determine the percentage of IFN-$\gamma$ produced by CD8$^+$ T cells. It is expected that upon activation of the A2A receptor with CGS-21680, a specific agonist, the percentage of IFN-$\gamma$ producing by CD8$^+$ T cells will decrease and when ZM-241385 -a specific antagonist- is used, the levels of IFN-$\gamma$ are similar to basal point. A significant decrease in the percentage of IFN-$\gamma$ producing CD8$^+$ T cells at C0 was observed in N-CHR patients when stimulating the A2A receptor. Furthermore, no differences were detected between C0 and C4 when comparing the percentage of IFN-$\gamma$ producing CD8$^+$ T cells (**Figure 5B**). On the other hand, in the group of CHR patients, a decrease in the percentage of IFN-$\gamma$ producing CD8$^+$ T cells was observed at C0 and C4 when pre-stimulated with CD3/CD28. However, no difference was found in the percentage of cells when stimulating the A2A receptor at C4, which was observed at C0 (**Figure 5C**). Similar results in CHR patients were observed in the group of patients classified as triple-negative (**Figure 5D**).

Additionally, we performed an analysis of the A2A receptor function in patients with T2DM. BRCA patients with T2DM did not show a decrease in the percentage of IFN-$\gamma$ producing CD8$^+$ T cells when stimulating the A2A receptor (**Figure 5E**). The function of A2A was detected only in N-T2DM patients (**Figure 5F**).

## P2X7+/A2A + RATIO IN CD8 T CELLS OF BREAST CANCER PATIENTS

The expression and function results suggest a key role of the P2X7 and A2A receptors in CD8$^+$ T cells from patients with BRCA. Then, we analyzed the P2X7/A2A ratio, and a significant increase only in N-CHR patients between C0 and C4 was detected (**Figure 6A**). Finally, the correlation between the P2X7/A2A ratio and the percentage of response of each patient was determined, where at C0 a positive and significant correlation was obtained ($p = 0.0448$, $R = 0.285$, **Figure 6B**), but at C4 was lost ($p = 0.4514$, $R = 0.1089$, **Figure 6C**).

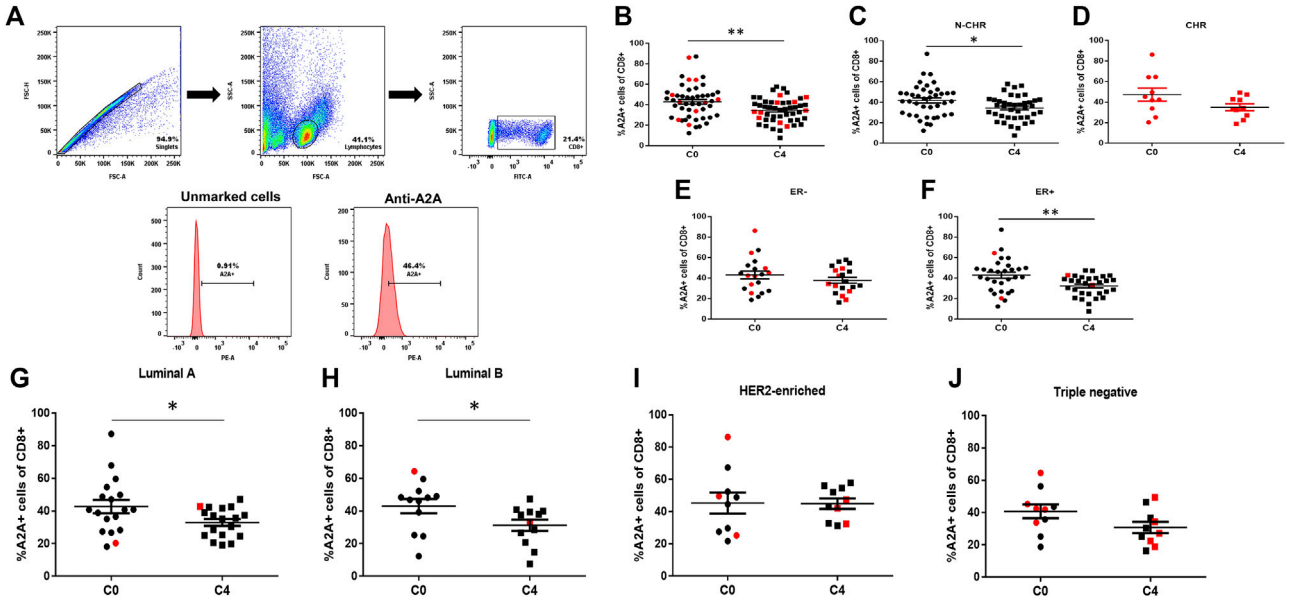


**FIGURE 4 |** Expression of the A2A purinergic receptor in CD8$^+$ T cells from BRCA patients by flow cytometry. Flow cytometric analysis was carried out using the following strategy; the singlets were first selected and then the lymphocyte population, based on cell size and granularity characteristics (FSC and SSC, respectively). The population of CD8$^+$ T cells was determined using specific CD8 staining, and the expression levels of the A2A receptor were obtained **(A)**. The A2A expression levels in CD8$^+$ T cells of the total samples **(B)**, the group of N-CHR **(C)**, or CHR **(D)** patients. The expression of the A2A receptor in CD8$^+$ T cells in different groups according to their molecular type; absence of the estrogen receptor (ER-) **(E)**; presence of estrogen receptor (ER+) **(F)**, luminal A **(G)**, luminal B **(H)**, human epidermal growth factor receptor 2 (HER2)-enriched **(I)**, and triple-negative **(J)**. The results correspond to the mean ± SEM. *p<0.05, **p<0.01.

## DISCUSSION

A growing body of evidence indicates that purinergic signaling plays a key role during tumorigenesis and tumor growth (Di Virgilio and Adinolfi, 2017). Among the purinergic receptors, the P2X7 receptor is one of the most studied as it promotes cancer cell proliferation, angiogenesis, and migration (Di Virgilio and Adinolfi, 2017; Di Virgilio et al., 2018). Besides, the P2X7 receptor participates in immune cells activation response, differentiation, and production of proinflammatory cytokines, and it promotes cell death by forming a non-selective pore, mainly in cells with high expression of the receptor as monocytes/macrophages (Surprenant and North, 2009; Di Virgilio et al., 2017; Adinolfi et al., 2018). Therefore, it is of great interest to determine whether the P2X7 receptor expressed in CD8$^+$ T lymphocytes plays a role in the chemoresistance of BRCA patients. Here, we showed that CD8$^+$ T cells present an increase in P2X7 receptor expression and a decrease in the A2A content only in patients that positively responded to neoadjuvant chemotherapy. In contrast, patients that developed chemoresistance showed no change in the expression of P2X7 and A2A in CD8$^+$ T cells.

Our results showed that the administration of first-line neoadjuvant chemotherapy significantly increased the expression of P2X7 in CD8$^+$ T cells. This effect might be caused by the release of molecules such as HMGB1 or ATP from cancer cells treated with drugs used in chemotherapy, which then activate dendritic cells to promote the presentation of an antigen (Aymeric et al., 2010), causing activation of CD8$^+$ T cells and elevated the expression of the P2X7 receptor (Borges da Silva et al., 2018). Therefore, this increase in extracellular ATP causes stimulation of the P2X7 receptor in CD8$^+$ T lymphocytes, which further favors its activation. On the other hand, in CHR patients, there was no increase in P2X7 receptor expression, which could indicate that the immune response against the tumor triggered after chemotherapy administration is not optimal. In fact, mouse models with deficient P2X7 expression developed accelerated tumorigenesis, lower infiltration of CD8$^+$ T cells into the tumor tissue, and reduced chemotherapy efficiency (Ghiringhelli et al., 2009; Adinolfi et al., 2015). Some isoforms of P2X7 have been reported related to cancer (Adinolfi et al., 2010), which could be participating in the mechanisms of chemotherapy efficacy. However, the relationship of each isoform with chemoresistance in BRCA is still unknown.

We also observed altered function of P2X7 receptor in patients who presented chemoresistance, as evidenced by no change in the percentage of CD62L positive cells from CD8$^+$ T cells as well as the lower production of IFN-$\gamma$ in the presence of ATP. These results might be related to the reduced expression of P2X7 receptors in cells from CHR patients. This observation is consistent with published results showing that changes in the expression of P2X7 alter CD8$^+$ T cells maturation and its production of IFN-$\gamma$ that impairs tumor infiltration (Borges da Silva et al., 2018; De Marchi et al., 2019). The shedding of CD62L is dependent on the activity of P2X7 (Mahnke et al., 2017); therefore, low shedding of CD62L reflects diminished function and expression of the P2X7 receptor. In the case of CHR patients, no significant change in the expression of CD62L occurred when

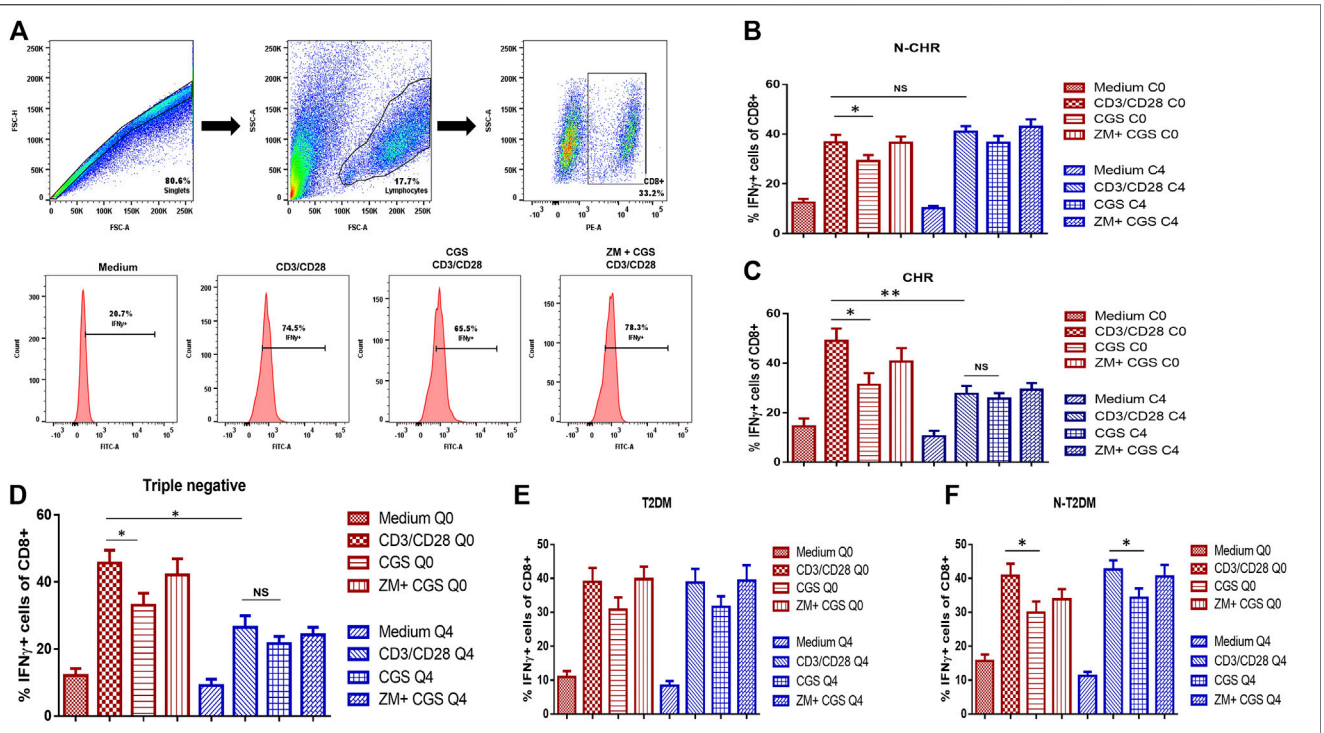


**FIGURE 5 |** Function of the A2A receptor in CD8$^+$ T cells from patients with BRCA by inhibiting IFN-$\gamma$ production. The analysis strategy to determine IFN-$\gamma$ expression in CD8$^+$ T cells included the following culture conditions: RPMI-1640 medium or pre-stimulation with the CD3/CD28 antibodies. Then, the A2A agonist was added (CGS-21680), or a combination of an agonist and an antagonist (CGS-21680 and ZM-241385) **(A)**. The IFN-$\gamma$ expression in CD8$^+$ T cells at C0 and C4 in N-CHR patients **(B)** or CHR patients **(C)**, triple-negative patients **(D)**, BRCA patients with type 2 diabetes mellitus (T2DM) **(E)**, and N-T2DM patients **(F)**. Values are shown as the mean ± SEM. *p<0.05, **p<0.01.

stimulated with ATP, as well as low shedding of CD62L at C0. Therefore, these results suggest that an adequate response to chemotherapy largely depends on the level of expression of the P2X7 receptor. However, further assays need to be performed to confirm this hypothesis.

Although it is known that there are differences in the survival of BRCA patients according to the expression of hormonal receptors, such as estrogen, progesterone, or the HER2 receptor (DeSantis et al., 2019), our results showed no changes in the expression of P2X7 and the CD62L marker, as well as low production of IFN-$\gamma$ in patients classified as triple-negative or HER2-enriched. In the case of luminal B patients, expression levels P2X7 were not modified after chemotherapy, and there were no changes in the CD62L marker. However, the analysis with the data from estrogen receptor-negative (ER−) or positive (ER+) patients showed that only RE−patients presented this alteration in the function of P2X7 (**Supplementary Figure S3E,F**). Therefore, these results could corroborate previously published information showing a relationship between disease-free survival or overall survival in patients with ER−and triple-negative BRCA (Liu et al., 2012) or HER2+ (Hou et al., 2018) and the presence of CD8$^+$ T lymphocytes infiltrated in the tumor, which could indicate that changes in the expression of P2X7 in these BRCA subtypes could be used as a marker of worse prognosis and the survival of these patients.

Metabolic disorders, such as T2DM, overweight obesity, are known as some of the main risk factors that increase the probability of developing cancer (Sun et al., 2017). As our study group was obese or overweight (76%) or had T2DM (30.9%), a significant correlation between P2X7 expression and the BMI of patients before chemotherapy administration was detected, but this correlation was lost during the fourth cycle of chemotherapy. This was possibly due to the side effects of chemotherapy that occasionally produce weight loss. However, when analyzing patients in normal weight, overweight, and obese (excluding patients with T2DM), we observed that in the obese or overweight group, the expression of P2X7 was not modified, and the function was altered. Our results confirm the previously reported relationship between obesity and BRCA, demonstrating the involvement of adipose tissue and the promotion of BRCA metastasis (Sabol et al., 2019). In this sense, we previously reported that purinergic signaling in adipose tissue and peripheral blood participates in generalized low-grade inflammation during overweight or obesity (Ruiz-Rodriguez et al., 2019). Furthermore, BRCA patients with T2DM showed no alteration in the P2X7 expression, which is consistent with previously reported showing that the expression and function of P2X7 on CD8$^+$ T cells is not modified in patients with T2DM (Garcia-Hernandez et al., 2011).

On the other hand, one of the variables that are normally considered to determine the progression of cancer, or as an

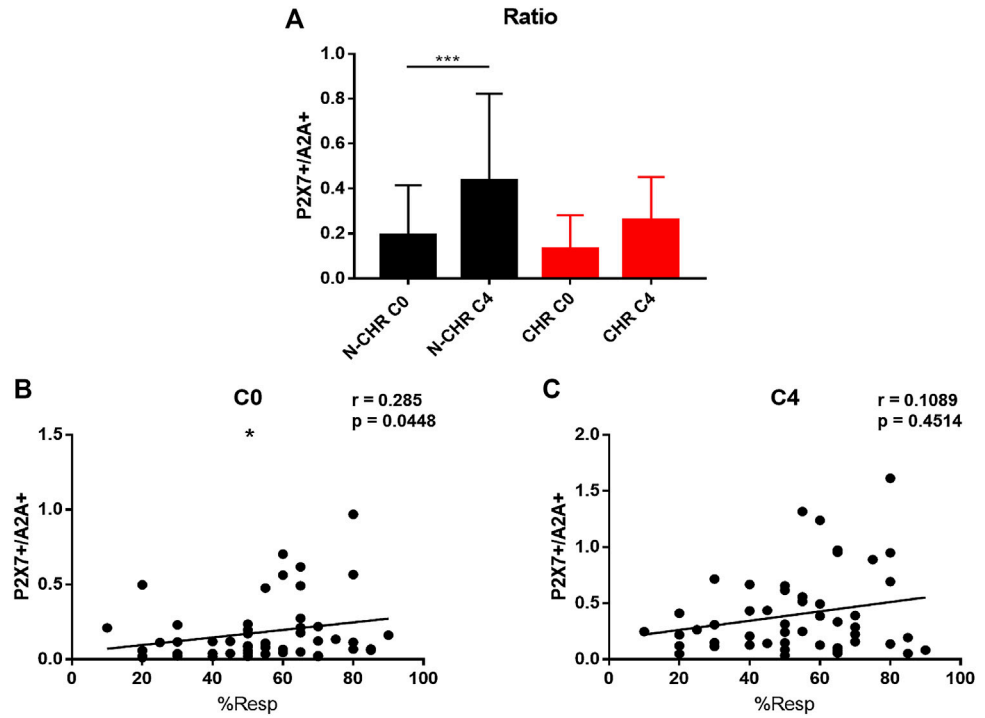


**FIGURE 6 |** P2X7/A2A ratio in CD8$^+$ T cells from patients with BRCA. Analysis of the P2X7/A2A ratio in CD8$^+$ T cells from N-CHR and CHR patients at C0 and C4 **(A)**. Correlation analysis between the percentage of response and the P2X7/A2A ratio at C0 **(B)** and C4 **(C)**. Values are shown as the mean ± SEM. *p<0.05, ***p<0.001.

indicator of treatment efficacy, is the tumor size. We found that only patients with a initial tumor size less than or equal to 5 cm presented an increase in the expression of P2X7 in CD8$^+$ T cells. These results might indicate a possible relationship between the P2X7 receptor and tumor size, BRCA subtype, and the number of lymphocytes infiltrated in the reported tumor, as was previously reported (Liu et al., 2012; Huang et al., 2015). The possible association between the variations in the percentage of P2X7 in CD8$^+$ T cells and chemoresistance, in patients with small initial tumor size (≤ 5 cm), could be a preliminarily indicator of chemoresistance and aid doctors during the decision-making when administering the first-line chemotherapy regimen. In this sense, one question that emerges in the context of our results is how does the expression of the P2X7 and A2A receptors change in the tumor during chemotherapy.

We also evaluated the A2A adenosine receptor, since it participates in the regulation or inhibition of the immune response (Linden and Cekic, 2012; Takenaka et al., 2016). It promotes the development and progression of BRCA tumor cells (Kutryb-Zajac et al., 2018). We found that CD8$^+$ T lymphocytes showed a decreased expression of the A2A receptor after the administration of chemotherapy, which may be related to the activation of CD8$^+$ T lymphocytes caused by the chemotherapy administration. Dendritic cells play an important role promoting the activation of CD8$^+$ T lymphocytes, coupled with an increase in extracellular ATP, possibly causing an increase in the expression of transcription factors such as NF-kB, which has been described as requiring activation in T lymphocytes for adequate control of tumor development (Barnes et al., 2015). Besides, the activation of NF-kB has a negative regulatory role for the A2A receptor (Zhang and Li, 2018; Silva et al., 2019). It has been shown the anergic CD8$^+$ T lymphocytes secrete low IFN-$\gamma$ production impairs NF-kB signaling (Clavijo and Frauwirth, 2012). These results could explain that the decrease in A2A receptor expression in patients after chemotherapy may be evidence for an adequate response to chemotherapy since CHR patients did not show a significant difference in receptor expression after chemotherapy. Also, we observed no changes in IFN-$\gamma$ production after chemotherapy administration in N-CHR patients. In contrast, in the case of CHR patients, a decrease in IFN-$\gamma$ production was detected, which supports the idea that no changes in A2A expression can continue to favor an inhibition in IFN-$\gamma$ production.

Additionally, the expression of A2A did no change in ER–, HER2-enriched or triple-negative patients. A decrease in IFN-$\gamma$ production after chemotherapy was observed, which might confirm previous findings showing that triple-negative BRCA patients were resistant to chemotherapy with doxorubicin and expressed the ectonucleotidase CD73 (Loi et al., 2013). The CD73 protein favors an increase in extracellular adenosine concentrations, and A2A receptor activation is involved.

BRCA patients with metabolic alterations comorbidity such as for overweight, obesity, or T2DM, significant changes in the modulation of A2A expression, and possibly in its activity might occur. For example, in the case of T2DM, a lack of function in the A2A receptor was found between C0 and C4, which is consistent with previously published results with T2DM patients showing that

the A2A receptor has an altered function and a higher receptor expression compared to healthy people (Guzman-Flores et al., 2015). Another comorbidity, such as obesity, hampers the survival of residual tumor cells in a HER2+ BRCA model (Ecker et al., 2019), which may support the idea that obesity has a negative impact on the response to chemotherapy, where the A2A receptor could have a key role. However, a study focused on low-grade inflammation present in adipose tissue from overweight or obese subjects showed that the A2A receptor does not have an important effect on this condition (Cortes-Garcia et al., 2018), which agrees with our results where we did not observe differences in the function of A2A in patients with alterations related to BMI (data not shown). However, obesity could play an important role in the response at the end of chemotherapy. Therefore, more studies are necessary to focus on patients with obesity after chemotherapy has been concluded, and searching for the role of purinergic receptors on residual tumor cells and the possible clinic relapse.

A ratio analysis between the expression or absence of CD16 in monocytes has been previously studied for some types of cancer such as lymphomas to determine possible biomarkers predictive of survival (Zhang et al., 2020). In our study, the P2X7/A2A ratio is proposed as a good prognosis marker related to chemoresistance, which was found only in N-CHR patients and a correlation with the percentage of response before starting chemotherapy. Therefore, it could be useful for decision-making in the use of the neoadjuvant FAC scheme for patients with BRCA, and it is also proposed as a possible marker of chemoresistance in patients with BRCA.

In conclusion, purinergic signaling of P2X7 and A2A receptors in $CD8^+$ T correlates with the response of BRCA patients to chemotherapy, and it can be utilized to implement personalized therapeutic strategies. Also, changes in the content of P2X7 and A2A receptors in $CD8^+$ T cells could serve as a sign of good prognosis in response to FAC chemotherapy for patients with BRCA, especially in patients with small tumors ($\leq$ 5 cm) and HER2-enriched or triple-negative patients. The metabolic alterations are a risk factor for cancer, but they also have implications for the chemoresistance of patients.

## DATA AVAILABILITY STATEMENT

All datasets generated for this study are included in the article/**Supplementary Material**.

## ETHICS STATEMENT

The studies involving human participants were reviewed and approved by Research Committee of the Central Hospital (COFEPRIS 14 CI 24 028 083) and the Committee of Ethics in Research (CONBIOETICA-24-CEI-001-20160427). The patients/participants provided their written informed consent to participate in this study.

## AUTHOR CONTRIBUTIONS

All authors contributed to the study conception and design. Material preparation, data collection, and analysis were performed by Victor Manuel Ruiz-Rodríguez and Eneida Turiján-Espinoza. The first draft of the manuscript was written by Victor Manuel Ruiz-Rodríguez, and all authors commented on previous versions of the manuscript. All authors read and approved the final manuscript. Diana Patricia Portales Perez studied the conception and design, contributed to the interpretation of the results, and drafted and critically revised the manuscript.

## FUNDING

This work was supported by Consejo Nacional de Ciencia y Tecnología (CONACYT) FOSEC SEP-INVESTIGACIÓN BÁSICA A1-S-26479 to AMES, as well as a doctoral fellowship awarded to VMRR (626561) by CONACYT, México.

## ACKNOWLEDGMENTS

The authors kindly acknowledge the nursing staff of Central Hospital Dr. Ignacio Morones Prieto for help in collecting samples.

## SUPPLEMENTARY MATERIAL

The Supplementary Material for this article can be found online at: https://www.frontiersin.org/articles/10.3389/fphar.2020.576955/full#supplementary-material

## REFERENCES

Adinolfi, E., Capece, M., Franceschini, A., Falzoni, S., Giuliani, A. L., Rotondo, A., et al. (2015). Accelerated tumor progression in mice lacking the ATP receptor P2X7. *Cancer Res* 75 (4), 635–644. doi:10.1158/0008-5472.CAN-14-1259

Adinolfi, E., Cirillo, M., Woltersdorf, R., Falzoni, S., Chiozzi, P., Pellegatti, P., et al. (2010). Trophic activity of a naturally occurring truncated isoform of the P2X7 receptor. *Faseb. J.* 24 (9), 3393–3404. doi:10.1096/fj.09-153601

Adinolfi, E., Giuliani, A. L., De Marchi, E., Pegoraro, A., Orioli, E., and Di Virgilio, F. (2018). The P2X7 receptor: a main player in inflammation. *Biochem. Pharmacol.* 151, 234–244. doi:10.1016/j.bcp.2017.12.021

Adinolfi, E., Raffaghello, L., Giuliani, A. L., Cavazzini, L., Capece, M., Chiozzi, P., et al. (2012). Expression of P2X7 receptor increases *in vivo* tumor growth. *Cancer Res* 72 (12), 2957–2969. doi:10.1158/0008-5472.CAN-11-1947

Apetoh, L., Ghiringhelli, F., Tesniere, A., Obeid, M., Ortiz, C., Criollo, A., et al. (2007). Toll-like receptor 4-dependent contribution of the immune system to anticancer chemotherapy and radiotherapy. *Nat. Med.* 13 (9), 1050–1059. doi:10.1038/nm1622

Arun, B. K., Dhinghra, K., Valero, V., Kau, S. W., Broglio, K., Booser, D., et al. (2011). Phase III randomized trial of dose intensive neoadjuvant chemotherapy with or without G-CSF in locally advanced breast cancer: long-term results. Oncologist 16 (11), 1527–1534. doi:10.1634/theoncologist.2011-0134

Aymeric, L., Apetoh, L., Ghiringhelli, F., Tesniere, A., Martins, I., Kroemer, G., et al. (2010). Tumor cell death and ATP release prime dendritic cells and efficient

anticancer immunity. *Cancer Res* 70 (3), 855–858. doi:10.1158/0008-5472.CAN-09-3566

Barnes, S. E., Wang, Y., Chen, L., Molinero, L. L., Gajewski, T. F., Evaristo, C., et al. (2015). T cell-NF-κB activation is required for tumor control *in vivo*. *J Immunother Cancer* 3 (1), 1. doi:10.1186/s40425-014-0045-x

Beavis, P. A., Divisekera, U., Paget, C., Chow, M. T., John, L. B., Devaud, C., et al. (2013). Blockade of A2A receptors potently suppresses the metastasis of CD73+ tumors. *Proc. Natl. Acad. Sci. U. S. A.* 110 (36), 14711–14716. doi:10.1073/pnas.1308209110

Borges da Silva, H., Beura, L. K., Wang, H., Hanse, E. A., Gore, R., Scott, M. C., et al. (2018). The purinergic receptor P2RX7 directs metabolic fitness of long-lived memory CD8(+) T cells. *Nature* 559 (7713), 264–268. doi:10.1038/s41586-018-0282-0

Breastcancer.org (2018). Molecular Subtypes of Breast Cancer. Available: https://www.breastcancer.org/symptoms/types/molecular-subtypes (Accessed 19 March 2019 ).

Buxton, I. L., Yokdang, N., and Matz, R. M. (2010). Purinergic mechanisms in breast cancer support intravasation, extravasation and angiogenesis. *Canc. Lett.* 291 (2), 131–141. doi:10.1016/j.canlet.2009.09.021

Clavijo, P. E., and Frauwirth, K. A. (2012). Anergic CD8+ T lymphocytes have impaired NF-kappaB activation with defects in p65 phosphorylation and acetylation. *J. Immunol.* 188 (3), 1213–1221. doi:10.4049/jimmunol.1100793

Cortes-Garcia, J. D., Briones-Espinoza, M. J., Vega-Cardenas, M., Ruiz-Rodriguez, V. M., Mendez- Mancilla, A., Gomez-Otero, A. E., et al. (2018). The inflammatory state of adipose tissue is not affected by the anti-inflammatory response of the A2a-adenosine system and miR-221/PTEN. *Int. J. Biochem. Cell Biol.* 100, 42–48. doi:10.1016/j.biocel.2018.04.020

Coskun, U., Gunel, N., Onuk, E., Yilmaz, E., Bayram, O., Yamac, D., et al. (2003). Effect of different neoadjuvant chemotherapy regimens on locally advanced breast cancer. *Neoplasma* 50 (3), 210–216.

De Marchi, E., Orioli, E., Pegoraro, A., Sangaletti, S., Portararo, P., Curti, A., et al. (2019). The P2X7 receptor modulates immune cells infiltration, ectonucleotidases expression and extracellular ATP levels in the tumor microenvironment. *Oncogene* 38 (19), 3636–3650. doi:10.1038/s41388-019-0684-y

DeSantis, C. E., Ma, J., Gaudet, M. M., Newman, L. A., Miller, K. D., Goding Sauer, A., et al. (2019). Breast cancer statistics, 2019. *CA Cancer J Clin* 69 (6), 438–451. doi:10.3322/caac.21583

Secretaría de Salud. (2017). Tratamiento del cancer de mama en segundo y tercer nivel de atención. Ciudad de México. Available: http://www.cenetec.salud.gob.mx/contenidos/gpc/catalogoMaestroGPC.html (Accessed 25 January 2020 ).

Di Virgilio, F., and Adinolfi, E. (2017). Extracellular purines, purinergic receptors and tumor growth. *Oncogene* 36 (3), 293–303. doi:10.1038/onc.2016.206

Di Virgilio, F., Dal Ben, D., Sarti, A. C., Giuliani, A. L., and Falzoni, S. (2017). The P2X7 receptor in infection and inflammation. *Immunity* 47 (1), 15–31. doi:10.1016/j.immuni.2017.06.020

Di Virgilio, F., Sarti, A. C., Falzoni, S., De Marchi, E., and Adinolfi, E. (2018). Extracellular ATP and P2 purinergic signalling in the tumour microenvironment. *Nat. Rev. Canc.* 18 (10), 601–618. doi:10.1038/s41568-018-0037-0

Ecker, B. L., Lee, J. Y., Sterner, C. J., Solomon, A. C., Pant, D. K., Shen, F., et al. (2019). Impact of obesity on breast cancer recurrence and minimal residual disease. *Breast Cancer Res.* 21 (1), 41. doi:10.1186/s13058-018-1087-7

Eisenhauer, E. A., Therasse, P., Bogaerts, J., Schwartz, L. H., Sargent, D., Ford, R., et al. (2009). New response evaluation criteria in solid tumours: revised RECIST guideline (version 1.1). *Eur. J. Canc.* 45 (2), 228–247. doi:10.1016/j.ejca.2008.10.026

Garcia-Hernandez, M. H., Portales-Cervantes, L., Cortez-Espinosa, N., Vargas-Morales, J. M., Fritche Salazar, J. F., Rivera-Lopez, E., et al. (2011). Expression and function of P2X(7) receptor and CD39/Entpd1 in patients with type 2 diabetes and their association with biochemical parameters. *Cell. Immunol.* 269 (2), 135–143. doi:10.1016/j.cellimm.2011.03.022

GCO (2018). Cancer Today: Breast Cancer. World Health Organization. Available: https://gco.iarc.fr/today/fact-sheets-cancers (Accessed 16 April 2019 ).

Gehring, M. P., Pereira, T. C., Zanin, R. F., Borges, M. C., Braga Filho, A., Battastini, A. M., et al. (2012). P2X7 receptor activation leads to increased cell death in a radiosensitive human glioma cell line. *Purinergic Signal.* 8 (4), 729–739. doi:10.1007/s11302-012-9319-2

Ghiringhelli, F., Apetoh, L., Tesniere, A., Aymeric, L., Ma, Y., Ortiz, C., et al. (2009). Activation of the NLRP3 inflammasome in dendritic cells induces IL-1beta-dependent adaptive immunity against tumors. *Nat. Med.* 15 (10), 1170–1178. doi:10.1038/nm.2028

Guzman-Flores, J. M., Cortez-Espinosa, N., Cortes-Garcia, J. D., Vargas-Morales, J. M., Catano-Canizalez, Y. G., Rodriguez-Rivera, J. G., et al. (2015). Expression of CD73 and A2A receptors in cells from subjects with obesity and type 2 diabetes mellitus. *Immunobiology* 220 (8), 976–984. doi:10.1016/j.imbio.2015.02.007

Haynes, N. M., van der Most, R. G., Lake, R. A., and Smyth, M. J. (2008). Immunogenic anti-cancer chemotherapy as an emerging concept. *Curr. Opin. Immunol.* 20 (5), 545–557. doi:10.1016/j.coi.2008.05.008

Hou, Y., Nitta, H., Wei, L., Banks, P. M., Lustberg, M., Wesolowski, R., et al. (2018). PD-L1 expression and CD8-positive T cells are associated with favorable survival in HER2-positive invasive breast cancer. *Breast J.* 24 (6), 911–919. doi:10.1111/tbj.13112

Huang, Y., Ma, C., Zhang, Q., Ye, J., Wang, F., Zhang, Y., et al. (2015). CD4+ and CD8+ T cells have opposing roles in breast cancer progression and outcome. *Oncotarget* 6 (19), 17462–17478. doi:10.18632/oncotarget.3958

INEGI Instituto Nacional de Estadística y Geografía (2016). Estadísticas a propósito del día mundial de la lucha contra el cáncer de mama. Available: https://www.inegi.org.mx/app/saladeprensa/noticia.html?id=2958 (Accessed 18 November 2019 ).

Ji, X., Lu, Y., Tian, H., Meng, X., Wei, M., and Cho, W. C. (2019). Chemoresistance mechanisms of breast cancer and their countermeasures. *Biomed. Pharmacother.* 114, 108800. doi:10.1016/j.biopha.2019.108800

Kutryb-Zajac, B., Koszalka, P., Mierzejewska, P., Bulinska, A., Zabielska, M. A., Brodzik, K., et al. (2018). Adenosine deaminase inhibition suppresses progression of 4T1 murine breast cancer by adenosine receptor-dependent mechanisms. *J. Cell Mol. Med.* 22 (12), 5939–5954. doi:10.1111/jcmm.13864

Linden, J., and Cekic, C. (2012). Regulation of lymphocyte function by adenosine. *Arterioscler. Thromb. Vasc. Biol.* 32 (9), 2097–2103. doi:10.1161/ATVBAHA.111.226837

Liu, S., Lachapelle, J., Leung, S., Gao, D., Foulkes, W. D., and Nielsen, T. O. (2012). CD8+ lymphocyte infiltration is an independent favorable prognostic indicator in basal-like breast cancer. *Breast Cancer Res.* 14 (2), R48. doi:10.1186/bcr3148

Loi, S., Pommey, S., Haibe-Kains, B., Beavis, P. A., Darcy, P. K., Smyth, M. J., et al. (2013). CD73 promotes anthracycline resistance and poor prognosis in triple negative breast cancer. *Proc. Natl. Acad. Sci. U. S. A.* 110 (27), 11091–11096. doi:10.1073/pnas.1222251110

Mahnke, K., Useliene, J., Ring, S., Kage, P., Jendrossek, V., Robson, S. C., et al. (2017). Down-regulation of CD62L shedding in T cells by CD39(+) regulatory T cells leads to defective sensitization in contact hypersensitivity reactions. *J. Invest. Dermatol.* 137 (1), 106–114. doi:10.1016/j.jid.2016.08.023

Mattarollo, S. R., Loi, S., Duret, H., Ma, Y., Zitvogel, L., and Smyth, M. J. (2011). Pivotal role of innate and adaptive immunity in anthracycline chemotherapy of established tumors. *Cancer Res.* 71 (14), 4809–4820. doi:10.1158/0008-5472.CAN-11-0753

Mittal, D., Young, A., Stannard, K., Yong, M., Teng, M. W., Allard, B., et al. (2014). Antimetastatic effects of blocking PD-1 and the adenosine A2A receptor. *Cancer Res.* 74 (14), 3652–3658. doi:10.1158/0008-5472.CAN-14-0957

Ruiz-Rodriguez, V. M., Cortes-Garcia, J. D., de Jesus Briones-Espinoza, M., Rodriguez-Varela, E., Vega-Cardenas, M., Gomez-Otero, A., et al. (2019). P2X4 receptor as a modulator in the function of P2X receptor in CD4+ T cells from peripheral blood and adipose tissue. *Mol. Immunol.* 112, 369–377. doi:10.1016/j.molimm.2019.06.009

Sabol, R. A., Beighley, A., Giacomelli, P., Wise, R. M., Harrison, M. A. A., O'Donnnell, B. A., et al. (2019). Obesity-altered adipose stem cells promote ER(+) breast cancer metastasis through estrogen independent pathways. *Int. J. Mol. Sci.* 20 (6). doi:10.3390/ijms20061419

Silva, R. L., Silveira, G. T., Wanderlei, C. W., Cecilio, N. T., Maganin, A. G. M., Franchin, M., et al. (2019). DMH-CBD, a cannabidiol analog with reduced cytotoxicity, inhibits TNF production by targeting NF-kB activity dependent on A2A receptor. *Toxicol. Appl. Pharmacol.* 368, 63–71. doi:10.1016/j.taap.2019.02.011

Spychala, J., Lazarowski, E., Ostapkowicz, A., Ayscue, L. H., Jin, A., and Mitchell, B. S. (2004). Role of estrogen receptor in the regulation of ecto-5'-nucleotidase and

adenosine in breast cancer. *Clin. Canc. Res.* 10 (2), 708–717. doi:10.1158/1078-0432.ccr-0811-03

Stoetzer, O. J., Fersching, D. M., Salat, C., Steinkohl, O., Gabka, C. J., Hamann, U., et al. (2013). Circulating immunogenic cell death biomarkers HMGB1 and RAGE in breast cancer patients during neoadjuvant chemotherapy. *Tumour Biol.* 34 (1), 81–90. doi:10.1007/s13277-012-0513-1

Sun, Y. S., Zhao, Z., Yang, Z. N., Xu, F., Lu, H. J., Zhu, Z. Y., et al. (2017). Risk factors and preventions of breast cancer. *Int. J. Biol. Sci.* 13 (11), 1387–1397. doi:10.7150/ijbs.21635

Surprenant, A., and North, R. A. (2009). Signaling at purinergic P2X receptors. *Annu. Rev. Physiol.* 71, 333–359. doi:10.1146/annurev.physiol.70.113006.100630

Takenaka, M. C., Robson, S., and Quintana, F. J. (2016). Regulation of the T cell response by CD39. *Trends Immunol.* 37(7), 427–439. doi:10.1016/j.it.2016.04.009

Xia, J., Yu, X., Tang, L., Li, G., and He, T. (2015). P2X7 receptor stimulates breast cancer cell invasion and migration via the AKT pathway. *Oncol. Rep.* 34 (1), 103–110. doi:10.3892/or.2015.3979

Zhang, H., and Li, W. (2018). microRNA-15 activates NF-kappaB pathway via down regulating expression of adenosine A2 receptor in ulcerative colitis. *Cell. Physiol. Biochem.* 51 (4), 1932–1944. doi:10.1159/000495718

Zhang, W., Ruan, J., Zhou, D., Han, X., Zhang, Y., Wang, W., et al. (2020). Predicting worse survival for newly diagnosed T cell lymphoma based on the decreased baseline CD16-/CD16 + monocyte ratio. *Sci. Rep.* 10 (1), 7757. doi:10.1038/s41598-020-64579-z

Zhou, J. Z., Riquelme, M. A., Gao, X., Ellies, L. G., Sun, L. Z., and Jiang, J. X. (2015). Differential impact of adenosine nucleotides released by osteocytes on breast cancer growth and bone metastasis. *Oncogene* 34 (14), 1831–1842. doi:10.1038/onc.2014.113

**Conflict of Interest:** The authors declare that the research was conducted in the absence of any commercial or financial relationships that could be construed as a potential conflict of interest.

frontiers in Pharmacology

ORIGINAL RESEARCH
published: 30 November 2020
doi: 10.3389/fphar.2020.585255

# A Prognostic Model Based on Immune-Related Long Non-Coding RNAs for Patients With Cervical Cancer

*Peijie Chen†, Yuting Gao†, Si Ouyang, Li Wei, Min Zhou, Hua You* and Yao Wang**

*Medical Oncology Department, Affiliated Cancer Hospital & Institute of Guangzhou Medical University, Guangdong, China*

**Objectives:** The study is performed to analyze the relationship between immune-related long non-coding RNAs (lncRNAs) and the prognosis of cervical cancer patients. We constructed a prognostic model and explored the immune characteristics of different risk groups.

**Methods:** We downloaded the gene expression profiles and clinical data of 227 patients from The Cancer Genome Atlas database and extracted immune-related lncRNAs. Cox regression analysis was used to pick out the predictive lncRNAs. The risk score of each patient was calculated based on the expression level of lncRNAs and regression coefficient (β), and a prognostic model was constructed. The overall survival (OS) of different risk groups was analyzed and compared by the Kaplan–Meier method. To analyze the distribution of immune-related genes in each group, principal component analysis and Gene set enrichment analysis were carried out. Estimation of STromal and Immune cells in MAlignant Tumors using Expression data was performed to explore the immune microenvironment.

**Results:** Patients were divided into training set and validation set. Five immune-related lncRNAs (H1FX-AS1, AL441992.1, USP30-AS1, AP001527.2, and AL031123.2) were selected for the construction of the prognostic model. Patients in the training set were divided into high-risk group with shorter OS and low-risk group with longer OS ($p = 0.004$); meanwhile, similar result were found in validation set ($p = 0.013$), combination set ($p < 0.001$) and patients with different tumor stages. This model was further confirmed in 56 cervical cancer tissues by Q-PCR. The distribution of immune-related genes was significantly different in each group. In addition, the immune score and the programmed death-ligand 1 expression of the low-risk group was higher.

**Conclusions:** The prognostic model based on immune-related lncRNAs could predict the prognosis and immune status of cervical cancer patients which is conducive to clinical prognosis judgment and individual treatment.

**Keywords: Cervical cancer, Long non-coding RNA, Immunology, Gene express, Prognosis**

OPEN ACCESS

***Edited by:***
*Xiaoping Lin,*
*Sun Yat-sen University Cancer Center (SYSUCC), China*

***Reviewed by:***
*Hong-Wu Xin,*
*Yangtze University, China*

****Correspondence:***
*Yao Wang*
*wangyao@gzhmu.edu.cn*
*Hua You*
*youhua307@163.com*

*†These authors have contributed equally to this work.*

***Specialty section:***
*This article was submitted to Pharmacology of Anti-Cancer Drugs, a section of the journal Frontiers in Pharmacology*

***Received:*** *20 July 2020*
***Accepted:*** *19 October 2020*
***Published:*** *30 November 2020*

***Citation:***
*Chen P, Gao Y, Ouyang S, Wei L, Zhou M, You H and Wang Y (2020) A Prognostic Model Based on Immune-Related Long Non-Coding RNAs for Patients With Cervical Cancer. Front. Pharmacol. 11:585255. doi: 10.3389/fphar.2020.585255*

## BACKGROUND

Cervical cancer is the fourth most common malignant tumor among women worldwide, both in morbidity and mortality (Bray et al., 2018). Approximately 90% of cervical cancer cases in recent years occurred in developing countries, with a higher rate of morbidity and mortality than in developed countries (WHO, 2018). Most of the early stage cervical cancer patients can be cured by surgery, and the primary treatment for locally advanced cervical cancer is chemo-radiotherapy. The

5-year overall survival (OS) rate of stage I cervical cancer patients is 92.1%, and that of stages II, III, and IV patients is 74.2, 52.0, and 29.8%, respectively (Nagase et al., 2019). While the drug resistance to patients leads to limited therapeutic response, including chemotherapeutics and radiation therapy; it has become a serious problem on cervical cancer therapy (Burger et al., 2011; Eskander and Tewari, 2014). With the advancement in tumor immunology, especially the development of immune checkpoint inhibitors (ICIs), the treatment of cervical cancer has made some progress in immunotherapy and targeted therapy (Menderes et al., 2016; De Felice et al., 2018). Evidence suggests that the objective response rate (ORR) of programmed death-ligand 1 (PD-L1) inhibitor is only about 14% (Chung et al., 2019). Nevertheless, the survival status and prognosis of recurrent and advanced cervical carcinoma patients is not yet satisfactory. Thus, performing risk stratification with immune factors for patients with cervical cancer may be helpful in predicting their survival and immunotherapeutic response.

Long non-coding RNA (lncRNA), a non-protein coding transcript, is more than 200 nucleotides in length. Previous research revealed that lncRNAs are extensively involved in different aspects of the immune system, including immune cell lineage development, immune cell activation, and immune-related diseases (Atianand et al., 2017). Notably, lncRNA is reported as a critical regulator in cancer immunity, covering antigen presentation, immune stimulation, tumor infiltration and so on (Yu et al., 2018). Numerous studies on cancer indicated that lncRNAs take part in tumorigenesis of cervical cancer, being closely correlated with the prognosis of patients. For instance, gastric carcinoma high expressed transcript 1 is considered a carcinogenic lncRNA that promotes proliferating, migrating and infiltrating in different kinds of cancer, including cervical cancer (Zhang et al., 2019). Another study demonstrated that lncRNA cancer susceptibility 15 plays a driving role in cell proliferation, invasion, cycle progression, and epithelial-to-mesenchymal signaling pathway of cervical cancer (Shan et al., 2019). LINC0051 also promote the progression of cervical cancer, as well as resistance to paclitaxel (Mao et al., 2019). Hence, lncRNA may act as a potential target in the treatment and prognosis of cervical cancer. However, we have not yet identified exactly what role the immune-related lncRNAs play in the prognosis of cervical cancer. Our study was, therefore, designed to explore the correlation between immune-related lncRNAs and the prognosis of cervical cancer, and construct a prognostic model by analyzing the gene expression profile in The Cancer Genome Atlas (TCGA) database.

# MATERIALS AND METHODS

## Samples and Datasets

In this research, we downloaded the gene expression profiles of tumor samples, and the corresponding prognostic information of 255 cervical cancer patients from the TCGA database (https://cancergenome.nih.gov/). Patients were excluded if the survival time was ≤30 days because they may have died of other fatal complications. Finally, 227 patients were enrolled in our research and each sample corresponded to one patient. The combination set were divided into training set 167 and validation set 60 randomly for the following study. Data collection date was January 10, 2020.

## Immune-Related Long Non-Coding RNAs Extraction and Mining

Extraction and mining methods of immune-related lncRNAs were described previously (Wang et al., 2018; Wei et al., 2019). We obtained the immune-related genes from Molecular Signatures Database 4.0.1 (Immune system process M13664, Immune response M19817) on Gene Set Enrichment Analysis (GSEA) website (http://software.broadinstitute.org/gsea/index.jsp) (Wang et al., 2018). LncRNAs were extracted by the GENCODE project (http://www.gencodegenes.org) (Derrien et al., 2012). We obtained the expression levels of immune genes and lncRNAs in each sample, and the cohort of immune-related lncRNAs was identified according to Pearson's correlation analysis by the cor. test function of R (correlation coefficient Cor > 0.6, $p < 0.001$).

## Prognostic Model Construction and Validation

The training set including 167 patients were used to construct the model. The Survival package of R (3.5.2) software was used for multivariate analysis of lncRNAs with statistically significant differences in univariate analysis, and the optimal prediction model was determined based on the Akaike Information Criterion (AIC). The risk score of each patient was determined by the lncRNAs' expression level and the regression coefficient ($\beta$) of the weighted linear combination in the multivariate analysis. The formula was listed as follows: Risk score = $\beta$ gene 1 × expr (gene 1) + $\beta$ gene 2 × expr (gene 2) + . . .+ $\beta$ gene N × expr (gene N). exprgene referred to the expression of lncRNAs. According to the median risk score, we divided all the patients into two groups: high-risk group and low-risk group. To evaluate the accuracy of this prognostic model, the same algorithm was performed in the validation set (60 patients) and combination set (227 patients) with the same coefficient ($\beta$), and also performed for further examination of cancer tissues from 56 cervical cancer patients in our center.

## Patient Eligibility and Evaluation

We enrolled 56 cervical cancer patients treated in Affiliated Cancer Hospital & Institute of Guangzhou Medical University between January 1, 2013 and December 30, 2017. All of the patients were diagnosed with postoperative histopathological examination. Primary cancer tissues were stored in RNA*later*™ Stabilization Solution (Invitrogen) immediately after resection at −80 °C. This study was approved by the Ethic Committee of Affiliated Cancer Hospital & Institute of Guangzhou Medical University, and written informed consent was obtained from each patient. Baseline characteristics were obtained from the patients' history. OSs were measured from the date of diagnosis to either the end of the follow-up period, to the date of death from any cause or to the date of loss to follow-up.

## Quantitative Real-Time PCR

Total RNA was extracted from tissue samples using TRIzol (Invitrogen) according to the manufacturer's protocol. Samples were treated with DNase using the RNase-free DNase Set (Qiagen) during the total RNA isolation. First strand complementary DNA (cDNA) was synthesized using the cDNA Synthesis kit (Thermo Fisher Scientific) according to the manufacturer's instructions. ABI prism 7900-HT sequence detection system (96-well, Applied Biosystems) was used to perform quantitative real-time PCR (RT-PCR) analysis. For RT-PCR, the following primers were used:

GAPDH: 5′- GACTCATGACCACAGTCCATGC-3′ (forward), 5′- AGAGGCAGGGATGATGTTCTG-3′ (reverse).

H1FX-AS1: 5′- GATGGGGAAGGGATTCGCTC-3′ (forward), 5′- TCTCCTTTGCTGTGTTCCCG-3′ (reverse).

AL441992.1: 5′- AAGAAGCTCTCGTGTGGCTC-3′ (forward), 5′- TGGCTTTGAAGCGAGGATGA-3′ (reverse).

USP30-AS1: 5′- AGCAATAGCTGACGGACCAC-3′ (forward), 5′- TGAAAACCAAGCAGCCCCA-3′ (reverse).

AP001527.2: 5′- ATTGGGAATGACTCATCTGTTTG-3′ (forward), 5′- AGCAGTAGACTCCCAGGAAAG-3′ (reverse).

AL031123.2: 5′- ACACACGTGGTCTGTAGCG-3′ (forward), 5′- GGGCCTTGCTTTCCCCATAA-3′ (reverse).

**TABLE 1 |** Characteristics of 227 patients with cervical cancer from The Cancer Genome Altas database.

| Characteristics | N (%) |
|---|---|
| Age | |
| <60 | 178 (78.4) |
| ≥60 | 49 (21.6) |
| Grade | |
| G1 | 10 (4.4) |
| G2 | 102 (44.9) |
| G3 | 92 (40.5) |
| G4 | 1 (0.4) |
| GX | 20 (8.8) |
| unknown | 2 (0.8) |
| FIGO stage | |
| I | 101 (44.5) |
| II | 50 (22.0) |
| III | 13 (5.7) |
| IV | 14 (6.2) |
| unknown | 49 (21.6) |
| Tumor | |
| T1 | 101 (44.5) |
| T2 | 53 (23.3) |
| T3 | 14 (6.2) |
| T4 | 9 (4.0) |
| Tis | 1 (0.4) |
| TX | 14 (6.2) |
| unknown | 35 (15.4) |
| Lymph node | |
| N0 | 93 (41.0) |
| N1 | 45 (19.8) |
| NX | 54 (23.8) |
| unknown | 35 (15.4) |
| Metastasis | |
| M0 | 88 (38.8) |
| M1 | 8 (3.5) |
| MX | 94 (41.4) |
| unknown | 37 (16.3) |

**TABLE 2 |** Immune-related LncRNAs with significant prognostic value identified by univariate Cox regression analysis.

| LncRNA | HR | *p* value |
|---|---|---|
| AL133215.2 | 0.413 | 0.017 |
| H1FX-AS1 | 0.416 | 0.012 |
| AC015922.2 | 1.306 | 0.025 |
| AC097468.3 | 0.445 | 0.007 |
| AL441992.1 | 0.600 | 0.019 |
| USP30-AS1 | 0.656 | 0.006 |
| AP001527.2 | 1.359 | 0.012 |
| AL031123.2 | 0.382 | 0.013 |
| AC024060.1 | 0.557 | 0.008 |

*LncRNA, Long non-coding RNA.*

All samples were processed in triplicate. The relative gene expression was determined using the $2^{-\Delta\Delta CT}$ method.

## Tumor Component Assessment

The distribution of immune-related genes was presented by principal component analysis (PCA). To identify whether the functional phenotypes were different between the high- and low-risk groups, GSEA was performed. Estimation of STromal and Immune cells in MAlignant Tumors using Expression data (ESTIMATE) was performed to evaluate the immune microenvironment, including the presence of stromal cell, tumor infiltration, and tumor purity in each sample (Yoshihara et al., 2013).

## Statistical Analysis

Kaplan–Meier curves were drawn to evaluate the OS and the data was statistically compared with the log rank test. The prognostic value of the immune-related lncRNAs was assessed by the univariate and multivariate cox proportional-hazards regression model. The receiver operating characteristic (ROC) curve was established to evaluate the reliability and accuracy of the prognostic model. All the statistical analyses were done using R software (version 3.5.2). $p$ value (two-sided) < 0.05 was taken as being statistically significant.

# RESULTS

## Patient Characteristics

We enrolled 227 patients with cervical cancer in our study, with an average age of 48.35 years (20–88 years) and sorted out their clinicopathological characteristics (**Table 1**).

**TABLE 3 |** The optimal immune-related prognostic LncRNAs screened out by multivariate cox regression analysis and the AIC value, five lncRNAs were used to construct the prognostic model.

| LncRNA | β | HR | *p* value |
|---|---|---|---|
| H1FX-AS1 | −0.70 | 0.50 | 0.040 |
| AL441992.1 | −0.61 | 0.54 | 0.003 |
| USP30-AS1 | −0.28 | 0.76 | 0.045 |
| AP001527.2 | 0.35 | 1.42 | 0.004 |
| AL031123.2 | −0.77 | 0.46 | 0.043 |

*LncRNA, Long non-coding RNA.*

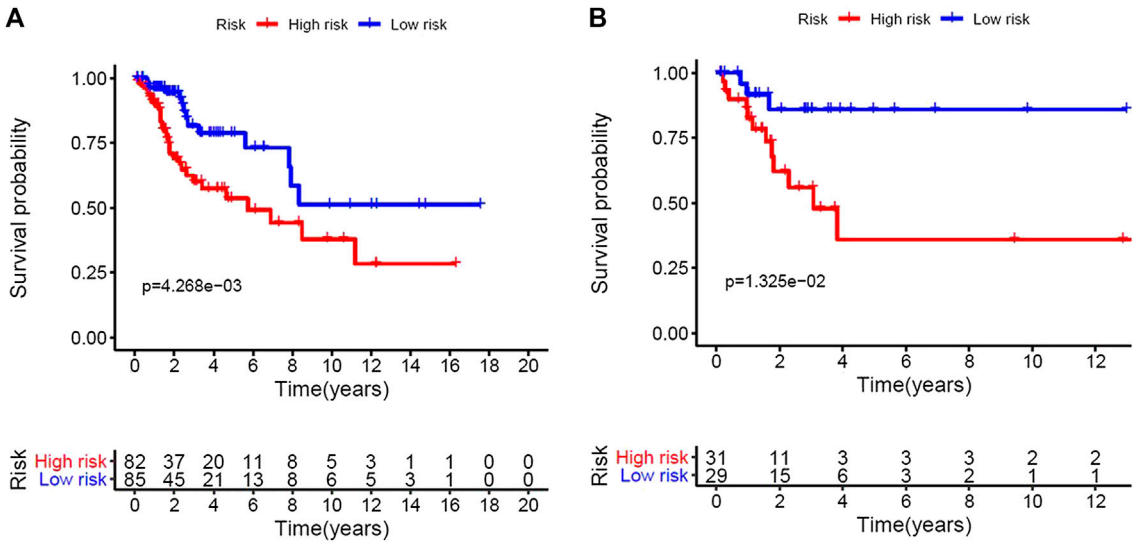


**FIGURE 1 |** Construction of the five immune-related Long non-coding RNAs prognostic model of cervical cancer patients. Based on the median risk score, we divided patients from the training set into high-risk group with 84 individuals and low-risk group with 83 individuals. **(A)**, Kaplan–Meier curve of the high-risk and low-risk groups of training set showed differences in survival rate. **(B)**, Kaplan–Meier curve of the high-risk and low-risk groups of validation set also showed differences in survival rate.

## Identification of Immune-Related Long Non-Coding RNAs With Prognostic Value

We extracted 331 immune-related protein-coding genes from Molecular Signatures Database and obtained 121 immune-related lncRNAs by the co-expression network (correlation coefficient Cor > 0.6, $p < 0.001$). Finally, univariate Cox regression analysis based on the training set revealed nine immune-related lncRNAs with the most significant prognostic value for cervical cancer patients (**Table 2**). Among all the lncRNAs, AC015922.2 and AP001527.2 were considered as perilous factors while the rest were protective factors.

## Construction and Verification of Prognostic Model

Based on the multivariate analysis and the AIC value, five lncRNAs were used to construct the prognostic model

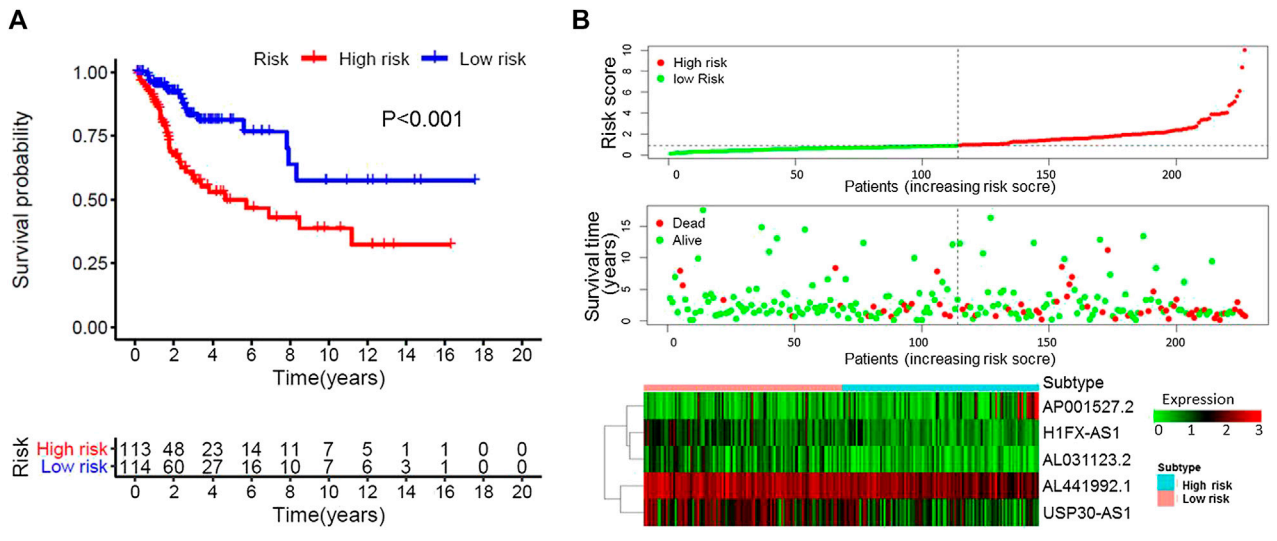


**FIGURE 2 |** Characteristics of the patients in the combination set based on the constructed model. **(A)**, Kaplan–Meier curve of the high-risk and low-risk groups of combination set showed differences in survival rate. **(B)**, Distribution of risk score, survival status of each patients, and heat map expression of five immune-related Long non-coding RNAs in high-risk and low-risk groups were presented.

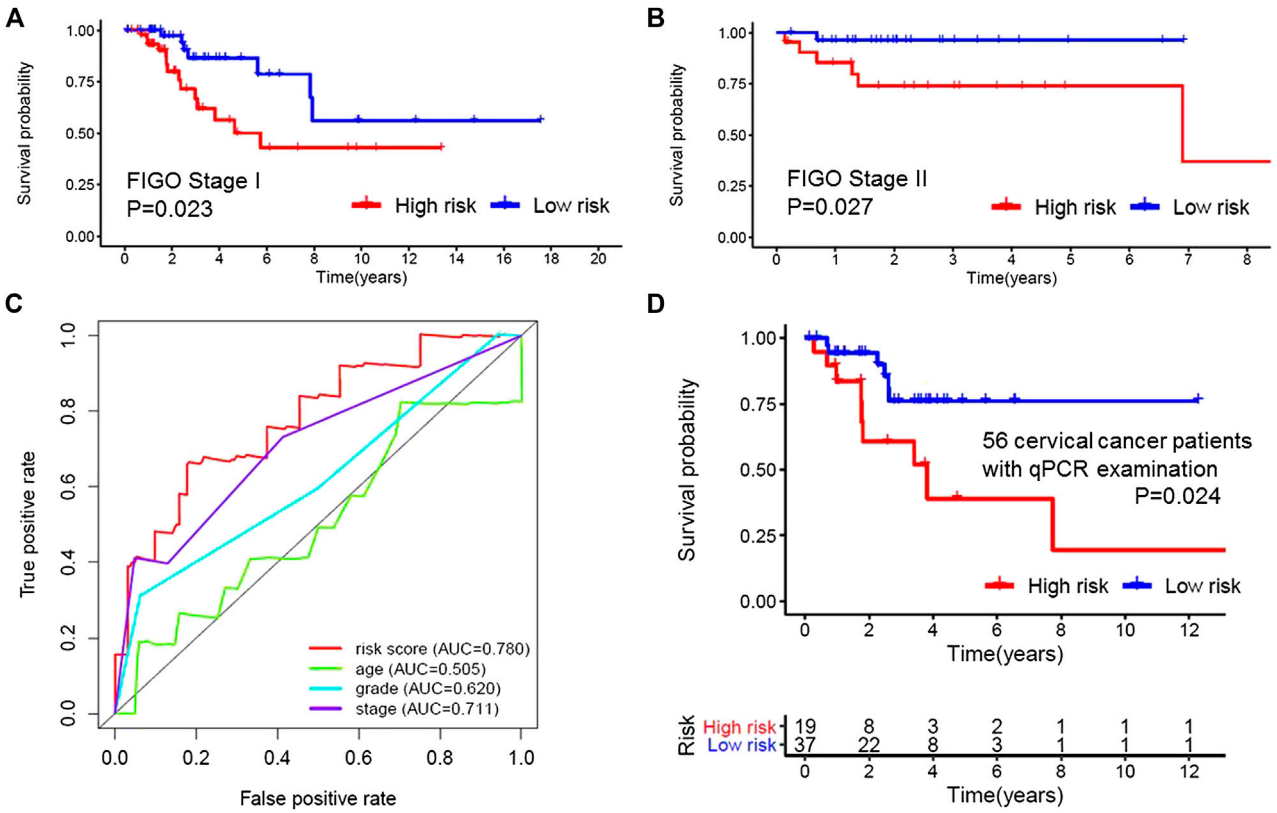


**FIGURE 3 |** Applicability and reliability of the prognostic model. **(A,B)** Kaplan–Meier curve of FIGO stages I and II of the high- and low-risk groups. **(C)**, Receiver operating characteristic (ROC) curve of the risk score, age, grade, and stage. The area under the ROC curve (AUC) of the prediction model was 0.780, which was much better than that of age (0.505), grade (0.620) and FIGO stage (0.711). **(D)** Kaplan–Meier curve of 56 cervical cancer patients. 56 patients from our cancer center were selected and QRT-PCR was used to calculate the expression level of five Long non-coding RNAs, finally the prognostic model was validated using their accordingly clinical data.

(**Table 3**). The expression level of lncRNAs and regression coefficient ($\beta$) were integrated to calculate the risk score for each patient. Based on the median risk score, we divided the patients from the training set into a high-risk group with 84 individuals and a low-risk group with 83 individuals. Kaplan-Meier plot showed differences in survival rate between the two groups ($p$ = 0.004, **Figure 1A**). We verified this model in the validation set ($p$ = 0.013, **Figure 1B**) and combination set ($p$ < 0.001, **Figure 2A**) with the similar result. In the combination set, the risk score and survival time of each risk group and the expression of five lncRNAs are shown in **Figure 2B**. To further investigate the value of this prognostic model in stratifying patients with different TNM stages, we carried out Kaplan-Meier analysis and showed that the risk subgroups differed significantly in both FIGO stage I and II ($p$ = 0.023 and $p$ = 0.027, respectively; **Figures 3A,B**). The area under the ROC curve (AUC) of the predictionmodel was 0.780, which was much better than that of age (0.505), grade (0.620), and FIGO stage (0.711) (**Figure 3C**). Moreover, 56 patients (**Table 4**) with cervical cancer were selected and QRTPCR was used to calculate the expression level of five lncRNAs, finally the prognostic modelwas validated using their accordingly clinical data. We found differences in survival rate between the two groups (p 0.024, **Figure 3D**).

**TABLE 4 |** Characteristics of 56 patients with cervical cancer, whom were enrolled from our cancer center for further q-PCR examination.

| Characteristics | N (%) |
|---|---|
| Age | |
| <60 | 40 (71.4) |
| ≥60 | 16 (28.6) |
| Grade | |
| G1 | 7 (12.5) |
| G2 | 29 (51.8) |
| G3 | 20 (35.7) |
| FIGO stage | |
| I | 17 (30.4) |
| II | 25 (44.6) |
| III | 9 (16.1) |
| IV | 5 (8.9) |
| Death | |
| Yes | 15 (26.8) |
| No | 41 (73.2) |
| Risk group | |
| High | 19 (33.9) |
| Low | 37 (66.1) |

## Immune Characteristics of High-Risk and Low-Risk Groups

Based on immune genes and whole gene expression profiles, we investigated the distribution mode of the high-risk and low-risk groups by PCA in the combination set. On whole gene expression profiles, PCA showed that the high- and low-risk groups were mixed up (**Figure 4A**). While based on the immune genes, these two groups were obviously different, indicating that the distribution of immune-related genes between the high- and low-risk groups was significantly different (**Figure 4B**). Further analysis by GSEA showed that the low-risk group had adequate immune response and immune system process pathways (**Figure 4C**). According to the ESTIMATE analysis, the immune score of the low-risk group was higher than that of the high-risk group (**Figure 5A**). The low-risk group had more immune and stromal cells but lower tumor purity (**Figure 5B**). Meanwhile, PD-L1 expression of the low-risk group was higher than that of the high-risk group (**Figure 5C**), presenting a potential target for immunotherapy. Moreover, GO and KEGG enrichment analysis found that the functions of this group were mainly concentrated in immune-related functions (**Table 5**).

## DISCUSSION

It has been reported that tumorigenesis is strongly associated with a series of cumulative genetic and epigenetic changes occurring in a normal cell; it is also closely related to the body's

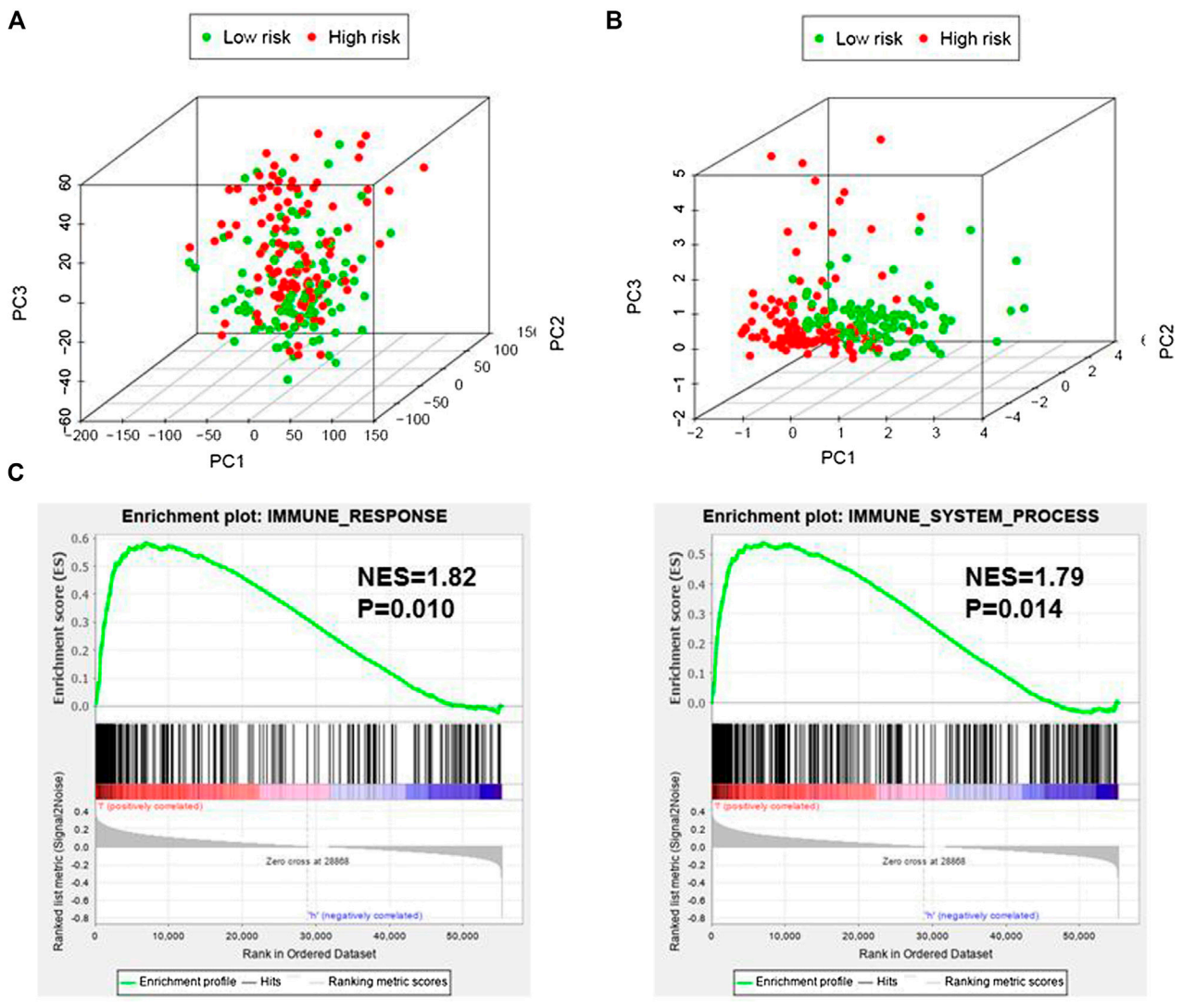


**FIGURE 4 |** Immune status of the high- and low-risk groups. **(A)**, Principal component analysis (PCA) showed that whole gene expression profiles between the high- and low-risk groups were mixed up. **(B)**, PCA indicated that the distribution of immune-related genes between the high- and low-risk groups were significantly different. **(C)**, Gene set enrichment analysis implied that the low-risk group had adequate immune response and immune system process pathways. NES, Normalized Enrichment Score.

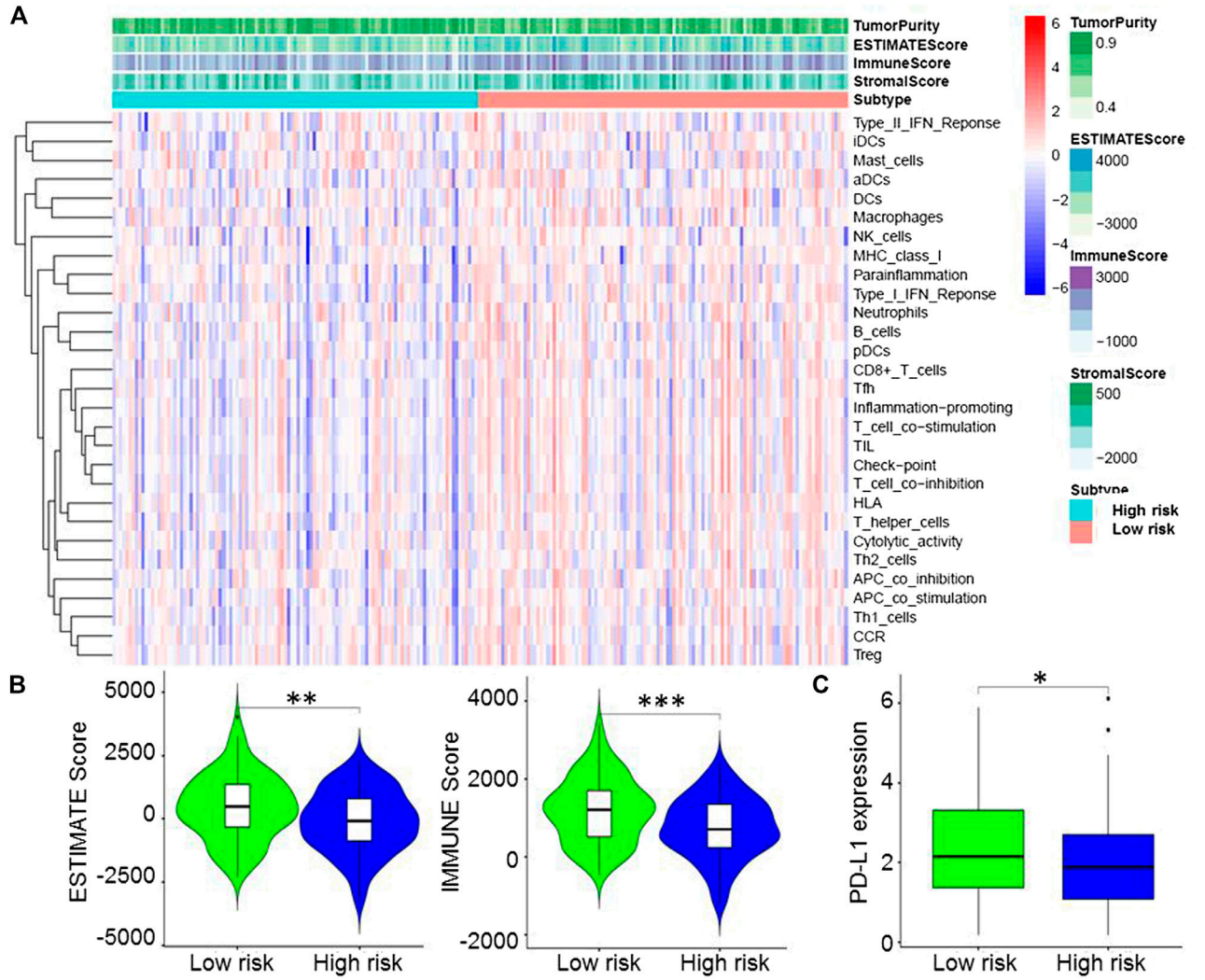


**FIGURE 5 |** Immune microenvironment of the high- and low-risk groups. **(A)**, Estimation of STromal and Immune cells in MAlignant Tumors using Expression data (ESTIMATE) analysis showed that the immune score of the low-risk group was higher than that of the high-risk group. **(B)**, ESTIMATE analysis indicated that the low-risk group had more immune and stromal cells but lower tumor purity. **(C)**, Programmed death-ligand 1 expression of the low-risk group was higher than that of the high-risk group.

microenvironment and immunity (Prendergast and Jaffee, 2007). The immune system recognizes and kills cancerous cells and their precursors, while cancerous cells develop strategies to escape from immune-surveillance thereby promoting tumorigenesis (Tesniere et al., 2006). Recently, lncRNA was proven to play an active part in the regulation of the immune system by affecting tumor microenvironment, epithelial-mesenchymal transition, dendritic cell and myeloid-derived stem cell regulation, and T and B cell activation and differentiation (Heward and Lindsay, 2014; Yu et al., 2015; Denaro et al., 2019). Immune-related lncRNAs, which were identified as a prognostic marker of various types of cancer (Wang et al., 2018), are markedly connected with immune cell infiltration (Li et al., 2020), and might be a potential target for cancer treatment.

Many lncRNAs have been shown to participate in the occurrence and progression of cervical cancer, either promoting (like SNHG7) or inhibiting (like GAS5) the disease (Cao et al., 2014; Zeng et al., 2019). Recent study identified a two-lncRNA signature (ILF3-AS1 and RASA4CP) as an independent biomarker which could predict the prognosis of cervical cancer based on the TCGA database and quantitative reverse transcription PCR (qRT-PCR) (Wu et al., 2019). This new finding further proved the importance of lncRNAs in cervical cancer, enlarged its application prospect on the prognosis of the disease, and emphasized the significance of future study on the function and mechanism of lncRNAs. In this study, we explored the connection between immune-related lncRNAs and prognosis of cervical cancer. Among the five immune-related lncRNAs used to construct the model, H1FX-AS1, AL441992.1, USP30-AS1, and AL031123.2 were protective factors, while AP001527.2 was a risk factor. As far as we know, all of these five immune-related lncRNAs have not been studied in clinical and fundamental

**TABLE 5 |** Significantly enriched GO terms and KEGG pathways of low risk group.

| GO | ID | Description | NSE | *p* |
|---|---|---|---|---|
| BP | GO: 0002704 | Regulation of leukocyte mediated immunity | 2.14 | 0.015 |
| BP | GO: 0032480 | Regulation of type I interferon production | 2.12 | 0.014 |
| BP | GO: 0002707 | Regulation of lymphocyte mediated immunity | 2.10 | 0.014 |
| BP | GO: 0002710 | Regulation of T cell mediated immunity | 2.08 | 0.016 |
| BP | GO: 0031312 | Extrinsic component of organelle membrane | 2.06 | 0.022 |
| KEGG | hsa04623 | Cytosolic DNA sensing pathway | 1.93 | 0.002 |
| KEGG | hsa00190 | Oxidative phosphorylation | 1.89 | 0.006 |
| KEGG | hsa05322 | Systemic lupus erythematosus | 1.87 | 0.002 |
| KEGG | hsa05320 | Autoimmune thyroid disease | 1.87 | 0.002 |
| KEGG | hsa04612 | Antigen processing and presentation | 1.80 | 0.012 |

*BP, biological process; CC, cellular component; GO, Gene Ontology; MF, molecular function.*

research. We hypothesized that the immune-related lncRNAs in our study might play a similar role in cervical cancer.

The prognostic model demonstrated superior ability in dividing patients into low- and high-risk groups. We found that patients in the low-risk group showed favourable prognosis, either the training set or the validation set, as well as in the combination set, which indicate that our model might be capable of risk stratification. The AUC for the prognostic model was 0.780, which was greater than the AUC of other clinicopathological factors. Moreover, this model can also distinguish the prognosis of patients in FIGO stages I and II, and could be an important supplement to FIGO stage. It is important that the value of the prognostic model was further verified with the tissue samples of patients.

There is evidence demonstrating that immunotherapy is a novel therapeutic strategy for cervical cancer treatment (Eskander and Tewari, 2015; Ventriglia et al., 2017). While the efficacy of immunotherapy varies from person to person, the ORR of nivolumab (ICI, anti-PD-1) in cervical cancer is 26.3% and the median OS is 21.9 months (Naumann et al., 2019). The efficiency of immunotherapy depends on the immunogenicity of the tumor microenvironment, therefore knowing more about the tumor microenvironment is the key to evaluating the probability of immunotherapy (Gasser et al., 2017). The predictive biomarkers of cancer immunotherapy mainly include PD-L1 expression, immune cell infiltration, tumor mutational burden, specific gene mutations, and so on (Chen et al., 2018; Darvin et al., 2018; Yi et al., 2018; Otoshi et al., 2019). Though the efficacy of immunotherapy is better than that for traditional treatment, only a few patients are suitable for it because of limited availability and high cost. It is essential to screen the appropriate individuals for immunotherapy. We found that the distribution of immune-related genes was significantly different in each group, the immune score and the PD-L1 expression of the low-risk group was higher, GSEA revealed that the low-risk group had abundant immune response and immune system process pathways. Thus, the low-risk group might be more suitable for immunotherapy because of possessing high immunogenicity but the mechanism remains unclear. Moreover, we ultimately look forward to verify the response rate of ICIs in different risk group, further work is needed to validate these findings in future.

## CONCLUSION

We constructed a prognostic model based on immune-related lncRNAs to evaluate the prognosis of patients with cervical cancer, the high- and low-risk groups displayed different immune states, indicating that immunogenicity might be a potential factor to determine the suitability of patients for immunotherapy. We expect this model to be helpful in clinical treatment, but its application value needs to be further verified by a multicenter, large-sample clinical study.

## DATA AVAILABILITY STATEMENT

The original contributions presented in the study are included in the article/supplementary material, further inquiries can be directed to the corresponding author/s.

## AUTHOR CONTRIBUTIONS

PC prepared and wrote the manuscript, searched literature; PC, YG and SO collected and interpreted the data; LW and MZ planned and designed the study; HY and YW analyzed the data and organized the logic of the paper.

## FUNDING

National Natural Science Foundation of China (81802723), Guangzhou Health and Family Planning Commission Technology Project (20191A011104), Clinical Key Specialty Construction Project of Guangzhou Medical University (YYPT202017).

## REFERENCES

Atianand, M. K., Caffrey, D. R., and Fitzgerald, K. A. (2017). Immunobiology of long noncoding RNAs. *Annu. Rev. Immunol.* 35, 177–198. doi:10.1146/annurev-immunol-041015-055459

Bray, F., Ferlay, J., Soerjomataram, I., Siegel, R. L., Torre, L. A., and Jemal, A. (2018). Global cancer statistics 2018: GLOBOCAN estimates of incidence and mortality worldwide for 36 cancers in 185 countries. *CA Cancer J. Clin.* 68 (6), 394–424. doi:10.3322/caac.21492

Burger, H., Loos, W. J., Eechoute, K., Verweij, J., Mathijssen, R. H. J., and Wiemer, E. A. C. (2011). Drug transporters of platinum-based anticancer agents and their clinical significance. *Drug Resist. Updates* 14 (1), 22–34. doi:10.1016/j.drup.2010.12.002

Cao, S., Liu, W., Li, F., Zhao, W., and Qin, C. (2014). Decreased expression of lncRNA GAS5 predicts a poor prognosis in cervical cancer. *Int. J. Clin. Exp. Pathol.* 7 (10), 6776–6783.

Chen, Q., Li, T., and Yue, W. (2018). Drug response to PD-1/PD-L1 blockade: based on biomarkers. *OncoTargets Therap.* 11, 4673–4683. doi:10.2147/ott.s168313

Chung, H. C., Ros, W., Delord, J.-P., Perets, R., Italiano, A., Shapira-Frommer, R., et al. (2019). Efficacy and safety of pembrolizumab in previously treated advanced cervical cancer: results from the phase II KEYNOTE-158 study. *J. Clin. Oncol.* 37 (17), 1470–1478. doi:10.1200/jco.18.01265

Darwin, P., Toor, S. M., Sasidharan Nair, V., and Elkord, E. (2018). Immune checkpoint inhibitors: recent progress and potential biomarkers. *Exp. Mol. Med.* 50 (12), 1–11. doi:10.1038/s12276-018-0191-1

De Felice, F., Marchetti, C., Palaia, I., Ostuni, R., Muzii, L., Tombolini, V., et al. (2018). Immune check-point in cervical cancer. *Crit. Rev. Oncol. Hematol.* 129, 40–43. doi:10.1016/j.critrevonc.2018.06.006

Denaro, N., Merlano, M. C., and Lo Nigro, C. (2019). Long noncoding RNAs as regulators of cancer immunity. *Mol. Oncol.* 13 (1), 61–73. doi:10.1002/1878-0261.12413

Derrien, T., Johnson, R., Bussotti, G., Tanzer, A., Djebali, S., Tilgner, H., et al. (2012). The GENCODE v7 catalog of human long noncoding RNAs: analysis of their gene structure, evolution, and expression. *Genome Res.* 22 (9), 1775–1789. doi:10.1101/gr.132159.111

Eskander, R. N., and Tewari, K. S. (2014). Chemotherapy in the treatment of metastatic, persistent, and recurrent cervical cancer. *Curr. Opin. Obstet. Gynecol.* 26 (4), 314–321. doi:10.1097/gco.0000000000000042

Eskander, R. N., and Tewari, K. S. (2015). Immunotherapy: an evolving paradigm in the treatment of advanced cervical cancer. *Clin. Therapeut.* 37 (1), 20–38. doi:10.1016/j.clinthera.2014.11.010

Gasser, S., Lim, L. H. K., and Cheung, F. S. G. (2017). The role of the tumour microenvironment in immunotherapy. *Endocr. Relat. Cancer* 24 (12), T283–T295. doi:10.1530/erc-17-0146

Heward, J. A., and Lindsay, M. A. (2014). Long non-coding RNAs in the regulation of the immune response. *Trends Immunol.* 35 (9), 408–419. doi:10.1016/j.it.2014.07.005

Li, Y., Jiang, T., Zhou, W., Li, J., Li, X., Wang, Q., et al. (2020). Pan-cancer characterization of immune-related lncRNAs identifies potential oncogenic biomarkers. *Nat. Commun.* 11 (1), 1000. doi:10.1038/s41467-020-14802-2

Mao, B. D., Xu, P., Zhong, Y., Ding, W. W., and Meng, Y. (2019). LINC00511 knockdown prevents cervical cancer cell proliferation and reduces resistance to paclitaxel. *J. Biosci.* 44 (2), 44. doi:10.1007/s12038-019-9851-0

Menderes, G., Black, J., Schwab, C. L., and Santin, A. D. (2016). Immunotherapy and targeted therapy for cervical cancer: an update. *Expet Rev. Anticancer Ther.* 16 (1), 83–98. doi:10.1586/14737140.2016.1121108

Nagase, S., Ohta, T., Takahashi, F., and Enomoto, T. (2019). Annual report of the committee on gynecologic oncology, the Japan Society of Obstetrics and Gynecology: annual patients report for 2015 and annual treatment report for 2010. *J. Obstet. Gynaecol. Res.* 45 (2), 289–298. doi:10.1111/jog.13863

Naumann, R. W., Hollebecque, A., Meyer, T., Devlin, M.-J., Oaknin, A., Kerger, J., et al. (2019). Safety and efficacy of nivolumab monotherapy in recurrent or metastatic cervical, vaginal, or vulvar carcinoma: results from the phase I/II CheckMate 358 trial. *J. Clin. Oncol.* 37 (31), 2825–2834. doi:10.1200/jco.19.00739

Otoshi, T., Nagano, T., Tachihara, M., and Nishimura, Y. (2019). Possible biomarkers for cancer immunotherapy. *Cancers* 11 (7), 935. doi:10.3390/cancers11070935

Prendergast, G. C., and Jaffee, E. M. (2007). Cancer immunologists and cancer biologists: why we didn't talk then but need to now. *Cancer Res.* 67 (8), 3500–3504. doi:10.1158/0008-5472.can-06-4626

Shan, S., Li, H. F., Yang, X. Y., Guo, Y., Guo, L., Chu, M. J., et al. (2019). Higher lncRNA CASC15 expression predicts poor prognosis and associates with tumor growth in cervical cancer. *Eur. Rev. Med. Pharmacol. Sci.* 23 (2), 507–512. doi:10.26355/eurrev_201901_16862

Tesniere, A., Zitvogel, L., and Kroemer, G. (2006). The immune system: taming and unleashing cancer. *Discov. Med.* 6 (36), 211–216.

Ventriglia, J., Paciolla, I., Pisano, C., Cecere, S. C., Di Napoli, M., Tambaro, R., et al. (2017). Immunotherapy in ovarian, endometrial and cervical cancer: state of the art and future perspectives. *Cancer Treat Rev.* 59, 109–116. doi:10.1016/j.ctrv.2017.07.008

Wang, W., Zhao, Z., Yang, F., Wang, H., Wu, F., Liang, T., et al. (2018). An immune-related lncRNA signature for patients with anaplastic gliomas. *J. Neuro Oncol.* 136 (2), 263–271. doi:10.1007/s11060-017-2667-6

Wei, C., Liang, Q., Li, X., Li, H., Liu, Y., Huang, X., et al. (2019). Bioinformatics profiling utilized a nine immune-related long noncoding RNA signature as a prognostic target for pancreatic cancer. *J. Cell. Biochem.* 120 (9), 14916–14927. doi:10.1002/jcb.28754

WHO (2018). Cervical cancer. Switzerland, Geneva: World Health Organization. Available at: http://www.who.int/cancer/prevention/diagnosis-screening/cervical-cancer/en/ (Accessed April 25, 2018).

Wu, W., Sui, J., Liu, T., Yang, S., Xu, S., Zhang, M., et al. (2019). Integrated analysis of two-lncRNA signature as a potential prognostic biomarker in cervical cancer: a study based on public database. *PeerJ* 7, e6761. doi:10.7717/peerj.6761

Yi, M., Jiao, D., Xu, H., Li, Q., Zhao, W., Han, X., et al. (2018). Biomarkers for predicting efficacy of PD-1/PD-L1 inhibitors. *Mol. Cancer* 17 (1), 129. doi:10.1186/s12943-018-0864-3

Yoshihara, K., Shahmoradgoli, M., Martinez, E., Vegesna, R., Kim, H., Torres-Garcia, W., et al. (2013). Inferring tumour purity and stromal and immune cell admixture from expression data. *Nat. Commun.* 4, 2612. doi:10.1038/ncomms3612

Yu, A. D., Wang, Z., and Morris, K. V. (2015). Long noncoding RNAs: a potent source of regulation in immunity and disease. *Immunol. Cell Biol.* 93 (3), 277–283. doi:10.1038/icb.2015.2

Yu, W.-D., Wang, H., He, Q.-F., Xu, Y., and Wang, X.-C. (2018). Long noncoding RNAs in cancer-immunity cycle. *J. Cell. Physiol.* 233 (9), 6518–6523. doi:10.1002/jcp.26568

Zeng, J., Ma, Y. X., Liu, Z. H., and Zheng, Y. L. (2019). LncRNA SNHG7 contributes to cell proliferation, invasion and prognosis of cervical cancer. *Eur. Rev. Med. Pharmacol. Sci.* 23 (21), 9277–9285. doi:10.26355/eurrev_201911_19420

Zhang, Q., Zhang, Y., and Wang, Y. (2019). GHET1 acts as a prognostic indicator and functions as an oncogenic lncRNA in cervical cancer. *Biosci. Rep.* 39 (4), BSR20182506. doi:10.1042/bsr20182506

**Conflict of Interest:** The authors declare that the research was conducted in the absence of any commercial or financial relationships that could be construed as a potential conflict of interest.

frontiers in Pharmacology

ORIGINAL RESEARCH
published: 09 December 2020
doi: 10.3389/fphar.2020.616251

# Berberine Improves Chemo-Sensitivity to Cisplatin by Enhancing Cell Apoptosis and Repressing PI3K/AKT/mTOR Signaling Pathway in Gastric Cancer

*Yingying Kou*[1], *Bending Tong*[2], *Weiqing Wu*[3]*, *Xiangqing Liao*[3] *and Min Zhao*[2]*

[1]GCP Office, Jiangsu Cancer Hospital, Jiangsu Institute of Cancer Research, The Affiliated Hospital of Nanjing Medical University, Nanjing, China, [2]Department of Pharmacy, Jiangsu Cancer Hospital, Jiangsu Institute of Cancer Research, The Affiliated Hospital of Nanjing Medical University, Nanjing, China, [3]Department of Health Management, First Affiliated Hospital of Southern University of Science and Technology, Second Clinical College of Jinan University, Shenzhen, China

OPEN ACCESS

**Edited by:**
*Zhe-Sheng Chen,*
*St. John's University, United States*

**Reviewed by:**
*Zhangang Xiao,*
*Southwest Medical University, China*
*Li Fu,*
*Shenzhen University, China*
*Jianwei Zhou,*
*Nanjing Medical University, China*

***Correspondence:**
*Min Zhao*
*jsch2020@163.com*
*Weiqing Wu*
*wweiqing007@sina.com*

**Specialty section:**
*This article was submitted to Pharmacology of Anti-Cancer Drugs, a section of the journal Frontiers in Pharmacology*

**Received:** *11 October 2020*
**Accepted:** *11 November 2020*
**Published:** *09 December 2020*

**Citation:**
*Kou Y, Tong B, Wu W, Liao X and Zhao M (2020) Berberine Improves Chemo-Sensitivity to Cisplatin by Enhancing Cell Apoptosis and Repressing PI3K/AKT/mTOR Signaling Pathway in Gastric Cancer. Front. Pharmacol. 11:616251. doi: 10.3389/fphar.2020.616251*

Gastric cancer is one of the most common malignancies ranks as the second leading cause of cancer-related mortality in the world. Cisplatin (DDP) is commonly used for gastric cancer treatment, whereas recurrence and metastasis are common because of intrinsic and acquired DDP-resistance. The aim of this study is to examine the effects of berberine on the DDP-resistance in gastric cancer and explore the underling mechanisms. In this study, we established the DDP-resistant gastric cancer cells, where the $IC_{50}$ values of DDP in the BGC-823/DDP and SGC-7901/DDP were significantly higher than that in the corresponding parental cells. Berberine could concentration-dependently inhibited the cell viability of BGC-823 and SGC-7901 cells; while the inhibitory effects of berberine on the cell viability were largely attenuated in the DDP-resistant cells. Berberine pre-treatment significantly sensitized BGC-823/DDP and SGC-7901/DDP cells to DDP. Furthermore, berberine treatment concentration-dependently down-regulated the multidrug resistance-associated protein 1 and multi-drug resistance-1 protein levels in the BGC-823/DDP and SGC7901/DDP cells. Interestingly, the cell apoptosis of BGC-823/DDP and SGC-7901/DDP cells was significantly enhanced by co-treatment with berberine and DDP. The results from animals also showed that berberine treatment sensitized SGC-7901/DDP cells to DDP *in vivo*. Mechanistically, berberine significantly suppressed the PI3K/AKT/mTOR in the BGC-823/DDP and SGC-7901/DDP cells treated with DDP. In conclusion, we observed that berberine sensitizes gastric cancer cells to DDP. Further mechanistic findings suggested that berberine-mediated DDP-sensitivity may be associated with reduced expression of drug transporters (multi-drug resistance-1 and multidrug resistance-associated protein 1), enhanced apoptosis and repressed PI3K/AKT/mTOR signaling.

**Keywords: gastric cancer, cisplatin, berberine, apoptosis, PI3K/AKT/mTOR 2**

## INTRODUCTION

Gastric cancer is one of the most common malignancies ranks as the second leading cause of cancer-related mortality in the world (Thrift and El-Serag, 2020). Around 30% of the total cases were diagnosed in China (Leung et al., 2008; Piñeros et al., 2017). Recently, great advancements have been made in early diagnosis and therapeutic treatments including surgical resection and chemo-/radio-therapy, whereas the clinical outcomes of the patients with this malignancy remains poor (Van Cutsem et al., 2016). Cisplatin (DDP) as a chemotherapeutic reagent has been widely used in the treatment for gastric cancer, and DDP-based therapy could significantly improve the survival of patients with gastric cancer (Wagner et al., 2017). Unfortunately, metastasis and recurrence of the gastric cancer are commonly existing in the patients due to the acquired and intrinsic DDP resistance (Haller and Misset, 2002; Baek et al., 2012; Choi et al., 2017). As DDP is still the standard chemotherapy for gastric cancer, developing effective way to reduce the DDP-resistance in gastric cancer is of great clinical significance.

The compounds from the herbal medicine have been attracting attentions due to their anti-cancer activities (Wang et al., 2018). Berberine is an iso-quinoline alkaloid and can be extracted from Beberis species (Imenshahidi and Hosseinzadeh, 2016; Wang et al., 2017). Studies have demonstrated that berberine possessed various pharmacological actions including anti-hypertensive, anti-arrhythmic, anti-bacterial and anti-cancer effects (Imenshahidi and Hosseinzadeh, 2016; Wang et al., 2017). Furthermore, studies found that berberine attenuated the radio-resistance of colon cancer cells via repressing P-gp expression (Guan et al., 2020). Gao et al., found that berberine could sensitize breast cancer cells to different chemotherapeutic drugs (Gao et al., 2019). Liu et al., showed that berberine could attenuate the DDP-resistance of ovarian cancer cells by targeting miR-21/programmed cell death 4 axis (Liu et al., 2013). Pre-treatment with berberine was effective to promote the anti-tumor effects of DDP in laryngeal cancer cells (Palmieri et al., 2018). Studies from Pandey et al., showed the potential actions of berberine to attenuate 5-fluoruracil-resistance in gastric cancer cells (Pandey et al., 2015); however, the exact actions of berberine in the DDP-resistance are not fully explored.

In the present study, we firstly established the DDP-resistant cellular model using two gastric cancer cell lines (BGC-823 and SGC-7901) under elevated concentrations of DDP. After that, we explored if berberine could attenuate the drug-resistance in these cell lines and deciphered the potential molecular mechanisms. This study may provide a novel strategy for managing the DDP-resistance in gastric cancer.

## MATERIALS AND METHODS

### Cell Lines and Generation of DDP-Resistant Cells

The BGC-823 and SGC-7901 cells were purchased from the Shanghai Institutes for Biological Sciences, Chinese Academy of Sciences (Shanghai, China) and the cells were cultured according to the instructions. For the generation of DDP-resistant BGC-823 (BGC-823/DDP) and DDP-resistant SGC-7901 (SGC-7901/DDP) cells, the parental cells (BGC-823 and SGC-7901) were initially treated with 0.5 μM DDP; and then the concentrations of DDP were gradually increased to 1, 3 and 10 μM (the highest concentration) every days. BGC-823 and SGC-7901 cells became resistant to DDP (10 μM) were chosen for further experimentation.

### Drug Treatments

The chemicals including DDP (catalogue #1134357) and berberine (catalogue #200275; purity ≥95%) were purchased from Sigma-Aldrich (St. Louis, United States). For the DDP treatments, the BGC-823, SGC-7901, BGC-823/DDP and SGC-7901/DDP cells were treated with increased concentrations of DDP (1, 3, 10, 30, 100 and 300 μM) for 24 h; for the berberine treatments, these cells were treated with increased concentrations of berberine (1, 3, 10, 30, 100, 300 and 1,000 μM) for 24 h; for the co-treatments, these cells were co-treated with DDP and berberine at different concentrations for 24 h. After the drug treatments, these cells were harvested for further *in vitro* analysis.

### 3-(4,5-Dimethylthiazol-2-yl)-2,5-Diphenyltetrazolium Bromide (MTT) Assay

The effects of DDP and berberine on the cell viability were determined by (3-(4,5-dimethylthiazol-2-yl)-2,5-diphenyltetrazolium bromide) MTT assay. Different cell lines with respective treatments were seeded in triplicate in a 96-well plate, and after incubating at 37°C for 24 h, the cells were incubated with 5 mg/ml MTT reagent in phosphate buffered saline at 37 °C for 2 h. After that, the 50% dimethyl formamide was added to solubilize the formazan crystals. Finally, the optical density (OD) values at 570 nm wavelength was determined using the microplate reader. Cell viability (%) was calculated as follows: (OD in the experimental group/OD in the control group) * 100. The $IC_{50}$ values were analyzed using the non-linear regression fit.

### Caspase-3 and Capsase-9 Activities Determination

Caspase-3 and caspase-9 activities of BGC-823/DDP and SGC-7901/DDP cells with respective treatments were assessed using the commercial caspase-3 and -9 activity kits, respectively (Beyotime, Beijing, China) according to the supplier's protocols.

### Flow Cytometry for Cell Apoptosis

Cell apoptosis of BGC-823/DDP and SGC-7901/DDP cells were assessed using the propidium iodide (PI) and fluorescein isothiocyanate (FITC)-Annexin V Apoptosis Detection kit (Thermo Fisher Scientific). BGC-823/DDP and SGC-7901/DDP cells with respective treatments were harvested and stained with PI and FITC-Annexin V according to the supplier's protocols. The percentage of Annexin V-positive population cells was assessed using a Calibur Flow cytometer

(BD Biosciences, Franklin Lake, United States), and the cell apoptotic rates were determined using Flow Jo software (Version 7.6.1, TreesStar, Ashland, United States).

## Western Blot Analysis

BGC-823/DDP and SGC-7901/DDP cells with respective treatments were lysed with Radioimmunoprecipitation assay buffer supplied with the protease inhibitors cocktail (Sigma, St. Louis, United States) on ice for at least 15 min. The protein samples were collected by obtaining the supernatants after centrifugation (12,000 *g*) for 20 min at 4°C. The concentration of the protein samples was determined using the bicinchoninic acid protein assay kit (Beyotime) according to the supplier's protocol. A total of 45 μg proteins were separated on the sodium dodecyl sulphate-polyacrylamide gel electrophoresis followed by transferring to the polyvinylidene difluoride membranes (Millipore) by using the electrophoretic method. After blocking with non-fat milk (5%) in Tris-buffered saline with 0.1% Tween-20 (TBST), the membrane was washed with TBST followed by incubating with corresponding primary antibodies at 4°C for 16 h. After that, the membrane was washed with TBST for 3 × 5 min followed by incubating with the membrane was then washed with TBST three times, followed by incubation with a horseradish peroxidase-conjugated secondary antibody (Cell Signaling Technology) at room temperature for 2 h. The blot bands on the membrane was detected using the enhanced chemiluminescence kit (Thermo Fisher Scientific) according to the supplier's protocol. The protein expression levels were evaluated using densitometric method using the Image J software. The concentrations and the sources of the primary antibodies were shown below: β-actin (1:2,000; Cell Signaling Technology, Danvers, United States), cleaved caspase-3 (1:1,000; Cell Signaling Technology), cleaved caspase-9 (1:1,000, Cell Signaling Technology), Bax (1:1,000; Cell Signaling Technology), multidrug resistance-associated protein 1 (MRP1; 1:1,000; Cell Signaling Technology), multi-drug resistance-1 (MDR1; 1:1,500; Cell Signaling Technology), phosphorylated (phospho)-PI3K (1:1,000; Cell Signaling Technology), PI3K (1:1,000; Cell Signaling Technology), phospho-AKT (1:1,000; Cell Signaling Technology), AKT (1:1,000; Cell Signaling Technology), phospho-mTOR (1:1,000; Cell Signaling Technology) and mTOR (1:1,000; Cell Signaling Technology). The protein levels were normalized to β-actin.

## *In vivo* Tumor Growth of SGC-7901/DDP Cells

The BALB/c-nu mice (5 weeks old; body weight: 15–19 g) were purchased from Guangdong Laboratory Experimental Animal Center (Guangzhou, China). The animals were housed in individual ventilated cage at 25.4 ± 2.2°C with 50.6 ± 8.8% humidity under controlled lighting (12 h light/day). All the animal experimental procedures were under the approval of Animal Ethic Committee of Nanjing Medical University. For the tumor inoculation and drug treatments, SGC-7901/DDP cells ($1\times10^7$ cells) were subcutaneously injected into the left flank of the nude mice. For the drug treatments, the mice from the vehicle group received phosphate buffered saline (2 ml/kg/day, i.p.); the mice from the DDP group received intraperitoneal DDP injection at 3 mg/kg/day; the mice from berberine group were treated with berberine (10 mg/kg/day); the mice from DDP + berberine group were injected with both DDP (3 mg/kg/day, i.p.) and berberine (10 mg/kg/day, i.p.). The tumor volume was measured every 5 days for 30 days. The formula for calculating tumor volume was as follow: volume = length × width × width/2. All treatments for 30 days, the animals were sacrificed by pentobarbitone (80 mg/kg, i.p.). The tumors were dissected and the weight of the tumors were weighed using a balance. The tumor tissues were then fixed for Ki-67 immunostaining and TUNEL assay.

## Ki-67 Immunostaining and TUNEL Assay

The proliferative potential of the tumor cells assessed by Ki-67 immunostaining. The Ki-67 immunostaining for the tumor tissues was performed according to previously published method (He et al., 2019). Briefly, the 4% paraformaldehyde-fixed tumor tissues were embedded in paraffin and sectioned into 4 μm thickness slices, and the slices were stained with Ki-67 (Cell Signaling Technology). The Ki-67-positive cells were analyzed using a confocal microscope by randomly choosing five fields. For the TUNEL assay, the sectioned tumor tissues (4 μm in thickness) were stained with TUENL *In Situ* Apoptosis Detection kit (Roche Diagnostic, Mannheim, Germany) according to previous studies (Ma et al., 2020). The TUNEL-positive cells were analyzed using a confocal microscope by randomly choosing five fields.

## Statistical Analysis

The statistical analyses were performed using GraphPad Prism Software (version 6.0; GraphPad Software, La Jolla, United States). Depending on the experiment type, two-tailed Student's t-test or one-way ANOVA followed by Bonferroni's multiple comparison tests was used for the analysis. The statistical significance was evaluated based on $p$ values, and $p < 0.05$ was considered to indicate statistical significance.

# RESULTS

## Effects of cisplatin and berberine on the cell viability gastric cancer cells and DDP-resistant gastric cancer cells

Firstly, we performed the MTT assay to examine the effects of DDP on the cell viability of the gastric cancer cells and DDP-resistant cells. In the BGC-823 and BGC-823/DDP cells, DDP dose-dependently inhibited the cell viability, and the $IC_{50}$ of DDP in BGC-823/DDP cells was significantly higher than that in BGC-823 cells (BGC-823: 21.37 ± 5.13 μM vs. BGC-823/DDP: 206.8 ± 55.98 μM; **Figure 1A**). Similarly, DDP reduced the cell viability of SGC-7901 and SGC-7901/DDP cells in a concentration-dependent manner with the $IC_{50}$ of DDP in the SGC-7901/DDP cells being remarkably higher than that in SGC-7901 cells (SGC-7901: 23.66 ± 2.14 μM vs. SGC-7901/DDP: 182.9 ± 32.71 μM; **Figures 1B**). These results suggest that BGC-823/DDP and SGC-7901/DDP exhibited resistance to the DDP

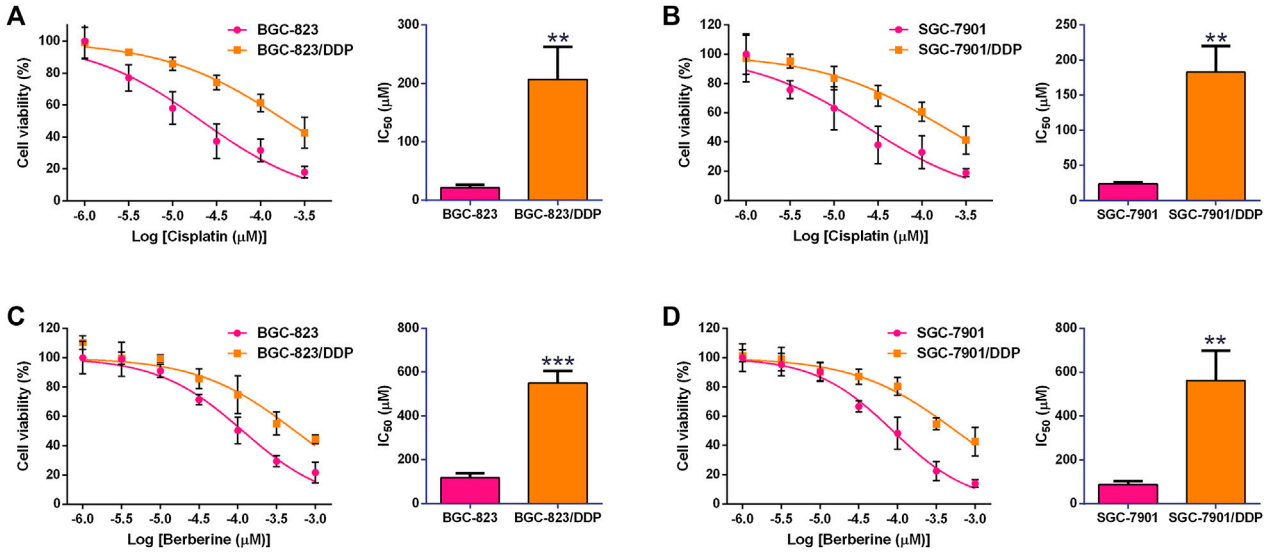


**FIGURE 1 |** Effects of cisplatin and berberine on the cell viability gastric cancer cells and DDP-resistant gastric cancer cells. MTT assay determined the cell viability of BGC-823 and BGC-823/DDP cells **(A)**, and SGC-7901 and SGC-7901/DDP cells **(B)** after being treated with different concentrations of cisplatin. MTT assay determined the cell viability of BGC-823 and BGC-823/DDP cells **(C)**, and SGC-7901 and SGC-7901/DDP cells **(D)** after being treated with different concentrations of cisplatin. $^{**}p < 0.05$ and $^{***}p < 0.001$ compared to the parental cell group ($n = 3$).

treatment. Furthermore, we explored the effects of berberine on the cell viability of BGC-823 and BGC-823/DDP cells, and berberine at 30 μM started to exhibit inhibitory effects on the cell viability of BGC-823 and BGC-823/DDP cells, and berberine concentration-dependently supressed the cell viability of these cells. The $IC_{50}$ of berberine in BGC-823/DDP cells was significantly higher than that in BGC-823 cells (BGC-823: 117.9 ± 20.49 μM vs. BGC-823/DDP: 549.6 ± 56.88 μM; **Figures 1C**). Consistent findings were observed in the SGC-7901 and SGC-7901/DDP cell lines (SGC-7901: 87.90 ± 15.23 μM vs. SGC-7901/DDP: 562.1 ± 135.9 μM; **Figures 1B**).

## Berberine Sensitizes DDP-Resistance Gastric Cancer Cells to Cisplatin Treatment

In order to examine if berberine could sensitize DDP-resistant gastric cancer cells to DDP, we co-treated BGC-823/DDP and SGC-7901/DDP cells with different concentrations of DDP and berberine. As shown in **Figure 2A**, 3 μM berberine treatment failed to significantly affect the $IC_{50}$ values of DDP in BGC-823/DDP cells; whereas berberine at 10 and 30 μM significantly reduced the $IC_{50}$ values of DDP in BGC-823/DDP cells when compared to BGC-823/DDP cells treated with DDP alone. Consistently, berberine at 10 and 30 μM significantly, but not 3 μM remarkably reduced the $IC_{50}$ values of DDP in SGC-7901/DDP cells when compared the cells treated with DDP alone (**Figure 2B**). To gain into the mechanistic actions of berberine on the DDP-resistance, the protein levels of MDR1 and MRP1 were determined in both BGC-823/DDP and SGC-7901/DDP cells using Western blot analysis. DDP at 30 μM and berberine at 30 μM both caused a significant reduction of MDR1 and MRP1 protein levels in BGC-823/DDP cells when compared to Blank control group (**Figure 2C**). Importantly, berberine concentration-dependently down-regulated MDR1 and MRP1 protein expression when compared to non-treated BGC-823/DDP cells (**Figure 2C**). Consistent results were also shown in the SGC-7901/DDP cells (**Figure 2D**). These data indicated that berberine could sensitize BGC-823/DDP and SGC-7901/DDP cells to DDP possibly via down-regulating MDR1 and MRP1 protein expression.

## Berberine Promoted Cell Apoptosis of DDP-Resistant Gastric Cells With DDP Treatment

The cell apoptosis of BGC-823/DDP and SGC-7901/DDP cells was evaluated by several experimental assays including flow cytometry, caspase-3 and -9 activities and western blot. DDP at 30 μM and berberine at 30 μM both slightly increased the cell apoptotic rates of BGC-823/DDP and SGC-7901/DDP cells when compared to Blank group (**Figures 3A**,**B**). Moreover, DDP and berberine co-treatment dramatically increased the BGC-823/DDP and SGC-7901/DDP cell apoptotic rates when compared to the other three groups (**Figures 3A**,**B**). Further examination of the capase-3 and -9 activities, we found that DDP and berberine co-treatment increased the caspase-3 and -9 activities by around two fold in BGC-823/DDP and SGC-7901/DDP cells; whereas DDP alone and berberine alone only caused a slightly increase in the capsase-3 and -9 activities of BGC-823/DDP and SGC-7901/DDP cells (**Figures 3C**–**F**). Moreover, the western blot analysis showed that the cleaved caspase-3,-9 and Bax protein levels were slightly increased after DDP or berberine treatment in both BGC-823/DDP and SGC-7901/DDP cells when compared to blank group (**Figures 3G**,H). Moreover, DDP and berberine co-

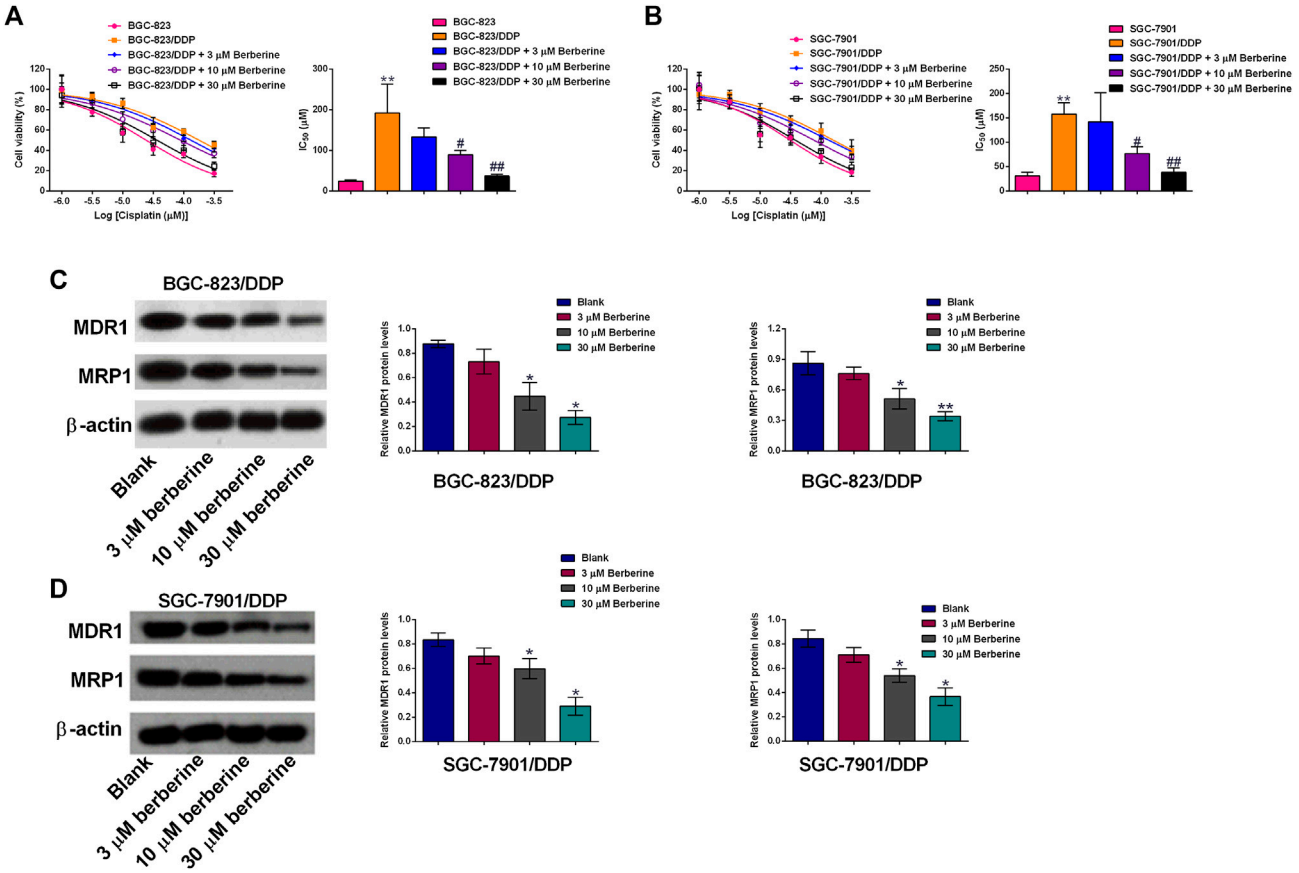


**FIGURE 2 |** Berberine sensitizes DDP-resistance gastric cancer cells to cisplatin treatment. **(A)** MTT assay determined the cell viability of BGC-823 cells after cisplatin treatment or BGC-823/DDP cells after cisplatin or cisplatin + berberine treatments. **(B)** MTT assay determined the cell viability of SGC-7901 cells after cisplatin treatment or SGC-7901/DDP cells after cisplatin or cisplatin + berberine treatments. $N = 3$; $^{**}p < 0.01$ compared to parental cell group; $^{\#}p < 0.05$ and $^{\#\#}p < 0.01$ compared to SGC-7901/DDP cells treated with DDP alone. **(C,D)** Western blot analysis of MDR1 and MRP1 protein levels in BGC-823/DDP and SGC-7901 cells after different concentrations of berberine treatments. $^{*}p < 0.05$ and $^{**}p < 0.01$ compared to Blank group ($n = 3$).

treatment dramatically enhanced the protein expression of cleaved caspase-3,-9 and Bax in both BGC-823/DDP and SGC-7901/DDP cells when compared to the other three groups (**Figures 3G**,H).

## Berberine Sensitizes DDP-Resistance Gastric Cancer Cells to Cisplatin Treatment *In Vivo*

The *in vivo* growth of SGC-7901/DDP cells were evaluated in a xenograft mice mode, DDP (3 mg/mg/day) or berberine (10 mg/kg/day) treatment caused a trivial suppression in the tumor growth of SGC-7901/DDP cells when compared to blank group (**Figure 4A**). Moreover, co-treatment with DDP and berberine suppressed the *in vivo* tumor growth of SGC-7901/DDP cells by around 50% when compared to blank group (**Figure 4A**). The examination of tumor weight showed the consistent results (**Figure 4B**). Further the proliferative potential and apoptosis of tumor tissues were assessed by Ki-67 immunostaining and TUENL assay. As shown in **Figures 4C**,D, DDP or berberine alone slightly suppressed the number of Ki-67-positive cells and increased the number of TUNEL-positive cells, when compared to blank group. Moreover, a dramatic reduction in the number of Ki-67-positive cells and an increase in the number of TUNEL-positive cells were observed in the tumor tissues from DDP and berberine co-treatment group (**Figures 4C**,D).

## Berberine inhibited PI3K/AKT/mTOR signaling in the DDP-resistant gastric cancer cells with cisplatin treatment

The effects of berberine on the PI3K/AKT/mTOR signaling were further examined by western blot assay. The phospho-PI3K,-AKT and -mTOR protein levels were slightly reduced after DDP or berberine treatment in both BGC-823/DDP and SGC-7901/DDP cells when compared to blank group (**Figures 3G**,H). Moreover, DDP and berberine co-treatment dramatically enhanced the protein expression of phospho-PI3K, -AKT and -mTOR in both BGC-823/DDP and SGC-7901/DDP cells when compared to the other three groups (**Figures 5A**,**B**).

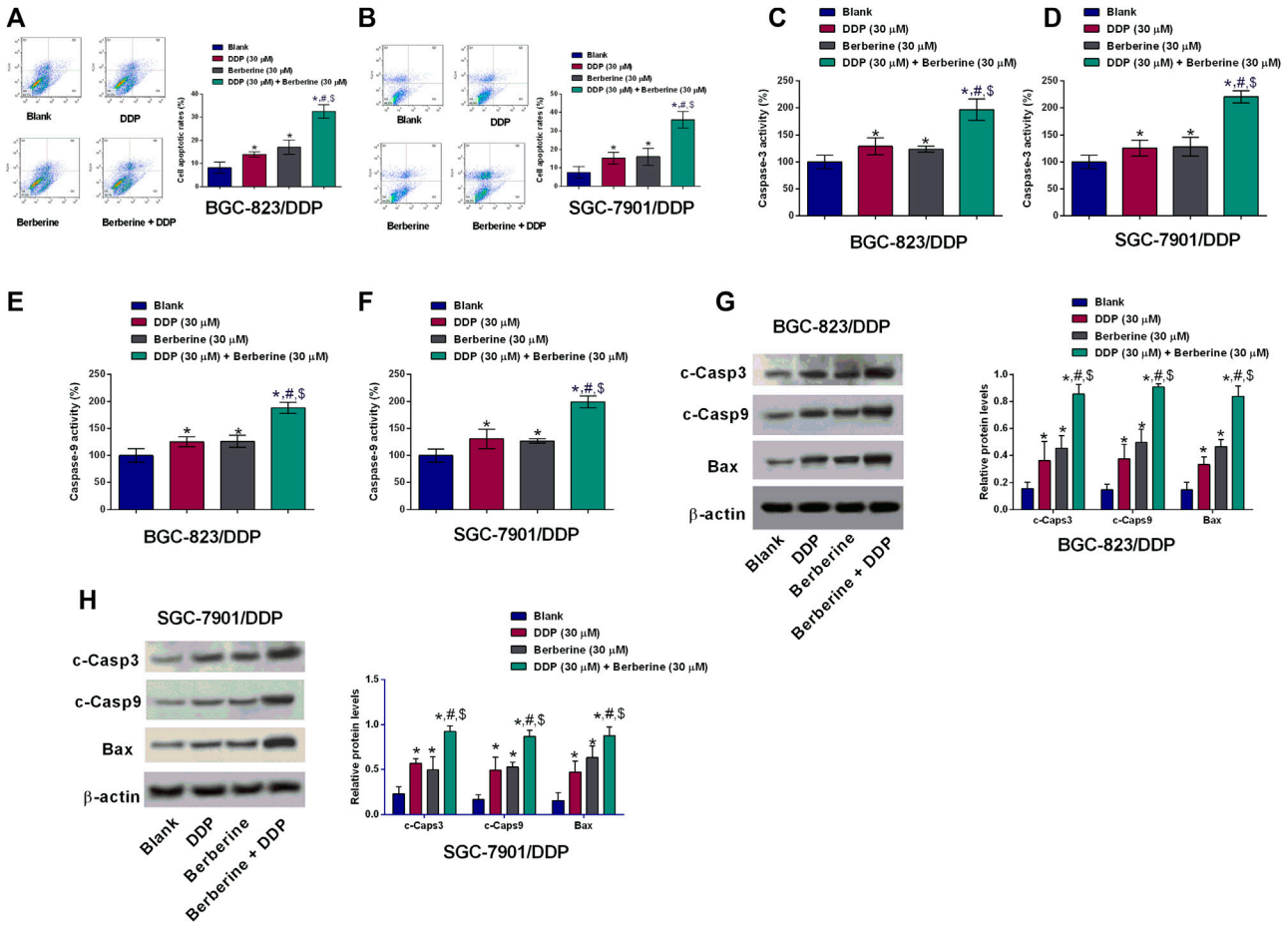


**FIGURE 3 |** Berberine promoted cell apoptosis of DDP-resistant gastric cells with DDP treatment. **(A,B)** Flow cytometry of apoptotic BGC-823/DDP and SGC-7901/DDP cells after treatment with DDP (30 μM), Berberine (30 μM) or DDP (30 μM) + Berberine (30 μM). **(C,D)** Caspase-3 activity kit determined caspase-3 activity of BGC-823/DDP and SGC-7901/DDP cells after treatment with DDP (30 μM), Berberine (30 μM) or DDP (30 μM) + Berberine (30 μM). **(E,F)** Caspase-9 activity kit determined caspase-9 activity of BGC-823/DDP and SGC-7901/DDP cells after treatment with DDP (30 μM), Berberine (30 μM) or DDP (30 μM) + Berberine (30 μM). **(G,H)** Western blot determined cleaved caspase-3 (c-Caps3), cleaved caspase-9 (c-Caps9) and Bax protein levels in BGC-823/DDP and SGC-7901/DDP cells after treatment with DDP (30 μM), Berberine (30 μM) or DDP (30 μM) + Berberine (30 μM). $^{*}p < 0.05$ compared to Blank group; $^{\#}p < 0.05$ compared to DDP (30 μM) group; $^{\$}p < 0.05$ compared to berberine (30 μM) group ($n = 3$).

## DISCUSSION

DDP has been widely used as the chemotherapeutic drugs for treating different types of human malignancies; however, the intrinsic and acquired DDP-resistance during the course of the chemotherapy largely hindered the clinical use of DDP in these patients (Venerito et al., 2018). On the other hand, the severe side effects of DDP are also an obstacle during the clinical application. Thus, identifying novel targets/strategies to promote the sensitivity of gastric cancer cells to DDP is of great importance. In this study, we established the DDP-resistant gastric cancer cells, where the $IC_{50}$ values of DDP in the BGC-823/DDP and SGC-7901/DDP were significantly higher than that in the corresponding parental cells. Berberine could concentration-dependently inhibited the cell viability of BGC-8203 and SGC-7901 cells; while the inhibitory effects of berberine on the cell viability were largely attenuated in the DDP-resistant cells. Berberine pre-treatment significantly sensitized BGC-823/DDP and SGC-7901/DDP cells to DDP. Furthermore, berberine treatment concentration-dependently down-regulated the MRP1 and MDR1 protein levels in the BGC-823/DDP and SGC7901/DDP cells. Interestingly, the cell apoptosis of BGC-823/DDP and SGC-7901/DDP cells was significantly enhanced by co-treatment with berberine and DDP. The results from animals also showed that berberine treatment sensitized SGC-7901/DDP cells to DDP *in vivo*. Mechanistically, berberine significantly suppressed the PI3K/AKT/mTOR in the BGC-823/DDP and SGC-7901/DDP cells treated with DDP. Taken together, our results indicated that berberine sensitized DDP-resistant gastric cancer cells to DDP via enhanced cell apoptosis and inhibited PI3K/AKT/mTOR signaling.

The anti-tumor effects of berberine in gastric cancer have been illustrated in various studies. Berberine was effective to induce cell cycle arrest and apoptosis in human gastric carcinoma SNU-5 cells (Lin et al., 2006), and berberine-induced gastric cancer cell

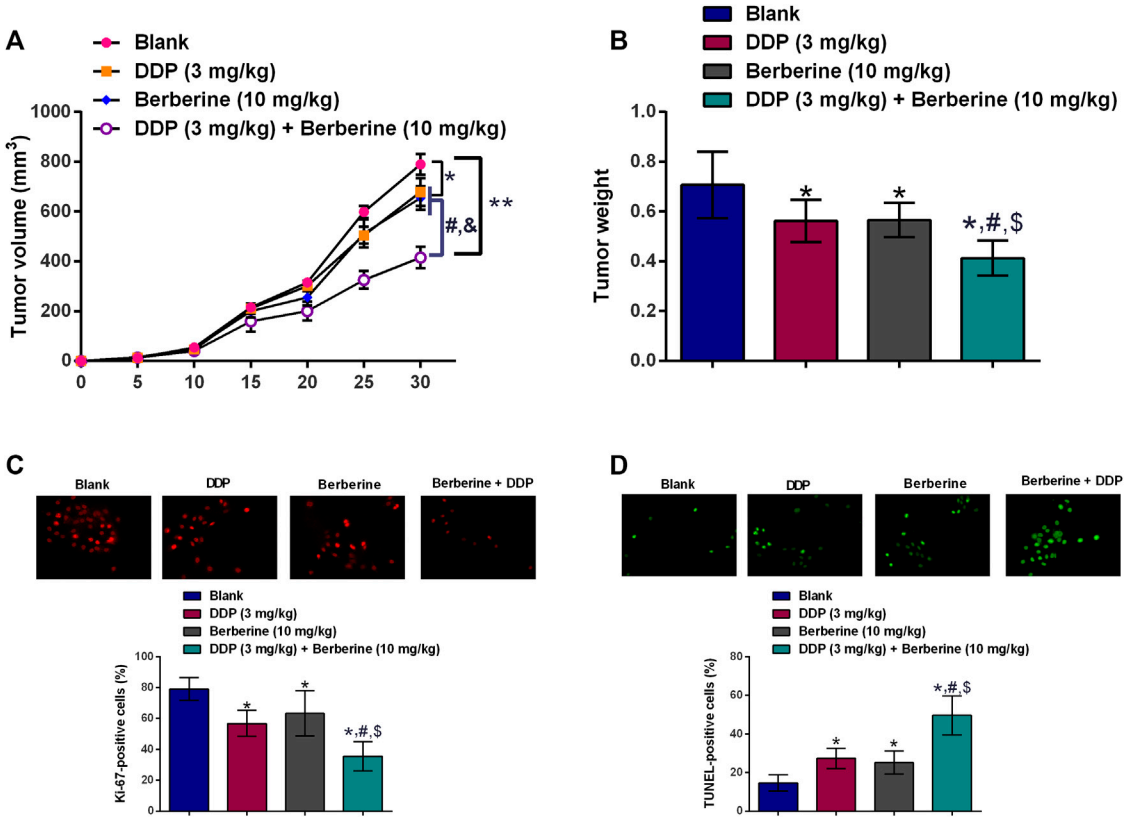


**FIGURE 4 |** Berberine sensitizes DDP-resistance gastric cancer cells to cisplatin treatment *in vivo*. **(A)** *In vivo* tumor growth of SGC-7901/DDP cells in the nude mice after treatment with DDP (3 mg/kg, i.p.), berberine (10 mg/kg, i.p.) or DDP (3 mg/kg, i.p.) + Berberine (10 mg/kg, i.p.). **(B)** Tumor weight dissected from the nude mice after treatment with DDP (3 mg/kg, i.p.), berberine (10 mg/kg, i.p.) or DDP (3 mg/kg, i.p.) + Berberine (10 mg/kg, i.p.). **(C)** Immunostaining of Ki-67 in the tumor tissues from the mice after treatment with DDP (3 mg/kg, i.p.), berberine (10 mg/kg, i.p.) or DDP (3 mg/kg, i.p.) + Berberine (10 mg/kg, i.p.). **(D)** TUNEL assay determined cell apoptosis in the tumor tissues from the mice after treatment with DDP (3 mg/kg, i.p.), berberine (10 mg/kg, i.p.) or DDP (3 mg/kg, i.p.) + Berberine (10 mg/kg, i.p.). $^{*}p < 0.05$ compared to Blank group; $^{\#}p < 0.05$ compared to DDP (3 mg/kg) group; $^{\$}p < 0.05$ compared to berberine (10 mg/kg) group ($n = 6$).

apoptosis is associated with Akt signaling (Yi et al., 2015). Moreover, berberine inhibited SNU-5 cell migration via down-regulating metalloproteinase-1, -2 and -9 expression (Lin et al., 2008). Wang et al., showed that berberine enhanced the anti-tumor effects of EGFR inhibitors in gastric cancer via supressing EGFR signaling (Wang et al., 2016). A recent study by Hu et al., showed that berberine attenuated gastric carcinoma proliferation, invasion, and migration by targeting the AMPK/HNF4α/WNT5A signaling (Hu et al., 2018). In agreement with previous findings, we also demonstrated the berberine exerted tumor-suppressive effects on the gastric carcinoma cell lines in a concentration-dependent manner. In the gastric cancer cells with drug-resistance, berberine could target surviving and STATs to sensitize gastric cancer cells to 5-Fluorouracil (Pandey et al., 2015). Consistently, our data showed that berberine sensitizes BGC-823/DDP and SGC-7901/DDP cells to DDP in a concentration-dependent manner. MDR1 is encoded by the ABCB1 gene with a molecular weight of 170 kDa, and studies found that MDR1 is highly expressed in tissues of the gastric carcinoma, and up-regulation of MDR1 was closed correlated with chemo-resistance of the gastric cancer cells (Lage, 2003). MDR1 exerted its effects via transporting toxic substances and intracellular drugs to extracellular space. MRP1 is encoded by the ABCC1 gene and belong to the superfamily of ATP-binding cassette transporters. MRP1 was also found to be up-regulated in the DDP-resistant gastric cancer cells, and MRP1 enhanced chemo-resistance via transporting chemotherapeutic drugs to extracellular space (Lage, 2003). To uncover the relationship of MDR1 and MRP1 with berberine-mediated DDP-sensitivity, we further examined the effects of berberine on the MDR1 and MRP1 protein expression. The expression of MDR1 and MRP1 proteins was significantly down-regulated by berberine in the BGC-823/DDP and SGC-7901/DDP cells. These results implied that MDR1/MRP1 pathway could participate in the berberine-mediated DDP-sensitivity in gastric cancer.

The effects of berberine on the cell apoptosis have been well-documented in various types of cancers. Berberine in combination with DDP induces apoptosis in ovarian cancer cells (Liu et al., 2019). Berberine enhances chemosensitivity by inducing apoptosis via dose-orchestrated AMPK signaling in breast cancer (Pan et al., 2017). More importantly, berberine promoted gastric cancer cell apoptosis via regulating Akt signaling (Yi et al., 2015). Further studies showed hat berberine-induced apoptosis was associated with caspase

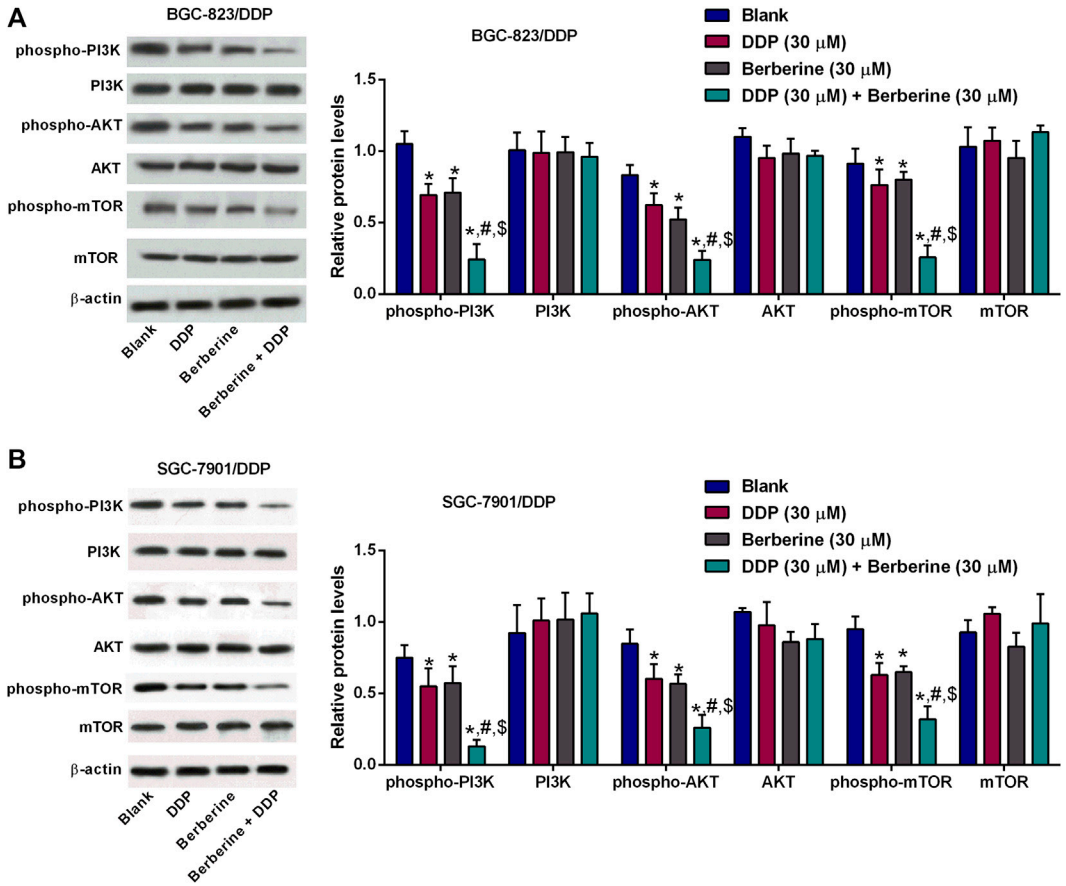


**FIGURE 5 |** Berberine inhibited PI3K/AKT/mTOR signaling in the DDP-resistant gastric cancer cells with cisplatin treatment. **(A,B)** Western blot determined phosphor-PI3K, PI3K, phospho-AKT, AKT, phosphor-mTOR or mTOR protein levels in BGC-823/DDP and SGC-7901/DDP cells after treatment with DDP (30 μM), Berberine (30 μM) or DDP (30 μM) + Berberine (30 μM). $^{*}p < 0.05$ compared to Blank group; $^{\#}p < 0.05$ compared to DDP (30 μM) group; $^{\$}p < 0.05$ compared to berberine (30 μM) group ($n = 3$).

activation (Wang et al., 2020). In the study, we consistently showed that berberine plus DDP significantly induced apoptosis in BGC-823/DDP and SGC-7901/DDP cells. In addition, the caspase-3 and -9 activities and protein levels were significantly increased in these cells upon berberine plus DDP treatment. These results implied that berberine-mediated DDP-sensitivity in gastric cancer cells may be associated with enhanced apoptosis by caspase-3 and -9 activation.

PI3K/Akt/mTOR signaling axis has been regarded as an important pathway in regulating drug-resistance in different cancer types including gastric cancer. Studies have demonstrated that phosphorylation of Akt and mTOR was increased in DDP-resistant gastric cancer cells and inhibition of PI3K/Akt pathway significantly attenuated CCL2-mediated DDP-resistance in gastric cancer (Xu et al., 2018). Dual inhibitor of PI3K and mTOR (NVP-BEZ235) promoted the drug resistance of gastric cancer cells to 5-fluorouracil (Li et al., 2018). TSPAN9 enhance the resistance of gastric cancer to 5-fluorouracil by activating PI3K/AKT/mTOR-mediated autophagy (Qi et al., 2020). On other hand, berberine could ameliorate diabetes-associated cognitive decline and hepatic ischemia/reperfusion injury via down-regulating PI3K/Akt/mTOR signaling pathway (Sheng et al., 2015; Chen et al., 2017). Berberine in combination with solid lipd curcumin particles could also increase cell death by inhibiting PI3K/Atk/mTOR pathway in glioblastoma cells (Maiti et al., 2019). In our results, the phosphorylation of PI3K, AKT and mTOR was remarkably repressed by the treatment with berberine plus DDP in BGC-823/DDP and SGC-7901/DDP cells. This indicated that berberine-mediated DDP-sensitivity of gastric cancer cells might be associated with inhibition of PI3K/AKT/mTOR signaling.

Our current findings are still at the preliminary stages, and further molecular mechanisms of berberine-mediated effects on the chemo-sensitivity should be investigated. Our results showed that berberine improved the DDP-sensitivity of gastric cancer cells, and berberine enhanced the chemo-sensitivity possibly via attenuating the expression of chemo-resistance associated mediators, which still require further examination. Recent studies also demonstrated that berberine exerted anti-tumor effects via regulating the expression of non-coding RNAs (Wei et al., 2016; Chang, 2017; Wang and Zhang, 2018), and further studies may use the non-coding RNA microarrays to determine the berberine-mediated downstream non-coding RNAs associated with chemosensitivity of the gastric cancer. The present study has not systematically examined the toxic effects of berberine, which may be considered in the future studies. Besides, berberine has also been reported to regulate the angiogenesis in the tumor tissues

(Jin et al., 2018; Luo et al., 2019; Lopes et al., 2020), whether berberine-mediated angiogenesis-associated mechanisms contributes to the chemo-sensitivity of the gastric cancer cells should be further explored.

In conclusion, we observed that berberine sensitizes gastric cancer cells to DDP. Further mechanistic findings suggested that berberine-mediated DDP-sensitivity may be associated with reduced expression of drug transporters (MDR1 and MRP1), enhanced apoptosis and repressed PI3K/AKT/mTOR signaling.

## DATA AVAILABILITY STATEMENT

The original contributions presented in the study are included in the article/**Supplementary Material**, further inquiries can be directed to the corresponding authors.

## ETHICS STATEMENT

The animal study was reviewed and approved by Animal Ethic Committee of Nanjing Medical University.

## AUTHOR CONTRIBUTIONS

WW and MZ conceived and designed the study; YK and BT performed the experiments; BT and WW contributed to the data analysis and the critical reading of manuscript. WW and MZ wrote the manuscript. All authors read and approved the final manuscript

## FUNDING

This work was supported by the Fund of Administration of Traditional Chinese Medicine of Jiangsu Province of China (YB201987).

## SUPPLEMENTARY MATERIAL

The Supplementary Material for this article can be found online at: https://www.frontiersin.org/articles/10.3389/fphar.2020.616251/full#supplementary-material.

## REFERENCES

Baek, S. K., Kim, S.-Y., Jeong, J.-h., Cho, K. S., and Yoon, H.-J. (2012). Second-line chemotherapy for advanced gastric cancer in Korea. *Gastric Cancer* 15, 345–354. doi:10.1007/s10120-011-0114-5

Chang, W. (2017). Non-coding RNAs and Berberine: a new mechanism of its anti-diabetic activities. *Eur. J. Pharmacol.* 795, 8–12. doi:10.1016/j.ejphar.2016.11.055

Chen, Q., Mo, R., Wu, N., Zou, X., Shi, C., Gong, J., et al. (2017). Berberine ameliorates diabetes-associated cognitive decline through modulation of aberrant inflammation response and insulin signaling pathway in DM rats. *Front. Pharmacol.* 8, 334. doi:10.3389/fphar.2017.00334

Choi, S. J., Jung, S. W., Huh, S., Chung, Y.-S., Cho, H., and Kang, H. (2017). Alteration of DNA methylation in gastric cancer with chemotherapy. *J. Microbiol. Biotechnol.* 27, 1367–1378. doi:10.4014/jmb.1704.04035

Gao, X., Wang, J., Li, M., Wang, J., Lv, J., Zhang, L., et al. (2019). Berberine attenuates XRCC1-mediated base excision repair and sensitizes breast cancer cells to the chemotherapeutic drugs. *J. Cell Mol. Med.* 23, 6797–6804. doi:10.1111/jcmm.14560

Guan, X., Zheng, X., Vong, C. T., Zhao, J., Xiao, J., Wang, Y., et al. (2020). Combined effects of berberine and evodiamine on colorectal cancer cells and cardiomyocytes *in vitro*. *Eur. J. Pharmacol.* 875, 173031. doi:10.1016/j.ejphar.2020.173031

Haller, D. G. and Misset, J.-L. (2002). Docetaxel in advanced gastric cancer. *Anti Canc. Drugs* 13, 451–460. doi:10.1097/00001813-200206000-00003

He, L., Yang, H., Tang, J., Liu, Z., Chen, Y., Lu, B., et al. (2019). Intestinal probiotics E. coli Nissle 1917 as a targeted vehicle for delivery of p53 and Tum-5 to solid tumors for cancer therapy. *J. Biol. Eng.* 13, 58. doi:10.1186/s13036-019-0189-9

Hu, Q., Li, L., Zou, X., Xu, L., and Yi, P. (2018). Berberine attenuated proliferation, invasion and migration by targeting the AMPK/HNF4α/WNT5A pathway in gastric carcinoma. *Front. Pharmacol.* 9, 1150. doi:10.3389/fphar.2018.01150

Imenshahidi, M. and Hosseinzadeh, H. (2016). Berberis vulgaris and berberine: an update review. *Phytother Res.* 30, 1745–1764. doi:10.1002/ptr.5693

Jin, F., Xie, T., Huang, X., and Zhao, X. (2018). Berberine inhibits angiogenesis in glioblastoma xenografts by targeting the VEGFR2/ERK pathway. *Pharm. Biol.* 56, 665–671. doi:10.1080/13880209.2018.1548627

Lage, H. (2003). Molecular analysis of therapy resistance in gastric cancer. *Dig. Dis.* 21, 326–338. doi:10.1159/000075356

Leung, W. K., Wu, M.-s., Kakugawa, Y., Kim, J. J., Yeoh, K.-g., Goh, K. L., et al. (2008). Screening for gastric cancer in Asia: current evidence and practice. *Lancet Oncol.* 9, 279–287. doi:10.1016/s1470-2045(08)70072-x

Li, L., Zhang, S., Xie, D., Chen, H., Zheng, X., and Pan, D. (2018). Dual inhibitor of PI3K and mTOR (NVP-BEZ235) augments the efficacy of fluorouracil on gastric cancer chemotherapy. *OncoTargets Ther.* 1111, 6111–6118. doi:10.2147/ott.s172957

Lin, J.-P., Yang, J.-S., Lee, J.-H., Hsieh, W.-T., and Chung, J.-G. (2006). Berberine induces cell cycle arrest and apoptosis in human gastric carcinoma SNU-5 cell line. *World J. Gastroenterol.* 12, 21–28. doi:10.3748/wjg.v12.i1.21

Lin, J. P., Yang, J. S., Wu, C. C., Lin, S. S., Hsieh, W. T., Lin, M. L., et al. (2008). Berberine induced down-regulation of matrix metalloproteinase-1, -2 and -9 in human gastric cancer cells (SNU-5) *in vitro*. *In Vivo* 22, 223–230.

Liu, L., Fan, J., Ai, G., Liu, J., Luo, N., Li, C., et al. (2019). Berberine in combination with cisplatin induces necroptosis and apoptosis in ovarian cancer cells. *Biol. Res.* 52, 37. doi:10.1186/s40659-019-0243-6

Liu, S., Fang, Y., Shen, H., Xu, W., and Li, H. (2013). Berberine sensitizes ovarian cancer cells to cisplatin through miR-21/PDCD4 axis. *Acta Biochim. Biophys. Sin.* 45, 756–762. doi:10.1093/abbs/gmt075

Lopes, T. Z., De Moraes, F. R., Tedesco, A. C., Arni, R. K., Rahal, P., and Calmon, M. F. (2020). Berberine associated photodynamic therapy promotes autophagy and apoptosis via ROS generation in renal carcinoma cells. *Biomed. Pharmacother.* 123, 109794. doi:10.1016/j.biopha.2019.109794

Luo, Y., Tian, G., Zhuang, Z., Chen, J., You, N., Zhuo, L., et al. (2019). Berberine prevents non-alcoholic steatohepatitis-derived hepatocellular carcinoma by inhibiting inflammation and angiogenesis in mice. *Am. J. Transl. Res.* 11, 2668–2682.

Ma, Y., Wang, R., Lu, H., Li, X., Zhang, G., Fu, F., et al. (2020). B7-H3 promotes the cell cycle-mediated chemoresistance of colorectal cancer cells by regulating CDC25A. *J. Canc.* 11, 2158–2170. doi:10.7150/jca.37255

Maiti, P., Plemmons, A., and Dunbar, G. L. (2019). Combination treatment of berberine and solid lipid curcumin particles increased cell death and inhibited PI3K/Akt/mTOR pathway of human cultured glioblastoma cells more effectively than did individual treatments. *PLoS One* 14, e0225660. doi:10.1371/journal.pone.0225660

Palmieri, A., Iapichino, A., Cura, F., Scapoli, L., Carinci, F., Mandrone, M., et al. (2018). Pre-treatment with berberine enhances effect of 5-fluorouracil and cisplatin in HEP2 laryngeal cancer cell line. *J. Biol. Regul. Homeost. Agents* 32, 167–177.

Pan, Y., Zhang, F., Zhao, Y., Shao, D., Zheng, X., Chen, Y., et al. (2017). Berberine enhances chemosensitivity and induces apoptosis through dose-orchestrated AMPK signaling in breast cancer. *J. Canc.* 8, 1679–1689. doi:10.7150/jca.19106

Pandey, A., Vishnoi, K., Mahata, S., Tripathi, S. C., Misra, S. P., Misra, V., et al. (2015). Berberine and curcumin target survivin and STAT3 in gastric cancer

cells and synergize actions of standard chemotherapeutic 5-fluorouracil. *Nutr. Canc.* 67, 1293–1304. doi:10.1080/01635581.2015.1085581

Piñeros, M., Ramos, W., Antoni, S., Abriata, G., Medina, L. E., Miranda, J. J., et al. (2017). Cancer patterns, trends, and transitions in Peru: a regional perspective. *Lancet Oncol.* 18, e573-e586. doi:10.1016/s1470-2045(17)30377-7

Qi, Y., Qi, W., Liu, S., Sun, L., Ding, A., Yu, G., et al. (2020). TSPAN9 suppresses the chemosensitivity of gastric cancer to 5-fluorouracil by promoting autophagy. *Canc. Cell Int.* 20, 4. doi:10.1186/s12935-019-1089-2

Sheng, M., Zhou, Y., Yu, W., Weng, Y., Xu, R., and Du, H. (2015). Protective effect of Berberine pretreatment in hepatic ischemia/reperfusion injury of rat. *Transplant. Proc.* 47, 275–282. doi:10.1016/j.transproceed.2015.01.010

Thrift, A. P. and El-Serag, H. B. (2020). Burden of gastric cancer. *Clin. Gastroenterol. Hepatol.* 18, 534–542. doi:10.1016/j.cgh.2019.07.045

Van Cutsem, E., Sagaert, X., Topal, B., Haustermans, K., and Prenen, H. (2016). Gastric cancer. *Lancet* 388, 2654–2664. doi:10.1016/s0140-6736(16)30354-3

Venerito, M., Vasapolli, R., Rokkas, T., and Malfertheiner, P. (2018). Gastric cancer: epidemiology, prevention, and therapy. *Helicobacter* 23 (Suppl. 1), e12518. doi:10.1111/hel.12518

Wagner, A. D., Syn, N. L., Moehler, M., Grothe, W., Yong, W. P., Tai, B. C., et al. (2017). Chemotherapy for advanced gastric cancer. *Cochrane Database Syst. Rev.* 8, CD004064. doi:10.1002/14651858.CD004064.pub4

Wang, J., Yang, S., Cai, X., Dong, J., Chen, Z., Wang, R., et al. (2016). Berberine inhibits EGFR signaling and enhances the antitumor effects of EGFR inhibitors in gastric cancer. *Oncotarget* 7, 76076–76086. doi:10.18632/oncotarget.12589

Wang, K., Feng, X., Chai, L., Cao, S., and Qiu, F. (2017). The metabolism of berberine and its contribution to the pharmacological effects. *Drug Metab. Rev.* 49, 139–157. doi:10.1080/03602532.2017.1306544

Wang, Y. and Zhang, S. (2018). Berberine suppresses growth and metastasis of endometrial cancer cells via miR-101/COX-2. *Biomed. Pharmacother.* 103, 1287–1293. doi:10.1016/j.biopha.2018.04.161

Wang, Y., Zhou, M., and Shang, D. (2020). Berberine inhibits human gastric cancer cell growth via deactivation of p38/JNK pathway, induction of mitochondrial-mediated apoptosis, caspase activation and NF-κB inhibition. *J. buon* 25, 314–318.

Wang, Z., Qi, F., Cui, Y., Zhao, L., Sun, X., Tang, W., et al. (2018). An update on Chinese herbal medicines as adjuvant treatment of anticancer therapeutics. *Biosci. Trends* 12, 220–239. doi:10.5582/bst.2018.01144

Wei, S., Zhang, M., Yu, Y., Lan, X., Yao, F., Yan, X., et al. (2016). Berberine attenuates development of the hepatic gluconeogenesis and lipid metabolism disorder in type 2 diabetic mice and in palmitate-incubated HepG2 cells through suppression of the HNF-4α miR122 pathway. *PLoS One* 11, e0152097. doi:10.1371/journal.pone.0152097

Xu, W., Wei, Q., Han, M., Zhou, B., Wang, H., Zhang, J., et al. (2018). CCL2-SQSTM1 positive feedback loop suppresses autophagy to promote chemoresistance in gastric cancer. *Int. J. Biol. Sci.* 14, 1054–1066. doi:10.7150/ijbs.25349

Yi, T., Zhuang, L., Song, G., Zhang, B., Li, G., and Hu, T. (2015). Akt signaling is associated with the berberine-induced apoptosis of human gastric cancer cells. *Nutr. Canc.* 67, 523–531. doi:10.1080/01635581.2015.1004733

**Conflict of Interest:** The authors declare that the research was conducted in the absence of any commercial or financial relationships that could be construed as a potential conflict of interest.

frontiers in Pharmacology

ORIGINAL RESEARCH
published: 13 January 2021
doi: 10.3389/fphar.2020.600994

# CPEB4-Promoted Paclitaxel Resistance in Ovarian Cancer *In Vitro* Relies on Translational Regulation of CSAG2

*Yaqing Zhang[1], Hongyun Gan[1], Fei Zhao[1], Xiaomei Ma[2], Xiaofeng Xie[1], Rui Huang[1] and Jin Zhao[1]**

[1]Medical College of Northwest Minzu University, Lanzhou, China, [2]Department of Gynecology, Gansu Provincial People's Hospital, Lanzhou, China

**Background:** Drug resistance is a major obstacle in chemotherapy for ovarian cancer, wherein the up regulation of drug-resistant genes plays an important role. The cytoplasmic polyadenylation element binding protein 4 (CPEB4) is an RNA binding protein that controls mRNA cytoplasmic polyadenylation and translation.

**Methods:** The expression of CPEB4 in paclitaxel-resistant ovarian cancer cell lines and recurrent ovarian tumors relative to counterparts was determined by qRT-PCR, Western blotting and immunohistochemistry. The response to paclitaxel treatment was evaluated by cellular viability test and colony formation assay. RNA immunoprecipitation and poly(A) tail test were applied to examine the levels of RNA binding and cytoplasmic polyadenylation.

**Results:** CPEB4 is elevated in paclitaxel-resistant ovarian cancer cells and recurrent ovarian tumors treated with paclitaxel-based chemotherapy. In addition, CPEB4 overexpression promotes paclitaxel resistance in ovarian cancer cells *in vitro*, and vice versa, CPEB4 knockdown restores paclitaxel sensitivity, indicating that CPEB4 confers paclitaxel resistance in ovarian cancer cells. Mechanistically, CPEB4 binds with the taxol (paclitaxel)-resistance-associated gene-3 (TRAG-3/CSAG2) mRNAs and induces its expression at a translational level. Moreover, CSAG2 expression is upregulated in paclitaxel-resistant ovarian carcinoma and cancer cell lines, and more importantly, siRNA-mediated CSAG2 knockdown overtly attenuates CPEB4-mediated paclitaxel resistance.

**Conclusion:** This study suggests that the drug-resistant protein CSAG2 is translationally induced by CPEB4, which underlies CPEB4-promoted paclitaxel resistance in ovarian cancer *in vitro*. Thus, interfering CPEB4/CSAG2 axis might be of benefit to overcome paclitaxel-resistant ovarian cancer.

**Keywords: CPEB4, paclitaxel, resistance, ovarian carcinoma, CSAG2**

OPEN ACCESS

***Edited by:***
*Dexin Kong,*
*Tianjin Medical University, China*

***Reviewed by:***
*Bolin Liu,*
*Louisiana State University, United States*
*Siying Chen,*
*First Affiliated Hospital of Xi'an Jiaotong University, China*

****Correspondence:***
*Jin Zhao*
*zhaojxbmu@163.com*

***Specialty section:***
*This article was submitted to Pharmacology of Anti-Cancer Drugs, a section of the journal Frontiers in Pharmacology*

***Received:*** *31 August 2020*
***Accepted:*** *09 November 2020*
***Published:*** *13 January 2021*

***Citation:***
*Zhang Y, Gan H, Zhao F, Ma X, Xie X, Huang R and Zhao J (2021) CPEB4-Promoted Paclitaxel Resistance in Ovarian Cancer* In Vitro *Relies on Translational Regulation of CSAG2. Front. Pharmacol. 11:600994. doi: 10.3389/fphar.2020.600994*

# INTRODUCTION

Ovarian cancer is the most lethal gynecologic malignancy, and approximate 22,440 new cases and 14,080 deaths have been estimated to occur in the United States in 2017 (Siegel et al., 2017). The standard first-line option for treating ovarian cancer is cytoreductive surgery followed by paclitaxel/platinum-based chemotherapy (Jayson et al., 2014). Although up to 80% of patients initially respond well to therapy, most of them develop recurrent ovarian cancer within 12–24 months and succumb to progressive refractory disease resistant to therapy, with a poor 5-years survival rate lower than 30% (Au Yeung et al., 2016). Therefore, there is an urgent need to develop a new therapeutic strategy targeting mechanisms leading to chemoresistance.

The development of resistance to paclitaxel is multifactorial and several mechanisms have been documented, including enhanced activity of xenobiotics transporter P-glycoprotein (Alam et al., 2019), alterations of β-tubulin (Yang et al., 2016) and remodeling of tumor microenvironment (Au Yeung et al., 2016). Recently, CSAG2, also known as the taxol resistance associated gene 3 (TRAG-3), has been identified to be overexpressed in a paclitaxel-resistant ovarian cancer cell line and also be a prognostic factor for predicting clinical outcome after paclitaxel-based chemotherapy (Lage and Denkert, 2007; Materna et al., 2007). Whereas, the specific role of CSAG2 in paclitaxel resistance is still unknown.

The reprogramming of gene expression *via* posttranscriptional regulation of specific mRNA subpopulations is an important mechanism underlying the broad modulation of expression of genes responsible for governing the malignant properties (Wurth et al., 2016; Hu et al., 2020). This regulation is primarily mediated by common *cis*-acting elements present in 3′ untranslated regions (UTRs), such as the cytoplasmic polyadenylation element (CPE) (Chen Y. et al., 2016), which is bound by the CPE binding proteins (CPEBs) (Harvey et al., 2018). To date, CPEBs have been found to act as either translational repressors or activators to regulate cell cycle, energy metabolism and senescence (Kang et al., 2020). Moreover, CPEB4, one member of CPEBs, has been shown to play a key role in the progression of pancreatic ductal adenocarcinoma, glioblastoma, glioma and gastric cancer (Ortiz-Zapater et al., 2011; Zhijun et al., 2017; Cao et al., 2018). In this study, we report that CPEB4 promotes paclitaxel resistance in ovarian cancer, and suggest that this effect depends on its translational regulation of CSAG2.

# MATERIALS AND METHODS

## Antibodies and Reagents

The antibodies and paclitaxel were purchased from the following sources: CPEB4 (Novus, NBP2-15984), CSAG2 (Invitrogen, PA5-25339), β-actin (Santa Cruz, sc-69879), goat anti-mouse IgG-HRP (Santa Cruz, sc-2302), goat anti-rabbit IgG-HRP (Santa Cruz, sc-2004), goat anti-rabbit peroxidase-conjugated IgG (Sigma-Aldrich, A0545), and paclitaxel (Sigma-Aldrich, T7191).

## Ovarian Tumor Specimens and Immunohistochemistry

Eighteen formalin-fixed and paraffin-embedded ovarian cancer specimens were obtained from Gansu Provincial Hospital under the ethical approval by the Ethics Committee of Medical College of Northwest Minzu University. Informed written consent was obtained from all patients, whose detailed clinical information was shown in **Supplementary Table S1**. Immunohistochemistry was performed to compare the expression levels of CPEB4 or CSAG2 in paired primary tumors before treatment and recurrent ovarian tumors post-chemotherapy, who received standard paclitaxel-based chemotherapy for three to six courses of treatment. Briefly, 5 μm specimen sections were prepared. Antigen retrieval was conducted by immersing slides in 0.1 M citrate (pH 6.0) at 120°C for 15 min. Slides were blocked with 5% goat serum for 1 h at room temperature (RT) prior to incubation with primary antibodies for overnight at 4°C. The isotype IgG antibody was used as negative control. After incubation, peroxidase-conjugated secondary antibodies were added onto slides for further 1 h incubation at RT. Eventual reactions were performed using diaminobenzidine (DAB) as chromogenic substrate [EnVision + System (DAKO)]. At last, sections were counterstained with haematoxylin, and visualized under a Leica DM6000 Digital microscope, and images were acquired using QWin software (Leica). The immunoreactivity was scored by the H score system (Wallin et al., 2016), ranging from zero to three, as assessed by two investigators based on the percentage of stained cells and intensity of staining.

## Cell Culture and Generation of Paclitaxel-Resistant Cells

Ovarian carcinoma cell lines SKOV3 and CaOV3, and human embryonic kidney 293T (HEK293T) cell line were obtained from the American Tissue Culture Center (Manassas, VA). All cell lines were cultured in a humidified incubator (ThermoFisher Scientific) at 37°C with 5% $CO_2$. SKOV3 and CaOV3 cell lines were maintained in complete RPMI-1640 medium (ThermoFisher Scientific) with 10% fetal bovine serum (FBS). HEK293T cell line was maintained in complete dulbecco's modified eagle's medium (DMEM) (ThermoFisher Scientific) with 10% FBS. The paclitaxel-resistant ovarian cancer cell lines SKOV3 (R) and CaOV3 (R) were established by over 7-months culture with increasing concentrations of paclitaxel, resulting in approximately 6.3-fold and 7.0-fold as compared with the parental cell lines, respectively. In brief, paclitaxel-resistant SKOV3 (R) and CaOV3 (R) were selected by culturing cells with paclitaxel in a dose-escalation manner using 72-h exposure. SKOV3 and CaOV3 cells were initially cultured with 5 nM paclitaxel. When sensitive cells were removed and surviving SKOV3 and CaOV3 cells repopulated the flask, the concentration of paclitaxel was increased to 10, 25, 50, 100, and 200 nM. After 7 and 8 months, the paclitaxel-resistant SKOV3 and CaOV3 cells were obtained, respectively. Meanwhile, naïve SKOV3 and CaOV3 cells were cultured with DMSO in the same manner. After resistance testing *via*

continuous 1-week culture with 200 nM paclitaxel, the resistant SKOV3 and CaOV3 cells were maintained in the presence of 10 nM paclitaxel, as compared with DMSO for naïve cells.

## Cellular Viability Test

Cells were harvested, then immersed in PBS, and stained with 0.4% trypan blue solution (Sigma-Aldrich, T8154). Trypan blue positive cells were defined as nonviable cells and excluded from the counting. The number of trypan blue negative cells were determined by TC20 Automated Cell Counter (Bio-Rad), and its percentage (%) within total cell number was calculated.

## Colony Formation Assay

Cells were harvested and counted by TC20 Automated Cell Counter as described before. A total of 1,000 viable cancer cells in each group were seeded in six-well plate and cultured with 2 ml medium. Three replicates were set for each treatment condition. The culture medium with or without paclitaxel was replaced with fresh medium every 3 days until the formed colonies were clearly visible for naked eyes. Eventually, colonies were washed with PBS, fixed with 4% paraformaldehyde solution (Santa Cruz, sc-281692), and stained by 0.05% crystal violet (Sigma-Aldrich, V5265). The final images were photographed and the ImageJ software was used to analyze the number of colonies in each well.

## Protein Extraction and Western Blotting

The whole cell proteins were extracted from cells lyzed in RIPA lysis buffer (Beyotime, P0013C) with protease inhibitor Cocktail (Roche, CO-RO) on ice for 10 min. The lysates were centrifuged with 12,000 × *g* at 4°C for 20 min. Protein samples in supernatants were denatured with 5× loading buffer at 100°C for 10 min. Equal amount of proteins were resolved by 10% SDS-PAGE, transferred onto Immobilon-P PVDF membrane (Millipore, IPVH00010), and then blocked by 5% bovine serum albumin (BSA) (Roche) saluted in tris buffered saline (TBS) supplemented with 0.1% Tween (TBST) for 1 h at RT. PVDF membrane were then incubated with primary antibodies overnight at 4°C. Next, membranes were washed with TBST for three times, and incubated further with secondary antibodies at RT for 1 h. Membranes were again washed with TBST for three times and reacted with the enhanced chemiluminescence (GE Healthcare, RPN2209) for protein detection under GE ImageQuant LAS 4000 instrument. The intensity of protein bands was quantified with ImageJ software.

## RNA Extraction and qRT-PCR Analysis

Cells were harvested and homogenized, and the total RNA were extracted with agents according to Trizol-based method (Thermo Fisher, 15596026). Procedures were performed as described in the manufacturer's instructions. The levels of target transcripts were determined by SYBR green real-time PCR kit (TakaRa, RR420A) and run by the 7500 Real-Time PCR System (Applied Biosystems). Data were analyzed based on the comparative Ct method. Human *ACTB* was used as an endogenous control. Primer sequences are listed as follows: CPEB4 sense 5′-TGG GGATCAGCCTCTTCATA-3′, antisense 5′-CAATCCGCCTAC AAACACCT-3′; CSAG2 sense 5′-CAACATCTCTGCCGCTAA CC-3′, antisense 5′-GTAGCCGCCGACATTACAAG-3′. ACTB sense 5′-ACGGGCATTGTGATGGACTC-3′, antisense 5′-GTG GTGGTGAAGCTGTAGCC-3′.

## Overexpression *via* Retrovirus Infection

Clone of human CPEB4 was constructed into pBABE-puro system (addgene, 1764), and empty vector construct was used as a control. Retrovirus expressing these retrovirus plasmids were packaged with HEK293T cells. Cancer cells were cultured and infected with retrovirus solution in the presence of 4 μg/ml polybrene for 18°h, and further cultured for 1°day in fresh medium. Cells infected with retrovirus were selected by culturing with 2 μg/ml puromycin for 1–2 weeks. The stably infected cells were maintained in culture medium containing 1 μg/ml puromycin. Overexpression was confirmed by qRT-PCR or Western blotting analysis.

## shRNA and siRNA-Mediated Knockdown

shRNA-mediated knockdown of human CPEB4 was implemented using a specific targeting sequence (5′-CCGGGC CTGCCTCATTTGGCGAATATTTCTCGAG AATATTCGC CAAATGAGGCAGGCTTTTTG-3′). A non-specific 'scrambled' shRNA was used as a control. These sequences were constructed into the pLKO.1-puro vector (Sigma, SHC201). For producing lentivirus, plasmids carrying these sequences were co-transfected with the packaging plasmids into HEK293T cells. At 2 days following transfection, supernatants containing lentivirus were harvested and stored at −80°C if not being used immediately. The cultured cancer cells were then infected with lentivirus solution for 18 h in the presence of 4 μg/ml polybrene. The stably infected cells were obtained by culturing them under the selective pressure of 2 μg/ml puromycin for 1–2 weeks. For gene knockdown mediated by siRNA transfection, cancer cells were transfected with 20 nM siRNAs targeting luciferase control (siCtrl), *CSAG2* (siCSAG2) using Lipofectamine RNAimax (Invitrogen, 13778150) for 24 h. Medium was replaced with fresh medium and cells were cultured for further 2 days. Gene knockdown was confirmed by qRT-PCR or Western blotting analysis.

## RNA Immunoprecipitation

RNA immunoprecipitation (RIP) was performed using a MagnaRIP Kit (Millipore) as described previously (Lu et al., 2016). Briefly, Cells were harvested and lyzed with RIP lysis buffer (10 mM HEPES, pH 7.0, 100 mM KCl, 5 mM MgCl2, 0.5% NP-40, 1 mM DTT) for 20 min on ice. After centrifuge, the whole cell lysates were incubated at 4°C overnight with magnetic protein A-protein G beads (Sigma-Aldrich) coupled with isotype IgG control or CPEB4 antibody to obtain RNA-protein immunocomplexes. Beads were washed three times with washing buffer, and incubated with proteinase K buffer for 45 min at constant 55°C, which was followed by RNA isolation from the immunoprecipitates according to the manufacturer's instructions. cDNA was reversely transcripted by First-strand cDNA Synthesis System (Thermo Scientific, K1621). qRT-PCR was performed by amplifying a 300-bp region in the 3′ UTR of each transcript.

## Poly(A) Tail Test

Poly(A) tail test was performed as described previously (Pique et al., 2008; Ortiz-Zapater et al., 2011). Briefly, 3 μg of total RNA were ligated to sense anchor primer (5′P-GGTCACCTCTGATCTGGAAGCGAC-$NH_2$-3′) and reversely transcribed with antisense anchor primer (GTCGCTTCCAGA TCAGAGGTGACCTTTTT). The product was then treated with 2 μg RNAse A. This final product was used as a template for PCR amplification with antisense anchor primer and a specific primer for each mRNA analyzed. FastStart Taq DNA polymerase (Roche, FPCRN-RO) was utilized as recommended by the manufacturer in the absence or presence of 5 μCi ($^{32}$P) α-dATP. PCR products were separated in a denaturing 8% polyacrylamide gel and visualized by autoradiography.

## Statistical Analyses

Statistical analyses were performed with GraphPad Prism 6. Data are presented as mean ± SEM. Statistical analyses comparing data between two groups were assessed by unpaired Student's *t* test, and ANOVA with a *post hoc* Dunnett's test was used for analyzing data among more than two groups. $p < 0.01$ and $p < 0.05$ indicate a statistical difference.

# RESULTS

## CPEB4 Is Upregulated in Paclitaxel-Resistant Ovarian Cancer Cells and Recurrent Ovarian Tumors

To explore whether CPEB4 plays a role in paclitaxel resistance in ovarian cancer, we compared its transcript levels between naive sensitive SKOV3 (S) cells and their paclitaxel-resistant counterparts SKOV3 (R) through qRT-PCR analysis. As depicted, the transcript level of CPEB4 in SKOV3 (R) was nearly twice than that of SKOV3 (S) (**Figure 1A**, left half). Additionally, similar tendency was obtained when comparing another pair of ovarian cancer cell lines, CaOV3 (S) and CaOV3 (R) (**Figure 1A**, right half). We next examined the protein level of CPEB4 by performing Western blotting analysis. As shown in **Figure 1B**, in consistent with its transcript level, the protein level of CPEB4 was upregulated in both SKOV3 (R) and CaOV3 (R), as compared with their naive sensitive counterparts. Of note, we further found that CPEB4 failed to be increased in SKOV3 (S) and CaOV3 (S) treated with paclitaxel for 72 h (**Figure 1C**). Overall, these results suggest that the upregulation of CPEB4 was associated with functional resistance

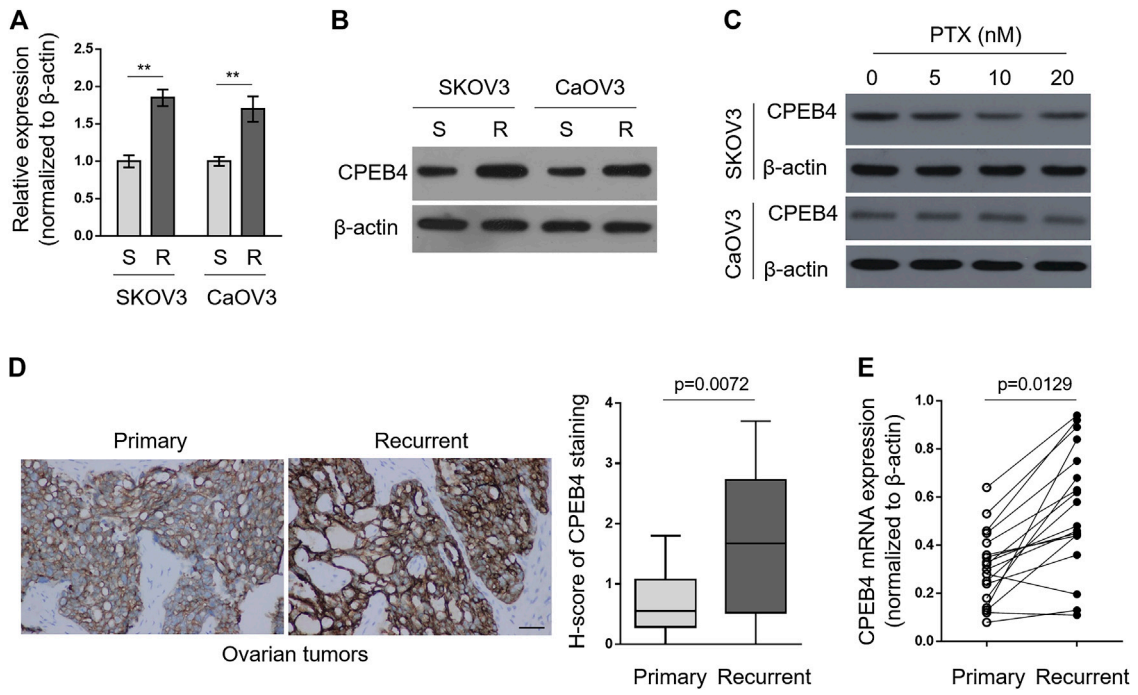


**FIGURE 1 |** CPEB4 is upregulated in paclitaxel-resistant ovarian cancer cells and recurrent ovarian tumors. **(A,B)** The paclitaxel-resistant ovarian cancer cell lines SKOV3 (R) and CaOV3 (R) were established with treatment of increasing concentrations of paclitaxel (PTX) for over 7 months. The mRNA **(A)** and protein **(B)** levels of CPEB4 in these cells were analyzed by qRT-PCR and Western blotting analysis, and compared with those of naive sensitive cells, SKOV3 (S) and CaOV3 (S). β-Actin was used as a loading and reference control. The representative images are shown. Data represent mean ± SEM. $n = 3$. $^{**}p < 0.01$. **(C)** SKOV3 **(upper)** and CaOV3 **(lower)** naive cells were treated with indicated concentrations of PTX for 72 h. The protein level of CPEB4 was analyzed by Western blotting. β-Actin was used as a loading control. The representative images are shown. **(D)** Representative images **(left)** of immunohistochemical staining of CPEB4 from matched primary and recurrent ovarian tumors treated with paclitaxel-based chemotherapy. Scale bar, 50 μm. H-score **(right)** is used to semi-quantify CPEB4 expression levels. The black line inside the box is the median, and the lines above and below the box indicate the maximum and minimum of the H-scores. Each group contained 18 paired samples. **(E)** The mRNA levels of CPEB4 in matched primary and recurrent ovarian tumors **(D)** were analyzed by qRT-PCR. β-Actin was used as a reference control. Each symbol represents the mean value of three replicates.

of ovarian cancer cells to paclitaxel and is impossibly due to acute inducible effect of paclitaxel in naive sensitive cells.

Next, we performed immunohistochemistry to compare CPEB4 expression between paired primary untreated ovarian tumors and recurrent tumors treated with paclitaxel-based chemotherapy. The result showed that CPEB4 had stronger immunoreactive staining in recurrent tumors than that of primary tumors (**Figure 1D**, left), and semi-quantification using H-score analysis proved the higher expression level of CPEB4 in recurrent ovarian tumors (**Figure 1D**, right). The transcript level of CPEB4 in these paired tumors was also quantified, and likewise, significant upregulation of CPEB4 was observed in recurrent ovarian tumors (**Figure 1E**). Collectively, these data indicate that CPEB4 is upregulated in paclitaxel-resistant ovarian cancer cells and recurrent ovarian tumors, and also imply an association of its upregulation with paclitaxel resistance.

## CPEB4 Promotes Paclitaxel Resistance in Ovarian Cancer Cells *In Vitro*

To understand the effect of CPEB4 upregulation on paclitaxel resistance, we enforced its expression in SKOV3 (S) and CaOV3 (S) *via* retrovirus infection (**Figure 2A**). The stable overexpression of CPEB4 did not obviously affect cell proliferation or survival (**Figure 2B**), however, it markedly increased the survival rate of both two ovarian cancer cell lines when treated with paclitaxel (**Figure 2C**). In addition, higher colony formation rate was also found in CPEB4-overexpressing cells compared with vector controls, in the presence of continuous paclitaxel exposure (**Figure 2D**). Therefore, these results support a promotive effect of CPEB4 overexpression on paclitaxel resistance in ovarian cancer cells, and also suggest that CPEB4 upregulation detected in paclitaxel-resistant cells (**Figures 1A,B**) may contribute to the development and maintenance of resistance. To test this idea, we performed shRNA-mediated CPEB4 stable knockdown in SKOV3 (R) and CaOV3 (R) cells (**Figure 2E**). Under untreated condition, CPEB4 knockdown had no obvious effect on cell proliferation or survival (**Figure 2F**). But, when cells were continuously treated with paclitaxel, CPEB4-deficient cells exhibited lower rates of survival (**Figure 2G**) and colony formation (**Figure 2H**) compared with shCtrl group, indicating that CPEB4 is essential for paclitaxel-resistant property. Together, these lines of evidence prove that CPEB4 upregulation promotes paclitaxel resistance in ovarian cancer cells *in vitro*.

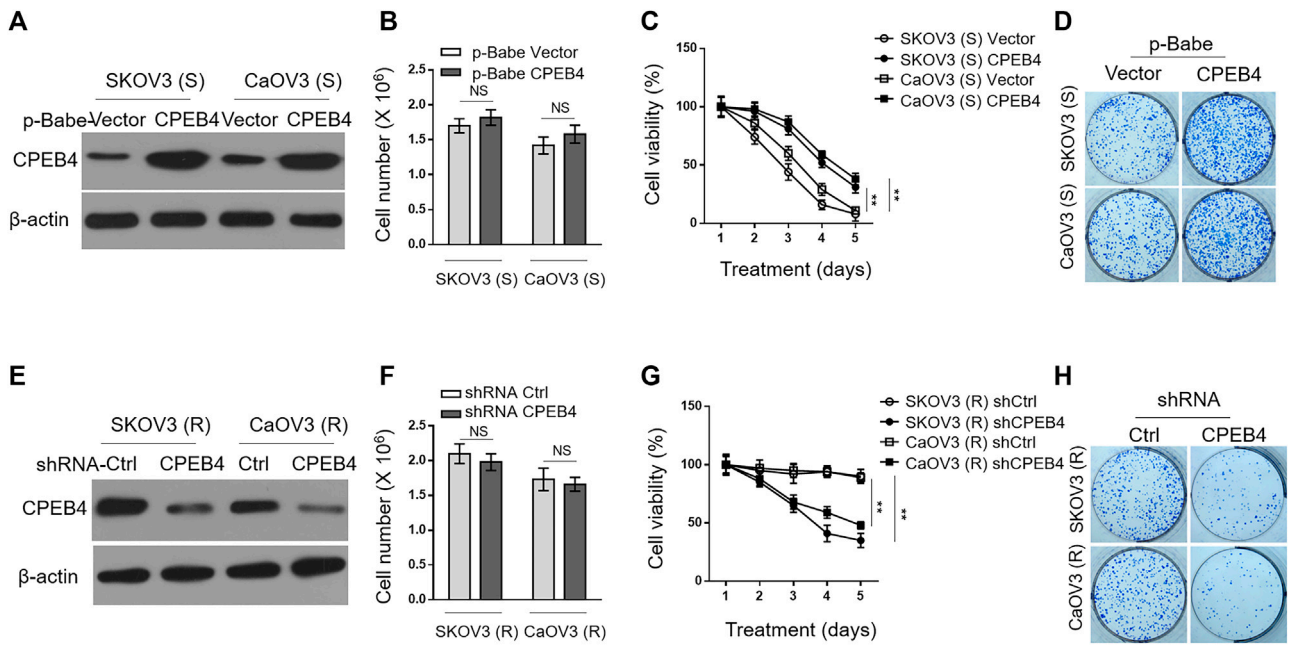


**FIGURE 2 |** CPEB4 promotes paclitaxel resistance in ovarian cancer cells *in vitro*. **(A)** The naive sensitive cells, SKOV3 (S) and CaOV3 (S), were stably infected with retrovirus expressing empty vector or human CPEB4, and the protein level of CPEB4 was analyzed by Western blotting. The representative images are shown. **(B)** The viable cell numbers of cells **(A)** cultured for 3 days with an initial $2 \times 10^6$ cell number. Trypan blue staining was used to exclude unviable cells. Data represent mean ± SEM. $n = 3$. NS, not significant. **(C)** Cells **(A)** were cultured with an initial $2 \times 10^6$ cell number and then treated with 20 nM PTX for indicated periods of time. The viable cell number relative to DMSO treated group is shown. Data represent mean ± SEM. $n = 3$. $^{**}p < 0.01$. **(D)** Representative images of cells **(A)** stained with crystal violet after 2-weeks culture with 20 nM PTX treatment **(left)**. The colony number was quantified by ImageJ **(right)**, and results relative to vector are shown. Data are mean ± SEM. $n = 3$. $^{**}p < 0.01$. **(E)** The paclitaxel-resistant cells, SKOV3 (R) and CaOV3 (R), were stably infected with lentivirus expressing shRNA targeting control or human CPEB4, and the protein level of CPEB4 was analyzed by Western blotting. The representative images are shown. **(F)** The viable cell numbers of cells **(E)** cultured for 3 days with an initial $2 \times 10^6$ cell number. Trypan blue staining was used to exclude unviable cells. Data represent mean ± SEM. $n = 3$. NS, not significant. **(G)** Cells **(E)** were cultured with an initial $2 \times 10^6$ cell number and then treated with 20 nM PTX for indicated periods of time. The viable cell number relative to DMSO treated group is shown. Data represent mean ± SEM. $n = 3$. $^{**}p < 0.01$. **(H)** Representative images of cells **(E)** stained with crystal violet after 2-weeks culture with 20 nM PTX treatment **(left)**. The colony number was quantified by ImageJ **(right)**, and results relative to control are shown. Data are mean ± SEM. $n = 3$. $^{**}p < 0.01$.

## CPEB4 Binds With CSAG2 mRNA and Induces Its Cytoplasmic Polyadenylation and Translation

CSAG2, also known as taxol (paclitaxel)-resistance-associated gene-3 (TRAG-3), is overexpressed in paclitaxel-resistant ovarian cancer cells (Duan et al., 1999), and also shown to be negatively associated with clinical outcome after paclitaxel treatment (Lage and Denkert, 2007; Materna et al., 2007). These clues imply a role of CSAG2 in paclitaxel resistance. Moreover, in a genome-wide screening study, CSAG2 was found to be coimmunoprecipitated with CPEB4 in pancreatic ductal adenocarcinoma cells line (Ortiz-Zapater et al., 2011), although remains to be validated further. These prompt us to investigate whether CSAG2 mediates the effect of CPEB4 on paclitaxel resistance. Firstly, we validated the binding between CPEB4 and CSAG2 in HEK293 cells which were enforced to express different amounts of exogenous CPEB4 (**Figure 3A**). The results from RNA immunoprecipitation (RIP) showed that CPEB4 indeed bound with the 3′ UTR of CSAG2 mRNA, and the binding intensity was positively correlated with the amount of CPEB4 (**Figures 3A,B**). To assess whether the cytoplasmic polyadenylation of CSAG2 mRNA was regulated by CPEB4, we measured the length of poly(A) tail of CSAG2 mRNA by anchored RT-PCR (Pique et al., 2008). In CPEB4-overexpressing HEK293 cells, the poly(A) tail was elongated along with increased CPEB4 level, which is in contrast to the short poly(A) tail observed in control cells (**Figure 3C**), illustrating that the CSAG2 mRNA is more polyadenylated when CPEB4 is overexpressed. Cytoplasmic polyadenylation plays a key role in the translational control of mRNAs (Mendez and Richter, 2001). Consistent with elongated poly(A) tail, the protein level of CSAG2 was induced upon CPEB4 overexpression (**Figure 3D**), in parallel, with its transcript level unaffected (**Figure 3E**). Together, these data show that CSAG2 expression is regulated by CPEB4-mediated translational control. We further examined whether this mechanism also exists in ovarian cancer cells. RIP assay showed that CPEB4 also bound with CSAG2 mRNA in SKOV3 (R) and CaOV3 (R) cells (**Figure 3F**). Moreover, shRNA-mediated CPEB4 knockdown resulted in shorter poly(A) tail of CSAG2 mRNA

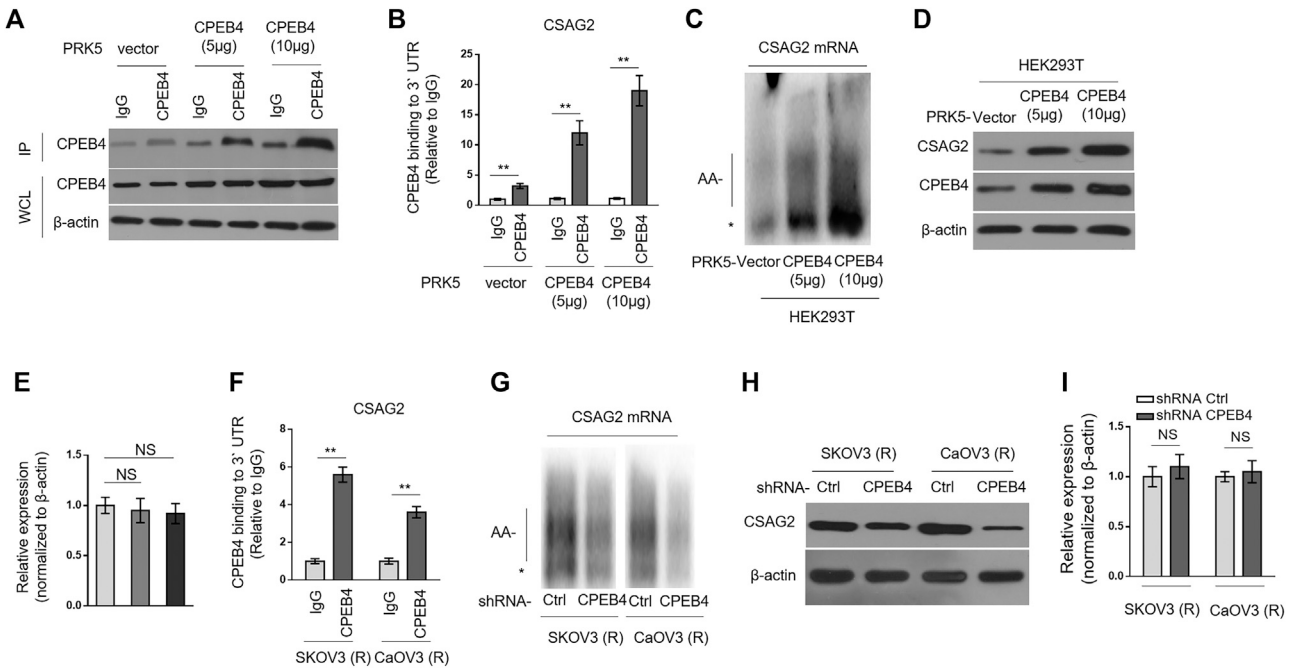


**FIGURE 3 |** CPEB4 binds with CSAG2 mRNAs and induces its cytoplasmic polyadenylation and translation **(A,B)** HEK293T cells were transfected with 5 or 10 μg plasmids expressing vector or human CPEB4 as indicated, and the cell lysates were immunoprecipitated with IgG isotype control antibody or CPEB4 antibody. The protein level of CPEB4 in whole cell lysates and IP products was analyzed by Western blotting **(A)**. Total RNAs bound with agarose beads were purified from immunoprecipitates and reversely transcribed to cDNA and analyzed by qRT-PCR to measure the level of CSAG2 transcript **(B)**. The results in each sample represent the mean value of three replicates. The enrichment value relative to IgG group is shown. Data are mean ± SEM. $^{**}p < 0.01$. **(C–E)** HEK293T cells were transfected with 5 or 10 μg plasmids expressing vector or human CPEB4 as indicated and cultured for 3 days. **(C)** Total RNAs were then extracted and the polyadenylation was measured by RNA ligation-coupled RT-PCR using ($^{32}$P) α-dATP and specific primers for CSAG2. Products were separated in a denaturing 8% polyacrylamide gel and visualized by autoradiography. *, non-adenylated RNAs; AA-, adenylated RNAs. **(D)** The whole cell lysates were analyzed by Western blotting for detecting the level of CSAG2. β-Actin was used as a loading control. Shown here are representative images. **(E)** The mRNA of CSAG2 was analyzed by qRT-PCR. β-Actin was used as a reference control. Data are mean ± SEM. $n = 3$. NS, not significant. **(F)** The cell lysates of SKOV3 (R) and CaOV3 (R) cells were immunoprecipitated with IgG isotype control antibody or CPEB4 antibody. The binding of 3′-UTR of CSAG2 mRNA with CPEB4 was analyzed as in **(B)**. Data are mean ± SEM. $^{**}p < 0.01$. **(G–I)** SKOV3 (R) and CaOV3 (R) cells stably expressing shRNA targeting control or human CPEB4 were routinely cultured for 3 days. The polyadenylation of CSAG2 mRNA **(G)**, and the protein level **(H)** and mRNA level **(I)** of CSAG2 were analyzed as in **(C–E)**. Data are mean ± SEM. $n = 3$. NS, not significant.

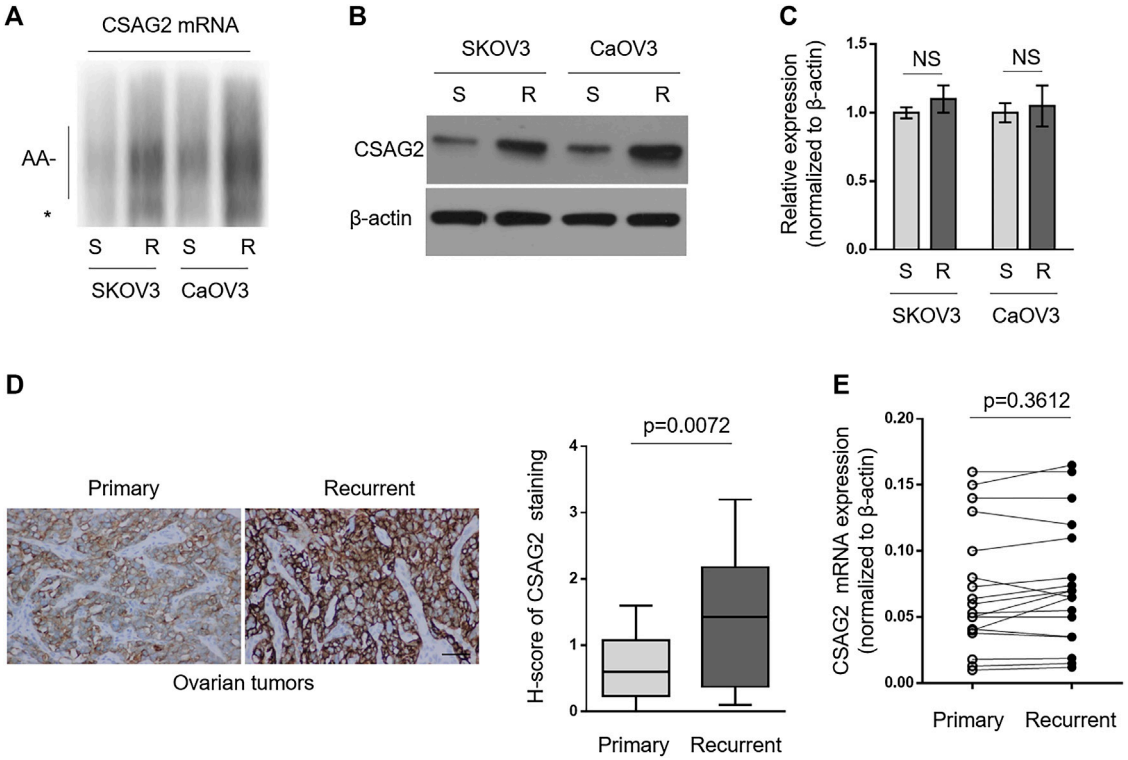


**FIGURE 4 |** CSAG2 is more polyadenylated and translated by CPEB4 in paclitaxel-resistant ovarian cancer cells and recurrent ovarian tumors. **(A–C)** Cells of SKOV3 (R), SKOV3 (S), CaOV3 (S), CaOV3 (R) were routinely cultured for 3 days. **(A)** Total RNAs were extracted and the polyadenylation was assessed as described before. *, non-adenylated RNAs; AA-, adenylated RNAs. **(B)** The protein level of CSAG2 in cell lysates was analyzed by Western blotting. β-Actin was used as a loading control, and representative images are shown. **(C)** The mRNA of CSAG2 was analyzed by qRT-PCR. β-Actin was used as a reference control. Data are mean ± SEM. $n = 3$. NS, not significant. **(D)** Representative images **(left)** of immunohistochemical staining of CSAG2 from matched primary and recurrent ovarian tumors treated with paclitaxel-based chemotherapy. Scale bar, 50 μm. H-score **(right)** of CSAG2 staining is used to semi-quantify its expression levels. The black line inside the box is the median, and the lines above and below the box indicate the maximum and minimum of the H-scores. Each group contained 18 paired samples. **(E)** The mRNA levels of CPEB4 in matched primary and recurrent ovarian tumors **(D)** were analyzed by qRT-PCR. β-Actin was used as a reference control. Each symbol represents the mean value of three replicates.

in these cells (**Figure 3G**), and accordingly, CSAG2 expression was decreased (**Figure 3H**), and its transcript level remained unchanged (**Figure 3I**). Therefore, these findings indicate that CPEB4 can bind with CSAG2 mRNA and induce cytoplasmic polyadenylation and translationally control its expression.

## CSAG2 Is More Polyadenylated and Translated by CPEB4 in Paclitaxel-Resistant Ovarian Cancer Cells and Recurrent Ovarian Tumors

Since paclitaxel-resistant ovarian cancer cells have higher expression level of CPEB4 (**Figures 1A,B**), together with the results mentioned above (**Figure 3**), we speculated that CSAG2 mRNA maybe more polyadenylated and expressed in paclitaxel-resistant ovarian cancer cells than that of naïve sensitive ones. As expected, anchored RT-PCR analysis revealed that poly(A) tail of CSAG2 mRNA was longer in KOV3 (R) and CaOV3 (R) cells (**Figure 4A**). Consistently, its protein level was increased (**Figure 4B**) and transcript level was not obviously affected (**Figure 4C**). Furthermore, keeping in line with these observations, CSAG2 showed stronger immunoreactive staining (**Figure 4D**, left) and higher H-score (**Figure 4D**, right) in recurrent tumors than that of primary tumors, and similarly, its transcript level did not show significant change (**Figure 4E**). Taken together, these data suggest that, due to different CPEB4 levels, CSAG2 expression is differentially regulated by CPEB4-mediated translational control in paclitaxel-resistant ovarian cancer cells and recurrent ovarian tumors compared with their counterparts, which leads to CSAG2 accumulation in resistant cells.

## CSAG2 Knockdown Attenuates CPEB4-Mediated Paclitaxel Resistance in Ovarian Cancer Cells

We then asked whether CSAG2 mediates the promotive effect of CPEB4 on paclitaxel resistance in ovarian cancer cells. CSAG2 was silenced by siRNA in KOV3 (S) cells

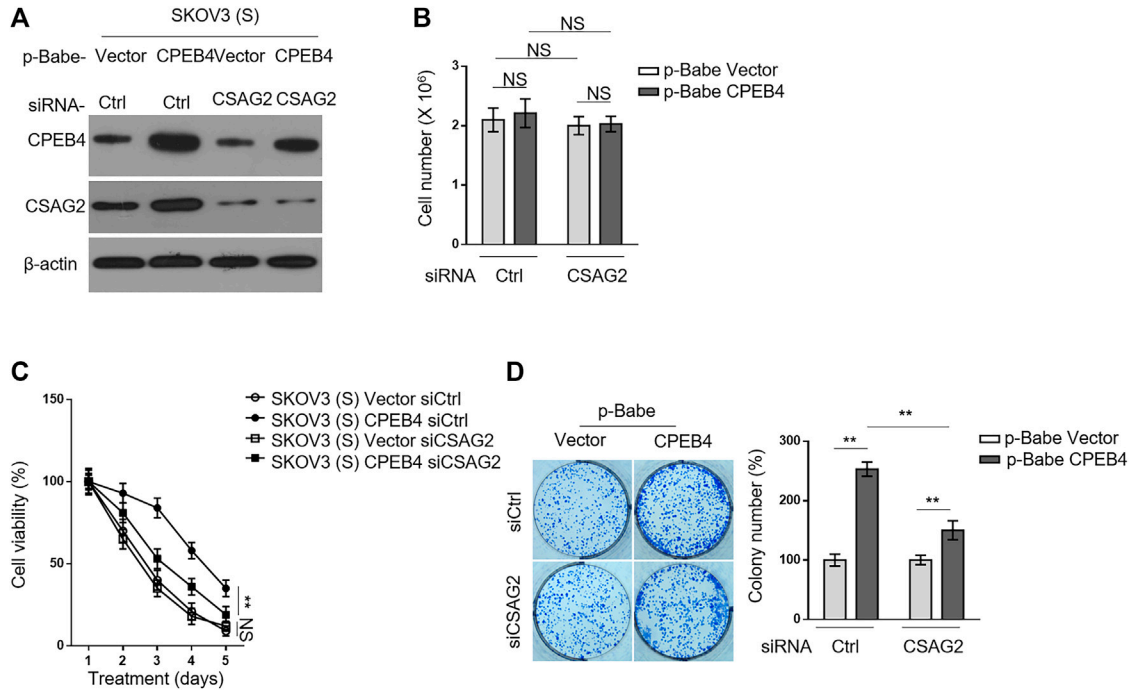


**FIGURE 5 |** CSAG2 knockdown attenuates CPEB4-mediated paclitaxel resistance in ovarian cancer cells. **(A)** Cells of SKOV3 (S) and CaOV3 (S) stably expressing empty vector or human CPEB4 were transfected with siRNA targeting control or CSAG2, and further cultured for 3 days. The protein levels of were analyzed by Western blotting. β-Actin was used as a loading control. The representative images are shown. **(B)** Cells were treated as in **(A)**, and the viable cell number was counted by Trypan blue staining to exclude unviable cells. Data represent mean ± SEM. $n = 3$. NS, not significant. **(C)** Cells were treated as in **(A)**, and then treated with 20 nM PTX for indicated periods of time. The viable cell number relative to DMSO treated group is shown. Data represent mean ± SEM. $n = 3$. $^{**}p < 0.01$; NS, not significant. **(D)** Cells were treated as in **(A)**, and then further cultured with 20 nM PTX for 2 weeks. Representative images of cells stained with crystal violet are shown **(left)**. The colony number was quantified by ImageJ **(right)**, and results relative to vector are shown. Data are mean ± SEM. $n = 3$. $^{**}p < 0.01$.

overexpressing CPEB4 (**Figure 5A**), and these manipulations did not *per se* affect cell proliferation or survival under untreated condition (**Figure 5B**). On the other side, CSAG2 silencing significantly attenuated the survival advantage conferred by CPEB4 overexpression when treated with paclitaxel, although did not completely reduce to the extent of two vector groups (**Figure 5C**), at any rate, suggesting that CSAG2 knockdown attenuates CPEB4-mediated paclitaxel resistance in ovarian cancer cells. Notably, this effect of CSAG2 seems contextual, since CSAG2 silencing did not apparently affect paclitaxel resistance in vector groups (**Figure 5C**). Consistently, similar tendency was obtained when examining the effect of CSAG2 knockdown on CPEB4-mediated advantages for colony formation (**Figure 5D**), further strengthening the notion that CSAG2 at least in part contributes to CPEB4-mediated paclitaxel resistance in ovarian cancer.

## DISCUSSION

Understanding the mechanisms of paclitaxel resistance is of great importance for developing effective therapeutic strategies to treat paclitaxel-resistant ovarian cancer. Our study provides biological basis and preclinical relevance that likely support a novel mechanism underpinning the paclitaxel resistance in ovarian cancer *in vitro*, in which CEPB4 is connected to the enhancement of paclitaxel resistance by its translational control of inducing CSAG2 expression, and thereby, uncovering the promotive function of CEPB4/CSAG2 axis in paclitaxel resistance in ovarian cancer. Deduced from our findings, it is possible that ovarian cancer cells may develop paclitaxel resistance through upregulating CEPB4 and thereafter inducing translational expression of CSAG2. Presumably, the higher levels of CEPB4 and CSAG2 this population of paclitaxel-resistant cells have, the more resistant these cells may respond to paclitaxel chemotherapy. If this is indeed the case and also applicable for paclitaxel resistance acquired by ovarian cancer after paclitaxel chemotherapy, the therapeutic strategy targeting CEPB4/CSAG2 axis, such as genetically reducing their expression or chemically inhibiting their activities, may thus be of potential clinical benefits for reducing paclitaxel resistance and enhancing the cytotoxic response of ovarian cancer to paclitaxel treatment.

The key aspect of the above proposition appears to rely on the activation of CEPB4 expression in ovarian cancer cells. In this study, in addition to paclitaxel-resistant ovarian cancer cell lines, SKOV3 and CaOV3, we also found that CPEB4 was upregulated at transcript and protein levels in recurrent ovarian tumors after treatment of paclitaxel-based chemotherapy, suggesting a molecular mechanism

that transcriptionally regulates its expression induction is announced in ovarian cancer in response to paclitaxel. However, cautions are needed here when drawing a further conclusion about its clinical relevance, because the recurrent ovarian tumors were obtained from patients treated with cisplatin and paclitaxel combination chemotherapy. To date, although no reports have associated cisplatin with paclitaxel resistance in ovarian cancer, its possible effect can not be easily excluded. Therefore, to better relate CEPB4 upregulation to paclitaxel resistance, examining CEPB4 expression in recurrent ovarian tumors receiving paclitaxel monotherapy may provide a more direct evidence to demonstrate the specificity of this phenotype. Alternatively, at an opposite direction, future studies investigating whether CEPB4 responds to cisplatin treatment could also aid the estimation of its effect on paclitaxel.

On the other hand, however, the appearance of CEPB4 upregulation in ovarian cancer cells treated with paclitaxel seems to take a relatively long period of time, since CPEB4 upregulation was not observed as an acute responding mechanism, at least within 72 h observed in our study, to paclitaxel exposure. In other words, certain responsive mechanisms occurring at later phase may be responsible for its induction. However, at present, much less is known concerning the mechanisms controlling CEPB4 transcription.

CEPB4 is an RNA binding protein that controls meiotic mRNA cytoplasmic polyadenylation and translation (Novoa et al., 2010). Its role in cancer is barely investigated, until recently its overexpression in pancreatic ductal adenocarcinomas and glioblastomas was reported, where it could support tumor growth, vascularization and invasion by translational activation of mRNAs including the tissue plasminogen activator (Ortiz-Zapater et al., 2011). In addition, its upregulated expression in human glioma (Hu et al., 2015), breast cancer (Sun et al., 2015), astrocytic tumor (Chen W. et al., 2016) hepatocellular carcinoma (Tsai et al., 2016), colorectal carcinoma (Cortes-Guiral et al., 2017), has been correlated with disease progression and poor prognosis. These studies suggest a pro-oncogenic role of CEPB4 in tumorigenesis. One previous study has shown that the enhancer region of CEPB4 gene binds with transcriptional factors Gata1 and Tal1, and during terminal erythroid differentiation, Gata1 and Tal1 induce its transcription (Hu et al., 2014). Moreover, CPEB4 gene could also be directed by p53 transcriptional targets (Zaccara et al., 2014). Whether these regulatory circuitries are responsible for CEPB4 upregulation in paclitaxel-resistant ovarian cancer cells and recurrent ovarian tumors needs intensive investigations. In functional studies, we found that CPEB4 promoted paclitaxel resistance in ovarian cancer cells *in vitro*. In despite of the largely unclear role of CPEB4 in ovarian cancer progression, our study reveals its connection to paclitaxel resistance in ovarian cancer.

By using RIP assay, followed by validation, we demonstrate that the mRNA of CSAG2, one protein closely related to paclitaxel resistance in ovarian cancer, binds with CEPB4. Although CSAG2 has been associated with paclitaxel resistance in ovarian cancer *in vitro* and in clinic study (Materna et al., 2007), its specific functions remain elusive and contradictory (Duan et al., 1999). In this study, we validate CSAG2 as a paclitaxel-resistant protein. CSAG2 is more polyadenylated and translated by CPEB4 in paclitaxel-resistant ovarian cancer cells and recurrent ovarian tumors, and this post-transcriptional regulation of CSAG2 by CPEB4 has a causal link to paclitaxel resistance, because CSAG2 knockdown attenuates CPEB4-mediated paclitaxel resistance in ovarian cancer cells. Nevertheless, the unsolved question is how CSAG2 exerts resistance response to paclitaxel treatment. In a latest study, CSAG2 was demonstrated necessary for proliferation and tumorigenesis *in vivo*, and CSAG2-stimulated SIRT1 activity to enhance p53 deacetylation was shown to inhibit p53 transcriptional activity, leading to improved cell survival under genotoxic stress (Yang and Potts, 2020). We speculate this regulatory circuit may be one of the mechanisms through which CSAG2 promotes paclitaxel resistance in ovarian cancer. Another critical issue needs to be addressed is whether CPEB4-regulated paclitaxel resistance *via* CSAG2 in ovarian cancer can be reproduced with *in vivo* scenarios. Elucidating these issues would not only help us to deeply understand paclitaxel resistance in ovarian cancer, but also develop a rational therapeutic treatment targeting active CEPB4/CSAG2 axis in paclitaxel-resistant ovarian cancer.

## DATA AVAILABILITY STATEMENT

The raw data supporting the conclusions of this article will be made available by the authors, without undue reservation.

## ETHICS STATEMENT

The studies involving human participants were reviewed and approved by Ethics Committee of Medical College of Northwest Minzu University. The patients/participants provided their written informed consent to participate in this study.

## AUTHOR CONTRIBUTIONS

Conception and design: JZ and YZ; Provision of study materials or patients: XM; Collection and assembly of data: RH; Data analysis and interpretation: XX; Manuscript writing and final approval of manuscript: All authors.

## FUNDING

This work was supported by Fundamental Research Funds for the Central Universities (Grant No. 31920200030 and 31920190210), the Science and Technology Development Project of Lanzhou city Chengguan District (No. 2018-1-10) and the National Natural Science Foundation of China (NSFC, No. 81860716).

## SUPPLEMENTARY MATERIAL

The Supplementary Material for this article can be found online at: https://www.frontiersin.org/articles/10.3389/fphar.2020.600994/full#supplementary-material.

## REFERENCES


Alam, A., Kowal, J., Broude, E., Roninson, I., and Locher, K. P. (2019). Structural insight into substrate and inhibitor discrimination by human P-glycoprotein. *Science*. 363 (6428), 753–756. doi:10.1126/science.aav7102

Au Yeung, C. L., Co, N. N., Tsuruga, T., Yeung, T. L., Kwan, S. Y., Leung, C. S., et al. (2016). Exosomal transfer of stroma-derived miR21 confers paclitaxel resistance in ovarian cancer cells through targeting APAF1. *Nat. Commun*. 7, 11150. doi:10.1038/ncomms11150

Cao, G., Chen, D., Liu, G., Pan, Y., and Liu, Q. (2018). CPEB4 promotes growth and metastasis of gastric cancer cells *via* ZEB1-mediated epithelial-mesenchymal transition. *OncoTargets Ther*. 11, 6153–6165. doi:10.2147/OTT.S175428

Chen, W., Hu, Z., Li, X. Z., Li, J. L., Xu, X. K., Li, H. G., et al. (2016). CPEB4 interacts with Vimentin and involves in progressive features and poor prognosis of patients with astrocytic tumors. *Tumor Biol*. 37 (4), 5075–5087. doi:10.1007/s13277-015-3975-0

Chen, Y., Tsai, Y. H., and Tseng, S. H. (2016). Regulation of the expression of cytoplasmic polyadenylation element binding proteins for the treatment of cancer. *Anticancer Res*. 36 (11), 5673–5680. doi:10.21873/anticanres.11150

Cortés-Guiral, D., Pastor-Iodate, C., Díaz Del Arco, C., Del Puerto-Nevado, L., and Fernández-Aceñero, M. J. (2017). CPEB4 immunohistochemical expression is associated to prognosis in stage IV colorectal carcinoma. *Pathol. Res. Pract*. 213 (6), 639–642. doi:10.1016/j.prp.2017.04.020

Duan, Z., Feller, A. J., Toh, H. C., Makastorsis, T., and Seiden, M. V. (1999). TRAG-3, a novel gene, isolated from a taxol-resistant ovarian carcinoma cell line. *Gene*. 229 (1–2), 75–81. doi:10.1016/s0378-1119(99)00042-6

Harvey, R. F., Smith, T. S., Mulroney, T., Queiroz, R. M. L., Pizzinga, M., Dezi, V., et al. (2018). Trans-acting translational regulatory RNA binding proteins. *Wiley Interdiscip. Rev. RNA*. 9 (3), e1465. doi:10.1002/wrna.1465

Hu, W., Yang, Y., Xi, S., Sai, K., Su, D., Zhang, X., et al. (2015). Expression of CPEB4 in human glioma and its correlations with prognosis. *Medicine (Baltimore)*. 94 (27), e979. doi:10.1097/MD.0000000000000979

Hu, W., Yuan, B., and Lodish, H. F. (2014). Cpeb4-mediated translational regulatory circuitry controls terminal erythroid differentiation. *Dev. Cell*. 30 (6), 660–672. doi:10.1016/j.devcel.2014.07.008

Hu, Y., Li, Y., Huang, Y., Jin, Z., Wang, C., Wang, H., et al. (2020). METTL3 regulates the malignancy of cervical cancer *via* post-transcriptional regulation of RAB2B. *Eur. J. Pharmacol*. 879, 173134. doi:10.1016/j.ejphar.2020.173134

Jayson, G. C., Kohn, E. C., Kitchener, H. C., and Ledermann, J. A. (2014). Ovarian cancer. *Lancet*. 384 (9951), 1376–1388. doi:10.1016/S0140-6736(13)62146-7

Kang, D., Lee, Y., and Lee, J. S. (2020). RNA-binding proteins in cancer: functional and therapeutic perspectives. *Cancers (Basel)*. 12 (9), 2699. doi:10.3390/cancers12092699

Lage, H., and Denkert, C. (2007). Resistance to chemotherapy in ovarian carcinoma. *Recent Results Cancer Res*. 176, 51–60. doi:10.1007/978-3-540-46091-6_6

Lu, Y., Li, T., Wei, G., Liu, L., Chen, Q., Xu, L., et al. (2016). The long non-coding RNA NEAT1 regulates epithelial to mesenchymal transition and radioresistance in through miR-204/ZEB1 axis in nasopharyngeal carcinoma. *Tumor Biol*. 37 (9), 11733–11741. doi:10.1007/s13277-015-4773-4

Materna, V., Surowiak, P., Kaplenko, I., Spaczyński, M., Duan, Z., Zabel, M., et al. (2007). Taxol-resistance-associated gene-3 (TRAG-3/CSAG2) expression is predictive for clinical outcome in ovarian carcinoma patients. *Virchows Arch*. 450 (2), 187–194. doi:10.1007/s00428-006-0346-7

Mendez, R., and Richter, J. D. (2001). Translational control by CPEB: a means to the end. *Nat. Rev. Mol. Cell Biol*. 2 (7), 521–529. doi:10.1038/35080081

Novoa, I., Gallego, J., Ferreira, P. G., and Mendez, R. (2010). Mitotic cell-cycle progression is regulated by CPEB1 and CPEB4-dependent translational control. *Nat. Cell Biol*. 12 (5), 447–456. doi:10.1038/ncb2046

Ortiz-Zapater, E., Pineda, D., Martínez-Bosch, N., Fernández-Miranda, G., Iglesias, M., Alameda, F., et al. (2011). Key contribution of CPEB4-mediated translational control to cancer progression. *Nat. Med*. 18 (1), 83–90. doi:10.1038/nm.2540

Piqué, M., López, J. M., Foissac, S., Guigó, R., and Méndez, R. (2008). A combinatorial code for CPE-mediated translational control. *Cell*. 132 (3), 434–448. doi:10.1016/j.cell.2007.12.038

Siegel, R. L., Miller, K. D., and Jemal, A. (2017). Cancer statistics, 2017. *CA Cancer J. Clin*. 67 (1), 7–30. doi:10.3322/caac.21387

Sun, H. T., Wen, X., Han, T., Liu, Z. H., Li, S. B., Wang, J. G., et al. (2015). Expression of CPEB4 in invasive ductal breast carcinoma and its prognostic significance. *OncoTargets Ther*. 8, 3499–3506. doi:10.2147/OTT.S87587

Tsai, L. Y., Chang, Y. W., Lee, M. C., Chang, Y. C., Hwang, P. I., Huang, Y. S., et al. (2016). Biphasic and stage-associated expression of CPEB4 in hepatocellular carcinoma. *PLoS One*. 11 (5), e0155025. doi:10.1371/journal.pone.0155025

Wallin, J. J., Bendell, J. C., Funke, R., Sznol, M., Korski, K., Jones, S., et al. (2016). Atezolizumab in combination with bevacizumab enhances antigen-specific T-cell migration in metastatic renal cell carcinoma. *Nat. Commun*. 7, 12624. doi:10.1038/ncomms12624

Wurth, L., Papasaikas, P., Olmeda, D., Bley, N., Calvo, G. T., Guerrero, S., et al. (2016). UNR/CSDE1 drives a post-transcriptional program to promote melanoma invasion and metastasis. *Cancer Cell*. 30 (5), 694–707. doi:10.1016/j.ccell.2016.10.004

Yang, C. H., Yap, E. H., Xiao, H., Fiser, A., and Horwitz, S. B. (2016). 2-(m-Azidobenzoyl) taxol binds differentially to distinct β-tubulin isotypes. *Proc. Natl. Acad. Sci. U.S.A*. 113 (40), 11294–11299. doi:10.1073/pnas.1613286113

Yang, X., and Potts, P. R. (2020). CSAG2 is a cancer-specific activator of SIRT1. *EMBO Rep*. 21 (9), e50912. doi:10.15252/embr.202050912

Zaccara, S., Tebaldi, T., Pederiva, C., Ciribilli, Y., Bisio, A., and Inga, A. (2014). p53-directed translational control can shape and expand the universe of p53 target genes. *Cell Death Differ*. 21 (10), 1522–1534. doi:10.1038/cdd.2014.79

Zhijun, L., Dapeng, W., Hong, J., Guicong, W., Bingjian, Y., and Honglin, L. (2017). Overexpression of CPEB4 in glioma indicates a poor prognosis by promoting cell migration and invasion. *Tumor Biol*. 39 (4), 1–9. doi:10.1177/1010428317694538


**Conflict of Interest:** The authors declare that the research was conducted in the absence of any commercial or financial relationships that could be construed as a potential conflict of interest.

frontiers in Pharmacology

ORIGINAL RESEARCH
published: 14 January 2021
doi: 10.3389/fphar.2020.584450

# IQGAP3 Overexpression Correlates With Poor Prognosis and Radiation Therapy Resistance in Breast Cancer

*Xin Hua*[1,2†], *Zhi-Qing Long*[1,2†], *Ling Guo*[1,3], *Wen Wen*[1,3], *Xin Huang*[1], *Wen-Wen Zhang*[1,2*] *and Huan-Xin Lin*[1,2*]

[1]State Key Laboratory of Oncology in South China, Collaborative Innovation Center for Cancer Medicine, Sun Yat-Sen University Cancer Center, Guangzhou, China, [2]Department of Radiotherapy, Sun Yat-Sen University Cancer Center, Guangzhou, China, [3]Department of Nasopharyngeal Carcinoma, Sun Yat-Sen University Cancer Center, Guangzhou, China

OPEN ACCESS

**Edited by:**
Dexin Kong,
Tianjin Medical University, China

**Reviewed by:**
Peir-In Liang,
Kaohsiung Medical University Hospital, Taiwan
Chia-Che Chang,
National Chung Hsing University, Taiwan

***Correspondence:**
Wen-Wen Zhang
zhangww@sysucc.org.cn
Huan-Xin Lin
linhx@sysucc.org.cn

[†]These authors have contributed equally to this work

**Specialty section:**
This article was submitted to Pharmacology of Anti-Cancer Drugs, a section of the journal Frontiers in Pharmacology

**Received:** 17 July 2020
**Accepted:** 15 October 2020
**Published:** 14 January 2021

**Citation:**
Hua X, Long Z-Q, Guo L, Wen W, Huang X, Zhang W-W and Lin H-X (2021) IQGAP3 Overexpression Correlates With Poor Prognosis and Radiation Therapy Resistance in Breast Cancer. Front. Pharmacol. 11:584450. doi: 10.3389/fphar.2020.584450

**Background:** IQ motif-containing GTPase activating protein 3 (IQGAP3), the latest identified member of the IQGAP family, may act as a crucial factor in cancer development and progression; however, its clinical value in breast cancer remains unestablished. We explored the correlation between IQGAP3 expression profile and the clinicopathological features in breast cancer.

**Methods:** IQGAP3 mRNA and protein levels were detected in breast cancer cell lines and tumor tissues by real-time PCR and western blotting and compared to the normal control groups. Protein expression of IQGAP3 was also evaluated immunohistochemically in archived paraffin-embedded specimens from 257 breast cancer patients, and the associations between IQGAP3 expression level, clinical characteristics, and prognosis were analyzed. We assessed the relationship between IQGAP3 expression and sensitivity to radiation therapy which was determined by subgroup analysis.

**Results:** IQGAP3 was significantly upregulated in breast cancer cell lines and human tumor tissues at both the mRNA and protein level compared to controls. Additionally, high levels of IQGAP3 expression were detected in 110/257 (42.8%) of archived paraffin-embedded breast cancer specimens. High IQGAP3 expression level was significantly related to clinical stage ($p$ = 0.001), T category ($p$ = 0.002), N category ($p$ = 0.001), locoregional recurrence ($p$ = 0.002), distant metastasis ($p$ = 0.001), and vital status ($p$ = 0.001). Univariate and multivariate statistical analysis showed that IQGAP3 expression was an independent prognostic factor among all 257 breast cancer patients in our cohort ($p$ = 0.003, $p$ = 0.001). Subgroup analysis revealed IQGAP3 expression correlated with radioresistance and was also an independent predictor of radiotherapy outcome.

**Conclusion:** Our findings suggest that high IQGAP3 expression predicts poor prognosis and radioresistance in breast cancer. Therefore, IQGAP3 may be a reliable prognostic biomarker in breast cancer and could be used to identify patients who may benefit from radiotherapy.

**Keywords: breast cancer, IQGAP3, prognosis, radiation therapy, resistance**

## INTRODUCTION

Breast cancer is the most frequent malignancy in women and the second leading cause of cancer-related deaths worldwide (Siegel et al., 2015). Radiotherapy (RT) is an indispensable part of the systemic therapeutic regimen for breast cancer, yet locoregional recurrence and distant metastasis remain key problems, resulting in poor survival (Gerber et al., 2010). Locoregional recurrence results from the presence or evolution of radioresistant tumor cells for which standard fractionated RT doses are sublethal (Speers et al., 2015). Currently, there is a dearth of clinically available predictive biomarkers to indicate the optimal radiation dosing in breast cancer, which leads to suboptimal treatment of these patients (Coates et al., 2015). Therefore, biomarkers associated with disease prognosis and RT sensitivity are required to optimize RT treatment plans and improve outcomes among breast cancer patients.

IQ motif-containing GTPase activating protein 3 (IQGAP3), the latest identified member of the IQGAP family, is an evolutionarily conserved GTPase-activating protein (Wang et al., 2007) and a hotspot for gene amplification in tumors. IQGAPs comprise five conserved domains: an IQ domain with four IQ motifs (IQ), a poly-proline protein-protein domain (WW), a calponin homology domain (CHD), a RasGAP-related domain (GRD), and a carboxy-terminal domain (RasGAPC) (Briggs and Sacks, 2003). Multiple proteins interact with these domains to regulate diverse cellular processes, including cell migration, cytokinesis, vesicle trafficking, cell proliferation, intracellular signaling, and cytoskeletal dynamics (Nojima et al., 2008).

Overexpression of IQGAP3 has been observed in lung, liver, pancreatic, and gastric cancer (Yang et al., 2014; Xu et al., 2016; Oue et al., 2017; Shi et al., 2017). Recently, IQGAP3 expression was found to be related to clinical stage and was an independent prognostic classifier of gastric cancer patients. Additionally, IQGAP3 knockdown was shown to reduce the number and size of the spheres formed by a gastric cancer cell line (MKN-74) and inhibited the phosphorylation of Akt and Erk1/2 (11). In hepatocellular carcinoma, IQGAP3 was reported to function as an important regulator of epithelial-mesenchymal transition (EMT) and metastasis by activating the transforming growth factor (TGF)-β signaling pathway (Shi et al., 2017). Regarding breast cancer, IQGAP3 knockdown inhibited cell proliferation and invasion in two breast carcinoma cell-lines (Hu et al., 2016). These reports provide some clues about IQGAP3 expression changes in several cancer types and the role of IQGAP3 in tumor development. However, the correlation between IQGAP3 expression and prognosis or RT sensitivity in breast cancer remained unclear.

Therefore, we investigated the expression pattern of IQGAP3 in breast cancer cell lines compared to control cell lines, as well as in patient tissues and matched adjacent normal tissues. We also analyzed the association of IQGAP3 protein expression with the survival outcomes and RT sensitivity in breast cancer patient cases.

## MATERIALS AND METHODS

### Microarray Data

We performed integrative analyses on the Cancer Genome Atlas (TCGA) data for Breast Invasive Carcinoma-BRCA (Ye et al., 2016). mRNA expression data [mRNA fragments per kilobase transcript per million mapped reads (FPKM)] and matched clinical metadata (n = 1,208, 113 normal breast samples and 1,095 breast cancer samples) were acquired from the TCGA data portal https://portal.gdc.cancer.gov/projects/TCGA-BRCA. The FPKM data were first transformed into transcripts per million data for better comparison and edgeR package was used to normalize gene expression, and then the IQGAP3 expression value was extracted (Lv et al., 2019). Breast cancer patients who received RT were then divided into a radioresistant group (n = 115, who showed disease progression via locoregional recurrence) and a radiosensitive group (n = 600, without disease progression) according to their response to RT treatment.

### Cell Lines

Breast cancer cell lines, including MCF-10A, ZR-75-1, SK-BR-3, MDA-MB-468, MDA-MB-453, MCF-7, BT-474, MDA-MB-231, BT-549, HCC1937, SUM159PT, Hs-578T, and ZR-75-30, were cultured in DMEM medium (Gibco, Grand Island, NY) supplemented with 10% fetal bovine serum (FBS; HyClone, Logan, UT).

### Patients and Tissue Specimens

A total of 257 paraffin-embedded breast cancer tissue samples with histologically confirmed invasive carcinoma of no-specific-type breast cancer were collected from 2006 to 2008 at Sun Yat-sen University Cancer Center (SYSUCC), Guangzhou, China. In addition, six paired breast cancer and adjacent normal tissues were collected from patients who had undergone surgery from 2017 to 2018 at our center. All samples were frozen and stored in liquid nitrogen until further use. All patients received surgery and 201 (78.2%) received RT after surgery. The recommended indications for postoperative RT were involvement of ≥4 axillary nodes, primary tumor ≥5 cm in size, post-breast-conserving surgery, positive surgical margins, the involvement of internal mammary node (in selected cases, n = 3), and the involvement of one to three axillary nodes (in selected cases, n = 15). Clinicopathological classification and staging were determined according to the criteria of the American Joint Committee on Cancer (AJCC 2010; seventh edition). This study was approved by the Clinical Research Ethics Committee of SYSUCC, and written informed consent was obtained from each patient.

### PCR

We used quantitative real-time PCR (qRT-PCR) to evaluate mRNA expression of IQGAP3 in 12 breast cancer cell lines and a control cell line (MCF-10A), as well as in six tumor tissues and adjacent normal control tissues obtained from breast cancer patients. Total RNA samples from cell lines and freshly frozen tissues were isolated using TRIzol reagent

(Invitrogen, Carlsbad, CA, USA) following the manufacturer's recommendations. qRT-PCR was performed according to previously described standard methods, using GADPH as a control (Liu et al., 2017). All primers were designed using Primer Express version 2.0 software (Applied Biosystems, Foster City, CA, USA) as follows: IQGAP3 forward: 5′-ATG AGCAGAGGCGGCAGAAT-3′, reverse: 5′-GAACCACGG AGGGTGCAAAA-3′, GAPDH forward: 5′-GTCTCCTCT GACTTCAACAGCG-3′, and reverse: 5′-ACCACCCTGTTG CTGTAGCCAA-3′. IQGAP3 expression levels were normalized to the geometric mean of GAPDH and calculated using $2^{-[(\text{Ct of IQGAP3})-(\text{Ct of GAPDH})]}$, where Ct represents the threshold cycle for each transcript. Each experiment was performed in triplicate.

## Western Blot

Western blot analysis was used to evaluate IQGAP3 protein expression in all 12 breast cancer cell lines and the control cell line (MCF-10A), as well as in six tumor tissue samples and adjacent normal tissues from breast cancer patients. Western blotting was carried out as described previously (Li et al., 2008) using the anti-IQGAP3 antibody (Abcam, Cambridge, MA). The membranes were stripped and reprobed with an anti-α-tubulin antibody (Sigma, Saint Louis, MI) as a loading control.

## Immunohistochemistry

Immunohistochemistry (IHC) and quantification of IQGAP3 expression were performed by two independent pathologists, as previously described (Song et al., 2012) using an anti-IQGAP3 antibody (1:1,000; Sigma, Saint Louis, MI). The percentage of cancer cells was scored as 1 (<10%), 2 (10–50%), 3 (50–75%), or 4 (>75%), and the staining intensity was sorted into four grades: 0 (no staining), 1 (weak staining, light yellow), 2 (moderate staining, yellow brown), and 3 (intense staining, brown). The scores for the staining intensity and proportion in each section were multiplied. The best cutoff value for IQGAP3 was defined by receiver operating curve (ROC) analysis with respect to overall survival: a staining score≥6 was classified as high expression and a score≤4 as low IQGAP3 expression.

## Gene Set Enrichment Analysis

Gene set enrichment analysis (GSEA, http://software.broadinstitute.org/gsea/index.jsp) was used to predict potential hallmarks using transcriptional sequences in the TCGA database. GSEA was performed on the gene list and ranked according to a moderated t-statistics (Ritchie et al., 2015), comparing patients with high and low IQGAP3 expression. A permutation test (of 1,000 times) was used to identify the significantly changed pathways (Subramanian et al., 2005).

## Statistical Analysis

All statistical analyses were conducted using SPSS (version 20.0; IBM Corporation, Armonk, NY, USA), and the survival curves were drawn using the GraphPad Prism 6.0 Software. The Pearson's $\chi^2$ tests or Fisher exact tests were used to analyze the associations between IQGAP3 expression and clinicopathological features. The Kaplan-Meier method and log-rank test were used to calculate and compare the curve survival curves. Multivariate analysis was performed via a Cox's proportional hazards model. A two-sided $p$-value of <0.05 was considered statistically significant.

# RESULTS

## IQGAP3 Expression Is Elevated in Breast Cancer Cell Lines

We found IQGAP3 mRNA levels were increased in tumor samples compared with normal tissues by analyzing the publicly available microarray TCGA data for breast cancer (**Figure 1A**). Additionally, we found IQGAP3 expression was elevated at both the mRNA and protein level in all 12 breast cancer cell lines compared with the MCF-10A control cell line (**Figure 2A**). Higher IQGAP3 expression was also detected at the mRNA and protein level in breast cancer tissues compared to adjacent normal tissues from six different patients (**Figure 2B**). Together, these results indicated IQGAP3 is overexpressed in breast cancer cell lines and tissues.

## IQGAP3 Overexpression Correlates With the Clinicopathological Features of Breast Cancer

Next, we investigated whether IQGAP3 overexpression levels in 257 cases of breast cancer specimens (detected via IHC) were associated with patients' clinicopathological features. Among the 257 breast cancer cases, 21 were in stage Ⅰ (8.2%), 32 were in stage Ⅱ (12.5%), and 204 were in stage Ⅲ (79.4%). A total of 110 samples (42.8%) had a higher level of IQGAP3 protein level expression (staining was strongly positive). A lower expression level (staining was weakly positive or negative) was found in 147 samples (57.2%, **Table 1**). Positive IQGAP3 staining was observed mainly in the cancer cell nuclei (**Figure 3**). IQGAP3 overexpression significantly correlated with the following characteristics: clinical stage ($p$ = 0.001), T category ($p$ = 0.010), N category ($p$ = 0.001), distant metastasis ($p$ = 0.001), locoregional recurrence ($p$ = 0.002), and vital status ($p$ = 0.001; **Table 1**).

## High IQGAP3 Expression Is Significantly Associated With Poor Prognosis in Breast Cancer

In the entire cohort, the 5-year overall survival (OS), locoregional recurrence-free survival (LRFS), and distant metastasis-free survival (DMFS) rates were as follows: 76.9%, 90.7%, and 71.9%, respectively. The cumulative 5-year OS, LRFS, and DMFS rates for patients with high IQGAP3 expression were 58.3%, 83.2%, and 50.8%, respectively, compared with 89.9%, 96.1%, and 88.2%, respectively, for patients with low IQGAP3 expression ($p$ = 0.001, **Figure 4A**; $p$ = 0.001, **Figure 4B**; and $p$ = 0.001, **Figure 4C**).

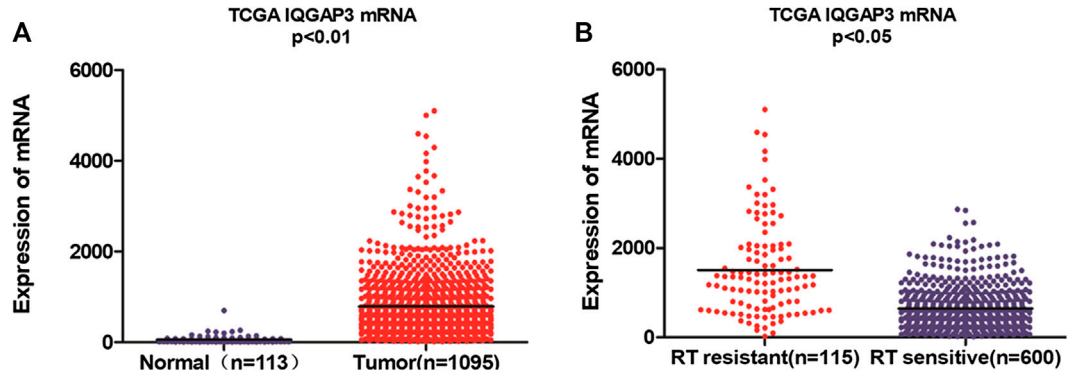


**FIGURE 1 |** Microarray data reveals IQGAP3 is upregulated in breast cancer patients and in cases that are resistant to radiotherapy (RT). **(A)** Expression of IQGAP3 in TCGA (breast invasive carcinoma) tumor and normal tissue data (Mann–Whitney test; $p < 0.01$). **(B)** Expression of IQGAP3 in TCGA (breast invasive carcinoma) including RT-resistant and RT-sensitive cases (Mann–Whitney test; $p < 0.05$).

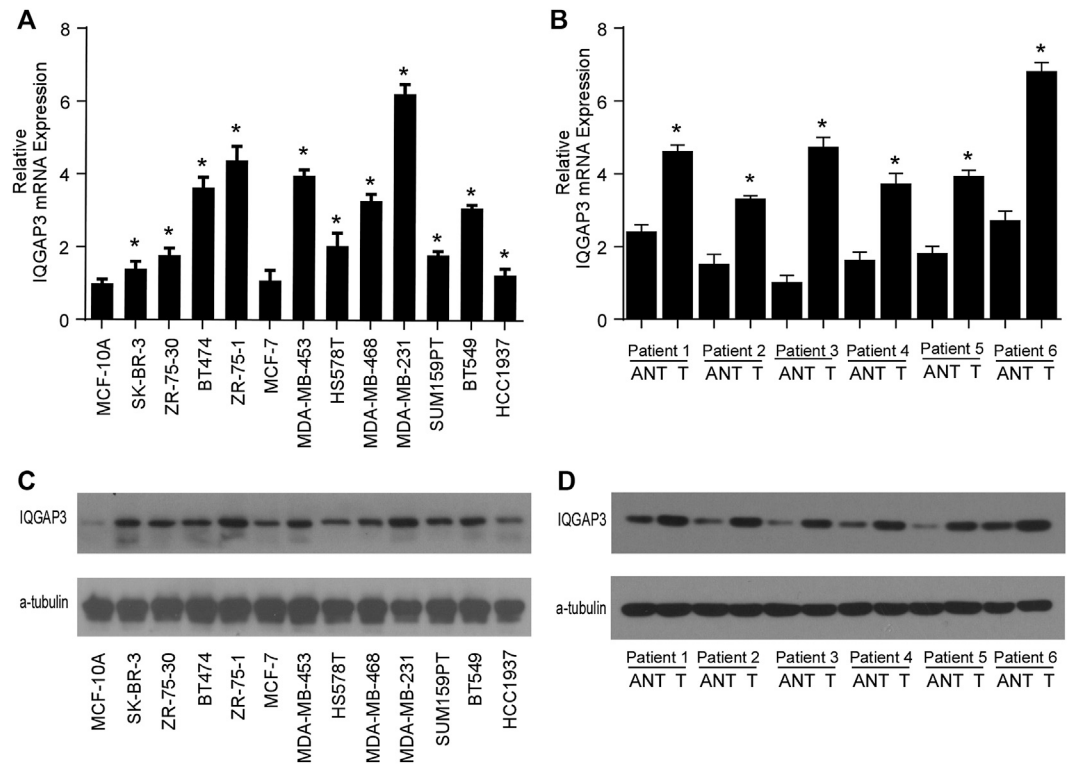


**FIGURE 2 |** IQGAP3 is upregulated in breast cancer cell lines and tissues. **(A)** Quantitative real-time PCR analysis of IQGAP3 mRNA expression in MCF-10A immortalized breast epithelial cells and twelve cultured breast cancer cell lines. GAPDH was used as a loading control. *$p < 0.05$. **(B)** Real-time PCR analysis of IQGAP3 mRNA expression in six paired breast cancer tumor tissues and adjacent normal tissues (ANT). GAPDH was used as a loading control. *$p < 0.05$. **(C)** Western blotting analysis of IQGAP3 protein expression in MCF-10A immortalized breast epithelial cells and twelve cultured breast cancer cell lines. α-tubulin was used as a loading control. **(D)** Western blotting analysis of IQGAP3 protein expression in six paired breast cancer tumor tissues and adjacent normal tissues (ANT). α-tubulin was used as a loading control.

We also evaluated the prognostic, predictive value of IQGAP3 overexpression in the RT subgroup (n = 201). IQGAP3 overexpression significantly correlated with poor OS, LRFS, and DMFS in patients who had undergone RT ($p = 0.001$, **Figure 4D**; $p = 0.003$, **Figure 4E**; and $p = 0.001$, **Figure 4F**). This data demonstrates that breast cancer patients with high levels of IQGAP3 show poor survival even after RT.

**TABLE 1 |** Association between IQGAP3 expression and clinicopathological features of breast cancer (n = 257).

| Feature | Total (n = 257) | IQGAP3 | | P |
|---|---|---|---|---|
| | | Low expression | High expression | |
| Age (y) | | | | |
| ≥45 | 138 (53.7%) | 78 (56.5%) | 60 (43.5%) | 0.899 |
| <45 | 119 (46.3%) | 69 (58.0%) | 50 (42.0%) | |
| T classification | | | | |
| 1 | 53 (20.6%) | 34 (64.2%) | 19 (35.8%) | **0.010** |
| 2 | 132 (51.4%) | 83 (62.9%) | 49 (37.1%) | |
| 3 | 42 (16.3%) | 20 (47.6%) | 22 (52.4%) | |
| 4 | 30 (11.7%) | 10 (33.3%) | 20 (66.7%) | |
| N classification | | | | |
| 0 | 38 (14.8%) | 27 (71.1%) | 11 (28.9%) | **0.001** |
| 1 | 28 (10.9%) | 21 (75.0%) | 7 (25.0%) | |
| 2 | 102 (39.7%) | 65 (63.7%) | 37 (36.3%) | |
| 3 | 89 (34.6%) | 34 (38.2%) | 55 (61.8%) | |
| Clinical stage | | | | |
| I | 21 (8.2%) | 14 (66.7%) | 7 (33.3%) | **0.001** |
| II | 32 (12.5%) | 27 (84.4%) | 5 (15.6%) | |
| III | 204 (79.4%) | 106 (52.0%) | 98 (48.0%) | |
| Locoregional recurrence | | | | |
| yes | 23 | 6 | 17 | **0.002** |
| no | 234 | 141 | 93 | |
| Distant metastasis | | | | |
| Yes | 72 | 18 | 54 | **0.001** |
| No. | 185 | 129 | 56 | |
| Vital status | | | | |
| Alive | 203 (79.0%) | 134 (66.0%) | 69 (34.0%) | **0.001** |
| Dead | 54 (21.0%) | 13 (24.1%) | 41 (75.9%) | |
| Treatment | | | | |
| Radiotherapy | 201 (78.2%) | 114 (56.7%) | 87 (43.2%) | 0.879 |
| | 56 (21.8%) | 33 (58.9%) | 23 (41.1%) | |
| Nonradiotherapy | | | | |

*P:* t *test with two independent samples.*

## IQGAP3 Overexpression Is an Independent Negative Prognostic Factor in Breast Cancer

Univariate Cox regression analysis showed that the T category, N category, estrogen receptor (ER) status, progesterone receptor (PR) status, and IQGAP3 expression were significantly associated with survival in breast cancer patients. Multivariate survival analysis also indicated IQGAP3 expression was indeed an independent prognostic factor for OS and progression-free survival (PFS; $p$ = 0.003 and $p$ = 0.001, respectively; **Table 2**) in the whole cohort breast cancer patients (n = 257). Multivariate survival analysis in the RT subgroup (n = 201) showed that IQGAP3 expression remained an independent prognostic factor for OS and PFS ($p$ = 0.002 and $p$ = 0.001, respectively; **Table 3**). These results suggest that IQGAP3 may be an independent prognostic factor of breast cancer treatment outcome, especially for patients who have undergone RT.

## IQGAP3 Overexpression Significantly Correlates With Radioresistance in Breast Cancer

Breast cancer patients who received RT were divided according to their response to treatment into a radioresistant group (who showed disease progression via locoregional recurrence) and a radiosensitive group (without disease progression). We first analyzed the public microarray TCGA data of breast cancer and found IQGAP3 was overexpressed in radioresistant samples (n = 115) compared to radiosensitive samples (n = 600; **Figure 1B**).

To confirm whether IQGAP3 is overexpressed in radioresistant breast cancer patients, we also examined IQGAP3 expression in 159 post-RT patients (radioresistant group n = 19; radiosensitive group n = 140) using IHC. IQGAP3 was overexpressed in radioresistant breast cancer patients compared to radiosensitive patients (**Figure 5**).

## IQGAP3 Overexpression Is an Independent Prognosis Factor for Radiation Therapy Outcome in Breast Cancer

Through subgroup analysis of the 159 post-RT cases, we discovered IQGAP3 overexpression was correlated with an obviously shorter radioresistance-free survival (RRFS). Univariate Cox regression analyses showed that IQGAP3 expression, T stage, N stage, ER, and PR were significant prognostic factors for RT outcome ($p$ = 0.012, $p$ = 0.005, $p$ = 0.005, $p$ = 0.001, and $p$ = 0.001, respectively; **Table 4**). IQGAP3 overexpression remained an independent prognostic factor for shorter RRFS in multivariate analysis (HR: 3.321; 95% CI: 1.135–9.716; $p$ = 0.028).

## IQGAP3 Overexpression May Promote DNA Damage Repair and Lead to Radiotherapy Resistance by Modulating the PI3K/AKT/mTOR Pathway

To examine the mechanism of IQGAP3 in the development of breast cancer radioresistance, we performed GSEA. We found IQGAP3 expression is positively correlated with DNA repair gene signatures (HALLMARK_DNA_REPAIR) and phosphatidylinositol-4,5-bisphosphate 3-kinase (PI3K) signaling-activated gene signatures (HALLMARK_PI3K_AKT_MTOR_SIGNALING) in TCGA published gene expression profiles (**Figure 6**).

# DISCUSSION

Growing evidence suggests IQGAP3 is overexpressed in various tumors, including melanoma, pancreatic cancer, gastric cancer, bladder cancer, hepatocellular carcinoma, and breast cancer (Yang et al., 2014; Hu et al., 2016; Xu et al., 2016; Oue et al., 2017; Shi et al., 2017). IQGAP3 has also been suggested to help in screening and diagnosis by acting as a biomarker in hepatocellular carcinoma (Qian et al., 2016). Furthermore, recent studies showed that IQGAP3 overexpression accelerates cell proliferation and invasion in several tumors, indicating it may play a role in cancer progression (Yang et al., 2014; Hu et al., 2016; Kumar et al., 2017). However, its role in breast cancer remained vague until now. To the best of our knowledge, this is the first

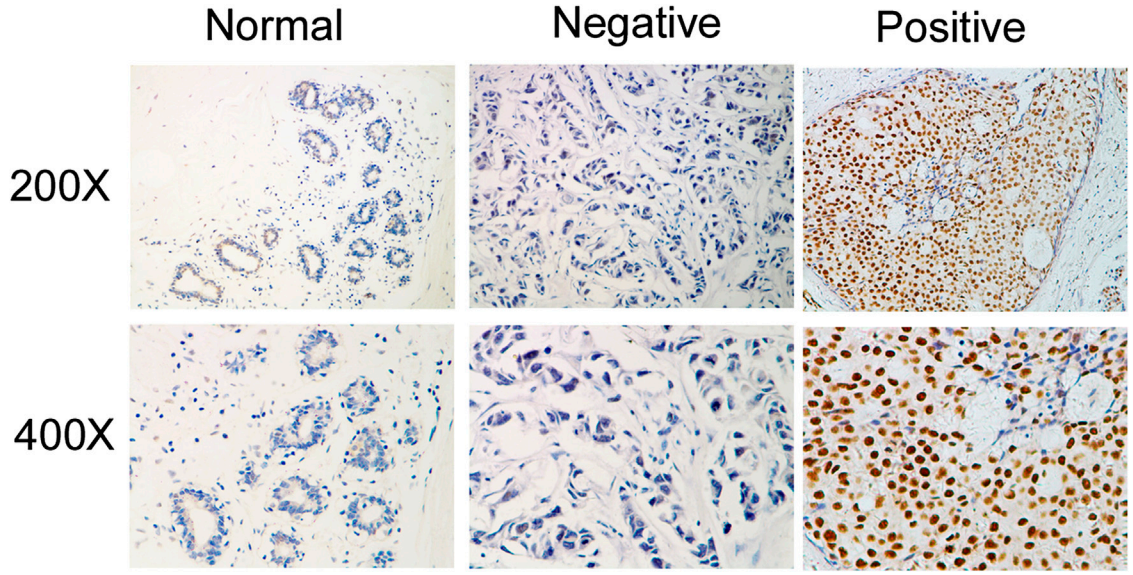


**FIGURE 3 |** Immunohistochemical detection of IQGAP3 expression in paraffin-embedded breast cancer tissues. Representative images of immunohistochemical staining for IQGAP3 in normal breast tissues (controls) and breast tumor tissues are shown.

**TABLE 2 |** Association of clinicopathological features with overall survival and progression-free survival in breast cancer patients (n = 257).

| Feature | Univariate analysis | *P* | Multivariate cox regression analysis | *P* |
|---|---|---|---|---|
| | Regression coefficient (SE) | | Hazard ratio (95% CI) | |
| OS | | | | |
| Age (y) | | | | |
| ≥45 vs. < 45 | 0.018 (0.014) | 0.197 | — | — |
| T stage | | | | |
| T 1 vs. 2 vs. 3 vs. 4 | 0.665 (0.143) | **0.001** | 1.823 (1.346–2.470) | **0.001** |
| N stage | | | | |
| N 0 vs. 1 vs. 2 | 0.984 (0.211) | **0.001** | 2.074 (1.395–3.084) | **0.001** |
| Estrogen receptor | | | | |
| ER (–) vs. (+) | –1.514 (0.309) | **0.001** | 0.206 (0.105–0.404) | **0.001** |
| Progesterone receptor | | | | |
| PR (–) vs. (+) | –0.810 (0.270) | **0.003** | 1.287 (0.712–2.326) | 0.403 |
| Human epidermal growth factor receptor type 2 | | | | |
| Her2 (–) vs. (+) | 0.382 (0.249) | 0.125 | — | — |
| IQGAP3 expression | | | | |
| Low vs. high | 1.606 (0.319) | **0.001** | 2.723 (1.419–5.224) | **0.003** |
| PFS | | | | |
| Age (y) | | | | |
| ≥45 vs. < 45 | 0.020 (0.011) | 0.0073 | — | — |
| T stage | | | | |
| T 1 vs. 2 vs. 3 vs. 4 | 0.585 (0.118) | **0.001** | 1.592 (1.238–2.047) | **0.001** |
| N stage | | | | |
| N 0 vs. 1 vs. 2 | 0.868 (0.163) | **0.001** | 1.866 (1.377–2.528) | **0.001** |
| ER | | | | |
| ER (–) vs. (+) | –1.315 (0.245) | **0.001** | 0.314 (0.177–0.559) | **0.001** |
| PR | | | | |
| PR (–) vs. (+) | –0.882 (0.226) | **0.001** | 1.023 (0.600–1.746) | 0.933 |
| Her2 | | | | |
| Her2 (–) vs. (+) | 0.467 (0.205) | **0.023** | 1.248 (0.750–2.076) | 0.393 |
| IQGAP3 expression | | | | |
| Low vs. high | 1.673 (0.265) | **0.001** | 3.160 (1.822–5.482) | **0.001** |

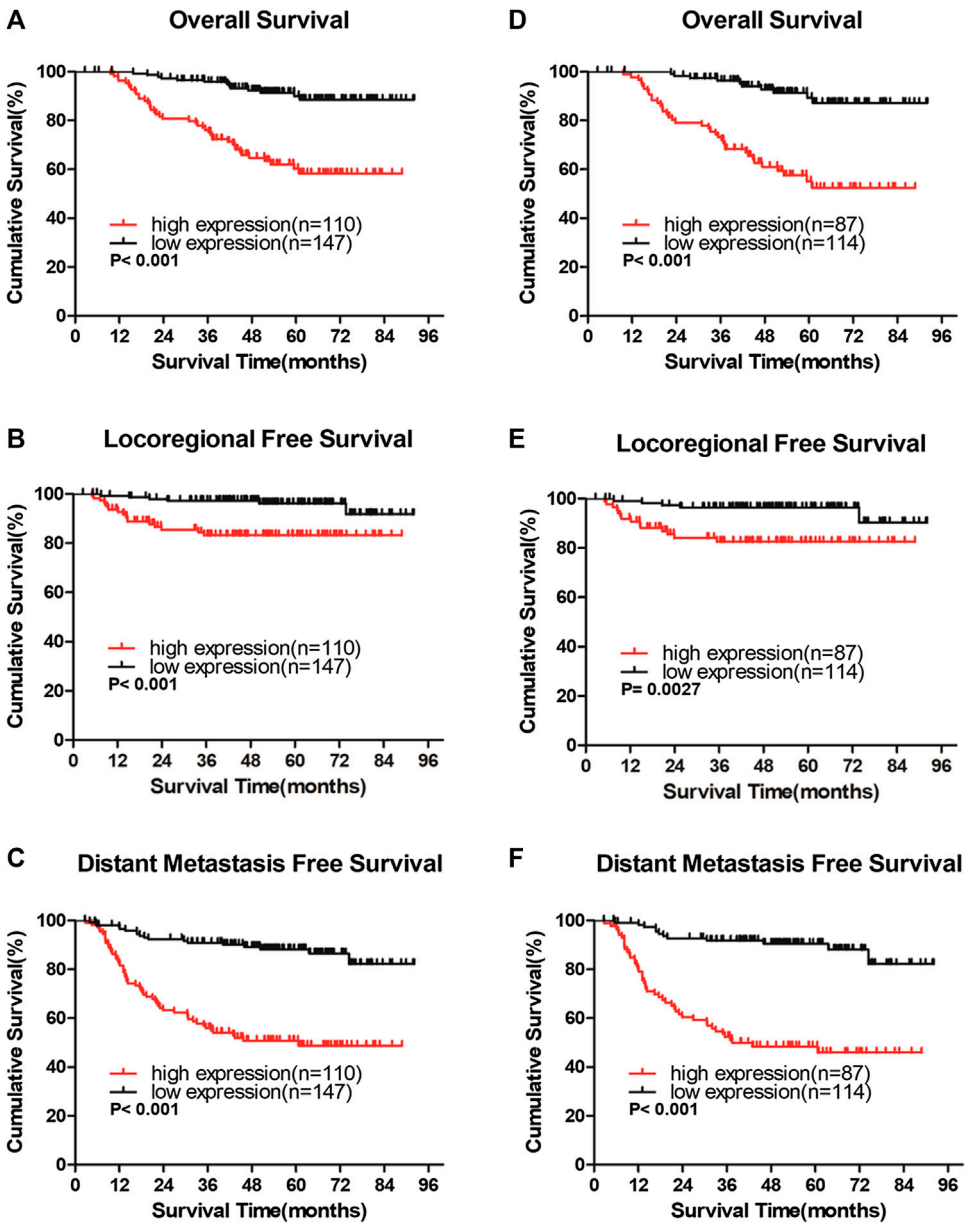


**FIGURE 4 |** IQGAP3 protein expression is associated with clinical outcomes in the whole cohort of breast cancer cases and in the radiotherapy (RT) subgroup **(A and B,C)**. Kaplan–Meier overall survival **(A)**, locoregional recurrence-free survival **(B)**, and distant metastasis-free survival **(C)** curves for all 257 patients with breast cancer stratified by high IQGAP3 expression (n = 110) vs. low IQGAP3 expression (n = 147) **(D and E,F)**. Kaplan–Meier overall survival **(D)**, locoregional recurrence-free survival **(E)**, and distant metastasis free survival **(F)** curves for RT subgroup of 201 patients stratified by high IQGAP3 expression (n = 87) vs. low IQGAP3 expression (n = 114). *p* values were calculated using the log-rank test.

study to confirm an association between IQGAP3 expression and disease prognosis and RT sensitivity in breast cancer.

Previous studies have shown that IQGAP3 may promote and accelerate cancer development *in vitro*. For example, IQGAP3 knockdown inhibited proliferation and ERK activity in cultured epithelial cells (Nojima et al., 2008); IQGAP3 was also found to activate EGFR–ERK signaling and, thus, promote the metastasis of lung cancer cells (Yang et al., 2014). Furthermore, in two pancreatic cancer cell lines (BXPC-3 and SW1990), IQGAP3 knockdown inhibited cell proliferation, migration, and invasion and induced cell apoptosis (Xu et al., 2016). Moreover, silencing IQGAP3 was found to inhibit the proliferation, motility, and invasion of breast cancer cell lines (Hu et al., 2016). Consistent with this study involving breast cancer cell lines, the present research provides evidence that IQGAP3 expression may have important clinical significance in breast cancer.

We confirmed IQGAP3 was overexpressed both at the mRNA level (transcriptionally) and protein level (translationally) in

**TABLE 3 |** Association of clinicopathological features with overall survival and progression-free survival in breast cancer patients undergoing radiotherapy (n = 201).

| Feature | Univariate analysis | *P* | Multivariate cox regression analysis | *P* |
|---|---|---|---|---|
| | Regression coefficient (SE) | | Hazard ratio (95%CI) | |
| **OS** | | | | |
| Age (y) | | | | |
| ≥45 vs. < 45 | −0.002 (0.015) | 0.909 | — | — |
| T stage | | | | |
| T 1 vs. 2 vs. 3 vs. 4 | 0.642 (0.160) | **0.001** | 1.851 (1.322–2.593) | **0.001** |
| N stage | | | | |
| N 0 vs. 1 vs. 2 | 0.863 (0.228) | **0.001** | 1.755 (1.156–2.662) | **0.008** |
| Estrogen receptor | | | | |
| ER (−) vs. (+) | −1.561 (0.345) | **0.001** | 0.181 (0.085–0.385) | **0.001** |
| Progesterone receptor | | | | |
| PR (−) vs. (+) | −0.852 (0.295) | **0.004** | 1.315 (0.689–2.509) | 0.406 |
| Human epidermal growth factor receptor type 2 | | | | |
| Her2 (−) vs. (+) | 0.227 (0.290) | 0.433 | - | - |
| IQGAP3 expression | | | | |
| Low vs. high | 1.745 (0.358) | **0.001** | 3.159 (1.515–6.586) | **0.002** |
| **PFS** | | | | |
| Age (y) | | | | |
| ≥45 vs. < 45 | 0.005 (0.013) | 0.702 | — | — |
| T stage | | | | |
| T 1 vs. 2 vs. 3 vs. 4 | 0.558 (0.137) | **0.001** | 1.611 (1.207–2.150) | **0.001** |
| N stage | | | | |
| N 0 vs. 1 vs. 2 | 0.836 (0.191) | **0.001** | 1.677 (1.183–2.377) | **0.004** |
| ER | | | | |
| ER (−) vs. (+) | −1.386 (0.285) | **0.010** | 0.293 (0.151–0.568) | **0.010** |
| PR | | | | |
| PR (−) vs. (+) | −0.994 (0.258) | **0.028** | 0.947 (0.515–1.739) | 0.860 |
| Her2 | | | | |
| Her2 (−) vs. (+) | 0.462 (0.245) | **0.023** | 1.216 (0.683–2.166) | 0.506 |
| IQGAP3 expression | | | | |
| Low vs. high | 1.867 (0.313) | **0.001** | 3.813 (1.995–7.286) | **0.001** |

**TABLE 4 |** Association of clinicopathological features with radioresistance-free survival in breast cancer cases resistant to radiation therapy (n = 159).

| Feature | Univariate analysis | *P* | Multivariate cox regression analysis | *P* |
|---|---|---|---|---|
| | Regression coefficient (SE) | | Hazard ratio (95%CI) | |
| RRFS | | | | |
| Age (y) | | | | |
| ≥45 vs. < 45 | 0.009 (0.023) | 0.690 | — | — |
| T stage | | | | |
| T 1 vs. 2 vs. 3 vs. 4 | 0.612 (0.245) | **0.012** | 1.613 (0.964–2.700) | 0.069 |
| N stage | | | | |
| N 0 vs. 1 vs. 2 | 1.029 (0.364) | **0.005** | 1.901 (0.973–3.715) | 0.060 |
| ER | | | | |
| ER (−) vs. (+) | −1.370 (0.493) | **0.005** | 0.445 (0.142–1.400) | 0.166 |
| PR | | | | |
| PR (−) vs. (+) | −1.801 (0.520) | **0.001** | 0.365 (0.107–1.240) | 0.106 |
| Her2 | | | | |
| Her2 (−) vs. (+) | 0.429 (0.441) | 0.331 | - | - |
| IQGAP3 expression | | | | |
| Low vs. high | 1.831 (0.521) | **0.001** | 3.321 (1.135–9.716) | **0.028** |

breast cancer cell lines and human tumor samples compared to noncancerous breast epithelial cells and tissues. IQGAP3 overexpression significantly correlated with the following characteristics: gender, clinical stage, T category, N category, vital status, and distant metastasis. Moreover, patients with high IQGAP3 expression were more likely to exhibit locoregional recurrence and distant metastasis, indicating that IQGAP3 protein expression promotes the

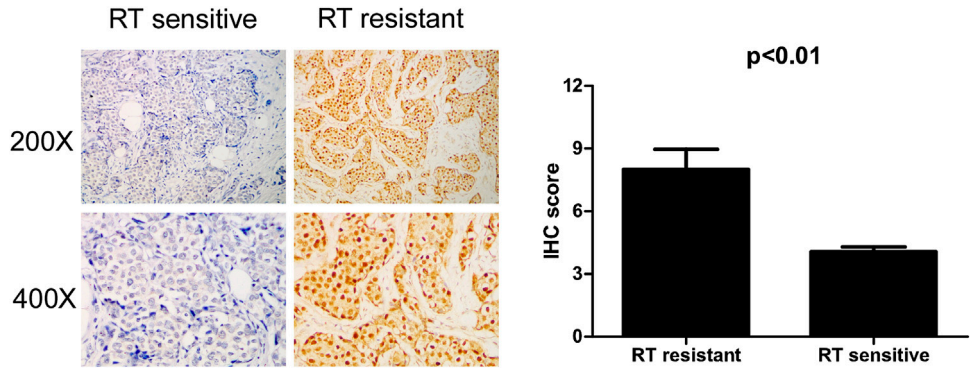


**FIGURE 5 |** Immunohistochemical (IHC) detection of IQGAP3 expression in paraffin-embedded breast cancer tissues in the radiotherapy- (RT-) sensitive and RT-resistant subgroups. Left panel: representative images of IHC staining for IQGAP3 in the RT-resistant and RT-sensitive tissues. Right panel: average IHC score of IQGAP3 in the RT-resistant (n = 19) and RT-sensitive tissues (n = 140).

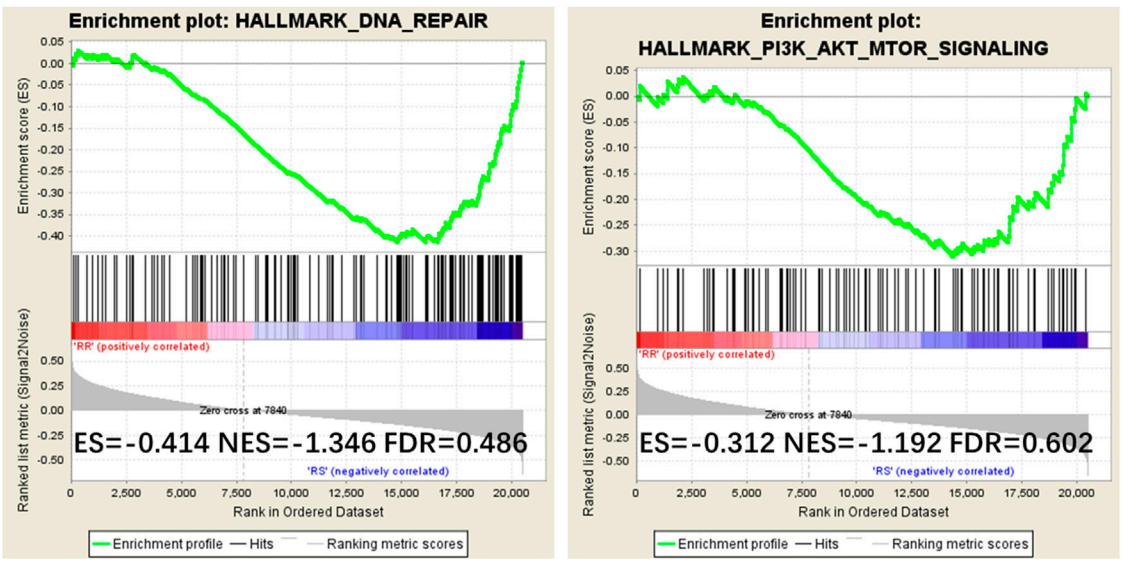


**FIGURE 6 |** Gene Set Enrichment Analysis (GSEA) plots showing that IQGAP3 expression correlates positively with DNA repair gene signatures (HALLMARK_DNA_REPAIR) and PI3K signaling-activated gene signatures (HALLMARK_PI3K_AKT_MTOR_SIGNALING) in the published Cancer Genome Atlas (TCGA) breast invasive carcinoma gene expression profiles.

progression of breast cancer. We also found a significant association between high IQGAP3 expression and poorer 5-year OS, LRFS, and DMFS in both the entire cohort and the RT-treated subgroup. Together, this evidence suggests that IQGAP3 contributes to the development and progression of breast cancer.

Breast cancer recurrence ranges from 10 to 41%, depending on T status, N status, and tumor grade (Pan et al., 2017). Compared to other thoracic tumors, innate or acquired radioresistance leads to locoregional recurrence and results in treatment failure. Therefore, radioresistance represents a formidable clinical problem in the systematic treatment regimen of breast cancer. However, no reliable biomarkers are currently available to identify patients who may be radioresistant before undergoing RT in breast cancer. We found IQGAP3 was strongly positively associated with radioresistance, and high IQGAP3 protein expression significantly correlated with shorter LRFS and OS, even after RT treatment. Therefore, IQGAP3 may be a valuable biomarker to identify specific patients who need a more aggressive RT therapeutic regimen (such as a higher dose of radiation) to reduce locoregional recurrence and improve survival. Moreover, our multivariate analysis confirmed IQGAP3 was an independent prognostic factor for RRFS in the subgroup analysis of radiosensitive breast cancer cases. In conclusion, IQGAP3 may be a reliable novel predictive biomarker of radioresistance and poor survival in breast cancer patients

following RT. It can be a potential marker to determine RT effect in the future, in addition to other traditional risk factors, like young age, vessel invasion, and a low number of examined axillary lymph nodes.

Tumor cellular exposure to radiation results in damage to DNA and other cellular structures, which then triggers a complex cascade of downstream response pathways in both the nucleus and cytoplasm, including DNA repair, cell cycle modulation, reactive oxygen species defense, cytokine production, and apoptosis (Pajic et al., 2018). In certain tumor cell subpopulations, these pathways can be innately biased towards a radioresistant, prosurvival phenotype (i.e., a phenotype with accelerated cell cycle arrest, reduced proliferation, more efficient or prolonged DNA repair, or dampened apoptotic signaling) (Gewirtz et al., 2009; Karar and Maity, 2009; Goldstein and Kastan, 2015). Indeed, IQGAP3 was found to bind to the Ras protein (Nojima et al., 2008), which plays a role in cell cycle arrest, DNA repair, proliferation, and antiapoptosis in human cancers (Simanshu et al., 2017). Studies have also shown that IQGAP3 can regulate certain signaling pathways and cellular functions (Hedman et al., 2015), including mitogen-activated protein kinase (MAPK) signaling, Ca2+/calmodulin signaling, cell–cell adhesion, β-catenin-mediated transcription, and microbial invasion.

To further examine the mechanism of IQGAP3 in the development of breast cancer radioresistance, we performed GSEA and found IQGAP3 expression positively correlates with DNA repair gene signatures (HALLMARK_DNA_REPAIR) and phosphatidylinositol-4,5-bisphosphate 3-kinase (PI3K) signaling-activated gene signatures (HALLMARK_PI3K_AKT_MTOR_SIGNALING) in published TCGA gene expression profiles. The PI3K signaling pathway is regulated by Ras; that is, the direct binding of Ras to the catalytic p110 subunit can directly activate PI3K. The PI3K pathway may contribute to the repair, regrowth, redistribution, and reoxidation of cells after RT. As per evidence, Fan et al. demonstrated that increased expression of PI3K in the breast cancer cell line MDA-DB-453 after RT not only protects cells from apoptosis but also significantly enhances their DNA repair ability (Fan et al., 2001). In addition, reducing PI3K signaling with a PI3K inhibitor (LY294002) after RT can lead to G2/M cell cycle arrest in a breast cell line MCF-7 (Shtivelman et al., 2002). Based on the above-mentioned evidence, we assume that high levels of IQGAP3, combined with Ras, may promote radioresistance in breast cancer by modulating the PI3K signaling pathway. Although many PI3K inhibitors are currently undergoing investigation in clinical trials, CAL-101 was the first PI3K inhibitor to be approved by the US Food and Drug Administration and the European Medicines Agency for the treatment of different types of leukemia in 2014 (Bendell et al., 2012; Shapiro et al., 2014).

There are some limitations to our study. First, it was a retrospective study, and the cohort size was not sufficiently large. Second, we lack direct evidence to support the role(s) of IQGAP3 in breast cancer progression and radioresistance. Therefore, further biochemical studies into the precise mechanism(s) of action of IQGAP3 are warranted.

## CONCLUSION

This study shows IQGAP3 is overexpressed in breast cancer cell lines and tissues and is associated with the clinicopathological features of the disease. Additionally, IQGAP3 overexpression correlates with radioresistance and significantly poorer prognosis. Therefore, IQGAP3 may be a reliable novel biomarker to provide personalized prognostication in breast cancer and could be used to identify patients who may benefit from more aggressive RT treatment to improve their survival.

## DATA AVAILABILITY STATEMENT

The data and materials of this study have been included at RDD (http://www.researchdata.org.cn/) with the number of RDDB2019000551.

## ETHICS STATEMENT

The studies involving human participants were reviewed and approved by the Clinical Research Ethics Committee of SYSUCC. The patients/participants provided their written informed consent to participate in this study.

## AUTHOR CONTRIBUTIONS

Conceptualization was done by W-WZ H-XL; methodology was conceptualized by XH and Z-QL; software was provided by XH Z-QL; validation was carried out by XH and WW; formal analysis was done by XH and H-XL; investigation was conducted by WW and W-WZ; resources were provided by LG, H-XL, and W-WZ; data curation was done by H-XL, WW, and Z-QL; writing (original draft preparation) was done by XH and Z-QL; writing (review and editing) was done by W-WZ and H-XL; visualization was carried out by LG and W-WZ; supervision was given by W-WZ and H-XL; W-WZ and H-XL was responsible for project administration; funding acquisition was carried out by LG, H-XL, and W-WZ; all authors have read and approved the paper.

## FUNDING

This work was partly supported by the National Natural Science Foundation of China (nos. 81773103, 81772877, and 81572848) and Natural Science Foundation of Guangdong Province (2017A030313617).

## ACKNOWLEDGMENTS

This manuscript has been released as a preprint at bioRxiv (Hua et al., 2018) and the abstract of this manuscript has been accepted as an oral presentation in ESMO ASIA annual meeting 2018. We would like to thank the native English speaking scientists of Elixigen Company (Huntington Beach, California) for editing our manuscript.

## REFERENCES


Bendell, J. C., Rodon, J., Burris, H. A., de Jonge, M., Verweij, J., Birle, D., et al. (2012). Phase I, dose-escalation study of BKM120, an oral pan-Class I PI3K inhibitor, in patients with advanced solid tumors. *J. Clin. Oncol.* 30 (3), 282–290. doi:10.1200/JCO.2011.36.1360

Briggs, M. W., and Sacks, D. B. (2003), IQGAP proteins are integral components of cytoskeletal regulation, *EMBO Rep*. 4 (6), 571–574. doi:10.1038/sj.embor.embor867

Coates, A. S., Winer, E. P., Goldhirsch, A., Gelber, R. D., Gnant, M., Piccart-Gebhart, M., et al. (2015). Tailoring therapies–improving the management of early breast cancer: st gallen international expert consensus on the primary therapy of early breast cancer 2015. *Ann. Oncol.* 26 (8), 1533–1546. doi:10.1093/annonc/mdv221

Fan, S., Ma, Y. X., Gao, M., Yuan, R. Q., Meng, Q., Goldberg, I. D., et al. (2001). The multisubstrate adapter Gab1 regulates hepatocyte growth factor (scatter factor)-c-Met signaling for cell survival and DNA repair. *Mol. Cell Biol.* 21 (15), 4968–4984. doi:10.1128/MCB.21.15.4968-4984.2001

Gerber, B., Freund, M., and Reimer, T. (2010). Recurrent breast cancer: treatment strategies for maintaining and prolonging good quality of life. *Dtsch Arztebl Int*. 107 (6), 85–91. doi:10.3238/arztebl.2010.0085

Gewirtz, D. A., Hilliker, M. L., and Wilson, E. N. (2009). Promotion of autophagy as a mechanism for radiation sensitization of breast tumor cells. *Radiother. Oncol.* 92 (3), 323–328. doi:10.1016/j.radonc.2009.05.022

Goldstein, M., and Kastan, M. B. (2015). The DNA damage response: implications for tumor responses to radiation and chemotherapy. *Annu. Rev. Med.* 66, 129–143. doi:10.1146/annurev-med-081313-121208

Hedman, A. C., Smith, J. M., and Sacks, D. B. (2015). The biology of IQGAP proteins: beyond the cytoskeleton. *EMBO Rep*. 16 (4), 427–446. doi:10.15252/embr.201439834

Hu, G., Xu, Y., Chen, W., Wang, J., Zhao, C., and Wang, M. (2016). RNA interference of IQ motif containing GTPase-activating protein 3 (IQGAP3) inhibits cell proliferation and invasion in breast carcinoma cells. *Oncol. Res*. 24 (6), 455–461. doi:10.3727/096504016x14685034103635

Hua, X., Long, Z-Q., Zhang, W-W., Lin, C., Sun, X-Q., Wen, W., et al. (2018). *IQGAP3 overexpression correlates with poor prognosis and radiation therapy resistance in breast cancer*. doi:10.1101/346163

Karar, J., and Maity, A. (2009). Modulating the tumor microenvironment to increase radiation responsiveness. *Canc. Biol. Ther*. 8 (21), 1994–2001. doi:10.4161/cbt.8.21.9988

Kumar, D., Hassan, M. K., Pattnaik, N., Mohapatra, N., and Dixit, M. (2017). Reduced expression of IQGAP2 and higher expression of IQGAP3 correlates with poor prognosis in cancers. *PloS One* 12 (10), e0186977. doi:10.1371/journal.pone.0186977

Li, J., Zhang, N., Song, L. B., Liao, W. T., Jiang, L. L., Gong, L. Y., et al. (2008). Astrocyte elevated gene-1 is a novel prognostic marker for breast cancer progression and overall patient survival. *Clin. Canc. Res*. 14 (11), 3319–3326. doi:10.1158/1078-0432.CCR-07-4054

Liu, S. L., Lin, H. X., Qiu, F., Zhang, W. J., Niu, C. H., Wen, W., et al. (2017). Overexpression of kinesin family member 20A correlates with disease progression and poor prognosis in human nasopharyngeal cancer: a retrospective analysis of 105 patients. *PloS One* 12 (1), e0169280. doi:10.1371/journal.pone.0169280

Lv, X., He, M., Zhao, Y., Zhang, L., Zhu, W., Jiang, L., et al. (2019). Identification of potential key genes and pathways predicting pathogenesis and prognosis for triple-negative breast cancer. *Canc. Cell Int*. 19, 172. doi:10.1186/s12935-019-0884-0

Nojima, H., Adachi, M., Matsui, T., Okawa, K., Tsukita, S., and Tsukita, S. (2008). IQGAP3 regulates cell proliferation through the Ras/ERK signalling cascade. *Nat. Cell Biol.* 10 (8), 971–978. doi:10.1038/ncb1757

Oue, N., Yamamoto, Y., Oshima, T., Asai, R., Ishikawa, A., Uraoka, N, et al. (2017). Overexpression of the transmembrane protein IQGAP3 is associated with poor survival of patients with gastric cancer, *Pathobiology* 85 (3), 192–200. doi:10.1159/000481890

Pajic, M., Froio, D., Daly, S., Doculara, L., Millar, E., Graham, P. H., et al. (2018). miR-139-5p modulates radiotherapy resistance in breast cancer by repressing multiple gene networks of DNA repair and ROS defense. *Canc. Res*. 78 (2), 501–515. doi:10.1158/0008-5472.CAN-16-3105

Pan, H., Gray, R., Braybrooke, J., Davies, C., Taylor, C., McGale, P., et al. (2017). 20-Year risks of breast-cancer recurrence after stopping endocrine therapy at 5 years. *N. Engl. J. Med*. 377 (19), 1836–1846. doi:10.1056/NEJMoa1701830

Qian, E. N., Han, S. Y., Ding, S. Z., and Lv, X. (2016). Expression and diagnostic value of CCT3 and IQGAP3 in hepatocellular carcinoma. *Canc. Cell Int*. 16, 55. doi:10.1186/s12935-016-0332-3

Ritchie, M. E., Phipson, B., Wu, D., Hu, Y., Law, C. W., Shi, W., et al. (2015). Limma powers differential expression analyses for RNA-sequencing and microarray studies. *Nucleic Acids Res*. 43 (7), e47. doi:10.1093/nar/gkv007

Shapiro, G. I., Rodon, J., Bedell, C., Kwak, E. L., Baselga, J., Brana, I., et al. (2014). Phase I safety, pharmacokinetic, and pharmacodynamic study of SAR245408 (XL147), an oral pan-class I PI3K inhibitor, in patients with advanced solid tumors. *Clin. Canc. Res*. 20 (1), 233–245. doi:10.1158/1078-0432.CCR-13-1777

Shi, Y., Qin, N., Zhou, Q., Chen, Y., Huang, S., Chen, B., et al. (2017). Role of IQGAP3 in metastasis and epithelial-mesenchymal transition in human hepatocellular carcinoma. *J. Transl. Med*. 15 (1), 176. doi:10.1186/s12967-017-1275-8

Shtivelman, E., Sussman, J., and Stokoe, D. (2002). A role for PI 3-kinase and PKB activity in the G2/M phase of the cell cycle. *Curr. Biol*. 12 (11), 919–924. doi:10.1016/s0960-9822(02)00843-6

Siegel, R. L., Miller, K. D., and Jemal, A. (2015). Cancer statistics. *CA Cancer J. Clin*. 65 (1), 5–29. doi:10.3322/caac.21254

Simanshu, D. K., Nissley, D. V., and McCormick, F. (2017). RAS proteins and their regulators in human disease. *Cell* 170 (1), 17–33. doi:10.1016/j.cell.2017.06.009

Song, L., Gong, H., Lin, C., Wang, C., Liu, L., Wu, J., et al. (2012). Flotillin-1 promotes tumor necrosis factor-alpha receptor signaling and activation of NF-kappaB in esophageal squamous cell carcinoma cells. *Gastroenterology* 143 (4), 995–e12. doi:10.1053/j.gastro.2012.06.033

Speers, C., Zhao, S., Liu, M., Bartelink, H., Pierce, L. J., and Feng, F. Y. (2015). Development and validation of a novel radiosensitivity signature in human breast cancer. *Clin. Canc. Res*. 21 (16), 3667–3677. doi:10.1158/1078-0432.CCR-14-2898

Subramanian, A., Tamayo, P., Mootha, V. K., Mukherjee, S., Ebert, B. L., Gillette, M. A., et al. (2005). Gene set enrichment analysis: a knowledge-based approach for interpreting genome-wide expression profiles. *Proc. Natl. Acad. Sci. USA*. 102 (43), 15545–15550. doi:10.1073/pnas.0506580102

Wang, S., Watanabe, T., Noritake, J., Fukata, M., Yoshimura, T., Itoh, N., et al. (2007). IQGAP3, a novel effector of Rac1 and Cdc42, regulates neurite outgrowth. *J. Cell Sci*. 120 (Pt 4), 567–577. doi:10.1242/jcs.03356

Xu, W., Xu, B., Yao, Y., Yu, X., Cao, H., Zhang, J., et al. (2016). Overexpression and biological function of IQGAP3 in human pancreatic cancer. *Am. J. Transl. Res*. 8 (12), 5421–5432.

Yang, Y., Zhao, W., Xu, Q. W., Wang, X. S., Zhang, Y., and Zhang, J. (2014). IQGAP3 promotes EGFR-ERK signaling and the growth and metastasis of lung cancer cells. *PLoS One* 9 (5), e97578. doi:10.1371/journal.pone.0097578

Ye, L., Guo, L., He, Z., Wang, X., Lin, C., Zhang, X., et al. (2016). Upregulation of E2F8 promotes cell proliferation and tumorigenicity in breast cancer by modulating G1/S phase transition. *Oncotarget* 7 (17), 23757–23771. doi:10.18632/oncotarget.8121


**Conflict of Interest:** The authors declare that the research was conducted in the absence of any commercial or financial relationships that could be construed as a potential conflict of interest.

frontiers in Pharmacology

ORIGINAL RESEARCH
published: 25 January 2021
doi: 10.3389/fphar.2020.610772

# Isorhamnetin Enhances the Radiosensitivity of A549 Cells Through Interleukin-13 and the NF-κB Signaling Pathway

*Yarong Du*[1,2], *Cong Jia*[1], *Yan Liu*[1], *Yehua Li*[1], *Jufang Wang*[2,3] *and Kun Sun*[1]*

[1]College of Life Science, Northwest Normal University, Lanzhou, China, [2]Key Laboratory of Space Radiobiology of Gansu Province & CAS Key Laboratory of Heavy Ion Radiation Biology and Medicine, Institute of Modern Physics, Chinese Academy of Sciences, Lanzhou, China, [3]School of Nuclear Science and Technology, University of Chinese Academy of Sciences, Beijing, China

Isorhamnetin (ISO), a naturally occurring plant flavonoid, is widely used as a phytomedicine. The major treatment modality for non-small-cell lung carcinoma (NSCLC) is radiotherapy. However, radiotherapy can induce radioresistance in cancer cells, thereby resulting in a poor response rate. Our results demonstrated that pretreatment with ISO induced radiosensitizing effect in A549 cells using colony formation, micronucleus, and γH2AX foci assays. In addition, ISO pretreatment significantly enhanced the radiation-induced incidence of apoptosis, the collapse of mitochondrial membrane potential, and the expressions of proteins associated with cellular apoptosis and suppressed the upregulation of NF-κBp65 induced by irradiation in A549 cells. Interestingly, the expression of interleukin-13 (IL-13), an anti-inflammatory cytokine, was positively correlated with the ISO-mediated radiosensitization of A549 cells. The knockdown of IL-13 expression by RNA interference decreased the IL-13 level and thus reduced ISO-mediated radiosensitivity in cells. We also found that the IR-induced NF-κB signaling activation was inhibited by ISO pretreatment, and it was abrogated in IL-13 silenced cells. We speculated that ISO may confer radiosensitivity on A549 cells via increasing the expression of IL-13 and inhibiting the activation of NF-κB. To our knowledge, this is the first report demonstrating the effects of ISO treatment on the responsiveness of lung cancer cells to irradiation through IL-13 and the NF-κB signaling pathway. In summary, ISO is a naturally occurring radiosensitizer with a potential application in adjuvant radiotherapy.

**Keywords: isorhamnetin, IL-13, NF-kB, radiosensitivity, radiotherapy**

OPEN ACCESS

***Edited by:***
*Xiaoping Lin,*
*Sun Yat-sen University Cancer Center (SYSUCC), China*

***Reviewed by:***
*Ali Sak,*
*Essen University Hospital, Germany*
*Carmela Spagnuolo,*
*National Research Council (CNR), Italy*

***Correspondence:**
*Kun Sun*
*kunsun@nwnu.edu.cn*

***Specialty section:***
*This article was submitted to Pharmacology of Anti-Cancer Drugs, a section of the journal Frontiers in Pharmacology*

***Received:*** *27 September 2020*
***Accepted:*** *11 December 2020*
***Published:*** *25 January 2021*

***Citation:***
*Du Y, Jia C, Liu Y, Li Y, Wang J and Sun K (2021) Isorhamnetin Enhances the Radiosensitivity of A549 Cells Through Interleukin-13 and the NF-κB Signaling Pathway. Front. Pharmacol. 11:610772. doi: 10.3389/fphar.2020.610772*

## INTRODUCTION

Isorhamnetin (ISO), a flavonoid isolated from traditional Chinese medicine (*Hippophae L.*), has been known to have antioxidative and anti-inflammatory effects and immunomodulatory properties (Echeverry et al., 2004; Seo et al., 2014). In addition, ISO can play a tumor-suppressive role in diverse human tumors as well (Teng et al., 2006; Manu et al., 2015). Zhang et al. reported that ISO could induce mitotic block in non-small-cell lung carcinoma cells (NSCLC), thus enhancing carboplatin- and cisplatin-induced G2/M arrest (Zhang et al., 2015), suggesting that ISO might be a potential

clinical chemotherapeutic drug for NSCLC. ISO restrains the proliferation and colony formation and induces the apoptosis of A549 cells, which may be related to mitochondrial dependent pathway. Through disrupting mitochondrial membrane potential (MMP), ISO promoted the release and activation of cytochrome c and caspases 3 and 9 and then induced A549 cells apoptosis (Li et al., 2015).

Lung cancer is one of the most frequently diagnosed cancers in terms of both incidence and mortality, with almost 1.38 million deaths every year worldwide (Alberg et al., 2005; Smith et al., 2019). NSCLC accounts for almost 80% of lung cancers, among which the most common subtypes are lung adenocarcinoma (LUAD) and lung squamous cell carcinoma (LUSC) (Posther and Harpole, 2006; Chen et al., 2017). Radiotherapy is a widely used therapeutic modality for patients in NSCLC. However, NSCLC has been historically considered as a radioresistant malignancy; therefore, conventional chemotherapy or radiotherapy is usually poor in cure rate for cancer patients. More attentions have been attracted to radiosensitizers because of their abilities to increase the radiosensitivity of cancer cells and reduce the side effects on normal cells. In order to identify promising radiosensitivity agents, a large number of natural products with anti-inflammatory, antioxidant, and antitumor activations have been considered (Li et al., 2017; Sun et al., 2017). ISO, a natural product, has these features and is also safe, easily available, and of better efficacy. Can it be potentially served as a radiosensitizer for cancer treatment?

The transcription factor Nuclear Factor-κB (NF-κB) is retained in the cytoplasm in a form of primary heterodimer containing P50 and P65 subunits bound to I-κB. When I-κB is phosphorylated and degraded, NF-κB would be activated, and p50 and p65 translocate to the nucleus and bind to its specific DNA site, which results in a series of key downstream proteins mediating antiapoptosis and attenuates radiation-induced apoptosis (Wang et al., 1996). Several reports have shown that NF-κB activation was associated with worse survival and radioresistance in multiple types of cancers (Magne et al., 2006; Bai et al., 2015; Wu et al., 2015). Thus, the therapeutic effect of radiotherapy is closely related to the active state of NF-κB and the level of inflammatory factor. Inhibition of NF-κB, therefore, has the potential to improve radiotherapeutic efficacy by enhancing radiation-induced cell kill. ISO, as a candidate to inhibit inflammation, has been shown to regulate immune responses via blocking the activation of NF-κB signal and downregulating the secretion of proinflammatory cytokines (TNF-α, IL-1β, and IL-6) (Chi et al., 2016; Li et al., 2016), which may suggest the potential of ISO as a radiosensitizer.

In the present study, we investigated the effects of treatments with ISO alone, irradiation (IR) alone, and combination of ISO + IR on cell viability, DNA damage repair, and apoptosis to determine the radiosensitivity of ISO. Meanwhile, we investigated the mechanisms underlying this effect likely involving NF-κB pathway. Our results demonstrated that ISO could sensitize A549 cells to radiation via inhibition of NF-κB activation mediated by upregulating the level of anti-inflammatory interleukin-13 (IL-13).

# MATERIALS AND METHODS

## Cell Culture

The non-small-cell lung carcinoma A549 and H460 cells were obtained from Shanghai Cell Bank of Chinese Academic of Science and maintained in RPMI 1640 medium (Gibco, United States) containing 10% heat-inactivated fetal bovine serum (Hyclone, United States) and 1% penicillin/streptomycin at 37°C in a humidified atmosphere containing 95% air and 5% $CO_2$.

## Chemical Treatment

ISO was purchased from Baoji Herbest Bio-Tech Company (CAS No: 480-19-3, China; with purity >98%) and stored as 100 mM stock solution in DMSO, protected from light at −20°C.

## Irradiation

Cells were incubated with or without ISO at concentration of 20 μM for 24 h and then irradiated with the indicated dose of X-rays, which were generated by XRad225 (PRECISION X-RAY) operated at 50 kVp energy. The dose rate was about 1.3 Gy/min.

## MTT Assay

Cells were seeded in a 96-well plate at a density of $5 \times 10^3$ cells/well and treated with various concentrations of ISO (0, 5, 10, 20, 40, 50, 60, or 80 μM). The control group was treated with an equal volume of DMSO. At the appropriate timepoints, cell proliferation assay was performed by the addition of 50 μl of 3-(4,5-dimethylthiazol-2-yl)-2,5-diphenyltetrazolium bromide (MTT) stock solution (2 mg/ml). After 4 h, the formazan crystals in each well were dissolved by addition of DMSO (150 μl). The absorbance was measured at 550 nm using an automated microplate reader.

## Colony Formation Assay

Cells were pretreated with or without 20 μM ISO for 24 h and then followed by irradiation at the exposure doses of 0, 0.5, 1, 2, 4, or 6 Gy. Cells were irradiated and then immediately reseeded at different densities to yield approximately 50–100 surviving colonies in the ϕ60 mm petri dish. After being cultured for 12–14 days, the colonies were stained with 0.5% crystal violet for 30 min and manually counted. The survival fraction was generated from three independent experiments with colony numbers normalized to Sham-treated controls.

## Micronucleus Assay

Micronucleus (MN) formation assay is another generally used biological endpoint for potential genotoxic study. Cells were pretreated with or without ISO for 24 h followed by X-rays. After being cultured for 48 h again, cells were fixed with methanol/acetic acid (3:1 v/v) for 20 min at room temperature and then air-dried cells were stained with 20 μl of Acridine Orange in an aqueous solution (10 μg/ml). The analyses were done under the fluorescence microscope (Axio Imager. Z2) at ×20 magnification and the scoring of MN was performed following

the criteria established by Fenech (Fenech, 2000). At least 500 cells were scored for each sample. Each experiment was repeated three times independently at least.

## Immunostaining

Immunochemical staining of cells was performed as described (Aten et al., 2004) for DNA double-strand breaks. The cells were reseeded at a density of $1 \times 10^5$ cells in 35 mm cell culture dishes overnight and were then pretreated with or without ISO for 24 h followed by X-rays. After irradiation, cells were fixed with 4% paraformaldehyde for 20 min at different time points. The fixed cells were permeabilized with 0.5% Triton X-100 in 10% BSA for 1 h. Subsequent experimental procedures followed the previous description (Jia et al., 2020). The cells were incubated with anti-γH2AX (surrogate of DSB) antibody (1: 5,000, Abcam, United States) for 1 h at room temperature, washed three times with PBS, and then incubated in buffer containing the FITC-conjugated goat anti-mouse secondary antibody (1:2,500, ZSGB-BIO, China) for 1 h. After washing with PBS for five times, cells were counterstained with DAPI (Invitrogen, United States). The fluorescent images were taken under a fluorescence microscope (Axio Imager Z2) at ×63 magnification and were analyzed. The fraction of cell with γ-H2AX foci was calculated (numbers of cells with DSBs/total cells) (d'Adda di Fagagna et al., 2003). At least 100 cells were counted for each sample.

## Western Blot Assay

Cells were pretreated with or without 20 μM ISO for 24 h followed by 2 Gy X-rays irradiation. After 12 h, cells were lysed with RIPA buffer (Beyotime, China) with Protease Inhibitor Cocktail Tablets (Roche, Switzerland). Equal amounts of total protein were denatured with 1× loading buffer (Beyotime, China) and subjected to 12% SDS-PAGE and then transferred to a methanol-activated PVDF membrane (Millipore, United States). The membranes were blocked and then probed overnight at 4°C with the following primary antibodies against: Bax, Bcl2, NF-κB, IL-13Rα2, and GAPDH (1:1,000, Proteintech, China); IL-13, IL-13Rα1, (1: 1,000, Affinity Biosciences, United States); p-IκBα and p-NF-κB (1:800, CST, United States). After three washes with TBS, membranes were probed with the horseradish peroxidase-(HRP-) labeled secondary antibody (1:2,500, ZSGB-BIO, China) for 1 h at room temperature. Staining was visualized using enhanced chemiluminescence (ECL) reagents, according to the manufacturer's recommendations. The intensity of protein bands on the western blot image was quantified by Image J software.

## Apoptosis Assays

The cells were incubated with or without 20 μM ISO for 24 h and then irradiated by 2 Gy X-rays. After 48 h, the cells (>$1 \times 10^5$ cells) were collected, washed, and stained with Annexin V-FITC and propidium iodide (PI) kit (BD, United States) for 15 min according to the manufacturer's protocol. The ratio of apoptosis was measured by a Coulter Epics on a flow cytometer FlowSight (Amnis, United States).

## Level of Cytokines Measurement by Meso Scale Discovery Assay

The A549 cells were pretreated with or without 20 μM ISO for 24 h and then exposed to 2 Gy X-rays. After 12 h, the supernatant was collected by the centrifuge and detected by MSD assay. According to the manufacturer's instruction of MSD kit, the MSD V-Plex Proinflammatory Panel 1 Human Kit (MSD platform) (Rockville, MD, United States) was used to measure IL-6, IL-8, IL-10, IL-13, IL-1β, IL-2, IL-4, IFN-γ, IL-12p70, and TNF-α concentrations in cell medium by MSD instrument. Ten kinds of cytokines can be detected simultaneously one-off in each well.

## Mitochondrial Membrane Potential Measurement

JC-1 (BD Biosciences), a dye that can selectively enter into mitochondria and reversibly change color from green to red, was used to detect the MMP levels according to the manufacturer's instruction. Briefly, after being pretreated with or without ISO for 24 h followed by X-rays irradiation and then being cultured for 24 h again, the cells (~$1 \times 10^6$ cells/ml) were loaded in 500 μl JC-1 working solution at 37°C for 20 min and then washed twice with 1× assay buffer. We detected the fluorescence intensity of JC-1 monomers green fluorescence (λex 488 nm, λem 530 nm) as well as JC-1aggregates red fluorescence (λex 525 nm, λem 590 nm). The ratio of fluorescence intensity was calculated to reflect the MMP.

## RNA Interference

IL13 siRNA-1 that targets IL-13 homo-205 (sense: 5′ GCAGCA UGGUAUGGAGCAUTT-3′, antisense: 5′ AUGCUCCAUACC AUGCUGCTT-3′) and IL13 siRNA-2 that targets IL-13 homo-25 (sense: 5′ UCCUCAAUCCUCUCCUGUUTT-3′, antisense: 5′ AACAGGAGAGGAUUGAGGATT-3′) were purchased from GenePharma (Guangzhou, China). A549 cells were transiently transfected with nontargeting siRNA or IL-13 siRNA oligos at a final concentration of 50 nM. The efficacy of interfering IL-13 expression was detected by western blot and quantitative real-time polymerase chain reaction (qRT-PCR). Twenty-four hours after transfection using jetPEI (Polyplus, United States), the cells were treated with or without 20 μM ISO for additional 24 h and then exposed to 2 Gy X-rays. The cells were further subjected to apoptosis detection, MN, and western blotting.

## Cell Growth Curve

The cells were transfected with IL-13 siRNA, pretreated with or without ISO for 24 h, and then exposed to 2 Gy X-rays. The cells were trypsinized soon after irradiation and reseeded in ϕ60 mm petri dish with $1 \times 10^5$ cells/dish for four days and counted by automated cell counter (Z2, Beckman, United States).

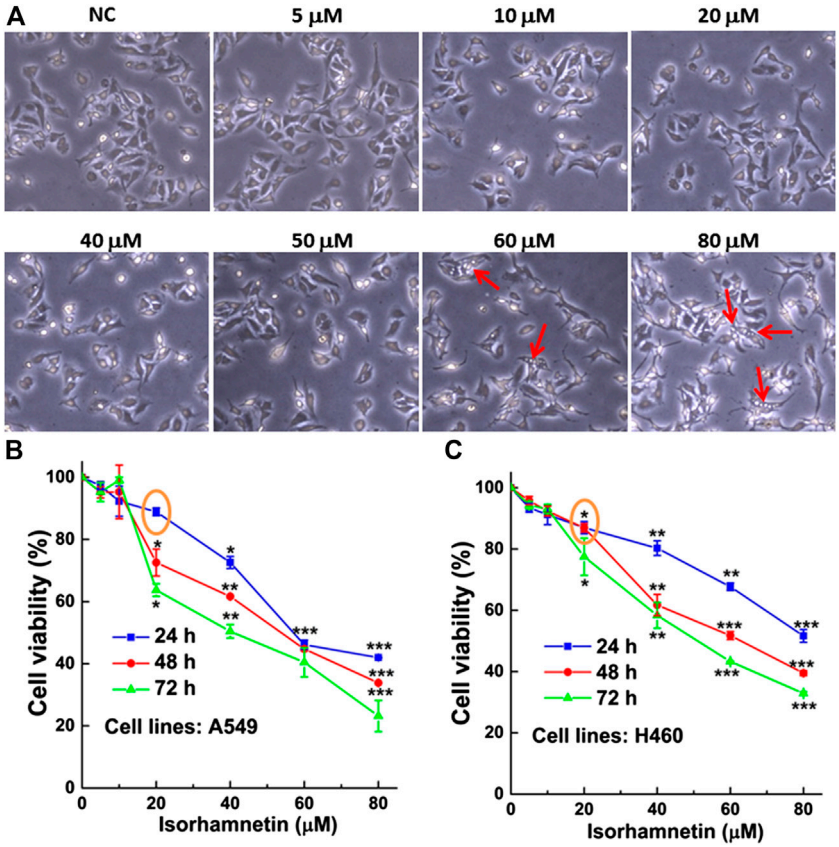


**FIGURE 1 |** ISO treatment induces vacuolation of NSCLC cells and inhibits cell proliferation. **(A)** The morphology of A549 cells after treatment with different concentrations (0, 5, 10, 20, 40, 50, 60, and 80 μM) of ISO for 24 h. The red arrow indicates the vacuolated A549 cells. The inhibitory effect of ISO was detected by MTT assay after different time of ISO treatment on the proliferations of A549 **(B)** and H460 **(C)** cell lines. $^{*}p < 0.05$, $^{**}p < 0.01$, $^{***}p < 0.001$ vs. the control groups.

## Quantitative Real-Time Polymerase Chain Reaction

According to manufacturer's instructions, total RNA was isolated using Trizol (Invitrogen). To obtain the cDNA, reverse transcription was conducted using a high-capacity Transcriptor First Strand cDNA synthesis kit (Roche, Switzerland). qRT-PCR was performed with SYBR Green Mix kit (Roche, Switzerland) by using Bio-Rad CFX system. The specific primer for detection of IL-13 gene was F: CAATGGCAGCATGGTATG; R: ATCCTCTGG GTCTTCTCG. The primer for GAPDH gene was F: GAAGGTGAA GGTCGGAGT; R: CATGGGTGGAATCATATTGGAA. The mRNA expression levels were normalized to GAPDH using the $2^{-\Delta\Delta Ct}$ method.

## Statistics

The results were presented as means ± standard errors (SE) from at least three independent experiments. The significance of differences ($p$ value) was determined by Student's $t$-test for single comparisons and analysis of variance (ANOVA) for statistical comparison between different groups. The $p$ values of 0.05 or less were regarded as significant in two sample's comparison.

# RESULTS

## Isorhamnetin Treatment Induces Vacuolation and Inhibits Cell Proliferation of Non-Small-Cell Lung Carcinoma Cells

After treatment with ISO (5, 10, 20, 40, 60, and 80 μM) for 24 h, the morphology of A549 cells was altered, and cells were round. Cell vacuolation and disintegration were observed in a dose-dependent manner (**Figure 1A**). The results of the MTT assay showed that the viability of ISO-treated A549 and H460 cells decreased in concentration- and time-dependent manners. The viability of both A549 (**Figure 1B**) and H460 (**Figure 1C**) cells was ~50% that of respective controls after treatment with 60 μM ISO for 24 h and >85% that of respective controls after treatment with 20 μM ISO, indicating that ISO inhibited cell proliferation.

## Isorhamnetin Enhances the Radiosensitivity of A549 Cells

To investigate whether ISO treatment could enhance the radiosensitivity of cells, two NSCLC cell lines were treated

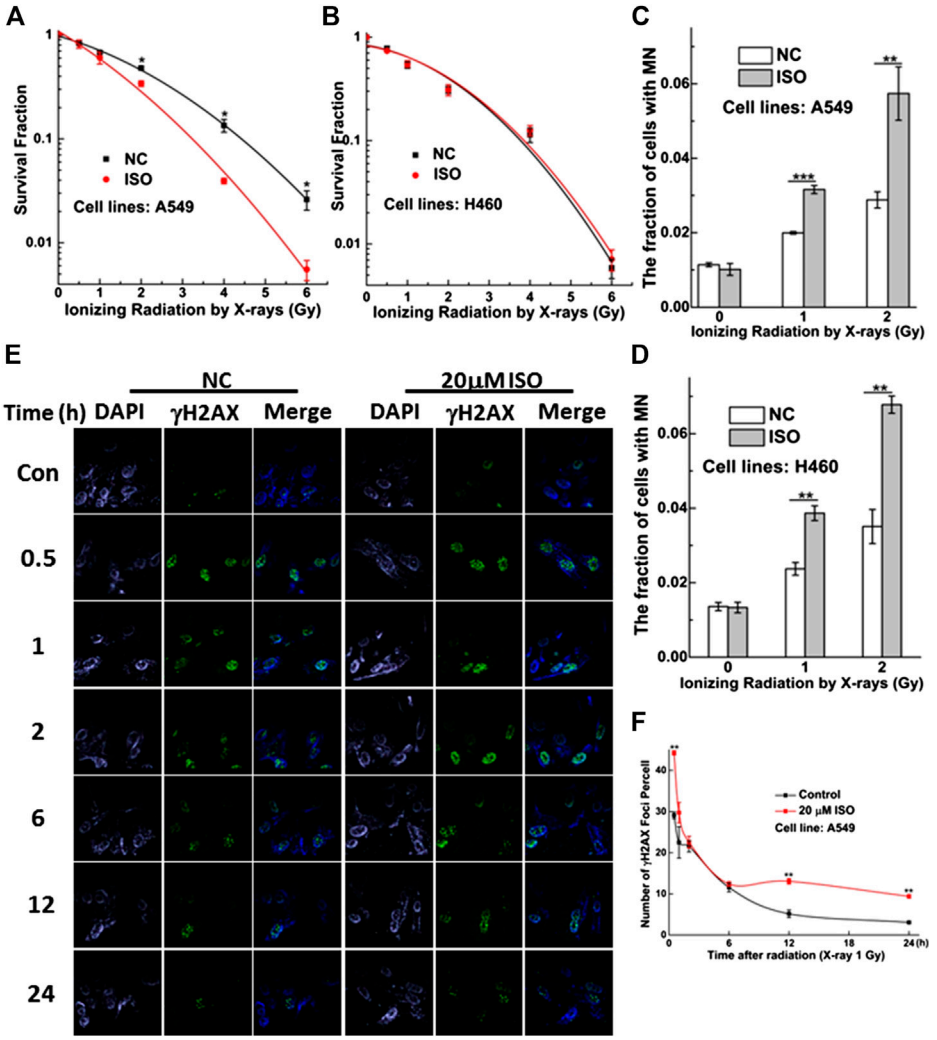


**FIGURE 2 |** ISO sensitized NSCLC cells to IR. Survivals measured by colony formation assay in A549 **(A)** and H460 **(B)** cells pretreated with/without ISO and followed by 0, 0.5, 1, 2, 4, and 6 Gy X-rays irradiation. The fraction of MN in A549 **(C)** and H460 **(D)** cells pretreated with/without ISO and followed by 0, 1, and 2 Gy X-rays irradiation. Five hundred cells were scored under microscopy to determine the frequency of cell with micronuclei. Representative images of γH2AX foci (green) in A549 **(E)** and H460 **(G)** cells pretreated with/without 20 μM ISO for 24 h and then exposed to 1 Gy X-rays, fixed at different time points, and detected by immunofluorescence staining assay. The numbers of γH2AX foci in 100 cells of each group were counted at each time point in A549 **(F)** and H460 **(H)** cells. Each data point represents the mean of three separate experiments. $^{*}p < 0.05$, $^{**}p < 0.01$, $^{***}p < 0.001$ vs. non-drug-treated cells.

with 20 μM ISO for 24 h and then irradiated with different doses of radiation. Colony formation, micronucleus, and γH2AX foci (a surrogate marker for DNA damage) assay were performed to examine the degree of radiosensitivity.

In A549 cells, treatment with ISO and irradiation decreased the viability (**Figure 2A**) and increased the MN fraction (**Figure 2C**) compared to the IR alone, especially at radiation doses of 2, 4, and 6 Gy. As shown in **Figures 2E,F**, treatment with ISO and irradiation significantly increased the numbers of γH2AX foci per cell, compared with IR alone at 1 Gy for 0.5 h ($p < 0.01$) in A549 cell lines. In addition, the dissolution of foci was faster in cells treated with ISO and irradiation from 0.5 to 6 h, compared to the IR alone. Interestingly, the number of γH2AX foci per cell in ISO + IR group was higher than that in the IR group from 12 to 24 h (**Figure 2F**).

As shown in **Figure 2D**, the MN fraction for H460 cells treated with ISO and irradiation was greater than that for cells treated with irradiation alone. However, this difference was not found by means of the colony formation assay (**Figure 2B**). As shown in **Figures 2G,H**, the number of γH2AX foci per cell in the ISO + IR group was higher than that in the IR group from 0.5 to 1 h after a radiation dose of 1 Gy ($p < 0.01$). However, this difference in the numbers of γH2AX foci per cell between ISO + IR and IR groups was not found in H460 cells after 2 h, indicating that ISO enhances the radiosensitivity of A549 cells and inhibits the repair of damaged DNA induced by irradiation.

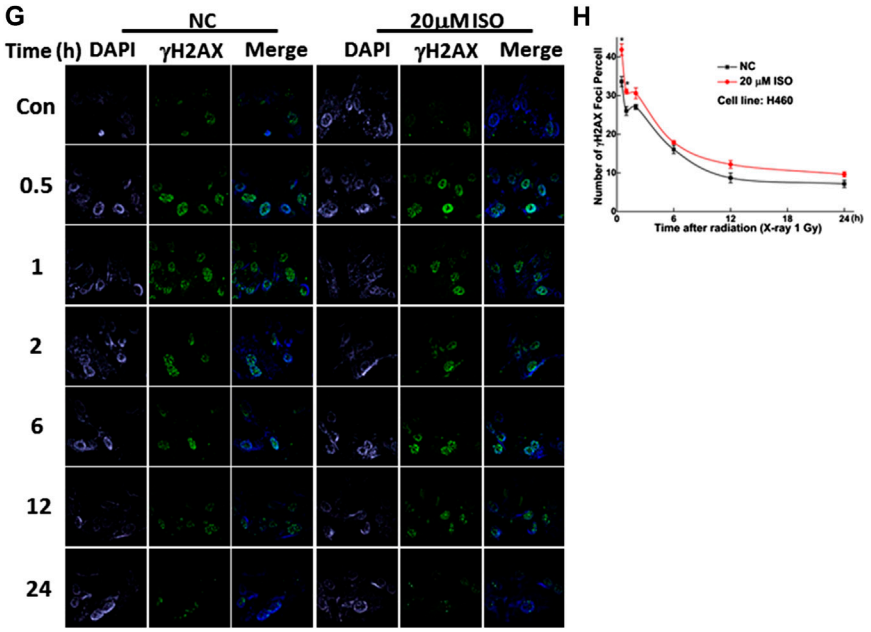


**FIGURE 2 | (Continued).**

## Treatment With Isorhamnetin Enhances Irradiation-Induced Cell Apoptosis and the Mitochondrial Membrane Potential

Apoptosis is one type of programmed cell death. We investigated the apoptosis rate in A549 and H460 cells treated with ISO and irradiation or irradiation alone using flow cytometry (**Figure 3A**). **Figure 3B** shows that the apoptosis rate was higher in A549 cells treated with ISO and irradiation than that in cells treated with irradiation alone. However, this difference in the apoptosis rate between ISO + IR and IR groups was not found in H460 cells (**Figure 3C**).

The MMP is a key indicator of mitochondrial function and activity, and mitochondrial depolarization has been reported to associate with apoptosis. Mitochondrial depolarization is indicated by decreased red fluorescence and increased green fluorescence after JC-1 staining, and the collapse of the MMP is revealed by the green/red fluorescence intensity ratio. We investigated whether the MMP was affected in cells treated with ISO and irradiation. **Figures 3D,E** show that ISO treatment significantly enhanced the radiation-induced collapse of MMP (increase in the green/red fluorescence intensity ratio) in both A549 and H460 cells.

We also examined the expression of proteins associated with apoptosis. As shown in **Figure 3F**, ISO treatment significantly suppressed the upregulation of radiation-induced NF-κBp65 expression in A549 and H460 cells. In addition, the expression of NF-κBp65 in A549 cells was higher than in H460 cells, which may be associated with the difference of radiosensitivity among different cell lines pretreated by ISO. Interestingly, ISO treatment decreased the Bcl2 level and increased the Bax level, compared to the irradiation alone (**Figure 3F**), indicating that ISO and irradiation accelerated the decrease of the of Bcl2/Bax ratio. Taken collectively, these results indicated that ISO treatment facilitated the apoptosis after irradiation.

The radiosensitization of ISO in H460 cells was not significant, reflected by clonogenic survival and apoptosis endpoints. Therefore, the mechanism of ISO radiosensitivity was widely investigated only in A549 cells in the following experiments.

## Treatment With Isorhamnetin Upregulates the Irradiation-Induced Interleukin-13 Level

To widely identify immune-related protein involved in the radiosensitization of ISO in A549 cells, the levels of 10 cytokines (IL-6, IL-8, IL-10, IL-13, IL-1β, IL-2, IL-4, IFN-γ, IL-12p70, and TNF-α) were measured using the Meso Scale Discovery (MSD) platform. MSD is a highly sensitive high-throughput electrochemiluminescence measurement system, which can detect as little as ~0.29 pg/ml of a target cytokine (Osuchowski et al., 2005). We found that the IL-13 level in the ISO + IR group (8.6886 ± 0.5642 pg/ml) was higher than that in the IR group (6.3332 ± 0.6143 pg/ml). The levels of IL-13 expression in negative control and ISO treatment groups were 3.9742 ± 0.1879 pg/ml and 3.6637 ± 0.6046 pg/ml, respectively (**Figure 4A**).

IL-13 can suppress the production of the inflammatory cytokine TNF and inhibit NF-κB activation by preventing degradation of IκBα (Lentsch et al., 1997; Manna and Aggarwal, 1998). A previous study has demonstrated that IL-13 is a mediator, and possibly a therapeutic target, in

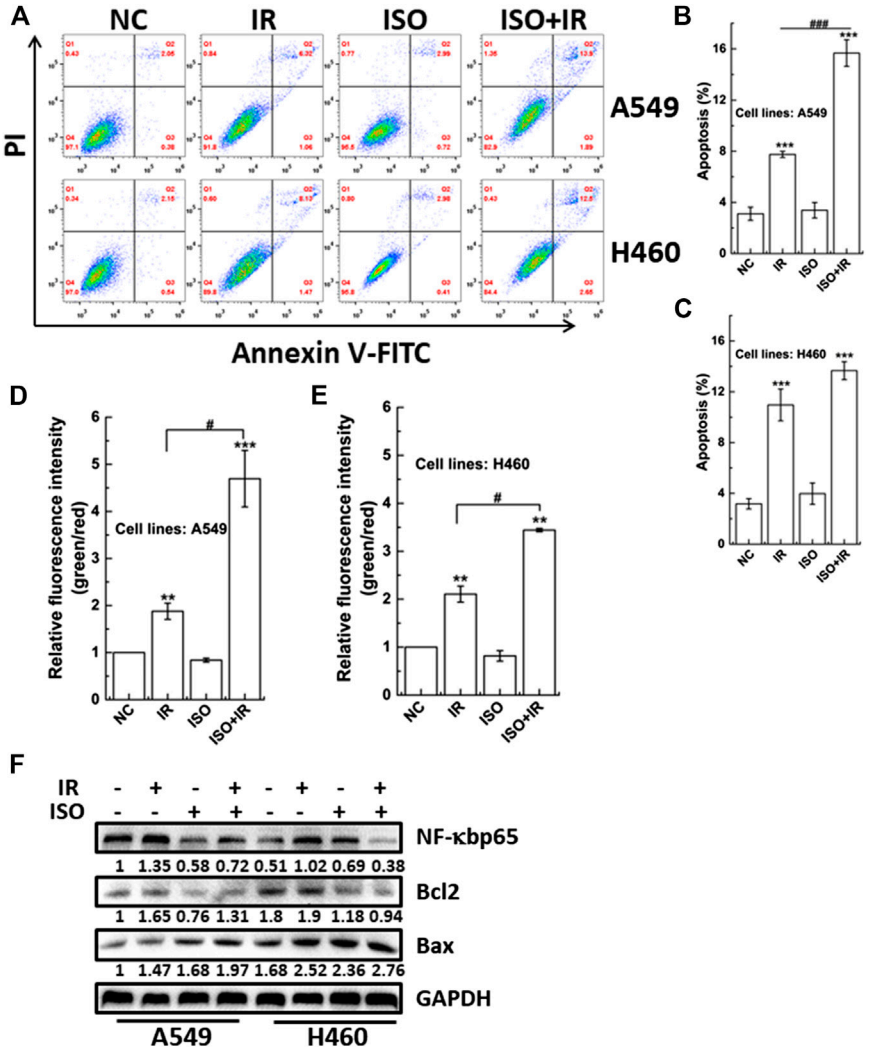


**FIGURE 3 |** The impact of ISO combined irradiation on cell apoptosis and the MMP. The levels of apoptosis in A549 **(A,B)** and H460 **(A,C)** cells pretreated with/without ISO and then exposed to 2 Gy X-rays irradiation. The irradiated cells were sequentially cultured for 48 h and then harvested to be analyzed by an Annexin V/PI flow cytometry analysis. The MMP was quantified by the microplate reader in A549 **(D)** and H460 **(E)** cells pretreated with/without ISO and followed by 2 Gy X-rays at 24 h after irradiation. **(F)** The expression levels of apoptosis-related proteins were assessed and quantified by western blotting in A549 and H460 cells. Cells were pretreated with/without ISO for 24 h and followed by 0 or 2 Gy X-rays and then analyzed by western blot after 12 h. $^{***}p < 0.001$ vs. the control group. $^{\#\#\#}p < 0.001$ vs. non-drug-treated cells.

radiation-induced lung injury, as shown by saturating fraction of the circulating decoy receptor IL-13Rα2 (Chung et al., 2016). Therefore, ISO may upregulate the expression of IL-13, thereby inhibiting NF-κB activation, inducing apoptosis, and triggering radiosensitivity.

IL-13 mRNA and protein expression were analyzed by qRT-PCR (**Figure 4B**) and western blot (**Figure 4C**), respectively. As shown in **Figure 4C**, ISO treatment upregulated the IL-13 mRNA levels compared to the negative control. Treatment with ISO and irradiation also significantly increased IL-13 mRNA and protein levels compared to irradiation alone. Furthermore, the expression of IL-13Rα2, the high affinity binding decoy receptor for IL-13, was significantly decreased in the ISO + IR group compared to the IR group (**Figure 4C**), indicating that ISO sensitizes cells to irradiation by affecting the function of IL-13.

## Interleukin-13 Is Required for the Radiosensitivity Mediated by Isorhamnetin

To confirm the effects of ISO on the radiosensitivity of cells through the increased expression of IL-13, we silenced IL-13 by RNA interference and measured several relevant biological endpoints. The most effective IL-13 siRNA, as confirmed by qRT-PCR and western blot (**Figure 5A**), was selected for further studies. As shown in **Figure 5B**, IL-13 knockdown (si-IL13 cells) failed to increase MN formation in ISO + IR group, compared to

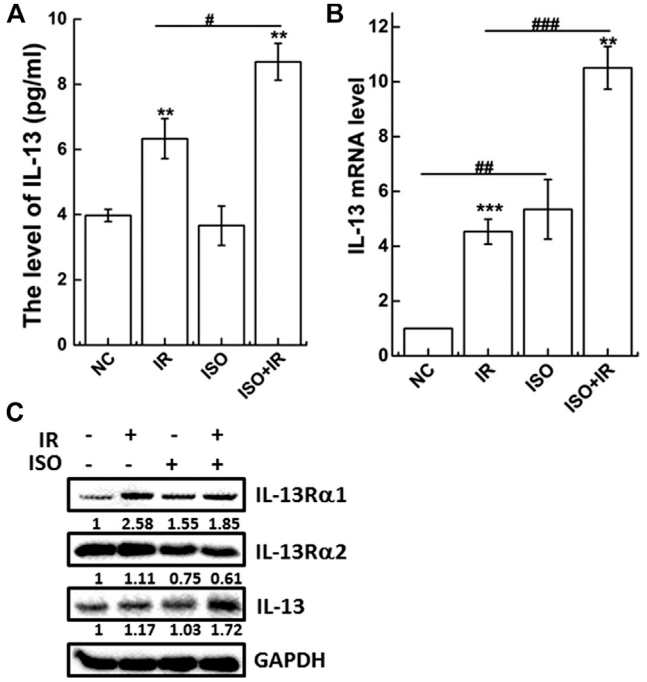


**FIGURE 4 |** ISO enhances the levels of anti-inflammatory IL-13 activated by IR in A549 cells. The level of IL-13 **(A)** in supernatant of cells pretreated with/without ISO for 24 h, exposed to 2 Gy X-rays, and then detected 12 h after irradiation by MSD assay. The expression of IL-13 gene **(B)** and associated receptor proteins **(C)** were analyzed at 12 h after irradiation by qRT-PCR and western blot, respectively, in A549 cells pretreated with/without ISO for 24 h and then exposed to 2 Gy X-rays. Fold changes over negative control were presented from $2^{-\Delta\Delta Ct}$ formula. $^{*}p < 0.05$, $^{**}p < 0.01$, $^{***}p < 0.001$ vs. the control group. $^{\#}p < 0.05$, $^{\#\#}p < 0.01$, and $^{\#\#\#}p < 0.001$ vs. non-drug-treated cells.

the IR group. When the cells were pretreated with 20 μM ISO and then irradiated with a radiation dose of 2 Gy, the cell number decreased to 80.9 ± 3.2% (green bar) compared with irradiation alone (set as 100%, purple bar) (**Figure 5C**). However, there was no significant toxicity in si-IL13 A549 cells after ISO treatment and irradiation (**Figure 5C**).

We measured the apoptosis rate in si-IL13 cells after ISO treatment and irradiation. **Figures 5D,E** show that irradiation did not increase the apoptosis rate in si-IL13 cells treated with ISO, compared to cells without ISO treatment. However, the apoptosis rate in IL-13 silenced control cells was higher than that in mock silenced cells (si-ctrl), which may be associated with the anti-inflammatory role of IL-13.

**Figure 5F** shows that ISO treatment significantly increased IR-induced IL-13 expression and inhibited the IR-induced activation of NF-κB by decreasing p-NF-κBp65 and the p-IκBα expression, compared to the IR group in si-ctrl group. Intriguingly, we observed that IL-13 knockdown also promoted the expression of p-IκBα and p-NF-κBp65 in control group, allowing for its nuclear translocation and regulation of gene expression. However, the upregulation of p-NF-κBp65 induced by IR was not suppressed by ISO in si-IL13 cells, suggesting that the gene of IL-13 pathway is required in the activation of NF-κB agitated by IR. Together, these results indicated that ISO treatment further increased the radiation-mediated upregulation of the IL-13 level, which inhibits the activation of NF-κB, thereby promoting apoptosis and enhancing radiosensitivity.

## DISCUSSION

Radiotherapy is commonly used to treat cancer, with more than 50% of cancer patients receiving radiotherapy during the clinical management of the disease. Unfortunately, the 5-year survival rate of radiotherapy alone is only 5–10% in lung cancer patients (Mauguen et al., 2012). The main cause of the poor response is the intrinsic or acquired resistance of lung cancer to radiotherapy (You et al., 2014). Radiosensitizers, sensitizing cancer cells to the effects of irradiation but protecting normal cells from its deleterious effects, play an important role in radiotherapy. For example, ISO (a 3′-O-methylated metabolite of quercetin) has been studied for its anticancer and antioxidant activity and anti-inflammatory properties, as well as its ability to induce chemosensitivity in several human cancer cells (Ramachandran et al., 2012; Saud et al., 2013; Yang et al., 2013; Li et al., 2014; Ahn and Lee, 2017). Due to its lower toxicity, ease of oral administration, and affordability, we investigated its mechanism of radiosensitization in order to provide a foundation for its development as a naturally occurring radiosensitizer of cancer cells. We selected A549 (lung adenocarcinoma) and H460 (large lung cell carcinoma) cell lines as representative models of NSCLC (Ji et al., 2018). We found that treatment with ISO, followed by irradiation, significantly decreases the surviving fraction in A549 cells and increases the MN fraction in A549 and H460 cells. In addition, we found that treatment with ISO + IR could significantly enhance DNA damage, the collapse of MMP, and the apoptotic rate, suggesting that ISO treatment can significantly enhance the radiosensitivity of A549 cells. We did not find the significant decrease of the survival and the increase of apoptosis in H460 cells after ISO pretreatment followed by IR. It may be because of the different biological endpoints having different sensitivity at certain timepoint after stress (Hu et al., 2005). In addition, this difference may be caused by the low expression of NF-κB in H460 cells, which weaken the role of ISO radiosensitivity. In A549 cells, NF-κB expression is high, the activation of NF-κB has a greater effect, and ISO treatment enhances more effective radiosensitivity.

Prior studies have indicated that ISO exerts its anti-inflammatory effects through the deactivation of NF-κB (Zhang et al., 2011; Yang et al., 2013). The activation of the NF-κB signaling pathway confers lung cancer cell radioresistance and thus survival by interfering with apoptotic signals. For example, c-IAP1 and c-IAP2 either directly block caspase function or indirectly induce ubiquitination in irradiated cancer cells (Varfolomeev et al., 2008). Furthermore, irradiation can induce DNA damage, which evokes a response where NF-κB is activated to protect cells from inflammation and subsequent death. Our results demonstrated that ISO treatment

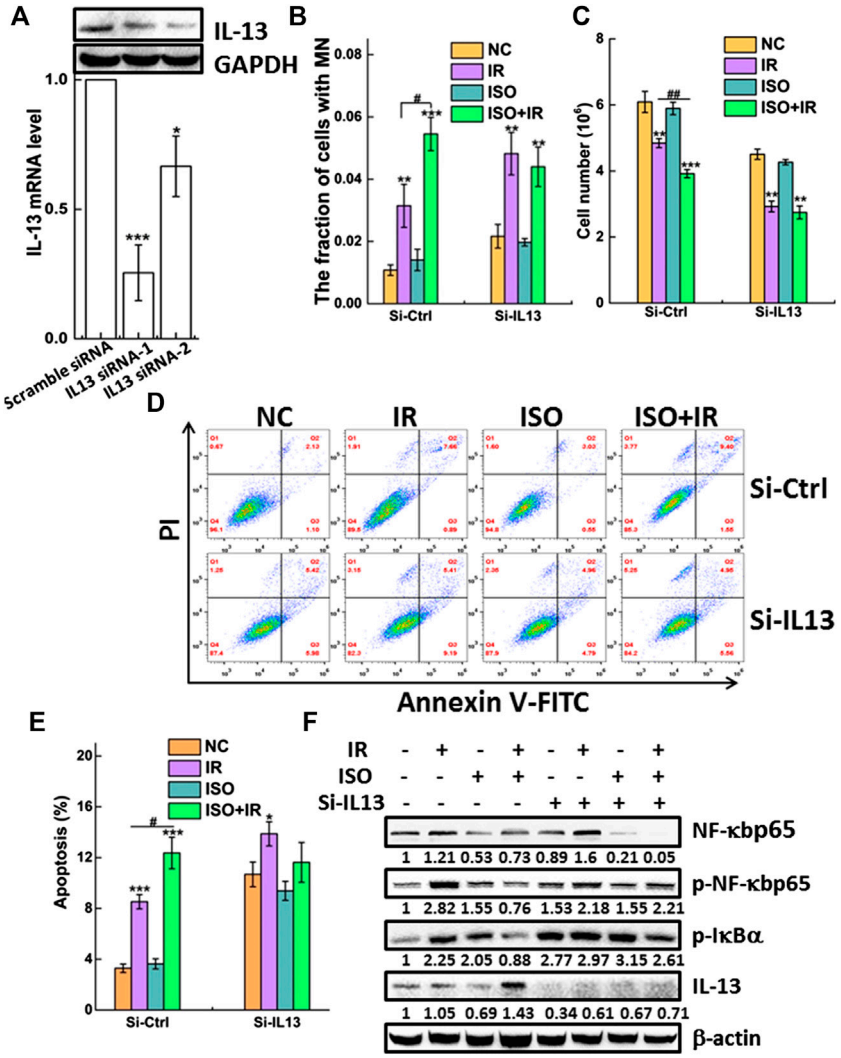


**FIGURE 5 |** IL-13 is required for the radiosensitivity mediated by ISO. **(A)** A549 cells were transiently transfected with IL-13 siRNA or scramble-siRNA as a control. Forty-eight hours after transfection the knockdown efficiency of IL-13 in cells was confirmed by western blot and qRT-PCR assays. Knockdown of IL-13 disturbed radiosensitivity mediated by ISO indicated in si-Ctrl or si-IL13 groups by micronucleus **(B)**, cell growth **(C),** and apoptosis assays **(D**,**E)**. **(F)** The expression of phosphorylated and total NF-κBp65 and p-IκBα, as well as IL-13 and β-actin, was assessed in negative vector or IL-13 silenced A549 cells by western blotting, respectively.

suppressed the irradiation-mediated activation of the NF-κB signaling pathway, which promoted programmed cell death.

IL-13, a pleiotropic immune regulatory cytokine, exhibits both immunomodulatory and anti-inflammatory properties. The anti-inflammatory effects of IL-13 are supported by its ability to downregulate the level of lipopolysaccharide-induced macrophage inflammatory protein-1α and the production of proinflammatory cytokines, namely, IL-1, TNF, IL-6, IL-8, IL-10, and IL-12 in monocytes (Yang et al., 2013). In addition, blocking the IL-13 mediated phosphorylation of STAT6 can protect breast cancer cells from developing sensitivity to irradiation (Rahal et al., 2018). In particular, IL-13 is a prominent feature in causing barrier effects and the epithelial apoptosis in cell models (Heller et al., 2005). Consistent with our findings in NSCLC cells, ISO treatment and irradiation increased the IL-13 level, which induced apoptosis of si-ctrl cells by downregulating p-IκBα and inhibiting NF-κB activation (p-NF-κBp65). IL-13 not only acts an apoptotic effector but also has a profound effect. We also found that the IR-induced NF-κB signaling activation was inhibited by ISO treatment, and it was abrogated in IL-13 silenced cells, which implied that NF-κB activation is inhibited by IL-13. Other studies have demonstrated IL-4 and IL-13 bind to the same receptors and exert similar biological functions by inhibiting NF-κB dependent transcription (Bennett et al., 1997; Shinozaki et al., 2010). In this study, the IL-4 expression was also upregulated in A549 cells after X-rays irradiation but not enhanced after treatment with ISO (data not shown). Transcriptional regulatory mechanisms are complex, and further studies are needed to completely understand the molecular mechanisms responsible for the

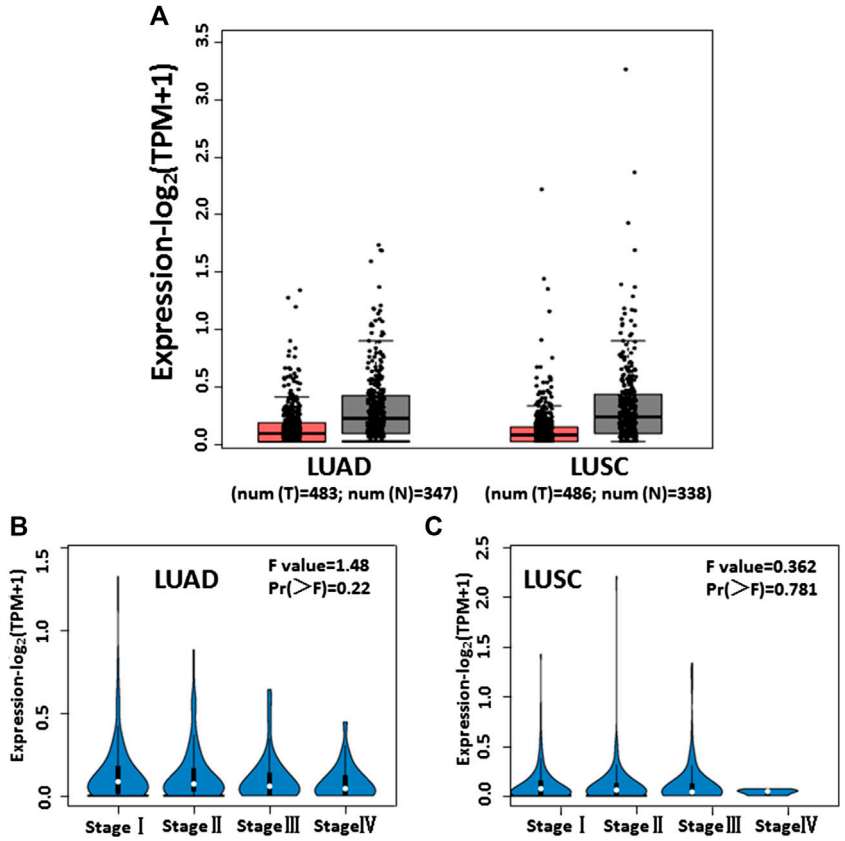


**FIGURE 6 |** The levels of IL-13 expression in NSCLC cells analyzed according to cancer public database. **(A)** IL-13 expression profile across tumor samples and adjacent normal tissues from GEPIA in LUAD and LUSC. **(B,C)** IL-13 expression levels in different stages of LUAD and LUSC from GEPIA database.

ISO-mediated increase in IL-13 expression and decrease in NF-κB activation after radiation.

Studies have proven that autophagy has been revealed as a novel response of cancer cells to ionizing radiation (Klionsky and Emr, 2000; Djavaheri-Mergny et al., 2006; Xiao, 2007). In our study, ISO treatment induces the formation of vacuolation in A549 cells, which may be involved in autophagic cell death. Therefore, we speculated the occurrence of mitochondrial dysfunction after ISO treatment and irradiation, resulting in autophagy in A549 cells. It is, therefore, necessary to further investigate the mechanism involved in sensitizing effect of ISO.

The GEPIA database (http://gepia.cancer-pku.cn/index.html) is a comprehensive web-based analysis tool that provides information on the expression of different genes in tumor and normal tissue specimens. We browsed the GEPIA database and observed low IL-13 expression in 483 LUAD and 486 LUSC tumor specimens, compared with 347 LUAD and 338 LUSC nontumor specimens (**Figure 6A**). From stage I to stage IV, the expression of IL-13 gradually decreased in LUAD (**Figure 6B**) and LUSC (**Figure 6C**) specimens, indicating that the changes in the IL-13 level can serve in evaluation of NSCLC. These results also suggested that IL-13 may be a biomarker of the disease and a therapeutic target in NSCLC.

## CONCLUSION

To our best knowledge, this is the first study to report that ISO treatment enhanced the radiosensitivity of lung cancer cells through IL-13 and the NF-κB signaling pathway, thereby promoting programmed cell death. These findings provided new insights into the mechanism responsible for the effects of ISO and may guide the development of novel therapeutic approaches for lung cancer.

## DATA AVAILABILITY STATEMENT

The raw data supporting the conclusions of this article will be made available by the authors, without undue reservation.

## AUTHOR CONTRIBUTIONS

YD designed and performed experiments, produced most data, analyzed all results, and wrote the manuscript. CJ and YaL were involved in the production and analysis of clonogenic assays and MN formation assays. JW and YeL reviewed and edited the manuscript. KS directed the study, provided most resources

and funding, and reviewed the manuscript. All authors critically read and approved the final content of the manuscript.

## FUNDING

This study was supported by the National Natural Science Foundation of China (11705248, 31660060) and the Science and Technology Research Project of Gansu Province (No. 145RTSA012 and 17JR5RA307).

## ACKNOWLEDGMENTS

The authors would also like to sincerely thank Burong Hu, Wenzhou Medical University, for his expert guidance.

## REFERENCES

Ahn, H., and Lee, G. S. (2017). Isorhamnetin and hyperoside derived from water dropwort inhibits inflammasome activation. *Phytomedicine* 24, 77–86. doi:10.1016/j.phymed.2016.11.019

Alberg, A. J., Brock, M. V., and Samet, J. M. (2005). Epidemiology of lung cancer: looking to the future. *J. Clin. Oncol.* 23 (14), 3175–3185. doi:10.1200/JCO.2005.10.462

Aten, J. A., Stap, J., Krawczyk, P. M., van Oven, C. H., Hoebe, R. A., Essers, J., et al. (2004). Dynamics of DNA double-strand breaks revealed by clustering of damaged chromosome domains. *Science* 303 (5654), 92–95. doi:10.1126/science.1088845

Bai, M., Ma, X., Li, X., Wang, X., Mei, Q., Li, X., et al. (2015). The accomplices of NF-κB lead to radioresistance. *Curr. Protein Pept. Sci.* 16 (4), 279–294. doi:10.2174/1389203716041504291523 28

Bennett, B. L., Cruz, R., Lacson, R. G., and Manning, A. M. (1997). Interleukin-4 suppression of tumor necrosis factor alpha-stimulated E-selectin gene transcription is mediated by STAT6 antagonism of NF-kappaB. *J. Biol. Chem.* 272 (15), 10212–10219. doi:10.1074/jbc.272.15.10212

Chen, M., Liu, X., Du, J., Wang, X. J., and Xia, L. (2017). Differentiated regulation of immune-response related genes between LUAD and LUSC subtypes of lung cancers. *Oncotarget* 8 (1), 133–144. doi:10.18632/oncotarget.13346

Chi, G., Zhong, W., Liu, Y., Lu, G., Lü, H., Wang, D., et al. (2016). Isorhamnetin protects mice from lipopolysaccharide-induced acute lung injury via the inhibition of inflammatory responses. *Inflamm. Res.* 65 (1), 33–41. doi:10.1007/s00011-015-0887-9

Chung, S. I., Horton, J. A., Ramalingam, T. R., White, A. O., Chung, E. J., Hudak, K. E., et al. (2016). IL-13 is a therapeutic target in radiation lung injury. *Sci. Rep.* 6, 39714. doi:10.1038/srep39714

d'Adda di Fagagna, F., Reaper, P. M., Clay-Farrace, L., Fiegler, H., Carr, P., Von Zglinicki, T., et al. (2003). A DNA damage checkpoint response in telomere-initiated senescence. *Nature* 426 (6963), 194–198. doi:10.1038/nature02118

Djavaheri-Mergny, M., Amelotti, M., Mathieu, J., Besançon, F., Bauvy, C., Souquère, S., et al. (2006). NF-kappaB activation represses tumor necrosis factor-alpha-induced autophagy. *J. Biol. Chem.* 281 (41), 30373–30382. doi:10.1074/jbc.M602097200

Echeverry, C., Blasina, F., Arredondo, F., Ferreira, M., Abin-Carriquiry, J. A., Vasquez, L., et al. (2004). Cytoprotection by neutral fraction of tannat red wine against oxidative stress-induced cell death. *J. Agric. Food Chem.* 52 (24), 7395–7399. doi:10.1021/jf040053q

Fenech, M. (2000). The *in vitro* micronucleus technique. *Mutat. Res.* 455 (1–2), 81–95. doi:10.1016/s0027-5107(00)00065-8

Heller, F., Florian, P., Bojarski, C., Richter, J., Christ, M., Hillenbrand, B., et al. (2005). Interleukin-13 is the key effector Th2 cytokine in ulcerative colitis that affects epithelial tight junctions, apoptosis, and cell restitution. *Gastroenterology* 129 (2), 550–564. doi:10.1016/j.gastro.2005.05.002

Hu, B., Han, W., Wu, L., Feng, H., Liu, X., Zhang, L., et al. (2005). *In situ* visualization of DSBs to assess the extranuclear/extracellular effects induced by low-dose alpha-particle irradiation. *Radiat. Res.* 164 (3), 286–291. doi:10.1667/rr3415.1

Ji, K., Sun, X., Liu, Y., Du, L., Wang, Y., He, N., et al. (2018). Regulation of apoptosis and radiation sensitization in lung cancer cells via the Sirt1/NF-kappaB/Smac pathway. *Cell. Physiol. Biochem.* 48 (1), 304–316. doi:10.1159/000491730

Jia, R., Chen, Y., Jia, C., Hu, B., and Du, Y. (2020). Suppression of innate immune signaling molecule, MAVS, reduces radiation-induced bystander effect. *Int. J. Radiat. Biol.* 1–9. doi:10.1080/09553002.2020.1807642

Klionsky, D. J., and Emr, S. D. (2000). Autophagy as a regulated pathway of cellular degradation. *Science* 290 (5497), 1717–1721. doi:10.1126/science.290.5497.1717

Lentsch, A. B., Shanley, T. P., Sarma, V., and Ward, P. A. (1997). *In vivo* suppression of NF-kappa B and preservation of I kappa B alpha by interleukin-10 and interleukin-13. *J. Clin. Invest.* 100 (10), 2443–2448. doi:10.1172/JCI119786

Li, C., Yang, X., Chen, C., Cai, S., and Hu, J. (2014). Isorhamnetin suppresses colon cancer cell growth through the PI3K-Akt-mTOR pathway. *Mol. Med. Rep.* 9 (3), 935–940. doi:10.3892/mmr.2014.1886

Li, G., Wang, Z., Chong, T., Yang, J., Li, H., and Chen, H. (2017). Curcumin enhances the radiosensitivity of renal cancer cells by suppressing NF-κB signaling pathway. *Biomed. Pharmacother.* 94 974–981. doi:10.1016/j.biopha.2017.07.148

Li, Q., Ren, F. Q., Yang, C. L., Zhou, L. M., Liu, Y. Y., Xiao, J., et al. (2015). Anti-proliferation effects of isorhamnetin on lung cancer cells *in vitro* and *in vivo*. *Asian Pac. J. Cancer Prev.* 16 (7), 3035–3042. doi:10.7314/apjcp.2015.16.7.3035

Li, Y., Chi, G., Shen, B., Tian, Y., and Feng, H. (2016). Isorhamnetin ameliorates LPS-induced inflammatory response through downregulation of NF-κB signaling. *Inflammation* 39 (4), 1291–1301. doi:10.1007/s10753-016-0361-z

Magné, N., Toillon, R. A., Bottero, V., Didelot, C., Houtte, P. V., Gérard, J. P., et al. (2006). NF-kappaB modulation and ionizing radiation: mechanisms and future directions for cancer treatment. *Canc. Lett.* 231 (2), 158–168. doi:10.1016/j.canlet.2005.01.022

Manna, S. K., and Aggarwal, B. B. (1998). IL-13 suppresses TNF-induced activation of nuclear factor-kappa B, activation protein-1, and apoptosis. *J. Immunol.* 161 (6), 2863–2872.

Manu, K. A., Shanmugam, M. K., Ramachandran, L., Li, F., Siveen, K. S., Chinnathambi, A., et al. (2015). Isorhamnetin augments the anti-tumor effect of capeciatbine through the negative regulation of NF-κB signaling cascade in gastric cancer. *Cancer Lett.* 363 (1), 28–36. doi:10.1016/j.canlet.2015.03.033

Mauguen, A., Le Péchoux, C., Saunders, M. I., Schild, S. E., Turrisi, A. T., Baumann, M., et al. (2012). Hyperfractionated or accelerated radiotherapy in lung cancer: an individual patient data meta-analysis. *J. Clin. Oncol.* 30 (22), 2788–2797. doi:10.1200/JCO.2012.41.6677

Osuchowski, M. F., Siddiqui, J., Copeland, S., and Remick, D. G. (2005). Sequential ELISA to profile multiple cytokines from small volumes. *J. Immunol. Methods* 302 (1–2), 172–181. doi:10.1016/j.jim.2005.04.012

Posther, K. E., and Harpole, D. H., Jr (2006). The surgical management of lung cancer. *Cancer Invest.* 24 (1), 56–67. doi:10.1080/07357900500449611

Rahal, O. M., Wolfe, A. R., Mandal, P. K., Larson, R., Tin, S., Jimenez, C., et al. (2018). Blocking interleukin (IL)4- and IL13-mediated phosphorylation of STAT6 (Tyr641) decreases M2 polarization of macrophages and protects against macrophage-mediated radioresistance of inflammatory breast cancer. *Int. J. Radiat. Oncol. Biol. Phys.* 100 (4), 1034–1043. doi:10.1016/j.ijrobp.2017.11.043

Ramachandran, L., Manu, K. A., Shanmugam, M. K., Li, F., Siveen, K. S., Vali, S., et al. (2012). Isorhamnetin inhibits proliferation and invasion and induces apoptosis through the modulation of peroxisome proliferator-activated receptor γ activation pathway in gastric cancer. *J. Biol. Chem.* 287 (45), 38028–38040. doi:10.1074/jbc.M112.388702

Saud, S. M., Young, M. R., Jones-Hall, Y. L., Ileva, L., Evbuomwan, M. O., Wise, J., et al. (2013). Chemopreventive activity of plant flavonoid isorhamnetin in colorectal cancer is mediated by oncogenic Src and β-catenin. *Cancer Res.* 73 (17), 5473–5484. doi:10.1158/0008-5472.CAN-13-0525

Seo, K., Yang, J. H., Kim, S. C., Ku, S. K., Ki, S. H., and Shin, S. M. (2014). The antioxidant effects of isorhamnetin contribute to inhibit COX-2 expression in

response to inflammation: a potential role of HO-1. *Inflammation*. 37 (3), 712–722. doi:10.1007/s10753-013-9789-6

Shinozaki, S., Mashima, H., Ohnishi, H., and Sugano, K. (2010). IL-13 promotes the proliferation of rat pancreatic stellate cells through the suppression of NF-kappaB/TGF-beta1 pathway. *Biochem. Biophys. Res. Commun.* 393 (1), 61–65. doi:10.1016/j.bbrc.2010.01.078

Smith, R. A., Andrews, K. S., Brooks, D., Fedewa, S. A., Manassaram-Baptiste, D., Saslow, D., et al. (2019). Cancer screening in the United States, 2019: a review of current American Cancer Society guidelines and current issues in cancer screening. *CA Cancer J. Clin.* 69 (3), 184–210. doi:10.3322/caac.21557

Sun, M., Pan, D., Chen, Y., Li, Y., Gao, K., and Hu, B. (2017). Coroglaucigenin enhances the radiosensitivity of human lung cancer cells through Nrf2/ROS pathway. *Oncotarget* 8 (20), 32807–32820. doi:10.18632/oncotarget.16454

Teng, B. S., Lu, Y. H., Wang, Z. T., Tao, X. Y., and Wei, D. Z. (2006). *In vitro* anti-tumor activity of isorhamnetin isolated from *Hippophae rhamnoides* L. against BEL-7402 cells. *Pharmacol. Res.* 54 (3), 186–194. doi:10.1016/j.phrs.2006.04.007

Varfolomeev, E., Goncharov, T., Fedorova, A. V., Dynek, J. N., Zobel, K., Deshayes, K., et al. (2008). c-IAP1 and c-IAP2 are critical mediators of tumor necrosis factor alpha (TNFalpha)-induced NF-kappaB activation. *J. Biol. Chem.* 283 (36), 24295–24299. doi:10.1074/jbc.C800128200

Wang, C. Y., Mayo, M. W., and Baldwin, A. S., Jr (1996). TNF- and cancer therapy-induced apoptosis: potentiation by inhibition of NF-kappaB. *Science* 274 (5288), 784–787. doi:10.1126/science.274.5288.784

Wu, D., Wu, P., Zhao, L., Huang, L., Zhang, Z., Zhao, S., et al. (2015). NF-κB expression and outcomes in solid tumors: a systematic review and meta-analysis. *Medicine* 94 (40), e1687. doi:10.1097/MD.0000000000001687

Xiao, G. (2007). Autophagy and NF-κB: fight for fate. *Cytokine Growth Factor Rev.* 18 (3–4), 233–243. doi:10.1016/j.cytogfr.2007.04.006

Yang, J. H., Kim, S. C., Shin, B. Y., Jin, S. H., Jo, M. J., Jegal, K. H., et al. (2013). O-Methylated flavonol isorhamnetin prevents acute inflammation through blocking of NF-κB activation. *Food Chem. Toxicol.* 59, 362–372. doi:10.1016/j.fct.2013.05.049

You, S., Li, R., Park, D., Xie, M., Sica, G. L., Cao, Y., et al. (2014). Disruption of STAT3 by niclosamide reverses radioresistance of human lung cancer. *Mol. Canc. Therapeut.* 13 (3), 606–616. doi:10.1158/1535-7163.MCT-13-0608

Zhang, B. Y., Wang, Y. M., Gong, H., Zhao, H., Lv, X. Y., Yuan, G. H., et al. (2015). Isorhamnetin flavonoid synergistically enhances the anticancer activity and apoptosis induction by cis-platin and carboplatin in non-small cell lung carcinoma (NSCLC). *Int. J. Clin. Exp. Pathol.* 8 (1), 25–37.

Zhang, N., Pei, F., Wei, H., Zhang, T., Yang, C., Ma, G., et al. (2011). Isorhamnetin protects rat ventricular myocytes from ischemia and reperfusion injury. *Exp. Toxicol. Pathol.* 63 (1–2), 33–38. doi:10.1016/j.etp.2009.09.005

**Conflict of Interest:** The authors declare that the research was conducted in the absence of any commercial or financial relationships that could be construed as a potential conflict of interest.

frontiers in Pharmacology

REVIEW
published: 08 February 2021
doi: 10.3389/fphar.2020.629266

# DNA Repair Pathways in Cancer Therapy and Resistance

*Lan-ya Li*[1,2], *Yi-di Guan*[1], *Xi-sha Chen*[1], *Jin-ming Yang*[3] *and Yan Cheng*[1]*

[1]Department of Pharmacy, The Second Xiangya Hospital, Central South University, Changsha, China, [2]Xiangya School of Pharmaceutical Sciences, Central South University, Changsha, China, [3]Department of Cancer Biology and Toxicology, Department of Pharmacology, College of Medicine, Markey Cancer Center, University of Kentucky, Lexington, KY, United States

DNA repair pathways are triggered to maintain genetic stability and integrity when mammalian cells are exposed to endogenous or exogenous DNA-damaging agents. The deregulation of DNA repair pathways is associated with the initiation and progression of cancer. As the primary anti-cancer therapies, ionizing radiation and chemotherapeutic agents induce cell death by directly or indirectly causing DNA damage, dysregulation of the DNA damage response may contribute to hypersensitivity or resistance of cancer cells to genotoxic agents and targeting DNA repair pathway can increase the tumor sensitivity to cancer therapies. Therefore, targeting DNA repair pathways may be a potential therapeutic approach for cancer treatment. A better understanding of the biology and the regulatory mechanisms of DNA repair pathways has the potential to facilitate the development of inhibitors of nuclear and mitochondria DNA repair pathways for enhancing anticancer effect of DNA damage-based therapy.

**Keywords: DNA damage, DNA repair pathways, mitochondrial DNA, drug resistance, cancer therapy**

OPEN ACCESS

***Edited by:***
*Zhe-Sheng Chen,*
*St. John's University, United States*

***Reviewed by:***
*Dongmei Zhang,*
*Jinan University, China*
*Guanghui Wang,*
*Xiamen University, China*

***Correspondence:**
*Yan Cheng*
*yancheng@csu.edu.cn*

***Specialty section:***
*This article was submitted to Pharmacology of Anti-Cancer Drugs, a section of the journal Frontiers in Pharmacology*

***Received:*** *14 November 2020*
***Accepted:*** *31 December 2020*
***Published:*** *08 February 2021*

***Citation:***
*Li L, Guan Y, Chen X, Yang J and Cheng Y (2021) DNA Repair Pathways in Cancer Therapy and Resistance. Front. Pharmacol. 11:629266. doi: 10.3389/fphar.2020.629266*

## THE DNA REPAIR PATHWAYS

A variety of endogenous and exogenous DNA-damaging agents such as UV light, ionizing radiation (IR) and chemotherapeutic agents can lead to DNA lesions, including mismatches, single-strand breaks (SSBs), double-strand breaks (DSBs), chemical modifications of the bases or sugars, and interstrand or intrastrand cross-links. If the damage is not corrected, it will cause genomic instability and mutation, which is one of the cancer hallmarks (Hanahan and Weinberg, 2011). In order to prevent this situation, cells have evolved a series of mechanisms called DNA damage response (DDR) in order to deal with such lesions. DDR is a complex network that functions in different ways to target various DNA lesions, including signal transduction, transcriptional regulation, cell-cycle checkpoints, induction of apoptosis, damage tolerance processes, and multiple DNA repair pathways (**Figure 1**) (Giglia-Mari et al., 2011; Tian et al., 2015).

In mammalian cells, the two main organelles containing DNA are nucleus and mitochondria. Nuclear DNA (nDNA) repair systems are divided into the following major pathways: 1) direct reversal, which mainly repairs the lesion induced by alkylating agents, 2) base excision repair (BER), aiming at DNA breaks (SSBs) and non-bulky impaired DNA bases, 3) nucleotide excision repair (NER), correcting bulky, helix-distorting DNA lesions, 4) mismatch repair (MMR), repair of insertion/deletion loops (IDLs) and base-base mismatch, 5) recombinational repair, which is further divided into homologous recombination repair (HRR) and non-homologous end joining (NHEJ), primarily functioning at DNA double strand breaks, 6) alternative nonhomologous end joining (alt-NHEJ, MMEJ), involved in repair of DSBs, 7) translesion synthesis (TLS), which is more likely to be a DNA damage tolerance mechanism (Jackson and Bartek, 2009; Hosoya and Miyagawa, 2014). Mitochondrial DNA (mtDNA) repair pathways, including the direct reversal, BER, MMR,

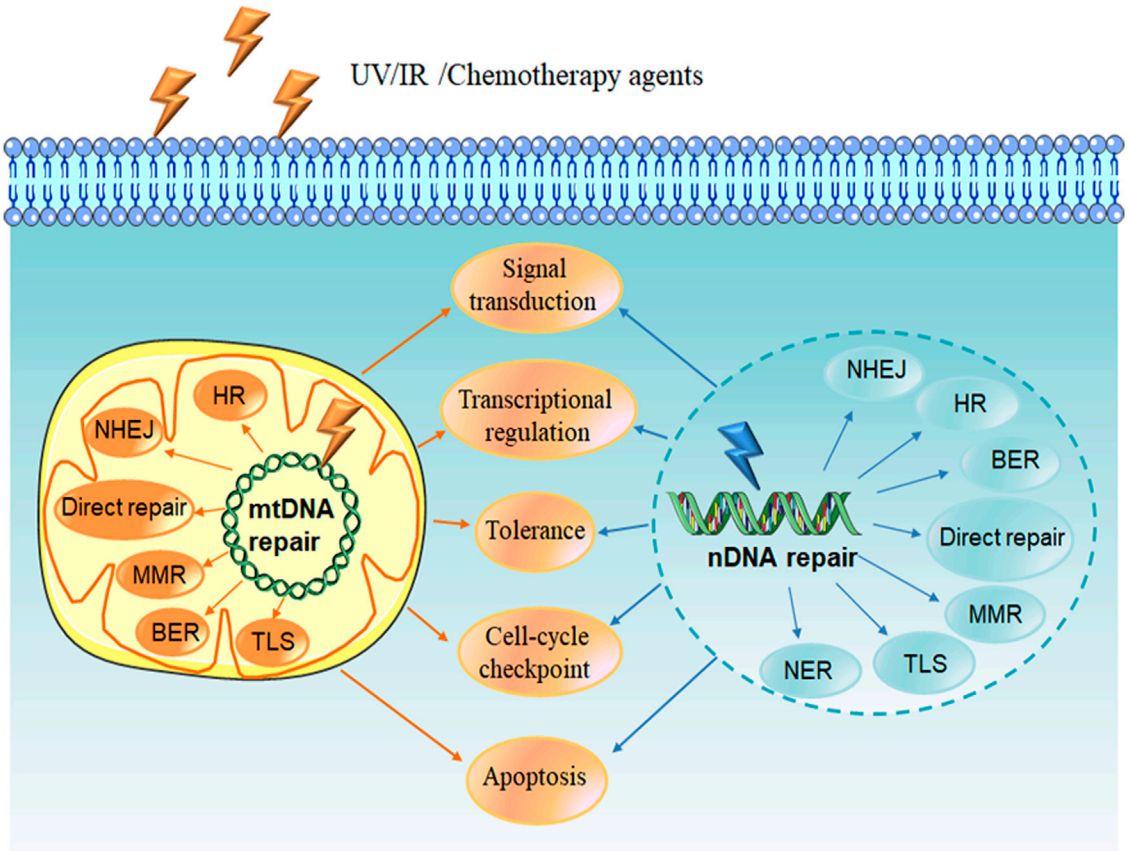


**FIGURE 1 |** DNA damage response. DNA damage is caused by endogenous agent oxygen species (ROS) or exogenous agents such as UV light, ionizing radiation (IR) and chemotherapy agents. DNA damage response (DDR) is induced to deal with the lesions, including signal transduction, transcriptional regulation, cell-cycle checkpoints, induction of apoptosis, multiple DNA repair pathways as well as damage tolerance processes. DNA repair pathways include nuclear and mitochondrial DNA repair pathways. Direct repair, BER, MMR and recombinational repair (HR and NHEJ) are existence in both nuclear and mitochondrial repair systems. NER has been reported only appearance in nucleus, and the existence of TLS pathway in mitochondria is unknown. NDNA, nuclear DNA; MtDNA, mitochondrial DNA; BER, base excision repair; HR, homologous recombination repair; NHEJ, non-homologous end joining; MMR, mismatch repair; TLS, translesion synthesis; NER, nucleotide excision repair.

TLS and double-strand break repair (DSBR), can repair damaged DNA to maintain mitochondria genetic integrity, protect mtDNA against oxidative damage, and promote cell survival (Ohta, 2006; Saki and Prakash, 2017).

## ROLE OF DNA REPAIR PATHWAYS IN CANCER BIOLOGY

DNA repair pathways play an important role in the maintenance of genome stability and integrity through correcting the impaired DNA that may contribute to carcinogenesis (Clementi et al., 2020). Numerous studies have indicated that certain cancers are associated with the defect or mutation in the proteins of nuclear or mitochondrial DNA repair pathways (Pearl et al., 2015; Cerrato et al., 2016). For example, the defect in the ATM–Chk2–p53 pathway, which plays a crucial role in DNA double-strand breaks repair, promoted glioblastoma multiforme (GBM) formation and contributed to GBMs radiation resistance (Squatrito et al., 2010). The human syndrome hereditary nonpolyposis colorectal cancer (HNPCC), which connects with high degrees of microsatellite instability, is caused by germline mutations in MMR genes, and the tumorigenesis of this disease is connected with the defect in the MMR pathway (Hampel et al., 2005). People who carry an MMR gene mutation have the increased risk of a wide variety of cancers than their noncarrier relatives (Win et al., 2012). Two important homologous recombination (HR) DNA repair-related genes, BRCA1 and BRCA2 germline mutant confer the genetic predisposition to breast, ovarian cancer and pancreatic cancer (Riaz et al., 2017). In addition, the tumor microenvironment characteristic of hypoxia, low pH and nutrient deficiency, can give rise to genomic instability and tumor progress through downregulating DNA repair pathway. It has been reported that hypoxic circumstance can result in the reduction of MLH1 expression, a core protein in the MMR pathway (Mihaylova et al., 2003). The downregulation of RAD51, a key mediator of HRR, was observed in multiple cancer cell types

induced by hypoxia, suggesting that the hypoxic tumor microenvironment can suppress the HRR pathway to cause genetic instability (Bindra et al., 2004; Lu et al., 2011). Tumor hypoxia also regulated the DDR by driving alternative splicing (Memon et al., 2016). Study in human pulmonary epithelial cells has found that the acidic conditions delayed DNA damaging compounds benzo[a]pyrene (B[a]P) metabolism and inhibited NER capacity, ultimately enhanced B[a]P-induced DNA damage (Shi et al., 2017). Recent studies have shown that extracellular nutrients have significant effects on genome integrity. Glutamine is the main source of carbon and nitrogen for tumor cells. Lack of glutamine led to DNA alkylation damage by inhibiting ALKBH activity and increased the sensitivity of cancer cells to alkylating agents (Tran et al., 2017). Glucose starvation also enhanced radiosensitivity of tumor cells by reducing DNA double-strand break (DSB) repair (Ampferl et al., 2018). Thus, the dysregulation of DNA repair pathways can contribute to the development of cancer by promoting genomic instability and mutation in mammal cells.

## TARGETING DNA REPAIR PATHWAYS IN CANCER THERAPY

The most common cancer treatments, including chemo- or radiotherapy, are designed to induce cell death by direct or indirect DNA damage. However, tumor cells can initiate DNA repair pathways to resist these anticancer agents during chemo- or radiotherapy. Therefore, combination of the nuclear or mitochondrial DNA repair pathway inhibitors with anticancer agents may increase the tumor cell sensitivity to these agents.

### O-6-Methylguanine-DNA Methyltransferase (MGMT)

The role of MGMT is to remove alkyl adducts from the $O^6$ position of guanine. Thus, the protective effect of MGMT could diminish the cytotoxic effects of alkylating agents (Middleton and Margison, 2003), suggesting that MGMT activity is likely to be a useful marker of the sensitivity of cancer cells to alkylating agents. It has been reported that high MGMT expression in tumor cell is associated with the resistance to 1,3- bis- (2-chloroethyl) -1-nitrosourea (BCNU) and temozolomide (TMZ) (Happold et al., 2018; Hsu et al., 2018), which target the $O^6$-position of guanine, resulting in cytotoxic and mutagenic DNA adducts (Rabik et al., 2006). Recently, researchers found that MGMT-mediated the resistance to DNA alkylating agents in cancer cell is profoundly dependent on the DNA repair enzyme PARP. Combination of temozolomide with PARP inhibitors (PARPi) in MGMT-positive cancer cells enhanced the anticancer effects (Erice et al., 2015; Jue et al., 2017).

The inactivation of MGMT in tumor cells has been appreciated as a therapeutic target for sensitizing cells to $O^6$-alkylating agents (Maki et al., 2005). *In vitro* and *in vivo* studies demonstrated that $O^6$-Benzylguanine ($O^6$-BG), a typical pseudo-substrate that was developed to inactivate MGMT, in combination with $O^6$-alkylating agents increased the therapeutic efficacy of chemotherapeutic alkylating agents (Maki, Murakami, 2005). Lomeguatrib (called $O^6$-(4-bromothenyl) guanine, as well as PaTrin-2), another pseudo-substrate tested in clinical trials, has been shown to increase the therapeutic index of methylating agent temozolomide in nude mice bearing A375M human melanoma xenografts and patients with advanced solid tumors (Middleton et al., 2002; Ranson et al., 2006). Bobustuc GC et al. demonstrated that inhibition of MGMT suppressed the expression of survivin and enhanced the cytotoxicity of gemcitabine in pancreatic cancer (Bobustuc et al., 2015). Another approach to MGMT inactivation is to silence the MGMT gene expression through its promoter methylation. Several studies in animal models have suggested that the therapy of MGMT gene silence was able to overcome TMZ resistance and increase tumor cell death (Viel et al., 2013). Clinical study indicated that patients with glioblastoma containing a methylated MGMT promoter obtained more benefits from TMZ than those who did not have a methylated MGMT promoter (Hegi et al., 2005). Lately, it has been confirmed that MGMT gene methylation can be a biomarker for temozolomide (TMZ) treatment and a potent prognostic factor in patients with GBM (Kim et al., 2012; Iaccarino et al., 2015; Zhao et al., 2016; Binabaj et al., 2018). However, according to the data from National *Cancer* database (NCDB) indicated that only 4.9% of GBM patients have MGMT promoter methylation. Even though MGMT promoter methylation status has prognostic value, it is ignored in the United States (Lee et al., 2018). More researches need to conduct to identify the prognostic value of MGMT promoter methylation in tumor patients responding to alkylating agents.

### Base Excision Repair

A number of investigations have shown that inhibition of BER pathway can enhance the sensitivity of cancer cells to alkylating agents and radiotherapy (Neijenhuis et al., 2005; Gao et al., 2019). The primary methods to prevent the activity of BER pathway focus on the development of AP endonuclease 1 (APE1) or Poly (ADP-ribose) polymerase (PARP) inhibitors.

Several studies indicated that methoxyamine (MX), a small alkoxyamine that can bind with the free aldehyde of AP site to prevent APE1 cleavage at AP sites, thereby inhibiting APE-1 endonuclease activity. Combined treatment with chemotherapeutic alkylating agent such as TMZ and BCNU could reinforce the cytotoxicity of alkylating agent by targeting BER pathway (Liu et al., 2003; Montaldi and Sakamoto-Hojo, 2013). Recently, based on preclinical studies, several clinical trials were conducted, for example combination therapy with MX and TMZ in patients with advanced solid tumors has completed (NCT00892385). Currently, phase I clinical trials of MX in combination of TMZ is undergoing in patients with relapsed solid tumors and lymphomas (NCT01851369). MX combination with pemetrexed disodium, cisplatin, is now investigating in phase I/II stage in patients with advanced malignant solid neoplasm (NCT02535312). Lucanthone, a topoisomerase II inhibitor as well as an APE1 endonuclease inhibitor, has been

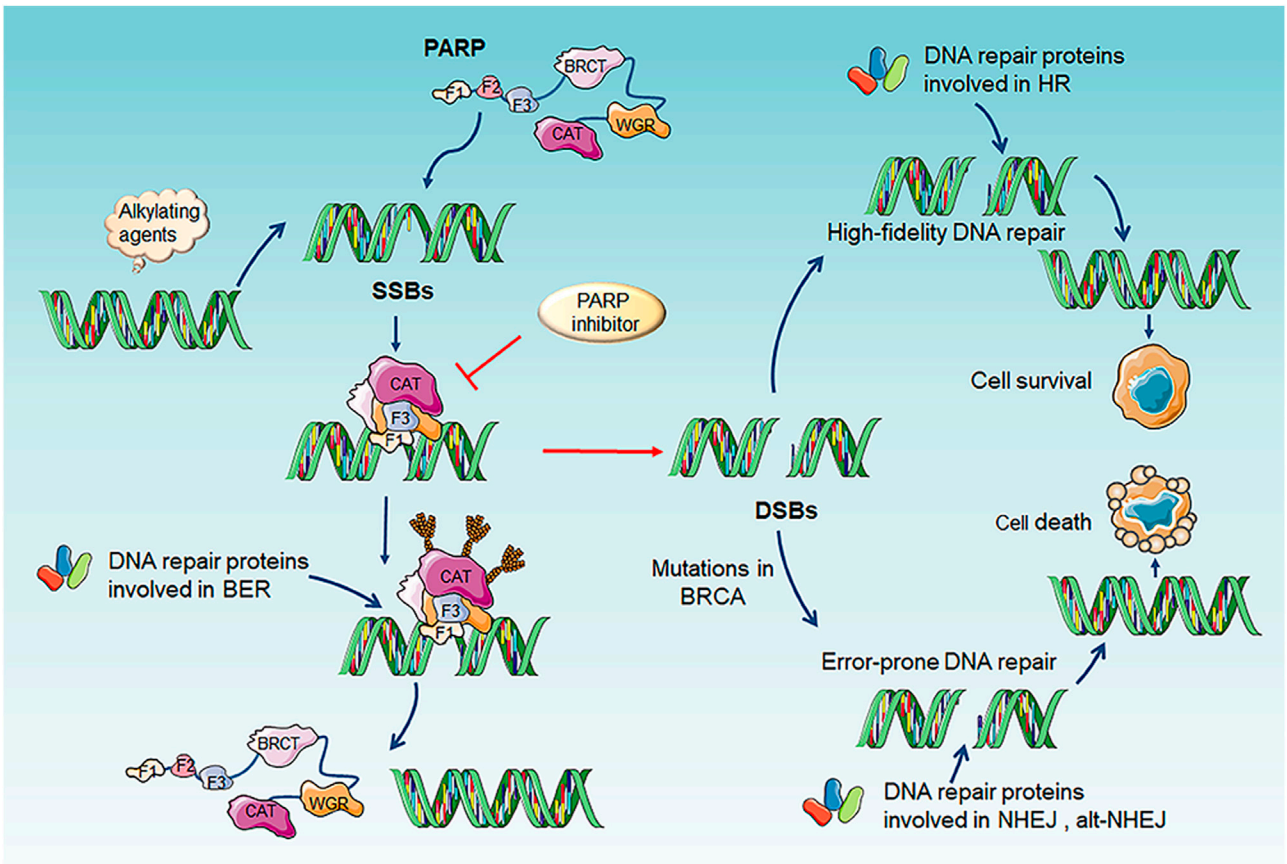


**FIGURE 2 |** Mechanism and function of PARP and PARP inhibitors. The catalytic function of PARP1 is activated through binding to the SSBs site cuased by alkylating agents. Activated PARP1 undergo PARylation and recruitment of a serials of key DNA repair effectors involved in BER to repair DNA lesion. Finally, PARP1 release from DNA and regain inactive state. PARP inhibitors binds the catalytic site of PARP and impaired of the enzymatic activity of PARP which "trap" PARP1 on DNA, results in suppression of the catalytic cycle of PARP1 and BER. Trapping PARP1 on DNA lesion also collapses DNA replication fork, therefore transforming SSBs into genotoxic DSBs. This type of DNA lesion would normally induce HR for repairing damaged DNA. However, if HR-defective exist in tumor cells, including BRCA1/2 deficiency or mutation, another less effective and error-prone DSBs repair pathway NHEJ or alt-NHEJ could be utilized, which causing genomic instability, chromosomal fusions/translocations and subsequently inducing cell death. SSBs, single-strand breaks; DSB, double-strand break; BER, base excision repair; alt-NHEJ, alternative nonhomologous end joining; NHEJ, non-homologous end joining; HR, homologous recombination repair.

shown to reinforce the cell killing effect of alkylating agents in human breast cancer cell line MDA-MB-231 (Luo and Kelley, 2004). Lucanthone combination with radiation and TMZ in GBM patients was tested in phase II clinical trial (NCT01587144). However, it was terminated in 2016. Another phase II clinical trial investigating lucanthone combination with radiation in patients with brain metastases from non-small cell lung cancer was withdrawn due to drug issues (NCT02014545).

PARP family is composed of 17 members, of which PARP1 and PARP2 are well-recognized DNA damage sensors, especially PARP1. PARP1 detect the region of damaged DNA and play a key role in several DNA repair pathway including BER, HHR and MMEJ (Konecny and Kristeleit, 2016). While PARP1 is best studied in BER and the mechanism of PARP inhibitor (PARPi) is based on trapping PARP1 on SSBs DNA site to inhibit BER repair. Finally, it converted SSBs into DSBs and impelled cell death in HR-deficiency tumor, for example BRCA1/2 mutations, RAD51 deficiency (**Figure 2**) (Konecny and Kristeleit, 2016; Brown et al., 2017; Lord and Ashworth, 2017; Oplustil O'Connor et al., 2016). In 2005, two pre-clinical researches published in nature indicated that BRCA1 or BRCA2 deficient cells highly sensitized to PARP inhibition (Farmer et al., 2005; Bryant et al., 2005). Based on the concept of "synthetic lethality"-targeting either gene alone in a synthetic lethal pair is tolerated, but simultaneous targeting both genes is lethal, researchers applied PARPi to BRCA mutation tumors (Dhillon et al., 2016). Several clinical trials using PARPi including Olaparib, Veliparib, Rucaparib (**Table 1**) as monotherapy for the treatment of patients with germline BRCA1/2 mutation tumors including advanced breast cancer, ovarian cancer, pancreatic cancer and prostate cancer presented significantly antitumor effect (Kaufman et al., 2015; Robson et al., 2017; Moore et al., 2018; Golan et al., 2019). Olaparib as maintenance therapy also significantly prolonged progression-free survival in advanced ovarian cancer patients with HRD-positive tumors who have achieved first-line standard therapy including bevacizumab. It has been approved by FDA for utilization of Olaparib in patients with advanced germline

**TABLE 1 |** DNA repair pathway inhibitors in current clinical trials.

| Targeting protein | DNA repair pathway | Inhibitors | Clinical status | Disease state | Intervention/treatment | NCT number | Status |
|---|---|---|---|---|---|---|---|
| PARP1/ PARP2 | BER | Olaparib (AZD-2281) | Phase II | Metastatic renal cell carcinoma with DNA repair gene mutations | Olaparib | NCT03786796 | Recruiting |
| | | | Phase II | Mesothelioma with homologous recombination deficiency | Olaparib | NCT04515836 | Not yet recruiting |
| | | | Phase II | Non-BRCA metastatic breast cancer (MBC) | Olaparib | NCT03367689 | Recruiting |
| | | | Phase II | Metastatic urothelial cancer with somatic DNA damage response (DDR) alterations | Olaparib | NCT03448718 | Recruiting |
| | | | Phase II | Metastatic breast cancer with BRCA1 and/or 2 promoter methylation | Olaparib | NCT03205761 | Recruiting |
| | | | Phase II | Cisplatin-resistant germ cell tumor | Olaparib | NCT02533765 | Active, not recruiting |
| | | | Phase I | Advanced cancer | Olaparib, AZD5363 | NCT02338622 | Completed |
| | | | Phase I | Triple negative breast cancer (TNBC) | Olaparib, radiation therapy | NCT03109080 | Active, not recruiting |
| | | | Phase III | HER2-ve metastatic breast cancer patient | Olaparib | NCT03286842 | Active, not recruiting |
| | | | Phase IV | BRCA or HRR + mutated ovarian cancer | Olaparib | NCT02476968 | Active, not recruiting |
| | | Niraparib | Phase I | Advanced solid tumors | Niraparib | NCT03497429 | Completed |
| | | | Phase II | Uterine serous carcinoma | Niraparib | NCT04080284 | Recruiting |
| | | | Phase I | EGFR-mutated advanced lung cancer | Niraparib, osimertinib | NCT03891615 | Recruiting |
| | | | Phase II | Pancreatic cancer | Niraparib | NCT03601923 | Recruiting |
| | | | Phase I | Solid tumors | SYD985, niraparib | NCT04235101 | Recruiting |
| | | | Phase III | Ovarian cancer | Nirapairb | NCT03709316 | Recruiting |
| | | Talazoparib | Phase I | BRCA mutation-associated breast and ovarian cancers, pancreatic and small cell lung cancer | Talazoparib | NCT01286987 | Completed |
| | | | Phase I | Leukemia with cohesin complex mutation | Talazoparib | NCT03974217 | Recruiting |
| | | | Phase II | Advanced cancer with DNA repair variations | Talazoparib | NCT04550494 | Not yet recruiting |
| | | | Phase II | Triple negative breast cancer | Talazoparib, ZEN003694 | NCT03901469 | Recruiting |
| | | Veliparib (ABT-888) | Phase I | Pancreatic cancer | Veliparib, gemcitabine, radiation | NCT01908478 | Completed |
| | | | Phase I | Refractory Solid Tumors | Veliparib, VX-970, cisplatin | NCT02723864 | Active, not recruiting |
| | | | Phase II | Malignant glioma without H3 K27M or BRAFV600 mutations | Radiation, temozolomide, veliparib | NCT03581292 | Recruiting |
| | | | Phase II | Metastatic breast cancer with BRCA1/2 gene mutation | ABT-888, temozolomide | NCT01009788 | Active, not recruiting |
| | | | Phase II | Refractory testicular germ cell cancer | Gemcitabine, carboplatin, veliparib | NCT02860819 | Active, not recruiting |
| | | | Phase I | Advanced malignant solid neoplasm | Dinaciclib, veliparib | NCT01434316 | Recruiting |
| | | Rucaparib | Phase I | Advanced solid tumor | Rucaparib, camsylate | NCT03521037 | Active, not recruiting |
| | | | Phase II | Nonmetastatic, hormone-sensitive prostate cancer | Rucaparib | NCT03533946 | Recruiting |
| | | | Phase I | Metastatic castration resistant prostate cancer | Rucaparib, enzalutamide, abiraterone | NCT04179396 | Recruiting |
| | | | Phase II | High-grade serous or endometroid ovarian cancer | Rucaparib, nivolumab | NCT03824704 | Active, not recruiting |
| | | | Phase II | Solid tumors and with deleterious mutations in HRR genes | Rucaparib | NCT04171700 | Recruiting |
| | | 2X-121 | Phase II | Metastatic breast cancer | 2X-121 | NCT03562832 | Active, not recruiting |
| APE1 | BER | Methoxyamine (TRC102) | Phase I/II | Relapsed solid tumors and lymphomas | TRC102 | NCT01851369 | Recruiting |
| | | | Phase I/II | Solid tumors or mesothelioma | Cisplatin, methoxyamine, pemetrexed disodium | NCT02535312 | |
| | | | Phase I | Stage IIIA-IV non-small cell lung cancer | Radiation, cisplatin | NCT02535325 | Active, not recruiting |
| APE1/Ref-1 | BER | APX3330 (E3330) | Phase I | Advanced solid tumors | APX3330 | NCT03375086 | Completed |
| DNA-PK | NHEJ | MSC2490484A (M3814) | Phase I | Locally advanced rectal cancer | M3814, avelumab, radiation | NCT03724890 | Recruiting |
| | | | Phase I | Advanced solid tumor | Radiation, cisplatin, MSC2490484A | NCT02516813 | Recruiting |
| | | | Phase I/II | Locally advanced rectal cancer | M3814, capecitabine, radiation | NCT03770689 | Recruiting |
| | | VX-984 (M9831) | Phase I | Advanced solid tumor | IV pegylated liposomal doxorubicin, VX-984 | NCT02644278 | Completed |
| DNA-PK/ mTOR | NHEJ | CC-115 | Phase I | Advanced solid tumors, hematologic malignancies | CC-115 | NCT01353625 | Active, not recruiting |

(Continued on following page)

**TABLE 1 |** (*Continued*) DNA repair pathway inhibitors in current clinical trials.

| Targeting protein | DNA repair pathway | Inhibitors | Clinical status | Disease state | Intervention/treatment | NCT number | Status |
|---|---|---|---|---|---|---|---|
| ATM | HR | AZD0156 | Phase I | Advanced solid tumors | AZD0156, olaparib, irinotecan, fluorouracil, folinic acid | NCT02588105 | Active, not recruiting |
| | | AZD1390 | Phase I | Brain cancer | Radiation, AZD1390 | NCT03423628 | Recruiting |
| | | | Phase I | Non small cell lung cancer | Radiation, olaparib, AZD1390 | NCT04550104 | Not yet recruiting |
| ATR | HR | AZD6738 (Ceralasertib) | Phase II | Biliary tract cancer | AZD6738, durvalumab | NCT04298008 | Recruiting |
| | | | Phase I | Leukemia, myelodysplastic syndrome | AZD6738 | NCT03770429 | Recruiting |
| | | | Phase II | Relapsed small cell lung cancer subjects | Durvalumab, AZD6738 | NCT04361825 | Enrolling by invitation |
| | | | Phase II | Clear cell renal cell carcinoma, locally advanced pancreatic cancer, locally advanced malignant solid neoplasm | AZD6738, olaparib | NCT03682289 | Recruiting |
| | | | Phase I | Refractory cancer | AZD6738, paclitaxel | NCT02630199 | Recruiting |
| | | | Phase II | Recurrent ovarian cancer | Olaparib pill, AZD6738 | NCT03462342 | Recruiting |
| | | | Phase II | IDH1 and IDH2 mutant tumors | Ceralasertib, olaparib | NCT03878095 | Recruiting |
| | | VE-822 (VX-970, M6620, berzosertib) | Phase II | Solid tumor, leiomyosarcoma, osteosarcoma | M6620 | NCT03718091 | Recruiting |
| | | | Phase1/II | Small cell cancers and extrapulmonary small cell cancers | Topotecan, VX-970 | NCT02487095 | Recruiting |
| | | | Phase I | Refractory solid tumors | Veliparib, VX-970, cisplatin | NCT02723864 | Active, not recruiting |
| | | | Phase II | Small cell lung cancers and small cell cancers outside of the lungs | Berzosertib, topotecan hydrochloride | NCT03896503 | Recruiting |
| | | | Phase II | Metastatic urothelial cancer | Berzosertib, cisplatin, gemcitabine hydrochloride | NCT02567409 | Active, not recruiting |
| CHK1 | HR | Prexasertib | Phase II | Triple negative breast cancer | LY3023414, prexasertib | NCT04032080 | Recruiting |
| | | | Phase II | Recurrent or refractory solid tumors | Prexasertib | NCT02808650 | Active, not recruiting |
| | | | Phase I/II | Desmoplastic small round cell tumor, rhabdomyosarcoma | Prexasertib, irinotecan | NCT04095221 | Recruiting |
| | | | Phase II | Platinum-resistant or refractory recurrent ovarian cancer | Prexasertib | NCT03414047 | Active, not recruiting |
| | | | Phase I | Advanced solid tumors | Prexasertib, olaparib | NCT03057145 | Active, not recruiting |
| | | MK-8776 | Phase I | Acute leukemias | MK-8776, cytarabine | NCT00907517 | Terminated |
| | | SRA737 | Phase I/II | Advanced solid tumors | SRA737, gemcitabine, cisplatin | NCT02797977 | Completed |
| WEE1 | HR | Adavosertib (AZD1775) | Phase II | Uterine serous carcinoma | Adavosertib | NCT04590248 | Not yet recruiting |
| | | | Phase I | Advanced solid tumors | Adavosertib | NCT04462952 | Recruiting |
| | | | Phase I/II | Relapsed or refractory solid tumors | Adavosertib, irinotecan hydrochloride | NCT02095132 | Active, not recruiting |
| | | | Phase I | Newly diagnosed or recurrent glioblastoma | Adavosertib, radiation therapy, temozolomide | NCT01849146 | Active, not recruiting |

*Abbreviations: PARP, Poly (ADP-ribose) polymerase; APE1, AP endonuclease 1; Ref-1, redox factor-1; DNA-PK, DNA-dependent protein kinase; mTOR, mammalian target of rapamycin; ATM, ataxia telangiectasia mutated; ATR, ataxia telangiectasia and Rad3-related; CHK1, checkpoint kinase 1; WEE1, Wee1-like protein kinase.*

BRCA-mutated ovarian cancer following three or more prior lines of chemotherapy (Kim et al., 2015). On May 19, 2020, the FDA also approved Olaparib for patients with metastatic castration-resistant prostate cancer (mCRPC) carrying HRR gene-mutated based on NCT02987543. PAPR1 inhibitors in combination with IR or with other different anticancer agents are currently undergoing clinical trials for treatment of patients with BRCA1/2 mutation or HRR-deficiency advanced solid tumors, which shown promising clinical activity (Bang et al., 2017; Wilson et al., 2017; Loibl et al., 2018; Coleman et al., 2019; Farago et al., 2019; Konstantinopoulos et al., 2019; Liu et al., 2019).

## Double Strand Breaks Repair

Among various DNA lesions, DSBs is the leading lethal damage that leads to cell death and genetic mutations. DNA-dependent protein kinase (DNA-PK), a member of the PI3K-related protein kinase (PIKK) family, is involved in DSBs repair pathway via non-homologous end joining (NHEJ) (Jette and Lees-Miller, 2015). It has been reported that DNA-PK activity plays a role in chemo-radiotherapy resistance (Wang Y. et al., 2018; Stefanski et al., 2019; Alikarami et al., 2017; Liu et al., 2015). Selective DNA-PK inhibitor have been developed, including NU7026 (Dolman et al., 2015), NU7441 (Yang et al., 2016), IC87361 and SU11752 (Shinohara et al., 2005). They could inhibit DSBs repair pathway and enhance the sensitivity of cancer cells to ionizing radiation or/and chemo-potentiation such as doxorubicin (Ciszewski et al., 2014). The combination of DNA-PK inhibitor M3814 with type II topoisomerase inhibitors, including doxorubicin, etoposide and pegylated liposomal doxorubicin, enhanced the efficacy of type II

topoisomerase inhibitors in ovarian cancer xenografts (Wise et al., 2019). Several novel DNA-PK inhibitors including MSC2490484A, VX-984 (M9831), M3814 are under clinical trial as single-agent or combination with Chemo-radiotherapy (**Table 2**). Alexander K. Tsai *et al.* recently found that NU7441 combination with a multikinase inhibitor regorafenib altered immune microenvironment of melanomas and enhanced the efficacy of various immunotherapies (Tsai et al., 2017).

Ataxia-teleangectasia mutated (ATM) and ATM-RAD3-related (ATR) protein, like DNA-PK protein, are the members of PIKK family. They work as a transducer of the DSB signal, and are involved in the repair of DNA DSBs (Weber and Ryan, 2015). A large of ATM inhibitors, including KU-55933, KU-60019, KU-59403, CP-466722, AZ31, AZ32, AZD0156, and AZD1390, have been developed and their antitumor effects have been investigated (Jin and Oh, 2019). It has been reported that human tumor cells treated with KU-55933, a specific inhibitor of the ATM kinase, could sensitize tumor cells to the cytotoxic effects of IR and DNA DSBs-inducing chemotherapeutic agents such as etoposide, doxorubicin, and camptothecin (Hickson et al., 2004; Hoey et al., 2018). KU-60019, an improved ATM kinase inhibitor, acts as a highly effective radio-sensitizer in human glioma cells (Biddlestone-Thorpe et al., 2013). AZD0156, a newly discovered ATM inhibitor, has the potential to promote the survival of leukemia-bearing mice and now is under clinical trial (Morgado-Palacin et al., 2016). Preclinical study demonstrated that ATM inhibitor AZD1390 enhanced the radiosensitivity of tumor cells and extended animal survival in preclinical brain tumor models (Durant et al., 2018). AZD1390, as a radiosensitizer, is now undergoing two clinical trials in patients with brain cancer (NCT03423628) or non small cell lung cancer (NCT04550104). Many inhibitors aiming at both ATM and DNA-PK have been reported to have great potential as a chemo- and radiotherapy sensitizing agents in cancer therapy (Powell and Bindra, 2009).

The cell cycle checkpoint kinases CHK1 and CHK2 are downstream substrates of ATM /ATR, which act as the "central transducers" of the DDR (Pilie et al., 2019). Activation of these pathways is essential for the proper regulation of checkpoint and DNA repair (Smith et al., 2010). The ATM–Chk2 and ATR–Chk1 pathways respond to different DNA damages, ATM is activated at DSBs, whereas ATR is recruited to tracts of ssDNA (Di Benedetto et al., 2017). Subsequently, CHK1 and CHK2 activated by ATR and ATM respectively upon their recruitment to DNA damage sites. Protein kinase WEE1 functioned as furthest downstream in ATR/CHK1 pathway, which is indirectly regulated by DNA damage (Cleary et al., 2020). WEE1 actives the G2/M cell cycle checkpoint by impeding cyclin-dependent kinase 1 and 2 (CDK1/2) activity, thereby inducing cell cycle arrest and promoting DNA damage repair. Inhibition of WEE1 causes aberrant DNA replication and replication-dependent DNA damage in cells by suppressing CDK2 (Guertin et al., 2013). Recently, compounds targeting CHK1 are currently in clinical trials (**Table 1**). The first-in-class WEE1 kinase inhibitor AZD1775 is also undergoing a series of clinical trials as monotherapy or in combination with other therapies (**Table 1**).

## mtDNA Repair Pathway

Recently, the exploration of novel anticancer strategies aiming at the differences in mitochondrial function and structure between normal cells and cancer cells has received intensive attention (Porporato et al., 2018). However, there are few studies that have discovered new anticancer approaches via targeting mtDNA repair pathway.

Like nDNA, efficient mtDNA repair pathway, especially BER pathway that mainly repairs ROS-induced lesion, may play an important role in cellular resistance to cancer therapeutic agents. MtDNA D-loop mutations were common in gastrointestinal cancer and correlated with carcinoma progression (Wang B. et al., 2018). It has been found that human breast cancer cells defective of mtDNA repair are more sensitive to oxidative damage than the control cells (Shokolenko et al., 2003). Grishko V I *et al* indicated that mtDNA repair pathways played an important role in protecting cells against ROS in normal HA1 Chinese hamster fibroblasts (Grishko et al., 2005). Another study clarified that mtDNA repair capacity was important for cellular resistance to oxidative damage by increasing their viability following exposure to oxidative stress (Shokolenko et al., 2003). Ueta E *et al* demonstrated that downregulation of the mtDNA repair-associated molecules, mitochondrial transcription factor A (mtTFA) and Poly by using inhibitors of PI3K/Akt signaling in oral squamous cell carcinoma cells (OSC) increased the susceptibility of radio-sensitive OSC cells and radio-resistant OSC cells to gamma-rays (Ueta et al., 2008). This observation implied that PI3K/Akt signal inhibitors can suppress mtDNA repair capacity. Thus, these inhibitors combined with ionizing irradiation or chemotherapeutic drugs may be utilized as an effective strategy in cancer therapy.

DNA glycosylases are involved in the initiation step of BER that recognizes and removes the abnormal base (Anderson and Friedberg, 1980). 8-OxoG-recognizing DNA glycosylase 1 (OGG1) is an important DNA glycosylase for repair of 8-oxoguanine (8-oxoG), which is one of the major DNA lesions both of the nDNA and mtDNA, especially in mtDNA (Rachek et al., 2002). It has been found that tumor cells harboring overexpressed recombinant OGG1 were more proficient at repairing of oxidative damage to mtDNA, and had increased cellular survival under oxidative stress (Rachek et al., 2002; Yuzefovych et al., 2016). We previously found that Sirt3, a major mitochondrial $NAD^+$-dependent deacetylase, physically associated with OGG1 and deacetylated this DNA glycosylase, and that deacetylation by Sirt3 prevented the degradation of the OGG1 protein and controlled its incision activity (Cheng et al., 2013). We further showed that regulation of the acetylation and turnover of OGG1 by Sirt3 played a critical role in repairing mitochondrial DNA (mtDNA) damage, protecting mitochondrial integrity, and preventing apoptotic cell death under oxidative stress. We observed that following ionizing radiation, human tumor cells with silencing of Sirt3 expression exhibited oxidative damage of mtDNA, as measured by the accumulation of 8-oxoG and 4,977 common deletion, showed more severe mitochondrial dysfunction, and underwent greater apoptosis, in comparison to the cells without silencing of Sirt3 expression. Our results not only reveal a new function and mechanism for Sirt3 in defending the mitochondrial genome against oxidative damage and in protecting from the

**TABLE 2 |** Inhibitors of DNA repair pathway recently under preclinical studies.

| Inhibitor | DNA repair pathway | Target | Application | References |
|---|---|---|---|---|
| Lomeguatrib (PaTrin-2) | Direct repair | MGMT | Pancreatic cancer cells; combination with HDACis in ovarian cancer | Wu et al. (2019), Shi et al. (2020) |
| Lucanthone | BER | APE1 | Glioblastoma multiforme (GBM) cell | Chowdhury et al. (2015) |
| CRT0044876 | BER | APE1 | Colon cancer cell lines | Seo and Kinsella (2009) |
| Methoxyamine | BER | APE1 | Combination with pemetrexed in non-small-cell lung cancer cells and xenografts | Oleinick et al. (2016) |
| APX3330 (E3330) | BER | APE1/Ref-1 | Bladder cancer | (Fishel et al., 2019) |
| RI-1 | HR | RAD51 | Combination with olaparib in breast cancer cells with wild-type PTEN; combination with radiation in glioma stem cells | King et al. (2017), Zhao et al. (2017) |
| B02 | HR | RAD51 | Combination with radiation in glioma stem cells; combination with clinically approved anticancer agents in breast cancer cell | Huang and Mazin (2014), King et al. (2017) |
| AG-14361 | BER | PARP1 | Combination with lestaurtinib in breast cancer cells | Vazquez-Ortiz et al. (2014) |
| A-966492 | BER | PARP1/2 | Combination with topotecan and radiotherapy on glioblastoma spheroids | Koosha et al. (2017) |
| KU-55933 | HR | ATM | Combination with radiotherapy on glioblastoma spheroids | Carruthers et al. (2015) |
| ETP-46464 | HR | ATM/ATR, mTOR | Single or combination with cisplatin in platinum-sensitive and -resistant ovarian, endometrial and cervical cancer cell lines | Teng et al. (2015) |
| VE-821 | HR | ATR | Combination with BETi in myc-induced lymphoma cells | Muralidharan et al. (2016) |
| AZ20 | HR | ATR | Colorectal adenocarcinoma tumor cells | Foote et al. (2013) |
| CGK733 | HR | ATM/ATR | Human breast cancer cells | Alao and Sunnerhagen (2009) |
| NU7026 | NHEJ | DNA-PK | Combination with carbon ion irradiation in non-small cell lung cancer cell | Ma et al. (2015) |
| NU7441 | NHEJ | DNA-PK | Combination with radiotherapy in non-small cell lung cancer cell | Sunada et al. (2016) |

*Abbreviations: MGMT, O-6-methylguanine-DNA methyltransferase; APE1, AP endonuclease 1; Ref-1, redox factor-1; RAD51, DNA repair protein RAD51 homolog 1; PARP, Poly (ADP-ribose) polymerase; ATM, ataxia telangiectasia mutated; ATR, ataxia telangiectasia and Rad3-related; mTOR, mammalian target of rapamycin; DNA-PK, DNAdependent protein kinase; BETi, BET inhibitors.*

genotoxic stress-induced apoptotic cell death, but also provide evidence supporting a new mtDNA repair pathway. Recently, researchers also proved that overexpression of mitochondrial OGG1 decreased breast cancer progression and metastasis (Yuzefovych et al., 2016).

In conclusion, combination of DNA repair pathway inhibitors with anticancer agents may enhance the tumor sensitivity to certain chemotherapeutic drugs and radiation. More effective and less toxic DNA-damaging agents have been developed and carried out in preclinical studies (**Table 2**). Based on the preclinical data, a number of clinical trials have been launched to test whether targeting DNA repair pathways can reinforce the efficacy of some anticancer drugs and benefit cancer patients (**Table 1**).

## THE RELATIONSHIP BETWEEN DNA REPAIR PATHWAYS AND CANCER THERAPEUTIC RESISTANCE

Resistance to cancer therapy remains the leading cause of treatment failure in cancer patients. DNA repair capacity (DRC) of tumor cells has been known to involve in drug resistance, including chemoradiotherapy, targeted therapy and immunotherapy. DNA damage inducing drug cisplatin is one of the most widely employed chemotherapeutic drugs. In a murine model of human lung cancer, tumor cells were initially effective with cisplatin treatment, but resistant emerged after prolonged treatment (Oliver et al., 2010). Cisplatin-resistant tumor cells exhibited higher level of DNA damage repair related genes and DRC, inhibition of NER pathway significantly enhanced the sensitivity of tumor cells to cisplatin (Oliver, Mercer, 2010; Wang et al., 2011). Low expression of 53BP1, a DDR protein involved in NHEJ, was associated with higher local recurrence in triple negative breast cancers (TNBC) patients treated with breast-conserving surgery and radiotherapy, indicating that 53BP1 may be a predictor of radio-resistance (Neboori et al., 2012). PTEN Y240 phosphorylation induced by ionizing radiation (IR), a standard treatment for glioblastoma (GBM) patients, promoted therapeutic resistance by enhancing DNA repair (Ma et al., 2019). Inhibiting DNA repair kinases could also prevent doxorubicin (DOX) resistance in breast cancer cells (Stefanski et al., 2019). Abnormal DNA repair activity was found in CDK4/6 inhibitors palbociclib-resistant breast cancer cells, whereas PARP inhibitors, olaparib and niraparib treatment could significantly inhibit palbociclib-resistant cancer cell viability (Kettner et al., 2019). In the recent years, immunotherapy is a major breakthrough in the field of cancer treatment. Therefore, the role of DDR in tumor immunotherapy has attracted much attention. Studies have shown deficiency of a specific DNA repair pathway was associated with immune checkpoint blockade (ICB) response. For example, MMR has been reported as a critical biomarker of response to immune checkpoint inhibitors in cancer (Le et al., 2017). Alterations in genes encoding MMR proteins often contribute to frameshift mutations, resulting in neoantigen generation (Germano et al., 2017). Phase II clinical trials proved that mismatch repair–deficient tumors exhibited higher responsive to PD-1 blockade compared with mismatch repair–proficient tumors(Asaoka et al., 2015). Based on lines of pre-clinical

and clinical evidence, the US Food and drug Administration (FDA) has approved anti-PD-1 antibodies for the treatment of patients with MMR-deficient (Ruiz-Bañobre and Goel, 2019). On the contrary, researchers also found that colorectal cancer (CRC) patient with DNA mismatch repair deficiency (dMMR)/a high-level of microsatellite instability (MSI-H) exhibited intrinsic resistance to immune checkpoint immune checkpoint inhibitor (Gurjao et al., 2019). Metastatic urothelial carcinoma (mUC) shown relatively low response rates to PD-1/PD-L1 blockade (15–24%), whereas the presence of DDR gene mutations is a potential marker of clinical benefit from anti-PD-1/PD-L1 immune checkpoint inhibitors in mUC (Teo et al., 2018). Preclinical studies have also revealed that suppression of PARP induced PD-L1 expression and consequently caused immunosuppression (Jiao et al., 2017). Researches also elucidated that PARP inhibitor olaparib enhanced $CD8^+$ T-cell recruitment and activation by activating the cGAS/STING pathway in BRCA1-deficient triple-negative breast cancer (Pantelidou et al., 2019). Therefore, multiple combination studies involving immune checkpoint inhibitors with DDR inhibitors are undergoing clinical trials, such as combination PARP inhibitor Niraparib and anti-PD-1 antibody pembrolizumab in patients with triple-negative breast cancer or ovarian cancer (NCT02657889). In the phase I, multi-center, dose-escalation study, patients with advanced solid tumors will receive WEE1 inhibitor AZD1775 (Adavosertib) in combination with MEDI4736 (durvalumab) (NCT02546661). These studies suggest that DRC plays a key role in cancer therapy resistance, therefore, evaluation of DNA repair phenotype before treatment could be of great value in clinical management of clinical therapeutic drugs or modalities.

A number of DDR inhibitors have currently come to market or under clinical development. PARP inhibitors are the first clinically approved DDR drugs based on the concept of "synthetic lethal" (Lord and Ashworth, 2017). PARP inhibitors have been widely used for cancer patients with BRCA1/2 mutation or HRR deficiency and showed promising clinical activity. However, resistance inevitably developed in the majority of patients and led to treatment failure. The mechanism of resistance to PARP inhibitors can be innate or acquired though clinical and preclinical studies. Preclinical studies demonstrated that overexpression of P-glycoprotein drug efflux transporter implicated in intrinsic resistance to Olaparib (Henneman et al., 2015). Resumption of PARformation due to poly (ADP-ribose) glycohydrolase (PARG) depletion conferred acquired resistance to PARP inhibition in BRCA2-deficient tumor cells (Gogola et al., 2018). PARP1 p. T910A mutation could override PARP1 inhibition promoted the secondary failure of Olaparib treatment (Gröschel et al., 2019). Another mechanism leading to resistance may restoration of HRR function or re-construction of replication fork stability by increasing RAD51 expression or re-expressing BRCA1/2 (Ter Brugge et al., 2016; Quigley et al., 2017; Clements et al., 2018; Lim et al., 2018; Marzio et al., 2019). Upregulation of certain oncogenic pathways such as Wnt/β-catenin signaling pathway or DDR related protein may also confer cancer cells insensitive to PARP inhibitors and providing some rationale for combination strategies with PARP inhibitors (Fukumoto et al., 2019; Watson et al., 2019; Liu et al., 2020).

## CONCLUSION AND PERSPECTIVES

Based on the relationship between DNA repair pathways and cancer development and progression, a new therapeutic strategy has emerged to increase the efficacy of DNA damaging agents through combination with inhibitors of DNA repair pathways. The inhibitors of several DNA repair pathways have been developed, and some of them are currently undergoing clinical trials. The therapeutic benefits of these agents should be further evaluated in cancer treatment, and the more specific inhibitors should be developed to reduce the adverse effect on normal tissues and cells. Many studies have demonstrated that the inhibition of DNA repair pathways may be an important way in anticancer therapies. However, we should realize that use of certain inhibitors of DNA repair pathways may have potential drawbacks. The combination of IR or chemotherapeutic agents with inhibitors of DNA repair pathway may increase the mutagenic lesions in surviving cells and lead to the development of secondary tumors. More attentions have been paid to the relationship between defective nuclear DNA repair pathway and therapeutic resistance but less about the association between the mitochondrial repair pathway and cancer cells. Due to the difference in mtDNA between cancer cells and normal cells, the development of mtDNA repair pathway inhibitors that can reduce the adverse effects to normal cells may be a more effective strategy to enhance the anticancer therapy than targeting nDNA. A better understanding on the mechanisms of mtDNA repair pathways shall facilitate the development of new effective chemo- and radiosensitizers by targeting mtDNA repair pathway in cancer therapy.

## AUTHOR CONTRIBUTIONS

LL drafted the manuscript. YG and XC designed the figure and table. JY and YC designed, reviewed, and finalized the manuscript. All authors contributed to the article and approved the submitted version.

## FUNDING

This work was supported by grants from the National Natural Science Foundation of China 81422051, 81472593, and 31401208 (YC).

## REFERENCES


Alao, J. P., and Sunnerhagen, P. (2009). The ATM and ATR inhibitors CGK733 and caffeine suppress cyclin D1 levels and inhibit cell proliferation. *Radiat. Oncol.* 4, 51. doi:10.1186/1748-717x-4-51

Alikarami, F., Safa, M., Faranoush, M., Hayat, P., and Kazemi, A. (2017). Inhibition of DNA-PK enhances chemosensitivity of B-cell precursor acute lymphoblastic leukemia cells to doxorubicin. *Biomed. Pharmacother.* 1077–1093. doi:10.1016/j.biopha.2017.08.022

Ampferl, R., Rodemann, H. P., Mayer, C., Hofling, T. T. A., and Dittmann, K. (2018). Glucose starvation impairs DNA repair in tumour cells selectively by blocking histone acetylation. *Radiother. Oncol.* 3, 465–470. doi:10.1016/j.radonc.2017.10.020

Anderson, C. T., and Friedberg, E. C. (1980). The presence of nuclear and mitochondrial uracil-DNA glycosylase in extracts of human KB cells. *Nucleic Acids Res.* 4, 875.

Asaoka, Y., Ijichi, H., and Koike, K. (2015). PD-1 blockade in tumors with mismatch-repair deficiency. *N. Engl. J. Med.* 20, 1979. doi:10.1056/NEJMc1510353

Bang, Y. J., Xu, R. H., Chin, K., Lee, K. W., Park, S. H., Rha, S. Y., et al. (2017). Olaparib in combination with paclitaxel in patients with advanced gastric cancer who have progressed following first-line therapy (GOLD): a double-blind, randomised, placebo-controlled, phase 3 trial. *Lancet Oncol.* 12, 1637–1651. doi:10.1016/s1470-2045(17)30682-4

Biddlestone-Thorpe, L., Sajjad, M., Rosenberg, E., Beckta, J. M., Valerie, N. C., Tokarz, M., et al. (2013). ATM kinase inhibition preferentially sensitizes p53-mutant glioma to ionizing radiation. *Clin. Cancer Res.* 12, 3189–3200. doi:10.1158/1078-0432.ccr-12-3408

Binabaj, M. M., Bahrami, A., ShahidSales, S., Joodi, M., Joudi Mashhad, M., Hassanian, S. M., et al. (2018). The prognostic value of MGMT promoter methylation in glioblastoma: a meta-analysis of clinical trials. *J. Cell. Physiol.* 1, 378–386. doi:10.1002/jcp.25896

Bindra, R. S., Schaffer, P. J., Meng, A., Woo, J., Maseide, K., Roth, M. E., et al. (2004). Down-regulation of Rad51 and decreased homologous recombination in hypoxic cancer cells. *Mol. Cell Biol.* 19, 8504–8518. doi:10.1128/mcb.24.19.8504-8518.2004

Bobustuc, G. C., Patel, A., Thompson, M., Srivenugopal, K. S., Frick, J., Weese, J., et al. (2015). MGMT inhibition suppresses survivin expression in pancreatic cancer. *Pancreas.* 4, 626–635. doi:10.1097/mpa.0000000000000299

Brown, J. S., O'Carrigan, B., Jackson, S. P., and Yap, T. A. (2017). Targeting DNA repair in cancer: beyond PARP inhibitors. *Canc. Discov.* 1, 20–37. doi:10.1158/2159-8290.CD-16-0860

Bryant, H. E., Schultz, N., Thomas, H. D., Parker, K. M., Flower, D., Lopez, E., et al. (2005). Specific killing of BRCA2-deficient tumours with inhibitors of poly(ADP-ribose) polymerase. *Nature.* 7035, 913–917. doi:10.1038/nature03443

Carruthers, R., Ahmed, S. U., Strathdee, K., Gomez-Roman, N., Amoah-Buahin, E., Watts, C., et al. (2015). Abrogation of radioresistance in glioblastoma stem-like cells by inhibition of ATM kinase. *Mol. Oncol.* 1, 192–203. doi:10.1016/j.molonc.2014.08.003

Cerrato, A., Morra, F., and Celetti, A. (2016). Use of poly ADP-ribose polymerase [PARP] inhibitors in cancer cells bearing DDR defects: the rationale for their inclusion in the clinic. *J. Exp. Clin. Cancer Res.* 1, 179. doi:10.1186/s13046-016-0456-2

Cheng, Y., Ren, X., Gowda, A. S., Shan, Y., Zhang, L., Yuan, Y. S., et al. (2013). Interaction of Sirt3 with OGG1 contributes to repair of mitochondrial DNA and protects from apoptotic cell death under oxidative stress. *Cell Death Dis.* 4, e731. doi:10.1038/cddis.2013.254

Chowdhury, S. M., Surhland, C., Sanchez, Z., Chaudhary, P., Suresh Kumar, M. A., Lee, S., et al. (2015). Graphene nanoribbons as a drug delivery agent for lucanthone mediated therapy of glioblastoma multiforme. *Nanomedicine* 1, 109–118. doi:10.1016/j.nano.2014.08.001

Ciszewski, W. M., Tavecchio, M., Dastych, J., and Curtin, N. J. (2014). DNA-PK inhibition by NU7441 sensitizes breast cancer cells to ionizing radiation and doxorubicin. *Breast Cancer Res. Treat* 1, 47–55. doi:10.1007/s10549-013-2785-6

Cleary, J. M., Aguirre, A. J., Shapiro, G. I., and D'Andrea, A. D. (2020). Biomarker-guided development of DNA repair inhibitors. *Mol. Cell.* 6, 1070–1085. doi:10.1016/j.molcel.2020.04.035

Clementi, E., Inglin, L., Beebe, E., Gsell, C., Garajova, Z., and Markkanen, E. (2020). Persistent DNA damage triggers activation of the integrated stress response to promote cell survival under nutrient restriction. *BMC Biol* 1, 36. doi:10.1186/s12915-020-00771-x

Clements, K. E., Thakar, T., Nicolae, C. M., Liang, X., Wang, H. G., and Moldovan, G. L. (2018). Loss of E2F7 confers resistance to poly-ADP-ribose polymerase (PARP) inhibitors in BRCA2-deficient cells. *Nucleic Acids Res.* 17, 8898–8907. doi:10.1093/nar/gky657

Coleman, R. L., Fleming, G. F., Brady, M. F., Swisher, E. M., Steffensen, K. D., Friedlander, M., et al. (2019). Veliparib with first-line chemotherapy and as maintenance therapy in ovarian cancer. *N. Engl. J. Med.* 25, 2403–2415. doi:10.1056/NEJMoa1909707

Dhillon, K. K., Bajrami, I., Taniguchi, T., and Lord, C. J. (2016). Synthetic lethality: the road to novel therapies for breast cancer. *Endocr. Relat. Cancer.* 10, T39–T55. doi:10.1530/erc-16-0228

Di Benedetto, A., Ercolani, C., Mottolese, M., Sperati, F., Pizzuti, L., Vici, P., et al. (2017). Analysis of the ATR-Chk1 and ATM-Chk2 pathways in male breast cancer revealed the prognostic significance of ATR expression. *Sci. Rep.* 1, 8078. doi:10.1038/s41598-017-07366-7

Dolman, M. E., van der Ploeg, I., Koster, J., Bate-Eya, L. T., Versteeg, R., Caron, H. N., et al. (2015). DNA-dependent protein kinase as molecular target for radiosensitization of neuroblastoma cells. *PLoS One.* 12, e0145744. doi:10.1371/journal.pone.0145744

Durant, S. T., Zheng, L., Wang, Y., Chen, K., Zhang, L., Zhang, T., et al. (2018). The brain-penetrant clinical ATM inhibitor AZD1390 radiosensitizes and improves survival of preclinical brain tumor models. *Sci. Adv.* 6, eaat1719. doi:10.1126/sciadv.aat1719

Erice, O., Smith, M. P., White, R., Goicoechea, I., Barriuso, J., Jones, C., et al. (2015). MGMT expression predicts PARP-mediated resistance to temozolomide. *Mol. Cancer Ther.* 5, 1236–1246. doi:10.1158/1535-7163.mct-14-0810

Farago, A. F., Yeap, B. Y., Stanzione, M., Hung, Y. P., Heist, R. S., Marcoux, J. P., et al. (2019). Combination olaparib and temozolomide in relapsed small-cell lung cancer. *Cancer Discov.* 10, 1372–1387. doi:10.1158/2159-8290.cd-19-0582

Farmer, H., McCabe, N., Lord, C. J., Tutt, A. N., Johnson, D. A., Richardson, T. B., et al. (2005). Targeting the DNA repair defect in BRCA mutant cells as a therapeutic strategy. *Nature.* 7035, 917–921. doi:10.1038/nature03445

Fishel, M. L., Xia, H., McGeown, J., McIlwain, D. W., Elbanna, M., Craft, A. A., et al. (2019). Antitumor activity and mechanistic characterization of APE1/ref-1 inhibitors in bladder cancer. *Mol. Cancer Ther.* 11, 1947–1960. doi:10.1158/1535-7163.mct-18-1166

Foote, K. M., Blades, K., Cronin, A., Fillery, S., Guichard, S. S., Hassall, L., et al. (2013). Discovery of 4-{4-[(3R)-3-Methylmorpholin-4-yl]-6-[1-(methylsulfonyl)cyclopropyl]pyrimidin-2-y l}-1H-indole (AZ20): a potent and selective inhibitor of ATR protein kinase with monotherapy *in vivo* antitumor activity. *J. Med. Chem.* 5, 2125–2138. doi:10.1021/jm301859s

Fukumoto, T., Zhu, H., Nacarelli, T., Karakashev, S., Fatkhutdinov, N., Wu, S., et al. (2019). N(6)-Methylation of adenosine of FZD10 mRNA contributes to PARP inhibitor resistance. *Cancer Res.* 11, 2812–2820. doi:10.1158/0008-5472.can-18-3592

Gao, X., Wang, J., Li, M., Wang, J., Lv, J., Zhang, L., et al. (2019). Berberine attenuates XRCC1-mediated base excision repair and sensitizes breast cancer cells to the chemotherapeutic drugs. *J. Cell Mol. Med.* 10, 6797–6804. doi:10.1111/jcmm.14560

Germano, G., Lamba, S., Rospo, G., Barault, L., Magrì, A., Maione, F., et al. (2017). Inactivation of DNA repair triggers neoantigen generation and impairs tumour growth. *Nature.* 7683, 116–120. doi:10.1038/nature24673

Giglia-Mari, G., Zotter, A., and Vermeulen, W. (2011). DNA damage response. *Cold Spring Harb. Perspect. Biol.* 1, a000745. doi:10.1101/cshperspect.a000745

Gogola, E., Duarte, A. A., de Ruiter, J. R., Wiegant, W. W., Schmid, J. A., de Bruijn, R., et al. (2018). Selective loss of PARG restores PARylation and counteracts PARP inhibitor-mediated synthetic lethality. *Cancer Cell.* 6, 1078–1093.e12. doi:10.1016/j.ccell.2018.05.008

Golan, T., Hammel, P., Reni, M., Van Cutsem, E., Macarulla, T., Hall, M. J., et al. (2019). Maintenance olaparib for germline BRCA-mutated metastatic pancreatic cancer. *N. Engl. J. Med.* 4, 317–327. doi:10.1056/NEJMoa1903387

Grishko, V. I., Rachek, L. I., Spitz, D. R., Wilson, G. L., and LeDoux, S. P. (2005). Contribution of mitochondrial DNA repair to cell resistance from oxidative stress. *J. Biol. Chem*. 10, 8901–8905. doi:10.1074/jbc.M413022200

Gröschel, S., Hübschmann, D., Raimondi, F., Horak, P., Warsow, G., Fröhlich, M., et al. (2019). Defective homologous recombination DNA repair as therapeutic target in advanced chordoma. *Nat. Commun*. 1, 1635. doi:10.1038/s41467-019-09633-9

Guertin, A. D., Li, J., Liu, Y., Hurd, M. S., Schuller, A. G., Long, B., et al. (2013). Preclinical evaluation of the WEE1 inhibitor MK-1775 as single-agent anticancer therapy. *Mol. Cancer Ther*. 8, 1442–1452. doi:10.1158/1535-7163.MCT-13-0025

Gurjao, C., Liu, D., Hofree, M., AlDubayan, S. H., Wakiro, I., Su, M. J., et al. (2019). Intrinsic resistance to immune checkpoint blockade in a mismatch repair-deficient colorectal cancer. *Cancer Immunol. Res*. 8, 1230–1236. doi:10.1158/2326-6066.CIR-18-0683

Hampel, H., Frankel, W. L., Martin, E., Arnold, M., Khanduja, K., Kuebler, P., et al. (2005). Screening for the Lynch syndrome (hereditary nonpolyposis colorectal cancer). *N. Engl. J. Med*. 18, 1851–1860. doi:10.1056/NEJMoa043146

Hanahan, D., and Weinberg, R. A. (2011). Hallmarks of cancer: the next generation. *Cell*. 5, 646–674. doi:10.1016/j.cell.2011.02.013

Happold, C., Stojcheva, N., Silginer, M., Weiss, T., Roth, P., Reifenberger, G., et al. (2018). Transcriptional control of O(6) -methylguanine DNA methyltransferase expression and temozolomide resistance in glioblastoma. *J. Neurochem*. 6, 780–790. doi:10.1111/jnc.14326

Hegi, M. E., Diserens, A. C., Gorlia, T., Hamou, M. F., de Tribolet, N., Weller, M., et al. (2005). MGMT gene silencing and benefit from temozolomide in glioblastoma. *N. Engl. J. Med*. 10, 997–1003. doi:10.1056/NEJMoa043331

Henneman, L., van Miltenburg, M. H., Michalak, E. M., Braumuller, T. M., Jaspers, J. E., Drenth, A. P., et al. (2015). Selective resistance to the PARP inhibitor olaparib in a mouse model for BRCA1-deficient metaplastic breast cancer. *Proc. Natl. Acad. Sci. U.S.A*. 27, 8409–8414. doi:10.1073/pnas.1500223112

Hickson, I., Zhao, Y., Richardson, C. J., Green, S. J., Martin, N. M., Orr, A. I., et al. (2004). Identification and characterization of a novel and specific inhibitor of the ataxia-telangiectasia mutated kinase ATM. *Cancer Res*. 24, 9152–9159. doi:10.1158/0008-5472.can-04-2727

Hoey, C., Ray, J., Jeon, J., Huang, X., Taeb, S., Ylanko, J., et al. (2018). miRNA-106a and prostate cancer radioresistance: a novel role for LITAF in ATM regulation. *Mol. Oncol*. 8, 1324–1341. doi:10.1002/1878-0261.12328

Hosoya, N., and Miyagawa, K. (2014). Targeting DNA damage response in cancer therapy. *Cancer Sci*. 4, 370–388. doi:10.1111/cas.12366

Hsu, S. H., Chen, S. H., Kuo, C. C., and Chang, J. Y. (2018). Ubiquitin-conjugating enzyme E2 B regulates the ubiquitination of O(6)-methylguanine-DNA methyltransferase and BCNU sensitivity in human nasopharyngeal carcinoma cells. *Biochem. Pharmacol*. 158, 327–338. doi:10.1016/j.bcp.2018.10.029

Huang, F., and Mazin, A. V. (2014). A small molecule inhibitor of human RAD51 potentiates breast cancer cell killing by therapeutic agents in mouse xenografts. *PLoS One*. 6, e100993. doi:10.1371/journal.pone.0100993

Iaccarino, C., Orlandi, E., Ruggeri, F., Nicoli, D., Torricelli, F., Maggi, M., et al. (2015). Prognostic value of MGMT promoter status in non-resectable glioblastoma after adjuvant therapy. *Clin. Neurol. Neurosurg*. 132, 1–8. doi:10.1016/j.clineuro.2015.01.029

Jackson, S. P., and Bartek, J. (2009). The DNA-damage response in human biology and disease. *Nature*. 7267, 1071–1078. doi:10.1038/nature08467

Jette, N., and Lees-Miller, S. P. (2015). The DNA-dependent protein kinase: a multifunctional protein kinase with roles in DNA double strand break repair and mitosis. *Prog. Biophys. Mol. Biol*. 2-3, 194–205. doi:10.1016/j.pbiomolbio.2014.12.003

Jiao, S., Xia, W., Yamaguchi, H., Wei, Y., Chen, M. K., Hsu, J. M., et al. (2017). PARP inhibitor upregulates PD-L1 expression and enhances cancer-associated immunosuppression. *Clin. Cancer Res*. 14, 3711–3720. doi:10.1158/1078-0432.ccr-16-3215

Jin, M. H., and Oh, D. Y. (2019). ATM in DNA repair in cancer. *Pharmacol. Ther*. [Epub ahead of print]. doi:10.1016/j.pharmthera.2019.07.002

Jue, T. R., Nozue, K., Lester, A. J., Joshi, S., Schroder, L. B., Whittaker, S. P., et al. (2017). Veliparib in combination with radiotherapy for the treatment of MGMT unmethylated glioblastoma. *J. Transl. Med*. 1, 61. doi:10.1186/s12967-017-1164-1

Kaufman, B., Shapira-Frommer, R., Schmutzler, R. K., Audeh, M. W., Friedlander, M., Balmana, J., et al. (2015). Olaparib monotherapy in patients with advanced cancer and a germline BRCA1/2 mutation. *J. Clin. Oncol*. 3, 244–250. doi:10.1200/jco.2014.56.2728

Kettner, N. M., Vijayaraghavan, S., Durak, M. G., Bui, T., Kohansal, M., Ha, M. J., et al. (2019). Combined inhibition of STAT3 and DNA repair in palbociclib-resistant ER-positive breast cancer. *Clin. Cancer Res*. 13, 3996–4013. doi:10.1158/1078-0432.ccr-18-3274

Kim, G., Ison, G., McKee, A. E., Zhang, H., Tang, S., Gwise, T., et al. (2015). FDA approval summary: olaparib monotherapy in patients with deleterious germline BRCA-mutated advanced ovarian cancer treated with three or more lines of chemotherapy. *Clin. Cancer Res*. 19, 4257–4261. doi:10.1158/1078-0432.ccr-15-0887

Kim, Y. S., Kim, S. H., Cho, J., Kim, J. W., Chang, J. H., Kim, D. S., et al. (2012). MGMT gene promoter methylation as a potent prognostic factor in glioblastoma treated with temozolomide-based chemoradiotherapy: a single-institution study. *Int. J. Radiat. Oncol. Biol. Phys*. 3, 661–667. doi:10.1016/j.ijrobp.2011.12.086

King, H. O., Brend, T., Payne, H. L., Wright, A., Ward, T. A., Patel, K., et al. (2017). RAD51 is a selective DNA repair target to radiosensitize glioma stem cells. *Stem Cell Rep*. 1, 125–139. doi:10.1016/j.stemcr.2016.12.005

Konecny, G. E., and Kristeleit, R. S. (2016). PARP inhibitors for BRCA1/2-mutated and sporadic ovarian cancer: current practice and future directions. *Br. J. Cancer*. 10, 1157–1173. doi:10.1038/bjc.2016.311

Konstantinopoulos, P. A., Barry, W. T., Birrer, M., Westin, S. N., Cadoo, K. A., Shapiro, G. I., et al. (2019). Olaparib and α-specific PI3K inhibitor alpelisib for patients with epithelial ovarian cancer: a dose-escalation and dose-expansion phase 1b trial. *Lancet Oncol*. 4, 570–580. doi:10.1016/s1470-2045(18)30905-7

Koosha, F., Neshasteh-Riz, A., Takavar, A., Eyvazzadeh, N., Mazaheri, Z., Eynali, S., et al. (2017). The combination of A-966492 and Topotecan for effective radiosensitization on glioblastoma spheroids. *Biochem. Biophys. Res. Commun*. 4, 1092–1097. doi:10.1016/j.bbrc.2017.08.018

Le, D. T., Durham, J. N., Smith, K. N., Wang, H., Bartlett, B. R., Aulakh, L. K., et al. (2017). Mismatch repair deficiency predicts response of solid tumors to PD-1 blockade. *Science*. 6349, 409–413. doi:10.1126/science.aan6733

Lee, A., Youssef, I., Osborn, V. W., Safdieh, J., Becker, D. J., and Schreiber, D. (2018). The utilization of MGMT promoter methylation testing in United States hospitals for glioblastoma and its impact on prognosis. *J. Clin. Neurosci*. 51, 85–90. doi:10.1016/j.jocn.2018.02.009

Lim, K. S., Li, H., Roberts, E. A., Gaudiano, E. F., Clairmont, C., Sambel, L. A., et al. (2018). USP1 is required for replication fork protection in BRCA1-deficient tumors. *Mol. Cell*. 6, 925–941.e4. doi:10.1016/j.molcel.2018.10.045

Liu, J. F., Barry, W. T., Birrer, M., Lee, J. M., Buckanovich, R. J., Fleming, G. F., et al. (2019). Overall survival and updated progression-free survival outcomes in a randomized phase II study of combination cediranib and olaparib versus olaparib in relapsed platinum-sensitive ovarian cancer. *Ann. Oncol*. 4, 551–557. doi:10.1093/annonc/mdz018

Liu, L., Cai, S., Han, C., Banerjee, A., Wu, D., Cui, T., et al. (2020). ALDH1A1 contributes to PARP inhibitor resistance via enhancing DNA repair in BRCA2(-/-) ovarian cancer cells. *Mol. Cancer Ther*. 1, 199–210. doi:10.1158/1535-7163.mct-19-0242

Liu, L., Yan, L., Donze, J. R., and Gerson, S. L. (2003). Blockage of abasic site repair enhances antitumor efficacy of 1,3-bis-(2-chloroethyl)-1-nitrosourea in colon tumor xenografts. *Mol. Cancer Ther*. 10, 1061

Liu, Y., Zhang, L., Liu, Y., Sun, C., Zhang, H., Miao, G., et al. (2015). DNA-PKcs deficiency inhibits glioblastoma cell-derived angiogenesis after ionizing radiation. *J. Cell. Physiol*. 5, 1094–1103. doi:10.1002/jcp.24841

Loibl, S., O'Shaughnessy, J., Untch, M., Sikov, W. M., Rugo, H. S., McKee, M. D., et al. (2018). Addition of the PARP inhibitor veliparib plus carboplatin or carboplatin alone to standard neoadjuvant chemotherapy in triple-negative breast cancer (BrighTNess): a randomised, phase 3 trial. *Lancet Oncol*. 4, 497–509. doi:10.1016/s1470-2045(18)30111-6

Lord, C. J., and Ashworth, A. (2017). PARP inhibitors: synthetic lethality in the clinic. *Science*. 6330, 1152–1158. doi:10.1126/science.aam7344

Lu, Y., Chu, A., Turker, M. S., and Glazer, P. M. (2011). Hypoxia-induced epigenetic regulation and silencing of the BRCA1 promoter. *Mol. Cell Biol*. 16, 3339–3350. doi:10.1128/mcb.01121-10

Luo, M., and Kelley, M. R. (2004). Inhibition of the human apurinic/apyrimidinic endonuclease (APE1) repair activity and sensitization of breast cancer cells to DNA alkylating agents with lucanthone. *Anticancer Res*. 4, 2127

Ma, H., Takahashi, A., Yoshida, Y., Adachi, A., Kanai, T., Ohno, T., et al. (2015). Combining carbon ion irradiation and non-homologous end-joining repair inhibitor NU7026 efficiently kills cancer cells. *Radiat. Oncol*. 10, 225. doi:10.1186/s13014-015-0536-z

Ma, J., Benitez, J. A., Li, J., Miki, S., Ponte de Albuquerque, C., Galatro, T., et al. (2019). Inhibition of nuclear PTEN tyrosine phosphorylation enhances glioma radiation sensitivity through attenuated DNA repair. *Cancer Cell*. 3, 504–518.e7. doi:10.1016/j.ccell.2019.01.020

Maki, Y., Murakami, J., Asaumi, J., Tsujigiwa, H., Nagatsuka, H., Kokeguchi, S., et al. (2005). Role of O6-methylguanine-DNA methyltransferase and effect of O6-benzylguanine on the anti-tumor activity of cis-diaminedichloroplatinum(II) in oral cancer cell lines. *Oral Oncol*. 10, 984–993. doi:10.1016/j.oraloncology.2005.05.011

Marzio, A., Puccini, J., Kwon, Y., Maverakis, N. K., Arbini, A., Sung, P., et al. (2019). The F-box domain-dependent activity of EMI1 regulates PARPi sensitivity in triple-negative breast cancers. *Mol. Cell*. 2, 224–237.e6. doi:10.1016/j.molcel.2018.11.003

Memon, D., Dawson, K., Smowton, C. S., Xing, W., Dive, C., and Miller, C. J. (2016). Hypoxia-driven splicing into noncoding isoforms regulates the DNA damage response. *NPJ Genom. Med*. 1, 16020. doi:10.1038/npjgenmed.2016.20

Middleton, M. R., and Margison, G. P. (2003). Improvement of chemotherapy efficacy by inactivation of a DNA-repair pathway. *Lancet Oncol*. 1, 37–44. doi:10.1016/s1470-2045(03)00959-8

Middleton, M. R., Thatcher, N., McMurry, T. B., McElhinney, R. S., Donnelly, D. J., and Margison, G. P. (2002). Effect of O6-(4-bromothenyl)guanine on different temozolomide schedules in a human melanoma xenograft model. *Int. J. Cancer*. 5, 615–617. doi:10.1002/ijc.10532

Mihaylova, V. T., Bindra, R. S., Yuan, J., Campisi, D., Narayanan, L., Jensen, R., et al. (2003). Decreased expression of the DNA mismatch repair gene Mlh1 under hypoxic stress in mammalian cells. *Mol. Cell Biol*. 9, 3265–3273. doi:10.1128/mcb.23.9.3265-3273.2003

Montaldi, A. P., and Sakamoto-Hojo, E. T. (2013). Methoxyamine sensitizes the resistant glioblastoma T98G cell line to the alkylating agent temozolomide. *Clin. Exp. Med*. 4, 279–288. doi:10.1007/s10238-012-0201-x

Moore, K., Colombo, N., Scambia, G., Kim, B. G., Oaknin, A., Friedlander, M., et al. (2018). Maintenance olaparib in patients with newly diagnosed advanced ovarian cancer. *N. Engl. J. Med*. 26, 2495–2505. doi:10.1056/NEJMoa1810858

Morgado-Palacin, I., Day, A., Murga, M., Lafarga, V., Anton, M. E., Tubbs, A., et al. (2016). Targeting the kinase activities of ATR and ATM exhibits antitumoral activity in mouse models of MLL-rearranged AML. *Sci. Signal*. 445, ra91. doi:10.1126/scisignal.aad8243

Muralidharan, S. V., Bhadury, J., Nilsson, L. M., Green, L. C., McLure, K. G., and Nilsson, J. A. (2016). BET bromodomain inhibitors synergize with ATR inhibitors to induce DNA damage, apoptosis, senescence-associated secretory pathway and ER stress in Myc-induced lymphoma cells. *Oncogene*. 36, 4689–4697. doi:10.1038/onc.2015.521

Neboori, H. J., Haffty, B. G., Wu, H., Yang, Q., Aly, A., Goyal, S., et al. (2012). Low p53 binding protein 1 (53BP1) expression is associated with increased local recurrence in breast cancer patients treated with breast-conserving surgery and radiotherapy. *Int. J. Radiat. Oncol. Biol. Phys*. 5, e677–83. doi:10.1016/j.ijrobp.2012.01.089

Neijenhuis, S., Begg, A. C., and Vens, C. (2005). Radiosensitization by a dominant negative to DNA polymerase beta is DNA polymerase beta-independent and XRCC1-dependent. *Radiother. Oncol*. 2, 123–128. doi:10.1016/j.radonc.2005.06.020

Ohta, S. (2006). Contribution of somatic mutations in the mitochondrial genome to the development of cancer and tolerance against anticancer drugs. *Oncogene*. 34, 4768–4776. doi:10.1038/sj.onc.1209602

Oleinick, N. L., Biswas, T., Patel, R., Tao, M., Patel, R., Weeks, L., et al. (2016). Radiosensitization of non-small-cell lung cancer cells and xenografts by the interactive effects of pemetrexed and methoxyamine. *Radiother. Oncol*. 2, 335–341. doi:10.1016/j.radonc.2016.10.007

Oliver, T. G., Mercer, K. L., Sayles, L. C., Burke, J. R., Mendus, D., Lovejoy, K. S., et al. (2010). Chronic cisplatin treatment promotes enhanced damage repair and tumor progression in a mouse model of lung cancer. *Genes Dev*. 8, 837–852. doi:10.1101/gad.1897010

Oplustil O'Connor, L., Rulten, S. L., Cranston, A. N., Odedra, R., Brown, H., Jaspers, J. E., et al. (2016). The PARP inhibitor AZD2461 provides insights into the role of PARP3 inhibition for both synthetic lethality and tolerability with chemotherapy in preclinical models. *Cancer Res*. 20, 6084–6094. doi:10.1158/0008-5472.CAN-15-3240

Pantelidou, C., Sonzogni, O., De Oliveria Taveira, M., Mehta, A. K., Kothari, A., Wang, D., et al. (2019). PARP inhibitor efficacy depends on CD8(+) T-cell recruitment via intratumoral STING pathway activation in BRCA-deficient models of triple-negative breast cancer. *Cancer Discov*. 6, 722–737. doi:10.1158/2159-8290.cd-18-1218

Pearl, L. H., Schierz, A. C., Ward, S. E., Al-Lazikani, B., and Pearl, F. M. (2015). Therapeutic opportunities within the DNA damage response. *Nat. Rev. Cancer*. 3, 166–180. doi:10.1038/nrc3891

Pilie, P. G., Tang, C., Mills, G. B., and Yap, T. A. (2019). State-of-the-art strategies for targeting the DNA damage response in cancer. *Nat. Rev. Clin. Oncol*. 2, 81–104. doi:10.1038/s41571-018-0114-z

Porporato, P. E., Filigheddu, N., Pedro, J. M. B., Kroemer, G., and Galluzzi, L. (2018). Mitochondrial metabolism and cancer. *Cell Res*. 3, 265–280. doi:10.1038/cr.2017.155

Powell, S. N., and Bindra, R. S. (2009). Targeting the DNA damage response for cancer therapy. *DNA Repair*. 9, 1153–1165. doi:10.1016/j.dnarep.2009.04.011

Quigley, D., Alumkal, J. J., Wyatt, A. W., Kothari, V., Foye, A., Lloyd, P., et al. (2017). Analysis of circulating cell-free DNA identifies multiclonal heterogeneity of BRCA2 reversion mutations associated with resistance to PARP inhibitors. *Cancer Discov*. 9, 999–1005. doi:10.1158/2159-8290.cd-17-0146

Rabik, C. A., Njoku, M. C., and Dolan, M. E. (2006). Inactivation of O6-alkylguanine DNA alkyltransferase as a means to enhance chemotherapy. *Cancer Treat Rev*. 4, 261–276. doi:10.1016/j.ctrv.2006.03.004

Rachek, L. I., Grishko, V. I., Musiyenko, S. I., Kelley, M. R., LeDoux, S. P., and Wilson, G. L. (2002). Conditional targeting of the DNA repair enzyme hOGG1 into mitochondria. *J. Biol. Chem*. 47, 44932–44937. doi:10.1074/jbc.M208770200

Ranson, M., Middleton, M. R., Bridgewater, J., Lee, S. M., Dawson, M., Jowle, D., et al. (2006). Lomeguatrib, a potent inhibitor of O6-alkylguanine-DNA-alkyltransferase: phase I safety, pharmacodynamic, and pharmacokinetic trial and evaluation in combination with temozolomide in patients with advanced solid tumors. *Clin. Cancer Res*. 5, 1577–1584. doi:10.1158/1078-0432.ccr-05-2198

Riaz, N., Blecua, P., Lim, R. S., Shen, R., Higginson, D. S., Weinhold, N., et al. (2017). Pan-cancer analysis of bi-allelic alterations in homologous recombination DNA repair genes. *Nat. Commun*. 1, 857. doi:10.1038/s41467-017-00921-w

Robson, M., Im, S. A., Senkus, E., Xu, B., Domchek, S. M., Masuda, N., et al. (2017). Olaparib for metastatic breast cancer in patients with a germline BRCA mutation. *N. Engl. J. Med*. 6, 523–533. doi:10.1056/NEJMoa1706450

Ruiz-Bañobre, J., and Goel, A. (2019). DNA mismatch repair deficiency and immune checkpoint inhibitors in gastrointestinal cancers. *Gastroenterology*. 4, 890–903. doi:10.1053/j.gastro.2018.11.071

Saki, M., and Prakash, A. (2017). DNA damage related crosstalk between the nucleus and mitochondria. *Free Radic. Biol. Med*. 216–227. doi:10.1016/j.freeradbiomed.2016.11.050

Seo, Y., and Kinsella, T. J. (2009). Essential role of DNA base excision repair on survival in an acidic tumor microenvironment. *Cancer Res*. 18, 7285–7293. doi:10.1158/0008-5472.can-09-0624

Shi, Q., Maas, L., Veith, C., Van Schooten, F. J., and Godschalk, R. W. (2017). Acidic cellular microenvironment modifies carcinogen-induced DNA damage and repair. *Arch. Toxicol*. 6, 2425–2441. doi:10.1007/s00204-016-1907-4

Shi, Y., Wang, Y., Qian, J., Yan, X., Han, Y., Yao, N., et al. (2020). MGMT expression affects the gemcitabine resistance of pancreatic cancer cells. *Life Sci*. 259, 118148. doi:10.1016/j.lfs.2020.118148

Shinohara, E. T., Geng, L., Tan, J., Chen, H., Shir, Y., Edwards, E., et al. (2005). DNA-dependent protein kinase is a molecular target for the development of noncytotoxic radiation-sensitizing drugs. *Cancer Res*. 12, 4987–4992. doi:10.1158/0008-5472.can-04-4250

Shokolenko, I. N., Alexeyev, M. F., Robertson, F. M., LeDoux, S. P., and Wilson, G. L. (2003). The expression of Exonuclease III from *E. coli* in mitochondria of breast cancer cells diminishes mitochondrial DNA repair capacity and cell

survival after oxidative stress. *DNA Repair*. 2, 471–482. doi:10.1016/s1568-7864(03)00019-3

Smith, J., Tho, L. M., Xu, N., and Gillespie, D. A. (2010). The ATM-Chk2 and ATR-Chk1 pathways in DNA damage signaling and cancer. *Adv. Cancer Res*. 73–112. doi:10.1016/b978-0-12-380888-2.00003-0

Squatrito, M., Brennan, C. W., Helmy, K., Huse, J. T., Petrini, J. H., and Holland, E. C. (2010). Loss of ATM/Chk2/p53 pathway components accelerates tumor development and contributes to radiation resistance in gliomas. *Cancer Cell*. 6, 619–629. doi:10.1016/j.ccr.2010.10.034

Stefanski, C. D., Keffler, K., McClintock, S., Milac, L., and Prosperi, J. R. (2019). APC loss affects DNA damage repair causing doxorubicin resistance in breast cancer cells. *Neoplasia*. 12, 1143–1150. doi:10.1016/j.neo.2019.09.002

Sunada, S., Kanai, H., Lee, Y., Yasuda, T., Hirakawa, H., Liu, C., et al. (2016). Nontoxic concentration of DNA-PK inhibitor NU7441 radio-sensitizes lung tumor cells with little effect on double strand break repair. *Cancer Sci*. 9, 1250–1255. doi:10.1111/cas.12998

Teng, P. N., Bateman, N. W., Darcy, K. M., Hamilton, C. A., Maxwell, G. L., Bakkenist, C. J., et al. (2015). Pharmacologic inhibition of ATR and ATM offers clinically important distinctions to enhancing platinum or radiation response in ovarian, endometrial, and cervical cancer cells. *Gynecol. Oncol*. 3, 554–561. doi:10.1016/j.ygyno.2014.12.035

Teo, M. Y., Seier, K., Ostrovnaya, I., Regazzi, A. M., Kania, B. E., Moran, M. M., et al. (2018). Alterations in DNA damage response and repair genes as potential marker of clinical benefit from PD-1/PD-L1 blockade in advanced urothelial cancers. *J. Clin. Oncol*. 17, 1685–1694. doi:10.1200/jco.2017.75.7740

Ter Brugge, P., Kristel, P., van der Burg, E., Boon, U., de Maaker, M., Lips, E., et al. (2016). Mechanisms of therapy resistance in patient-derived xenograft models of BRCA1-deficient breast cancer. *J. Natl. Cancer Inst*. 112, 1075. doi:10.1093/jnci/djw148

Tian, H., Gao, Z., Li, H., Zhang, B., Wang, G., Zhang, Q., et al. (2015). DNA damage response--a double-edged sword in cancer prevention and cancer therapy. *Cancer Lett*. 1, 8–16. doi:10.1016/j.canlet.2014.12.038

Tran, T. Q., Ishak Gabra, M. B., Lowman, X. H., Yang, Y., Reid, M. A., Pan, M., et al. (2017). Glutamine deficiency induces DNA alkylation damage and sensitizes cancer cells to alkylating agents through inhibition of ALKBH enzymes. *PLoS Biol*. 11, e2002810. doi:10.1371/journal.pbio.2002810

Tsai, A. K., Khan, A. Y., Worgo, C. E., Wang, L. L., Liang, Y., and Davila, E. (2017). A multikinase and DNA-PK inhibitor combination immunomodulates melanomas, suppresses tumor progression, and enhances immunotherapies. *Cancer Immunol. Res*. 9, 790–803. doi:10.1158/2326-6066.CIR-17-0009

Ueta, E., Sasabe, E., Yang, Z., Osaki, T., and Yamamoto, T. (2008). Enhancement of apoptotic damage of squamous cell carcinoma cells by inhibition of the mitochondrial DNA repairing system. *Cancer Sci*. 11, 2230–2237. doi:10.1111/j.1349-7006.2008.00918.x

Vazquez-Ortiz, G., Chisholm, C., Xu, X., Lahusen, T. J., Li, C., Sakamuru, S., et al. (2014). Drug repurposing screen identifies lestaurtinib amplifies the ability of the poly (ADP-ribose) polymerase 1 inhibitor AG14361 to kill breast cancer associated gene-1 mutant and wild type breast cancer cells. *Breast Cancer Res*. 3, R67. doi:10.1186/bcr3682

Viel, T., Monfared, P., Schelhaas, S., Fricke, I. B., Kuhlmann, M. T., Fraefel, C., et al. (2013). Optimizing glioblastoma temozolomide chemotherapy employing lentiviral-based anti-MGMT shRNA technology. *Mol. Ther*. 3, 570–579. doi:10.1038/mt.2012.278

Wang, B., Qiao, L., Wang, Y., Zeng, J., Chen, D., Guo, H., et al. (2018). Mitochondrial DNA D-loop lesions with the enhancement of DNA repair contribute to gastrointestinal cancer progression. *Oncol. Rep*. 6, 3694–3704. doi:10.3892/or.2018.6724

Wang, Y., Xu, H., Liu, T., Huang, M., Butter, P. P., Li, C., et al. (2018). Temporal DNA-PK activation drives genomic instability and therapy resistance in glioma stem cells. *JCI Insight*. 3, e98096. doi:10.1172/jci.insight.98096

Wang, L. E., Yin, M., Dong, Q., Stewart, D. J., Merriman, K. W., Amos, C. I., et al. (2011). DNA repair capacity in peripheral lymphocytes predicts survival of patients with non-small-cell lung cancer treated with first-line platinum-based chemotherapy. *J. Clin. Oncol*. 31, 4121–4128. doi:10.1200/JCO.2010.34.3616

Watson, Z. L., Yamamoto, T. M., McMellen, A., Kim, H., Hughes, C. J., Wheeler, L. J., et al. (2019). Histone methyltransferases EHMT1 and EHMT2 (GLP/G9A) maintain PARP inhibitor resistance in high-grade serous ovarian carcinoma. *Clin. Epigenet*. 1, 165. doi:10.1186/s13148-019-0758-2

Weber, A. M., and Ryan, A. J. (2015). ATM and ATR as therapeutic targets in cancer. *Pharmacol. Ther*. 149, 124–138. doi:10.1016/j.pharmthera.2014.12.001

Wilson, R. H., Evans, T. J., Middleton, M. R., Molife, L. R., Spicer, J., Dieras, V., et al. (2017). A phase I study of intravenous and oral rucaparib in combination with chemotherapy in patients with advanced solid tumours. *Br. J. Cancer*. 7, 884–892. doi:10.1038/bjc.2017.36

Win, A. K., Young, J. P., Lindor, N. M., Tucker, K. M., Ahnen, D. J., Young, G. P., et al. (2012). Colorectal and other cancer risks for carriers and noncarriers from families with a DNA mismatch repair gene mutation: a prospective cohort study. *J. Clin. Oncol*. 9, 958–964. doi:10.1200/jco.2011.39.5590

Wise, H. C., Iyer, G. V., Moore, K., Temkin, S. M., Gordon, S., Aghajanian, C., et al. (2019). Activity of M3814, an oral DNA-PK inhibitor, in combination with topoisomerase II inhibitors in ovarian cancer models. *Sci. Rep*. 1, 18882. doi:10.1038/s41598-019-54796-6

Wu, X., Luo, Q., Zhao, P., Chang, W., Wang, Y., Shu, T., et al. (2019). MGMT-activated DUB3 stabilizes MCL1 and drives chemoresistance in ovarian cancer. *Proc. Natl. Acad. Sci. U.S.A*. 8, 2961–2966. doi:10.1073/pnas.1814742116

Yang, C., Wang, Q., Liu, X., Cheng, X., Jiang, X., Zhang, Y., et al. (2016). NU7441 enhances the radiosensitivity of liver cancer cells. *Cell. Physiol. Biochem*. 5, 1897–1905. doi:10.1159/000445551

Yuzefovych, L. V., Kahn, A. G., Schuler, M. A., Eide, L., Arora, R., Wilson, G. L., et al. (2016). Mitochondrial DNA repair through OGG1 activity attenuates breast cancer progression and metastasis. *Cancer Res*. 1, 30–34. doi:10.1158/0008-5472.can-15-0692

Zhao, H., Wang, S., Song, C., Zha, Y., and Li, L. (2016). The prognostic value of MGMT promoter status by pyrosequencing assay for glioblastoma patients' survival: a meta-analysis. *World J. Surg. Oncol*. 1, 261. doi:10.1186/s12957-016-1012-4

Zhao, Q., Guan, J., Zhang, Z., Lv, J., Wang, Y., Liu, L., et al. (2017). Inhibition of Rad51 sensitizes breast cancer cells with wild-type PTEN to olaparib. *Biomed. Pharmacother*. 165–168. doi:10.1016/j.biopha.2017.07.090

**Conflict of Interest:** The authors declare that the research was conducted in the absence of any commercial or financial relationships that could be construed as a potential conflict of interest.

frontiers in Oncology

ORIGINAL RESEARCH
published: 17 February 2021
doi: 10.3389/fonc.2020.576565

# Detailed Molecular Mechanism and Potential Drugs for COL1A1 in Carboplatin-Resistant Ovarian Cancer

*Feng Yang*[1], *Ziyu Zhao*[1], *Shaoyi Cai*[1], *Li Ling*[1,2], *Leying Hong*[1], *Liang Tao*[1]* *and Qin Wang*[1]*

[1] Zhongshan School of Medicine, Sun Yat-Sen University, Guangzhou, China, [2] School of Pharmacy, Sun Yat-Sen University, Guangzhou, China

Carboplatin resistance in ovarian cancer (OV) is a major medical problem. Thus, there is an urgent need to find novel therapeutic targets to improve the prognosis of patients with carboplatin-resistant OV. Accumulating evidence indicates that the gene COL1A1 (collagen type I alpha 1 chain) has an important role in chemoresistance and could be a therapeutic target. However, there have been no reports about the role of COL1A1 in carboplatin-resistant OV. This study aimed to establish the detailed molecular mechanism of COL1A1 and predict potential drugs for its treatment. We found that COL1A1 had a pivotal role in carboplatin resistance in OV by weighted gene correlation network analysis and survival analysis. Moreover, we constructed a competing endogenous RNA network (LINC00052/SMCR5-miR-98-COL1A1) based on multi-omics data and experiments to explore the upstream regulatory mechanisms of COL1A1. Two key pathways involving COL1A1 in carboplatin resistance were identified by co-expression analysis and pathway enrichment: the "ECM-receptor interaction" and "focal adhesion" Kyoto Encyclopedia of Genes and Genomes pathways. Furthermore, combining these results with those of cell viability assays, we proposed that ZINC000085537017 and quercetin were potential drugs for COL1A1 based on virtual screening and the TCMSP database, respectively. These results might help to improve the outcome of OV in the future.

**Keywords: carboplatin, ovarian cancer, ceRNA, KEGG, drugs, virtual screening**

OPEN ACCESS

***Edited by:***
*Dexin Kong,*
*Tianjin Medical University, China*

***Reviewed by:***
*Dong-Joo (Ellen) Cheon,*
*Albany Medical College, United States*
*Feng Wang,*
*Affiliated Hospital of Nantong University, China*

***Correspondence:**
*Liang Tao*
*taol@mail.sysu.edu.cn*
*Qin Wang*
*wangqin6@mail.sysu.edu.cn*

***Specialty section:***
*This article was submitted to Pharmacology of Anti-Cancer Drugs, a section of the journal Frontiers in Oncology*

***Received:*** *26 June 2020*
***Accepted:*** *21 December 2020*
***Published:*** *17 February 2021*

***Citation:***
*Yang F, Zhao Z, Cai S, Ling L, Hong L, Tao L and Wang Q (2021) Detailed Molecular Mechanism and Potential Drugs for COL1A1 in Carboplatin-Resistant Ovarian Cancer. Front. Oncol. 10:576565. doi: 10.3389/fonc.2020.576565*

## INTRODUCTION

Ovarian cancer (OV) is the leading cause of death among women with gynecological malignancies and is characterized by high recurrence and mortality rates (1). Each year, 225,500 new cases of ovarian cancer are diagnosed, with 140,200 cancer-specific deaths worldwide (2). Owing to the use of chemotherapy, which is the mainstay of OV treatment, the mortality rate has decreased in recent decades (1). Chemotherapy, especially carboplatin, is the primary treatment for OV and can improve patients'

**Abbreviations:** COL1A1, Collagen Type I Alpha 1 chain; TCGA, The Cancer Genome Atlas; OV, Ovarian cancer; KEGG, Kyoto Encyclopedia of Genes and Genomes; WGCNA, Weighted gene correlation network analysis; GSEA, Gene Set Enrichment Analysis; ceRNA, Competing endogenous RNA; FDR, False discovery rate.

overall survival and quality of life (3). However, most OV patients receiving carboplatin chemotherapy develop chemoresistance, which leads to treatment failure (4).

Recently, many studies have demonstrated that the COL1A1 (collagen type I alpha 1 chain) gene is a potential therapeutic target with an important role in chemoresistance (5, 6). Most of these studies focused on the relationship between the expression of COL1A1 and chemoresistance. Some researchers found that the expression of COL1A1 was associated with resistance of OV to taxol (7), cisplatin (8), paclitaxel, doxorubicin, topotecan, vincristine, and methotrexate (5). However, the molecular mechanism by which COL1A1 participates in carboplatin-resistant OV has remained unclear; thus, the development of potential targeted therapeutic drugs is challenging.

In the present study, we performed data mining based on large-scale multi-omics data to explore the detailed molecular mechanism of COL1A1 in carboplatin-resistant OV and to identify potential drugs to target COL1A1. Our study provides new insight into the chemoresistance of OV at the molecular level and explores potential therapeutic drugs to overcome carboplatin resistance in OV and improve the outcomes of OV patients.

# MATERIALS AND METHODS

## Data Collection

The gene expression count profile (transcriptome sequencing and microRNA [miRNA] profiles) and corresponding clinical data of OV patients were collected from The Cancer Genome Atlas (TCGA) database (accessed on September 21, 2019). Protein-coding genes and long non-coding RNAs (lncRNAs) were isolated from the transcriptome sequencing data. Based on their clinical data and previous study (9), 98 OV patients were categorized into a carboplatin-nonresistant group (complete response and partial response; n = 84) and a carboplatin-resistant group (stable disease and progressive disease; n = 14). Patients' clinical characteristics are shown in **Table S1**. The use of TCGA data in the present study was in accordance with TCGA publication guidelines. As the patient data originated from the TCGA database, no further ethical approval was required.

## Study Design

The workflow of this study is shown in **Figure 1**. In order to confirm the function of COL1A1 in carboplatin-resistant OV, we used weighted correlation network analysis (WGCNA), an unsupervised analysis method, to identify carboplatin-resistance-related genes. Then, we performed hub gene analysis and survival analysis to further validate the key role of COL1A1 in carboplatin-resistant OV. Subsequently, we explored the upstream regulatory mechanisms of COL1A1 by constructing a competing endogenous RNA (ceRNA) network. Moreover, we performed co-expression analysis and pathway enrichment to identify the downstream regulatory mechanisms of COL1A1. Finally, we identified candidates for drug-repurposing by virtual screening based on the structure of COL1A1 and the traditional Chinese medicines in the TCMSP database. Furthermore, we performed experiments to evaluate the results of the analysis.

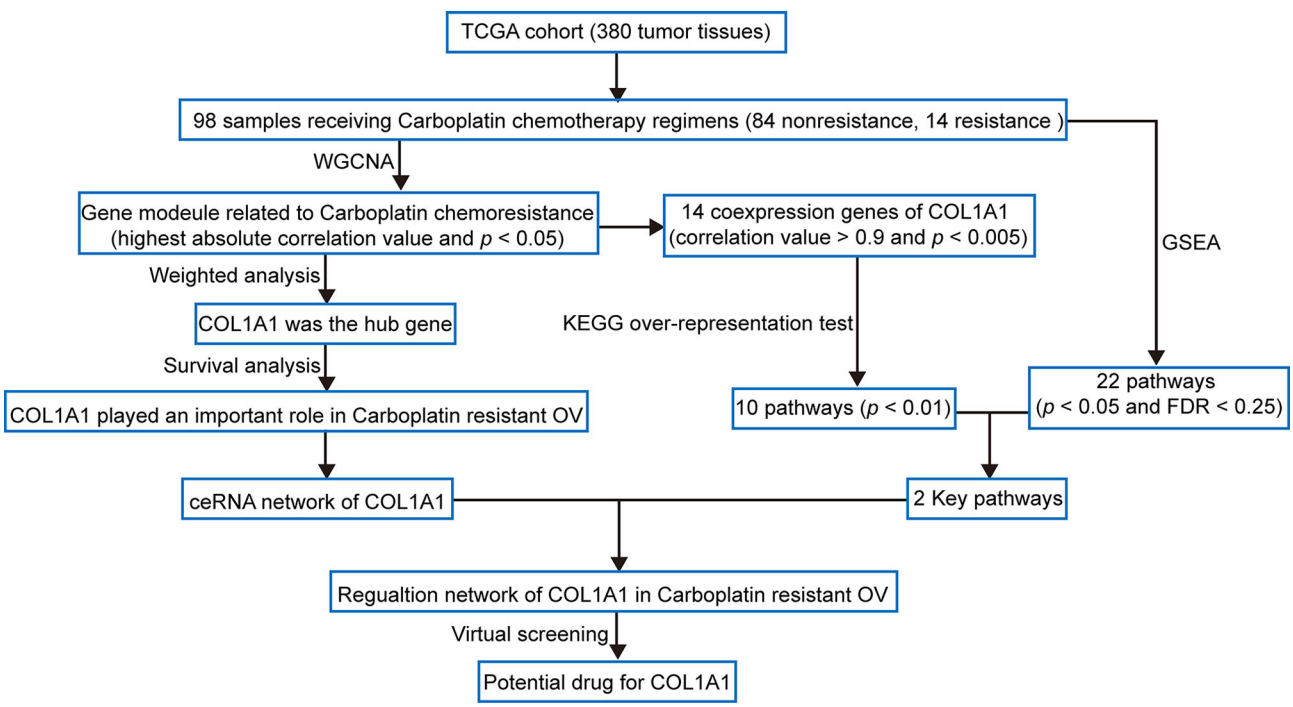


**FIGURE 1** | Flow diagram of the analysis procedure: data collection, preprocessing, analysis, and validation.

## Identification of the Hub Genes in Carboplatin-Resistant OV

To obtain modules related to carboplatin resistance in OV, WGCNA was performed using R package WGCNA (10). A total of 8,791 genes with the top 70% median absolute deviations were screened from the database (n = 98) based on carboplatin response. Gene expression modules with similar patterns were identified by the dynamic tree cut method (minModuleSize = 50, mergeCutHeight = 0.25, and deepSplit = 1). An unsigned network type was used to retain relationships between modules and sample type (nonresistant or resistant). Modules with the highest absolute correlation values and $p < 0.05$ were considered to be significantly related to carboplatin resistance. Then, the identified carboplatin resistance genes were used to construct a network based on WGCNA. Subsequently, we employed two different methods to determine the hub gene in the carboplatin resistance module obtained by WGCNA. We assumed that a biological network G = (V, E) is an undirected network, where V is the collection of nodes within the network and E is the edge set. We used another notation, G = (V[G], E[G]), to represent a network, where V(G) is the collection of nodes in a network G, and E(G) is the collection of edges in a network G. For a set S, we used |S| to denote its cardinality (i.e., the number of elements in the set). Given a node v, N(v) denotes the collections of its neighbors. The two methods were as follows.

1. Degree method (Deg)

$$Deg(v) = |N(v)|$$

2. Maximum neighborhood component (MNC)

$MNC(v) = |V(MC(v))|$, where $MC(v)$ is a maximum connected component of the G[N(v)] and G[N(v)] is the induced subgraph of G by N(v).

The gene ranked in first place by both methods was considered to be the hub gene in carboplatin-resistant OV. Finally, survival analysis was performed using KmPlot with an auto-selected best cutoff (11).

## Identification of Differentially Expressed mRNAs, miRNAs, and lncRNAs

We used the R package edgeR (12) to normalize and analyze significantly differentially expressed lncRNAs (DElncRNAs), miRNAs (DEmiRNAs), and mRNAs (DEmRNAs) between the carboplatin-resistant OV group (n = 14) and the carboplatin-nonresistant OV group (n = 84). According to the previous study (13), we wanted to obtain more candidates. So, the cutoff values were $|\log2 \text{ fold change}| \geq 0.4$ and $p < 0.05$. The DElncRNAs, DEmiRNAs, and DEmRNAs were identified based on these thresholds.

## Construction of the ceRNA Network for COL1A1

We constructed a ceRNA network based on the DEmRNAs, DEmiRNAs, and DElncRNAs as described previously (14). To construct the mRNA (COL1A1)-related ceRNA network, interactions between COL1A1 and miRNAs were predicted using TargetScan (http://www.targetscan.org/vert_71/), and lncRNA–miRNA relationships were identified using miRcode (http://mircode.org/). According to the ceRNA hypothesis (15), lncRNAs act as miRNA sponges and negatively regulate miRNA-mediated gene silencing. The COL1A1-related ceRNA network was constructed and visualized using Cytoscape 3.7.1 (16).

## Co-Expression Analysis of COL1A1 and Pathway Enrichment Analysis

To explore the downstream regulatory mechanism of COL1A1, we performed co-expression analysis between COL1A1 and genes related to carboplatin resistance according to WGCNA, with cutoff values of Pearson correlation coefficient > 0.9 and $p < 0.005$. After obtaining the genes co-expressed with COL1A1, a KEGG over-representation test was performed using R package clusterProfiler (17) with a cutoff of $p < 0.01$. Gene set enrichment analysis (GSEA) (18) was also used to explore the potential molecular mechanisms in the carboplatin-resistant (n = 14) and carboplatin-nonresistant (n = 84) groups based on the expression profiles of all protein-coding genes, with cutoff values of false discovery rate (FDR) < 0.25 and $p < 0.05$. These results were combined to obtain the key pathways involving COL1A1 in carboplatin-resistant OV.

## Potential Drug-Repurposing and Traditional Chinese Medicine

The three-dimensional (3D) structure of COL1A1 was downloaded from the Protein Data Bank (PDB; 5CVB, https://www.rcsb.org/), and its binding sites were identified by Schrodinger Maestro (19). Then, we built a library of 2,106 US Food and Drug Administration (FDA)-approved drugs obtained from the ZINC15 database (20). Finally, we performed virtual screening and molecular docking with Schrodinger Maestro to identify potential drug-repurposing. We also used TCMSP (http://www.tcmspw.com/tcmsp.php) (21) to find traditional Chinese medicines that might target COL1A1.

## Chemicals

Carboplatin (≥ 98% purity, CAS: 41575-94-4), ZINC000085537017 (Cangrelor; ≥ 95% purity, CAS: 163706-36-3), and quercetin (≥ 98.5% purity, CAS: 117-39-5) were purchased from Aladdin (China). Stock solutions were prepared in dimethyl sulfoxide (≥99.7% purity, CAS 67-68-5, Sigma-Aldrich) and stored at 4°C. The fresh stock solution was made on a weekly basis. Other chemicals used in the study were analytic grade.

## Cell Culture

Pairs of parental and resistant SKOV3 and A2780 cell lines were provided by Soochow University. Cells were cultured in DMEM (Gibco, 12800017) supplemented with 10% fetal bovine serum (Gibco, 10270-106) containing penicillin (100 IU/ml) and streptomycin (100 μg/ml) (Gibco, 15140122) at 37°C in a 5% $CO_2$ atmosphere.

## Real-Time Quantitative PCR

Total RNA was extracted using TRIzol reagent (Invitrogen). cDNA was synthesized using a cDNA synthesis kit (TIANGEN).

Quantitative real-time PCR analysis was performed in triplicate with SYBR Green (TIANGEN) and specific primers (**Table S2**) using a CFX Connect Real-Time PCR Detection System (Bio-Rad, USA). U6 was used as an internal control for miRNAs. The relative expression levels of mRNAs or lncRNAs were evaluated relative to glyceraldehyde 3-phosphate dehydrogenase (GAPDH). Relative expression values were calculated using the $2^{-\triangle\triangle Ct}$ method.

## Cell Viability

Cell viability was detected by cell counting kit-8 (CCK-8; TongRen) assay following the manufacturer's instructions. The CCK-8 test solution was added 30 min before the end of treatment, and the absorbance was measured at 450 nm using a microplate reader. Carboplatin-resistant cells were exposed to a concentration gradient (0, 0.01, 0.1, 1, 10, and 100 μM) of ZINC000085537017 or quercetin for 24 h. To understand the influence of ZINC000085537017 and quercetin on sensitivity to carboplatin, resistant cells were pretreated with 1 μM ZINC000085537017 or 10 μM quercetin for 24 h, followed by incubation with 20% maximal inhibitory concentration ($IC_{20}$) or $IC_{50}$ doses of carboplatin for 48 h, and then subjected to cell viability assays.

## Statistical Analysis

Statistical analysis was performed using R 3.6.3 (R Foundation for Statistical Computing, Vienna, Austria). Normal distribution and homogeneity of variance tests were performed before the statistical analysis. The Wilcoxon test was used to evaluate the expression of COL1A1 between the carboplatin-resistant (n = 14) and carboplatin-nonresistant groups (n = 84), and t-tests were used to compare data between the two groups; $p < 0.05$ was considered statistically significant.

# RESULTS

## COL1A1 Has an Important Role in Carboplatin-Resistant OV

A total of 98 samples (84 nonresistant to carboplatin and 14 resistant to carboplatin) were included in WGCNA. We selected β = 6 as the appropriate soft-thresholding value to ensure a scale-free network, and 16 modules were identified. These modules are shown in distinct colors in **Figure 2A**. Then, the correlations between module eigengenes and the clinical trait of interest (resistance to carboplatin) were determined (**Figure 2B**, **Table S3**). The modules with the highest absolute correlation values and $p < 0.05$ were considered to be significant carboplatin-resistance-related modules. Based on the cutoffs used, the yellow module was screened as significantly related to carboplatin resistance in OV (**Figure 2B**). A total of 412 genes of the yellow module (**Table S4**) were found to be significantly related to carboplatin resistance by WGCNA. Subsequently, we constructed a network based on these 412 genes, then used the Deg and MNC methods to identify the hub gene involved in carboplatin-resistant OV. COL1A1 was ranked first place in the hub gene analysis by both methods (**Table S5**). We also found that COL1A1 mRNA was significantly overexpressed in the carboplatin-resistant OV group ($p < 0.05$, **Figure 2C**). We used overall survival analysis with KmPlot to further validate the role of COL1A1 in carboplatin resistance. The results showed that high mRNA expression of COL1A1 was associated with poor prognosis in OV ($p < 0.05$, **Figure 2D**). Taken together, these results showed that COL1A1 plays an important part in carboplatin resistance in OV.

## Constructing of the ceRNA Network of COL1A1

We performed bioinformatics analysis to explore the ceRNA network of COL1A1 in carboplatin-resistant OV (**Figure 3A**). A total of 845 DElncRNAs (**Table S6**), 96 DEmiRNAs (**Table S7**), and 1,684 DEmRNAs (**Table S8**) were identified according to the cutoff values (|log2 fold change| ≥ 0.4 and $p < 0.05$). Then, based on the ceRNA hypothesis and online databases (TargetScan and miRcode), the ceRNA network of COL1A1 was constructed. According to the results of Targetscan (**Table S9**), the conserved sites of miR-98 and miR-143 on 3′ untranslated region (3′-UTR) of COL1A1 were 789–795 and 152–158, respectively. To make the results more creditable, we also did anther analysis by miRsystem. According to the results from miRsystem (**Table S10**), there were 6 hits and 4 hits for miR-98 and miR-143, respectively. Finally, several lncRNAs (FAM86C2P, LINC00315, WARS2-IT1, ATP11A-AS1, FOXP1-IT1, LINC00470, SMCR5, HERC2P4, DIRC3, LINC00052, HERC2P5, FLRT1, and ZNF876P) sponged has-mir-143 and has-mir-98 to regulate COL1A1 (**Figure 3B**). As determined by real-time PCR (**Figure 3C**), the expression levels of COL1A1 mRNA, miRNAs (miR-143 and miR-98), and lncRNAs (FLRT1, LINC00470, ZNF876P, SMCR5, DIRC3, LINC00052, FAM86C2P, and ATP11A-IT1) were all significantly different between the carboplatin-sensitive and carboplatin-resistant cell lines ($p < 0.05$), which was in line with our preliminary expectations. There was no change in mRNA expression of lncRNAs (HERC2P4, HERC2P5, LINC00315, WARS2-IT1, and FOXP1-IT1) (**Figure 3C**), inconsistent with the analysis results. Subsequently, we performed KmPlot analysis to examine the relationships between these candidates and the prognosis of OV patients. Consistent with our expectations, overexpression of miR-98 was associated with better outcomes in OV ($p < 0.05$, **Figure 3D**). However, overexpression of miR-143 was related to poor prognosis (**Figure S1**). As shown in **Figures 3E** and **F**, overexpression of LINC00052 or SMCR5 was significantly related to poor outcomes in OV, which was consistent with our expectations. The remaining lncRNA candidates did not show relationships in accordance with our expectations (**Figure S1**). Taken together, these results suggest that the ceRNA network of COL1A1 is LINC00052/SMCR5-miR-98-COL1A1.

## Identification of the Downstream Regulatory Mechanism of COL1A1

To explore the downstream mechanism of COL1A1 in carboplatin-resistant OV, we analyzed the genes co-expressed with COL1A1 among the 412 carboplatin-resistance-related genes. There were 14 genes co-expressed with COL1A1 (**Table S11**)

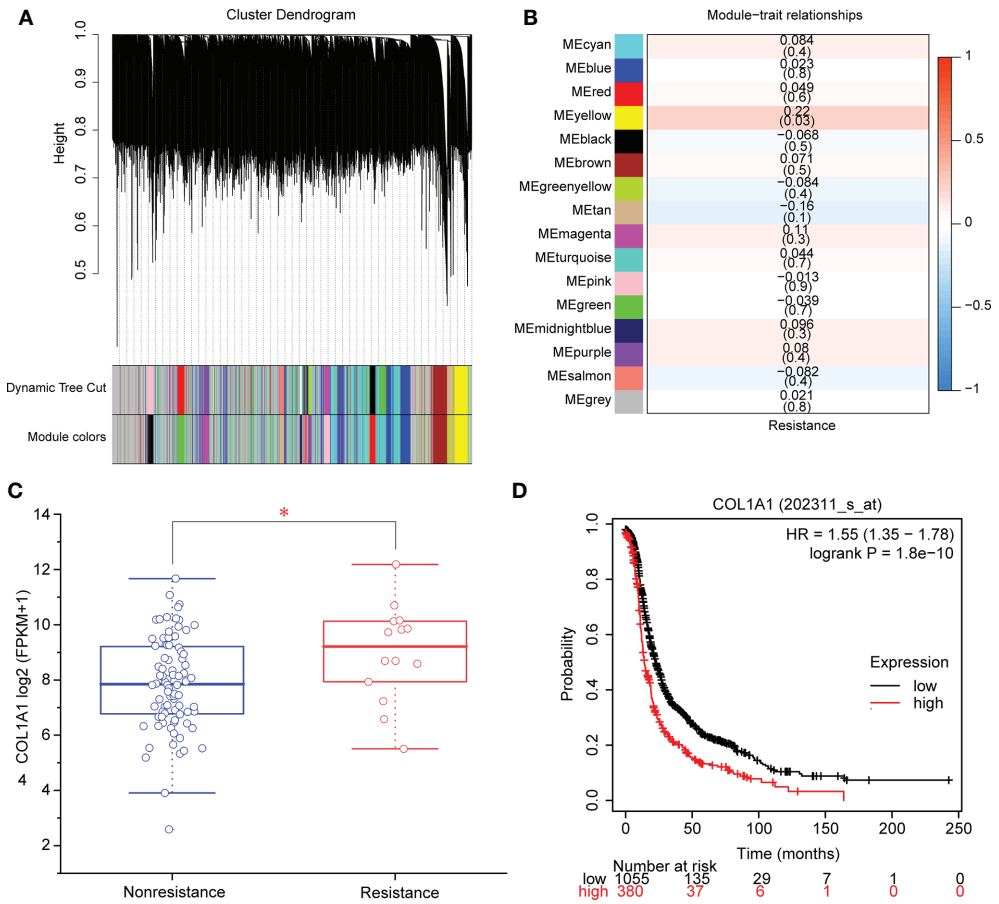


**FIGURE 2** | Identification of modules and genes associated with carboplatin-resistant OV. **(A)** Dendrogram of 8,791 genes in the top 70% median absolute deviations clustered based on a dissimilarity measure (1-TOM). **(B)** Heatmap of the correlation between module eigengenes and clinical traits. Each cell contains the correlation coefficient and *p*-value. **(C)** mRNA expression of COL1A1 in carboplatin-nonresistant OV (n = 84) and carboplatin-resistant OV (n = 14). *$p < 0.05$. **(D)** The overall survival of patients with high expression of COL1A1 was lower than that of patients with low expression ($p < 0.05$).

according to the cutoff values of absolute Pearson correlation coefficient > 0.9 and $p < 0.005$. In addition, 11 KEGG pathways were enriched in the KEGG over-representation test based on the co-expressed genes of COL1A1 (**Figure 4A**). Another method for pathway analysis, GSEA targets the expression across the whole genome. GSEA analysis produced a total of five pathways (**Table S12**) in the carboplatin-resistant group and 22 pathways (**Table S13**) in the carboplatin-nonresistant group, using cutoff values of FDR < 25% and $p < 0.05$. Based on the KEGG over-representation test and GSEA results (**Figure 4B**), two overlapping pathways, "ECM receptor interaction" and "focal adhesion," were identified.

## Potential Drug-Repurposing and Traditional Chinese Medicine

We used virtual screening with Schrodinger Maestro 2019-1 to identify potential drugs that could be repurposed to target COL1A1. The 3D protein structure of COL1A1 was downloaded from the PDB (5CVB, **Figure S2A**), and the active site was found by Schrodinger Maestro (**Figure S2B**). According to the glide scores (**Table S14**), ZINC000085537017 (Cangrelor) was the top hit from the structure-based virtual screening process. The 3D structure of ZINC000085537017 is shown in **Figure 5A**. There were six H-bonds and one pi–pi interaction in the ligand–protein complex (**Figure 5B**). The docking results for ZINC000085537017 and COL1A1 are shown in **Figure 5C**. Furthermore, we found that COL1A1 was targeted by quercetin based on the TCMSP database (**Table S15**). The docking results for quercetin and COL1A1 are shown in **Figure S2C**. To identify whether ZINC000085537017 or quercetin affected carboplatin sensitization in OV, first, carboplatin-resistant cell lines (A2780-carboplatin and SKOV3-carboplatin) were assayed for cell viability after treatment with a concentration gradient of ZINC000085537017 or quercetin (0, 0.01, 0.1, 1, 10, 100 μM) for 24 h. As shown in **Figures S3A–B and S3C–D**, 0.01–1.00 μM ZINC000085537017 and 0.01–10.0 μM quercetin did not significantly inhibit cell growth, but 10–100 μM ZINC000085537017 and 100 μM quercetin significantly

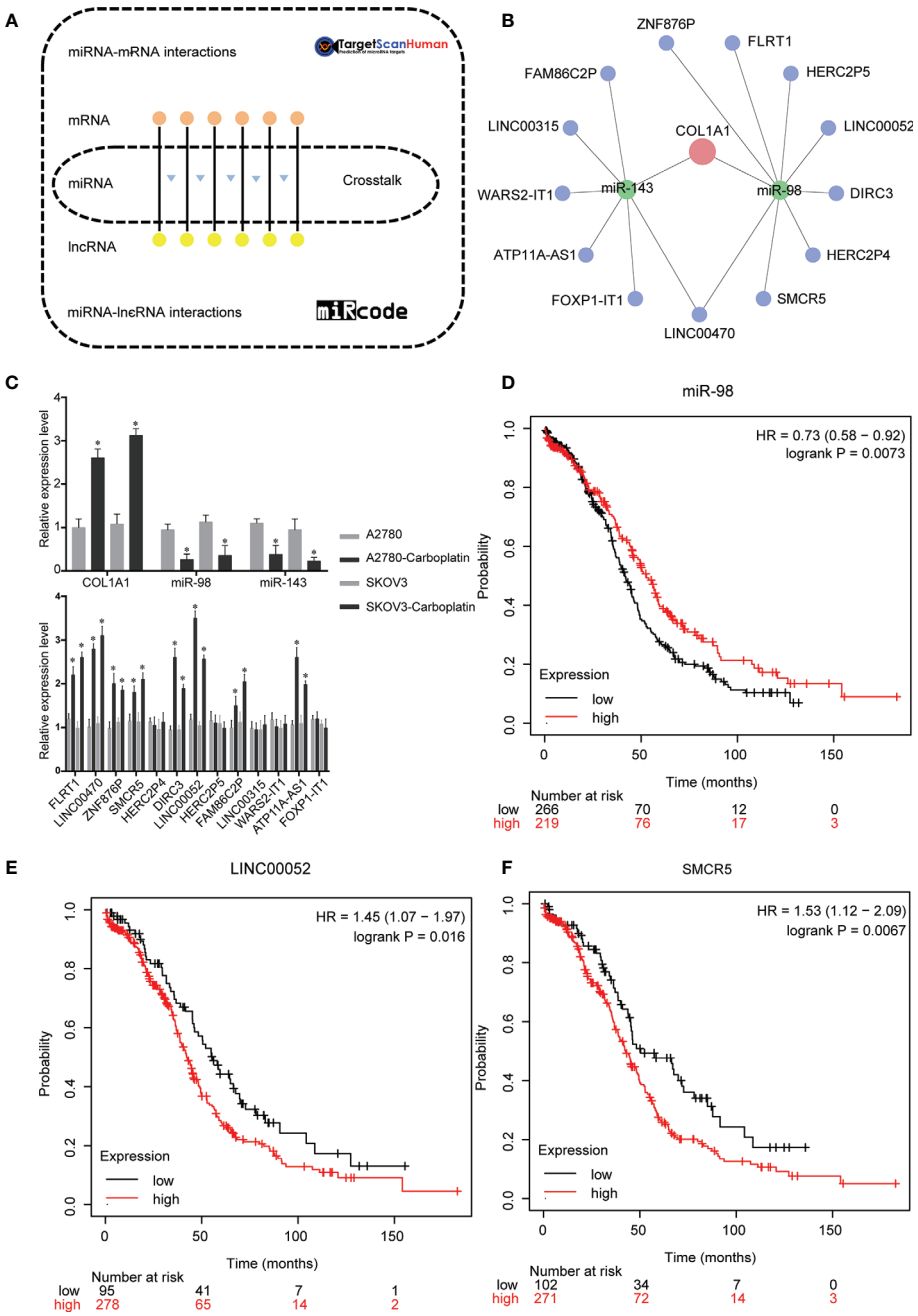


**FIGURE 3** | Upstream regulation mechanism of COL1A1 in carboplatin-resistant OV. **(A)** Bioinformatics methods were used to construct the ceRNA network of COL1A1. **(B)** ceRNA network of COL1A1. Red represents COL1A1, green represents miRNAs, blue represents lncRNAs. **(C)** Real-time PCR validation of candidates in ceRNA network. (mean ± SD, n =3). Asterisks indicate significant differences compared with the control group (*$p < 0.05$). Kaplan–Meier overall survival analyses for miR-98 **(D)**, LINC00052 **(E)**, and SMCR5 **(F)** in OV.

reduced cell viability ($p < 0.05$). Then, based on previous research (22, 23), we selected 1 μM ZINC000085537017 and 10 μM quercetin for subsequent studies. Second, we calculated the $IC_{50}$ values for carboplatin treatment for 48 h. The $IC_{50}$ values of A2780, A2780-carboplatin, SKOV3, and SKOV3-carboplatin were 19.03 μM (7.066 μg/mL), 91.28 μM (33.89 μg/mL), 15.18 μM (5.635 μg/mL), and 68.96 μM (25.6 μg/mL), respectively. As shown in **Figure 5D**, 1 μM ZINC000085537017 significantly enhanced the carboplatin sensitivity ($p < 0.05$) of carboplatin-resistant cells treated with $IC_{20}$ carboplatin, although it did not affect cell viability responses to $IC_{50}$ carboplatin (**Figure 5D**). Similarly, 10 μM quercetin significantly enhanced the sensitivity of carboplatin-resistant cells to carboplatin ($IC_{20}$ and $IC_{50}$) after 48 h of treatment ($p < 0.05$, **Figure 5E**).

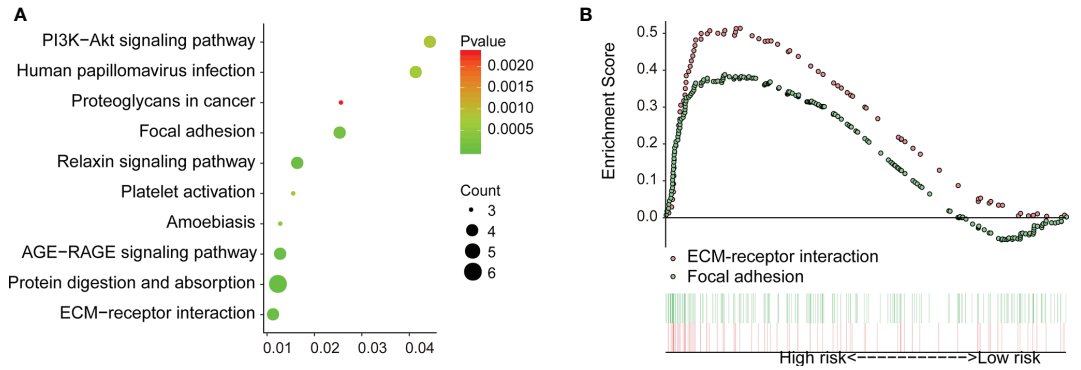


**FIGURE 4** | Downstream regulation mechanism of COL1A1 in carboplatin-resistant OV. **(A)** KEGG over-representation test pathway analysis of genes co-expressed with COL1A1 by clusterProfiler ($p < 0.01$). **(B)** Results of GSEA between carboplatin-resistant and nonresistant groups ($p < 0.05$ and FDR < 25%).

## DISCUSSION

Carboplatin is the cornerstone of chemotherapy for OV. However, drug resistance to this agent continues to present challenges, leading to a poor prognosis for OV patients with a 5-year survival rate of only 25–30% (4, 24). Therefore, the mechanism of resistance to carboplatin in OV has become a focus of research in recent years. Increasing evidence has shown that COL1A1 has an important role in chemoresistance and could represent a potential therapeutic target (5, 6), but the mechanism of COL1A1 in carboplatin-resistant OV has remained unclear. In the present study, we determined the detailed molecular mechanism involving COL1A1 in carboplatin resistance and identified potential targeted drugs (both traditional Chinese medicine and FDA-approved drugs). These results provide new information and supporting data that could help to improve the outcomes of OV patients.

Many hub genes involved in carboplatin resistance have been identified by screening of differentially expressed genes (25–28). However, they were selected by an artificially set threshold, potentially excluding some important genes. In the present study, carboplatin resistance genes were screened by WGCNA, an unsupervised analysis method, making our results potentially more realistic and objective. We first screened carboplatin-resistance-related genes by WGCNA, then used hub gene analysis to identify COL1A1 as the hub gene. Furthermore, the expression of COL1A1 mRNA was found to be higher in carboplatin-resistant OV ($p < 0.05$), and survival analysis showed that high expression of COL1A1 mRNA was correlated with poor prognosis ($p < 0.05$), further demonstrating the pivotal role of COL1A1 in carboplatin resistance. The mRNA expression of COL1A1 was also found to be increased significantly ($p < 0.05$) in two carboplatin-resistant cells by real-time PCR. Although many studies have reported that the expression of COL1A1 was related to chemoresistance in OV (5–8), this was the first time that COL1A1 had been shown to play an important part in carboplatin-resistant OV. Furthermore, as type I collagen is composed of COL1A1 and COL1A2 (29), we speculated that COL1A2 might also have an important role in carboplatin-resistant OV, although there have been no reports about the role of COL1A2 in carboplatin resistance. According to the WGCNA and hub gene analysis results, COL1A2 was found in the 412 carboplatin resistance gene sets and was ranked 12th and 20th by Deg and MNC, respectively. Previously, Januchowski et al. reported that mRNA levels of COL1A2 and COL1A1 were significantly increased in OV cell lines resistant to cisplatin, paclitaxel, doxorubicin, topotecan, vincristine, and methotrexate (5). Taken together, these results suggest that COL1A1 and COL1A2 could be used as molecular targets for new antitumor drugs against carboplatin-resistant OV.

Emerging evidence indicates that ceRNA networks have an important role in chemoresistance to cancers (30, 31) and can provide therapeutic targets. In the present study, we used bioinformatics analysis to identify the ceRNA network of COL1A1. We also performed real-time PCR and KmPlot analysis to further confirm that the ceRNA network was LINC00052/SMCR5-miR-98-COL1A1 (**Figure 6**). Moreover, COL1A1 was previously found to be regulated by miR-98 in hypertrophic scarring (32) and muscular dystrophies (33); overexpression of miR-98 could increase cell apoptosis and enhance sensitivity to cisplatin in lung adenocarcinoma (34); and low miR-98 expression was correlated with temozolomide resistance of glioma (35). Although there have been no reports on the relationship between LINC00052/SMCR5 and chemoresistance, high expression of LINC00052 was found to promote gastric cancer cell proliferation and metastasis (36) and progression of head and neck squamous cell carcinoma (37). However, some of the experimental results in this study were inconsistent with our expectations. We propose two possible reasons for this. First, the associations observed between dysregulated expression of some candidates and prognosis of OV might not have been causal. Second, false positive results may have been generated in our analysis. Overall, in this study, we identified a ceRNA network (LINC00052/SMCR5-miR-98-COL1A1), which expanded our understanding of the upstream regulatory mechanism of COL1A1 in carboplatin-resistant OV and could provide therapeutic targets to improve the prognosis of OV.

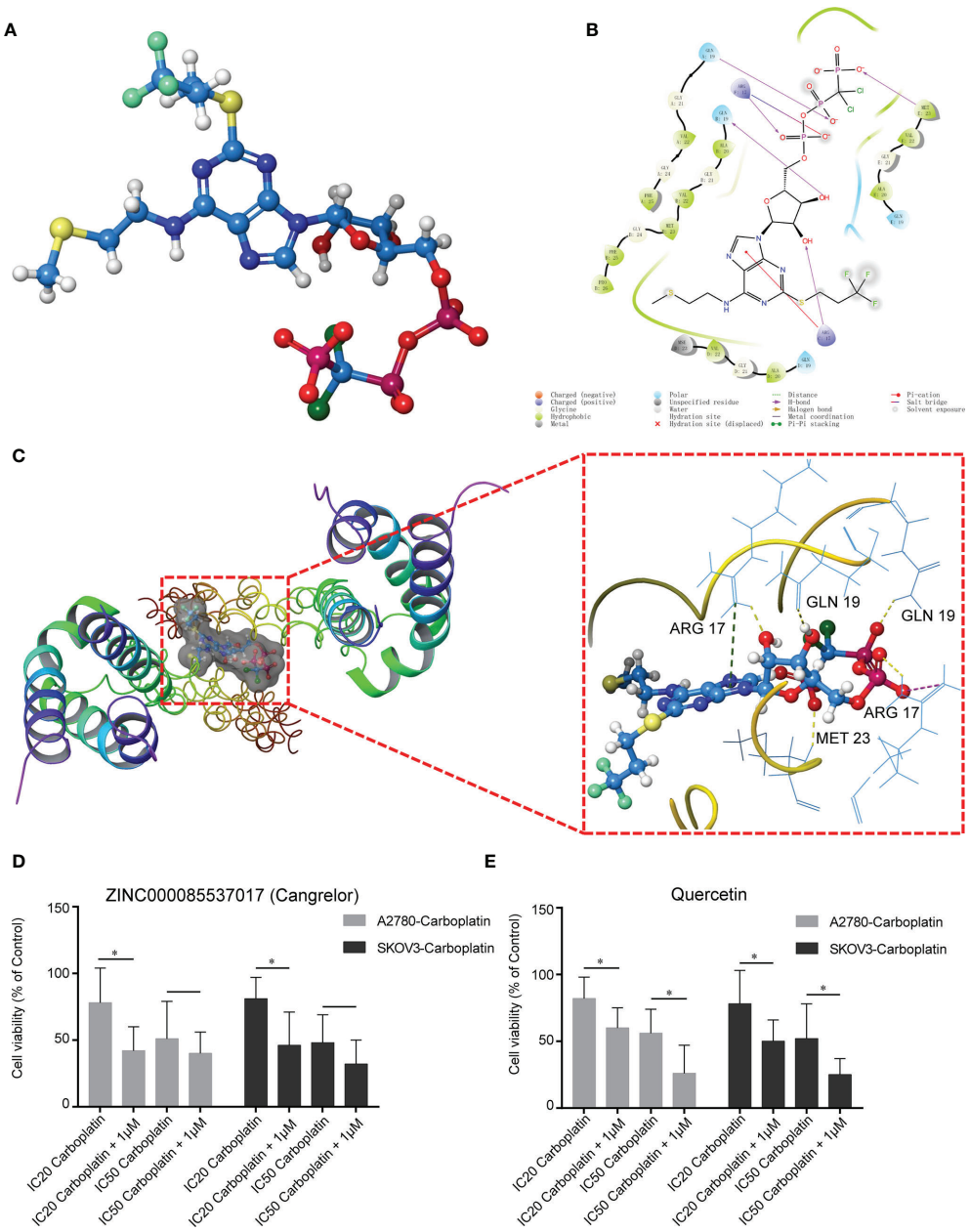


**FIGURE 5** | Potential drugs based on the structure of COL1A1. **(A)** Structure of ZINC000085537017. **(B)** 2D structure of ZINC000085537017's binding mode in COL1A1. **(C)** 3D structure of ZINC000085537017's binding mode in COL1A1. Yellow represents hydrogen bonds, green represents pi–pi interactions, and purple represents salt bridges. ZINC000085537017 **(D)** and quercetin **(E)** enhanced the cytotoxicity of carboplatin in resistant cells. Cells were pretreated with ZINC000085537017 or quercetin for 24 h, followed by incubation with carboplatin for 48 h, and were then subjected to cell viability assays. The results are presented as mean ± SD (n = 6) and were normalized to the control (*$p < 0.05$).

Furthermore, the "ECM-receptor interaction" and "focal adhesion" KEGG pathways were identified as downstream pathways of COL1A1 involved in carboplatin-resistant OV. We identified these two key pathways using the KEGG over-representation test based on the co-expressed genes of COL1A1 and GSEA, suggesting that COL1A1 promoted carboplatin resistance in OV through these pathways. According to previous studies, the "ECM-receptor interaction" pathway is involved in platinum- (38), paclitaxel-, and topotecan-resistant OV (39), trastuzumab-resistant gastric cancer (40), and temozolomide-resistant glioblastoma (41). Moreover, to date, many drug resistance mechanisms involving the extracellular

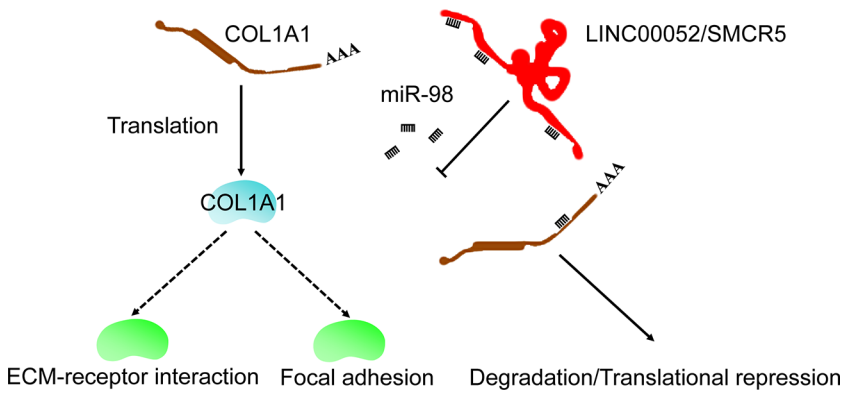


**FIGURE 6** | Possible mechanism of COL1A1 in carboplatin-resistant OV.

matrix have been identified across cancer types; these mechanisms have been classified into a range of categories including physical barriers to treatment (hypoxia, pH, and interstitial fluid pressure) and cell-adhesion-associated drug resistance (42). The "focal adhesion" KEGG pathway has been shown to be associated with taxol- (43) and cisplatin-resistant OV (44, 45). Taken together, these results indicated that COL1A1 was involved in carboplatin resistance in OV through the "ECM-receptor interaction" and "focal adhesion" KEGG pathways (**Figure 6**).

In the present study, we also explored potential drug-repurposing by virtual screening of FDA approved drugs and traditional Chinese medicines targeting COL1A1, which might expand potential therapeutic strategies for carboplatin-resistant OV treatment. We found that ZINC000085537017 and quercetin were potential drugs for treatment of COL1A1. Although 1 μM ZINC000085537017 did not affect cell viability in response to carboplatin, we expected that ZINC000085537017 and quercetin would enhance the sensitivity of carboplatin-resistant cells based on the cell viability assays. We speculated that the leaching toxicity of $IC_{50}$ carboplatin in resistant cells might have exceeded the influence of 1 μM ZINC000085537017, resulting in no significant differences being found when $IC_{50}$ carboplatin was combined with 1 μM ZINC000085537017 in these cells. Previous study showed that quercetin could increase the sensitivity of OV to cisplatin (46); however, in contrast to these studies, which focused on the relationship between the expression of COL1A1 and chemoresistance, we not only showed that COL1A1 was a therapeutic target but also identified some potential drugs. These results could help accelerate the development of drugs to improve the outcomes of carboplatin-resistant OV patients.

## CONCLUSION

In summary, we identified that COL1A1 has an important role in carboplatin-resistant OV by WGCNA; this result was further validated by survival analysis. Then, we constructed a ceRNA network for COL1A1 by bioinformatics analysis and experiments to expand understanding of the upstream regulatory mechanism of COL1A1 in carboplatin-resistant OV and identify potential therapeutic targets that could be used to improve the prognosis of OV. Moreover, we found that COL1A1 participated in carboplatin resistance in OV through the "ECM-receptor interaction" and "focal adhesion" KEGG pathways by co-expression analysis and pathway enrichment. Furthermore, combining these results with those of experiments, we found that ZINC000085537017 and quercetin were potential drugs for COL1A1 by virtual screening based on the structure of COL1A1 and the TCMSP database. These findings could accelerate drug development to improve the outcomes of carboplatin-resistant OV patients.

## DATA AVAILABILITY STATEMENT

The original contributions presented in the study are included in the article/**Supplementary Material**, further inquiries can be directed to the corresponding authors.

## AUTHOR CONTRIBUTIONS

LT and QW conceptualized and developed an outline for the manuscript and revised the manuscript. FY and ZZ conceived, designed, analyzed the data, and wrote the manuscript. LL and LH generated the figures and tables. SC collected the public data. All authors contributed to the article and approved the submitted version.

## FUNDING

This work was supported by the National Natural Science Foundation of China (Grant No. 81473234), the Joint Fund of

the National Natural Science Foundation of China (Grant No. U1303221), the Fundamental Research Funds for the Central Universities (Grant No.16ykjc01), and the grant from Department of Science and Technology of Guangdong Province (Grant No.20160908).

## SUPPLEMENTARY MATERIAL

The Supplementary Material for this article can be found online at: https://www.frontiersin.org/articles/10.3389/fonc.2020.576565/full#supplementary-material

## REFERENCES


1. Siegel RL, Miller KD, Jemal A. Cancer statistics, 2019. *CA Cancer J Clin* (2019) 69(1):7–34. doi: 10.3322/caac.21551
2. Matulonis UA, Sood AK, Fallowfield L, Howitt BE, Sehouli J, Karlan BY. Ovarian cancer. *Nat Rev Dis Primers* (2016) 2:16061. doi: 10.1038/nrdp.2016.61
3. Pignata S, CC S, Du Bois A, Harter P, Heitz F. Treatment of recurrent ovarian cancer. *Ann Oncol* (2017) 28(suppl_8):viii51–viii6. doi: 10.1093/annonc/mdx441
4. Damia G, Broggini M. Platinum Resistance in Ovarian Cancer: Role of DNA Repair. *Cancers (Basel)* (2019) 11(1):119. doi: 10.3390/cancers11010119
5. Januchowski R, Swierczewska M, Sterzynska K, Wojtowicz K, Nowicki M, Zabel M. Increased Expression of Several Collagen Genes is Associated with Drug Resistance in Ovarian Cancer Cell Lines. *J Cancer* (2016) 7(10):1295–310. doi: 10.7150/jca.15371
6. Leask A. A centralized communication network: Recent insights into the role of the cancer associated fibroblast in the development of drug resistance in tumors. *Semin Cell Dev Biol* (2020) 101:111–4. doi: 10.1016/j.semcdb.2019.10.016
7. Wang M, Wang J, Liu J, Zhu L, Ma H, Zou J, et al. Systematic prediction of key genes for ovarian cancer by co-expression network analysis. *J Cell Mol Med* (2020) 24(11):6298–307. doi: 10.1111/jcmm.15271
8. Yu PN, Yan MD, Lai HC, Huang RL, Chou YC, Lin WC, et al. Downregulation of miR-29 contributes to cisplatin resistance of ovarian cancer cells. *Int J Cancer* (2014) 134(3):542–51. doi: 10.1002/ijc.28399
9. Marchion DC, Cottrill HM, Xiong Y, Chen N, Bicaku E, Fulp WJ, et al. BAD phosphorylation determines ovarian cancer chemosensitivity and patient survival. *Clin Cancer Res* (2011) 17(19):6356–66. doi: 10.1158/1078-0432.CCR-11-0735
10. Langfelder P, Horvath S. Fast R Functions for Robust Correlations and Hierarchical Clustering. *J Stat Softw* (2012) 46(11):i11. doi: 10.18637/jss.v046.i11
11. Peng WX, Huang JG, Yang L, Gong AH, Mo YY. Linc-RoR promotes MAPK/ERK signaling and confers estrogen-independent growth of breast cancer. *Mol Cancer* (2017) 16(1):161. doi: 10.1186/s12943-017-0727-3
12. Robinson MD, McCarthy DJ, Smyth GK. edgeR: a Bioconductor package for differential expression analysis of digital gene expression data. *Bioinformatics* (2010) 26(1):139–40. doi: 10.1093/bioinformatics/btp616
13. Dangi A, Natesh NR, Husain I, Ji Z, Barisoni L, Kwun J, et al. Single cell transcriptomics of mouse kidney transplants reveals a myeloid cell pathway for transplant rejection. *JCI Insight* (2020) 5(20):e141321. doi: 10.1172/jci.insight.141321
14. Wang JD, Zhou HS, Tu XX, He Y, Liu QF, Liu Q, et al. Prediction of competing endogenous RNA coexpression network as prognostic markers in AML. *Aging (Albany NY)* (2019) 11(10):3333–47. doi: 10.18632/aging.101985
15. Thomson DW, Dinger ME. Endogenous microRNA sponges: evidence and controversy. *Nat Rev Genet* (2016) 17(5):272–83. doi: 10.1038/nrg.2016.20
16. Shannon P, Markiel A, Ozier O, Baliga NS, Wang JT, Ramage D, et al. Cytoscape: a software environment for integrated models of biomolecular interaction networks. *Genome Res* (2003) 13(11):2498–504. doi: 10.1101/gr.1239303
17. Yu G, Wang LG, Han Y, He QY. clusterProfiler: an R package for comparing biological themes among gene clusters. *Omics J Integr Biol* (2012) 16(5):284–7. doi: 10.1089/omi.2011.0118
18. Subramanian A, Tamayo P, Mootha VK, Mukherjee S, Ebert BL, Gillette MA, et al. Gene set enrichment analysis: a knowledge-based approach for interpreting genome-wide expression profiles. *Proc Natl Acad Sci USA* (2005) 102(43):15545–50. doi: 10.1073/pnas.0506580102
19. Salam NK, Nuti R, Sherman W. Novel method for generating structure-based pharmacophores using energetic analysis. *J Chem Inf Model* (2009) 49 (10):2356–68. doi: 10.1021/ci900212v
20. Irwin JJ, Sterling T, Mysinger MM, Bolstad ES, Coleman RG. ZINC: a free tool to discover chemistry for biology. *J Chem Inf Model* (2012) 52(7):1757–68. doi: 10.1021/ci3001277
21. Ru J, Li P, Wang J, Zhou W, Li B, Huang C, et al. TCMSP: a database of systems pharmacology for drug discovery from herbal medicines. *J Cheminform* (2014) 6:13. doi: 10.1186/1758-2946-6-13
22. Egan K, Crowley D, Smyth P, O'Toole S, Spillane C, Martin C, et al. Platelet adhesion and degranulation induce pro-survival and pro-angiogenic signalling in ovarian cancer cells. *PloS One* (2011) 6(10):e26125. doi: 10.1371/journal.pone.0026125
23. Koren Carmi Y, Mahmoud H, Khamaisi H, Adawi R, Gopas J, Mahajna J. Flavonoids Restore Platinum Drug Sensitivity to Ovarian Carcinoma Cells in a Phospho-ERK1/2-Dependent Fashion. *Int J Mol Sci* (2020) 21(18):6533. doi: 10.3390/ijms21186533
24. Cortes-Guiral D, Elias D, Cascales-Campos PA, Badia Yebenes A, Guijo Castellano I, Leon Carbonero AI, et al. Second-look surgery plus hyperthermic intraperitoneal chemotherapy for patients with colorectal cancer at high risk of peritoneal carcinomatosis: Does it really save lives? *World J Gastroenterol* (2017) 23(3):377–81. doi: 10.3748/wjg.v23.i3.377
25. Zhao H, Sun Q, Li L, Zhou J, Zhang C, Hu T, et al. High Expression Levels of AGGF1 and MFAP4 Predict Primary Platinum-Based Chemoresistance and are Associated with Adverse Prognosis in Patients with Serous Ovarian Cancer. *J Cancer* (2019) 10(2):397–407. doi: 10.7150/jca.28127
26. Wei L, Wen JY, Chen J, Ma XK, Wu DH, Chen ZH, et al. Oncogenic ADAM28 induces gemcitabine resistance and predicts a poor prognosis in pancreatic cancer. *World J Gastroenterol* (2019) 25(37):5590–603. doi: 10.3748/wjg.v25.i37.5590
27. Lian W, Jin H, Cao J, Zhang X, Zhu T, Zhao S, et al. Identification of novel biomarkers affecting the metastasis of colorectal cancer through bioinformatics analysis and validation through qRT-PCR. *Cancer Cell Int* (2020) 20:105. doi: 10.1186/s12935-020-01180-4
28. Ma Q, Xu Y, Liao H, Cai Y, Xu L, Xiao D, et al. Identification and validation of key genes associated with non-small-cell lung cancer. *J Cell Physiol* (2019) 234 (12):22742–52. doi: 10.1002/jcp.28839
29. Gelse K, Poschl E, Aigner T. Collagens–structure, function, and biosynthesis. *Adv Drug Delivery Rev* (2003) 55(12):1531–46. doi: 10.1016/j.addr.2003.08.002
30. Neve B, Jonckheere N, Vincent A, Van Seuningen I. Epigenetic Regulation by lncRNAs: An Overview Focused on UCA1 in Colorectal Cancer. *Cancers (Basel)* (2018) 10(11):440. doi: 10.3390/cancers10110440
31. Ogunwobi OO, Kumar A. Chemoresistance Mediated by ceRNA Networks Associated With the PVT1 Locus. *Front Oncol* (2019) 9:834:834. doi: 10.3389/fonc.2019.00834
32. Bi S, Chai L, Yuan X, Cao C, Li S. MicroRNA-98 inhibits the cell proliferation of human hypertrophic scar fibroblasts via targeting Col1A1. *Biol Res* (2017) 50(1):22. doi: 10.1186/s40659-017-0127-6
33. Mohamed JS, Hajira A, Lopez MA, Boriek AM. Genome-wide Mechanosensitive MicroRNA (MechanomiR) Screen Uncovers Dysregulation of Their Regulatory Networks in the mdm Mouse Model of Muscular Dystrophy. *J Biol Chem* (2015) 290(41):24986–5011. doi: 10.1074/jbc.M115.659375
34. Xiang Q, Tang H, Yu J, Yin J, Yang X, Lei X. MicroRNA-98 sensitizes cisplatin-resistant human lung adenocarcinoma cells by up-regulation of HMGA2. *Pharmazie* (2013) 68(4):274–81. doi: 10.1691/ph.2013.2759
35. Gu N, Wang X, Di Z, Xiong J, Ma Y, Yan Y, et al. Silencing lncRNA FOXD2-AS1 inhibits proliferation, migration, invasion and drug resistance of drug-resistant glioma cells and promotes their apoptosis via microRNA-98-5p/CPEB4 axis. *Aging (Albany NY)* (2019) 11(22):10266–83. doi: 10.18632/aging.102455

36. Shan Y, Ying R, Jia Z, Kong W, Wu Y, Zheng S, et al. LINC00052 Promotes Gastric Cancer Cell Proliferation and Metastasis via Activating the Wnt/beta-Catenin Signaling Pathway. *Oncol Res* (2017) 25(9):1589–99. doi: 10.3727/096504017X14897896412027
37. Ouyang T, Zhang Y, Tang S, Wang Y. Long non-coding RNA LINC00052 regulates miR-608/EGFR axis to promote progression of head and neck squamous cell carcinoma. *Exp Mol Pathol* (2019) 111:104321. doi: 10.1016/j.yexmp.2019.104321
38. Tassi RA, Gambino A, Ardighieri L, Bignotti E, Todeschini P, Romani C, et al. FXYD5 (Dysadherin) upregulation predicts shorter survival and reveals platinum resistance in high-grade serous ovarian cancer patients. *Br J Cancer* (2019) 121(7):584–92. doi: 10.1038/s41416-019-0553-z
39. Sterzynska K, Klejewski A, Wojtowicz K, Swierczewska M, Nowacka M, Kazmierczak D, et al. Mutual Expression of ALDH1A1, LOX, and Collagens in Ovarian Cancer Cell Lines as Combined CSCs- and ECM-Related Models of Drug Resistance Development. *Int J Mol Sci* (2018) 20(1):54. doi: 10.3390/ijms20010054
40. Yu C, Xue P, Zhang L, Pan R, Cai Z, He Z, et al. Prediction of key genes and pathways involved in trastuzumab-resistant gastric cancer. *World J Surg Oncol* (2018) 16(1):174. doi: 10.1186/s12957-018-1475-6
41. Zeng H, Xu N, Liu Y, Liu B, Yang Z, Fu Z, et al. Genomic profiling of long non-coding RNA and mRNA expression associated with acquired temozolomide resistance in glioblastoma cells. *Int J Oncol* (2017) 51(2):445–55. doi: 10.3892/ijo.2017.4033
42. Brown Y, Hua S, Tanwar PS. Extracellular matrix-mediated regulation of cancer stem cells and chemoresistance. *Int J Biochem Cell Biol* (2019) 109:90–104. doi: 10.1016/j.biocel.2019.02.002
43. McGrail DJ, Khambhati NN, Qi MX, Patel KS, Ravikumar N, Brandenburg CP, et al. Alterations in ovarian cancer cell adhesion drive taxol resistance by increasing microtubule dynamics in a FAK-dependent manner. *Sci Rep* (2015) 5:9529. doi: 10.1038/srep09529
44. Wei L, Yin F, Zhang W, Li L. STROBE-compliant integrin through focal adhesion involve in cancer stem cell and multidrug resistance of ovarian cancer. *Med (Baltimore)* (2017) 96(12):e6345. doi: 10.1097/MD.0000000000006345
45. Li J, Zhang Y, Gao Y, Cui Y, Liu H, Li M, et al. Downregulation of HNF1 homeobox B is associated with drug resistance in ovarian cancer. *Oncol Rep* (2014) 32(3):979–88. doi: 10.3892/or.2014.3297
46. Zhang Y, Chen S, Wei C, Rankin GO, Ye X, Chen YC. Flavonoids from Chinese bayberry leaves induced apoptosis and G1 cell cycle arrest via Erk pathway in ovarian cancer cells. *Eur J Med Chem* (2018) 147:218–26. doi: 10.1016/j.ejmech.2018.01.084

**Conflict of Interest:** The authors declare that the research was conducted in the absence of any commercial or financial relationships that could be construed as a potential conflict of interest.

frontiers in Oncology

MINI REVIEW
published: 18 February 2021
doi: 10.3389/fonc.2020.629422

# The Hypoxic Microenvironment of Breast Cancer Cells Promotes Resistance in Radiation Therapy

*Cordell Gilreath*[1], *Marjan Boerma*[2], *Zhiqiang Qin*[3], *M. Keith Hudson*[1]* *and Shanzhi Wang*[1]*

[1] Chemistry Department, University of Arkansas at Little Rock, Little Rock, AR, United States, [2] Pharmaceutical Sciences, University of Arkansas for Medical Sciences, Little Rock, AR, United States, [3] Department of Pathology, University of Arkansas for Medical Sciences, Little Rock, AR, United States

The American Cancer Society has estimated an expected 279,100 new breast cancer cases, and an expected 42,690 breast cancer deaths in the U.S. for the year 2020. This includes an estimated 276,480 women who are expected to be diagnosed. Radiation therapy, also called ionizing radiation therapy, is one of the most frequently used methods in the treatment of breast cancer. While radiation therapy is used in the treatment of more than 50% of all cancer cases, tumor resistance to ionizing radiation presents a major challenge for effective cancer treatment. Most tumor cells are in a hypoxic microenvironment that promotes resistance to radiation therapy. In addition to radiation resistance, the hypoxic microenvironment also promotes cancer proliferation and metastasis. In this review, we will discuss the hypoxic microenvironment of breast cancer tumors, related signaling pathways, breast cancer stem-like cells, and the resistance to radiation therapy. Recent developments in our understanding of tumor hypoxia and hypoxic pathways may assist us in developing new strategies to increase cancer control in radiation therapy.

**Keywords: breast cancer, radiation therapy, hypoxia, free radicals, superoxide ions, radiation resistance**

OPEN ACCESS

***Edited by:***
*Zhe-Sheng Chen,*
*St. John's University, United States*

***Reviewed by:***
*Shikha Kumari,*
*University of Nebraska Medical Center, United States*
*Xiang Zhou,*
*Fudan University, China*
*Weijia Wang,*
*Peking University First Hospital, China*

***Correspondence:**
*M. Keith Hudson*
*mkhudson@ualr.edu*
*Shanzhi Wang*
*sxwang2@ualr.edu*

***Specialty section:***
*This article was submitted to Pharmacology of Anti-Cancer Drugs, a section of the journal Frontiers in Oncology*

***Received:*** *14 November 2020*
***Accepted:*** *29 December 2020*
***Published:*** *18 February 2021*

***Citation:***
*Gilreath C, Boerma M, Qin Z, Hudson MK and Wang S (2021) The Hypoxic Microenvironment of Breast Cancer Cells Promotes Resistance in Radiation Therapy. Front. Oncol. 10:629422. doi: 10.3389/fonc.2020.629422*

## INTRODUCTION

Breast cancer is the second leading cause of cancer death in women. The American Cancer Society has estimated an expected 279,100 new breast cancer cases and an expected 42,690 breast cancer deaths in the U.S. for the year 2020 (1). There have been many advancements in the diagnosis and treatment of breast cancer in the past few decades. However, more research is still needed to overcome cancer resistance to therapy and improve the prognosis of advanced-stage breast cancer.

One significant obstacle to improve prognosis is breast cancer recurrence that is often associated with metastasis (2, 3). Breast cancer recurrence is the return of breast cancer months to years after the completion of initial treatment. Some cancer cells survive initial treatment and become undetected. These cancer cells may multiply and repopulate in nearby or distant areas. As such, the three types of breast cancer recurrence are local, regional, and metastatic recurrence. Local recurrence is the return of cancer in the same area of the breast as initial cancer; Regional recurrence is the return of cancer in the lymph nodes near the original cancer location; Metastatic recurrence,

also called distant recurrence, is the return of breast cancer in areas distant from the original cancer site (1). Common metastatic sites include the bone, lungs, or brain, and these metastatic recurrences are the foremost cause of breast cancer death (4).

Radiation therapy is used as an adjunct therapy for many primary cancers and is one of the most frequently used methods in breast cancer therapy. Ionizing radiation targeted at breast cancer cells causes an interaction with water and $O_2$ molecules near and inside the cells. This interaction produces free radicals and superoxide ions, which in turn cause damage to the cancer cell's DNA and other macromolecules, and potentially induces cell death (5). The primary purposes of radiation therapy are to improve prognosis of primary treatments, to treat metastasized cancer cells, and to decrease the chance of recurrence. However, tumor resistance to ionizing radiation presents a major challenge for effective breast cancer treatment. Tumor resistance may be in part due to a hypoxic microenvironment that is common in tumors. Here, we outline the cellular response to ionizing radiation and signal transduction pathways induced by hypoxic conditions as targets to identify novel strategies to increase the efficacy of radiation therapy.

## IONIZING RADIATION

Ionizing radiation in breast cancer therapy is greatly dependent on the damaging effects of low linear energy transfer (Low LET) radiation, such as X rays (5). There are direct and indirect effects of ionizing radiation. Direct effects of ionizing radiation are direct interactions between the particle and the targeted macromolecule, such as DNA (**Figure 1**), which eventually can lead to cell death (5, 6). Indirect effects of ionization consist of an intermediate step between radiation and the macromolecules, such as in water radiolysis. During water radiolysis in radiation therapy, water molecules are decompositioned by ionization radiation, and several types of free radicals are generated to damage macromolecules. These free radicals primarily include the hydrated electron ($e^-_{aq}$), the hydrogen radical (H•), and the hydroxyl radical (OH•), which are highly reactive to the adjacent macromolecules (5). During radiaton therapy, the majority of deposited radiation will be absorbed by cellular water. This makes indirect ionization of water the primary cause of biological damage from radiation exposure (5).

## THE HYPOXIC MICROENVIRONMENT

Tumor hypoxia, which is the lack of oxygen within a tumor, is one of the most common characteristics of the tumor microenvironment due to rapid cell growth and oxygen consumption (7). The hypoxic microenvironment in breast cancer requires the tumor to adapt in order to survive, and as such, tumor hypoxia has been closely associated with angiogenesis, metastasis, chemoresistance, and radiation resistance (8–10). Hypoxia has been recognized to activate many signaling transduction pathways, such as RAS/RAF/and mitogen-activated protein kinase (MAPK) (11). Hypoxia within the tumor microenvironment activates the heterodimer hypoxia-inducible factor 1 (HIF-1), a transcription factor consisting of two protein subunits, HIF-1α and HIF-1β. The expression and function of HIF-1α is regulated by oxygen concentration, while HIF-1β is constitutively expressed. Under normoxic conditions, HIF-1α is hydroxylated at proline residues 402 and 564, then ubiquitinated by prolyl-hydroxylase domain enzymes (PHD), which leads to proteasomal degradation (**Figure 2A**) (12–14). Under hypoxic conditions, HIF-1α is stabilized by dimerizing with HIF-1β (**Figure 2A**). Upon hypoxia, the HIF-1 heterodimer binds to the hypoxia response elements of multiple genes, which activates their transcription (**Figure 2A**) (8, 15). Many of these gene products participate in metabolism, such as, glycolytic enzymes, glucose transporters, antigenic growth factors, and carbonic anhydrases. The upregulation of these genes in breast cancer mediate a metabolic change from oxidative to glycolytic (11, 16, 17). Intratumoral hypoxia and alterations of the tumor microenvironmentare mechanisms that increase HIF-1α levels in breast cancer. In addition, the mutation and inactivation of tumor

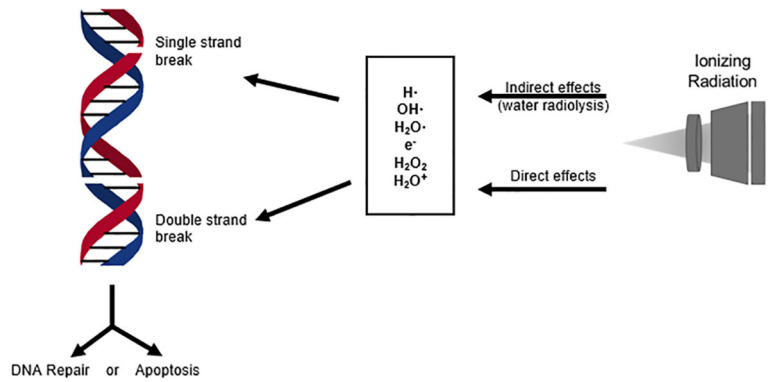


**FIGURE 1** | DNA breaks induced by direct and indirect effects of ionizing radiation activate cellular stress response mechanisms. These response mechanisms can either repair the DNA damage or signal the activation of apoptosis, which is the primary objective in cancer radiation therapy.

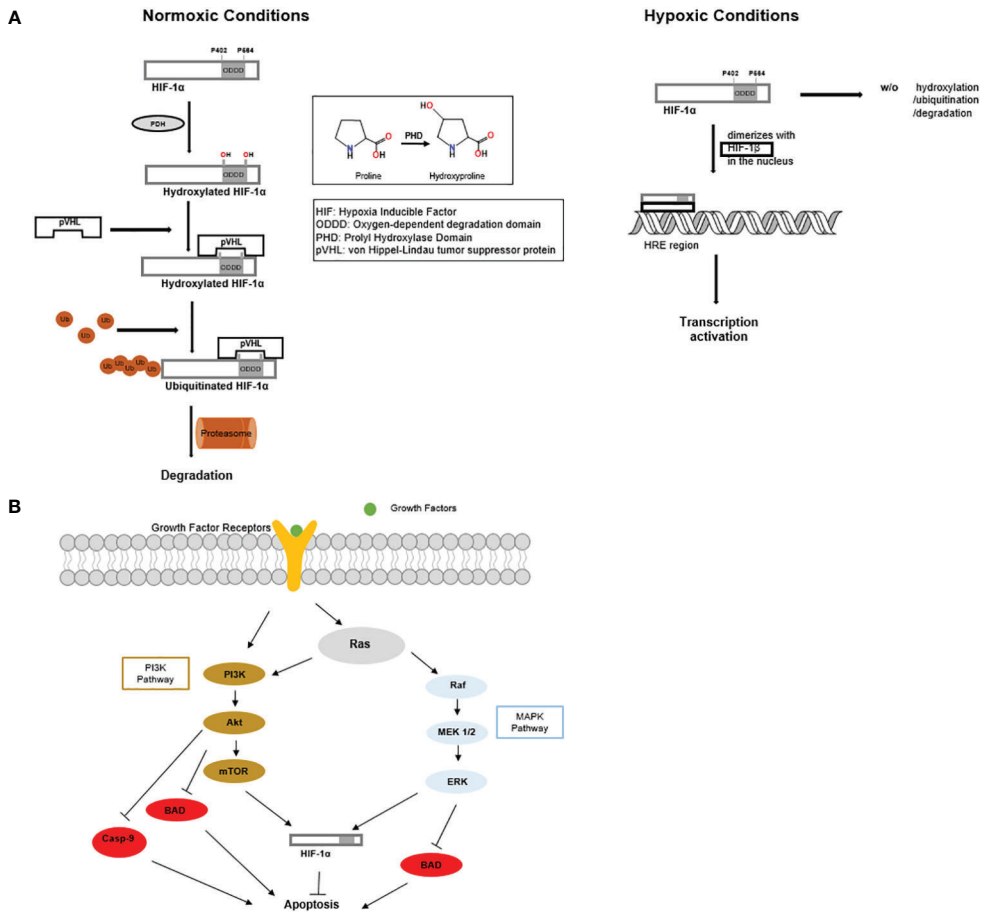


**FIGURE 2** | **(A)** Under normoxic conditions, HIF-1α is produced and rapidly undergoes hydroxylation, ubiquitination, and proteasomal degradation. While under hypoxic conditions, HIF-1α does not undergo proteasomal degradation. HIF-1α enters the nucleus and dimerizes with HIF-1β to form a stable heterodimer. The HIF-1 heterodimer promotes tumor growth and angiogenesis. **(B)** MAPK and PI3K signaling cascades inhibit apoptosis and promote the function of HIF1α.

suppressor genes such as the von Hippel-Lindau tumor suppressor (pVHL), tumor protein p53 (p53)), and phosphatase and tensin homolog (PTEN) are associated with increased HIF-1α activity (18). It is important to note that although HIF-1α is widely recognized as the main regulator in tumor hypoxia, many additional factors, such as histone acetyltransferase (p300) and the CREB-binding protein (CBP) (19, 20), are essential to promote the comprehensive hypoxic response within the tumor microenvironment (11).

## HYPOXIC AND ANTI-APOPTOTIC SIGNALING PATHWAYS

Hypoxic signaling within the tumor microenvironment is used by cancer cells to communicate with other cells and their extracellular environment. This communication within the hypoxic microenvironment is a highly explored area and is still not fully understood.

During hypoxia signaling, exosomes, the extracellular nanovesicles released by cells, play a vital role in communicating intercellular signals by way of paracrine signaling (7, 21). Tumor cells produce exosomes that contain several types of molecules from within the tumor cells, including miRNA, mRNA, DNA, proteins, and lipids that affect the activity of neighboring cells (21, 22). During hypoxia signaling, multiple pathways and even multiple cell types may crosstalk *via* exosomes. Boelens et al. showed that stromal cells released exosomes to communicate with breast cancer cells. This multi-signaling pathway uses both paracrine antiviral and juxtacrine neurogenic locus notch homolog protein 3 (NOTCH3) signaling to enhance breast cancer survival and therapy resistance. The communication is initiated by the stromal cells by increasing Ras-related protein Rab-27B (RAB27B) and transferring 5'-triphosphate RNA in exosomes. It results in the activation of retinoic acid-inducible gene 1 (RIG-l) antiviral signaling while simultaneously activates NOTCH3 receptors in breast cancer cells (23). The crosstalk between stromal and breast cancer cells signaling pathways converge as STAT1 promotes transcriptional responses to NOTCH3. This also promotes the

initiation of producing tumor cell subpopulations that are prone to therapeutic resistance. These findings also suggest that blocking the NOTCH pathway resensitizes tumor cells to radiation and may be a therapeutic target in the treatment of cancer (24). The role of exosomes in the breast cancer tumor microenvironment is still not fully understood, but there is an established correlation between the activation of hypoxic signaling and increased exosome production (7). Research is currently underway to determine whether tumor cell exosomes may be a novel target in cancer therapy.

Several signaling pathways participate in breast cancer resistance to radiation therapy, such as Ras/phosphoinositide 3-kinase (PI3K)/PTEN/protein kinase B (Akt)/mammalian target of rapamycin (mTOR) (**Figure 2B**) (25), and Ras/Raf/mitogen-activated protein kinase kinase (MEK)/extracellular signal-regulated kinase (ERK) (MAPK) (**Figure 2B**) (26, 27).

The activation of Akt, as part of PI3K pathway, could directly promote therapeutic resistance, including resistance to radiation (26). Akt is a kinase that is activated through the phosphorylation of its two residues, threonine 308 and serine 473 (28, 29). As a promoter of cell division and growth, Akt also plays a role in response to DNA damage (28). Akt can deactivate the BCL2 family member BAD by phosphorylation (30) and deactivate the cysteine protease Caspase-9. The deactivation of BAD and Caspase 9 is detrimental to the promotion of apoptosis, which is an essential factor of therapeutic resistance in breast cancer treatment. PI3-K/Akt signaling pathway is dysregulated in breast cancer. Söderlund et al. showed that the stimulation of the epidermal growth factor erbB2 (HER2)/PI3-K/Akt with heregulin-B1 triggered the resistance to radiation-induced apoptosis in breast cancer (28). Furthermore, it was found that the inhibition of the PI3K signaling resulted in sensitizing brease cancer cell line BT-474, which overactivates PI3K pathway by overexpressing human epidermal growth factor receptor 2 (HER2). Independently, Steelman et al. showed that the PI3-k/PTEN/Akt/mTOR signaling cascade pathway was activated in breast cancer, therefore promoting its resistance to therapy. Consistently, the elevated levels of Akt-1 promoted resistance to doxorubicin, tamoxifen, and radiation. Interestingly, cells that were resistant to chemotherapy or radiation therapy harbored p53 mutations and expression of the downstream cyclin-dependent kinase inhibitor 1 ($p21^{Cip1}$). Also, ERK, an enzyme associated with cell development and proliferation, was induced by Doxorubicin therapy (26). A better understanding of the mechanisms of these signaling cascades, the activation and inhibition of Akt, may present promising therapeutic targets in the treatment of breast cancer.

The MAPK signaling pathway is known to promote cancer cell survival and limit the effectiveness of radiation therapy (31). Criswell et al. showed that ionizing radiation activated the insulin-like growth factor -1 receptor (IGF-1R), which in turn activated the MAPK signaling pathway, which upregulates secretory clusterin (sCLU) expression, a stress induced pro-survival protein. The study presented evidence that AG1024, an IGF-1R inhibitor blocked the induction of sCLU after radiation (31). More research is necessary to fully understand the role of the delayed EGF-1R/MAPK signaling pathway, but inhibition of IGF-1R may be a potential target in cancer therapy.

The mammalian target of rapamycin (mTOR) is another signaling pathway closely related to radiation resistance in breast cancer. mTOR and ribosomal protein S6 Kinase Beta-1 (p-S6K1) were found to be elevated in breast cancer cells (32, 33). $CD44^{high}/CD24^{low}$ Michigan Cancer Foundation-7 (MCF-7) cells, a radioresistant breast cancer cell line, expresses higher levels of p-S6K1 than radiosensitive cells, suggesting a possible correlation between p-S6K1 and radiation resistance. Consistently, the inhibition of mTOR using everolimus increased radio-sensitivity in the $CD44^{high}/CD24^{low}$ MCF-7 cells (32). In radio-sensitivity prognosis, p-S6K1expression levels may be a predictor of therapeutic response and may also be a potential target to increase radiation therapy sensitivity (32).

Micro-RNA-21 (miR-21) suppresses the functions of many tumor suppressor genes, such as tropomyosin 1 (TPM1) and PTEN, which are associated with proliferation, apoptosis and metastasis (34–36). In the research study by Anastov et al., T47D, a radioresistant breast cancer cell line, and MDA-MB-361, a radiosensitive breast cancer cell line, were studied in parallel, miR-21 was found to be significantly elevated in the T47D cells, suggesting miR-21 contributes to radioresistance of breast cancers. The study presented evidence that miR-21 knockdown improved radiation induced apoptosis and growth arrest in radiation resistant cells comparable to that of radiation sensitive cells (35). It is well accepted that the overexpression of the anti-apoptotic miR-21 can stimulate cell cycle progression in the G2/M checkpoint. However, it is not established that the correlation between miR-21 and G2/M checkpoint arrest promotes radiation resistance. Nevertheless, the inhibition of miR-21 may be a potential therapeutic target and its overexpression a possible prognosis indicator (35).

Long non-coding RNA (lncRNA) HOX Transcript Antisense RNA (HOTAIR) has been shown in several studies to participate in the promotion and metastasis of breast cancer (37, 38), and its single nucleotide polymorphism is a marker for breast cancer. HOTAIR is upregulated in breast cancer, links DNA damage and nuclear factor kappa B (NF-κB) signaling and takes part in p53 regulated DNA damage response. The link between HOTAIR and the p53 and NF-κB pathways correlate with the promotion of breast cancer and radiation resistance. HOTAIR binds with many miRNAs in various cancer types, causing an upregulation of the miRNA targets and deviations in signaling transduction. Braunstein et al. showed that binding lncRNA HOTAIR with miR-218 resulted in a phenotypical radiation-sensitive breast tumor. The research suggested that the inhibition of HOTAIR could be a novel target in breast cancer treatment (39).

## CANCER STEM CELLS

In recent decades, a tumor cell population with cancer stem cell (CSC) phenotype has accumulated attention for its role in resistance to treatments. These cells have the ability to self-renew and initiate subpopulations of differentiated progeny (40). Cancer stem cells have been identified in a variety of tumors, including brain cancers, breast cancers, prostate, and melanoma (41). This population of cancer cells has presented evidence of

resistance to radiation therapy and chemotherapy (42–44). Research has presented evidence that the hypoxic tumor microenvironment is ideal for CSC survival (45). Further research is needed to better understand the role of the CSC phenotype subpopulation, but this subpopulation may be a new target to increase radiation sensitivity in cancer therapy.

Lin28 is a stem cell marker that is associated with radiation resistance in breast cancer (46). Apoptotic proteins poly(ADP-ribose) polymerase (PARP), caspase-3, and caspase-9 have significantly lower cleavage levels, thus less activation, in Lin28 overexpressing cells (46). As such, it was suggested that the overexpression of Lin28 mediated radioresistance by inhibiting radiation-induced apoptosis. Additionally, it has been shown that the Let-7 miRNA is downregulated in association with upregulation of Lin28 (47); and when the stabilized cells are transfected with Let-7 miRNA precursor, radiation sensitivity is resumed (46). Lin28 regulates Let-7 by directly interacting with the precesors of Let-7 family members (48). This suggests that Lin28 and Let-7 could be used as predictive biomarkers of response to radiation therapy.

The stem cell marker $CD44^+/CD24^-$ is recognized primarily in triple-negative breast cancer (TNBC) stem cells (49). $CD44^+/CD24^-$ has been associated with breast cancer resistance to ionizing radiation. In a 2011 study, Yin et al. showed that BRCA1 and Ataxia-Telangiectasia Mutated Kinase (ATM) activity are increased in $CD44^+/CD24^-$ cells (42). As an initiating factor for homologous recombination (HR), ATM is essential for the repair of radiation-induced double-strand DNA breaks (27, 50). ATM, a Ser/Thr kinase itself, is activated by autophosphorylation during double-strand DNA breaks. In $CD44^+/CD24^-$ cell lines and the primary culture of patient breast cancer cells, elevation in both expression and phosphorylation of ATM were found. Inhibition of ATM increased radiation sensitivity of the isolated $CD44^+/CD24^-$ cell, which suggests that ATM is a potential target to improve radiation sensitivity in breast cancer therapy (42).

Many studies have verified the breast cancer stem cell line with the $CD44^+/CD24^-/ALDH^+$ marker, and recently the high expression of aldehyde dehydrogenase ($ALDH^+$) was associated to therapeutic resistance. Croker et al. reported on the roles of $ALDH^+/CD44^+$ in breast cancer, where $ALDH^+/CD44^+$ was associated with chemoresistance, radiation resistance, poor prognosis, and played a role in metastasis (51). Considering that these stem cells are more resistant to therapy and promote proliferation in tumors (52), they may be more prone to distant metastasis. Additionally, it has been shown that this subset of cells expressed higher levels of therapy resistance proteins, p-glycoprotein, GSTpi, and/or CHK1 (51). Consistently, inhibition of $ALDH^+$ using diethylaminobenzaldehyde (DEAB) or all trans retinoic acid (ATRA) resulted in significantly improved radiation sensitivity, suggesting ALDH could be a potential target for improving therapeutic results (51).

## CONCLUSION

As one of the most used methods to treat breast cancer, ionizing radiation in radiation therapy creates reactive oxygen species that cause cell damage and induce cell death. The hypoxic microenvironment of breast cancer cells promotes tumor cell proliferation, apoptosis resistance, metastasis, and resistance to radiation as well as other therapeutics. The overexpression and stabilization of the protein HIF-1α do not only result from low oxygen levels within the microenvironment, but also promote the advancement of hypoxia and facilitates tumor cell survival within the hypoxic microenvironment. The cancer cell's capacity to survive in a low oxygen environment presents a major challenge to effective radiation therapy. In addition, the adaptation to the hypoxic microenvironment also promotes additional alterations, including metabolic changes, mutations, signaling pathways, upregulation and downregulation of various cellular components. Many of these adaptations decrease radiation sensitivity.

Extensive studies have been performed to elucidate the hypoxic response mechanisms, anti-apoptotic pathways, and cascades that lead to resistance to radiation. This led to the discovery of promising therapeutic targets for drug development to sensitize tumors to radiations. Importantly, the presence of the radiosensitizing targets will be critical to predict the prognosis after radiaotherpy. To achieve these goals, a deeper understanding of the development of radiation resistance in breast cancers, especially for the subgroups, is needed to develop specified and personalized therapy.

## AUTHOR CONTRIBUTIONS

All authors listed have made a substantial, direct, and intellectual contribution to the work and approved it for publication.

## FUNDING

This publication was made possible by the Arkansas INBRE program, supported by a grant from the National Institute of General Medical Sciences, (NIGMS), P20 GM103429 from the National Institutes of Health.

## REFERENCES

1. Siegel RL, Miller KD, Jemal A. Cancer statistics, 2020. *CA Cancer J Clin* (2020) 70(1):7–30. doi: 10.3322/caac.21590
2. Hagemeister FB, Buzdar AU, Luna MA, Blumenschein GR. Causes of death in breast cancer a clinicopathologic study. *Cancer* (1980) 46(1):162–7. doi: 10.1002/1097-0142(19800701)46:1<162::AID-CNCR2820460127>3.0.CO;2-B
3. Cristofanilli M, Hayes DF, Budd GT, Ellis MJ, Stopeck A, Reuben JM, et al. Circulating tumor cells: A novel prognostic factor for newly diagnosed metastatic breast cancer. *J Clin Oncol* (2005) 23(7):1420–30. doi: 10.1200/JCO.2005.08.140
4. Hara T, Iwadate M, Tachibana K, Waguri S, Takenoshita S, Hamada N. Metastasis of breast cancer cells to the bone, lung, and lymph nodes promotes resistance to ionizing radiation Takamitsu. *Strahlentherapie Und Onkol* (2017) 193(10):848–55. doi: 10.1007/s00066-017-1165-2

5. Dance DR, Christofides S, Maidment M, Mclean I, Ng KH. Diagnostic Radiology Physics: A handbook for teachers and students. *Iaea* (2014) 710.
6. Truong T, Sun G, Doorly M, Wang JYJ, Schwartz MA. Modulation of DNA damage-induced apoptosis by cell adhesion is independently mediated by p53 and c-Abl. *Proc Natl Acad Sci U S A* (2003) 100(18):10281–6. doi: 10.1073/pnas.1635435100
7. King HW, Michael MZ, Gleadle JM. Hypoxic enhancement of exosome release by breast cancer cells. *BMC Cancer* (2012) 12:421. doi: 10.1186/1471-2407-12-421
8. Krishnamachary B, Penet MF, Nimmagadda S, Mironchik Y, Raman V, Solaiyappan M, et al. Hypoxia Regulates CD44 and Its Variant Isoforms through HIF-1α in Triple Negative Breast Cancer. *PloS One* (2012) 7(8):1–9. doi: 10.1371/journal.pone.0044078
9. Park JE, Tan HS, Datta A, Lai RC, Zhang H, Meng W, et al. Hypoxic tumor cell modulates its microenvironment to enhance angiogenic and metastatic potential by secretion of proteins and exosomes. *Mol Cell Proteomics* (2010) 9 (6):1085–99. doi: 10.1074/mcp.M900381-MCP200
10. Dales JP, Garcia S, Meunier-Carpentier S, Andrac-Meyer L, Haddad O, Lavaut MN, et al. Overexpression of hypoxia-inducible factor HIF-1α predicts early relapse in breast cancer: Retrospective study in a series of 745 patients. *Int J Cancer* (2005) 116(5):734–9. doi: 10.1002/ijc.20984
11. Brennan DJ, Jirstrom K, Kronblad Å, Millikan RC, Landberg G, Duffy MJ, et al. CA IX is an independent prognostic marker in premenopausal breast cancer patients with one to three positive lymph nodes and a putative marker of radiation resistance. *Clin Cancer Res* (2006) 12(21):6421–31. doi: 10.1158/1078-0432.CCR-06-0480
12. Jokilehto T, Rantanen K, Luukkaa M, Heikkinen P, Grenman R, Minn H, et al. Overexpression and nuclear translocation of hypoxia-inducible factor prolyl hydroxylase PHD2 in head and neck squamous cell carcinoma is associated with tumor aggressiveness. *Clin Cancer Res* (2006) 12(4):1080–7. doi: 10.1158/1078-0432.CCR-05-2022
13. Lee G, Won HS, Lee YM, Choi JW, Oh TI, Jang JH, et al. Oxidative Dimerization of PHD2 is Responsible for its Inactivation and Contributes to Metabolic Reprogramming via HIF-1α Activation. *Sci Rep* (2016) 6 (November 2015):1–12. doi: 10.1038/srep18928
14. Zheng X, Linke S, Dias JM, Zheng X, Gradin K, Wallis TP, et al. Interaction with factor inhibiting HIF-1 defines an additional mode of cross-coupling between the Notch and hypoxia signaling pathways. *Proc Natl Acad Sci USA* (2008) 105(9):3368–73. doi: 10.1073/pnas.0711591105
15. Blancher C, Moore JW, Talks KL, Houlbrook S, Harris AL. Relationship of hypoxia-inducible factor (HIF)-1α and HIF-2α expression to vascular endothelial growth factor induction and hypoxia survival in human breast cancer cell lines. *Cancer Res* (2000) 60(24):7106–13.
16. Kim JW, Tchernyshyov I, Semenza GL, Dang CV. HIF-1-mediated expression of pyruvate dehydrogenase kinase: A metabolic switch required for cellular adaptation to hypoxia. *Cell Metab* (2006) 3(3):177–85. doi: 10.1016/j.cmet.2006.02.002
17. Jiang BH, Agani F, Passaniti A, Semenza GL. V-SRC induces expression of hypoxia-inducible factor 1 (HIF-1) and transcription of genes encoding vascular endothelial growth factor and enolase 1: Involvement of HIF-1 in tumor progression. *Cancer Res* (1997) 57(23):5328–35.
18. Semenza GL. Regulation of metabolism by hypoxia-inducible factor 1. *Cold Spring Harb Symp Quant Biol* (2011) 76:347–53. doi: 10.1101/sqb.2011.76.010678
19. Arany Z, Huang LE, Eckner R, Bhattacharya S, Jiang C, Goldberg MA, et al. An essential role for p300/CBP in the cellular response to hypoxia. *Proc Natl Acad Sci USA* (1996) 93(23):12969–73. doi: 10.1073/pnas.93.23.12969
20. Xenaki G, Ontikatze T, Rajendran R, Stratford IJ, Dive C, Krstic-Demonacos M, et al. PCAF is an HIF-1α cofactor that regulates p53 transcriptional activity in hypoxia. *Oncogene* (2008) 27(44):5785–96. doi: 10.1038/onc.2008.192
21. Zhang X, Sai B, Wang F, Wang L, Wang Y, Zheng L, et al. Hypoxic BMSC-derived exosomal miRNAs promote metastasis of lung cancer cells via STAT3-induced EMT. *Mol Cancer* (2019) 18(1):1–15. doi: 10.1186/s12943-019-0959-5
22. Jabbari N, Nawaz M, Rezaie J. Ionizing radiation increases the activity of exosomal secretory pathway in MCF-7 human breast cancer cells: A possible way to communicate resistance against radiotherapy. *Int J Mol Sci* (2019) 20 (15):3649. doi: 10.3390/ijms20153649
23. Ruivo CF, Melo SA. The emerging role of exosomes in cancer progression and their potential as therapy targets. In: Recent Trends in Cancer Biology: Spotlight on Signaling Cascades and MicroRNAs: Cell Signaling Pathways and MicroRNAs in Cancer Biology. (2018) 27–45. doi: 10.1007/978-3-319-71553-7_3
24. Boelens MC, Wu TJ, Nabet BY, Xu B, Qiu Y, Yoon T, et al. Exosome transfer from stromal to breast cancer cells regulates therapy resistance pathways. *Cell* (2014) 159(3):499–513. doi: 10.1016/j.cell.2014.09.051
25. Kim KW, Myers CJ, Jung DK, Lu B. NVP-BEZ-235 enhances radiosensitization via blockade of the PI3k/mTOR pathway in cisplatin-resistant non-small cell lung carcinoma. *Genes Cancer* (2014) 5(7–8):293–302. doi: 10.18632/genesandcancer.27
26. Steelman LS, Navolanic P, Chappell WH, Abrams SL, Wong EWT, Martelli AM, et al. Involvement of Akt and mTOR in chemotherapeutic and hormonal-based drug resistance and response to radiation in breast cancer cells. *Cell Cycle* (2011) 10(17):3003–15. doi: 10.4161/cc.10.17.17119
27. Ahmed KM, Dong S, Fan M, Li JJ. Nuclear factor-κB p65 inhibits mitogen-activated protein kinase signaling pathway in radioresistant breast cancer cells. *Mol Cancer Res* (2006) 4(12):945–55. doi: 10.1158/1541-7786.MCR-06-0291
28. Söderlund K, Pérez-Tenorio G, Stål O. Activation of the phosphatidylinositol 3-kinase/Akt pathway prevents radiation-induced apoptosis in breast cancer cells. *Int J Oncol* (2005) 26(1):25–32. doi: 10.3892/ijo.26.1.25
29. Kirkegaard T, Witton CJ, McGlynn LM, Tovey SM, Dunne B, Lyon A, et al. AKT activation predicts outcome in breast cancer patients treated with tamoxifen. *J Pathol* (2005) 207(2):139–46. doi: 10.1002/path.1829
30. Widmann C, Gibson S, Johnson GL. Caspase-dependent cleavage of signaling proteins during apoptosis. A turn-off mechanism for anti-apoptotic signals. *J Biol Chem* (1998) 273(12):7141–7. doi: 10.1074/jbc.273.12.7141
31. Criswell T, Beman M, Araki S, Leskov K, Cataldo E, Mayo LD, et al. Delayed activation of insulin-like growth factor-1 receptor/Src/ MAPK/Egr-1 signaling regulates clusterin expression, a pro-survival factor. *J Biol Chem* (2005) 280 (14):14212–21. doi: 10.1074/jbc.M412569200
32. Choi J, Yoon YN, Kim N, Park CS, Seol H, Park IC, et al. Predicting Radiation Resistance in Breast Cancer with Expression Status of Phosphorylated S6K1. *Sci Rep* (2020) 10(1)1–8. doi: 10.1038/s41598-020-57496-8
33. Lin HJ, Hsieh FC, Song H, Lin J. Elevated phosphorylation and activation of PDK-1/AKT pathway in human breast cancer. *Br J Cancer* (2005) 93 (12):1372–81. doi: 10.1038/sj.bjc.6602862
34. Iorio MV, Ferracin M, Liu CG, Veronese A, Spizzo R, Sabbioni S, et al. MicroRNA gene expression deregulation in human breast cancer. *Cancer Res* (2005) 65(16):7065–70. doi: 10.1158/0008-5472.CAN-05-1783
35. Anastasov N, Höfig I, Vasconcellos IG, Rappl K, Braselmann H, Ludyga N, et al. Radiation resistance due to high expression of miR-21 and G2/M checkpoint arrest in breast cancer cells. *Radiat Oncol* (2012) 7(1):1–12. doi: 10.1186/1748-717X-7-206
36. Ma X, Choudhury SN, Hua X, Dai Z, Li Y. Interaction of the oncogenic miR-21 microRNA and the p53 tumor suppressor pathway. *Carcinogenesis* (2013) 34(6):1216–23. doi: 10.1093/carcin/bgt044
37. Sørensen KP, Thomassen M, Tan Q, Bak M, Cold S, Burton M, et al. Long non-coding RNA HOTAIR is an independent prognostic marker of metastasis in estrogen receptor-positive primary breast cancer. *Breast Cancer Res Treat* (2013) 142(3):529–36. doi: 10.1007/s10549-013-2776-7
38. Özeş AR, Wang Y, Zong X, Fang F, Pilrose J, Nephew KP. Therapeutic targeting using tumor specific peptides inhibits long non-coding RNA HOTAIR activity in ovarian and breast cancer. *Sci Rep* (2017) 7(1):1–11. doi: 10.1038/s41598-017-00966-3
39. Hu X, Ding D, Zhang J, Cui J. Knockdown of lncRNA HOTAIR sensitizes breast cancer cells to ionizing radiation through activating miR-218. *Biosci Rep* (2019) 29(4):1–9. doi: 10.1042/BSR20181038
40. Lagadec C, Vlashi E, Della Donna L, Meng YH, Dekmezian C, Kim K, et al. Survival and self-renewing capacity of breast cancer initiating cells during fractionated radiation treatment. *Breast Cancer Res* (2010) 12(1):1–13. doi: 10.1186/bcr2479
41. Phillips TM, McBride WH, Pajonk F. The response of CD24-/low/CD44+ breast cancer-initiating cells to radiation. *J Natl Cancer Inst* (2006) 98 (24):1777–85. doi: 10.1093/jnci/djj495
42. Yin H, Glass J. The phenotypic radiation resistance of CD44 +/CD24 -or low breast cancer cells is mediated through the enhanced activation of ATM signaling. *PloS One* (2011) 6(9):1–11. doi: 10.1371/journal.pone.0024080

43. Griñán-Lisón C, Olivares-Urbano MA, Jiménez G, López-Ruiz E, del Val C, Morata-Tarifa C, et al. miRNAs as radio-response biomarkers for breast cancer stem cells. *Mol Oncol* (2020) 14(3):556–70. doi: 10.1002/1878-0261.12635
44. Qi XS, Pajonk F, McCloskey S, Low DA, Kupelian P, Steinberg M, et al. Radioresistance of the breast tumor is highly correlated to its level of cancer stem cell and its clinical implication for breast irradiation. *Radiother Oncol* (2017) 124(3):455–61. doi: 10.1016/j.radonc.2017.08.019
45. Lock FE, McDonald PC, Lou Y, Serrano I, Chafe SC, Ostlund C, et al. Targeting carbonic anhydrase IX depletes breast cancer stem cells within the hypoxic niche. *Oncogene* (2013) 32(44):5210–9. doi: 10.1038/onc.2012.550
46. Wang L, Yuan C, Lv K, Xie S, Fu P, Liu X, et al. Lin28 Mediates Radiation Resistance of Breast Cancer Cells via Regulation of Caspase, H2A.X and Let-7 Signaling. *PloS One* (2013) 8(6):6–11. doi: 10.1371/journal.pone.0067373
47. Wang L, Wang Y-X, Zhang D-Z, Fang X-J, Sun P-S, Xue H-C. Let-7a mimic attenuates CCL18 induced breast cancer cell metastasis through Lin 28 pathway. *BioMed Pharmacother* (2016) 78:301–7. doi: 10.1016/j.biopha.2016.01.028
48. Nam Y, Chen C, Gregory RI, Chou JJ, Sliz P. Molecular basis for interaction of let-7 MicroRNAs with Lin28. *Cell* (2011) 147(5):1080–91. doi: 10.1016/j.cell.2011.10.020
49. Ma F, Li H, Wang H, Shi X, Fan Y, Ding X, et al. Enriched CD44+/CD24- population drives the aggressive phenotypes presented in triple-negative breast cancer (TNBC). *Cancer Lett* (2014) 353(2):153–9. doi: 10.1016/j.canlet.2014.06.022
50. Burma S, Chen BP, Murphy M, Kurimasa A, Chen DJ. ATM Phosphorylates Histone H2AX in Response to DNA Double-strand Breaks. *J Biol Chem* (2001) 276(45):42462–7. doi: 10.1074/jbc.C100466200
51. Croker AK, Allan AL. Inhibition of aldehyde dehydrogenase (ALDH) activity reduces chemotherapy and radiation resistance of stem-like ALDH hiCD44 + human breast cancer cells. *Breast Cancer Res Treat* (2012) 133(1):75–87. doi: 10.1007/s10549-011-1692-y
52. Qiu Y, Pu T, Guo P, Wei B, Zhang Z, Zhang H, et al. ALDH+/CD44+ cells in breast cancer are associated with worse prognosis and poor clinical outcome. *Exp Mol Pathol* (2016) 100(1):145–50. doi: 10.1016/j.yexmp.2015.11.032

**Conflict of Interest:** The authors declare that the research was conducted in the absence of any commercial or financial relationships that could be construed as a potential conflict of interest.

frontiers in Oncology

BRIEF RESEARCH REPORT
published: 22 February 2021
doi: 10.3389/fonc.2020.624954

# Establishment and Characterization of an Irinotecan-Resistant Human Colon Cancer Cell Line

*Zhuo-Xun Wu[1], Yuqi Yang[1], Leli Zeng[1,2], Harsh Patel[1], Letao Bo[1], Lusheng Lin[3] and Zhe-Sheng Chen[1]**

[1] Department of Pharmaceutical Sciences, College of Pharmacy and Health Sciences, St. John's University, New York, NY, United States, [2] Precision Medicine Center, The Seventh Affiliated Hospital, Sun Yat-Sen University, Shenzhen, China, [3] Cell Research Center, Shenzhen Bolun Institute of Biotechnology, Shenzhen, China

Colorectal cancer (CRC) is a leading cause of cancer-related deaths worldwide. Irinotecan is widely used as a chemotherapeutic drug to treat CRC. However, the mechanisms of acquired resistance to irinotecan in CRC remain inconclusive. In the present study, we established a novel irinotecan-resistant human colon cell line to investigate the underlying mechanism(s) of irinotecan resistance, particularly the overexpression of ABC transporters. The irinotecan-resistant S1-IR20 cell line was established by exposing irinotecan to human S1 colon cancer cells. MTT cytotoxicity assay was carried out to determine the drug resistance profile of S1-IR20 cells. The drug-resistant cells showed about 47-fold resistance to irinotecan and cross-resistance to ABCG2 substrates in comparison with S1 cells. By Western blot analysis, S1-IR20 cells showed significant increase of ABCG2, but not ABCB1 or ABCC1 in protein expression level as compared to that of parental S1 cells. The immunofluorescence assay showed that the overexpressed ABCG2 transporter is localized on the cell membrane of S1-IR20 cells, suggesting an active efflux function of the ABCG2 transporter. This finding was further confirmed by reversal studies that inhibiting efflux function of ABCG2 was able to completely abolish drug resistance to irinotecan as well as other ABCG2 substrates in S1-IR20 cells. In conclusion, our work established an *in vitro* model of irinotecan resistance in CRC and suggested ABCG2 overexpression as one of the underlying mechanisms of acquired resistance to irinotecan. This novel resistant cell line may enable future studies to overcome drug resistance *in vitro* and improve CRC treatment *in vivo*.

**Keywords: chemotherapy, irinotecan, colorectal cancer, multidrug resistance, ABCG2**

OPEN ACCESS

***Edited by:***
*Xu Zhang,*
*Jiangsu University, China*

***Reviewed by:***
*Kaijian Hou,*
*Shantou University, China*
*Ru Li,*
*Stony Brook University, United States*

***Correspondence:**
*Zhe-Sheng Chen*
*chenz@stjohns.edu*

***Specialty section:***
*This article was submitted to Pharmacology of Anti-Cancer Drugs, a section of the journal Frontiers in Oncology*

***Received:*** *01 November 2020*
***Accepted:*** *21 December 2020*
***Published:*** *22 February 2021*

***Citation:***
*Wu Z-X, Yang Y, Zeng L, Patel H, Bo L, Lin L and Chen Z-S (2021) Establishment and Characterization of an Irinotecan-Resistant Human Colon Cancer Cell Line. Front. Oncol. 10:624954. doi: 10.3389/fonc.2020.624954*

## INTRODUCTION

Colorectal cancer (CRC), one of the most common type of malignant tumors, is the third leading cause of cancer-related deaths in the United States and fourth most deadly cancer worldwide (1). Currently, the mainstream therapeutic approaches to treat metastatic CRC are surgery, chemotherapy, irradiation, and targeted therapy (2). The first-line chemotherapy strategy is usually a combination of 5-fluorouracil, leucovorin, and either irinotecan or oxaliplatin (3).

The combination chemotherapy regimens have been shown to achieve greater efficacy as compared to single agent treatment (4). Irinotecan, derived from camptothecin, is a broad-spectrum chemotherapeutic agent targeting DNA topoisomerase I (topo I) (5). Topoisomerases are nuclear enzymes that are actively involved in the control of DNA topology during the replication and translation processes (6). It is well established that topo I levels are upregulated in some cancer types, and inhibiting topo I activity can affect the proliferation of tumor cells (7). Since its approval in 1996 by the United States Food and Drug Administration, irinotecan has been the first-line option in treating CRC, gastrointestinal cancers, lung cancer, and a variety of other malignancies (8). In the first-line treatment of mCRC, the combination of irinotecan with bolus or 5-fluorouracil/leucovorin can significantly increase patient survival compared with 5-fluorouracil/leucovorin alone, with an acceptable toxic profile (9). Furthermore, irinotecan-based combinations can be extremely diversified, including combination with kinase inhibitors and cell-cycle checkpoint inhibitors (10). Currently, new derivatives of irinotecan are still under development to improve anticancer efficacy and reduce side effects. After two decades of clinical usage, irinotecan remains a must-have drug in CRC treatment (11). However, one major obstacle of chemotherapy is inevitably the development of drug resistance. To date, the mechanism of irinotecan resistance is still inconclusive and requires further investigation. Studies have suggested several possible mechanisms that may lead to irinotecan resistance, including: 1) reduced topo I expression level, 2) mutation in the metabolizing enzyme or structure of topo I, 3) activation of NF-κB which suppresses the cell apoptosis, and 4) reduced intracellular drug accumulation by active drug efflux (12).

Several ATP-binding cassette (ABC) transporters are well-established mediators of multidrug resistance (MDR). Specifically, ABCB1, ABCG2, and ABCC1 are able to confer cancer cell MDR to a wide range of anticancer drugs with different chemical structures and mechanisms of action. These ABC transporters, by utilizing energy derived from ATP hydrolysis, extrude substrates from the cytoplasm to the extracellular matrix, resulting in decreased sensitivity of cancer cells to substrate drugs. *In vitro* model has been an ideal method to delineate the potential mechanisms contributing to drug resistance. The ABCB1 and ABCG2 transporters were first discovered from cells resistant to colchicine and mitoxantrone, respectively (13). The docetaxel-resistant cell lines were shown to overexpress ABCB1 transporter (14), and the arsenic trioxide-resistant cell line was shown to overexpress ABCB6 transporter (15). In the past few decades, a broad array of chemotherapeutic drugs as well as tyrosine kinase inhibitors (TKI) were identified as substrates of ABC transporters. The chemotherapeutic drugs paclitaxel, vincristine, and colchicine are substrates of ABCB1, while mitoxantrone, topotecan, and etoposide are substrates of ABCG2 (13, 16). In addition, TKIs such as imatinib (17), gefitinib (18), tivantinib (19), pevonedistat (20) are reported to be substrates of ABC transporters. Studies have resulted in mixed conclusions surrounding the role ABCG2 plays in mediating irinotecan resistance (21–24). Both irinotecan and its active metabolite SN-38 were reported to be substrates of ABCG2 (25). One exploratory analysis study was performed and suggested that the response to irinotecan is highly related to tumor *ABCG2* mRNA expression (26). In a retrospective study, it was found that ABCG2 level serves a predictive role for SN-38 resistance (27). In contrast, studies also suggested that ABCG2 was not a predictor of progression-free survival (PFS) in patients receiving irinotecan treatment and no significant correlation was found between ABCG2 level and treatment response (28, 29). Currently, the investigation of irinotecan and ABCG2 were mostly conducted by correlating ABCG2 expression level with response to irinotecan. However, whether irinotecan treatment can lead to ABC transporters overexpression remain inconclusive and should be further explored.

The present study aimed to facilitate the understanding of resistance mechanism of irinotecan in CRC. To achieve this, a colon cancer cell line resistant to irinotecan was established. It was found that, unlike ABCB1 or ABCC1, ABCG2 was overexpressed in irinotecan-resistant S1-IR20 cells. Furthermore, ABCG2 overexpression in S1-IR20 cells also conferred high levels of cross resistance to other ABCG2 substrates. Inhibiting the efflux function of ABCG2 significantly decreased the drug resistance to ABCG2 substrate drugs in S1-IR20 cells. Our results suggested that overexpression of ABCG2 is a key mediator of acquired resistance to irinotecan in CRC; thus, ABCG2 level may be monitored during irinotecan treatment.

# MATERIALS AND METHODS

## Chemicals

Chemicals were obtained from Sigma Chemical Co (St. Louis, MO) unless stated otherwise. Chemotherapeutic drugs used in this study were irinotecan, SN-38, mitoxantrone, topotecan, doxorubicin, colchicine, paclitaxel, and oxaliplatin. Ko143 was purchased from Enzo Life Sciences (Farmingdale, NY). Venetoclax was requested from Chemietek (Indianapolis, IN). Stock solutions (10 mM) were reconstituted in DMSO for all the drugs except oxaliplatin, which was dissolved in dimethylformamide.

## Development of Drug-Resistant S1-IR20 Cell Line

Human colon cancer S1 cell line was used as the parental cell line to establish the irinotecan-resistant subline. The parental S1 cells were initially cultured in medium with 0.5 μM of irinotecan for 48 h. Subsequently, the surviving cells were cultured in drug-free medium for 7 days and subjected to the next cycle of drug treatment. After 3–5 cycles of drug treatment, the cells were cultured with increased concentrations of irinotecan, a 50% increase each time. Finally, the resultant cell lines that grew exponentially in the presence of 20 μM of irinotecan were designated as drug-resistant subline and named S1-IR20. Established S1-IR20 cells were maintained in drug-free medium for 14 days before experiment.

## Cell Lines and Cell Culture

The human epidermoid carcinoma cell line KB-3-1 and its ABCB1-overexpressing subline KB-C2, ABCC1-overexpressing subline KB-CV60, human NSCLC NCI-H460 and its ABCG2-overexpressing subline NCI-H460/MX20, and human colon cancer cell line S1 and its irinotecan-resistant subline S1-IR20 were maintained in DMEM with 10% FBS. In addition, KB-C2 cells were maintained in the presence of 2 μg/ml of colchicine (30). NCI-H460/MX20 cells were maintained in the presence of 20 nM of mitoxantrone (31). KB-CV60 cells were maintained in the presence of 1 μg/ml of cepharanthine and 60 ng/ml of vincristine (32). All cell lines were maintained in a humid incubator (37°C, 5% $CO_2$) and subcultured at 80% confluency.

## Evaluation of S1-IR20 Drug Resistance Profile by MTT Assay

The MTT assay was used to determine the cytotoxicity of chemotherapeutic drugs as previously described (33). Cell viability curves were plotted as percentages relative to untreated controls. The half maximal inhibitory concentrations ($IC_{50}$) were calculated from the curves using GraphPad Prism 7.

## Western Blotting

Protein extraction and visualization were performed as previously described (19). The ABCG2-overexpressing NCI-H460/MX20, ABCB1-overexpressing KB-C2, and ABCC1-overexpressing KB-CV60 protein samples were used as positive control of ABCG2, ABCB1, and ABCC1, respectively. Immunoblotting was carried out with the following antibodies: anti-ABCG2, anti-ABCB1, anti-ABCC1, anti-topo I and anti-GAPDH (catalog number MAB4146, MA1-26528, MA5-16079, 44321M, MA5-15738, Thermo Fisher Scientific Inc., Waltham, MA) and anti-rabbit or anti-mouse secondary HRP-linked antibodies (catalog number 7074S and 7076S, 1:1,000 dilution, Cell Signaling Technology Inc., Danvers, MA). GAPDH was used as a loading control. The protein bands were visualized using an enhanced ECL Kit (Thermo Fisher Scientific Inc., Waltham, MA).

## Immunofluorescence Assay

The localization of ABCG2 transporter was visualized by immunofluorescent microscopy. Both S1 and S1-IR20 cells were seeded in 24-well plates ($1 \times 10^6$ cells per well). The immunofluorescence experiment was carried out as previously described (34). The antibodies used in this experiment were anti-ABCG2 (1:1,000, Thermo Fisher Scientific Inc., Waltham, MA) and Alexa Fluor 488 conjugated anti-mouse IgG antibody (1:1,000, Thermo Fisher Scientific Inc., Waltham, MA). The nuclei were counterstained with DAPI solution. The immunoreactivity was visualized using a Nikon TE-2000S fluorescence microscope (Nikon Instruments Inc., Melville, NY).

## Intracellular Accumulation of Irinotecan Determined by HPLC Assay

The HPLC assay was carried out with modified protocol as previously described (35, 36). Briefly, both S1 and S1-IR20 cells were seeded in six-well plates ($1 \times 10^6$ cells per well) and incubated overnight. On the following day, cells were pre-treated with or without Ko143 for 2 h. Subsequently, cells were further incubated with irinotecan in the presence or absence of Ko143 for another 2 h. At the end, cells were harvested and subjected to HPLC analysis.

## Statistical Analysis

All data are presented as the mean ± standard deviation from three independent experiments. Comparisons of differences in the quantitative data among groups were performed using one-way ANOVA. $P < 0.05$ was considered statistically significant.

# RESULTS

## Establishment of Irinotecan-Resistant Colon Cancer Cell Line and Its Drug Resistance Profile

To obtain the irinotecan-resistant subline, the colon cancer cell line S1 was exposed to increasing concentrations of irinotecan. The resistant subline S1-IR20 was obtained from the population growing in 20 μM of irinotecan. MTT assay was carried out to evaluate the drug resistance profile of S1-IR20 cells. Drug sensitivity of both parental S1 cells and drug-resistant S1-IR20 cells toward a panel of chemotherapeutic drugs is presented in **Table 1**. S1-IR20 showed no significant resistance to ABCB1 substrate drugs paclitaxel ($IC_{50}$ =

**TABLE 1** | The cytotoxicity of chemotherapeutic drugs in S1 and S1-IR20 cell lines.

| Drugs | Resistance mechanism | $IC_{50}$ value ± SD[a] (μM) | | Resistance-fold[b] |
|---|---|---|---|---|
| | | S1 | S1-IR20 | |
| **Irinotecan** | ABCG2 | 0.668 ± 0.157 | 31.78 ± 4.726 | 47.57* |
| **SN-38** | ABCG2 | 0.479 ± 0.039 | 22.60 ± 1.177 | 47.18* |
| **Topotecan** | ABCG2 | 0.679 ± 0.073 | 27.88 ± 3.087 | 41.06* |
| **Mitoxantrone** | ABCG2 | 0.070 ± 0.023 | 5.128 ± 1.126 | 37.14* |
| **Doxorubicin** | ABCG2, ABCB1 | 0.329 ± 0.054 | 5.955 ± 1.146 | 18.10* |
| **Oxaliplatin** | Non-ABC related | 13.62 ± 2.228 | 12.61 ± 1.262 | 0.93 |
| **Paclitaxel** | ABCB1, ABCC10 | 0.459 ± 0.084 | 0.624 ± 0.158 | 1.35 |
| **Colchicine** | ABCB1 | 0.277 ± 0.041 | 0.321 ± 0.028 | 1.16 |

[a] *$IC_{50}$ values are represented as mean ± SD of at least three independent experiments performed in triplicate.*
[b] *Resistance fold was calculated by dividing the $IC_{50}$ values of the resistant S1-IR20 cells by the $IC_{50}$ of parental S1 cells.*
**P < 0.05 versus the control group.*

0.459 and 0.624 μM for S1 and S1-IR20 lines, respectively), colchicine ($IC_{50}$ = 0.227 and 0.321 μM, respectively), or non-substrate drug oxaliplatin ($IC_{50}$ = 13.62 and 12.61 μM, respectively). In contrast, the resistant cells exhibited high resistance to irinotecan compared to the parental cells ($IC_{50}$ = 0.668 and 31.78 μM for S1 and S1-IR20 lines, respectively). The S1-IR20 cells also showed cross-resistance to SN-38 (47.18-fold), mitoxantrone (37.14-fold), topotecan (41.06-fold), and doxorubicin (18.10-fold) as compared to the parental cells. Therefore, the MTT results suggested that irinotecan-selected S1-IR20 cells may harbor the MDR phenotype.

## Western Blot Analysis

Since some ABC transporters have been well established to mediate MDR to a broad range of chemotherapeutic drugs, the expression level of ABCB1, ABCC1, and ABCG2 was evaluated by Western blotting (**Figure 1**). ABCG2 was overexpressed in S1-IR20 cells compared to the parental S1 cells, and the expression level was similar to the ABCG2-overexpressing NCI-H460/MX20 cells (**Figure 1A**). In contrast, both parental S1 and drug-resistant cells displayed no detectable levels of ABCB1 or ABCC1 as shown in **Figures 1B, C**. Since irinotecan's anticancer activity is by targeting topo I, we assessed the expression level of topo I in S1 and S1-IR20 cells. As shown in **Figure 1D**, topo I was expressed at the same level in both parental and resistant cells. Therefore, the high resistance to irinotecan as well as to mitoxantrone, topotecan, and doxorubicin in S1-IR20 cells may be associated with the overexpression of ABCG2.

## Immunofluorescence Assay

As a membrane transporter, ABCG2 requires membrane localization to exert its drug efflux function. Therefore, immunofluorescence assay was performed to confirm the overexpression of ABCG2 and visualize its localization in S1-IR20 cells (**Figure 2A**). In parental S1 cells, no detectable green fluorescence was observed, as S1 cells do not overexpress ABCG2. In contrast, strong green fluorescence was observed on the cell membrane of S1-IR20 cells, suggesting that the overexpressed ABCG2 transporter is localized on the cell membrane.

## Intracellular Accumulation of Irinotecan in S1 and S1-IR20 Cells

To evaluate the efflux activity of the overexpressed ABCG2 transporter, we measured the intracellular accumulation of

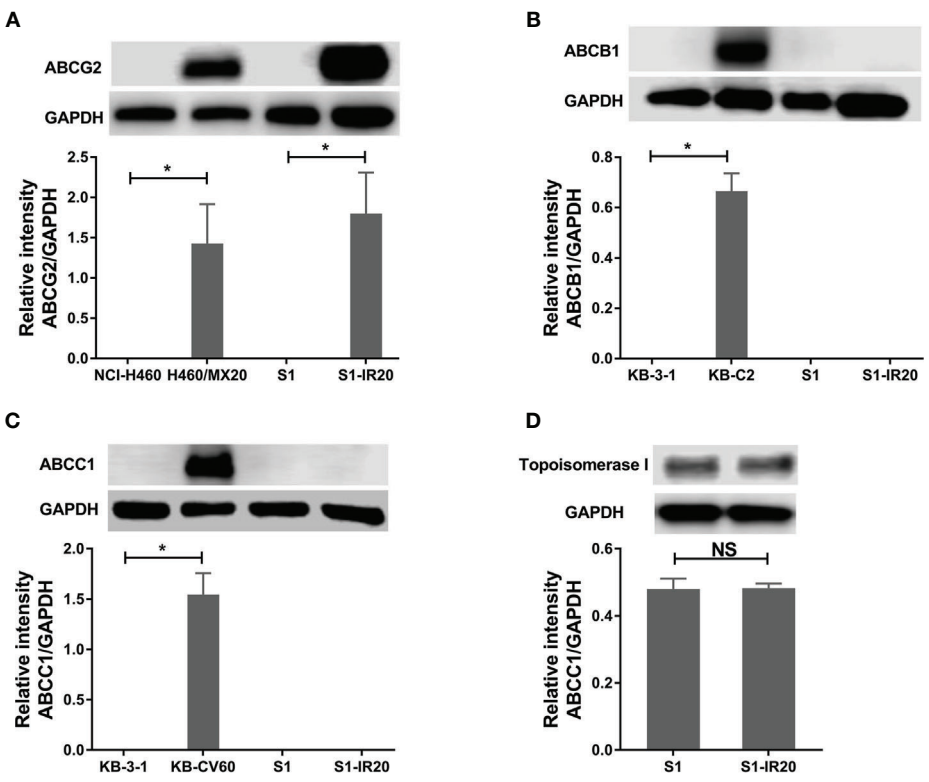


**FIGURE 1** | Protein expression profile of S1 and S1-IR20 cells. **(A)** The expression level of ABCG2 in S1 and S1-IR20 cells. The parental NCI-H460 and its ABCG2-overexpressing subline NCI-H460/MX20 were used as negative and positive control of ABCG2, respectively. **(B)** The expression level of ABCB1 in S1 and S1-IR20 cells. The parental KB-3-1 and its ABCB1-overexpressing subline KB-C2 were used as negative and positive control of ABCB1, respectively. **(C)** The expression level of ABCC1 in S1 and S1-IR20 cells. The parental KB-3-1 and its ABCC1-overexpressing subline KB-CV60 were used as negative and positive control of ABCC1, respectively. **(D)** The expression level of topoisomerase I in S1 and S1-IR20 cells. Data are expressed as mean ± SD derived from three independent experiments. *$p < 0.05$ *versus* the corresponding parental cells. NS, no significant.

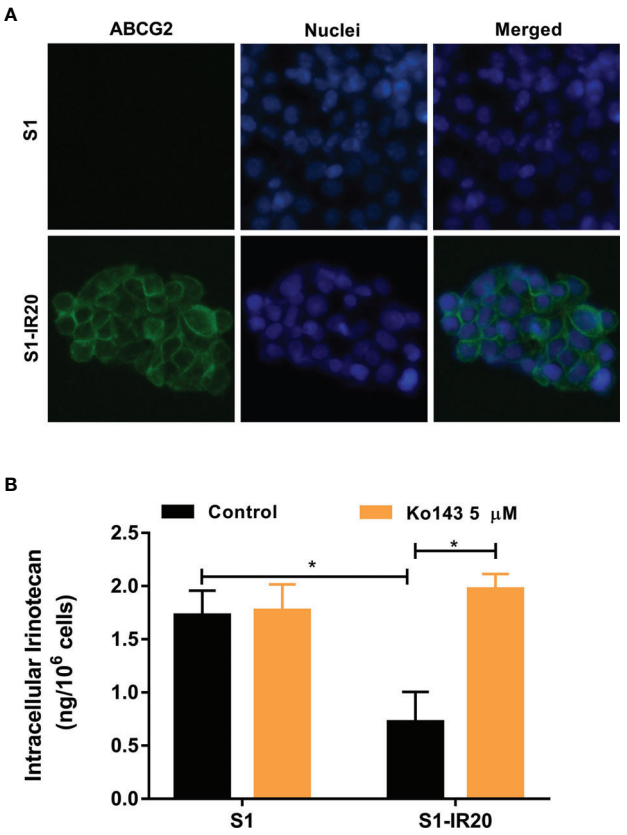


**FIGURE 2** | The localization of ABCG2 in S1-IR20 cells and intracellular accumulation of irinotecan in S1 and S1-IR20 cells. **(A)** Cellular membrane localization of the ABCG2 transporter in S1 and S1-IR20 cells. **(B)** The intracellular accumulation of irinotecan was determined in S1 and S1-IR20 cells *via* HPLC assay. Data are expressed as mean ± SD derived from three independent experiments. *$p < 0.05$ *versus* the control groups.

irinotecan in parental S1 and resistant S1-IR20 cells. If irinotecan is exported by the efflux function of the ABCG2 transporter, the intracellular accumulation will be lower in the drug-resistant cells than in the parental cells. As shown in **Figure 2B**, the S1-IR20 cells demonstrated a marked decrease of intracellular accumulation of irinotecan, which is 60% lower than that in the parental S1 cells. Furthermore, the intracellular accumulation of irinotecan in S1-IR20 cells was restored to the same level as S1 cells with the co-treatment of ABCG2 inhibitor Ko143.

## Drug Resistance Phenotype of S1-IR20 Cells Is Abolished by ABCG2 Inhibitor

To confirm that overexpression of ABCG2 is the major factor contributing to the resistance phenotype of S1-IR20 cells, we performed ABCG2-inhibition experiments using the MTT assay. The selective ABCG2 inhibitor Ko143 was used to inhibit the efflux function of ABCG2. As shown in **Figure 3**, resistance to irinotecan as well as to other ABCG2 substrate drugs was abolished by Ko143 in S1-IR20 cells, indicated by the overlapped cell viability curves with the parental cells. In the parental cells, the cell viability curves showed no significant difference in the presence or absence of Ko143. Notably, the cytotoxicity of non-substrate drug oxaliplatin was not altered by Ko143 in both parental and resistant cells. Therefore, these results further confirmed that ABCG2 is the major mediator of drug resistance in S1-IR20 cells. To determine whether S1-IR cells overexpress wild-type or mutant-type ABCG2, we performed reversal studies using venetoclax, an inhibitor of wild-type ABCG2. In S1-IR cells, venetoclax showed no effect to the cytotoxicity of mitoxantrone or irinotecan, suggesting that S1-IR cells may overexpress mutant-type ABCG2.

# DISCUSSION

Chemotherapy is the mainstream strategy for the treatment of CRC, and irinotecan is commonly used as part of the treatment strategies in treating CRC (37). However, chemotherapy inevitably leads to drug resistance, which decreases the anticancer efficacy of chemotherapeutic agents. Furthermore, chemotherapy resistance is often associated with MDR (38). Hence, great effort has been devoted to exploring the mechanisms of MDR in cancer, mostly by establishing drug-selected, acquired drug-resistant cell lines (30, 31). By studying the parental drug-sensitive cells to the drug-resistant cells by molecular biology and cellular methods, several MDR-associated molecules have been revealed (39). Numerous studies have suggested that ABCB1, ABCG2, and ABCC1 are key mediators of MDR through their drug efflux activity (40). In particular, ABCG2 has been reported to impact the pharmacokinetics of irinotecan (41). In contrast, the role of ABCG2 in predicting clinical response of or resistance to irinotecan in CRC is uncertain (22). To date, there are few studies describing the drug resistance mechanisms, e.g., overexpression of efflux pumps in irinotecan-selected resistant human CRC cell line (42, 43). In addition, whether irinotecan treatment will cause ABC transporter overexpression and lead to MDR is unknown. Previous study has established a mitoxantrone-selected drug-resistant S1-M1-80 subline from human S1 colon cancer cell line and suggested ABCG2 overexpression as the major resistance mechanism in the resistant subline (44). However, since mitoxantrone is not mainly used for CRC treatment, establishing an irinotecan-resistant subline would be more suitable to reveal the underlying drug resistance mechanisms and develop effective strategies to overcome the drug resistance. Although *in vivo* drug resistance mechanisms are more complicated than *in vitro*, investigating such *in vitro* drug resistance mechanisms can firstly provide strategies to circumvent or overcome acquired drug resistance in CRC.

In the present study, we established the irinotecan-resistant human colon cancer cell line (S1-IR20) through *in vitro* selection after exposing parental S1 human colon cancer cells to stepwise increasing concentrations of irinotecan. The characterization of the resistant subline S1-IR20 was performed by comparing it to the parental S1 cells. MTT assay was performed to evaluate the cytotoxic effect of irinotecan in parental S1 cells and drug-resistant S1-IR20 cells. This resistant subline exhibited over 40-

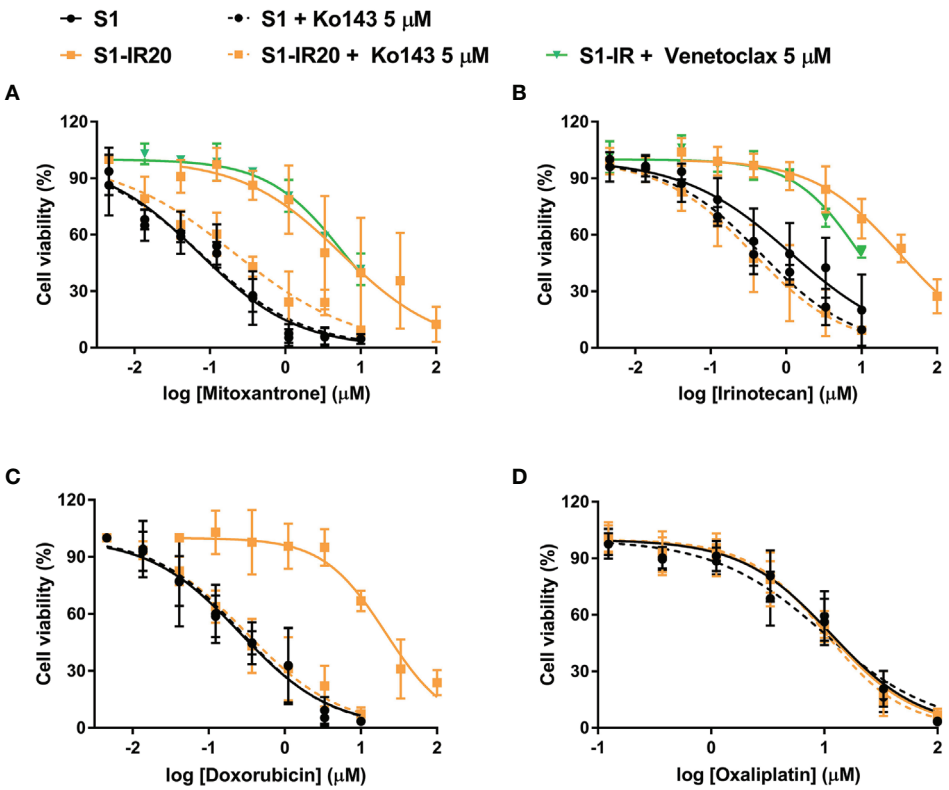


**FIGURE 3** | Reversal of ABCG2-mediated MDR using Ko143 in S1 and S1-IR20 cells. The effect of Ko143 and venetoclax on the cytotoxicity (i.e., cell viability curves) of **(A)** mitoxantrone, **(B)** irinotecan, **(C)** doxorubicin, and **(D)** oxaliplatin in S1 and S1-IR20 cells. Data are expressed as mean ± SD derived from three independent experiments.

fold resistance to irinotecan as compared with parental cells, and the drug resistance was stable after at least 2 months in the absence of irinotecan maintenance. Since ABCB1, ABCG2, and ABCC1 are major mediators of MDR, we explored whether these ABC transporters are involved in this irinotecan resistance. Subsequently, the cytotoxicity of a panel of chemotherapeutic drugs were assessed in S1 and S1-IR20 cells. Interestingly, the S1-IR20 cells showed significant cross resistance to SN-38 (47-fold), topotecan (41-fold), mitoxantrone (37-fold), doxorubicin (18-fold), which are known substrates of ABCG2 transporter (34, 45). In contrast, S1-IR20 cells did not exhibit any resistance to paclitaxel, colchicine, and oxaliplatin, suggesting that ABCG2 may be a major contributor to the drug resistance phenotype.

We then evaluated the protein expression level of ABCB1, ABCG2, and ABCC1 in both parental S1 cells and drug-resistant S1-IR20 cells. Our results showed that S1 cells did not have detectable expression levels of ABCB1, ABCG2, or ABCC1, which is consistent with previous studies (46). However, overexpression of ABCG2 but not ABCB1 or ABCC1 was observed in S1-IR20 cells. The expression level of ABCG2 in S1-IR20 cells is comparable to that of mitoxantrone-selected ABCG2-overexpressing NCI-H460/MX20 cells, suggesting that acquired resistance to irinotecan may be associated with ABCG2 overexpression. This result is in line with the drug resistance profile of S1-IR20 cell line. Furthermore, irinotecan exerted anticancer effects by targeting DNA topo I, therefore alteration of topo I expression may contribute to drug resistance (47). However, this is unlikely since S1 and S1-IR20 cells showed similar expression levels of topo I. This result is consistent with a previous study that demonstrated that SN-38 (active metabolite of irinotecan)-selected resistant cell line showed no change in topo I expression level (25). ABCG2 has been characterized as a transporter causing of MDR in many human cancers by actively transporting chemotherapeutic agents out of cancer cells (48). As irinotecan is reported as a substrate of ABCG2, exposing cancer cells to irinotecan may cause an up-regulation of both ABCG2 mRNA and protein expression level. Our results suggested that in the presence of irinotecan, ABCG2 is induced to export the drug from the cell and to prevent cytotoxicity.

Since ABCG2 transporter requires cell membrane localization in order to function as an efflux pump to extrude its substrates from intracellular space, we conducted an immunofluorescence assay to visualize the localization of ABCG2 in S1-IR20 cells. The results clearly showed that the overexpressed ABCG2 transporter is localized on the cell membrane of S1-IR20 cells, suggesting that ABCG2 can actively pump out substrate drugs from the cells, leading to decreased intracellular drug accumulation and thus decreasing drug efficacy. To further confirm that the irinotecan

resistance is caused by overexpression of ABCG2, we performed an HPLC assay to directly measure the intracellular accumulation of irinotecan in parental S1 cells and drug-resistant S1-IR20 cells in the presence or absence of ABCG2 inhibitor Ko143. It was observed that the intracellular amount of irinotecan in S1-IR20 cells was significantly lower than in S1 cells, with more than 60% of the drug being pumped out from S1-IR20 cells. In addition, co-treatment with Ko143 was able to restore the accumulation of irinotecan in S1-IR20 cells to the same level as that in the parental S1 cells. Ko143 demonstrated no effect on irinotecan accumulation in parental S1 cells, as the cell line does not overexpress ABCG2 transporter. This result was also validated by ABCG2-inhibition experiments. By performing an MTT assay, the cytotoxic effect of irinotecan as well as ABCG2 substrates mitoxantrone and doxorubicin was compared in the presence or absence of Ko143. Our results showed that Ko143 was able to abolish drug resistance to irinotecan, mitoxantrone, and doxorubicin. In contrast, Ko143 did not alter the cytotoxicity of oxaliplatin, a non-substrate drug, in S1 or S1-IR20 cells. In addition, venetoclax can reverse wild-type ABCG2-mediated MDR but has no inhibition effect to mutant-type ABCG2 (49). Our results showed that venetoclax did not affect to the cytotoxicity of irinotecan and mitoxantrone in S1-IR cells, suggesting that S1-IR cells may overexpress mutant-type ABCG2. However, the actual mutation site of ABCG2 in S1-IR cells remains to be determined.

In summary, our work revealed that overexpression of ABCG2 may be an important mechanism in acquired resistance to irinotecan in CRC. Although clinical data suggest an inconclusive relationship of irinotecan response with ABCG2 expression level, our finding reemphasized the importance of ABCG2 in the development of irinotecan-resistance. Therefore, tumor ABCG2 level may serve as a predictor for irinotecan resistance during long-term treatment. The establishment of this drug-resistant cell line may facilitate the understanding of other potential mechanisms contributing to irinotecan resistance in CRC and for developing effective strategy to improve therapeutic response in CRC patients.

## DATA AVAILABILITY STATEMENT

The original contributions presented in the study are included in the article/supplementary material. Further inquiries can be directed to the corresponding author.

## AUTHOR CONTRIBUTIONS

Z-XW, LL, and Z-SC conceptualized the study. Z-XW, YY, LZ, HP, and LB developed the methodology. Z-XW wrote and prepared the original draft. Z-XW, LL, and Z-SC wrote, reviewed, and edited the manuscript. Z-SC supervised the study. All authors contributed to the article and approved the submitted version.

## FUNDING

This study was partially supported by the Department of Pharmaceutical Sciences, St. John's University.

## ACKNOWLEDGMENTS

The authors would like to thank Drs. Robert W. Robey and Susan E. Bates (NCI, NIH, Bethesda, MD) for providing the NCI-H460 and NCI-H460/MX20 cell lines, Dr. Shin-Ichi Akiyama (Kagoshima University, Kagoshima, Japan) for the gift of KB-3-1 and KB-C2 cell lines, and Dr. Yangmin Chen for language editorial assistance (St. John's University, Queens, NY).

## REFERENCES

1. Dekker E, Tanis PJ, Vleugels JLA, Kasi PM, Wallace MB. Colorectal cancer. *Lancet* (2019) 394:1467–80. doi: 10.1016/S0140-6736(19)32319-0
2. Geng F, Wang Z, Yin H, Yu J, Cao B. Molecular Targeted Drugs and Treatment of Colorectal Cancer: Recent Progress and Future Perspectives. *Cancer Biother Radiopharm* (2017) 32:149–60. doi: 10.1089/cbr.2017.2210
3. Kuipers EJ, Grady WM, Lieberman D, Seufferlein T, Sung JJ, Boelens PG, et al. Colorectal cancer. *Nat Rev Dis Primers* (2015) 1:15065. doi: 10.1038/nrdp.2015.65
4. Van Cutsem E, Cervantes A, Nordlinger B, Arnold D. Metastatic colorectal cancer: ESMO Clinical Practice Guidelines for diagnosis, treatment and follow-up. *Ann Oncol* (2014) 25(Suppl 3):iii1–9. doi: 10.1093/annonc/mdu260
5. Fakih MG. Metastatic colorectal cancer: current state and future directions. *J Clin Oncol* (2015) 3:1809–24. doi: 10.1200/JCO.2014.59.7633
6. Fujita K-I, Kubota Y, Ishida H, Sasaki Y. Irinotecan, a key chemotherapeutic drug for metastatic colorectal cancer. *World J Gastroenterol* (2015) 21:12234–48. doi: 10.3748/wjg.v21.i43.12234
7. Armand JP, Ducreux M, Mahjoubi M, Abigerges D, Bugat R, Chabot G, et al. CPT-11 (Irinotecan) in the treatment of colorectal cancer. *Eur J Cancer* (1995) 31:1283–7. doi: 10.1016/0959-8049(95)00212-2
8. Rothenberg ML. Irinotecan (CPT-11): recent developments and future directions–colorectal cancer and beyond. *Oncologist* (2001) 6:66–80. doi: 10.1634/theoncologist.6-1-66
9. Fuchs C, Mitchell EP, Hoff PM. Irinotecan in the treatment of colorectal cancer. *Cancer Treat Rev* (2006) 32:491–503. doi: 10.1016/j.ctrv.2006.07.001
10. Wenjie W, Yuk-Ching T-D. Recent Advances in Use of Topoisomerase Inhibitors in Combination Cancer Therapy. *Curr Top Med Chem* (2019) 19:730–40. doi: 10.2174/1568026619666190401113350
11. Bailly C. Irinotecan: 25 years of cancer treatment. *Pharmacol Res* (2019) 148:104398. doi: 10.1016/j.phrs.2019.104398
12. Xu Y, Villalona-Calero MA. Irinotecan: mechanisms of tumor resistance and novel strategies for modulating its activity. *Ann Oncol* (2002) 13:1841–51. doi: 10.1093/annonc/mdf337
13. Robey RW, Pluchino KM, Hall MD, Fojo AT, Bates SE, Gottesman MM. Revisiting the role of ABC transporters in multidrug-resistant cancer. *Nat Rev Cancer* (2018) 18:452–64. doi: 10.1038/s41568-018-0005-8
14. Hill BT, Whelan RD, Shellard SA, McClean S, Hosking LK. Differential cytotoxic effects of docetaxel in a range of mammalian tumor cell lines and certain drug resistant sublines in vitro. *Invest New Drugs* (1994) 12:169–82. doi: 10.1007/BF00873957
15. Zhang Y-K, Dai C, Yuan C-G, Wu H-C, Xiao Z, Lei Z-N, et al. Establishment and characterization of arsenic trioxide resistant KB/ATO cells. *Acta Pharm Sin B* (2017) 7:564–70. doi: 10.1016/j.apsb.2017.04.001

16. Mo W, Zhang JT. Human ABCG2: structure, function, and its role in multidrug resistance. *Int J Biochem Mol Biol* (2012) 3:1–27.
17. Dohse M, Robey RW, Brendel C, Bates S, Neubauer A, Scharenberg C. Efflux of the Tyrosine Kinase Inhibitors Imatinib and Nilotinib (AMN107) Is Mediated by ABCB1 (MDR1)-Type P-Glycoprotein. *Blood* (2006) 108:1367–7. doi: 10.1182/blood.V108.11.1367.1367
18. Agarwal S, Sane R, Gallardo JL, Ohlfest JR, Elmquist WF. Distribution of gefitinib to the brain is limited by P-glycoprotein (ABCB1) and breast cancer resistance protein (ABCG2)-mediated active efflux. *J Pharmacol Exp Ther* (2010) 334:147–55. doi: 10.1124/jpet.110.167601
19. Wu ZX, Yang Y, Teng QX, Wang JQ, Lei ZN, Wang JQ, et al. Tivantinib, A c-Met Inhibitor in Clinical Trials, Is Susceptible to ABCG2-Mediated Drug Resistance. *Cancers* (2020) 12:186. doi: 10.3390/cancers12010186
20. Wei LY, Wu ZX, Yang Y, Zhao M, Ma XY, Li JS, et al. Overexpression of ABCG2 confers resistance to pevonedistat, an NAE inhibitor. *Exp Cell Res* (2020) 388:111858. doi: 10.1016/j.yexcr.2020.111858
21. Robey RW, Polgar O, Deeken J, To KW, Bates SE. ABCG2: determining its relevance in clinical drug resistance. *Cancer Metastasis Rev* (2007) 26:39–57. doi: 10.1007/s10555-007-9042-6
22. Nielsen DL, Palshof JA, Brünner N, Stenvang J, Viuff BM. Implications of ABCG2 Expression on Irinotecan Treatment of Colorectal Cancer Patients: A Review. *Int J Mol Sci* (2017) 18:1296. doi: 10.3390/ijms18091926
23. Palshof JA, Cederbye CN, Høgdall EVS, Poulsen TS, Linnemann D, Nygaard SB, et al. ABCG2 Protein Levels and Association to Response to First-Line Irinotecan-Based Therapy for Patients with Metastatic Colorectal Cancer. *Int J Mol Sci* (2020) 21:5027. doi: 10.3390/ijms21145027
24. de Jong FA, de Jonge MJ, Verweij J, Mathijssen RH. Role of pharmacogenetics in irinotecan therapy. *Cancer Lett* (2006) 234:90–106. doi: 10.1016/j.canlet.2005.04.040
25. Candeil L, Gourdier I, Peyron D, Vezzio N, Copois V, Bibeau F, et al. ABCG2 overexpression in colon cancer cells resistant to SN38 and in irinotecan-treated metastases. *Int J Cancer* (2004) 109:848–54. doi: 10.1002/ijc.20032
26. Jensen NF, Stenvang J, Beck MK, Hanáková B, Belling KC, Do KN, et al. Establishment and characterization of models of chemotherapy resistance in colorectal cancer: Towards a predictive signature of chemoresistance. *Mol Oncol* (2015) 9:1169–85. doi: 10.1016/j.molonc.2015.02.008
27. Therasse P, Arbuck SG, Eisenhauer EA, Wanders J, Kaplan RS, Rubinstein L, et al. New guidelines to evaluate the response to treatment in solid tumors. European Organization for Research and Treatment of Cancer, National Cancer Institute of the United States, National Cancer Institute of Canada. *J Natl Cancer Inst* (2000) 92:205–16. doi: 10.1093/jnci/92.3.205
28. Koopman M, Antonini NF, Douma J, Wals J, Honkoop AH, Erdkamp FL, et al. Sequential versus combination chemotherapy with capecitabine, irinotecan, and oxaliplatin in advanced colorectal cancer (CAIRO): a phase III randomised controlled trial. *Lancet (London England)* (2007) 370:135–42. doi: 10.1016/S0140-6736(07)61086-1
29. Silvestris N, Simone G, Partipilo G, Scarpi E, Lorusso V, Brunetti AE, et al. CES2, ABCG2, TS and Topo-I primary and synchronous metastasis expression and clinical outcome in metastatic colorectal cancer patients treated with first-line FOLFIRI regimen. *Int J Mol Sci* (2014) 15:15767–77. doi: 10.3390/ijms150915767
30. Lyall RM, Hwang JL, Cardarelli C, FitzGerald D, Akiyama S, Gottesman MM, et al. Isolation of human KB cell lines resistant to epidermal growth factor-Pseudomonas exotoxin conjugates. *Cancer Res* (1987) 47:2961–6.
31. Robey RW, Honjo Y, van de Laar A, Miyake K, Regis JT, Litman T, et al. A functional assay for detection of the mitoxantrone resistance protein, MXR (ABCG2). *Biochim Biophys Acta* (2001) 1512:171–82. doi: 10.1016/S0005-2736(01)00308-X
32. Aoki S, Chen ZS, Higasiyama K, Setiawan A, Akiyama S, Kobayashi M. Reversing effect of agosterol A, a spongean sterol acetate, on multidrug resistance in human carcinoma cells. *Jpn J Cancer Res Gann* (2001) 92:886–95. doi: 10.1111/j.1349-7006.2001.tb01177.x
33. Wu Z-X, Teng Q-X, Cai C-Y, Wang J-Q, Lei Z-N, Yang Y, et al. Tepotinib reverses ABCB1-mediated multidrug resistance in cancer cells. *Biochem Pharmacol* (2019) 166:120–7. doi: 10.1016/j.bcp.2019.05.015
34. Wu ZX, Yang Y, Wang G, Wang JQ, Teng QX, Sun L, et al. Dual TTK/CLK2 inhibitor, CC-671, selectively antagonizes ABCG2-mediated multidrug resistance in lung cancer cells. *Cancer Sci* (2020) 111:2872–82. doi: 10.1111/cas.14505
35. Tariq M, Negi LM, Talegaonkar S, Ahmad FJ, Iqbal Z, Khan AM. Liquid Chromatographic Method for Irinotecan Estimation: Screening of P-gp Modulators. *Indian J Pharm Sci* (2015) 77:14–23. doi: 10.4103/0250-474X.151577
36. Barilero I, Gandia D, Armand JP, Mathieu-Boué A, Ré M, Gouyette A, et al. Simultaneous determination of the camptothecin analogue CPT-11 and its active metabolite SN-38 by high-performance liquid chromatography: application to plasma pharmacokinetic studies in cancer patients. *J Chromatogr* (1992) 575:275–80. doi: 10.1016/0378-4347(92)80156-K
37. Gelibter AJ, Caponnetto S, Urbano F, Emiliani A, Scagnoli S, Sirgiovanni G, et al. Adjuvant chemotherapy in resected colon cancer: When, how and how long? *Surg Oncol* (2019) 30:100–7. doi: 10.1016/j.suronc.2019.06.003
38. Zhao W, Cong Y, Li HM, Li S, Shen Y, Qi Q, et al. Challenges and potential for improving the druggability of podophyllotoxin-derived drugs in cancer chemotherapy. *Natural Prod Rep* (2020). doi: 10.1039/D0NP00041H
39. Zhao Y, You H, Liu F, An H, Shi Y, Yu Q, et al. Differentially expressed gene profiles between multidrug resistant gastric adenocarcinoma cells and their parental cells. *Cancer Lett* (2002) 185:211–8. doi: 10.1016/S0304-3835(02)00264-1
40. Amawi H, Sim HM, Tiwari AK, Ambudkar SV, Shukla S. ABC Transporter-Mediated Multidrug-Resistant Cancer. *Adv Exp Med Biol* (2019) 1141:549–80. doi: 10.1007/978-981-13-7647-4_12
41. Li M, Seiser EL, Baldwin RM, Ramirez J, Ratain MJ, Innocenti F, et al. ABC transporter polymorphisms are associated with irinotecan pharmacokinetics and neutropenia. *Pharmacogenomics J* (2018) 18:35–42. doi: 10.1038/tpj.2016.75
42. Yang Y, Wang G, Zhu D, Huang Y, Luo Y, Su P, et al. Epithelial-mesenchymal transition and cancer stem cell-like phenotype induced by Twist1 contribute to acquired resistance to irinotecan in colon cancer. *Int J Oncol* (2017) 51:515–24. doi: 10.3892/ijo.2017.4044
43. Chen MC, Lee NH, Hsu HH, Ho TJ, Tu CC, Chen RJ, et al. Inhibition of NF-κB and metastasis in irinotecan (CPT-11)-resistant LoVo colon cancer cells by thymoquinone via JNK and p38. *Environ Toxicol* (2017) 32:669–78. doi: 10.1002/tox.22268
44. Miyake K, Mickley L, Litman T, Zhan Z, Robey R, Cristensen B, et al. Molecular Cloning of cDNAs Which Are Highly Overexpressed in Mitoxantrone-resistant Cells. Demonstration of Homology to ABC Transport Genes. *Cancer Res* (1999) 59:8–13.
45. Wu ZX, Peng Z, Yang Y, Wang JQ, Teng QX, Lei ZN, et al. M3814, a DNA-PK Inhibitor, Modulates ABCG2-Mediated Multidrug Resistance in Lung Cancer Cells. *Front Oncol* (2020) 10:674. doi: 10.3389/fonc.2020.00674
46. Ji N, Yang Y, Cai CY, Lei ZN, Wang JQ, Gupta P, et al. VS-4718 Antagonizes Multidrug Resistance in ABCB1- and ABCG2-Overexpressing Cancer Cells by Inhibiting the Efflux Function of ABC Transporters. *Front Pharmacol* (2018) 9:1236. doi: 10.3389/fphar.2018.01236
47. Kciuk M, Marciniak B, Kontek R. Irinotecan-Still an Important Player in Cancer Chemotherapy: A Comprehensive Overview. *Int J Mol Sci* (2020) 21:4919. doi: 10.3390/ijms21144919
48. Nakanishi T, Ross DD. Breast cancer resistance protein (BCRP/ABCG2): its role in multidrug resistance and regulation of its gene expression. *Chin J Cancer* (2012) 31:73–99. doi: 10.5732/cjc.011.10320
49. Wang JQ, Li JY, Teng QX, Lei ZN, Ji N, Cui Q, et al. Venetoclax, a BCL-2 Inhibitor, Enhances the Efficacy of Chemotherapeutic Agents in Wild-Type ABCG2-Overexpression-Mediated MDR Cancer Cells. *Cancers* (2020) 12:1466. doi: 10.3390/cancers12020466

**Conflict of Interest:** The authors declare that the research was conducted in the absence of any commercial or financial relationships that could be construed as a potential conflict of interest.

frontiers in Pharmacology

ORIGINAL RESEARCH
published: 25 February 2021
doi: 10.3389/fphar.2021.615889

# Artesunate Regulates Neurite Outgrowth Inhibitor Protein B Receptor to Overcome Resistance to Sorafenib in Hepatocellular Carcinoma Cells

*Wubin He[1†], Xiaoxu Huang[2†], Bradford K. Berges[3], Yue Wang[4], Ni An[2], Rongjian Su[2] and Yanyan Lu[5*]*

[1]Key laboratory of surgery of Liaoning Province of The First Affiliated Hospital of Jinzhou Medical University, Liaoning, China, [2]Key Laboratory of Molecular Cell Biology and New Drug Development of Jinzhou Medical University, Liaoning, Jinzhou, China, [3]Department of Microbiology and Molecular Biology of Brigham Young University, Provo, UT, United States, [4]Department of Pathlogy of The First Affiliated Hospital of Jinzhou Medical University, Liaoning, China, [5]Department of Orthopedic Spine Surgery of The First Affiliated Hospital of Jinzhou Medical University, Liaoning, China

OPEN ACCESS

**Edited by:**
Xiaoping Lin,
Sun Yat-sen University Cancer Center, China

**Reviewed by:**
Chia-Che Chang,
National Chung Hsing University, Taiwan
Runbi Ji,
Jiangsu University Affiliated People's Hospital, China

***Correspondence:**
Yanyan Lu
luyanyan@jzmu.edu.cn

[†]These authors share first authorship

**Specialty section:**
This article was submitted to Pharmacology of Anti-Cancer Drugs, a section of the journal Frontiers in Pharmacology

**Received:** 10 October 2020
**Accepted:** 19 January 2021
**Published:** 25 February 2021

**Citation:**
He W, Huang X, Berges BK, Wang Y, An N, Su R and Lu Y (2021) Artesunate Regulates Neurite Outgrowth Inhibitor Protein B Receptor to Overcome Resistance to Sorafenib in Hepatocellular Carcinoma Cells. Front. Pharmacol. 12:615889. doi: 10.3389/fphar.2021.615889

The multireceptor tyrosine kinase inhibitor sorafenib is a Food and Drug Administration-approved first-line drug for the treatment of advanced liver cancer that can reportedly extend overall survival in patients with advanced hepatocellular carcinoma (HCC). Primary and acquired resistance to sorafenib are gradually increasing however, leading to failure of HCC treatment with sorafenib. It is therefore crucial to study the potential mechanism of sorafenib resistance. The results of the current study indicate that neurite outgrowth inhibitor protein B receptor (NgBR) is overexpressed in cultured sorafenib-resistant cells, and that its expression is negatively correlated with the sensitivity of liver cancer cells to sorafenib. Artesunate can inhibit the expression of NgBR, and it may block sorafenib resistance. Herein we report that sorafenib treatment in combination with artesunate overcomes HCC resistance to sorafenib alone in a cell culture model.

**Keywords: artesunate, NGBR, sorafenib, resistance, hepatocellular carcinoma**

## INTRODUCTION

Hepatocellular carcinoma (HCC) is a primary solid tumor that develops chemoresistance. This limits the number of effective interventions for advanced HCC, leading to over 700,000 deaths annually around the world (Fukui et al., 2018). In early stages HCC can be treated using tumor resection, ablation, or liver transplantation (Díaz-González et al., 2020). The successful development of molecularly targeted drugs has reportedly extended the overall survival of patients with chronic liver cancer (Al-Salama et al., 2019).

The multityrosine kinase inhibitor sorafenib was the first small-molecule-targeted drug that demonstrably extended the overall survival of advanced HCC patients (Gramantieri et al., 2020). In the last decade it has been widely used as the first-line therapeutic drug for the treatment of chronic HCC (Wang et al., 2020). Most patients with advanced HCC develop resistance to sorafenib early during treatment, and thus do not benefit from it in the long term (Zhang et al., 2020). A previous report has demonstrated the role of mitogen-activated protein kinase 14 (MAPK14) activation in the development of sorafenib resistance in HCC (Rudalska et al., 2014). MAPK14 activation in HCC cells was associated with no response to sorafenib in a murine model of tumor development and treatment

with sorafenib (Hashiba et al., 2020). In other studies persistent activation of mitogen-activated protein kinase (MAPK kinase)/extracellular signal-regulated kinase (MEK/ERK) signaling pathways was evident in HCC due to the development of sorafenib resistance (Sung et al., 2018; Ghousein et al., 2020).

Artesunate is one of the derivatives of artemisinin, and it can inhibit tumor cell proliferation, tumor angiogenesis, tumor invasion, and metastasis. It can also induce tumor cell apoptosis, regulate cell signal transduction, reverse drug resistance, and enhance sensitization to anti-tumor chemotherapeutic drugs (Ji et al., 2019). The anti-cancer effects of artesunate have been confirmed in liver cancer (Yao et al., 2020), ovarian cancer, and breast cancer cells (Zhang et al., 2018). Previous work in our laboratory confirmed that artesunate can regulate and inactivate MEK/ERK signaling, and inhibit the propagation of liver cancer cells. Because sorafenib does not directly act on the MEK/ERK signaling pathway, we speculate that artesunate may synergistically enhance the sensitivity of liver cancer cells to sorafenib.

Reticulons are a relatively newly characterized eukaryotic gene family, and they are widely distributed in plants, animals, and yeasts (Oertle et al., 2003). Neurite outgrowth inhibitor (Nogo) proteins, also known as reticulon-4, are myelin-associated glycoproteins. Three Nogo protein subtypes are generated via differences in the transcription and splicing process, Nogo-A, Nogo-B, and Nogo-C, which contain 1,192, 373, and 199 residues respectively. These three translational products differ but they are all distributed in the endoplasmic reticulum (Josephson et al., 2002). Nogo-B is a shorter subtype than Nogo-A, and is widely distributed in various tissues and organs of the human body, but not in the central nervous system. It is expressed in the liver, lung, kidney, blood vessels, pancreas, and inflammatory cells (Long et al., 2017). (Oertle and Schwab, 2003) first discovered the Nogo-B-specific receptor (NgBR). NgBR is widely distributed in various tissues and organs in the body (Duff et al., 2015), and has specific effects on nervous system regeneration, cell chemotaxis, apoptosis, and propagation. It also plays key roles in cell apoptosis, epithelial-mesenchymal transition, and the development of drug resistance in tumor cells. The Nogo-B gene, also known as ASY (Li et al., 2001), is a human apoptosis-inducing gene but it has no known specific apoptosis-related motif. One study has shown that Nogo-B overexpression promotes endoplasmic reticulum stress and intracellular calcium disorder, and ultimately induces apoptosis (Teng and Tang, 2013). Schweigreiter et al. (2007) have shown that Nogo-B can regulate cell apoptosis through the caspase-7 pathway. NgBR can reportedly also directly bind to isoamylated Ras, stabilizing it on the envelope and promoting its function, which in turn enhances epidermal growth factor signal pathway activity, promoting tumor formation (Zhao et al., 2017).

This study was designed to identify the relationship between neurite outgrowth inhibitor protein B receptor (NgBR) and sorafenib resistance. Our results show that artesunate can inhibit NgBR expression, and in combination sorafenib artesunate can overcome the resistance to sorafenib in hepatocellular carcinoma cells.

# MATERIALS AND METHODS

## Cell Lines

The HepG2 human hepatoma cell line was purchased from the Shanghai Institute of Biochemistry and Cell Biology (Shanghai, China). All cell lines in the study were maintained in DMEM medium (Gibco, CA, United States) supplemented with 10% fetal bovine serum (Gibco, CA, United States), 50 μg/ml streptomycin, and 100 U/ml sodium penicillin at 37°C in an atmosphere containing 5% $CO_2$. HepG2 sorafenib-resistant cells (HepG2-SR) were generated by selection starting with sorafenib (Selleckchem, United States) at 2 μm, increasing to 10 μm over the course of 3 months.

## Quantitative Real-Time PCR

TRIzol reagent was used to extract total cellular RNA in accordance with the manufacturer's instructions (Thermo Fisher, United States). SYBR Green quantitative reverse transcription PCR (qRT-PCR) was used to evaluate NgBR mRNA expression levels. Primer NgBR F (5'-TGCCAGTTA GTAGCCCAGAAGCAA-3'); NgBR R (5'-AACCTGCCAAGT ATGATGAC-3')

## Cell Proliferation

The 3-(4,5-dimethylthiazol-2-yl)-2,5-diphenyltetrazolium bromide (MTT) assay and the 5-ethynyl-2'-deoxyuridine (EDU) immunofluorescence staining assay (Ribobio, Guangzhou, China) were used to test the propagation capacity of HCC cells. Sorafenib (99.15% purity) and artesunate (99.89% purity) were purchased from Selleck Chemical (United States). Briefly, for the MTT assay the cells were cultured at a density of 6,000 cells/well in 96-well plates in triplicate and treated with sorafenib and/or artesunate for 48 h. For the EDU immunofluorescence staining assay the cells were incubated with sorafenib for 24 h before permeabilization. EDU staining and fixation were performed in accordance with the manufacturer's instructions. A concentration of 1 mg/ml of 4′,6-diamidino-2-phenylindole (DAPI; Beyotime, China) was used to stain the cell nuclei for 15 min. Cell numbers were calculated via confocal laser scanning microscopy (Olympus, FV10i, Japan).

## Colony Formation Assay

Cells were seeded into six-well plates (103 cells per well) and cultured in complete media for two weeks. After two weeks, cells were fixed with methanol (1%), stained with 1% crystal violet, and imaged using a digital camera (Olympus, Japan). Cell colonies (cell clone diameter ≥1 mm) were counted in this experiment.

## Fluorescein Isothiocyanate-Terminal Deoxynucleotidyl Transferase-Mediated dUTP Nick-End Labeling

Cells in logarithmic growth phase were seeded into culture flasks ($1.5 \times 10^5$ cells/ml) and treated with sorafenib and/or artesunate in complete DMEM for 48 h. Paraformaldehyde (4%) in

phosphate-buffered saline was used to fix the cells for 30 min, followed by permeabilization in 0.3% Triton X-100 in phosphate-buffered saline for 5 min at room temperature. Cells were stained with terminal deoxynucleotidyl transferase-mediated dUTP nick-end labeling (TUNEL) reagent in the dark for 60 min, then the number of apoptotic cells was assessed via confocal laser scanning microscopy.

## Transfection

### siRNA

Cells were plated in a 6-well culture plate for 24 h and transfection reagents prepared. The control group was treated with 2 ml transfection medium, 2 μl RNAiMAX, and 2 μl siNC. The siNgBR group was treated with 2 ml transfection medium, 2 μl RNAiMAX, and 2 μl siNgBR. The siNC and siNgBR group was transfected using transfection reagents in a 6-well culture plate. The siRNA sequences used were: siNgBR F (GGAAAUACAUAG ACCUACA), R (UGUAGGUCUAUGUAUUUCC); and siNC F (UUCUCCGAACGUGUCACGU), R (ACGUGACACGUU CGGAGAA) (QIAGEN).

### Plasmids

NgBR overexpression plasmid transfection: cells were plated in 10-cm culture dishes for 24 h then 5 ml transfection medium, 20 μl Lipofectamine 2000 (Invitrogen), and 4 μg plasmid was prepared. Plasmid DNA and Lipofectamine 2000 were diluted in serum-free and antibiotic-free medium, respectively. Diluted DNA was added to diluted Lipofectamine 2000, mixed well, and incubated at room temperature for 20 min. NgBR overexpression group cells were transfected with the pIRES-NgBR-HA plasmid and control group cells were transfected with blank vector. The transfection efficiency was determined by western blot after 48 h incubation.

## Western Blotting

Radioimmunoprecipitation assay lysis buffer was used to prepare cell lysates for protein analysis. The BCA Assay Kit (Beyotime, China) was used to determine protein concentrations and achieve standardization among the samples. Aliquots of 40 μg of each lysate were prepared, run through SDS-PAGE, and transferred to a polyvinylidene difluoride membrane. The membrane was then blocked with 10% bovine serum albumin (Sigma, United States) and incubated at 4°C overnight with antibodies against the proteins of interest. The antibodies used were NgBR (ab168351, 1:1,000, Abcam, United Kingdom), Nogo-B (AF6034, 1:2,000, Imgenex, United States), phospho-Erk1/2 Thr202/Tyr204 (#4370, 1:1,000, Cell Signaling, United States), Erk1/2 p42/44 (#4696, 1:1,000, Cell Signaling), MEK1/2 (#8727, 1:1,000, Cell Signaling), phosphor-MEK1/2 Ser217/221 (#3958, 1: 1,000, Cell Signaling), and β-actin (#3700, 1:1,000, Cell Signaling).

## Xenotransplantation Studies

All xenotransplantation experiments were approved by the Experimental Animal Ethics Committee of Jinzhou Medical University (protocol 20170503) and conformed to the Guide for the Care and Use of Laboratory Animals published by the United States National Institutes of Health (eighth Edition, 2011). Cells ($1 \times 10^7$) were resuspended in 100 μl DMEM and injected into the dorsal flanks of female 6-week-old nu/nu mice subcutaneously. Two weeks later, 20 mice with tumor volumes of approximately 100 $mm^3$ were selected and dicided into four groups. The four group treatments were dimethylsulfoxide (DMSO) (Selleckchem, United States) with corn germ oil, artesunate (50 mg/kg) with corn germ oil, sorafenib (30 mg/kg) with corn germ oil, and artesunate/sorafenib (80 mg/kg/30 mg/kg) with corn germ oil. All treatments were administered once every 3 days for 21 days. The solvent used to dissolve the drugs was DMSO, with corn germ oil as a co-solvent.

## Data Analysis

All data were analyzed using GraphPad prism software 8.0. One-way analysis of variance and chi-square tests were used to compare single-factor groups. Inter-group analysis was performed using Student's *t*-tests. $p$ values $<0.05$ were considered statistically significant.

# RESULTS

## Artesunate Inhibition of Hepatocarcinoma Parent Cell and Sorafenib Resistant Cell Proliferation

HepG2 cells and HepG2-SR cells were treated with 0, 25, 50, or 100 μm concentrations of artesunate for 48 h, and artesunate alone inhibited the propagation of HepG2 and HepG2-SR liver tumor cells in a dose-dependent manner (**Figure 1A**). Cell viability was investigated via EDU immunofluorescence staining assays after 24 h, and several concentrations of artesunate inhibited the growth of HepG2 and HepG2-SR cells (**Figure 1B**). FITC-TUNEL staining apoptosis assays also revealed dose-dependent artesunate-induced apoptosis of HepG2 and HepG2-SR cells (**Figure 1C**).

## Artesunate Inhibition of NgBR Expression in Sorafenib-Resistant HCC Cells

In qRT-PCR and western blotting analyses there were significant increases in NgBR expression in sorafenib-resistant cells compared to normal cells (**Figurea 2A, B**). Sorafenib affected NgBR expression in a dose-dependent manner in sorafenib-resistant cells (**Figure 2C**). In experiments in which sorafenib-resistant cells were treated with various concentrations of artesunate for 48 h or a uniform concentration for various times, artesunate reduced NgBR expression in a dose-dependent manner (**Figure 2D**) and a time-dependent manner (**Figure 2E**).

## NgBR Knockdown and the Restoration of Sorafenib Sensitivity in Sorafenib-Resistant Liver Cancer Cells

Western blotting was used to determine NgBR knockdown efficiency (**Figure 3A**). MTT (72 h) and colony formation

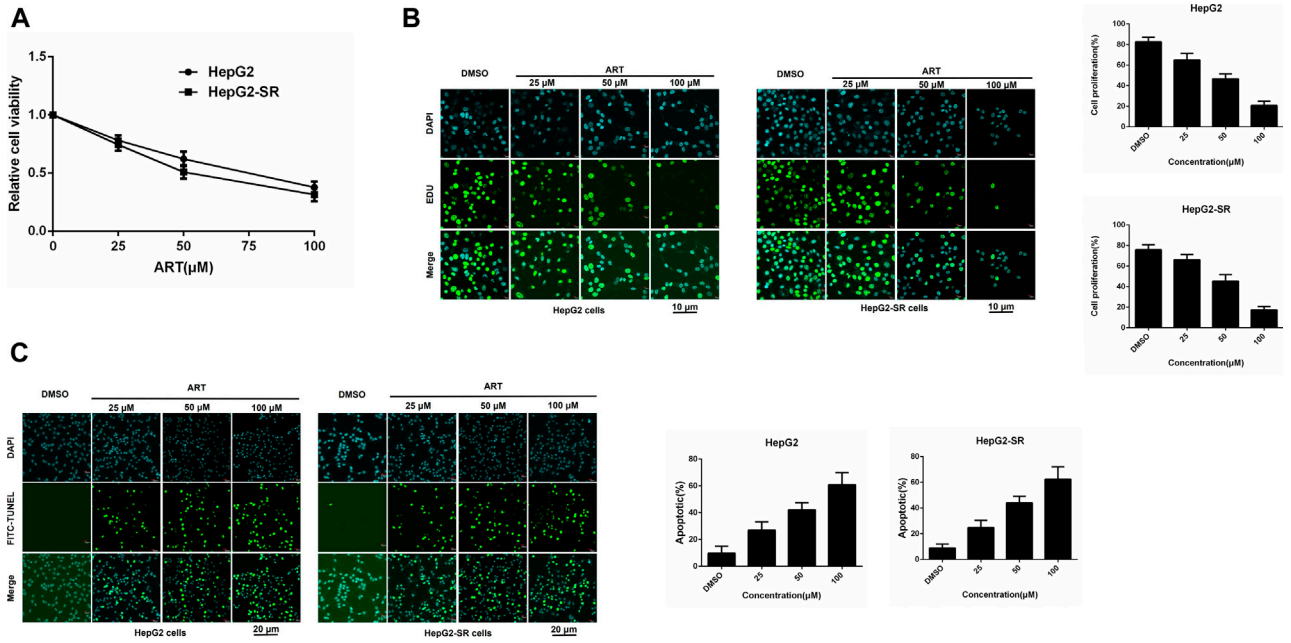


**FIGURE 1 |** Artesunate (ART) can effectively inhibit the propagation of sorafenib-resistant cells. **(A)**. HepG2-SR cells were treated with 0, 25, 50, or 100 μm artesunate, and 48 h later MTT assays were performed to detect artesunate sensitivity in the cells. **(B)**. Cell propagation detected by EDU assays. Cells were stained with DAPI (blue) for visualization of nuclei, and EDU (green) signifies proliferative cells. EDU-positive cells per field were quantified in multiple fields, and cell proliferation was measured relative to total cells. Scale bars = 10 μm. **(C)**. Apoptosis detected via FITC-TUNEL staining assays. Blue (DAPI) represents nuclei, and green (FITC-TUNEL) represents apoptotic cells. FITC-TUNEL-positive cells per field were quantified in multiple fields and the ratio of apoptotic cells was measured relative to total cells. Scale bars = 20 μm. Experiments were repeated three times.

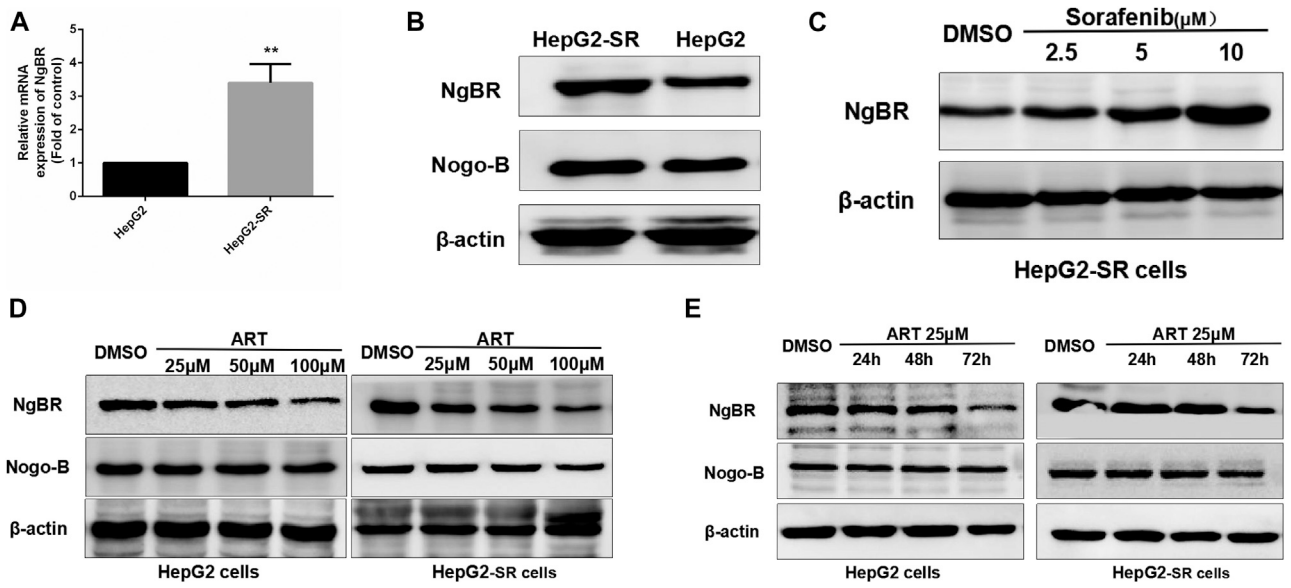


**FIGURE 2 |** Artesunate (ART) can inhibit NgBR expression in sorafenib-resistant HCC cells. NgBR expression was higher in HepG2-SR cells as determined by **(A)** qRT-PCR and **(B)** western blotting. Western blotting **(C)** indicated that NgBR expression increased in a dose-dependent manner in the presence of sorafenib in HepG2-SR cells. The experiment was performed in triplicate. Western blotting indicated that artesunate can inhibit the expression of NgBR in both HepG2 cells and sorafenib-resistant HCC cells, in a dose-dependent manner **(D)** and in a time-dependent manner **(E)**. Experiments were repeated three times, and data are expressed as means ± the standard error of the mean. Student's *t*-test was used to analyze the data. $^{*}p < 0.05$

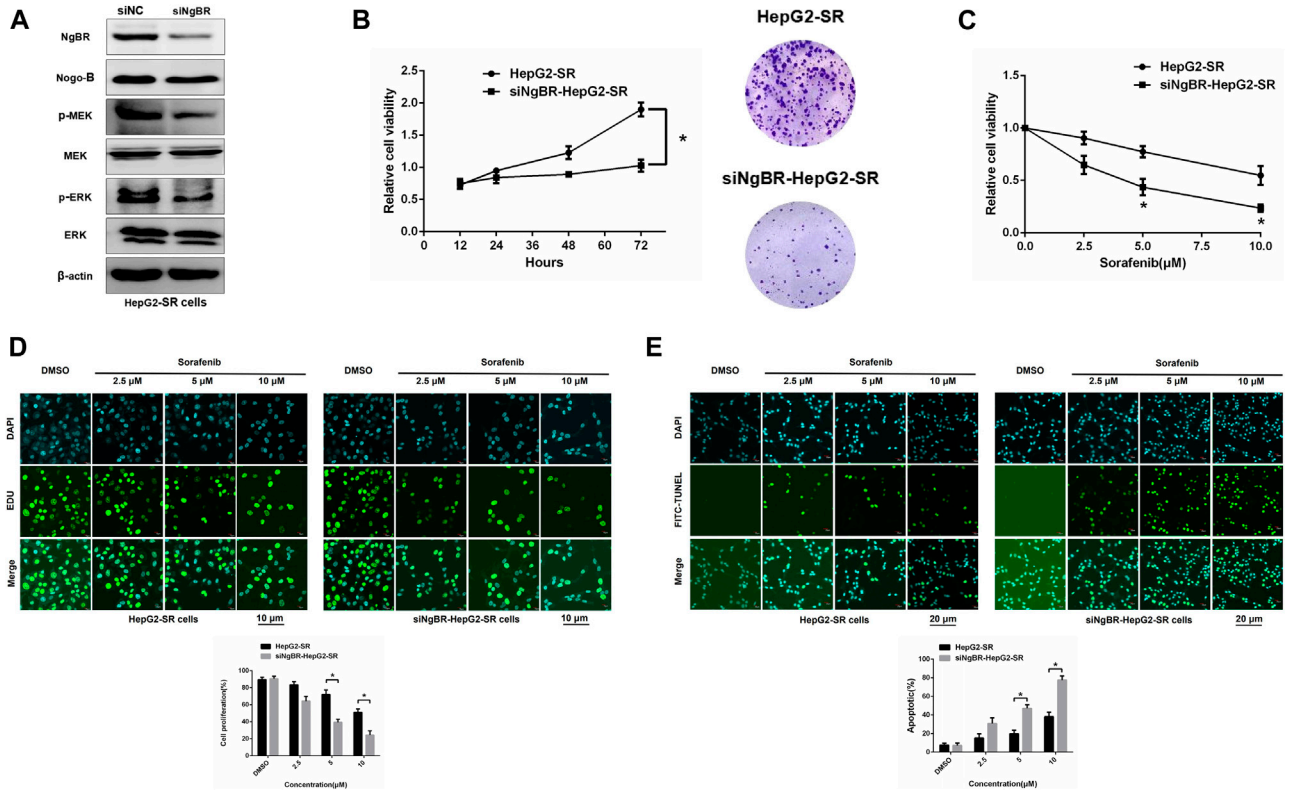


**FIGURE 3 |** NgBR knockdown reduces sorafenib resistance. **(A)**. NgBR knockdown efficiency of was assessed via western blotting. **(B)**. Cell growth of NgBR knockdown and normal control HepG2-SR cells was measured by MTT (72 h) and colony formation (14 days) assays. Data are presented as means ± standard deviation (SD). **(C)**. HepG2-SR cells were treated with various doses (0, 2.5, 5, and 10 μm) of sorafenib. After 48 h, the MTT assay was used to detect sorafenib sensitivity. **(D)**. Cell propagation was detected by EDU assays. Scale bars, 10 μm. **(E)**. Apoptosis was detected by FITC-TUNEL staining. Scale bars, 20 μm. Experiments were repeated three times and data are presented as mean ± SD. Student's *t*-test was used to analyze data. $^*p < 0.05$

(14 days) assays revealed that NgBR downregulation can reduce the viability of HepG2-SR cells (**Figure 3B**). Likewise, MTT (48 h) and EDU immunofluorescence staining (24 h) assays, after treatment with various sorafenib concentrations, revealed that NgBR knockdown significantly decreased cell proliferation in HepG2-SR cells. This effect was particularly evident with 5 and 10 μm sorafenib treatments (**Figures 3C, D**). FITC-TUNEL staining showed that sorafenib treatment at a lower concentrations (5 μm) caused significantly more apoptosis in NgBR-knockdown cells than in mock treated cells (**Figure 3E**).

## NgBR Overexpression in Hepatocarcinoma Parent Cells and the Promotion of Sorafenib Resistance in Liver Cancer Cells

NgBR was overexpressed in parental HepG2 cells (**Figure 4A**). MTT (72 h) and colony formation (14 days) assays revealed that NgBR overexpression can increase HepG2 cell viability (**Figure 4B**). We also found that, in HepG2 cells, NgBR overexpression significantly decreases the sensitivity of liver cancer cells to sorafenib at doses of either 5 μm or 10 μm (**Figures 4C, D**), and decreases rates of apoptosis following sorafenib (5 μm or 10 μm) treatment (**Figure 4E**).

## Effects of Artesunate Combined With Sorafenib on Sorafenib Resistance *in vitro*

The results of MTT assays conducted to determine appropriate concentrations of sorafenib alone or in combination with artesunate to achieve inhibitory effects on sorafenib-resistant liver cancer cells are shown in **Figure 5A**. In the combination study the sorafenib concentration was 2.5 μm and the artesunate concentration was 25 μm. HepG2-SR cells were treated with sorafenib (2.5 μm) and/or artesunate (25 μm) for 48 h, and artesunate rendered the cells significantly more sensitive to sorafenib. Inhibited proliferation and increased apoptosis were associated with sorafenib sensitivity (**Figures 5B, C**).

## Effects of Artesunate Combined With Sorafenib on Sorafenib Resistance *in vivo*

In experiments using xenografts derived from HepG2 and HepG2-SR cells to examine efficacy *in vivo*, after 3 weeks sorafenib alone and artesunate alone inhibited cancer growth as measured by tumor weight. The combination of artesunate and sorafenib resulted in greater growth inhibition than artesunate or sorafenib alone in both HepG2 and HepG2-SR xenograft models (**Figures 5D, E**). Thus, artesunate combined with sorafenib overcame NgBR-dependent sorafenib resistance in liver tumors *in vivo*.

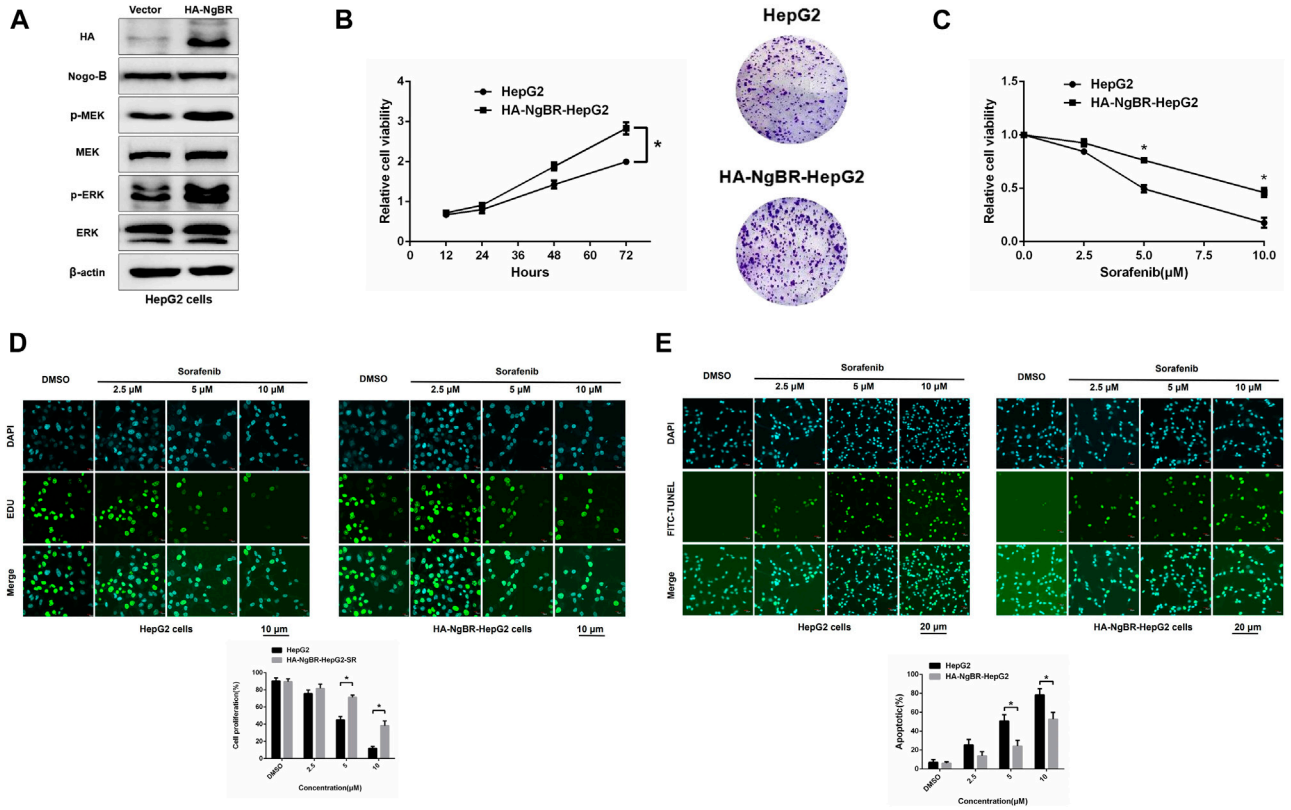


**FIGURE 4 |** NgBR overexpression promotes sorafenib resistance in liver cancer cells. **(A)**. NgBR overexpression was assessed via western blotting. **(B)**. Cell growth in NgBR overexpression and normal control HepG2 cells was detected by MTT (72 h) and colony formation (14 days) assays. The data are presented as means ± standard deviation (SD). **(C)**. MTT assay was employed to evaluate cellular proliferation, as a measure of sorafenib sensitivity in the cells, after 48 h. **(D)**. Cell proliferation was detected by EDU assays. Scale bars, 10 μm. **(E)**. Apoptosis was detected by FITC-TUNEL staining assays. Scale bars, 20 μm. Experiments were repeated three times and data are presented as mean ± SD. Student's *t*-test was used for data analysis. $^*p < 0.05$

## Artesunate can Block NgBR-Induced Sorafenib Resistance by Suppressing the MEK/ERK Pathway

The role of NgBR downregulation and overexpression in artesunate-induced sorafenib sensitization was examined. Firstly, The MTT assay was used to determine the appropriate concentrations of sorafenib alone, or in combination with artesunate, to use in HepG2-SR cells with downregulated NgBR and HepG2 cells with NgBR overexpression (**Figure 6A**). We found that artesunate can effectively inhibit cell proliferation in NgBR overexpressing cells only. To confirm that NgBR promotes HepG2 cell proliferation and survival through the activation of MEK/ERK signaling we examined the expression of relevant proteins. Activation of MEK/ERK signaling in HepG2 and HepG2-SR cells was examined by western blot. We found that, compared to HepG2 cells, the phosphorylation levels of MEK (p-MEK) and ERK (p-ERK) were significantly upregulated in HepG2-SR cells (**Figure 6B**). We then treated HepG2 and HepG2-SR cells with 10 μm U0126, a MEK 1/ inhibitor, for 7 days. Western blotting performed after U0126 treatment indicated that U0126 can inhibit p-MEK and p-ERK levels in both HepG2 and HepG2-SR cells (**Figure 6C**). MTT and EDU immunofluorescence staining (24 h) assays showed that in NgBR overexpressing HepG2 cells, artesunate-induced sorafenib sensitization was significantly decreased in U0126-treated cellscompared to U0126-untreated cells (**Figures 6D, E**).

## DISCUSSION

Sorafenib is a molecularly targeted drug available for the clinical management of liver cancer, but the development of resistance to sorafenib in liver cancer cells has reduced its therapeutic efficacy. Therefore, the current study investigated the mechanism of resistance of liver cancer to sorafenib. Increasing the cancer cells' sensitivity to therapeutic molecules is one of the main strategies for effective liver cancer treatment. Artesunate is a widely used effective anti-malarial agent, but studies have also confirmed that it has anti-tumor effects (Ye et al., 2020). Moreover, its cost-effectiveness and comparatively fewer adverse effects make it an ideal anti-tumor drug. The *in vitro* experimental results of the present study indicate that artesunate can prevent the propagation of hepatocarcinoma parent cells as well as cells resistant to sorafenib in a dose-dependent manner, and promote their apoptosis.

Previous studies suggest that NgBR upregulation may affect the occurrence and development of hormone receptor-positive

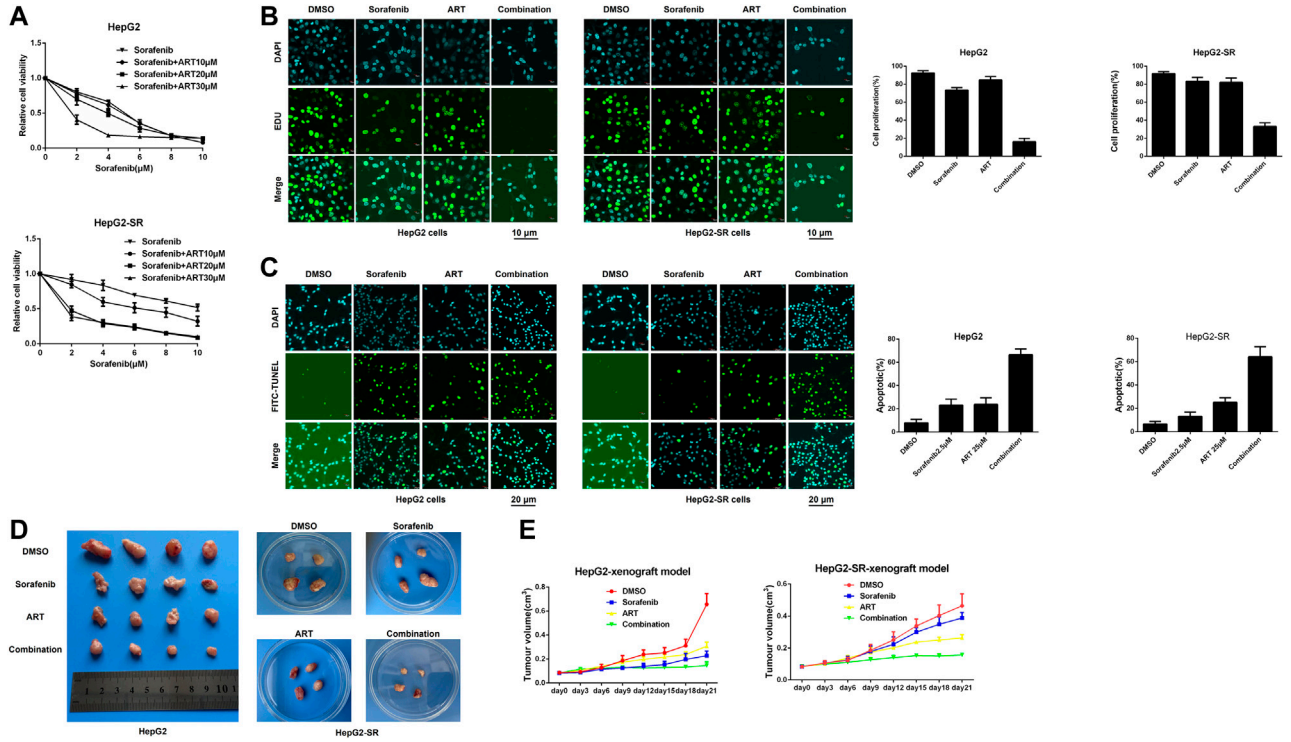


**FIGURE 5 |** Artesunate (ART) combined with sorafenib overcomes adaptive resistance to sorafenib *in vitro* and *in vivo*. **(A)**. Cells were treated with sorafenib alone or in combination with a fixed dose of artesunate, then MTT assays were conducted after 48 h. **(B)**. Sorafenib and artesunate alone or in combination were used in HepG2 cells and HepG2-SR cells after 24 h, and cell proliferation was detected via EDU assays. Scale bars = 10 μm. **(C)**. HepG2-SR cells and HepG2 cells were treated with sorafenib and artesunate alone or in combination for 48 h, then apoptosis was detected via FITC-TUNEL staining assays. Scale bars = 20 μm. **(D)**. ~1 × 107 HepG2 or HepG2-SR cells were injected into mouse flanks. When tumors reached ≥100 $mm^3$ in size the mouse was administered (1) DMSO with corn germ oil, (2) sorafenib (30 mg/kg) with corn germ oil, (3) artesunate (50 mg/kg) with corn germ oil, or (4) sorafenib (30 mg/kg) and artesunate (50 mg/kg) with corn germ oil once every 3 days via oral cannular. Tumor sizes were measured periodically with calipers, and tumor volumes were calculated using the formula volume = (width$^2$ × length)/2. **(E)**. After 21 days mice were killed by cervical dislocation, and the tumors were removed and weighed. Experiments were repeated three times.

breast cancer (Wang et al., 2013). Studies investigating tamoxifen resistance also indicate that epithelial-mesenchymal transition can play a key role (Liang et al., 2017). NgBR promotes epithelial-mesenchymal transition in breast and lung cancer (Zhao et al., 2015; Wu et al., 2018). The role of NgBR in the development of resistance to chemotherapy in HCC and breast cancer is clear, but whether NgBR can affect the development of sorafenib resistance has not been reported.

In this study, we investigated the correlation between NgBR and sorafenib resistance in HCC. To examine the correlation between sorafenib resistance and NgBR, we developed a sorafenib-resistant HCC cell line for *in vitro* studies. All sorafenib-resistant liver cancer cells showed strong propagation and reduced apoptosis in the presence of sorafenib. Additionally, NgBR was overexpressed in sorafenib-resistant cells, and sorafenib promoted NgBR expression in sorafenib-resistant liver cancer cells in a dose-dependent fashion. To study the role of NgBR in developing resistance to sorafenib, we knocked down NgBR in sorafenib-resistant cells. Sorafenib sensitivity increased in HepG2-SR knockdown cells, but not in mock-treated HepG2-SR cells. Then, we overexpressed NgBR in HCC parent cells and found that NgBR overexpression accounted for the observed sorafenib resistance in HCC. Therefore, we concluded that NgBR expression in sorafenib-resistant cells was correlated with resistance to sorafenib.

According to previous studies, artesunate can promote apoptosis and inhibit the propagation of sorafenib-resistant liver cancer cells. We speculated that artesunate functioned through inhibiting NgBR. Time and concentration-dependent studies confirmed that artesunate can inhibit the NgBR expression in sorafenib-resistant liver cancer cells.

Artesunate prevented the progression of sorafenib resistance in liver cancer cells by inhibiting NgBR expression, suggesting that artesunate, in combination with sorafenib, can increase the sensitivity of liver tumor cells to sorafenib. This study confirmed that artesunate can enhance the sensitivity of liver cancer cells to sorafenib both *in vivo* and *in vitro*. HepG2 cells overexpressing NgBR and HepG2-SR cells with downregulated NgBR were treated with different concentrations of sorafenib alone or in combination with artesunate. We found that artesunate can only effectively inhibit cell proliferation in NgBR overexpressing cells. This indicates that artesunate enhances the sensitivity of liver cancer cells to sorafenib by inhibiting the NgBR expression.

In a previous study, Gao et al. discovered that increased NgBR can enhance EGF-stimulated Ras activation and phosphorylation of AKT

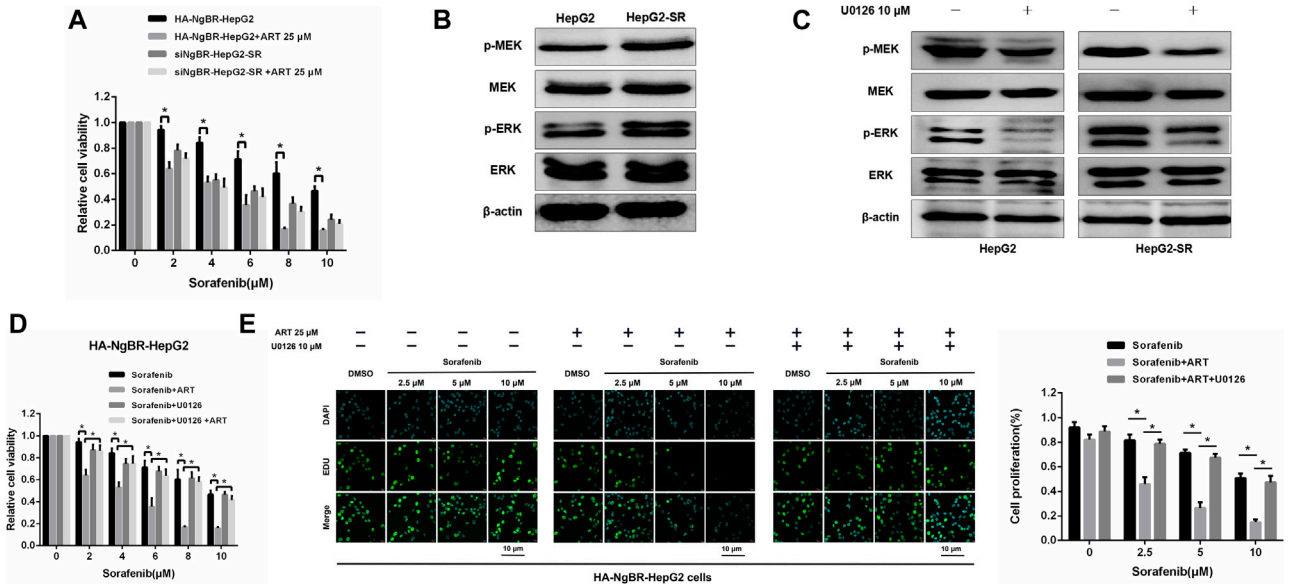


**FIGURE 6 |** Artesunate (ART) overcomes NgBR-induced sorafenib resistance by suppressing the MEK/ERK pathway. **(A)**. MTT assay detected proliferation in HepG2-SR cells with NgBR downregulation and HepG2 cells with NgBR overexpression after treatment with sorafenib alone or in combination with artesunate. **(B)**. Phosphorylation levels of MEK (p-MEK) and ERK (p-ERK) in HepG2 and HepG2-SR cells were detected by western blot. **(C)**. HepG2 and HepG2-SR cells were treated with 10 μm U0126 for 7 days to inhibit p-MEK and p-ERK. Western blot was used to determine inhibition efficiency. **(D)**. HepG2 cells with NgBR overexpression were treated with 10 μm U0126 for 7 days, and MTT assays were used to detect the artesunate-induced sorafenib sensitization. **(E)**. EDU assays were used to detect the proliferation in HepG2 cells overexpressing NgBR and treated with 10 μm U0126 for 7 days. Scale bars, 10 μm. Experiments were repeated three times and data are presented as means ± standard deviation (SD). Student's *t*-test was used for data analysis. $^*p < 0.05$

and ERK in tamoxifen-resistant breast cancer cells (Gao et al., 2018). Moreover, NgBR expression is associated with non-small cell lung cancer (NSCLC) development and increases Snail 1 expression in NSCLC cells by MEK/ERK pathway activation (Wu.et al., 2018). We examined the MRK/ERK pathway using western blot analysis. NgBR expression was positively correlated with the activation of phosphorylated MEK, confirming that the MEK/ERK pathway was significantly upstream in HepG2-SR cells. U0126-EtOH, a highly selective MEK1/2 inhibitor, was used to treat NgBR overexpressing HepG2 cells for 7 days. Compared to the non-treated U0126-EtOH group, the effects of artesunate-induced sorafenib sensitivity were inhibited by the MEK1/2 inhibitor. This result indicates that NgBR promotes HepG2 cell proliferation and survival through MEK/ERK pathway activation, and that artesunate can overcome NgBR-induced sorafenib resistance by suppressing the MEK/ERK pathway. The main limitation of this study is that it does not investigate the specific mechanism through which artesunate inhibits NgBR to increase the sensitivity of liver cancer cells to sorafenib. Thus, further studies focusing on the specific mechanism should be performed.

Taken together, the results of the current study demonstrate that NgBR is highly expressed in sorafenib-resistant HCC cells. NgBR is a functional marker that is essential for sorafenib resistance via activation of the MEK/ERK pathway. Artesunate can increase liver cancer cell sensitivity to sorafenib via inhibition of NgBR. Thus, targeting NgBR with a combination of artesunate and sorafenib can effectively overcome sorafenib resistance in HCC cells.

## DATA AVAILABILITY STATEMENT

The original contributions presented in the study are included in the article/Supplementary Material, further inquiries can be directed to the corresponding author.

## AUTHOR CONTRIBUTIONS

WH and XH contributed equally to this work. RS and YL designed the study. YW, NA, and XH performed the experiments and analyzed most of the data. WH contributed to data acquisition. BB assisted with manuscript writing and editing. All authors have read and approved the final manuscript.

## FUNDING

This work was supported by grants from the Natural Science Foundation of Liaoning Province, China (2019-ZD-0606).

## REFERENCES


Al-Salama, Z. T., Syed, Y. Y., and Scott, L. J. 2019). Lenvatinib: a review in hepatocellular carcinoma. *Drugs* 79 (6), 665–674. doi:10.1007/s40265-019-01116-x

Díaz-González, Á., Sanduzzi-Zamparelli, M., da Fonseca, L. G., Di Costanzo, G. G., Alves, R., Iavarone, M., et al. (2020). International and multicenter real-world study of sorafenib-treated patients with hepatocellular carcinoma under dialysis. *Liver Int.* 40 (6), 1467–1476. doi:10.1111/liv.14436

Duff, M. O., Olson, S., Wei, X., Garrett, S. C., Osman, A., Bolisetty, M., et al. (2015). Genome-wide identification of zero nucleotide recursive splicing in *Drosophila*. *Nature* 521 (7552), 376–379. doi:10.1038/nature14475

Fukui, N., Golabi, P., Otgonsuren, M., de Avila, L., Bush, H., and Younossi, Z. M. (2018). Hospice care in Medicare patients with primary liver cancer: the impact on resource utilisation and mortality. *Aliment. Pharmacol. Ther.* 47 (5), 680–688. doi:10.1111/apt.14484

Gao, P., Wang, X., Jin, Y., Hu, W., Duan, Y., Shi, A., et al. (2018). Nogo-B receptor increases the resistance to tamoxifen in estrogen receptor-positive breast cancer cells. *Breast Cancer Res.* 20 (1), 112. doi:10.1186/s13058-018-1028-5

Ghousein, A., Mosca, N., Cartier, F., Charpentier, J., Dupuy, J. W., Raymond, A. A., et al. (2020). miR-4510 blocks hepatocellular carcinoma development through RAF1 targeting and RAS/RAF/MEK/ERK signalling inactivation. *Liver Int.* 40 (1), 240–251. doi:10.1111/liv.14276

Gramantieri, L., Pollutri, D., Gagliardi, M., Giovannini, C., Quarta, S., Ferracin, M., et al. (2020). MiR-30e-3p influences tumor phenotype through MDM2/TP53 *Axis* and predicts sorafenib resistance in hepatocellular carcinoma. *Cancer Res.* 80 (8), 1720–1734. doi:10.1158/0008-5472.CAN-19-0472

Hashiba, T., Yamashita, T., Okada, H., Nio, K., Hayashi, T., Asahina, Y., et al. (2020). Inactivation of transcriptional repressor capicua confers sorafenib resistance in human hepatocellular carcinoma. *Cell Mol. Gastroenterol. Hepatol.* 10 (2), 269–285. doi:10.1016/j.jcmgh.2020.02.009

Ji, P., Huang, H., Yuan, S., Wang, L., Wang, S., Chen, Y., et al. (2019). ROS-mediated apoptosis and anticancer effect achieved by artesunate and auxiliary Fe(II) released from ferriferous oxide-containing recombinant apoferritin. *Adv. Healthc. Mater.* 8 (23), e1900911. doi:10.1002/adhm.201900911

Josephson, A., Trifunovski, A., Widmer, H. R., Widenfalk, J., Olson, L., and Spenger, C. (2002). Nogo-receptor gene activity: cellular localization and developmental regulation of mRNA in mice and humans. *J. Comp. Neurol.* 453 (3), 292–304. doi:10.1002/cne.10408

Li, Q., Qi, B., Oka, K., Shimakage, M., Yoshioka, N., Inoue, H., et al. (2001). Link of a new type of apoptosis-inducing gene ASY/Nogo-B to human cancer. *Oncogene* 20 (30), 3929–3936. doi:10.1038/sj.onc.1204536

Liang, Y. K., Zeng, D., Xiao, Y. S., Wu, Y., Ouyang, Y. X., Chen, M., et al. (2017). MCAM/CD146 promotes tamoxifen resistance in breast cancer cells through induction of epithelial-mesenchymal transition, decreased ERα expression and AKT activation. *Cancer Lett.* 386, 65–76. doi:10.1016/j.canlet.2016.11.004

Long, S. L., Li, Y. K., Xie, Y. J., Long, Z. F., Shi, J. F., Mo, Z. C., et al. (2017). Neurite outgrowth inhibitor B receptor: a versatile receptor with multiple functions and actions. *DNA Cell Biol.* 36 (12), 1142–1150. doi:10.1089/dna.2017.3813

Oertle, T., Huber, C., van der Putten, H., and Schwab, M. E. (2003). Genomic structure and functional characterisation of the promoters of human and mouse nogo/rtn4. *J. Mol. Biol.* 325 (2), 299–323. doi:10.1016/s0022-2836(02)01179-8

Oertle, T., and Schwab, M. E. (2003). Nogo and its paRTNers. *Trends Cell Biol.* 13 (4), 187–194. doi:10.1016/s0962-8924(03)00035-7

Rudalska, R., Dauch, D., Longerich, T., McJunkin, K., Wuestefeld, T., Kang, T. W., et al. (2014). *In vivo* RNAi screening identifies a mechanism of sorafenib resistance in liver cancer. *Nat. Med.* 20 (10), 1138–1146. doi:10.1038/nm.3679

Schweigreiter, R., Stasyk, T., Contarini, I., Frauscher, S., Oertle, T., Klimaschewski, L., et al. (2007). Phosphorylation-regulated cleavage of the reticulon protein Nogo-B by caspase-7 at a noncanonical recognition site. *Proteomics* 7 (24), 4457–4467. doi:10.1002/pmic.200700499

Sung, Y. C., Liu, Y. C., Chao, P. H., Chang, C. C., Jin, P. R., Lin, T. T., et al. (2018). Combined delivery of sorafenib and a MEK inhibitor using CXCR4-targeted nanoparticles reduces hepatic fibrosis and prevents tumor development. *Theranostics* 8 (4), 894–905. doi:10.7150/thno.21168

Teng, F. Y., and Tang, B. L. (2013). Nogo/RTN4 isoforms and RTN3 expression protect SH-SY5Y cells against multiple death insults. *Mol. Cell. Biochem.* 384 (1-2), 7–19. doi:10.1007/s11010-013-1776-6

Wang, B., Zhao, B., North, P., Kong, A., Huang, J., Miao, Q. R., et al. (2013). Expression of NgBR is highly associated with estrogen receptor alpha and surviving in breast cancer. *PloS One* 8 (11), e78083. doi:10.1371/journal.pone.0078083.e

Wang, H., Xu, H., Ma, F., Zhan, M., Yang, X., Hua, S., et al. (2020). Zinc finger protein 703 induces EMT and sorafenib resistance in hepatocellular carcinoma by transactivating CLDN4 expression. *Cell Death Dis.* 11 (4), 225. doi:10.1038/s41419-020-2422-3

Wu, D., Zhao, B., Qi, X., Peng, F., Fu, H., Chi, X., et al. (2018). Nogo-B receptor promotes epithelial-mesenchymal transition in non-small cell lung cancer cells through the Ras/ERK/Snail1 pathway. *Cancer Lett.* 418, 135–146. doi:10.1016/j.canlet.2018.01.030

Yao, X., Zhao, C.-r., Yin, H., Wang, K., and Gao, J.-j. (2020). Synergistic antitumor activity of sorafenib and artesunate in hepatocellular carcinoma cells. *Acta Pharmacol. Sin.* 41, 1609–1620. doi:10.1038/s41401-020-0395-5

Ye, R. R., Peng, W., Chen, B. C., Jiang, N., Chen, X. Q., Mao, Z. W., et al. (2020). Mitochondria-targeted artesunate conjugated cyclometalated iridium(iii) complexes as potent anti-HepG2 hepatocellular carcinoma agents. *Metallomics* 12 (7), 1131–1141. doi:10.1039/d0mt00060d

Zhang, S., Gao, W., Tang, J., Zhang, H., Zhou, Y., Liu, J., et al. (2020). The roles of GSK-3β in regulation of retinoid signaling and sorafenib treatment response in hepatocellular carcinoma. *Theranostics* 10 (3), 1230–1244. doi:10.7150/thno.38711

Zhang, S., Yuan, H., Guo, Y., Wang, K., Wang, X., and Guo, Z. (2018). Towards rational design of RAD51-targeting prodrugs: platinum IV-artesunate conjugates with enhanced cytotoxicity against BRCA-proficient ovarian and breast cancer cells. *Chem. Commun.* 54 (83), 11717–11720. doi:10.1039/c8cc06576d

Zhao, B., Hu, W., Kumar, S., Gonyo, P., Rana, U., Liu, Z., et al. (2017). The Nogo-B receptor promotes Ras plasma membrane localization and activation. *Oncogene* 36 (24), 3406–3416. doi:10.1038/onc.2016.484

Zhao, B., Xu, B., Hu, W., Song, C., Wang, F., Liu, Z., et al. (2015). Comprehensive proteome quantification reveals NgBR as a new regulator for epithelial-mesenchymal transition of breast tumor cells. *J. Proteomics.* 112, 38–52. doi:10.1016/j.jprot.2014.08.007


**Conflict of Interest:** The authors declare that the research was conducted in the absence of any commercial or financial relationships that could be construed as a potential conflict of interest.

frontiers in Oncology

ORIGINAL RESEARCH
published: 25 February 2021
doi: 10.3389/fonc.2021.590764

# Modulated Electro-Hyperthermia Facilitates NK-Cell Infiltration and Growth Arrest of Human A2058 Melanoma in a Xenograft Model

*Tamás Vancsik[1], Domokos Máthé[2], Ildikó Horváth[2], Anett Anna Várallyaly[3], Anett Benedek[3], Ralf Bergmann[2], Tibor Krenács[1], Zoltán Benyó[3] and Andrea Balogh[3]**

[1] 1st Department of Pathology and Experimental Cancer Research, Semmelweis University, Budapest, Hungary, [2] Department of Biophysics and Radiation Biology, Semmelweis University, Budapest, Hungary, [3] Institute of Translational Medicine, Semmelweis University, Budapest, Hungary

OPEN ACCESS

**Edited by:**
Xiaoping Lin,
Sun Yat-sen University Cancer Center (SYSUCC), China

**Reviewed by:**
Ana Stojanovic, Heidelberg University, Germany
Maxim Shevtsov, Technical University of Munich, Germany

***Correspondence:**
Andrea Balogh
balogh.andrea@med.semmelweis-univ.hu

**Specialty section:**
This article was submitted to Pharmacology of Anti-Cancer Drugs, a section of the journal Frontiers in Oncology

**Received:** 02 August 2020
**Accepted:** 13 January 2021
**Published:** 25 February 2021

**Citation:**
Vancsik T, Máthé D, Horváth I, Várallyaly AA, Benedek A, Bergmann R, Krenács T, Benyó Z and Balogh A (2021) Modulated Electro-Hyperthermia Facilitates NK-Cell Infiltration and Growth Arrest of Human A2058 Melanoma in a Xenograft Model. Front. Oncol. 11:590764. doi: 10.3389/fonc.2021.590764

Modulated electro-hyperthermia (mEHT), induced by 13.56 MHz radiofrequency, has been demonstrated both in preclinical and clinical studies to efficiently induce tumor damage and complement other treatment modalities. Here, we used a mouse xenograft model of human melanoma (A2058) to test mEHT (~42°C) both alone and combined with NK-cell immunotherapy. A single 30 min shot of mEHT resulted in significant tumor damage due to induced stress, marked by high hsp70 expression followed by significant upregulation of cleaved/activated caspase-3 and p53. When mEHT was combined with either primary human NK cells or the IL-2 independent NK-92MI cell line injected subcutaneously, the accumulation of NK cells was observed at the mEHT pretreated melanoma nodules but not at the untreated controls. mEHT induced the upregulation of the chemoattractant CXCL11 and increased the expression of the matrix metalloproteinase MMP2 which could account for the NK-cell attraction into the treated melanoma. In conclusion, mEHT monotherapy of melanoma xenograft tumors induced irreversible heat and cell stress leading to caspase dependent apoptosis to be driven by p53. mEHT could support the intratumoral attraction of distantly injected NK-cells, contributed by CXCL11 and MMP2 upregulation, resulting in an additive tumor destruction and growth inhibition. Therefore, mEHT may offer itself as a good partner for immunotherapy.

**Keywords: melanoma, hyperthermia, immunotherapy, NK-cell infiltration, tumor damage**

## INTRODUCTION

Modulated electro-hyperthermia (mEHT) is an effective and safe form of hyperthermia, which aims at selective heating of the extracellular matrix and cell membranes in the malignant tissues rather than homogenous heat delivery into tumors (1). The benefits of mEHT as a complementary therapy relies in its property to induce tumor-damage by direct cell killing, mediated by irreversible heat and cell stress and its tolerability by patients as it has almost no side-effects. In the recent years numerous

papers have described the growth inhibiting effect of mEHT in various tumor types, mostly in preclinical mouse models (2–6). These results provide evidence that besides the direct cell killing, mEHT has an immunomodulatory effect supporting the anti-tumor immune response (3, 4, 7). In the clinical setting, several case studies have revealed beneficial effects of mEHT (8, 9) including the on-going clinical phase studies which are expected to provide more details on the advantages of combining mEHT with radio- and chemotherapy (10). However, despite evidence supporting the rationale of hyperthermia for augmenting immunotherapy in pre-clinical models, these has not been implemented into the clinical practice (11). Natural killer (NK) cell therapy represents a promising novel treatment modality for both hematological malignancies and solid tumors (12). The cytotoxic activity of the NK cells is independent of tumor antigens, they are tolerant to cells expressing human leukocyte antigen class I (HLA class I) ligands but trigger cytotoxicity against altered cells of reduced HLA-I expression and, due to their short lifetime, the side effects of NK cell immunotherapy are negligible. Clinical trials have been performed with either primary NK cells derived from peripheral blood mononuclear cells (PBMCs) or commercially available clonal NK cell lines, which are easy to expand and maintain *in vitro* (12). The therapeutic outcomes of the adoptive transfer of NK cells was successful mainly in hematological malignancies, while in the case of solid tumors it has been disappointing due to impaired trafficking, infiltration and the immunosuppressive environment of the tumors (13). Several strategies have been proposed to overcome these obstacles and to augment NK cell activity in solid tumors (14). The treatment of NK cells with IL-15 helped to maintain anti-tumor activities in the context of an immunosuppressive microenvironment compared with IL-2 treated NK cells (15). Arming of NK cells with additional CXCR receptors to facilitate their migration toward various cytokine producing tumors (16) or engineering NK-92 cells to express T-cell receptors with tumor antigen specificity have also been proposed as promising strategies in different tumor models (17). In a recent study Yang et al. has reported that the focused ultrasound enhanced the accumulation of NK cells in ovarian cancer xenograft mainly by inducing CX3CL1 expression (18).

The effect of hyperthermia on NK cell mediated anti-tumor response has been extensively studied and reviewed (19). While the *in vitro* hyperthermia diminished the viability and cytotoxic activity of isolated NK cells (19, 20), *in vivo* treatment supported NK cell activity in several tumor models including the very first report about whole body hyperthermia on NK cell cytotoxicity in a patient treated for Ewing's sarcoma. Hyperthermia was shown to restore and enhance the NK cell activity possibly *via* inducing supportive interferon production (21). Ostberg et al. demonstrated that besides the NK activating pyrogenic cytokines (TNF-α, IFN-γ) secreted during hyperthermia, another possible mechanism behind enhanced NK cell cytotoxicity by fever range thermal stress is associated with plasma membrane NKG2D clustering and increased expression of MICA on target cells (22). Multhoff et al. reported recently that hyperthermia-induced hsp70 promoted NK cell activation, when used in combination with PD-1 inhibition, significantly increased the overall survival in preclinical models of glioblastoma and lung cancer (23, 24). The effectiveness of hyperthermia in melanoma treatment was demonstrated by us and others in several preclinical models (2, 25). Regarding its clinical application Overgard et al. reported that in a phase III clinical trial hyperthermia augmented significantly the fractionated radiotherapy (26).

In the present study we aimed at elucidating the effect of mEHT on A2058 human melanoma xenografts combined with adoptive transfer of primary or immortalized human NK-92MI cells. We demonstrate that mEHT, besides its tumor growth inhibiting effect, augments NK cell infiltration into the treated tumors and thus, it is a promising strategy to enhance the effectiveness of adoptive NK cell transfer.

# MATERIAL AND METHODS

## Cell Culture

A2058 human melanoma cell line originated from the American Type Culture Collection (ATCC; Rockville, MD, USA), a kind gift of Gabor Tigyi, Department of Physiology, UTHSC, Memphis) was maintained in DMEM with 10% fetal bovine serum in a humidified incubator with 5% $CO_2$ at 37°C. Primary human NK cells were isolated from PBMCs of a healthy donor by a density gradient with Ficoll-Paque Plus (Sigma-Aldrich; St. Louis, MO, USA) followed by purification using an NK cell isolation kit (Miltenyi Biotec; Teterow, Germany). Purified NK cells were expanded during 7 days in NK MACS medium (Miltenyi Biotec) supplemented with 2% human serum (Sigma-Aldrich) and 500 U of IL-2 (Miltenyi Biotec) under standard culture conditions in a humidified incubator. NK-92MI cell line purchased from ATCC was grown in NK MACS medium supplemented with 2% human serum and 10 U of IL-2. Cell staining of the NK cells for *in vivo* tracing was done with CellTrace Far Red Cell Proliferation Kit (Thermo Fisher Scientific; Waltham, MA, USA) as described by the manufacturer. For the co-culture experiments A2058 melanoma cells were plated in 12-well plates at 1 x $10^5$/ml in the culture medium described above. Next day graded doses of human primary NK cells were added to A2058 culture to reach the following ratio of 1:0, 1:0.25, 1:0.5, and 1:1 melanoma: NK cell and cultured for two h. Phase contrast microscopy images were taken with the Nikon TI2E microscope using the 20X objective.

## *In Vitro* mEHT Treatment

Sub-confluent cell-cultures were resuspended in fresh medium at $1 \times 10^6$ cells/ml density, then 1.5 ml cell suspension was used for each experimental group. Normothermic controls were treated in water bath for 30 min at 37°C, while 42°C treatment of mEHT was performed between two plan-parallel electric condenser plates using the Lab-EHY 100 device (Oncotherm Ltd; Budaörs, Hungary). Right after the treatment cells were cultured for 24 h at 1 x $10^6$ in a 60 mm diameter Petri dish or at $1.25 \times 10^5$ cells/well in a 6 well plate for RNA isolation or flow cytometry respectively.

## Quantitative RT-PCR

Total RNA was extracted 24 h after treatment of tumor cells using the NucleoSpin RNA Plus XS (Macherey-Nagel GmbH & Co. KG; Düren, Germany). Complementary DNA (cDNA) synthesis was done with RevertAid First Standard cDNA Synthesis Kit (Thermo Scientific). The primer sets used were as follows: RPS13 Fwd: CGAAAGCATCTTGAGAGGAACA, Rev: TCGAGCCAAAC GGTGAATC, CXCL-9 Fwd: AGTGCAAGGAACCCCAGTAG, Rev: AGGGCTTGGGGCAAATTGTT, CXCL-10 Fwd: AGCAG AGGAACCTCCAGTCT, Rev: AGGTACTCCTTGAAT GCCACT, CXCL-11 Fwd: GAGTGTGAAGGGCATGGCTA and Rev: ACATGGGGAAGCCTTGAACA (Merck KGaA; Darmstadt, Germany). Quantitative real-time PCR was performed with CFX Connect Real-Time PCR Detection System (Bio-Rad; California, USA) using the SsoAdvanced Universal SYBR Green Supermix (Bio-Rad). RPS13 was used as internal control, and the fold change in expression was calculated as $2^{-\Delta\Delta CT}$.

## Flow Cytometry

Dying cell fractions were identified and measured by flow cytometry. 24 h post-treatment the supernatants were collected and cells were trypsinized, then placed on ice for all further steps. The suspensions were centrifuged for 5 min at 300 × g, washed twice in PBS and resuspended in Annexin V Binding Buffer at a concentration of $1 \times 10^6$ cells/ml. To 100 µl of cell suspension 2.5 µl Alexa Fluor® 647 Annexin V stock solution (Biolegend; San Diego, CA, USA) and 1 µl of 1 mg/ml propidium-iodide (Sigma-Aldrich) was added. Samples were incubated in dark on ice for 20 min, then further diluted with 200 µl Annexin V Binding Buffer (Biolegend) and measured by flow cytometry. 638 nm wavelength excitation laser was used for Alexa Fluor® 647 Annexin V and 488 nm for PI fluorochrome. Based on its low forward and side scatter (FSC/SSC) properties, cell debris was excluded from the measurement, where $2 \times 10^4$ events per sample were counted by using flow cytometry (CytoFLEX Flow cytometer, Beckman Coulter Life Sciences; Indianapolis, USA). Obtained data were analyzed with CytExpertCell software (Beckman Coulter Life Science). For granzyme B detection primary NK cells were stained with FITC-labeled anti-human/mouse granzyme B antibody (#505403, Biolegend) according to the manufacturer's protocol. Cells were measured using 488 nm blue laser excitation wavelength and 525/40 nm bandpass filter for detection.

## *In Vivo* mEHT Treatment Model and *In Vivo* Imaging

The A2058 tumor cell suspension (1 million cells/100 µl) was inoculated subcutaneously into both flanks of NOD.CB-17-Prkdc scid/Rj mice (Janvier Labs; Le Genest-Saint-Isle, France). Depending on the follow-up timepoint different tumor sizes were used. When mice were sacrificed 24 post-treatment in order to characterize the early stress response, the tumors were treated when having 10 mm diameter while when the animals were used for 4-day follow-up the xenografts had 5-6 mm diameter (0.1–0.15 $cm^3$ volume).

Once the tumor had reached the desired volume, the right-side tumors were subjected to mEHT or sham treatment and the left-side ones were left untreated and used as controls. The mEHT treatment was performed as described before (2) by using the Lab-EHY 100 device (Oncotherm Ltd, Budaörs, Hungary). In the sham-treated mice the right-side tumors were placed between the electrodes and exposed to the same physical force like the treated ones. Tumor growth was monitored with ultrasound measurement (Philips Sonos 5500 Ultrasound; Amsterdam, Netherlands). Whole body imaging was performed to detect far red fluorescence with the fluorescent optical imaging system FOBI (CELLGENTEK Co., Ltd., Suwon, South Korea). Images were analyzed using VivoQuant software (inviCRO, LLC; Boston, USA). All animal work conducted during this study was approved by the Hungarian National Scientific Ethical Committee on Animal Experimentation under No.PE/EA/51-2/2019.

## Immunohistochemistry

Tumors were fixed in 4°C buffered 8% formalin for 48 h, dehydrated and embedded into paraffin wax. Then, 3 µm thick sections were cut, dewaxed and rehydrated prior to hematoxylin-eosin (H & E) staining or immunohistochemistry (IHC). Endogenous peroxidase activity was blocked for 15 min in methanol containing 3% $H_2O_2$. For antigen retrieval, rehydrated sections were heated at ~105°C in Tris-EDTA (TE) buffer pH 9.0 (0.1 M Trisbase and 0.01 M EDTA) for 20 min in a pressure cooker (2100 Antigen Retrieval, Aptum Biologics Ltd.; Southampton, United Kingdom) followed by 20 min cooling. After blocking non-specific protein-binding sites in 0.1 M Tris-buffered saline (TBS, pH7.4) containing 3% bovine serum albumin (BSA, Millipore; Kankakee, Illinois, USA), 0.1% TWEEN® 20 (Sigma-Aldrich) and 0,01% sodium-azide (BSA/TBST) for 20 min, slides were incubated in a humidity chamber at room temperature using antibodies (listed in **Table 1**) diluted in 1% BSA/TBST. HISTOLS® Labeled polymer-peroxidase (anti-rabbit Ig) detection system (Histopathology Ltd.; Hungary) was applied for rabbit monoclonal antibodies (mAbs) with an additional preliminary incubation step using rabbit anti-mouse Ig for mouse mAbs, for 40 min each. For the immunoperoxidase development a DAB chromogen/hydrogen peroxide kit (Leica-NovoCastra; Newcastle Up-on-Tyne, UK) was used. Samples were washed for 3 × 3 min in

**TABLE 1** | Antibodies and conditions used for immunohistochemistry and immunofluorescence.

| Antigen | Type | Reference no. | Dilution | Vendor |
|---|---|---|---|---|
| cC-3 | Rabbit, pAb | #9664 | 1:100 | Cell Signaling |
| Hsp70 | Rabbit, pAb | #4872 | 1:50 | Cell Signaling |
| CD57 | Mouse, mAb | #MAD-002084QD–7 | RTU | Master Diagnóstica |
| MMP-2 | Rabbit, pAb | # RB-9233-PO | 1:50 | Neomarkers |
| p53 | Mouse, mAb | #BP-53-12 | RTU | Genemed |
| p21 | Rabbit, mAB | #188224 | 1:500 | Abcam |
| AIF | Rabbit, pAb | #4642 | 1:25 | Cell Signaling |

*Vendor specification: Cell Signaling (Danvers, MA, USA), Neomarkers (Portsmouth, NH, USA), Genemed Biotechnologies, Inc. (San Francisco, CA, USA), Master Diagnóstica (Granada, Spain), Novus Biologicals (Centennial, CO, USA).*

TBST (pH 7.4) buffer between the incubations. Stained slides were digitalized and the immunoreactions were evaluated using modules of QuantCenter image-analysis software package (3DHISTECH; Budapest, Hungary). Positive immunoreactions for cleaved caspase-3, hsp70, p53, MMP-2, was determined as percentages within annotated tumor areas (HistoQuant module). In case of cleaved caspase-3 (cC-3), hsp70, p53, p21, and AIF the late apoptotic areas which might be lysed by metalloproteases, were excluded from the evaluation. For p53 and p21 evaluation nuclei with strong positive reaction were masked and calculated its area compared to the whole tumor area.

## Statistical Analysis

Statistical analysis was performed using GraphPad Prism software (v.6.07; GraphPad Software Inc.; La Jolla, CA, USA). Statistical significance between groups during the tumor growth follow-up was calculated using two-way ANOVA followed by Tukey's multiple comparisons. Mann–Whitney nonparametric test was performed for statistical comparison between treated and control groups. In experiments with more than two groups, statistical differences were assessed with ANOVA accompanied by Tukey's or Sidak's multiple comparisons test. p-values < 0.05 were considered significant.

# RESULTS

## mEHT Inhibits A2058 Melanoma Tumor Growth

To examine the effect of mEHT on A2058 melanoma, we have exposed established tumors to a single mEHT or sham treatment lasting for 30 min and monitored the tumor growth up to day four by using ultrasound. Mice were divided in two groups. In one group symmetrically grown tumors were either treated with mEHT or left untreated. In the other group, tumors were sham treated or left untreated. We found that already a single mEHT treatment had a marked effect on tumor growth. There was a significant difference manifested on the third- and fourth-day post treatment both between the mEHT-treated and its untreated counterpart (p=0.006) and also between mEHT-treated and the sham-treated tumors (p=0.01). There was no significant difference between the sham-treated and sham-untreated tumors at any timepoint (**Figure 1**).

## mEHT Activates p53 and Induces Caspase-3 Dependent Cell Death

Histological analysis of the tumors 24 h after a single mEHT treatment showed massive cell death in the treated side (**Figure 2A**). While in the non-treated tumors the percentage of the dead area is negligible, in the treated ones it reached 40% (*p=0.02). The cellular stress induced by mEHT was accompanied by abundant hsp70 expression which doubled one day post-treatment (*p=0.02) (**Figure 2B**).

In order to elucidate the cell killing mechanism of mEHT in A2058 melanoma xenografts, we used immunohistochemistry

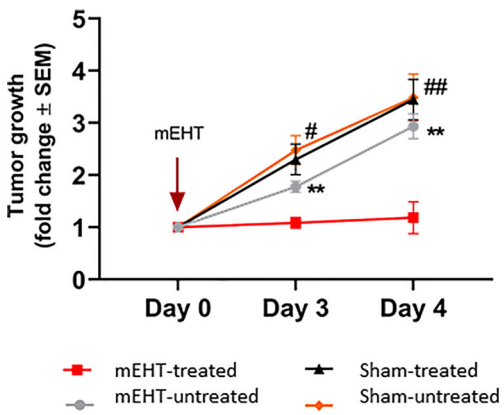


**FIGURE 1** | Tumor growth is arrested by modulated electro-hyperthermia (mEHT) treatment. N=6 for mEHT-treated and mEHT-untreated, n=5 for sham-treated and sham-untreated, **p=0.006 between mEHT-treated and untreated, #p=0.01 on day three and ##p=0.007 on day four between mEHT-treated and sham-untreated, *p=0.01 for mEHT and sham-treated on day three and four using two-way ANOVA followed by Tukey's multiple comparisons test.

(IHC) to detect the expression of several proteins involved in apoptosis. We reported before that mEHT stabilized and induced the nuclear translocation of p53 in B16F10 mouse melanoma cell line *in vitro* and *in vivo* (2). Regarding the p53 status, A2058 contains $TP53^{MUT}$ which is still functional as upon exposure to nutlin-3, the prototypic MDM2 antagonist, p53 increased and led to apoptosis (27). Using IHC we detected the expression level of p53 one day post-treatment. Our results demonstrate that in response to mEHT-induced stress the p53 protein level elevated and it was two-fold higher as compared to the non-treated, control side tumors (*p=0.02) (**Figure 3A**). Next, we investigated the expression of p21, the canonical p53 target gene, but it did not show any significant change (**Figure 3D**), which points to the fact that tumor cells at this timepoint (24 h post-treatment) are not in the cell cycle arrest phase but rather underwent apoptosis. To demonstrate this, we measured the level of cleaved caspase-3 and found that it was three times higher in the treated tumors compared to the non-treated counterparts (*p=0.02) (**Figure 3B**). It was shown before that mEHT could activate not only the caspase dependent but also the caspase independent apoptotic pathway characterized by high apoptosis inducing factor (AIF) expression (28). **Figure 3C** illustrates that in A2058, despite the fact that mEHT elicits significant increase of this protein, as its localization remains cytoplasmatic and not nuclear AIF is not contributing to mEHT-induced cellular death.

## mEHT Treatment Facilitates NK Cell Infiltration of Melanoma

We had reported previously that *in vivo* mEHT treatment causes downregulation of MHC-I expression in B16F10 mouse melanoma tumors (2). Our hypothesis was that this tumor phenotype was favorable to the cytotoxic activity of NK cells.

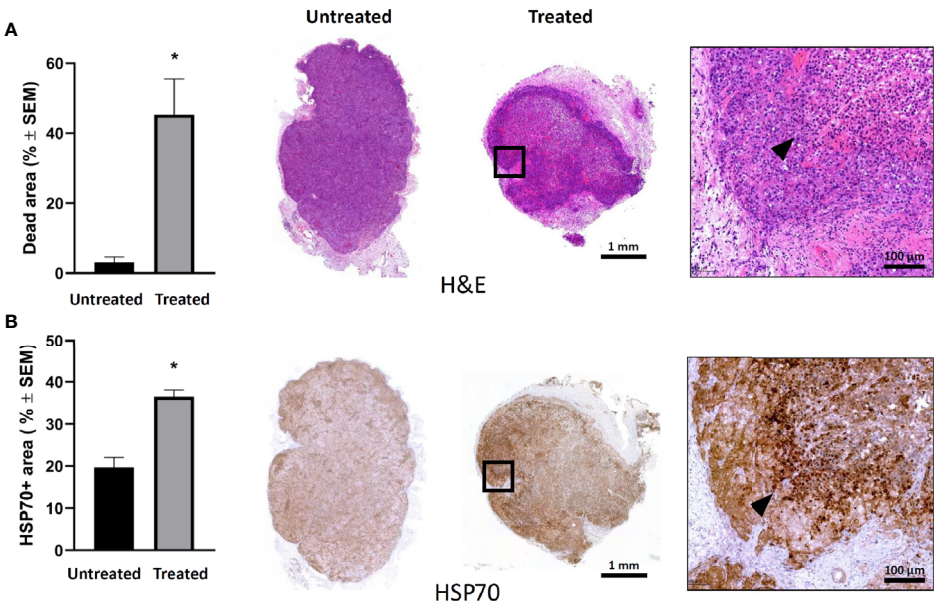


**FIGURE 2** | Modulated electro-hyperthermia (mEHT) monotherapy-induced cellular stress results in massive tumor destruction of established human A2058 xenografts**. (A)** Quantitative analysis and representative images of hematoxylin-eosin (H & E) staining reflecting live/death tumor areas of untreated and mEHT-treated tumors. **(B)** Heat stress response demonstrated by hsp70 expression. Arrowheads indicate characteristic staining of damaged tumor tissue and hsp70 expression in the mEHT-treated tumor sections. Samples were analyzed 24 h post-treatment, *p=0.02, n=4. Statistical significance was calculated using Mann-Whitney test.

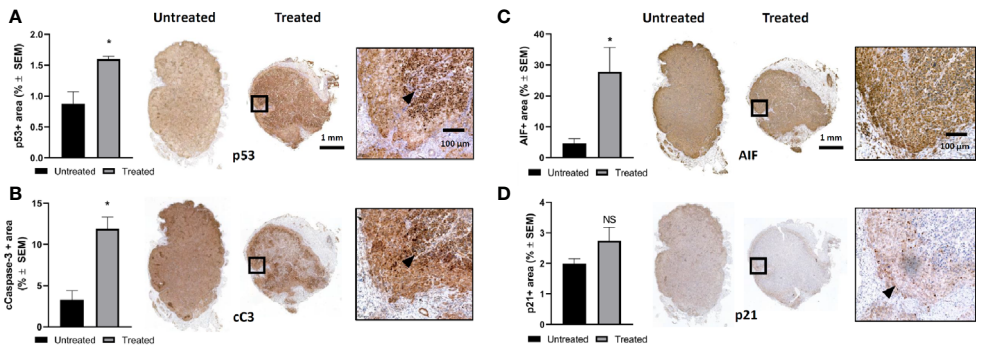


**FIGURE 3** | Modulated electro-hyperthermia (mEHT) treatment induces caspase dependent apoptosis *via* p53 activation in established human A2058 xenografts. **(A)** Quantitative analysis and representative images of immunostained tumor sections for p53, *p=0.02, n=4. **(B)** Cleaved caspase-3 (cC-3) *p=0.02, n=4. **(C)** AIF (apoptosis inducing factor) *p=0.04, n=6 and **(D)** D. p21 which is not significantly (NS) altered demonstrating that cellular senescence is not induced by mEHT. Arrowheads point to characteristic expression of the given protein on the mEHT treated tumor sections. Samples were analyzed 24 h post-treatment. Statistical significance was calculated using Mann-Whitney test.

Furthermore, the mEHT generated tumor microenvironment is rich in damage associated molecular pattern (DAMP) proteins (2–4), which are known to serve as chemoattractant to facilitate the recruitment of NK cells to the tumor site (4, 25). In the B16F10 mouse melanoma model we could not prove this unequivocally, at least not based on the frequency of the tumor infiltrating NK cells as there was no significant difference between the treated and control tumors. In order to address this question, we designed a different animal model, where we traced the distribution of *in vitro* expanded and fluorescently labeled primary NK cells or the immortalized NK-92MI cell line injected subcutaneously. Similar to the tumor growth model discussed above, we used mice implanted bilaterally and treated the right-side tumor only. One day after the mEHT treatment we injected the labeled NK cells at equal distance from both tumors subcutaneously above the lumbar region of the spine and traced their distribution daily using *in vivo*

imaging system. The fluorescence signal was detectable already on day one after NK cell injection and further intensified during the following days within the treated tumor (**Figures 4A, B**). The accumulation of NK cells was assessed based on the ratio of the fluorescence detected on day 0 and day 3 in untreated control and treated tumors. Measured signal on day three was significantly higher when mEHT was followed by adoptive NK cell transfer regardless of NK cell origin (**Figure 4E**), whereas in the untreated tumors low intensity was detected in the explanted tumors only (**Figures 4C, D**).

To characterize the cytotoxicity of the *ex vivo* expanded primary NK cells and the susceptibility of the A2058 melanoma cell line to NK cell killing we set up an *in vitro* co-culture of the two cell types by adding graded doses of NK cells to A2058 melanoma cells. The phase contrast microscopy images shown on **Figure 5A** demonstrate that our primary human NK cells are potent and strongly cytotoxic and as such they are capable of lysing the A2058 cells. Additionally, the granzyme B expression, what plays crucial role in the cytotoxic effect of the primary NK cells was also measured by flow cytometry and we found that 100% of the population stains positive for this specific marker (**Figure 5B**).

As we demonstrated above, based on the fluorescence signal intensity within *in vivo* conditions, the primary NK cells were able to sense and migrate toward the mEHT treated tumors. The intratumoral presence of the primary NK cells was further confirmed by immunostaining, using the NK specific CD57 marker (**Figure 5C**).

Next, we investigated the potential mechanism by which mEHT could enhance the migration of NK cells with respect to chemokines and MMP-2. The recruitment of NK cells in the inflamed tissues is regulated by the expression of several chemokine receptors, including CXCR3 that binds to the tumor-derived chemokine ligands (29). It has been shown that some of the inflammatory chemokines that recruit NK cells (CXCL9, CXCL10, CXCL11, and CXCL12) contain putative HSF1-binding sites and thus could be upregulated by thermal stress (30). To test whether mEHT can induce the expression of chemokines, we exposed A2058 cells to mEHT *in vitro* and measured the gene expression one day after treatment using qPCR. In order to confirm the effect of mEHT treatment first, we measured the extent of apoptosis using flow cytometry. As expected, mEHT was cytotoxic and resulted in a two-fold increase of the annexin V+ PI+ apoptotic population (*p=0.01) (**Figure 6A**). The qPCR result shows that mEHT had disparate effect on the tested chemokines as out of the three tested chemokines CXCL9 and CXCL10 were downregulated and CXCL11 was upregulated by thermal stress (*p=0.02) 24 h post-treatment (**Figure 6B**). Besides the chemoattractants, the migration of NK cells is determined by its ability to cross the ECM and

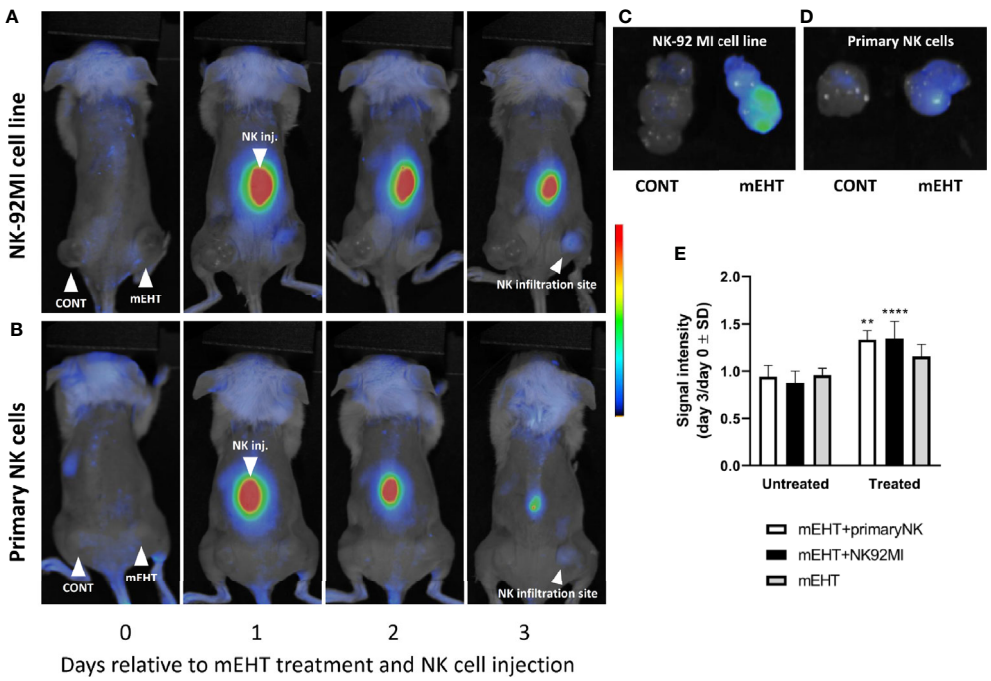


**FIGURE 4** | The modulated electro-hyperthermia (mEHT) treatment generated tumor microenvironment favors and permits NK infiltration of melanoma tumors regardless of natural killer (NK) cell origin. **(A, B)** *In vivo* imaging of tumor bearing mice with right side treated and left side control. Fluorescently labeled primary NK cells or NK92MI cells were injected subcutaneously one day post mEHT. *In vivo* imaging was done during 3 days to follow the NK cell trafficking. **(C, D)** Explanted control and mEHT-treated tumors infused by NK-92 MI or primary human NK cells. **(E)** Change of the signal intensity represented as ratio of the fluorescence detected on day 0 and day 3 in control and treated tumors infiltrated with fluorescent NK cells. Significance was calculated using two-way ANOVA followed by Sidak's multiple comparisons test. n=3 for untreated/treated + primary NK cells, n=6 for untreated/treated +NK92MI, n=5 for untreated/treated mEHT. *p between mEHT-untreated and treated counterparts; **p=0.001 for primary NK cell infused tumors, ****p<0.0001 for NK92MI cell line infiltrated tumors.

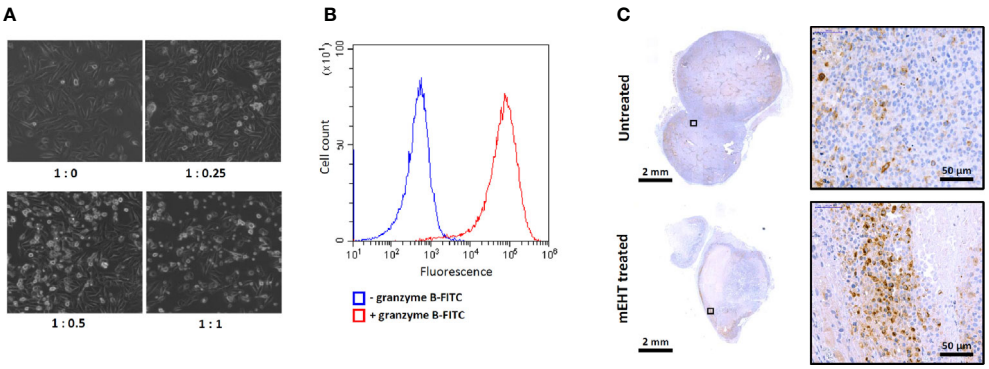


**FIGURE 5** | Characterization of ex vivo expanded primary NK cells. **(A)** Cytotoxic effect of primary NK cells and susceptibility of A2058 melanoma to natural killer (NK) cell killing demonstrated in co-culture. Graded doses of NK cells were added to A2058 culture in different ratios, phase contrast microscopy images were taken after 2 h of co-culture. Note the change in morphology of the melanoma culture from adherent to lysed, floating rounded dead cells in the presence of NK cells which indicates that tumor cells might have been eradicated by NK cells. **(B)** Flow cytometry analysis of granzyme B expression in primary NK cells. **(C)** Detection of CD57 positive primary NK-cells in modulated electro-hyperthermia (mEHT) treated and control tumors. Arrowheads emphasize the area where the average abundance of CD57+ marker can be seen on the control and an NK-infiltrated site of the mEHT samples.

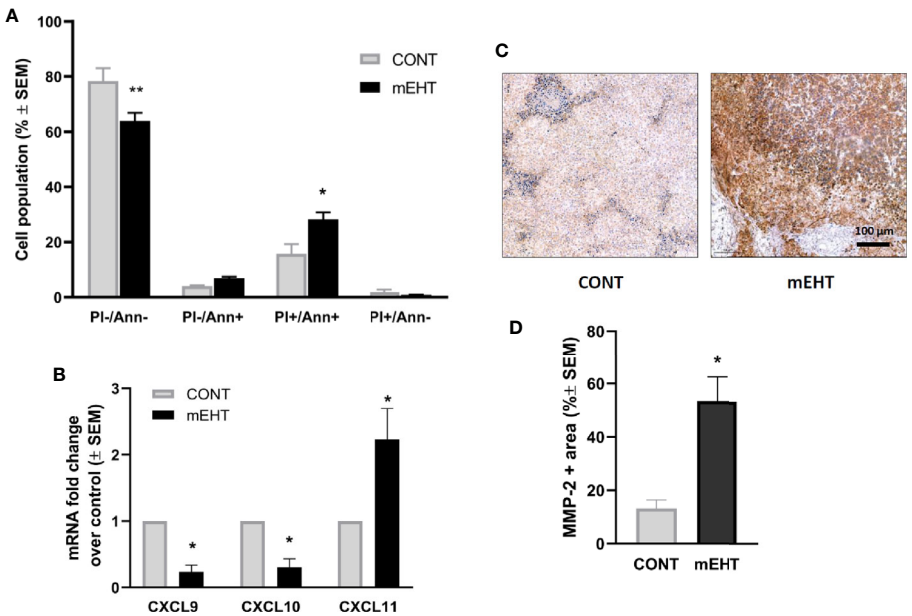


**FIGURE 6** | Tumor damage and the potential mechanism of natural killer (NK)-cell trafficking to modulated electro-hyperthermia (mEHT) treated melanoma. **(A)** *In vitro* mEHT treatment induces apoptosis of the A2058 cells marked by the elevated PI+/Ann+ population detected by flow-cytometry 24 h post-treatment, data shows the average of six experiments, *p=0.01, **p=0.003. **(B)** *In vitro* mEHT treatment regulates the expression of chemoattractants in A2058 cells detected by qPCR 24 h post-treatment, data shows the average of three experiments, *p=0.02 calculated with Mann-Whitney test. **(C, D)** mEHT upregulates MMP-2 expression detected by IHC 24 h post-treatment, n=4, *p=0.02 calculated with Mann-Whitney test.

basement membrane. These structures are degraded by MMPs produced by both the NK cells and the tumor cells. Using IHC we detected the MMP-2 protein expression and we show that one day after treatment the MMP-2 positive area was five times higher in the mEHT treated tumors as compared to the control group (*p=0.02) (**Figures 6C, D**).

## mEHT Induced Tumor Microenvironment Augments NK Cell Cytotoxic Activity

To assess the effect of combined mEHT and NK cell immunotherapy on tumor destruction, the explanted tumors were subjected to histology and immunostaining for cleaved caspase-3. Based on the H & E staining, both in the mEHT and

the mEHT combined with adoptive NK cell transfer cases, the treated tumors contain extensive damaged areas (**Figure 7A**). When the comparison was done between treated and untreated counterpart statistical significance was reached in each treatment group. The mEHT monotherapy resulted in massive cell death represented by 60% of the tumor area accounting for the strong statistical significance versus mEHT untreated ($^{\#}p < 0.0001$). The percentage of damaged tumor area escalated to almost 100% when the treatment was combined with the NK92MI cells and it was statistically significant not only when compared to its untreated counterpart ($^{\#}p < 0.0001$) but also versus monotherapy (***p=0.0007). When the primary NK cells were administered after the mEHT, we could not detect additive effect of the cell treatment versus the mEHT monotherapy (**Figure 7B**).

Next, we characterized more specifically the apoptotic response using cleaved caspase-3 staining (**Figure 8**). As expected, our findings correlate with the previous data: the caspase positive area is the highest in the mEHT+NK92MI treated group with statistical value of ***p=0.0005 between untreated and treated mEHT +NK92MI tumors. Strong cC-3 expression was detected also in the mEHT+primary NK cell-treated group, **p=0.003 between untreated mEHT+primary NK vs treated mEHT + primary NK cells, while no significant difference was noted in the mEHT treated/untreated groups.

## DISCUSSION

In a recently published paper, we described the effect of mEHT on B16F10, a mouse melanoma cell line, *in vitro* and *in vivo* (2, 31). The repeated mEHT treatment resulted in a delayed tumor growth marked by cell cycle arrest and senescence but without considerable immune activation of the host. In the present research, we make use of immunodeficient NOD/SCID mice to extend our studies on the effectiveness of mEHT on human melanoma using the A2058 cell line and, furthermore, to investigate the role of mEHT in combination with NK cell immunotherapy. First, we provided evidence of the cytotoxicity of mEHT on A2058 cells, showing that a single mEHT treatment was sufficient to elicit a significantly delayed growth of established tumors which were more susceptible to the deleterious effect of the treatment than the B16F10 mouse melanoma cell line. Dissecting

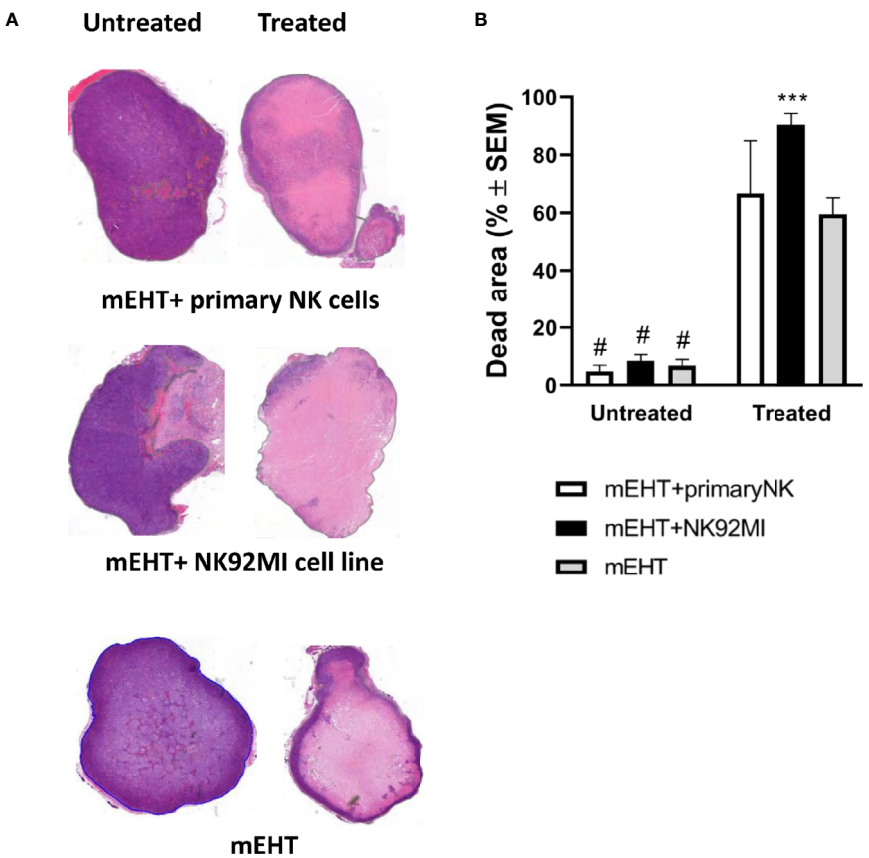


**FIGURE 7** | NK cell therapy effectively complements the modulated electro-hyperthermia (mEHT) treatment. **(A, B)** Additive effect of natural killer (NK) cell therapy is demonstrated by hematoxylin-eosin (H & E) staining and evaluation of the damaged tumor area. n=3 for untreated/treated + primary NK cells, n=6 for untreated/treated +NK92MI, n=5 for untreated/treated sham, n=8 for untreated/treated mEHT. Statistical significance was calculated using two-way ANOVA followed by Sidak's multiple comparisons test. ***p=0.0007 between mEHT +NK92MI cell line infiltrated and mEHT treated tumors and $^{\#}p < 0.0001$ between untreated tumors and treated counterparts.

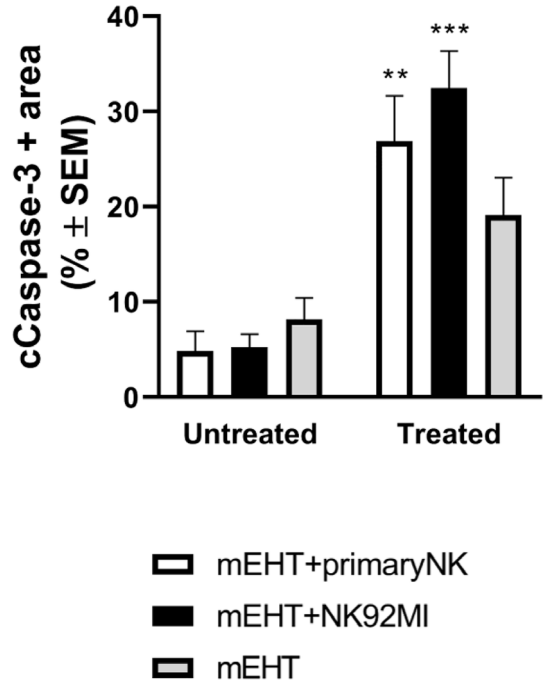


**FIGURE 8** | Caspase-3 expression is more increased in tumors treated with modulated electro-hyperthermia (mEHT) combined with primary or NK92MI cell line. Statistical significance was calculated using two-way ANOVA followed by Sidak's multiple comparisons test. **p=0.003 between mEHT-treated + primary natural killer (NK) cells and untreated + primary NK cells, ***p=0.0005 between untreated mEHT+NK92MI vs treated mEHT+NK92MI cell line.

the mechanism behind this effect we identified several key proteins. Similarly, to B16F10 mouse melanoma tumors, mEHT induced DNA damage and p53 activation but in contrary to B16F10, where this led to cell cycle arrest and senescence marked by high $p21^{waf1}$ expression without pronounced cell death (2) in the A2058 human melanoma xenografts the mEHT-induced p53 expression resulted in strong caspase-3 activation and subsequent apoptosis without significant p21 induction. This observation is in line with previous findings reported by Vancsik et al. (3, 32) who demonstrated that in C26 colorectal carcinoma the *in vitro* mEHT treatment induced p53 activation and caspase dependent cell death similarly to the *in vivo* experiments, where besides the caspase dependent cell death, they also detected the caspase independent pathway, marked by the elevated expression of apoptosis inducing factor (AIF) (28). In our present model the AIF protein was also upregulated by mEHT, but its nuclear translocation was inhibited, probably complexed by hsp70, recapitulating the findings we had described in the case of B16F10 mouse melanoma (2).

In the second part of our study, we investigated the effect of mEHT on the tumor microenvironment with respect to NK trafficking, homing and tumorigenic activity. While several lines of evidence indicate the effect of hyperthermia through hsp70 on the cytolytic activity of NK cells (20, 23), there is no evidence for the effect of hyperthermia on NK cell trafficking. We demonstrated that mEHT facilitated the migration and tumor infiltration of both the primary, *ex vivo* expanded NK cells and the genetically modified, IL-2 producing NK92-MI cells administered subcutaneously one day after loco-regional mEHT treatment of tumor bearing mice. We and others have shown previously that hyperthermia triggered immunogenic cell death accompanied by the release of DAMPs like ATP, HMGB1 and hsp70 which have cytokine-like effects attracting immune cells (2–4, 7, 25, 33). In a similar animal model with C26 colorectal cancer symmetrical allografts in immunocompetent mice Vancsik et al. showed that mEHT triggered a massive infiltration of autologous CD3+ T cells into the tumor (3). In the present study we propose that the mechanism of NK cell recruitment elicited by mEHT consists of multiple cellular events involving DAMP and chemokine secretion as well as extracellular matrix degradation, while NK cell activity is potentiated by increased susceptibility to NK-induced lysis of the target tumor cells. Nagarsekar et al. had proposed that CXC chemokines were a new family of heat-shock proteins. The analysis of the promoters of the CXC genes in both human and mouse showed that they share a common promoter organization with multiple copies of the HSF-1 binding sequence (heat shock response element) demonstrating a strong correlation between activation of HSPs and generation of CXC chemokines (34). In the present study we found that mEHT induced CXCL11 expression in A2058 cells, which has the strongest affinity to its receptor CXCR3, expressed on IL-2 activated primary NK cells and immortalized NK92MI cell line responsible for recruiting effector T cells. Surprisingly, the other two tested chemokines (CXCL9 and -10) were strongly downregulated at this timepoint. In order to gain a more precise overlook on the effect of mEHT on chemokine expression a time course experiment should be performed which then would allow the fine tuning of the therapeutic window of NK infusion depending on the highest peak of chemoattractants elicited by mEHT. Besides HSF1, p53 was also shown to cause tumor cells to secrete various chemokines with the potential to recruit NK cells. Antibody-mediated neutralization of the chemokine (C-C motif) ligand CCL2, but not CCL3, CCL4, or CCL5, prevented NK cell recruitment to the senescent tumors and reduced their elimination (35). It remains to be verified if the activation of p53 by mEHT in the A2058 melanoma contributes or not to NK recruitment *via* the induction of chemoattractant secretion.

Another factor which influences the amount and efficiency of NK cell delivery is the ECM of the tumor. ECM is a dynamic structure, defined by its synthesis by the particular cellular microenvironment and degradation by MMPs which enhance the migration of NK cells into the tumor. The role of hyperthermia in the MMP expression is not well established. It was shown that mild hyperthermia up-regulated matrix metalloproteinases and accelerated basement membrane degradation in experimental stroke (36). In breast cancer the extracellular hsp70 and heat shock protein 90 alpha were identified and shown to activate MMP-2 to facilitate cell migration and invasion (37). In the case of A2058 melanoma MMP-2 and MMP-9 expression was upregulated by various cytokines and inducers (38). We provide evidence that mEHT promotes the expression of MMP-2 and ECM

degradation of the A2058 melanoma *in vivo* facilitating the NK cell invasion of the tumor.

Once the NK cells have penetrated the tumor tissue, their cytolytic activity can effectively be manifested only in a permissive tumor microenvironment. Several lines of evidence prove that hyperthermia induces NK cell activity *via* either membrane bound or secreted hsp70 (23). We have previously shown that mEHT upregulated all the three forms (intracellular, secreted and membrane bound) of hsp70 in the B16F10 mouse melanoma (2). In the present study we detected the increase only in the intracellular form using IHC but as it was shown in repeated tumor models, we assume that the membrane bound form is also upregulated, resulting in enhanced cytolytic activity of NK cells. Based on histochemistry and detection of cC-3 expression, we show that the combined therapy results in higher tumor death rate proving the functionality of infiltrated NK cells. We noticed that this effect is more pronounced when mEHT is combined with NK92MI cell line most probably due to its stable expression of the IL-2 transgene rendering it IL-2 independent, while the primary NK cells rely on the host's IL-2 reservoir.

In summary, based on our results, mEHT might be an effective therapeutic approach in melanoma both *via* its direct inhibition of tumor growth, shown both earlier and here, and through its ability to promote the efficient intratumoral migration and homing of NK-cells. These together may ultimately lead to the complete eradication of melanoma when mEHT is combined with NK-cell therapy. Further preclinical studies using different molecular subclasses of melanomas and NK-cell species are required in combination with mEHT for establishing and efficient clinical translation of our results.

## DATA AVAILABILITY STATEMENT

The raw data supporting the conclusions of this article will be made available by the authors, without undue reservation.

## ETHICS STATEMENT

The animal study was reviewed and approved by Hungarian National Scientific Ethical Committee on Animal Experimentation under No. PE/EA/51-2/2019.

## AUTHOR CONTRIBUTIONS

Experimental model was set up by ABa who also wrote the original draft. The series of experimental tests were performed and analyzed by TV, ABe, AV, IH, DM, and RB. Statistical analysis was done by ABa. The review and editing of the manuscript was done by ZB and TK. All authors contributed to the article and approved the submitted version.

## FUNDING

This work was supported by the Hungarian National Research, Development and Innovation Office (NVKP_16-1-2016-0042) grant.

## REFERENCES

1. Hegyi G, Szasz O, Szasz A. Oncothermia: a new paradigm and promising method in cancer therapies. *Acupunct Electrother Res* (2013) 38(3-4):161–97. doi: 10.3727/036012913X13831832269243
2. Besztercei B, Vancsik T, Benedek A, Major E, Thomas MJ, Schvarcz CA, et al. Stress-Induced, p53-Mediated Tumor Growth Inhibition of Melanoma by Modulated Electrohyperthermia in Mouse Models without Major Immunogenic Effects. *Int J Mol Sci* (2019) 20(16). doi: 10.3390/ijms20164019
3. Vancsik T, Kovago C, Kiss E, Papp E, Forika G, Benyo Z, et al. Modulated electro-hyperthermia induced loco-regional and systemic tumor 1destruction in colorectal cancer allografts. *J Cancer* (2018) 9(1):41–53. doi: 10.7150/jca.21520
4. Andocs G, Meggyeshazi N, Balogh L, Spisak S, Maros ME, Balla P, et al. Upregulation of heat shock proteins and the promotion of damage-associated molecular pattern signals in a colorectal cancer model by modulated electrohyperthermia. *Cell Stress Chaperones* (2015) 20(1):37–46. doi: 10.1007/s12192-014-0523-6
5. Forika G, Balogh A, Vancsik T, Zalatnai A, Petovari G, Benyo Z, et al. Modulated Electro-Hyperthermia Resolves Radioresistance of Panc1 Pancreas Adenocarcinoma and Promotes DNA Damage and Apoptosis In Vitro. *Int J Mol Sci* (2020) 21(14). doi: 10.3390/ijms21145100
6. Danics L, Schvarcz CA, Viana P, Vancsik T, Krenacs T, Benyo Z, et al. Exhaustion of Protective Heat Shock Response Induces Significant Tumor Damage by Apoptosis after Modulated Electro-Hyperthermia Treatment of Triple Negative Breast Cancer Isografts in Mice. *Cancers (Basel)* (2020) 12(9). doi: 10.3390/cancers12092581
7. Tsang YW, Huang CC, Yang KL, Chi MS, Chiang HC, Wang YS, et al. Improving immunological tumor microenvironment using electro-hyperthermia followed by dendritic cell immunotherapy. *BMC Cancer* (2015) 15:708. doi: 10.1186/s12885-015-1690-2
8. Fiorentini G, Giovanis P, Rossi S, Dentico P, Paola R, Turrisi G, et al. A phase II clinical study on relapsed malignant gliomas treated with electro-hyperthermia. *Vivo* (2006) 20(6A):721–4. doi: 10.1177/1534735418812691
9. Fiorentini G, Sarti D, Milandri C, Dentico P, Mambrini A, Fiorentini C, et al. Modulated Electrohyperthermia in Integrative Cancer Treatment for Relapsed Malignant Glioblastoma and Astrocytoma: Retrospective Multicenter Controlled Study. *Integr Cancer Ther* (2019) 18:1534735418812691. doi: 10.1177/1534735418812691
10. Szasz AM, Minnaar CA, Szentmartoni G, Szigeti GP, Dank M. Review of the Clinical Evidences of Modulated Electro-Hyperthermia (mEHT) Method: An Update for the Practicing Oncologist. *Front Oncol* (2019) 9:1012. doi: 10.3389/fonc.2019.01012
11. Hurwitz MD. Hyperthermia and immunotherapy: clinical opportunities. *Int J Hyperthermia* (2019) 36(sup1):4–9. doi: 10.1080/02656736.2019.1653499
12. Hu W, Wang G, Huang D, Sui M, Xu Y. Cancer Immunotherapy Based on Natural Killer Cells: Current Progress and New Opportunities. *Front Immunol* (2019) 10:1205. doi: 10.3389/fimmu.2019.01205
13. Minetto P, Guolo F, Pesce S, Greppi M, Obino V, Ferretti E, et al. Harnessing NK Cells for Cancer Treatment. *Front Immunol* (2019) 10:2836. doi: 10.3389/fimmu.2019.02836
14. Chen Z, Yang Y, Liu LL, Lundqvist A. Strategies to Augment Natural Killer (NK) Cell Activity against Solid Tumors. *Cancers (Basel)* (2019) 11(7). doi: 10.3390/cancers11071040
15. Mao Y, van Hoef V, Zhang X, Wennerberg E, Lorent J, Witt K, et al. IL-15 activates mTOR and primes stress-activated gene expression leading to

prolonged antitumor capacity of NK cells. *Blood* (2016) 128(11):1475–89. doi: 10.1182/blood-2016-02-698027
16. Kremer V, Ligtenberg MA, Zendehdel R, Seitz C, Duivenvoorden A, Wennerberg E, et al. Genetic engineering of human NK cells to express CXCR2 improves migration to renal cell carcinoma. *J Immunother Cancer* (2017) 5(1):73. doi: 10.1186/s40425-017-0275-9
17. Mensali N, Dillard P, Hebeisen M, Lorenz S, Theodossiou T, Myhre MR, et al. NK cells specifically TCR-dressed to kill cancer cells. *EBioMedicine* (2019) 40:106–17. doi: 10.1016/j.ebiom.2019.01.031
18. Yang C, Du M, Yan F, Chen Z. Focused Ultrasound Improves NK-92MI Cells Infiltration Into Tumors. *Front Pharmacol* (2019) 10:326. doi: 10.3389/fphar.2019.00875
19. Dayanc BE, Beachy SH, Ostberg JR, Repasky EA. Dissecting the role of hyperthermia in natural killer cell mediated anti-tumor responses. *Int J Hyperthermia* (2008) 24(1):41–56. doi: 10.1080/02656730701858297
20. Hietanen T, Kapanen M, Kellokumpu-Lehtinen PL. Restoring Natural Killer Cell Cytotoxicity After Hyperthermia Alone or Combined with Radiotherapy. *Anticancer Res* (2016) 36(2):555–63. doi: 10.21873/anticanres.12269
21. Zanker KS, Lange J. Whole body hyperthermia and natural killer cell activity. *Lancet* (1982) 1(8280):1079–80. doi: 10.1016/S0140-6736(82)92142-0
22. Ostberg JR, Dayanc BE, Yuan M, Oflazoglu E, Repasky EA. Enhancement of natural killer (NK) cell cytotoxicity by fever-range thermal stress is dependent on NKG2D function and is associated with plasma membrane NKG2D clustering and increased expression of MICA on target cells. *J Leukoc Biol* (2007) 82(5):1322–31. doi: 10.1189/jlb.1106699
23. Shevtsov M, Pitkin E, Ischenko A, Stangl S, Khachatryan W, Galibin O, et al. Ex vivo Hsp70-Activated NK Cells in Combination With PD-1 Inhibition Significantly Increase Overall Survival in Preclinical Models of Glioblastoma and Lung Cancer. *Front Immunol* (2019) 10:454. doi: 10.3389/fimmu.2019.00454
24. Multhoff G, Pfister K, Gehrmann M, Hantschel M, Gross C, Hafner M, et al. A 14-mer Hsp70 peptide stimulates natural killer (NK) cell activity. *Cell Stress Chaperones* (2001) 6(4):337–44. doi: 10.1379/1466-1268(2001)006<0337:AMHPSN>2.0.CO;2
25. Werthmoller N, Frey B, Ruckert M, Lotter M, Fietkau R, Gaipl US. Combination of ionising radiation with hyperthermia increases the immunogenic potential of B16-F10 melanoma cells in vitro and in vivo. *Int J Hyperthermia* (2016) 32(1):23–30. doi: 10.3109/02656736.2015.1106011
26. Overgaard J, Gonzalez Gonzalez D, Hulshof MC, Arcangeli G, Dahl O, Mella O, et al. Randomised trial of hyperthermia as adjuvant to radiotherapy for recurrent or metastatic malignant melanoma. *Eur Soc Hyperthermic Oncol Lancet* (1995) 345(8949):540–3. doi: 10.1016/S0140-6736(95)90463-8
27. Ji Z, Njauw CN, Taylor M, Neel V, Flaherty KT, Tsao H. p53 rescue through HDM2 antagonism suppresses melanoma growth and potentiates MEK inhibition. *J Invest Dermatol* (2012) 132(2):356–64. doi: 10.1038/jid.2011.313
28. Meggyeshazi N, Andocs G, Balogh L, Balla P, Kiszner G, Teleki I, et al. DNA fragmentation and caspase-independent programmed cell death by modulated electrohyperthermia. *Strahlenther Onkol* (2014) 190(9):815–22. doi: 10.1007/s00066-014-0617-1
29. Susek KH, Karvouni M, Alici E, Lundqvist A. The Role of CXC Chemokine Receptors 1-4 on Immune Cells in the Tumor Microenvironment. *Front Immunol* (2018) 9:2159. doi: 10.3389/fimmu.2018.02159
30. Hasday JD, Thompson C, Singh IS. Fever, immunity, and molecular adaptations. *Compr Physiol* (2014) 4(1):109–48. doi: 10.1002/cphy.c130019
31. Dank M, Balogh A, Benedek A, Besztercei B, Danics L, Forika G, et al. [Preclinical and clinical investigation and development of electromagnetic oncological device - experience with solid tumors]. *Magy Onkol* (2019) 63(4):354–8.
32. Vancsik T, Forika G, Balogh A, Kiss E, Krenacs T. Modulated electro-hyperthermia induced p53 driven apoptosis and cell cycle arrest additively support doxorubicin chemotherapy of colorectal cancer in vitro. *Cancer Med* (2019) 8(9):4292–303. doi: 10.1002/cam4.2330
33. Lee S, Son B, Park G, Kim H, Kang H, Jeon J, et al. Immunogenic Effect of Hyperthermia on Enhancing Radiotherapeutic Efficacy. *Int J Mol Sci* (2018) 19(9). doi: 10.3390/ijms19092795
34. Nagarsekar A, Hasday JD, Singh IS. CXC chemokines: a new family of heat-shock proteins? *Immunol Invest* (2005) 34(3):381–98. doi: 10.1081/IMM-200067648
35. Iannello A, Thompson TW, Ardolino M, Lowe SW, Raulet DH. p53-dependent chemokine production by senescent tumor cells supports NKG2D-dependent tumor elimination by natural killer cells. *J Exp Med* (2013) 210(10):2057–69. doi: 10.1084/jem.20130783
36. Alam M, Mohammad A, Rahman S, Todd K, Shuaib A. Hyperthermia up-regulates matrix metalloproteinases and accelerates basement membrane degradation in experimental stroke. *Neurosci Lett* (2011) 495(2):135–9. doi: 10.1016/j.neulet.2011.03.056
37. Sims JD, McCready J, Jay DG. Extracellular heat shock protein (Hsp)70 and Hsp90alpha assist in matrix metalloproteinase-2 activation and breast cancer cell migration and invasion. *PloS One* (2011) 6(4):e18848. doi: 10.1371/journal.pone.0018848
38. Roomi MW, Kalinovsky T, Niedzwiecki A, Rath M. Modulation of MMP-2 and -9 secretion by cytokines, inducers and inhibitors in human melanoma A-2058 cells. *Oncol Rep* (2017) 37(6):3681–7. doi: 10.3892/or.2017.5597

**Conflict of Interest:** The authors declare that the research was conducted in the absence of any commercial or financial relationships that could be construed as a potential conflict of interest.

frontiers in Oncology

ORIGINAL RESEARCH
published: 25 February 2021
doi: 10.3389/fonc.2021.640656

# Overexpression of ABCC1 Confers Drug Resistance to Betulin

*Xuan-Yu Chen[1,2†], Yuqi Yang[2†], Jing-Quan Wang[2], Zhuo-Xun Wu[2], Jing Li[1*] and Zhe-Sheng Chen[2*]*

*[1] College of Integrated Chinese and Western Medicine, Hebei Medical University, Shijiazhuang, China, [2] Department of Pharmaceutical Sciences, College of Pharmacy and Health Sciences, St. John's University, New York, NY, United States*

Betulin is a lupane-type pentacyclic triterpene, which is isolated from birch bark. It has a broad spectrum of biological and pharmacological properties, such as anti-inflammatory, anti-tumor, anti-viral, and anti-bacterial activity. Herein, we explored the factors that may result in betulin resistance, especially with respect to its interaction with ATP-binding cassette subfamily C member 1 (ABCC1). ABCC1 is an important member of the ATP-binding cassette (ABC) transporter family, which is central to mediating multidrug resistance (MDR) in naturally derived anticancer agents. An MTT-based cell viability assay showed that ABCC1 overexpression has the ability to desensitize both cancer cell line and gene-transfected cell line to betulin and that this betulin-induced resistance can be antagonized by a known ABCC1 inhibitor MK571 at 25 μM. Additionally, betulin upregulates the ABCC1 protein expression level in both concentration-dependent and time-dependent manners, also blocks the transport function mediated by ABCC1. Subsequently, a high affinity score of betulin was achieved in a computational docking analysis, demonstrating a strong interaction of betulin with ABCC1.

**Keywords: betulin, ATP-binding cassette sub-family C member 1 (ABCC1), multidrug resistance-associated protein 1 (MRP1), multidrug resistance (MDR), natural product**

OPEN ACCESS

***Edited by:***
*Benyi Li,*
*University of Kansas Medical Center, United States*

***Reviewed by:***
*Ru Li,*
*Stony Brook University, United States*
*Abhijit Dey,*
*Presidency University, India*

****Correspondence:***
*Jing Li*
*lijingtiger@163.com*
*Zhe-Sheng Chen*
*chenz@stjohns.edu*

*†These authors have contributed equally to this work and share first authorship*

***Specialty section:***
*This article was submitted to Pharmacology of Anti-Cancer Drugs, a section of the journal Frontiers in Oncology*

***Received:*** *11 December 2020*
***Accepted:*** *13 January 2021*
***Published:*** *25 February 2021*

***Citation:***
*Chen X-Y, Yang Y, Wang J-Q, Wu Z-X, Li J and Chen Z-S (2021) Overexpression of ABCC1 Confers Drug Resistance to Betulin. Front. Oncol. 11:640656. doi: 10.3389/fonc.2021.640656*

## INTRODUCTION

To date, many drugs have originated from natural products, including vincristine, vinblastine, doxorubicin, and paclitaxel all have the potential to inhibit tumor progression (1). However, the effectiveness of these drugs can be restricted by multidrug resistance (MDR)-associated ATP-binding cassette (ABC) transporters (2). Specifically, vincristine, vinblastine, doxorubicin, and paclitaxel can be transported by ABC sub-family B member 1 (ABCB1, multidrug resistance protein 1/MDR1, P-glycoprotein/P-gp) (3); whereas, vincristine, vinblastine, and doxorubicin are substrate drugs of ABC sub-family C member 1 (ABCC1, multidrug resistance protein 1/MRP1) (4).

The 190 kDa MRP1, located in human chromosome locus *p13.11*, was firstly isolated from doxorubicin-resistance small cell lung cancer line H69AR, and was found to be associated with MDR in 1992 (5, 6). The protein structure of MRP1 has three membrane-spanning domains (MSDs), and two nucleotide-binding domains (NBDs) (7). Functionally, the NBDs serve as the energy source to produce hydrolyzed ATP, while the MSDs provide support for drug binding,

putative drug transport channel, dimerization, and trafficking (4). MRP1 has a wide distribution, for example throughout the adrenal gland, bladder, choroid plexus, helper T cells, and muscle cells (8).

Betulin, a lupane-type pentacyclic triterpene, is isolated from bark of birches. Due to its poor solubility in aqueous media, several more soluble derivatives and betulin nanoparticles were developed (9, 10). The chemical structure of betulin is presented in **Figure 1A**. Betulin and its derivatives have a broad spectrum of anti-cancer profile, such as against lung, breast, prostate, colon, colorectal, cervical, and pancreatic cancer, as well as melanoma and leukemia (11). The interaction between betulinic acid and ABCB1 or ABCG2 is conclusive (12, 13); however, the effect of ABCC1 on betulin efficacy needs to be elucidated. Interestingly, it has been documented that ABCC1 overexpression is correlated with lung, breast, prostate, and ovarian cancer, gastrointestinal carcinoma, melanoma, and leukemia (14, 15). Based on the overlapping cancer spectrum, we postulated that the overexpression of ABCC1 may attenuate the anticancer efficacy of betulin.

Herein, we focused on the interaction of betulin with ABCC1, and found that ABCC1 overexpression confers drug resistance to betulin. This finding may provide a valuable foundation for future preclinical and clinical investigations of betulin.

# MATERIALS AND METHODS

## Chemicals and Reagents

Betulin was kindly provided as a free sample from MedChemExpress (Purity > 98.0%, Monmouth Junction, NJ). Dulbecco's modified Eagle medium, trypsin-EDTA, penicillin/streptomycin, and fetal bovine serum were purchased from Corning (Corning, NY). Phosphate buffer saline (PBS) was obtained from VWR chemicals (Solon, OH). Vincristine, dimethyl sulfoxide (DMSO), and methylthiazolyldiphenyl-tetrazolium bromide (MTT) were obtained from Millipore-Sigma (Burlington, MA). MK571 and G418 were purchased from Enzo Life Sciences (Farmingdale, NY). Anti-MRP1/ABCC1 (D5C1X) antibody (product #72202), anti-GAPDH

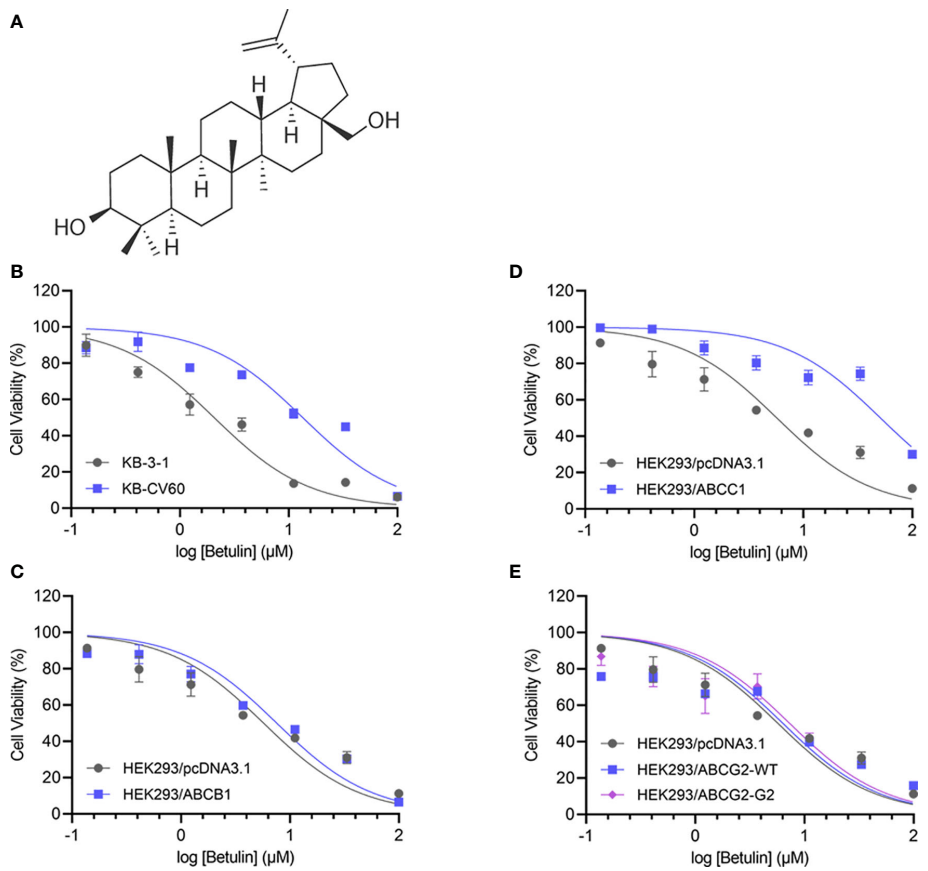


**FIGURE 1** | Chemical structure and cell viability-concentration curves. **(A)** The chemical structure of betulin. The cell viability-concentration curves for **(B)** KB-3-1 and KB-CV60 cells, **(C)** HEK293/pcDNA3.1 and ABCC1-tansfected HEK293 cells, **(D)** HEK293/pcDNA3.1 and ABCB1-tansfected HEK293 cells, **(E)** HEK293/pcDNA3.1 and HEK293 cells transfected with wild-type or R482G-mutant ABCG2 after treatment with serial concentrations of betulin. Each point is shown as mean ± SD, from the experiment that was repeated at least three times and performed independently.

(D16H11) antibody (product #5174), and HRP-conjugated anti-rabbit IgG secondary antibody (product #7074) were obtained from Cell Signaling Technology (Danvers, MA). [$^3$H]-Vincristine (0.7 Ci/mmol) was purchased from Moravek Biochemicals (Brea, CA). Liquid scintillation cocktail, and all other chemicals and reagents were purchased from ThermoFisher Scientific (Waltham, MA).

## Cell Lines and Cell Culture

Human epidermoid carcinoma cell line KB-3-1 was used as the drug-sensitive cell line, and its ABCC1-overexpressing cell line KB-CV60 was maintained in the medium with 1 μg/ml of cepharanthine and 60 ng/ml of vincristine (16). HEK293/pcDNA3.1, HEK293/ABCC1, HEK293/ABCB1, HEK293/ABCG2-WT, and HEK293/ABCG2-G2 were transfected with either an empty vector pcDNA3.1 or a pcDNA3.1 vector containing a full length ABCC1, ABCB1, or ABCG2 encoding arginine (R) or glycine (G) at position 482 (17). All transfected cells were selected in the medium with 2 mg/ml G418. All cell lines were cultured in medium supplemented with 10% serum and 1% antibiotics at 37°C under 5% $CO_2$. All drug resistant cell lines were cultured in drug-free medium for more than 2 weeks prior to further use.

## MTT-Based Cell Viability Assay

An established protocol of MTT assay was used to determine the cell viability of betulin with or without an inhibitor (18). DMSO was used as a solvent to prepare a stock solution (10 mM) of all compounds. As the highest concentration in the cell viability assay was 100 μM, the final concentration of DMSO was 1% in the treatment medium. Also, all control groups in the experiment were treated with solvent only. Briefly, 5,000 to 7,000 cells/well were evenly seeded in a 96-well plate, and incubated at 37°C overnight prior to further experiment. On the next day, a serial dilution of substrate drugs (0–100 μM) with or without inhibitors at the indicated concentration was added to the designated well. The cells were further incubated for 72 h. On the last day of treatment period, MTT solution was added to each well, and incubated for 4 h protected from light. After incubation, the supernatant was removed, and 100 μl/well DMSO was added to dissolve the formazan crystals. Subsequently, absorbance at 570 nm was measured by an UV/Vis microplate spectrophotometer (Fisher Science, Fair Lawn, NJ). The log scale curves in GraphPad (log inhibitor vs. responses) were used to fit cell viability curves and to calculate the $IC_{50}$ values. The values of resistance fold (RF) were calculated as previously stated (19).

## [$^3$H]-Vincristine Accumulation Assay

The transport function of MDR-associated ABC transporter was determined by tritium-labeled substrate accumulation assay (20). Briefly, $5\times10^5$ cells/well were seeded evenly in a 24-well plate, and incubated for 24 h. On the second day, cells were treated with betulin or MK571 at the indicated concentrations for 2 h. Then, [$^3$H]-vincristine was added to the designated wells at a final concentration of 36 nM. After 2 h incubation, cells were washed with PBS twice, and harvested and transferred into scintillation fluid. Subsequently, the intracellular radioactivity was measured by a liquid scintillation analyzer (Packard Instrument, Downers Grove, IL).

## Western Blot Analysis

As previously described, the protein expression level of ABCC1 was examined by a Western blot analysis (19). In short, cells were treated with or without betulin, and then the lysate was collected. This was followed by determining the protein concentration in the lysates, and equal amount of protein sample (12 μg) was separated by SDS-PAGE then transferred onto PVDF membrane. The membranes were blocked for 2 h with 5% non-fat milk at room temperature followed by incubation with primary antibody (anti-MRP1/ABCC1 and anti-GAPDH at 1:1000) overnight at 4°C. On the second day, after washing with TBST three times, the membranes were incubated with HPR-conjugated secondary antibody (at 1:1000) for 1 h at room temperature. Subsequently, the protein was visualized using an ECL substrate by a digital Western blot scanner (LI-COR, NE), and quantified and analyzed by Fiji software (NIH, Bethesda, MD).

## Molecular Docking Analysis of Betulin With Human ABCC1 Model

The betulin 3D structure was constructed for docking simulation with an ABCC1 model as previously described (21). ABCC1 protein model 5UJA ($LTC_4$ bound) was obtained from RCSB Protein Data Bank. The model is inward-facing ABCC1 with a resolution of 3.34 (22). Docking calculations were performed in AutoDock Vina (version 1.1.2) (23). Hydrogen atoms and partial charges were added using AutoDock Tools (ADT, version 1.5.4). Docking grid center coordinates were determined from the bound ligand $LTC_4$ provided in 5UJA PDB files. Receptor/ligand preparation and docking simulation were performed using default settings. The top-scoring pose (sorted by affinity score: kcal/mol) was selected for further analysis and visualization.

## Statistics

All data were presented as mean ± SD, and evaluated using a one-way or two-way ANOVA as appropriate by GraphPad software (La Jolla, CA). Statistical significance was considered when $p < 0.05$.

# RESULTS

## The Efficacy of Betulin Is Attenuated in ABCC1-Overexpressing Cells and That This Betulin-Induced Resistance Can Be Sensitized by ABCC1 Inhibitor

An MTT assay was performed to examine the cell viability of substrate drugs with or without an inhibitor. Herein, the RF values were used to assess the degree of attenuated effectiveness resulting from ABCC1 overexpression. As shown in **Figures 1B, C**, the

**TABLE 1** | MK571 at 25 μM sensitized ABCC1-overexpressing cells to betulin.

| Treatment | $IC_{50}$ ± SD[a] (RF[b]) (μM) | | | |
|---|---|---|---|---|
| | KB-3-1 | KB-CV60 | HEK293/pcDNA3.1 | HEK293/MRP1 |
| Betulin | 2.06 ± 0.29 (1.00) | 13.47 ± 0.89 (6.53)* | 5.73 ± 0.71 (1.00) | 51.06 ± 4.25 (8.92)* |
| + MK571 25 μM | 3.34 ± 0.42 (1.62) | 6.94 ± 0.61 (3.36) | 5.36 ± 0.42 (0.94) | 22.33 ± 1.57 (3.90) |
| Vincristine | 0.02 ± 0.01 (1.00) | 0.29 ± 0.03 (19.33)* | 0.39 ± 0.02 (1.00) | 9.28 ± 1.04 (23.79)* |
| + MK571 25 μM | 0.02 ± 0.01 (1.47) | 0.10 ± 0.01 (6.53) | 0.47 ± 0.03 (1.21) | 2.44 ± 0.41 (6.26) |

[a]*The half-maximal inhibitory concentration ($IC_{50}$) values are showed as mean ± SD from at least three independent experiments performed in triplicate.*
[b]*Resistance fold (RF) was calculated by dividing the $IC_{50}$ values of drug-sensitive cells with MK571 or cells expressed ABCC1 with or without MK571 by the $IC_{50}$ values of their corresponding parental cells without MK571.*
**p < 0.05 versus control group.*

efficacy of betulin was restricted in cells expressing ABCC1 as evidenced by higher $IC_{50}$ values in MDR cells mediated by ABCC1 compared to their corresponding drug-sensitive cell line counterparts. The RF value of betulin was significantly increased to 6.53-fold in KB-CV60 cells, and 8.93-fold in ABCC1-transfected HEK293 cells (**Table 1**). Importantly, the betulin-induced drug resistance can be antagonized by a known ABCC1 inhibitor MK571 at 25 μM. By contrast, vincristine serves as a reference substrate to compare the drug resistance conferred by ABCC1. Based on **Table 1**, vincristine had 19.33- and 23.79-fold resistance in drug-selected cancer cells and gene-transfected cells expressing ABCC1, and similarly, this resistance can be reversed by MK571 at 25 μM. Thus, betulin is less sensitive in ABCC1-overexpressing cells, and an established ABCC1 inhibitor could overcome the resistance effect induced by betulin.

## ABCB1 or ABCG2 Cannot Confer Resistance to Betulin in Cells Overexpressed ABCB1 or ABCG2

As overexpression of ABCB1 and ABCG2 are also central to MDR, cell lines expressing either ABCB1 or ABCG2 were investigated. Based on **Figures 1D, E**, the $IC_{50}$ values of betulin were 5.72, 7.56, 6.37, and 7.34 μM for HEK293/pcDNA3.1, HEK293/ABCB1, HEK293/ABCG2-WT, and HEK293/ABCG2-G2 cells, respectively. The RF values were 1.32, 1.11, and 1.28 in ABCB1-overexpressing cells, and wide-type or R482G-mutant ABCG2-overexpressing cell lines, respectively (**Figures 1D, E**). Given no significant difference in RF values between drug-sensitive and MDR cells mediated by ABCB1 or ABCG2, it is likely that ABCB1 and ABCG2 overexpression did not affect the effectiveness of betulin.

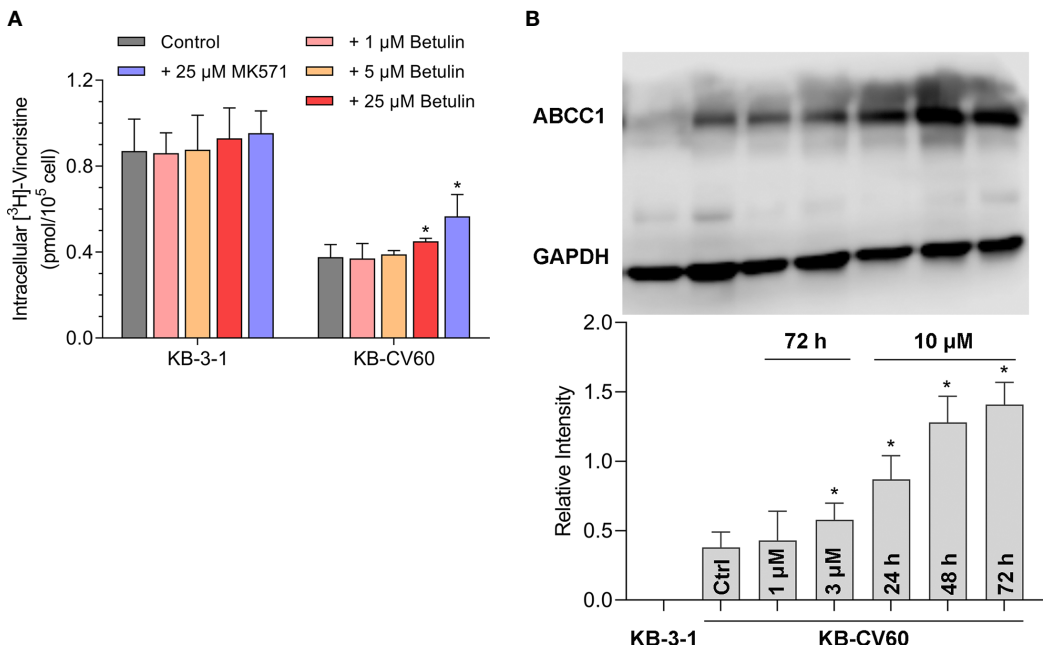


**FIGURE 2** | Effects of betulin on the transport function mediated by ABCC1 and the ABCC1 protein expression level. **(A)** [$^3$H]-vincristine intracellular accumulation in KB-3-1 and KB-CV60 cells after betulin or MK571 treatment at indicated concentrations. **(B)** The ABCC1 protein expression level after incubated with 1 μM or 3 μM betulin for 72 h, or with 10 μM betulin up to 72 h. All data are presented as mean ± SD. *indicates $p < 0.05$ compared with its corresponding control group.

## Betulin Blocks the Transport Function Mediated by ABCC1

A tritium-labeled drug accumulation analysis was conducted to assess the interaction between betulin and MDR-associated ABC transporter. Our results in **Figure 2A** showed that betulin at 25 μM enhanced the intracellular vincristine accumulation from 44% to 52% compared with KB-CV60 cells without an inhibitor. Herein, 25 μM MK571 acted as a reference ABCC1 inhibitor to increase substrate drug accumulation in KB-CV60 cells (from 44% to 65%). Therefore, betulin at a high concentration has the ability to impede the ABCC1 transport function resulting in increased level of intracellular accumulation of substrate drug.

## Betulin Induces ABCC1 Protein Expression Level

It is documented that upregulation of ABC transporter expression can induce MDR. A Western blot analysis was used to determine the ABCC1 protein expression level after betulin treatment. As shown in **Figure 2B**, 3 μM betulin had the ability to significantly induce ABCC1 expression after a 72 h incubation period. Also, the expression level of ABCC1 time-dependently increased following treatment with betulin at 10 μM up to 72 h. Betulin time- and concentration-dependently upregulated ABCC1 protein expression.

## Docking Simulation of Betulin in the Drug-Binding Pocket of ABCC1

To further validate the interaction of betulin and ABCC1 protein, an *in silico* analysis was conducted. Our results showed that betulin docked into the drug-binding site of ABCC1 with an affinity score of −6.8 kcal/mol. Overall, betulin binds in the pocket surrounded by the transmembrane domains of ABCC1 protein (**Figure 3A**), partially overlapping the leukotriene $C_4$ ($LTC_4$)-binding site (**Figure 3C**). Details of the ligand-receptor interaction are displayed in **Figure 3B**. The primary factor contributing to the binding affinity of betulin to the ABCC1 protein is *via* hydrophobic interactions. According to **Figures 3B, D**, betulin is positioned and stabilized in the hydrophobic cavity formed by Leu381, Phe385, Phe389, Tyr440, Thr439, Ile598, Phe594, Met1092, Thr1241, Tyr1242, Asn1244, and Tpr1245. Betulin was stabilized by a hydrogen bond formed with Trp553. Together, these results demonstrated that betulin has an interaction with the ABCC1 protein.

# DISCUSSION

Nowadays, many natural-derived drugs serve as sources of novel drug discovery and are tested clinically (24, 25). Unfortunately, the efficacy of certain natural products could be compromised by

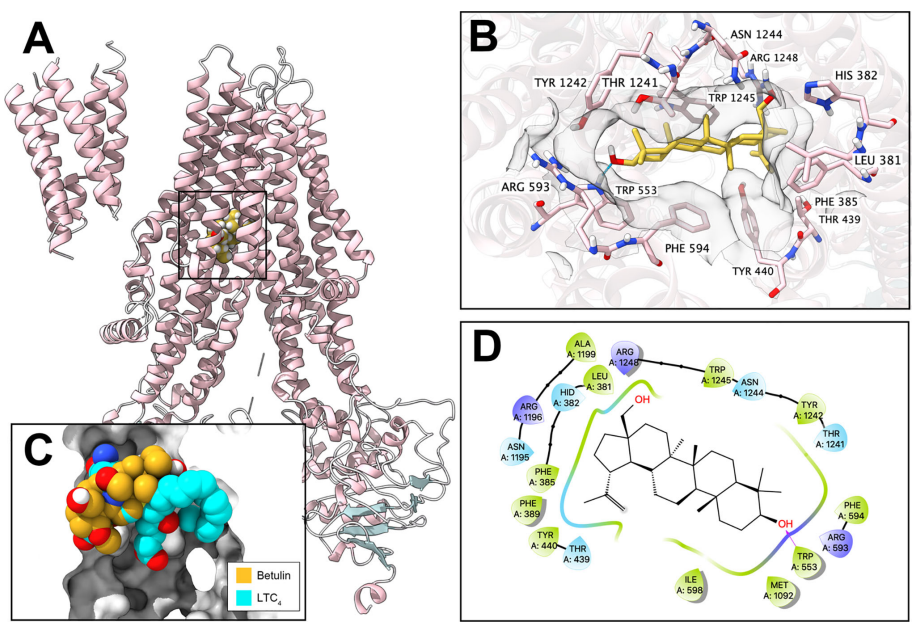


**FIGURE 3** | Interaction between betulin and human ABCC1 protein. **(A)** Overview of the best-scoring pose of betulin in the drug-binding pocket of ABCC1 protein (5UJA). ABCC1 was displayed as colored ribbons (helix: pink; strand: blue; coil: white). Betulin was displayed as colored balls. **(B)** Details of the interactions between betulin and ABCC1 (5UJA) binding pocket. ABCC1 helices were displayed as colored ribbons. Important residues were displayed as colored sticks (carbon: pink; oxygen: red; nitrogen: blue; hydrogen: white; fluoride: lime; chloride: light green). Surface formed by important residues were depicted as grey solid planes. Betulin was displayed as colored sticks (carbon: yellow; oxygen: red; nitrogen: blue; chloride: lime; fluoride: light green). Hydrogen bonds were displayed as blue dash lines. **(C)** Binding poses of betulin and ABCC1 substrate $LTC_4$ in ABCC1 binding pocket. **(D)** 2D diagram of the interaction between betulin and ABCC1. Amino acids within 3 Å from betulin were displayed as colored bubbles (green: hydrophobic; blue: polar). Purple solid lines with arrow indicate hydrogen bonds.

MDR-associated ABC transporters (3, 4). ABCC1 (MRP1), ABCB1 (MDR1, P-glycoprotein/P-gp), and ABCG2 (BCRP/MXR) are extensively studies, and are commonly responsible for MDR (18, 19). Betulin and betulinic acid derived from birch bark have a broad spectrum of pharmacological activity (11, 26). Researchers reported that betulinic acid inhibits ABCB1-, ABCG2-, and ABCB5-mediated MDR with similar effectiveness as counterparts in parental cell lines (12). Also, Zhao et al. found that betulinic acid nanoparticle exerts its anticancer efficacy *via* downregulating ABCG1 oncogene expression level (13). These provide us a clue that betulin may interact with MDR-associated ABC transporters. However, the interaction of betulin and ABCC1 remains inconclusive and needs to be determined. Considering the similar cancer spectrum between ABCC1 and betulin as described in the introduction section, we herein focused on the effectiveness of betulin influenced by ABCC1 overexpression.

Our experiments started from an MTT-based cell viability assay to assess the cytotoxicity of betulin and a reference substrate drug vincristine with or without an inhibitor. The results indicated that ABCC1 overexpression can confer resistance to betulin in cancer cells expressing ABCC1. As KB-3-1 is a human epidermoid carcinoma cell line, it is possible that, to some extent, developing other mechanism induces drug resistance apart from ABCC1 overexpression in the KB-CV60 cell line. Hence, the cell viability of betulin was determined on ABCC1-transfected HEK293 cells. Similarly, betulin resistance was found in HEK293/ABCC1 cells as evidenced by the higher RF value in cells transfected with ABCC1 compared with its corresponding sensitive HEK293/pcDNA3.1 cells counterpart. Vincristine, a vinca alkaloid isolated from the Madagascar periwinkle *Catharanthus roseus* (27), served as a reference substrate of ABCC1 (2). Although betulin does not have as high of an RF value as vincristine, it is still rather comparable to vincristine. Importantly, betulin-conferred drug resistance can be antagonized by a known ABCC1 inhibitor, MK571. Overexpression of ABCB1 and ABCG2 is also central to MDR, therefore cell viability of cells overexpressing ABCB1 or ABCG2 was also examined after betulin treatment. Given different cellular context, it is possible that switching arginine to glycine (R > G) in the ABCG2 gene at amino acid 482 could affect substrate specificity and different resistance levels to substrate drugs (17). Our results showed that no significant difference in $IC_{50}$ values was observed in drug-sensitive cells and corresponding MDR cells mediated by ABCB1, and wild-type or R482G-mutant ABCG2, which were consistent with results from Saeed et al (12).. Together, ABCC1 overexpression may promote betulin resistance, while overexpression of ABCB1 and ABCG2 could not confer resistance to betulin. Thus, we hypothesized that betulin is a, ABCC1 substrate.

Following mechanism-based studies, a Western blot analysis was conducted to assess the ABCC1 protein expression. Our results showed that within a 72 h incubation period, betulin upregulates ABCC1 expression level in time- and concentration-dependent manners. Interestingly, other researchers generated Pearson's correlation coefficients (R-values) to correlate the expression level of different genes and the $\log_{10}IC_{50}$ values for betulinic acid (12). Results from Saeed et al. demonstrated that there is no significant correlation between betulinic acid and ABCC1 gene expression. In the chemical structure, betulin and betulinic acid are different in hydroxymethyl and carboxyl groups, which may lead to differences in their pharmacological properties. We also postulated that this inconsistency may be the results from post-transcriptional and/or post-translational modification and regulation (28–31), which needs further validation.

Substrate drugs can occupy MDR-associated ABC transporters, and result in a competition with another drug substrate for transport function (20). As a result, a repurposed drug substrate acting as an inhibitor or a reversal agent has the ability to sensitize MDR-associated ABC transporter to another drug substrate (32). In our study, the [$^3$H]-vincristine accumulation in cancer cells was measured. Results from an accumulation assay demonstrated that betulin at 25 μM inhibits MDR-mediated by ABCC1. However, the inhibitory effect of betulin to ABCC1 is not as strong as 25 μM MK571, which might be the result of high resistance level caused by ABCC1 in KB-CV60 cells and/or the lower RF value difference of betulin relative to vincristine between KB-3-1 cells and KB-CV60 cells. Notably, the concentrations of betulin used in the accumulation assay are higher than the $IC_{50}$ values in corresponding cell lines, which can be toxic to the cells. However, the 4 h incubation of betulin with cells may not affect the cellular function. This is confirmed in the parental cells that no significant difference was observed between the vehicle group and the treatment groups. Of note, even the weaker inhibitory effect of betulin than MK571 counterpart, our findings do not warrant further investigation of betulin as a reversal agent or modulator to MDR mediated by ABCC1 overexpression.

The computational docking analysis serves as an efficient tool to predict the interaction of compound with protein models even though it indicates a virtual binding instead of an actual one (33, 34). Betulin received an affinity score of −6.8 kcal/mol with human ABCC1 protein model (5UJA). Also, it is known that leukotriene $C_4$ ($LTC_4$) can be pumped by ABCC1 (35). Our results revealed that betulin has binding interaction with human ABCC1 protein, and more importantly shares certain overlapping binding sites with $LTC_4$. Overall, betulin may exhibit a similar substrate behavior.

## CONCLUSIONS

Betulin is susceptible to drug resistance mediated by ABCC1 overexpression, and a known ABCC1 inhibitor, MK571, can sensitize the cells expressing ABCC1 to betulin. ABCC1-induced resistance to betulin can be explained by its upregulated protein expression of ABCC1. Additionally, betulin at high concentration

has the ability to inhibit ABCC1 transport function, which may affect the pharmacokinetic profile of other ABCC1 drug substrates, such as vincristine. These findings may be a valuable foundation for follow-up clinical investigation on the potential use of betulin.

## DATA AVAILABILITY STATEMENT

The raw data supporting the conclusions of this article will be made available by the authors, without undue reservation.

## AUTHOR CONTRIBUTIONS

Conceptualization: X-YC. Methodology: YY, X-YC, and J-QW. Writing-original draft: YY and X-YC. Writing-review and copyediting: X-YC, YY, Z-XW, and Z-SC. Supervision: JL and Z-SC. All authors contributed to the article and approved the submitted version.

## FUNDING

This research was funded by the National Natural Science Foundation of China (No.81973761).

## ACKNOWLEDGMENTS

Authors are grateful to Dr. Shin-Ichi Akiyama (Kagoshima University, Kagoshima, Japan) for providing KB-3-1 and KB-CV60 cell lines. We thank Drs. Susan E. Bates (NCI, NIH, Bethesda, MD) for kindly providing gene-transfected cell lines. We thank Dr. Yangmin Chen for editing the article. We thank for the supported from the National Natural Science Foundation of China (No. 81973761).

## REFERENCES

1. Muniraj N, Siddharth S, Sharma D. Bioactive Compounds: Multi-Targeting Silver Bullets for Preventing and Treating Breast Cancer. *Cancers* (2019) 11 (10):1563. doi: 10.3390/cancers11101563
2. Ji N, Yang Y, Cai CY, Lei ZN, Wang JQ, Gupta P, et al. Selonsertib (GS-4997), an ASK1 inhibitor, antagonizes multidrug resistance in ABCB1- and ABCG2-overexpressing cancer cells. *Cancer Lett* (2019) 440-441:82–93. doi: 10.1016/j.canlet.2018.10.007
3. Huang BY, Zeng Y, Li YJ, Huang XJ, Hu N, Yao N, et al. Uncaria alkaloids reverse ABCB1-mediated cancer multidrug resistance. *Int J Oncol* (2017) 51:257–68. doi: 10.3892/ijo.2017.4005
4. Yin JY, Huang Q, Yang Y, Zhang JT, Zhong MZ, Zhou HH, et al. Characterization and analyses of multidrug resistance-associated protein 1 (MRP1/ABCC1) polymorphisms in Chinese population. *Pharmacogenetics Genomics* (2009) 19:206–16. doi: 10.1097/FPC.0b013e328323f680
5. Cole SP, Bhardwaj G, Gerlach JH, Mackie JE, Grant CE, Almquist KC, et al. Overexpression of a transporter gene in a multidrug-resistant human lung cancer cell line. *Science (New York NY)* (1992) 258:1650–4. doi: 10.1126/science.1360704
6. Perdu J, Germain DP. Identification of novel polymorphisms in the pM5 and MRP1 (ABCC1) genes at locus 16p13.1 and exclusion of both genes as responsible for pseudoxanthoma elasticum. *Hum Mutat* (2001) 17:74–5. doi: 10.1002/1098-1004(2001)17:1<74::AID-HUMU14>3.0.CO;2-F
7. Higgins CF, Linton KJ. The ATP switch model for ABC transporters. *Nat Struct Mol Biol* (2004) 11:918–26. doi: 10.1038/nsmb836
8. Eckford PD, Sharom FJ. ABC efflux pump-based resistance to chemotherapy drugs. *Chem Rev* (2009) 109:2989–3011. doi: 10.1021/cr9000226
9. Zhao X, Wang W, Zu Y, Zhang Y, Li Y, Sun W, et al. Preparation and characterization of betulin nanoparticles for oral hypoglycemic drug by antisolvent precipitation. *Drug Deliv* (2014) 21:467–79. doi: 10.3109/10717544.2014.881438
10. Drąg-Zalesińska M, Drąg M, Poręba M, Borska S, Kulbacka J, Saczko J. Anticancer properties of ester derivatives of betulin in human metastatic melanoma cells (Me-45). *Cancer Cell Int* (2017) 17:4. doi: 10.1186/s12935-016-0369-3
11. Amiri S, Dastghaib S, Ahmadi M, Mehrbod P, Khadem F, Behrouj H, et al. Betulin and its derivatives as novel compounds with different pharmacological effects. *Biotechnol Adv* (2020) 38:107409. doi: 10.1016/j.biotechadv.2019.06.008
12. Saeed MEM, Mahmoud N, Sugimoto Y, Efferth T, Abdel-Aziz H. Betulinic Acid Exerts Cytotoxic Activity Against Multidrug-Resistant Tumor Cells via Targeting Autocrine Motility Factor Receptor (AMFR). *Front Pharmacol* (2018) 9:841. doi: 10.3389/fphar.2018.00481
13. Zhao H, Mu X, Zhang X, You Q. Lung Cancer Inhibition by Betulinic Acid Nanoparticles via Adenosine 5'-Triphosphate (ATP)-Binding Cassette Transporter G1 Gene Downregulation. *Med Sci Monit Int Med J Exp Clin Res* (2020) 26:e922092. doi: 10.12659/MSM.922092
14. Hipfner DR, Deeley RG, Cole SP. Structural, mechanistic and clinical aspects of MRP1. *Biochim Biophys Acta* (1999) 1461:359–76. doi: 10.1016/S0005-2736(99)00168-6
15. Shukla S, Ohnuma S, Ambudkar SV. Improving cancer chemotherapy with modulators of ABC drug transporters. *Curr Drug Targets* (2011) 12:621–30. doi: 10.2174/138945011795378540
16. Aoki S, Chen ZS, Higasiyama K, Setiawan A, Akiyama S, Kobayashi M. Reversing effect of agosterol A, a spongean sterol acetate, on multidrug resistance in human carcinoma cells. *Japanese J Cancer Research: Gann* (2001) 92:886–95. doi: 10.1111/j.1349-7006.2001.tb01177.x
17. Robey RW, Honjo Y, Morisaki K, Nadjem TA, Runge S, Risbood M, et al. Mutations at amino-acid 482 in the ABCG2 gene affect substrate and antagonist specificity. *Br J Cancer* (2003) 89:1971–8. doi: 10.1038/sj.bjc.6601370
18. Yang Y, Ji N, Cai CY, Wang JQ, Lei ZN, Teng QX, et al. Modulating the function of ABCB1: in vitro and in vivo characterization of sitravatinib, a tyrosine kinase inhibitor. *Cancer Commun (Lond Engl)* (2020) 40:285–300. doi: 10.1002/cac2.12040
19. Yang Y, Ji N, Teng QX, Cai CY, Wang JQ, Wu ZX, et al. Sitravatinib, a Tyrosine Kinase Inhibitor, Inhibits the Transport Function of ABCG2 and Restores Sensitivity to Chemotherapy-Resistant Cancer Cells in vitro. *Front Oncol* (2020) 10:700. doi: 10.3389/fonc.2020.00700
20. Wu ZX, Yang Y, Teng QX, Wang JQ, Lei ZN, Wang JQ, et al. Tivantinib, A c-Met Inhibitor in Clinical Trials, Is Susceptible to ABCG2-Mediated Drug Resistance. *Cancers* (2020) 12(1):186. doi: 10.3390/cancers12010186
21. Wang JQ, Li JY, Teng QX, Lei ZN, Ji N, Cui Q, et al. Venetoclax, a BCL-2 Inhibitor, Enhances the Efficacy of Chemotherapeutic Agents in Wild-Type ABCG2-Overexpression-Mediated MDR Cancer Cells. *Cancers* (2020) 12 (2):466. doi: 10.3390/cancers12020466
22. Johnson ZL, Chen J. Structural Basis of Substrate Recognition by the Multidrug Resistance Protein MRP1. *Cell* (2017) 168:1075–85.e9. doi: 10.1016/j.cell.2017.01.041
23. Trott O, Olson AJ. AutoDock Vina: improving the speed and accuracy of docking with a new scoring function, efficient optimization, and multithreading. *J Comput Chem* (2010) 31:455–61. doi: 10.1002/jcc.21334
24. Gezici S, Şekeroğlu N. Current Perspectives in the Application of Medicinal Plants Against Cancer: Novel Therapeutic Agents. *Anti Cancer Agents Medicinal Chem* (2019) 19:101–11. doi: 10.2174/1871520619666181224121004
25. Tao H, Zuo L, Xu H, Li C, Qiao G, Guo M, et al. Alkaloids as Anticancer Agents: A Review of Chinese Patents in Recent 5 Years. *Recent Pat Anticancer Drug Discov* (2020) 15:2–13. doi: 10.2174/1574892815666200131120618
26. Scheffler A. The Wound Healing Properties of Betulin from Birch Bark from Bench to Bedside. *Planta Med* (2019) 85:524–7. doi: 10.1055/a-0850-0224

27. Qu Y, Safonova O, De Luca V. Completion of the canonical pathway for assembly of anticancer drugs vincristine/vinblastine in Catharanthus roseus. *Plant J: Cell Mol Biol* (2019) 97:257–66. doi: 10.1111/tpj.14111
28. Dykes IM, Emanueli C. Transcriptional and Post-transcriptional Gene Regulation by Long Non-coding RNA. *Genomics Proteomics Bioinf* (2017) 15:177–86. doi: 10.1016/j.gpb.2016.12.005
29. Corbett AH. Post-transcriptional regulation of gene expression and human disease. *Curr Opin Cell Biol* (2018) 52:96–104. doi: 10.1016/j.ceb.2018.02.011
30. Tolsma TO, Hansen JC. Post-translational modifications and chromatin dynamics. *Essays Biochem* (2019) 63:89–96. doi: 10.1042/EBC20180067
31. Ho EA, Piquette-Miller M. Regulation of multidrug resistance by pro-inflammatory cytokines. *Curr Cancer Drug Targets* (2006) 6:295–311. doi: 10.2174/156800906777441753
32. Levy ES, Samy KE, Lamson NG, Whitehead KA, Kroetz DL, Desai TA. Reversible inhibition of efflux transporters by hydrogel microdevices. *Eur J Pharmaceutics Biopharmaceutics* (2019) 145:76–84. doi: 10.1016/j.ejpb.2019.10.007
33. Ferreira RJ, Bonito CA, Cordeiro M, Ferreira MU, Dos Santos D. Structure-function relationships in ABCG2: insights from molecular dynamics simulations and molecular docking studies. *Sci Rep* (2017) 7:15534. doi: 10.1038/s41598-017-15452-z
34. Lionta E, Spyrou G, Vassilatis DK, Cournia Z. Structure-based virtual screening for drug discovery: principles, applications and recent advances. *Curr Topics Medicinal Chem* (2014) 14:1923–38. doi: 10.2174/1568026614666140929124445
35. Cole SP. Multidrug resistance protein 1 (MRP1, ABCC1), a "multitasking" ATP-binding cassette (ABC) transporter. *J Biol Chem* (2014) 289:30880–8. doi: 10.1074/jbc.R114.609248

**Conflict of Interest:** The authors declare that the research was conducted in the absence of any commercial or financial relationships that could be construed as a potential conflict of interest.

frontiers in Oncology

ORIGINAL RESEARCH
published: 25 February 2021
doi: 10.3389/fonc.2021.603953

# Lung Metastases in Newly Diagnosed Esophageal Cancer: A Population-Based Study

*Jida Guo†, Shengqiang Zhang†, Huawei Li, Mohamed Osman Omar Hassan, Tong Lu, Jiaying Zhao and Linyou Zhang**

*Department of Thoracic Surgery, The Second Affiliated Hospital of Harbin Medical University, Harbin, China*

OPEN ACCESS

**Edited by:**
*Zhe-Sheng Chen,*
*St. John's University, United States*

**Reviewed by:**
*Jun Lyu,*
*First Affiliated Hospital of Jinan University, China*
*Xibao Yu,*
*Sun Yat-sen University Cancer Center (SYSUCC), China*
*Zhongbing Wu,*
*Hebei Medical University, China*

***Correspondence:**
*Linyou Zhang*
*hmulyzhang@outlook.com*

†*These authors have contributed equally to this work*

**Specialty section:**
*This article was submitted to Pharmacology of Anti-Cancer Drugs, a section of the journal Frontiers in Oncology*

**Received:** *04 December 2020*
**Accepted:** *11 January 2021*
**Published:** *25 February 2021*

**Citation:**
*Guo J, Zhang S, Li H, Hassan MOO, Lu T, Zhao J and Zhang L (2021) Lung Metastases in Newly Diagnosed Esophageal Cancer: A Population-Based Study. Front. Oncol. 11:603953. doi: 10.3389/fonc.2021.603953*

**Background:** Esophageal cancer is one of the most common cancer types, with its most common distant metastatic site being the lung. Currently, population-based data regarding the proportion and prognosis of patients with esophageal cancer with lung metastases (ECLM) at the time of diagnosis is insufficient. Therefore, we aimed to determine the proportion of patients with ECLM at diagnosis, as well as to investigate the prognostic parameters of ECLM.

**Methods:** This population-based observational study obtained data from the Surveillance, Epidemiology, and End Results (SEER) database registered between 2010 and 2016. Multivariable logistic regression was performed to identify predictors of the presence of ECLM at diagnosis. Multivariable Cox regression and competing risk analysis were used to assess prognostic factors in patients with ECLM. Median survival was estimated using Kaplan–Meier curves.

**Results:** Of 10,965 patients diagnosed with esophageal cancer between 2010 and 2016, 713 (6.50%) presented with initial lung metastasis at diagnosis. Lung metastasis represented 27.15% of all cases with metastatic disease to any distant site. Considering all patients with esophageal cancer, multivariable logistic regression indicated that pathology grade, pathology type, T staging, N staging, race, and number of extrapulmonary metastatic sites were predictive factors for the occurrence of lung metastases at diagnosis. The median survival time of patients with ECLM was 4.0 months. Patients receiving chemotherapy or chemoradiotherapy had the longest median overall survival, 7.0 months. Multivariable Cox regression indicated that age, histology type, T2 staging, number of extrapulmonary metastatic sites, and treatment (chemotherapy, radiotherapy, or chemoradiotherapy) were independent predictors for overall survival (OS). Multivariable competing risk analysis determined that age, number of extrapulmonary metastatic sites, and treatment were independent predictors for esophageal cancer-specific survival (CSS).

**Conclusion:** The findings of this study may provide important information for the early diagnosis of ECLM, as well as aid physicians in choosing appropriate treatment regimens for these patients.

**Keywords: esophageal cancer, lung metastases, survival, treatment, SEER program**

## INTRODUCTION

Esophageal cancer is the seventh most prevalent malignant tumor and has the sixth highest mortality rate worldwide (1). In 2019, 18,440 new esophageal cancer cases and 16,171 esophageal cancer-related deaths were registered in the United States (2). In Western countries, the incidence of esophageal cancer—especially esophageal adenocarcinoma—has increased over the recent decades (3–5). At the time of diagnosis, approximately 50% of patients with esophageal cancer have metastases to distant lymph nodes or other organs (6, 7). In general, the most common distant metastasis organs for esophageal cancer are, in descending order, the liver, lung, bone, and brain (8–10). The prognosis of esophageal cancer patients with distant metastases is very poor, with a 5-year survival rate <5% (11, 12). In recent years, the overall 5-year survival rate for patients with metastatic esophageal cancer may increase to approximately 20% in many countries owing to the development of new treatment methods and use of targeted drugs (13). Nonetheless, the establishment of an optimal treatment for esophageal cancer with distant metastasis (M1) requires further studies and clinical trials.

Wu et al. (13) suggested that surgery combined with radiotherapy could improve survival in patients with metastatic esophageal cancer; however, other studies had different perspectives (14, 15). Tanaka et al. (11) proposed chemoradiotherapy as an effective treatment for esophageal squamous cell carcinoma (ESCC) patients with distant metastasis. Additionally, the National Comprehensive Cancer Network (NCCN) guidelines recommend solely supportive and palliative care for these patients (16). Thus, treatment strategies for patients with M1 esophageal cancer remain controversial. To the best of our knowledge, a few population-based studies on esophageal cancer with distant metastasis have been published (17, 18). However, these studies did not provide population-level estimates of prognosis parameters for patients newly diagnosed with esophageal cancer with lung metastases (ECLM). Therefore, a population-based study providing detailed information about ECLM remains necessary to clarify the epidemiologic characteristics and prognosis associated with this disease.

The NCCN guidelines recommend using computed tomography (CT) and positron emission tomography (PET)/CT to estimate the clinical stage of esophageal cancer and determine whether distant metastases are present (16). For lung metastasis diagnosis, CT may be combined with fiberoptic bronchoscopy, endoscopic ultrasonography, and chest X-ray (19). Although CT is a routine imaging technique to monitor potential lung metastasis, its detection at the earliest stage remains a great challenge because of its small size and low density (20). With the advent of multidetector computed tomography (MDCT), especially 64-slice systems, the detection of small pulmonary nodules has improved (21). PET/CT has great advantages for excluding metastatic lesions; moreover, its positive and negative predictive values for distant metastatic diseases reached 68 and 99%, respectively (22). However, PET/CT is expensive, making it not cost-effective to use in diagnosis and evaluation. Therefore, identifying esophageal cancer patients who are at high-risk of lung metastases and determining predictive factors for ECLM occurrence are important. We believe that combining predictive factors with 64-slice MDCT may improve early and accurate diagnosis of ECLM.

In this population-based study, we used data of esophageal cancer patients with or without lung metastases from the Surveillance, Epidemiology, and End Results (SEER) database between 2010 and 2016 to determine the incidence of lung metastasis at diagnosis and to investigate predictive factors of lung metastasis detection at diagnosis on a population level. Additionally, we analyzed prognostic factors affecting the survival of ECLM patients and compared the effect of different treatments in disease prognosis.

## METHODS

### Cohort Selection and Data Collection

This retrospective study analyzed publicly available data from the SEER database. We used SEER*stat software version 8.3.4 (with additional treatment from 1975 to 2016) to extract data from the SEER-18 database, which includes information on cancer incidence, treatment, and survival for approximately 28% of the US population (23). The most recent datapoints available in the SEER database date from 2016 based on submissions up until November 2018; these became available in April 2019. Moreover, the SEER database did not include any information regarding metastases location until 2010. Therefore, we analyzed data from patients diagnosed with esophageal cancer between January 1, 2010 and December 31, 2016, including as many medical records as possible.

We screened the records of 28,213 patients who were initially diagnosed with esophageal cancer between 2010 and 2016. All patients were 18 years old or older. Exclusion criteria were as follows: 1) patients diagnosed based on death certificate or autopsy; 2) patients without active follow-up; 3) patients whose esophageal cancer was not the primary cancer; 4) lack of information about lung, liver, bone, and brain metastases at diagnosis; 5) patients whose esophageal cancer was stage T0; and 6) lack of information regarding histology grade, primary site, radiotherapy regimen, T staging, and N staging. A detailed data extraction flowchart is shown in **Figure 1**. Finally, 10,965

patients were included in the final study cohort. Of those, 2,626 patients were diagnosed with metastases to any distant site and 713 patients were diagnosed with lung metastases. Subsequently, we collected clinical and sociodemographic variables to conduct a descriptive statistical analysis and summarize the demographic and tumor characteristics of patients. Clinical variables included sex, age at diagnosis, tumor location, pathology grade, pathology type, tumor staging, T staging, N staging, treatment, race, and extra lung metastases number. Sociodemographic variables included insurance status, marital status, high school education, and median family income.

In this study, the optimal age cut-off points were determined using the X-tile program (http://www.tissuearray.org/rimmlab/), which can divide the cohort into three subsets and determine two optimal cut-off values using the minimum *p*-value from the log-rank $\chi^2$ statistics for patients' age based on survival rates (24). Therefore, we used X-tile to identify the optimal age cut-off based on the esophageal cancer-specific mortality rate of ECLM patients. As shown in **Figure 2**, the optimal age cut-off points were 58 and 74 years; thus, we stratified the cohort into three age groups: 18–58 years old, 59–74 years old, and ≥75 years old. Tumor locations included lesions in the upper, middle, and lower esophagus, as well as overlapping lesions. Cancer pathology grade was classified into three categories: well-differentiated (Grade I), moderately differentiated (Grade II), and poorly differentiated or undifferentiated (Grade III/IV). Histological types were determined using the International Classification of Diseases for Oncology, third edition (ICD-O-3) (adenocarcinoma: 8140, 8144, 8145, 8210, 8211, 8244, 8255, 8260–8263, and 8323; squamous carcinoma: 8051, 8052, 8070–8075, and 8083; others: 8000, 8010, 8013, 8020, 8033, 8041, 8046, 8094, 8480, 8490, 8560, 8574, and 8980).

TNM staging was based on the seventh edition of the Cancer Staging Manual of the American Joint Committee on Cancer (AJCC) (25). Because the eighth edition is the most commonly used classification at present, we converted the codes from the previous edition to their corresponding eighth-edition codes. T staging included T1, T2, T3, and T4; N staging included N0, N1, N2, and N3. Patients were also stratified according to treatment regimens: those who received radiotherapy (Ra), those who received chemotherapy (Che), those who received chemoradiotherapy (Che+Ra), and those who received none of these (No). In this study, the number and proportion of patients who received chemoradiotherapy were determined based on with/without chemotherapy patients number and with/without radiotherapy patients number.

Race contained white, black, and others. Insurance status was classified into insured, uninsured, and unknown. Marital status was divided into married, unmarried, and unknown. Educational levels were stipulated based on 10% increments with high school education as the base level. Median household income levels were defined using $20,000 increments. High school education

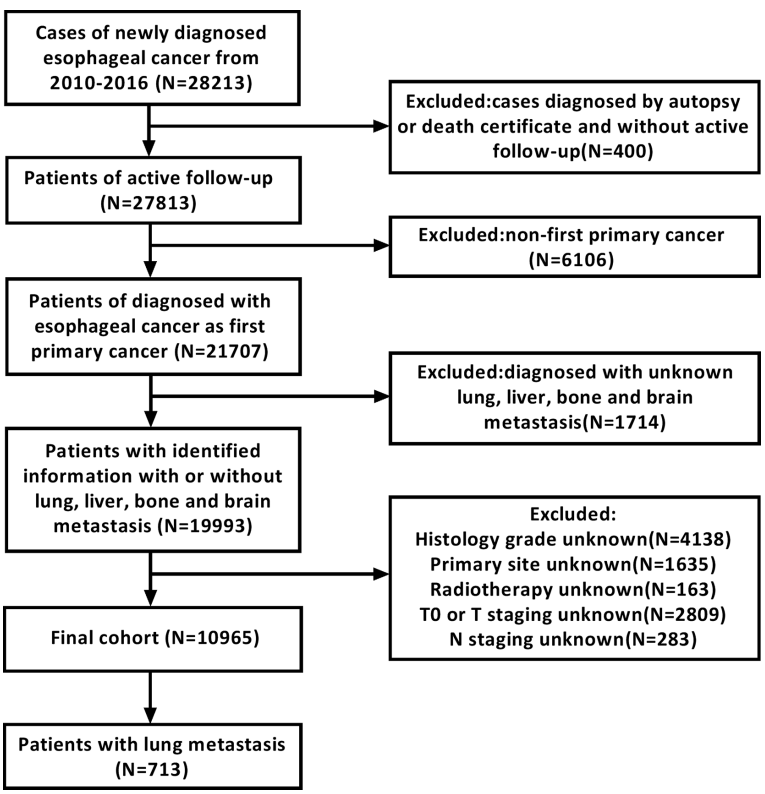


**FIGURE 1** | Flowchart of the esophageal cancer patients selection from SEER database.

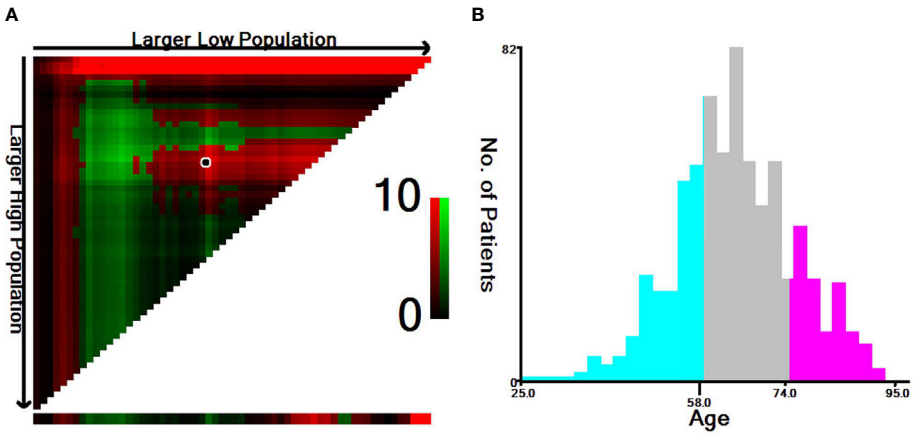


**FIGURE 2** | Identification of the optimal age cut-off points for esophageal cancer patients with lung metastasis. **(A)** X-tile plots based on age according to esophageal cancer-specific mortality. The plots show $\chi^2$ log-rank values; the brightest pixel represents the maximum $\chi^2$ log-rank value. **(B)** Distribution of patients according to age ranging from 25 to 95 years old. The optimal age cut-off of ECLM patients age is shown as 58 and 74 years old ($\chi^2 = 9.65$, $P < 0.001$).

and median family income were derived from the US Census American Community Survey obtained from the SEER*Stat software (26). Additionally, we investigated if the number of extrapulmonary metastases (in the liver, bone, brain, and other sites) at diagnosis was associated with the presence of metastasis in the lung and prognosis of ECLM patients.

## Statistical Analysis

We used descriptive statistics to calculate the absolute number, percentage, and median survival (in months) of patients with ECLM at diagnosis. ECLM incidence was determined based on the proportion of ECLM patients among the entire cohort, as well as among those diagnosed with metastatic esophageal cancer to any distant site. All data were stratified by sex, age, tumor location, and other variables. Multivariable logistic regression was used to determine predictive factors for the presence of lung metastases at diagnosis. The variables included in the multivariable logistic regression analysis were selected based on an univariable logistic regression analysis to identify statistically significant variables ($P < 0.05$).

Survival estimates were obtained using the Kaplan–Meier method and compared using the log-rank test. We conducted an univariable Cox regression model to identify statistically significant variables ($P < 0.05$); subsequently, these variables were included in the multivariable Cox regression model to determine the covariates associated with all-cause mortality. To analyze the variables that affected esophageal cancer-specific mortality, we conducted Fine and Gray's competing risk regression for univariable and multivariable analysis (27).

Statistical analyses were performed using SPSS (version 25.0; IBM Corp., Armonk, NY, USA) and R (version 3.3.2; R Foundation for Statistical Computing, Vienna, Austria) software. Logistic and Cox regression analyses were performed using SPSS. Prism 7.0 (GraphPad Software, San Diego, CA, USA) was used to plot Kaplan–Meier survival curves. R was used for competing risk analysis using the package "cmprsk" (version 2.2-72014). Two-sided *P*-values <0.05 were considered statistically significant.

# RESULTS

## Patient Characteristics

Overall, 10,965 patients were diagnosed with esophageal cancer between 2010 and 2016 in the USA. Of these, 8,867 (80.87%) were men and 2,098 (19.13%) were women, with a median age of 66 years (range, 18–102 years). The proportion of patients diagnosed with esophageal adenocarcinoma was more than two-fold of patients diagnosed with ESCC (64.30 *vs.* 28.15%). Patients' median survival was 11 months. Among all patients diagnosed with esophageal cancer, 2,626 presented with metastatic disease to any distant site and 713 presented with metastases in the lung. Regarding those with lung metastases, 594 (83.31%) were men and 119 (16.69%) were women. Moreover, those with lung metastases represented 6.50% of the entire cohort and 27.15% of patients with metastatic disease to any distant site. Patients' clinical and demographic characteristics are shown in **Table 1**.

## Predictors for the Presence of Lung Metastases

Univariable logistic regression analysis (**Supplementary Table 1**) identified 10 statistically significant variables ($P < 0.05$) among the entire cohort: age, tumor location, pathology grade, pathology type, T staging, N staging, race, insurance status, marital status, and number of extrapulmonary metastatic sites. These variables were included in the multivariable logistic regression analysis. As shown in **Table 2**, pathology grade, pathology type, T staging, N staging, race, and number of extrapulmonary metastatic sites were identified as statistically significant among the entire cohort.

**TABLE 1 |** Clinical Characteristics of Patients With Esophagus Cancer With Identified Lung Metastases at Diagnosis.

| Variable | Patients, No. | | | Proportion of Lung Metastases, % | | Survival Among Patients With Lung Metastases, Median (IQR), mo |
|---|---|---|---|---|---|---|
| | With Esophagus Cancer (n = 10,965) | With metastatic Disease (n = 2,626) | With Lung Metastases (n=713) | Among EntireCohort | Among Subset With Metastatic Disease | |
| Sex | | | | | | |
| Male | 8,867 | 2224 | 594 | 6.7 | 26.7 | 4.0 (1.0–9.0) |
| Female | 2,098 | 402 | 119 | 5.7 | 29.6 | 5.0 (1.0–10.0) |
| Age at diagnosis, Y | | | | | | |
| 18–58 | 2,830 | 835 | 205 | 7.2 | 24.6 | 5.0 (2.0–11.0) |
| 59–74 | 5,737 | 1,326 | 374 | 6.5 | 28.2 | 4.0 (1.0–9.3) |
| ≥75 | 2,398 | 465 | 134 | 5.6 | 28.8 | 3.0 (1.0–7.3) |
| Year at diagnosis | | | | | | |
| 2010 | 1,553 | 378 | 98 | 6.3 | 25.9 | 4.5 (2.0–9.5) |
| 2011 | 1,542 | 365 | 102 | 6.6 | 28.7 | 6.0 (2.0–11.0) |
| 2012 | 1,546 | 383 | 112 | 7.2 | 29.2 | 3.0 (1.0–8.0) |
| 2013 | 1,607 | 375 | 105 | 6.5 | 28.0 | 5.0 (1.5–11.5) |
| 2014 | 1,596 | 363 | 93 | 5.8 | 25.6 | 5.0 (2.0–12.0) |
| 2015 | 1,681 | 428 | 109 | 6.5 | 25.5 | 3.0 (1.0–8.5) |
| 2016 | 1,440 | 343 | 94 | 6.5 | 27.4 | 3.0 (1.0–6.0) |
| Tumor location | | | | | | |
| Upper | 739 | 112 | 51 | 6.9 | 45.5 | 4.0 (2.0–10.0) |
| Middle | 1,731 | 340 | 121 | 7.0 | 35.6 | 4.0 (2.0–10.0) |
| Lower | 7,988 | 2,008 | 485 | 6.1 | 24.2 | 4.0 (1.0–9.0) |
| Overlapping | 507 | 166 | 56 | 11.0 | 33.7 | 2.0 (1.0–7.75) |
| Pathology grade | | | | | | |
| Grade I | 730 | 69 | 18 | 2.5 | 26.1 | 5.0 (1.75–13.5) |
| Grade II | 4,670 | 917 | 284 | 6.1 | 31.0 | 5.0 (2.0–10.0) |
| Grade III/IV | 5,565 | 1,640 | 411 | 7.4 | 25.1 | 4.0 (1.0–9.0) |
| Histology type | | | | | | |
| Adenocarcinoma | 7,050 | 1,826 | 441 | 6.3 | 24.2 | 5.0 (2.0–10.0) |
| Squamous | 3,087 | 568 | 226 | 7.3 | 39.8 | 4.0 (1.0–9.0) |
| Others[a] | 828 | 232 | 46 | 5.6 | 19.8 | 1.5 (0.0–5.0) |
| Tumor staging[b] | | | | | | |
| I | 1,990 | 0 | 0 | 0 | 0 | NA |
| II | 2,453 | 0 | 0 | 0 | 0 | NA |
| III | 3,869 | 0 | 0 | 0 | 0 | NA |
| IV | 2,626 | 2,626 | 713 | 27.2 | 27.2 | 4.0 (1.0–9.0) |
| T staging[b] | | | | | | |
| T1 | 3,071 | 846 | 254 | 8.3 | 30.0 | 3.0 (1.0–9.0) |
| T2 | 1,435 | 188 | 31 | 2.2 | 16.5 | 6.0 (1.0–9.0) |
| T3 | 4,984 | 866 | 185 | 3.7 | 21.4 | 6.0 (3.0–13.0) |
| T4 | 1,475 | 726 | 243 | 16.5 | 33.5 | 3.0 (1.0–7.0) |
| N staging[b] | | | | | | |
| N0 | 5,107 | 584 | 175 | 3.4 | 30.0 | 3.0 (1.0–9.0) |
| N1 | 4,704 | 1471 | 413 | 8.8 | 28.1 | 4.0 (1.0–10.0) |
| N2 | 661 | 340 | 64 | 9.7 | 18.8 | 5.0 (2.0–9.0) |
| N3 | 493 | 231 | 61 | 12.4 | 26.4 | 3.0 (1.0–8.0) |
| Treatment[c] | | | | | | |
| No | 2,265 | 508 | 179 | 7.9 | 35.2 | 1.0 (0.0–2.0) |
| Ra | 727 | 294 | 102 | 14.0 | 34.7 | 2.0 (1.0–5.0) |
| Che | 1,303 | 854 | 204 | 15.7 | 23.7 | 7.0 (3.0–13.0) |
| Che+Ra | 6,670 | 970 | 228 | 3.4 | 23.5 | 7.0 (4.0–12.0) |
| Race | | | | | | |
| White | 9,349 | 2,239 | 570 | 6.1 | 25.5 | 4.0 (1.0–9.0) |
| Black | 995 | 235 | 94 | 9.4 | 40.0 | 3.0 (1.0–8.25) |
| Others[d] | 586 | 142 | 47 | 8.0 | 33.1 | 5.0 (2.0–11.0) |
| Unknown | 35 | 10 | 2 | 5.7 | 20.0 | 1.5 (0.0–NA) |
| Insurance status | | | | | | |
| Insured | 10,472 | 2,482 | 666 | 6.4 | 26.8 | 4.0 (1.0–9.25) |
| Uninsured | 335 | 113 | 36 | 10.7 | 31.9 | 3.0 (1.0–5.75) |
| Unknown | 158 | 31 | 11 | 7.0 | 35.5 | 3.0 (0.0–13.0) |
| Marital status | | | | | | |
| Married | 6,171 | 1,472 | 364 | 5.9 | 24.7 | 4.5 (2.0–10.0) |

*(Continued)*

**TABLE 1** | Continued

| Variable | Patients, No. | | | Proportion of Lung Metastases, % | | Survival Among Patients With Lung Metastases, Median (IQR), mo |
|---|---|---|---|---|---|---|
| | With Esophagus Cancer (n = 10,965) | With metastatic Disease (n = 2,626) | With Lung Metastases (n=713) | Among EntireCohort | Among Subset With Metastatic Disease | |
| Unmarried | 4,267 | 1,050 | 313 | 7.3 | 29.8 | 4.0 (1.0–9.0) |
| Unknown | 527 | 104 | 36 | 6.8 | 34.6 | 5.5 (1.25–13.0) |
| High school education | | | | | | |
| 0–10% | 3,235 | 753 | 191 | 5.9 | 25.4 | 5.0 (2.0–10.0) |
| 10–20% | 5,640 | 1,381 | 378 | 6.7 | 27.4 | 4.0 (1.0–9.0) |
| 20–30% | 1,950 | 426 | 137 | 7.0 | 29.7 | 4.0 (1.0–9.0) |
| 30–40% | 140 | 30 | 7 | 5.0 | 23.3 | 3.0 (3.0–13.0) |
| Median household income | | | | | | |
| 20,000–40,000 | 105 | 17 | 4 | 3.8 | 23.5 | 2.0 (0.25–3.0) |
| 40,000–60,000 | 2,291 | 574 | 166 | 7.2 | 28.9 | 4.0 (1.0–9.0) |
| 60,000–80,000 | 4,256 | 1,041 | 283 | 6.6 | 27.2 | 4.0 (1.0–9.0) |
| 80,000–100,000 | 2,821 | 636 | 160 | 5.7 | 25.2 | 5.0 (1.0–11.0) |
| >100,000 | 1,492 | 358 | 100 | 6.7 | 27.9 | 5.0 (2.0–9.75) |
| Extrapulmonary metastatic sites to liver, bone, brain, and others No. | | | | | | |
| 0 | 9,250 | 911 | 293 | 3.2 | 32.1 | 5.0 (2.0–11.0) |
| 1 | 1,353 | 1,353 | 294 | 21.7 | 21.7 | 4.0 (1.0–9.0) |
| 2 | 316 | 316 | 98 | 31.0 | 31.0 | 3.0 (1.0–6.0) |
| 3 | 46 | 46 | 28 | 60.9 | 60.9 | 2.0 (2.0–6.0) |

*IQR, interquartile range, CI, confidence interval;*
[a]*Including signet ring cell carcinoma, Mucinous carcinoma, etc.*
[b]*According to the eighth edition of the AJCC Cancer Staging manual.*
[c]*Including No, Without Radiotherapy or Chemotherapy; RA, Radiotherapy; Che, Chemotherapy; Ra+Che, Radiotherapy plus Chemotherapy.*
[d]*Including Hispanic, Asian, etc.*

Specifically, the following factors were associated with greater odds of lung metastasis presence at diagnosis: pathology grade II (*vs.* grade I; odds ratio [OR], 2.031; 95% confidence interval [CI], 1.222–3.375; $P = 0.006$), pathology grade III/IV (*vs.* grade I; OR, 1.975; 95% CI, 1.190–3.276; $P = 0.008$), squamous cell carcinoma (*vs.* adenocarcinoma; OR, 1.349; 95% CI, 1.064–1.710; $P = 0.013$), stage T4 (*vs.* T1; OR, 1.287; 95% CI, 1.040–1.592; $P = 0.020$), stage N1 (*vs.* N0; OR, 2.055; 95% CI, 1.682–2.512; $P < 0.001$), stage N2 (*vs.* N0; OR, 2.076; 95% CI, 1.482–2.909; $P < 0.001$), stage N3 (*vs.* N0; OR, 2.419; 95% CI, 1.695–3.452; $P < 0.001$), black race (*vs.* white; OR, 1.359; 95% CI, 1.028–1.797; $P = 0.031$), 1 extrapulmonary metastatic site (*vs.* 0 extrapulmonary metastatic site; OR, 6.294; 95% CI, 5.194–7.627; $P < 0.001$), 2 extrapulmonary metastatic sites (*vs.* 0 extrapulmonary metastatic site; OR, 10.187; 95% CI, 7.643–13.576; $P < 0.001$), and 3 extrapulmonary metastatic sites (*vs.* 0 extrapulmonary metastatic site; OR, 32.767; 95% CI, 17.187–62.472; $P < 0.001$). Conversely, the multivariable model indicated that sex, age, tumor location, insurance status, and marital status were not associated with the risk of lung metastasis presence at diagnosis. Additionally, stage T2 (*vs.* T1; OR, 0.297; 95% CI, 0.188–0.414; $P < 0.001$) and stage T3 (*vs.* T1; OR, 0.441; 95% CI, 0.355–0.547; $P < 0.001$) were associated with marginally lower odds of lung metastasis presence at diagnosis.

Considering these results, patients with esophageal cancer who presented with poor tumor grade, squamous cell carcinoma, T4 staging, late N staging, and presence of more metastatic sites, as well as black patients, had a higher risk of presenting with lung metastases at diagnosis, whereas T2 and T3 staging were considered protective factors for lung metastasis at diagnosis.

## Survival

For all-cause mortality among patients with metastatic disease to any distant site, univariable Cox regression analysis identified twelve variables that were significantly associated with overall survival ($P < 0.05$): sex, age, pathology type, T staging, N staging, number of extrapulmonary metastatic sites, race, insurance situation, marital status, high school education, median household income, and treatment (**Supplementary Table 2**). These variables were included in the multivariable Cox regression analyses. The statistics showed that eight variables were significantly associated with all-cause mortality for esophageal cancer patients with distant metastases ($P < 0.05$), including sex, age, pathology type, T staging, number of extrapulmonary metastatic sites, marital status, median household income, and treatment. Detailed statistical results are shown in **Supplementary Table 3**.

Univariable Cox regression analysis for all-cause mortality among patients with ECLM identified seven variables that were significantly associated with overall survival ($P < 0.05$): age, tumor location, pathology type, T staging, number of extrapulmonary metastatic sites, median household income, and treatment type. Regarding esophageal cancer-specific mortality, univariable competing risk analysis identified four variables that were significantly associated with cancer-specific survival ($P < 0.05$): age, pathology type, number of extrapulmonary metastatic sites, and treatment type. Details of the univariable analysis of mortality among patients with ECLM are displayed in **Supplementary Table 4**.

The variables identified using univariable analyses were included in multivariable analyses (**Table 3**). Multivariable Cox regression

**TABLE 2 |** Multivariable Logistic Regression for the Presence of Lung Metastases at Diagnosis of Esophagus Cancer.

| Variable | Patients, No | | Among Entire Cohort | |
|---|---|---|---|---|
| | Patients (n = 10,965) | With Lung Metastases (n = 713) | OR (95% CI) | *P* Value |
| Sex | | | | |
| Male | 8,867 | 594 | NA | NA |
| Female | 2,098 | 119 | NA | NA |
| Age at diagnosis (Year) | | | | |
| 18–58 | 2,830 | 205 | 1 (reference) | NA |
| 59–74 | 5,737 | 374 | 1.131 (0.930–1.375) | 0.218 |
| ≥75 | 2,398 | 134 | 1.142 (0.891–1.465) | 0.293 |
| Tumor location | | | | |
| Upper | 739 | 51 | 1 (reference) | NA |
| Middle | 1,731 | 121 | 1.003 (0.694–1.450) | 0.986 |
| Lower | 7,988 | 485 | 0.880 (0.614–1.261) | 0.485 |
| Overlapping | 507 | 56 | 1.295 (0.826–2.032) | 0.260 |
| Pathology grade | | | | |
| Grade I | 730 | 18 | 1 (reference) | NA |
| Grade II | 4,670 | 284 | 2.031 (1.222–3.375) | 0.006 |
| Grade III/IV | 5,565 | 411 | 1.975 (1.190–3.276) | 0.008 |
| Histology type | | | | |
| Adenocarcinoma | 7,050 | 441 | 1 (reference) | NA |
| Squamous | 3,087 | 226 | 1.349 (1.064–1.710) | 0.013 |
| Others[a] | 828 | 46 | 0.831 (0.591–1.168) | 0.286 |
| T staging[b] | | | | |
| T1 | 3,071 | 254 | 1 (reference) | NA |
| T2 | 1,435 | 31 | 0.297 (0.188–0.414) | <0.001 |
| T3 | 4,984 | 185 | 0.441 (0.355–0.547) | <0.001 |
| T4 | 1,475 | 243 | 1.287 (1.040–1.592) | 0.020 |
| N staging[b] | | | | |
| N0 | 5,107 | 175 | 1 (reference) | NA |
| N1 | 4,704 | 413 | 2.055 (1.682–2.512) | <0.001 |
| N2 | 661 | 64 | 2.076 (1.482–2.909) | <0.001 |
| N3 | 493 | 61 | 2.419 (1.695–3.452 | <0.001 |
| Race | | | | |
| White | 9,394 | 570 | 1 (reference) | NA |
| Black | 995 | 94 | 1.359 (1.028–1.797) | 0.031 |
| Others[c] | 586 | 47 | 1.293 (0.912–1.832) | 0.149 |
| Unknown | 35 | 2 | 0.768 (0.166–3.546) | 0.735 |
| Insurance status | | | | |
| Insured | 10,472 | 666 | 1 (reference) | NA |
| Uninsured | 335 | 36 | 1.120 (0.749–1.674) | 0.581 |
| Unknown | 158 | 11 | 1.090 (0.557–2.134) | 0.802 |
| Marital status | | | | |
| Married | 6,171 | 364 | 1 (reference) | NA |
| Unmarried | 4,267 | 313 | 1.161 (0.973–1.384) | 0.097 |
| Unknown | 527 | 36 | 1.455 (0.987–2.143) | 0.058 |
| High school education (per 10% increase) | 10,965 | 713 | NA | NA |
| Median household income (per 20,000 increase) | 10,965 | 713 | NA | NA |
| Extrapulmonary metastatic sites to liver, bone, brain, and others No. | | | | |
| 0 | 9,250 | 293 | 1 (reference) | NA |
| 1 | 1,353 | 294 | 6.294 (5.194–7.627) | <0.001 |
| 2 | 316 | 98 | 10.187 (7.643–13.576) | <0.001 |
| 3 | 46 | 28 | 32.767 (17.187–62.472) | <0.001 |

*CI, confidence interval; OR, odds ratio*

[a]*Including signet ring cell carcinoma, Mucinous carcinoma, etc.*

[b]*According to the eighth edition of the AJCC Cancer Staging manual.*

[c]*Including Hispanic, Asian, etc.*

analysis indicated that the following factors were associated with an increase in all-cause mortality among patients with ECLM: age ≥75 years (*vs.* 18–58 years; hazard ratio [HR], 1.481; 95% CI, 1.168–1.877; $P = 0.001$), other pathology types (*vs.* adenocarcinoma; HR, 1.769; 95% CI, 1.275–2.454; $P = 0.001$), 1 extrapulmonary metastatic site (*vs.* 0 extrapulmonary metastatic site; HR, 1.190; 95% CI, 1.333–1.107; $P=0.002$), and ≥2 extrapulmonary metastatic sites (*vs.* 0 extrapulmonary metastatic site; HR, 1.822; 95% CI, 1.419–2.339;

$P < 0.001$). Conversely, stage T2 (*vs.* T1; HR, 0.633; 95% CI, 0.404–0.992; $P = 0.046$), Ra treatment (*vs.* No treatment; HR, 0.648; 95% CI, 0.500–0.839; $P = 0.001$), Che treatment (*vs.* No treatment; HR, 0.260; 95% CI, 0.209–0.325; $P < 0.001$), and Che+Ra treatment (*vs.* No treatment; HR, 0.259; 95% CI, 0.206–0.325; $P < 0.001$) were significantly associated with a decrease in all-cause mortality. Tumor location and median household income were not significantly associated with all-cause mortality ($P > 0.05$).

Multivariable competing risk analysis for esophageal cancer-specific mortality among patients with ECLM identified the following factors associated with an increase in esophageal cancer-specific mortality: age ≥75 years (*vs.* 18–58 years; HR, 2.359; 95% CI, 1.346–4.135; $P = 0.003$), 1 extrapulmonary metastatic site (*vs.* 0 extra-pulmonary metastatic site; HR, 1.278; 95% CI, 1.026–1.593; $P=0.029$), ≥2 extrapulmonary metastatic sites (*vs.* 0 extrapulmonary metastatic site; HR, 1.469; 95% CI, 1.099–1.963; $P = 0.009$). Conversely, Che treatment (*vs.* No treatment; HR, 0.169; 95% CI, 0.098–0.391; $P < 0.001$) and Che+Ra treatment (*vs.* No treatment; HR, 0.223; 95% CI, 0.117–0.423; $P < 0.001$) were significantly associated with a decrease in esophageal cancer-specific mortality. Pathology type (including squamous cell carcinoma, adenocarcinoma, and others) and Ra treatment were not associated with esophageal cancer-specific mortality.

Multivariable Cox regression analysis indicated that other histology types were associated with poor overall survival, whereas T2 staging was associated with improved overall survival. Furthermore, considering the results of both multivariable models, patients with ECLM who were 75 years old or older had a worse prognosis, which was consistent with the optimal age cut-off points for patients with ECLM (**Figure 2**). Moreover, the multivariable analyses indicated that those with an extensive systemic disease at diagnosis had poor survival, while those who received positive treatment (radiotherapy, chemotherapy, or chemoradiotherapy) had improved survival.

Survival estimates obtained using the Kaplan–Meier method indicated that the median survival of patients with ECLM was 4.0 months (interquartile range [IQR], 1.0–9.0 months) (**Figure 3A**). The median survival of patients with ECLM aged 18–58 years was 5.0 months (IQR, 2.0–11.0 months); 59–74 years, 4.0 months (IQR, 1.0–9.3 months); and ≥75 years, 3.0 months (IQR, 1.0–7.3 months) (**Figure 3B**). The median survival of those with no extrapulmonary metastatic site was 5.0 months (IQR, 2.0–11.0 months); 1 extrapulmonary metastatic site, 4.0 months (IQR, 1.0–9.0 months); with ≥2 extrapulmonary metastatic sites, 3.0 months (IQR, 1.0–6.0 months) (**Figure 3C**). Finally, the median survival of patients with ECLM who received No treatment was 1.0 month (IQR, 0.0–2.0 months); Ra treatment, 2.0 months (IQR, 1.0–5.0 months); Che treatment, 7.0 months (IQR, 3.0–13.0 months); and Che+Ra treatment, 7.0 months (IQR, 4.0–12.0 months) (**Figure 3D**). In summary, those treated with chemotherapy or chemoradiotherapy had the best prognosis, while those who received no treatment had the worst prognosis.

Among all patients with ECLM, 102 (14.31%) received radiotherapy, 204 (28.61%) received chemotherapy, and 228 (31.98%) received chemoradiotherapy. Among the entire cohort, 727 (6.63%) patients received radiotherapy, 1,303 (11.88%) received chemotherapy, and 6,670 (60.83%) received chemoradiotherapy. Therefore, those who received chemoradiotherapy represented the majority in the entire cohort and among patients with ECLM.

## DISCUSSION

To the best of our knowledge, this is the first population-based study to describe the incidence proportion of ECLM and analyze the predictive and prognostic factors associated with the outcomes of patients with ECLM at diagnosis. We used the most recent data on esophageal cancer available in the SEER database, identifying and including 713 patients with ECLM in our study—possibly the largest number of patients with ECLM included in a study. We used descriptive statistical and logistic regression analyses to investigate the factors associated with ECLM at diagnosis. Moreover, we used three statistical methods (Kaplan–Meier curves, Cox regression, and competing risk analyses) to obtain survival estimates. The results presented in this study may aid physicians in timely detecting lung metastases and choosing appropriate treatment methods.

We demonstrated that 6.50% of patients with esophageal cancer had lung metastases at diagnosis, and 27.15% of esophageal cancer patients with any distant metastases at diagnosis had lung metastases. These results were similar to those of a previous study that also used data from the SEER database (17); conversely, our results were higher than those reported by another study based on the SEER database (28). This discrepancy may be caused by the use of different exclusion criteria. Nonetheless, our study included a larger cohort than the abovementioned studies, indicating that our analysis had greater statistical power. A previous study reported that lung metastases represented 20% of all metastatic esophageal cancer cases (14), a proportion slightly lower than that found in our study. This difference may be explained by an increase in the proportion of metastatic diseases over the past 20 years, as well as the development of diagnostic technologies that can detect the presence of lung metastases more efficiently. An autopsy-based study reported that 52% of patients had lung metastases, the largest proportion ever reported (29). The authors of this study hypothesized that differences in race and sex between patients included in their cohort and those included in other studies were the main reason for this discrepancy, as well as the use of data with very few postoperative deaths.

Our and other studies have shown that patients with squamous cell carcinoma were more likely to develop lung metastasis compared with those with other esophageal cancer histological types (17, 28). The aforementioned autopsy-based study (29) was based solely on autopsy findings of patients with ESCC, representing an additional reason for the high proportion of lung metastases found in their study. Another autopsy-based study reported that 31% of patients with metastatic esophageal cancer had lung metastases (30), a proportion slightly higher than that found in our study. Their autopsy series included patients with recurred or post-treatment lung metastases, whereas we exclusively included those with lung metastases at diagnosis. In addition,

**TABLE 3 |** Multivariable Cox Regression for All-Cause Mortality and Esophageal Cancer Specific Mortality Among Patients With Lung Metastases.

| Variable | Patients, No. | | All-cause mortality | | Cancer-specific mortality | |
|---|---|---|---|---|---|---|
| | Patients (n = 10,965) | With Lung Metastases (n = 713) | Hazard Ratio (95% CI) | *P* Value | Hazard Ratio (95% CI) | *P* Value |
| Sex | | | | | | |
| Male | 8,867 | 594 | NA | NA | NA | NA |
| Female | 2,098 | 119 | NA | NA | NA | NA |
| Age at diagnosis, Y | | | | | | |
| 18–58 | 2,830 | 205 | 1 (reference) | NA | 1 (reference) | NA |
| 59–74 | 5,737 | 374 | 1.147 (0.954–1.379) | 0.144 | 1.341 (0.771–2.334) | 0.300 |
| ≥75 | 2,398 | 134 | 1.481 (1.168–1.877) | 0.001 | 2.359 (1.346–4.135) | 0.003 |
| Tumor location | | | | | | |
| Upper | 739 | 51 | 1 (reference) | NA | NA | NA |
| Middle | 1,731 | 121 | 1.159 (0.818–1.641) | 0.407 | NA | NA |
| Lower | 7,988 | 485 | 1.117 (0.788–1.584) | 0.502 | NA | NA |
| Overlapping | 507 | 56 | 1.385 (0.917–2.093) | 0.121 | NA | NA |
| Pathology grade | | | | | | |
| Grade I | 730 | 18 | NA | NA | NA | NA |
| Grade II | 4,670 | 284 | NA | NA | NA | NA |
| Grade III/IV | 5,565 | 411 | NA | NA | NA | NA |
| Histology type | | | | | | |
| Adenocarcinoma | 7,050 | 441 | 1 (reference) | NA | 1 (reference) | NA |
| Squamous | 3,087 | 226 | 1.117 (0.905–1.378) | 0.421 | 1.155 (0.745–1.739) | 0.520 |
| Others[a] | 828 | 46 | 1.769 (1.275–2.454) | 0.001 | 1.468 (0.760–2.907) | 0.250 |
| T staging[b] | | | | | | |
| T1 | 3,071 | 254 | 1 (reference) | NA | NA | NA |
| T2 | 1,435 | 31 | 0.633 (0.404–0.992) | 0.046 | NA | NA |
| T3 | 4,984 | 185 | 0.864 (0.696–1.071) | 0.183 | NA | NA |
| T4 | 1,475 | 243 | 1.095 (0.911–1.318) | 0.334 | NA | NA |
| N staging[b] | | | | | | |
| N0 | 5,107 | 175 | NA | NA | NA | NA |
| N1 | 4,704 | 413 | NA | NA | NA | NA |
| N2 | 661 | 64 | NA | NA | NA | NA |
| N3 | 493 | 61 | NA | NA | NA | NA |
| Extrapulmonary metastatic sites to liver, bone, brain, and others No. | | | | | | |
| 0 | 9,250 | 293 | 1 (reference) | NA | 1 (reference) | NA |
| 1 | 1,353 | 294 | 1.333 (1.107–1.605) | 0.002 | 1.278 (1.026–1.593) | 0.029 |
| ≥2 | 362 | 126 | 1.822 (1.419–2.339) | <0.001 | 1.469 (1.099–1.963) | 0.009 |
| Race | | | | | | |
| White | 9,394 | 570 | NA | NA | NA | NA |
| Black | 995 | 94 | NA | NA | NA | NA |
| Others[c] | 586 | 47 | NA | NA | NA | NA |
| Unknown | 35 | 2 | NA | NA | NA | NA |
| Insurance status | | | | | | |
| Insured | 10,472 | 666 | NA | NA | NA | NA |
| Uninsured | 335 | 36 | NA | NA | NA | NA |
| Unknown | 158 | 11 | NA | NA | NA | NA |
| Marital status | | | | | | |
| Married | 6,171 | 364 | NA | NA | NA | NA |
| Unmarried | 4,267 | 313 | NA | NA | NA | NA |
| Unknown | 527 | 36 | NA | NA | NA | NA |
| High school education (per 10% increase) | 10,965 | 713 | NA | NA | NA | NA |
| Median household income (per 20000 increase) | 10,965 | 713 | 0.958 (0.882–1.040) | 0.307 | NA | NA |
| Treatment[d] | | | | | | |
| No | 2,265 | 179 | 1 (reference) | NA | 1 (reference) | NA |
| Ra | 727 | 102 | 0.648 (0.500–0.839) | 0.001 | 0.965 (0.620–1.500) | 0.870 |
| Che | 1,303 | 204 | 0.260 (0.209–0.325) | <0.001 | 0.196 (0.098–0.391) | <0.001 |
| Che+Ra | 6,670 | 228 | 0.259 (0.206–0.325) | <0.001 | 0.223 (0.117–0.423) | <0.001 |

*CI, confidence interval*

[a]*Including signet ring cell carcinoma, Mucinous carcinoma, etc.*

[b]*According to the eighth edition of the AJCC Cancer Staging manual.*

[c]*Including Hispanic, Asian, etc.*

[d]*Including No, Without Radiotherapy or Chemotherapy; RA, Radiotherapy; Che, Chemotherapy; Ra+Che, Radiotherapy plus Chemotherapy.*

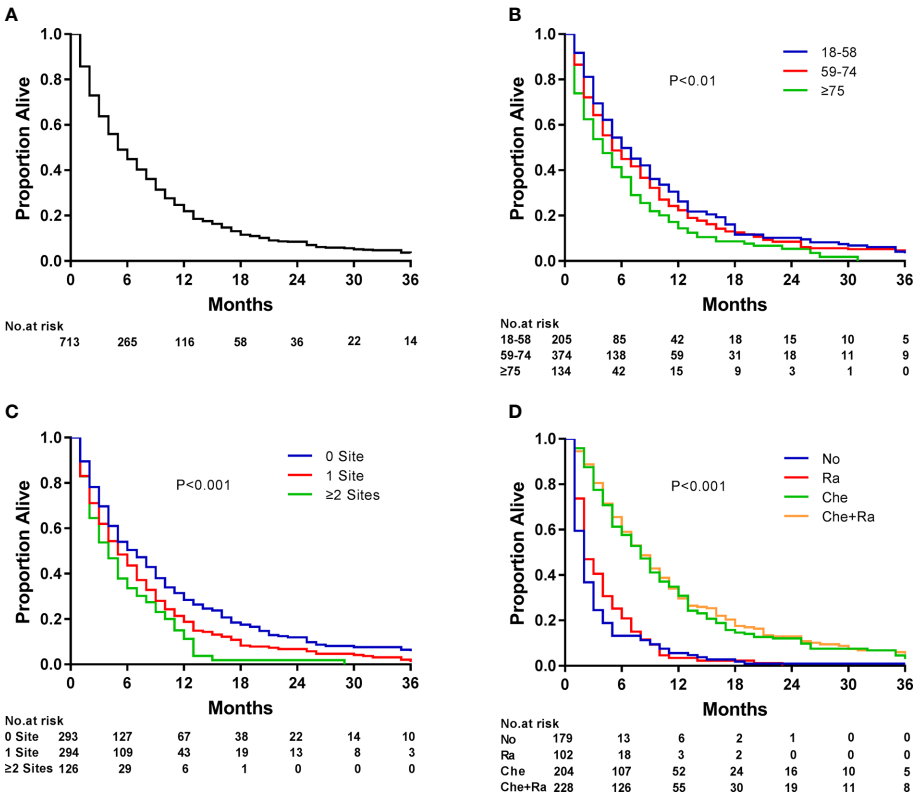


**FIGURE 3** | Kaplan–Meier analysis of overall survival among esophageal cancer patients with lung metastasis at diagnosis. **(A)** overall, **(B)** stratified by age, **(C)** stratified by the extent of extrapulmonary metastatic disease, and **(D)** stratified by type of treatment.

metastases are more easily detected during autopsy than during physical and imaging examinations performed at the time of esophageal cancer diagnosis. Accordingly, the proportion of patients with ECLM found in our study and in other SEER-based studies are consistently lower than those found in autopsy-based studies (17, 28–30).

In our study, we used multivariable logistic regression analysis to determine predictive factors for the presence of lung metastasis at diagnosis and identify those at increased risk of having lung metastases. We showed that patients with poor tumor grade, squamous cell carcinoma histological type, T4 staging, late N staging, and more extrapulmonary metastatic sites, as well as black patients, had an increased risk of having lung metastases at diagnosis compared with the entire cohort. Regarding pathology grades, among the entire cohort, 6.66, 42.59, and 50.75% of patients with lung metastases had diseases grade I, II, and III/IV, respectively. Among those with metastatic esophageal cancer, 2.63, 34.92, and 62.45% of patients with lung metastases had diseases grade I, II, and III/IV, respectively. Those with disease grade II and III/IV had a significantly greater likelihood of presenting with lung metastases at diagnosis than those with disease grade I. These results are in accordance with previous studies (17, 31, 32). Higher pathology grades are considered more malignant; accordingly, several studies have demonstrated that pathology grade is a strong survival predictor, with higher grades indicating a poor prognosis (33, 34). Nonetheless, the mechanism behind the association between higher pathology grades and lung metastasis occurrence requires further elucidation.

Regarding tumor pathology types, patients diagnosed with squamous cell carcinoma had a higher proportion of lung metastases than those diagnosed with adenocarcinoma. This finding is in accordance with previously mentioned studies (17, 28), as well as with other Japanese studies that reported the lung as the most common distant metastasis site in ESCC (35, 36). We hypothesized that the higher proportion of lung metastasis in ESCC may be related with tumor location because most esophageal adenocarcinomas were located in the lower esophagus, whereas ESCC was more evenly distributed throughout the upper, middle, and lower esophagus, with the middle esophagus representing the largest proportion (8, 31). However, the underlying mechanisms of distant metastasis responsible for the differences observed between these two pathology subtypes remain unclear.

Regarding T staging, tumors in T4 stage had a significantly higher percentage of lung metastasis compared with those of tumors in T2 and T3 stages. Furthermore, tumors in late N staging had a higher proportion of lung metastasis than that of tumors in early N staging. Accordingly, a previous study reported that T and N staging were the greatest contributors in metastasis prediction (32). Sakanaka et al. (37) demonstrated that patients with larger metastatic lymph nodes were at a higher risk of developing

diseases with distant metastases. Therefore, many studies have recognized late T staging and N staging as important factors for the occurrence of distant metastasis in esophageal cancer. In our study, T2 and T3 staging were associated with a lower risk of lung metastasis at diagnosis. Most T and N staging included in the SEER database were based on clinical staging using CT and other imaging examinations; consequently, the staging may be less accurate than pathological and autopsy-based staging used in other studies (38).

Black patients had a significantly greater likelihood of presenting with lung metastases at diagnosis than white patients. The reason for this difference remains unknown and requires further elucidation (38). In our study, esophageal cancer patients with more extrapulmonary metastatic sites had a significantly higher risk of lung metastasis. This finding is similar to those of studies on other metastatic malignant tumors, such as breast and gastric cancers (38, 39). We hypothesized that hematogenous and lymphatic dissemination caused by metastatic sites may increase the occurrence of distant metastases. Further studies focusing on this topic are warranted.

In clinical practice, CT scanning is often used to detect lung metastases; however, the detection of early metastatic lesions in the lung using this imaging technique is challenging (20). Conversely, 64-slice MDCT has great advantages for detecting small lung nodules (21). Patients poor tumor grade, squamous cell carcinoma histological type, T4 staging, late N staging, and more extrapulmonary metastatic sites, as well as black patients, should receive increased attention during clinical examination. Specifically, we suggest that these patients should undergo 64-slice MDCT scanning for lung nodules screening and, if necessary, pulmonary puncture pathology to ensure the early diagnosis of lung metastases. Timely diagnosis is important to assure that patients will receive appropriate treatment as soon as possible, significantly prolonging their survival and improving their quality of life (11, 17, 31).

In our study, we used competing risks analysis to identify variables affecting esophageal cancer-specific mortality. This analysis is based on events that occurred prior to the primary event of interest. Therefore, when predicting disease-specific outcomes, competing risk analysis provides a better estimation for the clinical prognosis of patients, helping clinicians to apply appropriate therapy strategies (40). Multivariable Cox regression analysis among patients with lung metastases indicated that patients with other histology types (e.g., signet ring cell carcinoma) had poorer OS than those with adenocarcinoma owing to their more aggressive biological behaviors (41). Interestingly, patients with T2-stage tumors had a better prognosis than those with T1-stage tumors. This finding may have been influenced by T staging inaccuracies in the SEER database.

Our study showed that patients who were 75 years old or older and with more extrapulmonary metastatic sites had a significantly lower overall survival and cancer-specific survival, while patients who received positive treatment (radiotherapy, chemotherapy, or chemoradiotherapy) had better prognoses. Patients aged ≥75 years had a shorter survival time than those aged 18–58 years. This discrepancy may be a result of poorer physical fitness and reduced natural life expectancy of older adults. Furthermore, from our findings, we observed that more extrapulmonary metastatic sites were consistently associated with poorer survival, which is in accordance with the results of other studies (17, 18). This trend is similar to that observed in other malignant tumors (38, 39). Therefore, a higher number of metastatic sites may indicate a poor prognosis in malignant diseases in general.

As evidenced by the Kaplan–Meier curves, radiotherapy, chemotherapy, and chemoradiotherapy treatment increased the median survival of patients with ECLM by 1, 6, and 6 months, respectively, compared with no treatment. The median survival of patients who received chemotherapy or chemoradiotherapy did not differ significantly ($P = 0.366$). Furthermore, patients who received radiotherapy had a better prognosis than patients who received no therapy ($P < 0.01$). However, similarly to the results of another SEER-based study (42), radiotherapy did not significantly affect cancer-specific mortality. In contrast, other studies have reached different conclusions (12, 43). Differently from these studies, we focused on patients with ECLM and their cancer-specific mortality, which may explain the result discrepancy. A prospective study suggested that chemoradiotherapy was superior to radiotherapy alone for treating patients with esophageal cancer (44). Another retrospective study showed that patients with stage IV B ESCC who underwent multimodality therapy, especially chemoradiotherapy, had significantly better survival than those who underwent single-modality therapy and supportive care (11). Similarly, we also found that chemoradiotherapy was superior to radiotherapy alone ($P < 0.01$). Furthermore, Wang et al. (45) reported that local therapy with radiation (median dose, 5,040 cGy) after initial palliative chemotherapy could achieve better local control and long-term survival in patients with stage IV B esophageal cancer. Guttmann et al. (46) demonstrated that chemotherapy combined with definitive dose radiotherapy (≥5,040 cGy) to the primary tumor could improve survival in patients with metastatic esophageal cancer compared with chemotherapy alone, whereas chemotherapy combined with palliative dose radiotherapy (<5,040 cGy) had a slightly worse prognosis than that of chemotherapy alone. Thus, radiation dose has a significant impact on the prognosis of patients with metastatic esophageal cancer. Because the SEER database did not provide radiation dose information, we were unable to evaluate this aspect. This lack of radiotherapy dose data may also explain why we observed no differences in prognosis between chemotherapy and chemoradiotherapy.

The NCCN guidelines recommend solely palliative and supportive care for patients with metastatic esophageal cancer (16). Previous studies also indicated that patients with stage IV esophageal cancer should not undergo esophagectomy (14, 15). In our study, among 713 patients with ECLM, only 22 underwent surgery for primary tumor treatment. Thus, the number patients in the surgery sub-cohort was insufficient to perform a survival analysis and assess the effect of surgery on patients' outcomes. Other studies have encountered this same limitation (18, 47). Therefore, randomized controlled and multicenter trials are required to determine whether surgery is an effective treatment option for patients with M1 esophageal cancer.

Presently, treatment strategies for esophageal cancer with distant metastasis remain controversial. Several studies, as well as the NCCN

guidelines, demonstrated that surgery was inappropriate for M1 esophageal cancer because of patients' short life expectancy and attendant risks (14–16). Moreover, no large-scale prospective studies have demonstrated whether surgery has a beneficial effect on the prognosis of patients with M1 esophageal cancer. Conversely, many studies showed that multimodality therapy (chemoradiotherapy) provided better treatment results for these patients (11, 43–45). In our study, most patients received chemoradiotherapy, achieving a median survival of 7 months. Over the past 10 years, targeted therapy (e.g., trastuzumab) for treating HER2-positive advanced and metastatic esophageal cancer has received increased attention and achieved positive results (13, 48). Thus, non-surgical multimodality treatments may represent the most appropriate choices for treating M1 esophageal cancer, including ECLM.

## LIMITATION

This study has some limitations. First, we utilized information from the SEER database, which is derived from a retrospective study and may carry inherent biases. Second, we only considered patients who had lung metastasis at initial diagnosis because data regarding patients who developed lung metastases during their disease course was not included in the SEER database. Third, all statistical analyses were based on the population of the United States and may not represent the population of other countries or regions. Fourth, education level and median family income were determined at a county level instead of a patient level, which may have affected the results of the uni- and multivariate analysis conducted in this study. Fifth, the SEER database did not include information regarding recurrence rate and mortality after treatment, which may have affected the evaluation of treatment effects. Finally, the SEER database did not provide details regarding chemotherapy drugs or radiotherapy dose and target. The incomplete information may have affected grouping accuracy, as well as the results derived from these groupings.

## CONCLUSION

To the best of our knowledge, this population-based study was the first to analyze patients with ECLM at initial diagnosis. Our study provided information regarding the epidemiology of lung metastases in these patients. Considering the factors that may predict the occurrence of lung metastasis at diagnosis, high-risk patients should undergo a 64-slice MDCT examination for small lung nodules screening. According to our findings, chemotherapy or chemoradiotherapy may represent the most advantageous treatments for patients with ECLM. Therefore, our study may provide useful information to help physicians in early diagnosis and selection of appropriate treatment for patients with ECLM, ultimately improving the outcomes of these patients.

## DATA AVAILABILITY STATEMENT

Publicly available datasets were analyzed in this study. This data can be found here: https://seer.cancer.gov/.

## AUTHOR CONTRIBUTIONS

JG, SZ, HL, and LZ contributed to the conception and design of this research. JG, SZ, HL, and LZ performed the data acquisition and analysis. JG and SZ wrote the first draft of the manuscript. MH, TL, and JZ wrote sections of the manuscript. All authors contributed to the article and approved the submitted version.

## ACKNOWLEDGMENTS

We would like to thank the staff members of the National Cancer Institute and the researchers who have been involved with the Surveillance, Epidemiology, and End Results (SEER) Program.

## SUPPLEMENTARY MATERIAL

The Supplementary Material for this article can be found online at: https://www.frontiersin.org/articles/10.3389/fonc.2021.603953/full#supplementary-material

## REFERENCES

1. Bray F, Ferlay J, Soerjomataram I, Siegel RL, Torre LA, Jemal A. Global cancer statistics 2018: GLOBOCAN estimates of incidence and mortality worldwide for 36 cancers in 185 countries. *CA Cancer J Clin* (2018) 68(6):394–424. doi: 10.1002/ijc.31937
2. Siegel RL, Miller KD, Jemal A. Cancer statistics, 2020. *CA Cancer J Clin* (2020) 70(1):7–30. doi: 10.3322/caac.21590
3. Coleman HG, Xie SH, Lagergren J. The Epidemiology of Esophageal Adenocarcinoma. *Gastroenterology* (2018) 154:390–405. doi: 10.1053/j.gastro.2017.07.046
4. Rubenstein JH, Shaheen NJ. Epidemiology, diagnosis, and management of esophageal adenocarcinoma. *Gastroenterology* (2015) 149(2):302–17. doi: 10.1053/j.gastro.2015.04.053
5. Arnold M, Soerjomataram I, Ferlay J, Forman D. Global incidence of oesophageal cancer by histological subtype in 2012. *Gut* (2015) 64(3):381–7. doi: 10.1136/gutjnl-2014-308124
6. Enzinger PC, Mayer RJ. Esophageal cancer. *N Engl J Med* (2003) 349 (23):2241–52. doi: 10.1056/NEJMra035010
7. Horner MJ, Ries LAG, Krapcho M, Aminou R, Howlader N, Altekruse SF, et al. *SEER Cancer Statistics Review, 1975–2006*. Bethesda, MD: National Cancer Institute (2009). Available at: http://seer.cancer.gov/csr/1975_2006/.
8. Mariette C, Balon JM, Piessen G, Fabre S, Van Seuningen I, Triboulet JP. Pattern of recurrence follow-ing complete resection of esophageal carcinoma and factors predictive of recurrent disease. *Cancer* (2003) 97(7):1616–23. doi: 10.1002/cncr.11228
9. D'Journo XB. Clinical implication of the innovations of the 8 edition of the TNM classification for esophageal and esophago-gastric cancer. *J Thorac Dis* (2018) 10:S2671–81. doi: 10.21037/jtd.2018.03.182
10. Chen MQ, Xu BH, Zhang YY. Analysis of prognostic factors for esophageal squamous cell carcinoma with distant organ metastasis at initial diagnosis. *J Chin Med Assoc* (2014) 77(11):562–6. doi: 10.1016/j.jcma.2014.05.014
11. Tanaka T, Fujita H, Matono S, Nagano T, Nishimura K, Murata K, et al. Outcomes of multimodalitytherapy for stage IVB esophageal cancer with

distant organ metastasis (M1-Org). *Dis Esophagus* (2010) 23(8):646–51. doi: 10.1111/j.1442-2050.2010.01069.x
12. Wu SG, Xie WH, Zhang ZQ, Sun JY, Li FY, Lin HX, et al. Surgery combined with radiotherapy improved survival in metastatic esophageal cancer in a surveillance epidemiology and end results population-based study. *Sci Rep* (2016) 6:28280. doi: 10.1038/srep28280
13. Forde PM, Kelly RJ. Chemotherapeutic and targeted strategies for locally advanced and metastatic eso-phageal cancer. *J Thorac Oncol* (2013) 8(6):73–84. doi: 10.1097/JTO.0b013e31828b5172
14. Quint LE, Hepburn LM, Francis IR, Whyte RI, Orringer MB. Incidence and distribution of distant metastases from newly diagnosed esophageal carcinoma. *Cancer* (1995) 76(7):1120–5. doi: 10.1002/1097-0142(19951001)76:7<1120::aid-cncr2820760704>3.0.co;2-w
15. Saddoughi SA, Reinersman JM, Zhukov YO, Taswell J, Mara K, Harmsen SW, et al. Survival After Surgical Resection of Stage IV Esophageal Cancer. *Ann Thorac Surg* (2017) 103(1):261–6. doi: 10.1016/j.athoracsur.2016.06.070
16. Ajani JA, D'Amico TA, Bentrem DJ, Chao J, Corvera C, Das P, et al. Esophageal and EsophagogastricJunction Cancers, Version 2.2019, NCCN Clinical Practice Guidelines in Oncology. *J Natl Compr Canc Netw* (2019) 17(7):855–83. doi: 10.6004/jnccn.2019.0033
17. Ai D, Zhu H, Ren W, Chen Y, Liu Q, Deng J, et al. Patterns of distant organ metastases in esophageal cancer: a population-based study. *J Thorac Dis* (2017) 9(9):3023–30. doi: 10.21037/jtd.2017.08.72
18. Wu SG, Zhang WW, He ZY, Sun JY, Chen YX, Guo L. Sites of metastasis and overall survival in esophageal cancer: a population-based study. *Cancer Manag Res* (2017) 9:781–8. doi: 10.2147/CMAR.S150350
19. van Vliet EP, Steyerberg EW, Eijkemans MJ, Kuipers EJ, Siersema PD. Detection of distant metastases inpatients with oesophageal or gastric cardia cancer: a diagnostic decision analysis. *Br J Cancer* (2007) 97(7):868–76. doi: 10.1038/sj.bjc.6603960
20. Chen H, Huang S, Zeng Q, Zhang M, Ni Z, Li X, et al. A retrospective study analyzing missed diagnosis of lung metastases at their early stages on computed tomography. *J Thorac Dis* (2019) 11(8):3360–8. doi: 10.21037/jtd.2019.08.19
21. Xie X, Willemink Martin J, de Jong Pim A, van Ooijen PM, Oudkerk M, Vliegenthart R, et al. Small irregular pulmonary nodules in low-dose CT: observer detection sensitivity and volumetry acc-uracy. *AJR Am J Roentgenol* (2014) 202(3):202–9. doi: 10.2214/AJR.13.10830
22. Noble F, Bailey DSWCIS Upper Gastrointestinal Tumour Panel, , Tung K, Byrne JP. Impact of integrated PET/CT in the staging of oesophageal cancer: a UK population-based cohort study. *Clin Radiol* (2009) 64(7):699–705. doi: 10.1016/j.crad.2009.03.003
23. Surveillance Epidemiology and End Results (SEER) Program. (2019). Available at: http://www.seer.cancer.gov (Accessed October 27, 2019).
24. Camp RL, Dolled-Filhart M, Rimm DL. X-tile:a new bio-informatics tool for biomarker assessment and outcome-based cut-point optimization. *Clin Cancer Res* (2004) 10(21):7252–9. doi: 10.1158/1078-0432.CCR-04-0713
25. Edge SB, Compton CC. The American Joint Committee on Cancer: the 7th Edition of the AJCC Cancer Staging Manual and the Future of TNM. *Ann Surg Oncol* (2010) 17(6):1471–4. doi: 10.1245/s10434-010-0985-4
26. US Census Bureau. *US Census 2000 Gateway* (2019). Available at: http://www.census.gov/main/www/cen2000.html (Accessed October 27, 2019).
27. Fine JP, Gray RJ. A proportional hazards model for the subdistribution of a competing risk. *J Am Stat Assoc* (1999) 94:496–509. doi: 10.1080/01621459.1999.10474144
28. Wu SG, Zhang WW, Sun JY, Li FY, Lin Q, He ZY, et al. Patterns of Distant Metastasis Between Histological Types in Esophageal Cancer. *Front Oncol* (2018) 8:302:302. doi: 10.3389/fonc.2018.00302
29. Anderson LL, Lad TE. Autopsy findings in squamous-cell carcinoma of the esophagus. *Cancer* (1982) 50(8):1587–90. doi: 10.1002/1097-0142(19821015)50:8<1587::aid-cncr2820500820>3.0.co;2-s
30. Mandard AM, Chasle J, Marnay J, Villedieu B, Bianco C, Roussel A, et al. Autopsy findings in 111cases of esophageal cancer. *Cancer* (1981) 48(2):329–35. doi: 10.1002/1097-0142(19810715)48:2<329::aid-cncr2820480219>3.0.co;2-v
31. Ai D, Chen Y, Liu Q, Deng J, Zhao K. The effect of tumor locations of esophageal cancer on themetastasis to liver or lung. *J Thorac Dis* (2019) 11(10):4205–10. doi: 10.21037/jtd.2019.09.67
32. Zhu C, You Y, Liu S, Ji Y, Yu J. A Nomogram to Predict Distant Metastasis for Patients with Esophageal Cancer. *Oncol Res Treat* (2020) 43:2–9. doi: 10.1159/000503613
33. Rice TW, Rusch VW, Apperson-Hansen C, Allen MS, Chen LQ, Hunter JG, et al. Worldwide esophageal cancer collaboration. *Dis Esophagus* (2009) 22(1):1–8. doi: 10.1111/j.1442-2050.2008.00901.x
34. Dickson GH, Singh KK, Escofet X, Kelley K. Validation of a modified GTNM classification in peri-junctional oesophago-gastric carcinoma and its use as a prognostic indicator. *Eur J Surg Oncol* (2001) 27(7):641–4. doi: 10.1053/ejso.2001.1200
35. Natsugoe S, Okumura H, Matsumoto M, Uchikado Y, Setoyama T, Uenosono Y, et al. The role of salvagesurgery for recurrence of esophageal squamous cell cancer. *Eur J Surg Oncol* (2006) 32(5):544–7. doi: 10.1016/j.ejso.2006.02.014
36. Sugiyama M, Morita M, Yoshida R, Ando K, Egashira A, Takefumi O, et al. Patterns and time of re-currence after complete resection of esophageal cancer. *Surg Today* (2012) 42(8):752–8. doi: 10.1007/s00595-012-0133-9
37. Sakanaka K, Ishida Y, Itasaka S, Ezoe Y, Aoyama I, Miyamoto S, et al. Identification of a predictive factor for distant metastasis in esophageal squamous cell carcinoma after definitive chemoradiotherapy. *Int J Clin Oncol* (2016) 21(5):899–908. doi: 10.1007/s10147-016-0967-z
38. Sun Z, Zheng H, Yu J, Huang W, Li T, Chen H, et al. Liver Metastases in Newly Diagnosed Gastric Cancer:A Population-Based Study from SEER. *J Cancer* (2019) 10(13):2991–3005. doi: 10.7150/jca.30821
39. Martin AM, Cagney DN, Catalano PJ, Warren LE, Bellon JR, Punglia RS, et al. Brain Metastases in Newly Diagnosed Breast Cancer: A Population-Based Study. *JAMA Oncol* (2017) 3(8):1069–77. doi: 10.1001/jamaoncol.2017.0001
40. Austin PC, Lee DS, Fine JP. Introduction to the Analysis of Survival Data in the Presence of Competing Risks. *Circulation* (2016) 133(6):601–9. doi: 10.1161/CIRCULATIONAHA.115.017719
41. Nafteux PR, Lerut TE, Villeneuve PJ, Dhaenens JM, De Hertogh G, Moons J, et al. Signet ring cells in esophageal and gastroesophageal junction carcinomas have a more aggressive biological behavior. *Ann Surg* (2014) 260(6):1023–9. doi: 10.1097/SLA.0000000000000689
42. Wu XX, Chen RP, Chen RC, Gong HP, Wang BF, Li YL, et al. Nomogram predicting cancer-specific mortality in patients with esophageal adenocarcinoma: a competing risk analysis. *J Thorac Dis* (2019) 11(7):2990–3003. doi: 10.21037/jtd.2019.07.56
43. Wojcieszynski AP, Berman AT, Wan F, Plastaras JP, Metz JM, Mitra N, et al. The impact of radiation therapy sequencing on survival and cardiopulmonary mortality in the combined modality treatment of patients with esophageal cancer. *Cancer* (2013) 119(11):1976–84. doi: 10.1002/cncr.27970
44. Herskovic A, Martz K, al-Sarraf M, Leichman L, Brindle J, Vaitkevicius V, et al. Combined chemotherapy and radiotherapy compared with radiotherapy alone in patients with cancer of the esophagus. *N Engl J Med* (1992) 326(24):1593–8. doi: 10.1056/NEJM199206113262403
45. Wang J, Suri JS, Allen PK, Liao Z, Komaki R, Ho L, et al. Factors Predictive of Improved Outcomes With Multimodality Local Therapy After Palliative Chemotherapy for Stage IV Esophageal Cancer. *Am J Clin Oncol* (2016) 39(3):228–35. doi: 10.1097/COC.0000000000000066
46. Guttmann DM, Mitra N, Bekelman J, Metz JM, Plastaras J, Feng W, et al. Improved Overall Survival with Aggressive Primary Tumor Radiotherapy for Patients with Metastatic Esophageal Cancer. *J Thorac Oncol* (2017) 12(7):1131–42. doi: 10.1016/j.jtho.2017.03.026
47. Liu M, Wang C, Gao L, Lv C, Cai X. A nomogram to predict long-time survival for patients with M1 diseases of esophageal cancer. *J Cancer* (2018) 9(21):3986–90. doi: 10.7150/jca.27579
48. Bang YJ, Van Cutsem E, Feyereislova A, Chung HC, Shen L, Sawaki A, et al. Trastuzumab in combination with chemotherapy versus chemotherapy alone for treatment of HER2-positive advanced gastric or gastro-oesophageal junction cancer (ToGA): a phase 3, open-label, randomised controlled trial. *Lancet* (2010) 376(9742):687–97. doi: 10.1016/S0140-6736(10)61121-X

**Conflict of Interest:** The authors declare that the research was conducted in the absence of any commercial or financial relationships that could be construed as a potential conflict of interest.

frontiers in Pharmacology

ORIGINAL RESEARCH
published: 13 April 2021
doi: 10.3389/fphar.2021.629264

# Radioresistant Nasopharyngeal Carcinoma Cells Exhibited Decreased Cisplatin Sensitivity by Inducing SLC1A6 Expression

*Wenwen Hao[1,2†], Lisha Wu[3†], Linhui Cao[4], Jinxiu Yu[5], Li Ning[2], Jingshu Wang[3], Xiaoping Lin[6*†] and Yanfeng Chen[2*]*

[1]Department of Nasopharyngeal Carcinoma, State Key Laboratory of Oncology in South China, Collaborative Innovation Center for Cancer Medicine, Guangdong Key Laboratory of Nasopharyngeal Carcinoma Diagnosis and Therapy, Sun Yat-sen University Cancer Center, Guangzhou, China, [2]Department of Head and Neck Surgery, State Key Laboratory of Oncology in South China, Collaborative Innovation Center for Cancer Medicine, Sun Yat-sen University Cancer Center, Guangzhou, China, [3]Department of Oncology, Sun Yat-sen Memorial Hospital, Sun Yat-sen University, Guangzhou, China, [4]Department of Traditional Chinese Medicine, Sun Yat-sen Memorial Hospital, Sun Yat-sen University, Guangzhou, China, [5]Department of Radiotherapy, The Second Affiliated Hospital of Guangzhou Medical University, Guangzhou, China, [6]Department of Nuclear Medicine, State Key Laboratory of Oncology in South China, Collaborative Innovation Center for Cancer Medicine, Sun Yat-sen University Cancer Center, Guangzhou, China

OPEN ACCESS

**Edited by:**
David A. Gewirtz,
Virginia Commonwealth University,
United States

**Reviewed by:**
Hisashi Harada,
Virginia Commonwealth University,
United States
Jingwen Xu,
Guangdong Pharmaceutical
University, China

***Correspondence:**
Yanfeng Chen
chenyf@sysucc.org.cn
Xiaoping Lin
linxp@sysucc.org.cn

†These authors have contributed equally to this work

**Specialty section:**
This article was submitted to Pharmacology of Anti-Cancer Drugs, a section of the journal Frontiers in Pharmacology

**Received:** 14 November 2020
**Accepted:** 02 March 2021
**Published:** 13 April 2021

**Citation:**
Hao W, Wu L, Cao L, Yu J, Ning L, Wang J, Lin X and Chen Y (2021) Radioresistant Nasopharyngeal Carcinoma Cells Exhibited Decreased Cisplatin Sensitivity by Inducing SLC1A6 Expression. Front. Pharmacol. 12:629264. doi: 10.3389/fphar.2021.629264

Cisplatin-based regimens are commonly used for the treatment of nasopharyngeal carcinoma (NPC) in patients who receive concurrent chemoradiotherapy. The sensitivity of NPC cells to cisplatin is closely associated with the efficacy of radiation therapy. In this study, we established two radioresistant NPC cell lines, HONE1-IR and CNE2-IR, and found that both cell lines showed reduced sensitivity to cisplatin. RNA-sequence analysis showed that SLC1A6 was upregulated in both HONE1-IR and CNE2-IR cell lines. Downregulation of SLC1A6 enhanced cisplatin sensitivity in these two radioresistant NPC cell lines. It was also found that the expression of SLC1A6 was induced during radiation treatment and correlated with poor prognosis of NPC patients. Notably, we observed that upregulation of SLC1A6 led to elevating level of glutamate and the expression of drug-resistant genes, resulted in reduced cisplatin sensitivity. Our findings provide a rationale for developing a novel therapeutic target for NPC patients with cisplatin resistance.

**Keywords: nasopharyngeal carcinoma, SLC1A6, cisplatin, radiation-resistance, glutamate**

## INTRODUCTION

Nasopharyngeal carcinoma (NPC) is a malignant tumor in the head and neck with high incidence in southern China and Southeast Asia (Chen et al., 2019; Ji et al., 2019). According to the guidelines of the National Comprehensive Cancer Network (NCCN), radiotherapy and cisplatin-based regimens are the main treatments for NPC patients (Pfister et al., 2020). The cisplatin-based concurrent chemoradiotherapy has been proven to improve the outcome of early and locally advanced NPC (Chen et al., 2011). However, there are a small portion of patients who did not response effectively or became recurrent to these treatments, and their prognosis remains poor (Chen et al., 2011; Karam et al., 2016).

The antitumor mechanism of cisplatin is to form covalent DNA adducts thus interfering with DNA repair (Wang and Lippard, 2005). The combination of cisplatin provides a synergetic effect for

radiotherapy for the reason that cisplatin could enhance the sensitivity to radiation (Boeckman et al., 2005). Interestingly, some studies have revealed that cancer cells could acquire cisplatin resistance after radiation therapy (Eichholtz-Wirth, 1995; Zhuang et al., 2019). Based on our clinical observations, the phenomenon of cisplatin resistance is commonly seen in NPC patients who also resistant to radiotherapy. However, the association of cisplatin and radiation resistance is elusive.

The SLC1A6 (Solute Carrier Family 1 Member 6) is a member of the SLC1A family, which consists of the excitatory amino acid transporters EAAT1–EAAT5 (designated as SLC1A1-3, 6-7) and the alanine serine cysteine transporters ASCT1-ASCT2 (designated as SLC1A4-5) in mammals (Freidman et al., 2020). This transmembrane transporter encoded by SLC1A6 mediates the uptake of L-glutamate and L/D-aspartate (Fairman et al., 1995; Ryan et al., 2009; Vandenberg and Ryan, 2013; Guskov et al., 2016). Although the role of SLC1A6 in cancers was not well documented, other members of the SLC1A family were reported to be overexpressed in multiple tumors and predict poor prognosis. For example, expression of SLC1A1, SLC1A2 or SLC1A3 contributed to promoting tumor progression in solid tumors, such as lung cancer, glioma, and gastric cancer (Ye et al., 1999; de Groot et al., 2005; Tao et al., 2011; Xu et al., 2020; Guo et al., 2021). Besides, the SLC1A members were also reported to be associated with drug resistance. SLC1A1 was upregulated in oxaliplatin-resistant colorectal cancers (Pedraz-Cuesta et al., 2015), and SLC1A3 was associated with L-asparaginase resistance in acute lymphoblastic leukemia (Sun et al., 2019). As mammalian transporters of amino acids, members of the SLC1A family are implicated to impact drug-related metabolic profiles in tumor cells.

In the present study, we established two radioresistant NPC cell lines, HONE1-IR and CNE2-IR. We found that the radioresistant NPC cells acquired the characteristic of reduced cisplatin sensitivity, which was associated with the upregulation of SLC1A6. By inducing SLC1A6, HONE1-IR and CNE2-IR cells increased the cellular glutamate level and drug resistance genes, leading to reduced cisplatin sensitivity.

# MATERIALS AND METHODS

## Ethical Statement

The approval of this study was obtained from the Ethics Committee of Sun Yat-sen University Cancer Center (SYSUCC, Guangzhou, China). This study met the ethical standard of the Declaration of Helsinki. The nasopharyngeal biopsy was performed in all patients who have submitted their informed consent.

## Patients and Specimens

A total of 78 NPC patients treated in Sun Yat-sen University Cancer Center were recruited and completely followed up from February 2011 to August 2014. The NPC biopsy specimens were fixed in 4% paraformaldehyde and paraffin-embedded and used for immunohistochemical (IHC) analysis of SLC1A6 expression. SLC1A6 expression was scored according to the staining intensity and percentage of positively stained cells. The staining intensity score of SLC1A6 was graded as follows: 0, no staining; 1, weak staining (light yellow); 2, moderate staining (yellow-brown); 3, intense staining (brown). The staining percentage score of SLC1A6 was graded as follows: 1, percentage of positive cells less than 30%; 2, percentage of positive cells between 30 and 60%; 3, percentage of positive cells more than 60%. The total-score was calculated as the formula: Total score = $\sum$ (Intensity score × percentage score)=(1 × percentage score) + (2 × percentage score) + (3 × percentage score). Finally, the intensity score, percentage score, and total score were used to verify the prognostic value of SLC1A6 expression for overall survival (OS).

## Immunohistochemistry

The 5-μm paraffin sections were deparaffinized with xylene and rehydrated in graded ethanol. Antigen retrieval was achieved by placing the sections in sodium citrate buffer (pH 6.0) at 95°C for 20 min. The sections were blocked with 5% goat serum in PBS and incubated with primary antibody against SLC1A6 (1:100, Thermo fisher, the United States) overnight at 4°C. The next day, the sections were stained with SP-9000 Detection Kits (Biotin-Streptavidin HRP Detection Systems, ZSGB-Bio, China) and the DAB Kit (ZSGB-Bio, China) was used for color development according to the manufacturer's manual. The sections were counterstained with hematoxylin and observed with a light microscope.

## Cells and Cell Culture

Human NPC cell lines CNE2 and HONE1 were gifted from Professor Chaonan Qian (SYSUCC) (Guo et al., 2020). Both the CNE2 and HONE1 cell lines, and their radioresistant cell lines HONE1-IR and CNE2-IR, were cultured in RPMI-1640 medium (Gibco, Thermo fisher, United States), supplemented with 10% fetal bovine serum (FBS, Gibco) and 1% antibiotics (Penicillin-Streptomycin). Another head and neck cell line SCC9 was cultured in F12-Dulbecco's modified Eagle's medium (Gibco, Thermo fisher, United States), supplemented with 10% FBS and 1% antibiotics (Penicillin-Streptomycin). Customized RPMI-1640 (deprived glutamic acid or aspartic acid) was ordered from Weiga Biotechnology Company (Guangzhou, China), supplemented with 10% dialyzed FBS (Gibco, Thermo fisher, United States). All cells were incubated in a humidified atmosphere with 5% $CO_2$ at 37°C.

## Establishment of Radioresistant Cell Lines

According to our previous study (Guo et al., 2020), HONE1 cells were cultured in RPMI-1640 medium supplemented with 10% FBS and reached approximately 50% confluence in 25-$cm^2$ flasks. Cells were treated with a dose of 6Gy radiation using an X-rays generator. After radiation, the culture medium was replaced with complete fresh medium and cells were returned to the incubator. Cells were passaged until they reached approximately 90% confluence. The fractionated irradiations were repeated five times and reached a total dose of 30Gy. The interval between each radiation was at least 2-weeks for all cells. Radioresistant cell population were selected and were referred as HONE1-IR cells.

The parental cells without irradiation were used as control cells. The CNE2-IR cells were kindly provided by Professor Yunfei Xia (SYSUCC).

## Quantitative Real-Time PCR

The total RNAs were extracted by the TRIzol reagents (RNAiso PLUS, Invitrogen, US) following the manufacturer's manuals. The isolated RNAs were assessed by Bioanalyzer 2,200 (Agilent, Uunited States) to determine their concentrations and quality before conversion to cDNA. Quantitative RT-PCR was carried out using the Real-Time PCR Detection System (Lightcycler 480 II, Roche, United States) based on the manufacturer's manual. Values were expressed as fold changes of the controls using the $2e^{-\Delta\Delta Ct}$ method.

## RNA-Seq Transcriptome Analysis

NPC Cells (HONE1 and HONE1-IR, CNE2, and CNE2-IR) were cultured and their total RNAs were extracted as described above and kept at −80°C. Sequencing and bioinformatic analysis were performed by DESeq2 and edgeR platforms with the aid of Novogene Company (Beijing, China). The intensity was used to generate the heatmap by Novomagic platform (Novogene Company). Differentially expressed genes were determined when $p < 0.05$ and the absolute log2 fold change of expression was greater than 3.

## MTS Assay

HONE1 (HONE1-IR and NC cells) and CNE2 (CNE2-IR and NC cells) were planted into 96-well plates at $1–2 \times 10^3$ cells/200 μl/well, treated with increasing concentration of cisplatin for 24 h. In the last 2 h of incubation, 20 μL of MTS tetrazolium (Promega, United States) was added to each well based on the manufacturer's protocols. Cell viability was examined by assessing the light absorbance at 490–500 nm. The cell survival curves were drawn based on the results obtained.

## Colony Formation

HONE1 (HONE1-IR cells and NC cells) and CNE2 (CNE2-IR and NC cells) were planted into 6-well plates at $5 \times 10^2$ cells/well. Subsequently, cisplatin was added to the cultured medium at the concentration of 20 μM for 24 h of treatment. After that, the culture medium was replaced by a fresh medium. The cells were cultured for 2 weeks. Crystal violet was used to stain the colonies.

## Small Interfering RNA Transfection

HONE1-IR and CNE2-IR cells were planted into 6-well plates one day before transfection to reach about 60–70% confluence. The siRNAs targeting SLC1A6 gene were purchased from Ruibo Company (Guangzhou, China). Transient transfection of HONE1-IR and CNE2-IR cells was performed using Lipofectamine RNAiMax (Invitrogen, United States) according to the manufacturer's protocols. Cells were transfected with a total of 50 pmol siRNA and subjected to Western blot and MTS assays after 24–48 h post-transfection. The siRNA sequences for SLC1A6 were as follows:

SLC1A6-siRNA-1 : 5′-AUGAAAACUGCAAUGACUGUA-3′
SLC1A6-siRNA-2 : 5′-AAGGAAUAAGCCAACGAUGAC-3′

## Establishment of SLC1A6 Overexpressed Stable Cell Lines

The cDNA of SLC1A6 was synthesized according to the human full-length open reading frame of SLC1A6 mRNA (NM_001,272,087) and integrated into pcDNA3.1 plasmid. The lentiviral expression plasmid was used to transfect 293T cells for packaging. The culture media of transfected 293T cells was harvested and used to transfect HONE1 or CNE2 cells. Cells expressing SLC1A6 were selected with puromycin (Sigma-Aldrich, United States) in the concentration of 2 μg/ml. SLC1A6-overexpressed stable cells were established after 10 days selection.

## Western Blotting Analysis

Following treatments, cells were lyzed by RIPA buffer (Beyotime, China) containing protease and phosphatase inhibitors (Life Technologies, United States). Protein concentrations were detected by a BCA kit (Thermo Fisher, United States). Proteins of samples were subjected to 8–10% SDS-PAGE and transferred to PVDF membranes (Biorad, United States). After being blocked with 5% non-fat milk for 1 h, membranes were incubated with primary antibodies at 4°C overnight. Primary antibodies against SLC1A6 (1:1,000, Thermo fisher), γH2AX (1:1,000, Cell Signaling), Beta-actin (1:1,000, Cell Signaling) were used. Then the membranes were washed with TBS containing 0.1% Tween-20, followed by incubation with HRP anti-rabbit (1:1,000, Cell Signaling) secondary antibody. The band intensity values were normalized to that of Beta-actin.

## Measurement of Glutamate or Aspartate Level

A total of $10 \times 10^6$ cells were collected and lyzed by ultrasonication (low frequency, 3s, 20 times), glutamate or aspartate content was extracted by glutamate assay kit (Solarbio, China) or aspartate assay kit (Abnova, Taiwan). The level of glutamate or aspartate was detected by comparing the light absorbance value with the standard solution curve. The absorbance value was measured at 340 nm or 570 nm, respectively.

## Online and Public Database

The correlation of SLC1A6 expression and survival outcome in patients with head and neck squamous cell carcinoma (HNSCC) in the TCGA database was analyzed on the GEPIA website (http://gepia.cancer-pku.cn/).

## Statistical Analysis

The data were expressed as the mean ± SD (the standard deviation). Comparisons between two groups were analyzed by unpaired Student's $t$ test. Comparisons among groups were performed by one-way analysis of variance (ANOVA) followed by Tukey's test. Significant $p$ value was considered as $< 0.05$. In all cases, $^*p < 0.05$, $^{**}p < 0.01$, $^{***}p < 0.001$.

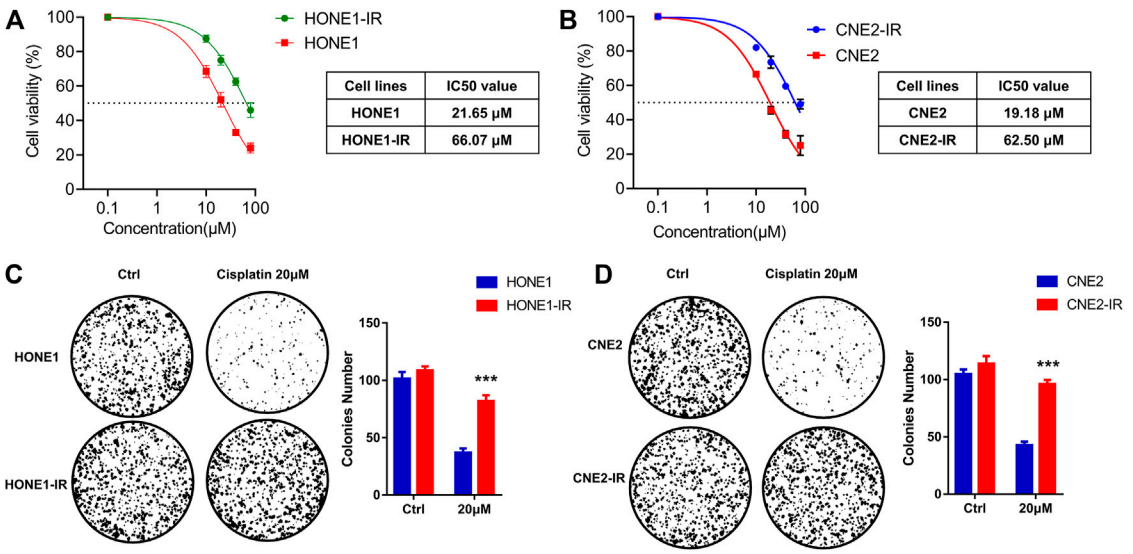


**FIGURE 1 |** Radioresistant HONE1-IR and CNE2-IR cells showed reduced sensitivity to cisplatin. **(A–B)** MTS assay on the IC50 values of radioresistant NPC cell lines HONE1-IR and CNE2-IR, as well as their parental cell lines HONE1 and CNE2 with cisplatin treatment. ANOVA test **(C–D)** Colony formation assay on the radioresistant NPC cell lines and their parental cell lines. Unpaired Student's t test. $^{*}p < 0.05$, $^{**}p < 0.01$, $^{***}p < 0.001$.

# RESULTS

## Radioresistant HONE1-IR and CNE2-IR Cells Showed Reduced Sensitivity to Cisplatin

Two radioresistant human NPC cell lines, HONE1-IR and CNE2-IR, were generated and their resistance to radiation was verified by survival assay (Guo et al., 2020). As the sensitivity to cisplatin is closely associated with radiotherapy efficacy, we compared the sensitivity to cisplatin in radioresistant NPC and their parental cells. MTS assay supported that radioresistant NPC cells exhibited reduced sensitivity to cisplatin compared to their parental cells. Subsequent analysis of chemosensitivity indicated that the cisplatin IC50 of HONE1-IR cells was significantly higher than that of their parental cells (66.07 vs. 21.65 μM)). Similarly, CNE2-IR cells also showed higher IC50 than that of their parental cells (62.50 vs. 19.18 μM) (**Figures 1A,B**). Colony formation assay showed that cisplatin treatment significantly reduced tumor cell proliferation in HONE1 and CNE2 cells, but not in HONE1-IR and CNE2-IR cells (**Figures 1C,D**). These findings indicated that radioresistant NPC cells reduced cisplatin sensitivity.

## SLC1A6 Gene was Up-Regulated in Both HONE1-IR and CNE2-IR Cells

To explore the potential regulators of cisplatin sensitivity in radioresistant NPC cells, RNA-Sequence was performed to compare the transcriptome profile of HONE1-IR cells and their parental cells. The cutoff criteria were more than 3-fold or less than 3-fold for upregulation or downregulation, respectively. As for CHE2-IR cells and their parental cells, the same method was performed. Heatmap showed a total of 573 genes in HONE1 cells (HONE1-IR cells vs. their parental cells) and 404 genes in CNE2 cells (CNE2-IR cells vs. their parental cells) were identified to be differentially expressed (**Figures 2A,B**). There were 30 common genes upregulated in both HONE1-IR and CNE2-IR cells compared to their parental cells (**Figure 2C**). SLC1A6 gene was particularly noted in the top nine over-expressed genes (**Figure 2D**) and verified by qRT-PCR (**Figure 2E**). These results indicated that SLC1A6 might be a crucial gene associated with cisplatin or radiation sensitivity in radioresistant NPC cells.

## SLC1A6 Overexpression Conferred Reduced Cisplatin and Radiation Sensitivity in Radioresistant NPC Cells

Furthermore, the up-regulation of SLC1A6 has been verified by Western blots in both HONE1-IR and CNE2-IR cells compared to their parental cells (**Figure 3A**). To further investigate the role of SLC1A6 in NPC radioresistant cells, siRNA or SLC1A6 overexpression lentivirus was used to knock down or up regulate the expression of SLC1A6 in cells (**Figure 3B**). Results showed that downregulation of SLC1A6 gene re-sensitized radioresistant NPC cells to cisplatin treatment (**Figure 3C**). Moreover, overexpression of SLC1A6 decreased the sensitivity to cisplatin in parental cells (**Figure 3D**). Besides, modulation of the SLC1A6 also impacted the sensitivity to radiation in radioresistant NPC and parental cells (**Figures 3E,F**). Cisplatin and radiation both cause DNA damage. Increased gamma-H2AX (γH2AX) expression, a biomarker of DNA damage, was noticed in radioresistant NPC cells by

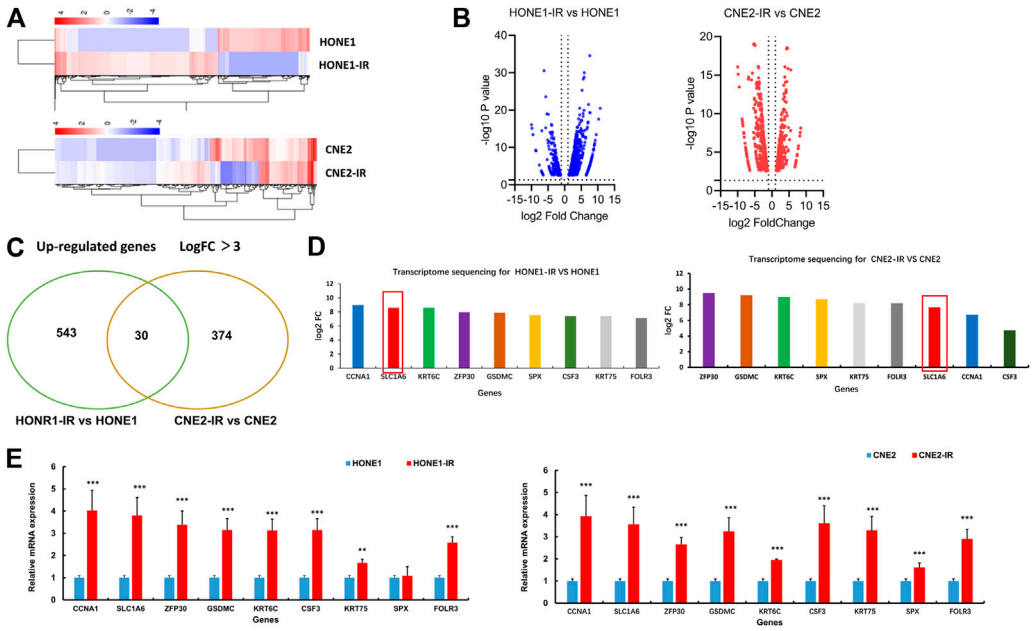


**FIGURE 2 |** SLC1A6 up-regulated in radioresistant NPC cells. **(A)** Heat maps showing the expression pattern of up-regulated and down-regulated genes in HONE1 cells (HONE1-IR vs. HONE1) and CNE2 cells (CNE2-IR vs. CNE2). Red or blue represents high or low expression, respectively (Raw Z score). **(B)** Volcano maps showing the expression pattern of genes. **(C)** Venn maps showing 573 up-regulated genes in HONE1R vs. HONE1 cells and 404 up-regulated genes in CNE2-IR vs. CNE2 cells, with 30 common genes. **(D)** Transcriptome sequencing showing the highest fold change in up-regulated nine genes, co-expressed in both radioresistant NPC cells, including SLC1A6. **(E)** qRT-PCR verified the different mRNA expression of the nine genes. Unpaired Student's t test. $^{*}p < 0.05$, $^{**}p < 0.01$, $^{***}p < 0.001$.

knocking down SLC1A6, followed by cisplatin or radiation treatment (**Figures 3G,H**). These results demonstrated that SLC1A6 contributed to reducing cisplatin and radiation sensitivity of radioresistant NPC cells.

## SLC1A6 Induced by Radiation Treatment and Correlated with Poor Prognosis

As SLC1A6 gene was up-regulated in the radioresistant NPC cells, we next investigated the impact of radiation on SLC1A6. We observed both RNA (**Figure 4A**) and protein levels (**Figure 4B**) of SLC1A6 increased during radiation treatment in NPC cells. As NPC belongs to HNSCC, another HNSCC cell line SCC9, was utilized to further verify the role of the SLC1A6 gene on the sensitivity to cisplatin. Similarly, SLC1A6 up-regulation was seen during radiation treatment in SCC9 cells (**Figures 4A,B**). SLC1A6 over-expressed SCC9 cells exhibited low sensitivity to cisplatin (**Figure 4C**). Analysis on TCGA database showed that high SLC1A6 expression was correlated with poor prognosis in HNSCC patients (**Figure 4D**). To further validate the prognostic role of the SLC1A6 in NPC patients, we collected 78 biopsies from NPC patients in Sun Yat-sen University Cancer Center. We demonstrated that high SLC1A6 expression was correlated with poor prognosis in these patients (**Figures 4E,F**). These results demonstrated that overexpression of SLC1A6 was associated with low therapeutic efficacy and poor survival in NPC patients.

## SLC1A6 Up-Regulated Glutamate Level and Drug Resistance Genes

Further experiments were conducted to elucidate the underlying mechanism of SLC1A6 in regulating cisplatin sensitivity in radioresistant NPC cells. SLC1A6 is one of the members of the EAATs family, which transport aspartate, glutamate, and cysteine. These amino acids serve as substrates in several biochemical and metabolic pathways in cancer cells. Previous studies have reported that the EAATs-mediated therapeutic resistance is related to altered tumor metabolic profiles (Ye et al., 1999; de Groot et al., 2005; Tao et al., 2011; Pedraz-Cuesta et al., 2015; Sun et al., 2019; Xu et al., 2020; Guo et al., 2021). It was found that the level of glutamate and aspartate increased in the radioresistant NPC cells compared to their parental cells (**Figure 5A**). In addition, deprivation of glutamate, not aspartate, in the culture medium re-sensitized radioresistant NPC cells to cisplatin treatment (**Figure 5B**). Moreover, PCR analysis revealed that the expression of CYP1A1, CYP2C8, CYP2D6, DHFR, GSTP1, and SULT1E1 genes, that are associated with drug catabolism, were significantly higher in radioresistant NPC cells compared to their parental cells (**Figure 5C**). ABCC1 and ABCC3, that are associated with drug transportation, were also elevated in radioresistant NPC cells (**Figure 5C**). The expressions of these genes were significantly decreased when SLC1A6 was knocked down in radioresistant NPC cells (**Figure 5D**). These results collectively supported that SLC1A6 overexpression reduced

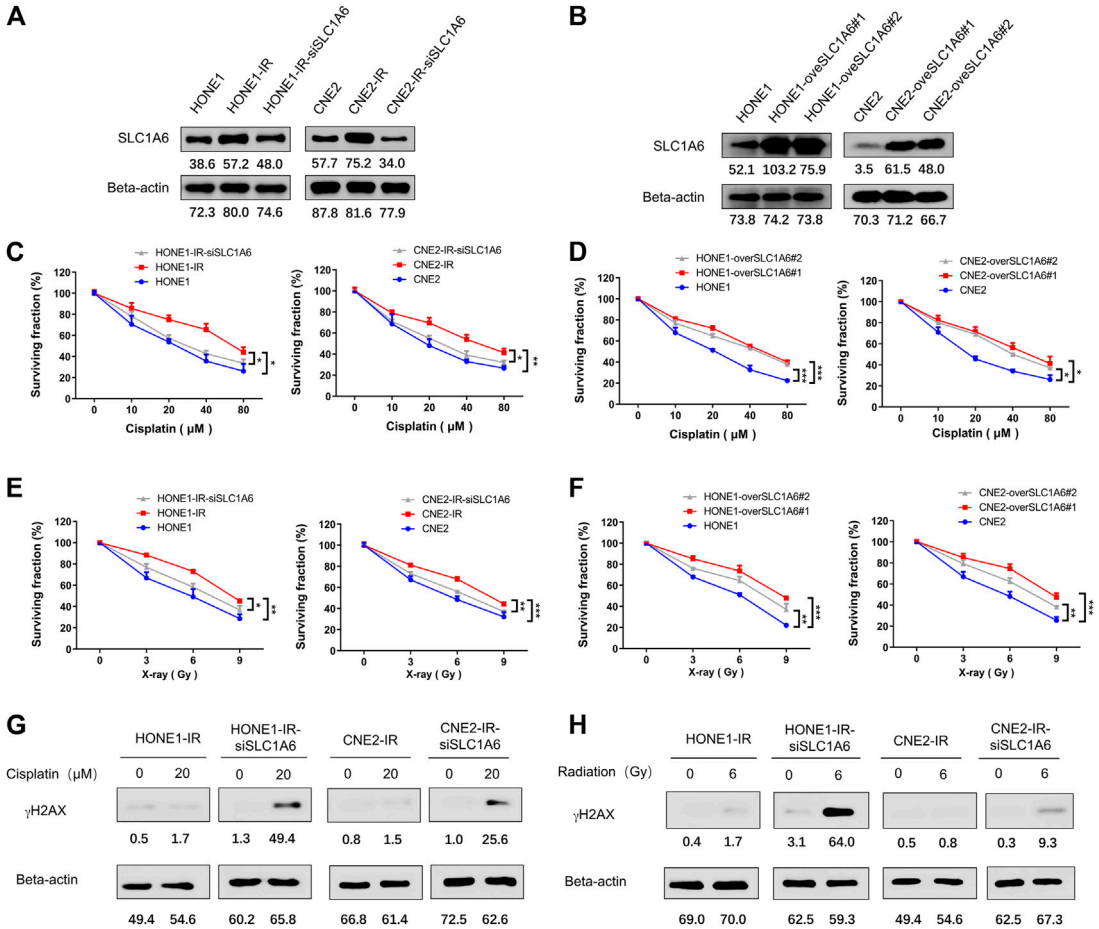


**FIGURE 3 |** SLC1A6 mediated reduced sensitivity to cisplatin and radiation in radioresistant NPC cells. **(A)** SLC1A6 and Beta-actin protein expression of HONE1, CNE2, HONE1-IR, CNE2-IR and radioresistant NPC SLC1A6 knockdown cell lines, detected by Western blots. **(B)** SLC1A6 and Beta-actin protein expression of HONE1, CNE2, HONE1-overSLC1A6 and CNE2-overSLC1A6 cell lines, detected by Western blots. **(C–D)** MTS assays conducted in HONE1, CNE2, HONE1-IR, CNE2-IR, radioresistant NPC SLC1A6 knockdown cell lines or SLC1A6 overexpressed cell lines, treated with cisplatin. The difference was analyzed by repeated ANOVA. **(E–F)** MTS assays conducted in HONE1, CNE2, HONE1-IR, CNE2-IR, radioresistant NPC SLC1A6 knockdown cell lines or SLC1A6 overexpressed cell lines, treated with fractional radiation. The difference was analyzed by repeated ANOVA. **(G–H)** The levels of γH2AX and Beta-actin analyzed by Western blots. $^{*}p < 0.05$, $^{**}p < 0.01$, $^{***}p < 0.001$.

cisplatin sensitivity in radioresistant NPC cells by increasing the level of glutamate and drug resistance genes.

## DISCUSSION

Radiation resistance has been a significant obstacle for the local control of NPC. Some patients who are resistant to radiotherapy are also not sensitive to cisplatin treatment. In this study, we observed the decreased sensitivity to cisplatin in radiation resistant NPC cells. Although previous studies have revealed the mechanism of radiation-resistance or cisplatin resistance, the relationship between radiation and cisplatin resistance is complicated and not elucidated. The cause of cisplatin resistance, included aberrant repair of DNA damage, apoptosis pathway defects, activation of drug export system, altered cellular metabolism, reduced oxidative stress, and cancer stem cell induction, etc. (Ikuta et al., 2005; Galluzzi et al., 2012; Zhang et al., 2012; Cruz-Bermúdez et al., 2019) As both radiation and cisplatin cause DNA damage in tumor cells, they might share the same biological pathway to reverse DNA damage. Cross-resistance mechanisms reported by studies include elevated GSH level, DNA repair enzymes, NFκB and TNFα, etc. (Chao et al., 1991; Poppenborg et al., 1997; Zhu et al., 2019)

Here, the identification of SLC1A6 as the crucial gene conferring reduced cisplatin sensitivity in radiation-resistant NPC cells is novel. In this study, it was found that SLC1A6 expression was upregulated in HONE1-IR and CNE2-IR cells. Down-regulating SLC1A6 expression could significantly rescue the cisplatin sensitivity in HONE1-IR and CNE2-IR cells. The SLC1A6 could be the common factor to reduce DNA damage from radiation or cisplatin treatment, which was confirmed by our study. Our results were in consistent with previous studies that described the radiation-induced cisplatin resistance (Eichholtz-Wirth et al., 1993; Eichholtz-Wirth, 1995; Zhuang et al., 2019). The cisplatin resistance acquired during radiation could explain the phenomenon that some patients with radio-resistance also didn't respond to cisplatin

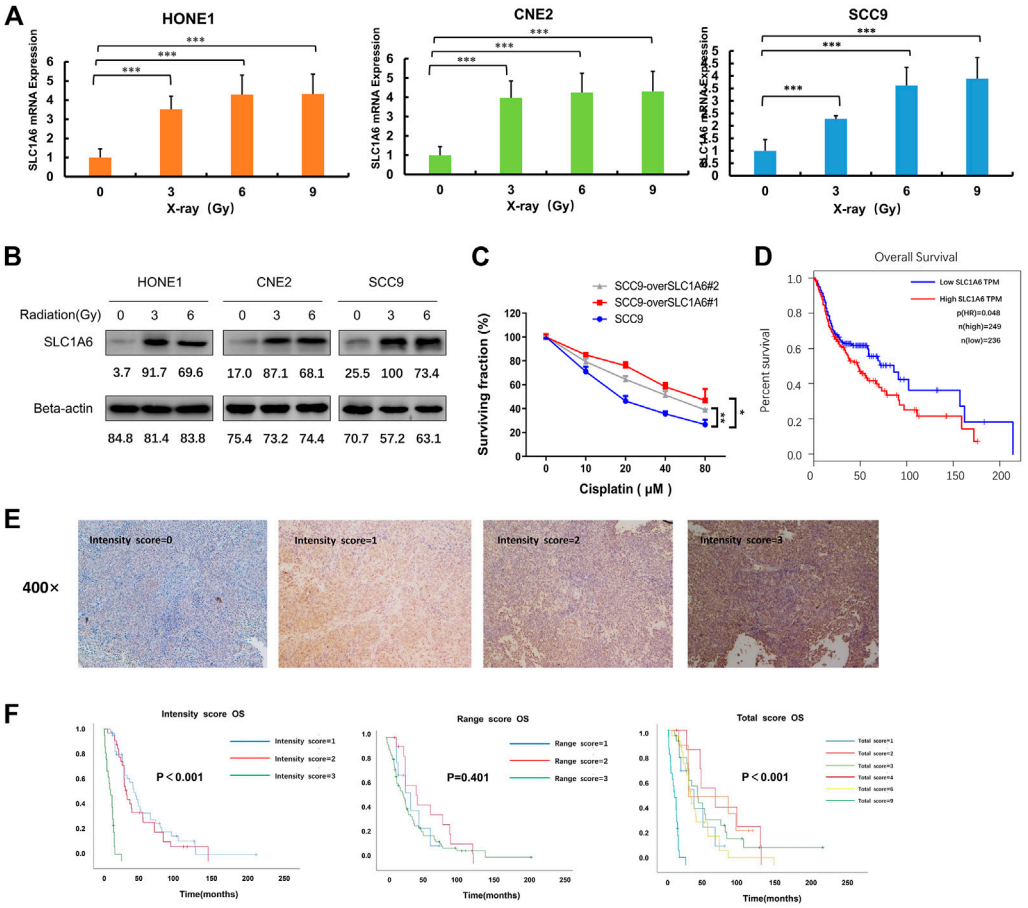


**FIGURE 4 |** SLC1A6 induced by radiation treatment and correlated with poor prognosis. **(A)** The mRNA expression of SLC1A6 in HONE1, CNE2, and SCC9 cells treated with increasing radiation doses. **(B)** The protein expression of SLC1A6 in HONE1, CNE2, and SCC9 cells treated with increasing doses of radiation. **(C)** Cell viability examined by MTS assays in SCC9 cells treated with cisplatin. **(D)** Patients with SLC1A6 overexpression showed poor overall survival analyzed with GEPIA websites. **(E)** Representative micrographs (400x). All images were acquired and processed at identical conditions. **(F)** OS curves on the SLC1A6 expression in validation set consisting of 78 patients with NPC from Sun Yat-sen University Cancer Center, using intensity score, percentage score, or total score, respectively. The differences were measured by Kaplan–Meier log-rank test. $^{*}p < 0.05$, $^{**}p < 0.01$, $^{***}p < 0.001$.

treatment and correlated with the radiation-induced SLC1A6 upregulation. However, the mechanism of radiation induced SLC1A6 overexpression remained far from understood. We hypothesized that genetic reprogramming happened in the process of DNA injury and repair upon radiation.

SLC1A family is thought to contribute to tumor progression by regulating microenvironments and metabolic profiles (Ye et al., 1999; de Groot et al., 2005; Tao et al., 2011; Pedraz-Cuesta et al., 2015; Sun et al., 2019; Freidman et al., 2020; Xu et al., 2020; Guo et al., 2021). SLC1A6 transports aspartate, glutamate, and cysteine, and regulation of these amino acids is essential for numerous biochemical and metabolic pathways such as the TCA cycle or nucleotide synthesis. For example, glutamate could be transformed into glutamine, facilitating nucleotide synthesis and repair DNA damage (Fu et al., 2019). The endocrine resistance breast cancer cells would increase aspartate and glutamate import to sustain DNA, lipid, and protein synthesis (Bacci et al., 2019). We found both glutamate and aspartate were elevated in radioresistant NPC cells. However, only glutamate played a vital role in resisting DNA injury from cisplatin treatment. These findings suggested that SLC1A6 contributed to metabolic reprogramming in radioresistant NPC cells.

We also uncovered that SLC1A6 promoted the upregulation of drug catabolic genes (CYP1A1, CYP2C8, CYP2D6, DHFR, GSTP1, and SULT1E1) and drug transport genes (ABCC1 and ABCC3). The CYP enzymes have been extensively investigated in drug metabolism, and their inhibitors were proven to be effective in reversing cisplatin sensitivity in cancer cells (Sonawane et al., 2019). Gstp1, a GST family member, is involved in the detoxification of cisplatin via cisplatin-glutathione adducts formation (Li et al., 2019). DHFR and SULT1E1 have been reported to be up-regulated in cisplatin-resistant cells (Marverti et al., 2009; Varamo et al., 2019). The ABC family of transporters is referred to as multidrug resistance proteins that transport substrates across the cellular membranes (Chen et al., 2016). These results implicated that SLC1A6 contributed to cisplatin resistance in radioresistant NPC cells through multiple factors.

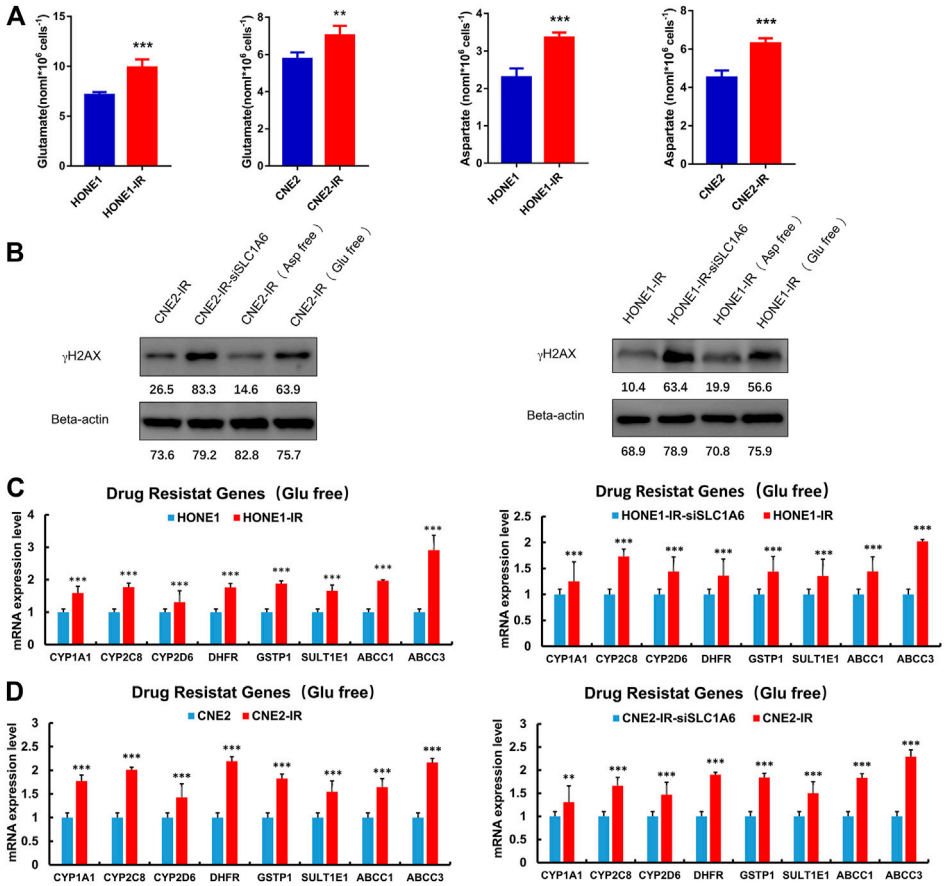


**FIGURE 5 |** SLC1A6 increased glutamate level and drug resistance gene expression. **(A)** The level of glutamate and aspartate in radioresistant NPC cells and their parental cells. **(B)** The level of γH2AX and Beta-actin in radioresistant NPC cells, radioresistant NPC SLC1A6 knockdown cells, radioresistant NPC cells cultured with glutamic acid free medium and radioresistant NPC cells cultured with aspartic acid free medium, treated with cisplatin. **(C–D)** RT-PCR on the mRNA expression of drug resistance genes in NPC cells, radioresistant NPC cells and radioresistant SLC1A6 knockdown cells. Unpaired Student's t test. $^{*}p < 0.05$, $^{**}p < 0.01$, $^{***}p < 0.001$.

In summary, we identified the upregulation of SLC1A6 in radioresistant NPC cells. Overexpression of SLC1A6 is correlated with reduced sensitivity to cisplatin by elevating the level of glutamate and drug resistance genes. Targeting SLC1A6 could be a potential strategy to enhance cisplatin sensitivity in NPC patients.

## DATA AVAILABILITY STATEMENT

The datasets presented in this study can be found in online repositories. The names of the repository/repositories and accession number(s) can be found below: NCBI SRA, PRJNA700383.

## ETHICS STATEMENT

This study was approved by the Ethics Committee of the Sun Yat-sen University Cancer Center, and met the ethical standard of the Declaration of Helsinki. Informed consent was obtained from each patient before obtaining the nasopharyngeal biopsy.

## AUTHOR CONTRIBUTIONS

WH, LW, LC, JY, JW and LN conducted experiments and acquired the data; WH, LW, LC and JY analyzed the data; WH, LW and LC wrote the paper; YC and XL conceived and designed the study. All authors read and agreed on the final manuscript.

## FUNDING

This study was supported by National Natural Science Foundation of China (81902928, 81702762), Natural Science Foundation of Guangdong Province (2021A1515010602), Beijing Xisike Clinical Oncology Research Foundation (Y-MX2016-062).

## REFERENCES


Bacci, M., Lorito, N., Ippolito, L., Ramazzotti, M., Luti, S., Romagnoli, S., et al. (2019). Reprogramming of amino acid transporters to support aspartate and glutamate dependency sustains endocrine resistance in breast cancer. *Cel Rep.* 28, 104–118. doi:10.1016/j.celrep.2019.06.010

Boeckman, H. J., Trego, K. S., and Turchi, J. J. (2005). Cisplatin sensitizes cancer cells to ionizing radiation via inhibition of nonhomologous end joining. *Mol. Cancer Res.* 3, 277–285. doi:10.1158/1541-7786.MCR-04-0032

Chao, C. C., Huang, S. L., Huang, H. M., and Lin-Chao, S. (1991). Cross-resistance to UV radiation of a cisplatin-resistant human cell line: overexpression of cellular factors that recognize UV-modified DNA. *Mol. Cel. Biol.* 11, 2075–2080. doi:10.1128/mcb.11.4.2075

Chen, Q.-Y., Wen, Y.-F., Guo, L., Liu, H., Huang, P.-Y., Mo, H.-Y., et al. (2011). Concurrent chemoradiotherapy vs radiotherapy alone in stage II nasopharyngeal carcinoma: phase III randomized trial. *J. Natl. Cancer Inst.* 103, 1761–1770. doi:10.1093/jnci/djr432

Chen, Y.-P., Chan, A. T. C., Le, Q.-T., Blanchard, P., Sun, Y., and Ma, J. (2019). Nasopharyngeal carcinoma. *The Lancet* 394, 64–80. doi:10.1016/S0140-6736(19)30956-0

Chen, Z., Shi, T., Zhang, L., Zhu, P., Deng, M., Huang, C., et al. (2016). Mammalian drug efflux transporters of the ATP binding cassette (ABC) family in multidrug resistance: a review of the past decade. *Cancer Lett.* 370, 153–164. doi:10.1016/j.canlet.2015.10.010

Cruz-Bermúdez, A., Laza-Briviesca, R., Vicente-Blanco, R. J., García-Grande, A., Coronado, M. J., Laine-Menéndez, S., et al. (2019). Cisplatin resistance involves a metabolic reprogramming through ROS and PGC-1α in NSCLC which can be overcome by OXPHOS inhibition. *Free Radic. Biol. Med.* 135, 167–181. doi:10.1016/j.freeradbiomed.2019.03.009

de Groot, J. F., Liu, T. J., Fuller, G., and Yung, W. K. A. (2005). The excitatory amino acid transporter-2 induces apoptosis and decreases glioma growth *in vitro* and *in vivo*. *Cancer Res.* 65, 1934–1940. doi:10.1158/0008-5472.CAN-04-3626

Eichholtz-Wirth, H., Reidel, G., and Hietel, B. (1993). Radiation-induced transient cisplatin resistance in murine fibrosarcoma cells associated with elevated metallothionein content. *Br. J. Cancer* 67, 1001–1006. doi:10.1038/bjc.1993.183

Eichholtz-Wirth, H. (1995). Reversal of radiation-induced cisplatin resistance in murine fibrosarcoma cells by selective modulation of the cyclic GMP-dependent transduction pathway. *Br. J. Cancer* 72, 287–292. doi:10.1038/bjc.1995.326

Fairman, W. A., Vandenberg, R. J., Arriza, J. L., Kavanaught, M. P., and Amara, S. G. (1995). An excitatory amino-acid transporter with properties of a ligand-gated chloride channel. *Nature* 375, 599–603. doi:10.1038/375599a0

Freidman, N., Chen, I., Wu, Q., Briot, C., Holst, J., Font, J., et al. (2020). Amino acid transporters and exchangers from the SLC1A family: structure, mechanism and roles in physiology and cancer. *Neurochem. Res.* 45, 1268–1286. doi:10.1007/s11064-019-02934-x

Fu, S., Li, Z., Xiao, L., Hu, W., Zhang, L., Xie, B., et al. (2019). Glutamine synthetase promotes radiation resistance via facilitating nucleotide metabolism and subsequent DNA damage repair. *Cel Rep.* 28, 1136–1143. doi:10.1016/j.celrep.2019.07.002

Galluzzi, L., Senovilla, L., Vitale, I., Michels, J., Martins, I., Kepp, O., et al. (2012). Molecular mechanisms of cisplatin resistance. *Oncogene* 31, 1869–1883. doi:10.1038/onc.2011.384

Guo, S.-S., Liu, R., Wen, Y.-F., Liu, L.-T., Yuan, L., Li, Y.-X., et al. (2020). Endogenous production of C-C motif chemokine ligand 2 by nasopharyngeal carcinoma cells drives radioresistance-associated metastasis. *Cancer Lett.* 468, 27–40. doi:10.1016/j.canlet.2019.10.008

Guo, W., Li, K., Sun, B., Xu, D., Tong, L., Yin, H., et al. (2021). Dysregulated glutamate transporter SLC1A1 propels cystine uptake via xc- for glutathione synthesis in lung cancer. *Cancer Res.* 81, 552–566. doi:10.1158/0008-5472.CAN-20-0617

Guskov, A., Jensen, S., Faustino, I., Marrink, S. J., and Slotboom, D. J. (2016). Coupled binding mechanism of three sodium ions and aspartate in the glutamate transporter homologue GltTk. *Nat. Commun.* 7, 13420. doi:10.1038/ncomms13420

Ikuta, K., Takemura, K., Kihara, M., Naito, S., Lee, E., Shimizu, E., et al. (2005). Defects in apoptotic signal transduction in cisplatin-resistant non-small cell lung cancer cells. *Oncol. Rep.* 13, 1229–1234.

Ji, M. F., Sheng, W., Cheng, W. M., Ng, M. H., Wu, B. H., Yu, X., et al. (2019). Incidence and mortality of nasopharyngeal carcinoma: interim analysis of a cluster randomized controlled screening trial (PRO-NPC-001) in southern China. *Ann. Oncol.* 30, 1630–1637. doi:10.1093/annonc/mdz231

Karam, I., Huang, S. H., McNiven, A., Su, J., Xu, W., Waldron, J., et al. (2016). Outcomes after reirradiation for recurrent nasopharyngeal carcinoma: north American experience. *Head Neck* 38 (Suppl. 1), E1102–E1109. doi:10.1002/hed.24166

Li, J., Ye, T., Liu, Y., Kong, L., Sun, Z., Liu, D., et al. (2019). Transcriptional activation of gstp1 by MEK/ERK signaling confers Chemo-Resistance to cisplatin in lung cancer stem cells. *Front. Oncol.* 9, 476. doi:10.3389/fonc.2019.00476

Marverti, G., Ligabue, A., Paglietti, G., Corona, P., Piras, S., Vitale, G., et al. (2009). Collateral sensitivity to novel thymidylate synthase inhibitors correlates with folate cycle enzymes impairment in cisplatin-resistant human ovarian cancer cells. *Eur. J. Pharmacol.* 615, 17–26. doi:10.1016/j.ejphar.2009.04.062

Pedraz-Cuesta, E., Christensen, S., Jensen, A. A., Jensen, N. F., Bunch, L., Romer, M. U., et al. (2015). The glutamate transport inhibitor DL-Threo-β-Benzyloxyaspartic acid (DL-TBOA) differentially affects SN38- and oxaliplatin-induced death of drug-resistant colorectal cancer cells. *BMC Cancer* 15, 411. doi:10.1186/s12885-015-1405-8

Pfister, D. G., Spencer, S., Adelstein, D., Adkins, D., Anzai, Y., Brizel, D. M., et al. (2020). Head and neck cancers, version 2.2020, NCCN clinical practice guidelines in Oncology. *J. Natl. Compr. Canc Netw.* 18, 873–898. doi:10.6004/jnccn.2020.0031

Poppenborg, H., Münstermann, G., Knüpfer, M. M., Hotfilder, M., and Wolff, J. E. (1997). C6 cells cross-resistant to cisplatin and radiation. *Anticancer Res.* 17, 2073–2077.

Ryan, R. M., Compton, E. L. R., and Mindell, J. A. (2009). Functional characterization of a Na+-dependent aspartate transporter from Pyrococcus horikoshii. *J. Biol. Chem.* 284, 17540–17548. doi:10.1074/jbc.M109.005926

Sonawane, V. R., Siddique, M. U. M., Gatchie, L., Williams, I. S., Bharate, S. B., Jayaprakash, V., et al. (2019). CYP enzymes, expressed within live human suspension cells, are superior to widely-used microsomal enzymes in identifying potent CYP1A1/CYP1B1 inhibitors: identification of quinazolinones as CYP1A1/CYP1B1 inhibitors that efficiently reverse B[a]P toxicity and cisplatin resistance. *Eur. J. Pharm. Sci.* 131, 177–194. doi:10.1016/j.ejps.2019.02.016

Sun, J., Nagel, R., Zaal, E. A., Ugalde, A. P., Han, R., Proost, N., et al. (2019). SLC 1A3 contributes to L-asparaginase resistance in solid tumors. *Embo J.* 38, e102147. doi:10.15252/embj.2019102147

Tao, J., Deng, N. T., Ramnarayanan, K., Huang, B., Oh, H. K., Leong, S. H., et al. (2011). CD44-SLC1A2 gene fusions in gastric cancer. *Sci. Translational Med.* 3, 77ra30. doi:10.1126/scitranslmed.3001423

Vandenberg, R. J., and Ryan, R. M. (2013). Mechanisms of glutamate transport. *Physiol. Rev.* 93, 1621–1657. doi:10.1152/physrev.00007.2013

Varamo, C., Peraldo-Neia, C., Ostano, P., Basiricò, M., Raggi, C., Bernabei, P., et al. (2019). Establishment and characterization of a new intrahepatic cholangiocarcinoma cell line resistant to gemcitabine. *Cancers* 11, 519. doi:10.3390/cancers11040519

Wang, D., and Lippard, S. J. (2005). Cellular processing of platinum anticancer drugs. *Nat. Rev. Drug Discov.* 4, 307–320. doi:10.1038/nrd1691

Xu, L., Chen, J., Jia, L., Chen, X., Awaleh Moumin, F., and Cai, J. (2020). SLC1A3 promotes gastric cancer progression via the PI3K/AKT signalling pathway. *J. Cel. Mol. Med.* 24, 14392–14404. doi:10.1111/jcmm.16060

Ye, Z.-C., Rothstein, J. D., and Sontheimer, H. (1999). Compromised glutamate transport in human glioma cells: reduction-mislocalization of sodium-dependent glutamate transporters and enhanced activity of cystine-glutamate exchange. *J. Neurosci.* 19, 10767–10777. doi:10.1523/JNEUROSCI.19-24-10767.1999

Zhang, Y., Wang, Z., Yu, J., Shi, J. z., Wang, C., Fu, W. h., et al. (2012). *Cancer* stem-like cells contribute to cisplatin resistance and progression in bladder cancer. *Cancer Lett.* 322, 70–77. doi:10.1016/j.canlet.2012.02.010

Zhu, R., Xue, X., Shen, M., Tsai, Y., Keng, P. C., Chen, Y., et al. (2019). NFκB and TNFα as individual key molecules associated with the cisplatin-resistance and radioresistance of lung cancer. *Exp. Cel Res.* 374, 181–188. doi:10.1016/j.yexcr.2018.11.022

Zhuang, H., Shi, S., Guo, Y., and Wang, Z. (2019). Increase of secondary mutations may be a drug-resistance mechanism for lung adenocarcinoma after radiation therapy combined with tyrosine kinase inhibitor. *J. Cancer.* 10, 5371–5376. doi:10.7150/jca.35247

**Conflict of Interest:** The authors declare that the research was conducted in the absence of any commercial or financial relationships that could be construed as a potential conflict of interest.

frontiers in Pharmacology

ORIGINAL RESEARCH
published: 13 April 2021
doi: 10.3389/fphar.2021.653306

# A New Chalcone Derivative C49 Reverses Doxorubicin Resistance in MCF-7/DOX Cells by Inhibiting P-Glycoprotein Expression

*Ting Wang[1†], Jingjing Dong[2†], Xu Yuan[1†], Haotian Wen[3], Linguangjin Wu[1], Jianwen Liu[4*], Hua Sui[5*] and Wanli Deng[1*]*

[1]Department of Medical Oncology, Putuo Hospital, Shanghai University of Traditional Chinese Medicine, Shanghai, China, [2]Shanghai Bailijia Health Pharmaceutical Technology, Shanghai, China, [3]Shuguang Hospital, Shanghai University of Traditional Chinese Medicine, Shanghai, China, [4]State Key Laboratory of Bioreactor Engineering and Shanghai Key Laboratory of New Drug Design, School of Pharmacy, East China University of Science and Technology, Shanghai, China, [5]Medical Experiment Center, Jiading Branch of Shanghai General Hospital, Shanghai Jiao Tong University School of Medicine, Shanghai, China

OPEN ACCESS

**Edited by:**
Xiaoping Lin,
Sun Yat-sen University Cancer Center (SYSUCC), China

**Reviewed by:**
Long Zhang,
Harvard Medical School, United States
Ruicai Gu,
University of Oklahoma Health Sciences Center, United States

***Correspondence:**
Jianwen Liu
liujian@ecust.edu.cn
Hua Sui
syh0808@163.com
Wanli Deng
tcmdwl@163.com

[†]These authors have contributed equally to this work and share first authorship

**Specialty section:**
This article was submitted to Pharmacology of Anti-Cancer Drugs, a section of the journal Frontiers in Pharmacology

**Received:** 14 January 2021
**Accepted:** 01 March 2021
**Published:** 13 April 2021

**Citation:**
Wang T, Dong J, Yuan X, Wen H, Wu L, Liu J, Sui H and Deng W (2021) A New Chalcone Derivative C49 Reverses Doxorubicin Resistance in MCF-7/DOX Cells by Inhibiting P-Glycoprotein Expression. Front. Pharmacol. 12:653306. doi: 10.3389/fphar.2021.653306

**Objective:** C49 is a chalcone derivative. The aim of the current study is to illuminate the efficacy of C49 in reversing multidrug resistance (MDR) in MCF-7/DOX cells and its underlying molecular mechanism.

**Methods:** The cytotoxic effects of C49 on MCF-7/DOX cells were evaluated by MTT assay using different concentration (0–250 μmol/L) of C49. Cell proliferation was evaluated by colony formation assay. Cell death was examined by morphological analysis using Hoechst 33,258 staining. Flow cytometry and immunofluorescence were utilized to evaluate the intracellular accumulation of doxorubicin (DOX) and cell apoptosis. The differentially expressed genns between MCF-7 and MCF-7/DOX cells were analyzed by GEO database. The expression of PI3K/Akt pathway proteins were assessed by Western blot The activities of C49 combined with DOX was evaluated via xenograft tumor model in female BALB/c nude mice.

**Results:** C49 inhibited the growth of MCF-7 cells ($IC_{50}$ = 59.82 ± 2.10 μmol/L) and MCF-7/DOX cells ($IC_{50}$ = 65.69 ± 8.11 μmol/L) with dosage-dependent and enhanced the cellular accumulation of DOX in MCF-7/DOX cells. The combination of C49 and DOX inhibited cell proliferation and promoted cell apoptosis. MCF-7/DOX cells regained drug sensibility with the combination treatment through inhibiting the expression of P-gp, p-PI3K and p-Akt proteins. Meanwhile, C49 significantly increased the anticancer efficacy of DOX *in vivo*.

**Conclusion:** C49 combined with DOX restored DOX sensitivity in MCF-7/DOX cells through inhibiting P-gp protein.

**Keywords: breast cancer, DOX, C49, multidrug resistance, P-gp, PI3K/akt signaling pathway**

## INTRODUCTION

Breast cancer has the highest mortality of female cancers and is the second cause of death in females (Siegel et al., 2020). Treatment for breast cancer includes surgery, chemotherapy, and radiotherapy, among them, chemotherapy plays a critical role (Harbeck et al., 2017; Waks and Winer, 2019). The first-line chemotherapeutic drug for breast cancer is doxorubicin (DOX), which is an anthracycline (Li et al., 2019b; Pondé et al., 2019; Tun et al., 2019; Zeinoddini et al., 2019). DOX represses DNA replication, interrupts cell cycle, and facilitates generation of intracellular reactive oxygen species (Meredith et al., 2016; Cui et al., 2018; Khaki-Khatibi et al., 2019) to induce tumor cell death (Marinello et al., 2018; El-Hamid et al., 2019). However, breast cancer cells generate DOX resistance and cause serious cardiotoxicity with increasing length of chemotherapy. These two factors are major causes for treatment failure and metastasis of breast cancer (Cappetta et al., 2017; Li et al., 2017; Ponnusamy et al., 2018; Wenningmann et al., 2019; Zheng et al., 2019; Al-Malky et al., 2020).

Numerous studies have found that P-glycoprotein (P-gp) expression is elevated in breast cancer patients who are insensitive to chemotherapy (Badowska-Kozakiewicz et al., 2016; Dyson et al., 2018; Mehrotra et al., 2018). This finding indicates that P-gp on cell membrane may participate in the development of drug resistance in breast cancer (Pokharel et al., 2016; Ge et al., 2017; Xiong et al., 2018). P-gp is a transmembrane protein encoded by ABCB1 gene, which is an ATP-dependent drug transport protein and is closely associated with multidrug resistance (MDR) of tumors. The function of P-gp protein is to excrete endogenous and exogenous substances and reduce the content of intracellular chemotherapeutics, as a result, chemotherapeutics fail to effectively kill tumor cells (Waghray et al., 2018; Guo et al., 2019). This defense mechanism is important for tumor cells to evade chemotherapeutic attack (Kartal-Yandim et al., 2016). A number of studies show that MDR can be reversed by inhibiting P-gp transport activity or competitively binding to P-gp protein binding site with chemotherapeutics (Li et al., 2016; Komoto et al., 2018; Chang et al., 2019).

Although several drugs can reverse drug resistance by repressing P-gp protein, their side effects have restricted the clinical application. For instance, verapamil may give rise to cardiotoxicity, and cyclosporin A may cause hepatotoxicity, nephrotoxicity, myelogenous toxicities and neurotoxicity (Joshi et al., 2017; Ding et al., 2018; Dong et al., 2019). Therefore, there is no approved MDR-reversing agent applied in clinical chemotherapy of cancers available at present. Thus, developing drugs with efficient reversal activity and few toxicities is urgently needed.

Chalcone derivatives extensively exist in plants, such as *glycyrrhiza* and *lupulus* (Watanabe et al., 2016; Gomes et al., 2017; Seliger et al., 2018; Wu et al., 2020). They have multiple biological activities, such as antioxidation and antivirus (Mateeva et al., 2017; Liang et al., 2018; Gupta et al., 2019; Lin et al., 2019; Maria Pia et al., 2019; Xu et al., 2019). Some researchers have designed a quinone chalcone compound, which can inhibit DNA topoisomerase I and has anti-inflammatory activity. The compound has a strong anti-tumor effect, and its inhibition rate on breast cancer cells is as high as 50% at the dose of 10 μg/ml. Natural chalcones have few side effects and high anti-tumor activity. Therefore, finding new natural chalcone derivatives has attracted a lot of interests. Studies have shown that chalcone derivatives have antitumor activity, such as facilitating apoptosis and autophagy of hepatocellular carcinoma cells and inhibiting proliferation of human bladder cancer cells (Wang et al., 2017; Hong et al., 2019; Pinto et al., 2019; Yang et al., 2019; Zhu et al., 2019). Previous studies have reported that some chalcone derivatives can repress the expression of P-gp protein, increase DOX accumulation in cells, and reverse MDR (Yin et al., 2019). In this study, we investigate a new chalcone, namely C49, for its ability to enhance the chemosensitivity of MCF-7/DOX cells to DOX and the possible mechanism of action. This study will provide a novel therapeutic option for breast cancer.

## MATERIALS AND METHODS

### Cell Culture

MCF-7/DOX and MCF-7 cells were obtained from the Cell Bank of Chinese Academy of Science (Shanghai, China). The cells were cultured in RPMI1640 medium containing 10% fetal bovine serum (FBS) at 37°C, in a humidified atmosphere with 5% $CO_2$. The resistance of MCF-7/DOX cells was maintained by using a medium containing DOX at a concentration of 50 ng/ml.

### Reagents and Chemicals

C49 (>99% purity) was synthesized in the School of Pharmacy of East China University of Science and Technology. DOX, 3-(4,5-Dimethylthiazol-2-yl)-2,5-diphenyltetrazolium bromide (MTT), and Hoechst 33,258 were purchased from Sigma Chemical Co. The primary antibodies, P-gp, Caspase-3, Caspase-9, Caspase-10, Bcl-2, Bcl-xL, p53, phospho-p53, PI3K, phospho-PI3K, Akt, phospho-Akt, β-actin, and Ki-67, were brought from Proteintech.

### Synthesis of C49

The method was performed as described previously (Tseng et al., 2013). Ccarboxylic acid (1.47 g, 5.0 mmol) was heated at 280°C for 4 h (TLC monitoring) and add hexane (50 ml), then the resulting precipitate was collected and purified by flash chromatography on silica gel (hexane/CH2Cl2 1/1). During extracted with CH2Cl2 and ethyl acetate (50 ml × 3), the crude product was purified and crystallized with EtOH to give quinolinyl chalcones.

### MTT Cell Viability Assay

The cell viability assays were performed by MTT method (Wang et al., 2016; Śliwka et al., 2016; Schröder et al., 2019). MCF-7 and MCF-7/DOX cells were seeded in 96-well plates ($1 \times 10^5$ cells/well) until they attached to the plate. Then, cells were treated with C49, DOX, or their combinations at different concentrations. After 24, 48 and 72 h, MTT assay was performed and the $IC_{50}$ of drug was calculated.

## Evaluating the Effect of Drug Combination

The drug combination index (CI) was calculated by Calcusyn (Biosoft, Cambridge, United Kingdom). CI reflects the synergistic effect of the drug combination (Liu et al., 2016; Bahri et al., 2019). The CI value <1, =1, and >1 represents synergy, addiction and antagonism, respectively.

## Colony-forming Assay

MCF-7/DOX cells were seeded in 24-well plates (100 cells per well). Cells were respectively treated with C49 (25 μmol/L), DOX (8 μmol/L) and their combination. After 7 days, they were washed, fixed, stained with 0.1% crystal violet at room temperature for 20 min, and photographed. ImageJ was utilized for quantitative analysis.

## Hoechst 33,258 Staining for Cell Morphology

MCF-7/DOX cells were inoculated into 12-well plates (approximately $2 \times 10^5$ cells/well) for 12 h and were respectively cultured with C49 (25 μmol/L), DOX (8 μmol/L) and their combination for 24 h. Then, they were fixed in paraformaldehyde (4%) for 15 min, stained with Hoechst 33,258 for 15 min with phosphate buffer saline (PBS) at room temperature, washed and photographed by a fluorescence microscope (Nikon, Tokyo, Japan).

## Western Blot Assay

WB assay was performed as described previously (Wang et al., 2019). MCF-7 and MCF-7/DOX cells were treated with C49 (25 μmol/L), DOX (8 μmol/L) and their combination for 24 and 48 h. The cells were washed twice with pre-cold PBS and were lyzed using RIPA lysate buffer with phosphatase inhibitor for 30 min. Then, the crude cell lysates were centrifuged at 12,000 rpm for 10 min at 4°C. Equal amounts of protein were separated with SDS-PAGE and transferred onto PVDF membranes. The resultants were blocked with BSA (50 mg/ml) and incubated overnight at 4°C with the primary antibodies of P-gp, Caspase-3, Caspase-9, Caspase-10, Bcl-2, Bcl-xL, p53, phospho-p53, PI3K, phospho-PI3K, Akt, phospho-Akt and β-actin. The PVDF was washed three times with TBST, incubated with horseradish peroxidase-conjugated secondary antibodies (1: 2000) for 2 h at the room temperature, and washed three times with TBST. Protein bands were obtained from WB detection system and quantitated using the ImageJ software.

## Gene Expression Profiles

GEO Series Accession Number GSE24460 (https://www.ncbi.nlm.nih.gov/geo/) contains the data of gene expression, which can be obtained from the database of the National Center for Biotechnology Information. It contains four samples including parental MCF-7 cell line vs. DOX-resistant MCF-7 cell sublines. Biological replicates include two parental controls and two drug resistance, which are independently grown and harvested.

## Screening Differentially Expressed Gene

Limma package, Hochberg False Discovery Rate and Benjamini were used to analyze the gene expression profiles and filter out the differentially expressed genes in MCF-7 and MCF-7/DOX cells using GSE24460. The differentially expressed genes was showed in heatmap, volcano and KEGG plot. The fold change threshold was >2, and the $p$ value was <0.05.

## Flow Cytometry

Flow cytometry (FCM) was used to detect cell apoptosis and intracellular DOX accumulation (Sui et al., 2017). The apoptosis was detected following the manual of Annexin V-FITC apoptosis detection kit (Invitrogen). MCF-7/DOX cells were seeded in 6-well plates ($1 \times 10^4$ cells/well). The cells were treated with C49 (25 μmol/L), DOX (8 μmol/L) and their combination for 48 h, collected and washed with PBS twice. Cells were re-suspended in PBS (250 μL) and then analyzed by FACS using flow cytometer (Becton Dickinson) to detect DOX intracellular accumulation.

## Drug Efflux Fluorescence Microscopy Assay

A FP-6200 spectrofluorometer (Jasco Corp., Tokyo, Japan) was used for measuring the emission spectrum of DOX in the presence and absence of DNA. Studies were carried out as described (Xiong et al., 2005). Briefly, MCF-7/DOX cells were plated in 24-well plates ($1 \times 10^4$ cells/well). When cells were attached, C49 (25 μmol/L) was used with or without DOX (8 μmol/L) for 48 h. Then, cells were exposed to DOX for 2 h, washed and fixed with 4% paraformaldehyde fixation solution for 15 min. DAPI staining was used to stain the nucleus. Cells were washed and photographed using a fluorescent microscope (Nikon, Tokyo, Japan).

## Tumor Xenografts

Female BALB/c nude mice (4–6 weeks old) were purchased from Shanghai Jiesijie Experimental Animal Company and maintained in a specific pathogen-free environment. The animal facility was authorized by the Ministry of Science and Technology of the PRC. MCF-7/DOX cells ($1 \times 10^6$) were suspended in 100 μL of PBS and injected into the right flank of nude mice. When the tumor size grew up to approximately 50 $mm^3$, the mice were randomly divided into 6 groups ($n$ = 5): 1) vehicle control (0.1 mL PBS), 2) C49 (5 mg/kg), 3) C49 (15 mg/kg), 4) DOX (2 mg/kg), 5) DOX (2 mg/kg) combined with C49 (5 mg/kg), and 6) DOX (2 mg/kg) combined with C49 (15 mg/kg). Then PBS and C49 were used by tail intravenous injection, and DOX was used by intraperitoneal injection every 2 days for 30 days. During the treatments, the tumor volumes were recorded using formula $(L \times D \times D) \times 0.5$, where "L" represents the length and "D" represents the breadth of the tumors. Experiments were terminated at the 30th day, and the animals were anesthetized and sacrificed. Tumors were fixed in 10% paraformaldehyde fixation solution for further analysis.

## Hematoxylin and Eosin Staining and Immunohistochemistry Staining

Histological analysis was performed on tissue samples isolated from mouse xenografts. Sections of 5 μm were cut from paraffin-embedded tissues and were prepared according to standard protocols for H&E (hematoxylin and eosin) and IHC (immunohistochemistry) staining. Images of sections were visualized using a microscope (Nikon, Tokyo, Japan).

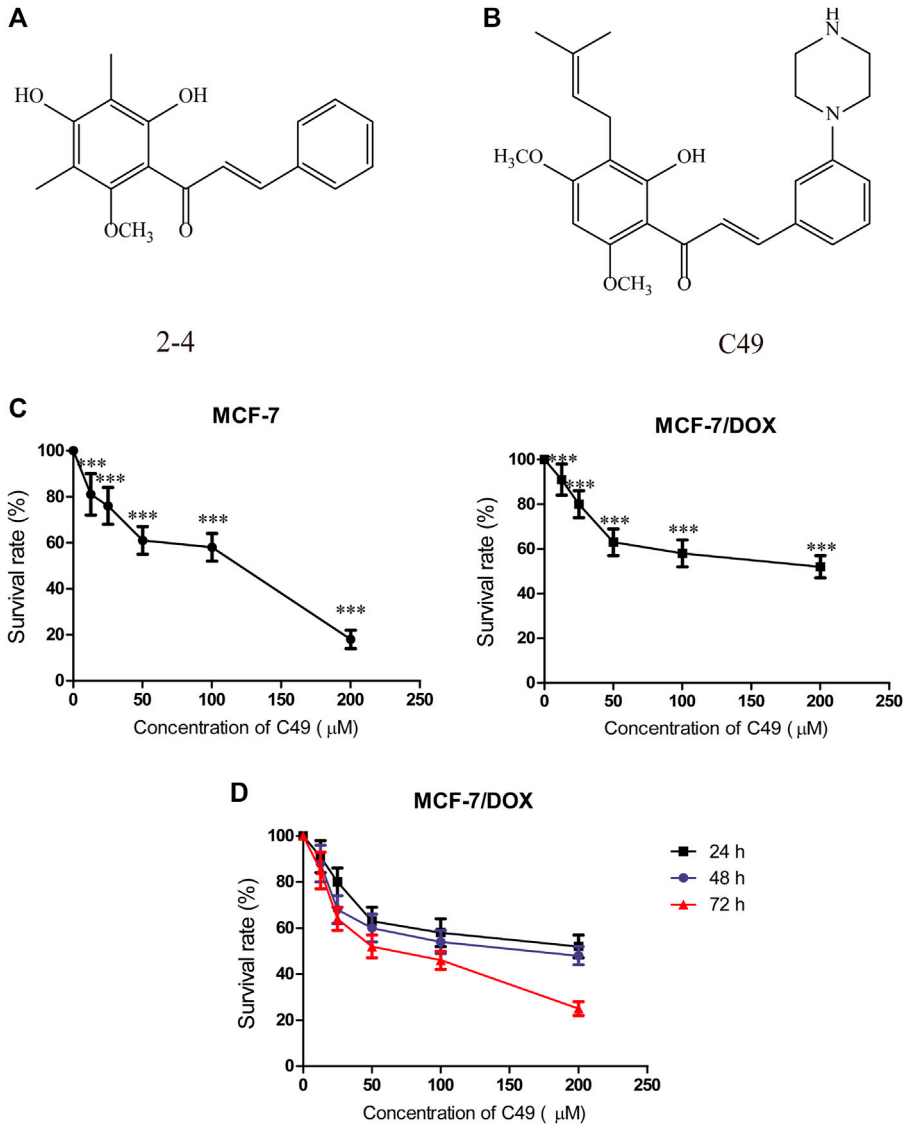


**FIGURE 1 |** Chemical structure of C49 and the effects of C49 on the viability of MCF-7 and MCF-7/DOX cells. **(A–B)** Chemical structures of C49 and its parent compound. **(C)** MCF-7 cells and MCF-7/DOX cells treated with DOX for 48 h, and the cell viability assessed by MTT assay. **(D)** MCF-7/DOX cells treated with C49 for 24, 48 and 72 h. Viability quantitated by the MTT assay. Each point represents mean ± SD, $n = 3$. $^{*}p < 0.05$, $^{**}p < 0.01$, and $^{***}p < 0.001$.

## Statistical Analysis

GraphPad Prism Software was used to analyze the experimental data. Values were denoted by the mean ± standard deviation or standard error of the mean. $p$ values of $^{*}p < 0.05$, $^{**}p < 0.01$, $^{***}p < 0.001$, $^{\#}p < 0.05$, $^{\#\#}p < 0.01$, $^{\#\#\#}p < 0.001$ represent significant difference.

# RESULTS

## Effect of C49 and DOX Treatment on MCF-7 and MCF-7/DOX Cells

C49 is a chalcone derivative, and its structure is shown in **Figures 1A,B**.

Before we investigated the anticancer efficiency of C49 with different dose of DOX, we first examined the doxorubicin-resistance of MCF-7 and MCF-7/DOX cells by MTT assay at 24 h. As showed in **Figure 1C**, the results indicated that DOX exerted significantly inhibit effect in MCF-7 cell when the dose of DOX exceed 5 μM. However, more than 90% of cells survived the concentration of 10 μM in MCF-7/DOX cell treated with DOX for 24 h (**Figure 1D**). Based on this resistance testing result, we then examined the cytotoxicity of C49 in MCF-7/DOX cell by CCK-8 assay at 48, and 72 h. C49 under concentration of 12.5 μmol/L was nontoxic through calculation based on $IC_{20}$ value. Thus, this dose was applied to the subsequent experiment to eliminate C49 toxicity interfering with drug-resistant cell strains.

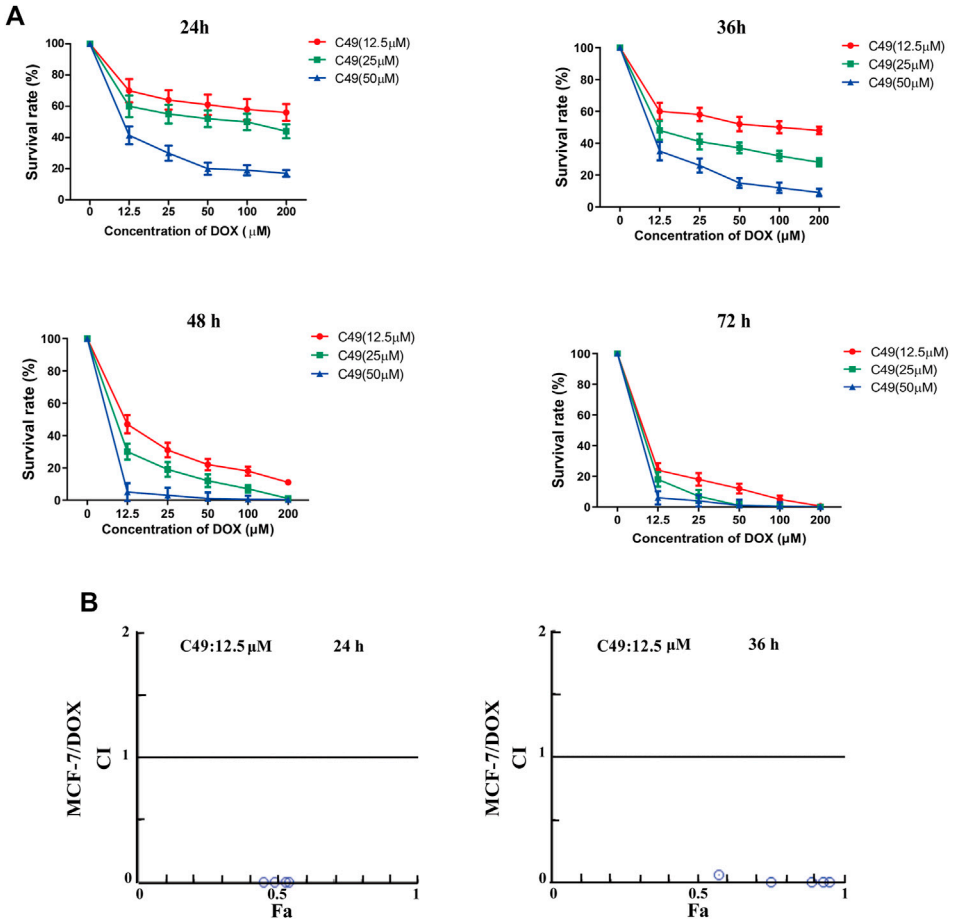


**FIGURE 2 |** The effect of C49 combined with DOX on the viability of MCF-7/DOX cell. **(A)** DOX or C49 combined with DOX inhibits the viability of MCF-7/DOX cells. Each point represents mean ± SD, $n = 3$. $^{*}p < 0.05$, $^{**}p < 0.01$ and $^{***}p < 0.001$ for DOX treated cells vs. combination treated cells. **(B)** Compusyn software used to compute the Combination Index (CI). CI values <1, =1, and >1 respectively represents synergic, addictive and antagonistic effect.

## Effect of C49 Combined With DOX on Proliferation of MCF-7/DOX Cells

MTT assay was performed to assess the proliferation of cells treated with different concentration of C49 and DOX. After combined treatment of C49 and DOX on MCF-7/DOX cells for 24, 36, 48 and 72 h, the anti-proliferative effect was remarkably lower in DOX single drug treatment group than that of C49 combined with DOX group. Compared with C49 (12.5 μM) combined with DOX group, the anti-proliferative effects of 25 and 50 μM C49 combined with DOX groups were markedly stronger than that of C49 low-dose group. The effects were dose and time dependent (**Figure 2A**). This result indicated that C49 could reverse the resistance of MCF-7/DOX cells against DOX, and a high C49 concentration is associated with a strong effect of reversing drug resistance. Meanwhile, the synergistic index of 12.5 μM C49 and DOX was evaluated using Calcusyn software. The CI values were smaller than 1 after their combined action for 24 and 36 h, suggesting that C49 and DOX exerted synergistic effect (**Figure 2B**).

## C49 Enhanced the Cytotoxicity of Doxorubicin to Repress Cell Proliferation and Induced Cell Apoptosis

Colony formation test, Hoechst 33,258 staining method, and FCM were used to examine the proliferation inhibitory effect of DOX, C49 (12.5 μM) or combination of both on MCF-7/DOX cells. **Figure 3A** showed that colony formation has no significant difference in C49 treatment group ($p > 0.05$). However, there was a difference in colony formation in DOX treatment group ($p < 0.05$) and significant difference was observed in C49 combined with DOX treatment group ($p < 0.01$) compared with the blank control group. Therefore, DOX and C49 in combination with DOX treatment could inhibit the proliferation of MCF-7/DOX cells, and the inhibiting effect of C49 combined with DOX group was remarkably stronger than that of DOX alone.

The cell nuclear morphology of the four groups were observed using Hoechst 33,258 staining at 48 h after cells treated with drugs. Usually, cells exhibited apoptotic features with chromatin condensation, nuclear condensation and DNA fragmentation

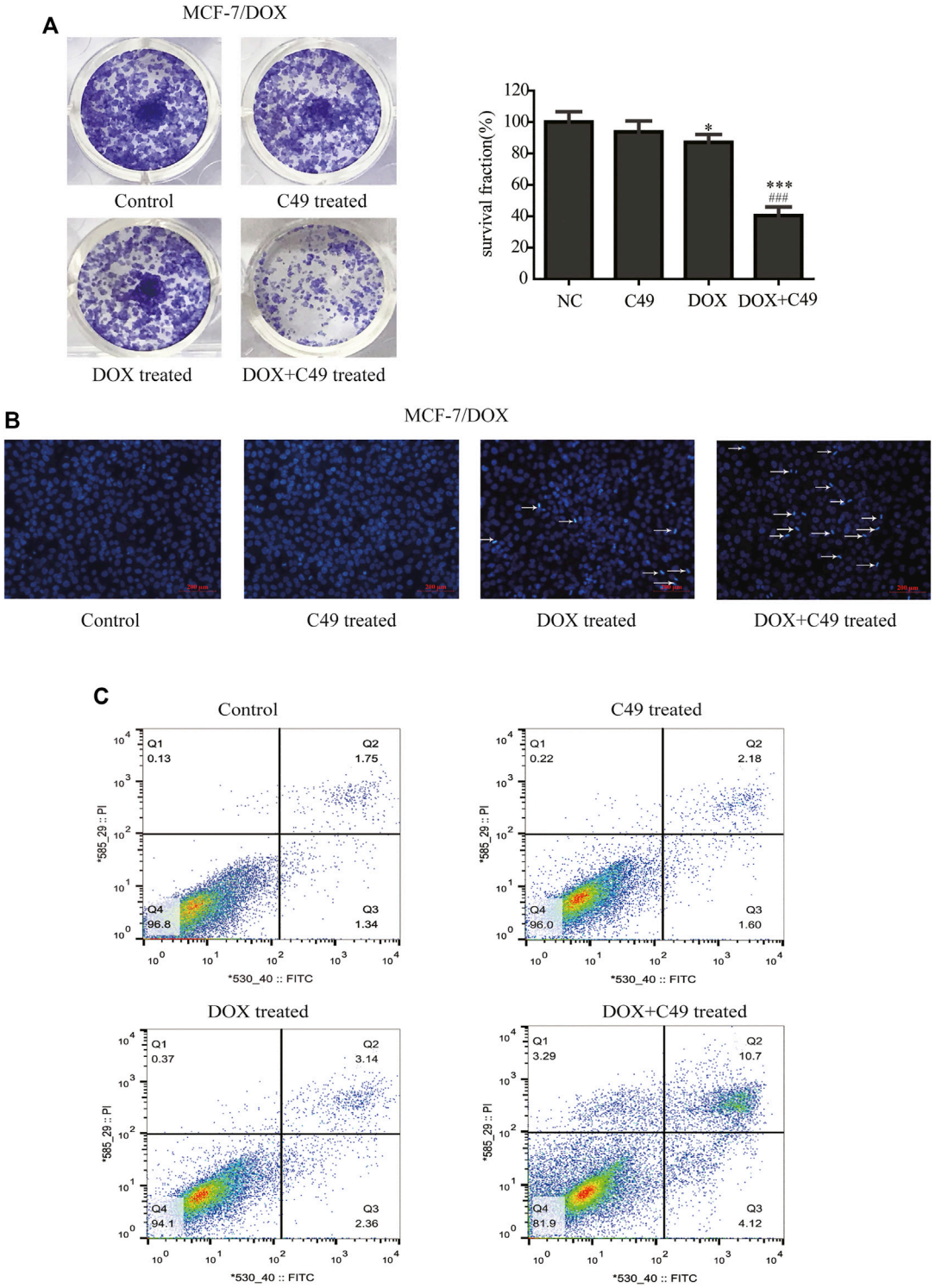


**FIGURE 3 |** C49 combined with DOX inhibited proliferation and promoted apoptosis of MCF-7/DOX cells. **(A)** Colony formation showed the proliferation of MCF7/DOX cells after DOX (8 μM) and/or C49 (12.5 μmol/L) treatment. The right panel was the quantitative analysis of colony formation experiment. Each bar represents mean ± SD, $n = 3$. $^{*}p < 0.05$, $^{**}p < 0.01$ and $^{***}p < 0.001$ for control cells vs. DOX and/or C49 treated cells. $^{###}p < 0.001$ for DOX treated cells vs. combination treated cells. **(B)** Hoechst 33,258 staining showing nuclear morphology of MCF-7/DOX cells 24 h after DOX (8 μmol/L) and/or C49 (12.5 μM) treatment. **(C)** Apoptotic cells detected by flow cytometry after DOX (8 μM) and/or C49 (12.5 μM) treatment for 48 h.

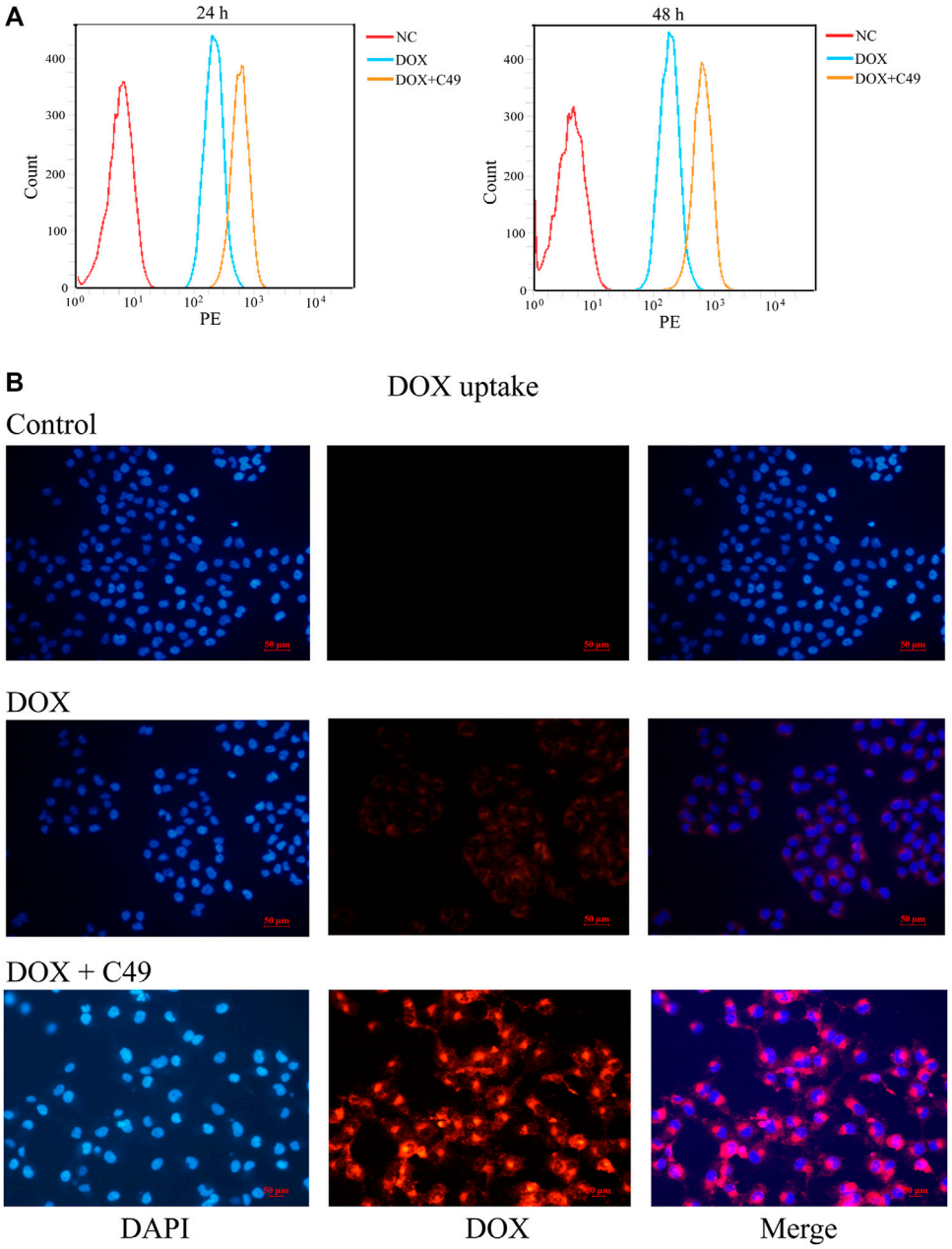


**FIGURE 4 |** C49 combined with DOX increased intracellular concentration of DOX in MCF-7/DOX cells. **(A)** Cells were treated with DOX (8 μM) and C49 (12.5 μM) for 24 or 48 h, and DOX accumulation in the cells were analyzed using flow cytometry. **(B)** Cells were treated with DOX (8 μM) and/or C49 (12.5 μM) for 48 h and stained with DAPI. DAPI: blue fluorescence, DOX: red fluorescence.

(Wang et al., 2011; Li et al., 2018). As shown in **Figure 3B**, the nuclear morphology of cells treated with C49 did not undergo marked changes, the cells treated with DOX showed increasing chromatin condensation and nuclear fragmentation, and a large number of cells treated with C49 combined with DOX are dying compared with cells in the blank control group. This result indicated that C49 combined with DOX could strengthen the DOX cytotoxicity in MCF-7/DOX cells. The cell apoptosis were detected by FCM. As shown in **Figure 3C**, the percentage of apoptotic cells (including the early and late apoptotic cells) was 1.05% in the control group, 3.23% in C49 group, 8.48% in DOX group and 57.4% in C49 combined with DOX group, indicating that the C49 and DOX alone had weak effect causing apoptosis of MCF-7/DOX cells, but C49 could enhance the sensitivity of DOX in MCF-7/DOX cells. These results suggested that C49 did not have marked cytotoxicity but could reverse drug resistance and enhance the cytotoxicity of DOX inhibit cell proliferation and induce cell apoptosis.

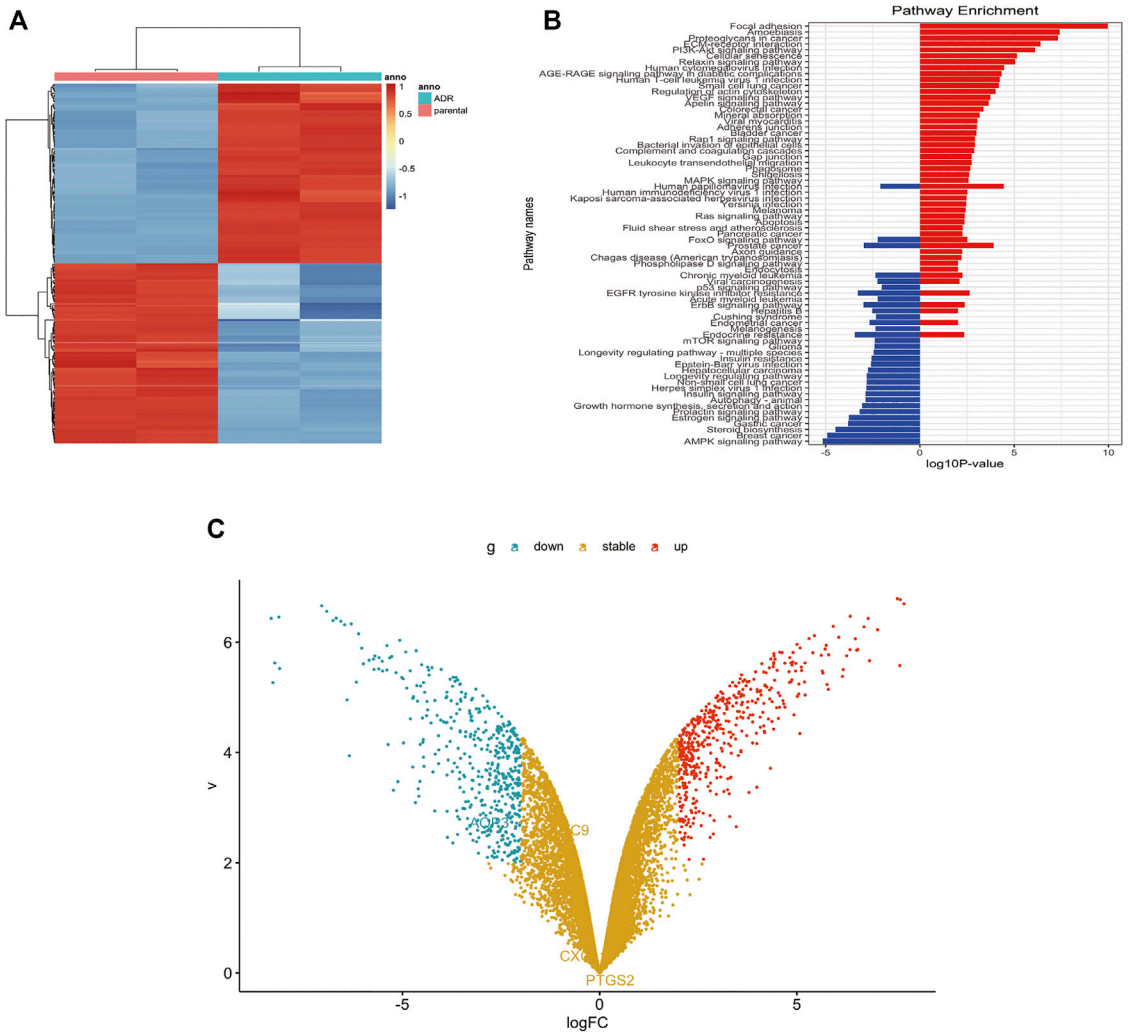


**FIGURE 5 |** P-gp upregulated in MCF-7/DOX cells. **(A)** Heatmap of differentially expressed genes in GEO dataset. **(B)** Analysis of pathways related to drug resistance revealed the PI3K/Akt signaling pathway is the fifth largest factor. **(C)** Volcano plot analyzed the differentially expressed gene between MCF-7 cells and MCF-7/DOX cells. The fold change threshold was >2, *p* value was <0.05.

## C49 Increased Intracellular Accumulation of Doxorubicin in MCF-7/Doxorubicin Cells

FCM assay and immunofluorescence (IF) assay were performed to examine the intracellular accumulation of DOX in MCF-7/DOX cells. Cells were treated with DOX or C49 combined with DOX for 24 and 48 h. FCM was adopted to detect intracellular DOX concentration. As shown in **Figure 4A**, intracellular DOX concentration in cells of DOX group was increased compared with that in the control group, and DOX concentration in C49 combined with DOX group was the highest among the three groups. This result indicated that C49 could facilitate intracellular accumulation of DOX in MCF-7/DOX cells. Immunofluorescent microscope was used to verify the result. As shown in **Figure 4B**, red fluorescence was increased in MCF-7/DOX cells in DOX (8 μM) group relative to the control group, while that in C49 (12.5 μM) combined with DOX (8 μM) group was significantly increased relative to DOX group. These results suggested that C49 increased the intracellular concentration of DOX in MCF-7/DOX cells.

## Differential Gene Expression Between MCF-7 and MCF-7/DOX Cells

GSE24460 gene chip was analyzed using Limma software package, Hochberg False Discovery Rate and Benjamini. Differential genes were screened through the expression of various chips, such as ABCB1, VIM, LDHB, NNMT, MMP1, FSTL1, CCN2, GPX1, ESR1, and AGR2 (**Supplementary Table S1**). Through the expression levels of the first 200 differential genes, heat maps were drawn to indicate differences of genes between the two cell lines (**Figure 5A**). KEGG graph showed that PI3K/Akt signaling pathway was activated in MCF-7/DOX cells (**Figure 5B**). Volcano plots embodied gene differences between

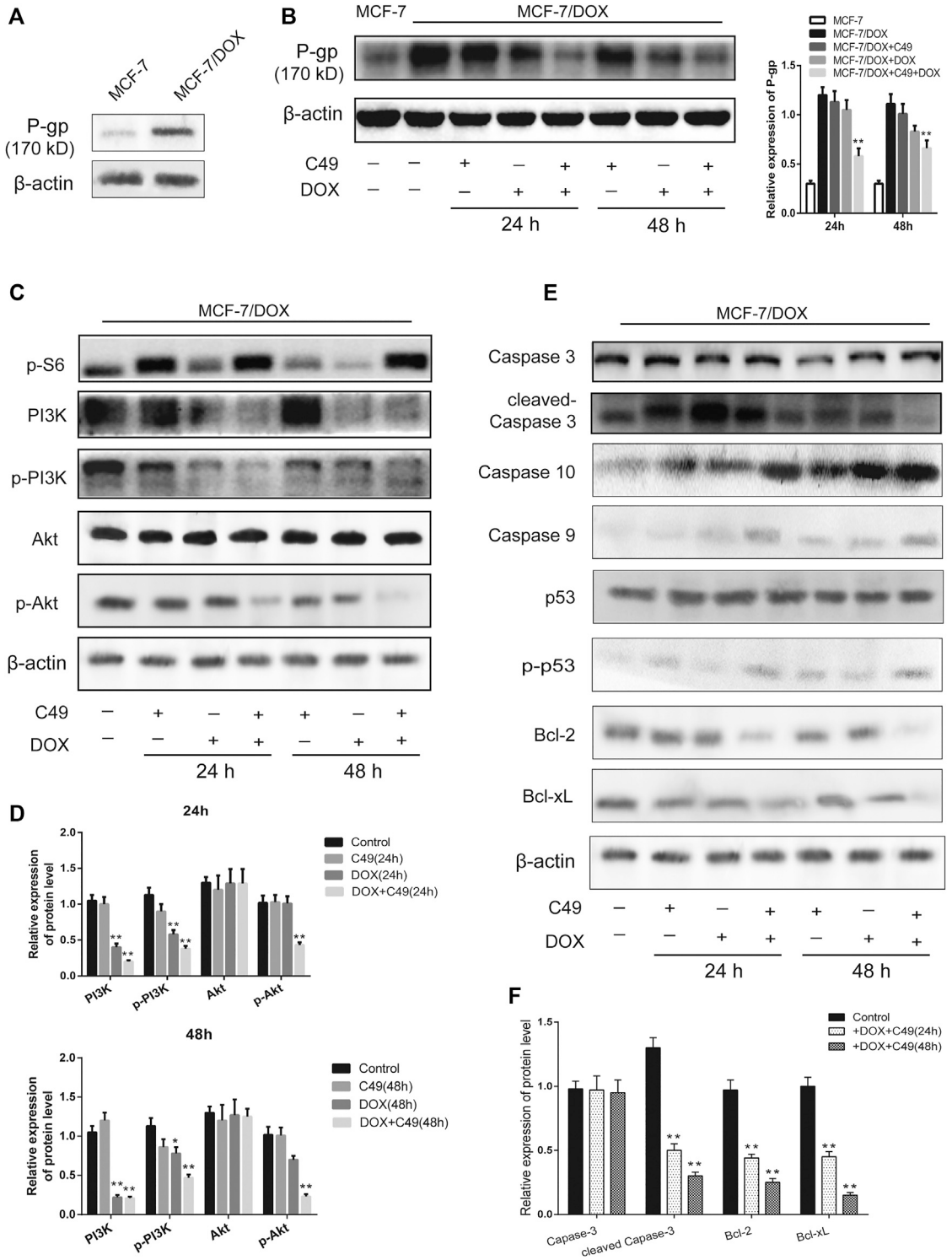


**FIGURE 6 |** The combination of C49 and DOX inhibited P-gp expression, apoptotic signaling pathway and the PI3K/Akt signaling pathway. **(A)** The P-gp expression in MCF-7 cells and MCF-7/DOX cells. **(B–F)** WB and quantitative analysis of P-gp, PI3K, p-PI3K, Akt, p-Akt, Caspase-3, Caspase-10, Caspase-9, p53, p-p53, Bcl-2, and Bcl-xL proteins expression compared with β-actin. $^{*}p < 0.05$, $^{**}p < 0.01$*vs.* MCF-7/DOX cells.

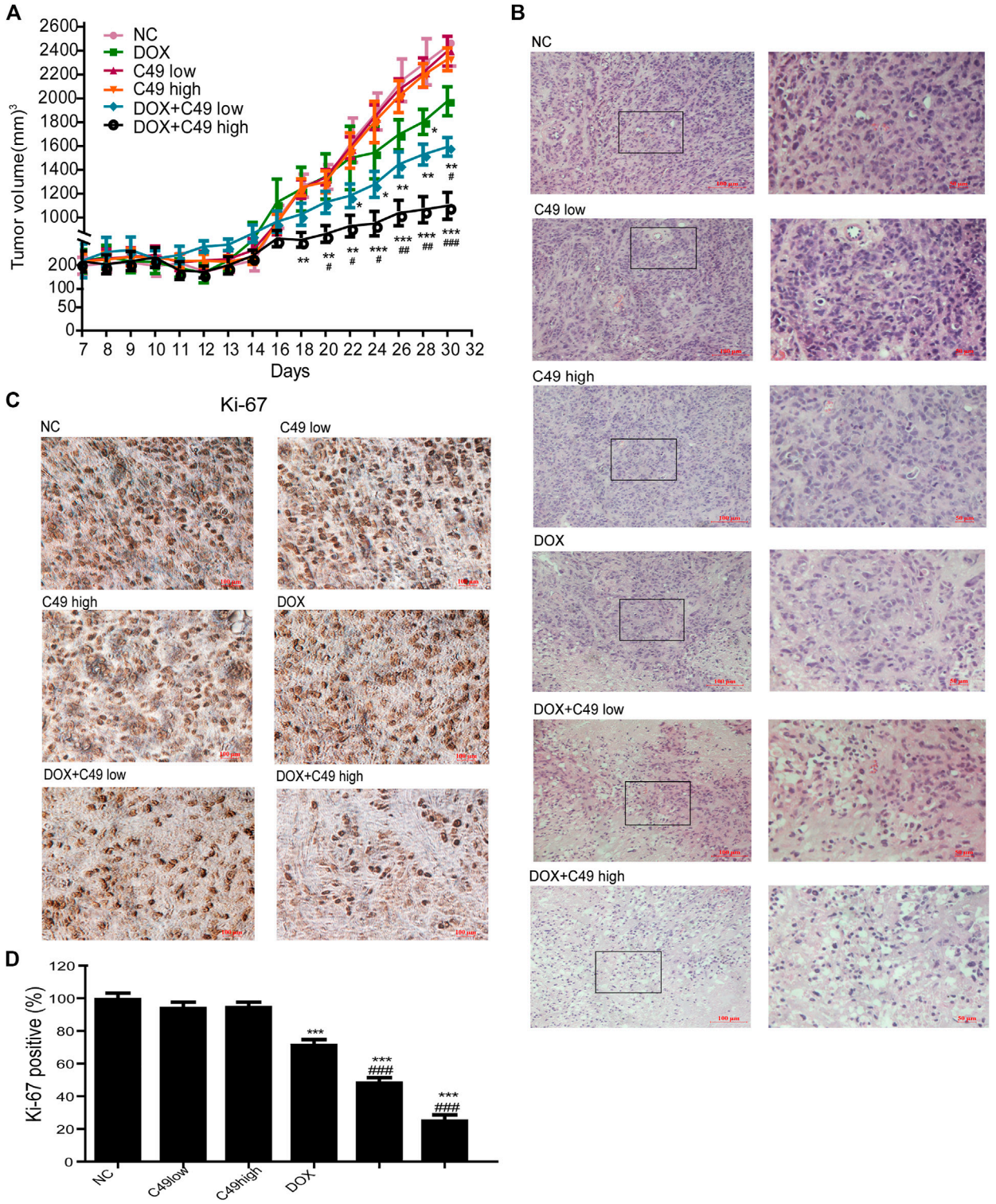


**FIGURE 7 |** C49 combined with DOX increased antitumor activity in MCF-7/DOX bearing nude mice. **(A)** Tumor volume in each group measured once every two days during drug treatment. Each bar represents mean ± SEM. Significant differences between control and DOX and/or C49 drug treatment group were indicated by $^{*}p < 0.05$, $^{**}p < 0.01$ and $^{***}p < 0.001$. Significant differences between DOX treatment group and combination treatment group were indicated by $^{\#}p < 0.05$, $^{\#\#}p < 0.01$ and $^{\#\#\#}p < 0.001$. **(B)** H&E staining showed the necrosis of the tumor xenografts. **(C)** Ki-67 immunostaining showed the proliferation of tumor xenografts. **(D)** Quantitative analysis of Ki-67 immunostaining assay.

the two cell lines (**Figure 5C**). The above-mentioned data indicated that PI3K/Akt signaling pathway and ABCB1 played dominant roles in the drug resistance of MCF-7/DOX cells.

## C49 Combined With Doxorubicin Repressed the Expression of P-gp, Phosphorylated-Phosphoinositide-3-kinase, and Phosphorylated-Protein Kinase B (p-Akt) proteins

Western blot analysis was used to detect the changes of protein expression in MCF-7/DOX cells before and after drug intervention. The results showed that the expression of P-gp protein in MCF-7/DOX cells was markedly higher than that in MCF-7 cells (**Figure 6A**). Following drug intervention for 24 and 48 h, C49 (12.5 μM) combined with DOX (8 μM) could remarkably reduce the level of P-gp protein in MCF-7/DOX cells compared with the control group (**Figure 6B**). As shown in **Figure 6C**, the expression levels of p-PI3K and p-Akt proteins in the combinational treatment group were significantly reduced, but the expression levels of total-PI3K and total-Akt did not obviously changed. The expression of apoptins in the downstream of PI3K/Akt signaling pathway was explored, and the results showed that the expression of Caspase-3 and Caspase-9 in the combinational treatment group were remarkably up-regulated while the expression of Bcl-2 was markedly down-regulated (**Figure 6D**). Some reports have shown an increase in phosphorylated p53 was induced by treatment with chemotherapeutic reagents *in vitro* and in murine xenograft models (Ohara et al., 2018). In our present study, there is no change in the expression level of p53 among the different groups, but its phosphorylated expression have been changed after C49 treatment in MCF-7/DOX cells (**Figure 6D**). The corresponding semi-quantitative results are showed in **Figure 6E**. Therefore, C49 combined with DOX could reverse MDR by repressing the expression of P-gp protein and PI3K/Akt signaling pathway.

## The Role of C49 on Breast Cancer Xenograft Mice

A breast cancer xenograft model was constructed on nude mouse to further verify the effect of C49 on the reversal of MDR *in vivo*. Consistent with previous results, no difference was noted in animal weight and hepatorenal toxicity among treatment groups during the experiment (**Supplementary Figures S1, S2**). After C49 or C49 combined with DOX intervention, C49 low and high-dose groups did not exert the effect of inhibiting tumor growth, DOX treatment group had a better inhibiting effect on tumor growth, and low and high-dose groups of combinational treatment remarkably inhibited tumor growth in a dose-dependent way compared with the control group (**Figure 7A**). H&E staining was implemented to detect the pathological change of tumor tissues in these mice. As shown in **Figure 7B**, tumor cells disorganization was evident in the control group with disorder cell arrangement and pathological nuclear mitotic figures. Compared to cells in the control group, those in the combination treatment group were sparsely arranged. Apart from nuclear fragmentation and dissolution, small vacuoles could be observed in the cytoplasm of many tumor cells. Nuclear fission was remarkably reduced. The cell proliferation of tumor tissues was examined by IHC staining. The expression of Ki-67 in tumor tissues was the highest in the control group, and lowest in the combinational treatment group compared to the control group (**Figure 7C**). These results showed that C49 had no significant antitumor effect but could significantly reverse the DOX resistance in grafted tumor of drug-resistant breast cancer. C49 combined with DOX could remarkably enhance the cytotoxicity of DOX to repress tumor growth and could thus realize the antitumor effect.

# DISCUSSION

The main treatment for breast cancer is surgery, which can lengthen the overall survival of patients when combined with chemotherapy. DOX is a first-line chemotherapeutic drug for breast cancer, which can kill tumor cells but it causes MDR if used for a long period of time, resulting in chemotherapy failure. Konieczkowski et al. (Konieczkowski et al., 2018) found that the mechanism of DOX in inducing MDR involved multiple processes, e.g., reducing drug absorption, increasing drug excretion and changing drug metabolism, where high expression of P-gp protein was the primary cause of drug resistance of tumors (Gao et al., 2018; Lowrence et al., 2019). In DOX-resistant breast cancer cells, P-gp protein can pump DOX out of MCF-7/DOX cells, as a result, DOX fails to exert effective cytotoxic effect (Cao et al., 2019) and breast cancer cells can evade attack of chemotherapeutics (Genovese et al., 2017). Reversal of drug resistance can be realized by repressing P-gp protein. For example, cryptotanshinone and dihydrotanshinone of *Salvia miltiorrhiza* can repress expression of P-gp protein to reverse drug resistance (Lee et al., 2018). Myrsinol diterpene can inhibit the excretory function of P-gp protein to reverse drug resistance of breast cancer (Wang et al., 2016). In our study, C49 combined with DOX could lower the expression of P-gp protein, leading to intracellular DOX accumulation in drug-resistant cells, inhibit cell proliferation and promote cell apoptosis.

MDR is associated with abnormal activation of relevant signaling pathways in drug-resistant cells. PI3K/Akt plays a critical role in regulating cell proliferation, survival, metabolism, and apoptosis of normal cells (Aoki et al., 2017; Tewari et al., 2019). This signaling pathway is abnormally activated in various tumors, e.g., breast, lung, ovarian, and prostate cancers (Lu et al., 2016; Gu et al., 2018; Ediriweera et al., 2019; Verret et al., 2019; Madsen et al., 2020) and participates in mediating tumor MDR (Guerrero-Zotano et al., 2016; Yang et al., 2017; Li et al., 2019a; Liu et al., 2020). For example, PI3K/Akt signaling pathway is involved in paclitaxel resistance when it is abnormally activated in prostate cancer. Meanwhile, abnormally activated PI3K/Akt signaling pathway can contribute to the phosphorylated activation of serine sites of Bcl-2 protein and change its spatial conformation to discourage apoptins from exerting normal functions and inhibiting cell apoptosis.

Previous studies show that the expression of some protein molecules in PI3K/Akt signaling pathway is up-regulated in chemotherapeutic-resistant cells, and the drug-resistant phenotypes could be reversed by inhibiting those proteins. For example, resveratrol and matrine can reverse the MDR of breast cancer by repressing PI3K/Akt signaling pathway (Chen et al., 2018; Zhou et al., 2018). Likewise, PI3K/Akt can target the anti-apoptotic genes like Bcl-2 and Bcl-xL, resulting in the suppression of apoptosis machinery. A report confirmed that a natural chalcone, has been shown to exert growth inhibitory effects on the human Hepatocellular carcinoma cells serves as a transcription suppressor of anti-apoptotic genes like Bcl-2 and Bcl-xL (Ji et al., 2019). In yet another study, Xanthohumol caused arrest of the cancer cells at the G2/M phase of the cell cycle, which was also accompanied with suppression of Caspase-family (Liu et al., 2019). Our study showed that the expression of p-PI3K, p-Akt and Bcl-2 proteins reduced remarkably in MCF-7/DOX cells treated with C49 in combination with DOX, indicating that PI3K/Akt signaling pathway was involved. In contrast, those of p-p53, Caspase-9, Caspase-3, and Caspase-10 were elevated. Therefore, this signaling pathway can promote or inhibit downstream signaling molecules, such as Bcl-2, Caspase-9 and p-p53, to regulate cell apoptosis.

In the DOX-resistant breast cancer xenograft mouse model, different concentrations of C49 or C49 combined with DOX were used for the treatment of tumors. The results showed that C49 combined with DOX could remarkably repress tumor growth, inhibit tumor cell proliferation, and accelerate tumor cell apoptosis. suggesting that C49 can enhance the chemotherapeutic effect of DOX *in vivo*.

## CONCLUSION

C49 combined with DOX can remarkably inhibit the proliferation of MCF-7/DOX cells and promote cell apoptosis both *in vitro* and *in vivo*. C49 may degrade the ability of P-gp protein to pump DOX out of cells by repressing the expression of P-gp protein, increasing the intracellular concentration of DOX. The combination of C49 and DOX may also repress the expression of p-PI3K and p-Akt proteins and reverse the drug resistance of breast cancer. Therefore, C49 can be a potential therapeutic drug for reversing DOX resistance in the treatment of breast cancer and other cancers.

## DATA AVAILABILITY STATEMENT

The original contributions presented in the study are included in the article/**Supplementary Material**, further inquiries can be directed to the corresponding authors.

## ETHICS STATEMENT

The animal study was reviewed and approved by the Animal Ethics Committee of Traditional Chinese Medicine at Shanghai University.

## AUTHOR CONTRIBUTIONS

TW, XY, JL, HS, and WD conceived and designed the experiments. TW, XY, PZ, HW, LW participated in the specific experimental process. TW, XY, PZ, HW, and LW performed the research and analyzed the data. TW wrote the paper. TW, XY,,HS, and WD drafted the manuscript. TW, XY, and JL revised the manuscript. All authors approved and agreed to be responsible for all aspects of the work.

## FUNDING

This research were supported by the Putuo District Science and Technology Innovation Project of Shanghai Province in China (ptkwws201715) and the Hospital-level project in Putuo hospital (2020306A).

## SUPPLEMENTARY MATERIAL

The Supplementary Material for this article can be found online at: https://www.frontiersin.org/articles/10.3389/fphar.2021.653306/full#supplementary-material.

## REFERENCES

Al-Malky, H. S., Al Harthi, S. E., and Osman, A. M. M. (2020). Major obstacles to doxorubicin therapy: cardiotoxicity and drug resistance. *J. Oncol. Pharm. Pract.* 26 (2), 434–444. doi:10.1177/1078155219877931

Aoki, M., and Fujishita, T. (2017). Oncogenic roles of the PI3K/AKT/mTOR axis. *Curr. Top. Microbiol. Immunol.* 407, 153–189. doi:10.1007/82_2017_6

Badowska-Kozakiewicz, A. M., Sobol, M., and Patera, J. (2017). Expression of multidrug resistance protein P-glycoprotein in correlation with markers of hypoxia (HIF-1α, EPO, EPO-R) in invasive breast cancer with metastasis to lymph nodes. *Arch. Med. Sci.* 13 (6), 1303–1314. doi:10.5114/aoms.2016.62723

Bahri, M., Fleurence, J., Faraj, S., Ben Mostefa Daho, M., Fougeray, S., and Birklé, S. (2019). Potentiation of anticancer antibody efficacy by antineoplastic drugs: detection of antibody-drug synergism using the combination index equation. *J. Visualized Exp.* 143. doi:10.3791/58291

Cao, A., Ma, P., Yang, T., Lan, Y., Yu, S., Liu, L., et al. (2019). Multifunctionalized micelles facilitate intracellular doxorubicin delivery for reversing multidrug resistance of breast cancer. *Mol. Pharm.* 16 (6), 2502–2510. doi:10.1021/acs.molpharmaceut.9b00094

Cappetta, D., De Angelis, A., Sapio, L., Prezioso, L., Illiano, M., Quaini, F., et al. (2017). Oxidative stress and cellular response to doxorubicin: a common factor in the complex milieu of anthracycline cardiotoxicity. *Oxid. Med. Cell Longev.* 2017, 1–13. doi:10.1155/2017/1521020

Chang, Y. T., Wang, C. C. N., Wang, J. Y., Lee, T. E., Cheng, Y. Y., Morris-Natschke, S. L., et al. (2019). Tenulin and isotenulin inhibit P-glycoprotein function and overcome multidrug resistance in cancer cells. *Phytomedicine* 53, 252–262. doi:10.1016/j.phymed.2018.09.008

Chen, J. M., Bai, J. Y., and Yang, K. X. (2018). Effect of resveratrol on doxorubicin resistance in breast neoplasm cells by modulating PI3K/Akt signaling pathway. *IUBMB Life* 70 (6), 491–500. doi:10.1002/iub.1749

Cui, Q., Wang, J. Q., Assaraf, Y. G., Ren, L., Gupta, P., Wei, L., et al. (2018). Modulating ROS to overcome multidrug resistance in cancer. *Drug Resist. Updat.* 41, 1–25. doi:10.1016/j.drup.2018.11.001

Ding, S., Patel, N., and Zhang, H. (2018). Ciclosporin A as a reversal agent against concurrent multidrug resistance in tumors with nanobubbles. *J. Biomed. Nanotechnol.* 14 (1), 190–197. doi:10.1166/jbn.2018.2494

Dong, Y., Liao, H., Yu, J., Fu, H., Zhao, D., Gong, K., et al. (2019). Incorporation of drug efflux inhibitor and chemotherapeutic agent into an inorganic/organic platform for the effective treatment of multidrug resistant breast cancer. *J. Nanobiotechnol* 17 (1), 125. doi:10.1186/s12951-019-0559-y

Dyson, J., Foll, F. L., Magal, P., Noussair, A., and Pasquier, J. (2019). Direct and indirect P-glycoprotein transfers in MCF7 breast cancer cells. *J. Theor. Biol.* 461, 239–253. doi:10.1016/j.jtbi.2018.10.040

Ediriweera, M. K., Tennekoon, K. H., and Samarakoon, S. R. (2019). Role of the PI3K/AKT/mTOR signaling pathway in ovarian cancer: biological and therapeutic significance. *Semin. Cancer Biol.* 59, 147–160. doi:10.1016/j.semcancer.2019.05.012

El-Hamid, E. S. A., Gamal-Eldeen, A. M., and Sharaf Eldeen, A. M. (2019). Liposome-coated nano doxorubicin induces apoptosis on oral squamous cell carcinoma CAL-27 cells. *Arch. Oral Biol.* 103, 47–54. doi:10.1016/j.archoralbio.2019.05.011

Gao, Y., Shi, W., Cui, J., Liu, C., Bi, X., Li, Z., et al. (2018). Design, synthesis and biological evaluation of novel tetrahydroisoquinoline derivatives as P-glycoprotein-mediated multidrug resistance inhibitors. *Bioorg. Med. Chem.* 26 (9), 2420–2427. doi:10.1016/j.bmc.2018.03.045

Ge, C., Cao, B., Feng, D., Zhou, F., Zhang, J., Yang, N., et al. (2017). The down-regulation of SLC7A11 enhances ROS induced P-gp over-expression and drug resistance in MCF-7 breast cancer cells. *Sci. Rep.* 7 (1), 3791. doi:10.1038/s41598-017-03881-9

Genovese, I., Ilari, A., Assaraf, Y. G., Fazi, F., and Colotti, G. (2017). Not only P-glycoprotein: amplification of the ABCB1- containing chromosome region 7q21 confers multidrug resistance upon cancer cells by coordinated overexpression of an assortment of resistance-related proteins. *Drug Resist. Updates* 32, 23–46. doi:10.1016/j.drup.2017.10.003

Gomes, M., Muratov, E., Pereira, M., Peixoto, J., Rosseto, L., Cravo, P., et al. (2017). Chalcone derivatives: promising starting points for drug design. *Molecules* 22 (8), 1210. doi:10.3390/molecules22081210

Gu, J. J., Qiao, K. S., Sun, P., Chen, P., and Li, Q. (2018). Study of EGCG induced apoptosis in lung cancer cells by inhibiting PI3K/Akt signaling pathway. *Eur. Rev. Med. Pharmacol. Sci.* 22 (14), 4557–4563. doi:10.26355/eurrev_201807_15511

Guerrero-Zotano, A., Mayer, I. A., and Arteaga, C. L. (2016). PI3K/AKT/mTOR: role in breast cancer progression, drug resistance, and treatment. *Cancer Metastasis Rev.* 35 (4), 515–524. doi:10.1007/s10555-016-9637-x

Guo, W., Dong, W., Li, M., and Shen, Y. (2019). Mitochondria P-glycoprotein confers paclitaxel resistance on ovarian cancer cells. *OncoTargets Ther.* 12, 3881–3891. doi:10.2147/OTT.S193433

Gupta, V. K., Gaur, R., Sharma, A., Akther, J., Saini, M., Bhakuni, R. S., et al. (2019). A novel bi-functional chalcone inhibits multi-drug resistant *Staphylococcus aureus* and potentiates the activity of fluoroquinolones. *Bioorg. Chem.* 83, 214–225. doi:10.1016/j.bioorg.2018.10.024

Harbeck, N., and Gnant, M. (2017). Breast cancer. *Lancet* 389, 1134–1150. doi:10.1016/S0140-6736(16)31891-8

Hong, S. H., Cha, H. J., Hwang-Bo, H., Kim, M. Y., Kim, S. Y., Ji, S. Y., et al. (2019). Anti-proliferative and pro-apoptotic effects of licochalcone A through ROS-mediated cell cycle arrest and apoptosis in human bladder cancer cells. *Int. J. Mol. Sci.* 20 (15), 3820. doi:10.3390/ijms20153820

Ji, X., Wei, X., Qian, J., Mo, X., Kai, G., An, F., et al. (2019). 2′,4′-Dihydroxy-6′-methoxy-3′,5′-dimethylchalcone induced apoptosis and G1 cell cycle arrest through PI3K/AKT pathway in BEL-7402/5-FU cells. *Food Chem. Toxicol.* 131, 110533. doi:10.1016/j.fct.2019.05.041

Joshi, P., Vishwakarma, R. A., and Bharate, S. B. (2017). Natural alkaloids as P-gp inhibitors for multidrug resistance reversal in cancer. *Eur. J. Med. Chem.* 138, 273–292. doi:10.1016/j.ejmech.2017.06.047

Kartal-Yandim, M., Adan-Gokbulut, A., and Baran, Y. (2016). Molecular mechanisms of drug resistance and its reversal in cancer. *Crit. Rev. Biotechnol.* 36 (4), 716–726. doi:10.3109/07388551.2015.1015957

Khaki-Khatibi, F., Ghorbani, M., Sabzichi, M., Ramezani, F., and Mohammadian, J. (2019). Adjuvant therapy with stattic enriches the anti-proliferative effect of doxorubicin in human ZR-75-1 breast cancer cells via arresting cell cycle and inducing apoptosis. *Biomed. Pharmacother.* 109, 1240–1248. doi:10.1016/j.biopha.2018.10.183

Komoto, T., Bernardes, T., Mesquita, T., Bortolotto, L., Silva, G., Bitencourt, T., et al. (2018). Chalcones repressed the AURKA and MDR proteins involved in metastasis and multiple drug resistance in breast cancer cell lines. *Molecules* 23 (8), 2018. doi:10.3390/molecules23082018

Konieczkowski, D. J., Johannessen, C. M., and Garraway, L. A. (2018). A convergence-based framework for cancer drug resistance. *Cancer Cell* 33 (5), 801–815. doi:10.1016/j.ccell.2018.03.025

Lee, G., Joung, J.-Y., Cho, J.-H., Son, C.-G., and Lee, N. (2018). Overcoming P-Glycoprotein-Mediated multidrug resistance in colorectal cancer: potential reversal agents among herbal medicines. *Evid.-Based Complement. Altern. Med.* 2018, 1–9. doi:10.1155/2018/3412074

Li, K., and Lai, H. (2017). TanshinoneIIA enhances the chemosensitivity of breast cancer cells to doxorubicin through down-regulating the expression of MDR-related ABC transporters. *Biomed. Pharmacother.* 96, 371–377. doi:10.1016/j.biopha.2017.10.016

Li, W., Zhang, H., Assaraf, Y. G., Zhao, K., Xu, X., Xie, J., et al. (2016). Overcoming ABC transporter-mediated multidrug resistance: molecular mechanisms and novel therapeutic drug strategies. *Drug Resist. Updates* 27, 14–29. doi:10.1016/j.drup.2016.05.001

Li, Y., Lin, Z., Guo, M., Zhao, M., Xia, Y., Wang, C., et al. (2018). Inhibition of H1N1 influenza virus-induced apoptosis by functionalized selenium nanoparticles with amantadine through ROS-mediated AKT signaling pathways. *Int. J. Nanomed.* 13, 2005–2016. doi:10.2147/IJN.S155994

Li, K., Liu, W., Zhao, Q., Wu, C., Fan, C., Lai, H., et al. (2019a). Combination of tanshinone IIA and doxorubicin possesses synergism and attenuation effects on doxorubicin in the treatment of breast cancer. *Phytotherapy Res.* 33 (6), 1658–1669. doi:10.1002/ptr.6353

Li, Y., Zhai, Z., Li, H., Wang, X., Huang, Y., and Su, X. (2019b). Guajadial reverses multidrug resistance by inhibiting ABC transporter expression and suppressing the PI3K/Akt pathway in drug-resistant breast cancer cells. *Chemico-Biological Interactions* 305, 98–104. doi:10.1016/j.cbi.2019.03.032

Liang, M., Li, X., Ouyang, X., Xie, H., and Chen, D. (2018). Antioxidant mechanisms of echinatin and licochalcone A. *Molecules* 24 (1), 3. doi:10.3390/molecules24010003

Lin, Y., Zhang, M., Lu, Q., Xie, J., Wu, J., and Chen, C. (2019). A novel chalcone derivative exerts anti-inflammatory and anti-oxidant effects after acute lung injury. *Aging* 11 (18), 7805–7816. doi:10.18632/aging.102288

Liu, M., Yin, H., Qian, X., Dong, J., Qian, Z., and Miao, J. (2016). Xanthohumol, a prenylated chalcone from hops, inhibits the viability and stemness of doxorubicin-resistant MCF-7/ADR cells. *Molecules* 22 (1), 36. doi:10.3390/molecules22010036

Liu, R., Chen, Y., Liu, G., Li, C., Song, Y., Cao, Z., et al. (2020). PI3K/AKT pathway as a key link modulates the multidrug resistance of cancers. *Cell Death Dis* 11 (9), 797. doi:10.1038/s41419-020-02998-6

Liu, X., An, L. J., Li, Y., Wang, Y., Zhao, L., Lv, X., et al. (2019). Xanthohumol chalcone acts as a powerful inhibitor of carcinogenesis in drug-resistant human colon carcinoma and these effects are mediated via G2/M phase cell cycle arrest, activation of apoptotic pathways, caspase activation and targeting Ras/MEK/ERK pathway. *J. BUON.* 24 (6), 2442–2447.

Lowrence, R. C., Subramaniapillai, S. G., Ulaganathan, V., and Nagarajan, S. (2019). Tackling drug resistance with efflux pump inhibitors: from bacteria to cancerous cells. *Crit. Rev. Microbiol.* 45 (3), 334–353. doi:10.1080/1040841X.2019.1607248

Lu, Q., Liu, Z., Li, Z., Chen, J., Liao, Z., Wu, W. R., et al. (2016). TIPE2 overexpression suppresses the proliferation, migration, and invasion in prostate cancer cells by inhibiting PI3K/Akt signaling pathway. *Oncol. Res.* 24 (5), 305–313. doi:10.3727/096504016X14666990347437

Madsen, R. R. (2020). PI3K in stemness regulation: from development to cancer. *Biochem. Soc. Trans.* 48 (1), 301–315. doi:10.1042/BST20190778

Maria Pia, G. D., Sara, F., Mario, F., and Lorenza, S. (2019). Biological effects of licochalcones. *Mrmc* 19 (8), 647–656. doi:10.2174/1389557518666180601095420

Marinello, J., Delcuratolo, M., and Capranico, G. (2018). Anthracyclines as topoisomerase II poisons: from early studies to new perspectives. *Int. J. Mol. Sci.* 19 (11), 3480. doi:10.3390/ijms19113480

Mateeva, N., Eyunni, S. V. K., Redda, K. K., Ononuju, U., Hansberry, T. D., Aikens, C., et al. (2017). Functional evaluation of synthetic flavonoids and chalcones for potential antiviral and anticancer properties. *Bioorg. Med. Chem. Lett.* 27 (11), 2350–2356. doi:10.1016/j.bmcl.2017.04.034

Mehrotra, M., Anand, A., Singh, K. R., Kumar, S., Husain, N., and Sonkar, A. A. (2018). P-glycoprotein expression in Indian breast cancer patients with reference to molecular subtypes and response to anthracycline-based chemotherapy-a prospective clinical study from a developing country. *Indian J. Surg. Oncol.* 9 (4), 524–529. doi:10.1007/s13193-018-0797-8

Meredith, A.-M., and Dass, C. R. (2016). Increasing role of the cancer chemotherapeutic doxorubicin in cellular metabolism. *J. Pharm. Pharmacol.* 68 (6), 729–741. doi:10.1111/jphp.12539

Ohara, K., Ohkuri, T., Kumai, T., Nagato, T., Nozaki, Y., Ishibashi, K., et al. (2018). Targeting phosphorylated p53 to elicit tumor-reactive T helper responses against head and neck squamous cell carcinoma. *Oncoimmunology* 7 (9), e1466771. doi:10.1080/2162402X.2018.1466771

Pinto, P., Machado, C. M., Moreira, J., Almeida, J. D. P., Silva, P. M. A., Henriques, A. C., et al. (2019). Chalcone derivatives targeting mitosis: synthesis, evaluation of antitumor activity and lipophilicity. *Eur. J. Med. Chem.* 184, 111752. doi:10.1016/j.ejmech.2019.111752

Pokharel, D., Padula, M., Lu, J., Jaiswal, R., Djordjevic, S., and Bebawy, M. (2016). The role of CD44 and ERM proteins in expression and functionality of P-glycoprotein in breast cancer cells. *Molecules* 21 (3), 290. doi:10.3390/molecules21030290

Pondé, N. F., Zardavas, D., and Piccart, M. (2019). Progress in adjuvant systemic therapy for breast cancer. *Nat. Rev. Clin. Oncol.* 16, 27–44. doi:10.1038/S41571-018-0089-9

Ponnusamy, L., Mahalingaiah, P. K. S., Chang, Y.-W., and Singh, K. P. (2018). Reversal of epigenetic aberrations associated with the acquisition of doxorubicin resistance restores drug sensitivity in breast cancer cells. *Eur. J. Pharm. Sci.* 123, 56–69. doi:10.1016/j.ejps.2018.07.028

Schröder, L., Marahrens, P., Koch, J. G., Heidegger, H., Vilsmeier, T., Phan-Brehm, T., et al. (2019). Effects of green tea, matcha tea and their components epigallocatechin gallate and quercetin on MCF-7 and MDA-MB-231 breast carcinoma cells. *Oncol. Rep.* 41 (1), 387–396. doi:10.3892/or.2018.6789

Seliger, J. M., Misuri, L., Maser, E., and Hintzpeter, J. (2018). The hop-derived compounds xanthohumol, isoxanthohumol and 8-prenylnaringenin are tight-binding inhibitors of human aldo-keto reductases 1B1 and 1B10. *J. Enzyme Inhib. Med. Chem.* 33 (1), 607–614. doi:10.1080/14756366.2018.1437728

Siegel, R. L., Miller, K. D., and Jemal, A. (2020). *Cancer* statistics, 2020. *CA A. Cancer J. Clin.* 70, 7–30. doi:10.3322/caac.21590

Śliwka, L., Wiktorska, K., Suchocki, P., Milczarek, M., Mielczarek, S., Lubelska, K., et al. (2016). The comparison of MTT and CVS assays for the assessment of anticancer agent interactions. *Plos. One.* 11 (5), e0155772. doi:10.1371/journal.pone.0155772

Sui, H., Duan, P., Guo, P., Hao, L., Liu, X., Zhang, J., et al. (2017). Zhi Zhen Fang formula reverses Hedgehog pathway mediated multidrug resistance in colorectal cancer. *Oncol. Rep.* 38 (4), 2087–2095. doi:10.3892/or.2017.5917

Tewari, D., Patni, P., Bishayee, A., Sah, A. N., and Bishayee, A. (2019). Natural products targeting the PI3K-Akt-mTOR signaling pathway in cancer: a novel therapeutic strategy. *Semin. Cancer Biol.* S1044-579X (19), 30405–5. doi:10.1016/j.semcancer.2019.12.008

Tseng, C. H., Chen, Y. L., Hsu, C. Y., Chen, T. C., Cheng, C. M., Tso, H. C., et al. (2013). Synthesis and antiproliferative evaluation of 3-phenylquinolinylchalcone derivatives against non-small cell lung cancers and breast cancers. *Eur. J. Med. Chem.* 59, 274–282. doi:10.1016/j.ejmech.2012.11.027

Tun, J. O., Salvador-Reyes, L. A., Velarde, M. C., Saito, N., Suwanborirux, K., and Concepcion, G. P. (2019). Synergistic cytotoxicity of renieramycin M and doxorubicin in MCF-7 breast cancer cells. *Mar. Drugs* 17 (9), 536. doi:10.3390/md17090536

Verret, B., Cortes, J., Bachelot, T., Andre, F., and Arnedos, M. (2019). Efficacy of PI3K inhibitors in advanced breast cancer. *Ann. Oncol.* 30 (Suppl. l_10), x12–x20. doi:10.1093/annonc/mdz381

Waghray, D., and Zhang, Q. (2018). Inhibit or evade multidrug resistance P-glycoprotein in cancer treatment. *J. Med. Chem.* 61 (12), 5108–5121. doi:10.1021/acs.jmedchem.7b01457

Waks, A. G., and Winer, E. P. (2019). Breast cancer treatment: A review. *JAMA* 321 (3), 288-300. doi:10.1001/jama.2018.19323

Wang, D., and Song, Q. (2017). Effect of levofloxacononone chalcone derivatives on the apoptosis and autophagy of HCC SMMC-7721 cells. *Pak. J. Pharm. Sci.* 30 (5(Special)), 1829–1832.

Wang, H., Chen, X., Li, T., Xu, J., and Ma, Y. (2016). A myrsinol diterpene isolated from a traditional herbal medicine, LANGDU reverses multidrug resistance in breast cancer cells. *J. Ethnopharmacol.* 194, 1–5. doi:10.1016/j.jep.2016.08.041

Wang, J., Chen, B., Cheng, J., Cai, X., Xia, G., Liu, R., et al. (2011). Apoptotic mechanism of human leukemia K562/A02 cells induced by magnetic iron oxide nanoparticles co-loaded with daunorubicin and 5-bromotetrandrin. *Int. J. Nanomedicine* 6, 1027–1034. doi:10.2147/IJN.S18023

Wang, X., Wang, T., Yi, F., Duan, C., Wanwg, Q., He, N., et al. (2019). Ursolic acid inhibits tumor growth via epithelial-to-mesenchymal transition in colorectal cancer cells. *Biol. Pharm. Bull.* 42 (5), 685–691. doi:10.1248/bpb.b18-00613

Watanabe, Y., Nagai, Y., Honda, H., Okamoto, N., Yamamoto, S., Hamashima, T., et al. (2016). Isoliquiritigenin attenuates adipose tissue inflammation *in vitro* and adipose tissue fibrosis through inhibition of innate immune responses in mice. *Sci. Rep.* 6 (1), 23097. doi:10.1038/srep23097

Wenningmann, N., Knapp, M., Ande, A., Vaidya, T. R., and Ait-Oudhia, S. (2019). Insights into doxorubicin-induced cardiotoxicity: molecular mechanisms, preventive strategies, and early monitoring. *Mol. Pharmacol.* 96 (2), 219–232. doi:10.1124/mol.119.115725

Wu, C.-P., Lusvarghi, S., Hsiao, S.-H., Liu, T.-C., Li, Y.-Q., Huang, Y.-H., et al. (2020). Licochalcone A selectively resensitizes ABCG2-overexpressing multidrug-resistant cancer cells to chemotherapeutic drugs. *J. Nat. Prod.* 83 (5), 1461–1472. doi:10.1021/acs.jnatprod.9b01022

Xiong, G., Chen, Y., and Arriaga, E. A. (2005). Measuring the doxorubicin content of single nuclei by micellar electrokinetic capillary chromatography with laser-induced fluorescence detection. *Anal. Chem.* 77 (11), 3488–3493. doi:10.1021/ac0500378

Xiong, H., Ni, J., Jiang, Z., Tian, F., Zhou, J., and Yao, J. (2018). Intracellular self-disassemble polysaccharide nanoassembly for multi-factors tumor drug resistance modulation of doxorubicin. *Biomater. Sci.* 6 (9), 2527–2540. doi:10.1039/C8BM00570B

Xu, M., Wu, P., Shen, F., Ji, J., and Rakesh, K. P. (2019). Chalcone derivatives and their antibacterial activities: current development. *Bioorg. Chem.* 91, 103133. doi:10.1016/j.bioorg.2019.103133

Yang, X., Ding, Y., Xiao, M., Liu, X., Ruan, J., and Xue, P. (2017). Anti-tumor compound RY10-4 suppresses multidrug resistance in MCF-7/ADR cells by inhibiting PI3K/Akt/NF-κB signaling. *Chemico-Biological Interactions* 278, 22–31. doi:10.1016/j.cbi.2017.10.008

Yang, X., Xie, J., Liu, X., Li, Z., Fang, K., Zhang, L., et al. (2019). Autophagy induction by xanthoangelol exhibits anti-metastatic activities in hepatocellular carcinoma. *Cell. Biochem. Funct.* 37 (3), 128–138. doi:10.1002/cbf.3374

Zeinoddini, S., Nabiuni, M., and Jalali, H. (2019). The synergistic cytotoxic effects of doxorubicin and Viola odorata extract on human breast cancer cell line T47-D. *J. Cancer Res. Ther.* 15 (5), 1073–1079. doi:10.4103/jcrt.JCRT_990_17

Zheng, G., Zheng, M., Yang, B., Fu, H., and Li, Y. (2019). Improving breast cancer therapy using doxorubicin loaded solid lipid nanoparticles: synthesis of a novel arginine-glycine-aspartic tripeptide conjugated, pH sensitive lipid and evaluation of the nanomedicine *in vitro* and *in*

*vivo*. *Biomed. Pharmacother.* 116, 109006. doi:10.1016/j.biopha.2019.109006

Zhou, B.-G., Wei, C.-S., Zhang, S., Zhang, Z., and Gao, H.-m. (2018). Matrine reversed multidrug resistance of breast cancer MCF-7/ADR cells through PI3K/AKT signaling pathway. *J. Cel. Biochem.* 119 (5), 3885–3891. doi:10.1002/jcb.26502

Zhu, H., Tang, L., Zhang, C., Wei, B., Yang, P., He, D., et al. (2019). Synthesis of chalcone derivatives: inducing apoptosis of HepG2 cells via regulating reactive oxygen species and mitochondrial pathway. *Front. Pharmacol.* 10, 1341. doi:10.3389/fphar.2019.01341

**Conflict of Interest:** The authors declare that the research was conducted in the absence of any commercial or financial relationships that could be construed as a potential conflict of interest.

## GLOSSARY

**Akt** protein kinase B

**Bcl-2** B cell lymphoma/leukemia-2

**Bcl-xL** B cell lymphoma-extra large

**BSA** bovine serum albumin

**Caspase-10** cysteinyl aspartate-specific proteinase -10

**Caspase-3** cysteinyl aspartate-specific proteinase -3

**Caspase-9** cysteinyl aspartate-specific proteinase -9

**CI** combination index

**DAPI** 2-(4-Amidinophenyl)-6-indolecarbamidine dihydrochloride

**DMSO** dimethyl sulfoxide

**DOX** doxorubicin

**FACS** fluorescence activating cell sorter

**FBS** fetal bovine serum

**FCM** flow cytometry

**FITC** fluoresceine isothiocyanate

**GEO** gene expression omnibus

**H&E** hematoxylin and eosin

**IC** inhibitory concentration

**$IC_{20}$** twenty percent of maximal inhibitory concentration

**$IC_{50}$** half maximal inhibitory concentration

**IF** immunofluorescence

**IHC** immunohistochemistry

**KEGG** kyoto encyclopedia of genes and genomes

**MCF-7** michigan cancer foundation-7

**MDR** multidrug resistance

**MTT** 3-(4,5-Dimethylthiazol-2-yl)-2,5-diphenyltetrazolium bromide

**PBS** phosphate buffer saline

**P-gp** p-glycoprotein

**PI3K** phosphatidylinositol 3-kinase

**PVDF** polyvinylidene fluoride

**RIPA** radio immunoprecipitation assay

**RPMI1640** roswell park memorial institute 1640

**SDS-PAGE** sodium dodecyl sulfate-polyacrylamide gel electrophoresis

**TBST** tris-buffered saline and tween 20

**WB** western blot

frontiers in Pharmacology

REVIEW
published: 15 April 2021
doi: 10.3389/fphar.2021.645864

# E3 Ubiquitin Ligase in Anticancer Drugdsla Resistance: Recent Advances and Future Potential

*Yuanqi Liu*[1,2], *Chaojun Duan*[1,2,3*†] *and Chunfang Zhang*[1,2,4*†]

[1]Department of Thoracic Surgery, Xiangya Hospital, Central South University, Changsha, China, [2]Hunan Engineering Research Center for Pulmonary Nodules Precise Diagnosis & Treatment, Changsha, China, [3]Department of Oncology, Xiangya Hospital, Central South University, Changsha, China, [4]National Clinical Research Center for Geriatric Disorders, Changsha, China

Drug therapy is the primary treatment for patients with advanced cancer. The use of anticancer drugs will inevitably lead to drug resistance, which manifests as tumor recurrence. Overcoming chemoresistance may enable cancer patients to have better therapeutic effects. However, the mechanisms underlying drug resistance are poorly understood. E3 ubiquitin ligases (E3s) are a large class of proteins, and there are over 800 putative functional E3s. E3s play a crucial role in substrate recognition and catalyze the final step of ubiquitin transfer to specific substrate proteins. The diversity of the set of substrates contributes to the diverse functions of E3s, indicating that E3s could be desirable drug targets. The E3s MDM2, FBWX7, and SKP2 have been well studied and have shown a relationship with drug resistance. Strategies targeting E3s to combat drug resistance include interfering with their activators, degrading the E3s themselves and influencing the interaction between E3s and their substrates. Research on E3s has led to the discovery of possible therapeutic methods to overcome the challenging clinical situation imposed by drug resistance. In this article, we summarize the role of E3s in cancer drug resistance from the perspective of drug class.

**Keywords: E3 ubiquitin ligase, cancer, cancer treatment, drugresistance, drug**

OPEN ACCESS

***Edited by:***
*Dexin Kong,*
*Tianjin Medical University, China*

***Reviewed by:***
*Pranav Gupta,*
*Albert Einstein College of Medicine, United States*
*Xiuping Yu,*
*Louisiana State University Health Shreveport, United States*

****Correspondence:***
*Chaojun Duan*
*duancjxy@126.com*
*Chunfang Zhang*
*zcf6169@outlook.com*

*†These authors have contributed equally to this work*

***Specialty section:***
*This article was submitted to Pharmacology of Anti-Cancer Drugs, a section of the journal Frontiers in Pharmacology*

***Received:*** *24 December 2020*
***Accepted:*** *24 February 2021*
***Published:*** *15 April 2021*

***Citation:***
*Liu Y, Duan C and Zhang C (2021) E3 Ubiquitin Ligase in Anticancer Drugdsla Resistance: Recent Advances and Future Potential. Front. Pharmacol. 12:645864. doi: 10.3389/fphar.2021.645864*

## INTRODUCTION

Cancer is a multifactorial disease and is considered the most severe public health issue worldwide (Siegel et al., 2019). Drug therapy is the main treatment for patients with advanced cancer. The drugs currently used for tumor treatment include platinum drugs, antitumor antibiotics, alkylating agents, hormones, molecular targeting agents, and immunotherapy. The use of tumor drugs will inevitably lead to drug resistance, which manifests as tumor recurrence (Glickman and Sawyers, 2012; Vasan et al., 2019).

Several mechanisms have been found to underlie anticancer drug resistance, including the effects of cancer stem cells (CSCs), epithelial-mesenchymal transition (EMT), and DNA damage repair (DDR) (Gong et al., 2018). Identifying the key molecules in these processes can help us understand the occurrence of drug resistance, and these key molecules play an essential role in predicting and reversing resistance to anticancer drugs. However, the mechanisms have not yet been elucidated.

### Ubiquitination and E3 Ubiquitin Ligases

Protein ubiquitination-based modification can regulate various signal-mediated cell death responses and plays an essential role in the occurrence, development, and outcome of cancer (Nalepa et al.,

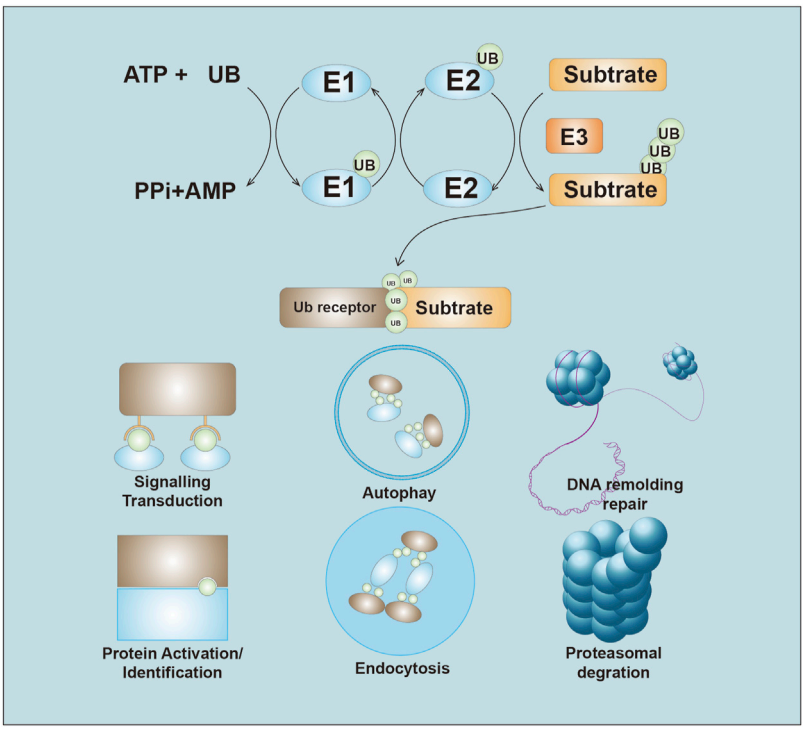


**FIGURE 1 |** Overview of the Ubiquitin system. Ubiquitin is initiate through the thioester bond with E1 in the ATP-depend manner. The activated ubiquitin then be transferred to the E2. E3 ligases recognize and transfer the ubiquitin to substrate. The ubiquitin chains lead to several ending, including proteasome-mediated degradation, ubiquitination signals transduction, autophagy, DNA remolding and repair, Protein identification, and endocytosis.

2006). Ubiquitination refers to the process by which ubiquitin is covalently bound to target proteins under the catalysis of a series of enzymes. The ubiquitination process usually requires the cooperation of the E1 ubiquitin-activating enzymes (E1s), E2 ubiquitin-coupling enzymes (E2s), and E3 ubiquitin ligases (E3s) (Buetow and Huang, 2016). Mechanistically, ubiquitin is activated in an ATP-dependent manner, inducing a thioester bond with an E1. The moieties are then transferred to the active site cysteine of the E2. The E3 binds to both the E2~Ub thioester and the substrate, catalyzing the transfer of ubiquitin from the active site cysteine of the E2 to the substrate lysine or N terminus (Tatham et al., 2013; Berndsen and Wolberger, 2014).

Ubiquitin chain topology determines the fate of ubiquitylated proteins (Ikeda and Dikic, 2008). Usually, ubiquitin-dependent proteolysis is associated with K48-linked and K11-linked ubiquitin chains. However, activation of signaling pathways is mainly dependent on K63-linked or M1-linked ubiquitin chains. Ubiquitin-mediated proteolysis is essential for the maintenance of protein homeostasis because it removes misfolded or unwanted proteins. The non-proteasomal ubiquitin-mediated assembly of signaling complexes also plays a pivotal role in several cellular processes, such as autophagy, DNA repair, and endocytosis (Bennett and Harper, 2008; Chen and Sun, 2009; Cappadocia and Lima, 2018). Given these phenomena, it is understandable that the dysregulation of ubiquitination can lead to genetic and epigenetic alterations in cancer.

E3s are critical components in the ubiquitination reaction owing to their strict control of both substrate affinity and specificity (Zheng and Shabek, 2017). E3s are a large class of proteins, and there are over 800 putative functional E3s (Ciechanover, 2015). E3s have been classified into three subgroups: E3s containing really interesting new gene (RING) and UFD2 homology (U-box) domains, the 28-member homologous to E6AP carboxyl terminus (HECT) E3 family, and the 14-member RING-between-RING (RBR) E3 family (Uchida and Kitagawa, 2016). The diversity of the E3 substrates contributes to the diverse functions of E3s (Li et al., 2014), and as a result, E3s are closely related to tumorigenesis because they regulate oncogenes and tumor suppressors (Senft et al., 2018). In addition, the substrate specificity of E3s suggests that they have promise as anticancer drug targets (Wang et al., 2017). Here, for the first time, we summarize the role of E3s in anticancer drug resistance from the perspective of drug class (**Figure 1**).

## Platinum Drugs

Platinum drugs are widely used in the treatment of human cancers. The zinc-finger E3s MUL1 and UBR5 was found to be involved in platinum resistance. The E3 UBR5 was amplified and overexpressed in ovarian cancer (OC). Higher UBR5 expression was observed in platinum-resistant OC tumor tissue than in normal tissues. Overexpression of UBR5 induced cisplatin resistance in OC cells both *in vivo* and

*in vitro*. Moreover, UBR5 knockdown via siRNA partly reversed platinum resistance in OC cells (O'Brien et al., 2008; Bradley et al., 2014). Mitochondrial E3 ubiquitin-protein ligase 1 (MUL1) is an E3 that interacts with and negatively regulates AKT. The degradation of AKT was found to lead to cisplatin sensitivity in OC cells (Lee et al., 2019). A decrease in EMT in cisplatin-resistant nasopharyngeal carcinoma (NPC) cells was observed after upregulation of NEDD4 in cells, suggesting that NEDD4 could be a novel therapeutic target for overcoming drug resistance in NPC (Feng et al., 2017).

Tripartite motif (TRIM) family proteins, most of which have E3 activities, control important cellular processes such as intracellular signaling, innate immunity, transcription, autophagy, and carcinogenesis (Hatakeyama, 2017). TRIM25 expression was identified to be significantly lower in the cisplatin-resistant non-small cell lung carcer (NSCLC) cell line A549 than in control cell lines (Qin et al., 2012). Overexpression of TRIM32 promoted degradation of Abi2, resulting in enhancement of cell growth, transforming activity, and cell motility. Moreover, TRIM32 suppressed the apoptosis induced by cisplatin in the hepatocellular carcinoma (HCC) cell line HEp2. Overexpression of TRIM32 in the HCC cell line also induced resistance to another platinum drug, oxaliplatin (Cui et al., 2016). Increased TRIM11 expression inhibits the apoptosis induced by cisplatin, and TRIM11 functions as an oncogene related to drug resistance both *in vivo* and *in vitro*. TRIM11 destabilized Daple in a p62-selective autophagic manner, further upregulating β-catenin expression to induce enhanced expression of ABCC9, which can transport chemotherapeutic drugs (Zhang et al., 2020). Autophagy can be a key mechanism of resistance to chemotherapy (Onorati et al., 2018). TRIM65 was found to be upregulated in NSCLC, and its overexpression promoted NSCLC cell resistance to cisplatin (Li et al., 2016). The inhibition of miR-138–5p attenuated the effects of TRIM65 knockdown on autophagy and cisplatin-induced apoptosis, suggesting that TRIM65 regulates cisplatin resistance in NSCLC by regulating miR-138–5p (Pan et al., 2019). TRIM59 was also found to be overexpressed in cisplatin-resistant A549 cells, and its overexpression in these cells resulted in increased cisplatin resistance. TRIM59 enhanced the ubiquitination of PTEN, a critical upstream regulator of HK2. The regulation of the PTEN/AKT/HK2 pathway induced by TRIM59 might provide insights into overcoming cancer resistance to cisplatin treatment (He and Liu, 2020).

Another type of RING-box-containing E3s, RING finger proteins (RNFs), play a role in platinum resistance. RNF38 was proposed as a biomarker of poor NSCLC prognosis, and its silencing increased the sensitivity of NSCLC cells to cisplatin (Wu et al., 2020). RNF138 was more highly expressed in cisplatin-resistant gastric cancer (GC) cell lines than in normal cell lines and modulated cisplatin resistance in these GC cells (Lu et al., 2018). Pellino family proteins (Pellino-1, 2, and 3) are E3s that contain C-terminal RING-like domains. Pellino-1 overexpression conferred NSCLC cells with resistance to the apoptosis induced by cisplatin or paclitaxel (Jeon et al., 2016).

The F-box-containing family member FBXW7 is one of the four subunits of the SKP1-cullin-F-box (SCF)-E3 complex, which functions in phosphorylation-dependent ubiquitination (Skaar et al., 2014). In NSCLC, FBXW7 upregulation significantly increased cisplatin chemosensitivity and abrogated the mesenchymal phenotype of NSCLC cell lines (Yu et al., 2013). Another report by Guodong X et al. indicated that FBXW7 could interact with Snai1 in NSCLC cell lines and directly degrade its expression, resulting in suppression of cisplatin and sorafenib resistance (Guodong et al., 2018). In colorectal carcinoma (CRC) cells, FBXW7 deficiency induced by mutation or loss can lead to the aberrant phosphorylation of p53 at serine 15 and further promote resistance to oxaliplatin. An understanding of the regulation of phospho-p53 (Ser15) by FBXW7 E3 activity could provide important clues for the clinical targetability of this axis (Perez-Losada et al., 2005; Li et al., 2015). In NPC, upregulation of FBXW7 significantly increased cisplatin-based chemosensitivity (Song et al., 2015). The CRL4 expression level was increased in cisplatin-resistant OC cells. CRL4 knockdown with shRNAs was able to reverse the cisplatin resistance of OC cells (Hu et al., 2019). In CRC, knockdown of CUL4A sensitized parental CRC cells to cisplatin (Englinger et al., 2017). CUL4B destabilized HP1α, a gene that suppresses the open confirmation of chromatin that is important for the DDR and DNA repair. The DDR and DNA repair are believed to be reasons for cisplatin resistance (Kim et al., 2017).

F-box-only proteins are the substrate-recognition component of the SCF-E3 complex. The relatively low level of FBXO22 in A549 cells contributes to an accumulation of CD147 and the cisplatin resistance of the cells (Wu et al., 2017). Additionally, FBXO21 was found to ubiquitinate and destabilized P-glycoprotein (P-gp), resulting in attenuation of multidrug resistance. However, a stem cell marker, CD44, was found to inhibit FBXO21-directed degradation of P-gp and promote multidrug resistance (Ravindranath et al., 2015). Using a microarray, another E3, FBXO32, was newly identified as a negative regulator of EMT in urothelial carcinoma (UC) tumors after they had acquired platinum resistance. FBXO32 dysregulation in platinum-resistant UC cells resulted in elevated expression of the EMT marker snail and decreased expression of E-cadherin (Tanaka et al., 2016).

SKP2, also known as F-box and leucine-rich repeat protein (FBXL1), is a member of the FBXL subfamily of F-box proteins and plays a pivotal role in cell cycle progression and proliferation. Evidence has shown that SKP2 can interact with Akt and facilitate its ubiquitination. K63-mediated AKT ubiquitination can be mediated by Skp2 and can regulate NPC to induce cisplatin resistance (Yu et al., 2019). Overexpression of SKP2 reduced the expression of p27Kip1, cyclin E, and p21Cip1, increased the proportion of S-phase cells, and increased resistance against cisplatin in NSCLC cell lines (Ishii et al., 2004).

E3s targeting P53 play a role in cisplatin resistance. MDM2, an important regulator of P53, controls cisplatin resistance in multiple cancers. MDM2 interacted and destabilized P53 and induced tumor cell resistance to cisplatin (Muscolini et al., 2011; Sheng et al., 2017). The genes encoding molecules that interfere with the interaction between MDM2 and p53 might also lead to drug resistance. Some genes, such as zinc-finger CCHC-type containing 10 (ZCCHC10) and NUMB, inhibit cisplatin

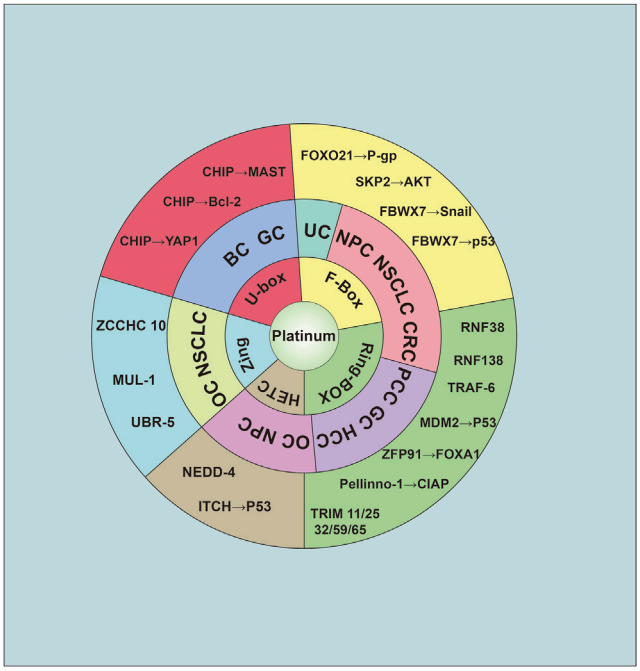


**FIGURE 2 |** The relationship of E3 ligase and platinum resistance. The E3 was cataloged as five group: U-box, F-box, Ring-Box, HETC, and Zing finger. Abbreviation was as follow: BC: Breast cancer; GC: Gastric cancer; UC, urothelial carcinoma; NPC, nasopharyngeal carcinoma; NSCLC, non-small cell lung cancer; CRC, colorectal carcinoma; PCC, pancreatic carcinoma; HCC, hepatocellular carcinoma; OC, ovarian cancer.

resistance by interfering with P53 ubiquitination mediated by MDM2 (Colaluca et al., 2008; Ning et al., 2019). TRAF6, an E3 that controls p53 mitochondrial translocation, was found to be overexpressed in CRC tissues. TRAF6 overexpression negatively correlates with apoptosis and predicts poor response to cisplatin-based chemotherapy and radiotherapy (Zhang et al., 2016). Cisplatin can enhance the FLIP-p53-Itch interaction, inducing FLIP ubiquitination and degradation in a p53-and Itch-dependent manner. These results suggest that the modulation of FLIP content may be an effective strategy for overcoming chemoresistance in OC (Abedini et al., 2008; Abedini et al., 2010).

The U-box domain-containing E3 CHIP has been studied to help understand drug sensitivity. CHIP knockdown increases the proportion of cisplatin-sensitive cells. CHIP can act as an activator of Bcl-2 expression levels to suppress breast cancer (BC) malignant progression (Tsuchiya et al., 2015). In addition to CHIP's role in BC, Dong-E Tang et al. revealed that CHIP could ubiquitinate YAP1 at the K280 site by K48-linked polyubiquitination and also generated a human GC cell line with resistance to cisplatin resistance (Tang et al., 2019). Microtubule-associated serine/threonine kinase 1 (MAST1) mediates cisplatin resistance in human cancers. Pan C et al. used a proteomics screen to identify CHIP-destabilized MAST1. The MAST1 destabilization resulted in hsp90B-induced sensitivity to cisplatin (Pan et al., 2019). ZFP91 knockdown reduced FOXA1 polyubiquitination, which decreased FOXA1 turnover and enhanced cellular sensitivity to cisplatin therapy (Tang et al., 2020). E3s and their corresponding substrates are summarized in **Figure 2**.

## Drugs Derived From Plants

Paclitaxel is an M-phase-specific plant drug initially derived from the Pacific yew and has become the first member of the taxane family to be used in cancer chemotherapy (Bernabeu et al., 2017). In a single-cell RNA sequencing analysis, protein ubiquitination was identified as the most differentially regulated pathway in docetaxel-resistant prostate cancer (PC) cells (Schnepp et al., 2020).

In NSCLC, BC and GC, silencing FBXW7 resulted in enhanced Taxol resistance (Yokobori et al., 2014; Gasca et al., 2016). However, in dormant BC cells, disruption of FBXW7 resulted in a shift of tumor cells from the quiescent state, rendering them susceptible to chemotherapy (Shimizu et al., 2019). miR-363 expression can promote chemoresistance by directly targeting FBXW7 (Zhang et al., 2016). Another Fox-containing E3, FBXW11, was also found to be involved in the development of Taxol resistance via associations with FOXO3a (Su et al., 2011). In PC, Skp2 silencing or using Skp2 inhibitors restored paclitaxel sensitivity in paclitaxel-resistant PC cells (Yang et al., 2016). EDD, an E3, promotes docetaxel resistance in hormone-refractory PC by regulating Wnt/β-Catenin signaling (Bian et al., 2020). In PC, SPOP knockout was found to confer resistance to cell death caused by docetaxel (Shi et al., 2019). Taxol decreased the expression of HDAC3 while increasing the expression of SIAH2 in melanoma cells. In addition, the E3 ligase SIAH2 can interact with HDAC3 and by so doing confers resistance to Taxol (Kim et al., 2015).

E3s targeting p53 also play roles in Taxol resistance. Pirh2, a RING finger-containing E3, can lead to polyubiquitination and proteasomal degradation of p53. The ectopic expression of Pirh2 enhanced cell proliferation, resistance to doxorubicin, and migration potential (Daks et al., 2016). The protease HAUSP is a critical component of the p53-Mdm2 pathway and acts as a specific deubiquitinase for p53 and Mdm2 and is thus essential for p53 regulation. HAUSP downregulation causes resistance to another plant-derived drug, camptothecin, and camptothecin-induced apoptosis (Becker et al., 2008). Parkin interferes with paclitaxel-induced microtubule assembly and stabilization by directly binding the microtubules on the outer cell surface. In addition, Parkin promotes the activity of paclitaxel to trigger multinucleation and apoptosis. Moreover, clinical data have revealed that the response of patients to preoperative paclitaxel therapy is correlated with Parkin expression (Wang et al., 2009).

## Antimetabolite Drugs

Fludarabine is a DNA synthesis inhibitor (Lukenbill and Kalaycio, 2013). *In vitro* and *in vivo* experiments showed that COP1 overexpression reduced HG3 cell sensitivity to fludarabine treatment by promoting ubiquitin-dependent p53 degradation (Fu et al., 2018). This result indicates that E3s promoting P53 degradation can also be related to fludarabine resistance.

5-Fluorouracil (5-FU) inhibits thymidylate synthase from activating thymine-induced cell death and functions mainly as

an S-phase antimetabolite (Longley et al., 2003). In BC, high preoperative expression of Skp2 was found to be associated with resistance to 5-FU therapy in 94% of patients (Davidovich et al., 2008). Cbl was decreased in 60% of human pancreatic ductal adenocarcinoma (PDAC) cases. Cbl knockdown increased PDAC resistance to gemcitabine and 5-FU (Kadera et al., 2015). TRIM47 is commonly overexpressed and related to poor prognosis in CRC patients. TRIM47 increases the ubiquitination and degradation of SMAD4. The overexpression of TRIM47 elevated CRC chemoresistance in response to 5-FU therapy (Liang et al., 2019). In CRC, high FBXW7 expression downregulated CRY2 through proteasomal degradation and increased CRC cell sensitivity to 5-FU (Fang et al., 2015). Cancer-associated fibroblasts (CAFs) play a pivotal role in creating the tumor microenvironment, which impacts adaptive resistance to chemotherapy (Kalluri, 2016). CRC cells cocultured with CAFs showed increased expression of RANBP2-type and C3HC4-type zinc-finger-containing 1 (RBCK1). Additionally, overexpression of RBCK1 was demonstrated in chemoresistant CRC tumors and CRC patients with poor prognosis. Exogenous expression of RBCK1 or RBCK1 inhibition was able to significantly influence 5-FU sensitivity in CRC cells (Liu et al., 2019).

Gemcitabine is another widely used S-phase antimetabolite drug (Mini et al., 2006). In pancreatic cancer (PCC) cells, FBW7 promoted gemcitabine sensitivity via upregulation of equilibrative nucleoside transporter 1 (ENT1) through lysosome inhibition (Hu et al., 2017). SMURF2 was downregulated in PCC tissues, and its expression was negatively associated with gemcitabine resistance. Upregulation of miR-15b was associated with degradation of SMURF2, and its expression was associated with EMT (Zhang et al., 2015). TRIM31 overexpression conferred gemcitabine resistance to PCC cells by promoting K63-linked polyubiquitination of tumor necrosis factor receptor-associated factor 2 (TRAF2) and sustained the activation of nuclear transcription factor kappa B (NF-κB) in PCC cells (Yu et al., 2018). Cul4A degraded TGFβ1, and its overexpression promoted resistance to gemcitabine in lung cancer. *In vivo* experiments, Cul4A-RNAi combined with gemcitabine chemotherapy inhibited lung cancer tumor growth, suggesting that this combination may provide a new approach for lung cancer treatment (Hung et al., 2015).

Asparaginase is a drug that selectively inhibits tumor cells by hydrolyzing asparagine (Asselin and Rizzari, 2015). FBXW7 overexpression can rescue Wnt-induced sensitization to asparaginase in FBXW7 mutant or wild-type leukaemias. In contrast, the FBXW7 R465C mutant, which has impaired binding to its canonical phosphodegron, abrogated this effect (Hinze et al., 2019).

## Alkylating Agents

Among various antitumour drugs, alkylating agents may be the most widely used category (Bhatt et al., 2017). Alkylating agents are cytotoxic drugs that combine with cell proteins and nucleic acids to kill tumor cells and have a direct toxic effect on cells (Lajous et al., 2019). Temozolomide (TMZ) is a DNA alkylating agent that can penetrate the blood-brain barrier. HERC3, an E3, promotes the ubiquitination-mediated degradation of SMAD7 and consequently activates the TGF-β pathway. Moreover, ectopic HERC3 expression was correlated with TMZ resistance in glioblastoma (GBM) cells (Li et al., 2019). Nucleolin (NCL) is overexpressed in GBM, and its overexpression was found to be positively relative to response to TMZ in GBM cells. The loss of MDM2-mediated NCL ubiquitination resulted in the inhibition of HDAC activity and sensitized GBM cells to TMZ (Ko et al., 2018).

## Anticancer Antibiotics

Doxorubicin is a cytotoxic anthracycline antibiotic that is often used as a tumor chemotherapy agent. Using mass spectrometry analysis, Kamran M et al. found that AURKA restricted FBXL7-induced survivin ubiquitination and degradation in GC, resulting in the promotion of doxorubicin resistance (Kamran et al., 2017). Doxorubicin-resistant HCC cells showed decreased expression of FBXW7. HSF1 was found to play an essential role in transcriptional activation of MDR1 via FBXW7-mediated degradation (Mun et al., 2020). Expression of P-gp on cancer cell surfaces is a critical determinant of anticancer drug resistance (Lin and Yamazaki, 2003). In other words, the reversal of drug resistance can be achieved by modulating the ubiquitination of P-gp (Zhang et al., 2004). Via mass spectrometry analyses, FBXO15/Fbx15 was found to interact with P-gp (Katayama et al., 2013). The downregulation of P-gp expression by UBE2R1-and FBXO15-mediated ubiquitination boosted sensitivity to vincristine and doxorubicin (Katayama et al., 2016).

Zeb1, an influential EMT-related transcription factor, mediated cell resistance to doxorubicin treatment. In HCC doxorubicin-resistant cells, the downregulation of SIAH1 mediated the stability of Zeb1, aiding resensitization of cells to doxorubicin treatment (Long et al., 2019). RNF8 activated K63 ubiquitination of Twist, which induced its translocation to the nucleus for subsequent EMT and CSC functions, thereby conferring doxorubicin resistance (Lee et al., 2016). SMO stabilizes and activates TRAF6, suggesting that the SMO/TRAF6 axis can contribute to doxorubicin resistance in lymphoma (Qu et al., 2018).

Dysregulated cholesterol metabolism in cancer cells may lead to drug resistance. Lower expression of the E3 Trc8 produced a decreased ubiquitination rate of 3-hydroxy-3-methylglutaryl-coenzyme A reductase (HMGCoAR), increased cholesterol synthesis, and increased cholesterol content in multidrug-resistant cells (Gelsomino et al., 2013). Overexpression of the E3 ubiquitin-protein ligase ZNRF2 improved cell survival in the presence of doxorubicin (Xiao et al., 2017). TRIM25 regulated p53 expression in NSCLC tissues and cell lines. Using TRIM25 RNAi increased the doxorubicin sensitivity of lung cancer cell lines (Qin et al., 2016). CUL2 knockdown enhanced cell sensitivity to doxorubicin treatment by regulating MAF1-mediated actin stress fiber integrity and apoptosis (Wang et al., 2019). MDM2, an E3 targeting p53 for degradation, can influence PC and BC cell sensitivity to doxorubicin (Lang et al., 2017; Cheteh et al., 2020). FKBP12 attenuated the cell toxicity of doxorubicin by binding to and degrading MDM2, disrupting the MDM2/MDM4 interaction, and inducing MDM2 self-ubiquitination (Liu et al., 2017). Cbl-b was found to be poorly

expressed in multidrug-resistant GC and GC cells. In addition, Cbl was also found to induce cell resistance to adriamycin (Xu et al., 2017; X CHe et al., 2017; Zhang et al., 2015).

## Endocrine Drugs

Endocrine therapy is an optional treatment for patients with hormone sensitivity, especially in PC and BC (Heinlein and Chang, 2004; Waks and Winer, 2019). Androgenic drugs such as abiraterone and enzalutamide can control the progression of PC.

Persistent androgen receptor (AR) activation leads to the loss of efficacy of anti-AR drugs in advanced PC. Reversal of this aberrant activation could be an ideal method for overcoming drug resistance. STUB1 disassociates AR/AR-V7 from HSP70, leading to AR/AR-V7 ubiquitination and degradation, which confers enzalutamide and abiraterone resistance (Liu et al., 2018). Inhibition of protein degradation by blocking Cullin-RING E3 complexes can interfere with the AR–ERG interaction, which is related to survival in PC (Rulina et al., 2016). AMFR can mediate the loss of 11b-hydroxysteroid dehydrogenase-2 (11b-HSD2), which inactivates cortisol, sustaining tumor cortisol concentrations to stimulate enzalutamide resistance. Reinstatement of 11b-HSD2 expression, or AMFR loss, reverses enzalutamide resistance in mouse xenograft tumors (Li et al., 2017).

Tamoxifen, a blocker of estrogen in breast cells, remains a cornerstone in the treatment of BC patients with estrogen receptor-positive tumors (Jordan, 2003). The RING finger protein TRIM2 is highly expressed in tamoxifen-resistant MCF-7 cells. TRIM2 was overexpressed in tamoxifen-resistant BC cells, which led to a reduction in Bim (Yin et al., 2017). The E3 HRD1 was downregulated in tamoxifen-resistant BC cells, and its knockdown significantly increased the survival of MCF7 cells treated with tamoxifen (Wang et al., 2017). The E3 RBCK1 regulated FKBPL stability at the posttranslational level via ubiquitination, and its downregulation increased sensitivity to tamoxifen treatment (Donley et al., 2014). The FBXW2-mediated downregulation of Sox2, a transcription factor conferring drug resistance, suppressed stem cell properties and overcame BC cell resistance to tamoxifen (Yin et al., 2019). The ubiquitin ligase c-Cbl was upregulated during tamoxifen-induced apoptosis of MCF-7 cells. Overexpression of c-Cbl significantly downregulated c-Src protein levels and tamoxifen-induced AKT activity (Yan et al., 2011). In addition, SIAH2 expression is significantly correlated with ER positivity in BC. SIAH2 sensitizes cells to tamoxifen through regulation of ER-a expression (Interiano et al., 2014).

## Targeted Drugs

The fusion of BCR (located on chromosome 22q11.2) and ABL1 (located on chromosome 9q34) leads to chronic myeloid leukemia (CML) (Baccarani et al., 2019). Imatinib is a tyrosine kinase inhibitor that can selectively inhibit BCR/ABL kinase activity and function as an effective therapy for CML. Smith PG et al. found that TGFβ played a key role in imatinib resistance by directly affecting c-Cbl-dependent Lyn ubiquitination and turnover, which resulted in bursts of Lyn kinase activity (Smith et al., 2012). TRAF6, an E3, facilitates the K63 ubiquitination of ULK1, resulting in reversal of imatinib resistance in CML cells (Han et al., 2019). LZTR1 acts as the regulator of RAS ubiquitination and MAPK pathway activation. Johannels W et al. reported that loss of LZTR1 expression could induce resistance to imatinib and rebastinib in CML cell lines (Bigenzahn et al., 2018).

Bortezomib is an effective proteasome inhibitor for cancer treatment that reversibly and selectively inhibits the 20S proteasome (Scott et al., 2016). Using an RNA microarray, researchers found that genes related to ubiquitination were differentially regulated in a bortezomib-resistant cell line (Park et al., 2014). NEDD4-1 ubiquitinates Akt and targets pAkt-Ser473 for proteasomal degradation. Low NEDD4-1 expression has been linked to poor prognosis in patients with multiple myeloma (MM), and NEDD4-1 knockdown results in bortezomib resistance *in vitro* and *in vivo* (Huang et al., 2020). Additionally, BAP1 depletion resulted in decreased gallbladder carcinoma (GBC) sensitivity to bortezomib (Hirosawa et al., 2018). Shen Y et al. demonstrated that silencing DTX3L improved the sensitivity to bortezomib in MM cell lines and increased the expression of apoptosis biomarkers (Shen et al., 2017). Malek E et al. observed increased CUL1 and SKP2 mRNA levels in patient CD138 + cells. Skp2 binds to Cullin-1 and Commd1 and synergistically enhances bortezomib-induced apoptosis (Malek et al., 2017).

Targeting HER2 with an inhibitor can be a treatment strategy for HER-2-positive BC or GC. c-Cbl and CHIP can interact and ubiquitinate HER2, which can be an effective strategy for combatting lapatinib resistance in HER2-positive cancer (Nunes et al., 2016; Huang et al., 2020). In addition, Skp2 silencing sensitized Her2-overexpressing tumors to trastuzumab treatment (Chan et al., 2012). MDM2 inhibition overcame lapatinib resistance in cells with either wild-type or mutant p53 and xenograft models, suggesting the potential of therapy directed against MDM2 for overcoming lapatinib resistance (Kurokawa et al., 2013). In GC, miR-223, which can regulate FBXW7, decreased GC cell sensitivity to trastuzumab (Eto et al., 2015). Jagged-1-mediated activation of Notch-1 can lead to trastuzumab resistance. The E3 Mindbomb-1 was required for Jagged-1 ubiquitination and subsequent Notch activation, which led to resistance to trastuzumab (Pandya et al., 2016).

Targeting aberrant EGFR expression in cancer cells is a promising treatment strategy for NSCLC. Activation of the Hippo-YAP pathway was correlated with EGFR inhibitor treatment (Kim and Myung, 2018). Wang H et al. identified tankyrase and its associated E3 RNF146 as positive YAP activity regulators by CRISPR screening. Tankyrase inhibition by RNF146 enhanced the growth inhibitory activity of EGFR inhibitors in NSCLC by inhibiting YAP signaling (Wang et al., 2016). FBXW7 regulated quiescence by targeting the c-MYC protein for ubiquitination. High levels of FBXW7 and low levels of c-MYC were observed in gefitinib-resistant cells with EGFR exon 19 deletion, suggesting that FBXW7 plays a pivotal role in the maintenance of gefitinib resistance in EGFR mutation-positive NSCLC (Hidayat et al., 2019). Cetuximab is a

**TABLE 1 |** Representative E3 ligase involved in non-platinum anti-cancer drug resistance.

| Classification | Drug | Cancer | E3 ligase | Mechanism | Role | Ref |
|---|---|---|---|---|---|---|
| Plants | Taxol | NSCLC | FBXW7 | FBXW7/MCL1/PLK1 | Sensitive | Gasca et al. (2016) |
| | | GC | FBXW7 | MiR-363/FBXW7 | Sensitive | Su et al. (2011) |
| | | BC/OC/NPC | FBXW11 | FBXW11/E1A/FOXO3 | Resistance | Yang et al. (2016) |
| | | NSCLC | Pirh2 | Pirh2/p53 | Resistance | Bian et al. (2020) |
| | | BC | Parkin | Microtubule assembly/stabilization | Sensitive | Kim et al. (2015) |
| | | Melanoma | SIAH2 | miR-335/SIAH2/HDAC3 | Resistance | Lukenbill and Kalaycio (2013) |
| | Docetaxel | PC | EDD | Wnt/β-Catenin | Resistance | Becker et al. (2008) |
| | | | SPOP | SPOP/Caprin | Sensitive | Wang et al. (2009) |
| | Camptothecin | CRC | HAUSP | p53/Mdm2 | Sensitive | Shi et al. (2019) |
| Anti-metabolite | Fludarabine | HCC | COP1 | COP1/p53-brn-3a/Bcl-2 | Sensitive | Longley et al. (2003) |
| | 5-Fluorouracil | BC | Skp2 | Skp2/$p27^{Kip1}$ | Resistance | Kadera et al. (2015) |
| | | PDACs | CBL | CBL/EGFR | Sensitive | Liang et al. (2019) |
| | | CRC | TRIM47 | TRIM47/SMAD4 | Resistance | Fang et al. (2015) |
| | | | FBXW7 | FBXW7/CRY2 | Sensitive | Kalluri, (2016) |
| | | | RBCK1 | Microenvironment/CAF | Resistance | Mini et al. (2006) |
| | Gemcitabine | PCC | FBXW7 | FBW7/ENT1 | Sensitive | Zhang et al. (2015) |
| | | | SMURF2 | miR-15b/SMURF2/EMT | Sensitive | Yu et al. (2018) |
| | | | TRIM31 | TRIM31/TRAF2/NF-κB | Sensitive | Hung et al. (2015) |
| | | NSCLC | Cul4A | Cul4A/TGFβ1 | Resistance | Asselin and Rizzari (2015) |
| | Asparaginase | Leukemias | FBXW7 | Wnt pathway | Sensitive | Bhatt et al. (2017) |
| Alkylating | Temozolomide | GBM | HERC3 | HERC3/SMAD7/TGFβ1 | Resistance | Ko et al. (2018) |
| | | GBM | MDM2 | MDM2/NCL/HDAC | Resistance | Kamran et al. (2017) |
| Antibiotics | Doxorubicin | GC | FBXL7 | AURKA/FBXL7/Survivin | Sensitive | Kamran et al. (2017) |
| | | CRC | FBXO15 | FBXO15/P-gp/mdr | Sensitive | Long et al. (2019) |
| | | HCC | CUL2 | CUL2/MAF-1 | Resistance | Cheteh et al. (2020) |
| | | HCC | FBXW7 | FBXW7/HSF1/MDR1 | Sensitive | Lin and Yamazaki, (2003) |
| | | HCC | SIAH1 | SIAH1/Zeb1/EMT | Resistance | Lee et al. (2016) |
| | | Lymphoma | TRAF6 | SMO/TRAF6 | Resistance | Gelsomino et al. 2013) |
| | | Colon cancer | Trc8 | Trc8/HMGCoAR/MDR | Resistance | Xiao et al. (2017) |
| | | Osteosarcoma | ZNRF2 | miR-100/ZNRF2 | Resistance | Qin et al. (2016) |
| | | NSCLC | TRIM25 | TRIM25/p53 | Resistance | Wang et al. (2019) |
| | | PC/BC | MDM2 | FKBP12/MDM2/p53 | Resistance | Xu et al. (2017) |
| | Adriamycin | BC/GC | Cbl-b | Cbl-b/EGFR/Akt-miR-200c-ZEB1 axis | Resistance | X CH et al. (2017); Zhang et al. (2015); Waks and Winer (2019) |
| Endocrine | Enzalutamide/ | PC | STUB1 | STUB1/ar/ar-v7/HSP70 | Resistance | Rulina et al. (2016) |
| | abiraterone | PC | Cullin-RING | AR–ERG/Wnt/β-catenin pathway/ NF-κB pathway | Resistance | Li et al. (2017) |
| | Enzalutamide | PC | AMFR | 11b-HSD2/cortisol | Resistance | Jordan (2003) |
| | Tamoxifen | BC | TRIM2 | Bim/cleaved PARP/caspase 3 | Resistance | Wang et al. (2017) |
| | | | HRD1 | S100A8/HRD1 | Sensitive | Donley et al. (2014) |
| | | | RBCK1 | RBCK1/FKBPL/ERa | Resistance | Yin et al. (2019) |
| | | | FBXW2 | FBXW2/Sox2 | Sensitive | Yan et al. (2011) |
| | | | c-Cbl | c-Cbl/c-src/AKT | Resistance | Interiano et al. (2014) |
| | | | SIAH2 | SIAH2/ER-a | Sensitive | Baccarani et al. (2019) |
| Targeted drugs | Imatinib | CML | c-Cbl | TGFβ/c-cbl/Lyn kinase activity | Resistance | Han et al. (2019) |
| | | | TRAF6 | TRAF6/ULK1 | Sensitive | Bigenzahn et al. (2018) |
| | Imatinib/rebastinib | CML | LZTR1 | LZTR1/RAS/MAPK pathway | Sensitive | Scott et al. (2016) |
| | Bortezomib | MM | NEDD4-1 | NEDD4-1/AKT | Sensitive | Hirosawa et al. (2018); Hirosawa et al. (2018) |
| | | | DTX3L | Cleaved PARP/caspase 3 | Resistance | Malek et al. (2017) |
| | | | Skp2 | Cullin-1/Commd1/caspase 3 | Resistance | Huang et al. (2020) |
| | Lapatinib | BC/GC | c-Cbl/CHIP | HER2 degration | Sensitive | Nunes et al. (2016); Chan et al. (2012) |
| | Trastuzumab | BC | Skp2 | AKT/Glut1/glucose uptake/ glycolysis | Resistance | Kurokawa et al. (2013) |
| | | GC | FBXW7 | miR-223/FBXW7 | Resistance | Pandya et al. (2016) |
| | | BC | Mindbomb-1 | Mindbomb-1/Jagged-1/Notch activation | Resistance | Kim and Myung (2018) |
| | Lapatinib | BC | MDM2 | P53 | Resistance | Eto et al. (2015) |
| | Erlotinib | NSCLC | RNF146 | RNF146/Hippo-YAP pathway | Resistance | Hidayat et al. (2019) |
| | Gefitinib | NSCLC | FBXW7 | FBXW7/c-MYC | Resistance | Yu et al. (2016) |
| | Cetuximab | GC | Cbl-b | Cbl-b/EGFR | Resistance | Tong et al. (2017) |
| | Sorafenib | HCC | FBXW8 | Nanog/CSCs | Resistance | Dai et al. (2017) |
| | JQ1/I-BET | PC | Cullin-3SPOP | Cullin-3SPOP/BET | Resistance | Janouskova et al. (2017); Kuske et al. (2018) |
| | BRAFi/MEKi | Melanoma | RNF44 | AMPK-α1/autophagy/metabolic | Resistance | Marzio et al. (2019) |
| | PARP inhibitors | BC | FBXO5 | SCF complex/RAD51 | Sensitive | Zhao et al. (2020) |

monoclonal antibody with a molecular target of EGFR. Specific silencing of Cbl-b expression increased the expression of EGFR and decreased the sensitivity of GC cells to cetuximab (Yu et al., 2016).

Regorafenib and sorafenib are multikinase inhibitors of RAS/RAF/MEK/ERK signaling that function to prevent tumors. CRC cells containing FBW7-inactivating mutations, including missense mutations in three arginine residues (R465, R479, and R505), were found to be insensitive to regorafenib and sorafenib (Tong et al., 2017). Nanog is a master transcriptional regulator of stemness in CSCs. The E3 FBXW8 ubiquitinates Nanog and suppresses Nanog expression, resulting in stemness enhancement and sorafenib resistance (Cao et al., 2019).

JQ1 and I-BET, two selective inhibitors of the bromodomain and extraterminal (BET) family, have shown promising early clinical trial outcomes. Xiangpeng Dai et al. found that cullin-3SPOP was responsible for promoting BET protein degradation. PC cell lines derived from individuals harboring SPOP mutations had increased resistance to BET inhibitor-induced cell growth arrest and apoptosis (Dai et al., 2017). Moreover, specific SPOP mutations could impair BET degradation (Janouskova et al., 2017).

BRAF inhibitors (BRAFi) and MEK inhibitors (MEKi) provide rapid disease control in patients with BRAF-mutant metastatic melanoma (Kuske et al., 2018). BRAFi/MEKi resistance triggers proteasomal degradation of AMPK-α1 and consequently drives autophagy and metabolic reprogramming in melanoma cells. Li YY et al. discovered that RING finger 44 (RNF44) could earmark AMPK-α1 for ubiquitination-mediated degradation in BRAFi-resistant melanoma cells (Li et al., 2017). PARP inhibitors (PARPi) are used clinically to treat BRCA-mutated breast tumors. FBXO5 assembles the active SCF ubiquitin ligase complex constitutively targeting RAD51 for degradation. This mechanism controls BC biology and sensitivity to PARPi (Marzio et al., 2019). The E3s involved in the response to non-platinum anticancer drugs are listed in **Table 1**.

# DISCUSSION

## "Druggability" of E3s

The purpose of studying the mechanisms of resistance is to identify strategies to combat resistance. E3s control tumor drug resistance by specifically binding to drug resistance-related genes and controlling their expression. Therefore, targeting E3 ligases can serve as a potential and effective strategy for combatting drug resistance. In the current environment, studying the resistance mechanisms of all existing E3s is challenging and impractical. However, some E3s have shown their ability to combat resistance. Several kinds of E3s have been deemed "druggable". First, E3s that target key pathway molecules, like Cbl, which targets EGFR, and NEDD4, which targets AKT, have potential (Zhao et al., 2020). Second, E3s targeting important oncogenes have also been proposed to be druggable. E3s like MDM2, which targets p53, FBXW2, which targets Sox2, and FBXW7, which targets MYC, have shown value in combating drug resistance.

## Targeting E3s to Combat Drug Resistance

Ongoing research mainly focuses on potential drugs that can be used in therapeutic applications targeting E3s. Such drugs must directly target the E3s to exert their effect; this requirement fits with several different tools, such as siRNAs, agonists, small molecule compounds that affect the binding of E3s to target proteins, and PROteolysis TArgeting Chimera (PROTAC) technology. Strategies targeting E3s include using small molecules or PROTACs that degrade E3s or interfere with the interaction between E3s and their substrates.

## Small Molecules Targeting E3s

Small molecules can target different E3s by directly binding with them and inhibiting their enzymatic activity. As mentioned above, MDM2 is a selective E3 that binds to P53. Agents that inhibit MDM2 include Nutlin-3a, RG7112, NVP-CGM097, AMG-232 and MI319. The combination of traditional anticancer drugs with novel agents was better for drug efficacy than monotherapy (Azmi et al., 1990; Kojima et al., 2006; Vu et al., 2013; Reuther et al., 2018) (**Figure 3**). These data suggest that targeting relevant E3s with small molecules to overcome drug resistance could be effective. Agonists have also been shown to be effective in controlling drug resistance. The PPAR$\gamma$ agonist pioglitazone inhibited EGFR/MDM2 signaling-mediated PPAR$\gamma$ degradation and increased cancer cell sensitivity to chemotherapy drugs (Shi et al., 2016).

## Interfering With the Interaction Between E3s and Their Substrates

Another strategy for combating drug resistance is interfering with the interaction between E3s and their target substrates. Using chemical library screens, E Malek et al. identified a novel compound, DT204, that reduced Skp2 binding to Cullin-1 and Commd1 and synergistically enhanced bortezomib-induced apoptosis (Malek et al., 2017). Small molecules have also been used to interfere with the interaction between EGFR and its E3. The downregulation of EGFR ubiquitination inhibits the internalization of EGFR, which is an essential mechanism of EGFR activation and drug resistance (Yu et al., 2020).

## Traditional Drugs Targeting E3s

Traditional drugs also facilitate the ubiquitination of E3s. Vitamin K3, an inhibitor of Siah2, promoted sensitivity of leukemia cells to imatinib (Huang et al., 2018). ATA is a molecular compound derived from Tanshinone IIA through chemical modification (Tian et al., 2010). A mechanistic study revealed that ATA promoted HER2 degradation by increasing c-Cbl and CHIP-mediated HER2 ubiquitination (Huang et al., 2020). Oridonin is a natural compound inducing oxidative stress that enhances CHIP targeting of BCR-ABL for ubiquitin-proteasome degradation, resulting in the enhancement of cancer cell death (Huang et al., 2017). Ginsenoside RD is another natural compound that increases the ubiquitination of multidrug resistance 1 (MDR1). Ginsenoside Rd treatment can reverse doxorubicin resistance in MCF-7/ADR cells (Pokharel et al., 2010).

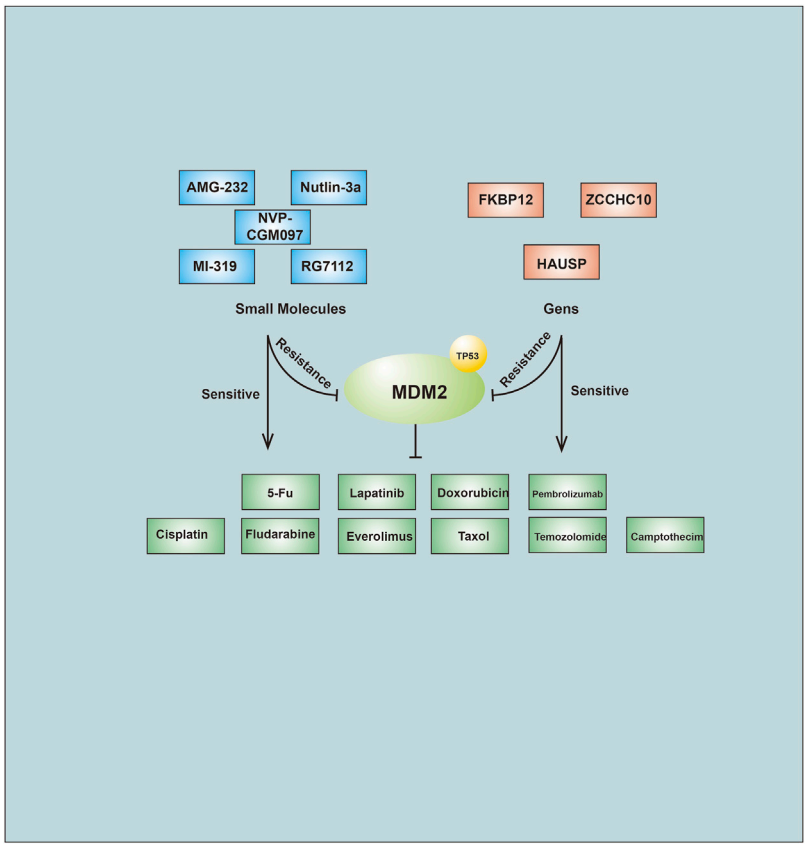


**FIGURE 3 |** Small molecules compounds and Genes affect anti-cancer drug through regulation of MDM2.

## PROTACs That Degrade E3s

PROTAC technology utilizes the ubiquitin-protease system to target a specific protein for ubiquitination and degradation (Sakamoto et al., 2001). PROTAC technology targets proteins, including transcription factors, skeletal proteins, enzymes, and regulatory factors (Zhang et al., 2018). Targeting oncogene family proteins using PROTACs to overcome drug resistance has recently become a popular area of research.

PROTACs directly targeting oncogenes are a tool for overcoming drug resistance. Ibrutinib resistance can occur due to a cysteine to serine mutation (C481S) in the site normally covalently bound by ibrutinib. Alexandru D. Buhimschi et al. introduced MT-802, which is a PROTAC that induces ubiquitination-dependent degradation of wild-type and C481S-mutant BTK from PROTAC, which could be a novel tool for overcoming ibrutinib resistance (Buhimschi et al., 2018). CP5V (apcin-A-PEG5-VHL ligand 1), as an efficient Cdc20 PROTAC, can mediate degradation of the oncogene Cdc20 through the ubiquitous pathway and overcome resistance to taxane chemotherapy in BC by inhibiting mitotic slippage (Chi et al., 2019). The SH2-U-box targets both native and T315I-mutant BCR-ABL for ubiquitination and degradation and thus may serve as a tool for treating both imatinib-sensitive and imatinib-resistant CML (Ru et al., 2016).

## Limitations of Targeting E3s to Combat Drug Resistance

In summary, E3s can play a role in tumor resistance by binding oncogenes or pathway proteins. Degrading E3s via different strategies or affecting their function can be used as strategies for anticancer treatment. However, E3s have some shortcomings in treating drug resistance. The first is the diversity of E3s, which prevents a complete understanding of all of the E3 functions and their corresponding target genes. The second is that E3s can bind to multiple different oncogenes. For example, TRIM family proteins perform different functions by binding to different oncogenes. The same E3 not only combines with one oncogene or tumor suppressor gene but also can interact with multiple oncogenes or tumor suppressor genes at the same time. Directly targeting E3s in anti-drug resistance research may lead to failure.

## CONCLUSION

Drug resistance has been a prominent factor negatively affecting clinical treatment. Various E3s target oncogenes or tumor suppressors, affecting the sensitivity of tumor cells to different drug treatments. Strategies that target E3s to combat drug resistance include interfering with E3 activators, degrading E3s and affecting the interaction between E3s and their substrates. Some famous E3s,

like MDM2, FBWX7, and SKP2, have been well studied and shown to have value for treating drug resistance. Research on E3s has led to the discovery of possible therapeutic methods to overcome the challenging clinical situation imposed by drug resistance.

## AUTHOR CONTRIBUTIONS

YL was contributed to the acquisition, analysis, and interpretation of data. CD and CZ was contributed to the conception and design; revising the article for important intellectual content; final approval of the version to be published.

## FUNDING

This work was supported by grants from National Natural Science Foundation of China (81372515), National Natural Science Youth Foundation of China (81602027,81702928), Natural Science Foundation General Program of Hunan Province (2018JJ3821), Natural Science Foundation Youth Program of Hunan Province (806288981033), Project of Scientific Research Plan of Hunan Provincial Health Commission (C2019185) and the Youth Foundation of Xiangya Hospital Central South University (2015Q01).

## REFERENCES

Abedini, M. R., Muller, E. J., Bergeron, R., Gray, D. A., and Tsang, B. K. (2010). Akt promotes chemoresistance in human ovarian cancer cells by modulating cisplatin-induced, p53-dependent ubiquitination of FLICE-like inhibitory protein. *Oncogene* 29 (1), 11–25. doi:10.1038/onc.2009.300

Abedini, M. R., Muller, E. J., Brun, J., Bergeron, R., Gray, D. A., and Tsang, B. K. (2008). Cisplatin induces p53-dependent FLICE-like inhibitory protein ubiquitination in ovarian cancer cells. *Cancer Res.* 68 (12), 4511–4517. doi:10.1158/0008-5472.Can-08-0673

Asselin, B., and Rizzari, C. (2015). Asparaginase pharmacokinetics and implications of therapeutic drug monitoring. *Leuk. Lymphoma* 56 (8), 2273–2280. doi:10.3109/10428194.2014.1003056

Azmi, A. S., Aboukameel, A., Banerjee, S., Wang, Z., Mohammad, M., Wu, J., et al. (1990). MDM2 inhibitor MI-319 in combination with cisplatin is an effective treatment for pancreatic cancer independent of p53 function. *Eur. J. Cancer*, 46 (6). Oxford, England, 1122–1131. doi:10.1016/j.ejca.2010.01.015

Baccarani, M., Rosti, G., and Soverini, S. (2019). Chronic myeloid leukemia: the concepts of resistance and persistence and the relationship with the BCR-ABL1 transcript type. *Leukemia* 33 (10), 2358–2364. doi:10.1038/s41375-019-0562-1

Becker, K., Marchenko, N. D., Palacios, G., and Moll, U. M. (2008). A role of HAUSP in tumor suppression in a human colon carcinoma xenograft model. *Cell Cycle (Georgetown, Tex)* 7 (9), 1205–1213. doi:10.4161/cc.7.9.5756

Bennett, E. J., and Harper, J. W. (2008). DNA damage: ubiquitin marks the spot. *Nat. Struct. Mol. Biol.* 15 (1), 20–22. doi:10.1038/nsmb0108-20

Bernabeu, E., Cagel, M., Lagomarsino, E., Moretton, M., and Chiappetta, D. A. (2017). Paclitaxel: what has been done and the challenges remain ahead. *Int. J. pharmaceutics* 526 (1-2), 474–495. doi:10.1016/j.ijpharm.2017.05.016

Berndsen, C. E., and Wolberger, C. (2014). New insights into ubiquitin E3 ligase mechanism. *Nat. Struct. Mol. Biol.* 21 (4), 301–307. doi:10.1038/nsmb.2780

Bhatt, L., Sebastian, B., and Joshi, V. (2017). Mangiferin protects rat myocardial tissue against cyclophosphamide induced cardiotoxicity. *J. Ayurveda Integr. Med.* 8 (2), 62–67. doi:10.1016/j.jaim.2017.04.006

Bian, P., Dou, Z., Jia, Z., Li, W., and Pan, D. (2020). Activated Wnt/β-Catenin signaling contributes to E3 ubiquitin ligase EDD-conferred docetaxel resistance in prostate cancer. *Life Sci.* 254, 116816. doi:10.1016/j.lfs.2019.116816

Bigenzahn, J. W., Collu, G. M., Kartnig, F., Pieraks, M., Vladimer, G. I., Heinz, L. X., et al. (2018). LZTR1 is a regulator of RAS ubiquitination and signaling. *Science (New York, NY)* 362 (6419), 1171–1177. doi:10.1126/science.aap8210

Bradley, A., Zheng, H., Ziebarth, A., Sakati, W., Branham-O'Connor, M., Blumer, J. B., et al. (2014). EDD enhances cell survival and cisplatin resistance and is a therapeutic target for epithelial ovarian cancer. *Carcinogenesis* 35 (5), 1100–1109. doi:10.1093/carcin/bgt489

Buetow, L., and Huang, D. T. (2016). Structural insights into the catalysis and regulation of E3 ubiquitin ligases. *Nat. Rev. Mol. Cel. Biol.* 17 (10), 626–642. doi:10.1038/nrm.2016.91

Buhimschi, A. D., Armstrong, H. A., Toure, M., Jaime-Figueroa, S., and Chen, T. L. (2018). Targeting the C481S ibrutinib-resistance mutation in bruton's tyrosine kinase using PROTAC-mediated degradation. *Biochemistry* 57 (26), 3564–3575.

Cao, J., Zhao, M., Liu, J., Zhang, X., Pei, Y., Wang, J., et al. (2019). RACK1 promotes self-renewal and chemoresistance of cancer stem cells in human hepatocellular carcinoma through stabilizing Nanog. *Theranostics* 9 (3), 811–828. doi:10.7150/thno.29271

Cappadocia, L., and Lima, C. D. (2018). Ubiquitin-like protein conjugation: structures, chemistry, and mechanism. *Chem. Rev.* 118 (3), 889–918. doi:10.1021/acs.chemrev.6b00737

Chan, C. H., Li, C. F., Yang, W. L., Gao, Y., Lee, S. W., Feng, Z., et al. (2012). The Skp2-SCF E3 ligase regulates Akt ubiquitination, glycolysis, herceptin sensitivity, and tumorigenesis. *Cell* 149 (5), 1098–1111. doi:10.1016/j.cell.2012.02.065

Chen, Z. J., and Sun, L. J. (2009). Nonproteolytic functions of ubiquitin in cell signaling. *Mol. Cel.* 33 (3), 275–286. doi:10.1016/j.molcel.2009.01.014

Cheteh, E. H., Sarne, V., Ceder, S., Bianchi, J., Augsten, M., Rundqvist, H., et al. (2020). Interleukin-6 derived from cancer-associated fibroblasts attenuates the p53 response to doxorubicin in prostate cancer cells. *Cell Death Discov* 6, 42. doi:10.1038/s41420-020-0272-5

Chi, J. J., Li, H., Zhou, Z., Izquierdo-Ferrer, J., Xue, Y., Wavelet, C. M., et al. (2019). A novel strategy to block mitotic progression for targeted therapy. *EBioMedicine* 49, 40–54. doi:10.1016/j.ebiom.2019.10.013

Ciechanover, A. (2015). The unravelling of the ubiquitin system. *Nat. Rev. Mol. Cel. Biol.* 16 (5), 322–324. doi:10.1038/nrm3982

Colaluca, I. N., Tosoni, D., Nuciforo, P., Senic-Matuglia, F., Galimberti, V., Viale, G., et al. (2008). NUMB controls p53 tumour suppressor activity. *Nature* 451 (7174), 76–80. doi:10.1038/nature06412

Cui, X., Lin, Z., Chen, Y., Mao, X., Ni, W., Liu, J., et al. (2016). Upregulated TRIM32 correlates with enhanced cell proliferation and poor prognosis in hepatocellular carcinoma. *Mol. Cell. Biochem.* 421 (1-2), 127–137. doi:10.1007/s11010-016-2793-z

Dai, X., Gan, W., Li, X., Wang, S., Zhang, W., Huang, L., et al. (2017). Prostate cancer-associated SPOP mutations confer resistance to BET inhibitors through stabilization of BRD4. *Nat. Med.* 23 (9), 1063–1071. doi:10.1038/nm.4378

Daks, A., Petukhov, A., Fedorova, O., Shuvalov, O., Merkulov, V., Vasileva, E., et al. (2016). E3 ubiquitin ligase Pirh2 enhances tumorigenic properties of human non-small cell lung carcinoma cells. *Genes & cancer* 7 (11-12), 383–393. doi:10.18632/genesandcancer.123

Davidovich, S., Ben-Izhak, O., Shapira, M., Futerman, B., and Hershko, D. D. (2008). Over-expression of Skp2 is associated with resistance to preoperative doxorubicin-based chemotherapy in primary breast cancer. *Breast cancer researchBCR* 10 (4), R63. doi:10.1186/bcr2122

Donley, C., McClelland, K., McKeen, H. D., Nelson, L., Yakkundi, A., Jithesh, P. V., et al. (2014). Identification of RBCK1 as a novel regulator of FKBPL: implications for tumor growth and response to tamoxifen. *Oncogene* 33 (26), 3441–3450. doi:10.1038/onc.2013.306

Englinger, B., Mair, M., Miklos, W., Pirker, C., Mohr, T., van Schoonhoven, S., et al. (2017). Loss of CUL4A expression is underlying cisplatin hypersensitivity in colorectal carcinoma cells with acquired trabectedin resistance. *Br. J. Cancer* 116 (4), 489–500. doi:10.1038/bjc.2016.449

Eto, K., Iwatsuki, M., Watanabe, M., Ishimoto, T., Ida, S., Imamura, Y., et al. (2015). The sensitivity of gastric cancer to trastuzumab is regulated by the miR-223/FBXW7 pathway. *Int. J. Cancer J. Int. du Cancer* 136 (7), 1537–1545. doi:10.1002/ijc.29168

Fang, L., Yang, Z., Zhou, J., Tung, J. Y., Hsiao, C. D., Wang, L., et al. (2015). Circadian clock gene CRY2 degradation is involved in chemoresistance of colorectal cancer. *Mol. Cancer Ther.* 14 (6), 1476–1487. doi:10.1158/1535-7163.Mct-15-0030

Feng, S., Yang, G., Yang, H., Liang, Z., Zhang, R., Fan, Y., et al. (2017). NEDD4 is involved in acquisition of epithelial-mesenchymal transition in cisplatin-resistant nasopharyngeal carcinoma cells. *Cel Cycle (Georgetown, Tex)* 16 (9), 869–878. doi:10.1080/15384101.2017.1308617

Fu, C., Shi, X., Gong, Y., Wan, Y., Sun, Z., Shi, H., et al. (2018). Constitutively photomorphogenic 1 reduces the sensitivity of chronic lymphocytic leukemia cells to fludarabine through promotion of ubiquitin-mediated P53 degradation. *Cell Physiol. Biochem. : Int. J. Exp. Cell. Physiol. Biochem. Pharmacol.* 50 (6), 2314–2328. doi:10.1159/000495092

Gasca, J., Flores, M. L., Giráldez, S., Ruiz-Borrego, M., Tortolero, M., Romero, F., et al. (2016). Loss of FBXW7 and accumulation of MCL1 and PLK1 promote paclitaxel resistance in breast cancer. *Oncotarget* 7 (33), 52751–52765. doi:10.18632/oncotarget.10481

Gelsomino, G., Corsetto, P. A., Campia, I., Montorfano, G., Kopecka, J., Castella, B., et al. (2013). Omega 3 fatty acids chemosensitize multidrug resistant colon cancer cells by down-regulating cholesterol synthesis and altering detergent resistant membranes composition. *Mol. Cancer* 12, 137. doi:10.1186/1476-4598-12-137

Glickman, M. S., and Sawyers, C. L. (2012). Converting cancer therapies into cures: lessons from infectious diseases. *Cell* 148 (6), 1089–1098. doi:10.1016/j.cell.2012.02.015

Gong, J., Zhou, Y., Liu, D., and Huo, J. (2018). F-box proteins involved in cancer-associated drug resistance. *Oncol. Lett.* 15 (6), 8891–8900. doi:10.3892/ol.2018.8500

Guodong, X., Yuan, L., Meng, W., Xiang, L., Sida, Q., Xin, S., et al. (2018). FBXW7 suppresses epithelial-mesenchymal transition and chemo-resistance of non-small-cell lung cancer cells by targeting snai1 for ubiquitin-dependent degradation. Xi'an, China. *Cell. Prolif.* 51 (5). e12473. doi:10.1111/cpr.12473

Han, S. H., Korm, S., Han, Y. G., Choi, S. Y., Kim, S. H., Chung, H. J., et al. (2019). GCA links TRAF6-ULK1-dependent autophagy activation in resistant chronic myeloid leukemia. *Autophagy*, 15. 2076-2090. doi:10.1080/15548627.2019.1596492

Hatakeyama, S. (2017). TRIM family proteins: roles in autophagy, immunity, and carcinogenesis. *Trends Biochemical Sciences* 42 (4), 297–311. doi:10.1016/j.tibs.2017.01.002

He, R., and Liu, H. (2020). TRIM59 knockdown blocks cisplatin resistance in A549/DDP cells through regulating PTEN/AKT/HK2. *Gene* 747, 144553. doi:10.1016/j.gene.2020.144553

Heinlein, C. A., and Chang, C. (2004). Androgen receptor in prostate cancer. *Endocr. Rev.* 25 (2), 276–308. doi:10.1210/er.2002-0032

Hidayat, M., Mitsuishi, Y., Takahashi, F., Tajima, K., Yae, T., Miyahara, K., et al. (2019). Role of FBXW7 in the quiescence of gefitinib-resistant lung cancer stem cells in EGFR-mutant non-small cell lung cancer. *Bosn J. Basic Med. Sci.* 19 (4), 355–367. doi:10.17305/bjbms.2019.4227

Hinze, L., Pfirrmann, M., Karim, S., Degar, J., McGuckin, C., Vinjamur, D., et al. (2019). Synthetic lethality of Wnt pathway activation and asparaginase in drug-resistant acute leukemias. *Cancer cell* 35 (4), 664–676. doi:10.1016/j.ccell.2019.03.004.e7

Hirosawa, T., Ishida, M., Ishii, K., Kanehara, K., Kudo, K., Ohnuma, S., et al. (2018). Loss of BAP1 expression is associated with genetic mutation and can predict outcomes in gallbladder cancer. *PloS one* 13 (11), e0206643. doi:10.1371/journal.pone.0206643

Hu, Q., Qin, Y., Zhang, B., Liang, C., Ji, S., Shi, S., et al. (2017). FBW7 increases the chemosensitivity of pancreatic cancer cells to gemcitabine through upregulation of ENT1. *Oncol. Rep.* 38 (4), 2069–2077. doi:10.3892/or.2017.5856

Hu, X., Meng, Y., Xu, L., Qiu, L., Wei, M., Su, D., et al. (2019). Cul4 E3 ubiquitin ligase regulates ovarian cancer drug resistance by targeting the antiapoptotic protein BIRC3. *Cel Death Dis.* 10 (2), 104. doi:10.1038/s41419-018-1200-y

Huang, B., Yip, W. K., Wei, N., and Luo, K. Q. (2020). Acetyltanshinone IIA is more potent than lapatinib in inhibiting cell growth and degrading HER2 protein in drug-resistant HER2-positive breast cancer cells. *Cancer Lett.* 490, 1–11. doi:10.1016/j.canlet.2020.06.010

Huang, H., Weng, H., Dong, B., Zhao, P., Zhou, H., and Qu, L. (2017). Oridonin triggers chaperon-mediated proteasomal degradation of BCR-ABL in leukemia. *Scientific Rep.* 7, 41525. doi:10.1038/srep41525

Huang, J., Lu, Z., Xiao, Y., He, B., Pan, C., Zhou, X., et al. (2018). Inhibition of Siah2 ubiquitin ligase by vitamin K3 attenuates chronic myeloid leukemia chemoresistance in hypoxic microenvironment. *Med. Sci. monitor : Int. Med. J. Exp. Clin. Res.* 24, 727–735. doi:10.12659/msm.908553

Huang, X., Gu, H., Zhang, E., Chen, Q., Cao, W., Yan, H., et al. (2020). The NEDD4-1 E3 ubiquitin ligase: a potential molecular target for bortezomib sensitivity in multiple myeloma. *Int. J. Cancer J. Int. du Cancer* 146 (7), 1963–1978. doi:10.1002/ijc.32615

Hung, M. S., Chen, I. C., You, L., Jablons, D. M., Li, Y. C., Mao, J. H., et al. (2015). Knockdown of Cul4A increases chemosensitivity to gemcitabine through upregulation of TGFBI in lung cancer cells. *Oncol. Rep.* 34 (6), 3187–3195. doi:10.3892/or.2015.4324

Ikeda, F., and Dikic, I. (2008). Atypical ubiquitin chains: new molecular signals. 'Protein Modifications: beyond the Usual Suspects' review series. *EMBO Rep.* 9 (6), 536–542. doi:10.1038/embor.2008.93

Interiano, R. B., Yang, J., Harris, A. L., and Davidoff, A. M. (2014). Seven in Absentia Homolog 2 (SIAH2) downregulation is associated with tamoxifen resistance in MCF-7 breast cancer cells. *J. Surg. Res.* 190 (1), 203–209. doi:10.1016/j.jss.2014.02.018

Ishii, T., Matsuse, T., Masuda, M., and Teramoto, S. (2004). The effects of S-phase kinase-associated protein 2 (SKP2) on cell cycle status, viability, and chemoresistance in A549 lung adenocarcinoma cells. *Exp. Lung Res.* 30 (8), 687–703. doi:10.1080/01902140490517818

Janouskova, H., El Tekle, G., Bellini, E., Udeshi, N. D., Rinaldi, A., Ulbricht, A., et al. (2017). Opposing effects of cancer-type-specific SPOP mutants on BET protein degradation and sensitivity to BET inhibitors. *Nat. Med.* 23 (9), 1046–1054. doi:10.1038/nm.4372

Jeon, Y. K., Kim, C. K., Koh, J., Chung, D. H., and Ha, G. H. (2016). Pellino-1 confers chemoresistance in lung cancer cells by upregulating cIAP2 through Lys63-mediated polyubiquitination. *Oncotarget* 7 (27), 41811–41824. doi:10.18632/oncotarget.9619

Jordan, V. C. (2003). Tamoxifen: a most unlikely pioneering medicine. *Nat. Rev. Drug Discov.* 2 (3), 205–213. doi:10.1038/nrd1031

Kadera, B. E., Toste, P. A., Wu, N., Li, L., Nguyen, A. H., Dawson, D. W., et al. (2015). Low expression of the E3 ubiquitin ligase CBL confers chemoresistance in human pancreatic cancer and is targeted by epidermal growth factor receptor inhibition. *Clin. Cancer Res. : official J. Am. Assoc. Cancer Res.* 21 (1), 157–165. doi:10.1158/1078-0432.Ccr-14-0610

Kalluri, R. (2016). The biology and function of fibroblasts in cancer. *Nat. Rev. Cancer* 16 (9), 582–598. doi:10.1038/nrc.2016.73

Kamran, M., Long, Z. J., Xu, D., Lv, S. S., Liu, B., Wang, C. L., et al. (2017). Aurora kinase A regulates Survivin stability through targeting FBXL7 in gastric cancer drug resistance and prognosis. *Oncogenesis* 6 (2), e298. doi:10.1038/oncsis.2016.80

Katayama, K., Fujiwara, C., Noguchi, K., and Sugimoto, Y. (2016). RSK1 protects P-glycoprotein/ABCB1 against ubiquitin-proteasomal degradation by downregulating the ubiquitin-conjugating enzyme E2 R1. *Scientific Rep.* 6, 36134. doi:10.1038/srep36134

Katayama, K., Noguchi, K., and Sugimoto, Y. (2013). FBXO15 regulates P-glycoprotein/ABCB1 expression through the ubiquitin--proteasome pathway in cancer cells. *Cancer Sci.* 104 (6), 694–702. doi:10.1111/cas.12145

Kim, H. B., and Myung, S. J. (2018). Clinical implications of the Hippo-YAP pathway in multiple cancer contexts. *BMB Rep.* 51 (3), 119–125. doi:10.5483/bmbrep.2018.51.3.018

Kim, J., Xu, S., Xiong, L., Yu, L., Fu, X., and Xu, Y. (2017). SALL4 promotes glycolysis and chromatin remodeling via modulating HP1α-Glut1 pathway. *Oncogene* 36 (46), 6472–6479. doi:10.1038/onc.2017.265

Kim, Y., Kim, H., Park, D., and Jeoung, D. (2015). miR-335 targets SIAH2 and confers sensitivity to anti-cancer drugs by increasing the expression of HDAC3. *Mol. Cell* 38 (6), 562–572. doi:10.14348/molcells.2015.0051

Ko, C. Y., Lin, C. H., Chuang, J. Y., Chang, W. C., and Hsu, T. I. (2018). MDM2 degrades deacetylated nucleolin through ubiquitination to promote glioma stem-like cell enrichment for chemotherapeutic resistance. *Mol. Neurobiol.* 55 (4), 3211–3223. doi:10.1007/s12035-017-0569-4

Kojima, K., Konopleva, M., McQueen, T., O'Brien, S., Plunkett, W., and Andreeff, M. (2006). Mdm2 inhibitor Nutlin-3a induces p53-mediated apoptosis by transcription-dependent and transcription-independent mechanisms and may overcome Atm-mediated resistance to fludarabine in chronic lymphocytic leukemia. *Blood* 108 (3), 993–1000. doi:10.1182/blood-2005-12-5148

Kurokawa, M., Kim, J., Geradts, J., Matsuura, K., Liu, L., Ran, X., et al. (2013). A network of substrates of the E3 ubiquitin ligases MDM2 and HUWE1 control apoptosis independently of p53. *Sci. signaling* 6 (274), ra32. doi:10.1126/scisignal.2003741

Kuske, M., Westphal, D., Wehner, R., Schmitz, M., Beissert, S., Praetorius, C., et al. (2018). Immunomodulatory effects of BRAF and MEK inhibitors: implications for Melanoma therapy. *Pharmacol. Res.* 136, 151–159. doi:10.1016/j.phrs.2018.08.019

Lajous, H., Lelièvre, B., Vauléon, E., Lecomte, P., and Garcion, E. (2019). Rethinking alkylating(-like) agents for solid tumor management. *Trends Pharmacological Sciences* 40 (5), 342–357. doi:10.1016/j.tips.2019.03.003

Lang, V., Aillet, F., Xolalpa, W., Serna, S., Ceccato, L., Lopez-Reyes, R. G., et al. (2017). Analysis of defective protein ubiquitylation associated to adriamycin resistant cells. *Cel Cycle (Georgetown, Tex)* 16 (24), 2337–2344. doi:10.1080/15384101.2017.1387694

Lee, H. J., Li, C. F., Ruan, D., Powers, S., Thompson, P. A., Frohman, M. A., et al. (2016). The DNA damage transducer RNF8 facilitates cancer chemoresistance and progression through twist activation. *Mol. Cel.* 63 (6), 1021–1033. doi:10.1016/j.molcel.2016.08.009

Lee, J., An, S., Jung, J. H., Kim, K., Kim, J. Y., An, I. S., et al. (2019). MUL1 E3 ligase regulates the antitumor effects of metformin in chemoresistant ovarian cancer cells via AKT degradation. *Int. J. Oncol.* 54 (5), 1833–1842. doi:10.3892/ijo.2019.4730

Li, G., Ci, W., Karmakar, S., Chen, K., Dhar, R., Fan, Z., et al. (2014). SPOP promotes tumorigenesis by acting as a key regulatory hub in kidney cancer. *Cancer cell* 25 (4), 455–468. doi:10.1016/j.ccr.2014.02.007

Li, H., Li, J., Chen, L., Qi, S., Yu, S., Weng, Z., et al. (2019). HERC3-Mediated SMAD7 ubiquitination degradation promotes autophagy-induced EMT and chemoresistance in glioblastoma. *Clin. Cancer Res. : official J. Am. Assoc. Cancer Res.* 25 (12), 3602–3616. doi:10.1158/1078-0432.Ccr-18-3791

Li, J., Alyamani, M., Zhang, A., Chang, K. H., Berk, M., Li, Z., et al. (2017). Aberrant corticosteroid metabolism in tumor cells enables GR takeover in enzalutamide resistant prostate cancer.*eLife* 6. e20183. doi:10.7554/eLife.20183

Li, N., Lorenzi, F., Kalakouti, E., Normatova, M., Babaei-Jadidi, R., Tomlinson, I., et al. (2015). FBXW7-mutated colorectal cancer cells exhibit aberrant expression of phosphorylated-p53 at Serine-15. *Oncotarget* 6 (11), 9240–9256. doi:10.18632/oncotarget.3284

Li, Y., Ma, C., Zhou, T., Liu, Y., Sun, L., and Yu, Z. (2016). TRIM65 negatively regulates p53 through ubiquitination. *Biochem. biophysical Res. Commun.* 473 (1), 278–282. doi:10.1016/j.bbrc.2016.03.093

Li, Y. Y., Wu, C., Shah, S. S., Chen, S. M., Wangpaichitr, M., Kuo, M. T., et al. (2017). Degradation of AMPK-α1 sensitizes BRAF inhibitor-resistant melanoma cells to arginine deprivation. *Mol. Oncol.* 11 (12), 1806–1825. doi:10.1002/1878-0261.12151

Liang, Q., Tang, C., Tang, M., Zhang, Q., Gao, Y., and Ge, Z. (2019). TRIM47 is up-regulated in colorectal cancer, promoting ubiquitination and degradation of SMAD4. *J. Exp. Clin. Cancer Res.* 38 (1), 159. doi:10.1186/s13046-019-1143-x

Lin, J. H., and Yamazaki, M. (2003). Role of P-glycoprotein in pharmacokinetics: clinical implications. *Clin. Pharmacokinet.* 42 (1), 59–98. doi:10.2165/00003088-200342010-00003

Liu, C., Lou, W., Yang, J. C., Liu, L., and Gao, A. C. (2018). Proteostasis by STUB1/HSP70 complex controls sensitivity to androgen receptor targeted therapy in advanced prostate cancer. *Nat. Commun.* 9 (1). 4700. doi:10.1038/s41467-018-07178-x

Liu, M. L., Zang, F., and Zhang, S. J. (2019). RBCK1 contributes to chemoresistance and stemness in colorectal cancer (CRC). *Biomed. Pharmacother.* 118, 109250. doi:10.1016/j.biopha.2019.109250

Liu, T., Xiong, J., Yi, S., Zhang, H., Zhou, S., Gu, L., et al. (2017). FKBP12 enhances sensitivity to chemotherapy-induced cancer cell apoptosis by inhibiting MDM2. *Oncogene* 36 (12), 1678–1686. doi:10.1038/onc.2016.331

Long, L., Xiang, H., Liu, J., Zhang, Z., and Sun, L. (2019). ZEB1 mediates doxorubicin (Dox) resistance and mesenchymal characteristics of hepatocarcinoma cells. *Exp. Mol. Pathol.* 106, 116–122. doi:10.1016/j.yexmp.2019.01.001

Longley, D. B., Harkin, D. P., and Johnston, P. G. (2003). 5-fluorouracil: mechanisms of action and clinical strategies. *Nat. Rev. Cancer* 3 (5), 330–338. doi:10.1038/nrc1074

Lu, Y., Han, D., Liu, W., Huang, R., Ou, J., Chen, X., et al. (2018). RNF138 confers cisplatin resistance in gastric cancer cells via activating Chk1 signaling pathway. *Cancer Biol. Ther.* 19 (12), 1128–1138. doi:10.1080/15384047.2018.1480293

Lukenbill, J., and Kalaycio, M. (2013). Fludarabine: a review of the clear benefits and potential harms. *Leuk. Res.* 37 (9), 986–994. doi:10.1016/j.leukres.2013.05.004

Malek, E., Abdel-Malek, M. A., Jagannathan, S., Vad, N., Karns, R., Jegga, A. G., et al. (2017). Pharmacogenomics and chemical library screens reveal a novel SCF(SKP2) inhibitor that overcomes Bortezomib resistance in multiple myeloma. *Leukemia* 31 (3), 645–653. doi:10.1038/leu.2016.258

Marzio, A., Puccini, J., Kwon, Y., Maverakis, N. K., Arbini, A., Sung, P., et al. (2019). The F-box domain-dependent activity of EMI1 regulates PARPi sensitivity in triple-negative breast cancers. *Mol. Cel.* 73 (2), 224–237. doi:10.1016/j.molcel.2018.11.003.e6

Mini, E., Nobili, S., Caciagli, B., Landini, I., and Mazzei, T. (2006). Cellular pharmacology of gemcitabine. *Ann. Oncol.* 17 (Suppl. 5), v7–12. doi:10.1093/annonc/mdj941

Mun, G. I., Choi, E., Lee, Y., and Lee, Y. S. (2020). Decreased expression of FBXW7 by ERK1/2 activation in drug-resistant cancer cells confers transcriptional activation of MDR1 by suppression of ubiquitin degradation of HSF1. *Cel Death Dis.* 11 (5), 395. doi:10.1038/s41419-020-2600-3

Muscolini, M., Montagni, E., Palermo, V., Di Agostino, S., Gu, W., Abdelmoula-Souissi, S., et al. (2011). The cancer-associated K351N mutation affects the ubiquitination and the translocation to mitochondria of p53 protein. *J. Biol. Chem.* 286 (46), 39693–39702. doi:10.1074/jbc.M111.279539

Nalepa, G., Rolfe, M., and Harper, J. W. (2006). Drug discovery in the ubiquitin-proteasome system. *Nat. Rev. Drug Discov.* 5 (7), 596–613. doi:10.1038/nrd2056

Ning, Y., Hui, N., Qing, B., Zhuo, Y., Sun, W., Du, Y., et al. (2019). ZCCHC10 suppresses lung cancer progression and cisplatin resistance by attenuating MDM2-mediated p53 ubiquitination and degradation. *Cel Death Dis.* 10 (6), 414. doi:10.1038/s41419-019-1635-9

Nunes, J., Zhang, H., Angelopoulos, N., Chhetri, J., Osipo, C., Grothey, A., et al. (2016). ATG9A loss confers resistance to trastuzumab via c-Cbl mediated Her2 degradation. *Oncotarget* 7 (19), 27599–27612. doi:10.18632/oncotarget.8504

O'Brien, P. M., Davies, M. J., Scurry, J. P., Smith, A. N., Barton, C. A., Henderson, M. J., et al. (2008). The E3 ubiquitin ligase EDD is an adverse prognostic factor for serous epithelial ovarian cancer and modulates cisplatin resistance *in vitro*. *Br. J. Cancer* 98 (6), 1085–1093. doi:10.1038/sj.bjc.6604281

Onorati, A. V., Dyczynski, M., Ojha, R., and Amaravadi, R. K. (2018). Targeting autophagy in cancer. *Cancer* 124 (16), 3307–3318. doi:10.1002/cncr.31335

Pan, C., Chun, J., Li, D., Boese, A. C., Li, J., Kang, J., et al. (2019). Hsp90B enhances MAST1-mediated cisplatin resistance by protecting MAST1 from proteosomal degradation. *J. Clin. Invest.* 129 (10), 4110–4123. doi:10.1172/jci125963

Pan, X., Chen, Y., Shen, Y., and Tantai, J. (2019). Knockdown of TRIM65 inhibits autophagy and cisplatin resistance in A549/DDP cells by regulating miR-138-5p/ATG7. *Cel Death Dis.* 10 (6), 429. doi:10.1038/s41419-019-1660-8

Pandya, K., Wyatt, D., Gallagher, B., Shah, D., Baker, A., Bloodworth, J., et al. (2016). PKCα attenuates jagged-1-mediated Notch signaling in ErbB-2-positive breast cancer to reverse trastuzumab resistance. *Clin. Cancer Res. : official J. Am. Assoc. Cancer Res.* 22 (1), 175–186. doi:10.1158/1078-0432.Ccr-15-0179

Park, J., Bae, E. K., Lee, C., Choi, J. H., Jung, W. J., Ahn, K. S., et al. (2014). Establishment and characterization of bortezomib-resistant U266 cell line: constitutive activation of NF-κB-mediated cell signals and/or alterations of ubiquitylation-related genes reduce bortezomib-induced apoptosis. *BMB Rep.* 47 (5), 274–279. doi:10.5483/bmbrep.2014.47.5.134

Perez-Losada, J., Mao, J. H., and Balmain, A. (2005). Control of genomic instability and epithelial tumor development by the p53-Fbxw7/Cdc4 pathway. *Cancer Res.* 65 (15), 6488–6492. doi:10.1158/0008-5472.Can-05-1294

Pokharel, Y. R., Kim, N. D., Han, H. K., Oh, W. K., and Kang, K. W. (2010). Increased ubiquitination of multidrug resistance 1 by ginsenoside Rd. *Nutr. Cancer* 62 (2), 252–259. doi:10.1080/01635580903407171

Qin, X., Chen, S., Qiu, Z., Zhang, Y., and Qiu, F. (2012). Proteomic analysis of ubiquitination-associated proteins in a cisplatin-resistant human lung

adenocarcinoma cell line. *Int. J. Mol. Med.* 29 (5), 791–800. doi:10.3892/ijmm.2012.912

Qin, Y., Cui, H., and Zhang, H. (2016). Overexpression of TRIM25 in lung cancer regulates tumor cell progression. *Techn. Cancer Res. Treat.* 15 (5), 707–715. doi:10.1177/1533034615595903

Qu, C., Kunkalla, K., Vaghefi, A., Frederiksen, J. K., Liu, Y., Chapman, J. R., et al. (2018). Smoothened stabilizes and protects TRAF6 from degradation: a novel non-canonical role of smoothened with implications in lymphoma biology. *Cancer Lett.* 436, 149–158. doi:10.1016/j.canlet.2018.08.020

Ravindranath, A. K., Kaur, S., Wernyj, R. P., Kumaran, M. N., Miletti-Gonzalez, K. E., Chan, R., et al. (2015). CD44 promotes multi-drug resistance by protecting P-glycoprotein from FBXO21-mediated ubiquitination. *Oncotarget* 6 (28), 26308–26321. doi:10.18632/oncotarget.4763

Reuther, C., Heinzle, V., Nölting, S., Herterich, S., Hahner, S., Halilovic, E., et al. (2018). The HDM2 (MDM2) inhibitor NVP-CGM097 inhibits tumor cell proliferation and shows additive effects with 5-fluorouracil on the p53-p21-Rb-E2F1 cascade in the p53wild type neuroendocrine tumor cell line GOT1. *Neuroendocrinology* 106 (1), 1–19. doi:10.1159/000453369

Ru, Y., Wang, Q., Liu, X., Zhang, M., Zhong, D., Ye, M., et al. (2016). The chimeric ubiquitin ligase SH2-U-box inhibits the growth of imatinib-sensitive and resistant CML by targeting the native and T315I-mutant BCR-ABL. *Scientific Rep.* 6, 28352. doi:10.1038/srep28352

Rulina, A. V., Mittler, F., Obeid, P., Gerbaud, S., Guyon, L., Sulpice, E., et al. (2016). Distinct outcomes of CRL-Nedd8 pathway inhibition reveal cancer cell plasticity. *Cel Death Dis.* 7 (12), e2505. doi:10.1038/cddis.2016.395

Sakamoto, K. M., Kim, K. B., Kumagai, A., Mercurio, F., Crews, C. M., and Deshaies, R. J. (2001). Protacs: chimeric molecules that target proteins to the Skp1-Cullin-F box complex for ubiquitination and degradation. *Proc. Natl. Acad. Sci. United States America* 98 (15), 8554–8559. doi:10.1073/pnas.141230798

Schnepp, P. M., Shelley, G., Dai, J., Wakim, N., Jiang, H., Mizokami, A., et al. (2020). Single-cell transcriptomics analysis identifies nuclear protein 1 as a regulator of docetaxel resistance in prostate cancer cells. *Mol. Cancer Res. : MCR* 18 (9), 1290–1301. doi:10.1158/1541-7786.Mcr-20-0051

Scott, K., Hayden, P. J., Will, A., Wheatley, K., and Coyne, I. (2016). Bortezomib for the treatment of multiple myeloma. *Cochrane Database Syst. Rev.* 4, Cd010816. doi:10.1002/14651858.CD010816.pub2

Senft, D., Qi, J., and Ronai, Z. A. (2018). Ubiquitin ligases in oncogenic transformation and cancer therapy. *Nat. Rev. Cancer* 18 (2), 69–88. doi:10.1038/nrc.2017.105

Shen, Y., Sun, Y., Zhang, L., and Liu, H. (2017). Effects of DTX3L on the cell proliferation, adhesion, and drug resistance of multiple myeloma cells. *Tumour Biol. : J. Int. Soc. Oncodevelopmental Biol. Med.* 39 (6), 1010428317703941. doi:10.1177/1010428317703941

Sheng, W., Dong, M., Chen, C., Wang, Z., Li, Y., Wang, K., et al. (2017). Cooperation of Musashi-2, Numb, MDM2, and P53 in drug resistance and malignant biology of pancreatic cancer. *FASEB J. : official Publ. Fed. Am. Societies Exp. Biol.* 31 (6), 2429–2438. doi:10.1096/fj.201601240R

Shi, J., Zhang, W., You, M., Xu, Y., Hou, Y., and Jin, J. (2016). Pioglitazone inhibits EGFR/MDM2 signaling-mediated PPARγ degradation. *Eur. J. Pharmacol.* 791, 316–321. doi:10.1016/j.ejphar.2016.09.010

Shi, Q., Zhu, Y., Ma, J., Chang, K., Ding, D., Bai, Y., et al. (2019). Prostate Cancer-associated SPOP mutations enhance cancer cell survival and docetaxel resistance by upregulating Caprin1-dependent stress granule assembly. *Mol. Cancer* 18 (1), 170. doi:10.1186/s12943-019-1096-x

Shimizu, H., Takeishi, S., Nakatsumi, H., and Nakayama, K. I. (2019). Prevention of cancer dormancy by Fbxw7 ablation eradicates disseminated tumor cells. *JCI Insight* 4 (4). doi:10.1172/jci.insight.125138

Siegel, R. L., Miller, K. D., and Jemal, A. (2019). *Cancer* statistics. *CA: a Cancer J. clinicians* 69 (1), 7–34. doi:10.3322/caac.21551

Skaar, J. R., Pagan, J. K., and Pagano, M. (2014). SCF ubiquitin ligase-targeted therapies. *Nat. Rev. Drug Discov.* 13 (12), 889–903. doi:10.1038/nrd4432

Smith, P. G., Tanaka, H., and Chantry, A. (2012). A novel co-operative mechanism linking TGFβ and Lyn kinase activation to imatinib resistance in chronic myeloid leukaemia cells. *Oncotarget* 3 (5), 518–524. doi:10.18632/oncotarget.500

Song, Y., Zhou, X., Bai, W., and Ma, X. (2015). FBW7 increases drug sensitivity to cisplatin in human nasopharyngeal carcinoma by downregulating the expression of multidrug resistance-associated protein. *Tumour Biol. : J. Int. Soc. Oncodevelopmental Biol. Med.* 36 (6), 4197–4202. doi:10.1007/s13277-015-3056-4

Su, J. L., Cheng, X., Yamaguchi, H., Chang, Y. W., Hou, C. F., Lee, D. F., et al. (2011). FOXO3a-Dependent mechanism of e1a-induced chemosensitization. *Cancer Res.* 71 (21), 6878–6887. doi:10.1158/0008-5472.Can-11-0295

Tanaka, N., Kosaka, T., Miyazaki, Y., Mikami, S., Niwa, N., Otsuka, Y., et al. (2016).Acquired platinum resistance involves epithelial to mesenchymal transition through ubiquitin ligase FBXO32 dysregulation. *JCI Insight* 1 (18), e83654. doi:10.1172/jci.insight.83654

Tang, D. E., Dai, Y., Lin, L. W., Xu, Y., Liu, D. Z., Hong, X. P., et al. (2019). STUB1 suppresseses tumorigenesis and chemoresistance through antagonizing YAP1 signaling. *Cancer Sci.* 110 (10), 3145–3156. doi:10.1111/cas.14166

Tang, D. E., Dai, Y., Xu, Y., Lin, L. W., Liu, D. Z., Hong, X. P., et al. (2020). The ubiquitinase ZFP91 promotes tumor cell survival and confers chemoresistance through FOXA1 destabilization. *Carcinogenesis* 41 (1), 56–66. doi:10.1093/carcin/bgz085

Tatham, M. H., Plechanovová, A., Jaffray, E. G., Salmen, H., and Hay, R. T. (2013). Ube2W conjugates ubiquitin to α-amino groups of protein N-termini. *Biochem. J.* 453 (1), 137–145. doi:10.1042/bj20130244

Tian, H. L., Yu, T., Xu, N. N., Feng, C., Zhou, L. Y., Luo, H. W., et al. (2010). A novel compound modified from tanshinone inhibits tumor growth *in vivo* via activation of the intrinsic apoptotic pathway. *Cancer Lett.* 297 (1), 18–30. doi:10.1016/j.canlet.2010.04.020

Tong, J., Tan, S., Zou, F., Yu, J., and Zhang, L. (2017). FBW7 mutations mediate resistance of colorectal cancer to targeted therapies by blocking Mcl-1 degradation. *Oncogene* 36 (6), 787–796. doi:10.1038/onc.2016.247

Tsuchiya, M., Nakajima, Y., Waku, T., Hiyoshi, H., Morishita, T., Furumai, R., et al. (2015). CHIP buffers heterogeneous Bcl-2 expression levels to prevent augmentation of anticancer drug-resistant cell population. *Oncogene* 34 (35), 4656–4663. doi:10.1038/onc.2014.387

Uchida, C., and Kitagawa, M. (2016). RING-, HECT-, and RBR-type E3 ubiquitin ligases: involvement in human cancer. *Curr. Cancer Drug Targets* 16 (2), 157–174. doi:10.2174/1568009616666151112122801

Vasan, N., Baselga, J., and Hyman, D. M. (2019). A view on drug resistance in cancer. *Nature* 575 (7782), 299–309. doi:10.1038/s41586-019-1730-1

Vu, B., Wovkulich, P., Pizzolato, G., Lovey, A., Ding, Q., Jiang, N., et al. (2013). Discovery of RG7112: a small-molecule MDM2 inhibitor in clinical development. *ACS Med. Chem. Lett.* 4 (5), 466–469. doi:10.1021/ml4000657

Waks, A. G., and Winer, E. P. (2019). Breast cancer treatment: a review. *Jama* 321 (3), 288–300. doi:10.1001/jama.2018.19323

Wang, D., Ma, L., Wang, B., Liu, J., and Wei, W. (2017). E3 ubiquitin ligases in cancer and implications for therapies. *Cancer Metastasis Rev.* 36 (4), 683–702. doi:10.1007/s10555-017-9703-z

Wang, H., Liu, B., Zhang, C., Peng, G., Liu, M., Li, D., et al. (2009). Parkin regulates paclitaxel sensitivity in breast cancer via a microtubule-dependent mechanism. *J. Pathol.* 218 (1), 76–85. doi:10.1002/path.2512

Wang, H., Lu, B., Castillo, J., Zhang, Y., Yang, Z., McAllister, G., et al. (2016). Tankyrase inhibitor sensitizes lung cancer cells to endothelial growth factor receptor (EGFR) inhibition via stabilizing angiomotins and inhibiting YAP signaling. *J. Biol. Chem.* 291 (29), 15256–15266. doi:10.1074/jbc.M116.722967

Wang, X., Rusin, A., Walkey, C. J., Lin, J. J., and Johnson, D. L. (2019). The RNA polymerase III repressor MAF1 is regulated by ubiquitin-dependent proteasome degradation and modulates drug resistance and apoptosis. *J. Biol. Chem.* 294. 19255-19268. 10.1074/jbc.RA119.008849

Wang, Y., Guo, A., Liang, X., Li, M., Shi, M., Li, Y., et al. (2017). HRD1 sensitizes breast cancer cells to Tamoxifen by promoting S100A8 degradation. *Oncotarget* 8 (14), 23564–23574. doi:10.18632/oncotarget.15797

Wu, B., Liu, Z. Y., Cui, J., Yang, X. M., Jing, L., Zhou, Y., et al. (2017). F-box protein FBXO22 mediates polyubiquitination and degradation of CD147 to reverse cisplatin resistance of tumor cells. *Int. J. Mol. Sci.* 18 (1). doi:10.3390/ijms18010212

Wu, C., Chen, L., Tao, H., Kong, L., and Hu, Y. (2020). Ring finger protein 38 induces the drug resistance of cisplatin in non-small cell lung cancer. *Cel Biol. Int.*. doi:10.1002/cbin.11423

X Che, X., Zhang, Y., Qu, X., Guo, T., Ma, Y., Li, C., et al. (2017). The E3 ubiquitin ligase Cbl-b inhibits tumor growth in multidrug-resistant gastric and breast cancer cells. *Neoplasma* 64 (6), 887–892. doi:10.4149/neo_2017_610

Xiao, Q., Yang, Y., An, Q., and Qi, Y. (2017). MicroRNA-100 suppresses human osteosarcoma cell proliferation and chemo-resistance via ZNRF2. *Oncotarget* 8 (21), 34678–34686. doi:10.18632/oncotarget.16149

Xu, L., Zhang, Y., Qu, X., Che, X., Guo, T., Cai, Y., et al. (2017).E3 ubiquitin ligase cbl-b prevents tumor metastasis by maintaining the epithelial phenotype in multiple drug-resistant gastric and breast cancer cells. *Neoplasia*, 19 (4). New York, NY, 374–382. doi:10.1016/j.neo.2017.01.011

Yan, S. C., Liu, Y. P., Zhang, L. Y., Qu, J. L., Xu, L., Liu, J., et al. (2011). Ubiquitin ligase c-Cbl is involved in tamoxifen-induced apoptosis of MCF-7 cells by downregulating the survival signals. *Acta Oncol.* 50 (5), 693–699. doi:10.3109/0284186x.2010.543144

Yang, Y., Lu, Y., Wang, L., Mizokami, A., Keller, E. T., Zhang, J., et al. (2016). Skp2 is associated with paclitaxel resistance in prostate cancer cells. *Oncol. Rep.* 36 (1), 559–566. doi:10.3892/or.2016.4809

Yin, H., Zhu, Q., Liu, M., Tu, G., Li, Q., Yuan, J., et al. (2017). GPER promotes tamoxifen-resistance in ER+ breast cancer cells by reduced Bim proteins through MAPK/Erk-TRIM2 signaling axis. *Int. J. Oncol.* 51 (4), 1191–1198. doi:10.3892/ijo.2017.4117

Yin, Y., Xie, C. M., Li, H., Tan, M., and Sun, Y. (2019). The FBXW2–MSX2–SOX2 axis regulates stem cell property and drug resistance of cancer cells. *Proc. Natl. Acad. ences* 116 (41), 201905973.

Yokobori, T., Yokoyama, Y., Mogi, A., Endoh, H., Altan, B., Kosaka, T., et al. (2014). FBXW7 mediates chemotherapeutic sensitivity and prognosis in NSCLCs. *Mol. Cancer Res. : MCR* 12 (1), 32–37. doi:10.1158/1541-7786.Mcr-13-0341

Yu, C., Chen, S., Guo, Y., and Sun, C. (2018). Oncogenic TRIM31 confers gemcitabine resistance in pancreatic cancer via activating the NF-κB signaling pathway. *Theranostics* 8 (12), 3224–3236. doi:10.7150/thno.23259

Yu, H. G., Wei, W., Xia, L. H., Han, W. L., Zhao, P., Wu, S. J., et al. (2013). FBW7 upregulation enhances cisplatin cytotoxicity in non- small cell lung cancer cells. *Asian Pac. J. Cancer Prev. : APJCP* 14 (11), 6321–6326. doi:10.7314/apjcp.2013.14.11.6321

Yu, J. J., Zhou, D. D., Yang, X. X., Cui, B., Tan, F. W., Wang, J., et al. (2020). TRIB3-EGFR interaction promotes lung cancer progression and defines a therapeutic target. *Nat. Commun.* 11 (1), 3660. doi:10.1038/s41467-020-17385-0

Yu, P., Fan, Y., Qu, X., Zhang, J., Song, N., Liu, J., et al. (2016). Cbl-b regulates the sensitivity of cetuximab through ubiquitin-proteasome system in human gastric cancer cells. *J. BUON : official J. Balkan Union Oncol.* 21 (4), 867–873.

Yu, X., Wang, R., Zhang, Y., Zhou, L., Wang, W., Liu, H., et al. (2019). Skp2-mediated ubiquitination and mitochondrial localization of Akt drive tumor growth and chemoresistance to cisplatin. *Oncogene* 38 (50), 7457–7472. doi:10.1038/s41388-019-0955-7

Zhang, P. F., Sheng, L. L., Wang, G., Tian, M., Zhu, L. Y., Zhang, R., et al. (2016). miR-363 promotes proliferation and chemo-resistance of human gastric cancer via targeting of FBW7 ubiquitin ligase expression. *Oncotarget* 7 (23), 35284–35292. doi:10.18632/oncotarget.9169

Zhang, R., Li, S. W., Liu, L., Yang, J., Huang, G., and Sang, Y. (2020). TRIM11 facilitates chemoresistance in nasopharyngeal carcinoma by activating the β-catenin/ABCC9 axis via p62-selective autophagic degradation of Daple. *Oncogenesis* 9 (5), 45. doi:10.1038/s41389-020-0229-9

Zhang, W. L., Zhang, J. H., Wu, X. Z., Yan, T., and Lv, W. (2015). miR-15b promotes epithelial-mesenchymal transition by inhibiting SMURF2 in pancreatic cancer. *Int. J. Oncol.* 47 (3), 1043–1053. doi:10.3892/ijo.2015.3076

Zhang, X., Lee, H. C., Shirazi, F., Baladandayuthapani, V., Lin, H., Kuiatse, I., et al. (2018). Protein targeting chimeric molecules specific for bromodomain and extra-terminal motif family proteins are active against pre-clinical models of multiple myeloma. *Leukemia* 32 (10), 2224–2239. doi:10.1038/s41375-018-0044-x

Zhang, X., Li, C. F., Zhang, L., Wu, C. Y., Han, L., Jin, G., et al. (2016). TRAF6 restricts p53 mitochondrial translocation, apoptosis, and tumor suppression. *Mol. Cel.* 64 (4), 803–814. doi:10.1016/j.molcel.2016.10.002

Zhang, Y., Qu, X., Teng, Y., Li, Z., Xu, L., Liu, J., et al. (2015). Cbl-b inhibits P-gp transporter function by preventing its translocation into caveolae in multiple drug-resistant gastric and breast cancers. *Oncotarget* 6 (9), 6737–6748. doi:10.18632/oncotarget.3253

Zhang, Z., Wu, J. Y., Hait, W. N., and Yang, J. M. (2004). Regulation of the stability of P-glycoprotein by ubiquitination. *Mol. Pharmacol.* 66 (3), 395. doi:10.1124/mol.104.001966

Zhao, L., Qiu, T., Jiang, D., Xu, H., Zou, L., Yang, Q., et al. (2020). SGCE promotes breast cancer stem cells by stabilizing EGFR. *Adv. Sci. (Weinh)* 7 (14), 1903700. doi:10.1002/advs.201903700

Zheng, N., and Shabek, N. (2017). Ubiquitin ligases: structure, function, and regulation. *Annu. Rev. Biochem.* 86, 129–157. doi:10.1146/annurev-biochem-060815-014922

**Conflict of Interest:** The authors declare that the research was conducted in the absence of any commercial or financial relationships that could be construed as a potential conflict of interest.

frontiers in Oncology

ORIGINAL RESEARCH
published: 22 April 2021
doi: 10.3389/fonc.2021.624811

# Cryptotanshinone Inhibits ERα-Dependent and -Independent BCRP Oligomer Formation to Reverse Multidrug Resistance in Breast Cancer

*Wenting Ni[1†], Hui Fan[1†], Xiuqin Zheng[1], Fangming Xu[1], Yuanyuan Wu[1], Xiaoman Li[1], Aiyun Wang[1,2], Shile Huang[3], Wenxing Chen[1,2*], Shijun Wang[4*] and Yin Lu[1,2*]*

[1] Jiangsu Key Laboratory for Pharmacology and Safety Evaluation of Chinese Materia Medica, School of Pharmacy, Nanjing University of Chinese Medicine, Nanjing, China, [2] Jiangsu Collaborative Innovation Center of Traditional Chinese Medicine (TCM) Prevention and Treatment of Tumor, Nanjing, China, [3] Department of Biochemistry and Molecular Biology, Louisiana State University Health Sciences Center, Shreveport, LA, United States, [4] Shandong Co-Innovation Center of Traditional Chinese Medicine (TCM) Formula, College of Traditional Chinese Medicine, Shandong University of Traditional Chinese Medicine, Jinan, China

OPEN ACCESS

**Edited by:**
Xiaoping Lin,
Sun Yat-sen University Cancer Center (SYSUCC), China

**Reviewed by:**
Xiaokun Wang,
Wayne State University, United States
Chaoyun Cai,
St. John's University, United States

***Correspondence:**
Wenxing Chen
chenwx@njucm.edu.cn
Yin Lu
luyingreen@njucm.edu.cn
Shijun Wang
wsj@sdutcm.edu.cn

[†] These authors have contributed equally to this work

**Specialty section:**
This article was submitted to Pharmacology of Anti-Cancer Drugs, a section of the journal Frontiers in Oncology

**Received:** 01 November 2020
**Accepted:** 19 February 2021
**Published:** 22 April 2021

**Citation:**
Ni W, Fan H, Zheng X, Xu F, Wu Y, Li X, Wang A, Huang S, Chen W, Wang S and Lu Y (2021) Cryptotanshinone Inhibits ERα-Dependent and -Independent BCRP Oligomer Formation to Reverse Multidrug Resistance in Breast Cancer. Front. Oncol. 11:624811. doi: 10.3389/fonc.2021.624811

Both long-term anti-estrogen therapy and estrogen receptor-negative breast cancer contribute to drug resistance, causing poor prognosis in breast cancer patients. Breast cancer resistance protein (BCRP) plays an important role in multidrug resistance. Here, we show that cryptotanshinone (CPT), an anti-estrogen compound, inhibited the oligomer formation of BCRP on the cell membrane, thus blocking its efflux function. The inhibitory effect of CPT on BCRP was dependent on the expression level of estrogen receptor α (ERα) in ERα-positive breast cancer cells. Furthermore, ERα-negative breast cancer cells with high expression of BCRP were also sensitive to CPT because CPT was able to bind to BCRP and inhibit its oligomer formation on the cell membrane, suggesting that the high level of BCRP expression is crucial for CPT to reverse drug resistance. The combination of CPT and chemotherapeutic agents displayed enhanced anticancer effects. The results suggest that CPT is a novel BCRP inhibitor *via* blocking the oligomer formation of BCRP on the cell membrane. CPT is able to inhibit the activity of BCRP in an ERα-dependent and -independent manner, sensitizing breast cancer cells to chemotherapy.

**Keywords: cryptotanshinone, breast cancer resistance protein (BCRP or ABCG2), estrogen receptor α, oligomer formation, multidrug resistance**

## BACKGROUND

Chemotherapy is one of the foremost approaches to treat cancer, but the occurrence of multidrug resistance (MDR) has weakened its clinical efficacy (1). MDR happens frequently in breast cancer, especially in estrogen receptor α-positive (ERα+) breast cancer. After receiving hormone therapy such as tamoxifen, about 70% of patients have recurrence of drug resistance in the late stages (2). Recently, many studies have shown a close relationship between the occurrence of breast cancer MDR and the expression of the ATP-binding cassette (ABC) transporter family, especially

P-glycoprotein (P-gp/ABCB1), multidrug-resistance-associated protein 1 (MRP1/ABCC1), and the breast cancer resistance proteins (BCRP/ABCG2) (3, 4).

ABCG2, a member of the human ABC transporter superfamily, was known as BCRP, having "drug pump" function (5). BCRP is structurally similar to P-gp and MRP (1), sharing certain homologous sequences (6). However, it still has its own unique conformation, a nucleotide-binding domain (NBD) at the C-terminus and a hydrophobic transmembrane domain (TMD) at the N-terminus, indicating BCRP as a semi-transporter (7). In general, P-gp and MRP1 that have two NBD and multiple TMD structures are called full transporters (8). Semi-transporters are commonly localized in the cytoplasm, but BCRP is the first reported semi-transporter localized on the cell membrane (9). Studies have demonstrated that BCRP is likely to form homodimers, tetramers, dodecamers, and even larger oligomer structures by intramolecular disulfide linkages, which significantly increase the efficiency of external pumping by increasing the formation of the outer channel cavity (10). Thus, inhibiting BCRP or blocking the efflux of therapeutic drugs has been considered a feasible strategy for eliminating the MDR, which boosts the development of BCRP inhibitors (11).

Cryptotanshinone (CPT) is a natural diterpenoid from the plant *Salvia miltiorrhiza*. Since CPT was shown to execute its anticancer action by inhibiting signal transducer and activator of transcription 3 (STAT3) dimerization (12), it has received great attention. We have demonstrated that CPT is able to inhibit the mammalian target of rapamycin (mTOR) signaling (13) and activate the mitogen-activated protein kinase (MAPK) pathways (14), leading to cell death. Of interest, CPT, unlike rapamycin and its derivatives, inhibits mTOR signaling *via* activating the AMP-activated protein kinase (AMPK)–tuberous sclerosis complex 2 (TSC2) axis (15). Most recently, we have observed that the anticancer activity of CPT is related to the status of ERα in breast cancer cells, as MCF7 (ERα-positive) cells are more sensitive to CPT than MDA-MB-231 (ERα-negative) cells (16). Also, MCF-7/ADR, a doxorubicin (DOX)-induced multidrug-resistant cell line, is also sensitive to CPT, and CPT is able to distinctly enhance the inhibitory effect of tamoxifen on MCF-7/ADR (16). MCF-7/ADR cell line is characterized by a high expression of ABC protein family and negative ERα expression induced by DOX to acquire MDR. Therefore, we hypothesized that CPT may target BCRP to reverse the MDR.

In this study, we, for the first time, showed that CPT could inhibit BCRP by interfering with the oligomer formation of BCRP on the cell membrane in both ERα-positive and -negative breast cancer cells. Our results indicate that CPT is a novel inhibitor of BCRP and has great potential to overcome MDR due to high expression of BCRP in both ERα-positive and -negative breast cancer.

**Abbreviations:** CPT, cryptotanshinone; BCRP, breast cancer resistance protein; ERα, estrogen receptor α; MDR, multidrug resistance; ABC, ATP-binding cassette; MRP1, multidrug resistance-associated protein; NBD, nucleotide-binding domain; TMD, transmembrane domain; MX, mitoxantrone; DOX, doxorubicin; TOPO, topotecan; FRET, fluorescence resonance energy transfer; STAT3, signal transducer and activator of transcription 3; AMPK, AMP-activated protein kinase; MAPK, mitogen-activated protein kinase; NRF2, nuclear factor erythroid-2 related factor 2.

# MATERIALS AND METHODS

## Chemicals and Reagents

CPT [purity 98%, high-performance liquid chromatography (HPLC), Xian Yuxuan Biotechnology Co., Ltd.], RPMI 1640, Dulbecco's Modified Eagle Medium (DMEM), fetal bovine serum (FBS), Opti MEM medium, trypsin-ethylenediamine tetraacetic acid (EDTA), and penicillin/streptomycin were purchased from Gibco (Grand Island, NY, USA). KO143 was obtained from MCE (Newark, NJ, USA). Mitoxantrone (MX) was brought from Meilunbio (Dalian, Liaoning, China). Rhodamine123 was purchased from Sigma-Aldrich (St. Louis, MO, USA). DOX was obtained from Bairui Biotechnology (Nanjing, China). Goat Anti-Rabbit IgG H&L fluorescein isothiocyanate (FITC) was from Abcam (Cambridge, UK). MTS and bovine serum albumin (BSA) were purchased from Biosharp (Hefei, Anhui, China), while radioimmunoprecipitation assay (RIPA) and phenylmethylsulfonyl fluoride (PMSF) were from Dingguo Biotechnology (Beijing, China).

## Cell Culture

Human breast cancer cells (MCF-7 and MDA-MB-231) were obtained from American Type Culture Collection (Manassas, VA, USA). MCF-7 cells were cultured in RPMI 1640 with 10% FBS, and MDA-MB-231 cells were cultured in DMEM with 10% FBS. DOX multidrug-resistant cell line MCF-7/ADR cells were purchased from Nanjing BERKE Biology (Nanjing, China). MCF-7/ADR cells were cultured in RPMI 1640 with 10% FBS and 1.25 μg/ml DOX. All cell lines were cultured in a humid incubator (37°C and 5% $CO_2$).

## Cell Viability Assay

MCF-7 cells, MDA-MB-231 cells, and MCF-7/ADR cells were seeded in a 96-well plate at a density of $1 \times 10^4$/well. After treating with agents, one solution reagent (MTS, 1:10 dilution in serum-free medium, Promega) was added and incubated at 37°C for 4 h. Finally, the cell viability was evaluated through measuring the optical density (OD) at 490 nm using the BioTek Synergy2 microplate reader (BioTek Instruments, VT, USA).

## High-Performance Liquid Chromatography Analysis

Cell lysates were prepared in the extraction buffer [containing methanol:water (1:1, v/v)] in the cold room for 15 min, followed by scraping and centrifuging at 17,000 g for 10 min. The concentration of CPT in the lysates was measured using HPLC (Waters E2695). Samples were injected into a 4.6 mm × 250 mm Stable Bond column (ZORBAX Eclipse Plus C18; Agilent, CA, USA). The chromatography was run starting with 45% solution A (methanol) and 55% solution B ($H_2O$), and the volume of solution A was raised to 50%, 90%, and 100% at 10, 30, and 35 min, respectively. Finally, 45% solution A was used at 45 min and until the end of the assay. Data were collected and analyzed by Analyst Software (AB Sciex).

**A**

| Cell | Drug Concentration | CPT-5μmol/L | CPT-10μmol/L | CPT-20μmol/L |
|---|---|---|---|---|
| MCF-7 | Intracellular | 4.268±0.111 | 9.377±0.189 | 19.898±0.327 |
| | Extracellular | 4.339±0.017 | 8.672±0.115 | 18.977±0.351 |
| MDA-MB-231 | Intracellular | 3.502±0.034 | 6.313±0.189 | 4.400±0.219 |
| | Extracellular | 4.845±0.496 | 9.063±1.795 | 18.747±0.243 |

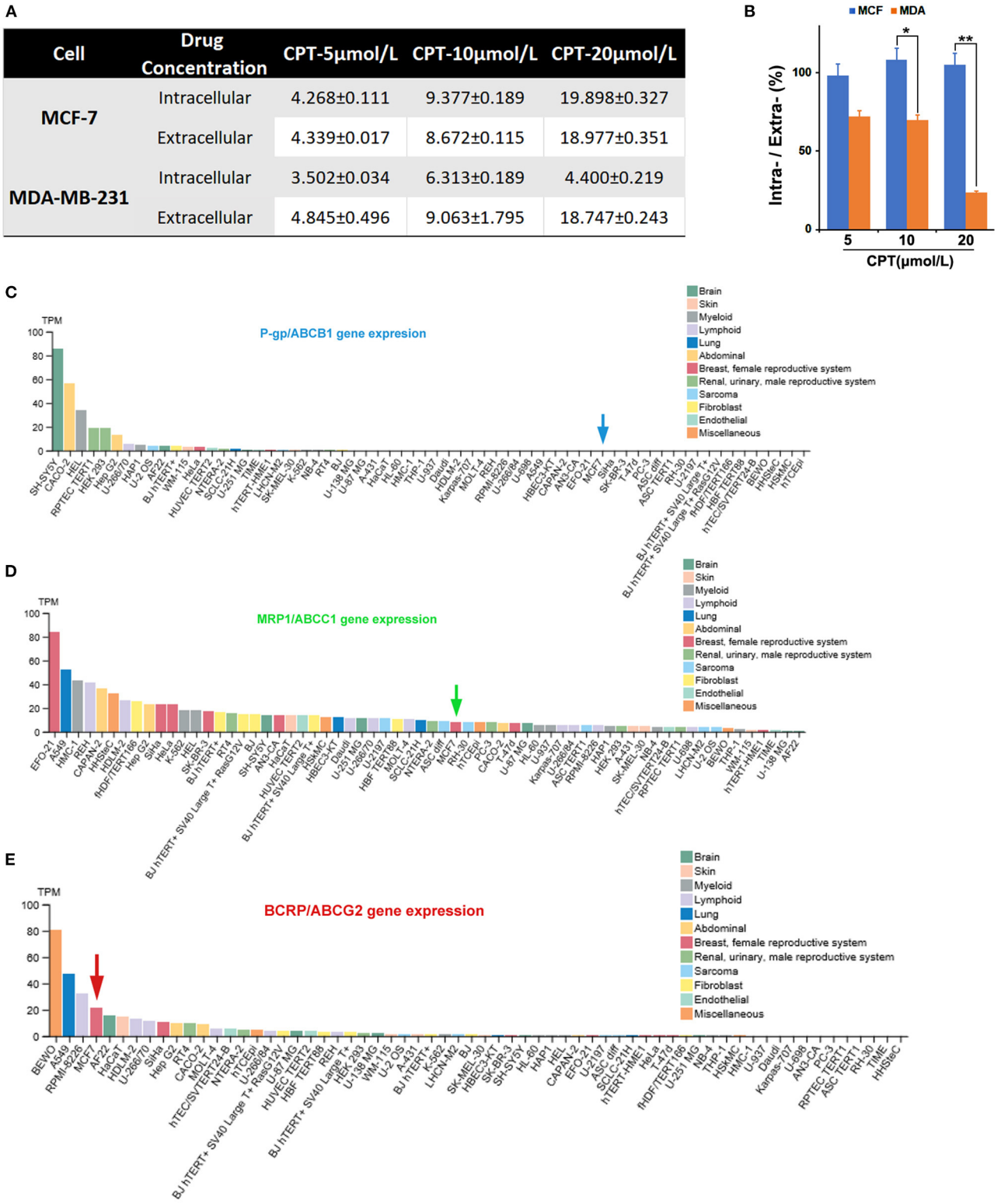


**FIGURE 1 |** Intracellular accumulation of cryptotanshinone (CPT) in MCF-7 cells is possibly related to breast cancer resistance protein (BCRP). **(A)** The indicated breast cancer cells were treated with CPT (5, 10, 20 μmol/L) for 8 h. Then, the medium was collected, and the intracellular and extracellular CPT concentrations (μmol/L) were detected by high-performance liquid chromatography (HPLC). The data are presented as mean ± SD ($n = 3$). **(B)** Statistical analysis of the ratio of intracellular CPT/extracellular CPT × 100%, $n = 3$, $^{*}P < 0.05$, $^{**}P < 0.01$. **(C–E)** The expression of ABCB1/ABCC1/ABCG2 mRNA levels in different cells based on the Human Protein Atlas database analysis.

## Molecular Docking Assay

The three-dimensional structures of CPT and MX were obtained from PubChem Compound database (https://www.ncbi.nlm.nih.gov/pccompound/). Meanwhile, the structure of BCRP/ABCG2 [Protein Data Bank (PDB) ID: 6FFC with resolution of 3.56 Å] was retrieved from the Research Collaborator for Structural Bioinformatics PDB (Anonymous, www.rcsb.org). The molecular docking between the two compounds and BCRP/ABCG2 was evaluated by Discovery Studio (DS) 3.5 using the CDOCKER Protocol under the protein–ligand interaction section after preparing the protein and ligands. The poses were scored by CDOCKER interaction energy, and the binding sites were also shown.

## Plasmids and Transient Transfection

The ERα shRNA (sense: 5′-GATCCCGCTACTGTTTGCTCCTAACCTCGAGGTTAGGAGCAAACAGTAGCTTTTTGGAT-3′; Antisense: 3′-AGCTATCCAAAAAGCTACTGTTTGCTCCTAACCTCGAGGTTAGGAGCAAACAGTAGCGG-5′) (16) was synthesized by Genechem (Shanghai, China). MCF-7 cells were planted in six-well plates at a density of $3 \times 10^5$ cells/well. The ERα shRNA plasmid (888 ng/μl) was diluted in Opti-MEM (100 μl) and then mixed with Lipofectamine 2000 reagent (Life Technologies, NY, USA). After 6-h transfection, culture medium was changed to normal medium and sequentially incubated in 37°C for 16 h. The Con-shRNA (535 ng/μl) was used as a negative control.

## Mitoxantrone/Rhodamine 123/Doxorubicin/Topotecan Efflux Experiment

The MX/rhodamine 123 (Rh123)/DOX/topotecan (TOPO) efflux experiment was performed as described (17). Briefly, breast cancer cells ($3 \times 10^5$ cells per well) were seeded in six-well plates and incubated overnight. At about 80% confluence, the cells were with CPT for 8 h. Then, the cells were collected by centrifugation in 2-ml tubes, and each tube was added with 1 ml of serum-free medium to homogenize the cells. All the cells except the blank group were added with the corresponding compounds and incubated in the dark under 37°C for 30 min (the MX-positive group was treated with KO143 10 μmol/L for 15 min in advance). Next, all cells were centrifuged (1,500 rpm, 4°C, 5 min), and the supernatants were discarded. The cells were washed with pre-cooled PBS twice. Finally, the cells were resuspended in 400 μl pre-cooled PBS. The fluorescence accumulation of MX/Rh123/DOX/TOPO is detected with a BD Accuri C6 Flow Cytometer (Becton, Dickinson and Company, NY, USA). The detection channel was FL-4/FL-1/FL-2. The wavelength of Ex/Em for MX/Rh123/DOX/TOPO is, respectively, 488/660 nm, 488/525 nm, 488/575 nm, and 488/525 nm.

## Non-Reducing Gradient Gel Electrophoresis

The non-reducing gradient gel electrophoresis was performed as described (18). Membrane and cytoplasmic proteins were extracted as described in *Extraction of Cell Membrane and Cytoplasmic Proteins*. The protein samples were denatured with a loading buffer containing no reducing agents such as dithiothreitol (DTT) or 2-mercaptoethanol (2-ME). Samples were boiled at 100°C for 15 min. The remaining steps were essentially identical to those in Western blotting. When detecting the BCRP polymer, membrane proteins were separated by 6% Tris-glycine sodium dodecyl sulfate-polyacrylamide gel electrophoresis (SDS-PAGE), and a multicolor broad range protein ladder ranging from 10 to 260 kDa (Thermo Scientific, Waltham, MA, USA) was used.

## Fluorescence Resonance Energy Transfer Microscopy Imaging

The fluorescence resonance energy transfer (FRET) was performed as described (19). The pCFP-ABCG2 and pYFP-ABCG2 plasmids were generously provided by Jun Wang (Shanghai Institute of Materia Medica, Chinese Academy of Sciences, Shanghai, China). Cells were seeded in a 35-mm confocal culture dish, and when the cell confluence reached 70%, the plasmid transfection was performed following the protocol provided by the manufacturer (Invitrogen, NY, USA). Plasmid pCFP-ABCG2 (191.3 ng/μl), pYFP-ABCG2 (399.3 ng/μl), and 3 μl Lipofectamine 2000 reagent (Life Technologies, NY, USA) were, respectively, mixed with 50 μl Opti-MEM medium. After incubating for 5 min at room temperature, the above two mixtures were lightly mixed and cultured for 10 min at room temperature. Finally, the 100 μl mixture was added dropwise to 1 ml serum-free medium, and 100 μl FBS was added 6 h later. After incubation for 16 h at 37°C, CPT was added. Finally, the living cell FRET images were collected under an inverted fluorescence microscope (Leica Microsystems, Solms, Germany) and analyzed by ImageJ software.

## Immunofluorescence Staining

Cells were plated on glass coverslips in six-well plates and then treated with corresponding compounds. The cell membrane was stained with 10 μmol/L DiI (Beyotime Biotechnology, Shanghai, China) for 10 min at 37°C. Then, cells were fixed in 4% paraformaldehyde for 20 min and blocked in BSA (1% BSA dissolved in PBS). The cells were incubated with the corresponding primary antibody (1:100 dilution) overnight at 4°C, followed by incubation with goat anti-rabbit IgG H&L FITC (1:1,000 dilution) for 2 h and Hoechst nuclear dye for 10 min in the dark. The images were obtained from a laser scanning confocal microscope (Leica TCS SP5 X, Solms, Germany).

## Extraction of Cell Membrane and Cytoplasmic Proteins

Cell membrane protein and cytoplasmic protein were extracted according to the protocol provided by the manufacturer (Beyotime Biotechnology, Shanghai, China). In brief, cells were seeded into 150-mm culture dishes (Lab services, Waltham, MA, USA) and treated with compounds when the cell coverage area reached about 80%. After treatment for 8 h, the cells were washed once with ice PBS and were then collected with a scraper,

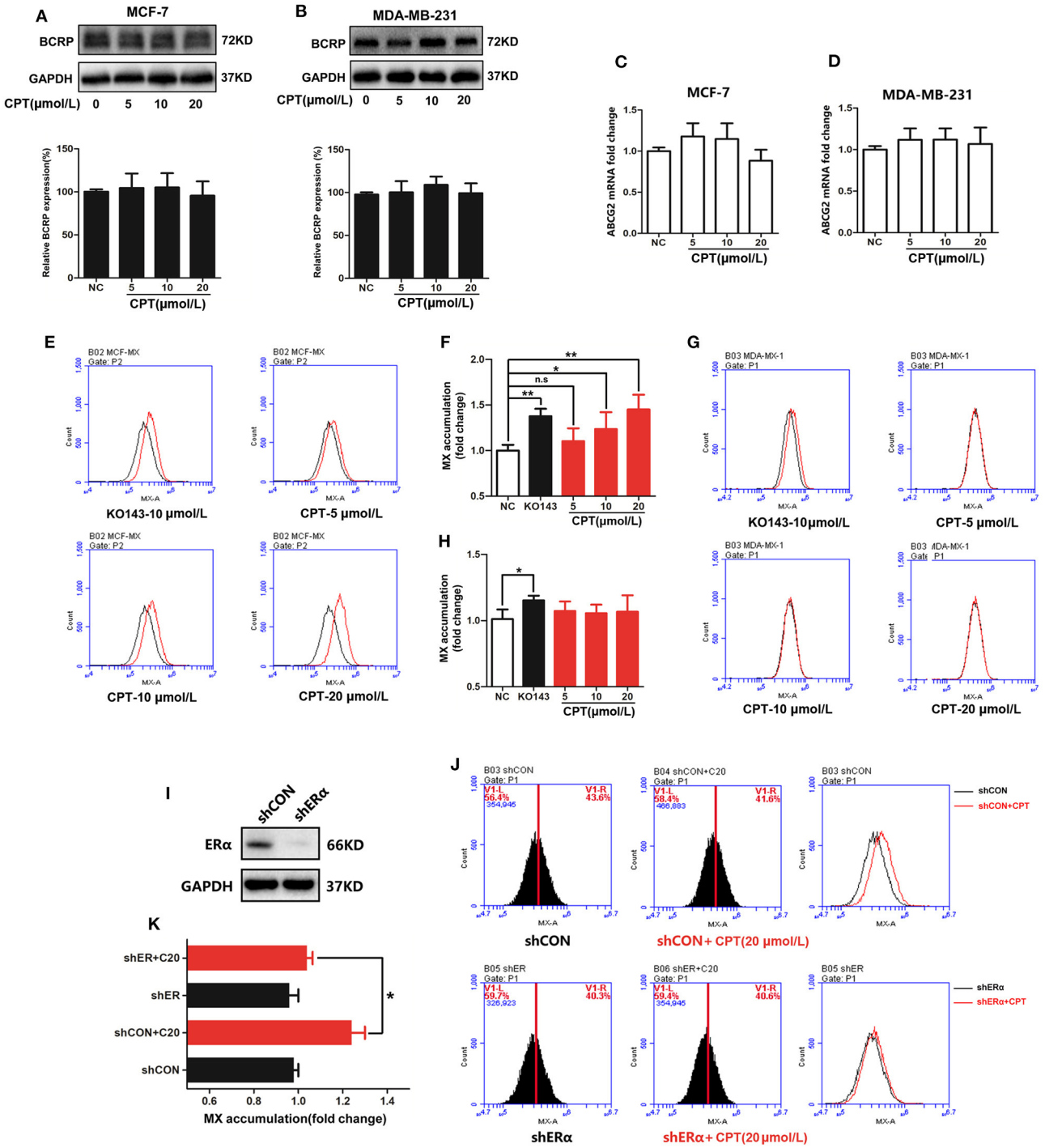


**FIGURE 2 |** Cryptotanshinone (CPT) inhibits the efflux function of breast cancer resistance protein (BCRP) in MCF-7 cells. Western blot analysis of the protein levels of BCRP in MCF-7 **(A)** and MDA-MB-231 cells **(B)** treated with CPT for 8 h. Q-PCR analysis of the mRNA levels of BCRP in MCF-7 **(C)** and MDA-MB-231 cells **(D)** treated with CPT for 8 h. The mitoxantrone (MX) fluorescence accumulation was detected in MCF-7 **(E)** and MDA-MB-231 cells **(G)** treated with CPT for 8 h by flow cytometry. The fluorescence intensity represents the activity of BCRP efflux. The quantitated results are shown in panels **(F,H)**, respectively, vs. negative control (NC), $n = 3$, $^{*}P < 0.05$, $^{**}P < 0.01$. **(I)** MCF-7 cells with shCON or with shERα were, respectively, treated with or without CPT (20 μmol/L) for 8 h and then **(J)** analyzed for MX fluorescence accumulation by flow cytometry. The quantitated results are shown in **(K)**, $n = 3$, $^{*}P < 0.05$.

followed by centrifuging (4°C, 600 g, 5 min). The supernatants were discarded, and the cells were resuspended in reagent A containing PMSF (1:100 dilution) and incubated in an ice bath for 10–15 min. Then, the cells were treated with liquid nitrogen, freezing and thawing twice, and centrifuged (4°C, 700 g, 10 min). The supernatants were collected and centrifuged (4°C, 14,000 g, 30 min) to precipitate cell membrane fragments. The supernatants contained cytoplasmic protein. The pellets were resuspended in reagent B and vortexed for 5 s and incubated in an ice bath for 5–10 min. After centrifugation (4°C, 14,000 g, 5 min), the supernatants contained cell membrane protein, which were stored at −80°C.

## Western Blotting Analysis

Western blot was performed and analyzed as described (15). The primary antibodies were used as follows: ERα, BCRP/ABCG2, MDR1/ABCB1 (Cell Signaling Technology, Danvers, MA, USA), and glyceraldehyde 3-phosphate dehydrogenase (GAPDH; Bioworld Technology, MN, USA). ABCC1 (Affinity, MA, USA) HRP-Goat Anti-rabbit IgG (H+L) was purchased from Bioworld Technology Company.

## RNA Isolation and Real-Time PCR

Total RNA was extracted from MCF-7 or MDA-MB-231 cells with TRIzol (Vazyme, Nanjing, China) according to the manufacturer's guidelines and reversely transcribed to cDNA by HiScript® II Reverse Transcriptase (Vazyme, Nanjing, China). Real-time PCR was executed of the ChamQTM SYBR® qPCR Master Mix (Vazyme, Nanjing, China) using Applied Biosystems 7500 Real-Time PCR Systems (Thermo Scientific, Waltham, MA, USA). GAPDH served as a reference control, and mRNA levels were expressed as fold changes after normalizing to GAPDH. The primers (Sangon Biotech, Shanghai, China) used are listed in **Supplementary Table 1**.

## Statistical Analysis

The results were determined using Student's *t*-test (two-group comparison) and ANOVA test by GraphPad Prism 5.0 software. $P < 0.05$ was considered statistically significant.

# RESULTS

## Intracellular Accumulation of Cryptotanshinone Is Possibly Related to Breast Cancer Resistance Protein

In order to understand why MCF-7 and MDA-MB-231 cells show different sensitivity to CPT except the status of the ERα, we first detected the intracellular and extracellular CPT levels in the two cell lines by HPLC. As shown in **Figure 1A**, treatment with CPT dose-dependently increased the intracellular and extracellular levels of CPT robustly and evenly in MCF-7 cells, but not in MDA-MB-231 cells. Of note, the increase in the intracellular CPT level was greatly less than that of the extracellular CPT level in MDA-MB-231 cells. This difference was significant when MDA-MB-231 cells were treated with CPT at 10 or 20 μmol/L (**Figure 1B**). The result suggests that there is a certain transporter that regulates the intake and pumping process of CPT in the cells. The most studied transporter proteins are ATP-binding transporters, such as P-gp, MRP1, and BCRP (5). We analyzed the expression of these three transporters in many cell lines from multi human tissues with the Human Protein Atlas Database. The results indicated that BCRP/ABCG2 was highly expressed in MCF-7 cells (**Figure 1C**), whereas P-gp/ABCB1 was almost not expressed and MRP1/ABCC1 was lowly expressed in the cells (**Figures 1D,E**). Accordingly, we speculated that BCRP may play an important regulatory role in transporting CPT across the membrane.

## Cryptotanshinone Inhibits Efflux Function of Breast Cancer Resistance Protein, Depending on the Expression Level of Estrogen Receptor α in Cells

The close relationship between CPT and BCRP led us to further explore the specific regulation of CPT on BCRP. Firstly, CPT had no significant effect on the total protein expression of BCRP in both MCF-7 and MDA-MB-231 cells (**Figures 2A,B**). In addition, CPT did not significantly affect ABCG2 mRNA levels in MCF-7 and MDA-MB-231 cells by q-PCR (**Figures 2C,D**; **Supplementary Table 1**). Considering that the most important ability of BCRP is to transport substrates, next we examined whether CPT influences the function of BCRP. For this, we evaluated the efflux function of BCRP through the MX efflux experiment (20). Compared with the positive control Ko143, a selective BCRP inhibitor, the fluorescence peak of CPT-treated group in MCF-7 cells was also significantly shifted to the right (**Figures 2E,F**). The increased fluorescence abundance of intracellular MX indicated that the efflux function of BCRP was inhibited. However, this effect was not observed in MDA-MB-231 cells (**Figures 2G,H**). So we wondered if the difference between the two cells might be related to the expression of ERα. To this end, the expression of ERα was silenced in MCF-7 cells, followed by treatment with CPT for 8 h (**Figure 2I**). Interestingly, knockdown of ERα partially decreased the accumulation of MX induced by CPT treatment (**Figures 2J,K**). These results indicate that CPT does not affect the cellular protein and mRNA levels of BCRP/ABCG2 but is able to inhibit the efflux function of BCRP in MCF-7 cells, and this effect is closely relevant with the presence of ERα.

## Cryptotanshinone Reduces the Level of Breast Cancer Resistance Protein on the Cell Membrane

BCRP is a semi-transporter on the cell membrane and functions as an oligomer (21). Next, we examined whether CPT affected the level and oligomerization of BCRP on the cell membrane. Our fractionation experiment showed that CPT treatment significantly reduced the level of BCRP on the cell membrane rather than in the cytoplasm in MCF-7 cells (**Figures 3A,B**). However, CPT treatment had no effect on the level of BCRP on the cell membrane or in the cytoplasm of MDA-MB-231 cells (**Figures 3C,D**). The results indicated an inhibitory effect of CPT on the function of BCRP in ER-positive breast cancer cells. This was further verified by our laser confocal scanning microscope

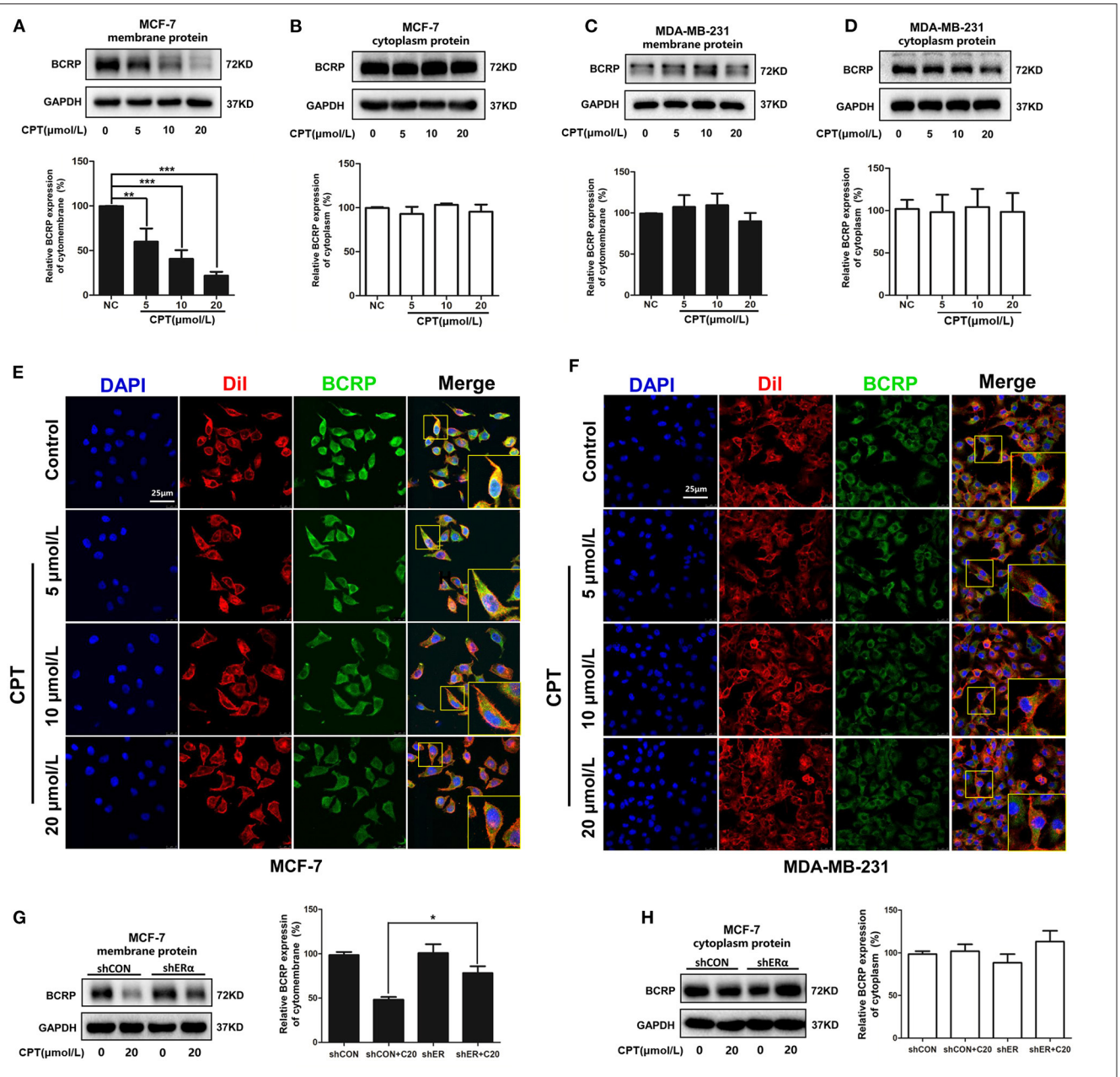


**FIGURE 3 |** Cryptotanshinone (CPT) reduces the expression and localization of breast cancer resistance protein (BCRP) on the cell membrane of MCF-7 cells. Western blot analysis of BCRP in the cell membrane and cytoplasm of MCF-7 **(A,B)** and MDA-MB-231 cells **(C,D)** treated with CPT for 8 h vs. negative control (NC), $n = 3$, $^{**}P < 0.01$, $^{***}P < 0.001$. Immunofluorescence staining for BCRP in MCF-7 **(E)** and MDA-MB-231 cells **(F)** treated with CPT for 8 h. Cell membrane was labeled with Dil. Scale bar, 25 μm. **(G,H)** MCF-7 cells with shCON or with shERα, were, respectively, treated with or without CPT (20 μmol/L) for 8 h, and then cell membrane protein and cytoplasmic protein were extracted to analyze the levels of BCRP. $n = 3$, $^{*}P < 0.05$.

(LCSM) experiment. As seen in **Figure 3E**, when MCF-7 cells were treated with high concentrations of CPT (10 and 20 μmol/L), the enrichment of FITC-BCRP on the cell membrane dyed with Dil was obviously inhibited. But this phenomenon was not observed in MDA-MB-231 cells (**Figure 3F**). Additionally, we confirmed the role of ERα during this process again. Compared with membrane BCRP expression in shCON MCF-7 cells, CPT inhibition of BCRP was partially enriched in ERα-silenced MCF-7 cells (**Figure 3G**). Cytoplasm BCRP had no significant change (**Figure 3H**). Collectively, our observations support the notion that CPT inhibits the efflux function of BCRP through reducing its expression on breast cancer cell

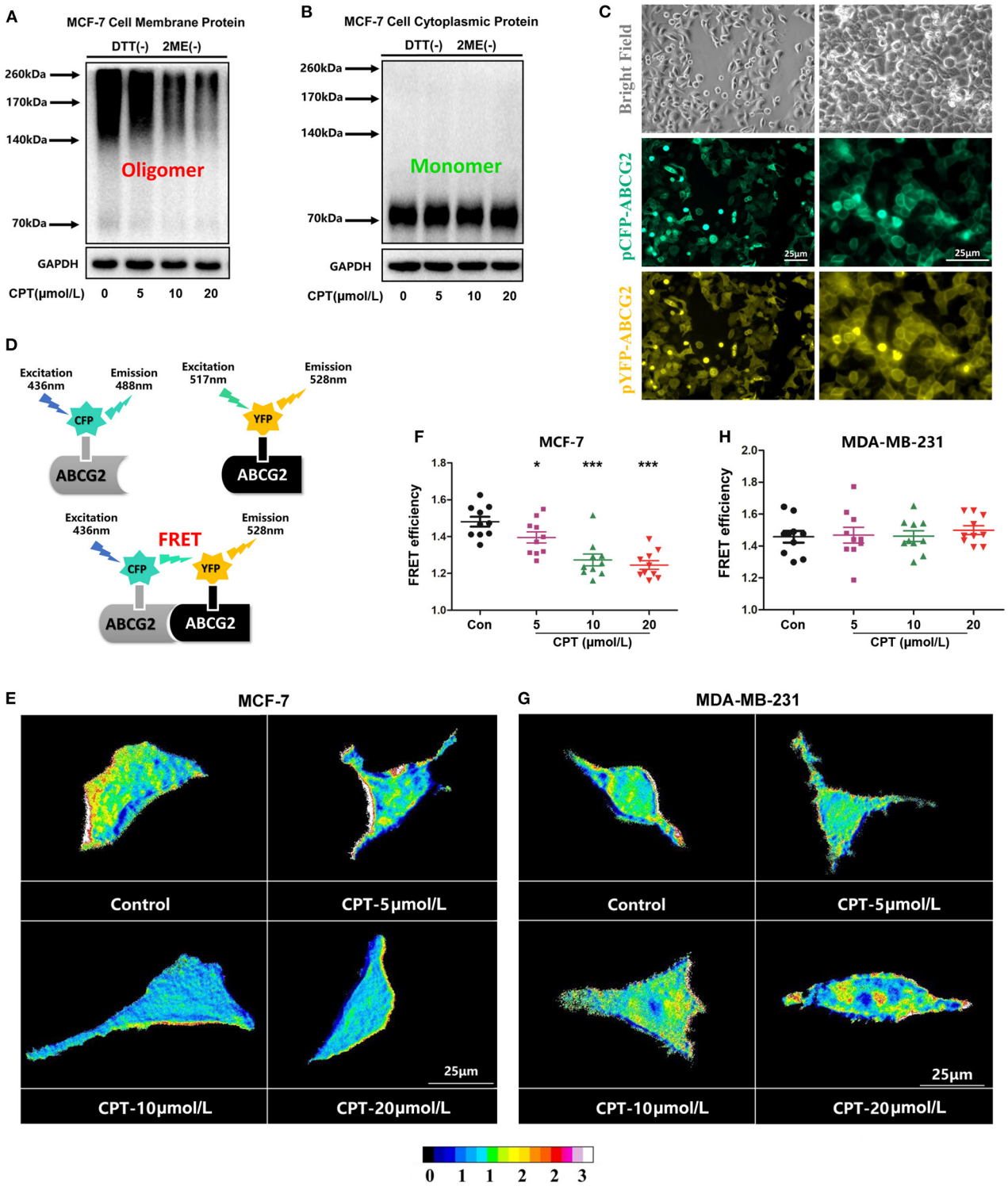


**FIGURE 4 |** Cryptotanshinone (CPT) inhibits breast cancer resistance protein (BCRP) oligomer formation in MCF-7 cells. **(A,B)** MCF-7 cells were treated with or without CPT (20 μmol/L) for 8 h. The membrane protein or cytoplasmic protein was extracted to detect the oligomer formation of BCRP under a non-reducing condition. **(C)** MCF-7 cells were transfected with pCFP-ABCG2 and pYFP-ABCG2 plasmids, respectively, for 24 h. The expression of BCRP on the cell membrane was observed under a microscope (200× and 400× magnification). **(D)** Schematic diagram of fluorescence resonance energy transfer (FRET) experiment; pCFP and pYFP are the donor and acceptor of fluorescence energy, respectively. When their distance reached within 10 nm, the FRET phenomenon would happen. FRET was applied to analyze the oligomer formation of BCRP in MCF-7 cells **(E,G)** and MDA-MB-231 cells **(F,H)** treated with CPT in the state of living cells. Images are shown as 16 colors map, and the color represents the degree of FRET efficiency. The quantitated data of FRET are vs. control, $n = 10$, $^{*}P < 0.05$, $^{***}P < 0.001$.

membrane, which is dependent on the presence of ERα in the cells.

## Cryptotanshinone Inhibits the Oligomer Formation of Breast Cancer Resistance Protein on the Cell Membrane

Next, we evaluated the effect of CPT on the oligomerization of BCRP using the assay of non-reducing gradient gel electrophoresis. As shown in **Figure 4A**, BCRP on the membrane of MCF-7 was primarily in the form of dimers and oligomers (molecular weight over 140 kDa). Oligomer formation was significantly inhibited by treatment with CPT (10 and 20 μmol/L). BCRP was also detected in the cytoplasm of MCF-7 cells, but its main form is a non-functional monomer with a molecular weight of 70 kDa (**Figure 4B**). Besides, after transfection, pCFP-ABCG2 and pYFP-ABCG2 were successfully expressed on the cell membrane of MCF-7 or MDA-MB-231 cells (**Figure 4C**). Our FRET assay revealed that CPT inhibited the BCRP oligomer formation on the cell membrane (**Figure 4D**), which was consistent with the observation from the non-reducing electrophoresis. CPT was able to interfere with BCRP oligomer formation in MCF-7 cells (**Figures 4E,F**), but not in MDA-MB-231 cells (**Figures 4G,H**). These data indicate that CPT inhibits the oligomer formation of BCRP on the cell membrane, thus impeding its efflux function.

## Cryptotanshinone Inhibits Breast Cancer Resistance Protein in Doxorubicin-Resistant Breast Cancer Cells Independent of Estrogen Receptor α

It has been noticed that DOX-resistant breast cancer cells MCF-7/ADR are sensitive to CPT (16). As indicated in **Figure 5A**, a high level of BCRP expression was detected in MCF-7/ADR cells, but very little in MDA-MB-231 cells. Next, we explored whether the cytotoxic effect of CPT on MCF-7/ADR cells is also dependent on inhibition of BCRP. Firstly, HPLC analysis showed that the concentration of intracellular CPT was nearly equivalent to that of extracellular CPT in MCF-7/ADR cells (**Figure 5B**). This result suggests that the transporters are involved in the inhibition of MCF-7/ADR cell proliferation by CPT. Despite the high expression of P-gp and MRP1 in MCF-7/ADR cells, CPT did not apparently alter the protein levels of P-gp and MRP1 either on the cell membrane or in the cytoplasm, as detected by Western blotting (**Supplementary Figures 1A–D**). In line with this, the flow cytometric assay indicated that CPT did not affect the efflux functions of P-gp and MRP1 (**Supplementary Figures 1E–G**). So, after excluding P-gp and MRP1 proteins, we focused on BCRP. Further experiments showed that CPT had no significant effect on the total cellular protein expression of BCRP in MCF-7/ADR cells (**Figure 5C**) but strongly inhibited the membrane protein expression of BCRP even at a low concentration (5 μmol/L) (**Figure 5D**). CPT treatment increased the BCRP content in the cytoplasm to some extent (**Figure 5E**). Similarly, the flow cytometry results showed that CPT inhibited the efflux function of BCRP in MCF-7/ADR cells, especially at a high concentration (20 μmol/L) (**Figures 5F,G**). FRET experiments also demonstrated that CPT inhibited the oligomer formation of BCRP in MCF-7/ADR cells (**Figures 5H,I**). It is worth noting that MCF-7/ADR cells have undergone many changes in morphology, characteristics, and functions compared with parental MCF-7 cells, especially MCF-7/ADR cells are ERα-negative. This suggests that CPT is also able to inhibit the function of BCRP in ERα-negative cells with high expression of BCRP.

BCRP consists of an NBD and a TMD (7), as well as substrate-binding regions TM1-3 (**Figure 5J**). To further determine whether CPT can be recognized by BCRP and extracellularly pumped out, molecular docking was used to dock MX, a substrate of BCRP, with the 3D structure of BCRP (**Supplementary Figures 2A,B**). After confirming the drug-binding pocket, the 3D structure of CPT was embedded for docking (**Figures 5K,L**). As shown in **Figure 5K** and **Supplementary Figure 2A**, through the intermolecular force comparison and calculation, the common binding sites were found to be VAL401, PHE439, LEU405, PHE432, and PHE439. The results indicated that CPT can be recognized by BCRP and pumped out of cells. The whole transport simulation process is shown in **Figure 5M**. When the substrate is bound into the cavity 1, the conformation of the protein changes with the transition from inward open to outward open. NDB combines with ATP hydrolysis to provide energy for conformational changes in the protein, while the substrate is transferred into the cavity 2, which has a relatively weak binding force, and the drug can finally be pumped out. Taken together, CPT can bind to BCRP and inhibit its efflux function, leading to an accumulation of CPT in MCF-7 cells.

## Cryptotanshinone Enhances the Sensitivity of Cancer Cells to Chemotherapeutic Drugs

Based on the above results, we reasoned that CPT may be synergistic with BCRP efflux anticancer drugs. To test this, we selected two of the most classic BCRP efflux drugs, MX and TOPO (22). At first, we screened the concentration of CPT and the positive control drug Ko143. Then, we carried out a 72-h co-incubation experiment at a concentration of 1 μmol/L, which had no significant effect on the proliferation of MCF-7/ADR cells (**Figures 6A,B**). Compared with the single treatment with MX (**Figure 6C**) or TOPO (**Figure 6D**), the co-treatment with CPT significantly attenuated drug resistance at higher doses (MX 10 μmol/L, TOPO 0.5 μmol/L), and the inhibition rate of proliferation was under 50%, close to the co-treatment with Ko143 (**Figures 6E,F**). And the $IC_{50}$ of CPT with MX is about 26 times of that of MX alone; CPT with TOPO is about 16 times of that of TOPO treatment alone. Meanwhile, subsequent flow cytometry showed that when MCF-7/ADR cells were co-treated with CPT and MX, the accumulation of MX increased in the cells, i.e., the functional inhibition of BCRP by CPT made the drug efflux reduced (**Figures 6G,H**). Similar results were observed in the co-treatment with CPT and TOPO (**Figures 6I,J**). The

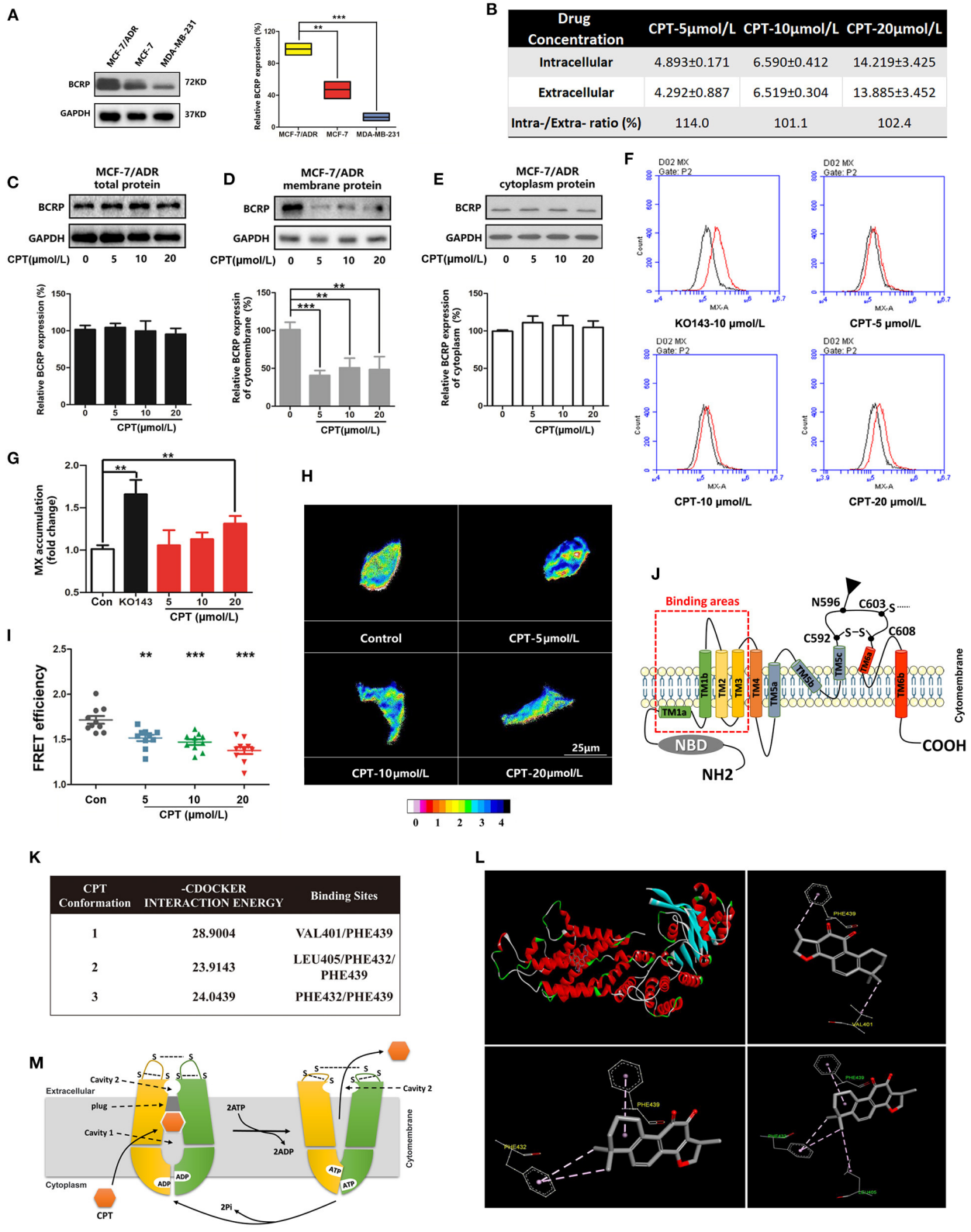


**B**

| Drug Concentration | CPT-5μmol/L | CPT-10μmol/L | CPT-20μmol/L |
|---|---|---|---|
| Intracellular | 4.893±0.171 | 6.590±0.412 | 14.219±3.425 |
| Extracellular | 4.292±0.887 | 6.519±0.304 | 13.885±3.452 |
| Intra-/Extra- ratio (%) | 114.0 | 101.1 | 102.4 |

**K**

| CPT Conformation | -CDOCKER INTERACTION ENERGY | Binding Sites |
|---|---|---|
| 1 | 28.9004 | VAL401/PHE439 |
| 2 | 23.9143 | LEU405/PHE432/ PHE439 |
| 3 | 24.0439 | PHE432/PHE439 |

**FIGURE 5 |** Cryptotanshinone (CPT) inhibits membrane expression and function of breast cancer resistance protein (BCRP) in MCF-7/ADR cells. **(A)** Western blot analysis of BCRP in different breast cancer cells. $n = 3$, $^{**}P < 0.01$. **(B)** High-performance liquid chromatography (HPLC) analysis of the intracellular and extracellular concentrations (μmol/L) of CPT in MCF-7/ADR cells treated with CPT for 8 h. The data are presented as mean ± SD. Western blot analysis of the BCRP total protein *(Continued)*

**FIGURE 5 | (C)**, membrane protein **(D)**, cytoplasm protein **(E)** expression in MCF-7/ADR cells treated with CPT for 8 h. **(F)** Mitoxantrone (MX) fluorescence accumulation was detected by flow cytometry in MCF-7/ADR cells treated with CPT for 8 h, and **(G)** the quantitated data were vs. control, $n = 3$, $^{**}P < 0.01$. **(H)** Fluorescence resonance energy transfer (FRET) analysis of the oligomer formation of BCRP in MCF-7/ADR cells treated with CPT in the state of living cells. Images are shown as 16 colors map, and the color represents the degree of FRET efficiency. **(I)** The quantitated data were vs. control, $n = 10$, $^{**}P < 0.01$, $^{***}P < 0.001$. **(J)** Schematic diagram of BCRP structure; TM1, TM2, TM3 are substrate-binding regions. **(K)** The molecular docking analysis about the sites of CPT docking with BCRP and their interaction energy. **(L)** The 3D structure of CPT docking with BCRP substrate-binding pocket, and three stable conformations and binding sites are listed. **(M)** The whole process of BCRP transporting substrates.

findings indicate that CPT is able to enhance the sensitivity of cancer cells to chemotherapeutic agents that can be pumped out by BCRP, reversing the MDR.

## DISCUSSION

The role of ERα in breast cancer is well-understood. ER expression is a critical factor for hormonal therapy and also considered as a prognostic marker. Overall, about 75% of breast cancer patients are ER-positive and treated with anti-estrogen drugs, such as the selective estrogen receptor modulator tamoxifen. However, a part of ERα-positive breast cancers can become resistant to hormone therapy partly due to loss of ERα expression, so a majority of these patients may suffer a relapse in 5 years (23). Furthermore, many researchers have also found that some chemotherapeutic agents may be less effective in ERα-positive breast cancer patients than ERα-negative ones (24). These bidirectional results imply the complex role of ERα in the resistant breast cancer.

Generally, breast cancer may develop MDR. Several factors including ABC transporters (5), mutations of targeted oncogenes, survived cancer stem cells (CSCs) (25), and activated cell growth factors are possibly involved in MDR. Especially BCRP, one type of the ABC transporters is an important factor controlling the breast cancer MDR. Indeed, the relationship between ERα and BCRP expression has been investigated (26). The estrogen response element (ERE) and progesterone response element (PRE) exist in the promoter region of BCRP (27). The excessive transcriptional expression of this type of response element may play a major role in the development of breast cancer MDR (11). The MDR is a multi-factor, multi-way, multi-stage, and comprehensive process (28). This study focused on BCRP primarily and expected to look for new applications of CPT to reverse breast cancer MDR.

In the previous research, we have proven that CPT is not a selective estrogen receptor inhibitor, though it can bind ERα and produce tamoxifen-like effects on cancers (16). More importantly, CPT inhibits DOX-resistant MCF-7/ADR cells, although it can activate MAPK and AKT, suggesting that CPT's overcoming the resistance is not through suppressing the activation of MAPK (29) and AKT (30) but by targeting other factors. So we studied if BCRP is the key molecule targeted by CPT. At present, numerous BCRP inhibitors including highly selective inhibitors and non-selective inhibitors have been identified, and some highly selective inhibitors should be prospectively applied in the clinic for reversing the MDR (31). However, the molecular mechanism of BCRP inhibition is complex. Some compounds inhibit BCRP through inhibiting its ATPase activity, such as FTC, Ko134, and Ko143, while others as BCRP substrates can bind to BCRP and competitively suppress the transport function of BCRP (9, 31). In this study, we found that CPT was able to interfere with the oligomer formation of BCRP on the cell membrane, thereby impeding its efflux function. On the one hand, in ERα-positive MCF-7 cells, inhibition of BCRP oligomer formation was dependent on the status of ERα, as downregulation of ERα attenuated CPT-induced accumulation of MX in the cells. How ERα mediates this process is unclear. On the other hand, in the ERα-negative MCF-7/ADR cells with a high expression of BCRP, the expression and oligomer formation of BCRP on the cell membrane were both inhibited by CPT. However, in the ERα-negative MDA-MB-231 cells with low expression of BCRP, CPT did not affect cell proliferation. These data suggest that CPT reversing resistance of breast cancer is dependent on the expression level of BCRP: the higher expression of BCRP, the stronger inhibitory effect of CPT on breast cancer cells. Although CPT is an anti-estrogen compound, it can directly bind BCRP and block its efflux function. It has been observed that breast cancer cells can switch between ERα and ErbB signaling to induce resistance, and combined inhibition of the two pathways can postpone the development of resistance (32). From MCF-7 to MCF-7/ADR, ERα is nearly undetectable but BCRP is overexpressed. Together, these observations suggest that there are two modes of CPT inhibition of BCRP: ERα-dependent and ERα-independent. CPT switches the targets between ERα and BCRP to attenuate MDR.

Increasing evidence indicates that a drug designed for individual molecular target is generally hard to conquer multigenic diseases such as cancer, diabetes, hypertension, and neural diseases (33, 34). So combined drugs that simultaneously affect multiple targets are more beneficial to control complex disease and reverse drug resistance. If a compound could target multiple proteins under various cell circumstances, the occurrence of resistance would also be decreased to minimal extent. We believed that CPT is a multi-target compound, since it has been shown to target a number of molecules such as STAT3 (12), AMPK (15), MAPK (14), ER (16), and nuclear factor erythroid-2 related factor 2 (NRF2) (35). Though different action mechanisms have been proposed for CPT, our findings indicate that ER and BCRP can be structurally bound with CPT. **Figure 7** illustrates the molecular process of CPT inhibition of BCRP in an ERα-dependent and -independent manner.

At present, designing the multi-target molecules based on the systems biology, structural biology, and chemical informatics has become an optimal way to develop a new drug (34). CPT as a multi-target compound is a potential candidate drug, particularly considering its selective inhibition of BCRP

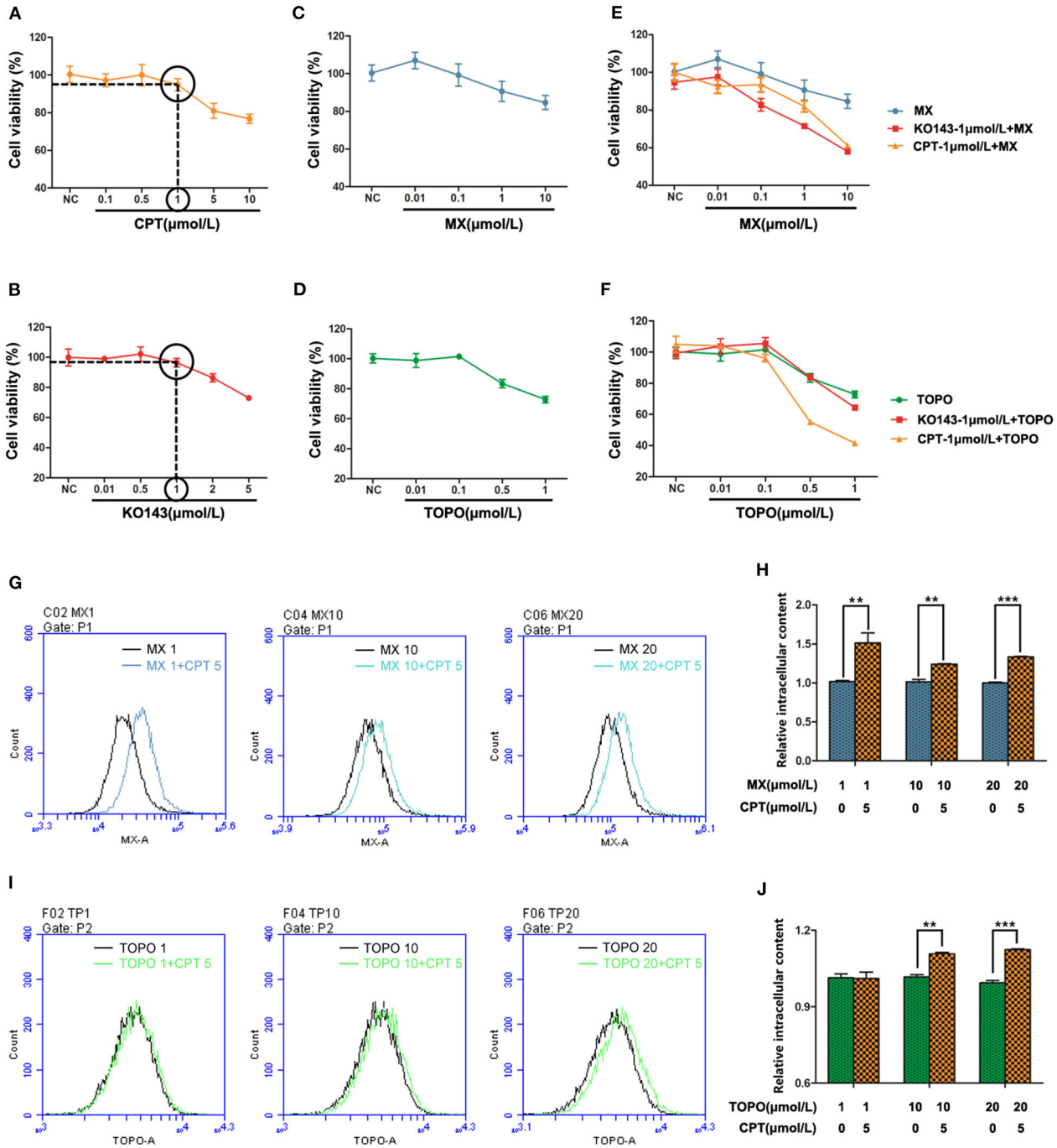


**FIGURE 6 |** Cryptotanshinone (CPT) synergizes with breast cancer resistance protein (BCRP) efflux anticancer drugs in cancer cells. MCF-7/ADR cells were, respectively, treated with CPT **(A)** or Ko143 **(B)** for 72 h to screen the highest concentration that does not significantly affect cell proliferation. MCF-7/ADR cells were treated with mitoxantrone (MX) **(C)** and topotecan (TOPO) **(D)** for 72 h to test cell viability. **(E)** Cell proliferation of MCF-7/ADR cells treated with MX and Ko143 1 μmol/L + MX and CPT-1 μmol/L + MX for 72 h. **(F)** Cell proliferation of MCF-7/ADR cells treated with TOPO and Ko143 1 μmol/L + TOPO and CPT 1 μmol/L + TOPO for 72 h. MX **(G)** and TOPO **(H)** fluorescence accumulation was detected by flow cytometry in MCF-7/ADR cells, respectively, treated with CPT + MX or CPT + TOPO for 8 h, and the fluorescence intensity reflects the relative content of intracellular drugs. **(I)** Comparison of intracellular MX content in CPT + MX group and MX alone group in MCF-7/ADR cells for 8 h. Results were vs. MX alone, respectively, $n = 3$, $^{**}P < 0.01$, $^{***}P < 0.001$. **(J)** Comparison of intracellular TOPO content in CPT + TOPO group and TOPO alone group in MCF-7/ADR cells for 8 h. Results were vs. TOPO alone, respectively, $n = 3$, $^{**}P < 0.01$, $^{***}P < 0.001$.

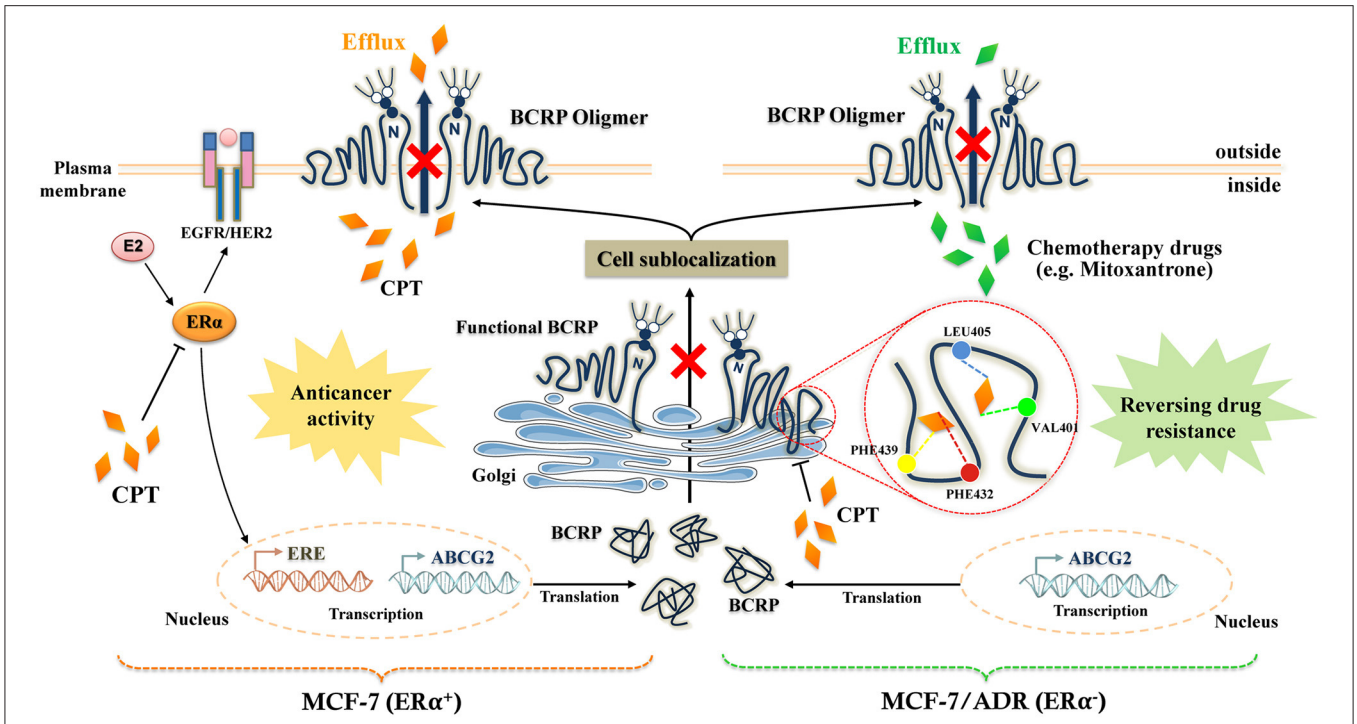


**FIGURE 7 |** The molecular mechanistic diagram of cryptotanshinone (CPT) reversing the multidrug resistance.

in ERα-negative breast cancer. Our observation that CPT is synergistic with anticancer drugs further highlights the great potential in clinical applications. Although the inhibitory activity of CPT is not dominant compared to some current BCRP inhibitors, CPT, as a lead natural compound, after appropriate optimization of the structure, may be developed into a highly effective and low-toxicity BCRP-specific inhibitor to serve clinical therapy.

## CONCLUSIONS

CPT is a novel natural BCRP inhibitor. It directly binds to BCRP and interferes with the oligomer formation of BCRP on the cell membrane, thereby blocking the efflux function of BCRP. In the ERα-positive cells, the inhibitory effect of CPT on BCRP is dependent on the expression level of BCRP. However, in the ERα-negative DOX-resistant breast cancer cells highly expressing BCRP, CPT can directly inhibit BCRP efflux function. So, CPT inhibits BCRP in an ERα-dependent and -independent manner. Our findings suggest that CPT has great potential to be explored for treatment of breast cancer with a high expression of BCRP regardless of the status of ERα.

## DATA AVAILABILITY STATEMENT

The raw data supporting the conclusions of this article will be made available by the authors, without undue reservation.

## AUTHOR CONTRIBUTIONS

WC and YL provided the study design and supervision and wrote the paper. WN and HF performed the experiments and analyses. SW and SH assisted with molecular analysis and interpretation. XZ assisted with data analysis and statistic. FX, YW, XL, and AW provided special reagents and/or helped in analyzing the experiments. All authors read and approved the final manuscript.

## FUNDING

This work was supported by the Natural Science Foundation of Higher School of Jiangsu Province (17KJA360003, 18KJA360007) and the National Natural Science Foundation of China (Nos. 81673648, 81973734, 81973587).

## SUPPLEMENTARY MATERIAL

The Supplementary Material for this article can be found online at: https://www.frontiersin.org/articles/10.3389/fonc.2021.624811/full#supplementary-material

**Supplementary Figure 1 |** Effect of CPT on P-gp and MRP1 protein expression and efflux function in MCF-7/ADR cells. Western blot analysis of P-gp and MRP1 cell membrane protein expression **(A)** and cytoplasmic protein expression **(C)** in MCF-7/ADR cells treated with CPT for 8 h, and the corresponding semi-quantitation analyses are shown in **(B,D)**. RH123 **(E)** and DOX **(F)** fluorescence accumulation in MCF-7/ADR cells treated with CPT for 8 h was, respectively, detected by flow cytometry, and the fluorescence intensity represents

the activity of P-gp and DOX efflux. RH123 and DOX were, respectively, the substrates of P-gp and MRP1. **(G)** The quantitated data of **(E)** and **(F)**.

**Supplementary Figure 2 |** The situation of mitoxantrone binding to BCRP. **(A,B)** The 3D structure of BCRP-specific substrate mitoxantrone (MX) is docked with BCRP to find substrate binding pocket, and three stable conformations, binding sites, and interaction energy are listed.

**Supplementary Figure 3 | (A)** The chemical structure of cryptotanshinone. **(B)** The HPLC chemoprofile of cryptotanshinone.

**Supplementary Table 1 |** Primers used for determination of ABCG2 mRNA expression levels in MCF-7 cells and MDA-MB-231 cells.

## REFERENCES


1. Wang J, Seebacher N, Shi H, Kan Q, Duan Z. Novel strategies to prevent the development of multidrug resistance (MDR) in cancer. *Oncotarget*. (2017) 8:84559–71. doi: 10.18632/oncotarget.19187
2. Richman J, Dowsett M. Beyond 5 years: enduring risk of recurrence in oestrogen receptor-positive breast cancer. *Nat Rev Clin Oncol*. (2019) 16:296–311. doi: 10.1038/s41571-018-0145-5
3. Kathawala RJ, Gupta P, Ashby CR, Chen ZS. The modulation of ABC transporter-mediated multidrug resistance in cancer: a review of the past decade. *Drug Resist Updat*. (2015) 18:1–17. doi: 10.1016/j.drup.2014.11.002
4. Mohammad IS, He W, Yin L. Understanding of human ATP binding cassette superfamily and novel multidrug resistance modulators to overcome MDR. *Biomed Pharmacother*. (2018) 100:335–48. doi: 10.1016/j.biopha.2018.02.038
5. Fletcher JI, Williams RT, Henderson MJ, Norris MD, Haber M. ABC transporters as mediators of drug resistance and contributors to cancer cell biology. *Drug Resist Updat*. (2016) 26:1–9. doi: 10.1016/j.drup.2016.03.001
6. Lefèvre F, Boutry M. Towards Identification of the substrates of ATP-binding cassette transporters. *Plant Physiol*. (2018) 178:18–39. doi: 10.1104/pp.18.00325
7. Taylor NMI, Manolaridis I, Jackson SM, Kowal J, Stahlberg H, Locher KP. Structure of the human multidrug transporter ABCG2. *Nature*. (2017) 546:504–9. doi: 10.1038/nature22345
8. Johnson ZL, Chen J. Structural basis of substrate recognition by the multidrug resistance protein MRP1. *Cell*. (2017) 168:1075–85.e9. doi: 10.1016/j.cell.2017.01.041
9. Mao Q, Unadkat JD. Role of the breast cancer resistance protein (BCRP/ABCG2) in drug transport–an update. *AAPS J*. (2015) 17:65–82. doi: 10.1208/s12248-014-9668-6
10. Horsey AJ, Cox MH, Sarwat S, Kerr ID. The multidrug transporter ABCG2: still more questions than answers. *Biochem Soc Trans*. (2016) 44:824–30. doi: 10.1042/BST20160014
11. Li W, Zhang H, Assaraf YG, Zhao K, Xu X, Xie J, et al. Overcoming ABC transporter-mediated multidrug resistance: molecular mechanisms and novel therapeutic drug strategies. *Drug Resist Updat*. (2016) 27:14–29. doi: 10.1016/j.drup.2016.05.001
12. Shin DS, Kim HN, Shin KD, Yoon YJ, Kim SJ, Han DC, et al. Cryptotanshinone inhibits constitutive signal transducer and activator of transcription 3 function through blocking the dimerization in DU145 prostate cancer cells. *Cancer Res*. (2009) 69:193–202. doi: 10.1158/0008-5472.CAN-08-2575
13. Chen W, Luo Y, Liu L, Zhou H, Xu B, Han X, et al. Cryptotanshinone inhibits cancer cell proliferation by suppressing Mammalian target of rapamycin-mediated cyclin D1 expression and Rb phosphorylation. *Cancer Prev Res*. (2010) 3:1015–25. doi: 10.1158/1940-6207.CAPR-10-0020
14. Chen W, Liu L, Luo Y, Odaka Y, Awate S, Zhou H, et al. Cryptotanshinone activates p38/JNK and inhibits Erk1/2 leading to caspase-independent cell death in tumor cells. *Cancer Prev Res*. (2012) 5:778–87. doi: 10.1158/1940-6207.CAPR-11-0551
15. Chen W, Pan Y, Wang S, Liu Y, Chen G, Zhou L, et al. Cryptotanshinone activates AMPK-TSC2 axis leading to inhibition of mTORC1 signaling in cancer cells. *BMC Cancer*. (2017) 17:34. doi: 10.1186/s12885-016-3038-y
16. Pan Y, Shi J, Ni W, Liu Y, Wang S, Wang X, et al. Cryptotanshinone inhibition of mammalian target of rapamycin pathway is dependent on oestrogen receptor alpha in breast cancer. *J Cell Mol Med*. (2017) 21:2129–39. doi: 10.1111/jcmm.13135
17. Montanari F, Cseke A, Wlcek K, Ecker GF. Virtual screening of DrugBank reveals two drugs as new BCRP inhibitors. *SLAS Discov*. (2017) 22:86–93. doi: 10.1177/1087057116657513
18. Xu J, Liu Y, Yang Y, Bates S, Zhang JT. Characterization of oligomeric human half-ABC transporter ATP- binding cassette G2. *J Biol Chem*. (2004) 279:19781–9. doi: 10.1074/jbc.M310785200
19. Ni Z, Mark ME, Cai X, Mao Q. Fluorescence resonance energy transfer (FRET) analysis demonstrates dimer/oligomer formation of the human breast cancer resistance protein (BCRP/ABCG2) in intact cells. *Int J Biochem Mol Biol*. (2010) 1:1–11.
20. Zhang YK, Wang YJ, Lei ZN, Zhang GN, Zhang XY, Wang DS, et al. Regorafenib antagonizes BCRP- mediated multidrug resistance in colon cancer. *Cancer Lett*. (2019) 442:104–12. doi: 10.1016/j.canlet.2018.10.032
21. Mo W, Zhang JT. Oligomerization of human ATP-binding cassette transporters and its potential significance in human disease. *Expert Opin Drug Metab Toxicol*. (2009) 5:1049–63. doi: 10.1517/17425250903124371
22. Krapf MK, Gallus J, Vahdati S, Wiese M. New inhibitors of breast cancer resistance protein (ABCG2) containing a 2,4-disubstituted pyridopyrimidine scaffold. *J Med Chem*. (2018) 61:3389–408. doi: 10.1021/acs.jmedchem.7b01012
23. Herynk MH, Fuqua SA. Estrogen receptors in resistance to hormone therapy. *Adv Exp Med Biol*. (2007) 608:130–43. doi: 10.1007/978-0-387-74039-3_10
24. Berry DA, Cirrincione C, Henderson IC, Citron ML, Budman DR, Goldstein LJ, et al. Estrogen-receptor status and outcomes of modern chemotherapy for patients with node-positive breast cancer. *JAMA*. (2006) 295:1658–67. doi: 10.1001/jama.295.14.1658
25. Koren E, Fuchs Y. The bad seed: cancer stem cells in tumor development and resistance. *Drug Resist Update*. (2016) 28:1–12. doi: 10.1016/j.drup.2016.06.006
26. Chang FW, Fan HC, Liu JM, Fan TP, Jing J, Yang CL, et al. Estrogen enhances the expression of the multidrug transporter gene ABCG2-increasing drug resistance of breast cancer cells through estrogen receptors. *Int J Mol Sci*. (2017) 18:163. doi: 10.3390/ijms18010163
27. Ee PL, Kamalakaran S, Tonetti D, He X, Ross DD, Beck WT. Identification of a novel estrogen response element in the breast cancer resistance protein (ABCG2) gene. *Cancer Res*. (2004) 64:1247–51. doi: 10.1158/0008-5472.CAN-03-3583
28. Yang M, Li H, Li Y, Ruan Y, Quan C. Identification of genes and pathways associated with MDR in MCF- 7/MDR breast cancer cells by RNA-seq analysis. *Mol Med Rep*. (2018) 17:6211–26. doi: 10.3892/mmr.2018.8704
29. Oh AS, Lorant LA, Holloway JN, Miller DL, Kern FG, El-Ashry D. Hyperactivation of MAPK induces loss of ERalpha expression in breast cancer cells. *Mol Endocrinol*. (2001) 15:1344–59. doi: 10.1210/mend.15.8.0678
30. Campbell RA, Bhat-Nakshatri P, Patel NM, Constantinidou D, Ali S, Nakshatri H. Phosphatidylinositol 3- kinase/AKT-mediated activation of estrogen receptor alpha: a new model for anti-estrogen resistance. *J Biol Chem*. (2001) 276:9817–24. doi: 10.1074/jbc.M010840200
31. Peña-Solórzano D, Stark SA, König B, Sierra CA, Ochoa-Puentes C. ABCG2/BCRP: specific and nonspecific modulators. *Med Res Rev*. (2017) 37:987–1050. doi: 10.1002/med.21428
32. Sonne-Hansen K, Norrie IC, Emdal KB, Benjaminsen RV, Frogne T, Christiansen IJ, et al. Breast cancer cells can switch between estrogen receptor alpha and ErbB signaling and combined treatment against both signaling pathways postpones development of resistance. *Breast Cancer Res Treat*. (2010) 121:601–13. doi: 10.1007/s10549-009-0506-y

33. Zimmermann GR, Lehár J, Keith CT. Multi-target therapeutics: when the whole is greater than the sum of the parts. *Drug Discov Today*. (2007) 12:34–42. doi: 10.1016/j.drudis.2006.11.008
34. Poornima P, Kumar JD, Zhao Q, Blunder M, Efferth T. Network pharmacology of cancer: from understanding of complex interactomes to the design of multi-target specific therapeutics from nature. *Pharmacol Res*. (2016) 111:290–302. doi: 10.1016/j.phrs.2016.06.018
35. Wang W, Wang X, Zhang XS, Liang CZ. Cryptotanshinone attenuates oxidative stress and inflammation through the regulation of Nrf-2 and NF-κB in mice with unilateral ureteral obstruction. *Basic Clin Pharmacol Toxicol*. (2018) 123:714–20. doi: 10.1111/bcpt.13091

**Conflict of Interest:** The authors declare that the research was conducted in the absence of any commercial or financial relationships that could be construed as a potential conflict of interest.

frontiers in Pharmacology

ORIGINAL RESEARCH
published: 29 April 2021
doi: 10.3389/fphar.2021.616529

# Systematic Investigation of DNA Methylation Associated With Platinum Chemotherapy Resistance Across 13 Cancer Types

*Ruizheng Sun[1,2†], Chao Du[1,2†], Jiaxin Li[1,2], Yanhong Zhou[1,2], Wei Xiong[1,2], Juanjuan Xiang[1,2], Jiheng Liu[3], Zhigang Xiao[4], Li Fang[1] and Zheng Li[1,2]**

[1]NHC Key Laboratory of Carcinogenesis, Hunan Cancer Hospital and the Affiliated Cancer Hospital of Xiangya School of Medicine, Central South University, Changsha, China, [2]The Key Laboratory of Carcinogenesis and Cancer Invasion of the Chinese Ministry of Education, Central South University, Changsha, China, [3]Department of Hematology and Oncology, The First Hospital of Changsha, Changsha, China, [4]Department of General Surgery, Hunan Provincial People's Hospital, The First Affiliated Hospital of Hunan Normal University, Changsha, China

OPEN ACCESS

**Edited by:**
Zhe-Sheng Chen,
St. John's University, United States

**Reviewed by:**
Majid Asadi-Samani,
Shahrekord University of Medical Sciences, Iran
Xibao Yu,
Sun Yat-sen University Cancer Center, China
Guolian Kang,
St. Jude Children's Research Hospital, United States

***Correspondence:**
Zheng Li
lizheng@csu.edu.cn

†These authors have contributed equally to this work

**Specialty section:**
This article was submitted to Pharmacology of Anti-Cancer Drugs, a section of the journal Frontiers in Pharmacology

**Received:** 12 October 2020
**Accepted:** 19 April 2021
**Published:** 29 April 2021

**Citation:**
Sun R, Du C, Li J, Zhou Y, Xiong W, Xiang J, Liu J, Xiao Z, Fang L and Li Z (2021) Systematic Investigation of DNA Methylation Associated With Platinum Chemotherapy Resistance Across 13 Cancer Types. Front. Pharmacol. 12:616529. doi: 10.3389/fphar.2021.616529

**Background:** Platinum resistance poses a significant problem for oncology clinicians. As a result, the role of epigenetics and DNA methylation in platinum-based chemoresistance has gained increasing attention from researchers in recent years. A systematic investigation of aberrant methylation patterns related to platinum resistance across various cancer types is urgently needed.

**Methods:** We analyzed the platinum chemotherapy response-related methylation patterns from different perspectives of 618 patients across 13 cancer types and integrated transcriptional and clinical data. Spearman's test was used to evaluate the correlation between methylation and gene expression. Cox analysis, the Kaplan-Meier method, and log-rank tests were performed to identify potential risk biomarkers based on differentially methylated positions (DMPs) and compare survival based on DMP values. Support vector machines and receiver operating characteristic curves were used to identify the platinum-response predictive DMPs.

**Results:** A total of 3,703 DMPs ($p$ value < 0.001 and absolute delta beta >0.10) were identified, and the DMP numbers of each cancer type varied. A total of 39.83% of DMPs were hypermethylated and 60.17% were hypomethylated in platinum-resistant patients. Among them, 405 DMPs (Benjamini and Hochberg adjusted $p$ value < 0.05) were found to be associated with prognosis in tumor patients treated with platinum-based regimens, and 664 DMPs displayed the potential to predict platinum chemotherapy response. In addition, we defined six DNA DMPs consisting of four gene members (mesothelin, protein kinase cAMP-dependent type II regulatory subunit beta, msh homeobox 1, and par-6 family cell polarity regulator alpha) that may have favorable prognostic and predictive values for platinum chemotherapy.

**Conclusion:** The methylation-transcription axis exists and participates in the complex biological mechanism of platinum resistance in various cancers. Six DMPs and four

associated genes may have the potential to serve as promising epigenetic biomarkers for platinum-based chemotherapy and guide clinical selection of optimal treatment.

**Keywords: methylation, DNA, drug resistance, neoplasm, platinum**

# INTRODUCTION

Platinum-based chemotherapy has been an indispensable anticancer therapy for nearly every cancer, but especially for urogenital, lung, and gastrointestinal cancers (Verhoeven et al., 2013; Dasari and Tchounwou, 2014; Rossi and Di Maio, 2016). Although the forms of platinum agents vary when it comes to treatment for specific cancer types, their pharmacological mechanisms are concentrated on inducing DNA damage and cell apoptosis (Dasari and Tchounwou, 2014). As a response to this extreme external stimulation, cancer cells will exert their full resources to escape and manage to survive the lethal strike, which induces genomic, epigenetic, and functional disorders and results in a platinum-resistant cellular biological phenotype (Fang et al., 2018a; Yu et al., 2020). This corresponds with clinical evidence that chemotherapy-treated patients tend to gradually develop platinum resistance, which leads to unsatisfactory clinical outcomes and survival (Agarwal and Kaye, 2003; Alcindor and Beauger, 2011; Fennell et al., 2016).

Epigenetics play a critical and profound role in the genesis, malignancy, and drug response of cancer by regulating DNA-based biological processes, such as replication, damage repair, and transcription (Dawson and Kouzarides, 2012; Peng and Zhong, 2015; Liu et al., 2018). DNA methylation was the first described and possibly the most extensive characteristic modification in human genetic materials. Accumulating evidence has shown that changes in DNA methylation have the potential to alter the platinum sensitivity of cancer cells and predict the chemotherapeutic response of patients (Vera et al., 2017; Fang et al., 2018a). Although several functional studies on specific methylation sites associated with chemoresistance have been conducted, there is an urgent need for a systematic investigation of DNA methylation affiliated with patients' platinum response via large-scale screening (Vera et al., 2017; Fang et al., 2018a; Fang et al., 2018b).

The Cancer Genome Atlas (TCGA) project collected the clinical and molecular characteristics of over 11,000 patients across different cancer types, making it the perfect database for analyzing and integrating pan-cancer methylation features of different platinum responses. Fang et al. and Zhu et al. provided a significant grouping method and detailed list of patients who received platinum-based treatment (Fang et al., 2018b; Zhu et al., 2020). This study aimed to provide a systematic landscape of DNA methylation associated with platinum treatment and its potential clinical applications across 13 TCGA cancer types.

# MATERIALS AND METHODS

## Data Collection and Processing

Profiles of 450 K beta value matrixes, transcriptional data and corresponding clinical information across 13 TCGA cancer types were downloaded by "TCGAbiolinks" (Colaprico et al., 2016). Filter, normalization, and annotation of methylation probes were all based on the functions of R package "ChAMP" (Tian et al., 2017). All methylation and transcriptional data were projected and annotated with hg19 (GRCH37). As described previously, we selected patients receiving platinum-based therapy and defined patients of "Complete Response" as platinum-sensitive group (CR) and other descriptions including "Clinical Progressive," "Stable Disease," and "Partial Response" as platinum-resistant group (PR) (Zhu et al., 2020). The integrated information of 618 patients with grouping information, cancer type, drug name and response can be seen in **Figures 1A,B**, and **Supplementary Table S1**.

Different methylated loci on the overall methylation level and the chromosome level were compared among medians by Wilcoxon rank sum test. Differentially methylated regions (DMRs) were identified by the method of "Bumphunter" and minimum cutoff adjusted $p$ value of 0.05 (Jaffe et al., 2012). Differentially methylated positions (DMPs) were defined as $p$ value <0.001 and absolute deltaBeta >0.10. Identification of DMRs and DMPs were implemented by functions in "ChAMP".

## Enrichment Analysis

The bias-free enrichment methods which directly calculate global tests and do gene set enrichment analysis (GSEA) were accomplished by Empirical Bayes gene set enrichment analysis (ebGSEA) method in "ChAMP" package. The results of ebGSEA were evaluated by two main parameters: area under curves (AUCs) from Wilcoxon test and P values detected for each pathway from Wilcoxon test. Gene Ontology (GO) and the Kyoto Encyclopedia of Genes and Genomes (KEGG) enrichment analysis based on corresponding genes of DMPs were conducted by R package "clusterProfiler" (Yu et al., 2012). Reactome pathway analyses were carried out by R package "ReactomePA" (Yu and He, 2016).

## Identification of Transcriptional-Affected DMPs

The corresponding gene names of DMPs were annotated by hg19 and expressions of DMP-related genes were scaled by transcripts per million (TPM) which may be the optimal form of transcriptional normalization. Correlations between methylation and transcriptional data were measured by the Spearman's test which is not limited to the distribution of data. Transcriptional-affected DMPs should meet the following criteria: 1.) absolute log Fold Change (logFC) of corresponding gene >1; 2.) correlations between values of DMPs and expressions of corresponding genes must be significantly negative (Rho of Spearman's test < −0.4, adjusted $P$ (Benjamini & Hochberg, BH) value of Spearman's test <0.05).

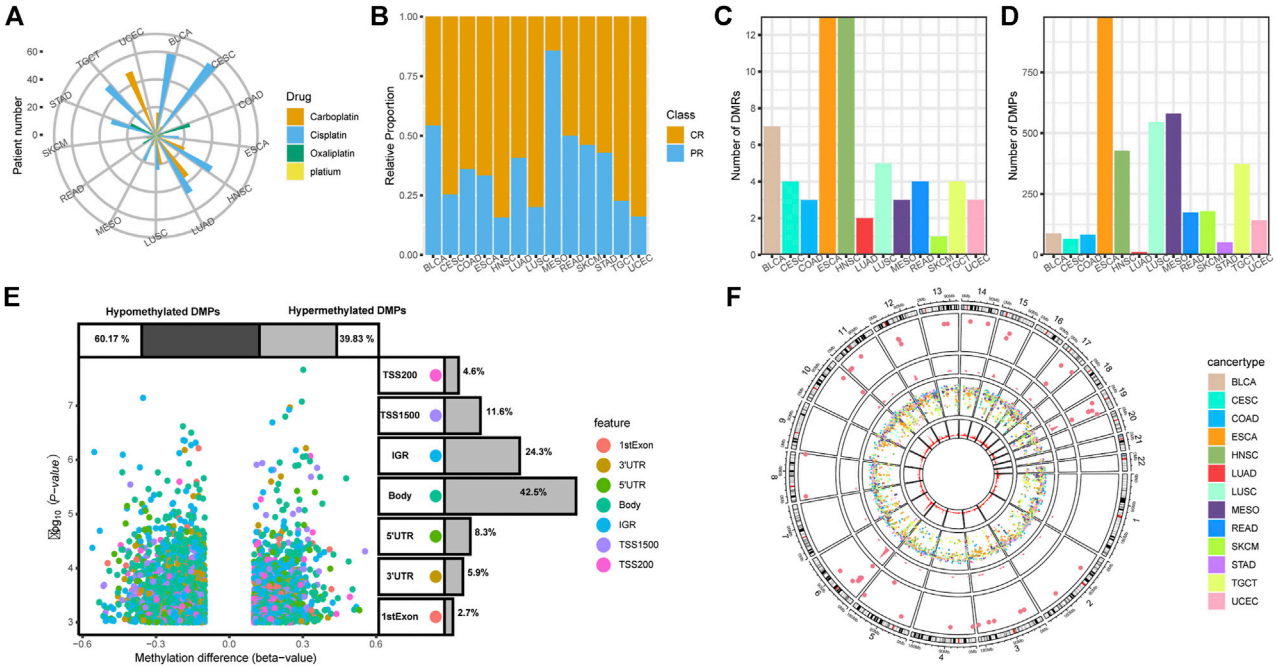


**FIGURE 1 |** Clinical information and DNA methylation patterns associated with platinum response. **(A)** Clinical application of platinum agents in 13 TCGA cancer types. **(B)** The platinum-sensitive group (CR)/platinum-resistant group (PR) relative proportion of 13 cancer types. **(C)** Number of differentially methylated regions (DMRs) in each cancer type. **(D)** Number of differentially methylated positions (DMPs) in each cancer type. **(E)** Volcano plots of DMPs with annotation of the methylation probe feature. **(F)** Rainfall and density plots of all DMRs and DMPs.

## Construction of Prognostic and Predictive Models

Screening prognostic DMPs across different cancer types were based on the results of univariate Cox analysis. Schoenfeld tests were conducted and all the Cox models shown in the main text did not violate the proportional hazard assumption. DMPs with adjusted $p$ value (BH) < 0.05 were defined as overall survival (OS) related prognostic DMPs. Multivariate Cox analysis of all prognostic DMPs were conducted to adjust for the potential covariates of age and gender (Gender is not a covariate in CESC and UCEC). Kaplan-Meier curves grouped by the value of specific prognostic DMPs were estimated and drawn using R package "survival" and "survminer".

Identification of platinum-response predictive DMPs were supported by support vector machines (SVMs), which is a binary classifier by maximizing the distance between the classes' closest points. C-classification method was used to predict the types of CR/PR based on the values of each DMP. Data of every cancer type were randomly split into train sets (2/3 of the total number) and test sets (1/3 of the total number) as described in R-project e1071. Accuracy and F1-measure of test sets by one-time split were used to evaluate predictive models constructed by train sets. AUCs of receiver operator characteristics (ROCs) according to the entire set and the leave-one-out-cross-validation (LOOCV) were used to see the robustness of predictive model. The platinum-response predictive DMPs were supposed to meet the following criteria: 1.) Accuracy >0.8; 2.) F1-measure > 0.8; 3.) AUC of the entire set >0.8; 4.) Mean AUC of LOOCV >0.6. SVMs, ROCs contribution and LOOCV were conducted respectively by R package "e1071," "pROC," and "cvms" (Robin et al., 2011).

# RESULTS

## Aberrant DNA Methylation Profiling Patterns Associated With Platinum Chemotherapy Across 13 Human Cancer Types

The platinum agents for chemotherapy and proportions of platinum-sensitive group (CR)/platinum-resistant group (PR) vary according to cancer type, as shown in **Figures 1A,B**. Cisplatin is the most widely used agent, and oxaliplatin is typically the only choice for gastrointestinal cancers. Carboplatin is used in uterine corpus endometrial carcinoma (UCEC), head-neck squamous cell carcinoma (HNSC), and lung cancers to different extents. There are also a few cases of platinum treatment without specifying agents.

The differences in overall methylation status between the CR and PR groups were observed, and PR groups were found to be in a lower methylation state compared with CR groups in most of tumors, especially in cervical squamous cell carcinoma and endocervical adenocarcinoma (CESC, $p$ < 0.05) (**Supplementary Figure S1**). From the chromosome

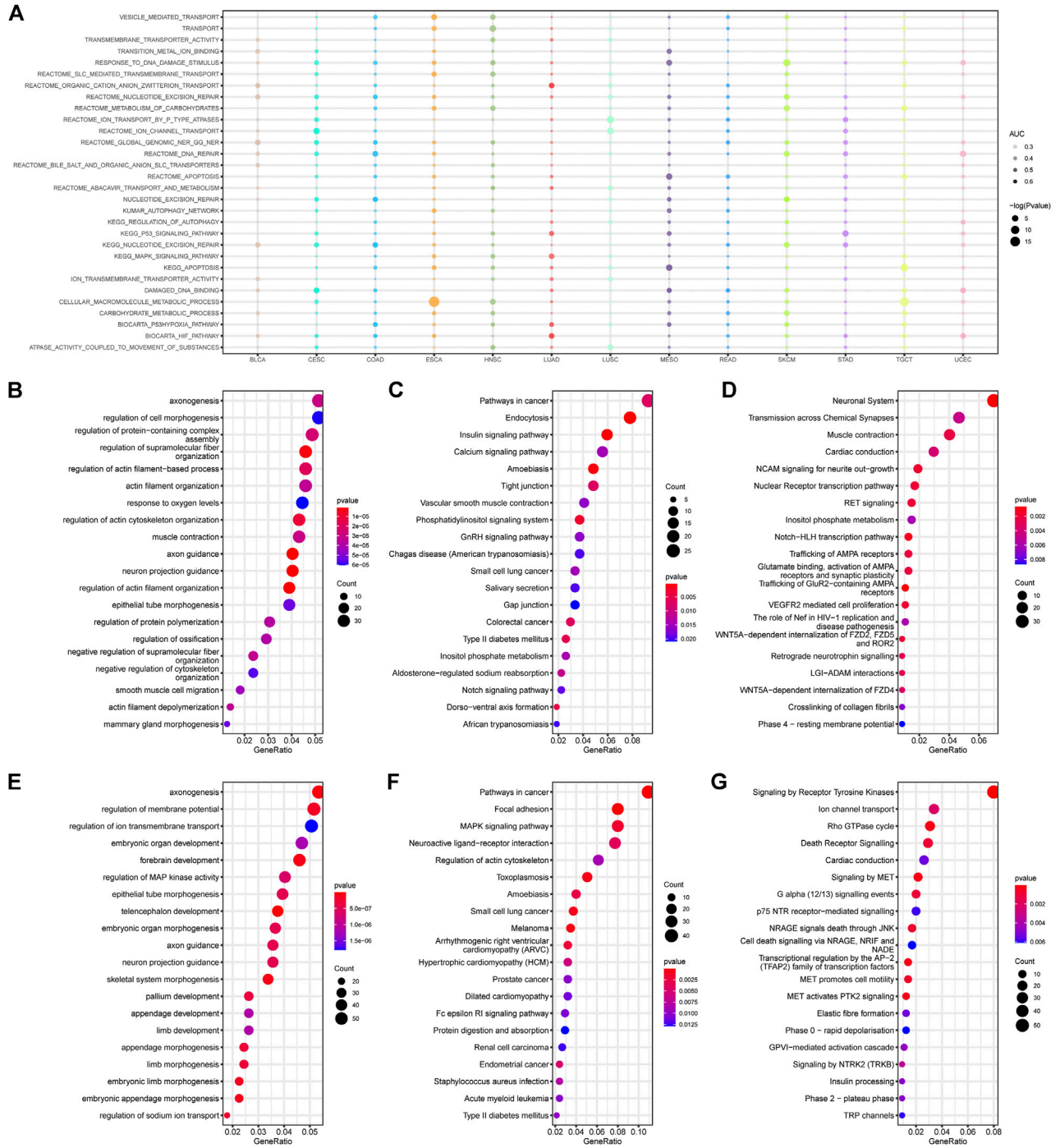


**FIGURE 2 |** Enrichment results of the methylation profiles correlated with platinum resistance. **(A)** Empirical Bayes gene set enrichment analysis (ebGSEA) results of 30 platinum response-related gene sets across 13 cancer types. **(B–D)** Gene Ontology (GO), the Kyoto Encyclopedia of Genes and Genomes (KEGG), and Reactome enrichment results of the hypermethylated DMPs in PR patients. **(E–G)** GO, KEGG, and Reactome results of the hypomethylated DMPs in PR patients.

perspective, 17 types of different methylated chromosomes ($p < 0.05$) also focused on the three cancer types including CESC, esophageal carcinoma (ESCA) and bladder urothelial carcinoma (BLCA). These results of the primary analysis indicated that DNA methylation may play a critical role in the platinum response (**Supplementary Figure S2**).

We screened 62 DMRs and 3,703 DMPs between CR and PR group across 13 TCGA cancer types. The total number of

identified DMRs and DMPs vary by cancer type due to the heterogeneity (**Figures 1C,D**). ESCA had the highest DMR and DMP values, which correspond with the overall and chromosome level results. Stomach adenocarcinoma (STAD) displayed no DMR and lung adenocarcinoma (LUAD) presented the lowest DMP value, which suggests that there is a weak connection between platinum resistance and DNA methylation in these two cancer types. Volcano plots revealed that 60.17% hypomethylated DMPs of 3,703 overall DMPs are more abundant than 39.83% hypermethylated DMPs, which may indicate that activation of specific genes is more powerful for gaining a platinum-resistant phenotype. Nearly half of the DMP features are gene body. The features of the intergenic region (IGR) and transcription start position (TSS) also take up over 10% (**Figure 1E**). From the genome perspective, the DMPs of all cancer types are distributed across the whole genome while DMRs are scattered among chromosomes according to rainfall plots. Density plots show that both DMPs and DMRs seem to form peaks on several chromosomes, including the sixth, nineteenth, and eleventh chromosomes, which may indicate the universal significance of methylation on specific genomic regions for platinum response (**Figure 1F**).

## Cancer Pathways Affected by Methylation and Correlated With Platinum Resistance

Various mechanisms are involved in platinum resistance, including pre-target, on-target, post-target, and off-target resistances (Galluzzi et al., 2012). In order to identify the methylation changes related to the drug response, we selected 30 typical platinum resistance gene sets in the molecular signatures database (MSigDB) and attempted to list the empirical Bayes Gene Set Enrichment Analysis (ebGSEA) results of the CR/PR groups among the 13 cancer types, aiming to obtain an overall landscape of resistance-related enrichment results regardless of DMRs and DMPs (**Figure 2A**). This shows that all 13 cancer types have significant platinum resistance enrichment on the DNA methylation level, which presents a promising chance to perform enrichment analysis based on DNA methylation data.

Both the hypermethylated and hypomethylated top GO results showed gene sets related to biological axon genesis, morphogenesis, and body development, indicating that some development-related genes may be involved in platinum response (**Figures 2B,E**). The KEGG results focused on cancer-related enrichment, including pathways in colorectal cancer, melanoma, prostate cancer, and renal cell carcinoma, which suggests that platinum-related phenotypes may be influenced by cancerous genes (**Figures 2C,F**). The Reactome results revealed hypermethylation of the neuronal system, transmission across chemical synapses, muscle contraction, and hypomethylation of ion channel transport, the Rho GTPase cycle, and death receptor signaling (**Figures 2D,G**). Generally speaking, pathways including the mitogen-activated protein kinase (MAPK) signaling, inositol phosphate metabolism, and neural genesis-related pathways, appeared more than twice in different enrichment results.

## Methylation and Transcription Characteristics of the Platinum Response in DMRs

To further investigate the common characteristics of DMRs, we downloaded the cytoband annotation of hg19 and projected DMRs onto the cytoband of each chromosome. Both q13.12 on the nineteenth chromosome and p22.1 on the sixth chromosome, which are the most frequent cytobands, had 6 DMRs (**Supplementary Table S2**). For p22.1 on the sixth chromosome, all DMRs were concentrated in the IGR genome region and did not correspond with any specific gene, suggesting that this region may affect the platinum response in a more complicated way rather than via transcription.

For the 6 DMRs on q13.12 of the nineteenth chromosome, the corresponding genes were all focused on the zinc finger protein (ZNF) family. In HNSC, the overall methylation status of PR was higher than that of CR, and the expression of the corresponding ZNF420 gene of PR was lower than that of CR, both of which follow a typical hypermethylation-transcription-repressive model (**Figures 3A–C**). In ESCA, the hypermethylation of PR and low expression of ZNF493 were more obvious (**Figures 3D–F**). In rectum adenocarcinoma (READ), the methylation status was the same as in HNSC and ESCA but did not induce significant transcriptional changes (**Supplementary Figure S3**). In CESC and lung squamous cell carcinoma (LUSC), the methylation value of CR was higher than that of PR, but none of the corresponding ZNF family gene expression levels were significantly different (**Supplementary Figure S3**). Although ZNF family genes have different methylation and expression patterns in different cancer types, all of the above results indicate the significance of methyl modification of ZNF genes in the platinum response of patients with different cancer types.

## Regulation of DMPs and Expression Profiles in Platinum-Treated Patients

It is a commonly accepted theory that hypermethylation or hypomethylation of DNA will induce silencing or activation of corresponding gene transcription, especially for CpG islands. We screened all DMPs using the Spearman correlation test criteria described in the Materials and methods and divided them into five different regions based on the delta beta probe values of CR/PR and log fold-change (FC) of corresponding mRNA, including transcriptional changes, DNA methylation changes, homodirectional changes, opposite changes, and subtle changes (**Figure 4A**). According to the methylation-transcription theory, we focused on the probes and genes with opposite changes.

To better demonstrate the relationship between DMPs and gene expression, we drew a lollipop plot of minus correlation coefficient Rho and P values for the top 20 probes ranked by absolute Rho (**Figure 4B**). There were 43 DMPs negatively associated with the expression of 28 genes (**Supplementary Table S3**). The proportions of DMPs in gene bodies, TSS1500, and TSS200 were 39.5, 32.6, and 20.9%, respectively, confirming their indispensable roles in transcription (**Figure 4C**). Features including islands and shores respectively accounted for 41.9 and 39.5% of the overall CpG islands

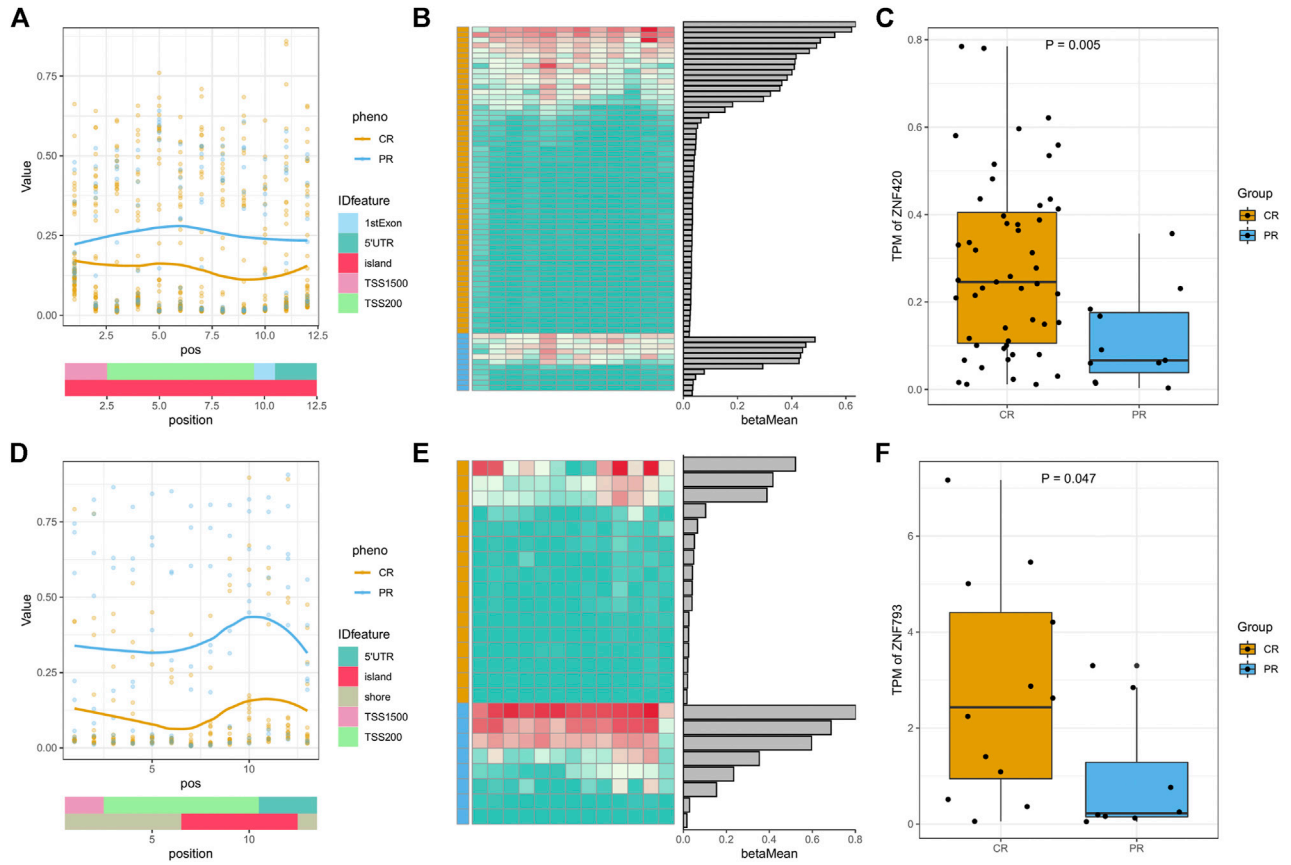


**FIGURE 3 |** Methylation and expression of ZNF family genes in the DMRs of HNSC and ESCA. **(A)** DMR plot of the methylation status of CR/PR patients with gene feature and CpG islands (CGI) information in head-neck squamous cell carcinoma (HNSC) DMR-8. **(B)** Heatmap of each DMP beta value and bar plots of the mean beta values in HNSC DMR-8. **(C)** Expression (TPM) of relevant genes in specific DMRs between the CR/PR groups in HNSC DMR-8. **(D–F)** DMR plot, heatmap, and gene expression in esophageal carcinoma (ESCA) DMR-8. *p* values were calculated using the Wilcoxon test.

(CGI) feature, respectively, which emphasizes the significance of the CpG theory (**Figure 4D**). As seen in **Supplementary Table S3**, there were 26 hypermethylated transcription-repressive genes and two hypomethylated transcription-activated genes. Hypermethylated deactivated pathways included negative regulation of protein phosphorylation, signaling by Hedgehog, and tight junctions. Hypomethylated activated pathways consisted of DNA damage-related pathways, the cellular response to hydroxyurea pathway, and metabolism-related pathways. These enrichment results share some of the same or similar gene sets as those in **Figure 2**, including tight junctions, DNA damage-related pathways, and metabolism-related pathways (**Supplementary Figure S4**), which indicates the significance of epigenetic-functional pathways in platinum resistance. Our data suggest the possibility of significant methylation-transcription connections of the genes in platinum-treated patients with different cancer types.

## DMP Patterns Associated With Clinical Prognosis and Platinum Response

Patient survival is one of the most important indications for assessing platinum-based chemotherapy responses. Since it is limited to the number of patients in each cancer type, overall survival (OS) is the most common and easiest available index of patient survival. There were 405 prognostic DMPs that could serve as risk factors and predictors of patient OS in four cancer types after univariate Cox screening (**Supplementary Table S4**). P values of over 99% (404/405) of the prognostic DMPs were less than 0.10 after adjusting for other potential clinical covariates using multivariate Cox analysis (**Supplementary Table S4**). HNSC, UCEC, BLCA, and CESC had more than 50 prognostic DMPs, which suggests that DMP values in these four cancer types can more easily play the role of survival-risk factors for OS in platinum-treated patients (**Figure 5A**).

Clinically, selection of treatment mainly depends on how the previous patients responded to various treatments. For chemotherapy patients, there is a strong need for valid biomarkers that can predict and assess the reaction of platinum drugs. SVMs provide an optimal method for identifying DMPs that are able to classify the CR and PR classes. As described previously, we defined response-predictive DMPs as potential biomarkers for classifying platinum response groups with promising accuracy, F1 measure, and the AUCs of ROCs. There were a total of

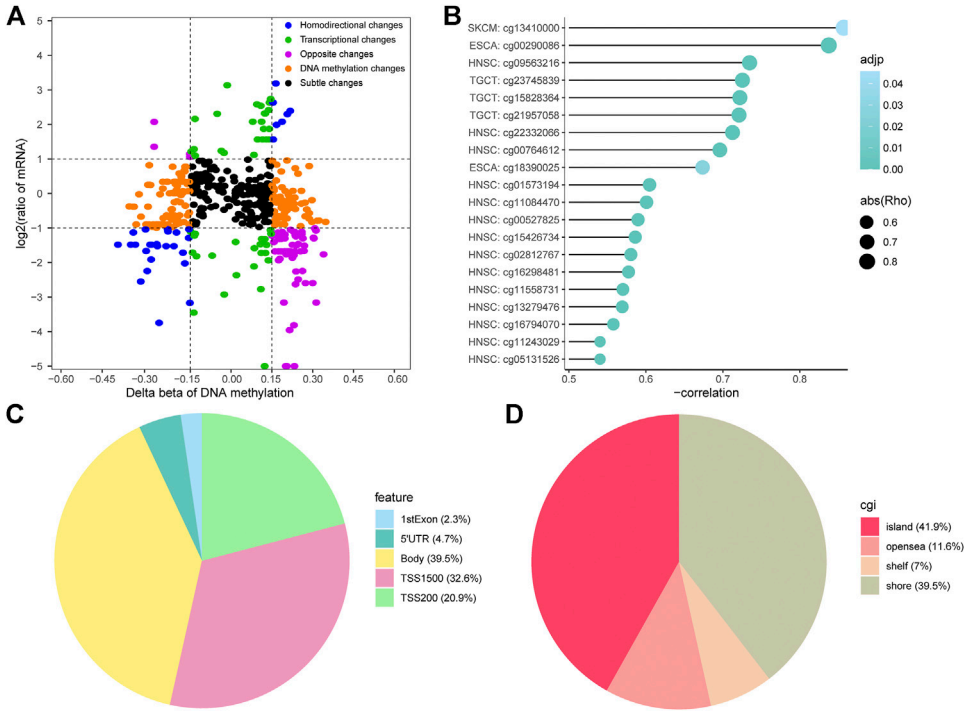


**FIGURE 4 |** Identification of the methylation-transcription axis in platinum-treated patients. **(A)** Methylation and transcription plots of transcription-regulative DMPs and corresponding genes in the CR/PR groups. **(B)** Top 20 DMPs with negative correlation coefficients in the opposite change fractions. **(C–D)** Proportion of genes and CpG islands (CGI) features of transcription-affective DMPs.

664 response-predictive DMPs distributed in eight cancer types, including COAD, ESCA, HNSC, LUSC, READ, SKCM, and UCEC (**Supplementary Table S5**; **Figure 5B**).

There were 12 potentially transcription-regulative DMPs that impacted the survival of patients treated with platinum-based methods (**Figure 5C**). Interestingly, there were three identified prognostic risk DMPs that also acted as response-predictive DMPs, including cg10398993, and cg00888463 in HNSC as well as cg00486340 in UCEC (**Figure 5C**). Coincidentally, they were all hypermethylated in PR patients and therefore followed the hypermethylation-deactivation patterns in platinum-treated samples. The independent P values of the Wilcoxon test were 0.0005, 0.0012, and 0.0014, respectively, which indicated significant differences in methylation (**Figures 5D–F**). The corresponding genes of these three DMPs were mesothelin (MSLN), protein kinase cAMP-dependent type II regulatory subunit beta (PRKAR2B), and msh homeobox 1 (MSX1), all of which correlated with tumor development, malignancy, and treatment (Yue et al., 2018b; Hilliard, 2018; Sha et al., 2018). Patients with hypermethylated status of these three genes were considered as the high-risk group and had poorer survival than those with hypomethylated status. The log-rank P values were calculated to be 0.031, 0.017, and 0.038, respectively, which showed well-performed prognostic distinctions between platinum-treated groups based on the specific methylation status of these four genes (**Figures 5G–I**). The AUCs of the ROC curves of the three DMPs were 0.834, 0.809, and 0.825, respectively, and all of the lower values of the 95% confidence intervals (CIs) were far greater than 0.5, which indicates promising predictive functions of the platinum-based chemotherapy response (**Figures 5J–L**). The mean AUCs of LOOCV of the three DMPs were 0.846, 0.627, and 0.780, respectively, which shows the predictive robustness of these three DMPs (**Supplementary Table S5**). This analysis emphasizes the potential biological and clinical significance of the methylation of these genes for platinum resistance in cancer.

It is worth mentioning that there were three methylation probes (cg15426734, cg01573194, and cg16794070) of the par-6 family cell polarity regulator alpha (PARD6A) significantly hypermethylated in the HNSC PR groups, which was proven by the *p* values of 0.0006, 0.0017, and 0.0011, respectively (**Figure 6A–C**). High-risk patients with hypermethylation showed poorer OS than low-risk patients with hypomethylation. The log-rank *p* values were 0.0068, 0.00021, and 0.00087, respectively, which revealed significant survival differences between the risk groups based on the values of the three PARD6A probes (**Figure 6D–F**). Although the three PARD6A probes were not defined as response-predictive DMPs because of their slightly inferior accuracy (0.783) and mean AUCs of LOOCV (0.716, 0.474, and 0.706), the AUCs of these entire sets were all over 0.8, which still indicate potential well-performed response-predictive functions (**Figure 6G-I**). Thus, our investigation suggests a novel clinical and biological understanding of PARD6A methylation.

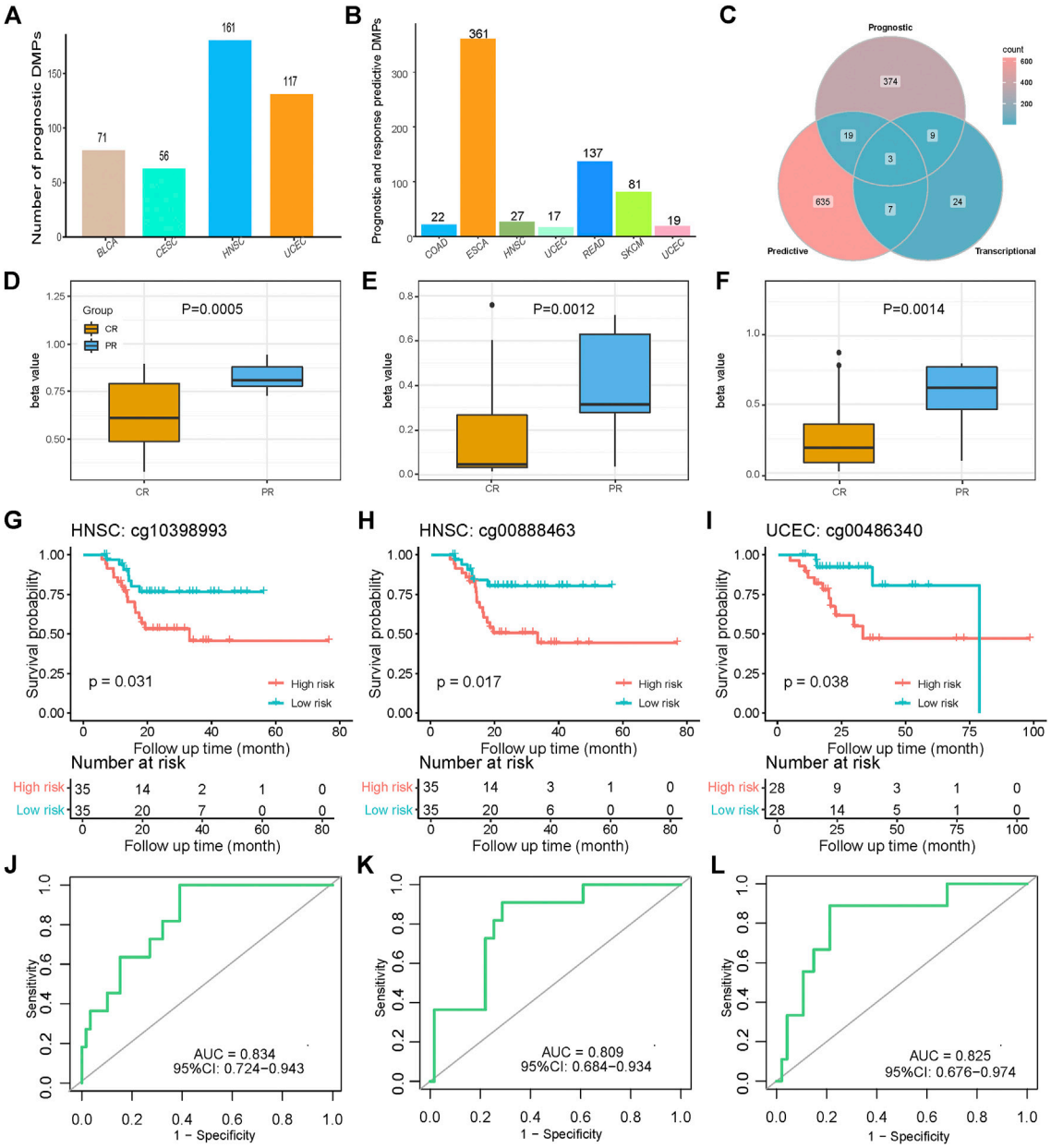


**FIGURE 5 |** Prognostic and platinum response-predictive DMP models. **(A)** Distribution of 405 prognostic DMPs among four cancer types. **(B)** Distribution of 664 platinum response-predictive DMPs among eight cancer types. **(C)** Intersection Venn plot of the prognostic, predictive, and transcriptional DMPs. **(D–F)** Different beta values of cg10398993, and cg00888463 in HNSC as well as cg00486340 in UCEC between the CR and PR groups. *p* values were calculated using the Wilcoxon test. **(G–I)** K-M survival plots grouped by the beta values of the three DMPs. *p* values were directly calculated using log-rank test. **(J–L)** Receiver operator characteristics (ROC) curves of the three DMPs.

## DISCUSSION

Platinum-based chemotherapy resistance has always been an intractable problem for oncology clinicians. TCGA provides a landmark platform for analyzing the epigenomic data related to chemotherapy, and several studies have focused on the role of a specific gene or site in chemoresistance for a specific cancer type (Grasse et al., 2018; Mase et al., 2019; Wang et al., 2019). In recent years, the importance of pharmacological epigenetics has received increasing attention from medical researchers and clinicians. DMRs and DMPs are worthwhile indicators to determine the molecular characteristics (Choudhury et al., 2020; Hernandez-Meza et al., 2020). In this study, we attempted to analyze the methylation profiles at various levels from the overall methylation status to the value of a single probe by integrating 618 platinum-treated patients across 13 TCGA cancer types. We screened 62 DMRs and 3,703 DMPs between CR and PR group, which included 2,232 hypomethylated DMPs and 1,471

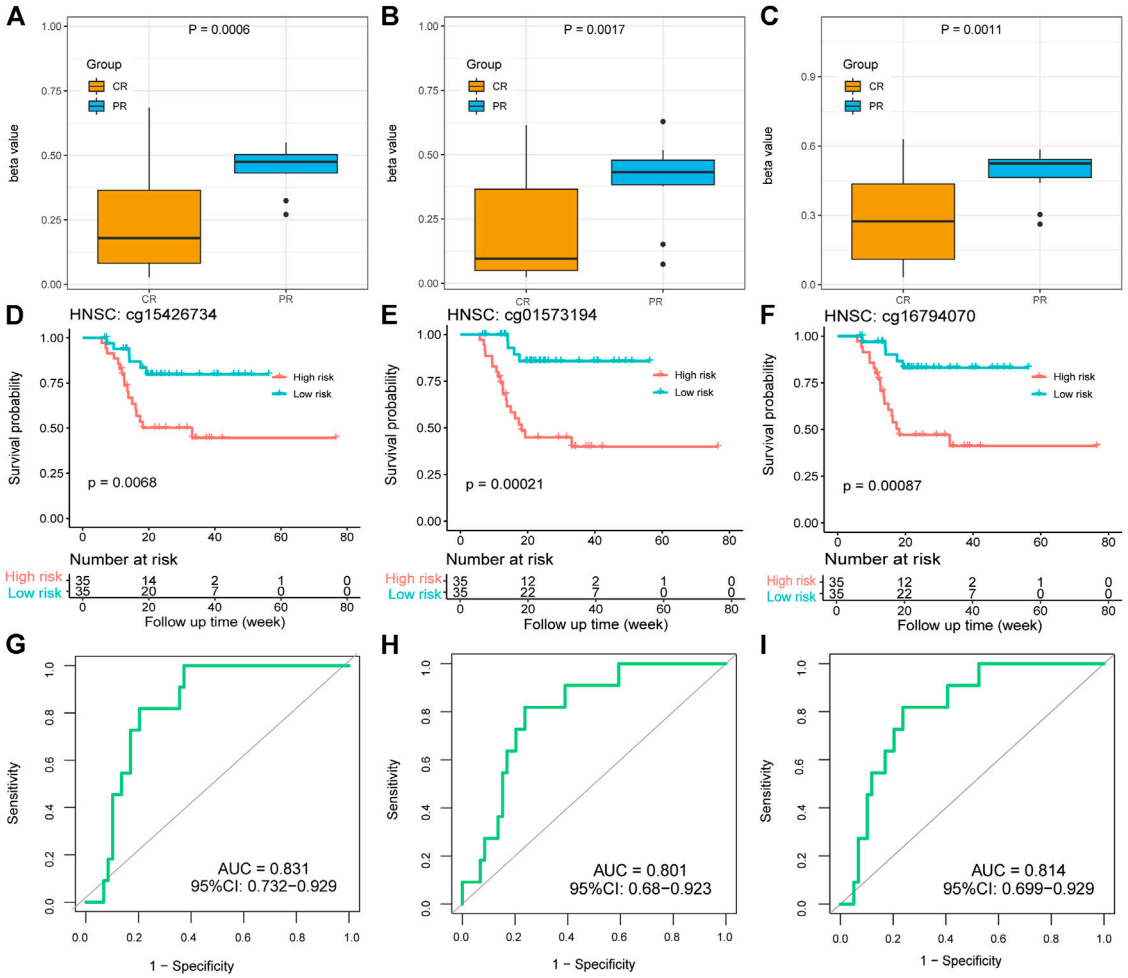


**FIGURE 6 |** Methylation and clinical values of PARD6A in platinum-treated patients with HNSC. **(A–C)** Different beta values of cg15426734, cg01573194, and cg16794070 between the CR and PR groups in HNSC. *p* values were calculated using the Wilcoxon test. **(D–F)** K-M survival plots grouped by the beta values of cg15426734, cg01573194, and cg16794070 in HNSC. *p* values were directly calculated using log-rank test. **(G–I)** ROC curves of the three DMPs.

hypermethylated DMPs. Enrichment results revealed methylation changes in platinum resistance-related pathways, though 13 cancer type had different outstanding enrichment results. Pathways including metabolism-related pathways, MAPK signaling, and neural genesis-related pathways might be epigenetically significant associated with platinum resistance. MAPK signaling is significant in ovarian patients with progression free survival over 6 months under platinum treatment (Matei et al., 2012). Inhibitors toward MAPK signaling are able to enhance sensitivity to platinum agents in melanoma cells (Makino et al., 2018). The role of MAPK signaling, which is specifically activated in platinum-based therapy, is biologically and clinically significant (Hernandez Losa et al., 2003; Makino et al., 2018). Our results indicate the activation of MAPK signaling under platinum-treatment might be driven by DNA hypomethylation of genes in MAPK pathway.

Corresponding transcriptional changes may be the most widely accepted biological mechanism of platinum response-related DNA methylation. Here, we identified the methylation and transcription characteristics of platinum response in DMRs. Leaving intergenic regions alone, q13.12 of the nineteenth chromosome is the most interesting cytoband and their corresponding genes of ZNF family might have extensive methylation patterns and potential biological significance across various cancer types. Recently, Mishra et al. revealed that methylation of ZNF genes could serve as a molecular clustering basis for pancreatic cancer (Mishra and Guda, 2017). A few analyses have focused on the clinical significance of ZNF genes' expression on drug resistance (Lee et al., 2013; Marzbany et al., 2019). Several functional studies on the role of mediating chemoresistance point out that ZNF genes may induce chemoresistance via DNA repair and activation of resistance genes' transcription (Rink et al., 2013; Chen et al., 2018). Our study of DMRs suggests that methylation and expression of ZNF genes may be associated with platinum resistance in multiple cancers.

As for potential transcription-affective abilities of DMPs, we integrated methylation and transcription profiles and identified

the typical genes/probes following widely known opposite directional patterns. We identified 26 hypermethylated transcription-repressive genes with 41 DMPs and two hypomethylated transcription-active genes with two DMPs in the profiles of platinum-resistant patients, which confirmed the existence and significance of the methylation-transcription axis in platinum response. These genes in methylation-transcription axis under platinum treatment might play a significant and functional role in platinum resistance, some of which has been reported. Overexpression of BLM RecQ like helicase (BLM) is able to induce DNA damage and increase sensitivity to platinum agents in triple-negative breast cancer and ovarian cancer (Birkbak et al., 2018). Overexpressed cyclin D1 (CCND1) can hyperactivate cyclin-dependent kinase 4 and 6 (CDK4/6) and induce cisplatin resistance in HNSC, TGCT and other cancers (Noel et al., 2010; Adkins et al., 2019). Our results might provide an interesting list of genes which participate in platinum resistance through methylation-transcription patterns.

DMPs are promising for identifying potential biological and clinical biomarkers. Regarding two of the most interesting questions, patient prognosis and response to platinum, we constructed models of 405 prognostic and 664 platinum response-predictive DMPs associated with platinum-based chemotherapy, which established a novel perspective of guiding clinical selection of optimal treatment based on pan-cancer methylation profiles. More importantly, six DMPs of four genes may have transcription-affected, prognostic, and platinum-response predictive functions in HNSC and UCEC, including MSLN (cg10398993), PRKAR2B (cg00888463), MSX1 (cg00486340), and PARD6A (cg15426734, cg01573194, and cg16794070). MSLN, a glycoprotein on the cell surface, is overexpressed in many cancers and is relevant to novel anti-cancer treatment by regulating the tumor microenvironment (Hilliard, 2018; Cerise et al., 2019). PRKAR2B plays a significant oncogenic and metastasis-promoting role in prostate cancer, especially in castration-resistant prostate cancers (Sha et al., 2018; Xia et al., 2020). MSX1 is associated with various malignant cancers and is frequently methylated in cervical and breast cancer (Yue et al., 2018a; Yue et al., 2018b). It should be pointed out that there are three PARD6A probes serving as survival risk factors with potential biological, prognostic, and response-predictive values in HNSC. PARD6A is a cell membrane protein that plays a pivotal role in enhancing the migration, invasion, and proliferation of cancer cells (Ruan et al., 2017). Methylation status and potential clinical values of PARD6A should capture the attention of researchers working on HNSC-related biomarkers. Our insufficient analytical methods might be a few minor flaws when identifying prognostic and platinum response-predictive DMPs. Other potential clinical covariates should be adjusted for further prognostic analysis and robustness of the response-predictive DMPs should be proved and verified in other external datasets. Anyway, our work provided a number of DMPs as potential biomarkers and candidates of further research. These five genes and methylation status may be promising candidates for further biological experiments and clinical studies.

Collectively, through systematic DNA methylation array analysis of 618 platinum-treated patients across 13 TCGA cancer types, we screened 62 DMRs and 3,703 DMPs between different responses to platinum-based chemotherapy. We constructed models of 405 prognostic and 664 platinum response-predictive DMPs associated with platinum-based chemotherapy, which may potentially help to guide the identification of additional clinical and epigenetic biomarkers as well as novel designs for molecular biological experiments related to platinum resistance.

## DATA AVAILABILITY STATEMENT

The original contributions presented in the study are included in the article/**Supplementary Material**, further inquiries can be directed to the corresponding author.

## AUTHOR CONTRIBUTIONS

ZL and RS conceived and designed the study. RS, CD, and JXL performed the computational and statistical analyses. YZ, WX, JX, JHL, ZX, and LF provide expertize technical guidance. RS, CD, and ZL wrote the manuscript, with extensive input from all authors. All authors have read and agreed to the published version of the manuscript.

## FUNDING

This study was supported by grants from the Overseas Expertize Introduction Project for Discipline Innovation (111 Project, No. 111-2-12), the National Natural Science Foundation of China (No.81972773), the Hunan Province Natural Sciences Foundation of China (No.2019JJ40395, 2019JJ40436 and 2019JJ40161), Scientific Research Project of Hunan Provincial Health Commission (No. 20200216), the Fundamental Research Funds for the Central South University (2020zzts765), and the Undergraduate Training Program for Innovation and Entrepreneurship (No.201910533180).

## ACKNOWLEDGMENTS

We would like to thank Editage (www.editage.cn) for English language editing. We would like to thank Jianming Zeng (University of Macau), and all the members of his bioinformatics team, biotrainee, for generously sharing their experience and codes. We would like to thank FigureYa (Blogger, WeChat Official Accounts) for the technical support in figure drafting and revision.

## SUPPLEMENTARY MATERIAL

The Supplementary Material for this article can be found online at: https://www.frontiersin.org/articles/10.3389/fphar.2021.616529/full#supplementary-material

## REFERENCES


Adkins, D., Ley, J., Neupane, P., Worden, F., Sacco, A. G., Palka, K., et al. (2019). Palbociclib and Cetuximab in Platinum-Resistant and in Cetuximab-Resistant Human Papillomavirus-Unrelated Head and Neck Cancer: a Multicentre, Multigroup, Phase 2 Trial. *Lancet Oncol.* 20 (9), 1295–1305. doi:10.1016/S1470-2045(19)30405-X

Agarwal, R., and Kaye, S. B. (2003). Ovarian Cancer: Strategies for Overcoming Resistance to Chemotherapy. *Nat. Rev. Cancer* 3 (7), 502–516. doi:10.1038/nrc1123

Alcindor, T., and Beauger, N. (2011). Oxaliplatin: a Review in the Era of Molecularly Targeted Therapy. *Curr. Oncol.* 18 (1), 18–25. doi:10.3747/co.v18i1.708

Birkbak, N. J., Li, Y., Pathania, S., Greene-Colozzi, A., Dreze, M., Bowman-Colin, C., et al. (2018). Overexpression of BLM Promotes DNA Damage and Increased Sensitivity to Platinum Salts in Triple-Negative Breast and Serous Ovarian Cancers. *Annals Oncol.* 29 (4), 903–909. doi:10.1093/annonc/mdy049

Cerise, A., Bera, T. K., Liu, X., Wei, J., and Pastan, I. (2019). Anti-Mesothelin Recombinant Immunotoxin Therapy for Colorectal *Cancer*. *Clinical Colorectal Cancer* 18 (3), 192–199. doi:10.1016/j.clcc.2019.06.006

Chen, G., Chen, J., Qiao, Y., Shi, Y., Liu, W., Zeng, Q., et al. (2018). ZNF830 Mediates Cancer Chemoresistance through Promoting Homologous-Recombination Repair. *Nucleic Acids Res.* 46 (3), 1266–1279. doi:10.1093/nar/gkx1258

Choudhury, S. R., Ashby, C., Tytarenko, R., Bauer, M., Wang, Y., Deshpande, S., et al. (2020). The Functional Epigenetic Landscape of Aberrant Gene Expression in Molecular Subgroups of Newly Diagnosed Multiple Myeloma. *J. Hematol. Oncol.* 13 (1), 108. doi:10.1186/s13045-020-00933-y

Colaprico, A., Silva, T. C., Olsen, C., Garofano, L., Cava, C., Garolini, D., et al. (2016). TCGAbiolinks: an R/Bioconductor Package for Integrative Analysis of TCGA Data. *Nucleic Acids Res.* 44 (8), e71. doi:10.1093/nar/gkv1507

Dasari, S., and Bernard Tchounwou, P. (2014). Cisplatin in Cancer Therapy: Molecular Mechanisms of Action. *European Journal of Pharmacology* 740, 364–378. doi:10.1016/j.ejphar.2014.07.025

Dawson, M. A., and Kouzarides, T. (2012). *Cancer* Epigenetics: from Mechanism to Therapy. *Cell* 150 (1), 12–27. doi:10.1016/j.cell.2012.06.013

Fang, F., Cardenas, H., Huang, H., Jiang, G., Perkins, S. M., Zhang, C., et al. (2018a). Genomic and Epigenomic Signatures in Ovarian *Cancer* Associated with Resensitization to Platinum Drugs. *Cancer Res.* 78 (3), 631–644. doi:10.1158/0008-5472.CAN-17-1492

Fang, L., Wang, H., and Li, P. (2018b). Systematic Analysis Reveals a lncRNA-mRNA Co-expression Network Associated with Platinum Resistance in High-Grade Serous Ovarian Cancer. *Invest. New Drugs* 36 (2), 187–194. doi:10.1007/s10637-017-0523-3

Fennell, D. A., Summers, Y., Cadranel, J., Benepal, T., Christoph, D. C., Lal, R., et al. (2016). Cisplatin in the Modern Era: The Backbone of First-Line Chemotherapy for Non-small Cell Lung Cancer. *Cancer Treatment Reviews* 44, 42–50. doi:10.1016/j.ctrv.2016.01.003

Galluzzi, L., Senovilla, L., Vitale, I., Michels, J., Martins, I., Kepp, O., et al. (2012). Molecular Mechanisms of Cisplatin Resistance. *Oncogene* 31 (15), 1869–1883. doi:10.1038/onc.2011.384

Grasse, S., Lienhard, M., Frese, S., Kerick, M., Steinbach, A., Grimm, C., et al. (2018). Epigenomic Profiling of Non-small Cell Lung Cancer Xenografts Uncover LRP12 DNA Methylation as Predictive Biomarker for Carboplatin Resistance. *Genome Med.* 10 (1), 55. doi:10.1186/s13073-018-0562-1

Hernandez-Meza, G., Von Felden, J., Gonzalez-Kozlova, E. E., Garcia-Lezana, T., Peix, J., Portela, A., et al. (2020). DNA Methylation Profiling of Human Hepatocarcinogenesis. *Hepatology*. doi:10.1002/hep.31659

Hilliard, T. (2018). The Impact of Mesothelin in the Ovarian *Cancer* Tumor Microenvironment. *Cancers* 10 (9), 277. doi:10.3390/cancers10090277

Jaffe, A. E., Murakami, P., Lee, H., Leek, J. T., Fallin, M. D., Feinberg, A. P., et al. (2012). Bump Hunting to Identify Differentially Methylated Regions in Epigenetic Epidemiology Studies. *Int. J. Epidemiol.* 41 (1), 200–209. doi:10.1093/ije/dyr238

Lee, E. J., Kang, G., Kang, S. W., Jang, K.-T., Lee, J., Park, J. O., et al. (2013). GSTT1 Copy Number Gain and ZNF Overexpression Are Predictors of Poor Response to Imatinib in Gastrointestinal Stromal Tumors. *PLoS One* 8 (10), e77219. doi:10.1371/journal.pone.0077219

Liu, D., Zhang, X.-X., Li, M.-C., Cao, C.-H., Wan, D.-Y., Xi, B.-X., et al. (2018). C/EBPβ Enhances Platinum Resistance of Ovarian Cancer Cells by Reprogramming H3K79 Methylation. *Nat. Commun.* 9 (1), 1739. doi:10.1038/s41467-018-03590-5

Losa, J. H., Cobo, C. P., Viniegra, J. G., Lobo, V. J. S.-A., Cajal, S. R. y., and Sánchez-Prieto, R. (2003). Role of the P38 MAPK Pathway in Cisplatin-Based Therapy. *Oncogene* 22 (26), 3998–4006. doi:10.1038/sj.onc.1206608

Makino, E., Gutmann, V., Kosnopfel, C., Niessner, H., Forschner, A., Garbe, C., et al. (2018). Melanoma Cells Resistant towards MAPK Inhibitors Exhibit Reduced TAp73 Expression Mediating Enhanced Sensitivity to Platinum-Based Drugs. *Cell Death Dis.* 9 (9), 930. doi:10.1038/s41419-018-0952-8

Marzbany, M., Bishayee, A., and Rasekhian, M. (2019). Increased Expression of ZNF 703 in Breast Cancer Tissue: An Opportunity for RNAi-NSAID Combinatorial Therapy. *Biotechnol. Applied Biochemistry* 66 (5), 808–814. doi:10.1002/bab.1790

Mase, S., Shinjo, K., Totani, H., Katsushima, K., Arakawa, A., Takahashi, S., et al. (2019). ZNF671 DNA Methylation as a Molecular Predictor for the Early Recurrence of Serous Ovarian Cancer. *Cancer Sci.* 110 (3), 1105–1116. doi:10.1111/cas.13936

Matei, D., Fang, F., Shen, C., Schilder, J., Arnold, A., Zeng, Y., et al. (2012). Epigenetic Resensitization to Platinum in Ovarian Cancer. *Cancer Res.* 72 (9), 2197–2205. doi:10.1158/0008-5472.CAN-11-3909

Mishra, N. K., and Guda, C. (2017). Genome-wide DNA Methylation Analysis Reveals Molecular Subtypes of Pancreatic Cancer. *Oncotarget* 8 (17), 28990–29012. doi:10.18632/oncotarget.15993

Noel, E. E., Yeste-Velasco, M., Mao, X., Perry, J., Kudahetti, S. C., Li, N. F., et al. (2010). The Association of CCND1 Overexpression and Cisplatin Resistance in Testicular Germ Cell Tumors and Other Cancers. *American Journal Pathol.* 176 (6), 2607–2615. doi:10.2353/ajpath.2010.090780

Peng, L., and Zhong, X. (2015). Epigenetic Regulation of Drug Metabolism and Transport. *Acta Pharmaceutica Sinica B* 5 (2), 106–112. doi:10.1016/j.apsb.2015.01.007

Rink, L., Ochs, M. F., Zhou, Y., Von Mehren, M., and Godwin, A. K. (2013). ZNF-mediated Resistance to Imatinib Mesylate in Gastrointestinal Stromal Tumor. *PLoS One* 8 (1), e54477. doi:10.1371/journal.pone.0054477

Robin, X., Turck, N., Hainard, A., Tiberti, N., Lisacek, F., Sanchez, J.-C., et al. (2011). pROC: an Open-Source Package for R and S+ to Analyze and Compare ROC Curves. *BMC Bioinformatics* 12, 77. doi:10.1186/1471-2105-12-77

Rossi, A., and Di Maio, M. (2016). Platinum-based Chemotherapy in Advanced Non-small-cell Lung Cancer: Optimal Number of Treatment Cycles. *Expert Review Anticancer Therapy* 16 (6), 653–660. doi:10.1586/14737140.2016.1170596

Ruan, L., Shen, Y., Lu, Z., Shang, D., Zhao, Z., Lu, Y., et al. (2017). Roles of Partitioning-Defective Protein 6 (Par6) and its Complexes in the Proliferation, Migration and Invasion of Cancer Cells. *Clin. Exp. Pharmacol. Physiol.* 44 (9), 909–913. doi:10.1111/1440-1681.12794

Sha, J., Han, Q., Chi, C., Zhu, Y., Pan, J., Dong, B., et al. (2018). PRKAR2B Promotes Prostate Cancer Metastasis by Activating Wnt/β-Catenin and Inducing Epithelial-Mesenchymal Transition. *J. Cel Biochem.* 119 (9), 7319–7327. doi:10.1002/jcb.27030

Tian, Y., Morris, T. J., Webster, A. P., Yang, Z., Beck, S., Feber, A., et al. (2017). ChAMP: Updated Methylation Analysis Pipeline for Illumina BeadChips. *Bioinformatics* 33 (24), 3982–3984. doi:10.1093/bioinformatics/btx513

Vera, O., Jimenez, J., Pernia, O., Rodriguez-Antolin, C., Rodriguez, C., Sanchez Cabo, F., et al. (2017). DNA Methylation of miR-7 Is a Mechanism Involved in Platinum Response through MAFG Overexpression in *Cancer* Cells. *Theranostics* 7 (17), 4118–4134. doi:10.7150/thno.20112

Verhoeven, R. H. A., Gondos, A., Janssen-Heijnen, M. L. G., Saum, K. U., Brewster, D. H., Holleczek, B., et al. (2013). Testicular Cancer in Europe and the USA: Survival Still Rising Among Older Patients. *Annals Oncol.* 24 (2), 508–513. doi:10.1093/annonc/mds460

Wang, X., Ghareeb, W. M., Zhang, Y., Yu, Q., Lu, X., Huang, Y., et al. (2019). Hypermethylated and Downregulated MEIS2 Are Involved in Stemness

Properties and Oxaliplatin-based Chemotherapy Resistance of Colorectal Cancer. *J. Cel Physiol* 234 (10), 18180–18191. doi:10.1002/jcp.28451

Xia, L., Han, Q., Chi, C., Zhu, Y., Pan, J., Dong, B., et al. (2020). Transcriptional Regulation of PRKAR2B by miR-200b-3p/200c-3p and XBP1 in Human Prostate Cancer. *Biomedicine & Pharmacotherapy* 124, 109863. doi:10.1016/j.biopha.2020.109863

Yu, C., Wang, Z., Sun, Z., Zhang, L., Zhang, W., Xu, Y., et al. (2020). Platinum-based Combination Therapy: Molecular Rationale, Current Clinical Uses, and Future Perspectives. *J. Med. Chem.* 63, 13397–13412. doi:10.1021/acs.jmedchem.0c00950

Yu, G., and He, Q.-Y. (2016). ReactomePA: an R/Bioconductor Package for Reactome Pathway Analysis and Visualization. *Mol. Biosyst.* 12 (2), 477–479. doi:10.1039/c5mb00663e

Yu, G., Wang, L.-G., Han, Y., and He, Q.-Y. (2012). clusterProfiler: an R Package for Comparing Biological Themes Among Gene Clusters. *OMICS: A Journal Integrative Biol.* 16 (5), 284–287. doi:10.1089/omi.2011.0118

Yue, Y., Yuan, Y., Li, L., Fan, J., Li, C., Peng, W., et al. (2018a). Homeobox Protein MSX1 Inhibits the Growth and Metastasis of Breast Cancer Cells and Is Frequently Silenced by Promoter Methylation. *Int. J. Mol. Med.* 41 (5), 2986–2996. doi:10.3892/ijmm.2018.3468

Yue, Y., Zhou, K., Li, J., Jiang, S., Li, C., and Men, H. (2018b). MSX1 Induces G0/G1 Arrest and Apoptosis by Suppressing Notch Signaling and Is Frequently Methylated in Cervical Cancer. *Ott* Vol.11, 4769–4780. doi:10.2147/OTT.S165144

Zhu, Y., Zhao, Y., Dong, S., Liu, L., Tai, L., and Xu, Y. (2020). Systematic Identification of Dysregulated lncRNAs Associated with Platinum-Based Chemotherapy Response across 11 Cancer Types. *Genomics* 112 (2), 1214–1222. doi:10.1016/j.ygeno.2019.07.007

**Conflict of Interest:** The authors declare that the research was conducted in the absence of any commercial or financial relationships that could be construed as a potential conflict of interest.

frontiers in Pharmacology

ORIGINAL RESEARCH
published: 10 May 2021
doi: 10.3389/fphar.2021.659735

# FMS-Related Tyrosine Kinase 3 Ligand Promotes Radioresistance in Esophageal Squamous Cell Carcinoma

*Zuoquan Zhu*[1†], *Jiahang Song*[1†], *Junjie Gu*[1], *Bing Xu*[1], *Xinchen Sun*[1*] and *Shu Zhang*[1,2*]

[1]Department of Radiotherapy, The First Affiliated Hospital of Nanjing Medical University, Nanjing, China, [2]Core Facility Center, The First Affiliated Hospital of Nanjing Medical University, Nanjing, China

**Aim:** The FMS-related tyrosine kinase 3 ligand (FL) has an important role in regulating FMS-related tyrosine kinase 3 (Flt-3) activity. Serum FL levels are markedly increased among patients with hematopoietic disease. However, its role in radiation treatment remains unclear. In this study, we investigated the effects of FL on radiotherapy for esophageal squamous cell carcinoma (ESCC).

**Methods:** KYSE150 and KYSE450 cells were stimulated with FL (200 ng/ml). mRNA expression was analyzed using qRT-PCR. Cell viability was checked using CCK-8 assay kits. Proliferation was determined using the EdU assay. Radiosensitivity was detected through a colony-forming assay. Flow cytometry was used to evaluate cell apoptosis. The number of γH2AX foci was verified using an immunofluorescence assay. The change in relative proteins was determined by western blot analysis. The growth of transplanted tumors was demonstrated in nude mice.

**Results:** Our results showed that FL increased the radiation resistance of ESCC cells by promoting clone formation, increasing EdU incorporation, enhancing DNA damage repair, and inhibiting apoptosis. Moreover, the Flt-3 receptor expression significantly increased in ESCC cells after radiation, which may have been an important factor in their radioresistance.

**Conclusion:** Our results suggest that FL increases the radioresistance of esophageal cancer cells and that FL-Flt-3 could be a potential target for enhancing radiosensitivity in ESCC.

**Keywords: fms-related tyrosine kinase 3 ligand, esophageal squamous cell carcinoma, apoptosis, radiotherapy, DNA damage**

OPEN ACCESS

***Edited by:***
*Xiaoping Lin,*
*Sun Yat-sen University Cancer Center (SYSUCC), China*

***Reviewed by:***
*Susanne Müller,*
*Goethe University Frankfurt, Germany*
*Mingliang You,*
*Hangzhou Cancer Hospital, China*

***Correspondence:**
*Shu Zhang*
*zhangshu@njmu.edu.cn*
*Xinchen Sun*
*sunxinchen2012@163.com*

*[†]These authors have contributed equally to this work*

***Specialty section:***
*This article was submitted to Pharmacology of Anti-Cancer Drugs, a section of the journal Frontiers in Pharmacology*

***Received:*** *28 January 2021*
***Accepted:*** *26 April 2021*
***Published:*** *10 May 2021*

***Citation:***
*Zhu Z, Song J, Gu J, Xu B, Sun X and Zhang S (2021) FMS-Related Tyrosine Kinase 3 Ligand Promotes Radioresistance in Esophageal Squamous Cell Carcinoma. Front. Pharmacol. 12:659735. doi: 10.3389/fphar.2021.659735*

## INTRODUCTION

Esophageal cancer (EC) is one of the most common cancers worldwide, with the distribution of its histologic subtypes—esophageal squamous cell carcinoma (ESCC) and esophageal adenocarcinoma (EA)—differing depending on geography (Siegel et al., 2020). More specifically, ESCC is a prevalent histological classification in East Asia (Colvin et al., 2017). Radiotherapy (RT) is recommended as an important and effective method for malignant treatment in about half of cancer patients during

clinical treatment (Mariette et al., 2015). ESCC patients who have contraindications for surgery or locally advanced disease have a treatment option through RT. However, radioresistance is a major cause of treatment failure, contributing to inadequate cure, relapse, and metastasis (Cohen and Leichman, 2015). Therefore, there is an urgent need to develop possible targets for radiosensitization to improve therapeutic effects on ESCC.

In 1993–1994, the FMS-related tyrosine kinase 3 ligand (FL) was cloned by two independent groups (Lyman et al., 1993; Hannum et al., 1994). FL is a type I transmembrane protein that can be secreted as a soluble dimeric protein. When the FMS-related tyrosine kinase 3 (Flt-3) receptor is activated by membrane-bound or cell-free forms, the growth of progenitor cells is promoted in the bone marrow and blood (Lisovsky et al., 1996a). There is also a strong synergy between FL and other hematopoietic growth factors (Sitnicka et al., 2003). Bone marrow hyperplasia, splenomegaly, lymphadenectasis, and hepatomegaly were evident in mice treated with FL (Tobón et al., 2010). In addition, FL remains at a high level in the majority of leukemias, and mutations in the Flt-3 gene are frequent genetic lesions in acute myeloid leukemia (Nakao et al., 1996; Stirewalt and Radich, 2003). In contrast, an increased FL plasma concentration can be used as a biomarker for radiation-induced marrow damage and residual hematopoiesis (Bertho et al., 2001; Prat et al., 2006). Moreover, plasma FL levels respond to radiation dose and time of collection (Sproull et al., 2013).

However, little is known about the role of FL in ESCC after RT. In the present study, we investigated the effect of FL on radiation-induced ESCCs and explored the underlying mechanisms.

# MATERIALS AND METHODS

## Cell Culture and Irradiation Methods

Human ESCC cell lines were obtained from the Shanghai Institute of Cell Biology (Shanghai, China). Cells were cultured in RPMI 1640 medium supplemented with 10% fetal bovine serum at 37°C in a humidified atmosphere with 5% $CO_2$. Cells were treated with PBS or recombinant human Flt-3 ligand (0, 5, 10, 20, 40, 80, 160, 320, 200, and 640 ng/ml) (PeproTech, United States), and the cells in the IR group were irradiated with 2, 4, 6, 8, or 10 Gy ionizing radiation ~~X-ray~~ from a medical linear accelerator (Precise accelerator, Elekta, Sweden).

## Quantitative Real-Time PCR

According to the manufacturer's instructions, mRNA was extracted from cells using Trizol (Invitrogen, Carlsbad, CA, United States) and was reverse transcribed using PrimeScript RT Master Mix (Takara Bio, Otsu, Japan). RT-PCR reactions were performed using a StepOnePlus Real-Time PCR System (Thermo Fisher Scientific, MA, United States) using SYBR Premix Ex Taq II (Takara Bio). The qRT-PCR primers were F: GGTGGGAATGGGTCAGAAGG (5′-3′) and R: GTACATGGC TGGGGTGTTGA (5′-3′) for ACTB, F: AGGGACAGTGTA CGAAGCTG (5′-3′) and R: GCTGTGCTTAAAGACCCA GAG (5′-3′) for Flt-3.

## Western Blot Analysis

Total protein was separated from cell lysates using RIPA buffer (Beyotime, Shanghai, China) supplemented with protease and phosphatase inhibitors (Kaygen, Nanjing, Jiangsu Province, China). The protein concentration was quantified using a BCA kit (Beyotime Biotechnology, Shanghai, China). The same amounts of proteins were separated by SDS-PAGE and then transferred to PVDF membranes (BioWorld, Saint Louis, MN, United States). The membranes were blocked with 5% skim milk for 2 h and then incubated overnight with primary antibodies against GAPDH, Flt-3, P-Flt-3, AKT, P-AKT, poly (ADP-ribose), polymerase1 (PARP1), Bad, and P-Bad (Cell Signaling Technology, Boston, MA, United States) at 4°C. On the second day, the membranes were incubated with secondary antibodies (Cell Signaling Technology, Boston, MA, United States) at room temperature for 1 h. Immunoblotted protein signals were detected using an enhanced chemiluminescence detection kit (Thermo Fisher Scientific) on the ChemiDoc XRS imaging system (Quantity One Quantitation software; Bio-Rad Laboratories, Hercules, CA, United States).

## Cell Viability Assay

Cell viability was measured using the CCK-8 assay. The cells were seeded into 96-well plates in triplicates at a density of 5,000 cells per well. After adherence, the cells were treated with or without a single dose of 8 Gy radiation and were stimulated with equal amounts of PBS and FL (200 ng/ml) after 24 h of radiation. At the designated time points after radiation (day 1, day 2, day 3, day 4), CCK-8 solution was added to each well according to the manufacturer's instructions. The absorbance was measured at a wavelength of 450 nm using a microplate reader (ELx800, BioTek, Winooski, VT, United States). The experiment was repeated thrice.

## Clonogenic Survival Assay

Cells were plated in triplicates into 6-well plates at a density of $1 \times 10^2$–$10^4$ cells/well and were allowed to adhere for 12 h. Then, the cells were irradiated at doses of 2, 4, 6, and 8 Gy and were cultured in a 5% $CO_2$ incubator at 37°C for an additional 10 days. After the end of the assay, cells were stained with Giemsa. Cell survival curves were fitted according to a multi-target single-hit model: $S = 1-(1- e^{-D/D0})^N$.

## EdU Assay

The EdU analysis kit (RiboBio, China) was used to assess cell proliferation. ESCC cells were seeded in confocal laser cuvette ~~ESCC plates~~ at a density of $5 \times 10^4$ cells/well. Next, the cells were incubated in a medium containing 50 μM EdU (C10310-1, RiboBio) for 6 h and processed according to the manufacturer's instructions. Images were acquired under fluorescence microscopy. The average proportion of EdU-positive cells in three random field of view was analyzed.

## Flow Cytometry Analysis

The cells were seeded in 6-well plates at a density of $1 \times 10^5$ cells/well. After 24 h treatment, apoptotic cells were detected using the FITC Annexin V Apoptosis Detection Kit (BD Biosciences,

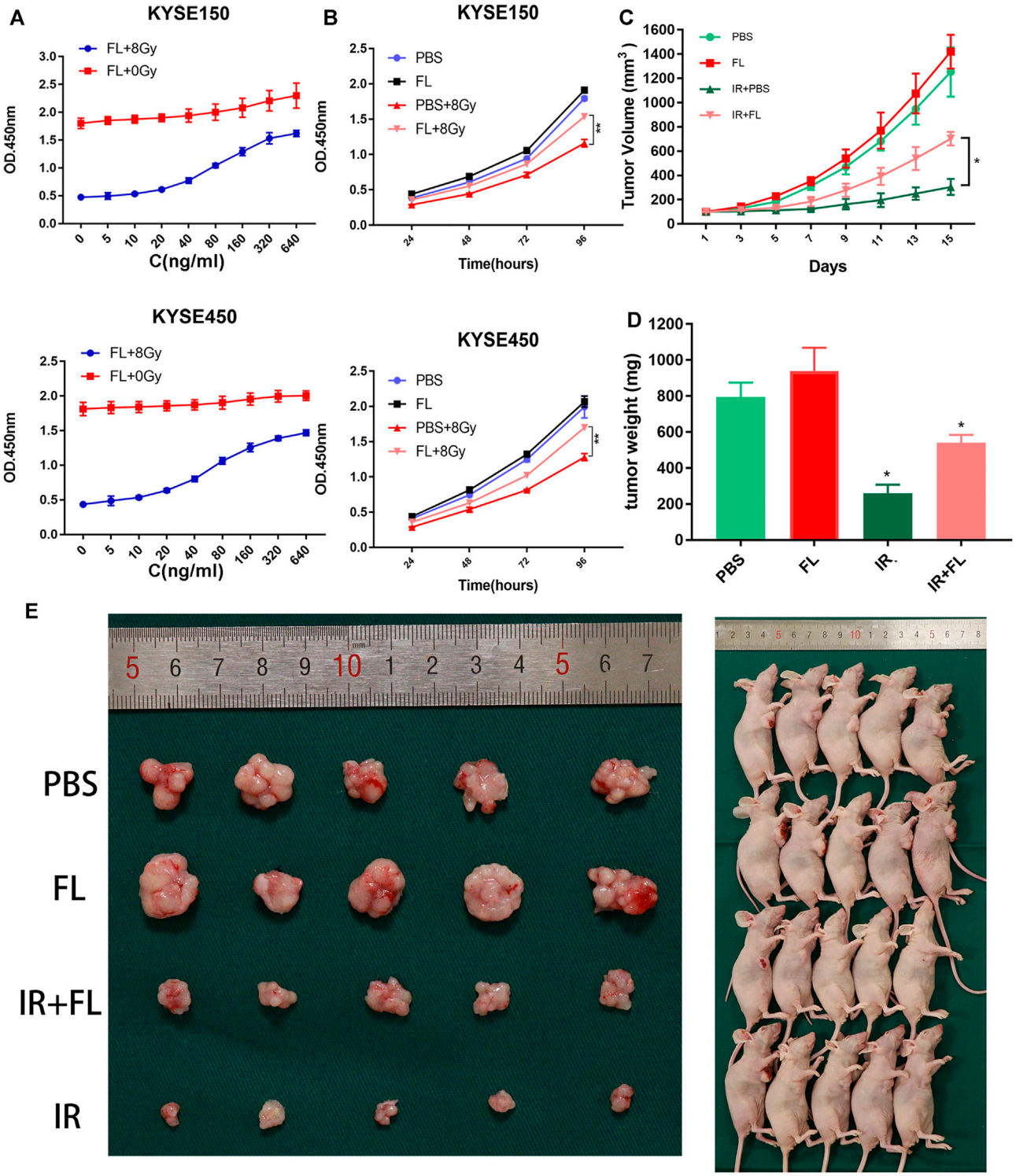


**FIGURE 1 |** FL promotes viability and tumor growth of ESCCs *in vitro* and *in vivo*. **(A)** The cell viability of ESCC cells in different concentration (0, 5, 10, 20, 40, 80, 160, 320, and 640 ng/ml) of FL (n = 3). **(B)** Cell viability of different time-point after 200 ng/ml FL treatment (n = 3). **(C)** The tumor volume assessed every 2 days (n = 5). **(D)** The tumor weight after sacrificed (n = 5). **(E)** Images of nude mice (n = 5). Mean ± SEM, $*p < 0.05$, $**p < 0$ 0.01.

Oxford, United Kingdom). We used flow cytometry to evaluate the rate of apoptosis and repeated all experiments thrice.

## Immunofluorescence Assay

The cells were seeded into a confocal laser cuvette at a concentration of $5 \times 10^4$ and were treated with a single dose of 8 Gy. After 24 h of radiation exposure, the cells were exposed to FL (200 ng/ml). The cells were harvested at 0, 2, 8, and 24 h after FL administration. The cells were then fixed in 4% paraformaldehyde for 30 min at room temperature and permeabilized in 0.1% Triton X-100 (Sigma, Santa Clara, CA, United States) for 15 min. The cells were blocked with 5% BSA (Gibco, NY, United States) for 1 h and incubated overnight with the primary antibody γH2AX (1 μg/ml; Abcam, Cambridge, Cambridgeshire, United Kingdom) at 4°C. The cells were washed thrice in TBST every 5 min and then incubated with secondary antibodies (Beyotime Biotechnology) for 1 h. Finally, the cells were treated with 2 μg/ml DAPI (Beyotime Biotechnology) for 5 min and then observed using a confocal fluorescence microscope (Leica, Frankfurt, Germany).

## Xenograft Tumors in Nude Mice

Nude mice (6 weeks old) were obtained from the Nanjing Medical University Animal Center (Nanjing, China). The mice were divided into four groups (n = 5): (a) PBS, (b) FL, (c) IR, and (d) IR + FL. KYSE150 cells were subcutaneously implanted into the right leg of each mouse. Approximately 20 days post-injection, mice in the IR group were exposed to irradiation (8 Gy) once, and 10 μg/d of PBS or FL was administered through intraperitoneal injections. The mice were sacrificed on day 35. Tumor diameters were measured every two days. Tumor volume was calculated according to the following formula: tumor volume (in $mm^3$) = (length [L] × width $[W]^2$)/2. IHC for P-Flt-3 and Ki 67 (Affinity Biosciences, United States) was also performed.

## Statistical Analyses

The data are expressed as the mean ± standard error of mean of at least three experiments. We used the *t*-test, one-way analysis of variance (ANOVA), and two-way ANOVA to determine the differences between treatment groups. Statistical analyses were performed using GraphPad Prism 5.0 (GraphPad Software, San Diego, CA, United States), and a $p$ value of $< 0.05$ was considered statistically significant.

# RESULTS

## FL Increased Radioresistance in Radiation-Induced ESCC *In Vitro* and *In Vivo*

KYSE150 and KYSE450 cells were treated with PBS or FL to verify whether FL was related to ESCC tumor growth. Cell viability was detected using a CCK-8 assay. As shown in **Figure 1A**, the optical density (OD) values significantly increased with the FL concentration (ranging from 5 to 640 ng/ml) in the ionizing radiation ~~X-ray~~ exposure group. Compared to the control, FL (640 ng/ml) increased cell viability up to 342.3 and 338.4% in KYSE150 and KYSE450, respectively. Without radiation, the maximum cell viability induced by FL (640 ng/ml) in KYSE150 and KYSE450 was 127.6 and 110.7%, respectively, compared to the control. In subsequent experiments, 200 ng/ml FL was used. Furthermore, cell viability was detected at 24, 48, 72, and 96 h, and after irradiation, the OD values of the FL group were higher than those of the PBS group (**Figure 1B**). At 48 h, the cell viability induced in KYSE150 and KYSE450 by FL (200 ng/ml) was 121.6 and 125.5% compared to the control, respectively; at 96 h, these values were 132.5 and 132.7%, respectively. However, there was no significant difference between the non-irradiated groups.

To confirm the effects of FL on ESCC cells *in vivo*, we injected nude mice with KYSE150 cells plus PBS or FL. As shown in **Figure 1C**, tumor growth significantly slowed in the IR group. The increase in tumor volume was much faster in the FL group than in the PBS group after radiation, and the mean tumor volumes after 15 days were 703 and 305 $mm^3$, respectively. By contrast, FL had no significant effect on tumor growth in the non-irradiated groups. Tumor weight was markedly greater in the non-irradiated group, and there was no difference between the FL- and PBS-alone groups. However, the mean tumor weight of the IR plus FL group was larger than that of the IR plus PBS group (540 and 260 g, respectively; **Figures 1D,E**). Our results indicate that FL weakened the effects of radiotherapy and increased radioresistance in ESCCs.

## FL Promoted Proliferation in ESCC Cell Lines ~~ESCC~~

The clonogenic survival assay revealed that ESCC cells in the FL plus radiation group had a higher survival fraction (SF) than those in the PBS plus radiation group (**Figures 2A,B**). In the FL group, the SF of KYSE150 and KYSE450 at 2 Gy was 0.59 and 0.56, whereas those of the control group was 0.5 and 0.43, respectively. In addition, the mean lethal dose ($D_0$) of KYSE150 and KYSE450 in the FL group was 2.34 and 1.66 Gy, compared to the 1.47 and 1.32 Gy in control group, respectively (Supplementary Table S1). Furthermore, we found that FL markedly increased the number of EdU incorporated in the KYSE150 and KYSE450 cells after ionizing radiation. However, there were no obvious changes in the groups without ionizing radiation (**Figures 2C,D**). So FL has no obvious impact in the groups without ionizing radiation, and it only promoted the proliferation under radiation. These results therefore indicate that FL exerts radiation resistance by promoting the proliferation of ESCC cells.

## FL Enhanced DNA Damage Repair in ESCC Cell Lines ~~ESCC~~

Irradiation can directly cause DNA double-strand breaks; therefore, radiosensitivity depends largely on the ability of tumor cells to repair DNA damage caused by irradiation (Sugase et al., 2017). To assess the effect of FL (200 ng/ml) on 8 Gy IR-induced DNA damage and repair in ESCC cells, we used immunofluorescence to detect the number of gamma-H2AX (γ-H2AX) at different time points (0, 2, 6, and 24 h) after FL administration in the ionizing radiation ~~X-ray~~ exposure group. As shown in **Figures 3A,B**, the number of γ-H2AX in the FL group was not different from that in the PBS group at 0 h. However, the number of γ-H2AX in the FL group was lower than that in the

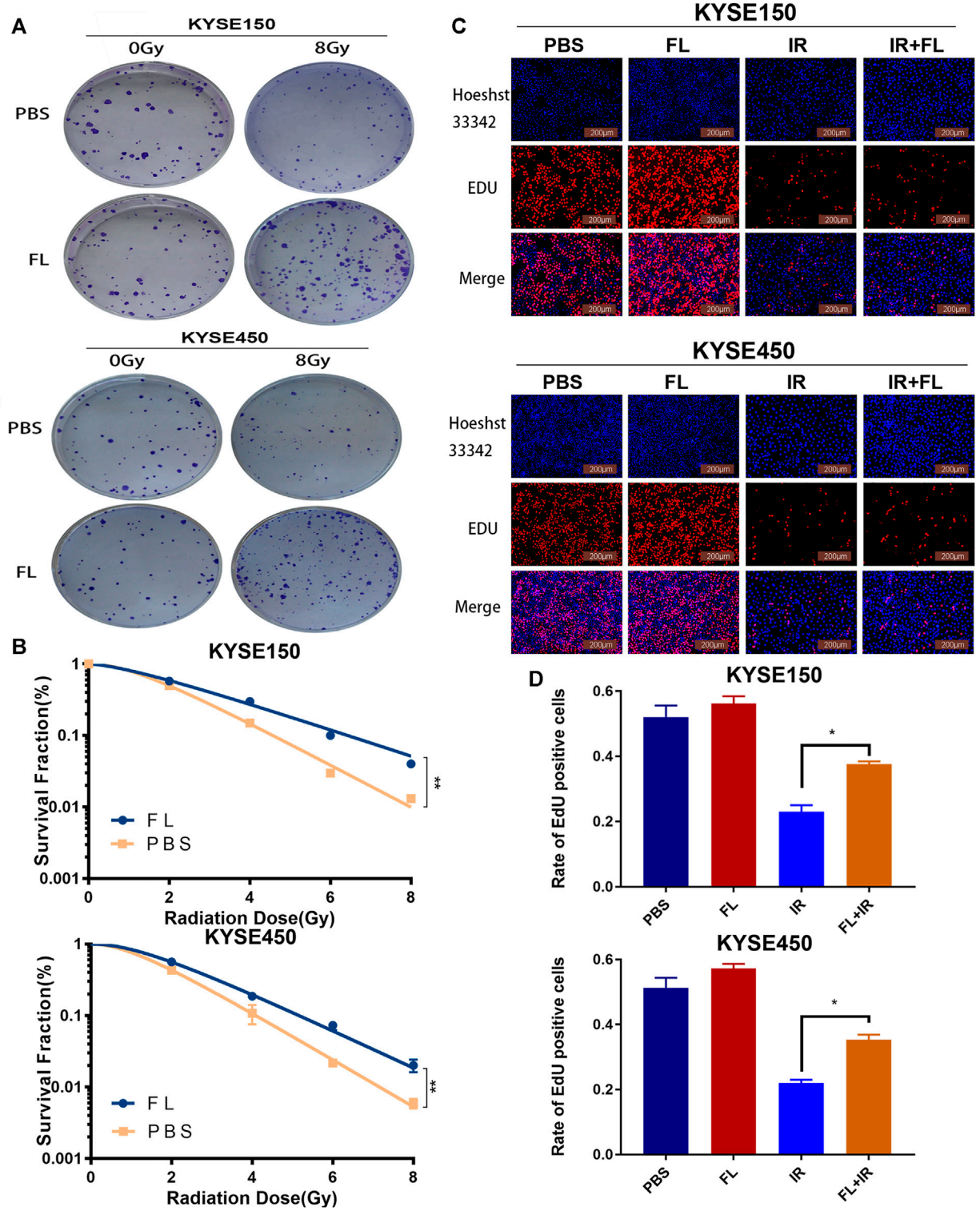


**FIGURE 2 |** FL promotes radioresistance of ESCC cells *in vitro*. **(A)** The clonogenic survival assays in PBS groups or 200 ng/ml FL administration for 24 h groups after 24 h of 8Gy radiation. **(B)** The survival curves calculated and fitted to a multi-target single-hit model from **(A)**. **(C)** the EdU incorporation assays in ESCC cells (Red fluorescence: EdU-positive cells; Blue fluorescence: total cells). **(D)** Mean rate of EdU positive cells in histogram. Mean ± SEM, N = 3, $^{*}p < 0.05$, $^{**}p < 0.01$.

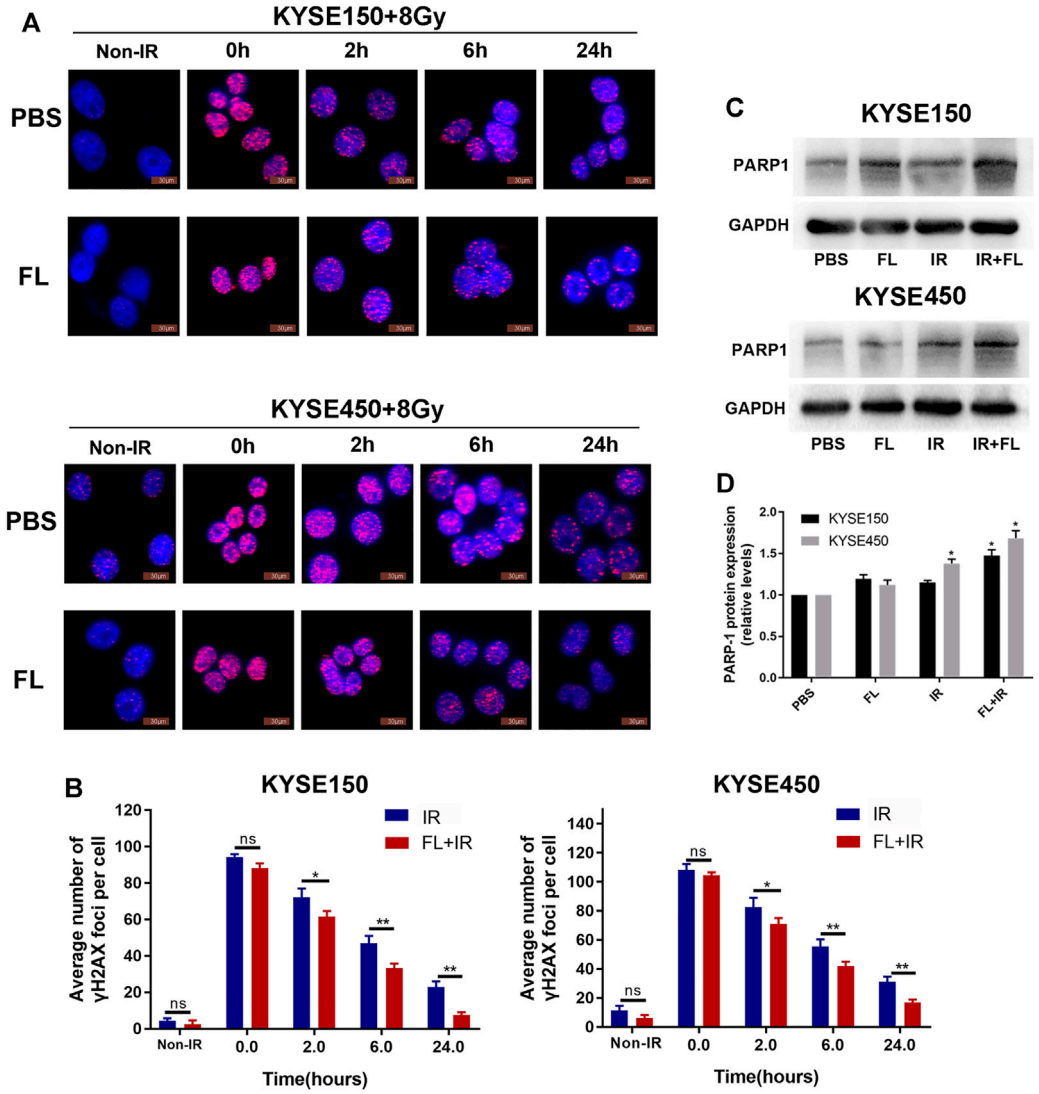


**FIGURE 3 |** FL reduces IR-induced DNA damage level and increases DNA repair. **(A,B)** Immunofluorescence detection of γH2AX foci in PBS groups or 200 ng/ml FL administration for 24 h groups after 8 Gy radiation different time. Mean ± SEM, N = 3, $^{*}p < 0.05$, $^{**}p < 0$ 0.01 **(C,D)** PARP1 protein expression in PBS groups or 200 ng/ml FL administration for 24 h groups after 24 h of 8 Gy radiation. GAPDH is an internal reference.

PBS group at 2, 6, and 24 h, especially at 24 h. Furthermore, our results showed that the number of descending γ-H2AX foci in the FL group was greater than that in the PBS group at the same time point after irradiation. Western blot assays showed that FL (200 ng/ml) increased PARP-1 expression in the 8 Gy radiation group. PARP-1 is a well-known regulator of DNA single-strand break excision repair (**Figures 3C,D**). These findings suggest that FL enhances DNA damage repair and is involved in the radiation resistance of ESCC cells.

## FL Decreased IR-Induced Apoptosis in ESCC Cell Lines ~~ESCC~~

Apoptosis is an important mechanism that regulates radiosensitivity. Flow cytometry analyses were used to further illustrate the role of FL in IR-induced apoptosis. The total apoptosis rate consisted of the early and late apoptosis populations. As shown in **Figures 4A,B**, radiation (8 Gy) induced apoptosis in KYSE150 and KYSE450 cells. Furthermore, FL (200 ng/ml) significantly decreased the IR-induced cell apoptosis rate of KYSE150 (from 26.55 to 20.49%) and KYSE450 (from 29.04 to 17.87%). However, without radiation, the apoptosis rate decreased only slightly in KYSE150 (from 6.68 to 5.49%) and KYSE450 (from 7.51 to 6.40%). These results show that FL decreased the IR-induced apoptosis rate to confer radioresistance to ESCC cells.

## Radiation Induced High Expression of the Flt-3 Receptor in ESCC Cell Lines ~~ESCC~~

FL can activate the Flt-3 receptor via membrane-bound forms; hence, we detected the mRNA and protein levels of the Flt-3

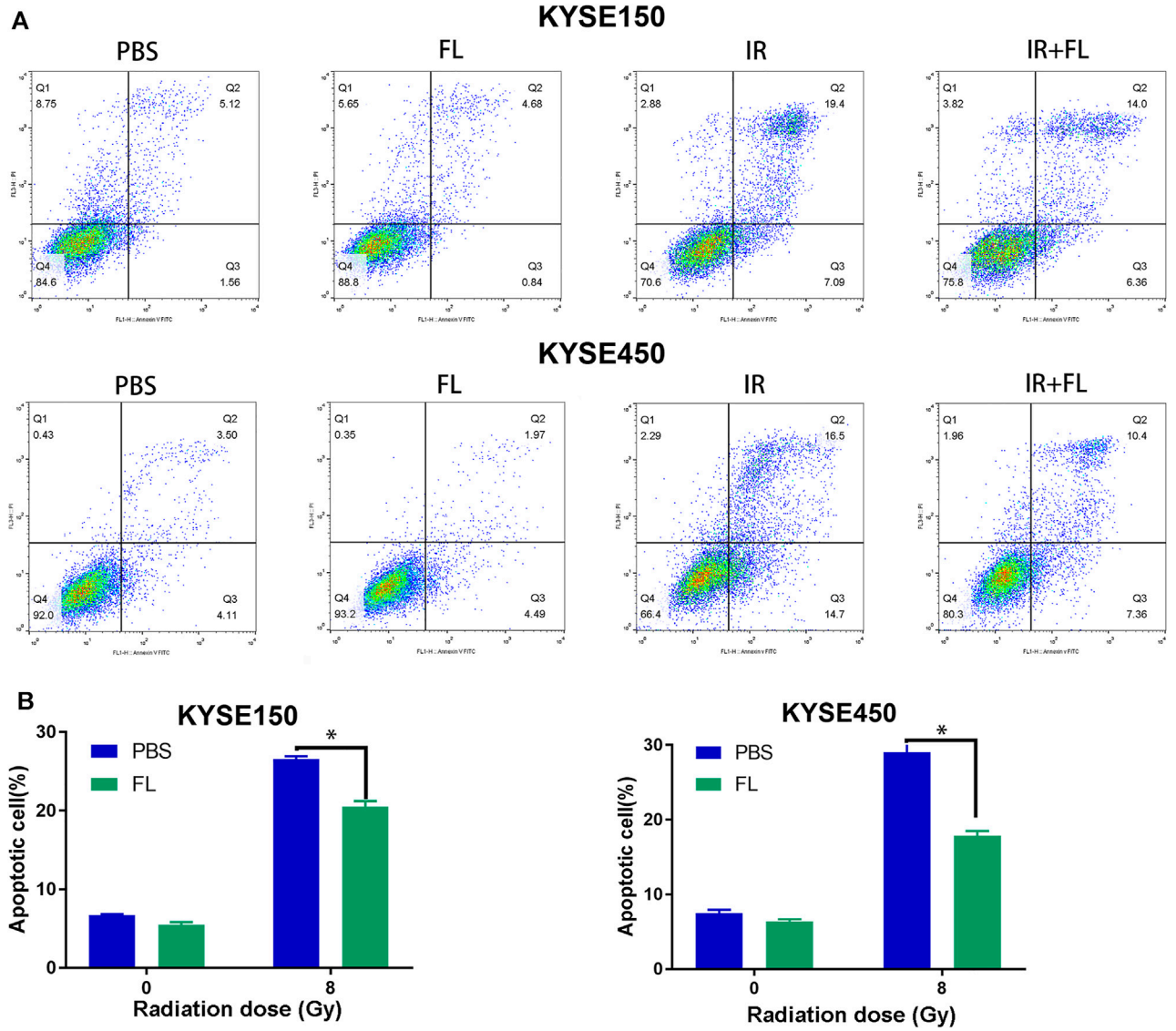


**FIGURE 4 |** FL decreases IR-induced apoptosis. **(A,B)** Apoptosis ratio in PBS groups or 200 ng/ml FL administration for 24 h groups after 24 h of 8 Gy radiation. Mean ± SEM, N = 3, $^{*}p < 0.05$.

receptor in ESCC cells. As shown in **Figure 5A**, irradiation (8 Gy) upregulated the expression of Flt-3 receptor mRNA in KYSE150 and KYSE450 cells. Furthermore, we found that this irradiation-induced upregulation of the Flt-3 receptor is dose-dependent (0, 2, 4, 6, and 8 Gy), whereas the Flt-3 receptor phosphorylation did not significantly change in either KYSE150 or KYSE450 cells 24 h after irradiation (**Figures 5B,C**). Furthermore, the time course experiments showed that 200 ng/ml FL led to a rapid and transient phosphorylation of Flt-3, with the peak level occurring at 15 min (**Figures 5D,E**); however, the Flt-3 receptor level did not change within 1 h after FL administration. These results suggest that IR-induced increased expression of the Flt-3 receptor may play a critical role in the FL-induced radioresistance of ESCC cells.

## FL Intensified IR-Induced Flt-3/PI3K/AKT Pathway Activation

Downstream-related proteins were analyzed further and we detected the Flt-3/PI3K/AKT signaling pathway and apoptosis-related proteins Bad (pro-apoptotic protein) and P-Bad (anti-apoptotic protein). As shown in **Figures 5F,G**, the phosphorylation of Flt-3, PI3K, and AKT significantly increased when FL was combined with IR, compared with FL alone. P-Bad (ser136) protein levels were upregulated in the FL

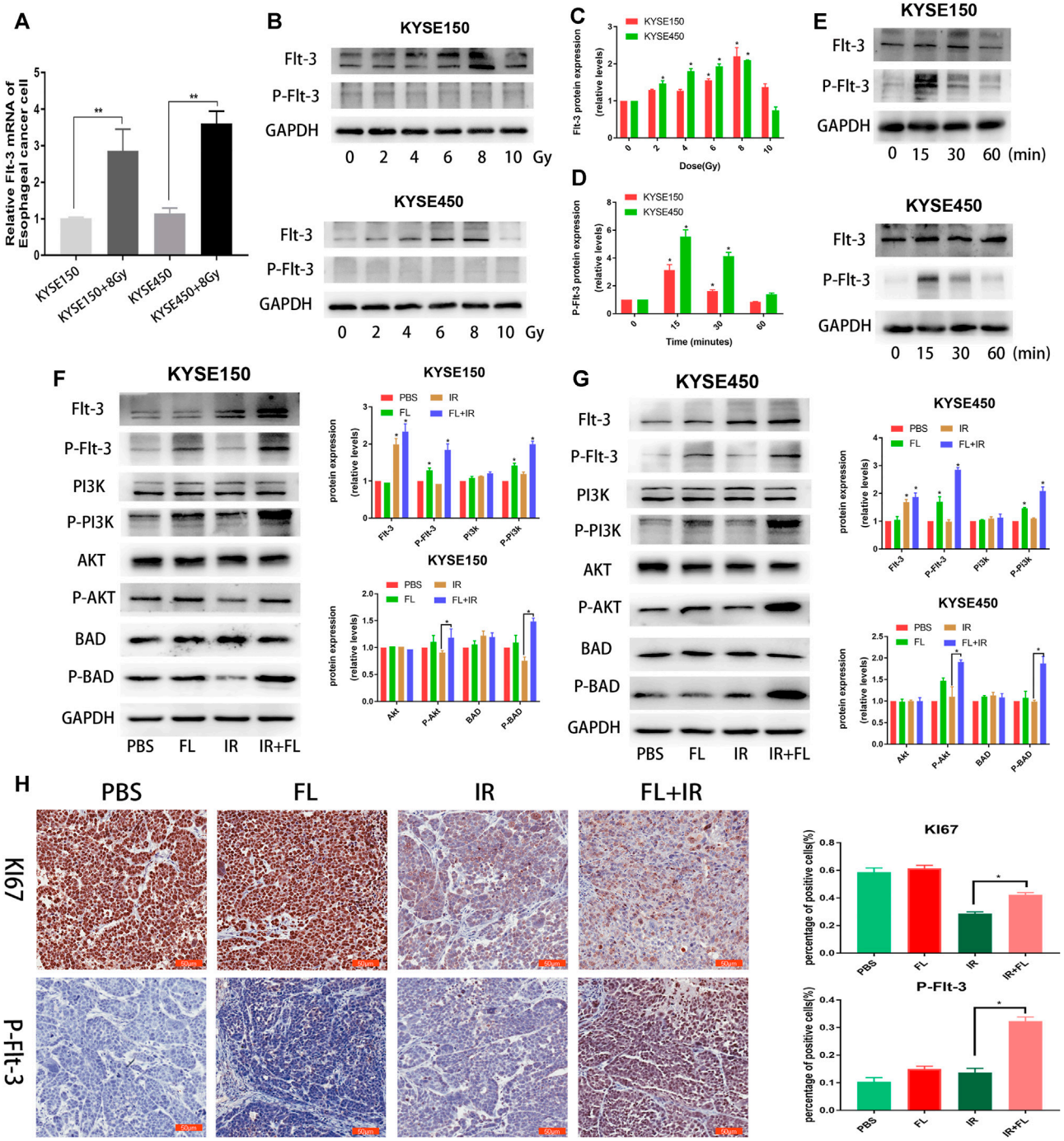


**FIGURE 5 |** FL induces radioresistance in ESCC cells through Flt-3/AKT/Bad signal pathway. **(A)** mRNA levels of Flt-3 receptor with or without IR in ESCC cells. **(B,C)** Expression and the quantitative analysis results of Flt-3 and P-Flt-3 in ESCC cells after different doses (0, 2, 4, 6, 8, and 10 Gy) radiation. **(D,E)** Expression and the quantitative analysis results of Flt-3 and P-Flt-3 in ESCC cells administrated with 200 ng/ml FL for different time after 24 h of 8 Gy radiation. **(F,G)** The levels and the quantitative analysis results of P-Flt-3/P-PI3K/P-AKT signal proteins and apoptosis-related proteins Bad and P-Bad in PBS groups or 200 ng/ml FL administration for 30 min groups after 24 h of 8 Gy radiation. GAPDH is an internal reference. **(H)** IHC images of nude mice and IHC analysis of P-Flt-3 and Ki 67 in tumor sections of KYSE150 bearing nude mice. Data show mean ± SEM $^{*}p < 0.05$.

plus IR group, compared to the FL alone group. Furthermore, IHC analysis of the xenograft nude mice tumor tissues showed that P-Flt-3 receptor expression significantly increased in the FL plus IR group compared to the control, FL, and IR alone groups. Moreover, Ki 67 expression in the FL plus IR group was significantly higher than that in the FL alone group

(**Figure 5H**). These results indicate that IR-induced upregulation of Flt-3 receptor and FL expression further activated the receptor and its downstream signaling pathway, which resulted in radioresistance in ESCC cells.

## DISCUSSION

Cytokines are increased in hematologic malignancies and FL has a vital role in the generation of mature peripheral leukocytes (McKenna et al., 2000), including the common lymphoid progenitor (Sitnicka et al., 2002). FL, a potent hematopoietic cytokine, mobilizes hematopoietic cells into the blood and lymphoid organs, and promotes the growth and differentiation of progenitor and stem cells both *in vivo* and *in vitro* (Antonysamy and Thomson, 2000). In addition to its effects to the hematopoietic progenitor and stem cells, FL also increases the number of dendritic cells in the peripheral blood and is involved in maintaining the viability of irradiated hematopoietic stem cells (MacVittie and Farese, 2002). In the current study, we found that FL increased the viability of KYSE150 and KYSE450 cells in a dose-dependent manner after radiation exposure. However, FL treatment did not affect cell viability in the non-irradiated group. By contrast, FL promoted tumor growth in the irradiation exposure group; nevertheless, there was no significant difference between this and the no irradiation exposure group *in vivo*. These results indicate that FL weakened the effects of radiotherapy on ESCC.

Furthermore, we explored the reasons behind FL's attenuation of radiotherapy effects. The clonogenic survival assay and the EdU incorporation assay were also employed for a more sensitive evaluation of proliferation after radiation (Feng et al., 2010; Li et al., 2017). We found that FL promoted colony formation and increased the number of EdU incorporated into KYSE150 and KYSE450 cells. On the other hand, previous studies have shown that FL expands the number of functionally competent human DCs *in vivo* (*Maraskovsky et al., 2000*). Ultimately, our results suggest that FL's promotion of cell proliferation ability plays a role in the radioresistance of ESCC cells.

We also found that FL reduced DNA damage, enhanced DNA damage repair, and further reduced radiation-induced apoptosis in KYSE150 and KYSE450 cells. DNA damage repair plays a significant role in radiosensitivity after radiation (Qian et al., 2014). The phosphorylated form of H2AX ($\gamma$H2AX) is used as a marker of DNA double-strand breaks (Sak and Stuschke, 2010). Poly (ADP-ribose) polymerase-1 (PARP-1) also participates in the modulation of cellular responses to DNA damage (Smith, 2001). Similarly, Veuger et al. revealed that the PARP-1 protein mediates the repair of both single- and double-strand DNA breaks after radiation (Veuger et al., 2003). Furthermore, evidence indicates that the apoptotic pathway is an essential mechanism for the regulation of radiosensitivity (Raleigh and Haas-Kogan, 2013). These results show that FL increased the radiation resistance of ESCC cells by promoting clone formation, increasing EdU incorporation, enhancing DNA damage repair, and inhibiting apoptosis in ESCCs.

FL can activate the Flt-3 receptor via membrane-bound and soluble forms to mobilize progenitor cells of the bone marrow (Tobón et al., 2010). In this study, we demonstrated for the first time that the expression of the Flt-3 receptor is significantly higher in ESCC cells after radiation. We inferred that IR-induced increased expression of the Flt-3 receptor is an important reason for the radioresistance of ESCC cells.

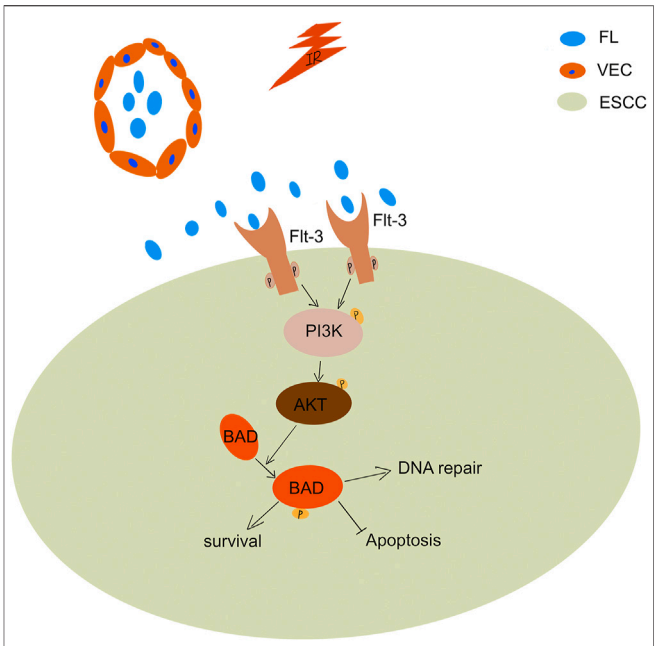


**FIGURE 6 |** Relevant mechanism of FL mediated the radioresistance of ESCCs during the radiotherapy. Radiation significantly increase Flt-3 receptor expression in ESCCs. FL phosphorylate the increased Flt-3 receptor, which further activate the PI3K/Akt pathway leading to BAD phosphorylation.

Previous studies have shown that FL induces phosphorylation of Flt-3 receptor signaling and enhances cell proliferation (Lisovsky et al., 1996b). Our study found that FL promoted the phosphorylation of the Flt-3 receptor after radiation to inhibit IR-induced apoptosis. Phosphorylation of the Flt-3 receptor reportedly activates PI3K and downstream AKT, and subsequently, the phosphorylation of BAD protein at Ser-136, leading to anti-apoptotic effects (Kim et al., 2006). Similar experimental results were obtained in our study. The BAD protein phosphorylation changes its binding ability to Bcl-2, resulting in a low ability to heterodimerize with relative survival proteins (Zha et al., 1996). In our study, radiation significantly increased Flt-3 receptor expression, which was phosphorylated by FL in ESCC cells. This phosphorylation of the Flt-3 receptor further activated PI3K/AKT/BAD signaling pathways and promoted clone formation, increased EdU incorporation, enhanced DNA damage repair, and inhibited apoptosis in IR-induced ESCC (**Figure 6**).

In conclusion, our results showed that FL boosted the radioresistance of ESCC cells both *in vitro* and *in vivo*. This radioresistance involves improving vitality, weakening DNA damage, enhancing DNA repair, and inducing anti-apoptosis. Moreover, Flt-3 receptor expression significantly increased in ESCC cells after radiation, which may be an important reason for the radioresistance. Therefore, FL-Flt-3 is a potential molecular target for enhancing radiosensitivity in ESCC.

## MANUSCRIPT CONTRIBUTION TO THE FIELD

In this manuscript, we found that the Fms-related tyrosine kinase 3 ligand (FL) boosted the radioresistance of ESCCs both *in vitro* and *in vivo*. The radioresistance of ESCCs involve in improving vitality, weakening DNA damage, enhancing DNA repair and inducing anti-apoptosis. Moreover, Flt-3 receptor expression increased significantly in ESCC cells after radiation, which is an important reason for the radioresistance of esophageal squamous cell carcinoma This is the first report that irradiation can promote the expression of Flt-3 receptor on tumor cells. We hypothesized that high expression of Flt-3 receptor was phosphorylated by FL. Phosphorylation of Flt-3 receptor further activated PI3K/AKT/BAD signal pathways and led to promote clone formation, increase EdU incorporation, enhance DNA damage repair and inhibit apoptosis in IR-induced ESCCs. Therefore, FL - Flt-3 is a potential molecular target for enhancing radiosensitivity of esophageal squamous cell carcinoma.

## DATA AVAILABILITY STATEMENT

The raw data supporting the conclusions of this article will be made available by the authors, without undue reservation.

## ETHICS STATEMENT

The animal study was reviewed and approved by Institutional Animal Care and Use Committee of NMU.

## AUTHOR CONTRIBUTIONS

ZZ carried out the study and drafted the manuscript. JS participated in cell culture experiments. JG and BX participated in the western blotting. XS and SZ conceived the study and participated in the study design. All authors read and approved the final manuscript.

## FUNDING

This study was supported by the Jiangsu Province Special Program for Young Medical Talent (grant no. QNRC2016571), and the National Natural Science Foundation of China (grant no. 82073344 and 81874217).

## ACKNOWLEDGMENTS

We would like to thank the Core Facility of Jiangsu Provincial People's Hospital for their help with the detection of experimental samples.

## REFERENCES

Antonysamy, M. A., and Thomson, A. W. (2000). Flt3 Ligand (FL) and its Influence on Immune Reactivity. *Cytokine*. 12 (2), 87–100. doi:10.1006/cyto.1999.0540

Bertho, J.-M., Demarquay, C., Frick, J., Joubert, C., Arenales, S., Jacquet, N., et al. (2001). Level of Flt3-Ligand in Plasma: a Possible New Bio-Indicator for Radiation-Induced Aplasia. *Int. J. Radiat. Biol.* 77 (6), 703–712. doi:10.1080/09553000110043711

Cohen, D. J., and Leichman, L. (2015). Controversies in the Treatment of Local and Locally Advanced Gastric and Esophageal Cancers. *J Clin Oncol.* 33 (16), 1754–1759. doi:10.1200/jco.2014.59.7765

Colvin, H., Mizushima, T., Eguchi, H., Takiguchi, S., Doki, Y., and Mori, M. (2017). Gastroenterological Surgery in Japan: The Past, the Present and the Future. *Ann. Gastroenterol. Surg.* 1 (1), 5–10. doi:10.1002/ags3.12008

Feng, X.-P., Yi, H., Li, M.-Y., Li, X.-H., Yi, B., Zhang, P.-F., et al. (2010). Identification of Biomarkers for Predicting Nasopharyngeal Carcinoma Response to Radiotherapy by Proteomics. *Cancer Res.* 70 (9), 3450–3462. doi:10.1158/0008-5472.Can-09-4099

Hannum, C., Culpepper, J., Campbell, D., McClanahan, T., Zurawski, S., Kastelein, R., et al. (1994). Ligand for FLT3/FLK2 Receptor Tyrosine Kinase Regulates Growth of Haematopoietic Stem Cells and Is Encoded by Variant RNAs. *Nature*. 368 (6472), 643–648. doi:10.1038/368643a0

Kim, K.-T., Levis, M., and Small, D. (2006). Constitutively Activated FLT3 Phosphorylates BAD Partially through Pim-1. *Br. J. Haematol.* 134 (5), 500–509. doi:10.1111/j.1365-2141.2006.06225.x

Li, Q., Li, Z., Wei, S., Wang, W., Chen, Z., Zhang, L., et al. (2017). Overexpression of miR-584-5p Inhibits Proliferation and Induces Apoptosis by Targeting WW Domain-Containing E3 Ubiquitin Protein Ligase 1 in Gastric Cancer. *J. Exp. Clin. Cancer Res.* 36 (1), 59. doi:10.1186/s13046-017-0532-2

Lisovsky, M., Braun, S. E., Ge, Y., Takahira, H., Lu, L., Savchenko, V. G., et al. (1996a). Flt3-ligand Production by Human Bone Marrow Stromal Cells. *Leukemia* 10 (6), 1012–1018.

Lisovsky, M., Estrov, Z., Zhang, X., Consoli, U., Sanchez-Williams, G., Snell, V., et al. (1996b). Flt3 Ligand Stimulates Proliferation and Inhibits Apoptosis of Acute Myeloid Leukemia Cells: Regulation of Bcl-2 and Bax. *Blood*. 88 (10), 3987–3997. doi:10.1182/blood.v88.10.3987.bloodjournal88103987

Lyman, S. D., James, L., Bos, T. V., de Vries, P., Brasel, K., Gliniak, B., et al. (1993). Molecular Cloning of a Ligand for the Flt3flk-2 Tyrosine Kinase Receptor: A Proliferative Factor for Primitive Hematopoietic Cells. *Cell* 75 (6), 1157–1167. doi:10.1016/0092-8674(93)90325-k

MacVittie, T. J., and Farese, A. M. (2002). Cytokine-based Treatment of Radiation Injury: Potential Benefits after Low-Level Radiation Exposure. *Mil. Med.* 167 (2 Suppl. l), 68–70. doi:10.1093/milmed/167.suppl_1.68

Maraskovsky, E., Daro, E., Roux, E., Teepe, M., Maliszewski, C. R., Hoek, J., et al. (2000). *In vivo* generation of Human Dendritic Cell Subsets by Flt3 Ligand. *Blood*. 96 (3), 878–884. doi:10.1182/blood.v96.3.878.015k15_878_884

Mariette, C., Robb, W. B., Piessen, G., and Adenis, A. (2015). Neoadjuvant Chemoradiation in Oesophageal Cancer. *Lancet Oncol.* 16 (9), 1008–1009. doi:10.1016/s1470-2045(15)00127-8

McKenna, H. J., Stocking, K. L., Miller, R. E., Brasel, K., De Smedt, T., Maraskovsky, E., et al. (2000). Mice Lacking Flt3 Ligand Have Deficient Hematopoiesis Affecting Hematopoietic Progenitor Cells, Dendritic Cells, and Natural Killer Cells. *Blood*. 95 (11), 3489–3497. doi:10.1182/blood.v95.11.3489.011k45_3489_3497

Nakao, M., Yokota, S., Iwai, T., Kaneko, H., Horiike, S., Kashima, K., et al. (1996). Internal Tandem Duplication of the Flt3 Gene Found in Acute Myeloid Leukemia. *Leukemia* 10 (12), 1911–1918.

Prat, M., Demarquay, C., Frick, J., Dudoignon, N., Thierry, D., and Bertho, J. M. (2006). Use of Flt3 Ligand to Evaluate Residual Hematopoiesis after Heterogeneous Irradiation in Mice. *Radiat. Res.* 166 (3), 504–511. doi:10.1667/rr0568.1

Qian, D., Zhang, B., Zeng, X.-L., Le Blanc, J. M., Guo, Y.-H., Xue, C., et al. (2014). Inhibition of Human Positive Cofactor 4 Radiosensitizes Human Esophageal Squmaous Cell Carcinoma Cells by Suppressing XLF-Mediated Nonhomologous End Joining. *Cell Death Dis.* 5 (10), e1461. doi:10.1038/cddis.2014.416

Raleigh, D. R., and Haas-Kogan, D. A. (2013). Molecular Targets and Mechanisms of Radiosensitization Using DNA Damage Response Pathways. *Future Oncol.* 9 (2), 219–233. doi:10.2217/fon.12.185

Sak, A., and Stuschke, M. (2010). Use of γH2AX and Other Biomarkers of Double-Strand Breaks during Radiotherapy. *Semin. Radiat. Oncol.* 20 (4), 223–231. doi:10.1016/j.semradonc.2010.05.004

Siegel, R. L., Miller, K. D., and Jemal, A. (2020). *Cancer* Statistics, 2020. *CA A. Cancer J. Clin.* 70 (1), 7–30. doi:10.3322/caac.21590

Sitnicka, E., Brakebusch, C., Martensson, I.-L., Svensson, M., Agace, W. W., Sigvardsson, M., et al. (2003). Complementary Signaling through Flt3 and Interleukin-7 Receptor α Is Indispensable for Fetal and Adult B Cell Genesis. *J. Exp. Med.* 198 (10), 1495–1506. doi:10.1084/jem.20031152

Sitnicka, E., Bryder, D., Theilgaard-Mönch, K., Buza-Vidas, N., Adolfsson, J., and Jacobsen, S. E. W. (2002). Key Role of Flt3 Ligand in Regulation of the Common Lymphoid Progenitor but Not in Maintenance of the Hematopoietic Stem Cell Pool. *Immunity*. 17 (4), 463–472. doi:10.1016/s1074-7613(02)00419-3

Smith, S. (2001). The World According to PARP. *Trends Biochemical Sciences* 26 (3), 174–179. doi:10.1016/s0968-0004(00)01780-1

Sproull, M., Avondoglio, D., Kramp, T., Shankavaram, U., and Camphausen, K. (2013). Correlation of Plasma FL Expression with Bone Marrow Irradiation Dose. *PloS one* 8 (3), e58558. doi:10.1371/journal.pone.0058558

Stirewalt, D. L., and Radich, . P. (2003). The Role of FLT3 in Haematopoietic Malignancies. *Nat. Rev. Cancer*. 3 (9), 650–665. doi:10.1038/nrc1169

Sugase, T., Takahashi, T., Serada, S., Fujimoto, M., Hiramatsu, K., Ohkawara, T., et al. (2017). SOCS1 Gene Therapy Improves Radiosensitivity and Enhances Irradiation-Induced DNA Damage in Esophageal Squamous Cell Carcinoma. *Cancer Res.* 77 (24), 6975–6986. doi:10.1158/0008-5472.Can-17-1525

Tobón, G. J., Renaudineau, Y., Hillion, S., Cornec, D., Devauchelle-Pensec, V., Youinou, P., et al. (2010). The Fms-like Tyrosine Kinase 3 Ligand, a Mediator of B Cell Survival, Is Also a Marker of Lymphoma in Primary Sjögren's Syndrome. *Arthritis Rheum.* 62 (11), 3447–3456. doi:10.1002/art.27611

Veuger, S. J., Curtin, N. J., Richardson, C. J., Smith, G. C., and Durkacz, B. W. (2003). Radiosensitization and DNA Repair Inhibition by the Combined Use of Novel Inhibitors of DNA-dependent Protein Kinase and poly(ADP-Ribose) Polymerase-1. *Cancer Res.* 63 (18), 6008–6015.

Zha, J., Harada, H., Yang, E., Jockel, J., and Korsmeyer, S. J. (1996). Serine Phosphorylation of Death Agonist BAD in Response to Survival Factor Results in Binding to 14-3-3 Not BCL-XL. *Cell.* 87 (4), 619–628. doi:10.1016/s0092-8674(00)81382-3

**Conflict of Interest:** The authors declare that the research was conducted in the absence of any commercial or financial relationships that could be construed as a potential conflict of interest.

frontiers in Oncology

ORIGINAL RESEARCH
published: 17 May 2021
doi: 10.3389/fonc.2021.668798

# Decitabine Sensitizes the Radioresistant Lung Adenocarcinoma to Pemetrexed Through Upregulation of Folate Receptor Alpha

*Yuqing Wang[1], Jie Huang[2], Qiong Wu[3], Jingjing Zhang[1], Zhiyuan Ma[1], Lucheng Zhu[2], Bin Xia[2], Shenglin Ma[2,4]* and Shirong Zhang[1]**

*[1] Translational Medicine Research Center, Key Laboratory of Clinical Cancer Pharmacology and Toxicology Research of Zhejiang Province, Affiliated Hangzhou First People's Hospital, Zhejiang University School of Medicine, Cancer Center, Zhejiang University, Hangzhou, China, [2] Department of Oncology, Affiliated Hangzhou Cancer Hospital, Zhejiang University School of Medicine, Hangzhou, China, [3] The Fourth College of Clinical Medicine, Zhejiang Chinese Medical University, Hangzhou, China, [4] Department of Cancer Medical Center, Affiliated Xiaoshan Hospital, Hangzhou Normal University, Hangzhou, China*

OPEN ACCESS

**Edited by:**
*Dexin Kong,*
*Tianjin Medical University, China*

**Reviewed by:**
*Fen Yang,*
*Nanjing Medical University, China*
*Humberto De Vitto,*
*University of Minnesota Twin Cities, United States*

***Correspondence:**
*Shirong Zhang*
*shirleyz4444@zju.edu.cn*
*Shenglin Ma*
*mashenglin@medmail.com.cn*

**Specialty section:**
*This article was submitted to Pharmacology of Anti-Cancer Drugs, a section of the journal Frontiers in Oncology*

**Received:** *17 February 2021*
**Accepted:** *29 April 2021*
**Published:** *17 May 2021*

**Citation:**
*Wang Y, Huang J, Wu Q, Zhang J, Ma Z, Zhu L, Xia B, Ma S and Zhang S (2021) Decitabine Sensitizes the Radioresistant Lung Adenocarcinoma to Pemetrexed Through Upregulation of Folate Receptor Alpha. Front. Oncol. 11:668798. doi: 10.3389/fonc.2021.668798*

Chemotherapy is the backbone of subsequent treatment for patients with lung adenocarcinoma (LUAD) exhibiting radiation resistance, and pemetrexed plays a critical role in this chemotherapy. However, few studies have assessed changes in the sensitivity of LUAD cells to pemetrexed under radioresistant circumstances. Therefore, the objectives of this study were to delineate changes in the sensitivity of radioresistant LUAD cells to pemetrexed and to elucidate the related mechanisms and then develop an optimal strategy to improve the cytotoxicity of pemetrexed in radioresistant LUAD cells. Our study showed a much lower efficacy of pemetrexed in radioresistant cells than in parental cells, and the mechanism of action was the significant downregulation of folate receptor alpha (FRα) by long-term fractionated radiotherapy, which resulted in less cellular pemetrexed accumulation. Interestingly, decitabine effectively reversed the decrease in FRα expression in radioresistant cells through an indirect regulatory approach. Thereafter, we designed a combination therapy of pemetrexed and decitabine and showed that the activation of FRα by decitabine sensitizes radioresistant LUAD cells to pemetrexed both *in vitro* and in xenografts. Our findings raised a question regarding the administration of pemetrexed to patients with LUAD exhibiting acquired radioresistance and accordingly suggested that a combination of pemetrexed and decitabine would be a promising treatment strategy.

**Keywords: lung adenocarcinoma (LUAD), radioresistance, pemetrexed, folate receptor α, decitabine**

## INTRODUCTION

Radiotherapy has been widely administered to patients with local lung adenocarcinoma (LUAD) patients to eliminate cancer cells (1). However, a majority of patients finally progress after radiation treatment due to either intrinsic insensitiveness or acquired radioresistance, which accelerates aggressive tumor growth or metastasis and further causes poor survival (2). Pemetrexed-based chemotherapy is currently commonly used as the first-line and second line treatment strategy for patients with recurrent or metastatic lung adenocarcinoma either alone or in combination with antiangiogenic drugs or immune checkpoint blockers, as recommended in various guidelines (3, 4). However, a prospective phase II study (5), which combined low-dose radiotherapy and pemetrexed in the treatment of recurrent NSCLC patients, found only 20% of all the previously irradiated patients showed a partial response, which suggested these previously irradiated tumor cells might have resistance to pemetrexed. Another clinic trial treated locally advanced NSCLC with carboplatin/pemetrexed plus radiotherapy and found three patients (20%) without distant metastases at registration developed distant metastases at a median time of 5 months, although these patients received consolidation carboplatin/pemetrexed for 2-3 cycles (6). These data suggested long-term fractionated radiotherapy may change the sensitivity of NSCLC cells to pemetrexed.

Radioresistant cancer cells display distinct gene-phenotypes with higher DNA repair and antioxidant capacities than their parental cells because of the complicated and repeated DNA damage repair process that occurs during the long-term radiation treatment (7, 8) and the dormancy-repopulation cycle of radioresistant cancer stem cells in the acidic tumor microenvironment (9), which may substantially alter the efficacy of chemotherapeutic drugs. For instance, radioresistant MDA-MB-231 breast cancer cells are resistant to paclitaxel (10). Radioresistant esophageal squamous cancer cells are resistant to paclitaxel through the upregulation of P-glycoprotein (11). Whereas, our recent study indicated that radioresistant LUAD cells showed increased sensitivity to SN-38, paclitaxel and docetaxel (12). However, the efficacy of pemetrexed on radioresistant LUAD cells was unclear and there were no basic studies, clinical trials or retrospective studies focused on this scenario. Thus, studies of changes in the cytotoxicity of pemetrexed toward radioresistant cancer cells are necessary.

Pemetrexed is a multitargeted antifolate drug that inhibits DHFR (dihydrofolate reductase), TYMS (thymidylate synthase), and GART (glycinamide ribonucleotide formyltransferase) in the folate pathway (13). Pemetrexed itself mainly relies on folate transporters and folate receptor proteins on the cell membranes to enter cells (13, 14), including reduced folate carrier (RFC), proton-coupled folate transporter (PCFT), folate receptor protein α (FRα), and folate receptor protein β (FRβ), of which FRα is expressed at high levels in epithelial cells of the placenta, female reproductive organs, breast, lung and various human solid tumors (15). FRα, as a high-affinity binding protein encoded by the gene FOLR1, mediates pemetrexed transport through endocytosis. Studies have indicated that patients with LUAD generally have high FRα expression levels (16–18), and the expression level of FRα directly affects the clinical efficacy of pemetrexed (19, 20). Therefore, FRα plays important role in the clinical outcomes of pemetrexed treatment. Interestingly, our study found most LUAD patients presented a significant reduction in serum FRα levels after receiving an average dose of more than 50 Gy radiotherapy, suggesting that long-term radiation treatment may change the expression of FRα and finally affect the efficacy of pemetrexed.

Given the importance of radiotherapy and pemetrexed in the clinical treatment of LUAD and the limited data on changes in FRα expression during long-term radiation treatment, the first aim of the present study was to delineate the altered sensitivity of radioresistant LUAD cells to pemetrexed based on the regulation of FRα. The secondary aim was trying to illustrate the potential regulatory mechanisms and develop a proper drug combination strategy that will increase the cytotoxicity of pemetrexed toward radioresistant lung adenocarcinoma.

## MATERIALS AND METHODS

### Cell Culture and Reagents

NCI-H1975, NCI-H1650, NCI-HCC827, NCI-H1299, A549 and PC9 cell lines were purchased from the Type Culture Collection of the Chinese Academy of Sciences (Shanghai, China). They were maintained in RPMI-1640 medium (Gibco-Life Technologies, NY, USA) supplemented with 10% fetal bovine serum (Gibco-Life Technologies), 100 μg/mL streptomycin and 100 U/mL penicillin (Gibco-Life Technologies). Cells were cultured at 37°C with a humid atmosphere of 5% $CO_2$ and 95% air. Pemetrexed, decitabine, and cycloheximide were obtained from Selleck Chemicals (Houston, TX, USA).

### Clinical Specimens

Surgical specimens from 18 patients with lung adenocarcinoma patients and paired serum samples collected within 3 days before and after radiotherapy alone from seven adenocarcinoma patients were obtained from Hangzhou First People's Hospital, which was approved by the Institutional Review Board of Hangzhou First People's Hospital. The relevant clinic pathological information of the enrolled patients was listed in **Supplementary Table 1**. All private information of each individual has been carefully blocked.

### Establishment of Radioresistant A549 Cells

Cell irradiation was performed with an X-RAD 225 irradiator provided by Precision (North Branford, USA). Briefly, a dose of 2 Gy (3.2 Gy/min, 13.3 mA, 225 kV, 2 mm Al filter) radiation was delivered to 50% confluent A549 cells at room temperature, and then the cells were maintained in culture. Cells were passaged to new flasks when they reached approximately 80% confluence. Afterwards, a repetitive 2 Gy dose of radiation was delivered to 50% confluent cells until a cumulative dose of 60 Gy was administered. A549 cells with acquired radioresistance were named A549R cells, and cells at passages 5-6 were used in all the subsequent experiments. The parental cells without irradiation were cultured and passaged simultaneously.

## Plasmid Constructs and Cell Transfection

For the knockdown of FRα, a short hairpin RNA was inserted into the lentiviral vector pLent-U6-GFP-Puro (Vigene Biosciences, Shandong, China). For FRα overexpression, the full-length FRα cDNA was inserted into the lentiviral vector pReceiver-Lv201 purchased from FulenGen Company (Guangzhou, China). Virus particles were packaged in HEK293T cells by transfection with Lipofectamine 3000 (Invitrogen, IL, USA). A549, A549R or H1299 cells were infected with the lentivirus-conditioned medium and 8 μg/mL polybrene (Sigma-Aldrich, MO, USA). Stably-transfected cells were screened by using puromycin (Sigma-Aldrich) at a concentration of 2.5 μg/mL. Target sequences of shRNAs are listed in **Supplementary Table 2**.

## RT-qPCR Analyses

Total RNA was extracted by using an AxyPrep Multisource RNA Miniprep Kit (Axygen, MA, USA) as described recently (12). The cDNA templates were synthesized from 500 ng of RNA using a commercially available reverse transcription kit (Takara, Japan). RT-qPCR was performed using a 7500 System (Applied Biosystems, Singapore) and TB Green Premix Ex Taq (Takara, Japan). All samples were analyzed in 3 biological replicates, with the GAPDH gene serving as an internal control. The relative expression of the target genes was calculated with the comparative threshold cycle (CT) method using the formula $2^{-\Delta CT}$. Fold changes of target genes were calculated using the formula $2^{-\Delta\Delta CT}$. The primers used for RT-qPCR are listed in **Supplementary Table 2**.

## Western Blot Analysis

Western blot analyses were performed to evaluate target protein expression. Briefly, protein lysates (~20 μg per sample) were loaded and run on 10% sodium dodecyl sulfate (SDS)-polyacrylamide gels, transferred to NC membranes (Millipore Corporation, MA, USA), and blocked with 5.0% nonfat milk for 3 h. The membranes were incubated with primary antibodies overnight at 4°C and then washed with Tris-buffered saline Tween-20 (TBST) three times for 10 min. Afterwards, membranes were incubated with the secondary antibodies for 2 h at room temperature and washed again. The bands on the membranes were visualized using an ECL system (Beyotime Institute of Biotechnology). Finally, membranes were exposed with an Odyssey infrared imaging system (LI-COR Biosciences, NE, USA). The following antibodies were used: anti-human FOLR1 (1:5000 dilution; Abcam, Cambridge, UK; CAT# ab221543), anti-human PCFT (1:300 dilution; Santa Cruz Biotechnology, Dallas, TX; CAT# sc-393460), anti-human RFC (1:300 dilution; Santa Cruz Biotechnology; CAT# sc-390948), anti-human GAPDH (1:5000 dilution; Abcam; CAT# ab181602), and HRP-labeled secondary antibodies (1:5000 dilution; Proteintech Group, Rosemont, IL).

## Immunofluorescence

A549 cells were fixed with 4% formaldehyde for 10 min, washed with PBS, and permeabilized with 0.1% Triton X-100 in PBS for 20 min. After washed with PBS and blocked with 5% BSA in PBS for 30 min, cells were incubated with primary antibody (anti-human FOLR1, 1:500 dilution) in 1% BSA-PBS overnight at 4°C, washed again, and incubated with fluorescent dye-conjugated secondary antibody for 1 h in the dark. Then, cells were washed with PBS for 3 times. Nuclei were stained with 4,6-diamidino-2-phenylindole (DAPI). Cells were analyzed by confocal microscopy (Zeiss, Stuttgart, Germany).

## Drug Treatment and Cell Viability Assay

For FRα induction, cells were cultured in medium supplemented with different concentrations of decitabine (0.1, 0.5, 2.5, 5 or 10 μM) for 72 h, or cells were treated with decitabine for different time (24, 48, 72 or 96 h). The medium was refreshed daily. Finally, total RNA or proteins were extracted. Cell viability was evaluated using the cell counting kit-8 (CCK-8) assay (MedChemExpress, NJ, USA) as described previously (12). Briefly, cells were seeded in 96-well plates at a density of 2000 cells/well. The medium was refreshed with drug-containing medium every 24 h. After 96 h, the cell survival rate was assessed. The absorbance was measured at 450 nm using a Multiskan Spectrum (Thermo Fisher Scientific, IL, USA). A concentration range of 0.005-2.0 μM pemetrexed and 0.05-20 μM decitabine was used to determine the $IC_{50}$ values. The $IC_{50}$ values of the concentration-response curves were calculated using CompuSyn software developed by Chou (21). Interactions between pemetrexed and decitabine were evaluated using CalcuSyn software and presented as the combination index (CI): CI < 1 indicates synergism, CI = 1 indicates an additive effect, and CI > 1 indicates antagonism.

## Pemetrexed Accumulation and LC-MS/MS Assay

Cells were seeded in 24-well plates to perform pemetrexed accumulation studies. Cells were washed with fresh medium once upon reaching 80% confluence, and then cells were incubated with drug-containing medium (50 μM pemetrexed) for 2, 4, 6, or 8 h at 37°C. Thereafter, the cells were gently washed with cold PBS 3 times and lysed with 0.1% SDS buffer. The pemetrexed concentration was quantified using a 4500 triple quadrupole mass spectrometer (AB Sciex, CA, USA) with a Turbo Ion Spray probe in positive mode. Multiple reaction monitoring (MRM) mode was used for quantitation based on the transitions of protonated molecular ions of pemetrexed at m/z 428.3−281.1 and anlotinib (internal standard) at m/z 408.3−304.2. The optimized mass spectrometric parameters were as follows: dwell time of 150 milliseconds, cell exit potential and entrance potential were 10 V and 12 V, respectively, collision energy (CE) of pemetrexed and anlotinib of27 V and 30 V, respectively, spray voltage temperature of 5500°C, and source temperature of 550°C. Data acquisition and processing were completed using Analyst software (version 1.6.2, AB Sciex, Framingham, MA). The chromatography analysis was performed using an LC-30AD system (Shimadzu Corporation, Kyoto, Japan) equipped with an ACQUITY UPLC BEH T3 column (2.1 mm×50 mm, 1.8 μm, Waters, USA) which was maintained at 40°C. A gradient elution program was conducted with mobile phase A (0.1% FA in 10 mM ammonium acetate/water) and mobile phase B (acetonitrile) as follows: 0 - 0.5 min, 90% of A; 0.5 - 1.5 min, 90% - 5% of A; 1.5 - 2.2 min, 5% of A; 2.3-3.8 min, 90% of A and finished at 3.8 min.

The flow rate of the mobile phase was 0.4 mL/min. The injection volume was 5 μL.

## Animal Study

Six-week-old male BALB/c nude mice were purchased from the Experimental Animal Center of the Zhejiang Academy of Medicinal Sciences (Hangzhou Medical College, Hangzhou, China). All procedures were approved by the Institutional Animal Care and Use Committee of Zhejiang University. Mice were inoculated subcutaneously in the flank with $5 \times 10^6$ A549 or A549R cells. When the volume of the formed tumor reached approximately 0.1 $cm^3$, mice were intraperitoneally injected with 2.5, 5.0, or 10 mg/kg decitabine three times at intervals of 3 h on day 0, and tumors were excised on day 4 and 7 to extract total proteins for immunoblot analyses. A dose of 5.0 mg/kg decitabine that effectively induced FRα expression was chosen for subsequent experiments. Mice were randomly divided into 4 groups with 6 mice in each group: (1) control group (Control): saline; (2) decitabine group (DAC): 5 mg/kg decitabine; (3) pemetrexed group (PEM): 100 mg/kg pemetrexed; (D) pemetrexed plus decitabine group (Combo): 100 mg/kg pemetrexed and 5 mg/kg decitabine. Decitabine was administered intraperitoneally three times at intervals of 3 h (22) on day 1, 8, and 15, and pemetrexed was administered intraperitoneally on day 5, 12, and 19 (23). The tumor size was measured once every 4 days, and the volumes were calculated as follows: $L \times W^2/2$, where L and W are the longest and shortest dimensions, respectively.

## Quantification of Serum FRα Levels

The concentrations of the FRα protein in human serum were determined using a Human FOLR1 ELISA kit (R&D Systems, Minneapolis, USA) according to the manufacturer's instructions.

## Statistical Analyses

GraphPad Prism version 8 for Windows (La Jolla, CA) was used to perform all statistical analyses, and data are expressed as the mean ± SE. When comparing two groups, Student's *t*-test (unpaired two-tailed) was used. For multiple comparisons, one-way analysis of variance (ANOVA) was used followed by Dunnett's or Tukey's *post hoc* test. A probability of $p < 0.05$ was considered as statistically significant.

# RESULTS

## Long-Term Fractionated Radiotherapy Downregulated the Expression of FRα in A549 Cells

We collected serum samples from seven patients with LUAD before and after radiotherapy. These patients received an average dose of more than 50 Gy radiotherapy with a fractionated dose of 2-3 Gy and had not received any other traditional chemotherapy before or during radiotherapy. Five patients presented a significant reduction in serum FRα levels after radiotherapy (**Figure 1A**), suggesting that long-term fractionated radiotherapy may downregulate the expression of FRα. Therefore, we screened several commonly used LUAD cell lines, including NCI-H1975, NCI-H1650, NCI-HCC827, NCI-H1299, A549 and PC9 cells, to determine the proper cell lines to construct radioresistant cell models. Most LUAD cell lines exhibited limited expression of both the FRα mRNA and protein (**Figures 1B, C**), except for A549 cells, which had a comparable FRα expression level to human LUAD tissues, consistent with a previous report that A549 cells were FRα-positive cells among 19 LUAD cell lines (24). We constructed the acquired radioresistant LUAD cell line A549R

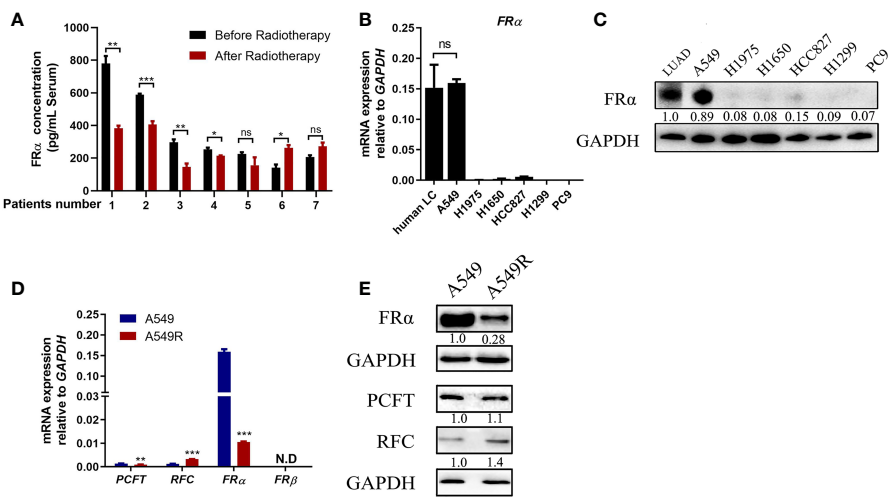


**FIGURE 1** | Long-term fractionated radiotherapy downregulated the expression of FRα in A549 cells. **(A)** Serum FRα concentration in 7 patients with LUAD. **(B)** The FRα mRNA expression level in human LUAD tissues and LUAD cell lines. **(C)** Expression of the FRα protein in human LUAD tumors (5 human tumors were pooled) and cell lines. **(D)** The mRNA expression of pemetrexed-related transporters and receptors. *PCFT* and *FRα* were significantly downregulated in A549R cells compared with A549 cells. *RFC* was upregulated and *FRβ* was not detected. **(E)** Expression of the FRα, PCFT and RFC proteins in A549 and A549R cells. Data are presented as the means ± SE, n =18 (human LUAD tissues) or 3 (cell lines or serum). Differences between A549 and A549R cells are denoted as *$p < 0.05$, **$p < 0.01$, and ***$p < 0.001$. ns, not significant. For immunoblots, densitometric values are shown as optical density after GAPDH normalization using Image J.

by treating A549 cells with fractionated irradiation at 60 Gy and then examined the expression of pemetrexed related transporters and receptors. As shown in **Figure 1D**, *FRα* was abundantly expressed in A549 cells, while the expression levels of *RFC*, *PCFT*, and *FRβ* were relatively low. After long-term fractionated irradiation, the level of the FRα transcript decreased approximately 15-fold and the RFC transcript level increased approximately 2-fold in A549R cells compared with the parental cells. Similarly, the level of the FRα protein was significantly decreased by long-term fractionated irradiation (**Figure 1E**).

## A Low-Expression Level of FRα Decreased Pemetrexed Efficacy in A549R Cells

FRα is abundantly expressed on the plasma membrane of A549 cells (**Figure 2A**) and facilitates pemetrexed to entry into cells 'slowly' through endocytosis. Notably, a high expression level of FRα exerts a substantial effect on the efficacy of pemetrexed; thus, we examined the $IC_{50}$ values of pemetrexed in A549 and A549R cells. Cell viability was evaluated after cells were treated with pemetrexed for 96 h. The dose-response curve significantly shifted to the right from A549 to A549R cells, and the $IC_{50}$ value was increased from 0.41 μM to 1.45 μM (**Figure 2B**). Meanwhile, pemetrexed accumulation was induced by incubating cells with 50 μM pemetrexed for 2, 4, 6, and 8 h, and the cellular contents of pemetrexed were detected using LC-MS/MS. The uptake study revealed that the cellular concentration of pemetrexed in A549 cells was 6-fold higher than that in A549R cells (**Figure 2C**). In addition, we excluded the possibility that the expression of pemetrexed target enzymes (including TYMS, DHFR, and GART) and folylpolyglutamate synthetase (FPGS), an important enzyme that increases the intracellular activity of pemetrexed (25), was perturbed by long-term fractionated irradiation (**Supplementary Figure 1A**).

Overexpression and knockdown experiments further validated our results that the low expression level of FRα led to decreased cytotoxicity of pemetrexed. As shown in **Figures 2D–F**, A549R cells overexpressed with FRα, the dose-response curve shifted to the left significantly from A549R-vector to A549R-FRα cells, and the $IC_{50}$ value was reduced from 1.27 μM to 0.5 μM (**Figure 2E**). Additionally, the intracellular pemetrexed concentration was increased in A549R-FRα cells (**Figure 2F**). Similar results were observed in H1299 cells with overexpression of FRα, the $IC_{50}$

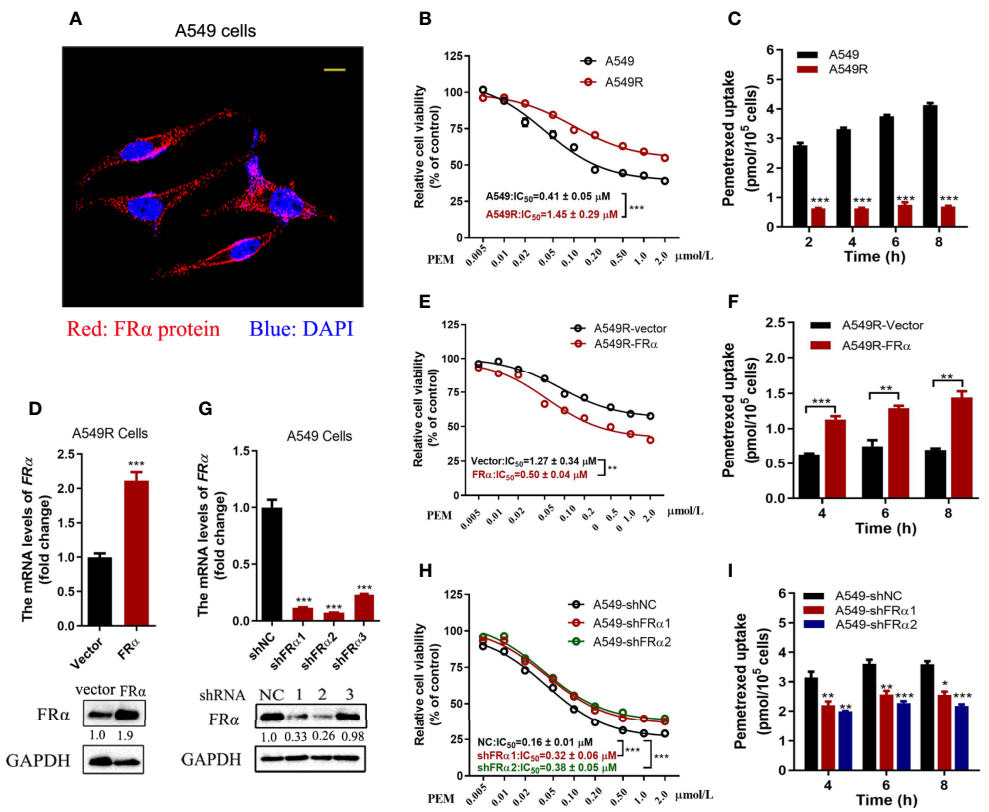


**FIGURE 2** | Low FRα expression decreased the efficacy of pemetrexed. **(A)** Confocal microscope image to determine the location of FRα in A549 cells. Bar = 10 μm. **(B, E, H)** Effect of pemetrexed on the viability of A549, A549R and their cell models. All cells were treated with pemetrexed at a concentration range of 0.005-2.0 μM for 96 h and then evaluated with the CCK-8 assay. Data are expressed as mean ± SE, n =5. **(D)** Cell models in which A549R cells stably overexpressing FRα or **(G)** A549 with stable knockdown of FRα. **(C, F, I)** Cellular accumulation of pemetrexed (50 μM) in A549, A549R and their cell models over 2, 4, 6 and 8 h. Data are presented as the means ± SE, n =3. Differences between A549 and A549R cells, A549R-vector and A549R-FRα cells, A549-shNC and A549-shFRα-1/shFRα-2 cells are denoted as: *p < 0.05, **p < 0.01, and ***p < 0.001, respectively.

value was reduced from 0.29 μM to 0.08 μM (**Supplementary Figure 2**). A549 cells were stably transfected with shRNA to knockdown FRα (**Figure 2G**). The dose-response curve shifted to the right from A549-shNC to A549-shFRα1/2 cells, and the $IC_{50}$ values were increased approximately 1-fold (**Figure 2H**). The intracellular pemetrexed concentration was decreased in A549 cells transfected with FRα-targeting shRNAs (**Figure 2I**). Based on these results, low FRα expression in cells decreased intracellular pemetrexed accumulation, thus reducing its cytotoxicity.

## Decitabine Partially Reversed FRα Expression in A549R Cells Through an Indirect Regulatory Mechanism

We analyzed the expression of FRα-related transcription factors to explore the possible mechanisms underlying the downregulation of FRα and found no difference in transcript levels between A549 and A549R cells (**Supplementary Figure 3**). Interestingly, when A549R cells were treated with decitabine, a demethylating reagent that blocks cellular DNA methyltransferases (DNMTs) (26), the expression of FRα was significantly upregulated. In addition, decitabine upregulated the expression of the FRα transcript in a concentration-dependent (**Figure 3A**) and time-dependent manner (**Figure 3B**) and the optimal concentration of decitabine was 0.5 μM. Similar results were observed for protein expression, as the level of the FRα protein was increased in A549R cells treated with increasing decitabine concentrations and treatment times (**Figure 3D**). However, decitabine did not affect FRα expression in A549 cells (**Figure 3E**) but weakly upregulated the expression of its mRNA (**Figure 3C**). Notably, although decitabine exerted a strong effect on reversing the change in FRα expression in A549R cells, it did not cause the expression of FRα to reach the original level (**Figure 3F**), indicating that decitabine only partially reversed the change in FRα expression.

Decitabine was used to globally inhibit DNA methylation in LUAD cells, thus we speculated that long-term fractionated radiotherapy might induce aberrant methylation in the promoter region of FRα, resulting in low FRα expression. Bisulfite sequencing PCR (BSP) was used to examine methylation of 15 CG sites (-2599 bp to -2152 bp), which contain the only one CpG island in the promoter region of the *FOLR1* gene (27). All CG sites were hypermethylated, and no significant difference in methylation was observed between A549 and A549R cells (**Supplementary Figure 4**). Another interesting phenomenon was the delayed induction of *FRα* expression by decitabine, which began between 24 h to 48 h and reached up to a 4-fold elevation at 96 h (**Figure 3B**). In addition, when decitabine was withdrawn at 12, 24, 36, and 48 h, the expression of the FRα mRNA further increased, as observed at 72 h (**Figure 4A**). This delayed regulation of *FRα* expression by decitabine suggests that this process is likely mediated indirectly through other productions of decitabine. Cycloheximide was used to inhibit *de novo* protein synthesis in the early stage (0-12 h) of decitabine treatment to confirm this hypothesis (**Figure 4B**). The delayed induction of the FRα mRNA observed at 72 h after only a 12-h treatment with decitabine was abrogated when cycloheximide was added (**Figure 4B**). These results indicated that decitabine reversed the change in FRα expression in A549R cells through

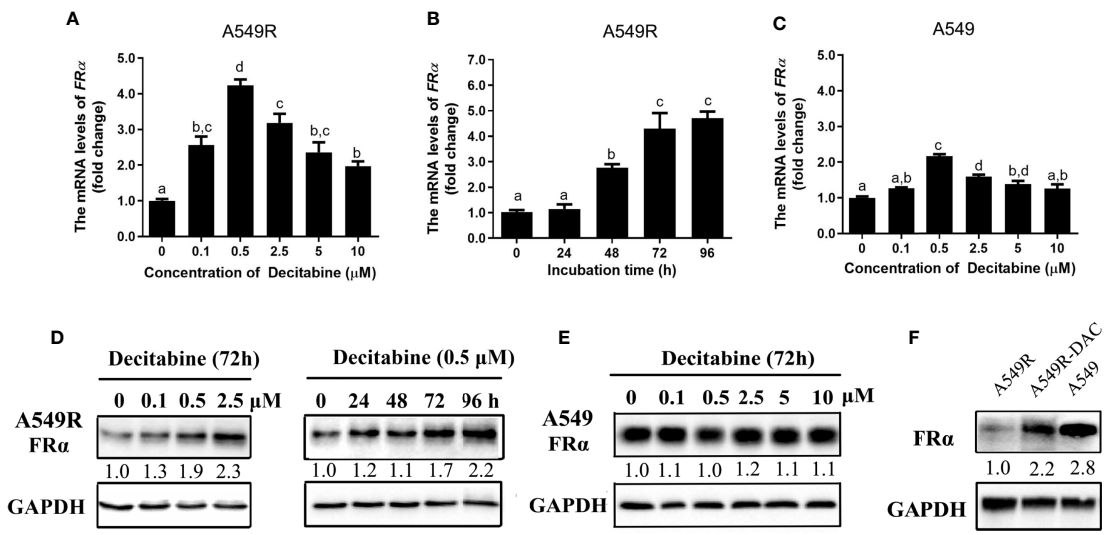


**FIGURE 3** | Decitabine upregulated the expression of FRα in A549R cells in a concentration-dependent and time-dependent manner. For the concentration-dependent study, cells were treated with different concentrations of decitabine (0.1-10 μM) for 72 h before RNA or protein was extracted. For the time-dependent study, cells were treated with 0.5 μM decitabine for 24, 48, 72 or 96 h before RNA or protein was extracted. **(A)** Decitabine upregulated *FRα* expression in A549R cells in a concentration-dependent manner. **(B)** Decitabine upregulated *FRα* expression in A549R cells in a time-dependent manner. **(C)** Decitabine slightly upregulated *FRα* expression in A549 cells. **(D)** Decitabine increased the expression of the FRα protein in a concentration-dependent and time-dependent manner. **(E)** Decitabine did not alter the expression of the FRα protein in A549 cells. **(F)** Levels of the FRα protein in A549, A549R and decitabine-treated A549R (A549R-DAC) cells that were exposed to 0.5 μM decitabine for 72 h before proteins were harvested. Data are presented as the means ± SE, n =3. Treatment groups with different letters shower significant differences using ANOVA followed by Tukey's test. For immunoblots, densitometric values are shown as optical density after GAPDH normalization using Image J.

indirect regulation by inducing the *de novo* synthesis of some other protein(s) instead of directly acting on the promoter of FRα.

## Cytotoxic Synergism of Pemetrexed and Decitabine

Next, the cytotoxicity of pemetrexed and decitabine alone or in combination was assessed. Based on the $IC_{50}$ values of pemetrexed and decitabine in A549R cells, a molar ratio of pemetrexed:decitabine of 1:10 was used for the drug combination studies. A549 cells treated with pemetrexed concurrently with decitabine exhibited increased cytotoxicity (**Figure 5A**). However, the combination index values increased as the concentrations of pemetrexed and decitabine increased and finally exceeded 1.0, indicating that the combination of high concentrations of pemetrexed and decitabine resulted in an antagonistic effect (**Figure 5E**). On the other hand, the growth inhibition effect of the combination of pemetrexed and decitabine was more potent than that of pemetrexed or decitabine alone in A549R cells (**Figure 5B**), with the sensitivity of A549R cells to pemetrexed increasing by 9.6-fold (**Figure 5H**). All the combination index (CI) values were less than 1.0 and consistently remained at low values as the cell growth inhibitory fraction increased (**Figure 5E**).

To further determine whether the synergistic effect depends on FRα activation by decitabine, we assessed the efficacy of combination therapy in A549R-NC and A549R-shFRα cells (**Figures 5C, D**). Drug combination analysis showed that FRα shRNA expression markedly inhibited the sensitivity of A549R cells to pemetrexed by DAC treatment (**Figure 5H**). In addition, cellular accumulation studies showed decitabine increased the concentration of pemetrexed in A549R cells (**Figure 5F**) and this concentration increase could be attenuated by shFRα (**Figure 5G**). We also assessed the synergistic effect of combination therapy on H1299 and H1975 cells that have low expression levels of FRα. Drug combination analysis showed there was no or a weak synergistic effect of pemetrexed and decitabine on H1299 cells and H1975 cells (**Supplementary Figure 5** and **Figure 5H**).

In summary, these results present a better cytotoxic synergistic effect of pemetrexed and decitabine on A549R cells than on other LUAD cells, and suggest decitabine sensitizes A549R cells to pemetrexed mainly through upregulation of FRα.

## Decitabine Enhanced the Cytotoxicity of Pemetrexed *In Vivo*

Based on the results described above, studies were performed to investigate the cytotoxic synergism of pemetrexed and decitabine *in vivo* by establishing A549 and A549R xenografts. First, we explored the effective concentration and treatment time of decitabine *in vivo*. Mice were intraperitoneally injected with different doses (2.5, 5 or 10 mg/kg) of decitabine on day 0 and tumors were collected on day 4 and 7. Treatment with 5 mg/kg and 10 mg/kg decitabine significantly upregulated FRα expression in A549R tumors on day 4 (**Figure 6A**), and this upregulation was more obvious on day 7 (**Figures 6B, C**). However, we did not observe the induction of FRα by decitabine in A549 xenografts (**Figures 6D, E**).

The drug administration timeline is shown in **Figure 7A**. Mice were treated with 100 mg/kg pemetrexed after injection of 5 mg/kg decitabine for 4 days. As showed in **Figure 7B**, compared to the saline-treated group, the tumor volume of A549 xenografts was decreased in the pemetrexed-treated group, but pemetrexed did not reduce the tumor volume of A549R xenografts (**Figure 7C**), consistent with the previous result that A549R cells were less sensitive to pemetrexed. As expected, the tumor volume in the combination group was significantly decreased in both A549 and A549R xenografts (**Figure 7D**) and similar results were observed for the tumor weight (**Figures 7F, G**). Moreover, the combination of pemetrexed and decitabine showed stronger growth inhibitory effects on A549R xenografts than on A549 xenografts. The concentrations of pemetrexed in tumors were detected by using LC-MS/MS, and the results indicated that decitabine increased the amount of pemetrexed by 2-fold in A549 tumors and 7-fold in A549R tumors (**Figure 7H**). Interestingly, although decitabine did not induce FRα expression in A549 tumors, the amount of pemetrexed in tumors of the combination group was also

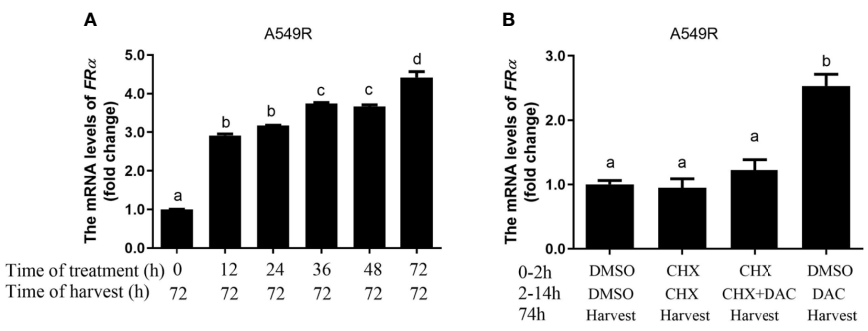


**FIGURE 4** | Decitabine delayed the induction of *FRα* expression in A549R cells. **(A)** The fold change in the expression of the FRα mRNA in A549R cells treated with 0.5 μM decitabine for the indicated periods. After decitabine treatment, cells were washed with decitabine-free media and replenished with new media that did not contain decitabine. At 72 h, all cells were collected for mRNA extraction. **(B)** A549R cells were pretreated with cycloheximide (CHX; 10 μM) followed by decitabine (DAC; 0.5 μM) as indicated. Twelve hours later, the cells were washed with decitabine/cycloheximide - free media and replenished with new media that did not contain decitabine/cycloheximide. All cells were harvested 60 h later, and total RNA was extracted for the quantification of the FRα mRNA by using RT-qPCR. Data are presented as the means ± SE, n =3. Treatment groups with different letters show statistically differences using ANOVA followed by Tukey's test.

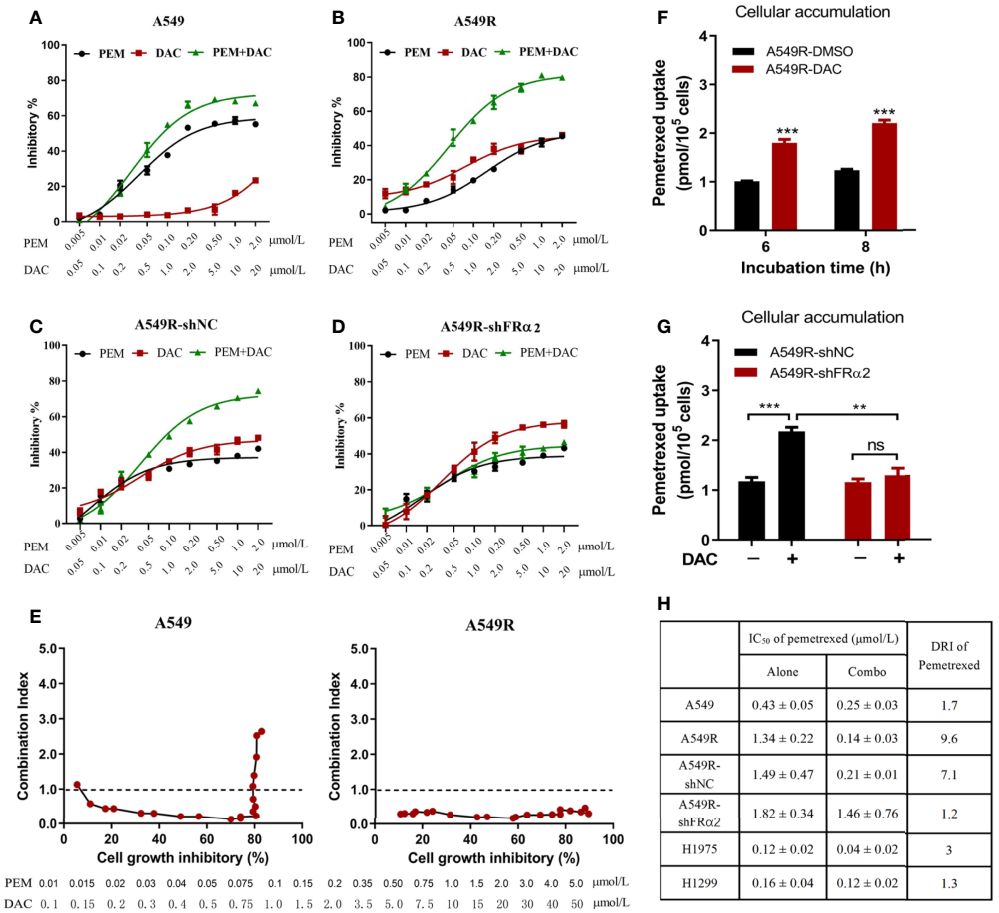


H

| | $IC_{50}$ of pemetrexed (μmol/L) | | DRI of Pemetrexed |
|---|---|---|---|
| | Alone | Combo | |
| A549 | 0.43 ± 0.05 | 0.25 ± 0.03 | 1.7 |
| A549R | 1.34 ± 0.22 | 0.14 ± 0.03 | 9.6 |
| A549R-shNC | 1.49 ± 0.47 | 0.21 ± 0.01 | 7.1 |
| A549R-shFRα2 | 1.82 ± 0.34 | 1.46 ± 0.76 | 1.2 |
| H1975 | 0.12 ± 0.02 | 0.04 ± 0.02 | 3 |
| H1299 | 0.16 ± 0.04 | 0.12 ± 0.02 | 1.3 |

**FIGURE 5** | Decitabine enhanced the cytotoxicity of pemetrexed *in vitro*. **(A–D)** A549, A549R, A549R-shNC and A549R-shFRα cells were treated with pemetrexed (PEM) and decitabine (DAC) alone or in combination, at the indicated concentrations for 96 h. The results are expressed as the percentage of surviving drug-treated cells relative to DMSO-treated control cells. **(E)** Combination index-fraction affected plots of pemetrexed and decitabine combinations in A549 and A549R cells. The concentration ranges of pemetrexed and decitabine are 0.01-5 and 0.1-50 μmol/L. A cytotoxicity index (CI) < 1, CI = 1, and CI > 1 indicates synergism, an additive effect, and antagonism, respectively. **(F)** Effects of decitabine on pemetrexed cellular accumulation. DMSO-treated and decitabine-treated (0.5 μM, 96h) A549R cells were incubated with 50 μM pemetrexed for 6 or 8 h. **(G)** Effects of FRα knockdown on pemetrexed cellular accumulation. DMSO-treated and decitabine-treated (0.5 μM, 96h) cells were incubated with 50 μM pemetrexed for 6 h. **(H)** $IC_{50}$ values and dose reduction index (DRI) of pemetrexed in cells receiving pemetrexed alone or combination treatment. DRI is the ratio of $IC_{50}$ (alone) to $IC_{50}$ (combo). **(A–D, H)**, data are presented as the means ± SE, n =5. E and F, data are presented as the means ± SE, n =3. Differences between cells are denoted as **p < 0.01 and ***p < 0.001. ns, not significant.

increased. By analyzing the levels of pemetrexed-related transporters, we found that the expression of *RFC* and *PCFT* was increased significantly (**Supplementary Figure 6**), which might account for the increased pemetrexed concentration detected in A549 tumors of the combination group. In addition, in the pemetrexed-treated group, the amount of pemetrexed in A549 tumors was much greater than that in A549R tumors, which explained the weaker growth inhibitory effect of pemetrexed on A549R xenografts (**Figure 7H**). H&E staining shows neither nephrotoxicity nor hepatotoxicity in mice undergoing different treatments (**Supplementary Figure 7**) and no significant weight loss was observed in each group (**Figure 7E**). Collectively, these results further indicated that decitabine enhanced the cytotoxicity of pemetrexed in A549R cells mainly by upregulating the expression of FRα *in vivo*.

## DISCUSSION

Many studies have focused on the mechanisms of radioresistance and the discovery of radiosensitizers. However, limited information is available on changes in the efficacy changes of chemotherapeutic drugs during long-term radiotherapy and, in particular, new drug strategies for patients with acquired radioresistance. In the present study, we showed that: 1) long-term fractionated irradiation downregulated FRα expression in LUAD cells, which directly decreased the intracellular accumulation of pemetrexed and resulted in low sensitivity of radioresistant cells to pemetrexed; 2) decitabine enhanced the cytotoxicity of pemetrexed *in vitro* and *in vivo* through the indirect upregulation of FRα; and 3) the combination of pemetrexed and decitabine showed strong synergetic cytotoxicity toward A549R

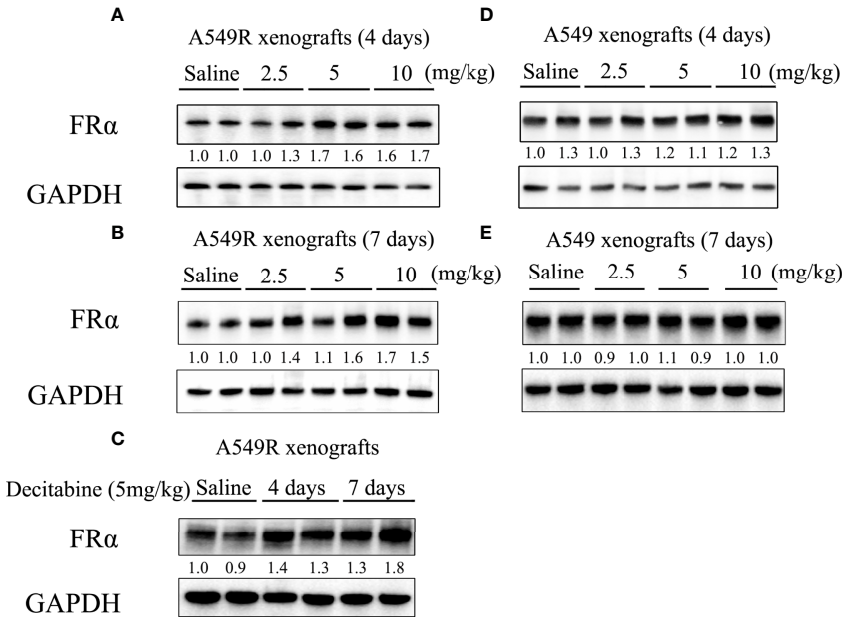


**FIGURE 6** | FRα protein expression in xenograft tumors from mice treated with decitabine. **(A, B)** FRα expression in A549R xenograft tumors. Mice were intraperitoneally injected with different doses (2.5, 5, or 10 mg/kg) of DAC on day 0, and tumors were collected on days 4 and 7. **(C)** Comparison of FRα expression in A549R xenograft tumors collected on day 4 and 7. **(D, E)** FRα expression in A549 xenograft tumors. Mice were intraperitoneally injected with different doses (2.5, 5, or 10 mg/kg) of DAC on day 0, and tumors were collected on day 4 and 7. Densitometric values are shown as optical density after GAPDH normalization using Image J and each band represents a mouse.

cells, which might provide a new strategy for patients with LUAD presenting with acquired radioresistance.

FRα was reported to be expressed at high levels in LUAD (17, 18, 28). However, its expression level in LUAD cell lines is not consistent. According to our study, only the A549 cell line was FRα-positive, and other LUAD cell lines had little or undetectable expression of FRα at the mRNA or protein level. This result was shown in another study in which the researchers analyzed the expression of FRα in 27 lung cancer cell lines, including 19 LUAD, 1 lung squamous cell carcinoma (SqCC), 1 lung adenosquamous carcinoma (ASC), 3 small cell lung cancer (SCLC) and 3 lung large cell carcinoma (LCC) cell lines, and only observed strong bands in the Western blots of A549 (LUAD), H647 (ASC), H460 (LCC) and SBC-5, KB (SCLC) cell lines, whereas other cell lines had faint or no bands, especially LUAD cell lines (24). Given the importance of pemetrexed in the clinical treatment of LUAD and the similar expression level of FRα to human LUAD, we constructed an A549 radioresistant cell model to study changes in the sensitivity of radioresistant cells to pemetrexed, which has been widely used in other studies to illustrate the internal mechanisms of acquired radioresistance (29, 30). Radioresistant isogenic cell models have been generated for many human cancer lines and have formed the basis for the identification of mechanisms of radioresistance (31, 32). When we searched the Gene Expression Omnibus (GEO) datasets for radioresistant cancer cells and FRα, we found that FRα was downregulated in radioresistant B-precursor acute lymphoblastic (ALL) tumor cells and the radioresistant squamous cell carcinoma cell line SCC61 (**Supplementary Figure 8**), suggesting that the downregulation of FRα in radioresistant cancer cells might be a universal phenomenon. Therefore, the efficiency of FRα-related chemotherapeutic drugs must be closely monitored in for patients with acquired radioresistance.

The membrane transport of pemetrexed in mammalian cells is mediated by several transporters and receptors. RFC, which belongs to the SLC19 family (*SLC19A1*), is widely distributed in various human tissues and functions as an anion exchanger, but its activity and folate-concentrating ability are limited in a low pH microenvironment (33, 34). Unlike RFC, PCFT which is encoded by *SLC46A1*, functions optimally at acidic rather than neutral pH. However, it is mainly expressed in the jejunum, duodenum, kidney, spleen, placenta, liver, and choroid plexus, but rarely in the lung (34). The folate receptors FRα and FRβ are high-affinity binding proteins that mediate the transport of pemetrexed through endocytosis. FRα is expressed at high levels in epithelial cells of the placenta, female reproductive organs, breast, lung and various human solid tumors (15, 35), whereas FRβ is mainly detected in hematopoietic tissues (35). Although FRα requires complex processes to facilitate pemetrexed to enter into cells, it has an affinity for preferred substrates more than 3 orders of magnitude greater than RFC (13, 36). In addition, various groups have documented high FRα expression in NSCLC (16, 17, 19, 37) and the results of our study also showed the highest expression level of FRα among the four transporters and receptors in A549 cells. Collectively, FRα may play a pivotal role in pemetrexed treatment of LUAD, and

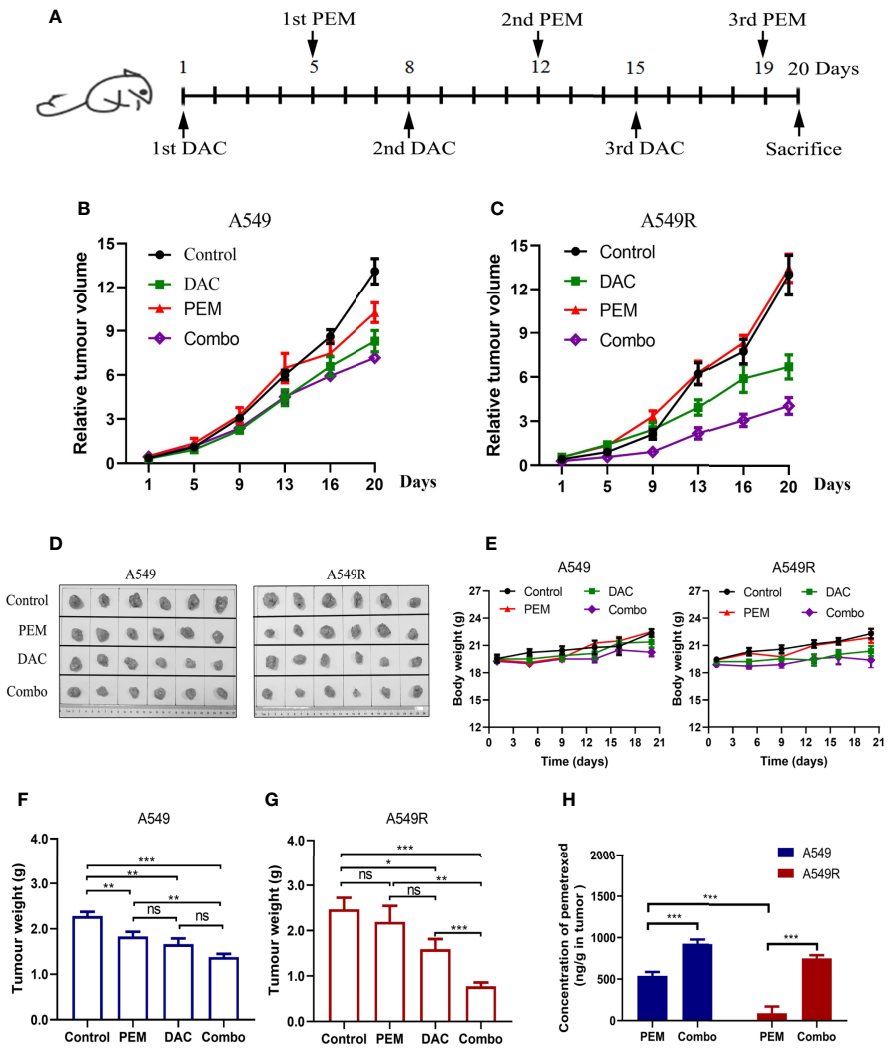


**FIGURE 7** | Decitabine sensitizes A549 and A549R cells to pemetrexed in xenograft models. **(A)** Experimental timeline and dosing schedule for xenograft models. **(B, C)** Tumor growth curves for A549 and A549R xenografts. **(D)** Tumors after resection from mice on day 20. **(E)** Body weight curves for A549 and A549R xenografts. **(F, G)** Tumor weight of A549 and A549R xenografts on day 20. **(H)** The concentration of pemetrexed in tumors of A549 and A549R xenografts. Data are presented as the means ± SE from 6 mice. Groups with different letters show significant differences using ANOVA followed by Tukey's test. Differences between the two groups are denoted as *$p < 0.05$, **$p < 0.01$ and ***$p < 0.001$. ns, not significant. Control, DAC, PEM, and Combo indicate mice treated with saline, decitabine alone, pemetrexed alone, and decitabine-pemetrexed combination, respectively.

downregulation of FRα inevitably leads to the low sensitivity of radioresistant LUAD cells to pemetrexed.

Drug combinations are currently the mainstream treatment strategy for cancer chemotherapy, and may produce favorable outcomes, including 1) increasing the efficacy of the therapeutic agent, 2) maintaining the same efficacy to avoid toxicity, and 3) minimizing or slowing the development of drug resistance (21). Decitabine was approved by Food and Drug Administration (FDA) as an epigenetic drug for patients with acute myeloid leukemia (AML) and myelodysplastic syndrome (MDS) (38). Although the antitumor mechanisms of decitabine are unclear, low doses of decitabine are efficacious against hematological neoplasms, rather than high doses that induced rapid DNA damage and cytotoxicity (39). Remarkably, low doses of decitabine exert durable antitumor effects on hematological and epithelial tumor cells but are not toxic to normal cells (39). In recent years, several clinical trials have reported the potential of decitabine as a single agent and in combination with other chemotherapeutics for NSCLC (40–44). However, single epigenetic agents had limited effects; thus, the investigative focus now lies on combination therapies of epigenetically active agents with conventional chemotherapy. Patients with lung cancer who are not eligible for aggressive chemotherapy might benefit from epigenetic therapy due to the lower number of side effects (43). In our study, the cytotoxicity of pemetrexed in radioresistant adenocarcinoma cells was decreased approximately 3-fold compared to that in the parental cells, suggesting that 4 times the dose of pemetrexed was needed to maintain the same efficacy, which may undoubtedly increase toxic

side effects. Interestingly, the combination of pemetrexed and decitabine effectively increased the accumulation of pemetrexed in radioresistant adenocarcinoma cells. Moreover, *in vivo* and *in vitro* studies indicated that the combination of pemetrexed and decitabine exerted a strong synergistic effect on H1975, A549 and A549R cells, consistent with preclinical studies showing that long-term and low-dose decitabine had remarkable chemotherapeutic potential for tumor therapy (40). According to a report, the mean maximum plasma concentration (Cmax) of decitabine in human is 64.8 - 77.0 ng/ml (0.28 μmol/L - 0.34 μmol/L) (45). In our study, a low dose of decitabine (0.2 μmol/L) increased pemetrexed sensitivity 1.2- and 3.1-fold in A549 and A549R cells, respectively, which suggests the good potential of a clinical combination of these two drugs. Unfortunately, the present study did not clarify the specific mechanism by which decitabine regulates the expression of FRα, but decitabine did not reduce CpG methylation in the FRα promoter, indicating that decitabine indirectly activated FRα expression through a mechanism that requires further study.

In conclusion, this study provides important basic data on the changes in pemetrexed-related transporters and receptors after long-term fractionated irradiation and suggests that the pemetrexed-decitabine combination is a promising treatment option that sensitizes radioresistant LUAD cells to pemetrexed by increasing the FRα-mediated accumulation of pemetrexed in cancer cells. By extension, we may provide a more individualized chemotherapy regimen for patients with LUAD presenting with acquired radioresistance. The FRα expression pattern in patients with LUAD acquired radioresistance is suggested to be closely monitored, thereby increased the survival of patients based on pemetrexed treatment. Of course, more preclinical studies are needed to optimize the safety and efficacy of pemetrexed-decitabine combination therapy.

## DATA AVAILABILITY STATEMENT

The original contributions presented in the study are included in the article/**Supplementary Material**. Further inquiries can be directed to the corresponding authors.

## ETHICS STATEMENT

The studies involving human participants were reviewed and approved by the Internal Review and the Ethics Board of Affiliated Hangzhou First People's Hospital, Zhejiang University School of Medicine. Written informed consent for participation was not required for this study in accordance with the national legislation and the institutional requirements. The animal study was reviewed and approved by The Institutional Animal Care and Use Committee of Zhejiang University.

## AUTHOR CONTRIBUTIONS

SZ, SM, and YW conceptualized the study. YW and JH designed the study and wrote the manuscript. YW, JH, QW, and JZ performed the experiments. ZM, LZ, and BX contributed to the editing of the manuscript. All authors contributed to the article and approved the submitted version.

## FUNDING

The work was supported by the Science and Technology Development Project of Hangzhou (grant. 20180533B98), Zhejiang Provincial Natural Science Foundation of China under Grant No. LQ19H310001 and LY19H160032, Zhejiang Provincial Medicine and Health Science Foundation (grant No. 2020RC027, 2020RC028) and National Natural Scientific Foundation of China (81803631).

## SUPPLEMENTARY MATERIAL

The Supplementary Material for this article can be found online at: https://www.frontiersin.org/articles/10.3389/fonc.2021.668798/full#supplementary-material

## REFERENCES

1. Collin SM, Metcalfe C, Refsum H, Lewis SJ, Zuccolo L, Smith GD, et al. Circulating Folate, Vitamin B12, Homocysteine, Vitamin B12 Transport Proteins, and Risk of Prostate Cancer: A Case-Control Study, Systematic Review, and Meta-Analysis. *Cancer Epidemiol Biomarkers Prev Publ Am Assoc Cancer Res Cosponsored Am Soc Prev Oncol* (2010) 19(6):1632–42. doi: 10.1158/1055-9965.EPI-10-0180
2. Skvortsova I, Debbage P, Kumar V, Slwortsov S. Radiation Resistance: Cancer Stem Cells (Cscs) and Their Enigmatic Pro-Survival Signaling. *Semin Cancer Biol* (2015) 35:39–44. doi: 10.1016/j.semcancer.2015.09.009
3. Costello LC, Franklin RB. Novel Role of Zinc in the Regulation of Prostate Citrate Metabolism and its Implications in Prostate Cancer. *Prostate* (1998) 35(4):285–96. doi: 10.1002/(SICI)1097-0045(19980601)35:4<285::AID-PROS8>3.0.CO;2-F
4. Bregenholt S, Brimnes J, Reimann J, Claesson MH. Accumulation of Immunoglobulin-Containing Cells in the Gut Mucosa and Presence of Faecal Immunoglobulin in Severe Combined Immunodeficient (Scid) Mice With T Cell-Induced Inflammatory Bowel Disease (IBD). *Clin Exp Immunol* (1998) 114(1):19–25. doi: 10.1046/j.1365-2249.1998.00691.x
5. Mantini G, Valentini V, Meduri B, Margaritora S, Balducci M, Micciche F, et al. Low-Dose Radiotherapy as a Chemo-Potentiator of a Chemotherapy Regimen With Pemetrexed for Recurrent non-Small-Cell Lung Cancer: A Prospective Phase II Study. *Radiother Oncol* (2012) 105(2):161–6. doi: 10.1016/j.radonc.2012.09.006
6. Shen X, Denittis A, Werner-Wasik M, Axelrod R, Gilman P, Meyer T, et al. Phase I Study of 'Dose-Dense' Pemetrexed Plus Carboplatin/Radiotherapy for Locally Advanced non-Small Cell Lung Carcinoma. *Radiat Oncol* (2011) 6:17. doi: 10.1186/1748-717X-6-17
7. Morgan MA, Lawrence TS. Molecular Pathways: Overcoming Radiation Resistance by Targeting Dna Damage Response Pathways. *Clin Cancer Res* (2015) 21(13):2898–904. doi: 10.1158/1078-0432.CCR-13-3229
8. Kim BM, Hong Y, Lee S, Liu P, Lim JH, Lee YH, et al. Therapeutic Implications for Overcoming Radiation Resistance in Cancer Therapy. *Int J Mol Sci* (2015) 16(11):26880–913. doi: 10.3390/ijms161125991
9. Huang J, Li JJ. Multiple Dynamics in Tumor Microenvironment Under Radiotherapy. *Adv Exp Med Biol* (2020) 1263:175–202. doi: 10.1007/978-3-030-44518-8_10
10. Ko YS, Jin H, Lee JS, Park SW, Chang KC, Kang KM, et al. Radioresistant Breast Cancer Cells Exhibit Increased Resistance to Chemotherapy and

Enhanced Invasive Properties Due to Cancer Stem Cells. *Oncol Rep* (2018) 40 (6):3752–62. doi: 10.3892/or.2018.6714
11. Wang Y, Chen Q, Jin S, Deng W, Li S, Tong Q, et al. Up-Regulation of P-glycoprotein is Involved in the Increased Paclitaxel Resistance in Human Esophageal Cancer Radioresistant Cells. *Scand J Gastroenterol* (2012) 47 (7):802–8. doi: 10.3109/00365521.2012.683042
12. Wang Y, Huang J, Wu Q, Zhang J, Ma Z, Ma S, et al. Downregulation of Breast Cancer Resistance Protein by Long-Term Fractionated Radiotherapy Sensitizes Lung Adenocarcinoma to SN-38. *Invest New Drugs* (2021) 39 (2):458–68. doi: 10.1007/s10637-020-01003-3
13. Chattopadhyay S, Moran RG, Goldman ID. Pemetrexed: Biochemical and Cellular Pharmacology, Mechanisms, and Clinical Applications. *Mol Cancer Ther* (2007) 6(2):404–17. doi: 10.1158/1535-7163.MCT-06-0343
14. Liang J, Lu T, Chen Z, Zhan C, Wang Q. Mechanisms of Resistance to Pemetrexed in non-Small Cell Lung Cancer. *Trans Lung Cancer Res* (2019) 8 (6):1107–18. doi: 10.21037/tlcr.2019.10.14
15. Kelley KM, Rowan BG, Ratnam M. Modulation of the Folate Receptor Alpha Gene by the Estrogen Receptor: Mechanism and Implications in Tumor Targeting. *Cancer Res* (2003) 63(11):2820–8.
16. Cagle PT, Zhai QJ, Murphy L, Low PS. Folate Receptor in Adenocarcinoma and Squamous Cell Carcinoma of the Lung: Potential Target for Folate-Linked Therapeutic Agents. *Arch Pathol Lab Med* (2013) 137(2):241–4. doi: 10.5858/arpa.2012-0176-OA
17. Shi H, Guo J, Li C, Wang Z. A Current Review of Folate Receptor Alpha as a Potential Tumor Target in non-Small-Cell Lung Cancer. *Drug Design Dev Ther* (2015) 9:4989–96. doi: 10.2147/DDDT.S90670
18. Driver BR, Barrios R, Ge YM, Haque A, Tacha D, Cagle PT. Folate Receptor Alpha Expression Level Correlates With Histologic Grade in Lung Adenocarcinoma. *Arch Pathol Lab Med* (2016) 140(7):682–5. doi: 10.5858/arpa.2015-0431-OA
19. Christoph DC, Asuncion BR, Hassan B, Tran C, Maltzman JD, O'Shannessy DJ, et al. Significance of Folate Receptor Alpha and Thymidylate Synthase Protein Expression in Patients With non-Small-Cell Lung Cancer Treated With Pemetrexed. *J Thorac Oncol Off Publ Int Assoc Study Lung Cancer* (2013) 8(1):19–30. doi: 10.1097/JTO.0b013e31827628ff
20. Iwakiri S, Sonobe M, Nagai S, Hirata T, Wada H, Miyahara R. Expression Status of Folate Receptor Alpha is Significantly Correlated With Prognosis in non-Small-Cell Lung Cancers. *Ann Surg Oncol* (2008) 15(3):889–99. doi: 10.1245/s10434-007-9755-3
21. Chou TC. Theoretical Basis, Experimental Design, and Computerized Simulation of Synergism and Antagonism in Drug Combination Studies. *Pharmacol Rev* (2006) 58(3):621–81. doi: 10.1124/pr.58.3.10
22. Liu Y, Zheng X, Yu Q, Wang H, Tan F, Zhu Q, et al. Epigenetic Activation of the Drug Transporter OCT2 Sensitizes Renal Cell Carcinoma to Oxaliplatin. *Sci Transl Med* (2016) 8(348):348ra97. doi: 10.1126/scitranslmed.aaf3124
23. Hatakeyama Y, Kobayashi K, Nagano T, Tamura D, Yamamoto M, Tachihara M, et al. Synergistic Effects of Pemetrexed and Amrubicin in non-Small Cell Lung Cancer Cell Lines: Potential for Combination Therapy. *Cancer Lett* (2014) 343(1):74–9. doi: 10.1016/j.canlet.2013.09.019
24. Kato T, Jin CS, Ujiie H, Lee D, Fujino K, Wada H, et al. Nanoparticle Targeted Folate Receptor 1-Enhanced Photodynamic Therapy for Lung Cancer. *Lung Cancer* (2017) 113:59–68. doi: 10.1016/j.lungcan.2017.09.002
25. Goldman ID, Zhao R. Molecular, Biochemical, and Cellular Pharmacology of Pemetrexed. *Semin Oncol* (2002) 29(6 Suppl 18):3–17. doi: 10.1053/sonc.2002.37461
26. Nie J, Liu L, Li X, Han W. Decitabine, a New Star in Epigenetic Therapy: The Clinical Application and Biological Mechanism in Solid Tumors. *Cancer Lett* (2014) 354(1):12–20. doi: 10.1016/j.canlet.2014.08.010
27. Notaro S, Reimer D, Fiegl H, Schmid G, Wiedemair A, Rossler J, et al. Evaluation of Folate Receptor 1 (FOLR1) mRNA Expression, its Specific Promoter Methylation and Global DNA Hypomethylation in Type I and Type II Ovarian Cancers. *BMC Cancer* (2016) 16:589. doi: 10.1186/s12885-016-2637-y
28. Scaranti M, Cojocaru E, Banerjee S, Banerji U. Exploiting the Folate Receptor Alpha in Oncology. *Nat Rev Clin Oncol* (2020) 17(6):349–59. doi: 10.1038/s41571-020-0339-5
29. Wang Y, He J, Zhang S, Yang Q. Intracellular Calcium Promotes Radioresistance of non-Small Cell Lung Cancer A549 Cells Through Activating Akt Signaling. *Tumour Biol J Int Soc Oncodev Biol Med* (2017) 39(3):1010428317695970. doi: 10.1177/1010428317695970
30. Zhang J, Zhou L, Nan Z, Yuan Q, Wen J, Xu M, et al. Knockdown of cMyc Activates Fas-mediated Apoptosis and Sensitizes A549 Cells to Radiation. *Oncol Rep* (2017) 38(4):2471–9. doi: 10.3892/or.2017.5897
31. McDermott N, Meunier A, Lynch TH, Hollywood D, Marignol L. Isogenic Radiation Resistant Cell Lines: Development and Validation Strategies. *Int J Radiat Biol* (2014) 90(2):115–26. doi: 10.3109/09553002.2014.873557
32. Kuwahara Y, Roudkenar MH, Urushihara Y, Saito Y, Tomita K, Roushandeh AM, et al. Clinically Relevant Radioresistant Cell Line: A Simple Model to Understand Cancer Radioresistance. *Med Mol Morphol* (2017) 50(4):195–204. doi: 10.1007/s00795-017-0171-x
33. Matherly LH. Molecular and Cellular Biology of the Human Reduced Folate Carrier. *Prog Nucleic Acid Res Mol Biol* (2001) 67:131–62. doi: 10.1016/S0079-6603(01)67027-2
34. Hou Z, Matherly LH. Biology of the Major Facilitative Folate Transporters SLC19A1 and SLC46A1. *Curr Topics Memb* (2014) 73:175–204. doi: 10.1016/B978-0-12-800223-0.00004-9
35. Matherly LH, Goldman DI. Membrane Transport of Folates. *Vitam Horm* (2003) 66:403–56. doi: 10.1016/s0083-6729(03)01012-4
36. Zhao R, Diop-Bove N, Visentin M, Goldman ID. Mechanisms of Membrane Transport of Folates Into Cells and Across Epithelia. *Annu Rev Nutr* (2011) 31:177–201. doi: 10.1146/annurev-nutr-072610-145133
37. Nunez MI, Behrens C, Woods DM, Lin H, Suraokar M, Kadara H, et al. High Expression of Folate Receptor Alpha in Lung Cancer Correlates With Adenocarcinoma Histology and EGFR [Corrected] Mutation. *J Thorac Oncol Off Publ Int Assoc Study Lung Cancer* (2012) 7(5):833–40. doi: 10.1097/JTO.0b013e31824de09c
38. Seelan RS, Mukhopadhyay P, Pisano MM, Greene RM. Effects of 5-Aza-2'-Deoxycytidine (Decitabine) on Gene Expression. *Drug Metab Rev* (2018) 50 (2):193–207. doi: 10.1080/03602532.2018.1437446
39. Tsai HC, Li H, Van Neste L, Cai Y, Robert C, Rassool FV, et al. Transient Low Doses of DNA-demethylating Agents Exert Durable Antitumor Effects on Hematological and Epithelial Tumor Cells. *Cancer Cell* (2012) 21(3):430–46. doi: 10.1016/j.ccr.2011.12.029
40. Momparler RL. Epigenetic Therapy of non-Small Cell Lung Cancer Using Decitabine (5-Aza-2'-Deoxycytidine). *Front Oncol* (2013) 3:188. doi: 10.3389/fonc.2013.00188
41. Vendetti FP, Rudin CM. Epigenetic Therapy in non-Small-Cell Lung Cancer: Targeting DNA Methyltransferases and Histone Deacetylases. *Expert Opin Biol Ther* (2013) 13(9):1273–85. doi: 10.1517/14712598.2013.819337
42. Forde PM, Brahmer JR, Kelly RJ. New Strategies in Lung Cancer: Epigenetic Therapy for non-Small Cell Lung Cancer. *Clin Cancer Res* (2014) 20(9):2244–8. doi: 10.1158/1078-0432.CCR-13-2088
43. Schiffmann I, Greve G, Jung M, Lubbert M. Epigenetic Therapy Approaches in non-Small Cell Lung Cancer: Update and Perspectives. *Epigenetics* (2016) 11 (12):858–70. doi: 10.1080/15592294.2016.1237345
44. Rodriguez-Paredes M, Esteller M. A Combined Epigenetic Therapy Equals the Efficacy of Conventional Chemotherapy in Refractory Advanced non-Small Cell Lung Cancer. *Cancer Discovery* (2011) 1(7):557–9. doi: 10.1158/2159-8290.CD-11-0271
45. Cashen AF, Shah AK, Todt L, Fisher N, DiPersio J. Pharmacokinetics of Decitabine Administered as a 3-H Infusion to Patients With Acute Myeloid Leukemia (AML) or Myelodysplastic Syndrome (MDS). *Cancer Chemother Pharmacol* (2008) 61(5):759–66. doi: 10.1007/s00280-007-0531-7

**Conflict of Interest:** The authors declare that the research was conducted in the absence of any commercial or financial relationships that could be construed as a potential conflict of interest.

frontiers in Pharmacology

ORIGINAL RESEARCH
published: 28 May 2021
doi: 10.3389/fphar.2021.607755



# Doxorubicin/Nucleophosmin Binding Protein-Conjugated Nanoparticle Enhances Anti-leukemia Activity in Acute Lymphoblastic Leukemia Cells *in vitro* and *in vivo*

*Donghui Gan*[1‡], *Yuwen Chen*[1‡], *Zhengjun Wu*[1‡], *Liping Luo*[1‡], *Shimuye Kalayu Yirga*[1], *Na Zhang*[1], *Fu Ye*[2], *Haijun Chen*[2†], *Jianda Hu*[1*†] and *Yingyu Chen*[1*†]

[1]Department of Hematology, Fujian Institute of Hematology, Fujian Provincial Key Laboratory of Hematology, Fujian Medical University Union Hospital, Fuzhou, China, [2]College of Chemistry, Fuzhou University, Fuzhou, China

Acute lymphoblastic leukemia (ALL) is an aggressive malignancy. Adults with ALL have more than 50% relapse rates. We have previously validated that overexpression of nucleophosmin (NPM) is involved in the multidrug resistance (MDR) development during ALL; and a synthetically engineered recombinant NPM binding protein (NPMBP) has been developed in our group; NPMBP and doxorubicin (DOX) can be conjugated in a nanoparticle-based drug delivery system named DOX-PMs-NPMBP to counteract MDR during ALL. Here, we evaluated the antileukemia potential of DOX-PMs-NPMBP in resistant ALL cells. This study demonstrates that DOX-PMs-NPMBP significantly enhances chemosensitivity to DOX in ALL cells. Despite at variable concentrations, both resistant and primary ALL cells from relapsed patients were sensitive to DOX-PMs-NPMBP. In detail, the half maximal inhibitory concentration (IC50) values of DOX-PMs-NPMBP were between 1.6- and 7.0-fold lower than those of DOX in cell lines and primary ALL cells, respectively; and apoptotic cells ratio was over 2-fold higher in DOX-PMs-NPMBP than DOX. Mechanistically, p53-driven apoptosis induction and cell cycle arrest played essential role in DOX-PMs-NPMBP-induced anti-leukemia effects. Moreover, DOX-PMs-NPMBP significantly inhibited tumor growth and prolonged mouse survival of ALL xenograft models; and no systemic toxicity occurrence was observed after treatment during follow-up. In conclusion, these data indicate that DOX-PMs-NPMBP may significantly exert growth inhibition and apoptosis induction, and markedly improve DOX antileukemia activity in resistant ALL cells. This novel drug delivery system may be valuable to develop as a new therapeutic strategy against multidrug resistant ALL.

**Keywords: acute lymphoblastic leukemia, p53, apoptosis, doxorubicin (dox), multidrug resistance (MDR), nanoparticle, nucleophosmin (NPM)**

OPEN ACCESS

***Edited by:***
*Zhe-Sheng Chen,*
*St. John's University, United States*

***Reviewed by:***
*Haishu Lin,*
*Shenzhen Technology University, China*
*Shen Li,*
*UCLA Department of Medicine, United States*

****Correspondence:***
*Yingyu Chen*
*chenyingyu@yahoo.com*
*Jianda Hu*
*drjiandahu@163.com*

[‡]*These authors contributed equally to this work*

***[†]ORCID:***
*Yingyu Chen*
*orcid.org/0000-0003-1243-3607*
*Jianda Hu*
*orcid.org/0000-0002-4438-2544*
*Haijun Chen*
*orcid.org/0000-0001-7945-2461*

***Specialty section:***
*This article was submitted to Pharmacology of Anti-Cancer Drugs, a section of the journal Frontiers in Pharmacology*

***Received:*** *18 September 2020*
***Accepted:*** *07 May 2021*
***Published:*** *28 May 2021*

***Citation:***
*Gan D, Chen Y, Wu Z, Luo L, Yirga SK, Zhang N, Ye F, Chen H, Hu J and Chen Y (2021) Doxorubicin/Nucleophosmin Binding Protein-Conjugated Nanoparticle Enhances Anti-leukemia Activity in Acute Lymphoblastic Leukemia Cells* in vitro *and* in vivo*. Front. Pharmacol. 12:607755. doi: 10.3389/fphar.2021.607755*

# INTRODUCTION

Acute lymphoblastic leukemia (ALL) is an aggressive, malignant disease. Improvements in multiagent chemotherapy treatments, along with tailored risk assessment, have raised survival rates in pediatric ALL. However, adult ALL patients still have a relapse rate exceeding 50%, and an overall survival rate of 20–40% (Sive et al., 2012; Tasian and Gardner, 2015; Richard-Carpentier et al., 2019). In recent years, a personalized treatment approach involving the following has contributed to the progress of adult ALL therapy: response to minimal residual disease and disease genetics; adopting pediatric-inspired regimens in younger adults; advances in transplantation; incorporation of new treatments and tyrosine kinase inhibitors found in frontline regimens; as well as adoptive cellular therapy (Aldoss and Stein, 2018; Pillai et al., 2019). In particular, antibody-based therapies, such as monoclonal antibodies and antibody-drug conjugates have shown promising activity profiles for the treatment of ALL (Phelan and Advani, 2018; Schmied et al., 2019). Introduction of these strategies in the frontline setting has been ongoing and will likely unravel significant benefits for ALL.

Nanomedicines is a unique treatment strategy that offers different methods of administering drugs and improvement of the therapeutic efficacy and poses less side effects to healthy cells and tissues. In the context of drug resistance, nanoparticles have been shown to improve P-glycoprotein (P-gp) efficacy, suggesting that nanomedicine might overcome multidrug resistance (MDR) (Dong and Mumper, 2010; Mattheolabakis et al., 2012). Nucleophosmin (NPM) is a multifunctional nucleolar protein involved in several biological processes, as well as the pathogenesis of malignancies in humans (Borer et al., 1989; Colombo et al., 2011). NPM mutations induce the nuclear export of the mutants, while aberrant cytoplasmic delocalization of NPM is of high importance for leukaemogenesis (Liso et al., 2008; Chen and Hu, 2020). We have previously validated that overexpression of NPM and nucleolin (NCL) is involved in the MDR development and an important indicator for prognosis evaluation in ALL (Hu et al., 2011). Additional research demonstrated that RNA interference causes a knockdown of NPM, which can reverse MDR in resistant leukemic cells (Lin et al., 2013; Wang et al., 2015), and a synthetically engineered recombinant NPM binding protein (NPMBP) has been developed. Furthermore, NPMBP and doxorubicin (DOX) were bound to nanoparticle-based drug delivery system named DOX-PMs-NPMBP (China patent application 2020103023956, 2020107395750), in the attempt to counteract MDR during ALL, but this requires pharmacological proof. Here, we evaluated the anti-leukemia potential of DOX-PMs-NPMBP for ALL. We report that such strategy can markedly improve the antileukemia effect of DOX, exposing a new therapeutic strategy for ALL, particularly multidrug resistant ALL.

# MATERIALS AND METHODS

## Cell Culture and the Induction of DOX-Resistant Nalm6 Cells

Nalm6 cells were obtained from Fujian Medical University (Fuzhou, China). The drug-resistance induction was as previous described (Wang et al., 2015). Briefly, Nalm6 cells were exposed to incrementally higher levels of DOX to establish a leukemia cell line that was resistant to DOX (Hanhui Pharmaceuticals Co., LTD., Shanghai, China). The drug sensitivity between the resistant cells and the parent cells was compared with a 3-(4,5-dimethylthiazol-2-yl)-2,5-diphenyltetrazolium bromide (MTT, Sigma, St. Louis, MO, United States) assay. Prior to each experiment, cells were grown in a culture medium free of DOX for a minimum of two weeks.

Either Nalm6 cells or Nalm6/DOX cells were further transduced with a lentiviral vector that encoded the luciferase (Luc) gene. The efficiency of the stable transduction was monitored by fluorescence microscopy. Both cell lines with stable luciferase expression were named as Nalm6-Luc cells and Nalm6-Luc/DOX cells, respectively.

## Primary Cell Isolation from Peripheral Blood

Peripheral blood (PB) samples were isolated from six ALL patients at our institute. All patients were diagnosed with ALL according to World Health Organization (WHO) and standard French-American-British (FAB) standards. All patients provided their informed consent according to the Helsinki declaration, while the institutional review board of the Ethics Committee of Fujian Medical University Union Hospital approved the study (2018–113). Primary ALL cells were isolated from PB samples as previously reported (Chen et al., 2014; Chen et al., 2020).

## Cloning, Protein Expression and Purification

NPMBP was produced in accordance with the standard procedure by Wuhan Institute of Biotechnology (Wuhan, China). Briefly, NPM truncation constructs were cloned in a pET28a vector, and recombinant his-tagged NPMBP was expressed in *E. coli* BL21 strain in medium with the presence of 50 mg/l Kanamycin. Bacterial cultures wore grown at 37°C to an optical density OD600 0.5–0.8. Protein expression was induced by the addition of 0.8 mM Isopropyl β-D-Thiogalactoside (IPTG, GoldBio, st. Louis, United States), the temperature was lowered to 25°C and the cultures were incubated for 12 h. Bacterial cultures were harvested by centrifugation and lysed by sonication on ice. NPMBP with high binding affinity was screened and isolated by phage display technology, which was further purified using Ni (2+) affinity chromatographic column. SDS-PAGE showed a highly pure 16 kD protein, in accordance with the expected molecular weight (**Figure 1A**). The peptide with best binding affinity towards NPM was identified (**Supplementary Figure 1**). Purified proteins were further concentrated and reconstituted in phosphate-buffered saline (PBS) containing 5% glycerol, pH 7.4 at −80°C.

## Preparation of DOX-PMs-NPMBP

Polyethylene glycol (PEG) was employed to modify the hydrophobic poly-(lactic acid) (PLA) to form the polymeric micelles (PMs) according to previous reports (Aliabadi et al., 2007; Duncan et al., 2019; Hoang et al., 2019). Equal

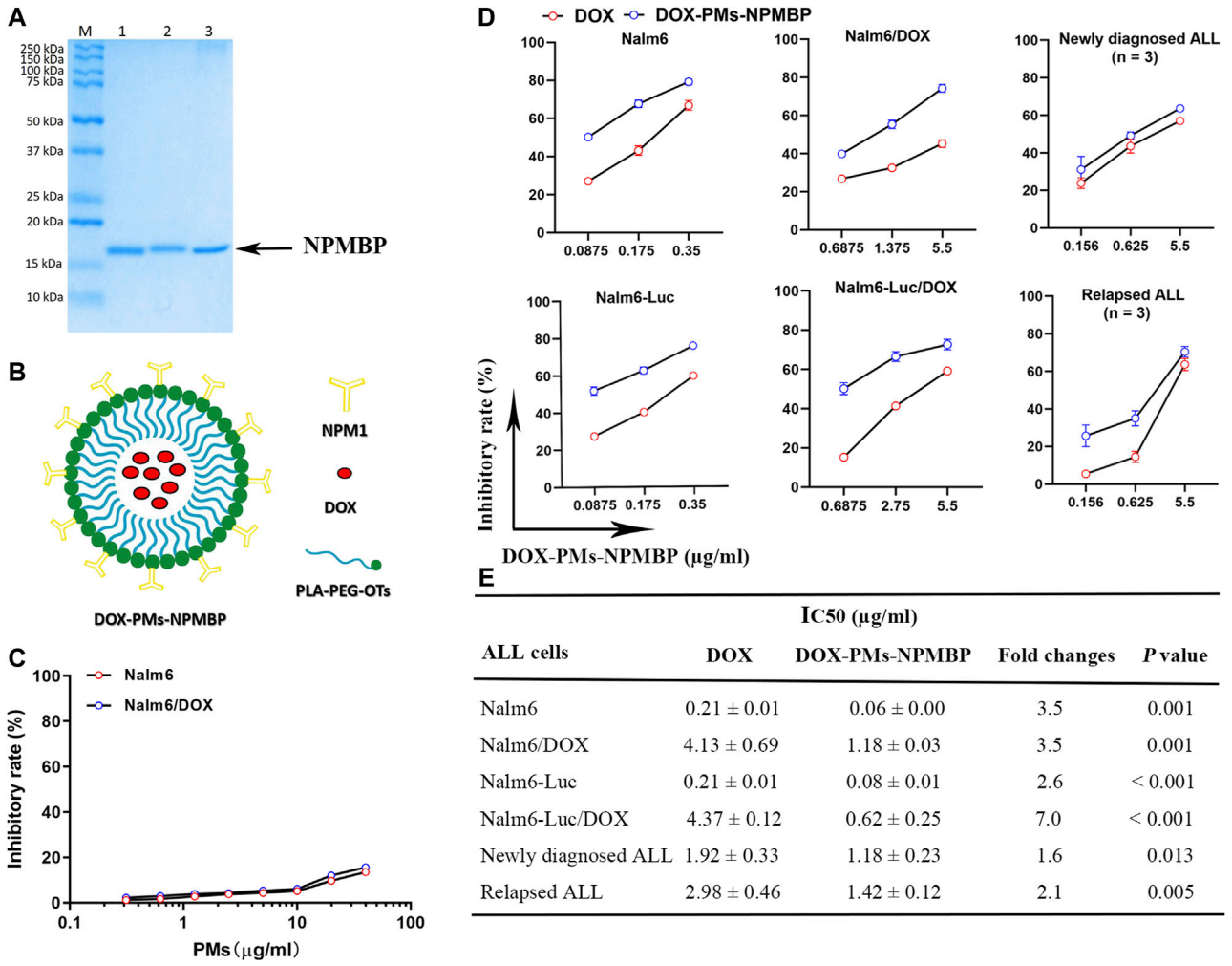


**E**

| ALL cells | IC50 (μg/ml) DOX | DOX-PMs-NPMBP | Fold changes | *P* value |
|---|---|---|---|---|
| Nalm6 | 0.21 ± 0.01 | 0.06 ± 0.00 | 3.5 | 0.001 |
| Nalm6/DOX | 4.13 ± 0.69 | 1.18 ± 0.03 | 3.5 | 0.001 |
| Nalm6-Luc | 0.21 ± 0.01 | 0.08 ± 0.01 | 2.6 | < 0.001 |
| Nalm6-Luc/DOX | 4.37 ± 0.12 | 0.62 ± 0.25 | 7.0 | < 0.001 |
| Newly diagnosed ALL | 1.92 ± 0.33 | 1.18 ± 0.23 | 1.6 | 0.013 |
| Relapsed ALL | 2.98 ± 0.46 | 1.42 ± 0.12 | 2.1 | 0.005 |

**FIGURE 1 |** IC50 values of DOX-PMs-NPMBP on multiple ALL cell lines and different primary ALL cells from patients as measured by MTT assay. **(A)** Representative gel demonstrating the expected molecular weight and purity of NPMBP. **(B)** Schematic illustration of the structure of DOX-PMs-NPMBP. **(C)** Quantitative evaluation of inhibitory rates in Nalm6-Luc cells and Nalm6-Luc/DOX cells with equivalent concentrations of polymeric micelles (PMs) for 48 h. **(D)** Quantitative evaluation of inhibitory rate in various ALL cells with DOX or DOX-PMs-NPMBP indicated concentration. **(E)** ALL cell lines or primary cells from six patients treated with increasing concentrations of DOX or DOX-PMs-NPMBP for 48 h. IC50 values of DOX and DOX-PMs-NPMBP were calculated. Data are presented as mean ± SD of three independent experiments.

concentrations of DOX and NPMBP at 0.3 mg/ml, achieving high drug-loading capacity and the high colloidal stability, were conjugated polymer-based nanoparticles and micelles. This drug- and binding protein-coated nanoparticle was named as DOX-PMs-NPMBP (**Figure 1B**, China Patent Application 2020103023956, 2020107395750). The DOX-PMs-NPMBP stock solutions in PBS at pH 7.4 were stored at −20°C.

## Cell Viability Assay

ALL cells ($4.0 \times 10^5$ cells/ml for cell lines and $2.5 \times 10^6$ cells/ml for primary cells) were seeded in 96-well plate. Cells were incubated directly after plating in triplicate with serial concentrations of DOX-PMs-NPMBP, DOX, and PMs. Cell viability was determined by MTT assay as we previously reported (Chen et al., 2020). The half maximal inhibitory concentration (IC50) was determined by the Logit way.

## Cell Apoptosis and Cell Cycle Distribution Assessed by Flow Cytometry

A total of $3.0 \times 10^5$ Nalm6/DOX cells were seeded in 6-well plate with 3 ml per well of medium. Cells were then treated with DOX, DOX-PMs-NPMBP and vehicle control for 24 h. The staining process of harvested cell pellets was manipulated using Annexin V Apoptosis Detection Kit (Becton Dickinson, CA, United States) according to the manufacturer's protocols. Frequency of apoptotic cells was analyzed by flow cytometry (BD FACSVerse™, Becton Dickinson, CA, United States). For cell cycle analysis, a total $3.0 \times 10^6$ cells were treated with DOX or

DOX-PMs-NPMBP for 24 h. Cell cycle distribution was examined as previously described (Chen et al., 2020). Propidium iodide used in this assay was purchased from BD Biosciences.

## Cellular Uptake of DOX

A total of $4.0 \times 10^5$ Nalm6/DOX cells per well were plated in 6-well plates in 2 ml of growth medium. Cells were then incubated with or without DOX, DOX-PMs-NPMBP at 37°C for 12 h, cells were twice washed with ice-cold PBS. Flow cytometer analysis was used to assess the cell-associated mean fluorescence intensity (MFI) of the DOX with excitation/emission wave lengths of 485/580 nm.

## Rhodamine123 (Rho123) Efflux Assay

Nalm6/DOX cells were seeded and treated with or without DOX, DOX-PMs-NPMBP as the procedures for the measurement of cellular uptake of DOX. Then, for the drug efflux ability analysis, Rho123 at 2 μM was added to each well and incubated for another 30 min at 37°C. After that, cells were twice washed with ice-cold PBS. Flow cytometer analysis was used to assess the MFI of Rho123 in the Nalm6/DOX cells through FITC channel.

## RNA Extraction and Sequencing

Nalm6/DOX cells were grown in the presence or absence of DOX or DOX-PMs-NPMBP for 12 h. After treatment, cells were pelleted by centrifugation and total RNA was extracted using TRIzol reagent (Invitrogen, CA) and quantified by UV spectrophotometry (Nanodrop). For each sample 1 μg RNA was inputted when preparing the RNA samples. A NEBNext® UltraTM RNA Library Prep Kit for Illumina® (NEB, United States) was used to create the sequencing libraries according to the manufacturer's instructions. We added index codes to designate sequences for each sample. A cBot Cluster Generation System with TruSeq PE Cluster Kit v3-cBot-HS (Illumina) was used to cluster the index-coded samples according to the manufacturer's instructions. After the clusters were generated, an Illumina Novaseq platform was used to sequence the library and 150 bp paired-end reads were created. The RNA sequencing and the bioinformatic analysis were done by Novogene Co., Ltd. (Beijing, China).

## Quantitative Real-Time Polymerase Chain Reaction

Quantitative real-time polymerase chain reaction (qRT-PCR) was performed on the ABI prism 7,700 sequence detection system (Applied Biosystems, CA, United States) using EvaGreen MasterMix-Low ROX kit (Richmond, BC, Canada). **Table 1** lists primer sequences for glyceraldehyde-3-phosphate dehydrogenase (GAPDH), NPM, proto-oncogene c-myc, TP53 (p53) and p14ARF, B-cell lymphoma 2 (bcl-2), $p21^{WAF1/CIP1}$, bcl-2 associated X (bax), mouse double minute 4 (MDM4), MDR, and phosphatase and tensin homolog (PTEN) detection by qRT-PCR. The relative mRNA amounts were calculated by the $2^{-\Delta\Delta Ct}$ method as we previously reported (Chen et al., 2020).

**TABLE 1 |** The primer sequences for qRT-PCR

| Gene | Sequence |
|---|---|
| GAPDH | F: 5′-CCACCATGGAGAAGGCTGGGGCTCA-3′ |
| | R: 5′-ATCACGCCACAGTTTCCCGGAGGGG-3′ |
| NPM | F: 5′-GTACAGCCAACGGTTTCCCTTG-3′ |
| | R: 5′-TTCACATCCTCCTCCTCTTCATCTTC-3′ |
| c-myc | F: 5′-TCCTGGCAAAAGGTCAGAGT-3′ |
| | R: 5′-TCTGACACTGTCCAACTTGAC-3 |
| p53 | F: 5′-CAGCACATGACGGAGGTTGT-3′ |
| | R: 5′-TCATCCAAATACTCCACACGC-3′ |
| bcl-2 | F: 5′-ACGACTTCTCCCGCCGCTAC-3′ |
| | R: 5′-CTGAAGAGCTCCTCCACCAC-3′ |
| p21 | F: 5′-CGATGGAACTTCGACTTTGTCA-3′ |
| | R: 5′-GCACAAGGGTACAAGACAGTG-3′ |
| bax | F: 5′-ATGGAGCTGCAGAGGATGATTG-3′ |
| | R: 5′-AATGTCCAGCCCATGATGGTTC-3′ |
| p14ARF | F: 5′-TCGCGATGTCGCACGGTA-3′ |
| | R: 5′-CAATCGGGGATGTCTGAGGGAC-3′ |
| MDM4 | F: 5′-TGGACAAATCAATCAGGTACGA-3′ |
| | R: 5′-CTCCTGCTGATCATAAAGTTGC-3′ |
| MDR | F: 5′-CCCATCATTGCAATAGCAGG-3′ |
| | R: 5′-GTTCAAACTTCTGCTCCTGA-3′ |
| PTEN | F: 5′-TGCAGTATAGAGCGTGCAGA-3′ |
| | R: 5′-TAGCCTCTGGATTTGACGGC-3′ |

## Western Blotting

Cells were cultured with or without DOX or DOX-PMs-NPMBP for 24 h. Western blot analysis was performed according to we previously described (Chen et al., 2014; Chen et al., 2020). Primary antibodies against Tublin, Actin and c-Myc were obtained from Santa Cruz Biotechnology, Inc. (Santa Gruz, CA, United States). NPM, P-gp, PTEN, Bcl-2, Bax, phospho-14ARF (p14ARF), $p21^{WAF1/CIP1}$, PI3 Kinase p85, phospho-p85 (p-p85), p53 and phospho-p53 (p-p53), Cyclin D, Cyclin E, phospho-retinoblastoma (p-Rb), mouse double minute 2 (MDM2) and MDM4 antibodies were provided by Cell Signaling Technology (Danvers, MA, United States). GAPDH antibody was purchased from Abcam (Cambridge, United Kingdom).

## *In vivo* Anti-leukemic Effects in Nalm6-Luc/DOX Xenograft Nude Mice

Around $5 \times 10^6$ Nalm6-Luc/DOX cells were subcutaneously transplanted to 6- to 8-week-old BALB/C-nude mice (Slac Laboratory Animal Co., Ltd. Shanghai, China). Twenty days after transplantation, the Nalm6-Luc/DOX xenograft models received either DOX, DOX-PMs-NPMBP, or PMs at maximal dose (equivalent to 3 mg/kg DOX) by intraperitoneal injection once daily for 3 days. PBS injection was administered as vehicle control. Animal body weight was monitored during the follow-up. Tumor size was measured during study course. Tumor inhibition rate were calculated as we previously reported (Chen et al., 2018). Nalm6-Luc/DOX xenograft models in response to treatment were monitored by IVIS LUMINA II Imaging system (Caliper Life Sciences, Hopkinton, MA, United States) at the 25th day after the initial treatment. The follow-up was completed at the 30th day, tumor tissues and

organs were carefully excised and fixed in 10% formalin, embedded in paraffin. Then, tumor tissue sections were sliced, adhered to slide, and stained with hematoxylin-eosin (HE).

## Therapy of NCG Mouse Xenografted With Nalm6-Luc/DOX Cells

NOD-Prkdc$^{em26}$Il2rg$^{em26}$Nju (NCG) mice (Nanjing Biomedical Research Institute of Nanjing University, Nanjing, China) aged six-to eight-week-old were inoculated intravenously in their tail veins with $1.0 \times 10^4$ Nalm6-Luc/DOX cells. Seven days later, recipient mice were intraperitoneally injected with either DOX or DOX-PMs-NPMBP at 1.5 mg/kg once daily for 3 days. Vehicle control mice were received PBS only. The mouse body weight was tracked and recorded. Either treated mice or vehicle control mice were monitored by IVIS LUMINA II Imaging System. Animals were sacrificed until the 14th day after start of the treatment. The liver and spleen were weighed. Bone marrow (BM) smears were obtained. Cell morphology was assessed microscopically upon Wright-Giemsa staining. BM cells were isolated and stained with anti-human CD19-APC monoclonal antibody (Becton Dickinson). CD19$^+$ Nalm6-Luc/DOX in BM were analyzed by flow cytometry.

The experiment was repeated and all recipients were closely monitored. Survival times were recorded. Follow-up was completed on days 42 post leukemia cell inoculation. All animals were maintained at the animal facility in Fujian Medical University. Animal experiments were performed according to previously reported procedures (Chen et al., 2020). All protocols were reviewed and approved by the Ethics Committee of Institutional Animal Care and Use in Fujian Medical University (2017–071).

## Statistical Analysis

The data listed is that of the mean ± the standard deviation (SD). Statistical significance was determined using the two-tailed Student's *t*-test or one-way analysis of variance (ANOVA). GraphPad Prism software (version 8.0) was used to conduct statistical analysis. Kaplan-Meier methods and a long-rank test were used to assess the life span of the mice. Statistically significant results were those $p < 0.05$, $p < 0.01$, $p < 0.001$, and $p < 0.0001$.

# RESULTS

## Increased DOX-PMs-NPMBP Sensitivity in ALL Cell Lines and Primary Cells Compared to DOX

We determined whether DOX-PMs-NPMBP may effectively inhibit cell growth in DOX-resistant cell lines (Nalm6/DOX cells and Nalm6-Luc/DOX cells) and their parental cell lines (Nalm6 cells and Nalm6-Luc cells). Overall, ALL cells were more sensitive to DOX-PMs-NPMBP compared with DOX (**Figure 1D, E**). Although the average IC50 value of DOX in resistant Nalm6 cells was around 20-fold higher than that of DOX in its parental cells, cell growth was significantly suppressed by DOX-PMs-NPMBP with a dose-dependent way. The average IC50 value of DOX-PMs-NPMBP was 0.08 ± 0.01 μg/ml and 0.62 ± 0.25 μg/ml in Nalm6-Luc cells and corresponding DOX-resistant cells, respectively, reflecting a 2.6- and 7.0-fold reduction compared to DOX alone. Similar results were found in Nalm6 cells and Nalm6/DOX cells. The average IC50 value of DOX-PMs-NPMBP was 3.5-fold lower than that of DOX in Nalm6 cells and Nalm6/DOX cells. Interestingly, DOX-PMs-NPMBP decreased cell proliferation more significantly than the effects of DOX alone in primary ALL cells. Primary ALL cells from newly diagnosed or relapsed patients, were more sensitive to DOX-PMs-NPMBP compared with DOX. The average IC50 value was significantly decreased from 1.92 ± 0.33 μg/ml and 2.98 ± 0.46 μg/ml in DOX group to 1.18 ± 0.23 μg/ml and 1.42 ± 0.12 μg/ml in DOX-PMs-NPMBP group in newly diagnosed and relapsed patients, respectively. Noticeably, as shown in **Figure 1C**, the blank PMs without NPMBP and DOX showed no significant toxicity in either Nalm6 cells or Nalm6/DOX cells. About 85% cell viability was observed at maximum polymer concentrations equivalent to 40 μg/ml DOX.

## DOX-PMs-NPMBP Induces Apoptosis in DOX-Resistant Nalm6 Cells and DOX-Sensitive Nalm6 Cells

We next assessed the role of DOX-PMs-NPMBP on apoptosis induction in Nalm6 cells and Nalm6/DOX cells. The results demonstrated that DOX-PMs-NPMBP induced apoptosis in both cell lines compared to DOX treatment alone (**Figure 2**). When treated with DOX-PMs-NPMBP for 24 h, the ratio of apoptotic cells was 16.8 ± 1.7 and 17.7 ± 3.2%, respectively, reflecting a 1.5-fold and 2.2-fold increase compared to Nalm6 cells and Nalm6/DOX cells following single DOX administration. These results indicate that DOX-PMs-NPMBP can increase DOX chemosensitivity in either DOX-responsive or DOX-resistant ALL cells.

## DOX-PMs-NPMBP promotes the intracellular retention of DOX in DOX-resistant Nalm6 cells

To illustrate the mechanisms of DOX-PMs-NPMBP growth inhibitory effect in drug-resistant Nalm6 cells, we monitored the intracellular accumulation of DOX after treatment. As shown in **Figure 3A**, it showed slightly increased the intracellular retention of DOX in Nalm6/DOX cells after treated with DOX. The MFI of DOX significantly increased in a dose-dependent manner in Nalm6/DOX cells after DOX-PMs-NPMBP administration. Compared with DOX alone, DOX uptake was dramatically increased by 1.4- and 2.0-fold in Nalm6/DOX cells, after 1.0 and 2.0 μg/ml DOX-PMs-NPMBP treatment, respectively.

## Biological evaluation shows significant accumulation of intracellular Rho123 in the Nalm6/DOX cells upon DOX-PMs-NPMBP administration

Flow cytometry analysis showed that the MFI of Rho123 was not significant different to that of untreated control in

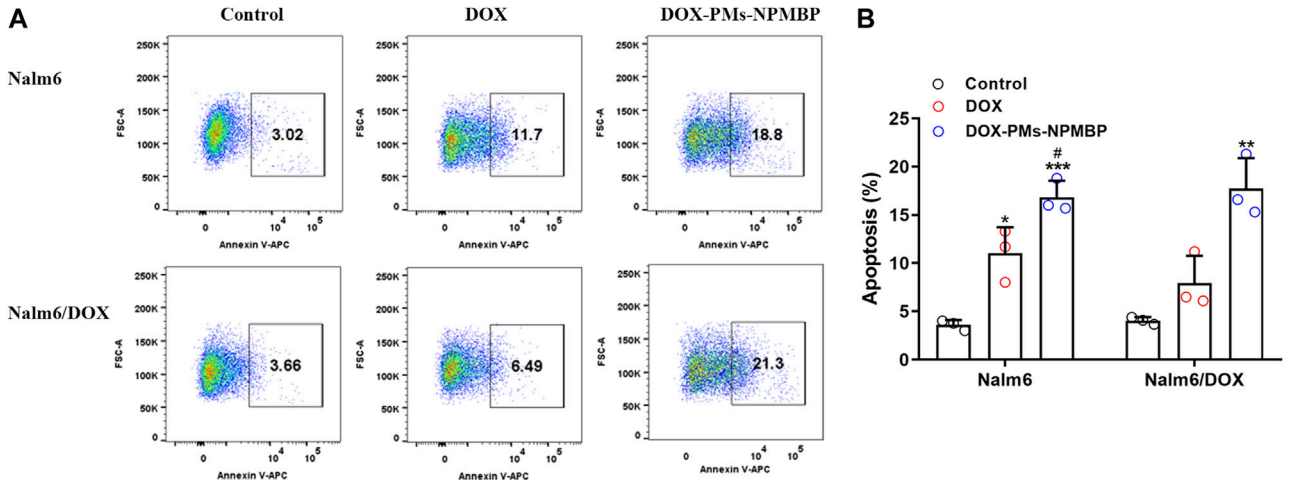


**FIGURE 2 |** DOX-PMs-NPMBP induces apoptosis in Nalm6/DOX cells. Nalm6/DOX cells were incubated with DOX or DOX-PMs-NPMBP for 24 h. Frequency of cells undergoing apoptosis was stained with Annexin V-APC and analyzed by flow cytometry. **(A)** Representative flow-cytograms of Annexin V$^+$ cells in each groups **(B)** Summary data for the frequency of apoptotic cells in each measured as in panel A. Data are generated from three independent experiments. $^*p < 0.05$, $^{**}p < 0.01$, $^{***}p < 0.001$ compared with control, $^{\#}p < 0.05$ compared with DOX.

Nalm6/DOX cells after treatment with DOX at 2.0 μg/ml ($p = 0.4419$), In contrast, DOX-PMs-NPMBP-treated resistant Nalm6/DOX cells dose-dependently increased intracellular accumulation of Rho123. As compared to DOX alone, the intracellular retention of Rho123 was significantly increased by 2.1- and 2.9-fold in Nalm6/DOX cells, after 1.0 and 2.0 μg/ml DOX-PMs-NPMBP treatment, respectively (**Figure 3B**).

## Bioinformation Analysis Shows Significant Transcriptional Changes in Nalm6/DOX cells Following DOX-PMs-NPMBP Treatment

To better understand the mechanisms driving DOX-PM-NPMBP increased anti-leukemia effects, we compared the transcriptional profiles of Nalm6/DOX cells following treatment with either DOX-PMs-NPMBP or DOX. **Figures 4A–C** show volcano plot of differential gene expressions (DEGs) in DOX-PMs-NPMBP-treated cells vs. vehicle control cells. We identified 2,414 upregulated genes, which are displayed as red dots, and 3,185 downregulated genes, which are displayed as green dots, between the vehicle control and the DOX-PMs-NPMBP treatment. We found 13 genes that were upregulated and 220 genes that were downregulated when compared DOX vs. DOX-PMs-NPMBP treatments. Next, we constructed the protein-protein interaction (PPI) and DEG network *via* the Search Tool for the Retrieval of Interacting Genes (STRING) repository (https://string-db.org/). The STRING diagram for the initial cohort of 400 gene proteins is shown in **Figure 4D**. This analysis displayed a clustering coefficient of 0.524 and a PPI enrichment *p*-value of 0. This suggests adequate connectivity and acceptable conclusions for analysis of the networks. To gain insight into the potential pathways that might be specifically associated with increased DOX-PMs-NPMBP-efficacy in Nalm6/DOX cells, we performed Kyoto Encyclopedia of Genes and Genomes (KEGG) enrichment analysis among different treatment groups. For DOX-PMs-NPMBP nanoparticle vs. vehicle control, 21 pathways were identified ($p < 0.05$, **Figure 4E**). Among those, p53 protein (gene symbol TP53) overlapped five pathways, e.g., Epstein-Barr virus infection, cell cycle, apoptosis, human T-cell leukemia virus one infection and p53 signaling pathway. The RNA-seq data regarding this study are available on the NCBI website database *via* the link: https://www.ncbi.nlm.nih.gov/Traces/study/?acc=PRJNA668604.

RNA-seq data was further validated by qRT-PCR. The relative gene expression levels of specific targets in Nalm6/DOX cells and primary ALL cells from patients were quantified (**Figures 5A, B**). Compared with either DOX or vehicle control, DOX-PMs-NPMBP conditioning significantly downregulated the mRNA levels of NPM, MDR, c-myc, bcl-2, MDM4 and PTEN, and markedly upregulated p53, bax, p21 and p14ARF. In line with the changes of mRNA expression after DOX-PMs-NPMBP treatment, we found that the protein expression of NPM, MDR, c-Myc, Bcl-2, MDM4 and PTEN dramatically decreased, while the p53, phospho-p53, Bax, p21 and p14ARF protein remarkably increased in the cells after administered DOX-PMs-NPMBP. In addition, DOX-PMs-NPMBP induced the protein expression of p85 and phospho-Rb, but reduced the levels of MDM2, phospho-p85, cyclin D, cyclin E in Nalm6/DOX cells (**Figure 5C**).

## DOX-PMs-NPMBP Induces the G0/G1 Cell Cycle Arrest in Nalm6/DOX Cells

We further explored the effects of DOX-PMs-NPMBP on cell cycle distribution of Nalm6/DOX cells. Compared to the control group, DOX-PMs-NPMBP remarkably increased the frequency of cells in the G0/G1 phase (52.82 ± 4.96% *vs* 39.76 ± 2.75%, $p = 0.016$), while decreased the proportion of cells in the S phase

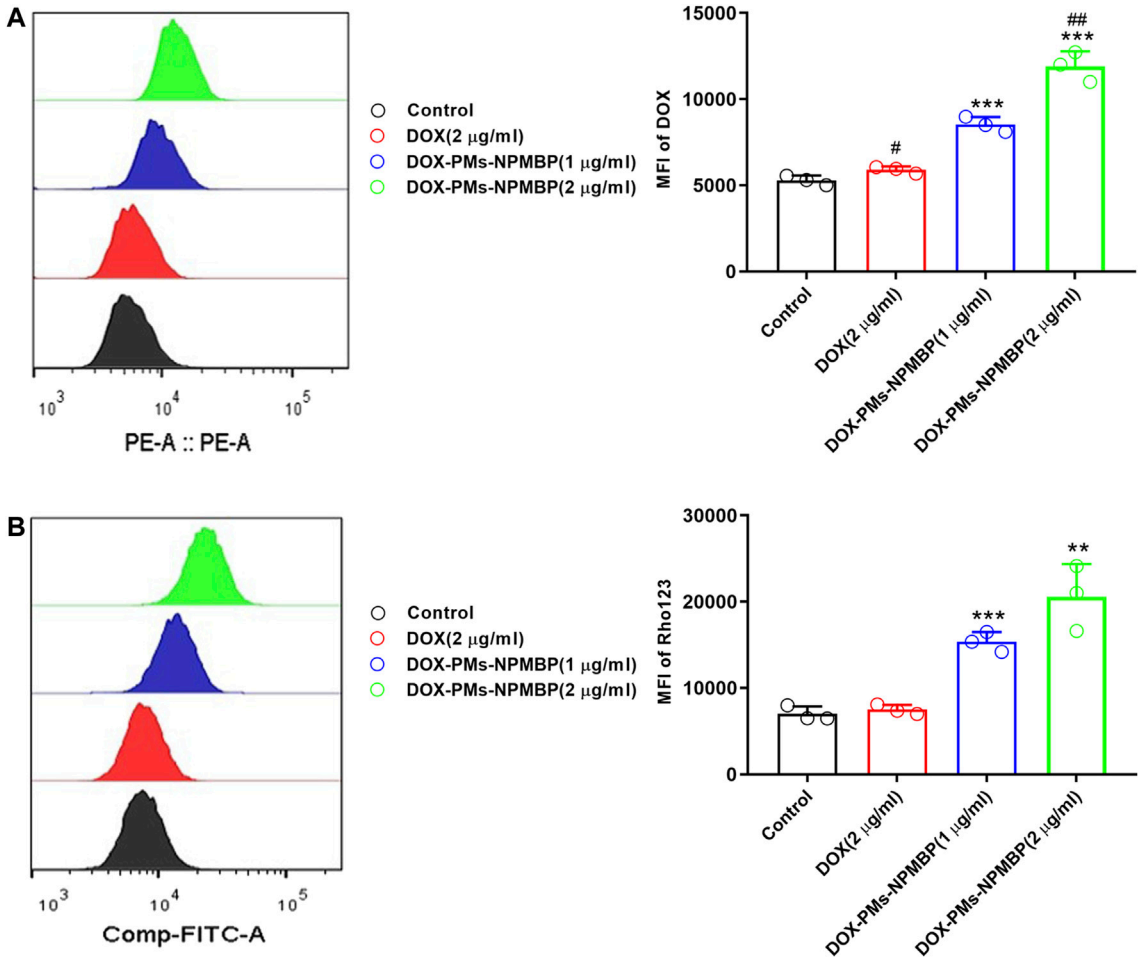


**FIGURE 3 |** DOX-PMs-NPMBP promotes intracellular accumulation of DOX or Rhodamine123 (Rho123) in Nalm6/DOX cells. Nalm6/DOX cells were treated with indicated concentration of DOX and DOX-PMs-NPMB for 12 h. The intracellular retention of DOX was evaluated by flow cytometry**(A)**. For the drug efflux ability assay, Rho123 at 2 μM was added to each well above and incubated for another 30 min at 37°C. After washed, flow cytometer analysis was used to assess the MFI of Rho123 in the Nalm6/ADR cells through FITC channel **(B)**. Data reflect the mean ± SD of three separate experiments. MFI: mean fluorescence intensity, $^{**}p < 0.01$, $^{***}p < 0.001$ compared with DOX, $^{\#}p < 0.05$ compared with control, $^{\#\#}p < 0.01$ compared with DOX-PMs-NPMBP (1 μg/ml).

(35.38 ± 4.33% *vs* 49.91 ± 2.20%, $p = 0.007$). In contrast, DOX alone slightly reduced cell amounts in the S phase, and increased frequency of G2/M phase cells. Moreover, the proportion of G0/G1 phase cells upon DOX-PMs-NPMBP administration was significantly increased in comparison with the DOX value (52.82 ± 4.96% *vs* 43.11 ± 3.11%, $p = 0.045$, **Figure 5D**).

## DOX-PMs-NPMBP Inhibits the Growth of Implanted Nalm6-Luc/DOX Cells in BALB/C-Nude Mice

To assess the impact of DOX-PMs-NPMBP *in vivo*, this compound was tested in Nalm6-Luc/DOX subcutaneous transplant model in BALB/C-nude mouse. Either DOX or DOX-PMs-NPMBP regimen was well tolerated when administered at 3 mg/kg once daily for 3 days during the follow-up. As shown in **Figure 6A**, the body weights in each group increased slightly with time after treatment. When normalized the body weight of PBS control group, the relative body weight in PMs group was similar to that of the controls. The relative body weight in both DOX- and DOX-PMs-NPMBP-treated group was slightly lower than that in PMs group; but without significant differences between the two regimens.

The average tumor volume in the DOX-treated animals was obviously smaller than that of PBS- and PMs-conditioned mice, but larger than that of DOX-PMs-NPMBP-administered recipients (**Figure 6B**). Animals bearing subcutaneous Nalm6-Luc/DOX tumor were imaged by IVIS SPECTRUM Imaging System pre- and post-initial treatment. Bioluminescent imaging demonstrated that Nalm6-Luc/DOX xenograft mice presented strong therapeutic response to DOX-PMs-NPMBP. Lower tumor burden was observed in the recipients which received DOX-PMs-NPMBP as compared to that DOX alone (**Figure 6C**). Following 30 days after initial regimen, DOX

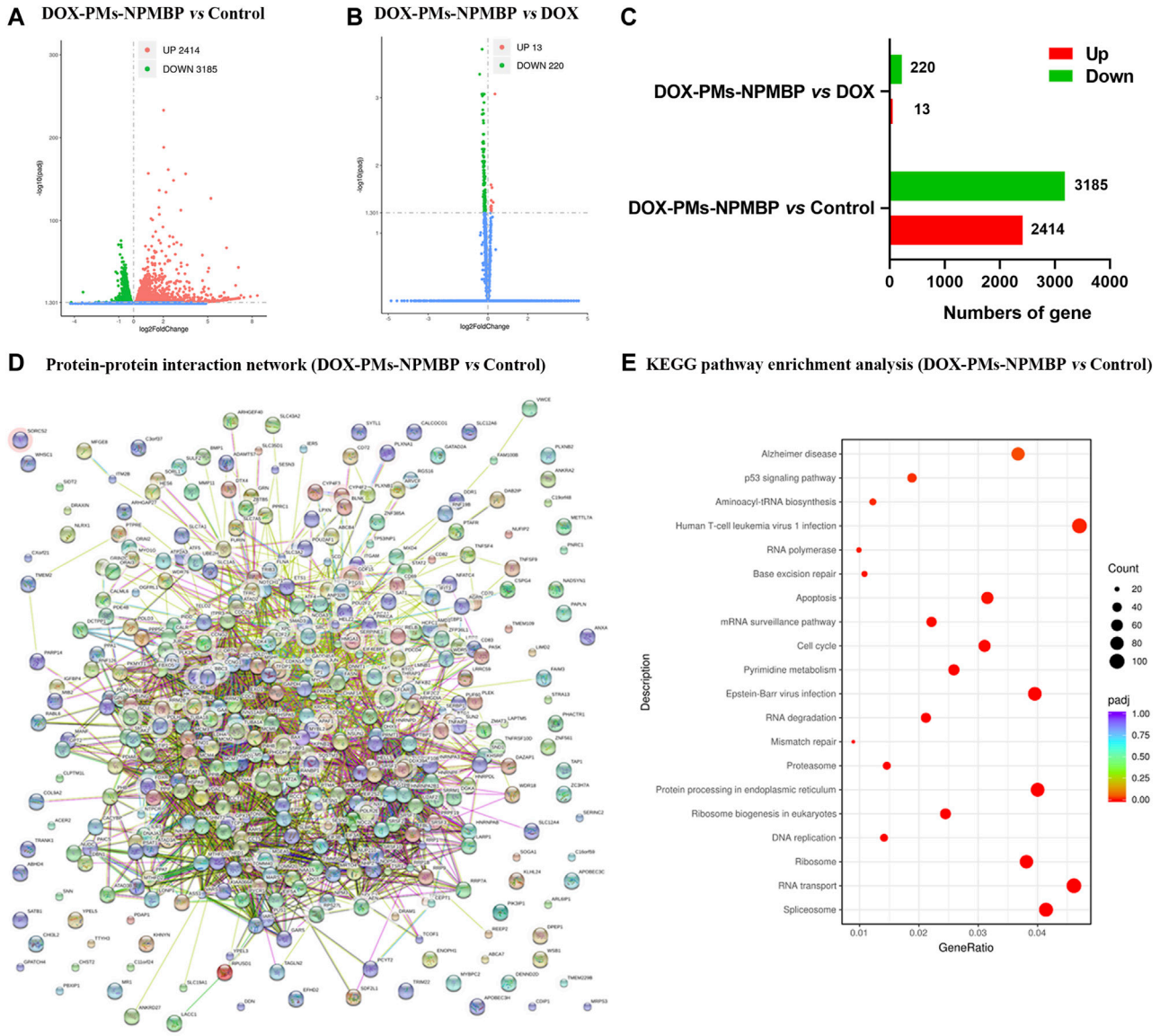


**FIGURE 4 |** Bioinformation analysis based on RNA-seq data. **(A–C)** Volcano plots of differentially expressed genes (DEGs) in Nalm6/DOX cells administered DOX, DOX-PMs-NPMBP, and vehicle control. **(D)** DOX-PMs-NPMBP-associated protein interaction network. Each circle means a protein/gene (node). **(E)**DOX-PMs-NPMBP-associated Kyoto Encyclopedia of Genes and Genomes (KEGG) pathway enrichment analysis.

-PMs-NPMBP group demonstrated an excellent antitumor activity with the inhibition rate of 79.2% compared to vehicle control, which remained the lowest among the three groups (**Figures 6C,D**).

Histologically, xenograft tumor in control group was characterized by high homogeneity and integrity, and unnormal proliferation state; Nalm6-Luc/DOX cells found in the vehicle control's subcutaneous tumor tissues were different sizes with the large stained nuclei, and were of a round shape. In contrast, the tumor sections of DOX and DOX-PMs-NPMBP showed different levels of inflammation and cell necrosis, depicted by a heterogeneous dyeing and messy cell morphology. Of note, less tumor cells, more erythrocytes and fibroblast cells were visible in the tumor tissues from DOX-PMs-NPMBP-treated mice (**Figure 6E**).

## DOX-PMs-NPMBP Enhances Antileukemia Activity in the NCG Nalm6-Luc/DOX Transplant Models

We further assessed the *in vivo* anti-leukemia activity of DOX-PMs-NPMBP in NCG mice. A total of $1.0 \times 10^4$ Nalm6-Luc/DOX cells were infused into NGG mice by tail vein injection. Seven days later, the mice were administered a single dose of DOX or DOX-PMs-NPMBP daily for 3 days. The day before initial

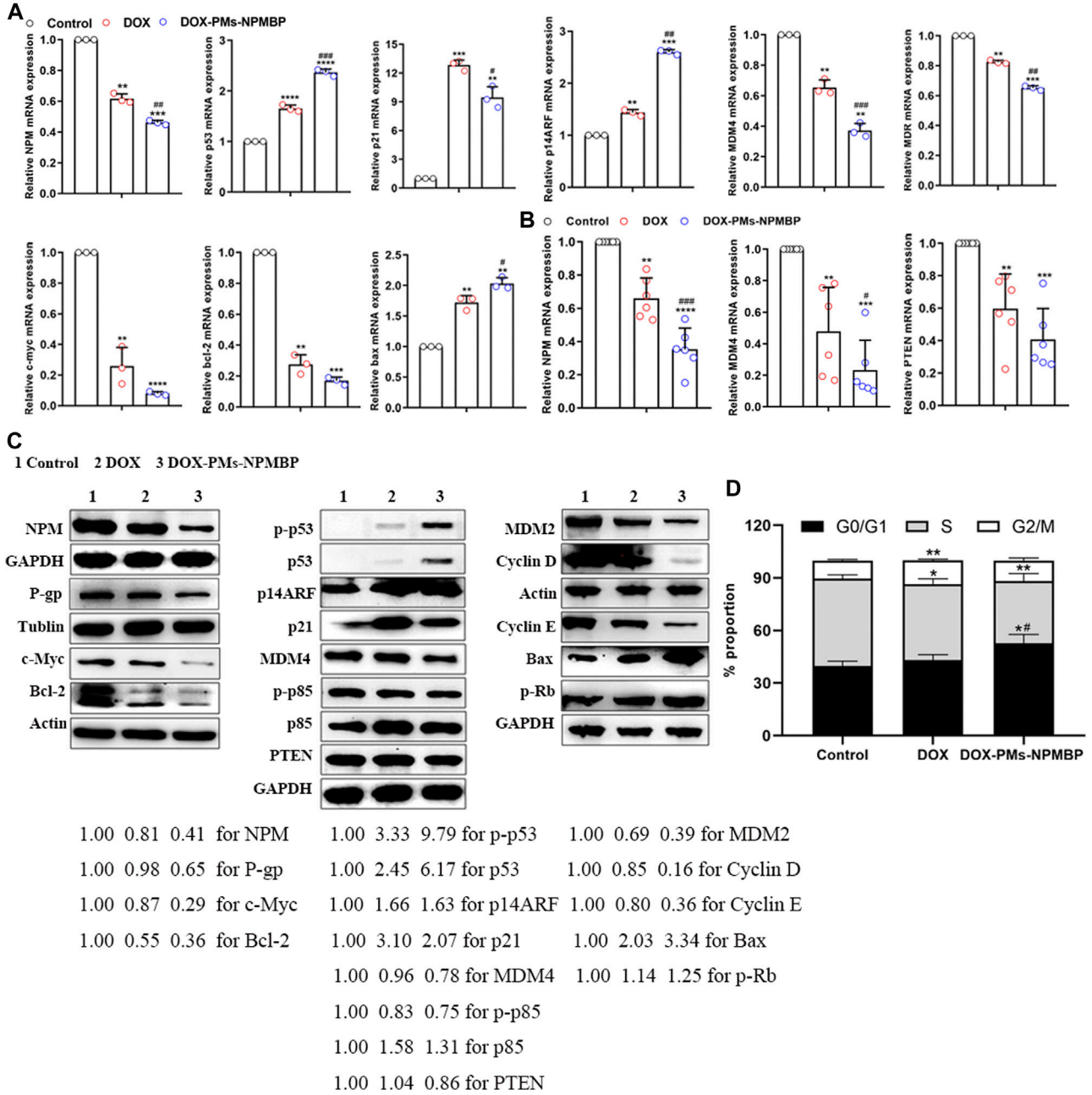


**FIGURE 5 |** Effects of DOX-PMs-NPMBP on mRNA and protein expression levels, and cell cycle distribution. Nalm6/DOX cells **(A)** and primary ALL cells from patients **(B)** were treated with DOX or DOX-PMs-NPMBP for 12 h, cells were harvested, and total RNA was isolated. Real-time PCR analysis was performed. All assays were repeated three times. $^{**}p < 0.01$, $^{***}p < 0.001$, $^{****}p < 0.0001$ compared with control, $^{\#}p < 0.05$, $^{\#\#}p < 0.01$, $^{\#\#\#}p < 0.001$ compared with DOX. **(C)** Protein expression levels in the Nalm6/DOX cells treated with DOX or DOX-PMs-NPMBP for 24 h as measured by western blotting. Tublin, Actin or GAPDH was employed as an internal reference. The experiments were repeated at least three times. The intensity of different protein bands was quantified and normalized with GAPDH, Tublin or Actin. Changes in protein expression levels are represented as percentage change from untreated control levels, which were set to 100% (1.00). **(D)** Cell cycle distribution analysis of Nalm6-Luc/DOX cells administered DOX or DOX-PMs-NPMBP for 24 h. Data are mean ± SD of three experiments performed independently. $^{*}p < 0.05$, $^{**}p < 0.01$ vs. control. $^{\#}p < 0.05$ vs. DOX.

regimen was designated as day 0. As shown in **Figure 7A**, DOX-PMs-NPMBP showed significant anti-leukemia activity, with less fluorescence signals 14 days after initial administration. In contrast, animals from vehicle control or DOX alone presented strong fluorescence signals, which widely spread to different organs. Body weights from each group mice were also monitored during the follow-up. Significant decreased body weight could be observed in control group; however, there was

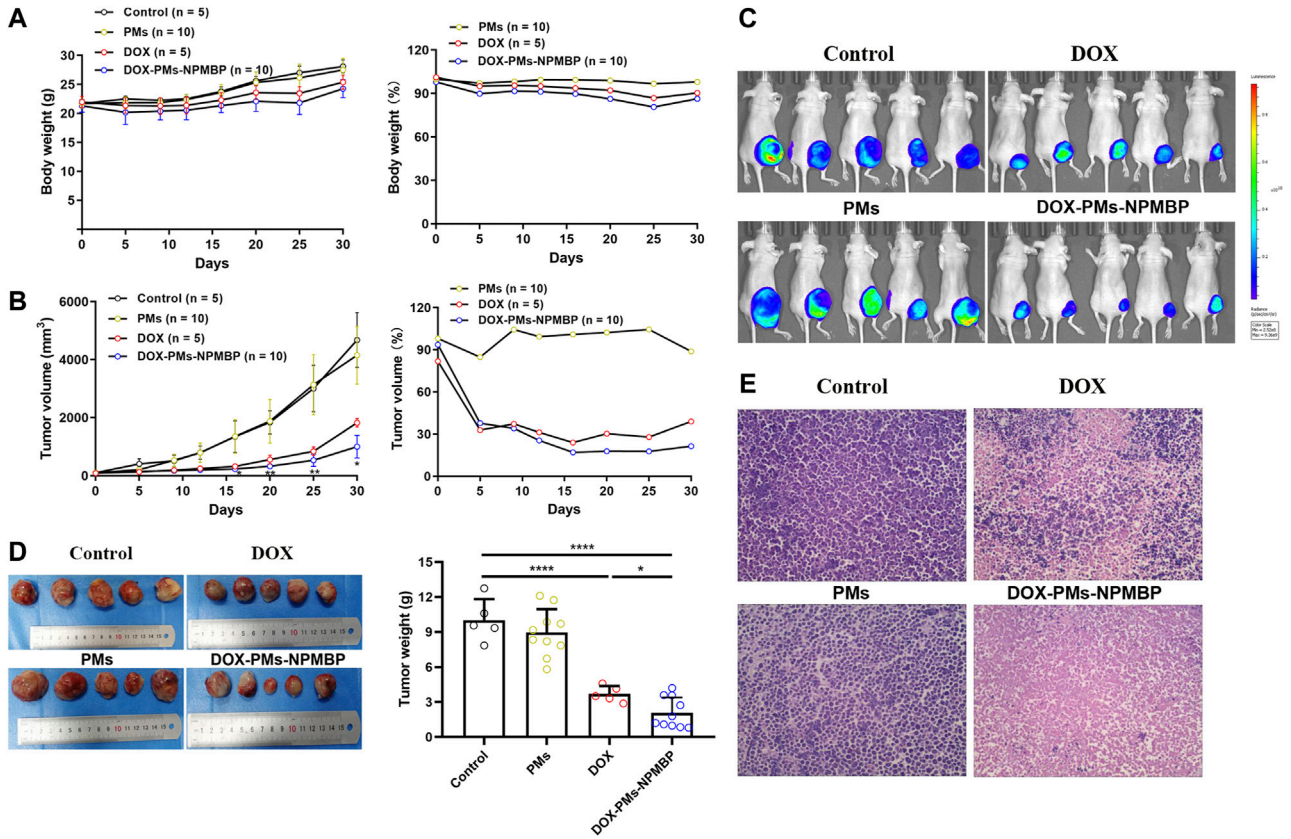


**FIGURE 6 |** DOX-PMs-NPMBP inhibits xenograft growth and enhances antileukemia activity in Nalm6-Luc/DOX xenograft nude mice. The nude mice with Nalm6-Luc/DOX xenografts were randomly divided into four groups and intraperitoneally administered DOX, DOX-PMs-NPMBP, PMs, or PBS once daily for 3 days. Body weights and tumor size were measured at the indicated time scheme by a caliper (tumor volume = shortest diameter$^2$ × longest diameter/2). **(A)** Body weight during follow-up. The relative levels of body weight are represented as percentage changes from vehicle control levels, which were set at 100%. **(B)** Tumor volume at each time point. The relative levels of tumor volume are represented as percentage changes from vehicle control levels, which were set to 100%. *$p < 0.05$, **$p < 0.01$ vs. DOX group. **(C)** Representative of whole-body luciferase reporter images from vehicle, DOX or DOX-PMs-NPMBP treated mice. **(D)** Representative of photographs of tumors excised from xenograft mice after completed the study. The tumor weight was measured. *$p < 0.05$, ****$p < 0.0001$. **(E)** Hematoxylin-eosin-stained sections of tumor tissue from representative control and treated mice.

no significant weight loss for DOX- and DOX-PMs-NPMBP-treated groups. Instead, the body weight of the mice from the nanoparticle conditioning group increased slightly during the study period, indicating the novel drug delivery system produced less systematic toxicity and reached higher therapeutic effect (**Figure 7B**). Moreover, larger liver and spleen were found in animals from either control group or DOX group compared to DOX-PMs-NPMBP-treatment (**Figures 7C, D**). Wright-Giemsa staining results demonstrated increased immature blast cells in the BM from vehicle control mice and DOX-treated mice. However, BM samples from DOX-PMs-NPMBP-conditioned mice showed more mature myeloid cells and lymphocytes (**Figure 7E**). Nalm6-Luc/DOX cells in the BM from individual mice were further confirmed by flow cytometric analysis. As shown in **Figures 7F,G**, the frequency of CD19$^+$ Nalm6-Luc/DOX cells was dramatically decreased upon DOX-PMs-NPMBP administration in comparison to either vehicle control or DOX-only treatment ($p < 0.0001$ *vs* control, $p < 0.01$ *vs* DOX).

## DOX-PMs-NPMBP Improves the Survival of Nalm6-Luc/DOX Xenograft NCG Mice

The overall survival of the animals with the different regimens was monitored. *In vivo*, administration of DOX in Nalm6-Luc/DOX cells yielded only partial improvement in overall survival, through partial delay but incomplete prevention of leukemia cell growth ($p > 0.05$ compared to PBS vehicle control). However, DOX-PMs-NPMBP regimen significantly reduced Nalm6-Luc/DOX leukemia burden and improved overall survival as compared with the control ($p < 0.05$). Thus, the *in vivo* results further confirm the enhanced therapeutic efficacy of DOX-PMs-NPMBP for resistant ALL (**Figure 8**).

## DISCUSSION

ALL is a hematologic malignant disease that occurs due to a buildup of lymphoid progenitor cells in various tissues,

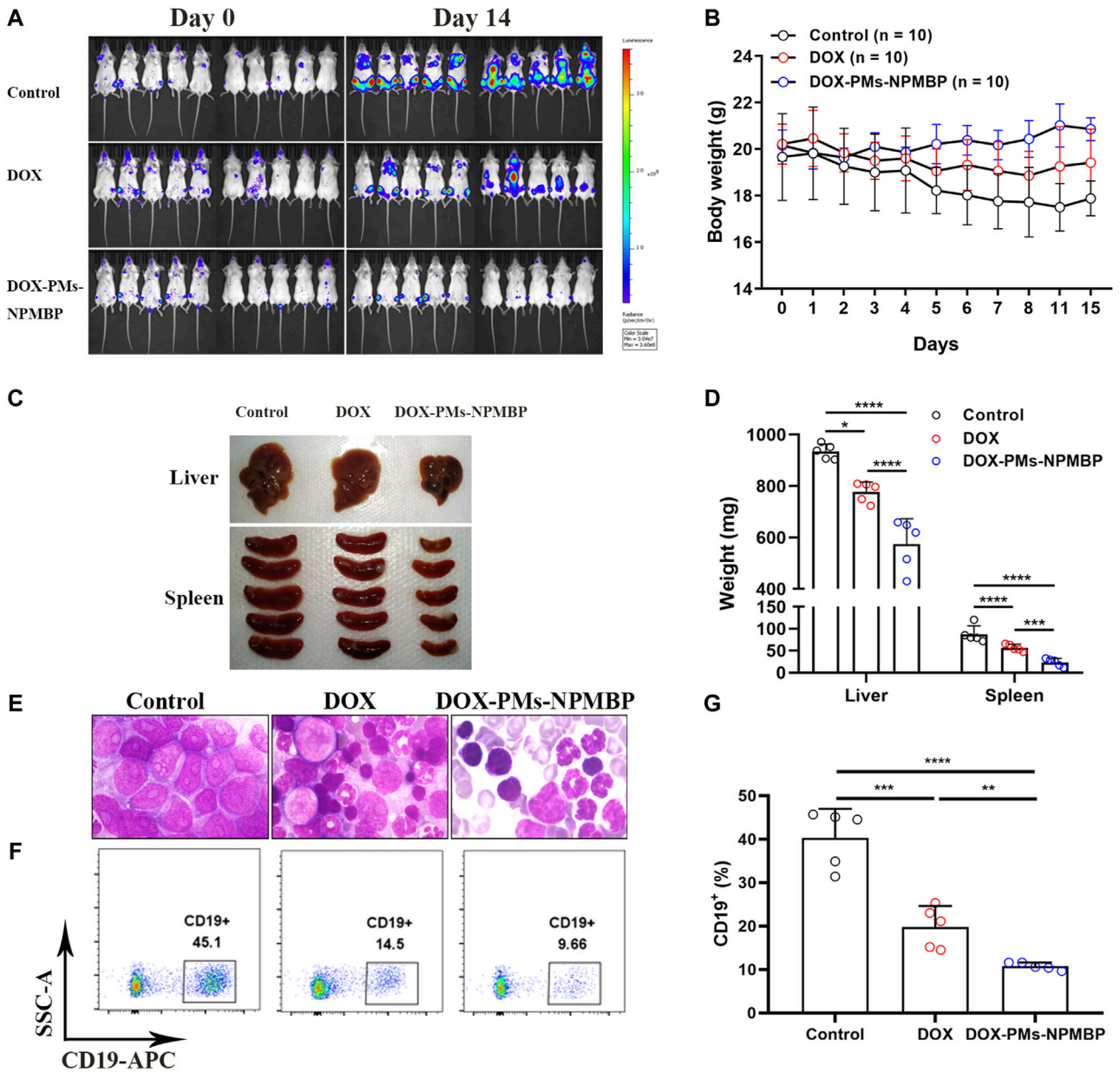


**FIGURE 7 |** DOX-PMs-NPMBP enhances antileukemia activity in NOD-Prkdc$^{em26}$Il2rg$^{em26}$Nju (NCG) mice implanted with Nalm6-Luc/DOX cells. A total of 1.0 × $10^4$ Nalm6-Luc/DOX cells were infused into NCG mice by tail vein injection. Seven days later, mice were intraperitoneally administered daily single dose of DOX, DOX-PMs-NPMBP, or PBS for 3 days. The day before initial regimen was designated as day 0. Animals were euthanized at the 14th day after the initial treatment. **(A)** Bioluminescence images of the ventral/dorsal area taken at pre- and post-treatment. **(B)** Body weights at each time point. **(C)** Representative photographs of liver and spleen excised from implanted NCG mice. **(D)** Liver and spleen weight changes in different conditioning group mice. **(E)** Representative Wright-Giemsa-stained sections of harvested bone marrow (BM) cells in each group mice. **(F)** Representative images of flow-cytogram illustrating the CD19$^+$ Nalm6-Luc/DOX cells in BM. Dot plots reflect CD19-APC vs. side scatters. *$p < 0.05$, ***$p < 0.001$, ****$p < 0.0001$. **(G)** The percentages of CD19$^+$ cells in BM were measured by flow cytometry. **$p < 0.01$, ***$p < 0.001$, ****$p < 0.0001$.

particularly bone marrow. The rate at which it is cured in adult ALL patients is between 20 and 40%, provided they undergo chemotherapy (Sive et al., 2012; Richard-Carpentier et al., 2019). There has been a significant increase in our collective understanding of the pathogenesis of ALL over the past decade, as well as novel approaches for treatment. In particularly, the administration of monoclonal antibodies, CAR-T cell therapies, and other novel targeted strategies in ALL show tremendous potential to improve cure and survival rates. For example, Inotuzumab ozogamicin is an anti-CD22 antibody drug conjugate that is set to deliver cytotoxic drugs to B-ALL cells expressing CD22, and shown great outcomes in

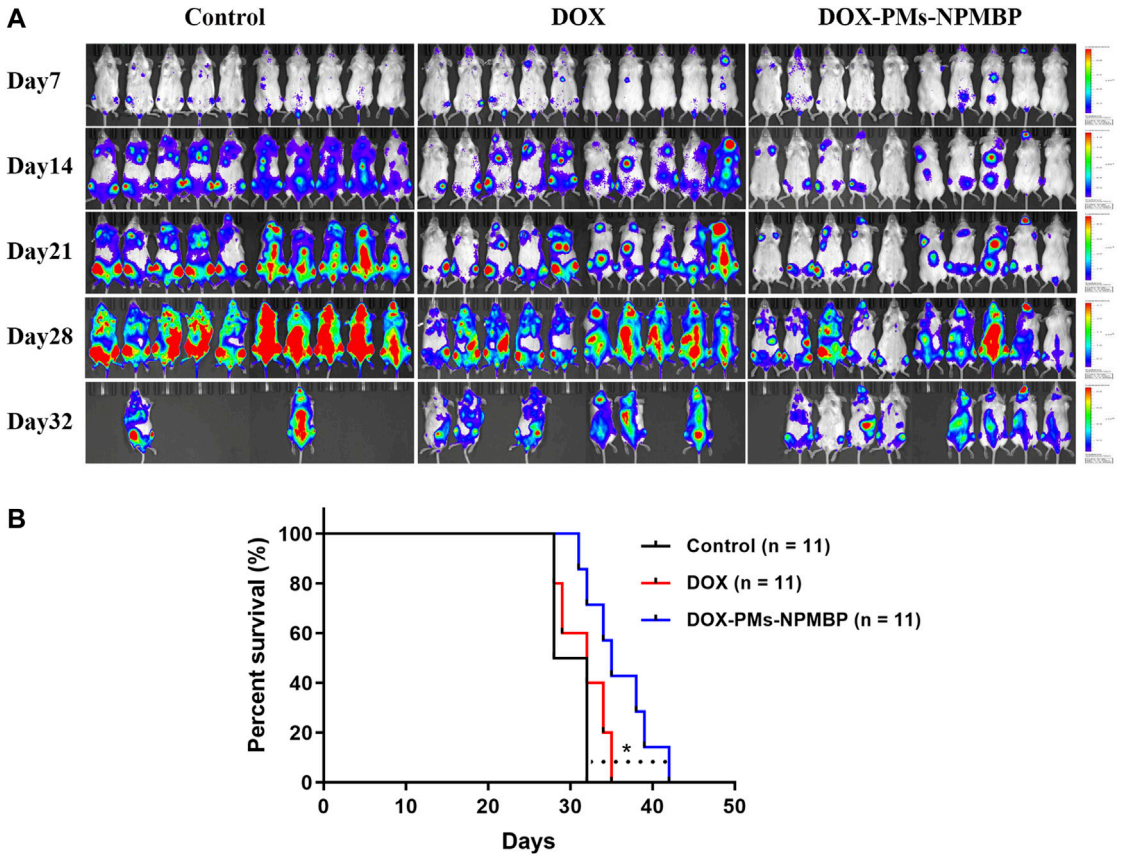


**FIGURE 8 |** DOX-PMs-NPMBP improves survival in NCG mice implanted with Nalm6-Luc/DOX cells. The day of implantation with Nalm6-Luc/DOX cells was designated as day 0. ALL xenograft models were monitored during the study period. Survival time of the recipients were recorded. **(A)** Representative bioluminescence images of the ventral/dorsal area taken on different time points during follow-up. **(B)** Kaplan-Meier survival curves. *$p < 0.05$ compared with control.

patients with relapsed or refractory ALL (Kantarjian et al., 2016). We previously confirmed that NPM overexpression was involved in MDR, and was associated with the prognosis of ALL (Hu et al., 2011; Lin et al., 2013; Wang et al., 2015). Engineered nanoparticles have certain chemical and physical characteristics that give them especially useful medical purposes. As such, in the present study, the antileukemia activity of NPM binding protein- and DOX-conjugated nanoparticle in ALL cells were evaluated, and the underlying mechanisms were fully elucidated.

Nanoparticles have high permeability and retention, allowing them to deliver drugs that can accumulate within the tumor (Markman et al., 2013). DOX-PMs-NPMBP is a novel method of delivery, in which adding PEG has refined the polymers. This avoids opsonization and increases *in vivo* circulation time. Nanoparticles also have wide surface areas, which provides ample space for the absorbed protein NPMBP to attach. Additionally, nanospheres have solid cores, which are optimal for the attachment of chemotherapeutic agent DOX. Moreover, the water-soluble polymer PLA can covalently bind to DOX, which raises the time of circulation and lowers toxicity in normal tissues (Markman et al., 2013). Furthermore, PLA is a polymeric biodegradable nanoparticle that can be used to create nanomedicines that have been approved by the Food and Drug Administration (FDA) in the United States (Mattheolabakis et al., 2012), which further inspired us to carry out an extensive investigation on the effects of the novel drug delivery system DOX-PMs-NPMBP in ALL cells.

Recently, Zhang and colleagues reported that Saporin, a strong cytotoxic compound, can significantly slow the growth of parental cancer cells and resistant ATP-binding cassette (ABC) transporter subfamily B member 1 (ABCB1)- and ABC transporter subfamily G member 2 (ABCG2)-overexpression cells when it has been encapsulated in lipid-based nanoparticles (Zhang et al., 2020). We found the resistant ALL cell lines, as well as the primary ALL cells from relapsed patients, were more sensitive to DOX/NPMBP-conjugated nanoparticles DOX-PMs-NPMBP. Although the resistant Nalm6/DOX cells showed a little effect in response to DOX-only administration, however, more than 2-fold increase in the frequency of apoptotic cells was observed in those cells responding to DOX-PMs-NPMBP vs. DOX alone. Consistently, a higher frequency of DOX-resistant ALL cells undergo G0/G1 phase arrest upon DOX-PMs-NPMBP administration. These observations suggest

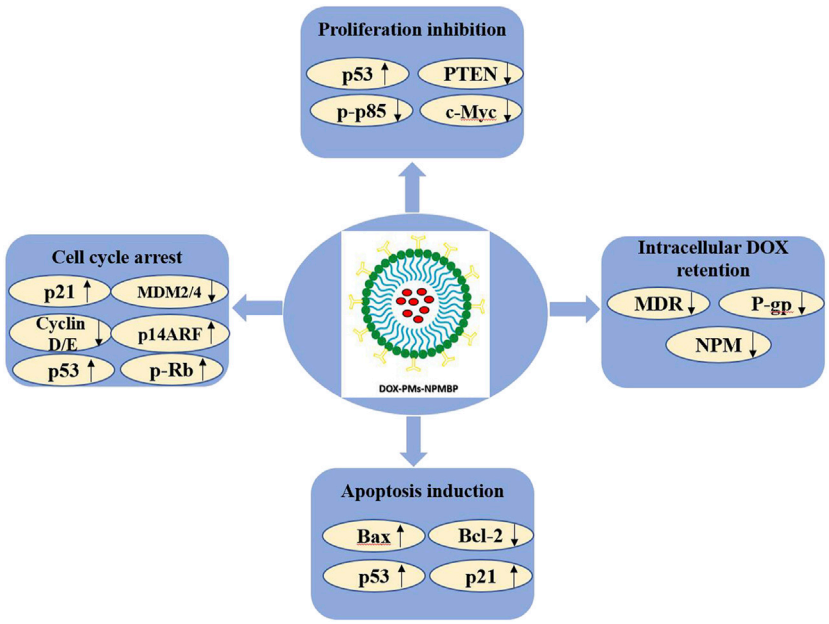


**FIGURE 9 |** The molecular mechanisms linking the anti-leukemia activity of DOX-PMs-NPMBP in DOX-resistant ALL cells.

that DOX and NPMBP conjugation into nanoparticles holds significant potential for enhancing DOX bioavailability and overcoming drug resistance in ALL cells.

When the gene expression profiles of Nalm6/DOX cells were analyzed comprehensively by RNA-seq technology, KEGG enrichment analysis of DEGs showed that 21 pathways were significantly different in following DOX-PMs-NPMBP treatment. Of note, TP53 overlapped in the five different pathways when compared the difference between DOX-PMs-NPMBP vs. vehicle control. And KEGG analysis didn't show that TP53 were significantly enriched in different biological process between DOX-PMs-NPMBP vs. DOX treatment (**Supplementary Figure 2,** https://www.ncbi.nlm.nih.gov/Traces/study/?acc=PRJNA668604), exposing p53 as an essential player in DOX-PMs-NPMBP biological activity. Previous studies revealed that the activation of p53 induces several protective reaction activities, such as cell cycle arrest, senescence or cell death. However, p53 inactivation, which is usually caused by TP53 gene mutation or negative regulation of wild type (wt) protein product, is commonly found in most human cancer (Ding et al., 2020; Jiang et al., 2020; Long et al., 2020). More recently, pharmacological manipulation of p53 has been a highly attractive strategy in the development of new anticancer treatments (Lazo, 2017; Duffy et al., 2020). Thus, the present study may be of great value to investigate the underlying mechanisms of DOX-PMs-NPMBP in the pre-B Nalm6 cells, which typically harbor with wt p53.

Furthermore, the underlying mechanisms of DOX-PMs-NPMBP-enhanced anti-leukemia and cell death effects were explored. DOX-PMs-NPMBP dramatically inhibited MDR as well as the targeting molecule NPM as compared to either DOX or vehicle control. Nanoparticle carrier has been reported to circumvent P-gp-mediated resistance, enhancing cellular drug-uptake through the forming of ion pairs and endocytosis, the lowering of ATP, regulating the function and expression of P-gp, as well as alterations in the P-gp downstream signaling pathways (Dong and Mumper, 2010; Zhang et al., 2020). This is a likely explanation for higher level of intracellular accumulation of DOX in the resistant cells when conditioned with DOX-PMs-NPMBP. Moreover, Rho123 efflux assay, a very sensitive functional assay for ABC-transporter P-gp, was further included in this study. The novel DOX-PMs-NPMBP nanoparticle system could markedly modulate the functional activity of P-gp, thereby reducing the drug pumping P-gp-mediated efflux of Rho123 in the resistant ALL cells in comparison to DOX, suggesting the classical MDR phenotype-dependent mechanism was involved in the action of DOX-PMs-NPMBP on DOX-resistant cells.

NPM plays important role for the nucleolar localization of oncogenic c-Myc and enhances c-Myc transformation. Constitutive NPM overexpression may stimulate c-Myc-mediated rRNA synthesis (Li and Hann, 2013). In line with these reports, our data delineates that DOX-PMs-NPMBP not only completely abolished the expression of c-Myc, but also markedly induced the activation of p14ARF, an important partner of NPM and a major tumor suppressor. P14ARF also has functions relating to nucleolar processes, as well as cell cycle arrest, *via* the MDM-p53 pathway (Lo et al., 2015). Additionally, NPM has been known to play key roles in maintaining p53 stability and regulating its transcriptional activation (Colombo et al., 2002). Interestingly, the presence of DOX-PMs-NPMBP in Nalm6/DOX cells results in the robust activation of p53 and cyclin-dependent kinase inhibitor one p21 coupled with the greatly suppression of MDM2 and MDM4, the

two key negative regulators of p53 (Jackson-Weaver et al., 2020; Li and Lozano, 2013). Previous study showed that p21 activation blocked cell cycle progression by function as the inhibitor of cyclin D/E kinases, which are required for the G1-S phase transition of cell cycle (Aubrey et al., 2018; Karimian et al., 2016; Kim and Choi, 2020). Thus, it is likely that we found the exposure of DOX-PMs-NPMBP markedly downregulated the expressions of cyclin D and cyclin E. Moreover, Hüllein J *et al* previously demonstrated the key role for tumor suppressor p53 in Burkitt lymphoma (BL) and identified MDM4 as a therapeutic target in various cancers. MDM4 knockdown activated p53, induced cell-cycle arrest, and lowered the growth of tumor in a xenograft model (Hullein et al., 2019). Recently, pharmaceutical inhibitors targeting MDM2 and MDM4 have been explored to reactive the p53/Rb tumor suppressor function; and the preliminary response data from the clinical trial in acute myeloid leukemia patients have been gaining increasing interest (Burgess et al., 2016; Vu et al., 2020). Likewise, our findings give an insight into the DOX-PMs-NPMBP-induced MDM2 and MDM4 dual inhibition, which might put forward the clinical perspectives of DOX-PMs-NPMBP to ALL therapy.

Nevertheless, compared with control or DOX alone, we found DOX-PMs-NPMBP-induced significant activation of p53, coinciding with the inhibition of PTEN as well as phospho-p85 and the PI3K regulatory subunit. PTEN is the negative regulator of PI3K/Akt signaling pathway, which is frequently activated in various cancer cells and associated with chemoresistance (Chen et al., 2014; Li et al., 2015; Chen et al., 2020; Yang et al., 2020). Along these lines, we observed the enhanced inhibitory effects on the anti-apoptotic Bcl-2, and the subsequent induction of proapoptotic Bax by DOX-PMs-NPMBP. Taken together and as the most straight forward interpretation of our data, we suggest that treatment with DOX-PMs-NPMBP-induced effects on cell viability mainly due to activated p53, leading to the subsequent p53-mediated apoptosis as well as cell cycle arrest. The graphical depiction regarding the molecular mechanisms of DOX-PMs-NPMBP working on resistant ALL cells were showed in **Figure 9**.

Nanoparticle-based therapy may offer multiple advantages over conventional therapeutics in various cancers, *e.g.* high carrier capacity, targeted delivery and therapy, improvement of biological properties, and reversal of MDR (Dong and Mumper, 2010; Sanna et al., 2014; Zhang et al., 2020). The therapeutic properties of DOX-PMs-NPMBP were further evaluated in a Nalm6-Luc/DOX xenograft BALB/C-nude and NCG ALL models. Lower tumor burden was observed in DOX-PMs-NPMBP-treated recipients as compared to the animals administered with DOX alone. Tumor inhibition rate achieved as high as 79.2% in DOX-PMs-NPMBP group when finished the following-up. Of note, the regimen of DOX-PMs-NPMBP significantly prolonged mouse survival. Similar findings have been recently reported in other PLA-PEG-based drug nanocarriers, demonstrating the potential of nanomedicine for cancer treatment. In particularly, PEG has been shown to enable site-specific delivery of drugs in various cancers (Xue et al., 2018; Duncan et al., 2019; Heshmati Aghda et al., 2020; Lundsten et al., 2020). Furthermore, no significant cytotoxicity of the blank PMs was observed in ALL cells *in vitro*, even when administered at maximum doses; and we didn't find obvious adverse reactions, such as gastrointestinal reactions, neurotoxicity, hepatoxicity and bone marrow suppression in the animals following DOX-PMs-NPMBP treatment. Compared with control or DOX alone, more mature cells were observed in the peripheral blood and bone marrow samples from DOX-PMs-NPMBP-treated animal. Herein, the *in vivo* experiments indicate that DOX-PMs-NPMBP regimen can enhance the sensitivity of ALL xenograft models to DOX and reach higher therapeutic effects with less systematic toxicity.

In conclusion, DOX-PMs-NPMBP nanoparticle can significantly inhibit leukemia cell growth and induce apoptosis; and markedly improve the antileukemia activity in resistant ALL cells *in vitro* and *in vivo*. Therefore, it is worthy of investigation in large animal models.

## DATA AVAILABILITY STATEMENT

The raw data supporting the conclusions of this article will be made available by the authors, without undue reservation. The RNA sequencing datasets presented in this study can be found in online repositories. The names of the repository/repositories and accession number(s) can be found below: https://www.ncbi.nlm.nih.gov/Traces/study/?acc=PRJNA668604&o=acc_s%3Aa.

## ETHICS STATEMENT

The studies involving human participants were reviewed and approved by the Ethics Committee of Fujian Medical University Union Hospital. The patients/participants provided their written informed consent to participate in this study. The animal study was reviewed and approved by the Ethics Committee of Institutional Animal Care and Use in Fujian Medical University.

## AUTHOR CONTRIBUTIONS

DG, YC, ZW and SKY performed the experiments and analyzed data. LL and NZ analyzed data and provided technical support. FY helped to synthesize DOX-PMs-NPMBP. HC assisted with the design and synthesis of DOX-PMs-NPMBP and made comments to the manuscript. JH supervised the project and reviewed the manuscript. YC designed and initiated the study, supervised the project, analyzed data, prepared the figures, wrote and reviewed the manuscript.

## FUNDING

This work was supported by the Joint Funds for the Innovation of Science and Technology in Fujian province (2016Y9029,

2016Y9032), Fujian Provincial Health Technology Project (2019-ZQN-42), Fujian Provincial Natural Science Foundation (2020J01996), the Program of New Century Excellent Talents in Fujian Province University (2016B032), the Cooperation Project of University and Industry (2017Y4005), National Natural Science Foundation of China (81500158, 81870135, U2005204), National and Fujian Provincial Key Clinical Specialty Discipline Construction Program, Provincial Key Laboratory Foundation of Hematology (2009J1004), and Construction Project of Fujian Medical Center of Hematology (Min201704).

## SUPPLEMENTARY MATERIAL

The Supplementary Material for this article can be found online at: https://www.frontiersin.org/articles/10.3389/fphar.2021.607755/full#supplementary-material

## REFERENCES

Aldoss, I., and Stein, A. S. (2018). Advances in Adult Acute Lymphoblastic Leukemia Therapy. *Leuk. Lymphoma* 59 (5), 1033–1050. doi:10.1080/10428194.2017.1354372

Aliabadi, H., Elhasi, S., Mahmud, A., Gulamhusein, R., Mahdipoor, P., and Lavasanifar, A. (2007). Encapsulation of Hydrophobic Drugs in Polymeric Micelles through Co-solvent Evaporation: the Effect of Solvent Composition on Micellar Properties and Drug Loading. *Int. J. Pharmaceutics* 329 (1-2), 158–165. doi:10.1016/j.ijpharm.2006.08.018

Aubrey, B. J., Kelly, G. L., Janic, A., Herold, M. J., and Strasser, A. (2018). How Does P53 Induce Apoptosis and How Does This Relate to P53-Mediated Tumour Suppression? *Cell Death Differ.* 25 (1), 104–113. doi:10.1038/cdd.2017.169

Borer, R. A., Lehner, C. F., Eppenberger, H. M., and Nigg, E. A. (1989). Major Nucleolar Proteins Shuttle between Nucleus and Cytoplasm. *Cell* 56 (3), 379–390. doi:10.1016/0092-8674(89)90241-9

Burgess, A., Chia, K. M., Haupt, S., Thomas, D., Haupt, Y., and Lim, E. (2016). Clinical Overview of MDM2/X-Targeted Therapies. *Front. Oncol.* 6, 7. doi:10.3389/fonc.2016.00007

Chen, Y., Gan, D., Huang, Q., Luo, X., Lin, D., and Hu, J. (2018). Emodin and its Combination with Cytarabine Induce Apoptosis in Resistant Acute Myeloid Leukemia Cells *In Vitro* and *In Vivo*. *Cell Physiol. Biochem.* 48 (5), 2061–2073. doi:10.1159/000492544

Chen, Y., and Hu, J. (2020). Nucleophosmin1 (NPM1) Abnormality in Hematologic Malignancies, and Therapeutic Targeting of Mutant NPM1 in Acute Myeloid Leukemia. *Ther. Adv. Hematol.* 11, 204062071989981. doi:10.1177/2040620719899818

Chen, Y., Li, J., Hu, J., Zheng, J., Zheng, Z., Liu, T., et al. (2014). Emodin Enhances ATRA-Induced Differentiation and Induces Apoptosis in Acute Myeloid Leukemia Cells. *Int. J. Oncol.* 45 (5), 2076–2084. doi:10.3892/ijo.2014.2610

Chen, Y., Zheng, J., Gan, D., Chen, Y., Zhang, N., Chen, Y., et al. (2020). E35 Ablates Acute Leukemia Stem and Progenitor Cells *In Vitro* and *In Vivo*. *J. Cel. Physiol.* 235 (11), 8023–8034. doi:10.1002/jcp.29457

Colombo, E., Alcalay, M., and Pelicci, P. G. (2011). Nucleophosmin and its Complex Network: a Possible Therapeutic Target in Hematological Diseases. *Oncogene* 30 (23), 2595–2609. doi:10.1038/onc.2010.646

Colombo, E., Marine, J.-C., Danovi, D., Falini, B., and Pelicci, P. G. (2002). Nucleophosmin Regulates the Stability and Transcriptional Activity of P53. *Nat. Cel. Biol.* 4 (7), 529–533. doi:10.1038/ncb814

Ding, H.-Y., Yang, W.-Y., Zhang, L.-H., Li, L., Xie, F., Li, H.-Y., et al. (2020). 8-Chloro-Adenosine Inhibits Proliferation of MDA-MB-231 and SK-BR-3 Breast Cancer Cells by Regulating ADAR1/p53 Signaling Pathway. *Cel. Transpl.* 29, 096368972095865. doi:10.1177/0963689720958656

Dong, X., and Mumper, R. J. (2010). Nanomedicinal Strategies to Treat Multidrug-Resistant Tumors: Current Progress. *Nanomedicine* 5 (4), 597–615. doi:10.2217/nnm.10.35

Duffy, M. J., Synnott, N. C., O'Grady, S., and Crown, J. (2020). Targeting P53 for the Treatment of Cancer. *Semin. Cancer Biol.* doi:10.1016/j.semcancer.2020.07.005

Duncan, S. A., Dixit, S., Sahu, R., Martin, D., Baganizi, D. R., Nyairo, E., et al. (2019). Prolonged Release and Functionality of Interleukin-10 Encapsulated within PLA-PEG Nanoparticles. *Nanomaterials* 9 (8), 1074. doi:10.3390/nano9081074

Heshmati Aghda, N., Abdulsahib, S. M., Severson, C., Lara, E. J., Torres Hurtado, S., Yildiz, T., et al. (2020). Induction of Immunogenic Cell Death of Cancer Cells through Nanoparticle-Mediated Dual Chemotherapy and Photothermal Therapy. *Int. J. Pharmaceutics* 589, 119787. doi:10.1016/j.ijpharm.2020.119787

Hoang, N. H., Sim, T., Lim, C., Le, T. N., Han, S. M., Lee, E. S., et al. (2019). A Nano-Sized Blending System Comprising Identical Triblock Copolymers with Different Hydrophobicity for Fabrication of an Anticancer Drug Nanovehicle with High Stability and Solubilizing Capacity. *Ijn* Vol. 14, 3629–3644. doi:10.2147/IJN.S191126

Hu, J., Lin, M., Liu, T., Li, J., Chen, B., and Chen, Y. (2011). DIGE-based Proteomic Analysis Identifies nucleophosmin/B23 and Nucleolin C23 as Over-expressed Proteins in Relapsed/refractory Acute Leukemia. *Leuk. Res.* 35 (8), 1087–1092. doi:10.1016/j.leukres.2011.01.010

Hüllein, J., Słabicki, M., Rosolowski, M., Jethwa, A., Habringer, S., Tomska, K., et al. (2019). MDM4 Is Targeted by 1q Gain and Drives Disease in Burkitt Lymphoma. *Cancer Res.* 79 (12), 3125–3138. doi:10.1158/0008-5472.CAN-18-3438

Jackson-Weaver, O., Ungvijanpunya, N., Yuan, Y., Qian, J., Gou, Y., Wu, J., et al. (2020). PRMT1-p53 Pathway Controls Epicardial EMT and Invasion. *Cel. Rep.* 31 (10), 107739. doi:10.1016/j.celrep.2020.107739

Jiang, L., Huang, S., Wang, J., Zhang, Y., Xiong, Y., Zeng, S. X., et al. (2020). Inactivating P53 Is Essential for Nerve Growth Factor Receptor to Promote Melanoma-Initiating Cell-Stemmed Tumorigenesis. *Cell Death Dis.* 11 (7), 550. doi:10.1038/s41419-020-02758-6

Kantarjian, H. M., DeAngelo, D. J., Stelljes, M., Martinelli, G., Liedtke, M., Stock, W., et al. (2016). Inotuzumab Ozogamicin versus Standard Therapy for Acute Lymphoblastic Leukemia. *N. Engl. J. Med.* 375 (8), 740–753. doi:10.1056/NEJMoa1509277

Karimian, A., Ahmadi, Y., and Yousefi, B. (2016). Multiple Functions of P21 in Cell Cycle, Apoptosis and Transcriptional Regulation after DNA Damage. *DNA Repair* 42, 63–71. doi:10.1016/j.dnarep.2016.04.008

Kim, S.-M., and Choi, K.-C. (2020). Acrylonitrile Induced Cell Cycle Arrest and Apoptosis by Promoting the Formation of Reactive Oxygen Species in Human Choriocarcinoma Cells. *J. Toxicol. Sci.* 45 (11), 713–724. doi:10.2131/jts.45.713

Lazo, P. A. (2017). Reverting P53 Activation after Recovery of Cellular Stress to Resume with Cell Cycle Progression. *Cell Signal.* 33, 49–58. doi:10.1016/j.cellsig.2017.02.005

Li, J., Chen, Y., Chen, B., Chen, C., Qiu, B., Zheng, Z., et al. (2015). Inhibition of 32Dp210 Cells Harboring T315I Mutation by a Novel Derivative of Emodin Correlates with Down-Regulation of BCR-ABL and its Downstream Signaling Pathways. *J. Cancer Res. Clin. Oncol.* 141 (2), 283–293. doi:10.1007/s00432-014-1820-2

Li, Q., and Lozano, G. (2013). Molecular Pathways: Targeting Mdm2 and Mdm4 in Cancer Therapy. *Clin. Cancer Res.* 19 (1), 34–41. doi:10.1158/1078-0432.CCR-12-0053

Li, Z., and Hann, S. R. (2013). Nucleophosmin Is Essential for C-Myc Nucleolar Localization and C-Myc-Mediated rDNA Transcription. *Oncogene* 32 (15), 1988–1994. doi:10.1038/onc.2012.227

Lin, M., Hu, J., Liu, T., Li, J., Chen, B., and Chen, X. (2013). Knockdown of Nucleophosmin by RNA Interference Reverses Multidrug Resistance in Resistant Leukemic HL-60 Cells. *Immunobiology* 218 (9), 1147–1154. doi:10.1016/j.imbio.2013.04.001

Liso, A., Bogliolo, A., Freschi, V., Martelli, M. P., Pileri, S. A., Santodirocco, M., et al. (2008). In Human Genome, Generation of a Nuclear export Signal through Duplication Appears Unique to Nucleophosmin (NPM1) Mutations

and Is Restricted to AML. *Leukemia* 22 (6), 1285–1289. doi:10.1038/sj.leu.2405045

Lo, D., Zhang, Y., Dai, M.-S., Sun, X.-X., Zeng, S. X., and Lu, H. (2015). Nucleostemin Stabilizes ARF by Inhibiting the Ubiquitin Ligase ULF. *Oncogene* 34 (13), 1688–1697. doi:10.1038/onc.2014.103

Long, J., Jia, M.-Y., Fang, W.-Y., Chen, X.-J., Mu, L.-L., Wang, Z.-Y., et al. (2020). FLT3 Inhibition Upregulates HDAC8 via FOXO to Inactivate P53 and Promote Maintenance of FLT3-Itd+ Acute Myeloid Leukemia. *Blood* 135 (17), 1472–1483. doi:10.1182/blood.2019003538

Lundsten, S., Hernández, V. A., Gedda, L., Sarén, T., Brown, C. J., Lane, D. P., et al. (2020). Tumor-Targeted Delivery of the P53-Activating Peptide VIP116 with PEG-Stabilized Lipodisks. *Nanomaterials* 10 (4), 783. doi:10.3390/nano10040783

Markman, J. L., Rekechenetskiy, A., Holler, E., and Ljubimova, J. Y. (2013). Nanomedicine Therapeutic Approaches to Overcome Cancer Drug Resistance. *Adv. Drug Deliv. Rev.* 65 (13-14), 1866–1879. doi:10.1016/j.addr.2013.09.019

Mattheolabakis, G., Rigas, B., and Constantinides, P. P. (2012). Nanodelivery Strategies in Cancer Chemotherapy: Biological Rationale and Pharmaceutical Perspectives. *Nanomedicine* 7 (10), 1577–1590. doi:10.2217/nnm.12.128

Phelan, K. W., and Advani, A. S. (2018). Novel Therapies in Acute Lymphoblastic Leukemia. *Curr. Hematol. Malig. Rep.* 13 (4), 289–299. doi:10.1007/s11899-018-0457-7

Pillai, V., Muralidharan, K., Meng, W., Bagashev, A., Oldridge, D. A., Rosenthal, J., et al. (2019). CAR T-Cell Therapy Is Effective for CD19-Dim B-Lymphoblastic Leukemia but Is Impacted by Prior Blinatumomab Therapy. *Blood Adv.* 3 (22), 3539–3549. doi:10.1182/bloodadvances.2019000692

Richard-Carpentier, G., Kantarjian, H., and Jabbour, E. (2019). Recent Advances in Adult Acute Lymphoblastic Leukemia. *Curr. Hematol. Malig. Rep.* 14 (2), 106–118. doi:10.1007/s11899-019-00503-1

Sanna, V., Pala, N., and Sechi, M. (2014). Targeted Therapy Using Nanotechnology: Focus on Cancer. *Int. J. Nanomedicine* 9, 467–483. doi:10.2147/IJN.S36654

Schmied, B. J., Lutz, M. S., Riegg, F., Zekri, L., Heitmann, J. S., Bühring, H.-J., et al. (2019). Induction of NK Cell Reactivity against B-Cell Acute Lymphoblastic Leukemia by an Fc-Optimized FLT3 Antibody. *Cancers* 11 (12), 1966. doi:10.3390/cancers11121966

Sive, J. I., Buck, G., Fielding, A., Lazarus, H. M., Litzow, M. R., Luger, S., et al. (2012). Outcomes in Older Adults with Acute Lymphoblastic Leukaemia (ALL): Results from the International MRC UKALL XII/ECOG2993 Trial. *Br. J. Haematol.* 157 (4), 463–471. doi:10.1111/j.1365-2141.2012.09095.x

Tasian, S. K., and Gardner, R. A. (2015). CD19-redirected Chimeric Antigen Receptor-Modified T Cells: a Promising Immunotherapy for Children and Adults with B-Cell Acute Lymphoblastic Leukemia (ALL). *Ther. Adv. Hematol.* 6 (5), 228–241. doi:10.1177/2040620715588916

Vu, T. T., Stölzel, F., Wang, K. W., Röllig, C., Tursky, M. L., Molloy, T. J., et al. (2020). miR-10a as a Therapeutic Target and Predictive Biomarker for MDM2 Inhibition in Acute Myeloid Leukemia. *Leukemia*. doi:10.1038/s41375-020-01095-z

Wang, L., Chen, B., Lin, M., Cao, Y., Chen, Y., Chen, X., et al. (2015). Decreased Expression of nucleophosmin/B23 Increases Drug Sensitivity of Adriamycin-Resistant Molt-4 Leukemia Cells through Mdr-1 Regulation and Akt/mTOR Signaling. *Immunobiology* 220 (3), 331–340. doi:10.1016/j.imbio.2014.10.015

Xue, X., Fang, T., Yin, L., Jiang, J., He, Y., Dai, Y., et al. (2018). Multistage Delivery of CDs-Dox/icg-Loaded Liposome for Highly Penetration and Effective Chemo-Photothermal Combination Therapy. *Drug Deliv.* 25 (1), 1826–1839. doi:10.1080/10717544.2018.1482975

Yang, F., Yan, Y., Yang, Y., Hong, X., Wang, M., Yang, Z., et al. (2020). MiR-210 in Exosomes Derived from CAFs Promotes Non-small Cell Lung Cancer Migration and Invasion through PTEN/PI3K/AKT Pathway. *Cell Signal.* 73, 109675. doi:10.1016/j.cellsig.2020.109675

Zhang, G.-N., Gupta, P., Wang, M., Barbuti, A. M., Ashby, C. R., Jr., Zhang, Y.-K., et al. (2020). Lipid-Saporin Nanoparticles for the Intracellular Delivery of Cytotoxic Protein to Overcome ABC Transporter-Mediated Multidrug Resistance *In Vitro* and *In Vivo*. *Cancers* 12 (2), 498. doi:10.3390/cancers12020498

**Conflict of Interest:** The authors declare that the research was conducted in the absence of any commercial or financial relationships that could be construed as a potential conflict of interest.

frontiers in Oncology

ORIGINAL RESEARCH
published: 03 June 2021
doi: 10.3389/fonc.2021.627856

# 3,3'-Diindolylmethane Enhances Paclitaxel Sensitivity by Suppressing DNMT1-Mediated KLF4 Methylation in Breast Cancer

*Fenfen Xiang[1†], Zhaowei Zhu[1†], Mengzhe Zhang[1†], Jie Wang[2], Zixi Chen[1], Xiaoxiao Li[1], Tao Zhang[1], Qing Gu[1], Rong Wu[1*] and Xiangdong Kang[1*]*

[1] Laboratory Medicine, Putuo Hospital, Shanghai University of Traditional Chinese Medicine, Shanghai, China, [2] General Surgery, Putuo Hospital, Shanghai University of Traditional Chinese Medicine, Shanghai, China

OPEN ACCESS

**Edited by:**
*Zhe-Sheng Chen,*
*St. John's University, United States*

**Reviewed by:**
*Sujie Jia,*
*Central South University, China*
*Shuaishuai Liu,*
*University of Maryland, Baltimore County, United States*

***Correspondence:**
*Xiangdong Kang*
*xd_kang@163.com*
*Rong Wu*
*rong701@126.com*

[†]*These authors have contributed equally to this work*

**Specialty section:**
*This article was submitted to Pharmacology of Anti-Cancer Drugs, a section of the journal Frontiers in Oncology*

**Received:** *17 February 2021*
**Accepted:** *12 May 2021*
**Published:** *03 June 2021*

**Citation:**
*Xiang F, Zhu Z, Zhang M, Wang J, Chen Z, Li X, Zhang T, Gu Q, Wu R and Kang X (2021) 3,3'-Diindolylmethane Enhances Paclitaxel Sensitivity by Suppressing DNMT1-Mediated KLF4 Methylation in Breast Cancer. Front. Oncol. 11:627856. doi: 10.3389/fonc.2021.627856*

Paclitaxel (PTX) is a first-line chemotherapeutic drug for the treatment of breast cancer, but drug resistance seriously limits its clinical use. The aim of the present work was to explore the effect of 3,3'-diindolylmethane (DIM) on PTX sensitivity and its possible mechanism in breast cancer. The expression of Krüppel-like factor 4 (KLF4) and DNA-methyltransferase 1 (DNMT1) in breast cancer tissues were assessed by immunohistochemistry and Western blotting. The methylation of *KLF4* was evaluated by the MassARRAY platform. The lentivirus carrying *KLF4* and *DNMT1* gene or shRNA targeting DNMT1 were used to overexpress KLF4 or knockdown DNMT1 in MCF-7 and T47D breast cancer cells and the role of KLF4 and DNMT1 in regulation of PTX sensitivity was investigated. The effect of PTX on inhibiting the proliferation of MCF-7 and T47D cells was measured by CCK-8 assay. Flow cytometry was used to examine cell apoptosis. The expression of mRNA and protein was evaluated by qRT-PCR and Western blotting analysis, respectively. Our data showed that the expression of DNMT1 was increased, and the methylation level of CpG sites (–148 bp) in the *KLF4* promoter was increased while the KLF4 expression was significantly decreased in breast cancer tissues. Overexpression of KLF4 increased the sensitivity of MCF-7 and T47D cells to PTX. DNMT1 increased the methylation of the KLF4 promoter and decrease the expression of KLF4. Knockdown of DNMT1 increased the sensitivity of MCF-7 and T47D cells to PTX. DIM enhanced the PTX sensitivity of MCF-7 and T47D cells, decreased the expression of DNMT1 and the methylation level of KLF4 promoter, thus increasing the level of KLF4. Furthermore, overexpression of DNMT1 attenuated the effect of DIM on the regulation of PTX sensitivity. Collectively, our data indicated that DNMT1-mediated hypermethylation of *KLF4* promoter leads to downregulation of KLF4 in breast cancer. The level of KLF4 is correlated with the sensitivity of MCF-7 and T47D cells to PTX. DIM could enhance the antitumor efficacy of PTX on MCF-7 and T47D cells by regulating DNMT1 and KLF4.

**Keywords: breast cancer, paclitaxel, sensitivity, KLF4, DNMT1, DIM**

## INTRODUCTION

Breast cancer is the leading cause of cancer-related death among women (1), which remains a challenging task for oncologists. One major obstacle to the successful treatment of patients who receive chemotherapy is drug resistant which resulted in treatment failure. As a well tolerate microtubule stabilizer, PTX is one of the most frequently used anticancer drugs, especially in the treatment of breast cancer; however, its clinical efficacy is limited by drug resistance (2). Therefore, to better understand the drug resistant mechanism of PTX and to enhance its sensitivity are critical for improving the treatment and prognosis of patients.

Krüppel-like factor 4 (KLF4) is a zinc-finger transcriptional factor which is mainly expressed in terminal differentiated epithelial cells and plays regulatory roles in cell proliferation, differentiation and pluripotency (3, 4). Clinically, loss of KLF4 function has been found in various types of cancers and is related to chemotherapeutic resistance (5–7). The low expression of KLF4 in tumor cells was shown to be caused by genetic and epigenetic alterations (8–10). Our preliminary work demonstrated that the expression of KLF4 is related to PTX sensitivity of breast cancer MCF-7 cells. However, the association of KLF4 expression, its functional alteration and PTX sensitivity in breast cancer are not well understood.

Abnormal methylation of genes is one of the epigenetic modifications involved in the development of tumors (11). DNA-methyltransferase (DNMT) is the principle enzyme responsible for maintaining CpG methylation (12), which mediates the transfer of the methyl group from S-adenosylmethionine to 5-methylcytosine base. Methylation of tumor suppressor genes plays critical roles in the pathogenesis of various cancers. It is generally considered that methylation of tumor suppressor gene is equivalent to gene loss or functional mutation (13–15). Therefore, reversing methylation of tumor suppressor genes may be a promising strategy for cancer prevention and treatment (16, 17). It was reported that inhibition of DNMT could enhance chemotherapeutic sensitivity of tumor cells (18, 19). Therefore, it is of great clinical significance to search for specific and low toxic anticancer agents that can reactivate silent cancer suppressor genes by targeting aberrant DNA methylation.

It was known that the bioactive substances in some foods can regulate epigenomes and possess anti-tumor activity. DIM is abundant in cruciferous vegetables, and was showed to have anticancer activities in some tumors, such as breast, cervical and prostate cancers (20, 21). Some clinical trials have been approved for using DIM in patients with premalignant or malignant lesions (22). However, whether DIM could increase the sensitivity of breast cancer cells to PTX and the underlying molecular mechanism remains poorly understood.

In this study, we showed that the KLF4 expression was downregulated in human breast cancer tissues, which was associated with hypermethylation of its promoter region. DIM could enhance PTX sensitivity in MCF-7 and T47D breast cancer cells by reducing the expression of DNMT1 and subsequently reducing the methylation level of *KLF4* and promoting the expression of KLF4. This work provides a new strategy for the improving chemotherapy and sheds a light for further clinical research in breast cancer treatment.

## MATERIALS AND METHODS

### Tissue Samples

Human breast cancer samples and the adjacent non-malignant breast samples were collected from the Putuo Hospital, Shanghai, China. Before sample collection, all patients signed the informed consent according to the institutional guidelines. This research was granted by the Ethical Review Committee of the Putuo Hospital, Shanghai University of Traditional Chinese Medicine. The procedures of the study were implemented according to the approved guidelines.

### Immunohistochemistry

Immunohistochemistry staining was performed according to the instructions. Briefly, the paraffin-embedded breast tumor tissues were continuously sectioned into sections of 5μm in thickness. The sections were dewaxed and rehydrated. The heat-mediated antigen retrieval was performed by boiling sections in Tris/EDTA at pH 9.0. Primary antibody against KLF4(1:300) or DNMT1 (1:200) was used to incubate with tissue sections overnight at 4°C, and then horseradish peroxidase-labeled antibody was used as a secondary antibody for 30 min. The color reaction was carried out with diaminobenzidine as a substrate.

### Cell Cultures

Human breast cancer cell lines (MDA-MB-231, MDA-MB-468, MCF-7 and T47D) were cultured in DMEM (Gibco Industries, Inc.) containing with 10% FBS and maintained at 37°C in a humidified atmosphere with 5% $CO_2$.

### Cell Proliferation Assays

MCF-7 and T47D Cells (8000 per well) were seeded onto 96-well plates and incubated overnight. Then, the cells were incubated with different concentrations of PTX (MedCham Express, dissolved in DMSO) alone or in combination with DIM (MedCham Express, dissolved in DMSO). The cells of the control group were treated with DMSO. After 48h of incubation, cell proliferation was measured using the Cell Counting Kit-8 (CCK-8, Dojindo, Japan). The light absorbance was measured at 450 nm.

### Quantitative Real-Time PCR

Total mRNA was isolated from MCF-7 and T47D cells by using TRIzol reagents (Takara Bio, Inc.), and the complementary DNA was synthesized by the PrimeScript RT reagent kit (Takara Bio, Inc.). Reactions were performed at 95°C, 2 min; 95°C, 15 sec and 60°C, 30 sec for 40 cycles in the real time PCR system (StepOne Plus; Applied Biosystems, USA). The relative expression levels of DNMT1 and KLF4 were normalized with GAPDH and calculated by $2^{-\Delta\Delta ct}$ method. The primers used in the research are shown in **Table 1**.

### Western Blotting

Tissues or cells were lysed by the RIPA (Beyotime Institute of Biotechnology, Beijing, China) containing with protease inhibitors. The amounts of protein of each sample were quantified. Protein

**TABLE 1** | Nucleotide sequences of primers used for qRT-PCR reactions.

| Gene | Forward | Reverse |
|---|---|---|
| GAPDH | 5'-ATGCTGCCCTTACCCCGG-3' | 5'-TTACTCCTTGGAGGCCATGTAGG-3' |
| DNMT1 | 5'-CGGCAGACCATCAGGCATTCTAC-3' | 5'-CACACCTCACAGACGCCACATC -3' |
| KLF4 | 5'-CCTTCAACCTGGCGGACATCAAC -3' | 5'-GCTGCTGCGGCGGAATGTAC-3' |
| Methylation (KLF4) | 5'-aggaagagagGTTGTATAGTGTTGGGTATT GTTTT -3' | 5'-cagtaatacgactcactatagggagaaggctTTACTATAACAAC TAAATCAACAAACTC-3' |

(50μg) was separated by polyvinylidene gel electrophoresis and transferred onto a polyvinylidene fluoride (PVDF) membrane (Merck Millipore). The membranes were blocked with 5% non-fat milk for 2 h and then hybridized with the KLF4 (CST) or DNMT1 (CST) antibody separately at 4°C overnight and with HRP-conjugated secondary antibodies for 1 h at room temperature. Finally, the immunoreactive bands were determined by enhanced chemiluminescence (Pierce Biotechnology).

## Analysis of Cell Apoptosis

Apoptosis of MCF-7 and T47D breast cancer cells were analyzed using the Annexin V-Phycoerythrin kit (BD Biosciences). After treatment with PTX alone or in combination with DIM for 48 h, MCF-7 and T47D cells were collected and stained with Annexin V-APC (BD Biosciences) in the dark for 20 min. Then, the stained cells were measured by flow cytometry using the Canto (BD Biosciences). The FlowJo software was used to analyze the data.

## Construction of KLF4 Lentiviral Vectors and DNMT1 Vectors

Human KLF4 cDNA was constructed by GenePharma (Shanghai, China), the overexpression of KLF4 and the negative control were named as KLF4-OE and KLF4-NC, respectively. Human DNMT1 cDNA synthesized by Genechem (Shanghai, China) was constructed with CMV-MCS-3FLAG-IRES-EGFP-SV40- neomycin plasmid, the overexpression of DNMT1 was named as DNMT1-OE and the control was named as DNMT1-NC. The shRNA sequence cgACTACA TCAAAGGCAGCAA targeted DNMT1 were subcloned with the hU6-MCS-CMV-GFP-SV40-Neomycin plasmid vector, the knockdown of DNMT1was named as DNMT1-KD and the control was named as DNMT1-NC.

## Mass Array Methylation Detection

Genomic DNA was obtained from the breast cancer tissues and cells using a QIAamp DNA kit and the bisulfite conversion reaction was implemented using the EpiTect Bisulfite Kit (Qiagen, Hilden, Germany). PCR primers (**Table 1**) were designed using EpiDesigner. Small RNA fragments with CpG sites were obtained from the PCR products through RNaseA digestion. DNA methylation of CpG was measured using the MassARRAY platform, and the methylation rate was calculated by Epityper software Version 1.0 (Agena, San Diego, CA, USA). The detection and analysis were conducted by the OE Biotech Co., Ltd.

## Statistical Analysis

The analyses of data were used by GraphPad Software, all data were expressed as the mean ± standard deviation from at least three independent experiments. The significance was calculated by Student's t-test, and $p<0.05$ was considered as statistically significant difference.

# RESULTS

## The Expression of KLF4 Decreased and Its Promoter Hypermethylated in Breast Cancer

Some previous studies showed that the expression of KLF4 was reduced (23–25), while others reported that KLF4 expression was increased in breast cancer tissues (26, 27). To determine the level of KLF4 in breast cancer tissues, we determined the KLF4 expression in 50 breast cancer and adjacent normal tissues by immunohistochemical (IHC) staining. The results showed that the expression of KLF4 was decreased in breast cancer tissues (**Figures 1A, B**). Also, the Western blot analysis showed that the KLF4 level was significantly lower in breast tumor tissues compared with normal tissues (**Figures 1C, D**).

The expression of KLF4 is regulated by the DNA methylation status of its promoter. Therefore, we explored whether the decreased expression of KLF4 was associated with the DNA methylation level of its promoter. The methylation level of *KLF4* promoter was measured in breast carcinoma tissues (n = 5) and adjacent normal tissues (n = 5) by the MassArray methylation assay. The selected regions for the bisulfifite sequencing and the CpG island in *KLF4* promoter region are shown in **Figure 1E**. The results showed that the methylation level of the CpG sites (−148 bp) in the *KLF4* promoter was significantly higher in breast tumor tissues than in adjacent normal tissues (**Figure 1F**).

Additionally, to investigate whether the downregulation of KLF4 was caused by the hypermethylation of its promoter, MCF-7 and T47D cells were treated with 5-Aza-2′-Deoxycytidine (5-AzaC), an inhibitor of DNA methyltransferase. The results showed that 5-AzaC significantly increase the expression level of KLF4 in MCF-7 and T47D cells (**Figures 1G, H**). This result confirmed that downregulation of KLF4 was caused by the hypermethylation of its promoter.

## The Expression of KLF4 Was Associated With PTX Sensitivity in Breast Cancer Cells

The KLF4 expression was evaluated in different breast cancer cells, including the MDA-MB-468, MDA-MB-231, MCF-7 and T47D breast cancer cells (**Figure 2A**) by immunofluorescent staining and Western blotting. It was found that the expression

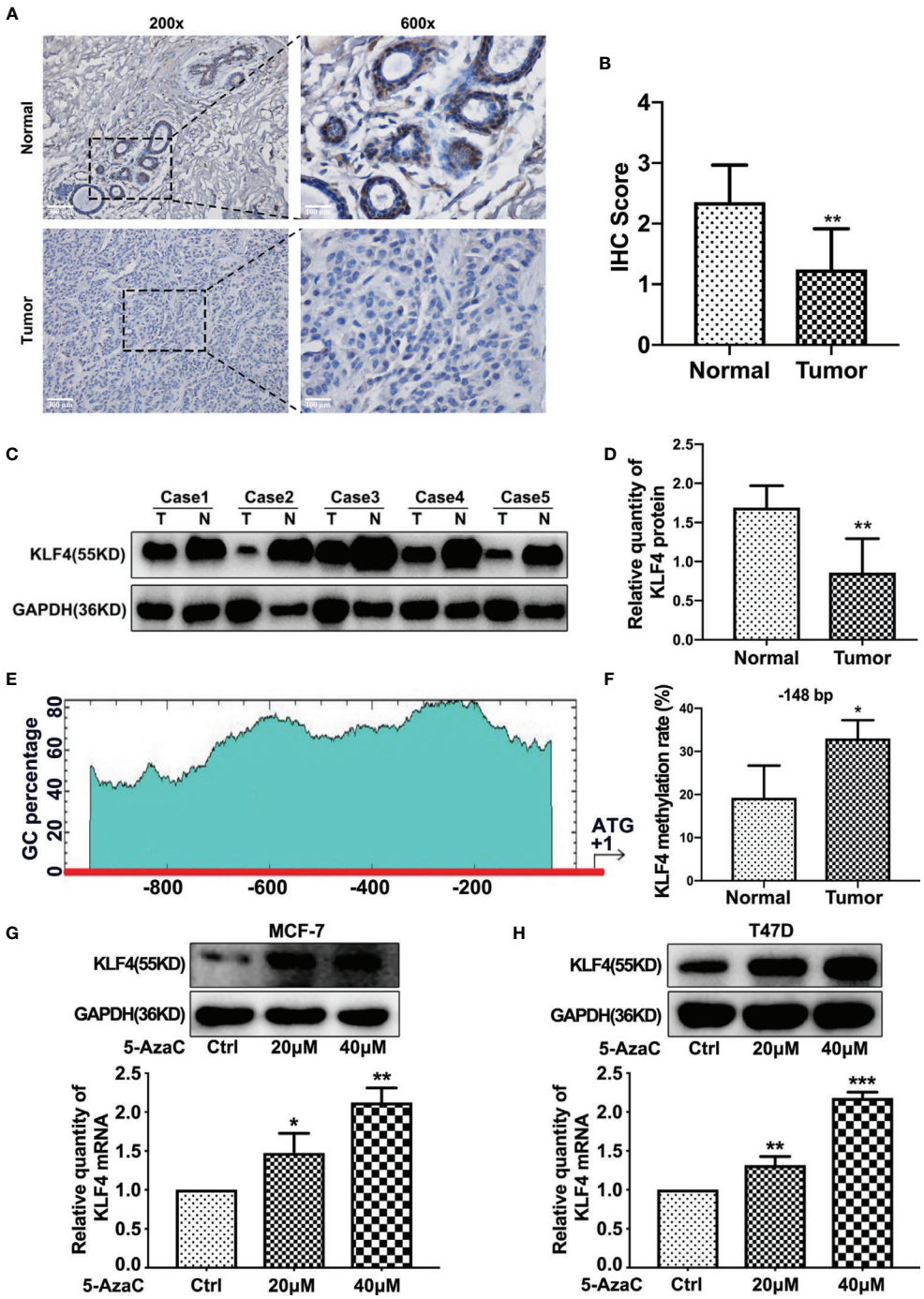


**FIGURE 1** | The expression of KLF4 decreased and its promoter hypermethylated in breast cancer **(A)** Immunohistochemical assessment of KLF4 expression in breast cancer tissues. **(B)** Average score of KLF4 immunostaining in breast cancer and adjacent tissues. **(C)** Western blotting analyses of KLF4 protein level in breast cancer and adjacent tissues. **(D)** Relative quantity of KLF4 protein in breast cancer and adjacent tissues. **(E)** The position of CpG sites in the promoter region of *KLF4*. **(F)** Methylation level of the *KLF4* promoter in breast cancer and adjacent tissues. **(G)** Real-time PCR and Western blotting analyses of KLF4 expression levels in MCF-7 cells treated with or without 5-AzaC (20 μmol/L) and 5-AzaC (40 μmol/L) for 48 h. **(H)** Real-time PCR and Western blot analyses of KLF4 expression in T47D cells treated with or without 5-AzaC (20 μmol/L) and 5-AzaC (40 μmol/L) for 48 h. **P*<0.05; ***P*<0.01; ****P*<0.001 versus control.

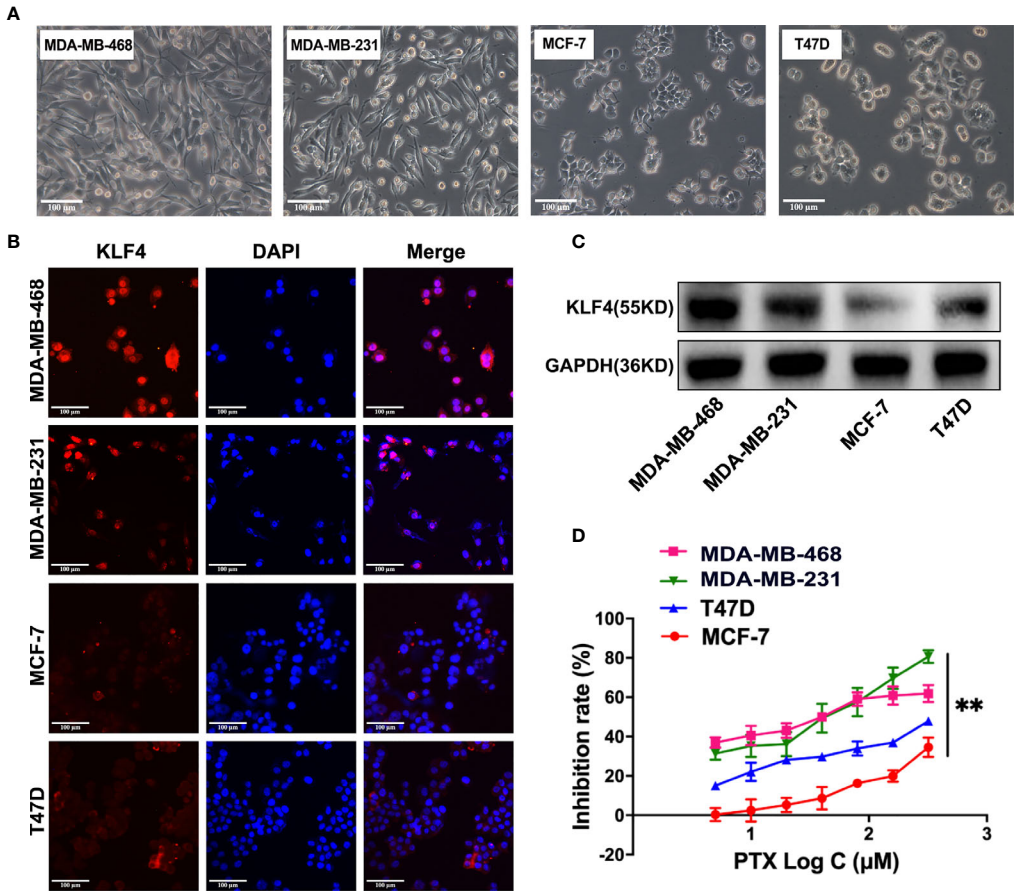


**FIGURE 2** | The expression of KLF4 was associated with PTX sensitivity in breast cancer. **(A)** Morphological images of cell lines. **(B)** Immunofluorescence analyses of KLF4 protein expression in MBA-MD-468, MBA-MD-231, MCF-7 and T47D cells. **(C)** Western blotting analyses of KLF4 protein expression in MBA-MD-468, MBA-MD-231, MCF-7 and T47D cells. **(D)** The inhibition of MBA-MD-468, MBA-MD-231, T47D and MCF-7 cell growth by PTX treatment. $^{**}P<0.01$ versus control.

of KLF4 was different in the different breast cancer cells (**Figures 2B, C**). To investigate the correlation between the KLF4 level and cell sensitivity to PTX, we evaluated the cell growth inhibition after treatment with PTX in these four cell lines. The results showed that the MDA-MB-468 and MDA-MB-231 cells had higher KLF4 level and are more sensitive to PTX than those of MCF-7 and T47D cells, that had lower KLF4 level and are less sensitive to PTX (**Figure 2D**). The results suggested that the level of KLF4 was related to the PTX sensitivity in breast cancer cells.

## Overexpression of KLF4 Increased the Sensitivity of Breast Cancer Cells to PTX

In order to determine whether KLF4 mediates PTX sensitivity in breast cancer cells, the lentiviral vector containing *KLF4* were used to overexpress KLF4 in MCF-7 and T47D breast cancer cells. The qRT-PCR and Western blot analysis showed that the KLF4 level was significantly higher in MCF-7 and T47D cells transfected with the *KLF4* lentiviral vector compared with the control cells (**Figures 3A, D**). The proliferation was decreased in of MCF-7 and T47D cells after overexpressing KLF4 (**Figures 3B, E**). Further, the proliferation was significantly inhibited by PTX in MCF-7 and T47D cells after overexpressing KLF4 compared with the control cells (**Figures 3C, F**). These results suggested that overexpression of KLF4 could increase the sensitivity of MCF-7 and T47D cells to PTX.

In order to investigate whether KLF4 could mediate apoptosis of MCF-7 and T47D cells after the PTX treatment, we tested apoptotic changes in MCF-7 and T47D cells using Annexin V-7AAD after PTX treatment for 48h. The results showed that the percentage of apoptotic cells was significantly increased in the cells overexpressed KLF4 (**Figures 3G–J**). This result suggested that the KLF4 overexpression was related to PTX-induced apoptosis in MCF-7 and T47D cells.

## DNMT1 Expression Was Negatively Correlated With KLF4 Expression and PTX Sensitivity in Breast Cancers

In order to find out the possible reason underlying hypermethylation of KLF4 promoter in breast cancer, we detected the expression of DNMT1 in these 50 breast carcinoma and adjacent normal tissues by IHC analysis. The results showed that the expression of DNMT1 was lower in breast normal tissues with relatively high KLF4

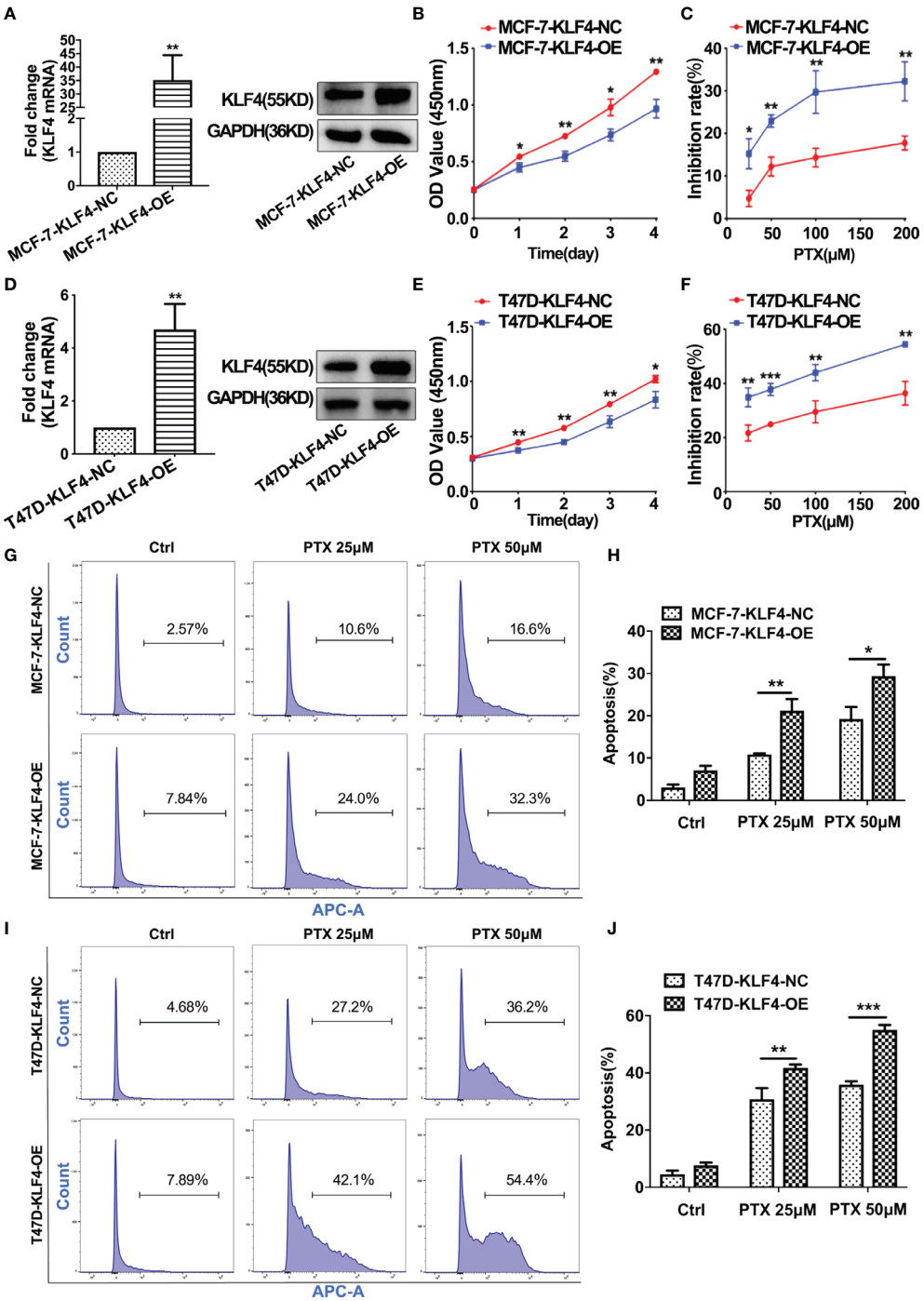


**FIGURE 3** | Overexpression of KLF4 increased the sensitivity of breast cancer cells to PTX. **(A)** Real-time PCR and Western blot analyses of KLF4 expression after transfection with the KLF4 overexpressing lentivirus in MCF-7 cells. **(B)** Growth curve of MCF-7 cells after overexpression of KLF4. **(C)** The inhibition of MCF-7 cell proliferation by PTX after KLF4 overexpression. **(D)** Real-time PCR and Western blot analyses on the expression of KLF4 after transfection with the KLF4 overexpressing lentivirus in T47D cells. **(E)** Growth curve of T47D cells after overexpression of KLF4. **(F)** The inhibition of T47D cell proliferation by PTX after KLF4 overexpression. **(G)** Apoptosis in MCF-7 cells treated with PTX after KLF4 overexpression. **(H)** Apoptotic cell percentage of MCF-7 cells treated with PTX. **(I)** Apoptosis of T47D cells treated with PTX after KLF4 overexpression. **(J)** Apoptotic cell percentage of T47D cells treated with PTX. *$P$<0.05; **$P$<0.01; ***$P$< 0.001 versus control.

expression, while DNMT1 was significantly increased in breast cancer tissues with relatively low KLF4 expression. These results indicated that DNMT1 expression was negatively correlated with KLF4 level in breast cancer (**Figures 4A, B**). Additionally, DNMT1 expression levels were significantly higher in carcinoma tissues than in adjacent tissues (**Figures 4C, D**). Similarly, the Western blot test showed that DNMT1 protein was significantly higher in carcinoma tissues (n = 5) than in adjacent normal tissues (n = 5) (**Figures 4E, F**).

To further confirm that the expression of KLF4 is regulated by DNA methyltransferase, DNMT1 shRNA was used to knockdown DNMT1 in MCF-7 and T47D cells. It was found that KLF4 mRNA and protein expression were significantly increased (**Figures 4G, J**), and the methylation of the CpG sites (−148 bp) in the *KLF4* promoter was significantly decreased (**Figures 4H, K**) upon decreasing DNMT1 expression. Additionally, the proliferation of MCF-7 and T47D cells was significantly inhibited by PTX after down-regulation of DNMT1 compared with that of the control cells (**Figures 4I, L**), suggesting that knockdown of DNMT1 could enhance the sensitivity of MCF-7 and T47D cells to PTX. These results indicated that DNMT1 and KLF4 play a critical effect in regulating the sensitivity of PTX in breast cancer cells.

## DIM Enhanced PTX Sensitivity in Breast Cancer

Furthermore, we explored whether DIM could enhance the effect of PTX on MCF-7 and T47D breast cancer cells. The concentrations of DIM used were chosen to be 50 μM and 80 μM for the MCF-7 cells, and 30 μM and 50 μM for T47D cells, and the CCK-8 results showed that DIM at a low toxic concentration significantly enhanced the efficacy of PTX in inhibition of cell growth in MCF-7 (**Figures 5A–C**) and T47D cells (**Figures 5D–F**). To confirm whether DIM can change the apoptotic rate of MCF-7 and T47D cells after PTX treatment, we tested the apoptotic changes of MCF-7 and T47D cells by Annexin V. It was found that the rate of apoptotic cells was increased significantly in cells treated with DIM in combination with PTX (**Figures 5G–J**). These results suggested that DIM can enhance PTX sensitivity in breast cancer cells.

## DIM Enhanced PTX Sensitivity by Inhibiting DNMT1 and Downregulating KLF4 Methylation

Studies have suggested that DIM plays an important role in regulating the expression of DNMT1 (28). Therefore, we evaluated whether DIM affects DNMT1 and KLF4 expression. Real-time PCR and Western blotting analysis revealed that DIM could significantly decrease the DNMT1 expression and increase the KLF4 expression in MCF-7 and T47D breast cancer cells (**Figures 6A, C**). To demonstrate the effect of DIM on enhancing PTX sensitivity through targeting DNMT1, we used a virus vector carrying DNMT1 to increase the expression of DNMT1 in MCF-7 and T47D cells. qRT-PCR and Western blot analysis showed that the DNMT1 levels were significantly higher in MCF-7 and T47D cells transfected with the DNMT1 vector compared with the control cells (**Figures 6B, D**). It was found that overexpression of DNMT1 reduced the inhibitory effect of proliferating MCF-7 and T47D cells after DIM and PTX combined treatment (**Figures 6E, F**). This result suggested that DIM was unable to enhance the sensitivity of MCF-7 and T47D cells to PTX when the expression of DNMT1 was increased. We further investigated whether DIM regulates the methylation level of *KLF4* promoter in breast cancer cells, and the results showed that compared with normal cells, the methylation level of CpG sites (−148 bp) in the *KLF4* promoter was decreased in breast cancer MCF-7 cells after treatment with DIM (**Figure 6G**). These results showed that DIM enhanced PTX sensitivity by inhibiting DNMT1 expression and subsequently upregulating the KLF4 level in the breast cancer cells (**Figure 6H**).

# DISCUSSION

PTX is commonly used in the treatment of breast cancer, but its clinical effect is limited due to the development of drug resistance. Therefore, there is an urgent need to find agents that can be used for effectively reversing PTX resistance in breast cancer. Here, we demonstrated that DNMT1 promoted the methylation of *KLF4* promoter and thus decreased KLF4 expression, which was correlated with the PTX sensitivity in breast cancer. In addition, DIM could effectively increase the sensitivity of MCF-7 and T47D breast cancer cells to PTX by downregulating KLF4 methylation through inhibiting DNMT1.

The role and expression of KLF4 in tumors are controversial. Some studies reported that KLF4 is upregulated in breast cancer tissues (26, 27), while others found that KLF4 is downregulated (23–25). In our study, we found that the expression of KLF4 was significantly decreased in breast cancer tissues. Studies have demonstrated that the expression of KLF4 was regulated by the DNA methylation status of its promoter (28). To determine whether the decrease in KLF4 expression is due to the increase in methylation level, we investigated the methylation status of the *KLF4* promoter in breast cancer tissues, and found that the methylation level of specific CpG site (−148 bp) in the *KLF4* promoter played a critical role in the regulation of KLF4 expression.

KLF4 plays a key role in chemotherapeutic treatments by regulating gene expression that required for signaling pathways (29). Furthermore, studies have shown that KLF4 affected chemoresistance of some chemotherapeutic drugs (30). However, the effect of KLF4 in PTX sensitivity of breast cancer cells has not been reported. Here, we demonstrated that the KLF4 expression was correlated with PTX sensitivity and that breast cancer cells with a lower KLF4 level were less sensitive to PTX. Moreover, we demonstrated that overexpression of KLF4 can increase PTX-induced inhibition of cell growth and promoted apoptosis of MCF-7 and T47D cells, which indicates that restoring KLF4 expression of breast cancer cells could be an effective way to overcome PTX resistance.

DNMT1 is required in maintaining CpG methylation and silencing of various tumor suppressor genes. Increased DNMT1 level often leads to the increased tumorigenesis and elevated DNMT1 expression was associated with PTX resistance (31, 32).

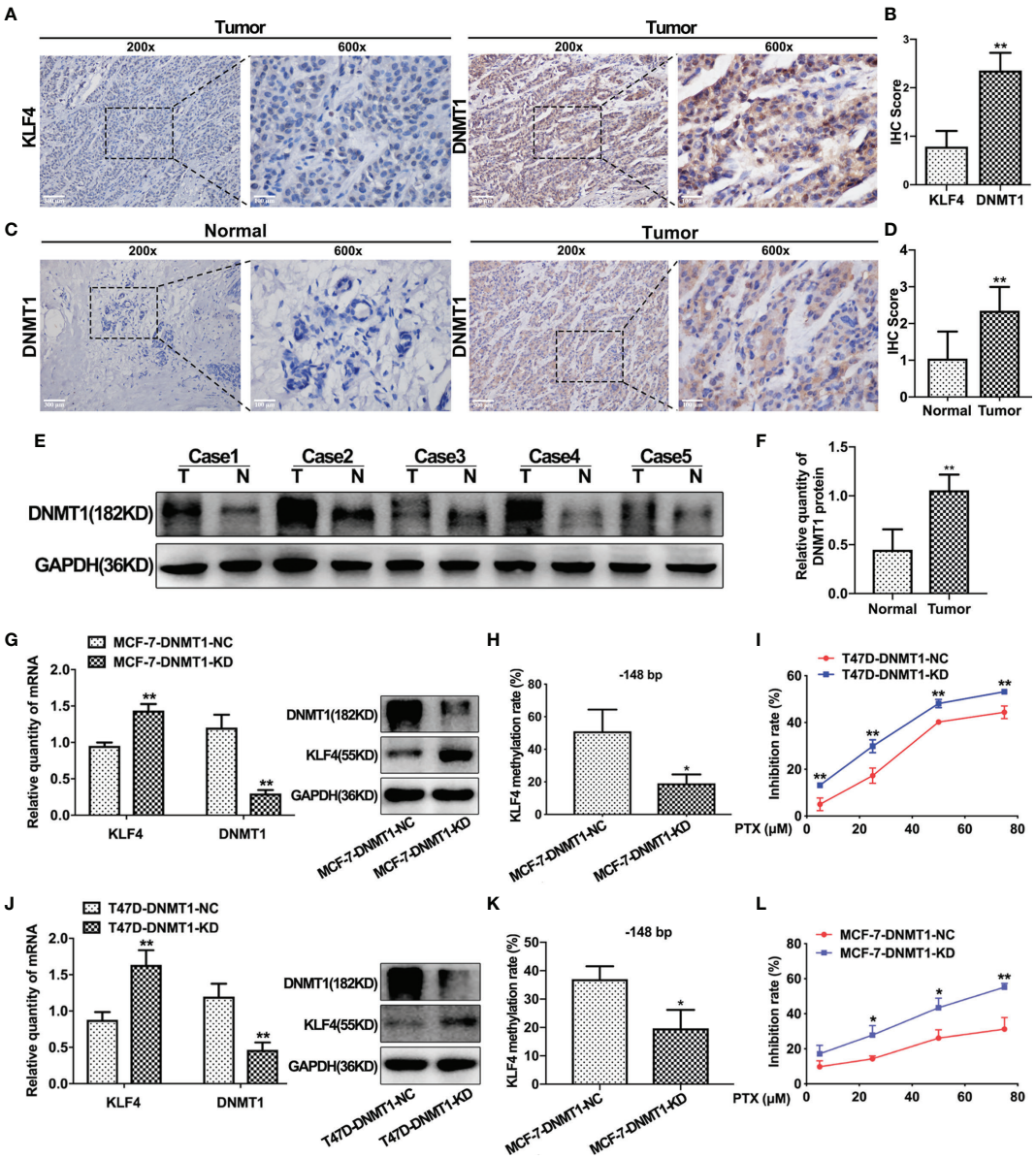


**FIGURE 4** | DNMT1 expression was negatively correlated with KLF4 expression and PTX sensitivity in breast cancers. **(A)** Immunohistochemical assessment of KLF4 and DNMT1 levels in breast cancer tissues. **(B)** Average score of KLF4 and DNMT1 immunostaining in breast cancer tissues. **(C)** Immunohistochemical assessment of DNMT1 expression in breast cancer and adjacent tissues. **(D)** Average score of DNMT1 immunostaining in breast cancer and adjacent tissues. **(E)** Western blotting analyses of DNMT1 protein expression in breast cancer and adjacent tissues. **(F)** Relative quantity of DNMT1 protein expression in breast cancer and adjacent tissues. **(G)** Real-time PCR and Western blot analysis of DNMT1 expression level in MCF-7 cells after transfection with the DNMT1 interference plasmid. **(H)** Methylation level of the KLF4 promoter in MCF-7 cells after transfection with the DNMT1 interference plasmid. **(I)** The viability of MCF-7 cells treated with PTX (5μM, 25μM, 50μM and 75μM) after transfection with the DNMT1 interference plasmid. **(J)** Real-time PCR and Western blot analysis of DNMT1 expression in T47D cells after transfection with the DNMT1 interference plasmid. **(K)** Methylation level of the KLF4 promoter in T47D cells after transfection with the DNMT1 interference plasmid. **(L)** The viability of T47D cells treated with PTX (5μM, 25μM, 50μM and 75μM) after transfection with the DNMT1 interference plasmid. *$P$<0.05; **$P$<0.01 versus control.

Studies have shown that DNMT1 reduced the expression of KLF4 by promoting methylation of its promoter (33, 34). In our present study, we found that DNMT1 expression increased in breast cancer tissues. Furthermore, after knockdown DNMT1 expression in MCF-7 and T47D breast cancer cells, the expression of KLF4 increased, and the sensitivity of breast cancer cells to PTX significantly increased. Our results demonstrated that DNMT1 plays a critical role in breast cancer development and PTX sensitivity.

It has been proved that DNA demethylation drug is effective in adjuvant therapy of some solid cancers and hematological malignancies (35). KLF4 is a major target of demethylation drugs

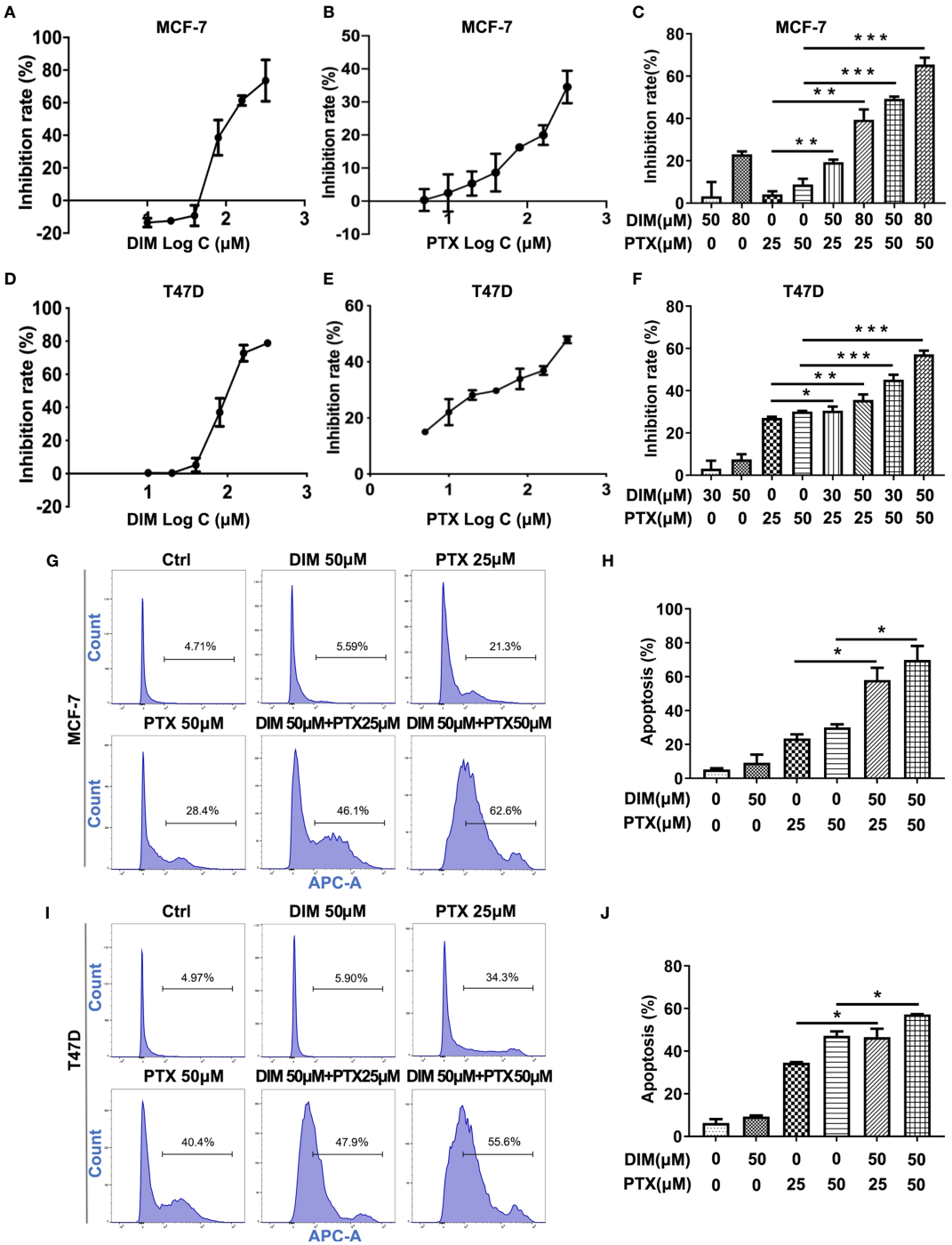


**FIGURE 5** | DIM enhanced PTX sensitivity in breast cancer cells. **(A)** The viability of MCF-7 cells after DIM (10μM, 20μM, 40μM, 80μM, 160μM and 320μM) treatment. **(B)** The viability of MCF-7 cell after PTX (5μM,10μM, 20μM, 40μM, 80μM, 160μM and 320μM) treatment. **(C)** The viability of MCF-7 cells treated with PTX after DIM pretreatment. **(D)** The viability of T47D cells after DIM (10μM, 20μM, 40μM, 80μM, 160μM and 320μM) treatment. **(E)** The viability of T47D cells after PTX (5μM,10μM, 20μM, 40μM, 80μM, 160μM and 320μM) treatment. **(F)** The viability of T47D cells treated with PTX after DIM pretreatment. **(G)** Apoptosis in MCF-7 cells treated with PTX after DIM pretreatment. **(H)** Percentage of apoptosis of MCF-7 cells treated with PTX after DIM pretreatment. **(I)** Apoptosis in T47D cells treated with PTX after DIM pretreatment. **(J)** Percentage of apoptosis of MCF-7 cells treated with PTX after DIM pretreatment. *$P$<0.05; **$P$<0.01; ***$P$< 0.001 versus control.

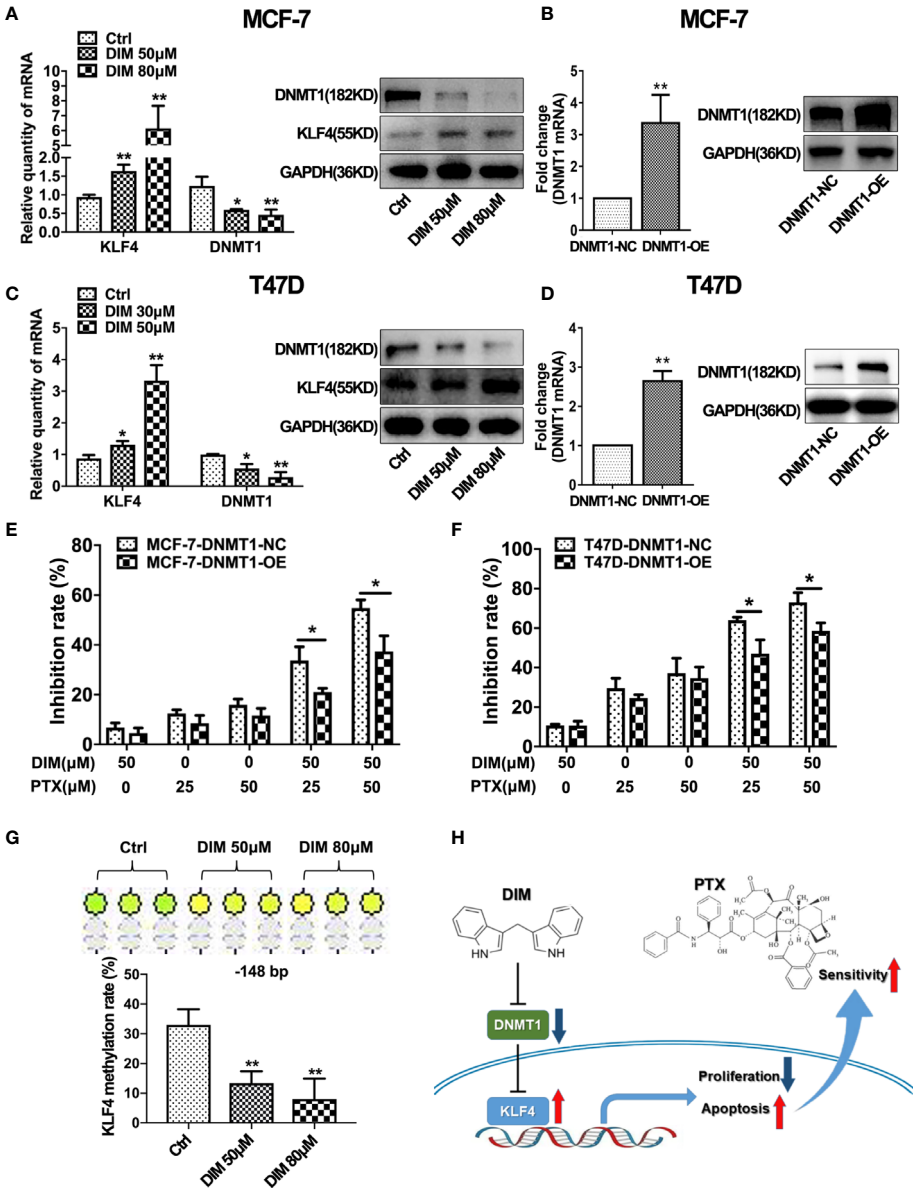


**FIGURE 6** | DIM enhanced PTX sensitivity by inhibiting DNMT1 and downregulating KLF4 methylation. **(A)** Real-time PCR and Western blotting analyses of KLF4 and DNMT1 expression in MCF-7 cells treated with or without DIM (50 μM or 80 μM) for 48 h. **(B)** Real-time PCR and Western blot analyses of DNMT1 expression after transfection with the DNMT1 overexpressing plasmid in MCF-7 cells. **(C)** Real-time PCR and Western blotting analyses of KLF4 and DNMT1 expression in T47D cells treated with or without DIM (30 μM or 50 μM) for 48 h. **(D)** Real-time PCR and Western blotting analyses of DNMT1 expression in T47D cells transfected with the DNMT1 overexpressing plasmid. **(E)** The viability of MCF-7 cells treated with PTX and DIM after overexpressing DNMT1. **(F)** The viability of T47D cells treated with PTX and DIM after overexpressing DNMT1. **(G)** Methylation levels of the *KLF4* gene in MCF-7 cells treated with or without DIM (50 μM or 80 μM) for 48 h. **(H)** Schematic model of DIM in enhancing PTX sensitivity by regulating the expression of KLF4 and DNMT1. *$P$<0.05; **$P$<0.01 versus control.

in enhancing the PTX sensitivity of breast cancer. Therefore, a drug that can inhibit DNMT1 expression and promote the expression of KLF4 would considerably improve the status of PTX resistance in the clinical treatment of breast cancer. Dietary DIM is a natural compound and has been proved to be a low toxic substance that can potentially inhibit the expression of DNMT1 (28), and can be used in the prevention and treatment of clinical cancer. Our study demonstrated that dietary DIM can significantly increase the sensitivity of MCF-7 and T47D cells to PTX. To further investigate the mechanism of action of DIM in enhancing PTX sensitivity, we determined the expression levels of DNMT1 and KLF4 in breast cancer MCF-7 and T47D cells after treatment with DIM. We found that DIM can increase the KLF4 expression and decrease the DNMT1 expression level in MCF-7 and T47D cells.

In summary, our findings demonstrate that the expression of DNMT1 and the methylation level of *KLF4* promoter increased, while the expression of KLF4 decreased in breast cancer tissues. Knockdown of DNMT1 can enhance PTX sensitivity by increasing KLF4 expression. DIM can effectively decrease the expression of DNMT1 and the methylation level of KLF4 in breast cancer cells, and then promote the expression of KLF4. Our study suggests that DIM can increase the sensitivity of PTX and therefore, combination of DIM and PTX could be an effective strategy to overcome drug resistance in breast cancer cells.

## DATA AVAILABILITY STATEMENT

The original contributions presented in the study are included in the article. Further inquiries can be directed to the corresponding authors.

## ETHICS STATEMENT

The studies involving human participants were reviewed and approved by Ethical Review Committee of the Putuo Hospital, Shanghai University of Traditional Chinese Medicine. The patients/participants provided their written informed consent to participate in this study.

## AUTHOR CONTRIBUTIONS

KX, WR and XF conceived and designed the project. XF, ZZ and ZM performed the experiments and acquired the data. WJ and ZZ collected tissue specimens. CZ and GQ analyzed the data. XF and ZM wrote the article. LX and ZT participated in writing the article. WR and KX commented and edited the article. All authors contributed to the article and approved the submitted version.

## FUNDING

This work was supported by the National Natural Science Foundation of China (No. 81703878), the Shanghai Rising Stars of Medical Talent Youth Development Program and the Putuo Hospital, Shanghai University of Traditional Chinese Medicine (No. 2020373B).

## REFERENCES

1. Siegel RL, Miller KD, Jemal A. Cancer Statistics, 2018. *CA Cancer J Clin* (2018) 68:7–30. doi: 10.3322/caac.21442
2. Jamdade VS, Sethi N, Mundhe NA, Kumar P, Lahkar M, Sinha N. Therapeutic Targets of Triple-Negative Breast Cancer: A Review. *Br J Pharmacol* (2015) 172:4228–37. doi: 10.1111/bph.13211
3. Wei D, Wang L, Yan Y, Jia Z, Gagea M, Li Z, et al. Klf4 Is Essential for Induction of Cellular Identity Change and Acinar-to-Ductal Reprogramming During Early Pancreatic Carcinogenesis. *Cancer Cell* (2016) 29:324–38. doi: 10.1016/j.ccell.2016.02.005
4. Sun H, Peng Z, Tang H, Xie D, Jia Z, Zhong L, et al. Loss of KLF4 and Consequential Downregulation of Smad7 Exacerbate Oncogenic TGF-beta Signaling in and Promote Progression of Hepatocellular Carcinoma. *Oncogene* (2017) 36:2957–68. doi: 10.1038/onc.2016.447
5. Liu HW, Su YK, Bamodu OA, Hueng DY, Lee WH, Huang CC, et al. The Disruption of the Beta-Catenin/TCF-1/STAT3 Signaling Axis by 4-Acetylantroquinonol B Inhibits the Tumorigenesis and Cancer Stem-Cell-Like Properties of Glioblastoma Cells, In Vitro and In Vivo. *Cancers (Basel)* (2018) 10:491. doi: 10.3390/cancers10120491
6. Hilakivi-Clarke L, Warri A, Bouker KB, Zhang X, Cook KL, Jin L, et al. Effects of In Utero Exposure to Ethinyl Estradiol on Tamoxifen Resistance and Breast Cancer Recurrence in a Preclinical Model. *J Natl Cancer Inst* (2017) 109:188. doi: 10.1093/jnci/djw188
7. Park CS, Lewis AH, Chen TJ, Bridges CS, Shen Y, Suppipat K, et al. A KLF4-DYRK2-Mediated Pathway Regulating Self-Renewal in CML Stem Cells. *Blood* (2019) 134:1960–72. doi: 10.1182/blood.2018875922
8. Katz JP, Perreault N, Goldstein BG, Actman L, McNally SR, Silberg DG, et al. Loss of Klf4 in Mice Causes Altered Proliferation and Differentiation and Precancerous Changes in the Adult Stomach. *Gastroenterology* (2005) 128:935–45. doi: 10.1053/j.gastro.2005.02.022
9. Zhao W, Hisamuddin IM, Nandan MO, Babbin BA, Lamb NE, Yang VW. Identification of Kruppel-Like Factor 4 as a Potential Tumor Suppressor Gene in Colorectal Cancer. *Oncogene* (2004) 23:395–402. doi: 10.1038/sj.onc.1207067
10. Zhang W, Chen X, Kato Y, Evans PM, Yuan S, Yang J, et al. Novel Cross Talk of Kruppel-Like Factor 4 and Beta-Catenin Regulates Normal Intestinal Homeostasis and Tumor Repression. *Mol Cell Biol* (2006) 26:2055–64. doi: 10.1128/MCB.26.6.2055-2064.2006
11. Klutstein M, Nejman D, Greenfield R, Cedar H. DNA Methylation in Cancer and Aging. *Cancer Res* (2016) 76:3446–50. doi: 10.1158/0008-5472.CAN-15-3278
12. Subramaniam D, Thombre R, Dhar A, Anant S. DNA Methyltransferases: A Novel Target for Prevention and Therapy. *Front Oncol* (2014) 4:80. doi: 10.3389/fonc.2014.00080
13. Patani H, Rushton MD, Higham J, Teijeiro SA, Oxley D, Cutillas P, et al. Transition to Naive Human Pluripotency Mirrors Pan-Cancer DNA Hypermethylation. *Nat Commun* (2020) 11:3671. doi: 10.1038/s41467-020-17269-3
14. Vernier M, McGuirk S, Dufour CR, Wan L, Audet-Walsh E, St-Pierre J, et al. Inhibition of DNMT1 and ERRalpha Crosstalk Suppresses Breast Cancer Via Derepression of IRF4. *Oncogene* (2020) 39:6406–20. doi: 10.1038/s41388-020-01438-1
15. Baylin SB, Herman JG. DNA Hypermethylation in Tumorigenesis: Epigenetics Joins Genetics. *Trends Genet* (2000) 16:168–74. doi: 10.1016/s0168-9525(99)01971-x
16. Tenen DG. Disruption of Differentiation in Human Cancer: AML Shows the Way. *Nat Rev Cancer* (2003) 3:89–101. doi: 10.1038/nrc989
17. Lomberk GA, Iovanna J, Urrutia R. The Promise of Epigenomic Therapeutics in Pancreatic Cancer. *Epigenomics* (2016) 8:831–42. doi: 10.2217/epi-2015-0016
18. Caiado F, Maia-Silva D, Jardim C, Schmolka N, Carvalho T, Reforco C, et al. Lineage Tracing of Acute Myeloid Leukemia Reveals the Impact of Hypomethylating Agents on Chemoresistance Selection. *Nat Commun* (2019) 10:4986. doi: 10.1038/s41467-019-12983-z
19. Romero-Garcia S, Prado-Garcia H, Carlos-Reyes A. Role of DNA Methylation in the Resistance to Therapy in Solid Tumors. *Front Oncol* (2020) 10:1152. doi: 10.3389/fonc.2020.01152
20. Higdon JV, Delage B, Williams DE, Dashwood RH. Cruciferous Vegetables and Human Cancer Risk: Epidemiologic Evidence and Mechanistic Basis. *Pharmacol Res* (2007) 55:224–36. doi: 10.1016/j.phrs.2007.01.009
21. Thomson CA, Ho E, Strom MB. Chemopreventive Properties of 3,3'-Diindolylmethane in Breast Cancer: Evidence From Experimental and Human Studies. *Nutr Rev* (2016) 74:432–43. doi: 10.1093/nutrit/nuw010

22. Fujioka N, Ainslie-Waldman CE, Upadhyaya P, Carmella SG, Fritz VA, Rohwer C, et al. Urinary 3,3'-Diindolylmethane: A Biomarker of Glucobrassicin Exposure and Indole-3-Carbinol Uptake in Humans. *Cancer Epidemiol Biomarkers Prev* (2014) 23:282–7. doi: 10.1158/1055-9965.EPI-13-0645
23. Jia Y, Zhou J, Luo X, Chen M, Chen Y, Wang J, et al. KLF4 Overcomes Tamoxifen Resistance by Suppressing MAPK Signaling Pathway and Predicts Good Prognosis in Breast Cancer. *Cell Signal* (2018) 42:165–75. doi: 10.1016/j.cellsig.2017.09.025
24. Wang B, Zhao MZ, Cui NP, Lin DD, Zhang AY, Qin Y, et al. Kruppel-Like Factor 4 Induces Apoptosis and Inhibits Tumorigenic Progression in SK-BR-3 Breast Cancer Cells. *FEBS Open Bio* (2015) 5:147–54. doi: 10.1016/j.fob.2015.02.003
25. Yori JL, Seachrist DD, Johnson E, Lozada KL, Abdul-Karim FW, Chodosh LA, et al. Kruppel-Like Factor 4 Inhibits Tumorigenic Progression and Metastasis in a Mouse Model of Breast Cancer. *Neoplasia* (2011) 13:601–10. doi: 10.1593/neo.11260
26. Yu F, Li J, Chen H, Fu J, Ray S, Huang S, et al. Kruppel-Like Factor 4 (KLF4) is Required for Maintenance of Breast Cancer Stem Cells and for Cell Migration and Invasion. *Oncogene* (2011) 30:2161–72. doi: 10.1038/onc.2010.591
27. Cittelly DM, Finlay-Schultz J, Howe EN, Spoelstra NS, Axlund SD, Hendricks P, et al. Progestin Suppression of miR-29 Potentiates Dedifferentiation of Breast Cancer Cells *Via* KLF4. *Oncogene* (2013) 32:2555–64. doi: 10.1038/onc.2012.275
28. Xie VK, Li Z, Yan Y, Jia Z, Zuo X, Ju Z, et al. Dna-Methyltransferase 1 Induces Dedifferentiation of Pancreatic Cancer Cells Through Silencing of Kruppel-Like Factor 4 Expression. *Clin Cancer Res* (2017) 23:5585–97. doi: 10.1158/1078-0432.CCR-17-0387
29. Rong Z, Luo Z, Zhang J, Li T, Zhu Z, Yu Z, et al. GINS Complex Subunit 4, a Prognostic Biomarker and Reversely Mediated by Kruppel-Like Factor 4, Promotes the Growth of Colorectal Cancer. *Cancer Sci* (2020) 111:1203–17. doi: 10.1111/cas.14341
30. Lee SI, Kim DK, Seo EJ, Choi EJ, Kwon YW, Jang IH, et al. Role of Kruppel-Like Factor 4 in the Maintenance of Chemoresistance of Anaplastic Thyroid Cancer. *Thyroid* (2017) 27:1424–32. doi: 10.1089/thy.2016.0414
31. Xiang S, Dauchy RT, Hoffman AE, Pointer D, Frasch T, Blask DE, et al. Epigenetic Inhibition of the Tumor Suppressor ARHI by Light at Night-Induced Circadian Melatonin Disruption Mediates STAT3-Driven Paclitaxel Resistance in Breast Cancer. *J Pineal Res* (2019) 67:e12586. doi: 10.1111/jpi.12586
32. Oghamian S, Sodir NM, Bashir MU, Shen H, Cullins AE, Carroll CA, et al. Reduction of Pancreatic Acinar Cell Tumor Multiplicity in Dnmt1 Hypomorphic Mice. *Carcinogenesis* (2011) 32:829–35. doi: 10.1093/carcin/bgr039
33. Yan J, Tie G, Wang S, Tutto A, DeMarco N, Khair L, et al. Diabetes Impairs Wound Healing by Dnmt1-Dependent Dysregulation of Hematopoietic Stem Cells Differentiation Towards Macrophages. *Nat Commun* (2018) 9:33. doi: 10.1038/s41467-017-02425-z
34. Lee E, Wang J, Yumoto K, Jung Y, Cackowski FC, Decker AM, et al. Dnmt1 Regulates Epithelial-Mesenchymal Transition and Cancer Stem Cells, Which Promotes Prostate Cancer Metastasis. *Neoplasia* (2016) 18:553–66. doi: 10.1016/j.neo.2016.07.007
35. Linnekamp JF, Butter R, Spijker R, Medema JP, van Laarhoven HWM. Clinical and Biological Effects of Demethylating Agents on Solid Tumours - a Systematic Review. *Cancer Treat Rev* (2017) 54:10–23. doi: 10.1016/j.ctrv.2017.01.004

**Conflict of Interest:** The authors declare that the research was conducted in the absence of any commercial or financial relationships that could be construed as a potential conflict of interest.

frontiers in Pharmacology

ORIGINAL RESEARCH
published: 26 August 2021
doi: 10.3389/fphar.2021.627935

# Increased Angiogenin Expression Correlates With Radiation Resistance and Predicts Poor Survival for Patients With Nasopharyngeal Carcinoma

*Shan-Shan Guo[1,2†], Yu-Jing Liang[1,2†], Li-Ting Liu[1,2†], Qiu-Yan Chen[1,2], Yue-Feng Wen[1,2,3], Sai-Lan Liu[1,2], Xue-Song Sun[1,2], Qing-Nan Tang[1,2], Xiao-Yun Li[1,2], Hai-Qiang Mai[1,2]* and Lin-Quan Tang[1,2]**

[1]State Key Laboratory of Oncology in South China, Guangdong Key Laboratory of Nasopharyngeal Carcinoma Diagnosis and Therapy, Sun Yat-sen University Cancer Center, Collaborative Innovation Center for Cancer Medicine, Guangzhou, China, [2]Department of Nasopharyngeal Carcinoma, Sun Yat-sen University Cancer Center, Guangzhou, China, [3]Department of Radiotherapy, Affiliated Cancer Hospital and Institute of Guangzhou Medical University, Guangzhou, China

OPEN ACCESS

**Edited by:**
*Zhe-Sheng Chen, John's University, United States*

**Reviewed by:**
*Feng Wang, Affiliated Hospital of Nantong University, China*
*Longyang Liu, Southern Medical University, China*

***Correspondence:**
*Lin-Quan Tang*
*tanglq@sysucc.org.cn*
*Hai-Qiang Mai*
*maihq@sysucc.org.cn*

*[†]These authors have contributed equally to this work*

**Specialty section:**
*This article was submitted to Pharmacology of Anti-Cancer Drugs, a section of the journal Frontiers in Pharmacology*

**Received:** *10 November 2020*
**Accepted:** *11 August 2021*
**Published:** *26 August 2021*

**Citation:**
*Guo S-S, Liang Y-J, Liu L-T, Chen Q-Y, Wen Y-F, Liu S-L, Sun X-S, Tang Q-N, Li X-Y, Mai H-Q and Tang L-Q (2021) Increased Angiogenin Expression Correlates With Radiation Resistance and Predicts Poor Survival for Patients With Nasopharyngeal Carcinoma. Front. Pharmacol. 12:627935. doi: 10.3389/fphar.2021.627935*

**Background:** Despite the development of such multiple therapeutic approaches, approximately 20% patients experience recurrence. Identification of molecular markers for stratifying the different risks of tumour recurrence and progression is considered imperative.

**Methods:** We used a RayBio Human Cytokine Antibody Array that simultaneously detected the levels of 297 proteins and profiled the conditioned medium of HONE1 cells and the radioresistant NPC cells HONE1-IR. We found Angiogenin(ANG) expression to be significantly increased in HONE1-IR and HONE1-IR cells exposed to 4-Gy X-ray radiation.

**Results:** We investigated the expression of ANG in NPC tissues and explored its prognostic significance in patients with NPC. We found that ANG expression was increased in recurrent NPC tissues. Elevated expression of ANG induced radio-resistance in NPC cells, in addition to being significantly associated with shorter PFS, OS, and LRFS in patients with NPC. Multivariate analysis results revealed that ANG was an independent prognostic factor that predicted PFS, OS, and LRFS. Furthermore, a nomogram model was generated to predict OS in terms of ANG expression.

**Conclusion:** Our results found the radioresistant function of ANG and proved the clinical prognostic significance of ANG, and the results could help predict radio-sensitivity and stratify high-risk patients or tumour recurrence.

**Keywords: angiongenin, biomarker, radio-resistance, nasopharyngeal carcinoma, prognosis**

**Abbreviations:** ANG, angiogenin; CCRT, concurrent chemoradiotherapy; PFS, progression-free survival; DMFS, distant metastasis-free survival; FBS, foetal bovine serum; IC, induction chemoradiotherapy; IHC, immunohistochemistry; IMRT, intensity-modulated radiotherapy; IV, intravenous; LRFS, locoregional recurrence-free survival; NPC, nasopharyngeal carcinoma; OS, overall survival; PFS, progression-free survival; RT, radiotherapy; SDS, sodium dodecyl sulphate; siRNA, small interfering RNA.

## BACKGROUND

Nasopharyngeal carcinoma (NPC) is endemic in southern China and South-East Asia (Chen et al., 2019). Radiotherapy (RT) is the primary treatment for the non-metastatic disease. For early-stage NPC, RT alone is the recommended treatment, whereas for locoregional NPC, concurrent chemoradiotherapy (CCRT) and induction chemoradiotherapy (IC) + CCRT constitute the standard treatment strategy (Lam and Chan, 2018). Despite the development of such multiple therapeutic approaches, approximately 20% patients experience recurrence (Lee et al., 2019). Although the American joint Committee on cancer (AJCC) staging system can differentiate the prognoses for patients with NPC, patients with the same tumour stage may also show heterogeneity in clinical outcomes. Therefore, identification of molecular markers for stratifying the different risks of tumour recurrence and progression is considered imperative. Development of novel biomarkers might enable better prediction of prognosis for patients with NPC and help develop potential therapeutic targets.

Angiogenin (ANG) is a secreted ribonuclease best known for its ability to promote blood vessel formation (Lyons et al., 2017). It has been reported to promote the metastasis of colorectal cancer cells (Li et al., 2019), proliferation and invasion of lung squamous carcinoma cells (Xu et al., 2016), and tumorigenesis in bladder cancer (Peres et al., 2016). Additionally, ANG can mediate tumour angiogenesis in prostate cancer and the proliferation in prostate cancer cells (Vanli and Guo-Fu, 2015). Recently, serum ANG level has been found to be a prognostic factor for numerous tumours, such as glioblastoma (Hu et al., 2019), non-Hodgkin lymphoma (Fang et al., 2011), cervical cancer (Landt et al., 2011), and laryngeal carcinoma (Marioni et al., 2010). Gino et al. investigated ANG by immunohistochemistry (IHC) in 15 Caucasian patients with NPC and found a trend towards significant inverse correlation between ANG expression and disease-free survival (Marioni et al., 2010). However, due to the very small sample size and all patients being of Caucasian origin, the results of this study would require further validation by other studies with larger sample size in prevalent districts. To date, no study has investigated the prognostic value of ANG in a prevalent district. Hence, exploring the prognostic significance of ANG for patients with NPC in a prevalent district was considered necessary.

In the present study, we used a RayBio Human Cytokine Antibody Array that simultaneously detected the levels of 297 proteins and profiled the conditioned medium of HONE1 cells and the radioresistant NPC cells HONE1-IR. We found ANG expression to be significantly increased in HONE1-IR and HONE1-IR cells exposed to 4-Gy X-ray radiation. Subsequently, we investigated the expression of ANG in NPC tissues and explored its prognostic significance in patients with NPC. Finally, we hypothesised that ANG expression could be a potential prognostic factor for patients with NPC.

**TABLE 1 |** Characteristics of the NPC patients.; Abbreviation: CCRT, concurrent chemoradiotherapy; ECOG, Eastern Cooperative Oncology Group; IC, induction chemotherapy; NPC, nasopharyngeal carcinoma; RT, radiotherapy; WHO, World Health Organization.

| Characteristics | Angiogenin | | *p* Value |
|---|---|---|---|
| | Low expression | High expression | |
| Age | | | 0.811 |
| ≤49 | 46 | 40 | |
| >49 | 46 | 43 | |
| Gender | | | |
| Female | 18 | 20 | 0.468 |
| Male | 74 | 63 | |
| T stage | | | 0.499 |
| 1 | 4 | 6 | |
| 2 | 11 | 15 | |
| 3 | 50 | 38 | |
| 4 | 27 | 24 | |
| N stage | | | 0.537 |
| 0 | 18 | 17 | |
| 1 | 26 | 29 | |
| 2 | 36 | 24 | |
| 3 | 12 | 13 | |
| Clinical stage | | | 0.327 |
| 1 | 2 | 2 | |
| 2 | 8 | 14 | |
| 3 | 41 | 36 | |
| 4 | 41 | 31 | |
| WHO Type | | | 0.06 |
| 1 | 0 | 1 | |
| 2 | 5 | 0 | |
| 3 | 87 | 80 | |
| ECOG score | | | 1.000 |
| 0 | 2 | 2 | |
| 1 | 90 | 81 | |
| Smoking history | | | 0.816 |
| 0 | 55 | 53 | |
| 1 | 37 | 30 | |
| EBV DNA | | | 0.811 |
| ≤4,000 | 46 | 40 | |
| >4,000 | 46 | 43 | |
| Treatment strategy | | | 0.43 |
| RT | 10 | 12 | |
| CCRT | 35 | 24 | |
| IC + CCRT | 47 | 47 | |

## MATERIALS AND METHODS

### Ethics Statement

This study was approved by the Institutional Review Board of Sun Yat-Sen University Cancer Center. All patients signed a written informed consent for the collection of tissue samples.

### Patient Recruitment and Follow-Up

The expression of ANG in tissue cells was evaluated in NPC tumour samples that were obtained before treatment from 175 histologically confirmed patients with NPC, who were prospectively enrolled between January 2010 and November 2011. Entry criteria for patients were as follows: histologically proven NPC, with stage I–IVa (according to the eighth edition of the AJCC/UICC staging system), no distant metastasis at

diagnosis, no anti-cancer treatment received prior to admission, no other tumour types or serious illness, and radical intensity-modulated radiotherapy (IMRT) received during treatment. Staging examinations included the following: magnetic resonance imaging of head and neck, chest radiograph, bone scintigraphy, and ultrasonography of the abdominal region of all patients. The median age of all the included patients was 49 years, ranging from 19 to 70 years. There were 137 male and 38 female patients, with a sex ratio of 3.6:1. The characteristics of the 175 patients with NPC were shown in **Table 1**.

The treatment regimens included RT alone, CCRT, and IC + CCRT. IMRT was performed for all the included patients, in accordance with the treatment policy for NPC at Sun Yat-Sen University Cancer Center (SYSUCC). The chemotherapy regimen used for IC was PF (intravenous (IV) administration of 80–100 mg/m$^2$ cisplatin on day 1 and that of 800 mg/m$^2$/d 5-Fu continuously over days 1–5). The chemotherapy regimen was repeated every 3 weeks for 2–3 cycles. Concurrent chemotherapy primarily included the IV administration of 80–100 mg/m$^2$ cisplatin every 3 weeks.

After the completion of treatment, patients were followed up every month for the first 3 months, every 3 months over 3 years, every 6 months for the next 2 years, and annually thereafter. Median follow-up time for the patients was 83 months (range, 5–106 months).

## IHC

The antibody used in the study was anti-ANG (cat. no. 0555–5,008, AbD Serotec, MorphoSys, Oxford, United Kingdom). Tissue sections were de-paraffinised with xylene and rehydrated with ethanol. Hydrogen peroxide (3%) was used to remove any endogenous peroxidase. Tissue slices were incubated with pepsin (no. ZLI-9013, ZSGB-Bio, Beijing, China) at 37°C for 20 min for antigen retrieval. The samples were incubated with the primary antibodies (1:100 dilution) overnight at 4°C. The sections were then washed with PBS and incubated with secondary antibodies (EnVision, Dako, Carpinteria, CA, United States) for 20 min at 37 °C; 3,3′-Diaminobenzidine was used to visualise the antigens. Sections were counterstained with haematoxylin. Hydrochloric acid-alcohol was used for differentiation. The scoring system for IHC, to generate the immunoreactivity score, was used as described previously (Waisberg et al., 2014). Two independent pathologists, without prior knowledge of the clinical origin of the specimen, evaluated each specimen.

## Cell Lines and Culture Conditions

The NPC cell line, HONE1, and the radioresistant NPC cell line, HONE1-IR, were cultured in RPMI 1640 medium (Gibco) supplemented with 5% foetal bovine serum (FBS; Gibco). The cell lines were cultured in a humidified incubator containing 5% $CO_2$ at 37°C. Regular morphological observations and tests for the absence of mycoplasma contamination (MycoAlert, Lonza) were conducted for the authentication of all the cell lines used in this study. The radioresistant NPC cell line HONE1-IR has been validated in our previous study (Guo et al., 2020).

## Small Interfering RNA Transfection

Transient transfection of HONE1-IR cells was performed using Lipofectamine RNAiMax (cat. no. 1795160; Invitrogen) according to the manufacturer's instructions. HONE1-IR cells were seeded onto six-well plates at a density of $1.5 \times 10^5$ cells/well 1 day prior to transfection. They were transfected with 50 pmol siRNA and subjected to clone formation at 24 h post-transfection. Scramble siRNA was purchased from Ruibo (Guangzhou, China). The siRNA sequences for *ANG* was 5′-CGTTGTTGTTGCTTGTGAA-3′.

## Western Blot Analysis

Cells were collected and lysed in sodium dodecyl sulphate (SDS) sample buffer (62.5 mM Tris-HCl [pH 6.8], 3% SDS, 10% glycerol, 50 mM DL-dithiothreitol, and 0.1% bromophenol blue) containing protease inhibitors (Roche, Indianapolis, IN, United States). Protein concentrations were tested using the BCA method (Pierce, Thermo Fisher Scientific, Rockford, IL, United States). Proteins (20 μg) were separated by SDS-polyacrylamide gel electrophoresis and transferred to polyvinylidene difluoride membranes. Bovine serum albumin (5%) in TBS-T (1 M Tris-HCl [pH 7.5], 0.8% NaCl, and 0.1% Tween 20) was used to block the membranes. The membranes were then incubated with primary antibodies (1:100 dilution) at 4°C overnight, followed by incubation with horseradish peroxidase-conjugated secondary antibodies (Pierce). Proteins were then visualised by enhanced chemiluminescence (Pierce). Antibodies against β-actin (cat. no. 66009-1-Ig; Proteintech) and ANG (cat. no. 0555–5,008, AbD Serotec, Kidlington, United Kingdom) were used in the experiments.

## Clonogenic Assay for Radio-Sensitivity and Irradiation

A total of $1 \times 10^3$ cells were seeded onto 3-cm dishes and incubated for 10 days after exposure to various doses of irradiation. After visual verification of colony formation, cells were briefly stained with 0.1% crystal violet in 100% methanol. Colonies that consisted of 100 or more cells were counted as clonogenic survivors. The surviving fraction was calculated by dividing the number of colonies by the number of seeded cells and then multiplying it by the plating efficiency, which is defined as the (number of colonies formed/number of cells seeded) × 100%. All the experiments were repeated independently at least thrice. An X-ray irradiation instrument with 4.2 kW X-rays (RS 2000; Rad Source Technologies Inc.), available at SYSUCC, was used to irradiate the cells. The uniformity of irradiation was appreciable, and the difference was less than 5%. Dose rate for irradiating the cells was 1.26 Gy/min.

## Cell Cycle and Cell Apoptosis Analysis

Cell cycle was studied on HONE1 cells as control and knock-down the expression of ANG by siRNA interfering at 48 h post-culture, the $5 \times 10^5$ cells plated in 6 wells plate were harvested, fixed in 70% ethanol over-night and stained with 500 μl of propidium iodure for 30 min at 37°C. Apoptosis analysis was performed by using FITC Annexin V Apoptosis Detection Kit with PI(Catalog: 556547, Lot: 4136994, BD Biosciences) according to the manufacturer's instructions. Samples were

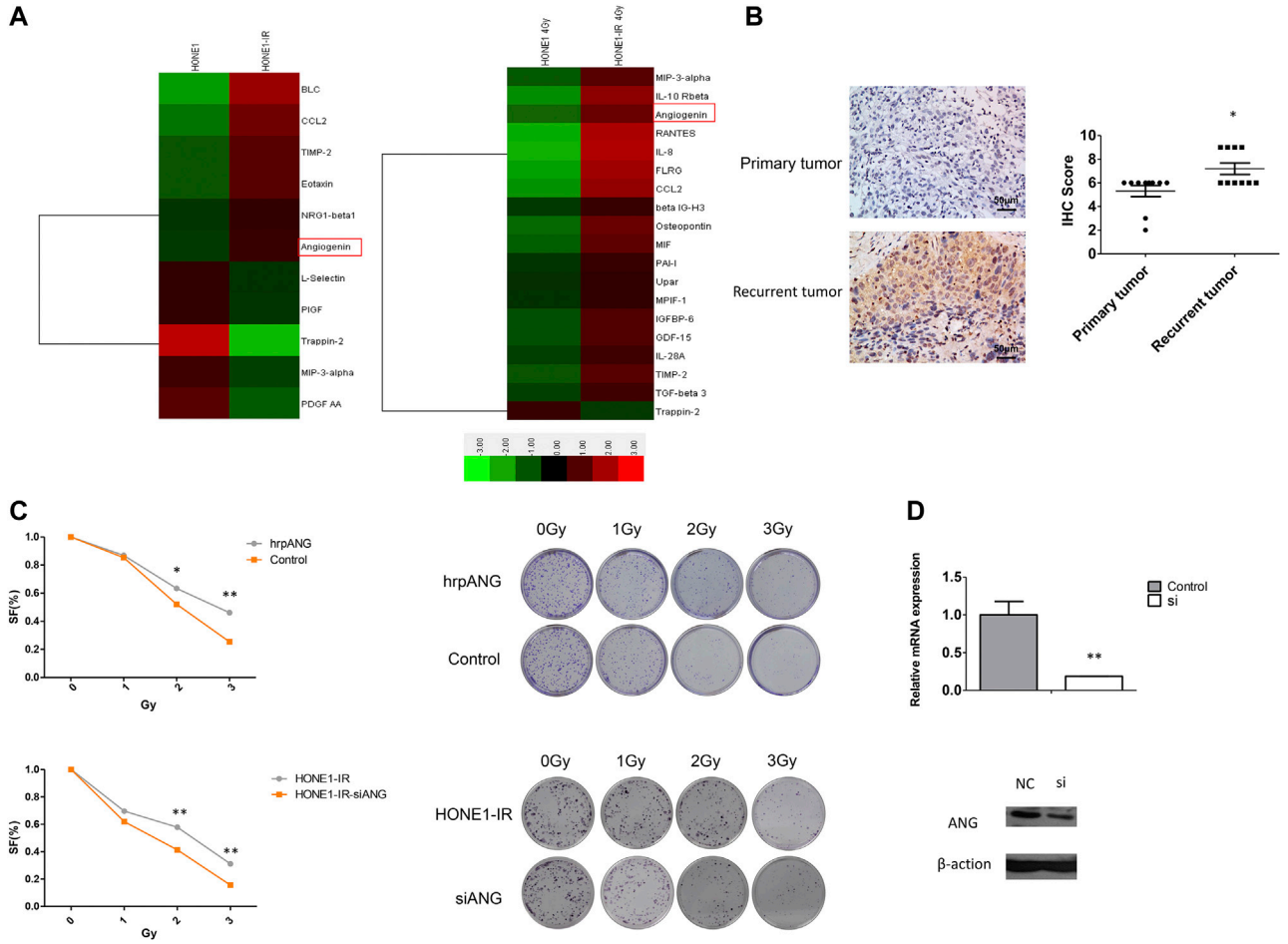


**FIGURE 1 |** Angiogenin (ANG) expression was elevated in radioresistant NPC cells and recurrent tumour tissues. **(A)** Heat maps show the expression pattern of 11 genes in HONE1 vs. HONE1-IR cells and 19 genes in HONE1 vs. HONE1-IR cells after 4-Gy irradiation, derived from unsupervised clustering analysis. Red or green reflects high or low expression, respectively, as indicated in the scale bar (Raw Z score). **(B)** The differential IHC scores of tumour tissues, regarding ANG expression, from 10 patients with NPC before initial treatment and after tumour recurrence in the same patients. * $p < 0.05$ following nonparametric tests. **(C)** The human recombinant protein ANG (hrp-ANG) led to increased radio-resistance, as seen by colony formation assays in HONE1 cells (upper panel). Radiation sensitivity was tested by colony formation assays in HONE1-IR cells and those transfected with CCL2-siRNAs (lower panel). Survival curves are constructed based on means ± SEM; * $p < 0.05$, ** $p < 0.001$. **(D)** ANG mRNA expression and protein expression were significantly decreased in HONE1-IR cells transfected with ANG-siRNAs.

analyzed by flow cytometry (FACS, AriaIII, and BD, United States) and all tests were repeated three times (in Triplicate).

## Statistical Analysis

A chi-squared analysis was used to compare the incidence rates with categorical variables. Survival rates were calculated using the Kaplan-Meier method and compared using log-rank tests. Multivariate analyses were performed using the Cox proportional hazards model. Hazard ratio point and interval (95% confidence interval) estimates were computed using the Cox proportional hazards model. ANG expression was adjusted for patient sex, age, T stage, N stage, UICC stage, and EBV DNA in the Cox proportional hazards model. Locoregional recurrence-free survival (LRFS) was defined as the time interval from the beginning of treatment to the date of first observation of local and/or regional recurrence or censored at the date of the last follow-up. Distant metastasis-free survival (DMFS) was defined as the time interval from the beginning of treatment to the date of first observation of distant lesions or censored at the date of last follow-up. Progression-free survival (PFS) was defined as the time interval from the beginning of treatment to the date of first observation of recurrence, distant metastasis, or death; alternatively, PFS was censored at the date of last follow-up. Overall survival (OS) was defined as the time interval from the beginning of treatment to the date of death or censored at the date of last follow-up.

The Statistical Package for Social Sciences version 18.0 software program (SPSS Inc., Chicago, IL, United States) was used for our analysis. A prognostic nomogram was established with significant variables for OS in the Cox regression model using the survival and rms package in R 4.0.0. The predictive accuracy and discriminative ability of this nomogram were evaluated using the C-index. All *p*-values were two sided, and $p < 0.05$ was considered statistically significant.

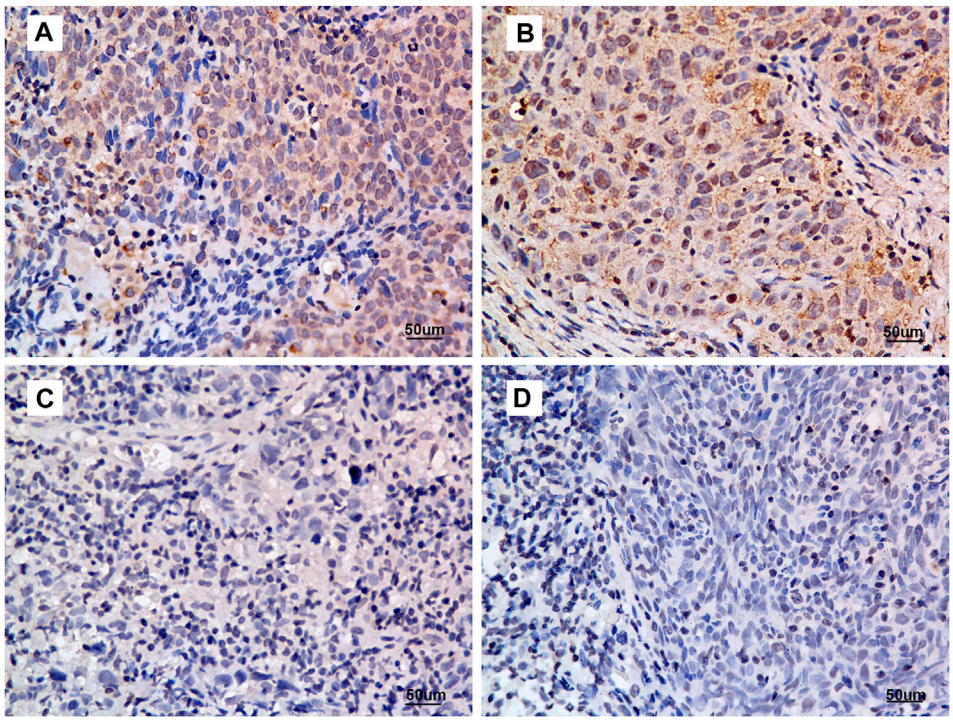


**FIGURE 2 |** Criteria for ANG expression intensity scoring. **(A)** intensity score = 3, **(B)** intensity score = 2, **(C)** intensity score = 1, and **(D)** intensity score = 0. Representative micrographs are shown (400×). All micrographs were collected and processed under identical conditions.

# RESULTS

## ANG-Mediated Radio-Resistance in NPC Cells *In vitro* and its Correlation With NPC Recurrence

Previously, we had used cytokine antibody array test on radioresistant NPC cell line HONE-IR and its original cell line HONE1, as mentioned in our previous study (Guo et al., 2020), and found ANG to be significantly elevated in HONE1-IR cells, and significantly increased further by radiation (**Figure 1A**). Therefore, we speculated ANG to be correlated with radio-resistance and tumour recurrence in NPC. Ten pairs of tumour tissues from primary NPC and normal tissues from the same patient, presenting tumour recurrence, were tested by IHC. The IHC scores showed ANG expression in recurrent NPC tissues to be significantly higher than that in primary tumour tissues (**Figure 1B**).

Since ANG is a secreted protein, we used hrp-ANG (cat. no. 265-AN; R&D Systems, Minneapolis, MN, USA) to investigate whether ANG could modulate radio-resistance in NPC cells. We found hrp-ANG-treated HONE1 cells to present increased resistance to IR than control cells (**Figure 1C** upper panel). In addition, we used specific siRNAs to knock down ANG in HONE1-IR cells; colony formation assays indicated ANG knockdown to markedly decrease colony formation after irradiation (**Figure 1C** lower panel). The efficacy of siRNAs for knocking down ANG expression is shown in **Figure 1D**.

## ANG as an Independent Prognostic Factor for Clinical Outcomes in Patients With NPC

The IHC scores of 175 primary tumour tissues were analysed to identify the prognostic value of ANG in NPC. **Figure 2** presents the intensity score of ANG expression in NPC tissues. The baseline data for patient characteristics were well balanced (**Table 1**). The study included 38 women (21.7%) and 137 men (78.3%), with a median age of 49 years (range, 19–78 years). Four patients (2.3%) were classified to be in stage I, 22 (12.6%) in stage II, 77 (44.0%) in stage III, and 72 (41.1%) in stage IV. The median follow-up time was 83 months (range, 5–106 months).

After regular follow-up, a total of 44 patients presented tumour progression, 31 presented distant metastasis, eight presented locoregional recurrence, and 31 died. For all the included patients, 5-years OS was 86.5%, 5-years PFS was 77.0%, 5-years LRFS was 91.1%, and 5-years DMFS was 83.3%.

Five-year LRFS was significantly better in the low ANG-expression group than in the high ANG-expression group (95.1 vs. 85.4%, $p = 0.026$). Similarly, 5-year PFS was significantly better in the low ANG-expression group than in the high ANG-expression group (83.6 vs. 68.5%, $p = 0.049$).

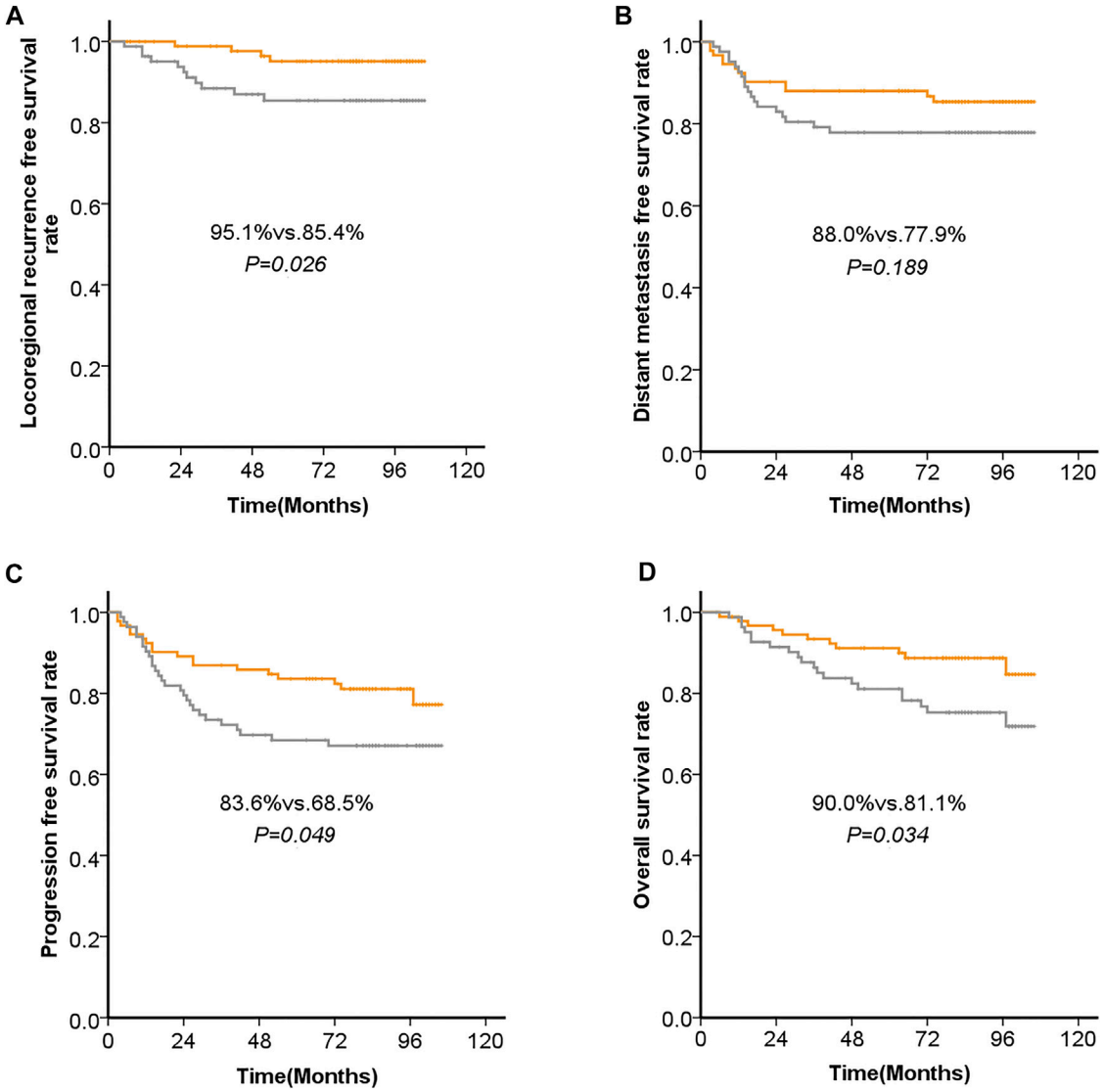


**FIGURE 3 |** Kaplan-Meier analysis of **(A)** the 5-years locoregional recurrence-free survival (LRFS), **(B)** 5-years distant metastasis-free survival (DMFS), **(C)** progression-free survival (PFS), and **(D)** overall survival (OS), with regard to the expression levels of ANG in patients with NPC before initial treatment.

Five-year OS was also significantly better in the low ANG-expression group than in the high ANG-expression group (90.0 vs. 81.1%, $p$ = 0.034). However, there was no significant difference between the low and high ANG-expression groups regarding 5-years DMFS. The survival curves based on Kaplan-Meier method, for patients with NPC, regarding ANG expression level, are shown in **Figure 3**.

In multivariate analysis, ANG expression was significantly associated with 5-years OS, PFS, and LRFS. Results from the multivariate Cox regression analysis are shown in **Table 2**. ANG expression was significantly associated with 5-years OS (p = 0.022), HR of 2.428 (95%CI, 1.134–5.200); PFS ($p$ = 0.014), HR of 2.160 (95%CI, 1.165–4.005); and LRFS ($p$ = 0.028), HR of 3.767 (95%CI, 1.153–12.309). Additionally, the results of multivariate analysis revealed that T stage, N stage, and EBV DNA were significantly associated with OS and DMFS, while T stage and N stage were significantly associated with PFS. The results of multivariate analysis of Cox proportional hazard regression were shown in **Table 2**.

## Prognostic Nomogram for OS

A prognostic nomogram for OS was established, containing significant prognostic variables such as T stage, N stage, EBV DNA, and ANG (**Figure 4A**). The nomogram showed T stage and N stage to contribute the most to the prognosis of OS, whereas ANG and EBV DNA were also found to play important roles. Each subtype of the aforementioned variables was assigned a grade-point score. A straight line could easily be drawn to determine the estimated proportion of OS rate at each time point by adding up the total score and positioning it on the

**TABLE 2 |** The multivariate analysis of Angiogenin in NPC patients.

| | HR | 95%CI | *p* Value |
|---|---|---|---|
| LRFS | | | |
| Age | 1.420 | 0.487–4.139 | 0.521 |
| Gender | 0.526 | 0.155–1.780 | 0.302 |
| T stage | 1.507 | 0.502–4.524 | 0.465 |
| N stage | 1.204 | 0.642–2.256 | 0.563 |
| Clinical stage | 1.867 | 0.546–6.386 | 0.320 |
| EBV DNA | 1.070 | 0.301–3.805 | 0.916 |
| Angiogenin | 3.767 | 1.153–12.309 | 0.028 |
| DMFS | | | |
| Age | 1.212 | 0.594–2.474 | 0.596 |
| Gender | 1.416 | 0.407–4.931 | 0.584 |
| T stage | 2.968 | 1.326–6.644 | 0.008 |
| N stage | 2.017 | 1.220–3.334 | 0.006 |
| Clinical stage | 0.698 | 0.270–1.802 | 0.457 |
| EBV DNA | 2.998 | 1.251–7.184 | 0.014 |
| Angiogenin | 1.636 | 0.772–3.468 | 0.199 |
| OS | | | |
| Age | 1.044 | 0.511–2.133 | 0.906 |
| Gender | 1.408 | 0.407–4.874 | 0.589 |
| T stage | 4.581 | 1.752–11.978 | 0.002 |
| N stage | 1.987 | 1.236–3.196 | 0.005 |
| Clinical stage | 0.480 | 0.165–1.398 | 0.178 |
| EBV DNA | 2.793 | 1.243–6.278 | 0.013 |
| Angiogenin | 2.428 | 1.134–5.200 | 0.022 |
| PFS | | | |
| Age | 1.168 | 0.647–2.109 | 0.606 |
| Gender | 0.792 | 0.354–1.772 | 0.570 |
| T stage | 2.387 | 1.251–4.557 | 0.008 |
| N stage | 1.661 | 1.140–2.422 | 0.008 |
| Clinical stage | 1.103 | 0.529–2.297 | 0.794 |
| EBV DNA | 1.877 | 0.959–3.674 | 0.066 |
| Angiogenin | 2.160 | 1.165–4.005 | 0.014 |

*Abbreviations: CI, confidence interval; DMFS, distant metastasis free survival; GPS, glasgow prognostic score; HR, hazard ratio; LRFS, locoregional recurrence free survival; OS, overall survival; PFS, progression free survival.*

total score scale. Harrell's C-index of the established nomogram (to predict OS) was 0.80 (95% CI, 0.73–0.87), displaying a model with favourable discriminative capacity. Calibration curves for the 3-years and 5-years OS probabilities displayed optimal agreement between the actual observed survival rate and nomogram prediction (**Figure 4B**).

## DISCUSSION

Although the local control of NPC can be increased by IMRT rather than conventional radiotherapy, approximately 20% of the patients still present locoregional recurrence following radical IMRT (Lee et al., 2019). Survival of the recurrent patients with NPC remains low, and the side effects after re-radiotherapy as a treatment for recurrent NPC are severe (e.g., bleeding) (Karam et al., 2016). Tumour recurrence has been recommended to have relationship strong association with radio-resistance (Barker et al., 2015). Any biomarker that can help identify radio-sensitivity would be useful in this context; therefore, possible candidates for predicting tumour recurrence and progression are urgently required.

In the present study, we found ANG to promote radio-resistance in NPC cells. In addition, we found ANG to be an independent prognostic factor for OS, PFS, and LRFS. To the best of our knowledge, this is the first study to identify the radioresistant function and prognostic significance of ANG in NPC. The results of our study could help stratify patients with different degrees of risk and guide clinical treatment strategies.

The possible mechanism underlying ANG-promoted radio-resistance in NPC cells is as follows: Since microvesicles derived from mesenchymal stem cells are known to promote angiogenesis, Chen et al. (2014) used an antibody array and found that Angiogenin, VEGF, IGF, Tie-2/TEK, and IL-6 which were higher in microvesicles under hypoxic conditions than under normoxic conditions, which revealed that ANG might be responsible for the hypoxia-augmented proangiogenic effects of microvesicles. In addition, Chang et al. (2017) found several angiogenic cytokines in the medium, including ANG, which promoted the formation of tubules across human umbilical cord vein endothelial cells and protected the cells against radiation-induced apoptosis *in vitro*. Yamasaki et al. (2009) showed ANG and tiRNAs to participate in a process of stress-induced translational repression. ANG may be a stress-induced factor that protects adjacent or distant cells from the deleterious effects of environmental stress. Studies have demonstrated ANG to induce cell survival, proliferation, endothelial tube formation, xenograft angiogenesis, cell migration, angiogenesis, and tumour suppressor gene expression (Miyake et al., 2015; Peres et al., 2016). Hence, ANG may protect NPC cells from the radiation-induced hypoxia-modulated environmental stress and induce cell survival, proliferation, and radio-resistance. However, the exact mechanism warrants further study. As we further did experiments of cell cycle showed that more cells stayed in S and G2/M phase after siRNA interfered ANG in HONE1 cells (**Supplementary Figure S1A**). So we speculated that knocked down ANG lead to more cells stayed in G2/M to be more radiosensitive, as previous studies mentioned that cells being most radiosensitive in the G (2)-M phase, less sensitive in the G (1) phase (Pawlik and Keyomarsi, 2004). In addition, knocked down the expression of ANG contributed to cell apoptosis as shown in **Supplementary Figure S1B**, revealed that ANG's anti-apoptosis function, which was in accordance with previous studies (Li et al., 2014; Shu-Ping and Guo-Fu, 2015). It is possible that the function on cell cycle and apoptosis of ANG results in the radioresistant function of ANG. We also tested the cell migration after knocked down ANG expression and found that ANG promoted cell migration, which was in accordance with previous studies (Schwartz et al., 2007; Li et al., 2019) and maybe it is associated with its angiogenesis function and accelerated metastasis. Further studies are in urgently need to explain this results.

In the current study, we found the IHC scores of ANG in recurrent NPC tissues to be significantly higher than those in primary tumour tissues, and ANG expression was significantly associated with tumour recurrence in NPC. Since previous studies have indicated tumour recurrence to be related to radio-resistance (Chen et al., 2014; Yang et al., 2020), these findings collectively indicate that ANG expression may be an important biomarker of radio-resistance in patients with NPC.

Previous studies on other tumours have found ANG expression to be a prognostic factor for tumour recurrence,

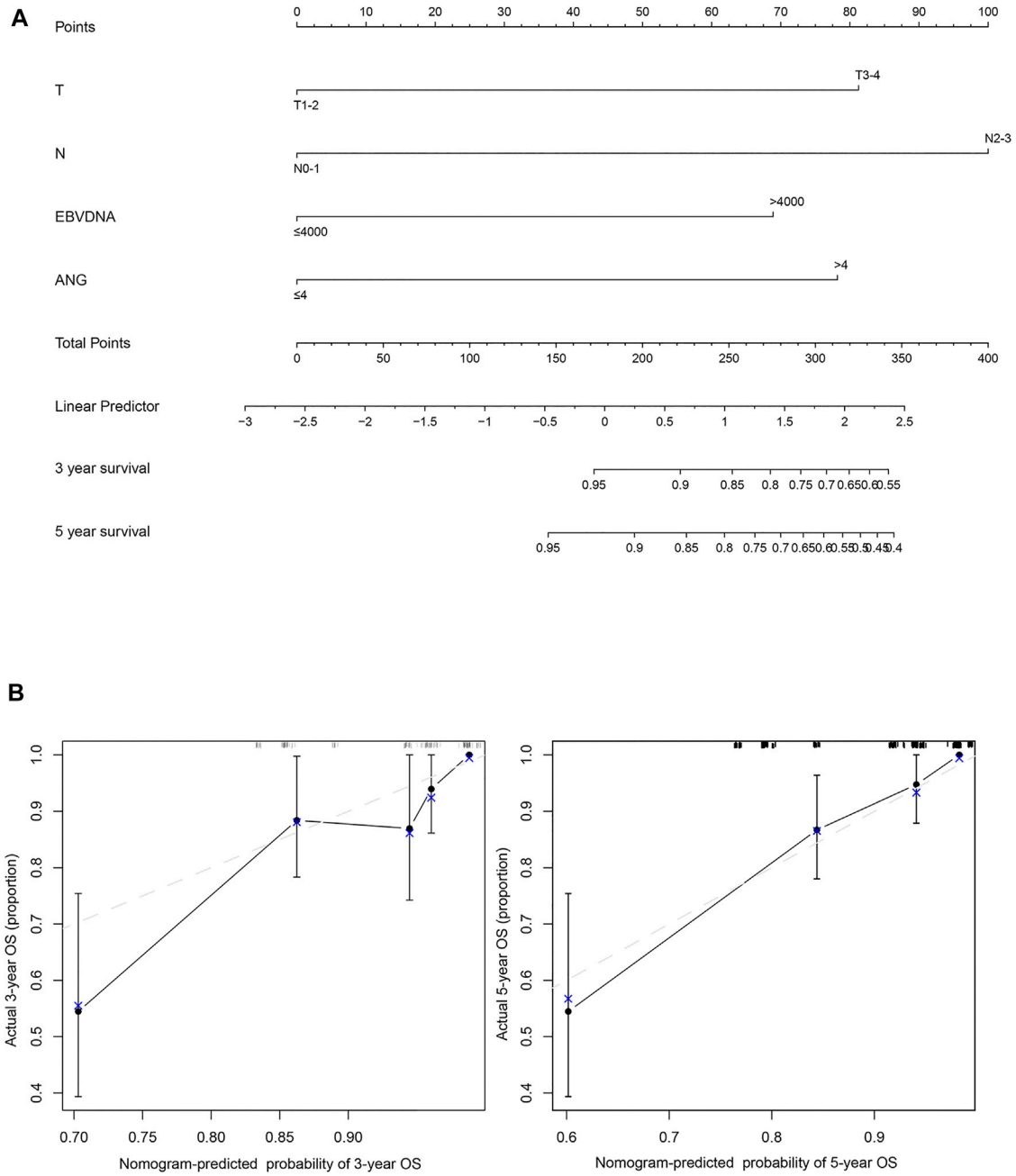


**FIGURE 4 |** The nomogram and model calibration curve. **(A)** Nomogram including T stage, N stage, EBV DNA, and ANG expression levels in patients with nasopharyngeal carcinoma. **(B)** Model calibration curve showing the predicted and actual probabilities of ANG expression.

tumour progression, and OS. For example, a study analysed ANG expression in 108 operable laryngeal squamous cell carcinoma tissues and found ANG expression to be related to carcinoma recurrence rate and disease-free survival (DFS) (Marioni et al., 2010). Previous studies have found ANG expression to be significantly high in cases with loco-regional recurrent disease in laryngeal squamous cell carcinoma (Marioni et al., 2014; Lovato et al., 2015); ANG expression ≥ 5.0% is considered a significant, independent, negative prognostic factor in terms of DFS (Chen et al., 2014; Yang et al., 2020). Hu et al. found high ANG expression to be an independent indicator of shorter OS in proneural glioblastoma (Chen et al., 2014; Yang et al., 2020). Eppenberger et al. tested 305 primary breast tumours and found ANG levels to be positively correlated with disease relapse in patients with breast cancer (Eppenberger et al., 1998). Our results, regarding ANG being an independent prognostic factor for OS, PFS, and LRFS are in accordance with the results reported by previous studies. These results collectively recommended ANG as

an effective prognostic factor for predicting clinical outcomes in patients with NPC. Since most studies have reported the prognostic significance of ANG on LRFS, PFS, and OS, but not on DMFS, the finding that ANG could not predict DMFS was in accordance with previous studies.

Based on the significant impact of ANG on the survival of patients with NPC and the excellent quantitative ability of the nomogram, a simple and easy-to-use clinical prediction model was established to clinically predict OS in NPC. The nomogram demonstrated favourable discriminative capacity and satisfactory agreement between the predicted and actual results.

There are a few limitations of our study. First, the present study did not explore the exact biological mechanisms underlying ANG-induced radio-resistance. Secondly, the samples of NPC tissues were extracted from a single centre; therefore, further studies incorporating tumour samples from multiple cancer centres should be conducted to validate our results in the future.

In the present study, we found ANG expression to be increased in recurrent NPC tissues. Elevated expression of ANG induced radio-resistance in NPC cells, in addition to being significantly associated with shorter PFS, OS, and LRFS in patients with NPC. Multivariate analysis results revealed that ANG was an independent prognostic factor that predicted PFS, OS, and LRFS. Furthermore, we designed a nomogram model to predict OS in terms of ANG expression. Our results provided a new perspective on the therapeutic strategies of NPC; it could help predict radio-sensitivity and stratify high-risk patients or tumour recurrence.

## DATA AVAILABILITY STATEMENT

The raw data supporting the conclusion of this article will be made available by the authors, without undue reservation. The authenticity of this article has been validated by uploading the key raw data onto the Research Data Deposit public platform (www.researchdata.org.cn), with the approval RDD number as RDDB2020000965.

## ETHICS STATEMENT

The studies involving human participants were reviewed and approved by Sun Yat-sen University Cancer Center. The patients/participants provided their written informed consent to participate in this study.

## AUTHOR CONTRIBUTIONS

Study concepts: L-QT, H-QM, and S-SG. Study design: S-SG and H-QM. Data acquisition: S-SG, L-QT, L-TL, Y-FW, X-SS, S-LL, Q-NT, X-YL, and LG. Quality control of data and algorithms: S-SG, L-QT, and Q-YC. Data analysis and interpretation: S-SG, L-TL, X-YL, X-SS, and S-LL Statistical analysis: S-SG. Manuscript preparation: S-SG and L-TL. Manuscript editing: S-SG, L-QT, and H-QM. Manuscript review: H-QM.

## FUNDING

This work was supported by grants from the National Key R&D Program of China (2017YFC1309003, 2017YFC0908500), the National Natural Science Foundation of China (No. 81425018, No. 81672868, No. 81802775, No. 82002852, No. 82003267), the Sci-Tech Project Foundation of Guangzhou City (201707020039), the Sun Yat-sen University Clinical Research 5,010 Program, the Special Support Plan of Guangdong Province (No. 2014TX01R145), the Natural Science Foundation of Guangdong Province (No. 2017A030312003, No. 2018A0303131004), the Natural Science Foundation of Guangdong Province for Distinguished Young Scholar (No. 2018B030306001), the Sci-Tech Project Foundation of Guangdong Province (No. 2014A020212,103), the Health & Medical Collaborative Innovation Project of Guangzhou City (No. 201400000001, No.201803040003), Pearl River S&T Nova Program of Guangzhou (No. 201806010135), the Planned Science and Technology Project of Guangdong Province (2019B020230002), the National Science and Technology Pillar Program during the Twelfth Five-year Plan Period (No. 2014BAI09B10), Natural Science Foundation of Guangdong Province (2017A030312003,and the Fundamental Research Funds for the Central Universities.

## SUPPLEMENTARY MATERIAL

The Supplementary Material for this article can be found online at: https://www.frontiersin.org/articles/10.3389/fphar.2021.627935/full#supplementary-material

**Supplementary Figure S1** | **(A)** Typical flow cytometry of HONE1 cells cycle arrest, **(B)** apoptosis analysis by flow cytometry of HONE1 cells. **(C)** Transwell assay showed the cell migration of HONE1 cells. **(D)** The relative mRNA expression of HONE1 cells.

## REFERENCES

Barker, H. E., Paget, J. T., Khan, A. A., and Harrington, K. J. (2015). The Tumour Microenvironment after Radiotherapy: Mechanisms of Resistance and Recurrence. *Nat. Rev. Cancer* 15 (7), 409–425. doi:10.1038/nrc3958

Chang, P. Y., Zhang, B. Y., Cui, S., Qu, C., Shao, L. H., Xu, T. K., et al. (2017). MSC-derived Cytokines Repair Radiation-Induced Intra-villi Microvascular Injury. *Oncotarget* 8 (50), 87821–87836. doi:10.18632/oncotarget.21236

Chen, J., Liu, Z., Hong, M. M., Zhang, H., Chen, C., Xiao, M., et al. (2014). Proangiogenic Compositions of Microvesicles Derived from Human Umbilical Cord Mesenchymal Stem Cells. *PLoS One* 9 (12), e115316. doi:10.1371/journal.pone.0115316

Chen, Y. P., Chan, A. T. C., Le, Q. T., Blanchard, P., Sun, Y., and Ma, J. (2019). Nasopharyngeal Carcinoma. *Lancet* 394 (10192), 64–80. doi:10.1016/s0140-6736(19)30956-0

Eppenberger, U., Kueng, W., Schlaeppi, J. M., Roesel, J. L., Benz, C., Mueller, H., et al. (1998). Markers of Tumor Angiogenesis and Proteolysis Independently Define High- and Low-Risk Subsets of Node-Negative Breast Cancer Patients. *J. Clin. Oncol.* 16 (9), 3129–3136. doi:10.1200/jco.1998.16.9.3129

Fang, S., Repo, H., Joensuu, H., Orpana, A., and Salven, P. (2011). High Serum Angiogenin at Diagnosis Predicts for Failure on Long-Term Treatment

Response and for Poor Overall Survival in Non-hodgkin Lymphoma. *Eur. J. Cancer* 47 (11), 1708–1716. doi:10.1016/j.ejca.2011.02.018

Guo, S. S., Liu, R., Wen, Y. F., Liu, L. T., Yuan, L., Li, Y. X., et al. (2020). Endogenous Production of C-C Motif Chemokine Ligand 2 by Nasopharyngeal Carcinoma Cells Drives Radioresistance-Associated Metastasis. *Cancer Lett.* 468, 27–40. doi:10.1016/j.canlet.2019.10.008

Hu, J.-l., Luo, W.-J., and Wang, H. (2019). Angiogenin Upregulation Independently Predicts Unfavorable Overall Survival in Proneural Subtype of Glioblastoma. *Technol. Cancer Res. Treat.* 18, 153303381984663. doi:10.1177/1533033819846636

Karam, I., Huang, S. H., McNiven, A., Su, J., Xu, W., Waldron, J., et al. (2016). Outcomes after Reirradiation for Recurrent Nasopharyngeal Carcinoma: North American Experience. *Head Neck* 38 (Suppl. 1), E1102–E1109. doi:10.1002/hed.24166

Lam, W. K. J., and Chan, J. Y. K. (2018). Recent Advances in the Management of Nasopharyngeal Carcinoma. *F1000Res* 7, 1829. doi:10.12688/f1000research.15066.1

Landt, S., Mordelt, K., Schwidde, I., Barinoff, J., Korlach, S., Stöblen, F., et al. (2011). Prognostic Significance of the Angiogenic Factors Angiogenin, Endoglin and Endostatin in Cervical Cancer. *Anticancer Res.* 31 (8), 2651–2655.

Lee, A. W. M., Ng, W. T., Chan, J. Y. W., Corry, J., Mäkitie, A., Mendenhall, W. M., et al. (2019). Management of Locally Recurrent Nasopharyngeal Carcinoma. *Cancer Treat. Rev.* 79, 101890. doi:10.1016/j.ctrv.2019.101890

Li, L., Pan, X. Y., Shu, J., Jiang, R., Zhou, Y. J., and Chen, J. X. (2014). Ribonuclease Inhibitor Up-Regulation Inhibits the Growth and Induces Apoptosis in Murine Melanoma Cells through Repression of Angiogenin and ILK/PI3K/AKT Signaling Pathway. *Biochimie* 103, 89–100. doi:10.1016/j.biochi.2014.04.007

Li, S., Shi, X., Chen, M., Xu, N., Sun, D., Bai, R., et al. (2019). Angiogenin Promotes Colorectal Cancer Metastasis via tiRNA Production. *Int. J. Cancer* 145 (5), 1395–1407. doi:10.1002/ijc.32245

Lovato, A., Lionello, M., Staffieri, A., Blandamura, S., Tealdo, G., Giacomelli, L., et al. (2015). A Higher Angiogenin Expression Is Associated with a Nonnuclear Maspin Location in Laryngeal Carcinoma. *Clin. Exp. Otorhinolaryngol.* 8 (3), 268–274. doi:10.3342/ceo.2015.8.3.268

Lyons, S. M., Fay, M. M., Akiyama, Y., Anderson, P. J., and Ivanov, P. (2017). RNA Biology of Angiogenin: Current State and Perspectives. *RNA Biol.* 14 (2), 171–178. doi:10.1080/15476286.2016.1272746

Marioni, G., Blandamura, S., Lionello, M., Giacomelli, L., Lovato, A., Favaretto, N., et al. (2014). Indications for Postoperative Radiotherapy in Laryngeal Carcinoma: a Panel of Tumor Tissue Markers for Predicting Locoregional Recurrence in Surgically Treated Carcinoma. A Pilot Study. *Head Neck* 36 (11), 1534–1540. doi:10.1002/hed.23493

Marioni, G., Koussis, H., Scola, A., Maruzzo, M., Giacomelli, L., Karahontziti, P., et al. (2010). Expression of MASPIN and Angiogenin in Nasopharyngeal Carcinoma: Novel Preliminary Clinico-Pathological Evidence. *Acta Otolaryngol.* 130 (8), 952–958. doi:10.3109/00016480903518034

Marioni, G., Marino, F., Blandamura, S., D'Alessandro, E., Giacomelli, L., Guzzardo, V., et al. (2010). Neoangiogenesis in Laryngeal Carcinoma: Angiogenin and CD105 Expression Is Related to Carcinoma Recurrence Rate and Disease-free Survival. *Histopathology* 57 (4), 535–543. doi:10.1111/j.1365-2559.2010.03664.x

Miyake, M., Goodison, S., Lawton, A., Gomes-Giacoia, E., and Rosser, C. J. (2015). Angiogenin Promotes Tumoral Growth and Angiogenesis by Regulating Matrix Metallopeptidase-2 Expression via the ERK1/2 Pathway. *Oncogene* 34 (7), 890–901. doi:10.1038/onc.2014.2

Pawlik, T. M., and Keyomarsi, K. (2004). Role of Cell Cycle in Mediating Sensitivity to Radiotherapy. *Int. J. Radiat. Oncol. Biol. Phys.* 59 (4), 928–942. doi:10.1016/j.ijrobp.2004.03.005

Peres, R., Furuya, H., Pagano, I., Shimizu, Y., Hokutan, K., and Rosser, C. J. (2016). Angiogenin Contributes to Bladder Cancer Tumorigenesis by DNMT3b-Mediated MMP2 Activation. *Oncotarget* 7 (28), 43109–43123. doi:10.18632/oncotarget.10097

Schwartz, B., Shoseyov, O., Melnikova, V. O., McCarty, M., Leslie, M., Roiz, L., et al. (2007). ACTIBIND, a T2 RNase, Competes with Angiogenin and Inhibits Human Melanoma Growth, Angiogenesis, and Metastasis. *Cancer Res.* 67 (11), 5258–5266. doi:10.1158/0008-5472.can-07-0129

Shu-Ping, L. I., and Guo-Fu, H. U. (2015). Mechanism and Function of Angiogenin in Apoptosis Regulation. *Zhongguo Sheng Wu Hua Xue Yu Fen Zi Sheng Wu Xue Bao* 31 (12), 1258–1260. doi:10.13865/j.cnki.cjbmb.2015.12.05

Vanli, N., and Guo-Fu, H. U. (2015). Mechanism and Function of Angiogenin in Prostate Cancer. *Zhongguo Sheng Wu Hua Xue Yu Fen Zi Sheng Wu Xue Bao* 31 (12), 1261–1266. doi:10.13865/j.cnki.cjbmb.2015.12.06

Waisberg, J., De Souza Viana, L., Affonso Junior, R. J., Silva, S. R., Denadai, M. V., Margeotto, F. B., et al. (2014). Overexpression of the ITGAV Gene Is Associated with Progression and Spread of Colorectal Cancer. *Anticancer Res.* 34 (10), 5599–5607.

Xu, L., Liao, W. L., Lu, Q. J., Li, C. G., Yuan, Y., Xu, Z. Y., et al. (2016). ANG Promotes Proliferation and Invasion of the Cell of Lung Squamous Carcinoma by Directly Up-Regulating HMGA2. *J. Cancer* 7 (7), 862–871. doi:10.7150/jca.14440

Yamasaki, S., Ivanov, P., Hu, G. F., and Anderson, P. (2009). Angiogenin Cleaves tRNA and Promotes Stress-Induced Translational Repression. *J. Cel Biol* 185 (1), 35–42. doi:10.1083/jcb.200811106

Yang, S. S., Yu, D. Y., Du, Y. T., Wang, L., Gu, L., Zhang, Y. Y., et al. (2020). Inhibition of Delta-like Ligand 4 Enhances the Radiosensitivity and Inhibits Migration in Cervical Cancer via the Reversion of Epithelial-Mesenchymal Transition. *Cancer Cel Int* 20, 344. doi:10.1186/s12935-020-01434-1

**Conflict of Interest:** The authors declare that the research was conducted in the absence of any commercial or financial relationships that could be construed as a potential conflict of interest.

**Publisher's Note:** All claims expressed in this article are solely those of the authors and do not necessarily represent those of their affiliated organizations, or those of the publisher, the editors and the reviewers. Any product that may be evaluated in this article, or claim that may be made by its manufacturer, is not guaranteed or endorsed by the publisher.

frontiers in Pharmacology

REVIEW
published: 17 December 2021
doi: 10.3389/fphar.2021.720474

# Emerging Significance of Ginsenosides as Potentially Reversal Agents of Chemoresistance in Cancer Therapy

*Jin-Feng Xu*[1], *Yan Wan*[1], *Fei Tang*[1], *Lu Chen*[1], *Yu Yang*[1], *Jia Xia*[1], *Jiao-Jiao Wu*[1], *Hui Ao*[1,2]* *and Cheng Peng*[1]*

[1]State Key Laboratory of Characteristic Chinese Medicine Resources in Southwest China, Pharmacy College, Chengdu University of Traditional Chinese Medicine, Chengdu, China, [2]Innovative Institute of Chinese Medicine and Pharmacy, Chengdu University of Traditional Chinese Medicine, Chengdu, China

Chemoresistance has become a prevalent phenomenon in cancer therapy, which alleviates the effect of chemotherapy and makes it difficult to break the bottleneck of the survival rate of tumor patients. Current approaches for reversing chemoresistance are poorly effective and may cause numerous new problems. Therefore, it is urgent to develop novel and efficient drugs derived from natural non-toxic compounds for the reversal of chemoresistance. Researches *in vivo* and *in vitro* suggest that ginsenosides are undoubtedly low-toxic and effective options for the reversal of chemoresistance. The underlying mechanism of reversal of chemoresistance is correlated with inhibition of drug transporters, induction of apoptosis, and modulation of the tumor microenvironment(TME), as well as the modulation of signaling pathways, such as nuclear factor erythroid-2 related factor 2 (NRF2)/AKT, lncRNA cancer susceptibility candidate 2(CASC2)/ protein tyrosine phosphatase gene (PTEN), AKT/ sirtuin1(SIRT1), epidermal growth factor receptor (EGFR)/ phosphatidylinositol 3-kinase (PI3K)/AKT, PI3K/AKT/ mammalian target of rapamycin(mTOR) and nuclear factor-κB (NF-κB). Since the effects and the mechanisms of ginsenosides on chemoresistance reversal have not yet been reviewed, this review summarized comprehensively experimental data *in vivo* and *in vitro* to elucidate the functional roles of ginsenosides in chemoresistance reversal and shed light on the future research of ginsenosides.

**Keywords: ginsenosides, reverse, chemoresistance, chemotherapy, cancer**

OPEN ACCESS

***Edited by:***
*Dexin Kong,*
*Tianjin Medical University, China*

***Reviewed by:***
*Inamul Hasan Madar,*
*Korea University, South Korea*
*Yang Shao,*
*Fudan University, China*

***Correspondence:**
*Hui Ao*
*aohui2005@126.com*
*Cheng Peng*
*pengchengcxy@126.com*

***Specialty section:***
*This article was submitted to Pharmacology of Anti-Cancer Drugs, a section of the journal Frontiers in Pharmacology*

***Received:*** *04 June 2021*
***Accepted:*** *03 December 2021*
***Published:*** *17 December 2021*

***Citation:***
*Xu J-F, Wan Y, Tang F, Chen L, Yang Y, Xia J, Wu J-J, Ao H and Peng C (2021) Emerging Significance of Ginsenosides as Potentially Reversal Agents of Chemoresistance in Cancer Therapy. Front. Pharmacol. 12:720474. doi: 10.3389/fphar.2021.720474*

## 1 INTRODUCTION

Chemoresistance is regarded as the capability of cancer cells to evade or to cope with the presence of therapeutics, and a vital challenge that researchers manage to reverse. Chemoresistance occurs before treatment and is acquired after therapy, which causes disease relapse and metastasis and worsens the clinical outcome of the cancer patients in most cases (Gottesman et al., 2016; Hamed et al., 2019). As reported, more than 90% of cancer patients died from metastatic cancer in different degrees, which was related to chemoresistance to varying degrees (Wilson et al., 2009). Notably, occurrence of chemoresistance is attributed to multiple targets and pathways, including inhibition in drug transporter proteins expression and membrane fluidity, alteration in the drug target, apoptosis

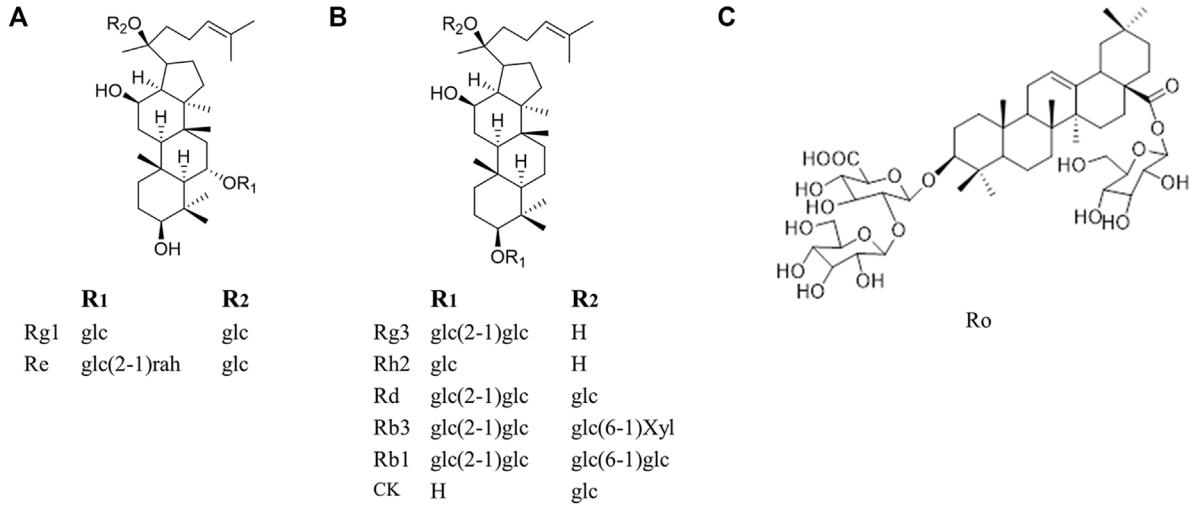


| | R1 | R2 |
|---|---|---|
| Rg1 | glc | glc |
| Re | glc(2-1)rah | glc |

| | R1 | R2 |
|---|---|---|
| Rg3 | glc(2-1)glc | H |
| Rh2 | glc | H |
| Rd | glc(2-1)glc | glc |
| Rb3 | glc(2-1)glc | glc(6-1)Xyl |
| Rb1 | glc(2-1)glc | glc(6-1)glc |
| CK | H | glc |

**FIGURE 1 |** Molecular structures of representative ginsenosides separated from ginseng in our study. **(A)** Protopanaxatriol ginsenosides **(B)** Protopanaxadiol ginsenosides **(C)** Oleanane.

induction, and modulation of autophagy. Mechanically, the occurrence of multiple factors such as drug efflux, apoptosis, autophagy and microenvironment, are related to multiple pathways and targets, including NRF2/AKT, CASC2/PTEN, AKT/SIRT1, EGFR/PI3K/AKT, PI3K/AKT/mTOR, and NF-κB (Grossman and Altieri, 2001; Vadlapatla et al., 2013). In recent years, chemoresistance reversal has attracted attention worldwide but is still in a bottleneck period. Until now, three measures including chemical drugs, biological therapy and hyperthermia are taken to reverse chemoresistance. Unfortunately, these methods are not suitable for clinical promotion because of their single target and function property, serious side effects, expensive cost, and high technical requirements. Furthermore, these strategies have no anti-cancer effects themselves, but bring new problems to cancer therapy (Baird and Kaye, 2003). Thus, better therapeutic approaches with multiple targets, multi-functions, higher efficiency, and lower cost and toxicity are needed to overcome chemoresistance.

Fortunately, natural products, are one of the most promising options for the management of cancer chemoresistance. It is reported that 49% of anti-cancer drugs which are characterized as multiple targets, high effectiveness, and low toxicity and availability, come directly or indirectly from natural products (Newman and Cragg, 2016). Among these natural products as cancer therapy, none has probably enjoyed as much worldwide prestige and attention as ginseng (Qi et al., 2010). Ginseng is often used in combination with chemotherapeutic drugs to promote chemotherapy. Patients taking ginseng had a 50% lower risk of cancer recurrence compared to patients who do not take ginseng (Yun and Choi, 1995). Shenmai formulation, which contains ginseng, has been proved as a marketed drug in the complementary treatment of cancer chemoresistance, indicating the great treatment potential of ginsenosides when combined with chemotherapeutic agents (Wu et al., 2021; Yang et al., 2020). Ginsenosides, the main active ingredient of ginseng, are usually used in cancer treatment when combined with chemotherapy and this combination provides a better therapeutic intervention than a single usage of ginsenosides or chemotherapy. They are a special group of triterpenoid saponins and composed of 17 carbons and classified into three kinds according to their chemical structure of aglycones: Protopanaxadiol (PPD), protopanaxatriol (PPT) and oleanane (**Figure 1**). Notably, ginsenoside Rg3 and Rh2, both of which belong to PPD type, are the most intensively researched ginsenosides which possess chemoresistance reversal activity with PPD type. For instance, Li et al. (Li et al., 2016) found that co-treatment of epidermal growth factor receptor-tyrosine kinase inhibitor (EGFR-TKI) and Rg3 may be a promising strategy to delay acquired resistance in clinical treatment. However, to our best knowledge, the chemoresistance-reversal effects of ginsenosides have not been systematically reviewed, which will hamper the usage of ginsenosides in cancer treatment, especially in the development of chemoresistance reversals.

Here, the medicinal potential and the underlying mechanisms behind the reversal effects of ginsenosides on chemoresistance related to alterations in membrane transporters, apoptosis, autophagy and TME are systematically reviewed and analyzed (**Figure 2**), and the view that ginsenosides can be used as supplements to reverse chemoresistance is pointed out. We hope this review will lay the foundation for the in-depth investigation of the biochemical mechanisms and pharmacological properties of ginsenosides and benefit the future development and utilization of ginsenosides.

## 2 INHIBITING MEMBRANE TRANSPORTERS

Overexpression of drug transporters on the plasma membrane has been demonstrated to be a key mechanism

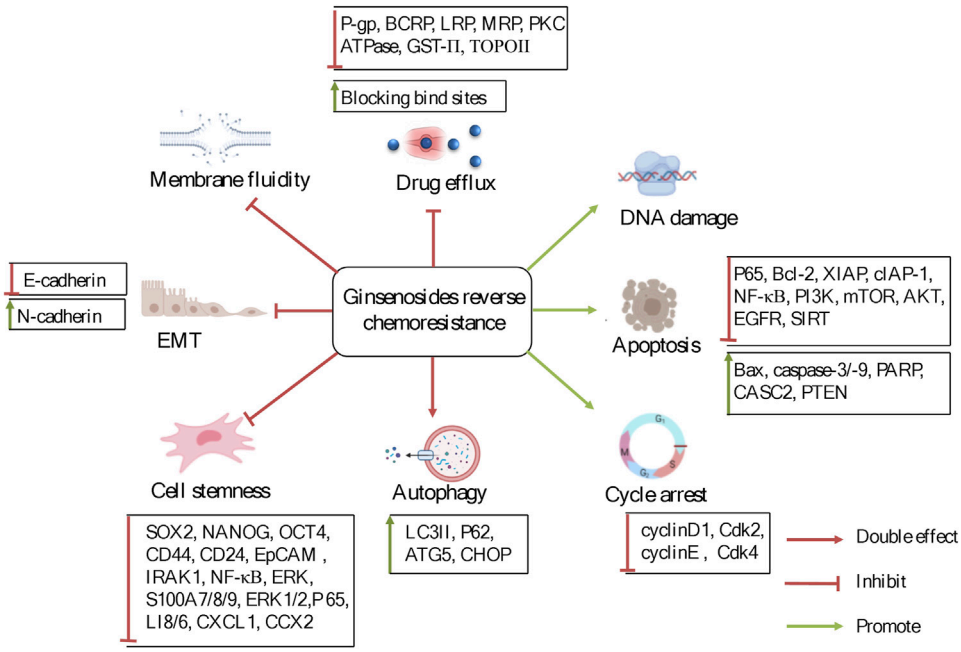


**FIGURE 2 |** The potentially reversal effects and mechanisms of ginsenosides on chemoresistance in cancer therapy. Ginsenosides were used to treat chemoresistance mainly through the regulation of factors and signaling pathways related to drug transporters, apoptosis, autophagy, and tumor microenvironment.

conferring chemoresistance (Wu et al., 2008). Generally speaking, these transporters can be classified into ATP-binding cassette (ABC) and non-ABC transporters. Among them, P-glycoprotein (P-gp, gene symbol ABCB1), breast cancer resistance protein (BCRP, gene symbol ABCG2) and multidrug resistance-related protein (MRP, gene symbol ABCC), belong to the ABC transporters family while lung resistance-related protein (LRP) is a non-ABC transporter (Vadlapatla et al., 2013). Additionally, topoisomerase II (TOPO II), glutathione-S-transferase (GST) and protein kinase C (PKC) may also be connected to reverse chemoresistance. However, they usually act as supplements for chemoresistance mediated by drug transporter proteins and genes. Hence, there were few studies to explore their effect alone (Kunze et al., 1991; Daniel, 1993; Beck et al., 1998). Currently, it is recognized that overexpression of these proteins facilitates the efflux of chemotherapeutic agents. The mechanism behind this is that these proteins act as the drug transport barriers between the nucleus and the cytoplasm, inhibit redistribution of drugs as well as prevent chemotherapeutic agents from binding to targets, and in turn directly or indirectly decrease drugs concentration at intracellular targets (Meschini et al., 2002; Thomas and Coley, 2003; Mao and Unadkat, 2015).

Therefore, overexpression and overactivation of these above proteins are considered as the most important reasons resulting in chemoresistance. And an important approach to reverse chemoresistance is to inhibit the expression of drug transporter proteins. And the following mechanisms were involved in the inhibitory effects of ginsenosides on P-gp and non-P-gp transporter proteins.

## 2.1 Inhibiting P-gp-Mediated Chemoresistance

P-gp, which is firstly discovered in Chinese hamster ovarian cancer cells and is closely related to drug-resistant cells, is mainly located in the cell membrane, and account for a low proportion in the endoplasmic reticulum, mitochondrial, and Golgi body (Juliano and Ling, 1976; Szabó et al., 2000). But it is worth noting that P-gp in the mitochondria pumps the drug from the cytoplasm into the mitochondria, whereas P-gp on the cell membrane pumps the drug out of the cells (Munteanu et al., 2006). Therefore, overexpression of P-gp in different locations may result in drug redistribution and accumulation at targets. Moreover, as a classic mechanism of chemoresistance, the activation of P-gp is associated with chemoresistance to several types of chemotherapeutic agents, such as anthracycline, vincristine and paclitaxel (Gottesman et al., 2002; Bikadi et al., 2011). At present, P-gp mediated chemoresistance can be reversed by three generation inhibitors (Chen Z et al., 2016). Although these inhibitors exert an inhibitory effect on P-gp, their adverse effects limit their implication, such as low specificity and affinity, undesirable drug-drug interactions and toxicity to normal cells in clinical trials (Daenen et al., 2004; Kelly et al., 2011; Syed and Coumar, 2016). Therefore, it is of great necessity to seek out novel P-gp inhibitors that are not only highly effective and low toxic but also obviously potentially reversal agents of P-gp mediated chemoresistance.

Ginsenosides can efficiently reverse chemoresistance as P-gp inhibitors (Chen et al., 2014). Compared to classic P-gp inhibitors, ginsenosides appear to be multi-targeted P-gp inhibitors, whose mechanisms include downregulating the expression of P-gp, competitively or non-competitively blocking the binding site of P-gp and suppressing the cell membrane fluidity.

### 2.1.1 Downregulating Expression of P-gp

The pharmacological mechanism of chemoresistance is mainly attributed to a decreased accumulation of intracellular drugs mediated by P-gp overexpression. Thereby, inhibiting overexpression of P-gp and MDR1 can result in reversal of chemoresistance (Fu et al., 2013).

Studies have found that ginsenosides in combination with chemotherapeutic agents exert a remarkably inhibitory effect on chemoresistance through inhibiting overexpression of P-gp and MDR1 and consequently suppressing drug effluxes. For example, Fu et al. found that ginsenosides might facilitate Eca109/DDP cells more sensitive to cisplatin (DDP). And their study showed that co-treatment of ginsenoside Rg3 and DDP decreased expression of P-gp more than treatment of DDP alone, suggesting the decreased expression of P-gp might be responsible for ginsenoside Rg3-mediated reversal of chemoresistance. Similarly, Ma and his coworkers (Ma et al., 2019) demonstrated that ginsenoside Rh2 could be a potential agent to reverse chemoresistance when co-treated with oxaliplatin in LoVo/L-OHP cells through decreasing the protein and mRNA levels of P-gp. Also, another study by Li and Chen (Li and Chen, 2013) indicated that ginsenoside Rh2 significantly decreased adriamycin (ADM/Adr) or fluorouracil (FU) efflux in MCF-7/ADM cells. Further, Rh2 could reverse chemo-resistant cells to chemotherapeutic agents by depressing the expression of P-gp. Additionally, ginsenosides can inhibit overexpression of P-gp especially in the nuclei and mitochondria, and thereby change drug distribution. Zhang et al. (Zhang et al., 2012c) showed that treatment of 20 (S)-Rh2 not only decreased $IC_{50}$ of MCF-7/Adr cells by inhibiting expression of P-gp but also promoted the redistribution of ADM. With the suppressive effect on expressions of P-gp, 20 (S)-Rh2 could up-regulate the rate and amount of ADM entering intracellular sites in MCF-7/Adr cells, especially in the nuclei and mitochondria where P-gp was over-expressed, which ultimately contributed to reverse chemoresistance and enhance cell apoptosis induced by ADM.

Further studies also revealed the underlying mechanism which contributed to the regulation of ginsenosides on overexpression of P-gp. Ginsenosides could also reverse chemoresistance through inhibiting the expression of MDR1 gene and increasing the ubiquitination of MDR1. MDR1 stability is dependent on ubiquitin-dependent protein degradation (Zhang et al., 2004). A study (Pokharel et al., 2010) firstly found that ginsenoside Rd, Re, Rb1, and Rg1, especially Rd, decreased MDR1 protein levels in MCF-7/ADR cells, which could be reversed by MG-132, a proteasome inhibitor, suggesting that the proteasomal degradation pathway was responsible for turnover of Rd-mediated MDR1. However, further study showed that Rd did not change mRNA or nuclear protein levels of key transcription factors including hypoxia-inducible factor-1 $\alpha$ (HIF-1 $\alpha$), C/-enhancer-binding protein $\beta$ (C/EBP $\beta$), forkhead box-containing protein, O subfamily1(FoxO1), or Y-box binding protein-1(YB-1), which regulated human MDR1 gene transcription or affected the pregnane X receptor (PXR) dependent transcription activity, showing that the effect of Rd on chemoresistance was not related to the transcription of MDR1 gene. Additionally, Rd increased ubiquitination of MDR1 and consequently reversed doxorubicin (DOX)-resistance in MCF-7/Adr cells, which increased MDR1 protein levels. Further study by Zhang et al. (Zhang et al., 2012a) aimed to elucidate the key factors that decreased ABCB1 expression, and altered cellular pharmacokinetics of Adr, revealing the synergistic mechanism of 20 (S)-Rh2 on MCF-7/Adr cells when co-treated with Adr. The mitogen-activated protein kinase (MAPK)/nuclear factor (NF)-$\kappa$B pathway, translocation and binding activity of NF-$\kappa$B and the binding capability of NF-$\kappa$B to the human MDR1 promoter were inhibited by 20 (S)-Rh2 in MCF-7/Adr cells. Moreover, inhibiting the MAPK/NF-$\kappa$B pathway brought about a decrease in the expression of ABCB1 and the cellular pharmacokinetics regulated by Adr was also significantly altered by inhibiting NF-$\kappa$B. Overall, 20 (S)-Rh2 might down-regulate Adr-induced overexpression of ABCB1 in MCF-7/Adr cells by alleviating the MAPK/NF-$\kappa$B pathway.

### 2.1.2 Blocking the Binding Site of Chemotherapeutic Agents

In addition, blocking the binding site of chemotherapeutic drugs and P-gp is efficient to reverse chemoresistance. There are two types of blockers, including competitive and non-competitive ones. The competitive blockers have high affinity and refer to the ones that leave little place for the binding of P-gp to other chemotherapeutic agents, which result in decreased activity of P-gp (Srivalli and Lakshmi., 2012). In contrast, the non-competitive blockers, substrates of P-gp, are highly effective, reversible, and non-competitive inhibitors of P-gp (Dewanjee et al., 2017).

At present, there were lots of studies showing that ginsenosides could decrease drug effluxes through competitively or non-competitively inhibiting drugs from being bound with P-gp. On one hand, ginsenosides always inhibit chemotherapeutic agents from being bound to these proteins by competitively blocking their binding site and therefore resisting drug efflux, without any effects on the mRNA and protein expressions of drug-related proteins. For example, Choi et al. (Choi et al., 2003) found that protropanaxatriol ginsenosides (PTG) including ginsenoside Rg1 and Re had the potential to reverse MDR by competitively blocking the [$^3$H]-azidopine binding site in DOX resistant AML-2/DX100 cells. Similarly, Gao et al. (Gao et al., 2002) found that Rg3 improved the sensitivity of K562/ADM cells to ADM but failed to affect the growth of K562/ADM cells expressing P-170. Thus, it was speculated that 20 (R)-ginsenoside Rg3 could reverse P-gp-mediated MDR through direct interaction with P-gp in breast cancer treatment. Kim et al. (Kim et al., 2003) revealed that $IC_{50}$ values of vincristine

(VCR), DOX, colchicine (COL) and VP-16 in KBV20C were decreased and the intracellular accumulation of drugs was increased in KBV20C cells following Rg3 treatment. Without any effect on MDR1 gene expression or P-gp level, Rg3 resisted vinblastine efflux and reversed chemoresistance to those drugs in KBV20C cells, properly owing to its competition with [$^3$H] azidopine for binding to the P-gp. It was suggested Rg3 could specifically inhibit P-gp-mediated drug accumulation. Thus, reversal of chemoresistance mediated by Rg3 was redounded to its competition with anticancer drugs for binding to P-gp thereby blocking drug efflux. In addition, Rb1, a major component of ginseng, exerted a synergistic effect with vincristine on chemoresistance in HL60/VCR cells but failed to inhibit the expression of MDR1 (Li et al., 2005). It was worth noting that a membrane breaker was used for the first time in this study to explore the mechanism of why P-gp activity was decreased by Rb1. Although P-gp on the cell membrane was decreased significantly in the presence of Rb1 before cell membrane integrity was broken, the total P-gp was unaffected, indicating that Rb1 has no effect on P-gp expression but P-gp function. Hence, the P-gp inhibitory effect of Rb1 was possibly dependent on the calcium channel since Rb1 was a blocker of the calcium channel, similar to Vp. Consistently, Chen et al. (Chen G et al., 2016) explored the reason why PPD 12, a derivative of 20(S)-protopanaxadiol (PPD), enhanced the sensitivity of MDR cells to ADM. This new compound strengthened the accumulation of ADM and Rho123 *via* blocking the efflux. As a substrate of P-gp, PPD12 inhibited the transport function of ABCB1 by stimulating the ATPase activity but failed to alter mRNA or protein expression, indicating that PPD is a substrate of P-gp as the first generation of P-gp inhibitor. Moreover, a predicted binding mode showed hydrophobic interactions of PPD12 within the large drug-binding cavity of ABCB1. Residues in the drug-binding pocket of ABCB1 were bound with P-gp stably through hydrogen bonding and hydrophobic interactions. Notably, PPD12 in non-toxic concentrations sensitized chemo-resistant cells to their anticancer substrates better than either the PPD. Additionally, co-treatment of PPD12 and ADM treated in the KB/VCR xenograft mice model inhibited tumor growth without decreasing weight. Similarly, Rg5 could reverse chemoresistance through inhibiting the function of ABCB1 by stimulating the ATPase activity both in A2780/T cells and A549/T cells (Feng et al., 2020). The underlying mechanism was partially attributive to its upregulation on the activity of ABCB1 ATPase. As Rg5 activated the ATPase of ABCB1, it might be a substrate of ABCB1. However, it inhibited Vp stimulated ATPase activity, which showed that Rg5 was bound to P-gp with high affinity and prevented other agents from being bound to the transporters, resulting in decreased activity of ABCB1 transporter. On the other hand, ginsenosides exerted an inhibitory effect on chemoresistant cells by non-competitively blocking the activity of P-gp. For instance, 20 (S)-Rh2 was a non-competitive P-gp inhibitor (Zhang et al., 2010). It significantly inhibited the efflux rates of three typical P-gp inhibitors, involving digoxin, fexofenadine and etoposide and the inhibitory action of 20 (S)-Rh2 on the function of P-gp could persist for 3 h at least after washed in MCF-7/Adr cells. Unlike P-gp substrates, 20 (S)-Rh2 reduced the Vp-stimulated P-gp ATPase activity close to the basal level and UIC2 binding fluorescence. Furthermore, 20 (S)-Rh2 promoted absorption and bioavailability of etoposide significantly without affecting terminal elimination half-time and P-gp expression *in situ* and *in vivo*. Collectively, 20 (S)-Rh2 exerted an inhibitory effect in a noncompetitive instead of a competitive manner. Similarly, Zhao et al. (Zhao et al., 2009) held that aPPD, the final deglycosylation metabolite of the PPD group in the gastrointestinal tract, was exactly a non-competitive and reversible inhibitor of P-gp with high efficiency. This study revealed that $IC_{50}$ values of aPPD-induced cytotoxicity in drug sensitive P388wt and drug resistant P388adr cells were similar, suggesting that aPPD is impossible to be a substrate of P-gp. In addition, the level of calcein accumulation was enhanced and a similar inhibitory effect on the activity of P-gp was observed in MCF-7/Adr and P388/Adr cells in the presence of aPPD. Differently from 20 (S)-Rh2, the activity of P-gp immediately returned to the control levels after removal of aPPD and aPPD exerted no effect on ATPase. Another study (Liu et al., 2004) also indicated that the blockage of P-gp activity was highly reversible after aPPD was washed out, which suggested recovery of P-gp activity. Furthermore, aPPD did not affect ATPase activity of P-gp. Also, the activity of aPPD on chemoresistance was observed *in vivo*. Paradoxically, although both aPPD and 20 (S)-Rh2 were not substrates of P-gp, the recovery time of P-gp activity was different when aPPD and 20 (S)-Rh2 was removed due to their different chemical structures.

### 2.1.3 Suppressing the Lipid Fluidity and Modulating Lipid Rafts

The fluidity of the membrane refers to the extent of the molecular disorder and molecular motion within a lipid bilayer. Cholesterol, the main ingredient of a lipid bilayer, is responsible for lipid fluidity owing to its function and activity (Yeagle, 1991). Moreover, cholesterol is a key factor to maintain the complete structure and function of lipid rafts. Depletion of cholesterol leads to rupture of lipid rafts and confusion of cell function (Li et al., 2006). Lipid rafts are detergent-resistant microdomains of the plasma membrane with low-density and enriched in cholesterol and glycosphingolipids. Structurally, quantities of drug transporters, such as P-gp, are located in the cell membrane and lipid rafts. Therefore, lipid fluidity and lipid rafts play a central role in chemoresistance in cancers though affecting the function of drug transporters.

Ginsenosides-induced reversal of chemoresistance mediated by P-gp has been achieved through alteration of lipid fluidity and modulation of lipid rafts. For instance, a study performed by Kwon et al. (Kwon et al., 2008) showed that because of the structural similarity of Rg3 and cholesterol, Rg3 decreased the membrane fluidity and in turn blocked drug efflux induced by P-gp in drug resistant KB V20C cells but not in drug sensitive KB V20 cells, which resulted in reversal of P-gp-mediated

chemoresistance. Moreover, Rg3 induced a significant increase of fluorescence anisotropy in KB V20C cells, suggesting that Rg3 significantly decreased cellular lipid membrane fluidity in KB V20C cells, thereby decreasing drug effluxes. Notably, the inhibitory effect could be reversed when Rg3 was removed. Also, the longevity of mice implanted with Adr-resistant P388 leukemia cells was remarkably promoted by Rg3. Collectively, Rg3 exerted an inhibitory effect on the membrane fluidity of drug-resistant cells, consequently reversing chemoresistance. Also, ginsenoside Rp1, a novel semi-synthesized agent from Rg5 and Rk1, had an inhibitory effect on lipid fluidity (Yun et al., 2013) By competing with cholesterol for incorporation into lipid rafts, ginsenoside Rp1 induced lipid raft clustering and accordingly decreased membrane fluidity in drug resistant NCI/ADR-RES and DXR cells, which caused translocation of MDR-1 out of lipid rafts, inhibited the activity of MDR1 and augmented an accumulation of DOX or rho 123. Moreover, the inactivation of Src, a kinase located in lipid rafts, led to a decrease of MDR1 in DXR cells treated by co-treatment of Rp-1 and actinomycin D(ActD). Overall, as a cholesterol depletor, Rp1 reversed chemoresistance *via* modulating lipid rafts and inactivating Src and MDR1.

## 2.2 Downregulating Expression of Non-P-gp Proteins

Three transporters, involving MRP, BCRP, and LRP, belong to non-P-gp proteins. MRP functions as the major exporter of organic anions and overexpression of MRP can confer resistance to platinum-containing chemotherapeutic drugs, such as DDP (Surowiak et al., 2006) BCRP, a semi-transport protein, delivers chemotherapeutic drugs through forming homodimers or oligomers and consequently develops transmembrane channels. Overexpression of BCRP is reported to confer chemoresistance for a wide range of chemotherapeutics such as MX, camptothecin derivates, flavopiridol, and methotrexate (Ross et al., 1999). LRP mediates resistance of certain drugs that cannot be mediated by P-gp and MRP, such as carboplatin and alkylating agents, all of which target DNA (Meschini et al., 2002). Collectively, overexpression of one or multiple proteins mentioned above may lead to chemoresistance. Interestingly, the suppression of these proteins and P-gp are observed simultaneously.

Ginsenosides Rg3 and Rh2 are the most studied saponins that can inhibit the expression of transporters. Zhang et al. (Zhang et al., 2002) found that Rg3 might act as a promising candidate for chemoresistance in human lung adenocarcinoma (A549/DDP cells) time–dependently through inhibiting expression of chemoresistance-related proteins, including MDR1, MRP and LRP. Co-treatment of DDP and Rg3 decreased not only $IC_{50}$ values of DDP in A549/DDP cells but also the mRNA and protein levels of MDR1, MRP and LRP. Liu et al. (Liu Cet al., 2018) obtained similar results from the previous findings. Moreover, the nude mice bearing human lung adenocarcinoma that received co-treatment of DDP and Rg3 had obviously reduced tumor volumes and weights compared with animals treated with DDP alone. Moreover, Rg3 treatment enhanced uptake of technetium-99m labeled hexakis-2-methoxyisobutylisonitrile (99mTc-MIBI) suggesting that Rg3 can sensitize chemotherapy *in vivo*. Consistently, another study (Liu GW et al., 2018) showed that ginsenoside Rh2 reversed resistance of chemotherapeutic agents through inhibiting multiple drug resistance related proteins in HCT-8/5-FU and LoVo/5-FU cells. Expressions of MRP1, MDR1, LRP and GST were obviously inhibited in the presence of Rh2.

Furthermore, the metabolites of ginsenosides exert inhibitory effects on MDR tumor cells synergistically as well. Jin et al. (Jin et al., 2006) suggested that PPD is a useful ingredient to improve chemotherapy responsiveness as a novel BCRP inhibitor. PPD reinforced the antiproliferative action of MX on human breast carcinoma MCF-7/MX cells that overexpressed BCRP. And MX retention was lower in MCF-7/MX cells than MCF-7 cells, suggesting that the extruding MX ability in MCF-7/Adr cells might be related to BCRP. Additionally, uptake of MX was obviously enhanced and the activity of BCRP ATPase was inhibited in the presence of PPD in MCF-7/MX cells. Therefore, it was indicated that PPD significantly reverses the resistance of MCF-7/MX cells to MX as a BCRP inhibitor in a synergistic fashion. In conclusion, overexpression of chemoresistance-related proteins (P-gp, MRP, LRP, BCRP and GST) could be reversed by co-treatment of chemotherapeutic agents and ginsenosides.

# 3 REGULATING APOPTOSIS AND AUTOPHAGY

Apoptosis and autophagy are two different forms of programmed cell death, and there may be a functional relationship between them. Presently, studies have found that there are roughly three relationships between autophagy and apoptosis. 1) Autophagy usually precedes apoptosis and then activates apoptosis(Cui et al., 2007). 2) In some cases, such as mitochondrial damage caused by stimulation by oxidation, ischemia/reperfusion and toxic compounds, etc. (Kanzawa et al., 2003), autophagy can protect cells from apoptosis and necrosis. 3) Autophagy and apoptosis promote cell death together (Yanagisawa et al., 2003). In short, autophagy not only has been suggested as a possible mechanism for non-apoptotic death but also represents a survival strategy. However, the specific transformation mechanism between the two types of cell death is not remains unclear. To our best knowledge, ginsenosides reversed chemoresistance by modulating both of apoptosis and autophagy. Therefore, the chemoresistance-reversal mechanism involved in ginsenosides induced apoptosis and autophagy were introduced together as follow.

## 3.1 Inducing Cancer Cell Apoptosis

Apoptosis, known as programmed death, is one of the important life phenomena in the biological world. Generally, the Fas pathway, mitochondrial passage, adenylyl-cyclase pathway and p53 activation pathway

mediate apoptosis. They target Bax and suppress anti-apoptotic proteins such as Bcl-2, finally triggering apoptosis (Lee et al., 2020). Data has suggested that inducing apoptosis sensitized cancer cells to chemotherapeutic drugs, such as 5-FU, DOX and ActD (Boyer et al., 2004; Fulda and Debatin, 2004). Therefore, inducing apoptosis can contribute to the suppression of chemoresistance (Schmitt and Lowe, 2001).

Ginsenosides act as apoptosis inducers to reverse chemoresistance. Investigations had indicated that ginsenosides induced apoptosis in different cancer cell lines, resulting in the reversal of chemoresistance *in vitro* and *in vivo*. For instance, Hu et al. (Hu et al., 2010) revealed that the chemoresistance reversal effect of Rh2 in A549/DDP cells could be achieved through the mitochondrial apoptosis pathway. Intracellular calcium ion concentration was higher after DDP treatment than after co-treatment of DDP and Rh2. After co-treatment of Rh2 and DDP, the expression of cyto C in the cytoplasm was higher than that in mitochondria. Moreover, caspase 3 was motivated and highly expressed in A549/DDP cells. In contrast, the expression of cyto C was higher in the mitochondria than that in the cytoplasm and the nucleus was reduced after treatment of Rh2 or DDP alone. Therefore, the combination of Rh2 and DDP significantly increased cell apoptosis in the drug resistant cancer cells. Consistently, Ma et al. (Ma et al., 2019) showed that the reversal effect of Rh2 on oxaliplatin-resistant colon cancer cells was correlated with apoptosis activation as well. Rh2 could reverse L-OHP induced resistance in LoVo/L-OHP cells through inhibiting proliferation and protein and mRNA levels of Bax and promoting protein and mRNA levels of Bax and caspase-3.

More importantly, further in-depth studies showed that inducing apoptosis can be mediated by different signaling pathways which could be clarified as follows.

### 3.1.1 Modulating the CASC2/PTEN/Akt Signaling Pathway

LncRNA cancer susceptibility candidate 2 (CASC2) and protein tyrosine phosphatase gene (PTEN) have been characterized as tumor suppressors and efficient suppressive regulators of cancers. Regulation of CASC2 and PTEN induced by AKT is closely associated with chemoresistance of tumors. For example, Feng et al. (Feng et al., 2017) found that inhibition of the CASC2/PTEN/Akt pathway sensitized DDP-resistant cervical cancer cells to DDP since overexpression of CASC2 reduced $IC_{50}$ values in HeLa/DDP and CaSki/DDP cells, while CASC2 knockdown promoted $IC_{50}$ values. Furthermore, CASC2 inhibits miR-21 and p-AKT protein level and promotes PTEN protein level, indicating that CASC2 might sensitize cancer cells to drugs through regulating PTEN and Akt pathways. Similarly, PTEN has also been regarded as a therapeutic target for reversing chemoresistance (Xia et al., 2013). Therefore, suppression of the CASC2/PTEN/Akt pathway plays an important role in the reversal of chemoresistance.

Co-treatment of Rg3 and gemcitabine (GEM) can inhibit the growth of drug-resistant cells through the CASC2/PTEN/Akt pathway. Zou et al. (Zou et al., 2020) found that inhibition of the PTEN/Akt signaling was involved in the reversal effect of Rg3 in GEM-resistant pancreatic cancer. The cell growth and colony formation of Panc-1/GEM and SW1990/GEM cells were suppressed after treatment of GEM and Rg3. At the same time, Rg3 could activate the CASC2/PTEN signaling, inhibit cell growth and induce cells apoptosis concentration-dependently in Panc-1/GEM cells and SW1990/GEM cells. Moreover, the expression of PTEN was positively related to CASC2, suggesting that Rg3 modulates PTEN signaling through activating CASC2 expression. Additionally, a significant decrease in tumor volume and weight were observed in the nude mice implanted with GEM-resistant pancreatic cancer cells when treated by Rg3. Overall, Rg3 increased cell apoptosis and consequently reversed chemoresistance through modulating the CASC2/PTEN signaling pathway in GEM-resistant pancreatic cancer.

### 3.1.2 Modulating the AKT/SIRT1 Pathway

Sirtuin1 (SIRT1) can deacetylate various histone and non-histone substrates, such as p53, c-MYC and FOXO, therefore altering DNA repair, cell cycle, apoptosis and development of chemoresistance (Chen et al., 2011; Wang et al., 2013; Mao et al., 2014). Also, SIRT1 inactivates the AKT pathway in a SIRT1 deacetylase-dependent manner (Wang et al., 2015). Therefore, regulation of the SIRT1/AKT pathway could be a possible strategy for reversing chemoresistance.

There was a study confirming that the combination of ginsenoside Rp1 and ActD exerted a synergistic sensitization on the drug resistant cancer lines by modulating the AKT/SIRT1 pathway (Yun et al., 2020). Treatment of ActD or Rp1 alone mildly inhibited the cell growth while the inhibitory effect of co-administration of Rp1 and ActD was significantly promoted in drug-resistant LS513 colon cancer. Importantly, Rp1 re-sensitized the drug resistant cells to ActD through increasing apoptosis and aggravating DNA damage. Further researches suggested that Rp1 could attenuate the up-regulation of SIRT1 caused by ActD and consequently increase apoptosis through enhancing p53 acetylation in drug resistant cells. Meanwhile, co-treatment of Rp1 and ActD also decreased AKT activation to downregulate the expression of SIRT1, and ultimately activated cells apoptosis as well as reversed chemoresistance in tumor cells. More, tumor growth was significantly inhibited when ActD combined with Rp1 in nude mice implanted with LS513 cells as well. Taken together, modulation of the AKT/SIRT1 pathway was involved in Rp1-reversed drug resistance.

### 3.1.3 Modulating the EGFR/PI3K/AKT Signaling Pathway

Epidermal growth factor receptor (EGFR), known as a key factor in the development of tumor, can bind with a ligand, which leads to autophosphorylation of the receptor, activate downstream signal transduction and activity, involving Ras/MAPK, PI3K/AKT, STAT, and Src family kinases, and promote proliferation, survival, invasion, and migration of tumor cells (Wieduwilt and Moasser, 2008). Among them, the EGFR/PI3K/AKT pathway indirectly regulates tumor cell apoptosis through maintaining the balance between cell proliferation and apoptosis

(Hong and Fan, 2019). Therefore, inhibition of the EGFR/PI3K/AKT pathway could be a viable strategy for overcoming chemoresistance through affecting apoptosis.

Rg3-mediated inactivation of the EGFR/PI3K/AKT pathway is an efficient method to induce cancer cell apoptosis, which has been proved by Jiang and his coworkers (Jiang et al., 2017). The sensitivity of erlotinib to pancreatic cancer cells was significantly enhanced when co-treatment with Rg3 *in vitro* and *in vivo*. The cell viability, growth and formation of cell colonies in BxPC-3 and AsPC-1 cells were inhibited when exposed to different concentrations of Rg3 and erlotinib. Likewise, apoptosis induced by erlotinib and cleavage of caspase-3, caspase-9 and PARP were obviously promoted by Rg3 in BxPC-3 and AsPC-1 cells. Furthermore, lower expression levels of p-EGFR, p-PI3K and p-AKT were observed when combined with Rg3, which revealed that Rg3 downregulates expressions of p-EGFR, p-PI3K, and p-AKT, thereby sensitizing pancreatic cancer cells to erlotinib. Similarly, the study *in vivo* showed Rg3 inactivated the EGFR/PI3K/AKT signal pathway. Moreover, the tumor volume was decreased by co-treatment of erlotinib and Rg3 in nude mice implanted with BxPC-3 cells. In conclusion, downregulating the EGFR/PI3K/AKT signal pathway, which induced cell apoptosis, was a vital mechanism related to Rg3-mediated reversal of chemoresistance.

### 3.1.4 Modulating the PI3K/AKT/mTOR Pathway

Activation of the PI3K/AKT/mTOR pathway is a common feature of a wide range of human cancers (Brown et al., 2008). Upregulation of the PI3K/AKT/mTOR pathway contributes to cancer cell survival, acquires chemoresistance, which was related to inhibition of apoptosis and cell cycle progression, differentiation and growth (Choo and Blenis, 2006). Thus, it is believable that activating the PI3K/AKT/mTOR signaling can effectively result in chemoresistance reversal.

Ginsenoside Rg1 could induce apoptosis in paclitaxel-resistant nasopharyngeal cancer cells which might be correlated to suppression of the mTOR/PI3K/AKT pathway (Li et al., 2019). Rg1 increased Bax and decreased Bcl-2 expression and induced cycle arrest in the S phase in SUNE1 cells. Additionally, Rg1 decreased the phosphorylation of mTOR, PI3K in a concentration dependent manner without apparent effects on the total PI3K, AKT and mTOR, suggesting that Rg1 inactivated the TOR/PI3K/AKT pathway in SUNE1 cells. Taken together, Rg1 is considered as a supplementary anticancer agent to reverse chemoresistance due to its inactivation of the TOR/PI3K/AKT pathway in paclitaxel-resistant nasopharyngeal carcinoma.

### 3.1.5 Modulating the NF-κB Pathway

Constitutive activation of nuclear factor-κB (NF-κB) in cancer treatment induces tumor promotion, angiogenesis, metastasis, apoptosis, and resistance to anticancer drugs (Garg and Aggarwal, 2002; Pikarsky et al., 2004). Therefore, inhibition of NF-κB is an efficient approach to increase apoptosis and reverse chemoresistance.

Growing evidence implied that the combination of ginsenosides and chemotherapeutic agents exerted an inhibitory effect *via* inactivation of the NF-κB pathway in cancer cells. For instance, ginsenoside Rg3 combined with the conventional drugs, involving docetaxel (TXT), paclitaxel, DDP and Adr, resisted the growth of HCT116 and SW620 colon cancer cells and induced apoptosis *via* inhibiting NF-κB (Kim et al., 2009). Co-treatment of Rg3 and TXT obviously induced apoptosis through regulating apoptotic related genes, including inhibiting the expression level of Bcl-2, XIAP and cIAP-1 and promoting the expression of Bax, caspase-3 and caspase-9. In agreement with this, Rg3 resisted the NF-κB DNA binding activity, TNF-α-induced transcriptional activation of NF-κB and AP-1 activity and notably promoted apoptosis and sensitivity of chemotherapeutic drugs in colon cancer cells. Similarly, Kim et al. (Kim et al., 2010) found that higher doses of Rg3 could enhance the sensitivity of prostate cancer to TXT through downregulation of the NF-κB pathway. Inhibition of NF-κB pathway and cells growth and induction of apoptosis was observed after Rg3 treatment in prostate cells (LNCaP, PC-3, and DU145), especially LNCaP cells. Importantly, co-treatment of Rg3 and TXT caused a significant reduction in the expression of G0/G1 regulators cyclin D1, cyclin E, Cdk2, and Cdk4. Moreover, another study by Yuan et al. (Yuan et al., 2017) found that the synergistic inhibitory effect of the combination of Rg3 and paclitaxel in triple-negative breast cancer (TNBC) cells, including three cancer cell lines MDA-MB-231, MDA-MB-453, and BT-549, resulted from regulation of apoptotic proteins and genes and inactivation of NF-κB. Additionally, reduction of tumor volumes and weights in the nude mice implanted with TNBC cells *in vivo* after co-treatment of Rg3 and paclitaxel was observed. Therefore, the treatment of ginsenoside Rg3 could serve as a novel strategy in treating a line of cancers with a high incidence and mortality *via* inhibiting the NF-κB pathway.

## 3.2 Modulating Cell Autophagy

Autophagy is a lysosome-mediated protein and organelle degradation process that is characterized by the formation of autophagosomes (Mizushima and Klionsky, 2007). Intensive studies have suggested that autophagy can serve as both an inhibitor and a motivator of cancer cells relying on the degree of induction (autophagic flux) and stage of tumor progression (Eskelinen, 2011). Similarly, the chemo-resistant mechanism associated with autophagy is separated into two aspects. Some cases maintain high basal autophagic flux, resulting in intrinsic resistance to chemotherapeutic drugs while others gradually acquire chemoresistance by increasing autophagic fluxes in response to the treatment of chemotherapeutic drugs. Paradoxically, an increase in autophagic flux may also induce tumor cell death in some cases, leading to remarked inconsistency across studies (Sheng et al., 2018). In brief, a better understanding of the dual role of autophagy in cancer is necessary to figure out the acquirement of chemoresistance.

Ginsenosides can activate autophagy to reverse chemoresistance. For example, Rp1 was efficient to resist proliferation in paclitaxel-resistant nasopharyngeal cancer by promoting autophagic cell death (Li et al., 2019). The data showed that Rg1 increased the protein levels of LC3-II and decreased the expression of p62 in SUNE1 cells. Taken

together, the activation of autophagy was correlated with the reversal of chemoresistance mediated by Rg1.

In contrast, autophagy inhibition is critical for ginsenosides to reverse chemoresistance. Wang et al. (Wang et al., 2019) found that 20(S)-Rg3 sensitized PC-9-resistant (PC-9R) and HCC827-resistant (HCC827R) cells to icotinib through suppressing the late maturation or degradation stage of autophagy. The levels of LC3II protein, p62 protein and the number of LC3II puncta in PC-9 and HCC827 cells were increased by Rg3. However, protein levels of LC3II and p62 were not increased anymore when Rg3 combined with CQ, which indicated that the increased LC3 puncta formation accompanied by increased p62 levels in Rg3-treated cells may attribute to suppression of the late maturation or degradation stage of autophagy. Consistently, their results showed that inhibition of autophagy by Rg3 could reverse chemoresistance in PC-9R xenograft models. Another study performed by Kim et al. (Kim et al., 2014) showed that autophagy was often regarded as a cell survival mechanism in cancer cells exposed to DOX while 20 (S)-Rg3 sensitized hepatocellular carcinoma to DOX through inhibiting autophagy, which resulted in cell death. More importantly, CHOP as well as the ATG-5 dependent autophagic pathway was involved in Rg3-inhibited autophagy. Rg3 did not increase LC3II and p62 protein levels anymore when ATG5 gene was abolished. Moreover, knockdown of CHOP repressed 20 (S)-Rg3-induced death of HepG2 cells while upregulation of CHOP could promote TRAIL-induced apoptosis. Additionally, a decrease in tumor weight and volume was observed after treatment of Rg3 *in vivo*. Collectively, 20 (S)-ginsenoside Rg3 was a novel inhibitor of autophagy through increasing LC3II and p62 protein levels in a CHOP and ATG-5 dependent autophagic manner and thus sensitized hepatocellular carcinoma to doxorubicin.

## 4 MODULATING TUMOR MICROENVIRONMENT (TME)

Tumor microenvironment (TME), including smooth muscle cells, endothelial cells, fibroblasts of various phenotypes, myofibroblasts, mast cells, T cells, B cells, natural killer, neutrophils, granulocyte, and antigen-presenting cells is a complex and constantly changing matrix surrounding tumor cells. The interaction of these components in TME has affected the biological behavior of tumors including epithelial-mesenchymal transition (EMT), characteristics maintenance of cancer stem cells (CSCs), invasion, metastasis, and chemoresistance (Polyak et al., 2009; Hale et al., 2013). CSCs, typical cells in TME, show a high degree of uncertainty and instability. They regulate the expression of transporters and apoptotic genes, the activity of microsomal multifunctional oxidases, DNA damage repair, and activation of key cell signaling pathways, which have become one of the main theories that produce chemoresistance. EMT is a phenomenon produced by epithelial cells under the action of matrix metalloproteinases, adhesion molecules, selectins and other factors. It is one of the initial development methods of CSCs and has the potential to endow CSCs with chemoresistance, viability and metastatic ability (Huang et al., 2012). Additionally, hypoxia is the most prominent sign of TME and results from tumor cell proliferation that is faster than angiogenesis or abnormal new blood vessels (Challapalli et al., 2017). Studies have revealed that hypoxia can promote EMT and cancer cell stemness, which facilitates cell survival and acquires chemoresistance (Cosse and Michiels, 2008; Bharti et al., 2016). Therefore, it is important to modulate the resistance of solid tumors to chemotherapeutic agents by modulating TME.

Studies showed that ginsenosides suppressed the ovarian stem cancer cells through inhibiting the process of EMT. For example, Kala et al. (Kala, 2014) found that Rb1 or CK combined with DDP or paclitaxel significantly reversed chemoresistance in a dose and time dependent manner through inhibiting ovarian stem cancer cells. Co-treatment of ginsenosides and chemotherapeutic agents obviously inhibited tumor sphere forming ability and cell viability through downregulating E-cadherin and up-regulating N-cadherin in HEYA8 and SKOV-3 cells. Therefore, modulating EMT to inhibit the cell stemness was the reason why Rb1 or CK enhanced the sensitivity of cancer cells to chemotherapeutic agents. In another case, Wang et al. (Wang et al., 2018) found co-treatment of Rg3 and DDP exerted an important role in hypoxic lung cancer therapy. Rg3 could sensitize hypoxia human NSCLC cells to DDP by inhibiting the NF-$\kappa$B pathway thereby retaining the progress of EMT and stemness evidenced as reduced expressions of E-cadherin, N-cadherin, sex determining region Y-box 2 (SOX2), NANOG, OCT4, and CD44. Moreover, consistent results both *in vivo* and *in vitro* were observed. Collectively, Rg3 could sensitize hypoxic lung cancer cells to DDP through preventing NF-$\kappa$B induced EMT and stemness. Also, Rg3 (Tan et al., 2020) could target CSCs and reverse osimertinib resistance in H1975 and H1975/OR cells by activating the Hippo pathway, which was key cancer signaling in association with cell proliferation, cell death, and cancer metastasis (Kulkarni et al., 2020). Co-treatment of Rg3 and osimertinib could promote expressions of the active components of the Hippo pathway, such as MST1/2 and LATS1/2, and depress the expression of the negative executor or effector. In addition, ginsenoside panaxatriol (GPT) (Wang et al., 2020) sensitized MDA-MB-231 PTX resistant (MB231-PR) cells to PTX through reducing the characteristics of stem cells, which was correlated with the IRAK1/NF-$\kappa$B and the ERK pathways. Co-treatment of GPT and PTX inhibited expressions of CSC related genes including octamer-binding transcription factor 4 (OCT4), sex determining region Y-box 2 (SOX2), NANOG, aldehyde dehydrogenase 1 (ALDH1), and CD44 gene expression, indicating that cell stemness-mediated invasion and tumor growth were inhibited by GPT and PTX. And IRAK1 and S100A7/8/9 formed a feedback loop to drive the malignancy of TNBC cells (Goh et al., 2017). The combination inhibited phosphorylation of IRAK1, P65 and ERK1/2, and promoted I$\kappa$B-alpha as well as inhibited S100A7/9 mRNA expression. In addition, the combination therapy also exerted an inhibitory effect on expressions of NF-$\kappa$B targeted genes including interleukin 6 (IL6), IL8, chemokine (C-X-C motif) ligand 1 (CXCL1), and chemokine (C-C motif) ligand 2 (CCL2). Thus, GPD could overcome PTX resistance by

**TABLE 1 |** Summary of the reversal effect of ginsenosides when combined with chemotherapeutic agents on chemoresistance in cancer treatment.

| Cancer type | Drugs | Ginsenosides | Cell type | Effect | Mechanism | References |
|---|---|---|---|---|---|---|
| Esophageal cancer | Cisplatin | Rg3 | Eca109/DDP | Reverse drug resistance<br>Inhibit tumor growth | ↓ p-gp expression<br>↑cell cycle arrest in G1/S phase | Li and Chen (2013) |
| Colon cancer | Oxaliplatin | Rh2 | LoVo/L-OHP, LoVo cell | Reverse drug resistance<br>Inhibit proliferation<br>Induce apoptosis | ↓ p-gp expression, Bcl-2<br>↑ Bax, caspase-3 and Smad4 | Ma et al. (2019) |
| Breast cancer | Adriamycin, Fluorouracil | Rh2 | MCF-7/Adr, MCF-7 | Reverse drug resistance | ↓P-gp activity<br>↑Drug accumulation | Li and Chen (2013) |
| Breast cancer | Adriamycin | 20(S)-Rh2 | MCF-7/Adr, MCF-7 | Reverse drug resistance<br>Induce apoptosis | ↓P-gp activity<br>↑Drug accumulation and distribution | Zhang et al., 2012c |
| Breast cancer | Adriamycin | Rd | MCF-7/Adr | Reverse drug resistant | ↓ MDR1 *via* ubiquitination-dependent protein degradation | Pokharel et al. (2010) |
| Breast cancer | Adriamycin | 20(S)-Rh2 | MCF-7/Adr | Reverse drug resistant | ↓ ABCB1 expression, NF-κB/MAPK pathway | Zhang et al., 2012a |
| Acute myelogenous leukemia | Daunorubicin | Protopanaxatriol ginsenosides, Protopanaxatriol ginsenosides, Rb1, Rb2, Rc, Rg1, Re | AM-2/D100, AM-2/DX100 | Reverse drug resistance | ↓Drugs inteact with P-gp<br>↑Drugs accumulation | Choi et al. (2003) |
| Human myeloid leukemia | Adriamycin | 20(R)-Rg3 | K562/ADM | Reverse drug resistant<br>Induce apoptosis | ↓P-gp | Gao et al. (2002) |
| Fibroblast carcinoma | Vincristine, Doxorubicin | Rg3 | KB V20C, P388/DOX | reverse drug resistant<br>Increase life span of mice | ↑Drugs toxicity, competitively blocking bind site | Kim et al. (2003) |
| Acute promyelocytic leukemia | Vincristine | Rb1 | HL60, HL60/VCR | Reverse drug resistant | ↓ Drug bind to P-gp<br>↑Cellular drug accumulation | Li et al. (2005) |
| Breast Cancer<br>Fibroblast carcinoma | Adriamycin | 20(S)-protopanoxadiol derivative | KB/VCR, MCF-7/ADM | Reverse drug resistant<br>Induce apoptosis<br>Decrease the volume of tumor | ↓ Drug bind to P-gp<br>↑ABCB1 ATPase activation | Chen G et al. (2016) |
| Ovarian cancer; Lung cancer | Docetaxel, Doxorubicin, Paclitaxel, Daunorubicin | Rg5 | A2780/T, A549/T, A549 | Reverse drug resistance<br>Induce apoptosis<br>Increase cycle arrest in G2/M<br>Increase cytotoxicity | ↓Drugs bind to P-gp, Nrf2/AKT pathways<br>↑Cellular drug accumulation, ABCB1 ATPase | Feng et al. (2020) |
| Breast cancer | Digoxin, Fexofenadine, Etoposide | 20(S)-ginsenoside Rh2 | MCF-7/ADR, Caco-2 cells (HTB-37) | Reverse drug resistance<br>Increase efficiency of anticancer | ↓ P-gp, ATPase activity; change the binding sites | Zhao et al. (2009) |
| Murine leukemia<br>Breast cancer | Adriamycin | 20(S)-Protopanaxadiol | P388, P388adr, MCF-7/ADR | Reverse multidrug resistance | ↓P-gp activity<br>↑ Cytotoxicity, cellular drug accumulation | Zhao et al. (2009) |
| | | aglycon 20(S)-protopanaxadiol | | Induce apoptosis | ↓ P-gp<br>↑ Caspase 3, 8, and 9, cytotoxicity | Liu et al. (2004) |
| Murine leukemia, Human fibroblast cancer | Adriamycin, Vincristine | 20(S)-Rg3 | P388/Adr, KBV20C | Reverse drug resistance<br>Decrease the volume of tumor | ↓ Membrane fluidity, P-gp function<br>↑Cytotoxicity | Kwon et al. (2008) |
| Ovarian cancer | Actinomycin D, Paclitaxel, Doxorubicin | Rp1 | OVCAR-8, NCI/ADR-RES, DXR | Reverse drug resistance<br>Induce apoptosis | ↓ MDR-1 protein expression and Src activition<br>↑Redistribute lipid rafts, MDR-1 protein, DNA damage | Yun et al. (2013) |
| | Cisplatin | Rg3 | A549/DDP | | | |

(Continued on following page)

**TABLE 1 |** (*Continued*) Summary of the reversal effect of ginsenosides when combined with chemotherapeutic agents on chemoresistance in cancer treatment.

| Cancer type | Drugs | Ginsenosides | Cell type | Effect | Mechanism | References |
|---|---|---|---|---|---|---|
| Lung adenocarcinoma | | | | Reverse drug resistance | ↓MDR1, LRP, MRP expression | Zhang et al. (2002) |
| Lung cancer | Cisplatin | 20(S)-Rg3 | A549, A549/DDP | Reverse drug resistance<br>Decrease tumor weight | ↓P-gp, MPR1, LPR1 expression | Liu C et al. (2018) |
| Colorectal Cancer | 5-FU | Rh2 | LoVo, LoVo/5-FU, HCT, HCT-8/5-FU | Reverse drug resistance<br>Induce apoptosis<br>Increase cell cycle arrest: G0/G1 phase<br>Inhibit proliferation, migration and EMT | ↓ MRP1, MDR1, LRP and GST expression, cyclin D1, CDK2, p-Rb, Bcl-2<br>↑ Cleaved-caspase 3 | Liu C et al. (2018) |
| Breast cancer | Mitoxantrone, Doxorubicin | Protopanaxadiol-containing ginsenosides (Rg3, Rh2, and PPD) and protopanaxatriol-containing ginsenosides (Rg1, Rh1, and PPT) | MCF-7, MCF-7/MX, MCF-7/Adr | Reverse drug resistance<br>Inhibit drug efflux<br>Increase drug uptake | ↓ BCRP-associated vanadate sensitive ATPase activity | Jin et al. (2006) |
| Lung adenocarcinoma | Cisplatin | Rh2 | A549/DDP | Inhibit tumor growth<br>Reverse drug resistance<br>Induce apoptosis | ↑Mitochondrial permeability, transmemtal potential, cytochrom C, caspase-3 | Hu et al. (2010) |
| Pancreatic cancer | Gemcitabine | Rg3 | Panc-1, SW 1990, Panc-1/GEM, SW1990/GEM | Inhibit tumor growth<br>Induce apoptosis | ↑CASC2, PTEN | Zou et al. (2020) |
| Colon cancer, Ovarian cancer, Lung cancer | Actinomycin D | Rp1 | LS513, OVCAR8-DXR, A549-DXR | Induce apoptosis<br>Inhibit tumor growth<br>Reverse drug resistance | ↓SIRT1, AKT<br>↑DNA damage, 53 acetylation, PARP clevage | Yun et al. (2020) |
| Pancreatic cancer | Erlotinib | Rg3 | BxPC-3, AsPC-1 | Inhibit proliferation<br>Induce apoptosis<br>Increase tumor cells sensitivity<br>Decrease tumor growth | ↓p-EGFR, p-PI3K, p-Akt<br>↑ Caspase-3, caspase-9, PARP cleavage | Jiang et al. (2017) |
| Nasopharyngeal cancer | Paclitaxel | Rg1 | SUNE1 cells, NP460 | Inhibit cell viability<br>Inhibit cell growth<br>Induce autophagy<br>Induce apoptosis | ↓p62, Bcl-2<br>↑LC3II, Bax,ROS, cycle arrest in S phase | Li et al. (2019) |
| Colon cancer | Docetaxel | Rg3 | HCT116, SW620 | Inhibit proliferation<br>Induce apoptosis<br>Reverse drug resistance | ↓DNA binding activity of NF-κB, Bcl-2, XIAP and cIAP-1<br>↑ Bax, caspase-3, caspase-9 | Kim et al. (2009) |
| Prostate cancer | Docetaxel | Rg3 | LNCaP, PC-3, DU145 | Inhibit tumor growth<br>Reverse drug resistance<br>Induce apoptosis | ↓Activity of NF-κB transcriptional activity, DNA binding activity of NF-κB, Bcl-2, XIAP, cIAP-1<br>↑Cell cycle arrest: G0/G1 phase, Bax, caspase-3, caspase-9, cleaved PARP | Kim et al. (2009) |
| Triple-negative breast cancer | Paclitaxel | Rg3 | MDA-MB-231, MDA-MB453, BT-549 | Inhibit cell viability<br>Induce apoptosis | ↓ NF-κB activation, p65, Bcl-2<br>↑Bax, Caspase-3, cytotoxicity | Yuan et al. (2017) |
| | Icotinib | 20(S)-Rg3 | | | | |

(Continued on following page)

**TABLE 1 |** (*Continued*) Summary of the reversal effect of ginsenosides when combined with chemotherapeutic agents on chemoresistance in cancer treatment.

| Cancer type | Drugs | Ginsenosides | Cell type | Effect | Mechanism | References |
|---|---|---|---|---|---|---|
| Human non-small cell lung cancer | | | PC-9, HCC827, PC-9R, HCC827R | Reverse drug resistance<br>Inhibit autophagy<br>Inhibit cell proliferation<br>Inhibit tumor growth | ↑ LC3-II, LC3II puncta formation, P62 | Wang et al. (2019) |
| Hepatocellular cancer | Doxorubicin | 20(S)-Rg3 | SK-Hep1, HepG2 | Inhibite autophagy<br>Induce cell death<br>Inhibit tumor weight and volume<br>Reverse drug resistance | ↑ LC3 II, LC3II puncta formation, GFP-LC3 puncta formation, CHOP, P62 | Kim et al. (2014) |
| Ovarian cancer | Paclitaxel or cisplatin | Rb1, CK | SKOV-3, HEY A8 CSCs | Inhibit proliferation<br>Inhibit CSC self-renewal<br>Inhibit EMT | ↓Snail, Slug, E-cadherin, p-Akt, p-ERK1/2, Wnt/$\beta$-catenin signaling<br>↑cytotoxicity, caspase-3, N-cadherin | Kala (2014) |
| Hypoxic lung cancer | Ciaplatin | Rg3 | SPC-A1, H1299 cells | Inhibit EMT and stemness<br>Inhibit tumor growth<br>Induce apoptosis<br>Inhibit tumor growth, weight and volume | ↓Bcl-2 and survivin, Snail, N-cadherin, and Vimentin, NF-$\kappa$B DNA binding and p-p65, p65, p-IKK, IKK<br>↑Caspase-3, -8, -9 and Bax,E-cadherin | Wang et al. (2018) |
| Non-small cell lung cancer | Osimertinib | Rg3 | H1975 | Reverse drug resistance | ↓Cell stemness<br>↑ Hippo pathway | Tan et al. (2020) |
| Triple-negative breast cancer | Paclitaxel | Panaxatriol | MB231-PR; SUM159-PR | Induce apoptosis<br>Inhibits cancer stemness<br>Inhibit cell growth | ↓BCL-2, MCL-1, p-IRAK1, P65, ERK1/2, S100A7, S100A9<br>↑Bax, IκB-alpha, cytotoxicity | Wang et al. (2020) |

mediating stemness of tumor cells which resulted from an inhibition of the IRAK1/NF-κB/ERK pathway.

## 5 DISCUSSION

Chemoresistance is a common phenomenon and the main barrier in cancer chemotherapy. Modern scientific studies have explained the causes of cancer chemoresistance from multi-perspectives and multi-dimensions, which has built a foundation for the development of chemoresistance-reversal agents. Currently, ginsenosides, originated from ginseng, have received much attention as potential preventive and therapeutic strategies against all kinds of tumors, particularly as supplements of chemotherapy in reversing chemoresistance. According to the previous reports, it is notable that Rg3 and Rh2, have the unique advantage over chemotherapeutic drugs and function as multi-targeted and multi-pathway chemoresistance-reversal agents. In this article, the inhibitory effect and mechanisms of ginsenosides on chemoresistance are summarized (**Tables 1** and **2**). The underlying mechanisms may be correlated with inhibition of drug transport proteins, modulation of autophagy, induction of apoptosis as well as alterations of TME (**Figure 2**). Further researches suggested that multiple signal pathways are involved in reversing chemoresistance, such as CASC2/PTEN/Akt, AKT/SIRT1, EGFR/PI3K/AKT, PI3K/AKT/mTOR, Nrf2/PI3K/AKT, and MAPK/NF-κB pathways (**Figures 3** and **4**). Also, these studies revealed the structure-activity relationship of ginsenosides. The differences between the chemical structures of those ginsenosides might have quite a substantial influence on the mechanism of reversing chemoresistance. For instance, the P-gp inhibitory effect of 20 (S)-Rh2 and 20 (S)-PPD was more pronounced than that of 20 (R)-Rh2 and 20 (R)-PPD, respectively (Zhang et al., 2012b). Moreover, ginsenosides with higher molecular weights, including Rg3, PTG, Rb1, PPD12, and Rg5, were more likely to reverse chemoresistance

**TABLE 2 |** Summary of molecular mechanisms of main ginsenosides against chemo-resistance.

| Ginsenosides | Inhibiting the drug transporters expression | Competitively blocking the binding sites of P-gp | Non-competitively blocking the binding sites of P-gp | Inhibiting lipid efflux and lipid raft | Inducing apoptosis | Modulating autophagy | Altering TME |
|---|---|---|---|---|---|---|---|
| Rg3 | + | + | — | + | + | — | + |
| 20(S)-Rg3 | + | + | — | — | — | + | — |
| Rh2 | + | — | — | — | + | — | — |
| 20(R)-Rh2 | — | — | + | — | — | — | — |
| PPD | + | + | — | — | — | — | — |
| PPD12 | — | + | — | — | — | — | — |
| aPPD | — | — | + | — | — | — | — |
| PTG | — | + | — | — | — | — | — |
| Rb1 | — | + | — | — | — | — | + |
| Rg5 | — | + | — | — | — | — | — |
| Rd | + | — | — | — | — | — | — |
| Rp1 | — | — | — | — | + | — | — |
| Rg1 | + | — | — | + | + | + | — |
| GPT | — | — | — | — | — | — | + |

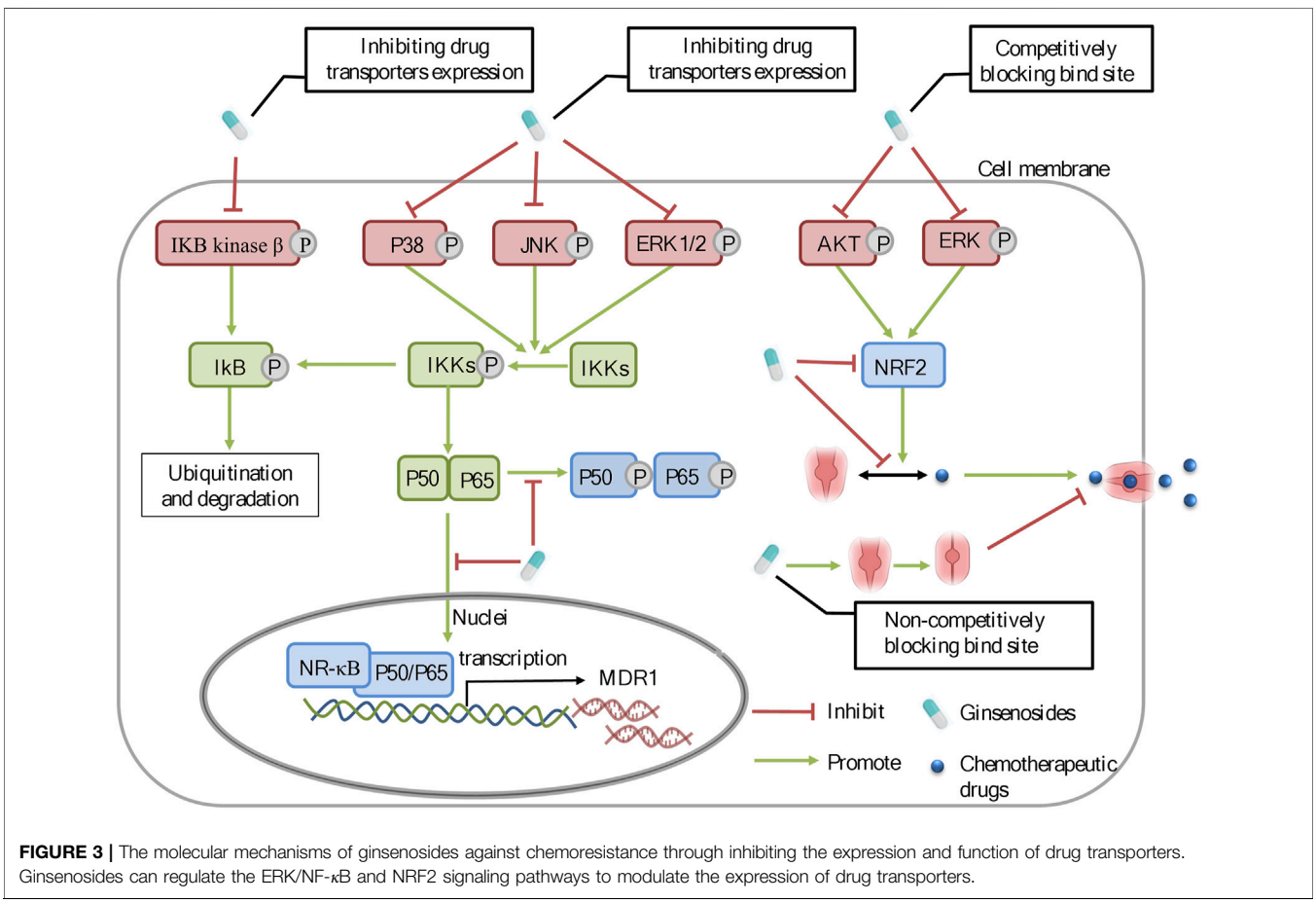


**FIGURE 3 |** The molecular mechanisms of ginsenosides against chemoresistance through inhibiting the expression and function of drug transporters. Ginsenosides can regulate the ERK/NF-κB and NRF2 signaling pathways to modulate the expression of drug transporters.

through competitively blocking the binding site of P-gp whereas smaller molecules like 20(S)-Rh2 and aPPD in a non-competitively blocking manner (**Table 2**).

Substantial evidence *in vitro* and *in vivo* reveal the benefits of the combination of ginsenosides and chemotherapy on chemoresistance. However, according to the current studies in this field, these findings also have certain limitations. Firstly, ginsenosides are characterized by low oral bioavailability caused by poor oral absorption, usually <5% in the rodent model (Xu et al., 2003). Therefore, various drug delivery systems and routes

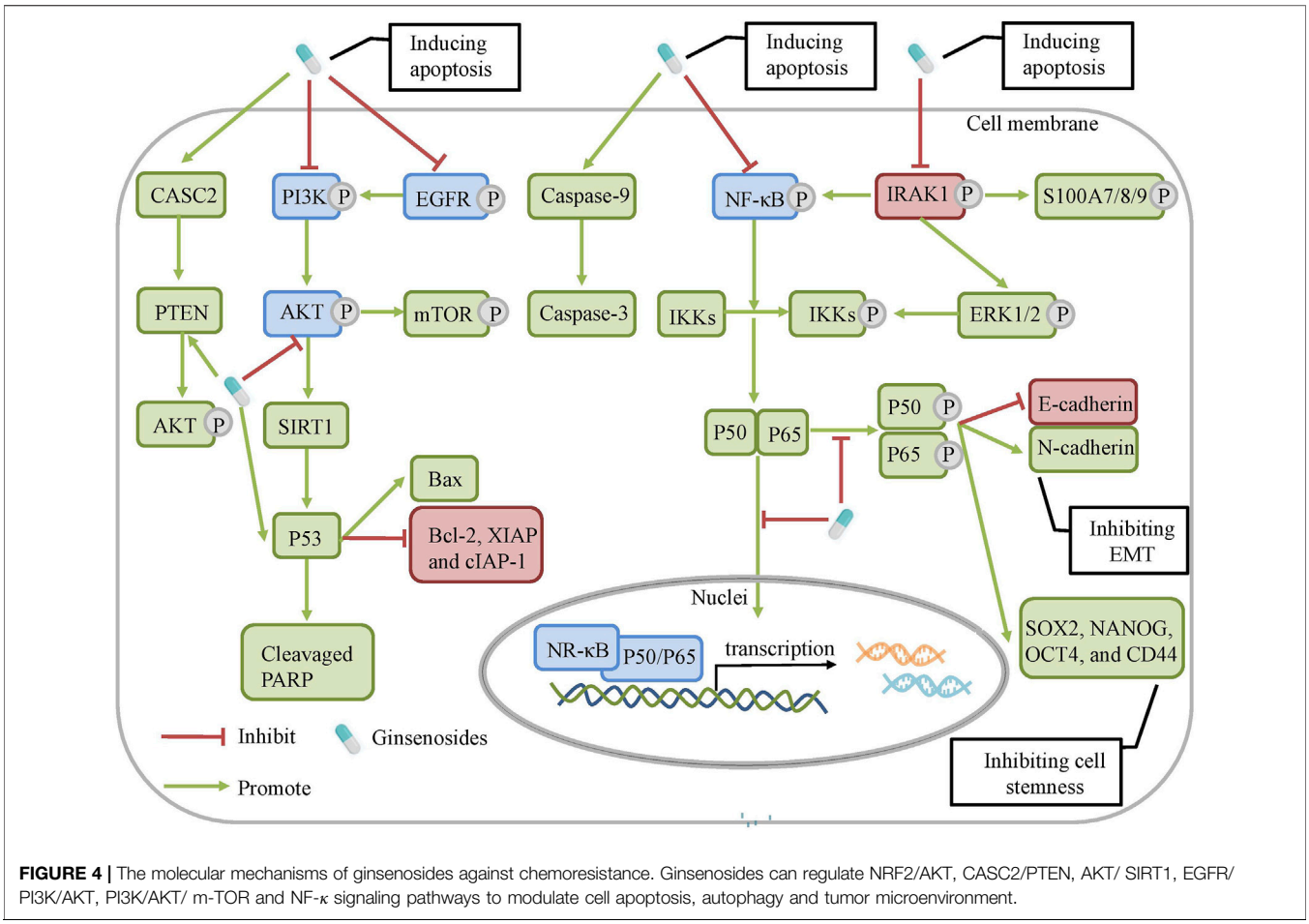


**FIGURE 4 |** The molecular mechanisms of ginsenosides against chemoresistance. Ginsenosides can regulate NRF2/AKT, CASC2/PTEN, AKT/ SIRT1, EGFR/ PI3K/AKT, PI3K/AKT/ m-TOR and NF-$\kappa$ signaling pathways to modulate cell apoptosis, autophagy and tumor microenvironment.

should be taken to improve oral bioavailability or exert a novel effect (Hong et al., 2019). Such as the multifunctional liposome system, ginsenosides functioned as not only the chemotherapy adjuvant to exert their inherent anticancer activity, but also the functional membrane material to promote effectiveness in cancer therapy in this system. Furthermore, although studies showed that poor oral bioavailability and absorption, as well as the potency of the anti-tumor effects of ginsenosides, were related to their molecular weights and structure (Zhang et al., 2012b), the structure-activity relationship of ginsenosides has not been completely illuminated. Hence, some measures, such as chemical synthesis and structural modification should be taken to improve the chemoresistance reversal activity of ginsenosides. Secondly, there are a high proportion of studies on classical mechanisms of ginsenosides-induced chemoresistance reversal, mainly involving P-gp and apoptosis mediated chemoresistance, whereas a low proportion of studies on non-classical mechanisms, which are attributed to regulation of GST-$\pi$, Topo II, CSCs, et al. Therefore, the metabonomics and molecular docking techniques are needed in the further studies. Also, the quartz crystal microbalance (QCM) (Zhou et al., 2012), a novel monitor method is a preferable choice compared to MTT to real-time monitor the chemotherapy induced death process of tumor cells. Finally, most of the current studies focus on the effect of ginsenosides on chemoresistance through animal models and cells, but there are insufficient clinical researches of such benefits. Thus, large sample-sized, randomized, controlled, and clinical studies should be carried out to investigate their actual effects on chemoresistance, setting a higher level of evidence for the therapeutic effects of ginsenosides.

This article systematically summarizes the therapeutic potential of ginsenosides in reversing chemoresistance *in vivo* and *in vitro* and illuminates the mechanisms by which ginsenosides alleviate chemoresistance. The underlying molecular mechanism can be partially elucidated by the roles of the expression and function of P-gp, MDR1, BCRP, LRP, apoptosis, autophagy, and microenvironment as well as CASC2/PTEN/AKT, AKT/SIRT1, EGFR/PI3K/AKT, PI3K/AKT/mTOR and MAPK/NF-$\kappa$B signaling pathways. Given that ginsenosides can also reduce side effects caused by chemotherapy and elicit anti-cancer activities and little toxicity, they have demonstrated promises as an indispensable strategy for reversing chemoresistance. We look forward to further revealing their reversal mechanisms and widespread clinical applications.

## AUTHOR CONTRIBUTIONS

J-FX contributed to the drafting of the manuscript. HA and CP obtained funding, designed, conceived and supervised process, and revised the manuscript. Others were involved in searching, screening the search results, translation, and data collection. All the authors have read and approved the final manuscript.

## FUNDING

This work was supported by Program of National Natural Science Foundation of China (81503272, 81630101), Application Foundation Research Project of Sichuan Provincial Department of Science and Technology (2017JY0187), and Xinglin Scholar Research Promotion Project of Chengdu University of TCM (2018016).

## REFERENCES

Baird, R. D., and Kaye, S. B. (2003). Drug Resistance Reversal-Aare We Getting Closer? *Eur. J. Cancer* 39 (17), 2450–2461. doi:10.1016/s0959-8049(03)00619-1

Beck, J., Bohnet, B., Brügger, D., Bader, P., Dietl, J., Scheper, R. J., et al. (1998). Multiple Gene Expression Analysis Reveals Distinct Differences between G2 and G3 Stage Breast Cancers, and Correlations of PKC Eta with MDR1, MRP and LRP Gene Expression. *Br. J. Cancer* 77 (1), 87–91. doi:10.1038/bjc.1998.13

Bharti, R., Dey, G., and Mandal, M. (2016). Cancer Development, Chemoresistance, Epithelial to Mesenchymal Transition and Stem Cells: A Snapshot of IL-6 Mediated Involvement. *Cancer Lett.* 375 (1), 51–61. doi:10.1016/j.canlet.2016.02.048

Bikadi, Z., Hazai, I., Malik, D., Jemnitz, K., Veres, Z., Hari, P., et al. (2011). Predicting P-Glycoprotein-Mediated Drug Transport Based on Support Vector Machine and Three-Dimensional crystal Structure of P-Glycoprotein. *PLoS One* 6 (10), e25815. doi:10.1371/journal.pone.0025815

Boyer, J., McLean, E. G., Aroori, S., Wilson, P., McCulla, A., Carey, P. D., et al. (2004). Characterization of P53 Wild-type and Null Isogenic Colorectal Cancer Cell Lines Resistant to 5-fluorouracil, Oxaliplatin, and Irinotecan. *Clin. Cancer Res.* 10 (6), 2158–2167. doi:10.1158/1078-0432.ccr-03-0362

Brown, V. I., Seif, A. E., Reid, G. S., Teachey, D. T., and Grupp, S. A. (2008). Novel Molecular and Cellular Therapeutic Targets in Acute Lymphoblastic Leukemia and Lymphoproliferative Disease. *Immunol. Res.* 42 (1-3), 84–105. doi:10.1007/s12026-008-8038-9

Challapalli, A., Carroll, L., and Aboagye, E. O. (2017). Molecular Mechanisms of Hypoxia in Cancer. *Clin. Transl. Imaging* 5 (3), 225–253. doi:10.1007/s40336-017-0231-1

Chen, H. C., Jeng, Y. M., Yuan, R. H., Hsu, H. C., and Chen, Y. L. (2011). SIRT1 Promotes Tumorigenesis and Resistance to Chemotherapy in Hepatocellular Carcinoma and its Expression Predicts Poor Prognosis. *Ann. Surg. Oncol.* 19 (6), 2011–2019. doi:10.1245/s10434-011-2159-4

Chen, S., Wang, Z., Huang, Y., O'Barr, S. A., Wong, R. A., Yeung, S., et al. (2014). Ginseng and Anticancer Drug Combination to Improve Cancer Chemotherapy: a Critical Review. *Evid. Based Complement. Alternat. Med.* 2014, 168940. doi:10.1155/2014/168940

Chen G, G., Liu, J., Chen, W., Xu, Q., Xiao, M., Hu, L., et al. (2016). A 20(S)-protopanoxadiol Derivative Overcomes Multi-Drug Resistance by Antagonizing ATP-Binding Cassette Subfamily B Member 1 Transporter Function. *Oncotarget* 7 (8), 9388–9403. doi:10.18632/oncotarget.7011

Chen Z, Z., Shi, T., Zhang, L., Zhu, P., Deng, M., Huang, C., et al. (2016). Mammalian Drug Efflux Transporters of the ATP Binding Cassette (ABC) Family in Multidrug Resistance: A Review of the Past Decade. *Cancer Lett.* 370 (1), 153–164. doi:10.1016/j.canlet.2015.10.010

Choi, C. H., Kang, G., and Min, Y. D. (2003). Reversal of P-Glycoprotein-Mediated Multidrug Resistance by Protopanaxatriol Ginsenosides from Korean Red Ginseng. *Planta Med.* 69 (3), 235–240. doi:10.1055/s-2003-38483

Choo, A. Y., and Blenis, J. (2006). TORgeting Oncogene Addiction for Cancer Therapy. *Cancer Cell* 9 (2), 77–79. doi:10.1016/j.ccr.2006.01.021

Cosse, J. P., and Michiels, C. (2008). Tumour Hypoxia Affects the Responsiveness of Cancer Cells to Chemotherapy and Promotes Cancer Progression. *Anticancer Agents Med. Chem.* 8 (7), 790–797. doi:10.2174/187152008785914798

Cui, Q., Tashiro, S., Onodera, S., Minami, M., and Ikejima, T. (2007). Autophagy Preceded Apoptosis in Oridonin-Treated Human Breast Cancer MCF-7 Cells. *Biol. Pharm. Bull.* 30 (5), 859–864. doi:10.1248/bpb.30.859

Daenen, S., van der Holt, B., Verhoef, G. E., Löwenberg, B., Wijermans, P. W., Huijgens, P. C., et al. (2004). Addition of Cyclosporin A to the Combination of Mitoxantrone and Etoposide to Overcome Resistance to Chemotherapy in Refractory or Relapsing Acute Myeloid Leukaemia: a Randomised Phase II Trial from HOVON, the Dutch-Belgian Haemato-Oncology Working Group for Adults. *Leuk. Res.* 28 (10), 1057–1067. doi:10.1016/j.leukres.2004.03.001

Daniel, V. (1993). Glutathione S-Transferases: Gene Structure and Regulation of Expression. *Crit. Rev. Biochem. Mol. Biol.* 28 (3), 173–207. doi:10.3109/10409239309086794

Dewanjee, S., Dua, T. K., Bhattacharjee, N., Das, A., Gangopadhyay, M., Khanra, R., et al. (2017). Natural Products as Alternative Choices for P-Glycoprotein (P-Gp) Inhibition. *Molecules* 22 (6), 871. doi:10.3390/molecules22060871

Eskelinen, E. L. (2011). The Dual Role of Autophagy in Cancer. *Curr. Opin. Pharmacol.* 11 (4), 294–300. doi:10.1016/j.coph.2011.03.009

Feng, Y., Zou, W., Hu, C., Li, G., Zhou, S., He, Y., et al. (2017). Modulation of CASC2/miR-21/PTEN Pathway Sensitizes Cervical Cancer to Cisplatin. *Arch. Biochem. Biophys.* 623-624, 20–30. doi:10.1016/j.abb.2017.05.001

Feng, S. L., Luo, H. B., Cai, L., Zhang, J., Wang, D., Chen, Y. J., et al. (2020). Ginsenoside Rg5 Overcomes Chemotherapeutic Multidrug Resistance Mediated by ABCB1 Transporter: *In Vitro* and *In Vivo* Study. *J. Ginseng Res.* 44 (2), 247–257. doi:10.1016/j.jgr.2018.10.007

Fu, L. F., Wang, Y. S., Liu, Y. W., and Xu, B. Z. (2013). Reversing Cisplatin-Resistant of Eca109/DDP Cell Line by Ginsenoside Rg3. *Anat. Res.* 35 (05), 351–354.

Fulda, S., and Debatin, K. M. (2004). Sensitization for Anticancer Drug-Induced Apoptosis by the Chemopreventive Agent Resveratrol. *Oncogene* 23 (40), 6702–6711. doi:10.1038/sj.onc.1207630

Gao, C. Z., Yang, P. M., Lu, G. G., and Qu, S. X. (2002). Studies of 20(R)-ginsenoside Rg3 on Reversal Multidrug Resistance (MDR) and Induction of Apoptosis in K562/ADM Cell Line. *Prog. Anatomical Sci.* 8 (1), 31–35. doi:10.16695/j.cnki.1006-2947.2002.01.011

Garg, A., and Aggarwal, B. B. (2002). Nuclear Transcription Factor-kappaB as a Target for Cancer Drug Development. *Leukemia* 16 (6), 1053–1068. doi:10.1038/sj.leu.2402482

Goh, J. Y., Feng, M., Wang, W., Oguz, G., Yatim, S. M. J. M., Lee, P. L., et al. (2017). Chromosome 1q21.3 Amplification Is a Trackable Biomarker and Actionable Target for Breast Cancer Recurrence. *Nat. Med.* 23 (11), 1319–1330. doi:10.1038/nm.4405

Gottesman, M. M., Fojo, T., and Bates, S. E. (2002). Multidrug Resistance in Cancer: Role of ATP-dependent Transporters. *Nat. Rev. Cancer* 2 (1), 48–58. doi:10.1038/nrc706

Gottesman, M. M., Lavi, O., Hall, M. D., and Gillet, J. P. (2016). Toward a Better Understanding of the Complexity of Cancer Drug Resistance. *Annu. Rev. Pharmacol. Toxicol.* 56, 85–102. doi:10.1146/annurev-pharmtox-010715-103111

Grossman, D., and Altieri, D. C. (2001). Drug Resistance in Melanoma: Mechanisms, Apoptosis, and New Potential Therapeutic Targets. *Cancer Metastasis Rev.* 20 (1-2), 3–11. doi:10.1023/a:1013123532723

Hale, M. D., Hayden, J. D., and Grabsch, H. I. (2013). Tumour-microenvironment Interactions: Role of Tumour Stroma and Proteins Produced by Cancer-Associated Fibroblasts in Chemotherapy Response. *Cel Oncol. (Dordr)* 36 (2), 95–112. doi:10.1007/s13402-013-0127-7

Hamed, A. R., Abdel-Azim, N. S., Shams, K. A., and Hammouda, F. M. (2019). Targeting Multidrug Resistance in Cancer by Natural Chemosensitizers. *Bull. Natl. Res. Cent.* 43, 8. doi:10.1186/s42269-019-0043-8

Hong, Y., and Fan, D. (2019). Ginsenoside Rk1 Induces Cell Death through ROS-Mediated PTEN/PI3K/Akt/mTOR Signaling Pathway in MCF-7 Cells. *J. Funct. Foods* 57, 255–265. doi:10.1016/j.jff.2019.04.019

Hong, C., Wang, D., Liang, J., Guo, Y., Zhu, Y., Xia, J., et al. (2019). Novel Ginsenoside-Based Multifunctional Liposomal Delivery System for Combination Therapy of Gastric Cancer. *Theranostics* 9 (15), 4437–4449. doi:10.7150/thno.34953

Hu, S., Yu, J. Y., Xiong, L. J., Hu, C. P., and Zhang, Y. X. (2010). Research on the Mechanism of Ginsenoside Rh2 Reversing the Resistance of Lung

Adenocarcinoma Cells to Cisplatin. *Zhonghua Yi Xue Za Zhi* 90 (4), 264–268. Chinese.

Huang, R. Y., Chung, V. Y., and Thiery, J. P. (2012). Targeting Pathways Contributing to Epithelial-Mesenchymal Transition (EMT) in Epithelial Ovarian Cancer. *Curr. Drug Targets* 13 (13), 1649–1653. doi:10.2174/138945012803530044

Jiang, J., Yuan, Z., Sun, Y., Bu, Y., Li, W., and Fei, Z. (2017). Ginsenoside Rg3 Enhances the Anti-proliferative Activity of Erlotinib in Pancreatic Cancer Cell Lines by Downregulation of EGFR/PI3K/Akt Signaling Pathway. *Biomed. Pharmacother.* 96, 619–625. doi:10.1016/j.biopha.2017.10.043

Jin, J., Shahi, S., Kang, H. K., van Veen, H. W., and Fan, T. P. (2006). Metabolites of Ginsenosides as Novel BCRP Inhibitors. *Biochem. Biophys. Res. Commun.* 345 (4), 1308–1314. doi:10.1016/j.bbrc.2006.04.152

Juliano, R. L., and Ling, V. (1976). A Surface Glycoprotein Modulating Drug Permeability in Chinese Hamster Ovary Cell Mutants. *Biochim. Biophys. Acta* 455 (1), 152–162. doi:10.1016/0005-2736(76)90160-7

Kala, S. (2014). *Role of Ginsenoside Rb1 and its Metabolite Compound K in Attenuating Chemoresistance and Tumour-Initiating Properties of Ovarian Cancer Cells*. Pokfulam, Hong Kong SAR: The University of Hong Kong. doi:10.5353/th_b5334847

Kanzawa, T., Kondo, Y., Ito, H., Kondo, S., and Germano, I. (2003). Induction of Autophagic Cell Death in Malignant Glioma Cells by Arsenic Trioxide. *Cancer Res.* 63 (9), 2103–2108.

Kelly, R. J., Draper, D., Chen, C. C., Robey, R. W., Figg, W. D., Piekarz, R. L., et al. (2011). A Pharmacodynamic Study of Docetaxel in Combination with the P-Glycoprotein Antagonist Tariquidar (XR9576) in Patients with Lung, Ovarian, and Cervical Cancer. *Clin. Cancer Res.* 17 (3), 569–580. doi:10.1158/1078-0432.CCR-10-1725

Kim, S. W., Kwon, H. Y., Chi, D. W., Shim, J. H., Park, J. D., Lee, Y. H., et al. (2003). Reversal of P-Glycoprotein-Mediated Multidrug Resistance by Ginsenoside Rg(3). *Biochem. Pharmacol.* 65 (1), 75–82. doi:10.1016/s0006-2952(02)01446-6

Kim, S. M., Lee, S. Y., Yuk, D. Y., Moon, D. C., Choi, S. S., Kim, Y., et al. (2009). Inhibition of NF-kappaB by Ginsenoside Rg3 Enhances the Susceptibility of colon Cancer Cells to Docetaxel. *Arch. Pharm. Res.* 32 (5), 755–765. doi:10.1007/s12272-009-1515-4

Kim, S. M., Lee, S. Y., Cho, J. S., Son, S. M., Choi, S. S., Yun, Y. P., et al. (2010). Combination of Ginsenoside Rg3 with Docetaxel Enhances the Susceptibility of Prostate Cancer Cells via Inhibition of NF-kappaB. *Eur. J. Pharmacol.* 631 (1-3), 1–9. doi:10.1016/j.ejphar.2009.12.018

Kim, D. G., Jung, K. H., Lee, D. G., Yoon, J. H., Choi, K. S., Kwon, S. W., et al. (2014). 20(S)-Ginsenoside Rg3 Is a Novel Inhibitor of Autophagy and Sensitizes Hepatocellular Carcinoma to Doxorubicin. *Oncotarget* 5 (12), 4438–4451. doi:10.18632/oncotarget.2034

Kulkarni, A., Chang, M. T., Vissers, J. H. A., Dey, A., and Harvey, K. F. (2020). The Hippo Pathway as a Driver of Select Human Cancers. *Trends Cancer* 6 (9), 781–796. doi:10.1016/j.trecan.2020.04.004

Kunze, N., Yang, G. C., Dölberg, M., Sundarp, R., Knippers, R., and Richter, A. (1991). Structure of the Human Type I DNA Topoisomerase Gene. *J. Biol. Chem.* 266 (15), 9610–9616. doi:10.1016/s0021-9258(18)92864-4

Kwon, H. Y., Kim, E. H., Kim, S. W., Kim, S. N., Park, J. D., and Rhee, D. K. (2008). Selective Toxicity of Ginsenoside Rg3 on Multidrug Resistant Cells by Membrane Fluidity Modulation. *Arch. Pharm. Res.* 31 (2), 171–177. doi:10.1007/s12272-001-1137-y

Lee, G.-Y., Lee, J.-S., Son, C.-G., and Lee, N.-H. (2020). Combating Drug Resistance in Colorectal Cancer Using Herbal Medicines. *Chin. J. Integr. Med.* 27, 551–560. doi:10.1007/s11655-020-3425-8

Li, P., and Chen, S. (2013). Study of the Ginsenoside Rh2 Reversal MCF-7/ADM Multidrug Resistance. *Zhong Guo Yi Yao Zhi Nan* 11 (21), 8–10. doi:10.15912/j.cnki.gocm.2013.21.064

Li, Y., Wang, Z. Z., and Yu, T. F. (2005). *In Vitro* study on the Reversal of Multidrug Resistance (MDR) in HL60/VCR Cell Line with Ginsenoside-Rb1. *J. Radioimmunol.* 5, 362–365.

Li, Y. C., Park, M. J., Ye, S. K., Kim, C. W., and Kim, Y. N. (2006). Elevated Levels of Cholesterol-Rich Lipid Rafts in Cancer Cells Are Correlated with Apoptosis Sensitivity Induced by Cholesterol-Depleting Agents. *Am. J. Pathol.* 168 (4), 1107–1115. doi:10.2353/ajpath.2006.050959

Li, Y., Wang, Y., Niu, K., Chen, X., Xia, L., Lu, D., et al. (2016). Clinical Benefit from EGFR-TKI Plus Ginsenoside Rg3 in Patients with Advanced Non-small Cell Lung Cancer Harboring EGFR Active Mutation. *Oncotarget* 7 (43), 70535–70545. doi:10.18632/oncotarget.12059

Li, W., Li, G., She, W., Hu, X., and Wu, X. (2019). Targeted Antitumor Activity of Ginsenoside (Rg1) in Paclitaxel-Resistant Human Nasopharyngeal Cancer Cells Are Mediated through Activation of Autophagic Cell Death, Cell Apoptosis, Endogenous ROS Production, S Phase Cell Cycle Arrest and Inhibition of M-TOR/PI3K/AKT Signalling Pathway. *J. BUON* 24 (5), 2056–2061.

Liu C, C., Gong, Q., Chen, T., Lv, J., Feng, Z., Liu, P., et al. (2018). Treatment with 20(S)-ginsenoside Rg3 Reverses Multidrug Resistance in A549/DDP Xenograft Tumors. *Oncol. Lett.* 15 (4), 4376–4382. doi:10.3892/ol.2018.7849

Liu, G., Zhao, Y., Yan, H., Bu, X., and Jia, W. (2004). An Aglycon Ginsenoside Induces Apoptosis and Blocks P-Glycoprotein in Multidrug Resistance Cancer Cells. *Cancer Res.* 64 (7 Suppl), 689–690.

Liu GW, G. W., Liu, Y. H., Jiang, G. S., and Ren, W. D. (2018). The Reversal Effect of Ginsenoside Rh2 on Drug Resistance in Human Colorectal Carcinoma Cells and its Mechanism. *Hum. Cel* 31 (3), 189–198. doi:10.1007/s13577-017-0189-3

Ma, J., Gao, G., Lu, H., Fang, D., Li, L., Wei, G., et al. (2019). Reversal Effect of Ginsenoside Rh2 on Oxaliplatin-Resistant colon Cancer Cells and its Mechanism. *Exp. Ther. Med.* 18 (1), 630–636. doi:10.3892/etm.2019.7604

Mao, Q., and Unadkat, J. D. (2015). Role of the Breast Cancer Resistance Protein (BCRP/ABCG2) in Drug Transport-Aan Update. *AAPS J.* 17 (1), 65–82. doi:10.1208/s12248-014-9668-6

Mao, B., Hu, F., Cheng, J., Wang, P., Xu, M., Yuan, F., et al. (2014). SIRT1 Regulates YAP2-Mediated Cell Proliferation and Chemoresistance in Hepatocellular Carcinoma. *Oncogene* 33 (11), 1468–1474. doi:10.1038/onc.2013.88

Meschini, S., Marra, M., Calcabrini, A., Monti, E., Gariboldi, M., Dolfini, E., et al. (2002). Role of the Lung Resistance-Related Protein (LRP) in the Drug Sensitivity of Cultured Tumor Cells. *Toxicol. Vitro* 16 (4), 389–398. doi:10.1016/s0887-2333(02)00035-8

Mizushima, N., and Klionsky, D. J. (2007). Protein Turnover via Autophagy: Implications for Metabolism. *Annu. Rev. Nutr.* 27, 19–40. doi:10.1146/annurev.nutr.27.061406.093749

Munteanu, E., Verdier, M., Grandjean-Forestier, F., Stenger, C., Jayat-Vignoles, C., Huet, S., et al. (2006). Mitochondrial Localization and Activity of P-Glycoprotein in Doxorubicin-Resistant K562 Cells. *Biochem. Pharmacol.* 71 (8), 1162–1174. doi:10.1016/j.bcp.2006.01.006

Newman, D. J., and Cragg, G. M. (2016). Natural Products as Sources of New Drugs from 1981 to 2014. *J. Nat. Prod.* 79 (3), 629–661. doi:10.1021/acs.jnatprod.5b01055

Pikarsky, E., Porat, R. M., Stein, I., Abramovitch, R., Amit, S., Kasem, S., et al. (2004). NF-kappaB Functions as a Tumour Promoter in Inflammation-Associated Cancer. *Nature* 431 (7007), 461–466. doi:10.1038/nature02924

Pokharel, Y. R., Kim, N. D., Han, H. K., Oh, W. K., and Kang, K. W. (2010). Increased Ubiquitination of Multidrug Resistance 1 by Ginsenoside Rd. *Nutr. Cancer* 62 (2), 252–259. doi:10.1080/01635580903407171

Polyak, K., Haviv, I., and Campbell, I. G. (2009). Co-evolution of Tumor Cells and Their Microenvironment. *Trends Genet.* 25 (1), 30–38. doi:10.1016/j.tig.2008.10.012

Qi, F., Li, A., Inagaki, Y., Gao, J., Li, J., Kokudo, N., et al. (2010). Chinese Herbal Medicines as Adjuvant Treatment during Chemo- or Radio-Therapy for Cancer. *Biosci. Trends* 4 (6), 297–307.

Ross, D. D., Yang, W., Abruzzo, L. V., Dalton, W. S., Schneider, E., Lage, H., et al. (1999). Atypical Multidrug Resistance: Breast Cancer Resistance Protein Messenger RNA Expression in Mitoxantrone-Selected Cell Lines. *J. Natl. Cancer Inst.* 91 (5), 429–433. doi:10.1093/jnci/91.5.429

Schmitt, C. A., and Lowe, S. W. (2001). Apoptosis Is Critical for Drug Response *In Vivo*. *Drug Resist. Update* 4 (2), 132–134. doi:10.1054/drup.2001.0188

Sheng, J., Qin, H., Zhang, K., Li, B., and Zhang, X. (2018). Targeting Autophagy in Chemotherapy-Resistant of Hepatocellular Carcinoma. *Am. J. Cancer Res.* 8 (3), 354–365.

Srivalli, K. M. R., and Lakshmi, P. K. (2012). Overview of P-Glycoprotein Inhibitors: A Rational Outlook. *Braz. J. Pharm. Sci.* 48, 353–367. doi:10.1590/S1984-82502012000300002

Surowiak, P., Materna, V., Kaplenko, I., Spaczynski, M., Dolinska-Krajewska, B., Gebarowska, E., et al. (2006). ABCC2 (MRP2, cMOAT) Can Be Localized in the Nuclear Membrane of Ovarian Carcinomas and Correlates with Resistance to Cisplatin and Clinical Outcome. *Clin. Cancer Res.* 12 (23), 7149–7158. doi:10.1158/1078-0432.CCR-06-0564

Syed, S. B., and Coumar, M. S. (2016). P-glycoprotein Mediated Multidrug Resistance Reversal by Phytochemicals: A Review of SAR & Future

Perspective for Drug Design. *Curr. Top. Med. Chem.* 16 (22), 2484–2508. doi:10.2174/1568026616666160212123814

Szabó, D., Keyzer, H., Kaiser, H. E., and Molnár, J. (2000). Reversal of Multidrug Resistance of Tumor Cells. *Anticancer Res.* 20 (6B), 4261–4274. doi:10.1097/00001813-200011000-00012

Tan, Q., Lin, S., Zeng, Y., Yao, M., Liu, K., Yuan, H., et al. (2020). Ginsenoside Rg3 Attenuates the Osimertinib Resistance by Reducing the Stemness of Non-small Cell Lung Cancer Cells. *Environ. Toxicol.* 35 (6), 643–651. doi:10.1002/tox.22899

Thomas, H., and Coley, H. M. (2003). Overcoming Multidrug Resistance in Cancer: an Update on the Clinical Strategy of Inhibiting P-Glycoprotein. *Cancer Control* 10 (2), 159–165. doi:10.1177/107327480301000207

Vadlapatla, R. K., Vadlapudi, A. D., Pal, D., and Mitra, A. K. (2013). Mechanisms of Drug Resistance in Cancer Chemotherapy: Coordinated Role and Regulation of Efflux Transporters and Metabolizing Enzymes. *Curr. Pharm. Des.* 19 (40), 7126–7140. doi:10.2174/13816128113199990493

Wang, Z., Yuan, H., Roth, M., Stark, J. M., Bhatia, R., and Chen, W. Y. (2013). SIRT1 Deacetylase Promotes Acquisition of Genetic Mutations for Drug Resistance in CML Cells. *Oncogene* 32 (5), 589–598. doi:10.1038/onc.2012.83

Wang, G., Wang, J. J., To, T. S., Zhao, H. F., and Wang, J. (2015). Role of SIRT1-Mediated Mitochondrial and Akt Pathways in Glioblastoma Cell Death Induced by Cotinus Coggygria Flavonoid Nanoliposomes. *Int. J. Nanomedicine* 10, 5005–5023. doi:10.2147/IJN.S82282

Wang, J., Tian, L., Khan, M. N., Zhang, L., Chen, Q., Zhao, Y., et al. (2018). Ginsenoside Rg3 Sensitizes Hypoxic Lung Cancer Cells to Cisplatin via Blocking of NF-κB Mediated Epithelial-Mesenchymal Transition and Stemness. *Cancer Lett.* 415, 73–85. doi:10.1016/j.canlet.2017.11.037

Wang, X. J., Zhou, R. J., Zhang, N., and Jing, Z. (2019). 20(S)-ginsenoside Rg3 Sensitizes Human Non-small Cell Lung Cancer Cells to Icotinib through Inhibition of Autophagy. *Eur. J. Pharmacol.* 850, 141–149. doi:10.1016/j.ejphar.2019.02.023

Wang, P., Song, D., Wan, D., Li, L., Mei, W., Li, X., et al. (2020). Ginsenoside Panaxatriol Reverses TNBC Paclitaxel Resistance by Inhibiting the IRAK1/NF-κB and ERK Pathways. *PeerJ* 8, e9281. doi:10.7717/peerj.9281

Wieduwilt, M. J., and Moasser, M. M. (2008). The Epidermal Growth Factor Receptor Family: Biology Driving Targeted Therapeutics. *Cell Mol. Life Sci.* 65 (10), 1566–1584. doi:10.1007/s00018-008-7440-8

Wilson, T. R., Johnston, P. G., and Longley, D. B. (2009). Anti-apoptotic Mechanisms of Drug Resistance in Cancer. *Curr. Cancer Drug Targets* 9 (3), 307–319. doi:10.2174/156800909788166547

Wu, C. P., Calcagno, A. M., and Ambudkar, S. V. (2008). Reversal of ABC Drug Transporter-Mediated Multidrug Resistance in Cancer Cells: Evaluation of Current Strategies. *Curr. Mol. Pharmacol.* 1 (2), 93–105. doi:10.2174/1874467210801020093

Wu, L., Liu, J., Hou, J., Zhan, T., Yuan, L., Liu, F., et al. (2021). Interactions of the Major Effective Components in Shengmai Formula with Breast Cancer Resistance Protein at the Cellular and Vesicular Levels. *Biomed. Pharmacother.* 133, 110939. doi:10.1016/j.biopha.2020.110939

Xia, H., Ooi, L. L., and Hui, K. M. (2013). MicroRNA-216a/217-induced Epithelial-Mesenchymal Transition Targets PTEN and SMAD7 to Promote Drug Resistance and Recurrence of Liver Cancer. *Hepatology* 58 (2), 629–641. doi:10.1002/hep.26369

Xu, Q. F., Fang, X. L., and Chen, D. F. (2003). Pharmacokinetics and Bioavailability of Ginsenoside Rb1 and Rg1 from Panax Notoginseng in Rats. *J. Ethnopharmacol.* 84 (2-3), 187–192. doi:10.1016/s0378-8741(02)00317-3

Yanagisawa, H., Miyashita, T., Nakano, Y., and Yamamoto, D. (2003). HSpin1, a Transmembrane Protein Interacting with Bcl-2/Bcl-xL, Induces a Caspase-independent Autophagic Cell Death. *Cell Death Differ.* 10 (7), 798–807. doi:10.1038/sj.cdd.4401246

Yang, L., Zhang, C., Chen, J., Zhang, S., Pan, G., Xin, Y., et al. (2020). Shenmai Injection Suppresses Multidrug Resistance in MCF-7/ADR Cells through the MAPK/NF-κB Signalling Pathway. *Pharm. Biol.* 58 (1), 276–285. doi:10.1080/13880209.2020.1742167

Yeagle, P. L. (1991). Modulation of membrane function by cholesterol. *Biochimie*, 73 (10), 1303–1310. doi:10.1016/0300-9084(91)90093-g

Yuan, Z., Jiang, H., Zhu, X., Liu, X., and Li, J. (2017). Ginsenoside Rg3 Promotes Cytotoxicity of Paclitaxel through Inhibiting NF-κB Signaling and Regulating Bax/Bcl-2 Expression on Triple-Negative Breast Cancer. *Biomed. Pharmacother.* 89, 227–232. doi:10.1016/j.biopha.2017.02.038

Yun, T. K., and Choi, S. Y. (1995). Preventive Effect of Ginseng Intake against Various Human Cancers: a Case-Control Study on 1987 Pairs. *Cancer Epidemiol. Biomarkers Prev.* 4 (4), 401–408.

Yun, U. J., Lee, J. H., Koo, K. H., Ye, S. K., Kim, S. Y., Lee, C. H., et al. (2013). Lipid Raft Modulation by Rp1 Reverses Multidrug Resistance via Inactivating MDR-1 and Src Inhibition. *Biochem. Pharmacol.* 85 (10), 1441–1453. doi:10.1016/j.bcp.2013.02.025

Yun, U. J., Lee, I. H., Lee, J. S., Shim, J., and Kim, Y. N. (2020). Ginsenoside Rp1, A Ginsenoside Derivative, Augments Anti-cancer Effects of Actinomycin D via Downregulation of an AKT-SIRT1 Pathway. *Cancers (Basel)* 12 (3), 605. doi:10.3390/cancers12030605

Zhang, W., Liu, X., Wang, J., Jiang, W., Zhang, Y., Liu, Y. L., et al. (2002). Reversal Effect of Ginsenoside Rg3 on Cisplatin-Resistant Human Lung Adenocarcinoma Cell Line (A549DDP) and its Mechanisms. *Chin. J. Respir. Crit. Care* (02), 41–44. Chinese.

Zhang, Z., Wu, J. Y., Hait, W. N., and Yang, J. M. (2004). Regulation of the Stability of P-Glycoprotein by Ubiquitination. *Mol. Pharmacol.* 66 (3), 395–403. doi:10.1124/mol.104.001966

Zhang, J., Zhou, F., Wu, X., Gu, Y., Ai, H., Zheng, Y., et al. (2010). 20(S)-ginsenoside Rh2 Noncompetitively Inhibits P-Glycoprotein *In Vitro* and *In Vivo*: a Case for Herb-Drug Interactions. *Drug Metab. Dispos.* 38 (12), 2179–2187. doi:10.1124/dmd.110.034793

Zhang, J., Lu, M., Zhou, F., Sun, H., Hao, G., Wu, X., et al. (2012a). Key Role of Nuclear Factor-κB in the Cellular Pharmacokinetics of Adriamycin in MCF-7/Adr Cells: the Potential Mechanism for Synergy with 20(S)-ginsenoside Rh2. *Drug Metab. Dispos.* 40 (10), 1900–1908. doi:10.1124/dmd.112.045187

Zhang, J., Zhou, F., Niu, F., Lu, M., Wu, X., Sun, J., et al. (2012b). Stereoselective Regulations of P-Glycoprotein by Ginsenoside Rh2 Epimers and the Potential Mechanisms from the View of Pharmacokinetics. *PLoS One* 7 (4), e35768. doi:10.1371/journal.pone.0035768

Zhang, J., Zhou, F., Wu, X., Zhang, X., Chen, Y., Zha, B. S., et al. (2012c). Cellular Pharmacokinetic Mechanisms of Adriamycin Resistance and its Modulation by 20(S)-ginsenoside Rh2 in MCF-7/Adr Cells. *Br. J. Pharmacol.* 165 (1), 120–134. doi:10.1111/j.1476-5381.2011.01505.x

Zhao, Y., Bu, L., Yan, H., and Jia, W. (2009). 20S-protopanaxadiol Inhibits P-Glycoprotein in Multidrug Resistant Cancer Cells. *Planta Med.* 75 (10), 1124–1128. doi:10.1055/s-0029-1185477

Zhou, B., Xiao, X., Xu, L., Zhu, L., Tan, L., Tang, H., et al. (2012). A Dynamic Study on Reversal of Multidrug Resistance by Ginsenoside $Rh_2$ in Adriamycin-Resistant Human Breast Cancer MCF-7 Cells. *Talanta* 88, 345–351. doi:10.1016/j.talanta.2011.10.051

Zou, J., Su, H., Zou, C., Liang, X., and Fei, Z. (2020). Ginsenoside Rg3 Suppresses the Growth of Gemcitabine-Resistant Pancreatic Cancer Cells by Upregulating lncRNA-CASC2 and Activating PTEN Signaling. *J. Biochem. Mol. Toxicol.* 34 (6), e22480. doi:10.1002/jbt.22480

**Conflict of Interest:** The authors declare that the research was conducted in the absence of any commercial or financial relationships that could be construed as a potential conflict of interest.

**Publisher's Note:** All claims expressed in this article are solely those of the authors and do not necessarily represent those of their affiliated organizations, or those of the publisher, the editors and the reviewers. Any product that may be evaluated in this article, or claim that may be made by its manufacturer, is not guaranteed or endorsed by the publisher.

## GLOSSARY

**ABC** ATP-binding cassette

**ActD** actinomycin D

**ADM** Adriamycin

**BCRP**

**Breast cancer resistance protein**

**CK** Compound K; CQ, Chloroquine

**CSCs** Cancer stem cells

**DDP** Cisplatin

**DOX** Doxorubicin

**EGFR** Epidermal growth factor receptor

**EGFR-TKI** Epidermal growth factor receptor-tyrosine kinase inhibitor

**EMT** Epithelial-mesenchymal transition

**FU** Fluorouracil

**GEM** Gemcitabine

**GST** Glutathione-S-transferase

**HCQ** Hydroxychloroquine

**IL** Interleukin; L-OHP, Oxaliplatin

**LRP** Lung resistance-related protein

**MAPK** Mitogen-activated protein kinase

**MDR1** Multi-drug resistance 1

**MRP** Multidrug resistance-related protein

**m-TOR** Mammalian target of rapamycin

**MX** Mitoxantrone

**NF-κB** Nuclear factor-κb

**NRF2** Nuclear factor erythroid-2 related factor 2

**P-gp** P-glycoprotein

**PI3K** Phosphatidylinositol 3-kinase

**PKC** protein kinase C

**PPD** Protopanoxadiol

**PPT** Protopanaxatriol

**PTEN** protein tyrosine phosphatase gene

**PTG** Protropanaxatriol ginsenosides

**Rho123** Rhodamine 123

**SIRT1** Sirtuin1

**TME** Tumor microenvironment

**TNBC** Triple-negative breast cancer

**TOPOII** Topoisomerase II

**TXT** Docetaxel

**VCR** Vincristine

**Vp** Verapamil

# Advantages of publishing in Frontiers

**OPEN ACCESS**
Articles are free to read for greatest visibility and readership

**FAST PUBLICATION**
Around 90 days from submission to decision

**HIGH QUALITY PEER-REVIEW**
Rigorous, collaborative, and constructive peer-review

**TRANSPARENT PEER-REVIEW**
Editors and reviewers acknowledged by name on published articles

**Frontiers**
Avenue du Tribunal-Fédéral 34
1005 Lausanne | Switzerland

**Visit us:** www.frontiersin.org
**Contact us:** frontiersin.org/about/contact

**REPRODUCIBILITY OF RESEARCH**
Support open data and methods to enhance research reproducibility

**DIGITAL PUBLISHING**
Articles designed for optimal readership across devices

**FOLLOW US**
@frontiersin

**IMPACT METRICS**
Advanced article metrics track visibility across digital media

**EXTENSIVE PROMOTION**
Marketing and promotion of impactful research

**LOOP RESEARCH NETWORK**
Our network increases your article's readership